2011-2018

Research Highlights

CCFS

The Australian Research Council Centre of Excellence for Core to Crust Fluid Systems

- CCFS information is accessible on WWW at:

  http://www.ccfs.mq.edu.au/

- Contact CCFS via email at:

  ccfs.admin@mq.edu.au

The CCFS Annual Report is available from our website http://www.ccfs.mq.edu.au/ as a downloadable pdf file or in html format, and by mail on USB on request.

Front Cover: These balls and dendrites of native vanadium are enclosed in crystals of hibonite ($CaAl_{12}O_{19}$) ejected from Cretaceous volcanoes on Mt Carmel in northern Israel. The balls nucleated as droplets on the faces of growing hibonite crystals, when a vanadium melt became immiscible with the Ca-Al silicate melt that was crystallising hibonite, grossite ($CaAl_4O_7$) and spinel, in a magma chamber near the crust-mantle boundary. The dendrites grew out into the silicate melt, and were overgrown by the hibonite. The presence of vanadium melts testifies to the most reduced conditions yet recognised on Earth, equivalent to the oxygen fugacity of the early solar nebula, where the atmosphere was dominated by hydrogen. See Research highlight pp. 315-317.

QR code to view 3D images

Cover and Report design by Sally-Ann Hodgekiss.

Contents

Australian Government
Australian Research Council

Established and supported under the Australian Research Council's Research Centres Program

Research highlights:
A new conceptual framework

Following the new conceptual framework outlined on page 3 of the 2013 CCFS Annual Report, Research highlights are identified as contributing to understanding Earth Architecture (the roadmap for fluids) and/or Fluid Fluxes (the "traffic report"), with logos for easy attribution. For a full description of the foundation programs, see *CCFS 2013 Annual Report Appendix 1*.

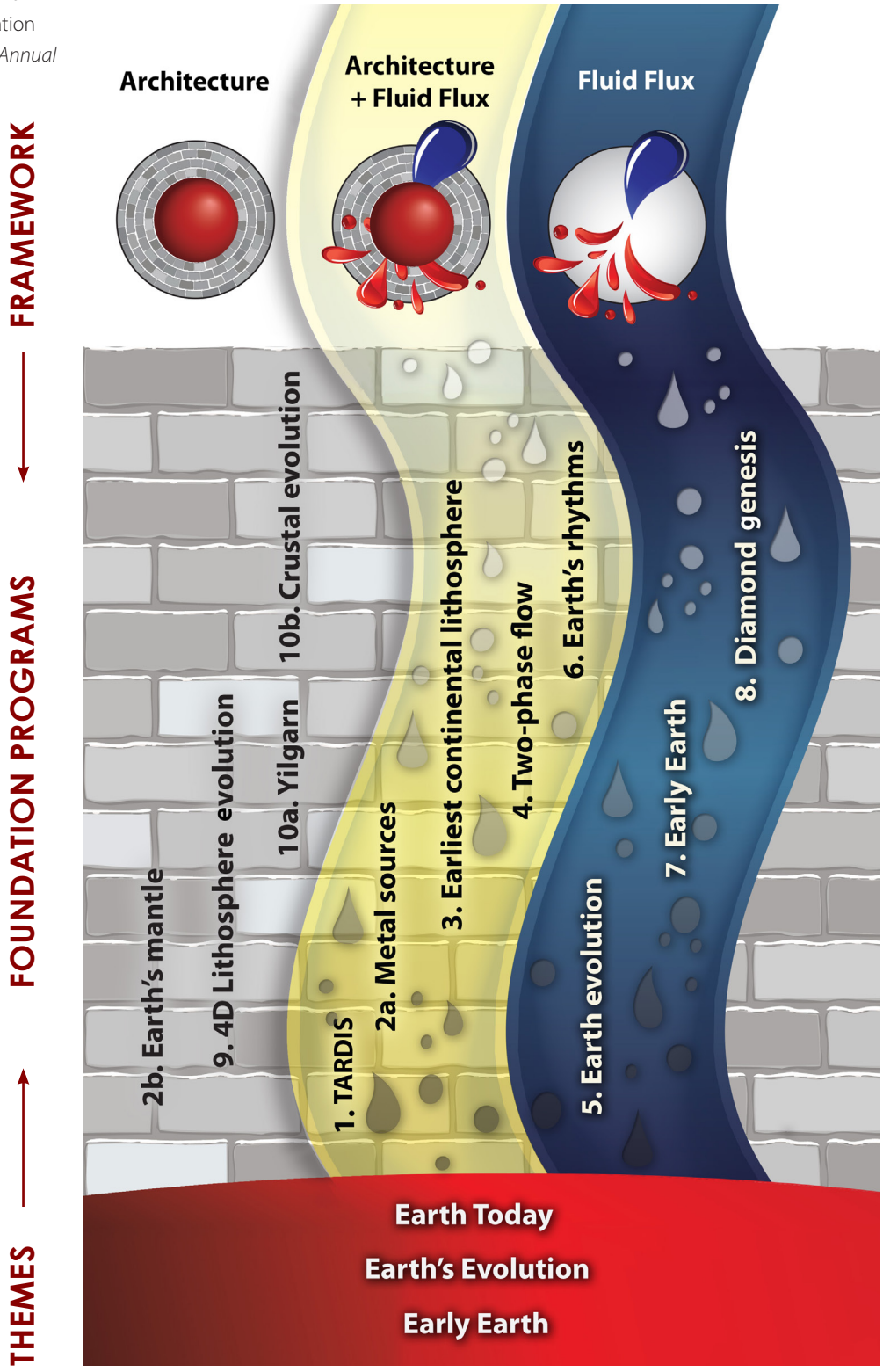

Research highlights 2011

Contents

Moon impacts on origin of Earth and Solar System

Material from the Moon can provide insights into the early history of the solar system and help us to understand the mechanisms of planetary differentiation. On Earth, traces of early differentiation have been erased by tectonic events, whereas the Moon has been relatively inactive for almost 4 billon years. Therefore the Moon provides a unique opportunity to study early differentiation processes on a planetary scale. In addition, the early solar system was affected by intense meteoritic bombardment. The heavily cratered surface of the Moon testifies to this bombardment, which is still ongoing. Evidence of the early bombardment is difficult to find as the lunar surface is continuously reshaped and modified by the influx of meteorites.

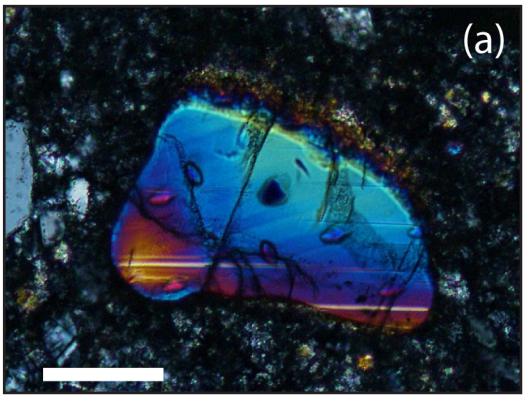

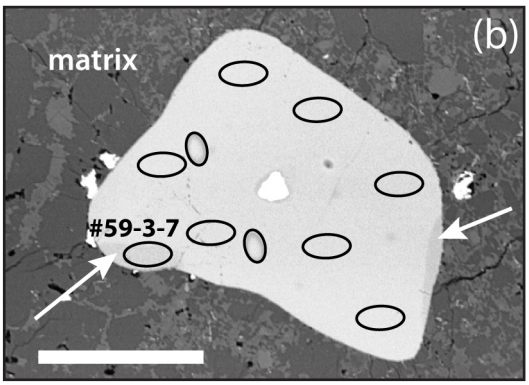

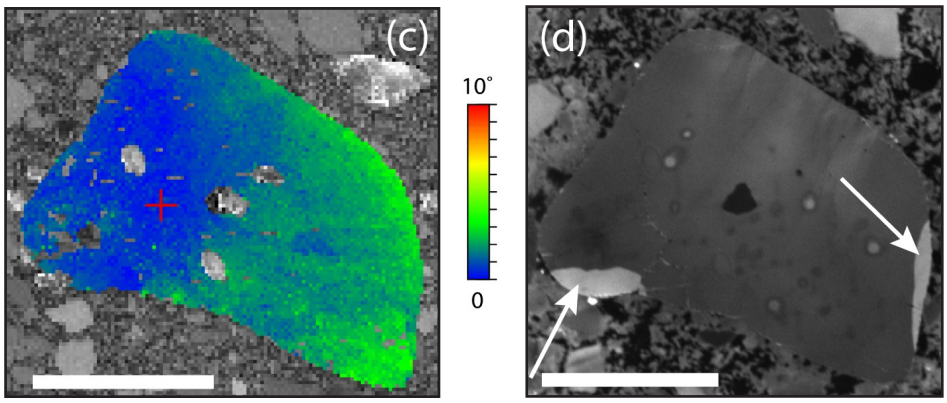

Figure 1. Images of zircon grain 73235-59#3 (the tiger).

One source of information is old grains of zircon, which can be extracted from lunar rocks and soils.

Lunar zircons are useful because they can give information about both differentiation (as they crystallised in deep-seated plutonic bodies) and impact processes. They are not easily destroyed by impact metamorphism, but often carry signs of partial reworking during the impacts. They are found in impact melt breccias, which are rocks composed of pieces of broken rocks, loose minerals (or pieces of broken minerals) set in a matrix made up of crystallised impact melt. Zircons found in thin sections are imaged using an optical microscope and then a scanning electronic microscope (SEM) to reveal their internal features (Fig. 1). They are then dated *in situ* by the U-Pb technique using an ion microprobe: this allows us to target specific areas of the zircon grains and extract ages related either to magmatic events or impact deformation.

One special zircon grain, nicknamed "Tiger" because of its striped appearance, shows several features that are often observed in lunar zircons and are especially significanct for the interpretation of their history. The stripes are Planar Deformation Features (or PDFs) corresponding to defects in the crystalline lattice that can only be created at the very high pressures generated by an impact. These PDFs are visible in the optical microscope (Fig. 1a) and with the SEM. In addition, the zircon grain is plastically deformed, testifying to deformation that occured during the heating generated by the impact (Fig. 1c). The Tiger grain also shows some recrystallised areas (Fig. 1 arrows); as no fluids are known to be available on the Moon, these recrystallised zones probably were generated following changes induced by an impact. These recrystallised zones in lunar zircon provide a unique way of dating the impact that generated them. In the case of the Tiger grain, the area is large enough to fit an ion probe spot on it. This zone proved to be ~250 million years younger than the main part of the zircon, which records the time of the zircon's original crystallisation from the melt (Fig. 2).

This study shows that many zircon grains can be used to determine both the time of their magmatic crystallisation and the timing of their modification by impacts. Study of the relationships between different impact features preserved in some grains allows us to reconstruct the P-T paths followed by these grains in the immediate aftermath of the impact. We hope that in the future we will be able to use this information to link individual zircon cont...

grains to specific impact craters on the Moon and determine from which part of the crater this zircon was excavated. For more of this story, see *CCFS publications #126 and #147.*

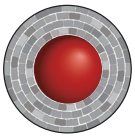

This project is part of CCFS Theme 1, Early Earth, and contributes to understanding Earth's Architecture.

Contacts: Alexander Nemchin, Marion Grange
Funded by: CCFS, Curtin University, ARC Discovery (from 2012)

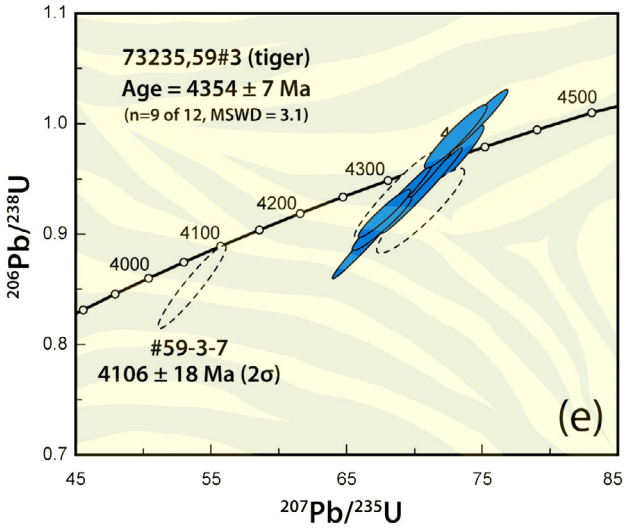

Figure 2. Concordia plot showing ages of primary zircon (filled symbols) and PDFs.

Sulfur in unique ancient Australian rocks may unlock Earth and life secrets

The relationship between the evolution of Earth's atmosphere and hydrosphere during the Archean, and the beginning of life are major questions in Earth Science. The mass-independent fractionation (MIF) of sulfur isotopes (expressed as $\delta^{34}S$, $\Delta^{33}S$ and $\Delta^{36}S$) was caused by ultraviolet photolysis of atmospheric SO_2 in the Archean when the atmosphere was oxygen-poor and the ocean was sulfur-poor. There are significant variations in the degree of mass-independent fractionation during the Archean; it was lowest in the Mesoarchean (from 3.3 to 2.8 Ga), and these variations carry very important information. This low point has been suggested to be a result of an early rise in atmospheric oxygen. However, more recent studies (Farquar et al., 2007 *Nature*) show there is no clear evidence that oxygen rose then. The strongest Mesoarchean $\Delta^{33}S$ MIF values ranged from -0.13 to 1.31 between 2.96 Ga and 2.9 Ga (Fig. 1); this coincides with the only major volcanic events during this period, after the stabilisation of the first cratons (Kaapvaal and Pilbara). These events are linked to the start of plate tectonics and subduction (from 3.1 to 2.95 Ga), which poured volcanic gasses into the atmosphere, contributing to the development of sulfur isotope MIF and the high levels of Mesoarchean sulfur. Prior to 2.7 Ga there is a very limited rock record, and most samples showing sulfur MIF from the Mesoarchean are from continental-margin sedimentary ocean basins on the two new cratons; therefore the lack of significant negative $\Delta^{33}S$ values is not really evidence for oceanic sulfate (or atmospheric oxygen) during this period.

Australia is the only place where a wide variety of marine deposits of this key age occur, that can fill the gap in the existing global database. Recently, we have obtained the first excellent Mesoarchean results from deep ocean environments in the 2.9 Ga Lake Johnston Belt and the Murchison province of the Yilgarn. Those samples show key evidence for variations in the sulfur cycle through this time range, rather than just minor oxygen-fugacity variations before the Great Oxidation Event (Figs. 2-4). However, the ~2.9 Ga Lake Johnston Greenstone belt in the Yilgarn Craton is a marine rift with submarine volcanic rocks (basalts, felsic volcanics and komatiites) shales andbanded iron formations (BIFs); it also contains low-temperature volcanogenic massive sulfides (VMS) and the Maggie Hays komatiite-hosted Ni sulfide

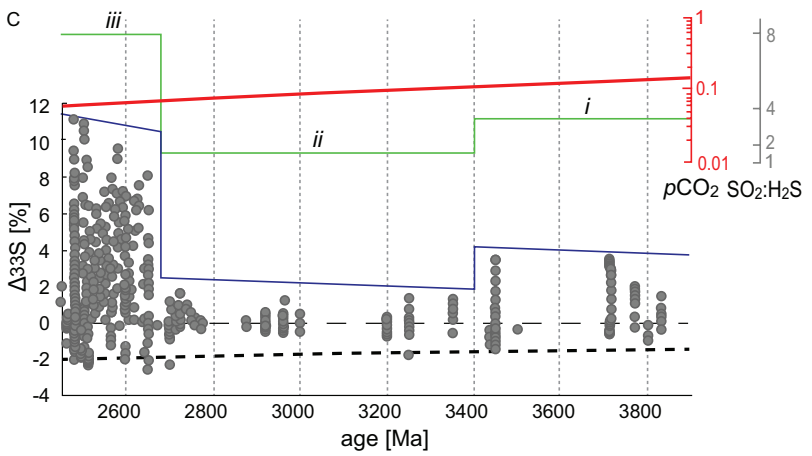

Figure 1. The global SMIF database 2010 showing the first significant Mesoarchean positive SMIF data from the margins of the first stable cratons. (Halvey et al. 2010, Science).

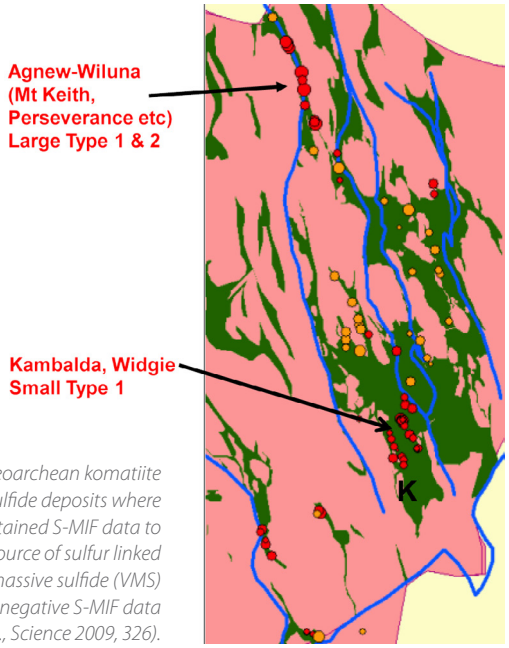

Figure 2. Neoarchean komatiite hosted Ni sulfide deposits where we have obtained S-MIF data to define the source of sulfur linked to volcanic massive sulfide (VMS) deposits with negative S-MIF data (Bekker et al., Science 2009, 326).

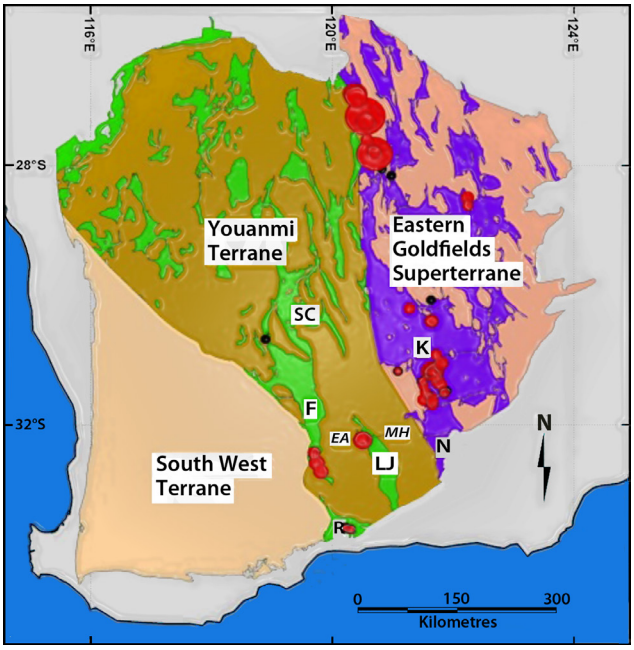

Figure 3. Similar-looking komatiite hosted Ni Sulfide deposits, with adjacent VMS deposits and banded iron formations, where we have found the only significant Mesoarchean negative S-MIF data.

deposit. The new $\Delta^{33}S$ values we recently obtained from a key set of samples from this belt range from -1.7 to 0.1, providing the first and only strongly negative $\Delta^{33}S$ data from the Mesoarchean. These observations are consistent with the reduction of inorganic sulfate, similar to that observed in the Neoarchean VMS, komatiite-hosted Ni sulfides (Figs. 2, 3 and 4) and BIFs. This provides the only evidence for a Mesoarchean sulfate reservoir linked to a subaerial volcanic plume and an oceanic volcanic plume with volcanic island eruptions. These data show that the strongest positive and negative $\Delta^{33}S$ variations in the Mesoarchean sulfur MIF record are lower than the range of sulfur MIF variations in the Paleoarchean and Neoarchean. They are linked to the only preserved evidence for Measoarchean Large Igneous Province volcanic events with some subaerial volcanism producing the key volcanic gas. Our new data from the largest 2.95 Ga Mesoarchean deep submarine volcanic massive sulfide deposit, Golden Grove, are evidence for major suphur recycling after plate tectonics started.

This project is part of CCFS Themes 1 and 2, Early Earth and Earth Evolution and contributes to understanding Earth's Fluid Fluxes.

Contacts: Mark Barley, Marco Fiorentini
Funded by: ARC Discovery (initial work until relinquished in early 2011), CCFS Foundation Program 5

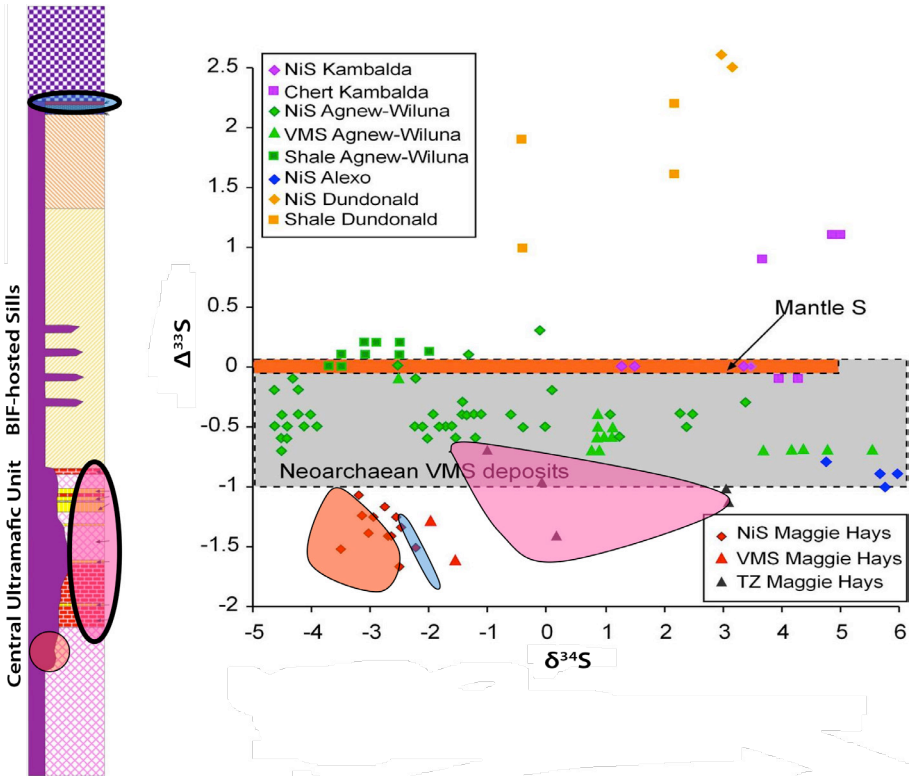

Figure 4. Our 2.9 Ga Lake Johnson SMIF data from Maggie Hays compared to our first 2.7 Ga Neoarchean data.

A new tectonic history for the Yilgarn predicts eastward expansion of gold prospects

The Albany–Fraser Orogen is an arcuate orogenic belt along the southern and southeastern margins of the Archean Yilgarn Craton in Western Australia. Previous studies ascribed the main tectonic and metamorphic features of the belt to the Mesoproterozoic Albany–Fraser Orogeny. However, a significant tectonomagmatic event is now known to have taken place during the Paleoproterozoic within the Biranup Zone of the orogen, and also suggests an allochthonous setting for much of the orogen. Magmatism in the Biranup Zone commenced at ca 1710 Ma, and the Hf-isotope signature indicates that the magmas were derived predominantly by melting of an Archean (Yilgarn craton) source (Fig. 1a). Younger intrusions, with crystallisation ages between 1680–1665 Ma, show a progressively higher proportion of juvenile mantle–derived material in their source. Lu–Hf and U–Pb data from individual zircons, as well as data from entire intrusive bodies, indicate more juvenile additions through time. This rapidly-evolving tectonomagmatic history, and the original Yilgarn-like Hf-isotope signature modified by juvenile material, suggests that an extensional setting, possibly a back-arc, on the margin of the Yilgarn Craton is a feasible tectonic setting for the Biranup Zone of the Albany–Fraser Orogen. Thus, the Hf- isotope data imply an autochthonous origin for much of the orogen. New Lu–Hf results indicate that the Fraser Zone represents addition of juvenile (mantle-derived) material into the crust of the Biranup Zone. This implies that basement to the Fraser Zone is Biranup Zone material, and the extent of rocks considered to be prospective for gold mineralisation probably increases eastward further than previously suspected.

Lu–Hf isotopes also provide information on the growth mechanism of zircon (Fig. 1b), which is important for linking the growth of dateable minerals to the development of other minerals in the rocks. Metamorphic zircon rims produced during Stage II of the Albany–Fraser Orogeny consistently show more radiogenic Hf-isotope signatures, and lower Lu/Hf ratios, than those of igneous zircons. This relationship is best explained by breakdown of igneous zircon and the growth of garnet, depleting the metamorphic reservoir in heavy rare-earth elements (HREE). This metamorphic reservoir, with high $^{176}Hf/^{177}Hf$ but low Lu/Hf, was the source from which metamorphic zircon grew. This indicates that Stage II metamorphic zircon growth occurred under amphibolite-facies (or higher-grade) conditions.

Hf-isotope data from zircons in intrusive rocks of the western Musgrave Province indicate apparent crustal reworking following juvenile input events at ca 1900 and 1600–1550 Ma. Although no juvenile material is known from the older event, radiogenic addition into the crust is required to account for consistent Hf (and Nd) isotope evolution patterns, which show no indication of mixing processes. The timing of juvenile addition and the lack of similarity to Albany–Fraser and Arunta crust suggests that the ca 1900 Ma event reflects development of a mafic underplate on the margin of an Archean Craton. Oxygen isotopes in zircons with ca 1950–1900 Ma model ages indicate that their parent melts were not contaminated by near-surface material, so these model ages represent crustal generation. Correspondence in time between extraction of material from the mantle and the reworking of Archean material strongly supports a coupled response of the upper and lower crust to a juvenile crustal-generation event at ca 1900 Ma. The crustal evolution defined by Hf (and Nd) isotopes allows refinement of paleogeographic reconstructions and has implications for mineralisation styles.

This project is part of CCFS Themes 1 and 3, Early Earth, and Earth Today contributes to understanding Earth's Architecture and Fluid Fluxes.

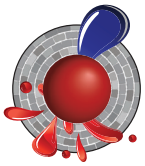

Contact: Michael Wingate

Funded by: GSWA

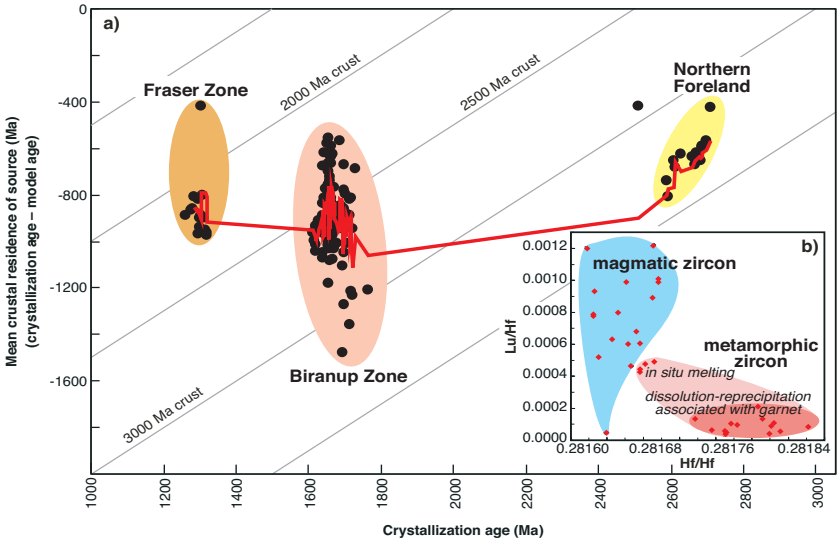

Figure 1. Lu–Hf data used to determine tectonic affiliations of Albany–Fraser Orogen rocks. (a) Event signature diagram showing the general trend with time produced by reworking (downwards), mixing (horizontal), or juvenile input (upwards). The vertical axis shows the "crustal residence time" (age) of the magma sources. The data are from three lithostratigraphic domains: the Biranup and Fraser Zones and the Northern Foreland. The Northern Foreland shows crustal-residence times consistent with an Eastern Goldfields Superterrane (Yilgarn Craton) heritage. The Biranup Zone displays a range of crustal residence times, from old signatures similar to the Eastern Goldfields Superterrane to values considerably less negative, suggesting juvenile addition to the crust. The Fraser Zone Hf is situated mainly between the 2.0 and 2.2 Ga crustal evolution lines and is compatible with the Fraser Zone having reworked Biranup Zone material. (b) Differences in Hf isotopes and Lu/Hf of magmatic zircon, and metamorphic zircon linked to garnet growth.

Tracking water in the Earth's mantle

Water is a very efficient fluxing agent, and is likely to have a strong influence on both the distribution and styles of melting within the Earth's mantle. Knowledge about its distribution and behaviour is critical for our understanding of geochemical fractionation within the Earth's mantle. However, other factors, including pressure and temperature, are also critical because the effects of water in real magmas can be difficult to distinguish from those produced by P and T. To unravel these effects, we have compared the compositional and structural properties of clinopyroxene (an important mantle phase) crystallised from both water-rich and water-poor magmas.

High-pressure experiments have been performed at 1.0-3.5 GPa and 1025-1190 ºC on a hydrous, intraplate magma (nepheline-basanite). Water contents ranging from 5.8 to 16.3 wt % were dissolved in the co-existing melts. Clinopyroxenes (Fig. 1) crystallised from these hydrous experiments were analysed for major elements using an electron microprobe at the GEMOC Analytical Facility. Crystal-chemical structural data for the these pyroxenes, including structure refinements and lattice parameters, were obtained by Fernando Camera and Roberta Oberti using single-crystal X-ray diffractometry at the CNR-Institute of Geoscience and Georesources, University of Pavia, Italy. Water concentrations in the melts were estimated from mass balances between run products and starting materials.

Increasing pressure of formation has a marked effect on both the compositions and structural properties of the clinopyroxenes crystallised from the hydrous melts. Crystals become more jadeite-rich ($NaAlSi_2O_6$) but less calcic and Ti-rich as pressures of synthesis increase. These changes are accompanied by a systematic decrease in cell volumes. Higher temperature causes increases in both the clino-enstatite/clino-ferrosalite components ($(Mg, Fe)_2SiO_6$) and the Ca-Tschermaks component ($CaAl.AlSiO_6$). Inclusion of these latter components also reduces cell volumes.

We evaluated the effects of H_2O by applying the single-crystal clinopyroxene barometer of Nimis and Ulmer *(Contrib. Mineral. Petrol., 133: 122-135, 1998)* to our data. This barometer is based on the overall response of the crystal structure (principally cell volume) to pressure, rather than to specific compositional changes. It was also calibrated primarily for anhydrous melt compositions. When applied to our data, the Nimis and Ulmer barometer systematically underestimates the pressures of synthesis, and the underestimation increases at higher pressure. This is due to the comparatively large volumes of the crystals grown in our experiments. Thus at constant pressure, clinopyroxenes crystallised from H_2O-rich melts have larger volumes than those crystallised from equivalent anhydrous systems. At least in part, this can be attributed to the effects of H_2O on the activity coefficients of pyroxene-forming melt components such as jadeite (Fig. 2). When compared to anhydrous experiments, the data also reflect changes in the activity coefficients of components within the clinopyroxene

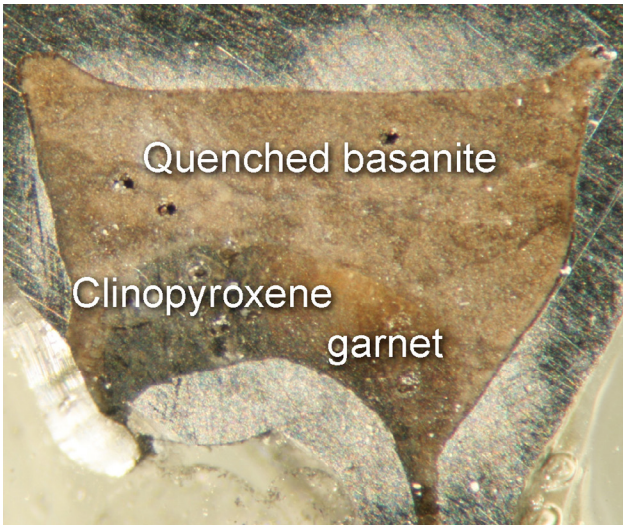

Figure 1. Experimentally grown crystals of dark green clinopyroxene and brown garnet in a quenched, hydrous, basanite melt. The experiment was conducted at 1190 ºC and 3.5 GPa.

crystal structure (e.g. Tschermaks, clino-enstatite and clino-ferrosalite) caused by the lower temperatures of the hydrous experiments. Further work is underway to evaluate these effects quantitatively and link them to water concentrations in mantle-derived hydrous magmas.

This project is part of CCFS Theme 3, Earth Today, and contributes to understanding Earth's Fluid Fluxes.

Contacts: John Adam, Trevor Green, Tracy Rushmer
Funded by: Macquarie University Development Grant, ARC Discovery, MQ

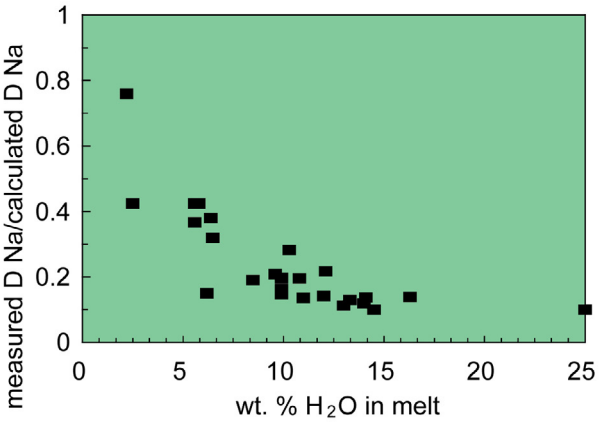

Figure 2. The effect of water on the partitioning of sodium between clinopyroxene and melt. The vertical axis shows the ratios of measured partition coefficients for hydrous melts and values calculated for anhydrous melts.

Minute but noble mineral grains yield insights into mantle processes

Pods of monomineralic chromite (chromitites) often occur in the zone between the mantle and the crustal sections of ophiolites, pieces of oceanic lithosphere that were emplaced on land during the closure of oceanic basins. These "podiform chromitites" usually contain high levels of the platinum-group elements (PGE: Os, Ir, Ru, Rh, Pt, Pd). The PGE concentrate in mantle rocks and minerals, and can be used to trace the mechanism of mass transfer between the upper mantle and the crust, and the recycling of crust into the mantle. Podiform chromitites are of particular interest since they tend to concentrate the most incompatible PGE (i.e. Os, Ir, Ru), which are found as minute inclusions of platinum-group minerals (PGM) made up mostly of these elements [e.g. Os-Ir alloys; erlichmanite (OsS_2), osarsite (OsAsS), laurite (Ru, Os)S_2].

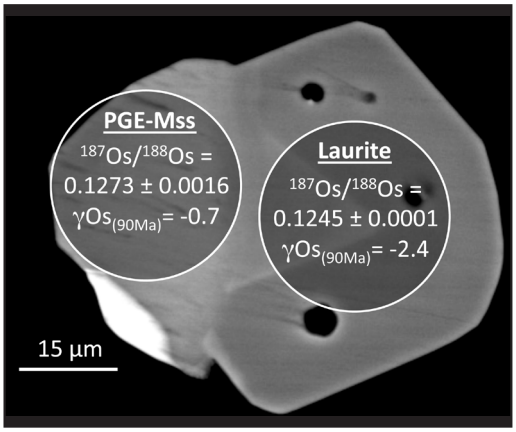

Figure 1. Re-Os systematics in the analyzed sulfides of the Caridad chromitite (Mayarí-Baracoa Ophiolitic Belt, eastern Cuba). Black spots correspond to minute inclusions of millerite and/or chalcocite; the brighter mineral associated with PGE-rich Mss is cuproiridsite.

The development of micro-analytical techniques of laser ablation at CCFS enables measurement of Re-Os isotopes *in situ* on single grains of PGM ~5 µm across. The application of this approach to primary PGM inclusions in podiform chromitites from the Mayarí-Baracoa Ophiolitic Belt (eastern Cuba) has let us decipher heterogeneities in $^{187}Os/^{188}Os$ at the km, hand-sample, thin-section, and even single-grain scales (Fig. 1). These observations lead directly to the conclusion that the observed Os-isotope heterogeneity in PGM reflects the presence in the upper mantle of melts derived from rock volumes with widely varying Os-isotope composition, perhaps even bodies of ancient subducted crust. This isotopic heterogeneity also suggests that the Os-isotope compositions of PGM hosted in the podiform chromitites may be representative of the large volumes of the convecting mantle that would need to be melted to accumulate these concentrations of Cr and PGEs (see *CCFS publication #13)*.

However, podiform chromitites, like their mantle-derived host rocks (i.e. dunite, harzburgite, lherzolite), can be altered by fluids during post-magmatic events, such as serpentinisation or metamorphism. During these processes the PGM can be released and exposed to the circulating solutions as the host chromite reacts. Pre-existing PGM may be partially or completely replaced by secondary PGM (e.g. sulfides reduced to alloys or

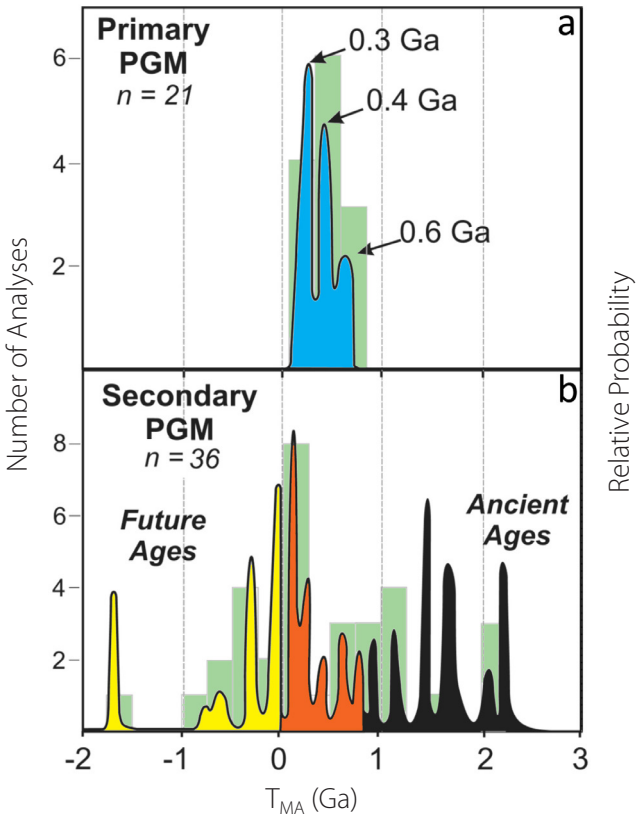

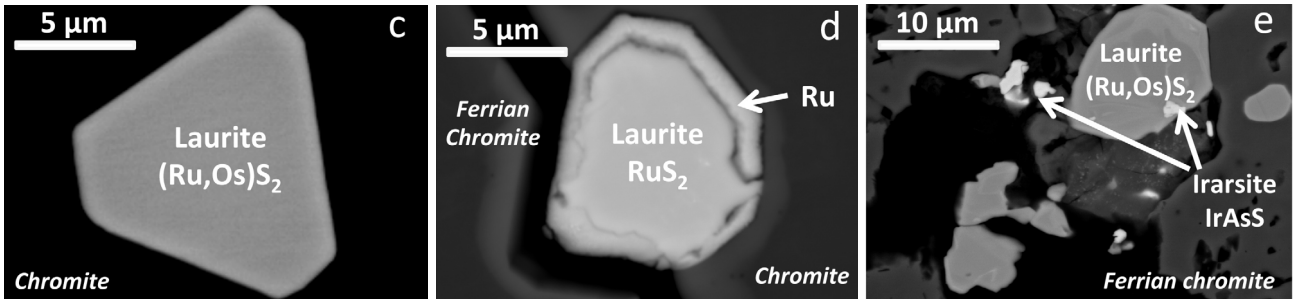

Figure 2. Isotopic heterogeneity in PGM suites. T_{MA} model ages of primary (a) and secondary (b) PGM grains from the Dobromirtsi chromitites. Photos are backscattered electron images of primary PGM (c) hosted in unaltered chromite, and altered (secondary) PGM (d, e) found in altered zones of the chromitites. Note scale bars - these are tiny, but analysable, grains.

oxides; Fig. 2) and/or new secondary PGM can be formed, stable at the conditions imposed by the alteration. The *in situ* laser ablation analysis of PGM from metamorphosed chromitites in Bulgaria (*CCFS Publication #42)* reveals that primary PGM hosted in unaltered chromite are isotopically different from secondary PGM related to the metamorphic overprint (Fig. 2).

These differences between primary and secondary PGM indicates that a significant part of the Os-isotope heterogeneity described in many PGM suites, and interpreted to be mantle-derived, is actually due to post-magmatic disturbance by hydrothermal processes. The fact that secondary PGM in the metamorphosed chromitites of Dobromirtsi yield $^{187}Os/^{188}Os$ within the range of depleted to enriched mantle sources suggests that much of the Os-isotopic variability previously reported for PGM taken out of their microstructural setting (e.g. mineral concentrates or detrital grains collected from streams), and interpreted as a magmatic feature, may instead be related to secondary alteration processes. Therefore, interpretations of mantle events based on the *in situ* analysis of PGM nuggets from placers may be need to be re-considered. Moreover, the observation that metamorphosed chromitites may carry primary and secondary PGM with very distinct $^{187}Os/^{188}Os$ suggests that previously reported Os-isotope compositions of metamorphosed chromitites, which were determined using whole-rock analysis, might reflect mixing of primary (magmatic) and secondary Os remobilised during metamorphism, rather than primary magmatic values.

Once again, *in situ* microanalysis is providing insights impossible to derive from bulk analysis – and providing grounds for caution about our understanding of some mantle processes!

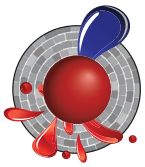

This project is part of CCFS Themes 1, 2 and 3, Early Earth, Earth Evolution and Earth Today and contributes to understanding Earth's Architecture and Fluid Fluxes.

Contacts: José María González-Jiménez, Bill Griffin, Norman Pearson, Sue O'Reilly
Funded by: ARC, CCFS Foundation Program

The perfect conditions for gold in the West Qinling Orogen

The West Qinling orogenic belt in Central China has an abundant supply of gold ore, but most discoveries of gold deposits in the region only took place during the last four decades. Located between the North China and South China cratons, this orogen now represents one of the most prospective gold provinces in China. With over 500 tonnes of gold reserves identified, it holds a great deal of potential for the future. However the nature of gold formation in this region remains a contentious issue.

Previous research in this region has examined the conditions behind gold formation with a view to aiding exploration targeting efforts, but has not considered factors affecting preservation of the deposits within the Earth's crust. Gold ore is formed underground and over millions of years through a combination of uplift and surface erosion, bringing the ore to within mining levels (exhumation). It is therefore not sufficient for industry to simply conclude that an area has the right conditions for gold mineralisation. If there has been too much erosion the gold will have been destroyed, but if there has not been enough it is inaccessible. Part of Qingtao Zeng's research tests this link between different mineralisation styles and the exhumation history of their host rocks.

The two major gold mineralisation styles that have been reported in the West Qinling Orogen are (1) orogenic gold and (2) Carlin-type gold mineralisation. The Liba goldfield and the Dashui gold deposit are selected to represent these two styles. The work on the Liba and Dashui gold deposits has been published online and submitted to Mineralium Deposita.

The exhumation history of the deposits has been examined through thermochronology and a comparative study was conducted to understand how and why there were such huge differences in mineralisation profiles. Thermochronology cont...

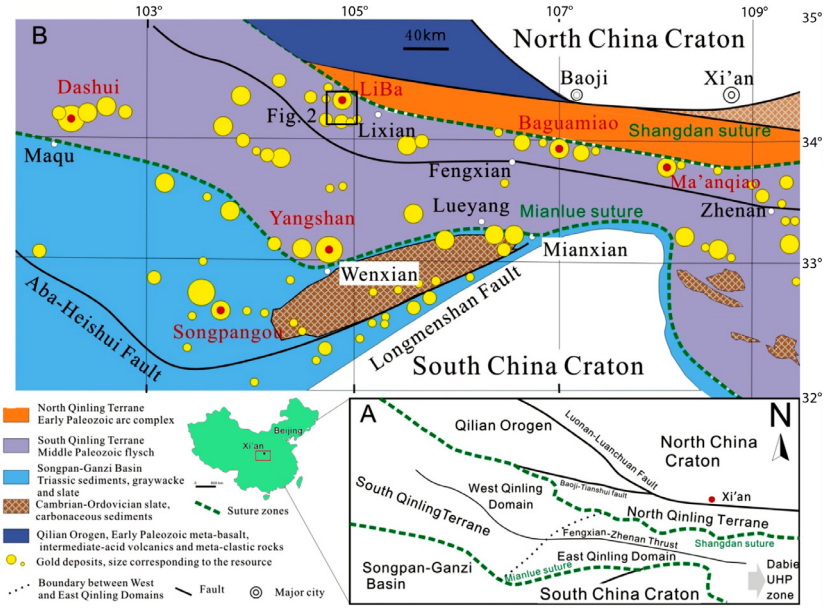

Figure 1.

is a subfield of geology where the time that a sample has spent at a particular depth in the Earth's crust can be determined. The technique combines radiometric dating and a knowledge of the closure temperature for different isotopic systems in individual minerals, to derive a geothermal gradient. The results from this research tell us that in the Liba area, exploration should focus on relatively deep expressions of gold mineralisation, because approximately 5 km of overburden has been eroded away. In the Dashui area, however, erosion has been much less, and a higher priority for gold exploration in the region should be given to shallow mineralisation styles.

By using the knowledge acquired through this research, exploration companies can determine both whether the ore is accessible and what style it will be. After all, "you can only find what you are looking for". In summary, Qingtao's study has increased our understanding of the localisation of gold mineralisation in terms of both genesis and preservation, providing a tool for designing exploration strategy in the West Qinling Orogen.

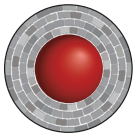

This project is part of CCFS Theme 3, Earth Today, and contributes to understanding Earth's Architecture.

Contacts: Qingtao Zeng, Cam McCuaig
Funded by: Peking University

Zircons reveal 3.5 billion-year old crust beneath central Spain

Our first results on zircons from the lower-crustal granulite xenoliths of the Variscan orogenic belt of central Spain provide evidence for the existence of Paleoproterozoic-Archean (up to 3.5 Ga) components in the deep crust, even though the exposed crust is much younger (GEMOC/CCFS *Publication #721)*. This is supported by both widespread Paleoproterozoic-Archean Hf model ages and the presence of inherited zircon cores with comparable U-Pb ages. Around 75% of zircon grains show inherited cores defining age clusters in Archean (3371-3453 Ma), Proterozoic (618-1680 Ma) and Early Paleozoic (440–573 Ma) time (Fig. 1).

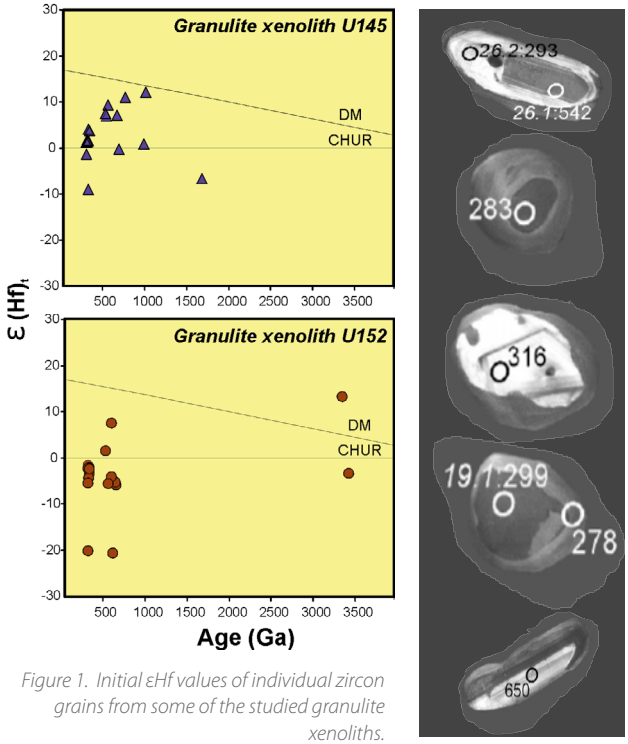

Figure 1. Initial εHf values of individual zircon grains from some of the studied granulite xenoliths.

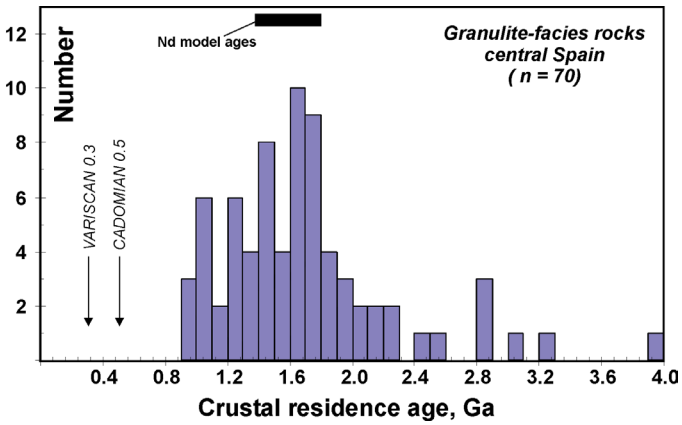

Figure 2. Histogram of Hf Model ages of zircons from the four studied granulite-facies rocks from central Spain. The range of whole-rock Nd model ages is shown for comparison.

Hf-isotope data are useful for estimating the timing of significant production and/or preservation of juvenile continental crust. Thus, the presence in an outcropping migmatite (the Cervatos anatexite) and in the granulite xenolith U152 of two old zircon cores showing markedly positive εHf values (+4.4 and +13.1, at 2180 and 3371 Ma, respectively; Fig. 1), suggests the possibility of juvenile addition during Palaeoproterozoic and Archean times. Figure 2 presents a summary of the Hf model-age data collected on the studied granulitic rocks as well as the range of whole-rock Nd model ages available for them. The resulting juvenile continental-growth histogram shows a continuum between 0.95 and 2.3 Ga, with a predominance of 1.0–1.8 Ga ages and a peak at 1.6–1.7 Ga. Nd and Hf model ages in the range of 1.4–1.7 Ga may represent mixing of Late Proterozoic juvenile components with variable proportions of older crust of Paleoproterozoic and possibly Archean age. The presence of very old crustal components in Neoproterozoic successions deserves a thorough debate in the future, when forthcoming data from metamorphic rocks of the Iberian Massif are available.

Some of the recent paleogeographic reconstruction models suggest northern African sources for the Mesoproterozoic inheritances in the metasediments of the Central Iberian Zone.

In this study age populations in the interval 800–1250 Ma are interpreted as evidence of the location of NW Iberia between the West African Craton and the Saharan and Arabian–Nubian shields (Fig. 3). The Hf-isotope data presented here record only a minor mantle input at 1.0–1.2 Ga in central Iberia, which is markedly younger than the more widespread crust-forming event at 1.3–1.6 Ga recorded in other continental blocks (e.g. Amazonia, Australia, Ukraine). On the other hand, crustal-generation events in central Africa at 1.0–1.3 Ma, reported recently for detrital zircons from central Africa (Congo Craton), match the distribution of Hf model ages of the granulite zircons from central Spain better than those from the Amazonian and West African cratons. This implies that during early Neoproterozoic and late Mesoproterozoic times, NW Iberia was far from the Amazonian Craton, and that its position to the north-east of the West African Craton might be a more reasonable option (Fig. 3). Furthermore, palaeogeographic reconstructions for Early Paleozoic time, based on benthic faunas, support the idea that NW Iberia was probably closer to the Algerian Sahara or Libya than to the Moroccan part of the North Gondwanan shelf.

This project is part of CCFS Themes 1 and 2, Early Earth and Earth Evolution and contributes to understanding Earth's Architecture.

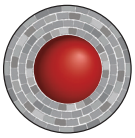

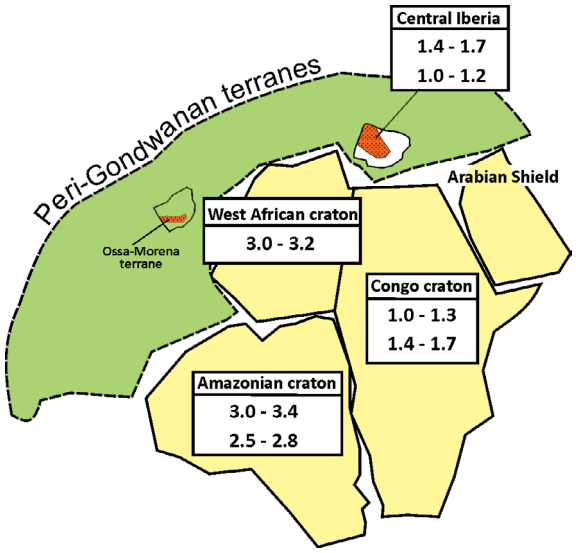

Figure 3. Hf-isotope data of granulite zircons agrees with recent palaeogeographical reconstruction models that show central Iberia as a Peri-Gondwanan terrane located between the West African craton and the Arabian shield, far from the Amazonia microplate. The main Hf-isotope T_{DM} peaks in relative-probability histograms are shown for different cratons (Amazonia, West Africa, central Africa).

Contacts: Elena Belousova, Carlos Villaseca (Universidad Complutense de Madrid)
Funded by: ARC Discovery (O'Reilly, Griffin, Pearson), Industry

Zircons from South China Block, reveal hot (non-glacial) origin

Low $\delta^{18}O$ signatures in supracrustal rocks have been regarded as a signal of cold paleoclimates such as glaciations. Unusually low $\delta^{18}O$ values in Neoproterozoic igneous rocks in parts of the South China Block have thus been genetically linked to Neoproterozoic glaciation events. However, the oxygen isotope compositions of Neoproterozoic magmatic zircons in central South China, measured using *in situ* techniques, argue against such an interpretation. Our results show that low-$\delta^{18}O$ magmatic zircons started to appear in South China from ca 870 Ma, coinciding with the tectonic switching from the Sibao Orogeny to post-orogenic extension, which occurred >150 Ma prior to the first glaciation event. The most abundant low-$\delta^{18}O$ magmatic zircons have ages of 800–700 Ma. 830–700 Ma magmatic zircons show a bimodal distribution of $\delta^{18}O$: mantle-like (+ 4.4 to +5.8‰) and high $\delta^{18}O$ (+9.3 to +10.8 ‰). A sharp temporal change in maximum zircon $\delta^{18}O$ values in South China coincided with the onset of continental rifting and the possible arrival of a plume head. No negative-$\delta^{18}O$ zircons have been identified in this study, contrary to previous studies (Figs. 1 and 2). These features strongly argue against a glaciation origin for low to negative $\delta^{18}O$ values in Neoproterozoic magmatic zircons from South China. We propose that two stages of high-temperature water-magma interaction during plume-driven magmatism and continental rifting best explain the low-$\delta^{18}O$ magmas. The most important implication of this study is that formation of such low $\delta^{18}O$ magmatic zircons was not necessarily related to glacial events and should not be used as a geochemical marker of a cold paleoclimate.

This study shows that the extremely negative $\delta^{18}O$ values from the Dabie-Sulu UHP metamorphic rocks are most likely due to metamorphic processes. The main evidence for this is the presence of extremely low-$\delta^{18}O$ metamorphic minerals including garnet ($\delta^{18}O$ = +5.6‰ to -10‰), omphacite ($\delta^{18}O$ = +7.0‰ to -9.4‰), and phengite ($\delta^{18}O$ = 1.3‰ to -9.1‰) (Zheng et al., 1998, *EPSL, v. 155, 113–129).* Air-abraded zircons gave higher $\delta^{18}O$ values (0.1‰–1.0‰) than those processed without air abrasion (Zheng et al., 2004). Recently, new oxygen-isotope and U-Pb age records of metamorphic zircon grains from UHP eclogites from the Dabie Sulu belt showed that $\delta^{18}O$ values of 850-720 Ma igneous zircon cores are similar to our results and all the negative $\delta^{18}O$ values are found in metamorphic rims on zircon grains (Chen et al., *GCA, v.75, 4877-4898, 2011).* We therefore propose a two-stage high-temperature alteration model to explain the extremely low $\delta^{18}O$ values found in the Dabie-Sulu metamorphic rocks. The first stage represents pre-glaciation high-temperature hydrothermal alteration as discussed earlier. The second cont...

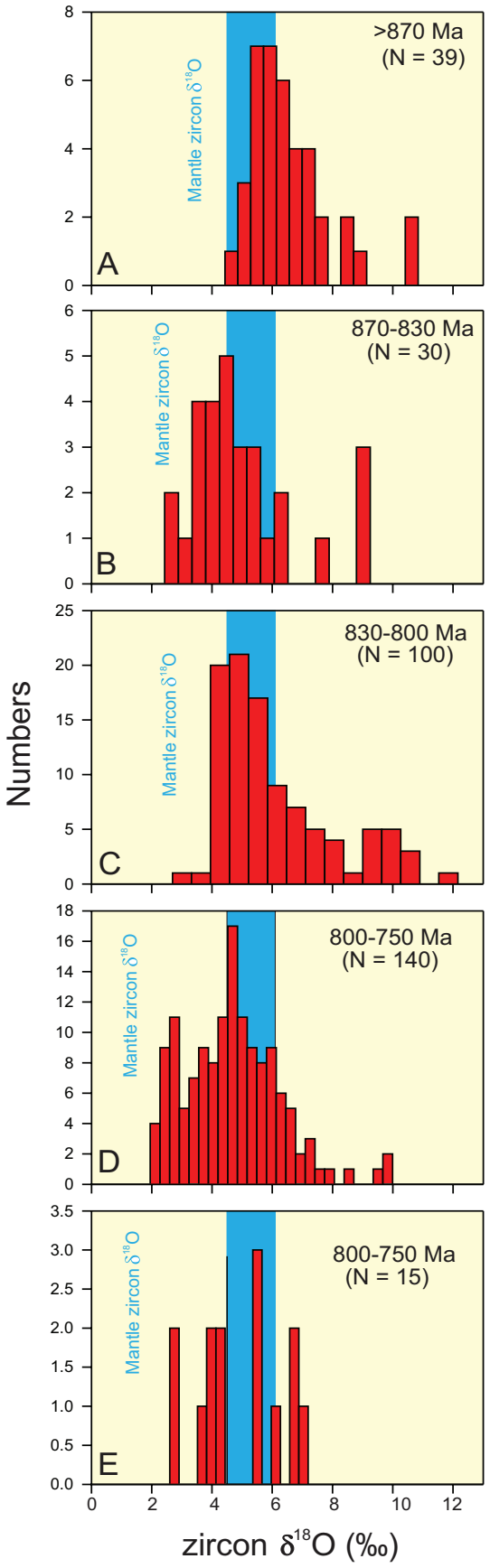

Figure 1. Oxygen isotope compositions of zircons with ages of (A) >870 Ma, (B) 870–830 Ma, (C) 830–800 Ma, (D) 800–750 Ma, and (E) 750–700 Ma. Number of bins in (D) is 25 and 15 for others (Modified after Wang et al., 2011, Geology, v. 39, no. 8, p. 735-738).

stage involves meteoric-hydrothermal alteration under ice age conditions at ≤720 Ma. The oxygen isotopes of pre-glaciation magmatic and sedimentary rocks preserved in the rift basins may have acquired negative $\delta^{18}O$ values during the second stage, although their magmatic zircons would have retained their primary features. Such altered rocks served as the protoliths of UHP metamorphic rocks, thus generating metamorphic minerals and zircon rims with extremely negative $\delta^{18}O$ values.

This project is part of CCFS Theme 2, Earth Evolution, and contributes to understanding Earth's Architecture.

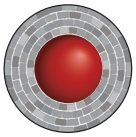

Contacts: Xuan-Ce Wang, Xian-Hua Li, Zheng-Xiang Li, Qiu-Li Li

Funded by: NSFC grant (CI: Professor Xian-Hua Li, commencing 2011, Partner Institution CAS)

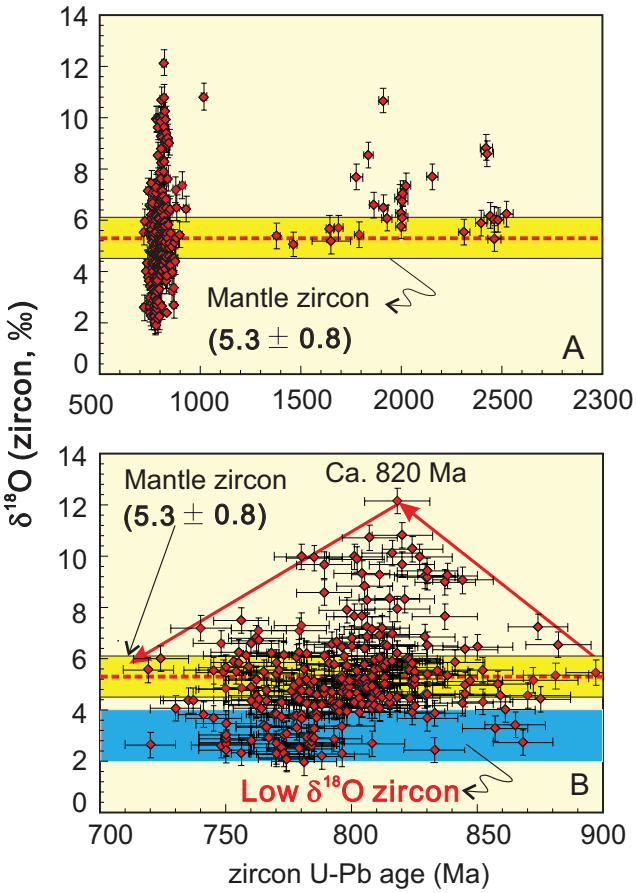

Figure 2. Zircon $\delta^{18}O$ values versus U-Pb ages for (A) all analysed grains and (B) 900–700 Ma grains. The thick arrow lines in (B) show the evolution of maximum oxygen isotopes (Wang et al., 2011, Geology, v. 39, no. 8, p. 735-738).

Copper can concentrate by collision

Porphyry copper deposits are in great demand with today's exploration industries, supplying nearly 70 percent of the world's copper, 50 percent of its molybdenum and 25 percent of its gold. Most of these deposits are formed above subduction zones, where one oceanic plate sinks beneath another continental or oceanic plate, such as in the Eastern Pacific. Traditionally, porphyry Cu deposits were found in subduction area such as in Chile and Peru. However in the last decade it has been discovered that porphyry copper deposits also can be found in continental collisional zones, where two continents collided after oceanic subduction terminated. However, our understanding of the processes of their creation remain limited.

Such deposits have been discovered mainly in the Alpine-Himalayan orogenic belt. Examples include the Eocene-Oligocene Yulong porphyry Cu-Mo belt of East Tibet, the mid-Miocene Gangdese porphyry Cu belt in southern Tibet, and the Neogene porphyry Cu-Au deposits of the southwest Pacific. Their formation involves distinct but as-yet poorly-understood processes unrelated to active subduction, ranging from deep generation of magmas and metal sources to exsolution and evolution of ore-forming fluids in the upper crust.

This CET study has examined porphyry copper systems in Western Yunnan, south-eastern Tibetan Plateau and resulted in new insights into the formation of porphyry Cu systems in continental collisional tectonic settings. The study reported the systems' geology, whole-rock geochemistry, Sr-Nd-Pb isotopes and Hf-O isotopes in zircon, to document the geochemical characteristics of three intrusive suites and determine their magma/metal sources and petrogenesis.

The results revealed a strong indication that continental collision zones hold potential for both porphyry Cu±Mo and Cu±Au deposits. There are five critical factors to this formation, in sequence: (1) an early phase of subduction-modification of continental lithospheric mantle; (2) decompressional melting of upwelling asthenosphere after orogenic delamination; (3) underplating of mafic magmas from the asthenosphere at Moho depths and partial melting of lower crust; (4) melts from residual metasomatised mantle lithosphere; and (5) collectively generating a bimodal suite where porphyry mineralisation is present in alkaline granitoids.

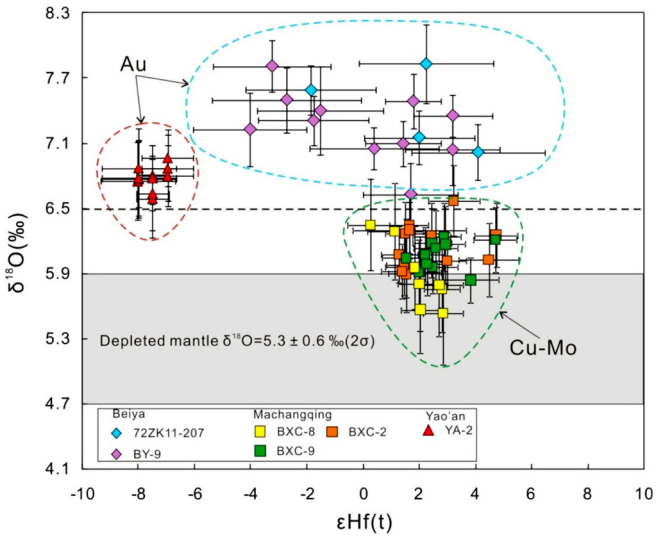

Figure 1. In situ zircon Hf-O isotope data for the Yao, Machangqing and Beiya intrusions.

This research shows that porphyry Cu deposits can certainly form in collisional settings apart from a subduction setting. However, the geological processes related to the formation of these collision zone deposits are still not fully understood. Future research will aim to understand the origin and evolution of the water, metal and sulfur in the collision-zone porphyry deposits.

This project is part of CCFS Theme 3, Earth Today, and contributes to understanding Earth's Architecture and Fluid Fluxes.

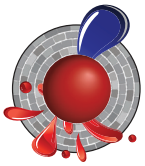

Contacts: Yongjun Lu, Cam McCuaig
Funded by: CAGS

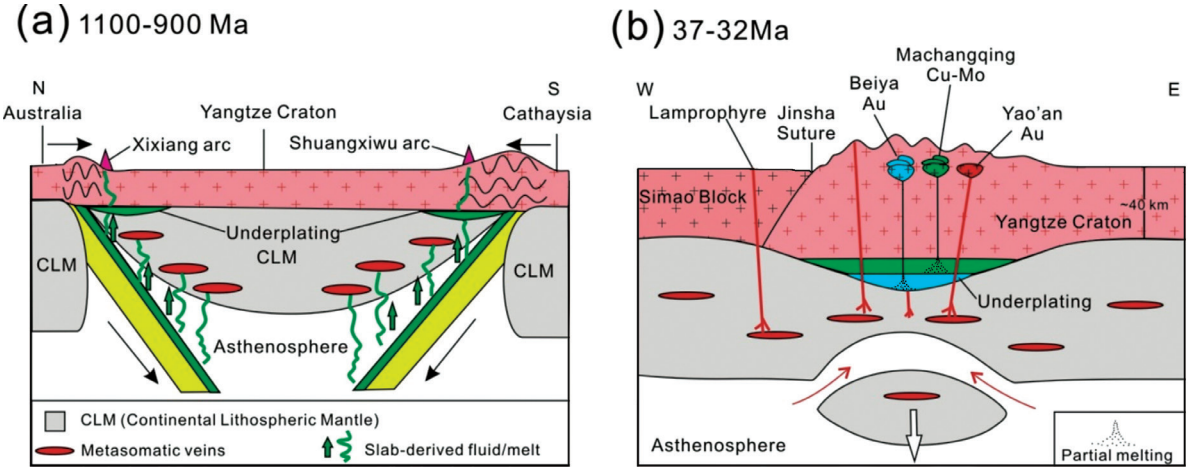

Figure 2. Metallogenic model for the formation of western Yunnan post-collisional porphyry Cu systems.

Coupling, decoupling and fluid infiltration: a torrid history of crust-mantle relationships beneath NW Spitsbergen

The Bockfjord area of NW Spitsbergen (Norwegian Arctic; Fig. 1) exposes a long history of crustal evolution, ending in the Caledonian (400-500 Ma) orogeny; prior to the opening of the North Atlantic Ocean, this area was part of the Laurentian (Greenland) side of the orogen. The N-striking Breibogen-Bockfjord (BB) fault marks the western margin of a large graben

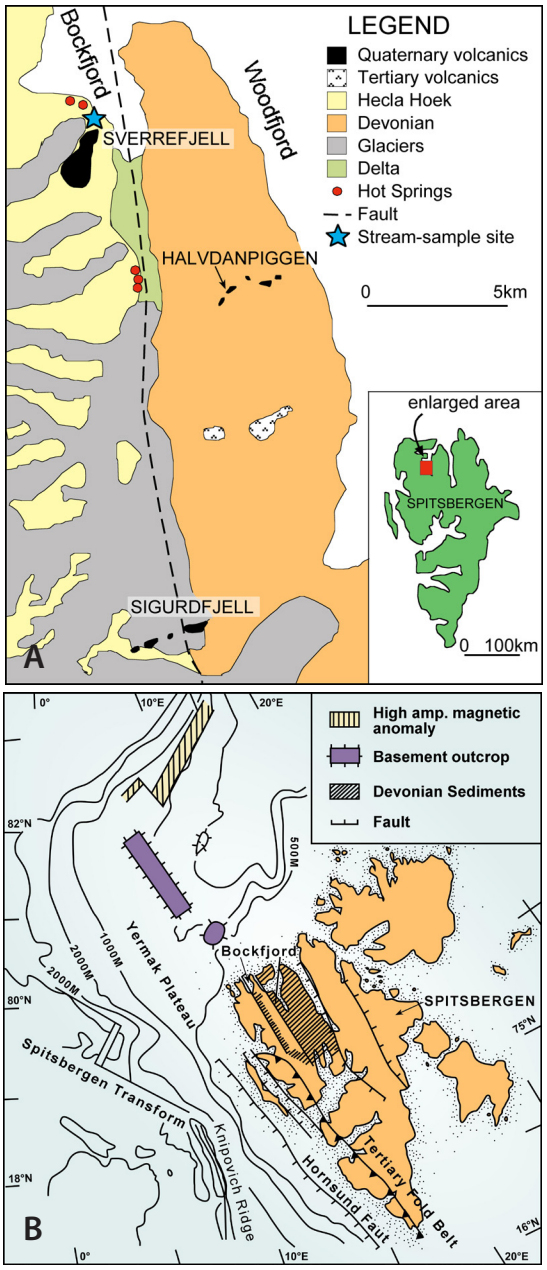

Figure 1. A) Map of the Bockfjord area, with the BB fault nd volcano locations. B) Regional setting, showing possible remnants of Spitsbergen lithosphere on the Yermak Plateau.

filled with Devonian redbeds (Fig. 2). West of the fault the basement consists of gneisses, schists and granites of the Hekla Hoek formation, apparently a Caledonian thrust sheet. U-Pb and Hf-isotope data for detrital zircons from this area show that the protoliths of the Hekla Hoek rocks formed ca 1.8 Ga ago, but were heavily reworked ca 800-1000 Ma ago, and again during the Caledonian orogeny.

Figure 2. Redbeds along Bockfjord.

Quaternary alkali-basalt volcanism has provided abundant xenoliths of mantle and crustal rocks from both sides of the BB fault. Sverrefjell, a large (but glaciated) cinder cone (Fig. 3) may be the world's single largest source of mantle- and crustally-derived xenoliths, with an estimated volume of about one-third of a cubic kilometer. Lower-crustal xenoliths are mainly mafic to intermediate granulites. Most zircons from eight xenoliths have Neoarchean/Paleoproterozoic and Paleozoic U-Pb ages; several also contain zircons with ages and/or Hf model ages >3.2 Ga.

Figure 3. Sverrefjell.

The peridotite xenoliths are mainly spinel lherzolites, metasomatised to varying extents. Xenoliths from basalts east of the BB fault commonly contain amphibole, phlogopite and apatite; peridotites from west of the fault rarely have these metasomatic phases. *In situ* Re-Os isotope analysis of sulfides in the peridotites shows another dichotomy. Xenoliths from west of the fault contain sulfides with Re depletion (T_{RD}) model ages

extending back to 3.3 Ga, with major populations at 2.4-2.6 Ga, 1.6-1.8 Ga and 1.2-1.3 Ga (Fig. 4); the Caledonian orogeny is only weakly represented. East of the BB fault the peaks in the T_{RD} spectrum are at 900-1100 Ma and 400-500 Ma; only a few grains have T_{MA} >2.5 Ga.

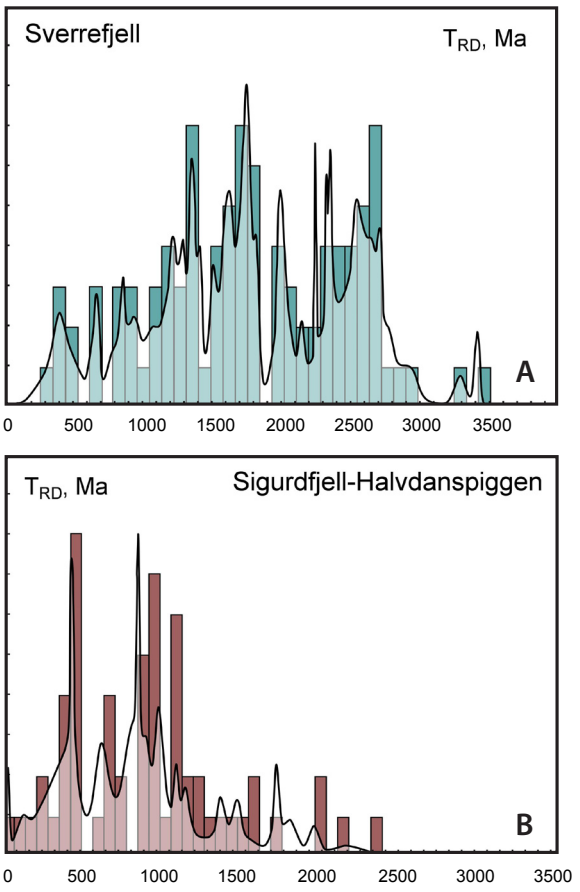

Figure 4. Distribution of Os model ages of sulfides in peridotite xenoliths from either side of the BB fault.

The data show a major disjunct, on both sides of the BB fault, between the Archean lower crust and a Proterozoic-Paleozoic upper crust; this suggests that the original Archean upper (and middle?) crust was detached and replaced by thrust sheets of younger material during the Caledonian orogeny (Fig. 5). The striking differences in the sub-continental lithospheric mantle (SCLM) across the BB fault suggest that major transcurrent movement has juxtaposed lithospheric sections that evolved independently. This may have happened during the long transport of these terranes from north of Greenland, during the opening of the Arctic Sea.

West of the BB fault, the presence of Archean lower crust overlying Archean SCLM suggests that the crust and mantle have remained coupled for ≥3 Ga. East of the fault, similar Archean lower crust overlies an apparently younger, more fertile SCLM. The pervasive melt-related metasomatism that refertilised the SCLM east of the BB fault may have obscured its Archean origin.

Typical Archean SCLM is 150-250 km thick, whereas the Bockfjord volcanoes carry no samples from deeper than 80 km.

The detached lower part of the Archean SCLM may now lie beneath the Gakkel Ridge to the NW (Fig. 1A), as proposed by Goldstein et al. (2008) on the basis of basalt geochemistry. This proposition is supported by the mean T_{RD} of the Sverrefjell sulfides (1740±718 Ma), which is similar to the oldest whole-rock T_{RD} values for peridotites dredged from the Gakkel Ridge (1.8-2.2 Ga; Liu et al., 2010).

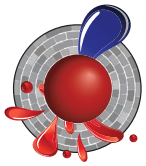

This project is part of CCFS Themes 1, 2 and 3, Early Earth, Earth Evolution and Earth Today, and contributes to understanding Earth's Architecture and Fluid Fluxes.

Contacts: Bill Griffin, Sue O'Reilly, Norman Pearson
Funded by: ARC and GEMOC, CCFS Foundation Program

Figure 5.

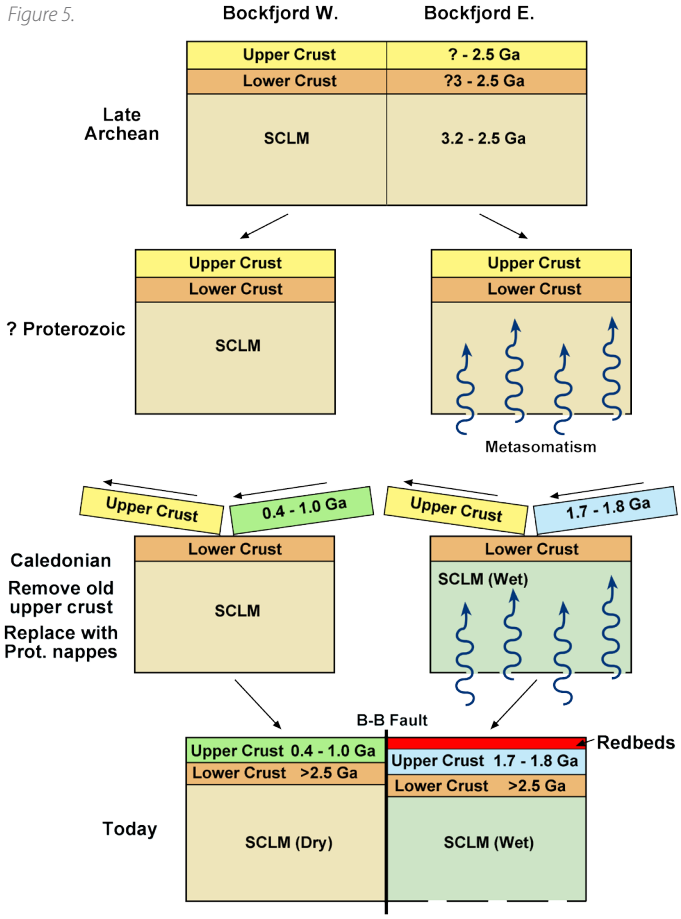

Remaking an old continent - A 40° twist between northern and southern Australia 600 million years ago

The basement rocks beneath the western two-thirds of Australia are mostly older than 1800 million years old (Ma) and host the vast majority of Australia's mineral wealth; the eastern one-third is younger than 540 Ma (Fig. 1). It has long been assumed that the older part of the continent has been in its present-day shape for at least 1000 Ma. However, a re-examination of the tiny magnetic needles trapped in some of Australia's old rocks has revealed a previously unknown 40° twist between the continent's two halves some 600 million years ago (Fig. 2).

Palaeomagnetism is a research method that measures the orientation of tiny magnetic particles trapped in rocks. These act as a fossil compass that records the movement of each continent on the Earth's surface in the deep past. Such fossil magnetic records, called apparent polar wander paths, work like a magnetic barcode for each continent or a piece of a continent. When two pieces of continent travel together on the Earth's surface, their bar codes match exactly. If the two continental pieces later moved apart, their previous palaeomagnetic 'barcodes' would split. This allows us to detect when continents joined together, when they broke apart, and how they moved relative to each other and to the geographic North Pole (Earth's rotation axis).

During a reanalysis of geological and palaeomagnetic data from Australia, we noticed that the palaeomagnetic 'bar codes' (i.e., apparent polar wander paths) between the northern and southern halves of the old Australian ontinent share comparable shapes but with a systematic offset in their present-day continental configuration. However, this offset disappears if we rotate southern Australia about 40° relative to northern Australia (Fig. 2a).

This disjunction between the two halves of the old Australian continent coincides with traces of a major 650–550 Ma mountain belt, which runs from the Paterson Ranges off the eastern boundary of the Pilbara to the Petermann and Musgrave ranges of Central Australia, and disappears into central Queensland (Figs. 1, 2b). This east-west trending zone probably was a mighty mountain range, comparable to the Tianshan ranges in central Asia. There are webs of locally molten rocks in the Musgrave Ranges (Fig. 1) caused by large earthquakes that occurred during this major upheaval. The rotation event would also have laterally

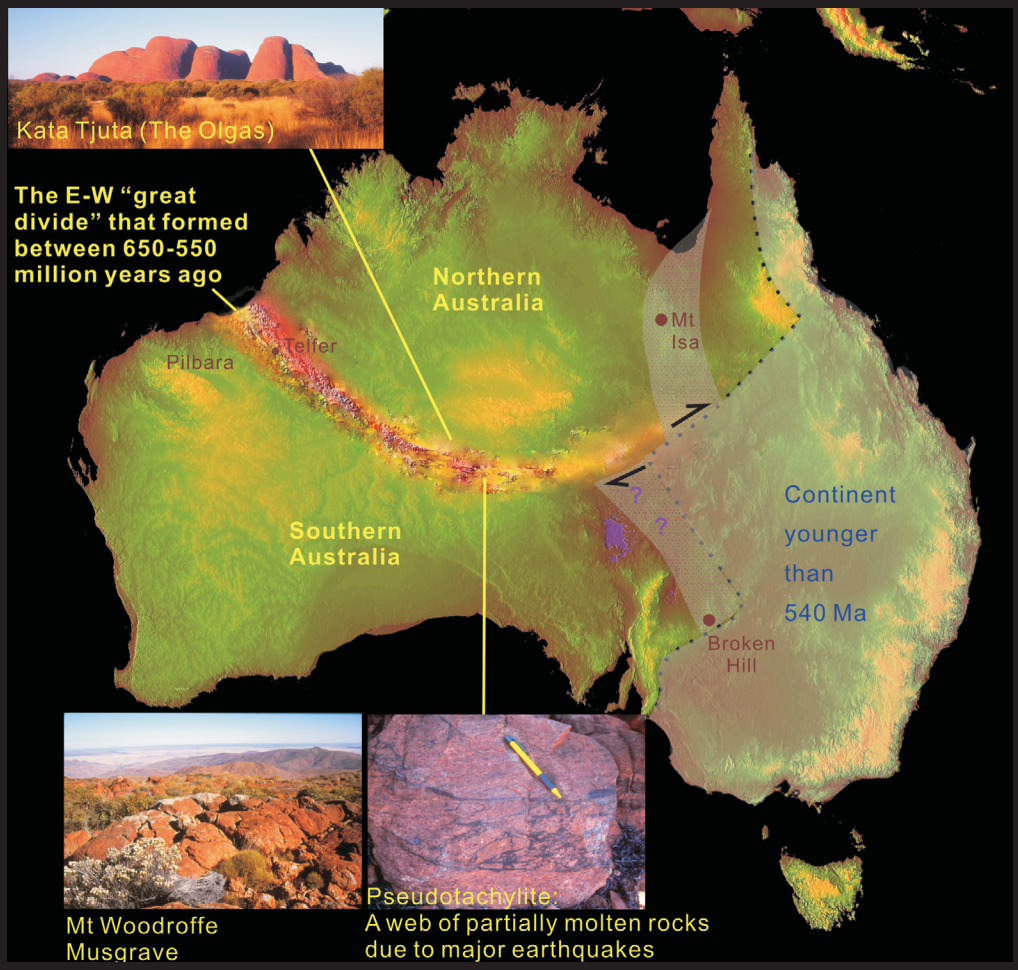

Figure 1. A cartoon of the mighty east-west trending mountain range formed between 650-550 million years ago placed on the present-day Australian landscape. Sediments shed from the northern slope of the mountains formed Uluru (Ayers Rock) and Kata Tjuta (The Olgas).

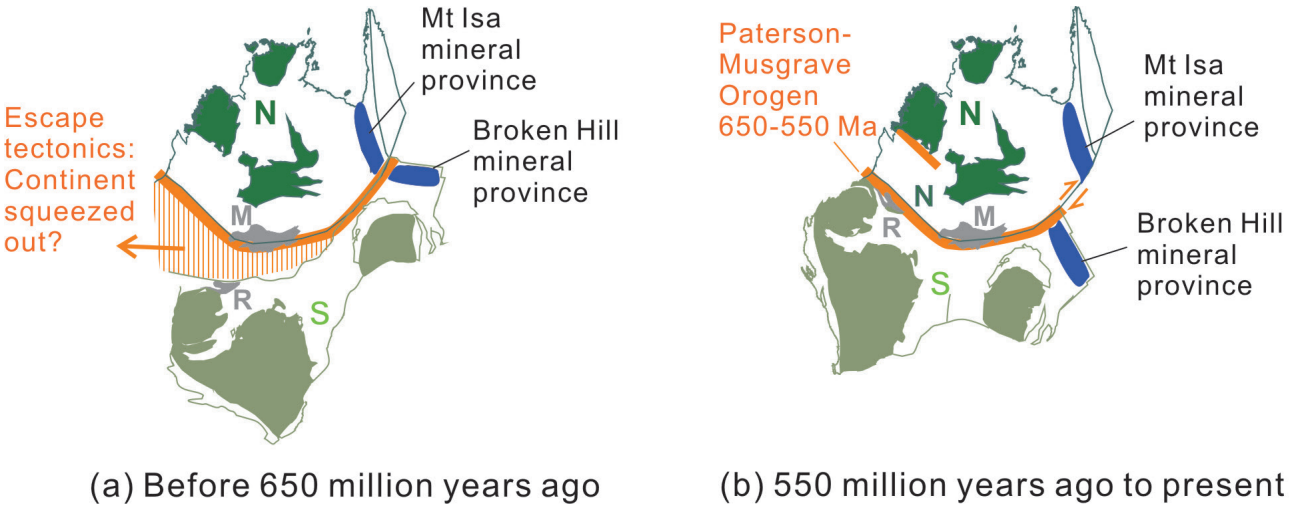

Figure 2. Maps of the old part (>540 million years old) of the Australian continent now (b) and before final tectonic assembly (a) – omitting the eastern third of the continent which had not yet formed. Dark green 'N' = northern Australia; Olive green 'S' = southern Australia; M = Musgrave Block; R = Rudall Complex of the Paterson orogen. Note that the two halves of an originally continuous Mt Isa-Broken Hill mineral province are now offset by ~550 km.

offset the northern and southern halves of the old continent by over 500 km, and would provide a setting for forming new mineral deposits. Sediments shed off the northern slope of this mighty mountain range formed the present-day cultural and landscape icons, Uluru (Ayers Rock) and Kata Tjuta (The Olgas) (Fig. 1).

Australia probably lost a bit of real-estate during this event, as land that used to fill in the narrow triangular gap in the western part of the continent was probably squeezed out to the west during the rotation. However, Australia did gain in mineral endowment, such as the large Telfer gold deposit in Western Australia. There is potential for finding more such deposits along this long mountain belt. This new interpretation also solves one of the long-standing puzzles about where the southern extension of the Mt Isa mineral zone went. Our work indicates that the two mineral belts may indeed, as previously speculated by geologists, have formed as parts of a single belt that was cut into two halves and offset by over 500 km during an intracontinental rotation some 650–550 million years ago (Figs. 1 and 2).

Our new geotectonic model also resolves a longstanding controversy surrounding the configuration and breakup history of the supercontinent Rodinia (lifespan ca 900–700 Ma), consisting of almost all continents that existed at the time. It implies that Rodinia didn't break up until much later than we thought, placing the breakup much closer to the time of the hypothesised first 'Snowball Earth' event. This makes it more plausible that the breakup of the supercontinent and accompanying geographical and chemical changes led to catastrophic global chilling events (opposite to global warming events) between 750 and 600 million years ago. Both events probably played roles in the Cambrian explosion of complex life on Earth. The formation and subsequent erosion of the mighty mountain range across Australia may also have contributed to the oxygenation of the atmosphere, thus making the Earth more habitable for complex life.

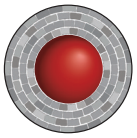

This project is part of CCFS Theme 2, Earth Evolution, and contributes to understanding Earth's Architecture.

Contacts: Zheng-Xiang Li, David Evans (Yale University)
Funded by: ARC Discovery

Arkansas was built over collision zone of Archean microcontinents

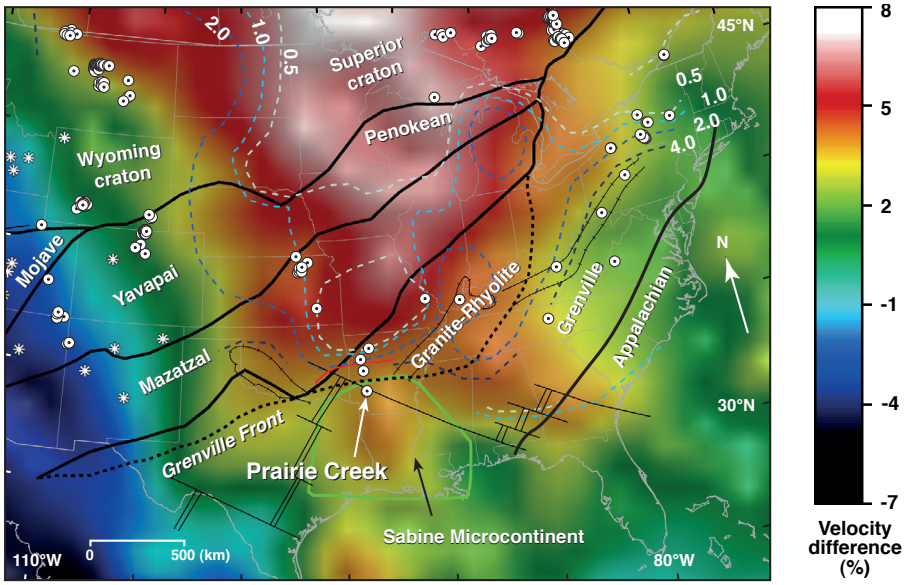

Figure 1. Seismic tomographic image (100-175 km depth slice, courtesy of Steve Grand) covering part of southern North America. The image highlights the spatial relationship between shear wave velocity (Vs) and crustal features. Reference velocity is 4.5 km/sec. "Hot" colours represent high Vs, while "cold" colours represent low Vs. The Prairie Creek lamproite field is indicated by an arrow. Solid thick black lines are crustal province boundaries of Whitmeyer and Karlstrom (2007). Short black dashes show the interpreted northwestern extent of Grenville lithospheric reworking. Green line shows approximate outline of the Sabine microcontinent, which is surrounded on its west, north and northeast sides by the Ouachita orogen thrust front. Ticked thin black lines are Late Neoproterozoic to Cambrian aulocogens. Thin black lines are the proposed latest Neoproterozoic rifts and transform faults for southernmost Laurentia (Thomas, 2006). Solid red line is the approximate northern extent of Ouachita Orogen thrusts. Long-dashed lines are contours of Phanerozoic sediment thickness (km indicated). Dots are kimberlites and lamproites, and asterisks are Quaternary volcanoes.

The upper crust across the southern half of North America consists of a series of Proterozoic orogenic belts (Fig. 1: the 1.6-1.8 Ga Yavapai and Mazatzal terranes, the 1.5-1.3 Ga Granite-Rhyolite Province, the 1.3-1.0 Ga Grenville Province, and finally the Phanerozoic Appalachian belt) successively accreted onto the Archean continental core. This pattern suggests a simple concentric growth of the continent over about a billion years. However, the seismic tomography in Figure 1 suggests that the situation is more complex – high-velocity anomalies like those typically associated with Archean continental roots are visible in a wide band stretching southward from the Canadian Shield. Although these anomalies become less prominent to the south, they are still obvious down to the Gulf of Mexico. What is high-velocity lithospheric mantle doing under young orogenic belts? Unfortunately, there are no volcanic rocks that sample the high-veolcity mantle, and the few that have intruded along the edges of the high-velocity volumes (Fig. 1) rarely carry xenoliths that could reveal the nature of the subcontinental lithospheric mantle (SCLM).

The Cretaceous Prairie Creek - Twin Knobs lamproites of southern Arkansas intrude Proterozoic crust near the boundary between the Granite-Rhyolite Province and the Grenville orogen. On the seismic tomography, they lie along the boundary between two blocks of high-velocity mantle. They carry xenocrysts and rare xenoliths derived from the SCLM and the deep crust; these were studied by Dr David Dunn for his PhD thesis, and he has collaborated with us to find out more about them. U-Pb dating of groundmass perovskite in the Prairie Creek lamproites gives a poorly constrained Cretaceous age, consistent with local stratigraphy. U-Pb dating and *in situ* Sr and Nd isotope data show that perovskite micronodules in the Twin Knobs 2 lamprophyre are ca 600 Ma old, and may represent samples of older rift-related alkalic magmas derived from a juvenile mantle. A lithologic section constructed from mantle-derived garnet xenocrysts (Fig. 2) shows a moderately depleted SCLM that has experienced a high degree of melt-related metasomatism, especially in the depth range 150-140 km. *In situ* Re-Os analysis

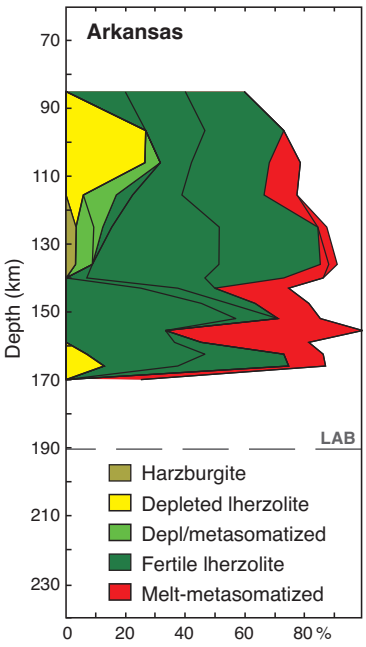

Figure 2. "Chemical Tomography" section showing the relative proportions of depleted and metasomatised rock types versus depth, as derived from Cr-pyrope xenocrysts. The relatively high proportion of fertile lherzolites is typical of the SCLM beneath many Proterozoic terranes. The figure is constructed by calculating the relative proportions of each garnet type at 50 °C intervals, using a sliding window 100 °C wide, to take account of probable uncertainties in the depth estimates.

of sulfide grains in the xenoliths (Fig. 3) yields model ages ranging up to 3.4 Ga, with major peaks at 1.4-1.5 Ga and 200-300 Ma. The scatter of Early Paleoproterozoic model ages appears to reflect mixing between residual Archean high-Os sulfides and later low-Os sulfide melts (Fig. 3b).

These data suggest that the SCLM beneath the Prairie Creek area formed in Archean time, and has been progressively refertilised by a series of magmatic events, which appear to correlate in time with events in the overlying crust. The Archean SCLM sampled by the lamproites may represent the mantle root of the Sabine microcontinent, which is recognisable in the seismic tomography (Fig. 1) as the higher-Vs feature (100-175 km depth) that lies mainly to the south of the lamproite field. Seismic tomography also shows several blocks with high Vs beneath the Grenville province to the east, which may represent other microcontinental blocks. These findings suggest that the growth of individual continents is significantly affected by the accretion of older microcontinental blocks, and that the extent of old SCLM, and of early continental crust, therefore may be greater than generally estimated.

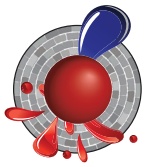

This project is part of CCFS Themes 1 and 2, Early Earth and Earth Evolution and contributes to understanding Earth's Architecture and Fluid Fluxes.

Contacts: Bill Griffin, Sue O'Reilly, Graham Begg
Funded by: ARC Discovery and Linkage Projects

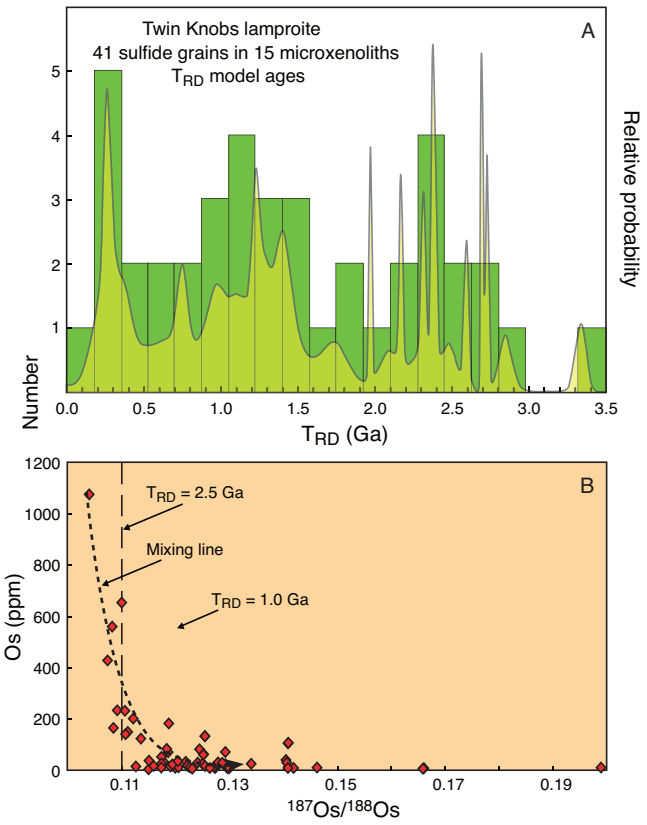

Figure 3. Re-Os data for sulfide grains in xenoliths from the Twin Knobs lamproite. (A) Cumulative-probability plot and histogram for Re-depletion ages (T_{RD}); (B) Plot of Os content vs $^{187}Os/^{188}Os$; the negative correlation at low $^{187}Os/^{188}Os$ suggests reaction (mixing) between old high-Os sulfides and younger sulfide melts with low Os and high $^{187}Os/^{188}Os$. Vertical dashed lines show $^{187}Os/^{188}Os$ corresponding to T_{RD} = 2.5 Ga and 1.0 Ga.

Yilgarn Seismic Reflection Survey released

The Youanmi deep seismic reflection survey, acquired across the Yilgarn Craton in May and June 2010, has been released on 22 February 2012 (http://www.dmp.wa.gov.au/13230.aspx). The deep seismic reflection data and the magnetotelluric data are part of a GSWA-led project within the Centre of Excellence for Core to Crust Fluid Systems, aimed at developing a 3D understanding of the lithospheric structure of the northwest Yilgarn Craton, its development through time, and the link to large-scale mineralisation.

The survey was funded through the Western Australian Government's Royalties for Regions Exploration Incentive Scheme (EIS). Terrex Seismic Pty Ltd (http://www.terrexseismic.com/), an Australian company based in Perth, carried out the seismic data acquisition, and Geoscience Australia (GA) managed acquisition, processing and interpretation.

The survey builds on the existing network of deep-crustal cont...

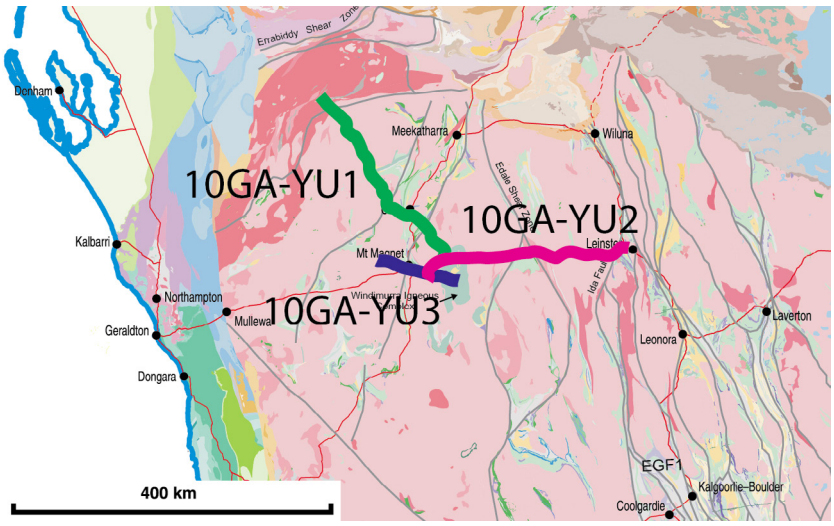

Figure 1. Location of the YU1, YU2 and YU3 seismic reflection lines in the Yilgarn Craton, Western Australia.

seismic surveys that have imaged the Yilgarn Craton and its margins, and will improve the understanding of the crustal structure of Western Australia. Three individual seismic lines (YU1, YU2 and YU3), along with complementary magnetotelluric data, were acquired as part of the survey.

The three lines cross the northern part of the Yilgarn Craton from the Narryer Terrane in the northwest, across major bounding and internal structures of the Youanmi Terrane and into the Kalgoorlie Terrane of the Eastern Goldfields Superterrane (Fig. 1). The eastern end of YU2 (Fig. 2)
crosses major structures on the western side of the Eastern Goldfields Superterrane, which were also imaged by the 2001 GA deep seismic reflection line (01AGS–NY1), about 120 km to the southeast.

The main objectives for the Youanmi deep seismic reflection survey are to:

- Image deep structure in the Narryer Terrane, the oldest component of the Yilgarn Craton, and the region that contains the oldest known crust in Australia;
- Image the contact between the Narryer Terrane and the adjacent, highly mineralised Murchison Domain of the Youanmi Terrane;
- Investigate the nature of granite–greenstone contacts and the overall shape, depth, and structure of greenstone belts;
- Compare the nature, orientation, and crustal penetration of mineralised and unmineralised structures;
- Develop a 3D image of the mafic–ultramafic Windimurra Igneous Complex;
- Image the Ida Fault, the boundary between the Youanmi Terrane and the Kalgoorlie Terrane in the Eastern Goldfields Superterrane, and compare the deep structure in the adjacent terranes;
- Link with previously acquired deep-crustal seismic traverses in the Eastern Goldfields Superterrane.

Interpretation of the seismic lines will be undertaken ahead of a public release workshop planned for October/November 2012.

This project is part of CCFS Themes 2 and 3, Earth Evolution and Earth Today, and contributes to understanding Earth's Architecture.

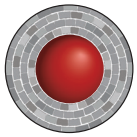

Contacts: Stephen Wyche (stephen.wyche@dmp.wa.gov.au), Klaus Gessner (klaus.gessner@dmp.wa.gov.au)
Funded by: NCRIS AuScope, Geoscience Australia, GSWA, CCFS Foundation Program

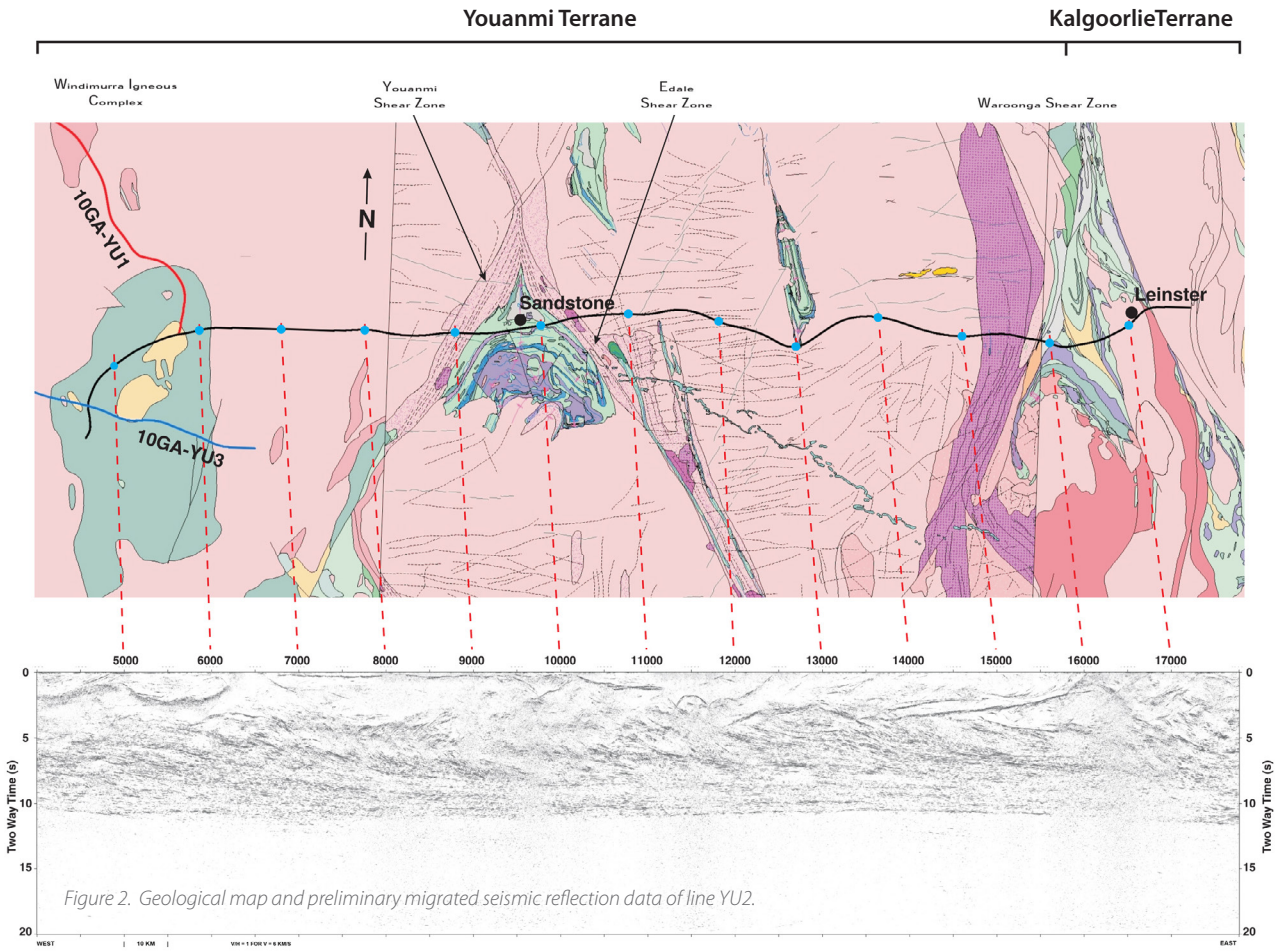

Figure 2. Geological map and preliminary migrated seismic reflection data of line YU2.

Mapping Earth's thermochemical structure in 3D

There are basically two sources of information we can use to constrain the compositional and temperature structure of Earth's mantle: geophysical data (e.g. gravity anomalies, travel-time data, surface heat flow, etc.) and studies of mantle samples (e.g. xenoliths, tectonically-exposed massifs). Experimental petrology and numerical simulations can complement these observations, but they cannot really constrain the physical state of the mantle. Both geophysical data and mantle samples have advantages and limitations when used to infer the physical and chemical structure of the mantle. The geophysical data offer a larger and more continuous spatial coverage, but their conversion into estimates of composition and temperature is full of difficulties -- and they only reflect present-day conditions. The mantle samples, on the other hand, carry direct information on the compositional and thermal structure of the mantle when they were erupted or exhumed, but their spatial and temporal coverage is limited.

The most reliable way to map the thermochemical structure of the Earth's interior would be via "multi-observable probabilistic inversions", using many types of data and an internally consistent thermodynamic/geophysical formulation. However, the theory and implementation of such inversion schemes still are immature and greatly understudied. None of the current methods can handle the simultaneous, internally consistent inversion of 3D data for surface heat flow, gravity and geoid anomalies, electrical conductivity, absolute elevation, seismic velocities and composition. Moreover, available methods/software used to model the Earth's interior cannot handle some major problems: i) the system is strongly non-linear, ii) the temperature effect on geophysical properties is much greater than the compositional effect, so the latter is hard to isolate, iii) the compositional data are non-unique (different compositions can fit seismic and potential-field data equally well), iv) strong correlations between physical parameters and geophysical observables complicate the inversion and their effects are poorly understood, and v) there are trade-offs between temperature and composition in seismic wave speeds.

We now have developed a new full-3D multi-observable inversion method particularly designed to circumvent these problems. Some key aspects of the method are: a) it combines multiple datasets (ambient noise tomography, receiver function analysis, body-wave tomography, magnetotelluric, geothermal, petrological, and gravity) in a single thermodynamic-geophysical framework, b) a general probabilistic (Bayesian) formulation is used to appraise the data, c) neither initial models nor well-defined *a priori* information are required, d) it provides realistic uncertainty estimates, e) it offers critical insights into the incompatibilities between traditional stand-alone methods, and f) it can incorporate geochemical/petrological information. The combination of different observables reduces the uncertainties because they are differently sensitive to shallow/deep, thermal/compositional anomalies. This allows a better control of the lateral and vertical variations of the bulk properties of the lithosphere and mantle.

The fundamental goal of this method is the conversion of observations into robust estimates of temperature and composition in the lithosphere and upper mantle. This requires the assessment of two different but related levels of functional relationships (or parameterisations). The first is between the raw observations and the set of governing physical parameters; e.g. the physical relationship between travel times and the subsurface seismic velocity structure or between variations in the surface electromagnetic field and the subsurface electrical conductivity structure. The second level of functional relationships is between the set of governing physical parameters (e.g. seismic velocity) and a more fundamental set of model parameters represented by the major-element composition and temperature of the rocks. Since this set of parameters (e.g. composition) controls the second set of governing physical parameters (e.g. shear velocity),

cont...

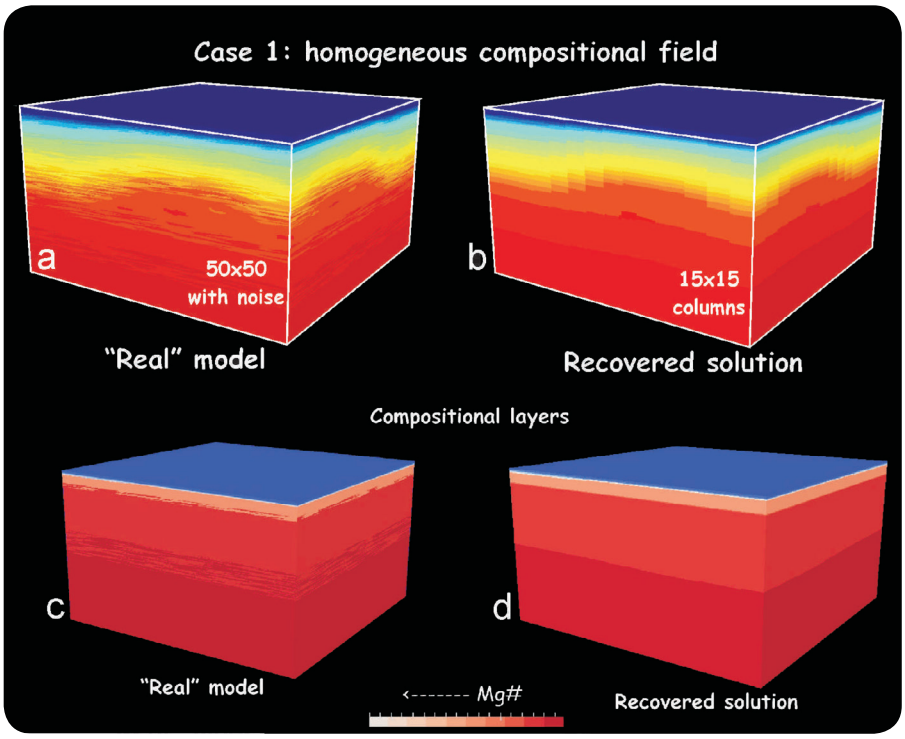

Figure 1.

they are commonly referred to as the primary and secondary parameters.

This first level is the simplest and most widely used in conventional inversion methods. Typically, we assume an appropriate physical theory (e.g. seismic wave propagation) and use that to relate the secondary model parameters to the observations during the inversion. The final result is one or more sets of secondary physical parameters (i.e. Earth models), such as shear velocity or electrical conductivity, that show an acceptable fit to the data. The second level of functional relationships is commonly ignored in inversion studies or treated as *a posteriori* independent (not self-consistent) corrections. Partly because of this, but also due to its intrinsic complexities (e.g. different compositions give the same seismic velocity), this functional level and its relationship with geophysical observables are less well-understood.

Figure 1 shows the comparison of a "real" input thermochemical model and the solution recovered after inverting surface and body waves, geoid and gravity anomalies, surface heat flow, and elevation. No magnetotelluric data have been included in this example. The input model and its observables were calculated with the software LitMod3D in a mesh of 50x50x204 nodes. The thermal structure is heterogeneous and contains added "noise" while the compositional structure is horizontally homogeneous, featuring three layers with distinct Mg#. Although the inversion mesh is much coarser (15x15x190), the two recovered structures are in excellent agreement with the original structure. This example shows that our probabilistic inversion scheme can distinguish between thermal and compositional signatures, something that other available methods cannot achieve.

Although the method still is being tested and benchmarked, our preliminary results are encouraging. They demonstrate that inversion of multiple geophysical and petrological data to obtain a thermochemical "tomography" of the upper mantle is possible and more reliable than other standard methods. This new approach opens the way to migrate from standard "parameter tomography" (e.g. seismic tomography) to future "multi-observable thermochemical tomography" schemes, the ultimate goal of geophysical methods.

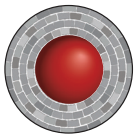

This project is part of CCFS Theme 3, Earth Today, and contributes to understanding Earth's Architecture.

Contact: Juan Carlos Afonso
Participants: Juan Carlos Afonso, Javier Fullea, Yingjie Yang, Bill Griffin, Sue O'Reilly, Alan G. Jones, James Connolly, Sergei Lebedev, Nick Rawlinson
Funded by: ARC Discovery

High strain below Tibet – mapping a mid-crustal low velocity zone

The Tibetan Plateau results from the convergence between the Indian and Eurasian plates, which has been going on since Late Cretaceous to Early Paleocene times. There is lively debate about the processes that have controlled the deformation of Tibet, particularly the potential localisation of deformation either in the vertical or horizontal directions. Two general models are commonly proposed. The first is the "rigid block" model in which deformation is primarily localised along active faults on the edges of the blocks. The second is the "internal deformation" model in which the crust is treated as a non-rigid continuum, like gummy candy, and deformation is spread across the blocks. In this model, strain disperses in the deeper crust into much broader ductile shear zones, in which the lithosphere may deform more or less homogeneously. This might be via "vertically coherent deformation" or by more rapid, ductile "channel flow" in the middle to lower crust.

Geophysical data can help us discriminate between these competing models. In particular, it is important to determine whether Tibet deforms in a way that mimics the surface expression of crustal blocks and faults, and whether we can

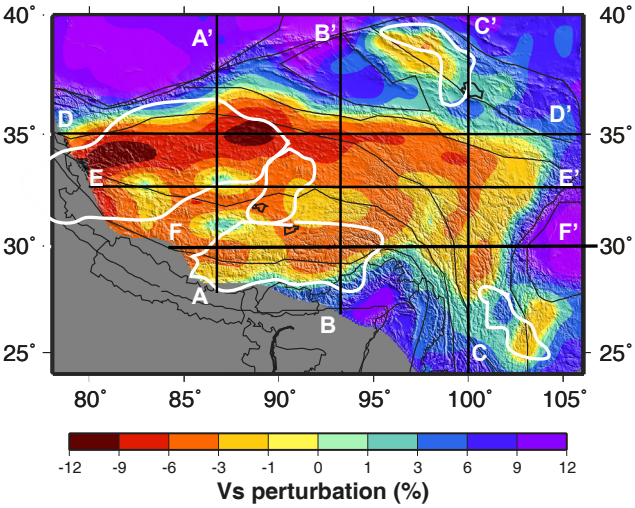

Figure 1. (a) Map of the amplitude of the crustal low-velocity zone across the region relative to 3.4 km/s. Yellows, oranges, and reds denote velocities at 30 km depth (relative to sea level) less than 3.4 km/s. White contours identify strong radial anisotropy found in the study of Shapiro et al. (2004). Note that the distribution of strong radial anisotropy is largely coincident with strong LVZs in western and central Tibet. Agreement is weaker in eastern Tibet, but this is probably due to the reduction of resolution in this region in the study of Shapiro et al (2004).

observe pervasive, interconnected weak layers or channels in the crust. There is a growing body of evidence that suggests the Tibetan crust is warm and thus presumably ductile. These observations are often taken as *prima facie* evidence for the

existence of partial melts or aqueous fluids in the middle or deep crust beneath Tibet. Some have argued for the decoupling or partitioning of strain between the upper crust and uppermost mantle. This raises several questions. How pervasive are the phenomena that support the existence of crustal partial melt? In particular, do we see mid-crustal low velocity zones (LVZs) across Tibet? If we do, what is the geometry or inter-connectivity of the crustal LVZs across Tibet?

We addressed these questions by producing a new 3-D model of crustal and uppermost mantle shear wave speeds (illustrated by Fig.1 and 2). We used the Rayleigh wave dispersion observed on cross-correlations of long time series of ambient seismic noise, recorded from about 600 stations in the Chinese Provincial networks, FDSN, and PASSCAL experiments.
The 3-D model shows significant, apparently inter-connected, zones of low shear velocity across most of the Tibetan Plateau at mid-crustal depths (20-40 km). These low-velocity zones (LVZs) do not correspond to surface faults and, significantly, are most prominent near the periphery of Tibet. The observations support the internal-deformation model in which strain is dispersed in the deeper crust into broad ductile shear zones, rather than being localised near the edges of rigid blocks. The prominent LVZs coincide with strong mid-crustal radial anisotropy (Shapiro et al., 2004) in western and central Tibet. The anisotropy probably results at least partially from the alignment of anisotropic minerals by deformation, which mitigates the need to invoke partial melts to explain the observations. Irrespective of their cause (partial melts or mineral alignment), mid-crustal LVZs reflect deformation, and their amplification near the edges of the Tibetan plateau provides new information about the mode of deformation across Tibet.

There are two specific seismic observations that are needed to extend and clarify inferences from the results presented here. First, higher-resolution Love wave phase velocity measurements obtained from ambient noise across all of Tibet are needed to infer Vsh in the middle crust. These observations will help to determine whether the observed LVZs result entirely or only partially from mineral alignment. Second, azimuthal anisotropy, observed both for the crust from ambient noise and for the uppermost mantle from earthquake records, will constrain the vertical continuity of the strain and will help to discriminate between channel flow and vertically coherent deformation. Both types of observations will be obtained in planned future studies.

This project is part of CCFS Theme 3, Earth Today, and contributes to understanding Earth's Architecture.

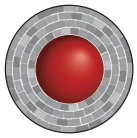

Contact: Yingjie Yang
Funded by: MQ New Staff Grant

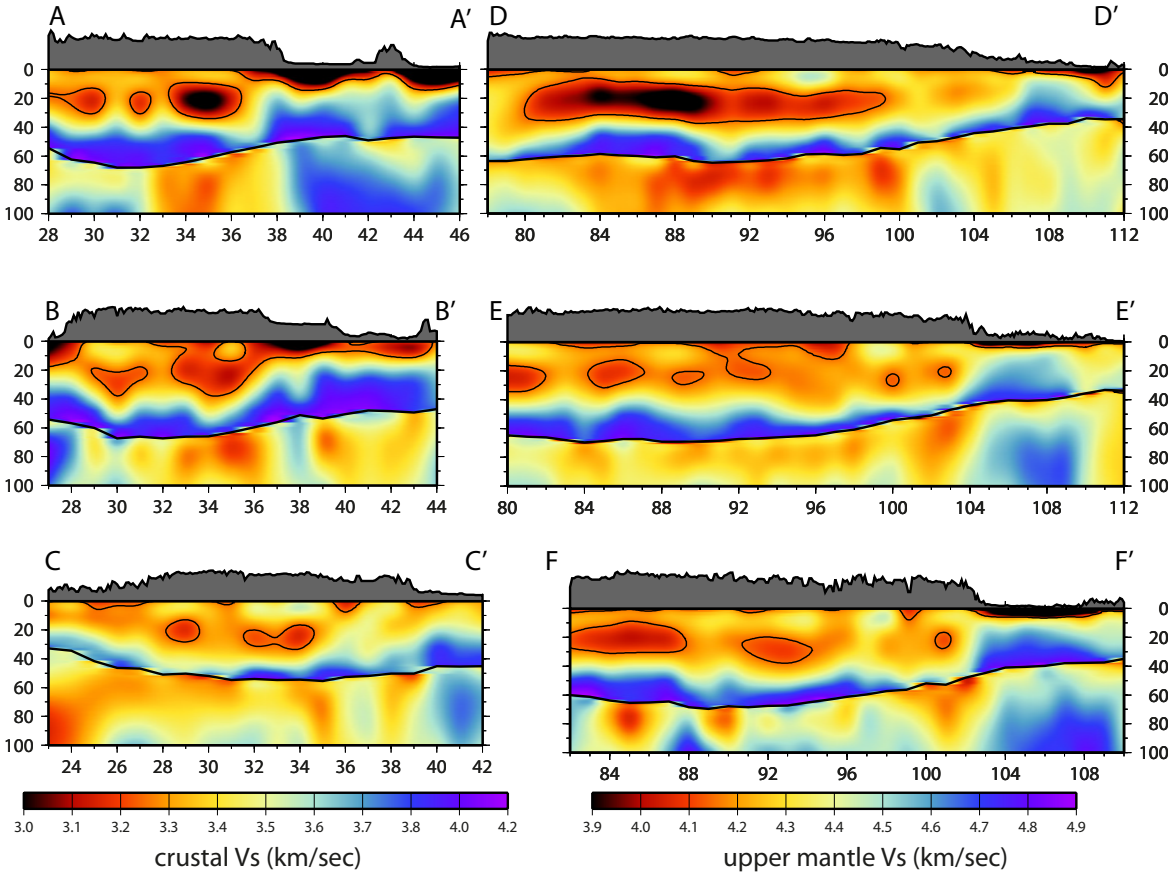

Figure 2. Vertical cross-sections of Vsv along the six profiles identified in Figure 1. Surface topography is shown at the top of each panel. Shear-wave speeds are presented in absolute units, but with different color scales in the crust and mantle. Very low shear-wave speeds in the crust (<3.25 km/s) are outlined by black contours. All depths are relative to sea level.

Water deep in the mantle-A key to transforming the Lithosphere?

Besides the visible H_2O on the Earth's surface, there is another unexpected and invisible H_2O reservoir at depth. This is the H_2O in the mantle, 'dissolved' as hydroxyl in the crystal structure of major mantle minerals. It relates not only to the probability of life, but also to geological processes.

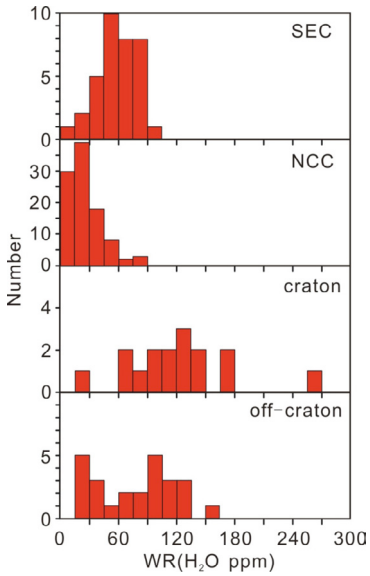

Figure 1. Comparison of H_2O contents whole-rock (WR) of the Cathaysia (SE China) xenoliths in this study with those of North China Craton (NCC), craton and off-craton peridotites. For the references of data for NCC, cratonic and off-cratonic peridotites see CCFS publication #2.

Refractory subcontinental lithospheric mantle (SCLM) is produced by the removal of partial melts from mantle rocks; this process includes the removal of this deep H_2O. The nature and evolution of the SCLM are strongly influenced by hydrous melts and fluids, which affect the physical and chemical properties of mantle minerals and rocks. Like some light rare earth elements (LREEs) (La, Ce) or large ion lithophile elements (LILs) (K), H_2O behaves as an extremely incompatible component (Dperidotite/melt = <0.01) in a melt/solid system, which makes it a sensitive tracer of melt-extraction and metasomatism in the SCLM. Thus an understanding of the H_2O inventory of the SCLM provides another tool to study the nature and the evolution of the SCLM, and the role H_2O has played during lithospheric modification.

Peridotite xenoliths in alkali basalts consist mainly of nominally-anhydrous minerals (e.g. olivine, pyroxene) and these can be analysed to measure the actual H_2O budget of the SCLM. This study has focused on determining the H_2O contents of peridotite xenoliths from four localities (Mingxi, Anyuan, Niutoushan and Qilin) in the Cathaysia block of SE China, using Fourier Transform Infrared Spectroscopy (FTIR). We studied (1) the homogeneity of water distribution within single pyroxene grains; (2) the partitioning of water between cpx and opx (mean Dcpx/opx = 2.3); and (3) the correlations between the H_2O contents and major element concentrations in cpx. From these data it appears that the pyroxenes have largely preserved the water content of their mantle sources.

The whole-rock water contents calculated from mineral modes range from 12 to 94 ppm (average 60±20 ppm). This is much higher than the previously-reported water contents of xenoliths from the North China Craton (NCC) (average 26±17 ppm). However, it is still quite low compared to those of continental lithospheric mantle worldwide, as inferred from analyses of typical cratonic (122±54 ppm) and off-craton (81±40 ppm) peridotites (Fig. 1). The present relatively low water budget has evolved through multiple geological events over the long history of this SCLM, e.g. hydration due to paleo-Pacific plate subduction, dehydration by melt extraction during Yanshanian magmatism (Fig. 2a) and subsequent rehydration due to the fluxing by low-degree asthenospheric melts after lithospheric

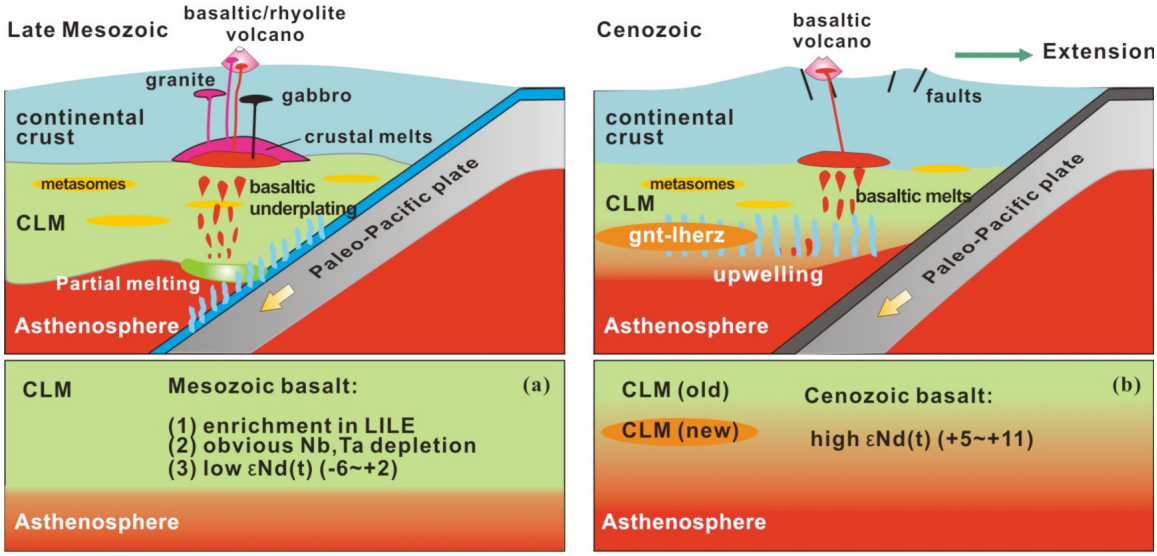

Figure 2. Cartoon showing (a) hydration due to water released from the subducted slab, and dehydration after melt extraction in Yanshanian magmatism. The enriched signatures in the Late Mesozoic basalts reflect contributions from the hydrated SCLM; (b) rehydration by low-degree asthenospheric melts after lithospheric thinning. The upwelling and decompressional melting of asthenosphere is supported by decreasing contribution from SCLM in basalts in SE China over time, with εNd (t) of −6~+2, and +5~+11 for Late Mesozoic and Cenozoic, respectively.

thinning *(CCFS Publication #2)* (Fig. 2b). This is evidenced by young basaltic volcanism at the surface. Water itself plays an important role during the modification of the subcontinental lithospheric mantle. The garnet lherzolites, which represent the deepest portion of the SCLM (~1.9 GPa) sampled in this study, have the highest water contents (>80 ppm). This fertile garnet-facies layer, at depths of 50-100 km, appears to have lost very little water. It may represent young lithosphere accreted at the bottom of the pre-existing lithosphere (Fig. 2b). It marks the completion of the lithospheric thinning episode and the upwelling of the asthenosphere.

A negative correlation between pyroxene water contents and oxygen fugacity has been found only in xenoliths from Niutoushan (Mg# < 90), which lies on the Changle–Nan'ao fault zone. The fault may have facilitated the infiltration of the Niutoushan peridotites by oxidised fluids (or hydrous melts) rising from the subducting Pacific plate.

This project is part of CCFS Theme 2, Earth Evolution, and contributes to understanding Earth's Fluid Fluxes.

Contacts: Yao Yu, Bill Griffin, Sue O'Reilly
Funded by: NSFC Grant 40730313, ARC Discovery and Linkage grants (O'Reilly and Griffin), iMQRES, EPS Postgraduate Fund

A window of opportunity for plate tectonics?

Plate tectonics is the machine that shapes the Earth's surface, from mountain ranges to ocean depths. It is the cornerstone of modern geology, yet it appears that the process only occurs on one known planet - Earth. Additionally, a serious debate continues as to when plate tectonics started on Earth - current estimates range from over 4.4 billion years ago - almost the age of the planet - to just one billion years ago – geologically speaking, our recent past.

It is fairly well accepted that as a planet cools, and its lithosphere - the strong, outer layer that carries the crust - gets thicker, the planet will develop a stagnant "lid". This is defined by the end of active surface tectonics on a planet. Mars, the Moon, and Mercury all seem to have passed into this twilight regime. However, recent work at CCFS/GEMOC has indicated that stagnant-lid tectonics can operate at the other end of the spectrum, too. For extremely hot planets, the high interior temperatures result in low internal viscosities. This breaks down the coupling between the convecting mantle and the plates, and tectonics again becomes unsustainable. A type example of this sort of hot stagnant lid model could be Io, the most volcanically active planetary body in the solar system.

This model predicts an evolution in tectonics over the course of a planet's slow cooling, from a hot stagnant mode in its early history, to an active tectonic regime, waning into a cold stagnant mode as the planet ages. Recent simulations at CCFS/GEMOC, presented at the American Geophysical Union meeting in December 2011, confirm this evolutionary trend. These models for the first time incorporated not only the decay in heat production in the mantle through time, but also realistically-evolving conditions in the core of the planet. The starting conditions were the results from equilibrium convection simulations under Hadean thermal conditions. These models commonly showed an evolution from hot stagnant behaviour initially, to an episodic subduction mode, where periods of quiescence are interspersed with periods of rapid, violent subduction. This progressed into a steadier plate tectonic mode, under mantle conditions similar to today. Eventually the lithosphere thickened beyond the point of sustainable surface behaviour, and the system progressed into a cold stagnant-lid regime. The exact timing and progress depend strongly on the simulation parameters and the initial conditions chosen. However, the results confirm that rather than an end-member tectonic regime, plate tectonics is a phase in a planet's tectonothermal evolution - which has large implications for exosolar planetary conditions.

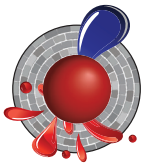

This project is part of CCFS Theme 1, Early Earth, and contributes to understanding Earth's Architecture and Fluid Fluxes.

Contact: Craig O'Neill
Funded by: ARC Discovery, Future Fellowship, MQ

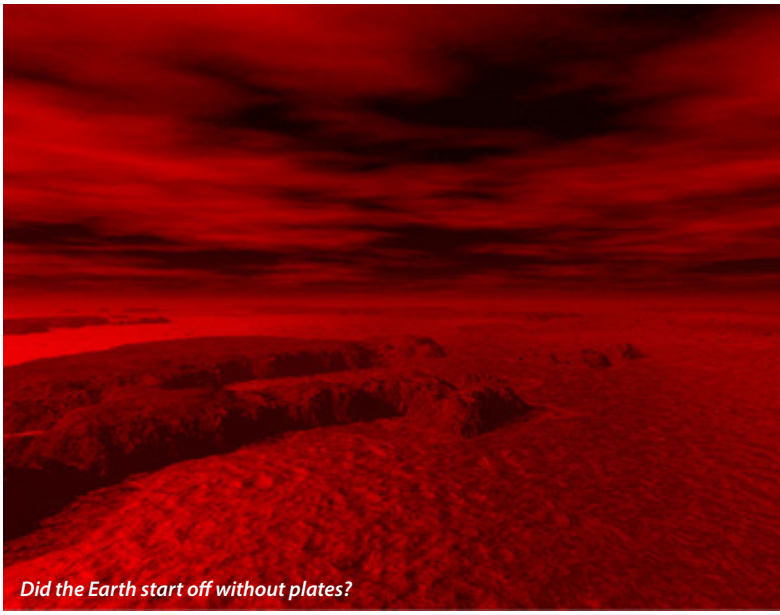

Did the Earth start off without plates?

Metasomatic highways - 200 km below Earth's surface

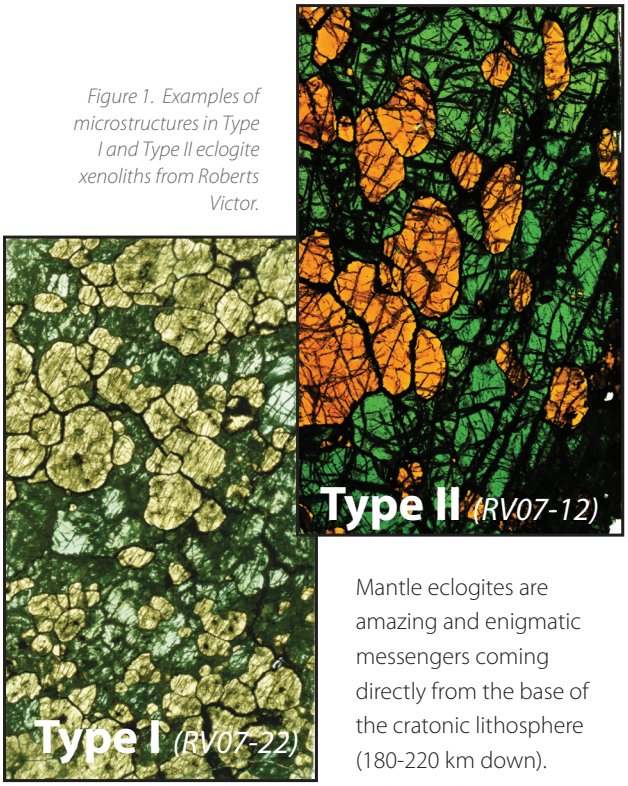

Figure 1. Examples of microstructures in Type I and Type II eclogite xenoliths from Roberts Victor.

Mantle eclogites are amazing and enigmatic messengers coming directly from the base of the cratonic lithosphere (180-220 km down). Although the processes that originally produced these rocks are yet to be fully understood, they are critical samples to constrain the dynamics of the sub-continental lithospheric mantle (SCLM). Because of their privileged position at the lithosphere-asthenosphere boundary (LAB), they are witnesses of the interactions between the lithospheric mantle and the asthenosphere.

Eclogite xenoliths recovered from the Roberts Victor kimberlite pipe (Kaapvaal Craton; South Africa) reveal peculiar features that indicate that the rocks have been modified since their emplacement. Recent studies done at CCFS/GEMOC *(CCFS/GEMOC Publication #003/772)* have shown that most of the Roberts Victor eclogites (Type I eclogites) underwent intensive metasomatism, provoked by substantial melt/fluid percolation not long before the kimberlite eruption (Fig. 1). Although this process was inferred from entirely metasomatised xenoliths, the transformation has also been recorded in some composite xenoliths that contain both original and metasomatised lithologies.

HRV77 is a remarkable example (Fig. 2), which highlights how metasomatic fluids have percolated through the eclogite body via metasomatic channels. This sample is composed of two parts. One is a clinopyroxene macrocryst associated with a few clear, ovoid garnet grains. The surrounding part is mostly bimineralic (grt+cpx) but also contains sulfide, phlogopite and

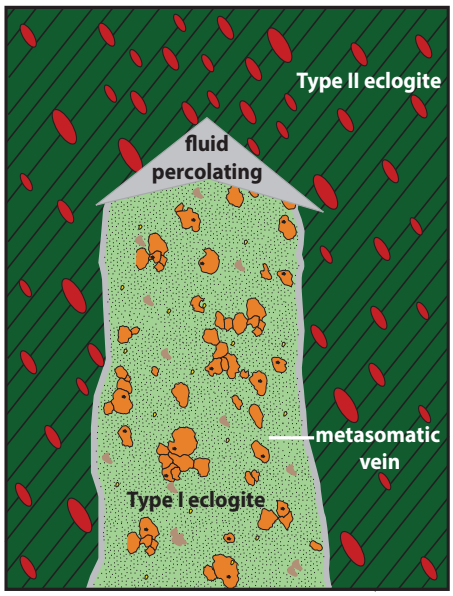

Figure 3. Cartoon showing the possible fluid percolation mechanism and the formation of (metasomatised) Type I eclogites at the expense of Type II.

calcite. In this part the garnets are cloudy, show irregular shapes (irregularity increasing with distance from the contact) and contain blebs similar to melt pockets. From these petrographic observations, we conclude that the bimineralic part represents a metasomatic channel, in which cpx and grt recrystallised and metasomatic minerals have been added. Supporting these observations, major- and trace-elements also show clear differences between the two parts. While the cpx macrocryst shows a LREE-depleted pattern similar to the un-metasomatised Type II eclogites, cpx from the bimineralic part shows enrichment in LREE, as observed in the dominant Type I metasomatised eclogites. *In situ* Sr-isotope analyses of the clinopyroxene also support such a dichotomy. The cpx macrocryst has $^{87}Sr/^{86}Sr$ = 0.7029 (cpx from Type II eclogites have $^{87}Sr/^{86}Sr$ = 0.7013 – 0.7030) while the bimineralic part with $^{87}Sr/^{86}Sr$ = 0.7068 is typical of Type I eclogites ($^{87}Sr/^{86}Sr$ = 0.7060 – 0.7064).

These obvious contrasts of chemistry and microstructure in such an intimate relationship imply that the bimineralic part witnessed the transit of a melt/fluid with which it interacted, while the macrocrystic part represents the wall-rock of this percolation vein (Fig. 3).

This kind of sample is of the greatest interest because they are the "missing link" between the two main types of eclogites recovered at Roberts Victor. They offer a spatial connection between the two types, indicating that their relationship is of a "mother-daughter" nature; they are not simply cousins as has been previously inferred in the literature.

This project is part of CCFS Theme 2, Earth Evolution and contributes to understanding Earth's Fluid Fluxes.

Contacts: Yoann Gréau, Jin-Xiang Huang, Bill Griffin, Sue O'Reilly

Funded by: ARC Discovery (O'Reilly, Griffin), iMURS, EPS postgraduate Fund

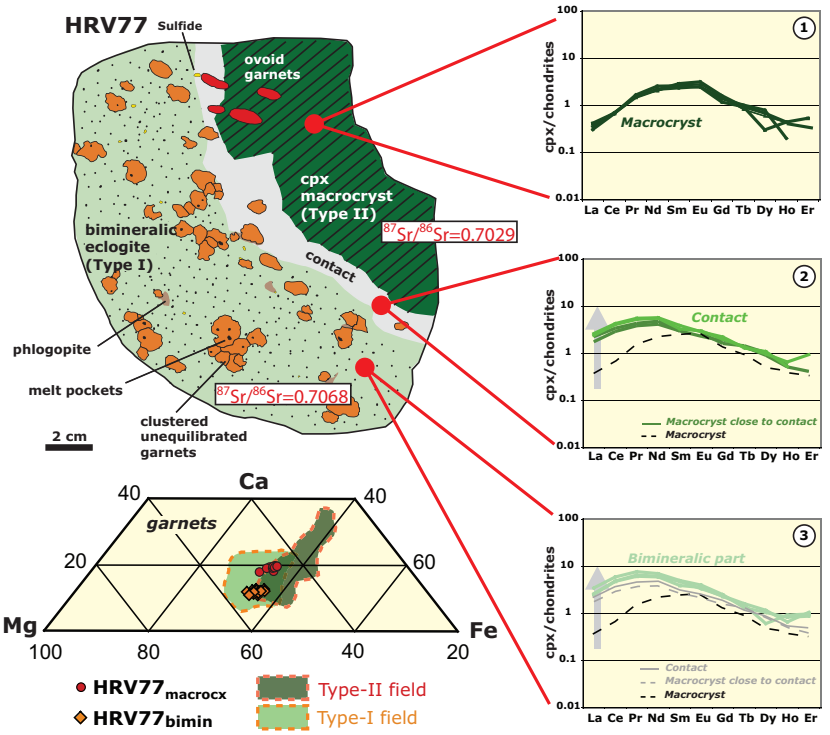

Figure 2. Sketch of the petrographic structure of composite xenolith HRV77 and the associated chemical variability. Cpx boundaries are not represented in the bimineralic part but grain-size is similar to garnet. Contact is composed of the macrocrystic cpx showing features of destabilisation. Bottom quadrilateral shows variations of major-element compositions between dusty garnets sitting in the bimineralic part (diamonds) and ovoid clear garnets sitting in the cpx macrocryst (circles). Right side REE patterns of cpx: (1) macrocrystic cpx; (2) macrocrystic cpx close to contact and contact itself; (3) cpx in the bimineralic part. Note the progressive enrichment in LREE from a Type II pattern to the typical Type I pattern.

Diamonds highlight mantle fluid processes

Diamonds are "time capsules" that can preserve the geochemical signatures of their formation environment and trap inclusions from their matrix, providing unique insights into the mantle environment. They are carried from the mantle to the surface by very deep-seated, violent volcanic eruptions, from depths greater than 150 km. It is very likely that COH fluids percolating through the deep mantle caused the eruptions and also were the source of carbon for diamond formation. Interaction of oxygen and carbon in mantle processes defines and controls diamond formation (for example, precipitation and dissolution of diamonds, transportation of incompatible elements).

This project aims to combine the information that can be extracted from diamonds and other minerals, formed in the mantle. Studying the internal structure, physical and chemical properties of diamonds and related minerals, we are trying to uncover the mystery of the carbon source, which still is a controversial subject. Using the diamond and coexisting minerals we can provide a better understanding of diamond formation processes, which are related to major mantle processes and mantle composition, and can help us to understand the geological evolution of our planet.

We use diamondiferous mantle xenoliths from African and Siberian kimberlites as a source of information about mantle processes. This work, combined with the PhD studies of Yoann Gréau and Jin-Xiang Huang (see *Research highlight, p. 26)* has shown that mantle metasomatism (chemical alteration by fluids) plays an important role in diamond formation and is responsible for changes in geochemistry of silicates. In 2011 a new approach was taken, looking at the genesis and evolution of polycrystalline diamond aggregates (diamondites; Fig 1). Using the Electron Backscattered Diffraction (EBSD) technique, we made the first observations and interpretations of diamondite microstructures. The technique produces maps of the crystallographic orientation of the different diamond crystals in the aggregate, and also maps the distribution of silicate minerals that occur as inclusions and interstitial grains (Fig. 2). The study demonstrated that most diamondites have been significantly modified by deformation and recrystallisation processes. Many originally crystallised as relatively coarse-grained diamonds with abundant silicate inclusions; as they recrystallised under stress the grain sizes were reduced and the silicate phases moved to grain boundaries. Using integrated datasets including microstructural observations and *in situ* analyses of trace elements, C-isotopes in diamond and O-isotopes in the silicates, we found that many diamondites have an extended mantle-residence history including deformation/crystallisation processes and fluid interaction after initial crystallisation. The fluids changed the crystallisation environment (chemical composition of silicates) and may have provided carbon for secondary diamond formation. Based on the differences in chemical composition of the enclosed and interstitial silicates and zoning in the carbon isotopic composition of diamonds we can conclude that the host fluids were Mg-rich. An important conclusion was that polycrystalline diamond aggregates should not be interpreted as the cont...

products of primary crystallisation shortly before eruption, and detailed observations of their internal structures must play an important role in the interpretation of their genesis.

This study offers us new insights into mantle processes including diamond formation, deformation and fluid/melt interaction, and illustrates the complexity of the mantle system and the important role of fluids in it. The understanding of the fluids' compositions and interactions in the mantle is probably a clue to the variation in the geochemistry of the mantle system itself.

This project is part of CCFS Theme 2, Earth Evolution, and contributes to understanding Earth's Fluid Fluxes.

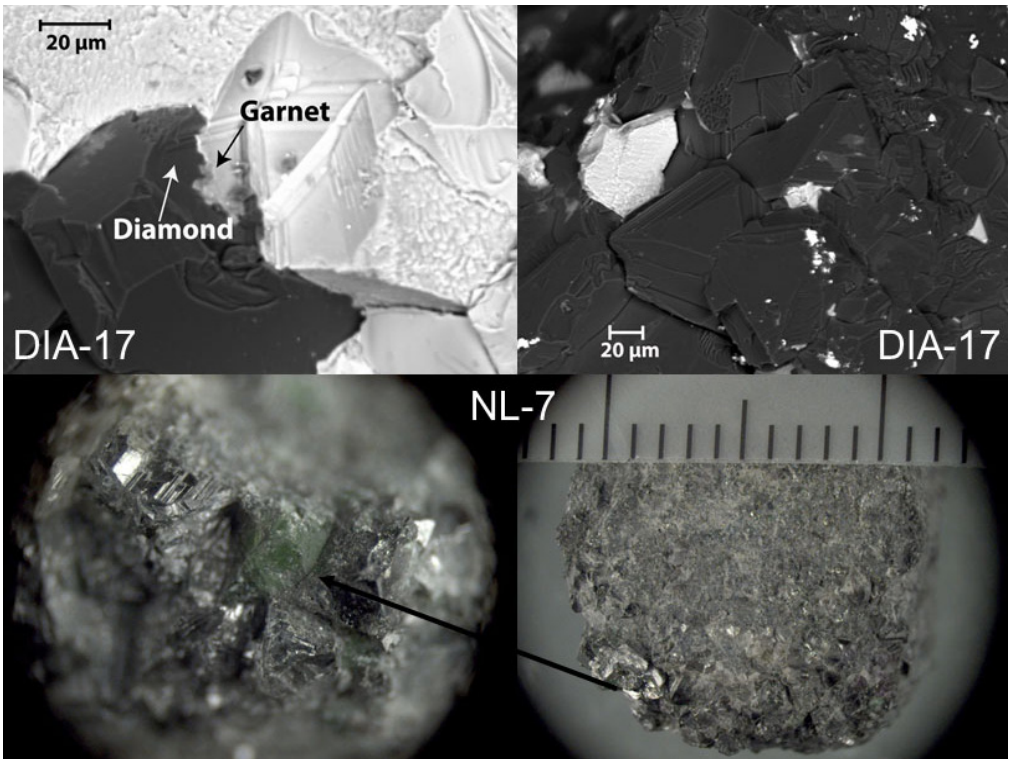

Contacts: Ekaterina Rubanova, Dan Howell, Bill Griffin, Sue O'Reilly, Norman Pearson

Funded by: ARC Discovery, CCFS Foundation Program, iMURS, EPS postgraduate fund

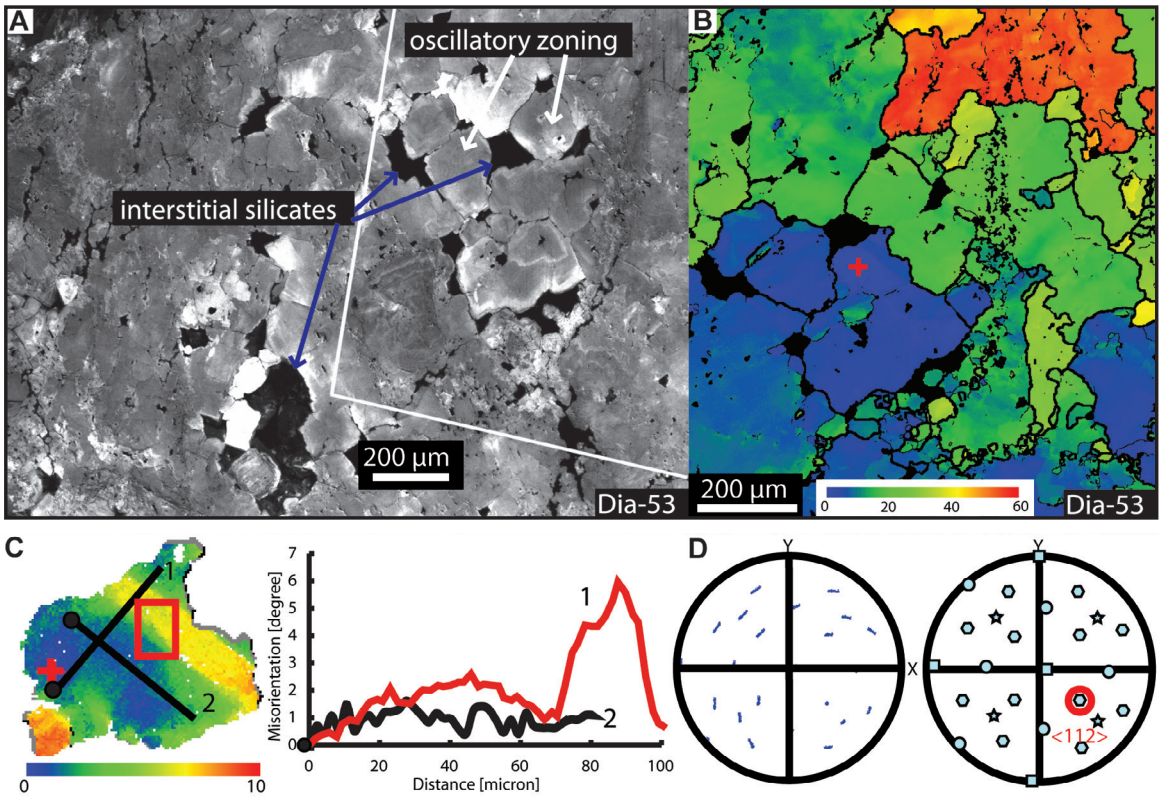

Figure 2. Photomicrograph (A) of a polished diamondite. (B) EBSD image of the field outlined in (A). Different colours show different crystallographic orientations. (C) Traverses across a weakly deformed diamond grain. (D) Orientations of diamonds in (B).

Unveiling fluid histories in deep mantle eclogites with sulfide compositions

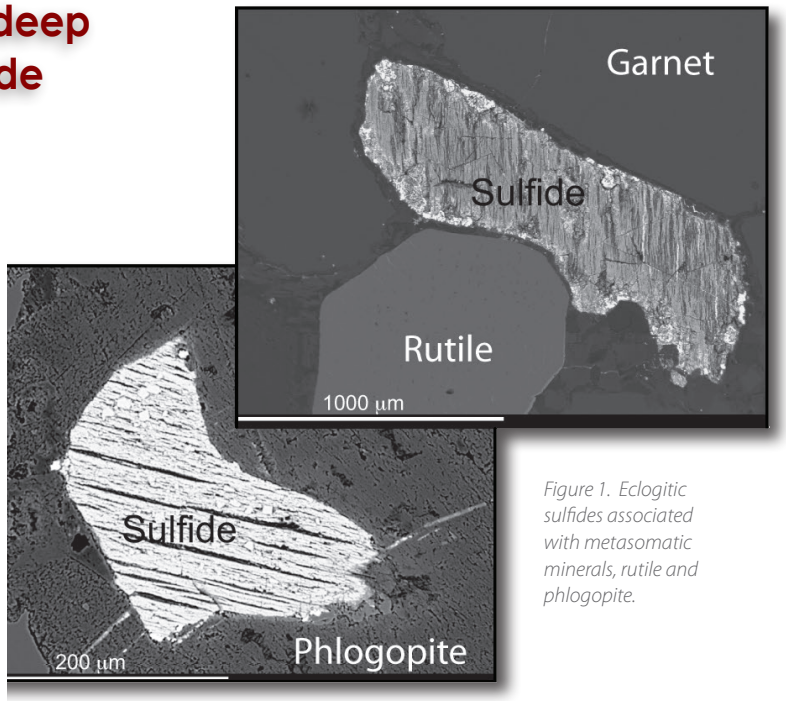

Figure 1. Eclogitic sulfides associated with metasomatic minerals, rutile and phlogopite.

Eclogite xenoliths are commonly found in kimberlites that erupted in cratonic areas. These rocks, sampled by the ascending magma, are minor but important constituents of the sub-continental lithospheric mantle (SCLM). However a long-lived debate still rages about why such mafic lithologies occur in the SCLM. The currently dominant line of argument sees mantle eclogites as remnants of subducted oceanic slabs stored in the cratonic SCLM, while other researchers regard mantle eclogites as deep-seated mafic melts trapped near the lithosphere-asthenosphere boundary (LAB). A recent study (*CCFS Publication #003)* pointed out that the "subuction" hypothesis was mostly based on the study of the more common Type I eclogites (defined by higher levels of the minor elements Na and K in garnet and clinopyroxene, respectively). These eclogites were shown to possibly not be the best choice as their microstructures and lithophile-element geochemistry indicate that they have been intensively over-printed by at least one metasomatic event. The less common Type II eclogites may represent primary, or at least less-altered, compositions.

Type I eclogite xenoliths recovered from Roberts Victor kimberlite (Kaapvaal Craton; South Africa) contain abundant polyphase sulfides (up to several modal %). Although many of these sulfides have undergone supergene weathering (i.e. transformation to violarite, smythite and pyrite), some samples present fresh unaltered assemblages made of pyrrhotite (Po) + pentlandite (Pn) + chalcopyrite (Cp). This typical magmatic assemblage is similar to sulfide inclusions found in Roberts Victor eclogitic diamonds, and more generally the reconstructed bulk sulfides are similar to sulfide inclusions in eclogitic diamonds worldwide (Fig. 1).

In Roberts Victor eclogites, although sulfides are systematically lacking in Type II eclogites, they are ubiquitous in Type I, cont...

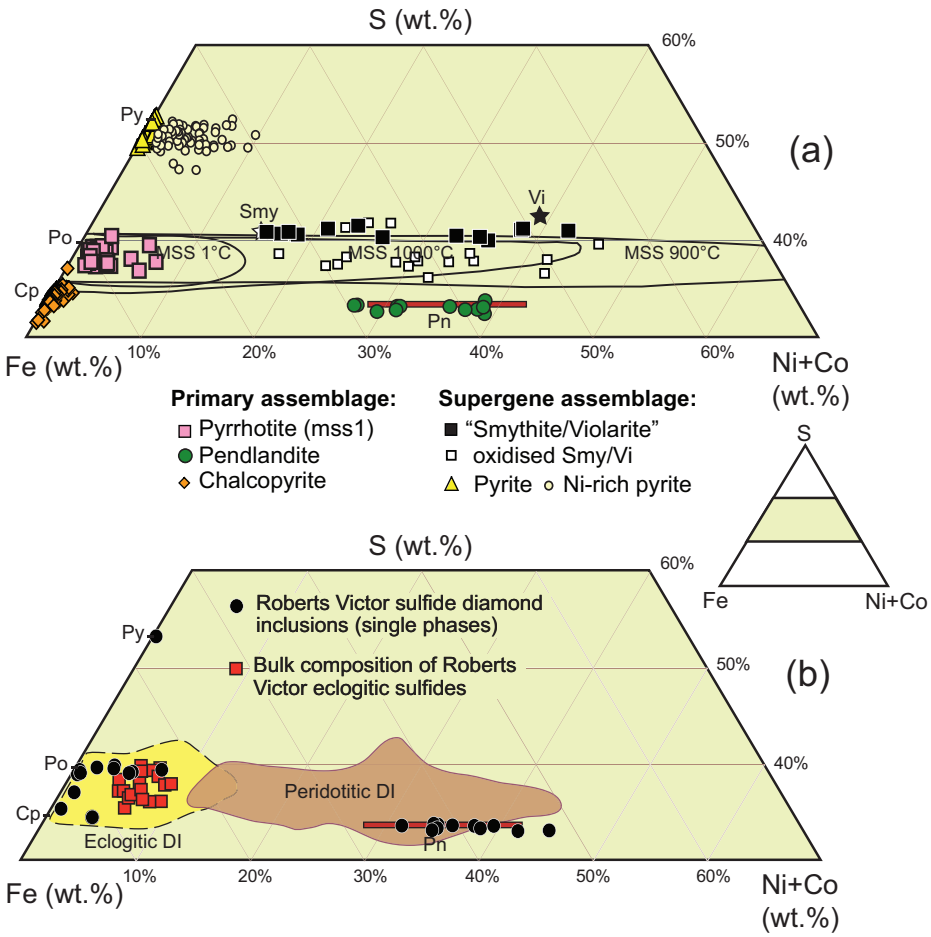

Figure 2. Electron-probe analyses of individual phases plotted on Fe-Ni-S diagrams.

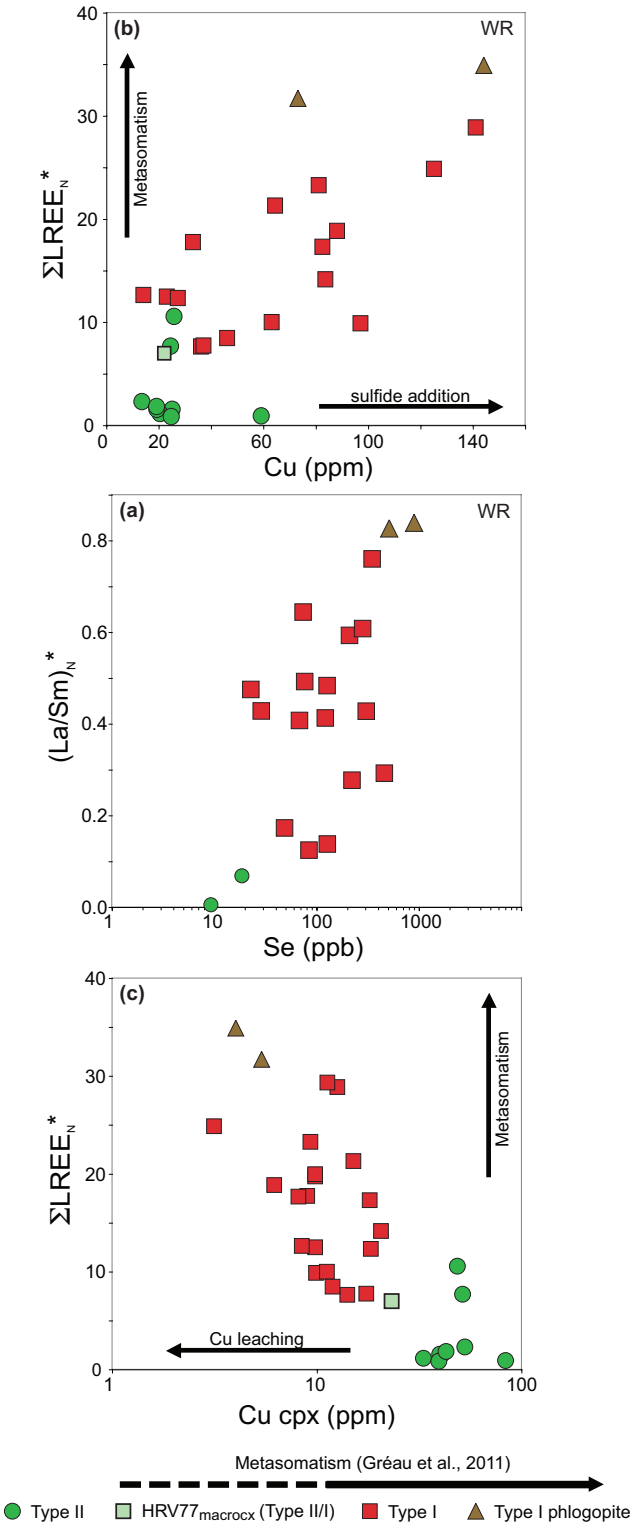

Figure 3. Correlations between metasomatic tracers and sulfide addition.

and are often found in close association with metasomatic minerals like phlogopite and rutile (Fig. 2). It is therefore perhaps not accidental that both diamonds and sulfides are only found in Type I eclogites. A growing body of evidence indicates that diamonds are metasomatic minerals, but is this the case for the eclogitic sulfides? Chalcophile elements (elements with affinities for sulfur) such as Cu or Se might be the clue; they will be mostly carried by sulfides, and they can therefore be used as proxies to trace their origin.

Correlations between the whole-rock budgets of these elements and typical metasomatic tracers such as (La/Sm) or ΣLREE (Fig. 3) clearly indicate that the sulfides are related to the metasomatism affecting the silicate assemblage. Furthermore, a negative correlation between the Cu content of clinopyroxene and ΣLREE shows how Cu is leached from the silicates during the crystallisation of sulfide associated with the metasomatic event. These data provide another line of evidence to confirm that Type I eclogites have been heavily over-printed by metasomatism, meaning that Type II are the only suitable rocks to constrain the origins of mantle eclogites.

Themes 2 and 3, Earth Evolution and Earth Today, and contributes to understanding Earth's Fluid Fluxes.

Contacts: Yoann Gréau, Bill Griffin, Sue O'Reilly, Olivier Alard (Montpellier)

Funded by: ARC Discovery (O'Reilly, Griffin), iMURS, EPS postgraduate Fund

The Hainan Plume samples an ancient mantle reservoir

Subduction of oceanic slabs to the core-mantle boundary (CMB) as part of plate tectonic processes, and hot mantle plumes that rise from the lower mantle, are two of the major phenomena that have operated through much of Earth's history. However, it is unclear how they interact with each other and whether

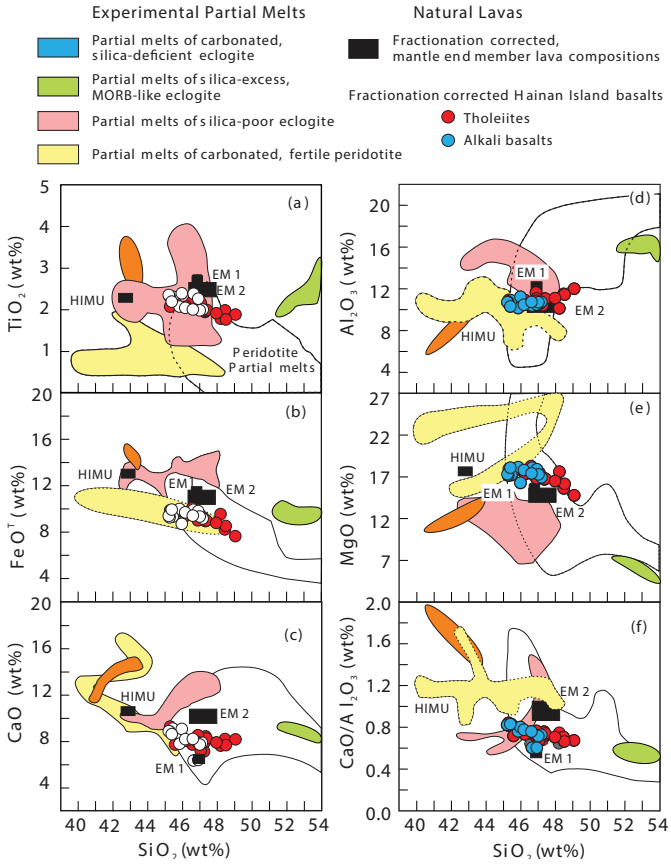

Figure 1. Comparison of fractionation-corrected Hainan basalts (compositions in equilibrium with Fo90.7, corrected for olivine addition), with experimental partial melts. Also shown for reference are the primary-melt estimates of HIMU, EM1, and EM2 mantle end members (CCFS Publication #24).

they are parts of a single geodynamic system; this is a gap in our understanding of how the Earth works. Southeast Asia is a unique site to test possible genetic linkages between deep subduction and plume generation because both phenomena have been seismically detected in the deep Earth in this region.

Recent geophysical studies made a surprising discovery: a plume-like low-velocity structure, called the Hainan plume, beneath Hainan Island and the Leizhou peninsula (Leiqiong) in Southeast Asia. This low-velocity structure goes down 1300–1900 km and may emanate from the lowermost mantle, making it one of perhaps a dozen postulated lower-mantle plumes worldwide. Global occurrences of mantle plumes and subducting slabs since the Mesozoic generally are found in different areas, with plumes in the broad Pacific and African mantle upwelling zones (commonly called superplumes) and subduction in mantle downwelling zones. However, seismic tomographic studies show that the plume-like Hainan low-velocity structure sits close to the subduction zones of the Pacific, Philippine Sea and South China Sea slabs to the east, and the Indo-Australian slab to the south and west, and is far from both superplumes. This suggests that the Hainan plume is unique in being linked to the subduction of tectonic plates; if so, it sheds new light on the workings of the global geodynamic system.

The primary melts for the Hainan basalts have been estimated using the most forsteritic olivine (Fo90.7) as the final olivine and less evolved bulk samples (MgO >9.0 wt% and CaO >8.0 wt%), assuming a constant Fe-Mg exchange partition coefficient of KD = 0.31 and $Fe^{3+}/FeT = 0.1$. The calculated primary melt compositions are similar to those of fractionation-corrected EM-1 and EM-2 type OIBs (Fig. 1) and plot within the overlapping experimental fields defined by partial melting of silica-deficient eclogites and peridotite (Fig. 1). According to the primary melt compositions, the effective melting pressures (Pf) and melting temperatures (T) form an array that plots systematically above the dry lherzolite solidus but below the base of the lithosphere (Fig. 2). The Pf-T array (Pf = 0.0105 × e0.0052T, R2 = 0.81) begins at about 18 kbar (about 60 km) and intersects the dry peridotite solidus at about 50 kbar (ca 160 km). This intersection translates into a mantle potential temperature beneath Hainan Island of about 1500–1600 °C, which is approximately 200 °C hotter than ambient mantle but typical of thermal mantle plumes such as the Hawaiian plume (Fig. 2). Pb-isotope analyses

cont...

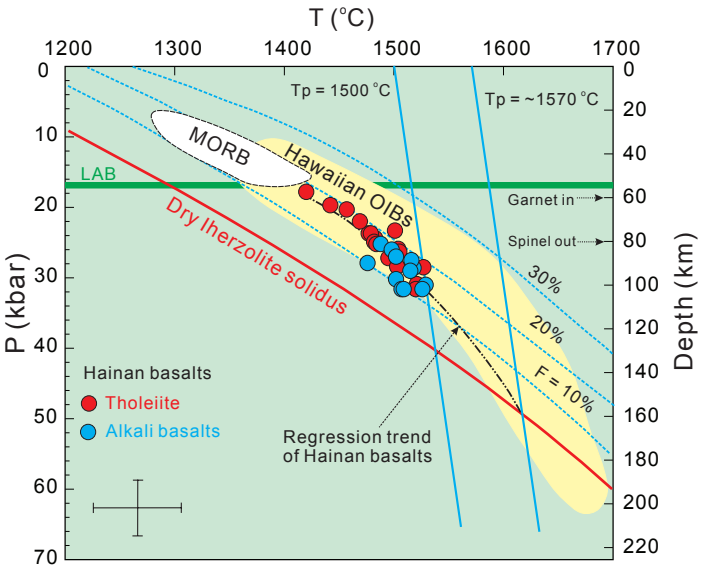

Figure 2. Temperatures and pressures calculated for the Hainan basalts. Curved lines represent melting adiabats where F(%) represents fraction of melting. Near-vertical lines represent solid mantle adiabats. The lithosphere-asthenosphere boundary (LAB) beneath Hainan Island is at about 55 km depth as constrained by geophysical data (CCFS Publication #24). Garnet-in and spinel-out reactions occur at about 60 and 80 km for a steady-state geotherm.

suggest that the Leiqiong flood basalts were derived mainly from an ancient (4.5–4.4 Gyr) primitive-mantle reservoir preserved near the core-mantle boundary (CMB). Their Nd- and Os-isotope compositions also suggest a lower-mantle origin. The lower-mantle isotopic compositions and high mantle potential T, together with the lower mantle-rooted plume-like seismic velocity structure, all point to the existence of a deep Hainan mantle plume. The Hainan plume thus provides a rare example of a young lower mantle plume close to deep slab subduction.

This project is part of CCFS Themes 1 and 2, Early Earth and Earth Evolution and contributes to understanding Earth's Fluid Fluxes.

Contacts: Xuan-Ce Wang, Zheng-Xiang Li, Xian-Hua Li
Funded by: NSFC grant, ARC CCFS, ECSTAR , Foundation grants

Nickel in natural diamonds

Diamonds, along with the mineral and fluid inclusions they can contain, represent the deepest direct samples from the Earth's mantle. Studying these diamond "capsules" as well as their contents has shed a lot of light on the chemistry of mantle fluids. An important tool for studying the chemistry of the fluids from which the diamonds grew is laser ablation mass spectrometry (LA-ICPMS), a technique pioneered at GEMOC for measuring trace elements in diamonds. This has been shown to be of most use for fibrous diamonds that contain abundant fluid micro-inclusions. Due to the low concentrations of trace elements in gem quality diamonds, a key requirement has been to trap a lot more material to analyse than is produced during a typical laser-ablation analysis.

To do this, we have had to develop a different way of ablating diamonds. Instead of passing the ablated material (suspended in gas) directly into the mass spectrometer, we pass it through a liquid. The gas bubbles off through the liquid and the ablated material is left behind in solution, where it can be analysed by ICP-MS. This allows us to ablate for several hours instead of minutes, capturing far more material than traditionally possible. Typical ablation pits made using this method measure 500 x 500 x 120 microns, compared with the 50-micron-diameter pits of most LAM-ICPMS analysis. While this method sacrifices the spatial resolution of regular LAM-ICPMS analysis, it achieves very low levels of detection for many trace elements.

Mixed-habit diamonds are those that show periods of smooth faceted octahedral growth and rough, hummocky cuboid growth, occurring at the same time. This often results in a center-cross feature, which may or may not be visible to the naked eye. These types of diamonds have been known to contain nickel, only in the cuboid sectors. This impurity is responsible for the green luminescence that is characteristic of these types of diamonds, but was something long thought to only occur in synthetic diamonds. While no measure of nickel concentrations in these diamonds has been made before, levels were estimated to be in the order of <0.1 ppm. Preliminary LA-ICPMS analysis performed here at GEMOC has revealed concentrations ranging between 2 and 20 ppm. These samples were the motivation to measure even smaller concentrations of trace elements, to see if any other elements were preferentially partitioned into the cuboid sectors rather than the octahedral ones. It is already know that nitrogen is preferentially taken up into the octahedral sectors and important question marks remain regarding variations of hydrogen.

For nickel to be found in diamond suggests an absence of any sulfide phases during the time of growth. This is because nickel is a chalcophile element – one that would rather react with sulfur than with oxygen (i.e. to form silicates). Sulfides are one of the most common types of inclusions found in diamonds, so their absence may be indicative of the physical and chemical growth conditions that resulted in this special type of diamond growth. Further analysis of the impurities in these types of diamonds should help reveal more information about the role of fluids in the mantle.

This project is part of CCFS Themes 2 and 3, Earth Evolution and Earth Today, and contributes to understanding Earth's Fluid Fluxes.

Contacts: Dan Howell, Bill Griffin, Sue O'Reilly, Norman Pearson
Funded by: ARC Discovery (relinquished), CCFS Foundation Program

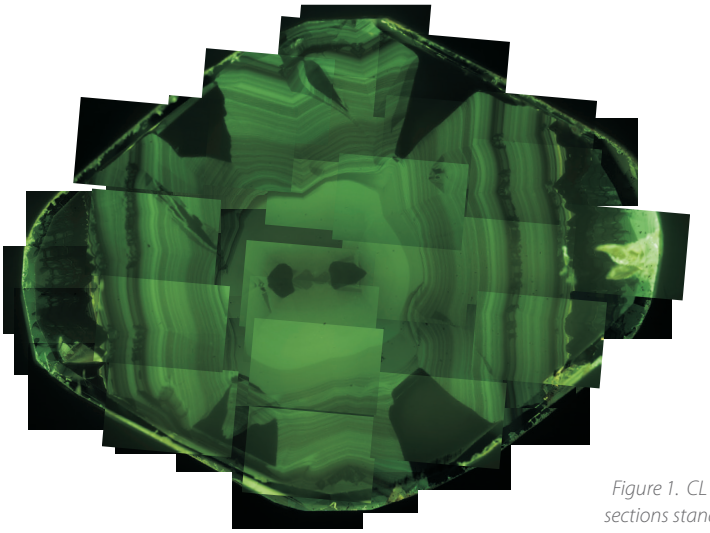

Figure 1. CL image of a complexly-zoned mixed-habit diamond - cuboid sections stand out in green colour.

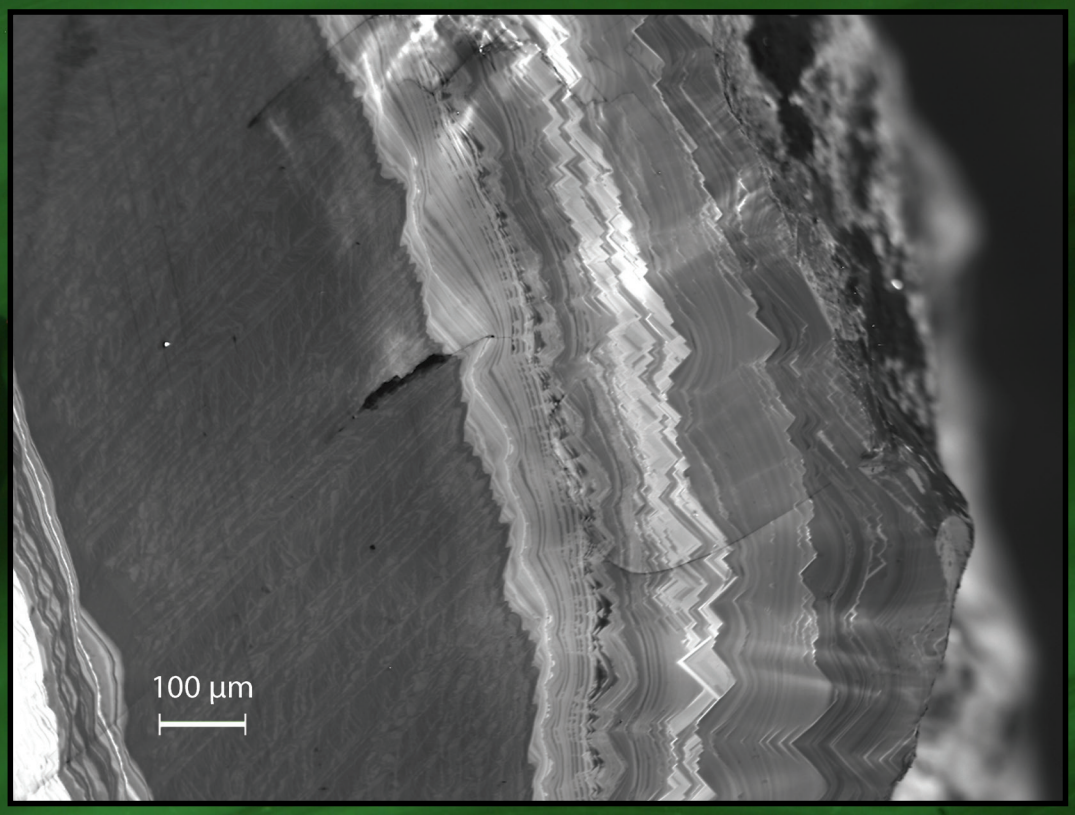
100 µm

Chromites from dirt - a new pathfinder for nickel deposits

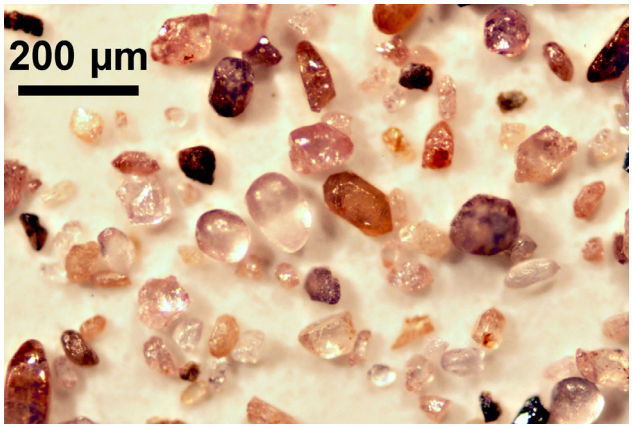

Figure 1. Black chromite grains in a heavy mineral concentrate. (photo: Elena Belousova).

The ever-increasing demand for global metal resources is creating many challenges for the metal exploration industry. Mineral deposits are not renewable and it is likely that all easily accessible giant deposits close to the surface have already been found. As a consequence, exploration for new 'hidden' deposits has to be extended to remote areas and deeper into the Earth itself, which is like looking for a needle in a haystack.

One way to aid exploration in a fast and cost-effective way is the analysis of resistate mineral phases from heavy mineral concentrates (Fig. 1). When water and wind erode rocks, mineral grains are liberated and may be deposited in nearby rivers. Minerals that are heavier and more resistant to destructive erosion than others are often trapped and concentrated in low-velocity parts of river beds and these "heavy mineral concentrates" provide an easily recovered sample of the entire catchment area of a drainage system. The minerals are analysed for their major- and trace-element compositions to identify element signatures that might indicate the nearby presence of a mineral deposit. This approach is used, for example, in diamond exploration, where garnet, chrome diopside and chromite are used as resistate indicator minerals to determine if a terrane is prospective for diamonds.

In 2011, GEMOC investigated the potential use of heavy mineral concentrates in the exploration for komatiite-hosted nickel-sulfide deposits. Komatiites contain some of the world's highest-grade nickel-sulfide deposits and the Archean Yilgarn Craton in Western Australia hosts several of these. The development of reliable prospectivity indicators to target exploration towards mineralised komatiite units has been a long-standing goal, particularly in Australia where komatiites rarely outcrop at the surface and geochemical exploration is often restricted to drill cores (Fig. 2a, b). Accordingly, the identification of an effective resistate indicator mineral for nickel-sulfide deposits that can be sampled at the surface could provide a major breakthrough in the exploration for mineralised komatiites.

Earlier research at GEMOC has shown that the ruthenium content of chromite can be used to discriminate mineralised

Figure 2a. Australian komatiite outcrops like this one are rare....

Figure 2b. ....therefore geochemical exploration is often restricted to diamond drill cores.

from barren komatiites in pristine rocks from deep drill cores. Chromites from mineralised komatiites have distinctly lower ruthenium contents than chromites from unmineralised environments (see *GEMOC Annual Report 2010)*. The research was extended in 2011 to see if the ruthenium content of chromites from heavy mineral concentrates can also be used in the exploration for nickel-sulfide deposits. As well as metamorphism and alteration, detrital chromites have inevitably undergone strong weathering, and primary ruthenium signatures may be obliterated by chemical modification of the chromite. To investigate how postmagmatic processes affect the ruthenium content of chromite, GEMOC's state-of-the-art laser ablation ICP-MS facility (Fig. 3) has been used to analyse more than 500 chromite grains from komatiites, komatiitic basalts and ferro-picrites from the Yilgarn Craton of Western Australia, the Superior Craton of Canada and the Fennoscandian Shield of Finland and Russia. The sample suite included rocks that have undergone different degrees of metasomatism and alteration, and sampling depths ranged from several hundred metres below the surface to near-surface rocks that have undergone extensive weathering.

Figure 3. GEMOC's state-of-the-art laser ablation ICP-MS facility.

The results show that ruthenium is essentially immobile during postmagmatic processes and that chromite cores (as opposed to their rims) are relatively resistant to destructive metamorphism and alteration, as well as lateritic weathering. Therefore, primary magmatic ruthenium signatures can be preserved in chromites. Based on currently available evidence, high-ruthenium chromites are largely, if not entirely, restricted to unmineralised komatiites. Hence the presence of mixtures of high- and low-ruthenium chromite, of appropriate major element chemistry, in detrital heavy mineral concentrates is a reliable signal of mineralised komatiite sequences, and varying proportions of high- and low-Ru grains may be an indicator of proximity.

As chromite is a widespread component of resistate heavy mineral suites, and large sample collections exist from previous diamond exploration programs, a prime opportunity has been created to investigate these sample collections, using an analytical technique that was unavailable when much of that material was originally investigated. Therefore, this technique could be an effective way to detect komatiite-hosted nickel-sulfide deposits, and could be used together with other geological, structural, geophysical and volcanological exploration techniques.

This project is part of CCFS Theme 3, Earth Today, and contributes to understanding Earth's Architecture and Fluid Fluxes.

Contacts: Marek Locmelis, Norman Pearson, Marco Fiorentini
Funded by: CCFS Foundation Program

Komatiites deliver volatiles to early Earth's surface

Komatiites are ancient volcanic rocks, mostly over 2.7 billion years old, which formed through high-degree partial melting of the mantle. Establishing the volatile content of komatiites is crucial to constraining the thermal evolution of the Early Earth and its primordial atmosphere. However, existing models are mainly based on evidence from komatiite flows, whereas komatiite intrusions have been neglected.

Our observations on komatiites from the Agnew-Wiluna greenstone belt of Western Australia show that komatiite flows must have degassed during emplacement, flow and crystallisation: flows ~150 metres thick contain vesicles, amygdales and segregation structures, showing a significant volatile content, but those less than 10 metres thick lack any textural or petrographic evidence of primary volatile contents. This implies that komatiite intrusions retained higher proportions of their primary volatile budget, and contain volatile-bearing mineral phases that reflect the presence of magmatic water in the parental magma. This means that evidence from komatiite intrusions, rather than lava flows alone, should be used to evaluate the thermal architecture of the Early Earth and the volatile inventory of the primordial atmosphere.

The results of this study indicate the possibility of a range of volatile contents in different komatiite types. In fact, our observations suggest that some komatiites were initially volatile-bearing and subsequently lost their volatiles. This would be facilitated by the low viscosity of komatiite magmas, allowing volatiles to bubble out more easily, and (or) by emplacement in shallow marine environments (i.e. low confining pressures). The diversity in the physical evidence for magmatic volatile contents may reflect different proportions of degassing caused by variable confining pressure and proximity to vent. Komatiite flows that lack hydrous magmatic minerals and textural or petrographic evidence of primary volatile interaction may be the degassed equivalents of volatile-bearing liquids. Alternatively, they could represent melts that were actually anhydrous. If so, the variable physical evidence for volatile content in komatiite units globally may reflect the presence of "wet" and "dry" komatiites, which were most likely emplaced in different geodynamic environments, just as a diversity of basalt types exist in more recent terrains.

The principal significance of the presence of magmatic amphiboles in some komatiitic and ferropicritic sills in the Agnew-Wiluna (Australia), Abitibi (Canada) and Pechenga (Russia) greenstone belts is that they reflect the crystallisation of hydrous parental magmas. The diverse nature of the physical evidence for magmatic volatiles in komatiite units that solidified at different distances from vent highlights means that we need to focus on evidence from proximal intrusions or thick flows, which may have retained a significant proportion of their primary volatile budget. Previous studies have mainly focused on thin lava flows without considering the effects of degassing, whereas thicker flows or intrusions have been generally neglected.

A re-assessment of the primary volatile content of komatiite magmas from intrusive settings has key implications for the thermal and petrological evolution of the Early Earth, localisation of nickel-sulfide ores, and development of the primordial atmosphere. The extreme Archean geothermal gradients advocated to explain the formation of komatiites in dry settings may have not been necessary to extract komatiites from volatile-bearing portions of the mantle. The localisation of "dry" and "wet" komatiites may reflect the presence of different Archean geodynamic environments (e.g. rift settings versus subduction zones). Correlation of H_2O contents and physical evidence of volatile content with proximity to Archean volcanic centres and intrusions could be significant in petrologic models and in mineral exploration. A relatively high water content, reflected by presence of magmatic amphibole, may reflect proximity to vents. Therefore, if komatiite-hosted nickel-sulfides form preferentially in proximal extrusive and dynamic intrusive environments, careful mapping of the physical evidence for volatile contents in different volcanic facies may help to identify areas with greater potential for nickel-sulfide deposits.

An Australian komatiite outcrop.

Finally, degassing of komatiites would have also contributed to the development of an early atmosphere, through volatile exchange at the ocean surface. Since komatiite flow fields were extremely voluminous and occupied extensive areas of the seafloor, volatile exsolution during their emplacement and crystallisation could have influenced physical

and chemical parameters in the primordial oceans, and indirectly contributed to the creation of a complex zonation at the interface between water and seafloor.

This project is part of CCFS Theme 1, Early Earth, and contributes to understanding Earth's Fluid Fluxes.

Contacts: Marco Fiorentini, Steve Beresford
Funded by: ARC Discovery

Research highlights 2012

Contents

Deep Earth recycling in the Hadean

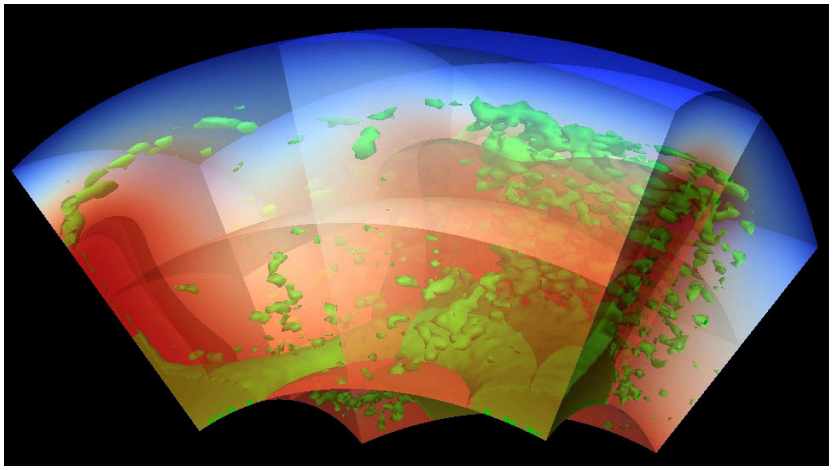

Could the mixing of Earth's earliest geochemical reservoirs constrain the geodynamics of the Earth during the Hadean period?

The Hadean has been referred to as a geological dark age – for the first 500 million years of Earth's history, there is a complete dearth of any geological record. The crust of this time was probably destroyed by meteorite bombardment, volcanic resurfacing, vigorous tectonic mixing or all three.

The Hadean was undoubtedly hellish – on top of the heat supplied by relentless meteorite bombardment, the mantle was efficiently heated by high rates of radioactive decay, including short-lived, and now extinct, isotopes like aluminium-26. The mantle also retained much of the substantial heat generated during accretion and the formation of the core.

Under this sort of hot mantle conditions, traditional wisdom has it that the interior viscosity of the Earth would be quite low, and mantle convection extremely vigorous. Mantle convection simulations have suggested that the mixing of early geochemical reservoirs should have been extremely efficient under these conditions, and should have been homogenised on timescales of less than 100 Myrs.

Recently, a number of lines of evidence have provided contrasting views on the Hadean. Model ages on the Nuvvuagittuq greenstone in Quebec suggest some Hadean crust has survived, and zircons from Jack Hills have been used to argue for subduction processes in the Hadean. However, the residence time for the mafic protolith for these Jack Hills zircons is ~400 Myrs – an inordinately long time for a thick mafic crust to survive on an active mantle.

The preservation of geochemical anomalies in younger Archaean rocks also suggests long survival times and inefficient mixing in the Hadean. Neodymium-142 anomalies reflect very early crustal extraction – and the identification of such anomalies in 2.666 Ga basalts from the Abitibi belt suggest these mantle anomalies survived for almost ~2 Gyr. Similarly, tungsten-182 anomalies reflect primordial partitioning events, yet are still observed in rocks as young as 2.8 Gyr from the Kostomuksha Greenstone belt in the Baltic Shield, Russia. Lastly, the present concentration of platinum-group elements in the Earth's mantle is thought to be due to a post-core meteoritic addition, called the late veneer. However, PGEs did not reach their present concentration in mafic lavas until ~2.9 Ga; prior to that they increase linearly from about 3.9 Ga onwards – suggesting they were being progressively mixed into the deep mantle and sampled during this time.

The mixing times of these independent geochemical reservoirs (~2 Gyr) are far longer than the anticipated mixing time from simple convection simulations (<~100 Myr), and so the question becomes – what is missing?

The answer may lie in the tectonic response of the Earth to its hot, early start. New work at CCFS by Craig O'Neill and colleagues suggests that for most of the Hadean the Earth may have been tectonically inactive – the low interior viscosities prevented the build-up of the stress required to fracture and mobilise plates, and the planet may have been in a "hot stagnant lid" regime. The evolution from this starting point into a tectonically episodic regime with rapid, recurring overturn events, has profound implications for Earth's mixing history and thermal evolution.

Three dimensional spherical-cap simulations (pictured), starting from a hot stagnant-lid state, suggest the mixing time in such a regime is an order of magnitude less than for either plate tectonics, or the simple convection calculations performed previously. This in itself can explain the discrepancy between observed mixing times, and those predicted by earlier models.

On top of that, the new simulations suggest that the early Earth lost its heat inefficiently. Previous thermal-evolution models for Earth invariably run into a problem called the "Archean thermal catastrophe" – where in order to match declining heat fluxes, internal temperatures would have been unreasonably high (i.e. global mantle melting) during the Archean. The new models prevent this thermal catastrophe, by demonstrating that Earth could have lost its heat inefficiently, and had lower global heat fluxes early in its history than previously assumed - meaning that internal temperatures could stay within reasonable bounds.

This project is part of CCFS Theme 1, Early Earth, and contributes to understanding Earth's Architecture and Fluid Fluxes.

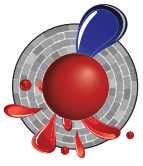

Contact: Craig O'Neill
Funded by: ARC Future Fellowship, MQ infrastructure funding

Synchronous pole dancing: the state of supercontinent Nuna before Rodinia

The idea that Earth's evolution has been dominated by cycles of supercontinent assembly and breakup has been debated for decades. However, our understanding of past supercontinents has mainly been limited to the last 1000 Ma; we could be more confident about the history of the ca 320-180 Ma supercontinent Pangea than the ca 900-700 Ma supercontinent Rodinia. Our knowledge of an even older supercontinent (Nuna or Columbia), formed around 1.8 Ga, has been more tenuous, and early papers were mostly based on intercontinental geological correlations that are intrinsically non-unique. Early attempts at Nuna-related continental reconstructions were hampered by the lack of high-quality palaeomagnetic results, or merely regional, rather than global considerations.

Recently (*CCFS publication#197)* we reported new palaeomagnetic results from North China, and by integrating recent results from Australia, India, and Amazonia and all previously reported results, we reconstructed the first near-complete reconstruction of Nuna (Fig. 1). Our work indicates that Nuna formed by ca 1750 Ma, and lasted at least until ca 1400 Ma (Fig. 1 and 2). This work was involved an ongoing international collaboration with Professor Shihong Zhang of China University of Geosciences, and Professor David Evans of Yale University.

Our reconstruction agrees with previously proposed, geologically based models, including the SAMBA connection between Baltica, Amazonia and Western Africa, the Nuna core connection between Laurentia, Baltica and Siberia, the proto-SWEAT connection between Laurentia, Mawson block and Australian blocks, and the North China-India connection. In addition, our reconstruction for the first time quantitatively merges these regional connections into a single and coherent supercontinent.

Our Nuna reconstruction, constrained by both our new results and an updated global paleomagnetic dataset, is also consistent with key geological features including the ca 1800 Ma orogenic belts leading to the assembly of Nuna (Fig. 2a) and Mesoproterozoic intraplate extensional basins and the Large Igneous Province (LIP) record that may be related to the breakup of Nuna (Fig. 2b). This breakup may have begun around 1400 Ma ago, but available paleomagnetic data are not yet complete enough to allow a more precise depiction of Nuna's fragmentation.

This research is directly related to CCFS Foundation Program 6: Detecting Earth's rhythms, and projects 2d and 9.

This project is part of CCFS Theme 2, Earth Evolution, and contributes to understanding Earth's Architecture.

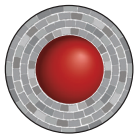

Contacts: Zheng-Xiang Li, Shihong Zhang, David Evans

Funded by: Chinese National Natural Science Foundation grants and 973 Program support, ARC DP (DP0770228), CCFS Foundation Program 6

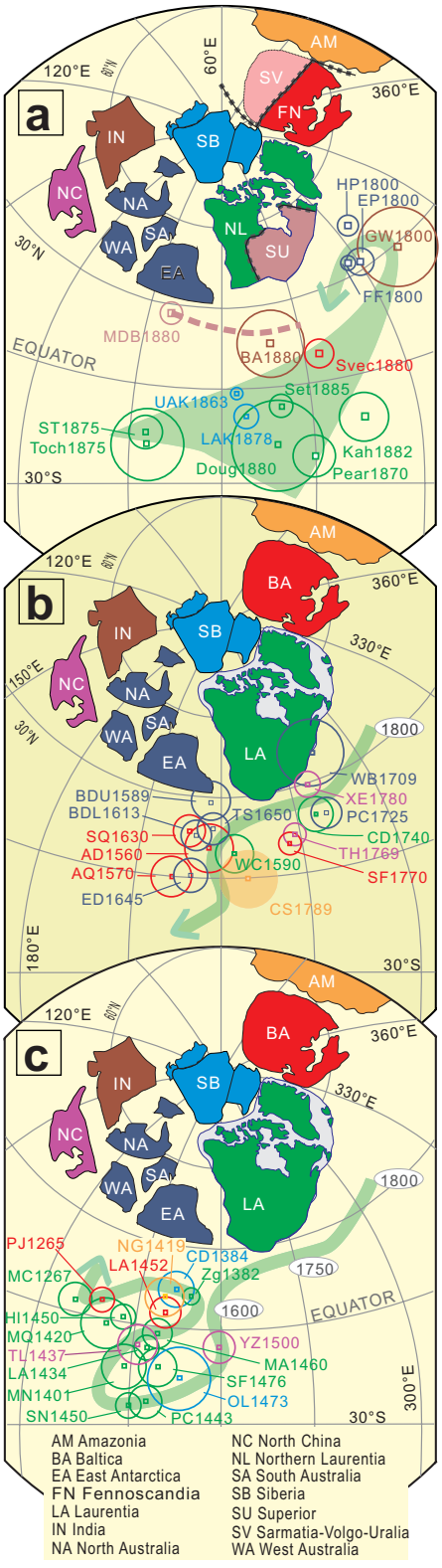

Figure 1. Presently available paleomagnetic datasets enabled the reconstruction of the first palaeomagnetically constrained complete Nuna supercontinent (Zhang et al., 2012; CCFS contribution #197), all in present North American coordinates. Cratons and their poles are colour coded, and ages following pole abbreviations are in millions of years before present (Ma). (a) Palaeomagnetic poles between 1880 and 1800 Ma, showing broad convergence (light-green swath) of poles from the Slave craton of Laurentia, Siberia, Baltica, India and Australia, which suggests that these blocks might commence to join together at ca 1800 Ma. Arrow points toward the position of younger poles. (b) Poles between 1780 Ma and 1600 Ma from Australian cratons, Laurentia, Baltica and NCB, define a common apparent polar wander path (APWP) for Nuna (green curve); arrow points toward the position of younger poles. (c) Palaeomagnetic poles for 1500 -1265 Ma from North China, Siberia, Laurentia, Baltica and Amazonia against the common APWP (green curve) that is defined by all poles between 1800 Ma and 1260 Ma, indicating common motion to at least 1380 Ma. Arrow points toward the position of younger (< 1200 Ma) poles from Laurentia and Baltica. See CCFS publication #197 for more details.

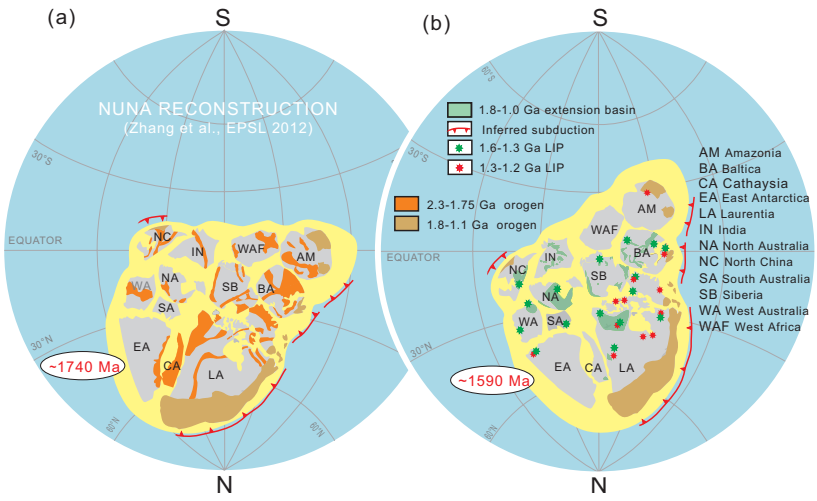

Figure 2. Configuration and palaeogeographic position of the supercontinent Nuna (a) at ca. 1740 Ma soon after its assembly, and (b) at ca. 1590 Ma, when large igneous provinces and extensional basins were extensively developed. Paleomagnetic poles from Laurentia were used to plot the paleolatitude of the supercontinent. Placing Laurentia in northern hemisphere was based on the likely westward trade-wind direction interpreted by Hoffman and Grotzinger (1993) from the 1950 -1860 Ma geological records in the Slave craton. We turned the world upside-down to make Australia and North America plotted upright, and therefore for easier viewing. See CCFS publication #197 for more details.

More insights from Earth's oldest zircons: ~4.45 Ga crust in the North Qinling Orogenic Belt, China

Most of what we know about Earth's earliest crust comes from Jack Hills in Western Australia, where hafnium-isotope data from old detrital zircons in a younger sandstone indicate that their parent magmas were melted from still older rocks that formed about 4.4-4.5 billion years (Ga) ago. These zircons provide our only means of exploring the Hadean period, the time between the formation of the Earth and the preservation of the oldest known rocks, formed about 3.8 Ga ago. However, Hadean zircons have been found in only four other localities; the Southern Cross belt in Western Australia, the Acasta gneiss complex in northwestern Canada, and China. The Chinese examples include a single 4.1 Ga grain from the Burang area of Tibet and another ~4.1 Ga grain from the North Qinling Orogenic Belt. The latter discovery comes from rocks in a Phanerozoic collisional belt developed between the North and South China cratons. The zircon was found in Ordovician volcanic rocks of the Caotangou Group, dated at 456 ± 2 Ma. These arc volcanic rocks penetrated the basement of the North China Craton, so the zircon xenocryst could have been picked up by the magma either in its source region or during its ascent; it is the first report of Hadean crustal material in a Phanerozoic igneous rock.

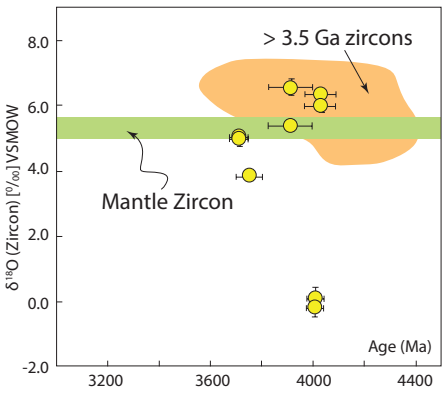

For this study, over 3000 zircon grains were separated from ignimbrite collected from the same outcrop as the initial discovery, and were analysed for U-Pb age using both SHRIMP and LA-ICP-MS techniques. In total, only three grains were identified with ages ≥3.9 Ga and these were selected for U-Pb and Hf-O isotopic analysis.

The magmatic cores in these zircons range in age from 3909 ± 45 Ma to 4080 ± 9 Ma and record Hf crustal model ages up to 4.5 Ga. Importantly, the latter lie on the same Lu/Hf trajectory as the least-disturbed Jack Hills zircons, so they are only the second example of the earliest known crustal rocks on Earth. The zircon cores also show a wide range in $\delta^{18}O$, both above and below the mantle value (Fig. 1); this is strong evidence that the source rocks of the magmas had been subjected to surficial processes such as weathering. The rims of two grains record new zircon growth at 3.7 Ga and, when combined with their presence in an Ordovician volcanic rock, suggest that ancient crust was still present in the basement of the North China Craton during the Paleozoic (*CCFS publication #301*).

This project is part of CCFS Theme 1, Early Earth, and contributes to understanding Earth's Architecture.

Contact: Simon Wilde

Funded by: CCFS Foundation Program 2; The National Basic Research Program of China (973 Program; grant No. 2012CB416601), the National Natural Science Foundation of China (NSFC; grant No. 41272004) and the MOST Special Funds from the State Key Laboratory of Continental Dynamics, Xi'an, China

Figure 1. Plot of $\delta^{18}O$ versus age for the xenocrystic zircons (yellow symbols) from the North Qinling Orogenic Belt, China. In green is the band for 'mantle zircon' (Valley et al., Contrib. Mineral. Petrol., 1998); the orange area shows the field of global >3.5 Ga zircons (from Valley et al., Contrib. Mineral. Petrol., 2005; Harrison et al., Science, 2005; Trail et al., Geochem. Geophys. Geosystems, 2007; Heiss et al., Geochimica et Cosmochimica Acta, 2007).

Unmasking xenolithic eclogites: sleuthing with the key samples

Xenolithic eclogites are high-temperature and high-pressure mafic rocks, generally brought up from 150-220 km depth to Earth's surface by kimberlites. They are minor but important constituents of the subcontinental lithospheric mantle (SCLM), and information on their evolution and origin can provide unique constraints on the history of the ancient lithospheric mantle.

Extensive studies of eclogite samples from all over the world have generated two contradictory hypotheses about their origin. One regards the eclogites as deep-seated magmatic rocks, while the other regards them as components of subducted oceanic slabs. To test these hypotheses, it is essential to find out whether the samples being studied actually contain the information we are after (i.e. what is the RIGHT sample).

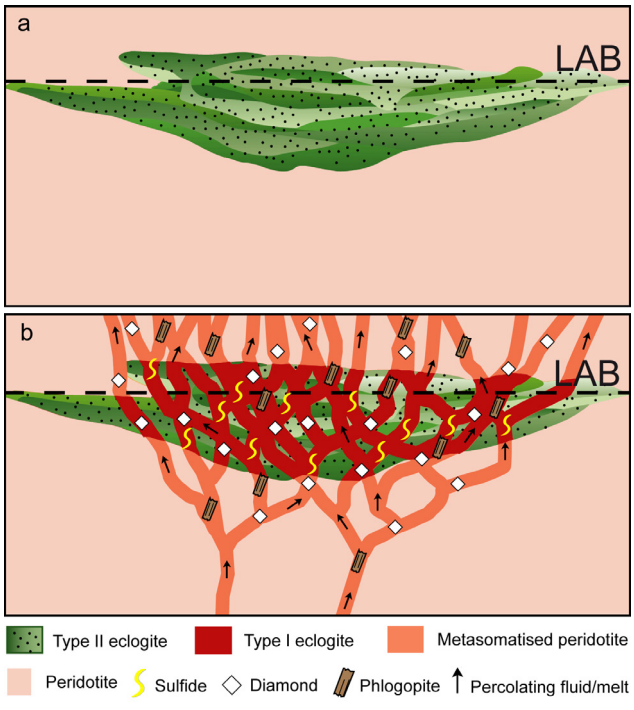

Figure 1. Cartoon of the Roberts Victor eclogite body at the base of SCLM before (a) and after (b) the metasomatism.

Previous work on the famous eclogite suite from the Roberts Victor kimberlite (South Africa) has divided the samples into Types I and II. Type I eclogites are heavily metasomatised by a sequence of melts/fluids in the carbonatitic-kimberlitic spectrum; Type II eclogites may be the protoliths of Type I (Fig. 1; *CCFS publications #3, 41*).

The progressive metasomatism inferred from studies of the whole eclogite suite has now been found within one hand specimen, RV07-17 (Fig. 2). From top to bottom, this sample becomes less equilibrated in terms of microstructure; grain boundaries that are smooth in the upper part become convolute and complex in the lower part, which also has more secondary minerals (e.g. phlogopite, sulfide) and more fluid inclusions.

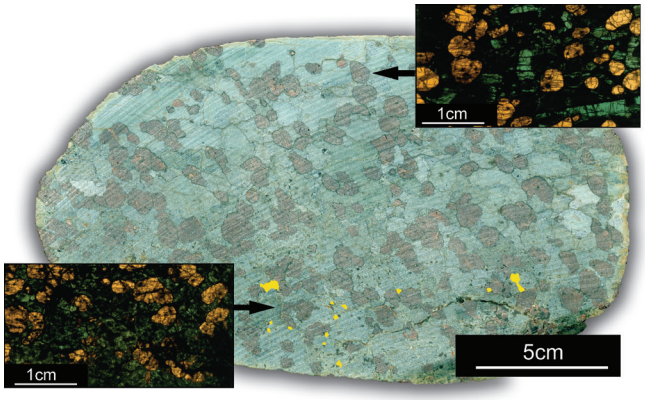

Figure 2. Handspecimen photo of RV07-17 and thin-section images of upper and lower parts of the sample.

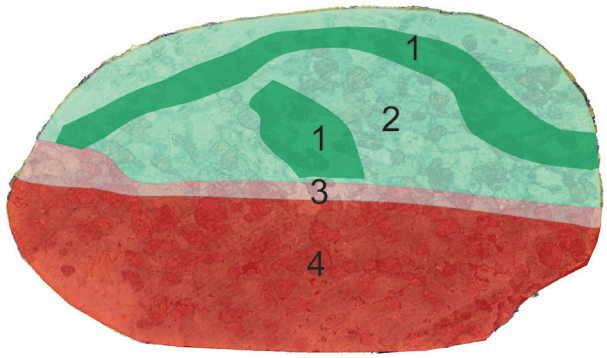

Figure 3. Drawing of RV07-17 showing four different zones.

Four zones (Zone 1, 2, 3, and 4) can be recognised using the chemical compositions of garnets (Fig. 3). From Zone 1 to Zone 4, the pyrope content of the garnets increases gradually from 0.47-0.62; cpx shows progressive enrichment in MgO (10.8-14%). The cross-cutting pattern strongly suggests that Zone 1 represents an early stage of the metasomatism, and Zone 4 the latest stage.

REE patterns of both garnet and cpx also show systematic changes (Fig. 4a-4b). The garnets of Zone 1 have flat REE patterns from Lu to Sm, but a strong depletion in the LREE. Toward Zone 4, the relative abundance of the MREE of the garnets drops significantly, giving smoother patterns. The large cpx grain in Zone 1 shows a strong depletion in the LREE, but the LREE/MREE of the cpx increases from Zone 1 to Zone 4. The Sr contents of cpx change sharply from ~230 ppm in Zone 1+2 to ~320 ppm in Zone 4, and the $^{87}Sr/^{86}Sr$ of cpx increases from ~0.7055 in Zone 1+2 to ~0.7063 in Zone 4. From Zone 1 to 4, $\delta^{18}O$ of the garnet decreases from ~8.5 ‰ to ~6.0 ‰ as the MgO content increases (Fig. 4c).

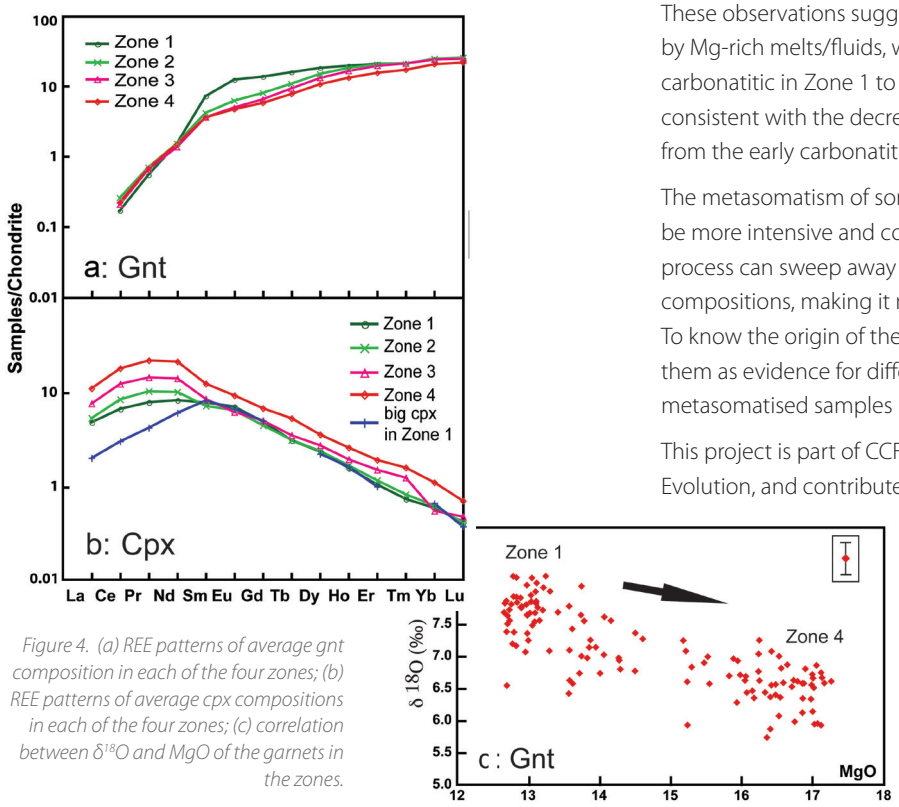

Figure 4. (a) REE patterns of average gnt composition in each of the four zones; (b) REE patterns of average cpx compositions in each of the four zones; (c) correlation between $\delta^{18}O$ and MgO of the garnets in the zones.

These observations suggest that the eclogite was metasomatised by Mg-rich melts/fluids, which changed through time from carbonatitic in Zone 1 to more kimberlite-like in Zone 4. This is consistent with the decrease of $\delta^{18}O$ in the metasomatic agent from the early carbonatitic fluids to the late kimberlitic melt/fluid.

The metasomatism of some mantle eclogites (e.g. Type I) may be more intensive and complete than previously thought. This process can sweep away all original information on chemical compositions, making it nearly impossible to define a protolith. To know the origin of the xenolithic eclogites, and to use them as evidence for different dynamic scenarios, the least-metasomatised samples must be studied.

This project is part of CCFS Theme 2, Earth Evolution, and contributes to understanding Earth's Fluid Fluxes.

Contacts: Jin-Xiang Huang, Yoann Gréau, Bill Griffin, Sue O'Reilly

Funded by: ARC Discovery (O'Reilly and Griffin), CCFS Foundation Program 8, MQRES, EPS Postgraduate Fund

Rare rocks – the smoking gun for lithosphere drop-off 435 million years ago

How can an orogen (mountain belt) form within a continental plate? Why do these episodes of crustal deformation end with widespread intraplate magmatism? These types of geological activity represent a "hole" in the Plate Tectonics paradigm, which emphasises activity along plate boundaries. The 2000 km-long intraplate Wuyi-Yunkai orogen, active in the early Palaeozoic South China, is well documented. It has high-grade metamorphic rocks in the orogenic core (Fig. 1a, dark grey area), and widespread, mostly late- to post-orogenic granites, in both the orogenic core and the foreland areas (light grey areas; Fig. 1a). Previous regional tectono-magmatic analyses suggested that this widespread late- to post-orogenic granitic cont...

Figure 1. (a) Simplified regional geological map highlighting the regional extent of the early Paleozoic Wuyi-Yunkai orogeny in South China, featuring high-grade metamorphic rocks (shown in green) in the orogenic core (shown in dark grey), and widespread late-to post-orogenic granites (shown in red) throughout the orogeny (after Li et al., GSA Bull. 2010). (b) Plot of La/Nb versus εNd(435 Ma) for the rare Chayuanshan basaltic rocks in northern Guangdong province, which point to a sub-continental lithospheric mantle (SCLM) source region.

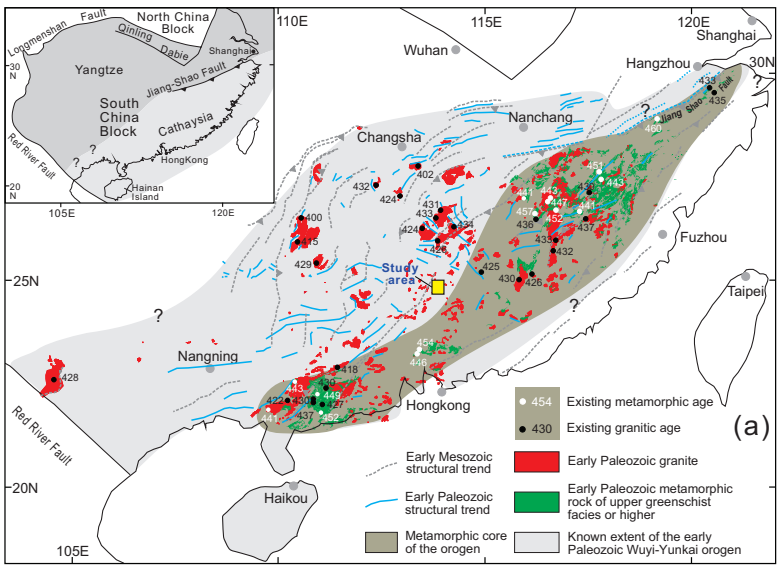

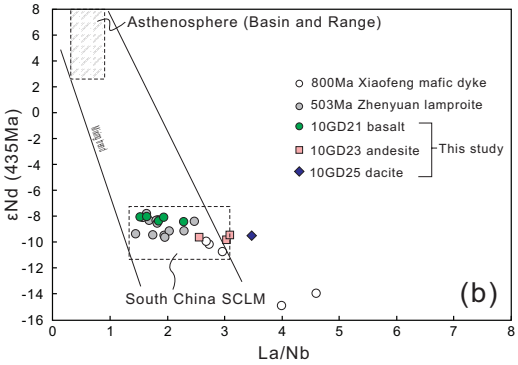

magmatism mostly occurred during orogenic collapse when the deep crust (the "root") of the orogen delaminated. However, the lack of any syn- to late-orogenic mafic rocks made it difficult to verify this or any other possible models.

The discovery of rare Silurian post-kinematic basaltic to andesitic volcanic rocks in northern Guangdong province (*CCFS publication #193*) has made it possible to study mantle-crust interactions during the intraplate orogenic event. The Chayuanshan volcanic rocks crop out on the northwestern margin of the orogenic core (Fig. 1a, marked as "Study area"). They unconformably overlie strongly-deformed Cambro-Ordovician strata, but are in low-angle unconformable contact with overlying post-orogenic mid-Devonian strata. LA-ICP-MS and SHRIMP U-Pb dating of zircons from two andesitic samples gave consistent magmatic ages of 434 ± 6 Ma and 435 ± 6 Ma, which are younger than the 460-440 Ma peak metamorphism of the orogeny but synchronous with the widespread un-deformed, late-orogenic (440-415 Ma) granitic intrusions.

Nine basaltic samples, with the least crustal contamination, have high MgO contents (12.3-19.2 wt.%). The Nd isotope and trace-element compositions of these high-Mg basalts point to a source region of an ancient sub-continental lithospheric mantle (SCLM; Fig. 1b), which is generally depleted in basaltic-melt components in comparison with the asthenospheric mantle, resulting in high mantle Mg# values. The calculated primary basaltic melt has ~50 wt% SiO_2, ~14 wt% MgO and ~9 wt% FeOT. The estimated potential temperature for the melts is close to 1400 ºC, much higher than that of a normal sub-continental lithosphere. The effective melting pressure for the melts is 1.0-1.4 GPa. This suggests that the magma was generated from partial melting of lithospheric peridotite heated by hot upwelling asthenosphere. The related high-Mg# andesites are interpreted as the products of differentiation and assimilation, fractionation and contamination processes from the same basaltic magma source, as supported by their negative zircon εHfT values (-21.7 to -6.3) and high zircon $\delta^{18}O$ values (7.3-9.0 permil).

Our results lend strong petrological support for the idea of an orogenic root delamination beneath the Wuyi-Yunkai orogeny. As shown in Figure 2, we interpret the Chayuanshan basaltic rocks as representing partial melts near the edge of the remaining sub-continental lithospheric mantle (SCLM). Heat from the upwelling asthenosphere as well as possible basaltic underplating, and regional decompression caused by orogenic collapse, can best explain the widespread synchronous granites along the orogen. In this model, the low- pressure and high-temperature melting of a hydrated subcontinental lithospheric mantle, as demanded by the basaltic magmas, can be satisfied by the delamination of the root, and the consequent orogenic collapse. The volcanic rocks unconformably overlie the strongly deformed Cambro-Ordovician succession, but are nearly parallel with the overlying, post-orogenic Devonian succession; this is consistent with a late-orogenic origin. The ca 435 Ma age of the volcanism post-dates the high-grade metamorphism at ca 460-440 Ma, but is synchronous with the widespread, dominantly post-kinematic felsic magmatism at ca 440-415 Ma. The underplating of mafic magmas, in combination with heat from the upwelling asthenosphere and decompression due to orogenic collapse, provides a plausible explanation for the widespread post-kinematic felsic magmatism.

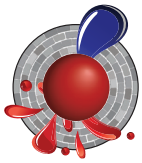

This project is part of CCFS Themes 2 and 3, Earth Evolution and Earth Today and contributes to understanding Earth's Architecture and Fluid Fluxes.

Contacts: Wei-Hua Yao, Zheng-Xiang Li, Xuan-Ce Wang, Xian-Hua Li
Funded by: Chinese Academy of SciencesAS SAFEA(KZCX2-YW-Q04-06), NNSFC (40973025), ARC (DP110104799)

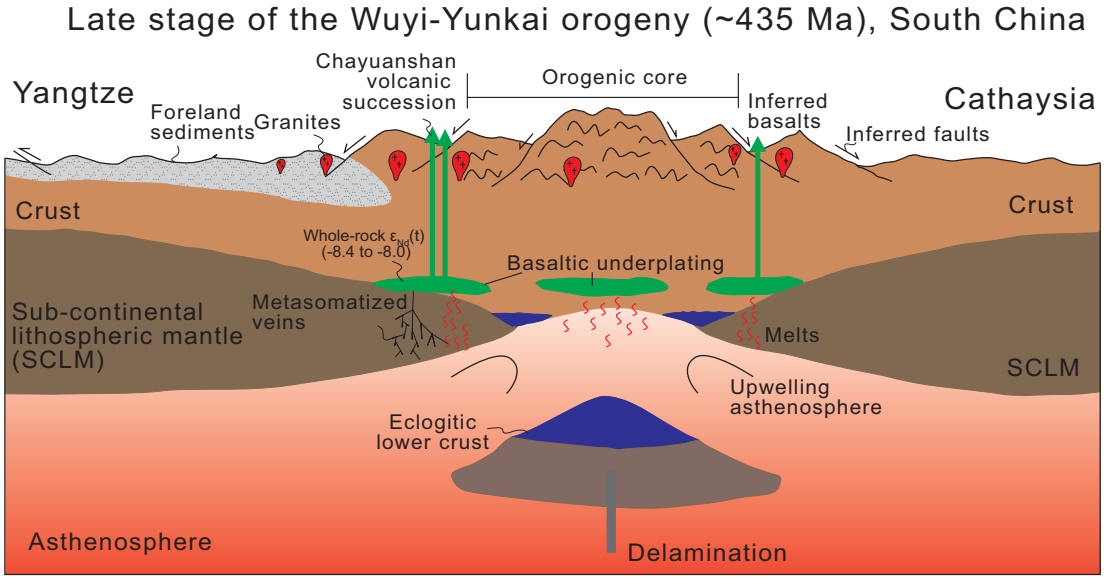

Figure 2. A cartoon diagram showing the delamination of the sub-continental lithospheric mantle (SCLM) and lower crust after crustal thickening during the intraplate Wuyi-Yunkai orogeny at ca 435 Ma.

Mobility of osmium unearthed: unexpected consequences for tracking mantle evolution

The Os-isotope compositions of platinum-group minerals (PGMs) in ophiolite chromitites are commonly regarded as resistant to fluid-related processes, and have been used to track the evolution of Earth's convecting mantle. However, we have found significant differences in $^{187}Os/^{188}Os$ between primary and secondary PGMs from metamorphosed ophiolite chromitites of the Dobromirtsi Ultramafic Massif, in the Central Rhodope Metamorphic Core Complex of southeastern Bulgaria (*CCFS publication #42)*. Primary (magmatic) PGMs hosted in unaltered chromite cores have $^{187}Os/^{188}Os$ from 0.1231 to 0.1270, and $^{187}Re/^{188}Os \leq 0.002$. T_{MA} and T_{RD} model ages, calculated relative to the Enstatite Chondrite Reservoir, cluster around three main peaks: ca. 0.3, 0.4, and 0.6 Ga. Secondary PGMs, produced by alteration of magmatic PGMs, have a wider range of variation ($^{187}Os/^{188}Os = 0.1124–0.1398$, $^{187}Re/^{188}Os \leq 0.024$); these grains yield T_{MA} and T_{RD} model ages from ~1.7 Ga up to 2.2 Ga. The larger range in $^{187}Os/^{188}Os$ in the secondary PGMs is interpreted as due to reactions between the primary PGMs and infiltrating metamorphic-hydrothermal fluids with a range of Os-isotope compositions. This redistribution of Os in PGMs during metamorphism has significant implications for the interpretation of both whole-rock and *in-situ* Os-isotopes.

The fact that secondary PGMs in the metamorphosed chromitites of Dobromirtsi yield $^{187}Os/^{188}Os$ within the range of depleted to enriched mantle sources suggests that much of the Os-isotopic variability previously reported for PGMs taken out of their microstructural setting (e.g. mineral concentrates or detrital grains collected from streams), and interpreted as a magmatic feature, may instead be related to secondary alteration processes. Therefore, interpretations of mantle events based on the *in-situ* analysis of PGM nuggets from placers may need to be reconsidered. On a more positive note, the Os-isotope data from the secondary Os-bearing phases in ophiolites can actually give a wider perspective on the sources and evolution of the host mantle peridotite.

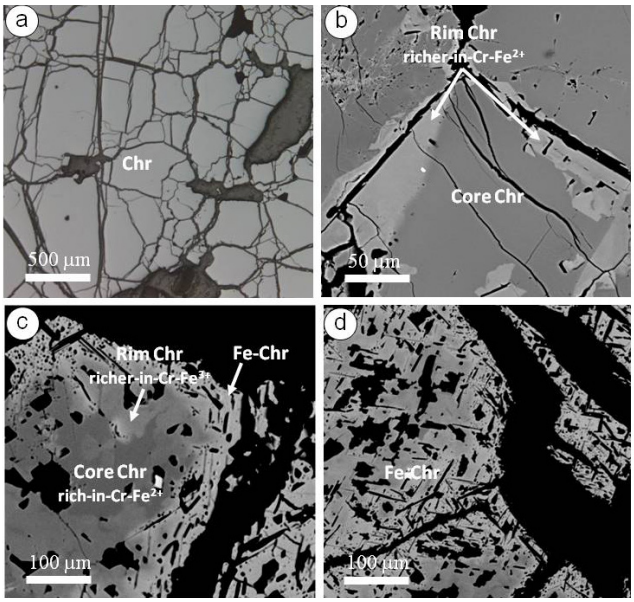

Figure 2. a. reflected-light image of massive chromitite. b. BSE image of zoned chromite; unaltered core mantled by secondary chromite enriched in Cr and Fe^{2+} and depleted in Mg and Al. c. Zoned chromite (BSE); modified core with two secondary rims: an inner rim of Cr- and Fe^{2+}-rich and Mg- and Al-depleted chromite, and an outer rim of Fe^{3+}- rich (ferrian) chromite. d. Homogenous grain (BSE) of secondary ferrian chromite.

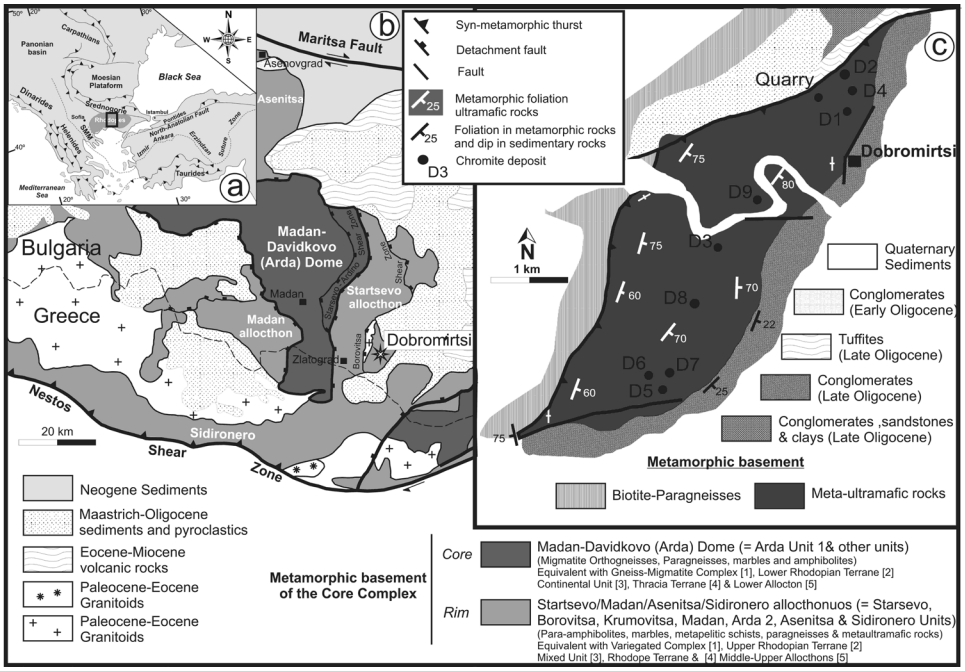

Figure 1. Location of the Dobromirtsi ultramafic massif in the Central Rhodope Core Complex in SE Bulgaria.

This project is part of CCFS Themes 2 and 3, Earth Evolution and Earth Today, and contributes to understanding Earth's Architecture and Fluid Fluxes.

Contacts: José María, González-Jiminéz, Bill Griffin, Norman Pearson, Sue O'Reilly

Funded by: ARC CoE CCFS Foundation Program 1, ARC Post-Award fund to CCFS, grants to international collaborators

Solving the biggest jigsaw puzzle in Solid-Earth Sciences

The conversion of geophysical data (e.g. seismic travel-time curves, gravity anomalies, surface heat flow, etc) into robust estimates of the true thermochemical structure of the Earth's interior is one of the most fundamental goals of the Geosciences. It is the physical state of the deep rocks that drives processes such as volcanism, seismic activity and tectonism. Detailed knowledge of the thermal and compositional structure of the upper mantle is an essential requirement for understanding the formation, deformation and destruction of continents, the physical and chemical interactions between the lithosphere and the convecting sublithospheric mantle, the long-term stability of ancient lithosphere, and the development and evolution of surface topography.

Our current knowledge of the thermal and compositional structure of the lithosphere and the sublithospheric mantle essentially derives from four independent sources.
(i) The most widely applied modelling approach uses gravity and/or surface heat flow data to obtain a model for the temperature and/or density structure of the lithosphere that fits the data to some acceptable level.
(ii) The second most common approach applied to the lithosphere and upper mantle is based on the modelling of seismic data. The aim here is to test thermal and mineralogical (or density) models that are compatible with seismic data (usually shear waves) by using either thermodynamic concepts and/or experimental data from mineral physics. Typically, these studies do not invert directly for composition but rather assume *a priori* "representative" compositional models.
(iii) A third source of independent information is provided by models and data derived from magnetotellurics (MT). MT is a natural-source electromagnetic method based on the relationship between the temporal variations of electric and magnetic fields at the Earth's surface and its subsurface electrical structure.
(iv) Finally, the only *direct* approach is the petrological-geochemical estimation of thermobarometric and chemical data from xenoliths (fragments of upper mantle brought up to the surface by volcanism) and exhumed mantle sections. Where specific mineral assemblages are present, xenoliths can be used to derive the compositional and paleo-thermal structure beneath specific localities.
At present, there are often significant discrepancies between the predictions from these four approaches. *The key to progress lies in integrating data from all of these sources into a single consistent model.*

Figure 1. Left: "True" and recovered solution from a full 3D inversion, including travel time residual tomography, using the new method/code for the compositional field. Note that although the absolute magnitudes are not well recovered, the general trend and geometries are correctly identified.

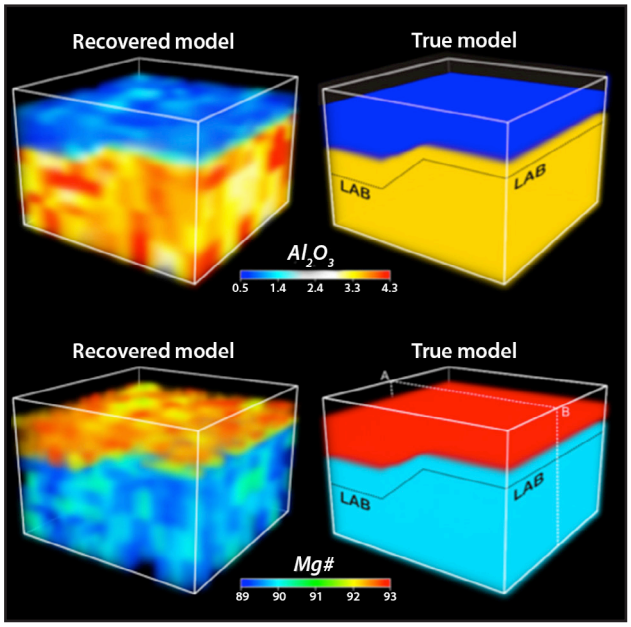

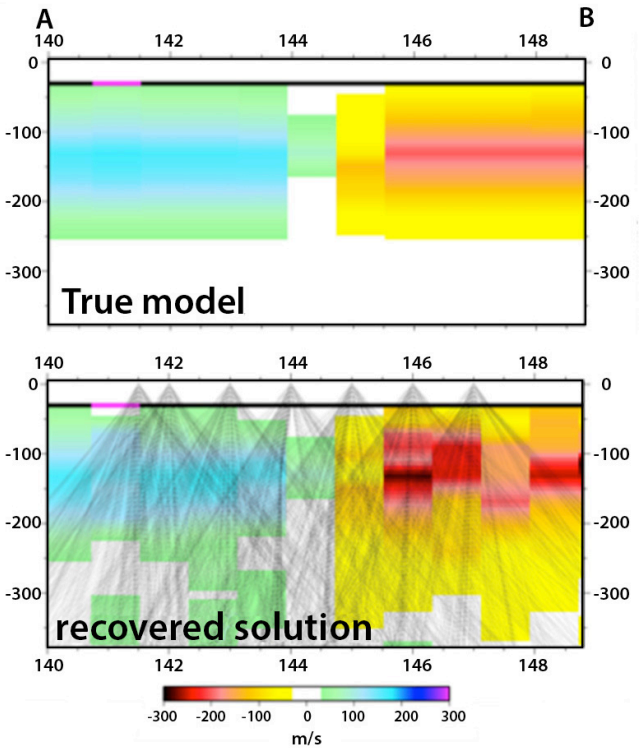

Figure 2. Top: Vertical slice from the 3D synthetic model (left) showing the Vp anomaly structure of the true model. Bottom: Recovered solution; ray traces used in the inversion are shown (modified from results presented at the AGU Fall meeting, 2012).

We have developed the first nonlinear, 3D, multi-observable inversion method, based on a probabilistic (Bayesian) inference approach, that can simultaneously invert Rayleigh and Love (seismic waves) dispersion curves, body-wave seismic tomography, and magnetotelluric, geothermal, petrological, gravity, elevation, and geoid datasets. Assembling this giant "jigsaw puzzle" problem has required a massive collaborative effort between thermodynamicists, geophysicists and

geochemists, and is the first step towards real thermochemical tomography of the Earth, which is undoubtedly the future of imaging techniques. Our preliminary results (recently published in *Journal of Geophysical Research, online Feb 2013)* indicate that we can expect to resolve temperature anomalies of $\Delta T >$ 150 °C and large anomalies of $\Delta Mg\# > 3$ (or bulk $\Delta Al_2O_3 > 1.5$) simultaneously when combining high-quality geophysical data. This resolving power is sufficient to explore some long-standing problems regarding the nature and evolution of the lithosphere (e.g. vertical stratification of cratonic mantle, compositional *vs* temperature signatures in seismic velocities, etc.) and offers new opportunities for joint studies of the structure of the upper mantle with unprecedented resolution.

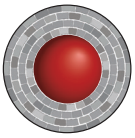

This project is part of CCFS Theme 3 Earth Today and contributes to understanding Earth's Architecture.

Contacts: Juan Carlos Afonso, Yingjie Yang
Funded by: Discovery Project DP120102372, MQ iPRS

Zircon multi-isotopic mapping: a robust roadmap to mineral discovery

Recent studies in the Yilgarn Craton of Western Australia have demonstrated that multi-isotopic maps, based on *in-situ* U-Pb and Lu-Hf analyses of zircon and whole-rock Sm-Nd data, are a powerful tool for mapping crustal growth, and for imaging lithospheric blocks and their margins.

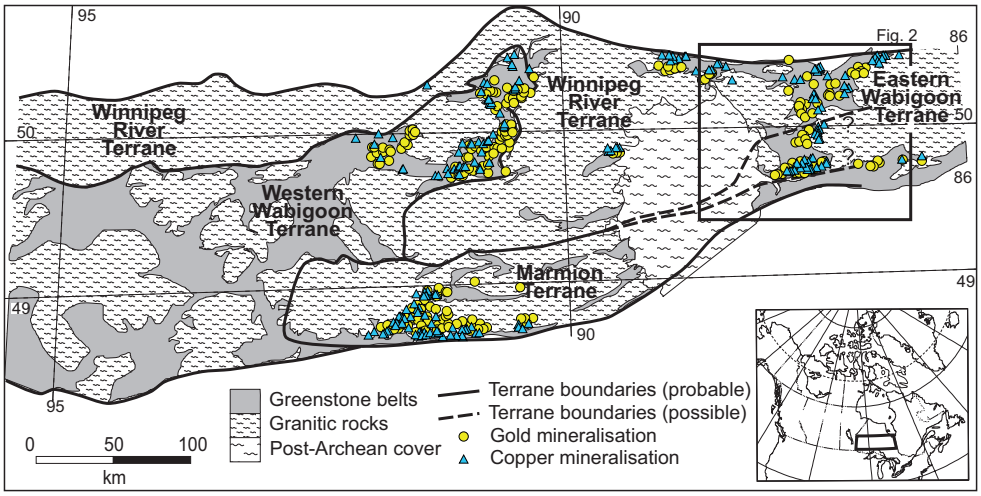

Figure 1. Simplified geological map of Wabigoon Subprovince in western Superior Craton, Canada. The inset shows the location of the study area. The subprovince has been divided into the Winnipeg River, Marmion, Western Wabigoon, and Eastern Wabigoon terranes based on whole-rock Nd-isotope data. The locations of gold and copper mineralisation are highlighted to show their relationship with terrane boundaries.

These studies pointed to a strong spatial correlation between lithospheric boundaries and the location of large concentrations of several styles of mineral deposit (e.g. Champion and Cassidy, 2007; McCuaig et al., 2010; Begg et al., 2010; Mole et al., 2012). The implication is that these isotopic boundaries mark lithosphere-scale structures that control fluid flux, and thus the location of large mineral systems through time. However, the only available case study in the Archaean is the Yilgarn of WA, and even that is only focused on the central portion of the craton. Therefore, it is critical to test this hypothesis in other parts of the world.

A comparative study has been started in the Wabigoon Subprovince in the western part of the Superior Craton of Canada. This project aims to: 1) apply multi-isotopic (U-Pb, Lu-Hf, O) analyses of zircon to map the lithospheric architecture in time and space; 2) determine if the distribution of mineral systems is controlled by this lithosphere architecture; 3) generate mappable exploration criteria for targeting various mineral systems at craton- to terrane scales.

The Wabigoon Subprovince can be subdivided into four terranes based on the whole-rock Sm-Nd isotopic data published by Tomlinson et al. (2004). Gold and copper mineralisation in the region appears to be controlled by the Winnipeg River and Western Wabigoon terrane boundaries (Fig. 1). However, the mineralisation within the Marmion and Eastern Wabigoon terranes does not follow the previously defined terrane boundaries (Fig. 1). In the Eastern Wabigoon Terrane, the assumed boundaries trend nearly E-W, whereas the gold and copper mineralisation forms a zone that trends northward. This discrepancy suggests that the terrane boundary may in fact strike northward (Fig. 2). Preliminary zircon Hf isotopic analysis shows that samples collected west of this hypothetcal boundary have older Hf model ages (3.5 Ga) than those from east of the boundary (3.1 Ga), suggesting that the western area has an older basement than the eastern area (Fig. 2). This difference in zircon Hf isotopes also suggests that the boundary of the East Wabigoon Terrane trends northward, which is consistent with the spatial arrangement of gold and copper mineralisation in the region. However, more data from both sides of this possible boundary are necessary to prove the case.

cont...

In the Marmion Terrane, the NE-trending mineralisation coincides with a NE-striking structure. There is contrasting in magnetic anomalies across this structure within the Marmion Terrane, which suggests that it is also a possible terrane boundary. The ongoing zircon mapping will test this hypothesis.

In summary, it appears that the spatial distribution of mineral systems (Au and Cu) in the Wabigoon Subprovince is controlled by the terrane boundaries (similar to the scenario in the Yilgarn Craton). The enhanced understanding of the interplay between lithospheric architecture potentially can help to bring about a paradigm shift in exploration strategy within the mineral industry, encouraging companies to use higher-precision multi-isotopic datasets to guide their area selection on the large scale.

This project is part of CCFS Themes 2 and 3, Earth Evolution and Earth Today, and contributes to understanding Earth's Architecture.

Contacts: Cam McCuaig, Yongjun Lu
Funded by: CCFS

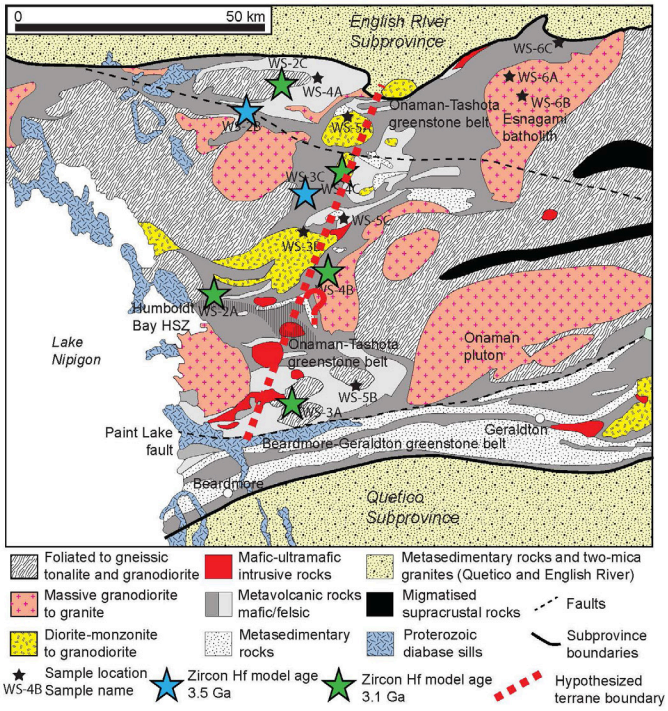

Figure 2. Geology of Eastern Wabigoon area. The preliminarily analysed zircon samples are shown by stars. The blue stars represent samples with older Hf model ages of 3.5 Ga, whereas the green stars having younger Hf model ages of 3.1 Ga. The hypothesised terrane boundary is highlighted by a red thick dashed line.

Cooking the lower crust: high-calorie ultramafic magmas in Arctic Norway

Most geologists are familiar with a wide range of mafic to felsic magmatic rocks, but the idea of ultramafic (high-Mg, low-Si) magmas is hard to assimilate, simply because laboratory experiments show that such magmas could only exist at temperatures that are not seen in the crust. Ultramafic lavas (komatiites) occurred widely in Archean time, but very rarely afterward; this has been used to argue for much higher mantle temperatures in the Archean. If ultramafic magmas do exist in the modern Earth, it would raise serious questions: how would they be generated, and how could they rise into the crust without crystallising?

The serendipity of a major continental collision, and

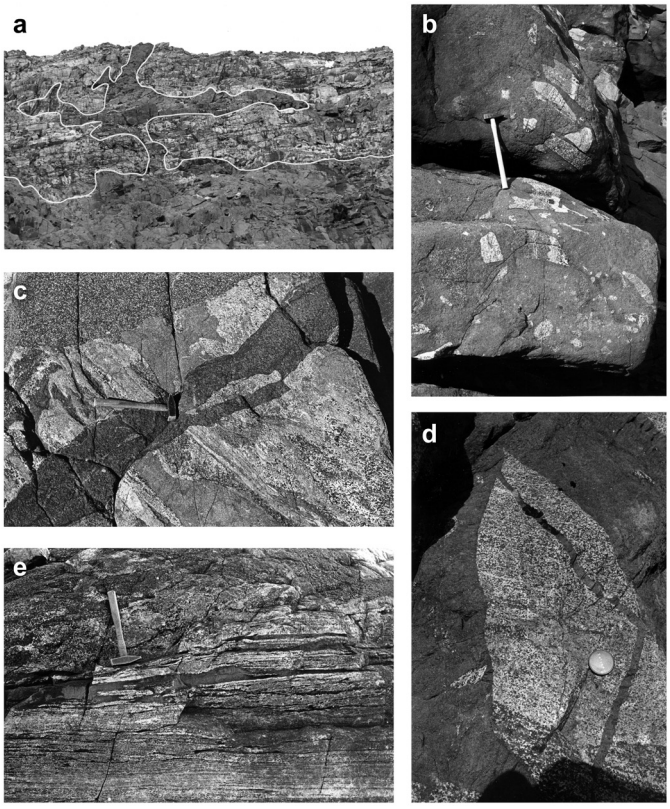

Figure 1. Intrusive relationships. (a) Overview of the roof zone of the Nordre Bumandsfjord pluton, showing the contact between the dunite (massive grey) and the layered gabbros, which are intruded by the dunite along the contact, and by dunite sills and dikes. Length of photo ca 200 meters. (b) Intrusive breccia, with angular blocks of variably remelted layered gabbros in matrix of contaminated peridotite, which is cut in turn by a more massive dunite dike on the right side of the view; hammer shaft = 60 cm. (c) Xenolith of partially remelted gabbro with dunite sill along the layering is cut by a dike of contaminated peridotite; the whole xenolith is enclosed in a strongly contaminated, plagioclase-rich peridotite; hammer shaft = 30 cm. (d) Thin dunite dikes cutting a gabbro xenolith, enclosed in dunite; coin = ca 2 cm. (e) Massive dunite penetrating as sills along the layering of a strongly foliated gabbro near the eastern contact; hammer shaft = 30 cm.

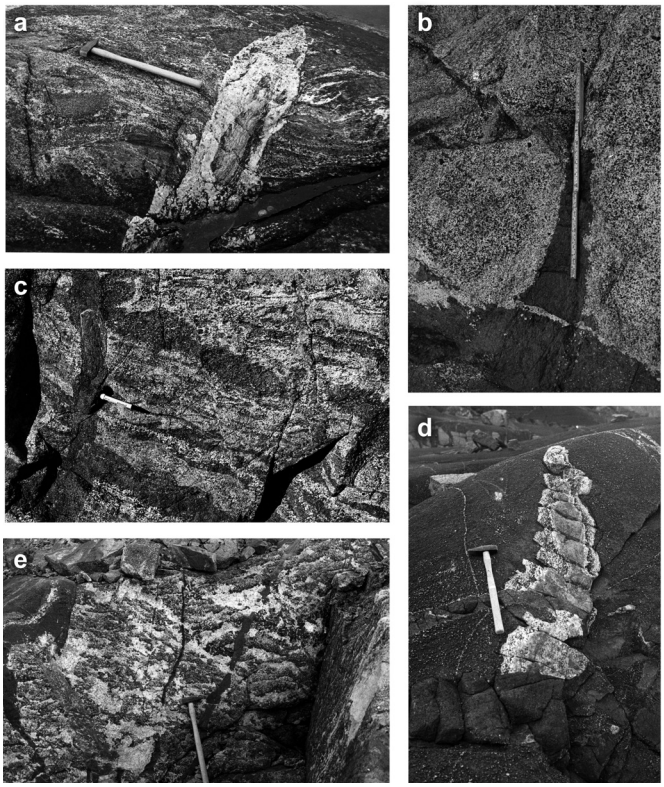

Figure 2. Anatectic phenomena. (a) Anorthositic dike, carrying xenolith of layered gabbro, crosscutting melted and strongly deformed gabbro; hammer shaft = 60 cm. (b) Bleaching at the rim of a gabbro xenolith, illustrating the removal of cpx-rich melts; note backveining of dunite by anorthositic melt issuing from rim of xenolith; ruler = 20 cm. (c) Wholesale melting of gabbroic xenolith (in peridotite visible at upper left), producing pegmatitic textures; hammer shaft =60 cm. (d) gabbro xenolith enclosed in contaminated peridotite, showing pegmatitic melting of xenolith rim; both xenolith and host peridotite are cut by dikes of less contaminated peridotite; hammer shaft = 60 cm. (e) Melting within gabbro xenolith, mimicking the pre-existing layering; gabbro is cut by dike of contaminated peridotite; pen = 15 cm.

the expansive exposures uncovered by a retreating icecap, the Caledonian nappe complex of Arctic Norway provides rare insights into the interaction between mafic-ultramafic magmas and the deep continental crust. The Kalak Nappe Complex contains >25,000 km^3 of mafic igneous rocks, mostly layered gabbros, making up the 570-560 Ma Seiland Igneous Complex. The Complex has been intruded by a series of ultramafic magmatic rocks, including the Nordre Bumandsfjord Pluton. Field relationships in this pluton (Fig. 1-3) show that extremely fluid, dry, relatively Fe-rich (Fo81) dunite magmas intruded a pile of cumulate gabbros, with extensive block stoping and intrusive brecciation. Diking on scales from mm to meters, and extensive melting and assimilation of the gabbros, attest to high temperatures, consistent with a 2 km-wide granulite-facies contact aureole.

Major- and trace-element trends show that the dunites were progressively contaminated by a clinopyroxene-rich partial melt of the gabbros, producing a range of lithologies from dunite through lherzolites to wehrlite. Experimental studies of natural samples at 0.8-1 GPa define the dunite solidus at 1650-1700 °C. In the average peridotite, contamination has dramatically lowered the solidus of the magma, producing a crystallisation interval of ca 400 °C (1600-1200 °C). This would provide large amounts of heat for melting and metamorphism, while the magmas remained fluid to relatively low T, consistent with the field relationships. Thermochemical and dynamic modelling shows that the dunitic primary magmas may represent the last melting of a rapidly ascending diapir of previously depleted subducted oceanic lithosphere. The mafic rocks of the Seiland Complex may already have been extracted from this diapir, and the late dikes of the province may reflect melting of the asthenosphere as the diapir spread out beneath the lithosphere. Ultramafic magmas, abundant in the Archean, may still be more common than usually assumed. However, they would only penetrate to the shallow crust under unusually extensional conditions, where ascent could outpace assimilation. See *CCFS publication #237.*

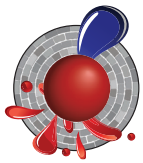

This project is part of CCFS Theme 2, Earth Evolution, and contributes to understanding Earth's Architecture and Fluid Fluxes.

Contacts: Bill Griffin, Sue O'Reilly, Craig O'Neill
Funded by: CCFS Foundation Program 2

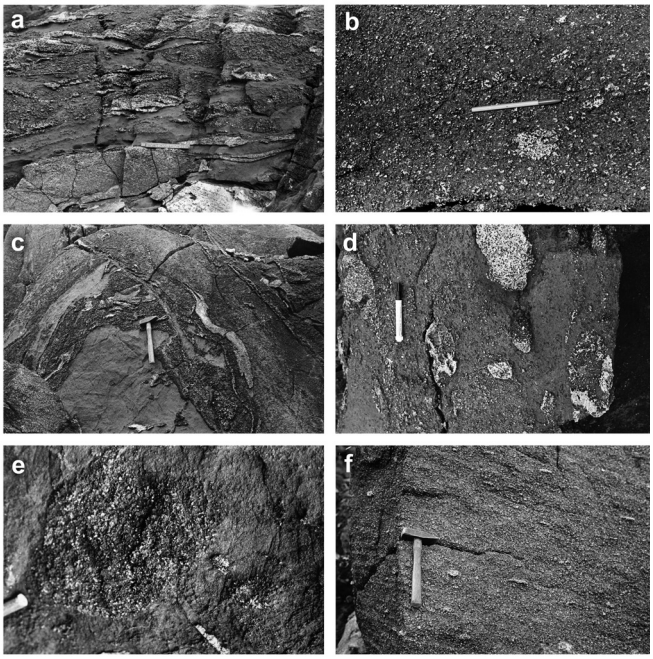

Figure 3. Contamination processes. (a) Dunite sills in heavily contaminated gabbro studded with fragments of residual anorthosite; scale ruler = 7 cm. (b) Residual clots of gabbroic plagioclase, scattered in heavily contaminated dunite; pen = 15 cm. (c) Heavily contaminated peridotite with folded schlieren of residual anorthosite, in sharp contact with relatively clean dunite, which appears to be intruded by the contaminated dunite; hammer shaft = 30 cm. (d) Ghost xenoliths, defined by residual plagioclase, enclosed in strongly foliated contaminated peridotite; pen = 15 cm. (e) Ghost xenolith of gabbro (10 cm diam.), defined by residual plagioclase, in moderately contaminated dunite. (f) Relatively homogeneous, strongly foliated and strongly contaminated peridotite, with relict knots of gabbroic plagioclase; hammer shaft = 30 cm.

Archean lower crustal rocks in southeastern Greenland: to hell and back

Figure 1. Field work in remote and rugged areas in southeastern Greenland relies on helicopter.

Ongoing work in CCFS suggests that many areas of relatively young crust are underlain by much older crust (*CCFS publications #37, 38, 75, 95, 97, 163, 190)*, but the lower crust is rarely available for direct study. Much of the upper crust is commonly interpreted as originating from the partial melting of the lower crust, but there is considerable debate as to how these magmas are produced and move through the lower crust to their ultimate sites of emplacement, at shallower levels.

The Thrym Complex in southeastern Greenland appears to represent a very rare example of a section through the Archean crust, which includes *ca* 2750 Ma granulite-facies and *ca* 2700 Ma greenschist-facies rocks. It is made up of highly metamorphosed rocks representing major multiphase granitic bodies and a wide range of felsic, intermediate, mafic and ultramafic intrusions. These rocks are located in a high-alpine terrain at altitudes of around 3500 m above sea level (Fig. 1), and is one of the least studied regions of high-grade Archean gneisses and granulites in the North Atlantic Craton (if not in the world). The CET is studying this remote region, in collaboration with the Geological Survey of Denmark and Greenland (GEUS), within the framework of the Foundation Program 'Metal Sources and Transport Mechanisms in the Deep Lithosphere' in the ARC Centre of Excellence for Core to Crust Fluid Systems (CCFS). This study took a regional approach in understanding the petrogenesis of the *ca* 2790-2700 Ma orthogneisses using new field data, petrology, whole rock geochemistry and U/Pb zircon age data on material collected in 2011. The principal aim was to understand the evolution of the early lower crust and to better decipher the regional geological history of the area.

Earlier studies have implied that the lower crust is predominantly mafic in nature. However, in the Archean lower-crustal section of the Thrym Complex, felsic gneisses predominate over mafic and ultramafic rocks.

The chemical and isotopic data suggest that the protoliths for the *ca* 2750 Ma orthogneiss in the Thrym Complex formed at the base of a tectonically thickened arc-like crust at temperatures between 800° and 1000 °C, and depths between 35 and 50 km. The mafic granulites and ultramafic rocks were metamorphosed at high grade, leading to partial melting with garnet and rutile present, consistent with the conditions expected in deep crustal levels or an arc root. With crustal thickening during continental collision, temperatures in this already hotter-than-normal crust can be amplified by increased radioactive heat production, leading to partial melting. This high-grade metamorphism was synchronous with similar metamorphism in western Greenland, suggesting that significant crustal thickening and possible relamination took place over much of the eastern part of the North Atlantic Craton in NeoArchean time (the Skjoldungen Orogeny; Fig. 2).

Our study of the Archean Thrym Complex in southeastern Greenland highlights the importance of integrating geochemical data with field observations in the development of geological models for high-grade gneiss terranes. For further information, see *CCFS publication #228*.

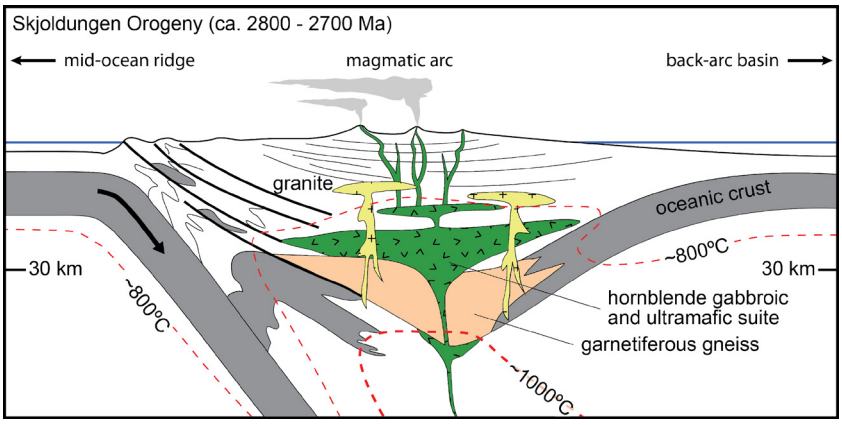

Figure 2. Model for the formation of the protoliths for gneisses in southeastern Greenland (from Bagas et al., Lithos 2013).

This project is part of CCFS Theme 2, Earth Evolution and contributes to understanding Earth's Architecture and Fluid Fluxes.

Contacts: Leon Bagas, Marco Fiorentini
Funded by: CCFS, Greenland BMP, GEUS, CET, UWA

Subduction switches: geochemistry as a proxy for paleogeophysics in South China

It is generally thought that late Mesozoic granite magmatism in the South China Block (SCB) shows an oceanward-younging migration. However, our new geochronological study of granites along the Pingtan-Dongshan Metamorphic Belt in the coastal part of the SCB, is not consistent with this trend. These late Mesozoic granites (and all those previously published) can be subdivided on their zircon U-Pb ages, into an early episode (194-140 Ma) and a later episode (140-66 Ma); the granites of the two episodes also have different geochemistry.

Both age groups of granites in this area are relatively depleted in Nb, Ta and Ti, but enriched in large-ion lithophile elements (e.g. Rb, Ba), with low Rb/Ba and Rb/Sr ratios and A/CNK values. These features are typical of I-type granitoids related to subduction. However, the early granites have higher Sr and K_2O contents and higher La/Yb, Sr/Y and Eu/Eu* ratios than the later ones (Fig. 1), suggesting that the former originated from a shallower source with higher geothermal gradients, probably in a back-arc extensional setting, whereas the later ones derived from a deeper source with lower geothermal gradients; this probably was related to a compressional continental arc setting.

Integrating all recent precise zircon U-Pb ages, we find that the early episode of late Mesozoic igneous rocks (194-140 Ma) in the southeastern SCB formed in three pulses: 194-175 Ma, 174-151 Ma and 150-140 Ma. These pulses of magmatism mainly occur in the Nanling Range with EW-striking trends, probably extending eastward to the coast (Fig. 2). The granites of the later episode (140-66 Ma) mainly are found in the coastal SCB along a SW-NE trend. The early (140-100 Ma) magmatism is characterised by calc-alkaline I-type granites and probably formed in a continental-arc setting, whereas late (99-66 Ma) magmatism features alkaline A-type granites and occurred in an extensional setting.

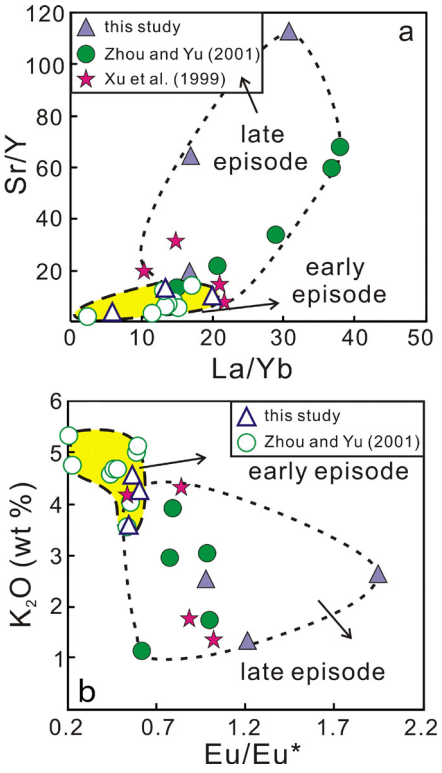

Figure 2. Simplified new distribution and genetic model for late Mesozoic igneous rocks in the South China Block. The subduction of the Paleo-Pacific plate is inferred by Engebretson et al. (1985), Maruyama and Seno (1986) and Maruyama et al. (1997).

The different distributions and tectonic settings of the late Mesozoic igneous rocks in the SCB contradict previous genetic models. Integrating our observations with previous studies on the subduction direction of Paleo-Pacific plate (Fig. 2), we propose that the early episode of late Mesozoic igneous rocks in the SCB were probably formed under extensional tectonics related to the northward subduction of the Paleo-Pacific plate in Jurassic time. In contrast, the granites of the later episode, running NE-SW along the coastal SCB, resulted from the NW-ward subduction of the Paleo-Pacific plate in Cretaceous time. This represents a major switch in the subduction direction. The oceanward-younging trend of the later episode probably was related to the rollback of the subducted plate.

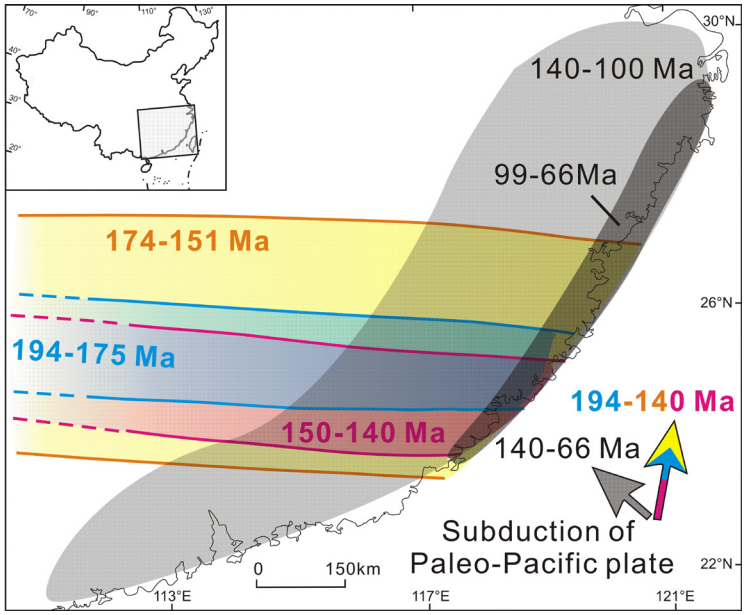

Figure 1. Geochemical differences between the early and late episode of late Mesozoic granites in the PDMB.

This project is part of CCFS Themes 2 and 3, Earth Evolution and Earth Today, and contributes to understanding Earth's Architecture.

Contacts: Qian Liu, Jinhai Yu, Sue O'Reilly
Funded by: NSF of China

Unveiling mantle fluids using diamonds

Diamond-bearing eclogite xenoliths are common in the Udachnaya kimberlite, Siberia. Three types of garnet (Gnt) can be recognised in these eclogites, with different major-, trace-element and O-isotope compositions and related to different stages of mantle metasomatism.

The major- and trace-element compositions of garnets from 25 xenoliths show a well-defined change from positive to negative ratios of the heavy to light rare-earth elements (HREE/LREE) at a CaO content of 7.8-8.7%. This suggests either a change in fluid

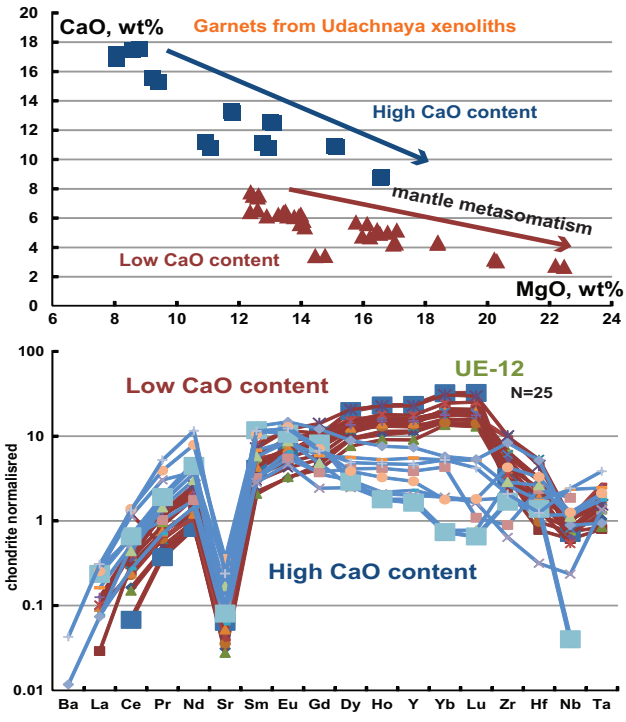

Figure 1. Major- and TE- element composition of garnets from Udachnaya xenoliths.

compositions or a change in garnet/fluid partitioning related to garnet composition. Both groups show similar trends of increasing MgO content in garnet due to mantle metasomatic processes. This is well evidenced by the difference in major-element, trace-element and oxygen isotope compositions between the original Garnet 1 and the metasomatic Garnet 2 in sample UE-12-2. Gnt1 and Gnt2 are usually found together with diamonds in metasomatic veins (Fig. 1). Garnet 2 forms Mg-rich rims on Garnet 1 (mg#=0.67-0.80 vs 0.57-0.58 for Garnet 1). The significant zoning in chemistry and its relationship to diamond with mantle-like carbon isotopes ($\delta^{13}C$ =-5.6 - -6.6‰) suggest that Garnet 2 (and the diamond?) were produced by mantle fluids/melts shortly before eruption. Garnet 2 has a wide range in oxygen isotope composition ($\delta^{18}O$ = 6.2-9.0‰), suggesting mixing of mantle fluids with the original isotopic system (Gnt1, $\delta^{18}O$ =11.1-12.0‰). This pattern of decreasing $\delta^{18}O$ with

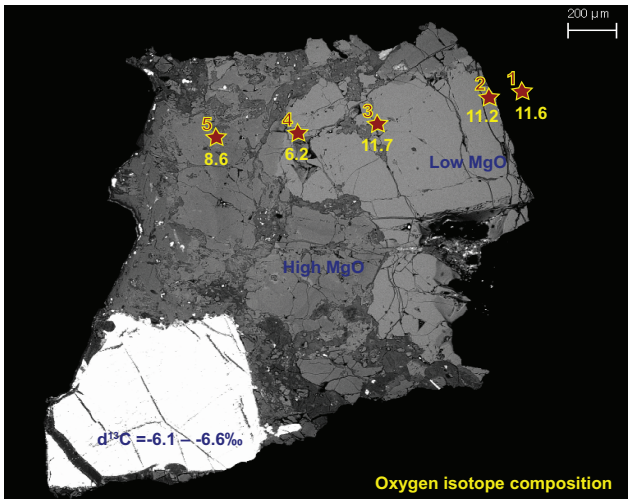

Figure 2. Oxygen isotope composition of Garnet 1 (original) and Garnet 2 (metasomatised); backscattered electron image of the sample (stars show traverse).

increasing mg# during metasomatism is similar to that identified in the Roberts Victor eclogite suite (see *Research highligh pp. 42-43*).

Garnet 3 is found in corundum-bearing eclogites and has much higher Ca (CaO=15.61-16.56 wt%) and different isotopic characteristics ($\delta^{13}C$ =-3.6 - -5.3‰; $\delta^{18}O$ =3.2-5.7‰). This suggests a different protolith, or a different metasomatic fluid from the one that produced Garnet 2. The Lu/Gd ratio increases significantly from Garnet (0.06-0.12) to Garnet 1 (4.0-4.2) to Garnet 2 (5.5-9.0). The demonstrated correlation between the oxygen composition of metasomatic garnet and high MgO contents, related to the formation of diamond with mantle-like carbon-isotope compositions, demonstrate the important role of mantle fluids. These fluids may also have been a trigger for the eruption.

This project is part of CCFS Themes 2 and 3, Earth Evolution and Earth Today and contributes to understanding Earth's Fluid Fluxes.

Contacts: Ekaterina Rubanova, Bill Griffin, Sue O'Reilly

Funded by: CoE CCFS Foundation Program 8, IPRS, MQ PGRF

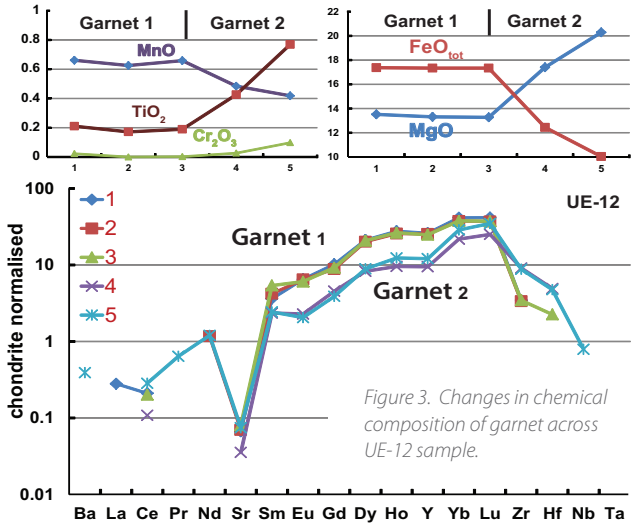

Figure 3. Changes in chemical composition of garnet across UE-12 sample.

Yilgarn dykes track details of supercontinent events: the transition from Nuna to Rodinia

It has been widely accepted that the supercontinent Nuna (also known as Columbia) formed about 1800 million years ago (Ma) (see *Research highlight pp. 40-41* for more information about Nuna). However, precisely when it broke up, and how the resulting continental blocks reassembled to form the next supercontinent (Rodinia), is less certain. Australia held key positions in both supercontinents, and high-quality paleomagnetic data for Mesoproterozoic Australia are therefore crucial for understanding this process.

Figure 1. A northeast-trending, ca. 1.2 Ga mafic dyke (the dark outcrop) intruding granitic gneiss at the southeast margin of the Yilgarn craton. Inset shows zircon grains from the dyke. (Photographs by Michael Wingate)

The Gnowangerup-Fraser mafic dyke swarm is part of the Marnda Moorn large igneous province (LIP) and runs subparallel to the southern and southeastern margins of the Yilgarn Craton. Some dykes towards the craton margin are strongly recrystallised and others are deformed within the orogen, implying that at least some dykes were emplaced before the youngest deformation in the Albany-Fraser Orogen. Five dykes have previously yielded U-Pb ages between 1203 and 1218 Ma, and a positive baked-contact test suggests a that the magnetic remanence in the dykes is primary. The fossil record of past geomagnetic direction, which reflects the orientation and palaeolatitude of the continent at the time the rock formed, had been retrieved from a 1212 Ma Fraser dyke. To check this result and to get a true, time-averaged palaeomagnetic record, we collected samples from 19 dykes, along the Phillips and Fitzgerald Rivers, and north of Ravensthorpe. Stepwise demagnetisation provided a stable bipolar remanence from 14 dykes. A block sample from one of them, a coarse-grained dolerite was collected from the centre of a 20 m wide, vertical, northeast-trending (043°) dyke exposed in the Fitzgerald River (Fig. 1). The GSWA's SHRIMP analysis of zircons from this sample indicated high and variable U and Th contents and Th/U ratios, typical of primary zircons in a mafic intrusion, and provided a preliminary crystallisation age of 1218 ± 6 Ma. A similar dyke, further east in the Phillips River, yielded a preliminary crystallisation age of 1211 ± 42 Ma, based on SHRIMP analyses of low-uranium baddeleyite.

The mean palaeomagnetic direction from the 14 dykes gives a palaeomagnetic pole at 55.8°N, 323.9°E, A95=6.5°, almost identical to the previously reported preliminary pole position from the 1212 Ma Fraser dyke. This robust paleopole, a rare key-pole for Mesoproterozoic Australia, places the West Australian Craton in a near-polar position at 1210 Ma (Fig. 2a). Comparison with coeval Laurentian paleopoles indicates that Laurentia and Australia would have been widely separated at that time (Fig. 2a). The two continents travelled very different paths between 1200 Ma and 1000 Ma (Fig. 2), and therefore could not have been parts of any supercontinent. This implies that the supercontinent Nuna must have broken apart before 1200 Ma, and Rodinia probably did not form until after 1070 Ma. Our concurrent geochemical analyses of this dyke swarm suggest a possible mantle plume connection for its formation. However, whether this swarm and coeval LIP events in other continents can be treated as parts of a single LIP to reconstruct palaeogeography, and how such plume event(s) are linked to supercontinent cycles, require further investigations.

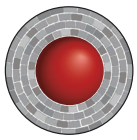

This project is part of CCFS Theme 2, Earth Evolution, and contributes to understanding Earth's Architecture.

Contacts: Zheng-Xiang Li, Sergei Pisarevsky, Xuan-Ce Wang, Michael Wingate
Funded by: CCFS Foundation Program 6

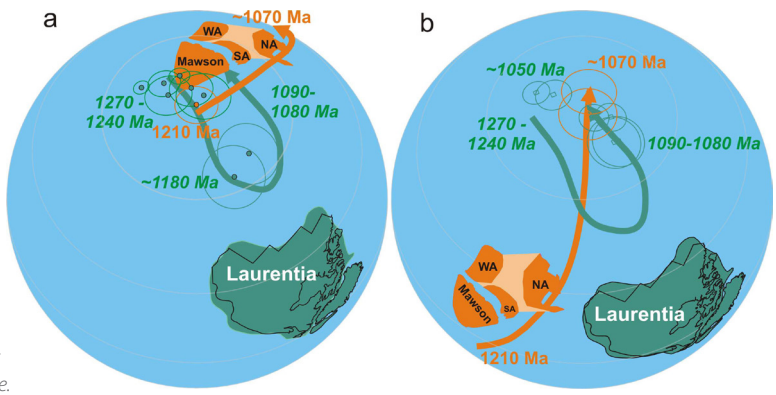

Figure 2. Palaeomagnetically permissive palaeolatitudes of Australia and Laurentia at ca 1210 ma (a) and ca 1070 Ma (b), respectively, illustrating rapid changes in both palaeolatitudes and relative positions during the transition time between supercontinents Nuna (ca. 1800-1400 Ma) and Rodinia (ca. 900-700 Ma). The ca 1200 Ma key pole for Australia is from this study. The distinctively different apparent polar wander paths for the two continents (the thick bands with arrows, with colours corresponding their respective continents) suggest that the two continents travelled different paths during that time interval; in other words, they could not have been part of a supercontinent at that time.

Stealth attacks in Earth's uppermost mantle: recognition of a new type of metasomatism and its consequences

Mantle metasomatism is a relatively recent concept, introduced in the early 1970s when detailed studies of lithospheric mantle rock fragments (xenoliths), brought to the surface in basaltic to kimberlitic magmas, became widespread. Two main types of metasomatism were defined: modal (or patent) metasomatism describes the introduction of new minerals; cryptic metasomatism describes changes in composition of pre-existing minerals without formation of new phases. A new type of metasomatism has now been documented (*CCFS publication #5*),

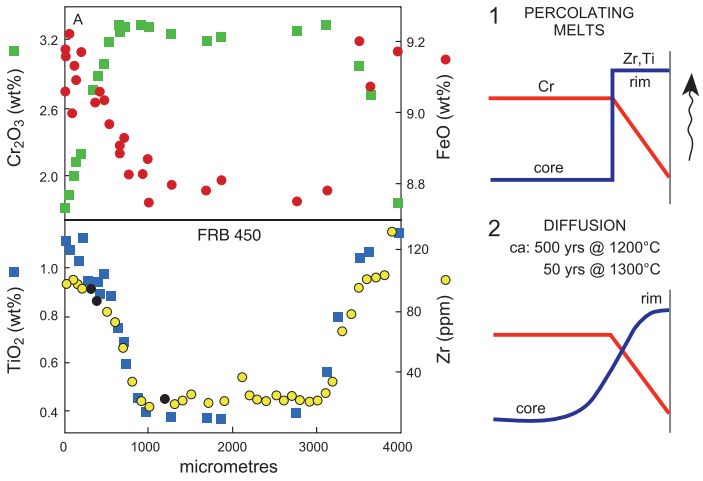

Figure 1. Zoning in a garnet from sheared lherzolite xenolith FRB450, and a model. (1) Instantaneous overgrowth of a garnet rim high in Zr and Ti, but low in Cr. (2) Diffusional modification of Zr and Ti profile. Chromium diffuses much more slowly, if at all (After Griffin et al. (1996)).

stealth metasomatism; this process involves the addition of new phases (e.g. garnet and/or clinopyroxene), but is a "deceptive" metasomatic process because it adds phases indistinguishable mineralogically from common mantle peridotite phases. The recognition of stealth metasomatism reflects the increasing awareness of the importance of refertilisation by metasomatic fluid fronts in determining the composition of mantle domains. Tectonically exposed peridotite massifs provide an opportunity to study the spatial relationships of metasomatic processes on scales of a metre to kilometers.

Mantle fluid types:

The nature of mantle fluids can be determined from the nature of fluid inclusions in mantle minerals and indirectly from changes in the chemical (especially trace-element) compositions of mantle minerals. Metasomatic fluids in off-craton regions cover a vast spectrum from silicate to carbonate magmas containing varying types and abundances of dissolved fluids and solutes.

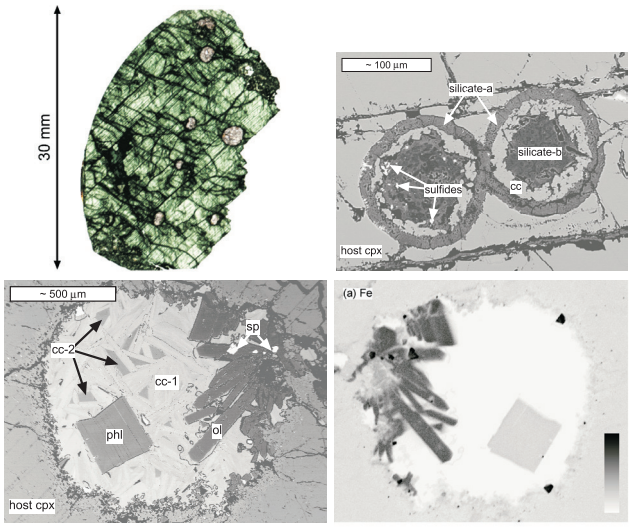

Figure 2. Inclusions of carbonatitic and silicic melts trapped in the Cr-diopside of megacrystalline lherzolite xenoliths from the A154 kimberlite, Slave Craton, Canada. Quench crystals of a Sr-rich carbonate and olivine show that these inclusions were molten at the time of kimberlite eruption, but that the melts had penetrated the pyroxene long enough before the eruption that the pyroxene was able to partially recrystallise and trap the melt inclusions. The lower two frames are mirror images at the same scale (After van Achterbergh et al. (2004)).

Fluid inclusions in diamond and deep xenoliths reveal the presence of high-density fluids with carbonatitic and hydro-silicic and/or saline-brine end-members. The data from deep cratonic xenoliths reinforce the importance of highly mobile melts spanning the kimberlite-carbonatite spectrum, which may become immiscible with changing conditions.

Effects of metasomatism on mantle geophysical properties:

A critical conceptual advance in understanding Earth's geodynamic behaviour is emerging from understanding the linkage between mantle metasomatism and the physical properties of mantle domains recorded by geophysical data. For example, metasomatic refertilisation of cratonic lithospheric mantle increases its density, lowers its seismic velocity and strongly affects its rheology. Introduction of radioactive

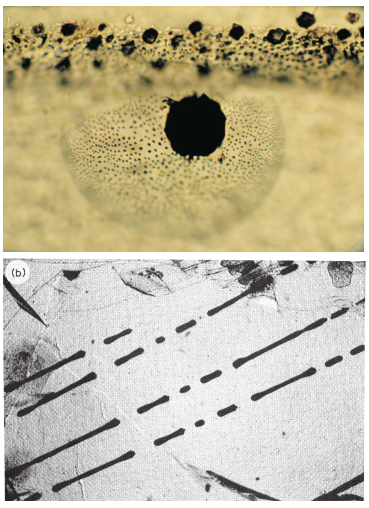

Figure 3. Photomicrographs of inclusions of sulfide melts, trapped in pyroxene from pyroxenite xenoliths from SE Australia. Left panel shows a single large inclusion that has expanded and fractured the pyroxene, sending molten sulfide and CO_2 into the crack, which has recrystallised to trap a swarm of microinclusions. Right panel shows sulfide melts that originally were trapped as elongate hollow rods filled with liquid CO_2, and then necked down to hollow spheres (After Andersen et al. (1987)).

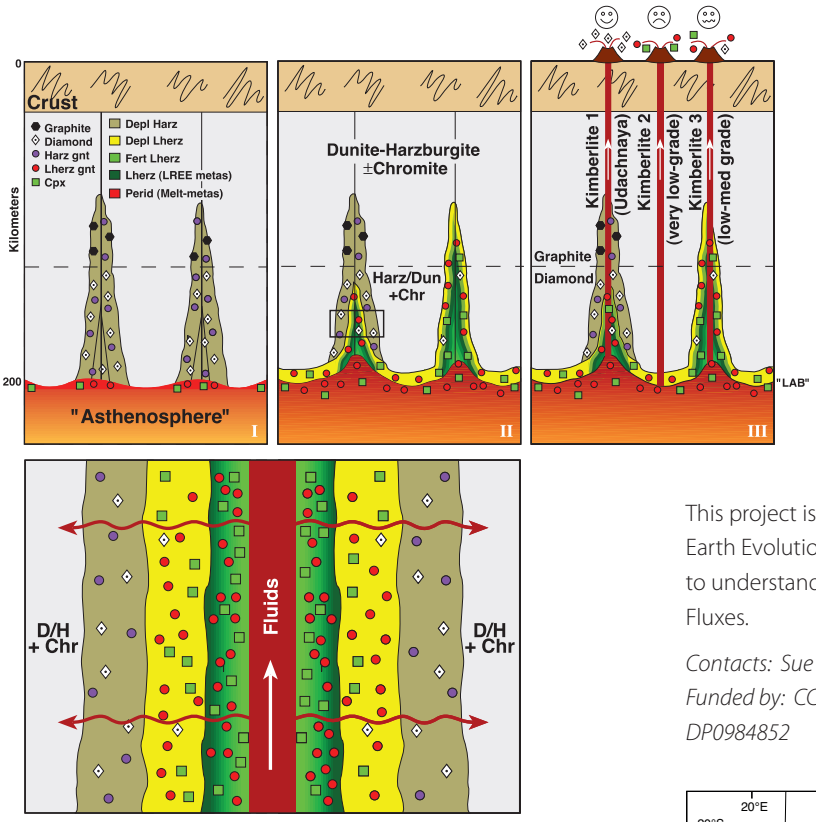

Figure 4. Cartoon illustrating a model for the early stages of cratonic metasomatism (After Malkovets et al. (2007)). (I) Primitive Archean SCLM, consisting of relatively oxidised harzburgite/dunite, is metasomatised by Si-bearing CH_4-rich fluids brought in by low-degree melts from the underlying "asthenosphere". Precipitation of diamond/graphite - harzburgitic garnet near fluid conduits. Melt-related metasomatism near the lithosphere-asthenosphere bound-ary (LAB) converts some harzburgites to lherzolite by addition of Ca, Fe, and Al. (II) Continued input of melts/fluids. Reduced harzburgite does not precipitate diamond/graphite. Melt-related metasomatism refertilises harzburgite to lherzolite at the base of the lithosphere and along conduits (weakly in left conduit, more extensively in right conduit). Relict harzburgitic diamonds in lherzolites. (III) Kimberlite eruption; high-grade pipes sample remnants of Stage-A modified mantle. Barren pipes sample least-metasomatised mantle and lack both harzburgitic garnets and diamonds. Some low-grade pipes sample highly metasomatised mantle with relict diamonds. The lower panel shows a detail of the melt conduit and the progressive metasomatism of the wall rocks, first by CH_4-rich fluids expelled from the melts, and then by the melts themselves. Dun dunite, Harz harzburgite, Lherz lherzolite, Fert (re)-fertilised, Perid peridotite, Cpx clinopyroxene, Gnt garnet, Chr chromite, LREE light rare earth elements, metas metasomatised.

elements (U, Th, K) increases heat production, and the key to understanding electromagnetic signals from mantle domains may be closely related to the distribution and type of fluids (e.g. carbonatitic, hydrous) and their residence in or between grains.

Consequences of mantle metasomatism through time:

The lithospheric mantle is a palimpsest recording the multiple fluid events that have affected each domain since it formed. Metasomatism is the mechanism that primes mantle regions for metallogenic fertility (see *Research highlight pp. 68-69*) and recognition of metasomatic processes is providing a potentially global predictive framework for the location of some ore deposits (e.g. as Ni. Cr, Au, Cu, diamond) in the crust. These metasomatic events, involving different fluids and compositions, have repeatedly overprinted variably depleted original mantle wall-rocks. This produces a complex, essentially globally metasomatised lithospheric mantle, heterogeneous on scales of microns to terranes and perhaps leaving little or no "primary" mantle wall-rock. Decoding this complex record by identifying significant episodes and processes is a key to reconstructing lithosphere evolution and the nature and origin of the volatile flux from the deep Earth through time.

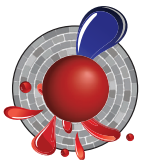

This project is part of CCFS Themes 2 and 3, Earth Evolution and EarthToday, and contributes to understanding Earth's Architecture and Fluid Fluxes.

Contacts: Sue O'Reilly, Bill Griffin
Funded by: CCFS Foundation Programs 1 and 8, relinquished DP DP0984852

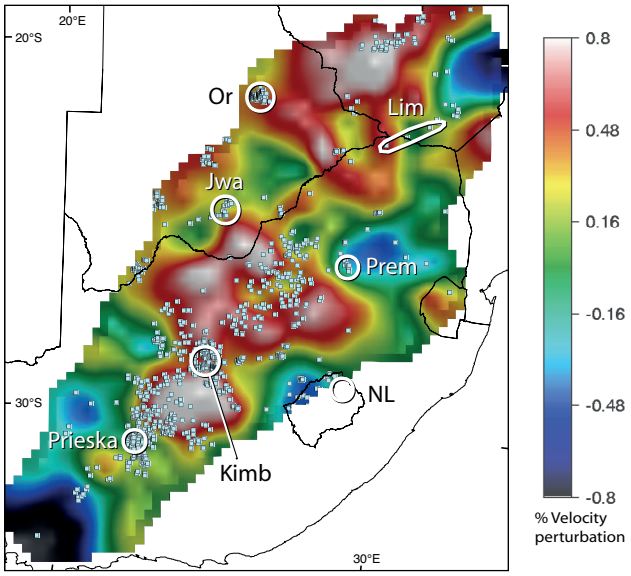

Figure 5. Detailed Vs tomography along a 1,000-km traverse at 200 km depth across the SW part of the Kalahari craton of southern Africa (Begg et al. 2009), with locations of kimberlites (Faure 2006). Circles and oval mark locations of well-studied xenolith and xenocryst suites. Lim Limpopo Belt, Prem Premier (Cullinan) Mine, NL northern Lesotho, Kimb Kimberley area, Or Orapa area, Jwa Jwaneng area, Prieska area lies across the craton margin. These suites clearly do not sample the highest-velocity (most depleted) parts of the SCLM root.

Figures reproduced from "Suzanne Y. O'Reilly, and W. L. Griffin. 2013. Mantle Metasomatism. In: Metasomatism and the Chemical Transformation of Rock, Lecture Notes in Earth System Sciences 2013, pp 471-533" with permission of Springer-Verlag.

Ancient reservoirs and recycled components: Linking plumes and plate tectonics

Whether mantle plumes and plate subduction are genetically linked is a fundamental question that impinges on our understanding of how Earth works. Earth's materials are circulated between the surface and the bottom of the mantle through mantle-plume and plate-tectonic processes. The late Cenozoic basalt province in southeastern Asia is the first example that may demonstrate direct links between a young mantle plume and deep subduction. The presence of a young mantle plume rooted in the lower mantle is suggested by low-velocity seismic structures and a thinned mantle transition zone. Our pilot work, led by Dr Xuan-Ce Wang, has demonstrated that these young basalts were generated by partial melting of unusually hot mantle (*CCFS publication #24*).

The synchronous less-contaminated basalts (εNd>+3) from the Leiqiong area, on the nearby Indochina peninsula, and the South China Sea seamounts (the LIS basalts) fall close to or within the range suggested for a FOZO (focal zone) mantle component, which is commonly proposed as a major component of the lower mantle (Fig. 1). The LIS basalts show a narrow range of $^{206}Pb/^{204}Pb$, but large variations in $^{207}Pb/^{204}Pb$, so they are bracketed by the 4.5- and 4.4 Gyr-old geochrons. This suggests the presence of a 4.5-4.4 Ga-old reservoir resulting from primordial differentiation of Earth mantle. This implies the presence of rocks that have been isolated from mantle convection currents since early in Earth's history. These isotopic signatures are consistent with previous observations that argue for the existence of a plume, rising from the lower mantle in the Hainan region.

An important feature of the LIS basalts is the decoupling between isotopic and elemental signatures. The trace- and major-elements are highly correlated with trace-element ratios.

Figure 2. Covariation of selected trace element ratios and major elements with Sm/Nd ratios in the LIS basalts. The chondritic bulk silicate Earth (BSE), nonmodal batch partial melting (solid lines with square or circle) and binary mixing (dark blue dashed lines) between recycled oceanic crust (ROC) and peridotitic source derived melts are shown.

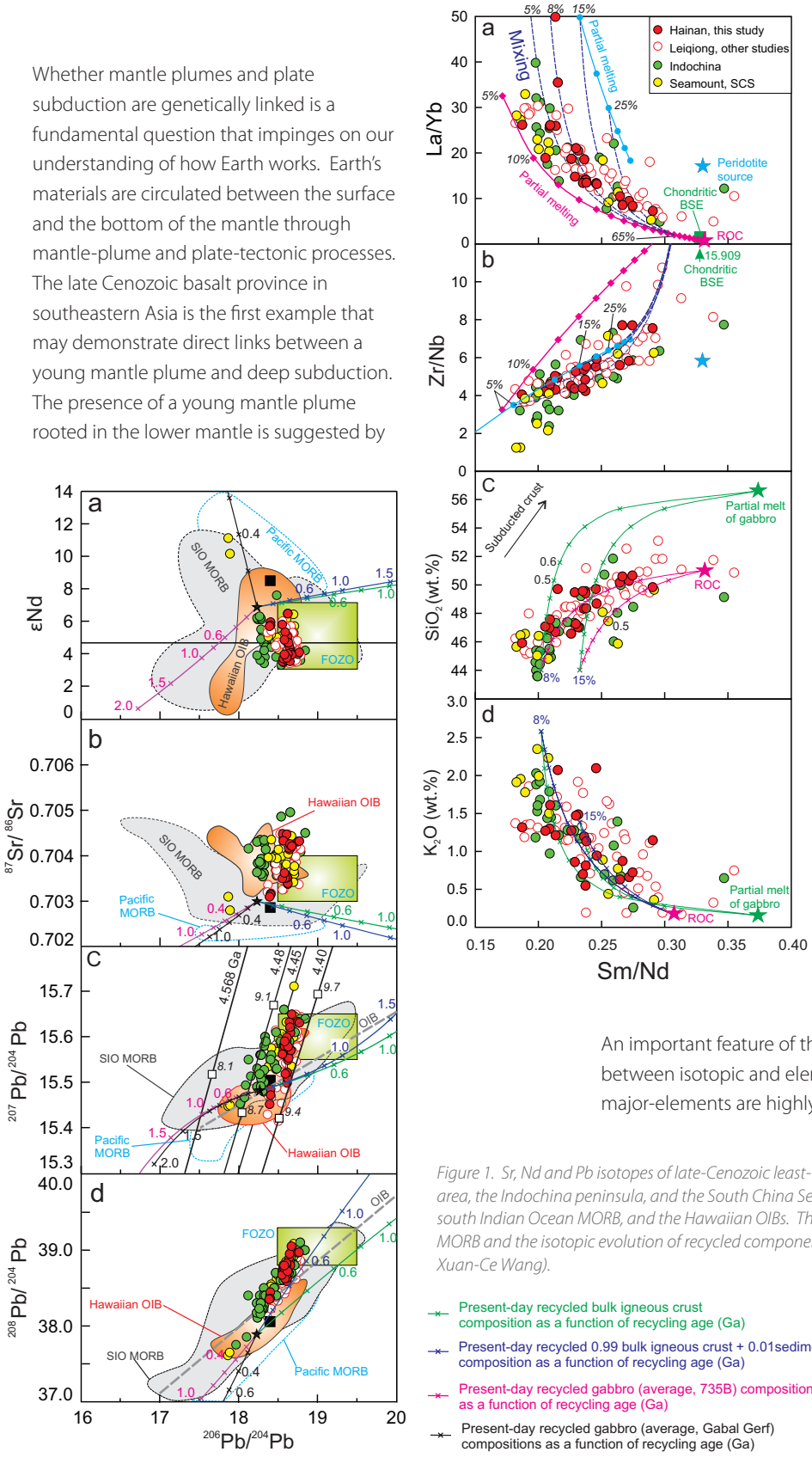

Figure 1. Sr, Nd and Pb isotopes of late-Cenozoic least-contaminated LIS basalts from the Leiqiong area, the Indochina peninsula, and the South China Sea seamounts compared with Pacific MORB, south Indian Ocean MORB, and the Hawaiian OIBs. The fields of Pacific and south Indian Ocean MORB and the isotopic evolution of recycled components are also shown (for detail, please contact: Xuan-Ce Wang).

Present-day recycled bulk igneous crust composition as a function of recycling age (Ga)

Present-day recycled 0.99 bulk igneous crust + 0.01sediment composition as a function of recycling age (Ga)

Present-day recycled gabbro (average, 735B) compositions as a function of recycling age (Ga)

Present-day recycled gabbro (average, Gabal Gerf) compositions as a function of recycling age (Ga)

Leiqiong area: (ε17 Ma) Hainan basalts, this study; Leiqiong basalts, other studies

ε17 Ma basalts, Indochina peninsula

0.4-22 Ma Seamount basalts, Sth China Sea

8.1 μ value ($^{238}U/^{204}Pb$)

Average global MORB

Average south Indian Ocean (SIO) MORB

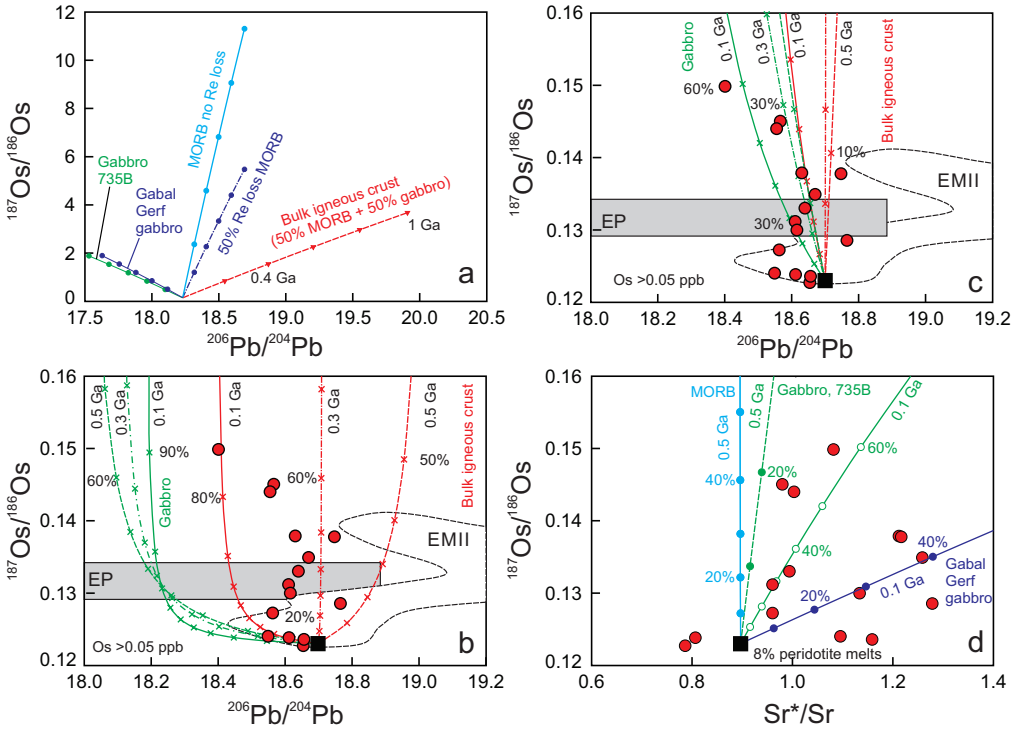

Figure 3. Comparison of the Os-Pb isotopes of the Hainan basalts with isotopic evolution of different recycled lithologies.

With crustal contamination excluded, the correlations presented in Figure 2 suggest two end-member (high- and low-silica) melts. The high-silica end-member is similar to the bulk recycled oceanic crust and experimental melts of oceanic gabbro. The low-silica end-member melt compares well with the composition of incipient partial melts of garnet peridotite. However, there are no prominent correlations between elements and isotopes identified in this study. This suggests that the source of the late Cenozoic basalts may also contain young recycled components.

These conclusions have been confirmed by modelling of the isotopic evolution of recycled components (Figs. 1 and 3). First, the recycled oceanic crust may be the dominant factor controlling Pb isotopic heterogeneities in OIBs sources. Second, extremely high $^{187}Re/^{188}Os$ ratios recently reported in oceanic crust (80-675) would lead to very radiogenic $^{187}Os/^{188}Os$ ratios ($^{187}Os/^{188}Os$ = 2-12) over 1 Ga (Fig. 3a), suggesting that such a component probably is absent in the LIS basalt source. Third, both ancient (>0.6 Ga) gabbro- and bulk oceanic crust-derived melts have distinctive Pb-Sr-Nd (Fig. 1) and Os (Fig. 3) isotopes that are significantly different from what we observed in the natural LIS basalts. Overall, our modelling results show that the maximum age for the recycled components in the source of the LIS basalts is <0.6 Ga.

These new findings, along with existing geophysical, petrological, geochemical evidence, confirm the coexistence of an ancient (4.5-4.4 Ga) mantle reservoir and young (0.2-0.5 Ga) recycled materials in the source region of the young Hainan plume. This study may provide the first observational support for dynamic linkages between deep subduction and the generation of mantle plumes (Fig. 4).

This project is part of CCFS Themes 2 and 3, Earth Evolution and Earth Today, and contributes to understanding Earth's Architecture and Fluid Fluxes.

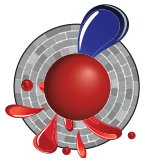

Contacts: Xuan-Ce Wang, Zheng-Xiang Li

Funded by: CCFS and NSFC

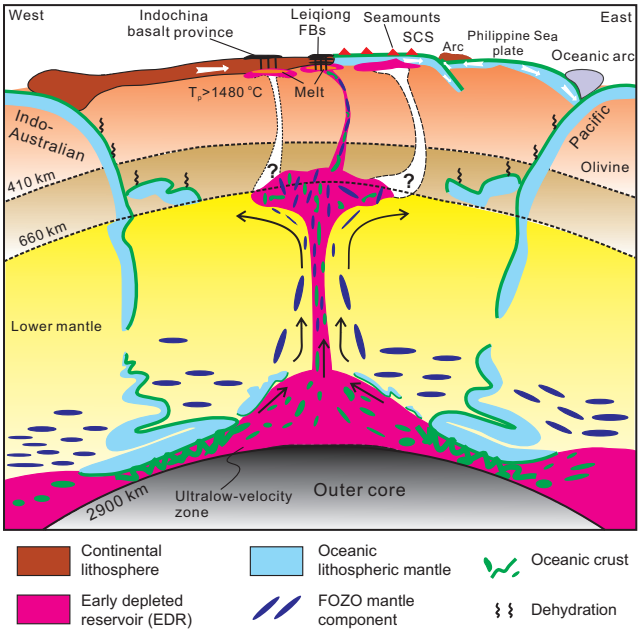

Figure 4. A cartoon illustrating the formation mechanism of the Hainan plume based on seismic imaging results and this study.

The end of the Archaean in the eastern Kaapvaal Craton: the 3.1 Ga Mpuluzi batholith

The Mpuluzi batholith forms part of the eastern Kaapvaal Craton in southeastern Africa - a piece of Archaean continental crust that has been stable for the past three billion years. The Mpuluzi outcrops over an area of approximately 2000 km^2, and dominates the landscape, forming a high plateau that rises above the African grasslands (Fig. 1). The Mpuluzi is one of several large bodies of similar age in the region, along with the Nelspruit, Piggs Peak and Heerenveen batholiths, which total approximately 10,000 km^2 (Fig. 2). These large granitoid intrusions were all emplaced at ~3.1 Ga, and are all unusual in form - they occur as 1-2 km thick sheets, rather than the deep-rooted batholiths common in Archean cratons. For half a billion years prior to their emplacement, the eastern Kaapvaal Craton was an active region, with large-scale melt emplacement events recorded at 3.51, 3.44 and 3.2 Ga. After the emplacement of the Mpuluzi and other 3.1 Ga granitoids, no major geological events were recorded in the region for another 600 Ma.

The Mpuluzi batholith.

The emplacement of the Mpuluzi batholith, marking such a turning point in the history of the Kaapvaal Craton, is thus an event of significant interest in terms of crustal evolution processes. Although the older crustal remnants beneath the granite sheets - the Barberton Greenstone Belt to the northeast and the Ancient Gneiss Complex to the southeast - have been extensively studied, the Mpuluzi itself is still poorly understood, and there are few constraints on either the melt generation or emplacement chronology. This project has been designed to tackle some major questions: What was the heat source for the magmas, and what was the source material? How many pulses of magma were involved, and over what timescale? Why did emplacement occur in this unusual sheet-like form?

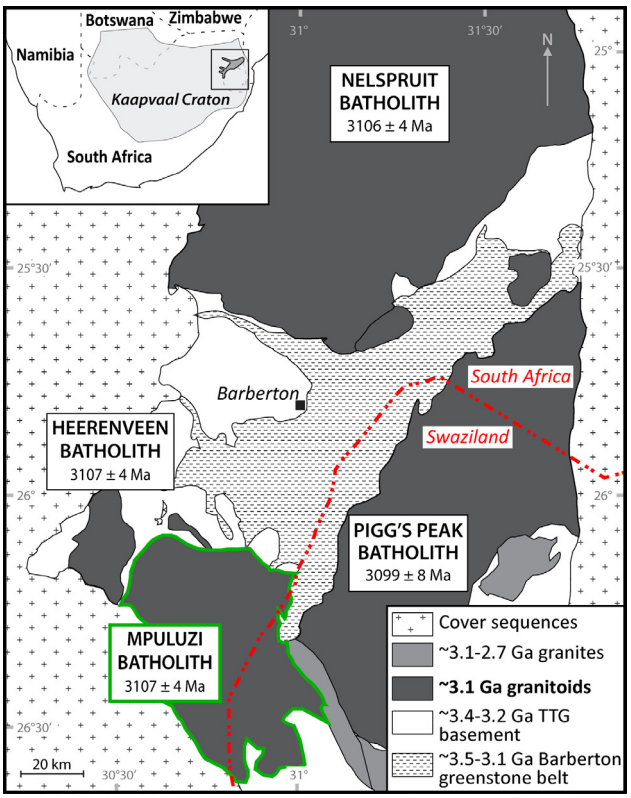

Dating the zircon from the Mpuluzi samples has proved to be a challenge, with many grains full of cracks and inclusions, leaving little 'clean' material to analyse. The high concentrations of the radioactive elements U and Th in the grains has meant that their 3 billion year life has been rather a hard one. Many have lost a lot of their radiogenic lead, as radiation damage progressively destroyed the crystal lattice.

The U-Pb ages obtained from Mpuluzi samples range from ~3.14 to ~3.09 Ga, with the main cluster of ages at 3.123 ± 7 Ga, emplacement may have occurred over a period as long as 50 million years. Some samples have a minor inherited population at ~3.5 Ga, which suggests that older crustal material was melted to produce the magmas. The Hf-isotope data provide further supporting evidence, with mean model ages of ~3.5 Ga, and in some samples extending back as far as ~4 Ga.

The Mpuluzi samples are currently being analysed for their Sr and Nd isotopic compositions, which will provide further constraints on the composition and age of the source material. The problems of the heat source and the unusual emplacement style will then be addressed through geodynamic modelling. Watch this space!

This project is part of CCFS Themes 2 and 3, Earth Evolution and Earth Today, and contributes to understanding Earth's Architecture and Fluid Fluxes.

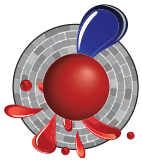

Contacts: Rosanna Murphy, Bill Griffin, Norman Pearson, Sue O'Reilly, Craig O'Neill

Funded by: CCFS Foundation Program 1, MQRES, EPS HDR Fund

Metals in dirty water – the genesis of ore deposits

Field evidence shows that metal ore bodies are deposited by fluids derived from deeper in the Earth – but we do not yet understand in any detail how the metals are picked up from the deeper lithosphere and transported in the fluids. We have begun a multi-scale integrated study to address this void in our understanding. One part of the study involves a set of key experiments designed to evaluate the chemical behaviour of fluid systems at the conditions of the lithospheric mantle and the asthenosphere. The current focus is on the complex transport and concentration mechanisms of siderophile-chalcophile elements such as Ni, Cu and PGE in the deep lithosphere. Researchers from Macquarie and The University of Western Australia are collaborating on this Foundation Program, which addresses Theme 3 (Earth Today - and its Resources) of the CCFS.

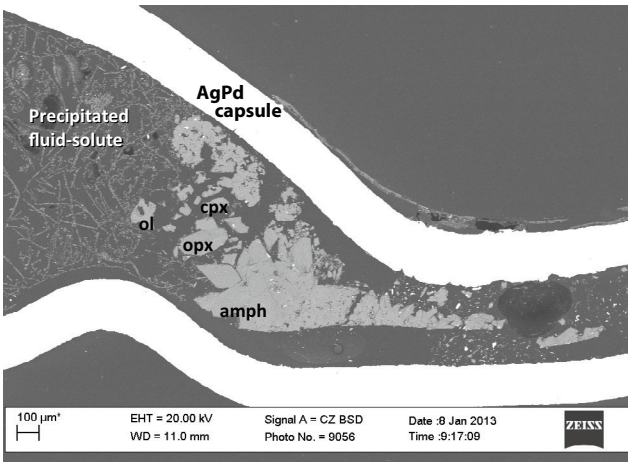

Figure 1. A longitudinal section of a capsule showing run products from a water-saturated experiment on a nepheline basanite at 950 °C and 2.0 GPa. The run products include solute precipitated from the quenched H_2O-fluid (seen as filamentous strands of fine beads) and crystals of clinopyroxene, orthopyroxene, olivine, ilmenite, mica and amphibole.

We have conducted twelve experiments at 0.5-3.0 GPa and 950-1100 °C to determine the partitioning of minor and trace elements (including chalcophile metals) between hydrous fluids, peridotite minerals and typical intraplate basanitic melts. Five experiments were also conducted under H_2O-undersaturated conditions on coexisting basanite and sulfide melts. The fluid/mineral/melt partitioning data, combined with previously obtained mineral/melt partition coefficients for the same basanite, provide information on the contrasting abilities of H_2O-fluids and silicate melts to transport metals and incompatible elements within the mantle lithosphere.
A particular feature of the experimental approach is that it avoids the use of fluid traps (including carbon spheres and fluid inclusions in solid minerals) commonly employed in

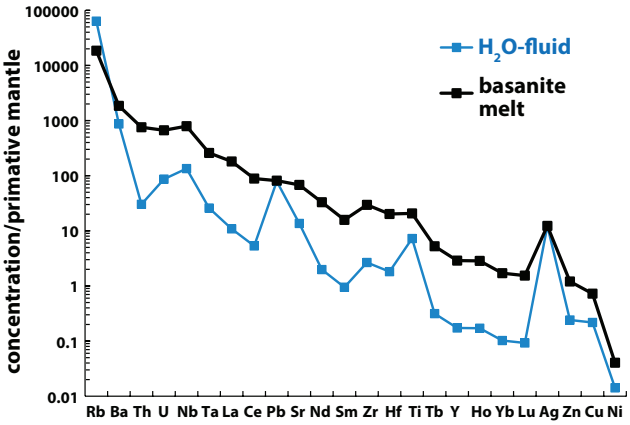

Figure 2. Mantle-normalised element concentrations in aqueous fluids and silicate melts equilibrated with a garnet lherzolite of Primitive Mantle composition. The fluid composition was calculated using partition coefficients from this study.

similar experiments. This allows the experimental run products produced to be unambiguously identified (see Fig. 1) and analysed by electron microprobe and LA-ICPMS.

The successful experiments have produced a small but unique data set for H_2O-fluids in equilibrium with mantle phases. There are very few equilibrium data on such very fluid-rich systems under these deep mantle conditions, so the data set is being carefully analysed. At 950-1100 °C and 2.0 GPa the fluids contain 15-25 wt % of dissolved solute. The solutes are enriched in SiO_2 (56-66 wt %), Al_2O_3, and alkalis (10.9-12.6 wt % $Na_2O + K_2O$) but depleted in TiO_2, FeO, MgO and CaO relative to the basanite. Overall the transport capacities of H_2O-fluids within the upper mantle are distinctly different from those of silicate melts (Fig. 2). Alkalis, Pb and Ag are relatively enriched in the aqueous fluids, whereas most chalcophile and incompatible elements are not. As we continue to analyze these unique experiments, more partitioning data will be available on the economically important elements. Currently the results suggest the silicate melts can transport sulfides much more efficiently than aqueous fluids, but fluids may be critical in transporting metals such as Ag.

This project is part of CCFS Theme 3, Earth Today, and contributes to understanding Earth's Fluid Fluxes.

Contacts: Marco Fiorentini, John Adam, Tracy Rushmer, Marek Locmelis
Funded by: CCFS Foundatio Project 2a

Decoding sulfur DNA solves how ancient ore deposits formed in Western Australia

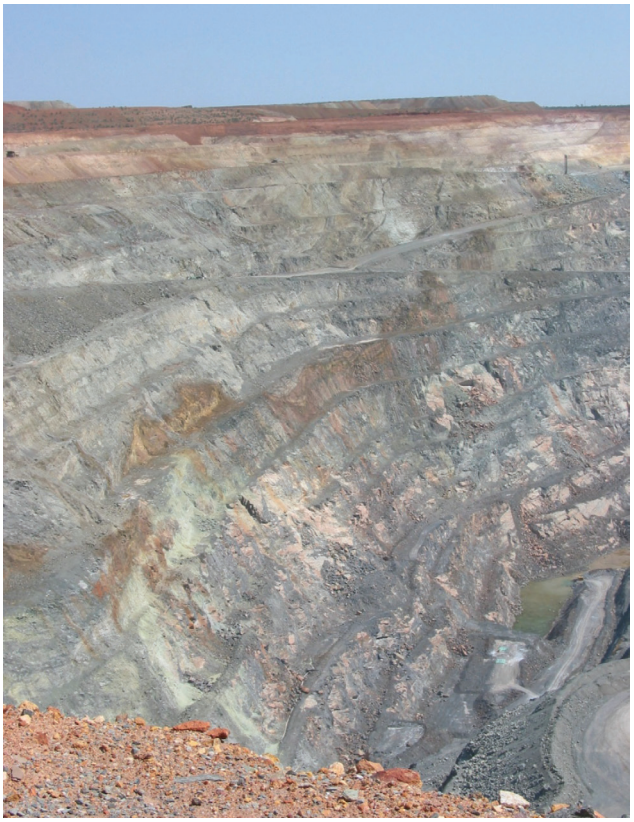

Figure 1. Exhalative sulfides in close spatial association with the largest komatiite-hosted nickel-sulfide deposit in the world, Mount Keith, Western Australia.

Magmatic hydrothermal oceanic vents represent places where metals accumulate in the form of exhalative and sedimentary sulfides associated with submarine felsic volcanoes. These are also loci where life can flourish in the form of a wide range of complex and diversified bacteria colonies. In the Archean Earth (more than 2.5 billion years ago), coeval to the emplacement of sulfide-bearing felsic magmas, komatiites locally erupted on the floor of the ocean. These hot and highly turbulent magmas assimilated previously formed volcanogenic exhalative and sedimentary sulfides, leading to the formation of discrete sulfide melts, which concentrated chalcophile and siderophile metals such as nickel, copper and the platinum group elements from the komatiite magma.

Multiple sulfur isotope data on sulfides from variably mineralised komatiite units in the Archean north Eastern Goldfields, Western Australia, provide new constraints on these assimilation and ore-forming processes. Although magmatic sulfides from komatiites display very similar $\Delta^{33}S$ signatures to volcanogenic exhalative and sedimentary sulfides, they have consistently lower $\delta^{34}S$ values relative to these sources. In other words, the sulfur-bearing compounds from the magmatic sulfides in the komatiites are on average isotopically lighter than the sulfur compounds contained in the volcanogenic exhalative and sedimentary sulfides. This lowering of the $\delta^{34}S$ signature is consistent with degassing of the komatiite-sulfide melt system. At the temperatures and oxygen fugacities relevant to komatiite magmatism, sulfur in the melt exists primarily as ^{34}S-poor sulfide species, while sulfur in the co-existing gas would be dominated by ^{34}S-rich SO_2. Continuous loss of this ^{34}S-enriched gas would lower the $\delta^{34}S$ values of coexisting sulfide melt, leading to magmatic sulfides with the isotopic compositions measured here.

Our results indicate that komatiites from the north Eastern Goldfields of Western Australia, irrespective of their initial sulfur content, degassed upon emplacement at Earth's surface. Komatiite degassing likely influenced physical and chemical parameters of the primordial oceans by the addition of heavy sulfur in the form of SO_2, thus contributing to the positive heavy S ocean signature. This then indirectly contributed to the creation of a complex chemical gradient at the interface between seawater and seafloor in the primordial Earth.

This project is part of CCFS Themes 1 and 2, Early Earth and Earth Evolution and contributes to understanding Earth's Fluid Fluxes.

Contacts: Carissa Isaac, Marco Fiorentini
Funded by: CCFS Foundation Program 5

Figure 2. Typical "komatiite country" in the Eastern Goldfields of Western Australia.

Slaking the Earth's thirst at mid-crust levels

Numerous studies have identified low-$\delta^{18}O$ fluids in ductile shear zones that dissect volumes of otherwise anhydrous crustal rocks. A prime example is the shear-zone network that dissects the Proterozoic granulite terranes in central Australia. The pronounced lowering of $\delta^{18}O$ values by up to 10‰ between rehydrated fault-zone rocks and their adjacent largely anhydrous equivalents precludes the involvement of internally-derived fluid sources. This is problematic because these shear zones typically post-date the high-grade regional metamorphism of their wall rocks by tens or hundreds of millions of years. As a consequence, in cases where calculated fluid compositions are below the mantle signature ($\delta^{18}O = 5.7 \pm 0.3$‰), such alteration patterns are typically interpreted as the product of deep crustal metasomatism driven by the influx of surface-derived fluids. However, models that propose the migration of a mobile fluid phase from the surface to the mid-crust are both mechanically and geochemically challenging.

We have used the Cameca 1280 ion microprobe at the University of Western Australia to analyse oxygen isotopes in garnet porphyroblasts from the mid-crustal Walter-Outalpa shear zone, southern Curnamona Province, South Australia. All the garnets have homogeneous $\delta^{18}O$ values of < 3‰. Integrated Lu-Hf geochronology and compositional mapping by electron microprobe demonstrate that the closed-system growth of these isotopically light garnets (Fig. 1) started as early as 531 Ma, prior to the peak of metamorphism and deformation during the Delamerian Orogeny (514–490 Ma). These new data have lead to the proposition that the prograde burial and dehydration of altered fault panels under thick sedimentary sequences during pre-orogenic basin formation has produced the observed lowering of the $\delta^{18}O$ values. This contrasts with established fluid transport models, where surficial fluid signatures are imposed at depth by large fluxes of downward-penetrating fluids. The existence of low $\delta^{18}O$ values in deeply-exhumed shear zones may therefore indicate that the fault structures had a pre-metamorphic history of near-surface exposure, weathering, burial/metamorphism and re-exposure.

This project is part of CCFS Theme 2, Earth Evolution, and contributes to understanding Earth's Fluid Fluxes.

Contacts: Chris Clark, John Cliff
Funded by: ARC Discovery

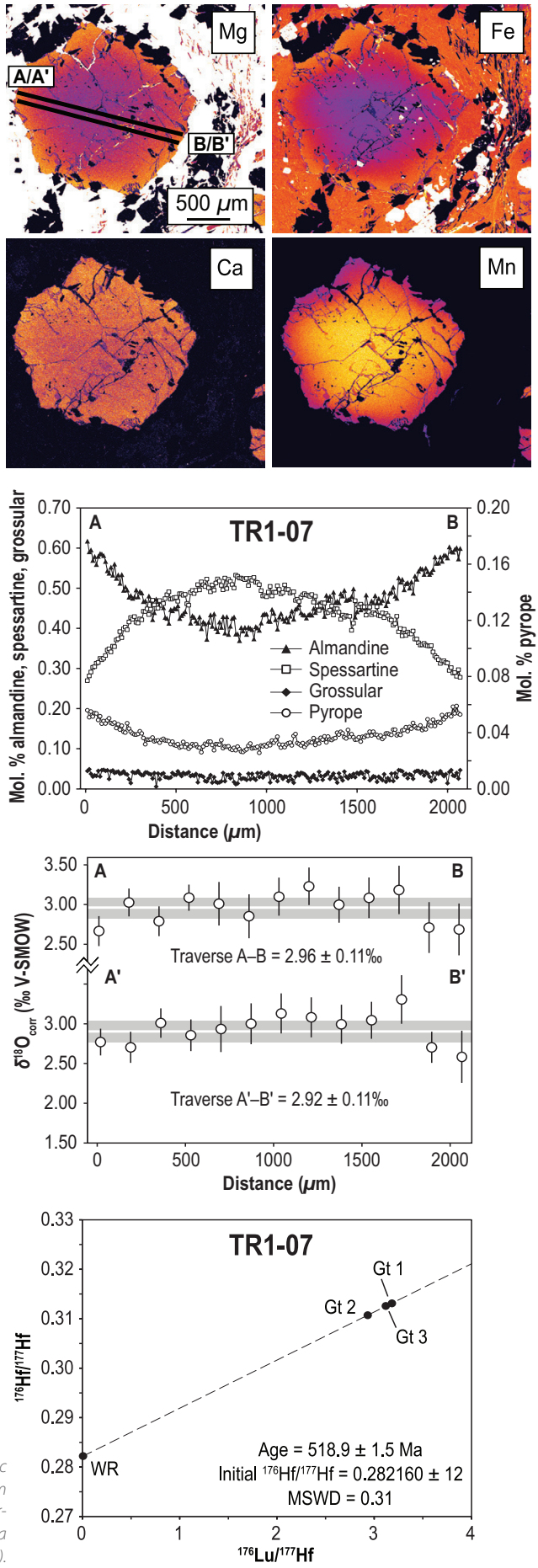

Figure 1. Major element chemical, O-isotopic and Lu-Hf geochronological dataset from a single garnet from within the Walter-Outalpa shear zone in central Australia (Raimondo et al., 2013, Geology, in press).

Unravelling the early Earth's record of biological fingerprints using sulfur isotopes

Multiple sulfur isotopes (^{32}S, ^{33}S, ^{34}S, ^{36}S) are becoming an increasingly important tool to investigate biological processes on the early Earth. They can tell us about the types of life present in Earth's earliest sedimentary environments and trace the transfer of sulfur species in fluids and gases from the interior of the Earth via the atmosphere, hydrosphere, and finally into the biosphere.

3.5 billion-year-old pillow lavas from the Barberton greenstone belt, South Africa, containing microtubes with microbially-mediated sulfide inclusions.

One problem in this type of study is the spatial resolution at which multiple sulfur isotopes are currently analysed. Traditional bulk analyses can lead to artificial homogenisation of sulfur-isotope signals in a sample and conceal evidence of processes on the micron scale (the scale where microbial mediation might be observed). Our work under the CCFS Theme: The Early Earth is using *in-situ* techniques (SIMS and NanoSIMS), where the spatial context of the analyses is retained, to gain new insights into this problem.

Using the CAMECA NanoSIMS at UWA in the past year, we have been able to extract sulfur-isotope data ($\delta^{34}S$) from tiny (<15 µm) pyrite grains within microtubes in ca 3.5 billion-year-old basalts. These record $\delta^{34}S$ values as low as ca -40 ‰, indicating that sulfur processing microbes were a likely component of the early Archean sub-seafloor biosphere (*CCFS publication #230*).

We have also used the CAMECA IMS1280 (see *Technology development* section of the 2011 Annual Report) to analyse some of Earth's oldest sedimentary sulfides from the 3.5 billion-year-old Dresser Formation of Western Australia. Here we have measured all 4 stable sulfur isotopes, and while the $\delta^{34}S$ and $\Delta^{33}S$ values appear to be similar to previous bulk analyses, the $\Delta^{36}S$ values have a much greater spread than previously reported. This could be significant for understanding the sources of sulfur on the early Earth, but more work is needed to test the robustness of SIMS $\Delta^{36}S$ data. As a result we are now collaborating with international experts such as James Farquhar (University of Maryland) to conduct further tests on these samples using both SIMS and more traditional techniques.

We are also implementing modern analogue experiments to discover the micron-scale distribution of multiple sulfur isotopes in microbially-precipitated sulfides. Here we are working in collaboration with microbiologists and isotope geochemists in Norway and USA, using cultures of different sulfur-processing microbes, in particular sulfate-reducers and sulfur-disproportionators. The isotopic compositions of the end products of these experiments will soon be analysed using SIMS and NanoSIMS. It is hoped that this will give us more accurate interpretations of Archean sulfur isotope data and help us understand the anomalous $\Delta^{36}S$ signatures seen in our data from the Dresser Formation.

This project is part of CCFS Theme 1, Early Earth, and contributes to understanding Earth's Fluid Fluxes.

Contacts: David Wacey, Mark Barley
Funded by: CCFS Foundation Program 7

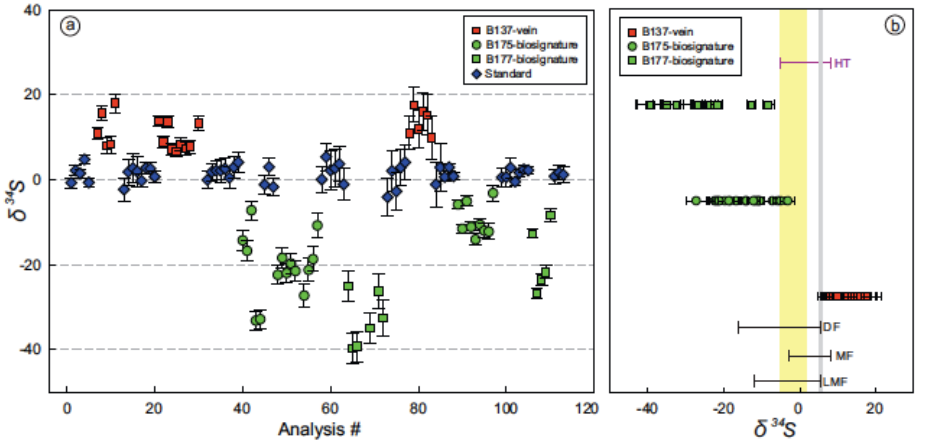

Nanoscale secondary ion mass spectrometry $\delta^{34}S$ sulfide data from ~3.5 Ga Hooggenoeg Formation South Africa shows vein sample (red), two candidate biotexture-bearing samples (green), and standard (blue). (a): Analyses in order performed: B137 ranges from +6.7‰ to +18‰ and is positively shifted from CMCA-S1 pyrite standard; B175 and B177 are negatively shifted from standard, with B175 ranging from −27.3‰ to −3.2‰ and B177 from −39.8‰ to −8.3‰ (error bars are 2σ). (b): Range in measured $\delta^{34}S$ values compared to other Archean sulfides. Candidate biotexture-bearing samples show largest range and most negatively shifted values yet measured, whereas vein sample is positively shifted and shows smaller range. For reference, yellow band indicates mantle sulfur, gray line indicates Archean seawater, and purple line (HT) indicates hydrothermal sulfides (from Mojzsis, 2007). For comparison, $\delta^{34}S$ range of sulfides from cherts and sediments of similar age are shown: 3.49.

How hot is the Earth, really?

The internal heat of the Earth drives plate tectonics, so the surface heat flux can give us an important constraint on the properties and behavior of the Earth through geologic history. The surface heat flow can be reliably measured over continents, but due to hydrothermal circulation in oceanic crust, measurements in ocean basins often do not reflect deep lithospheric heat flow. As such, estimates of lithospheric heat flow over ocean basins usually are based on geodynamic models. These models usually are simple, using constant thermal properties and boundary conditions – but are they useful? We have developed new thermal models that incorporate a petrologically and thermodynamically more complete view of lithospheric cooling. These models show that several thermal complexities are important as they change the predicted surface heat flow over ocean basins significantly while remaining compatible with reliable measurements. Specifically, we have shown that the effective thermal properties of the oceanic lithosphere depend strongly on age, and that this age-dependence is primarily due to the thermal insulation effect of oceanic crust. Therefore, heat flow over young seafloor is significantly lower than conventional models predict while predictions at older ages are similar.

This revision of conventional thermotectonic theory has several major implications. For example, lower heat flux over young seafloor indicates that the advective or hydrothermal component of heat transport has been significantly overestimated. This changes the hydrogeological regime of oceanic lithosphere and impacts on geochemical mass-balance problems related to the fluid interaction of lithosphere and oceans. Also, strongly age-dependent cooling affects the seafloor subsidence rate, and in this case our models are consistent with global topographic data. This shows that persistent features of lower magnitude than roughness in the data can be identified. In addition, the modeled net seafloor heat flow, and thus global heat flow, is lower than conventional models predict. Since the low conductivity of oceanic crust is the principal reason for the low heat flow over young seafloor, this effect is expected to be more important early in Earth history when the oceanic crust was thicker than it is now. This means that seafloor heat flow in the Archean may have been significantly lower than conventional models predict, or that plate velocity would have to be much higher to compensate for low-conductivity lithosphere.

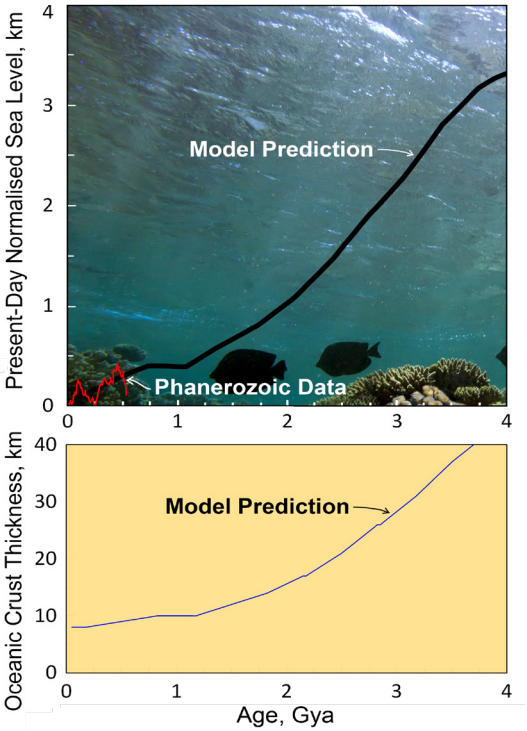

Figure 2. Predicted sea level and thickness of oceanic crust since the start of the Archean. The red line shows data for Phanerozoic sea level (Hallam, Phanerozoic sea-level changes, Columbia Univ. Press, 224p, 1992).

We also have coupled our revised thermotectonic model of oceanic lithosphere to an isostatic model of the Earth to predict eustatic sea level changes over Earth history. Remarkably, our model predicts systematic sea-level change in good agreement with the Phanerozoic record, and we calculate that sea level at the end of the Archean (2.5 Ga) was at least 2 km higher than it is now, although our estimates are highly dependent on the choice of melting model. Ongoing research in this project will refine these predictions.

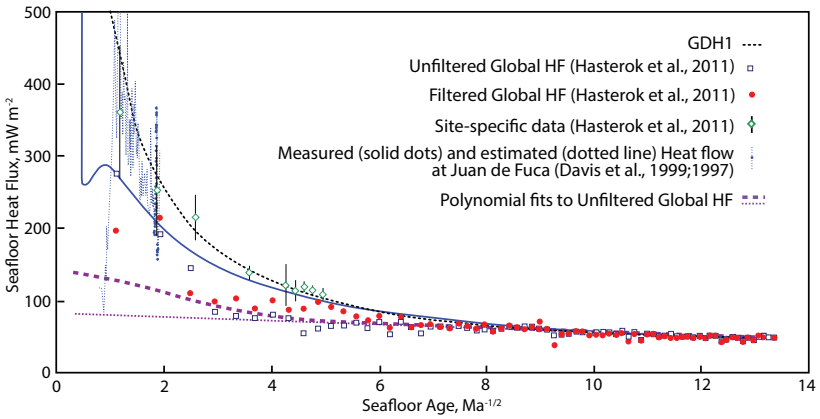

Figure 1. Predicted and measured seafloor heat flow. The thick blue line is our preferred model. The dashed red line is a conventional plate model, and the data points and dashed violet lines describe global heat flow data.

This project is part of CCFS Theme 3, Earth Today, and contributes to understanding Earth's Architecture

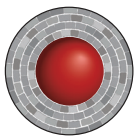

Contacts: Chris Grose, Juan Carlos Afonso
Funded by: ARC Discovery (JCA); ARC IPRS

Squeezing the mantle: between an ocean and a continent

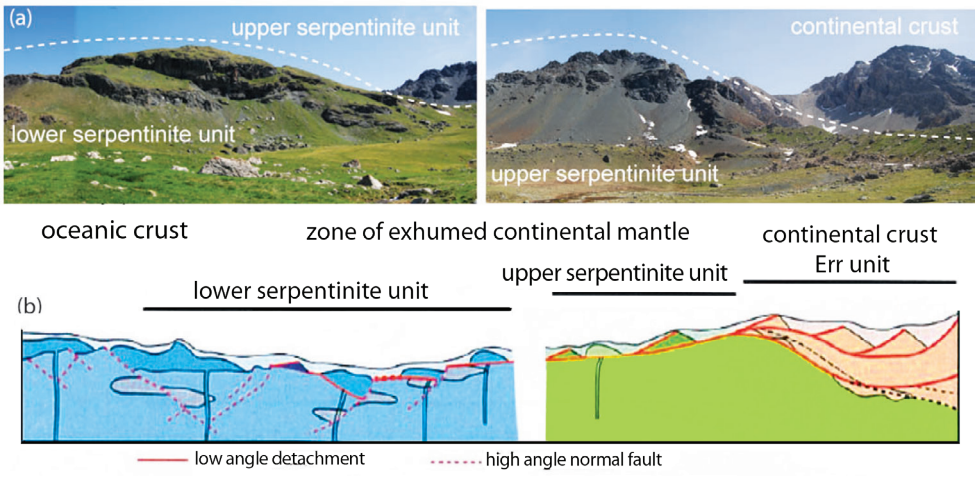

Figure 1. Palinspastic reconstruction of the Platta nappe (Desmurs et al. 2001, Geol Soc London Spec Publ). (a) Pictures showing the present observed Alpine structure. (b) Palinspastic section across the Platta-Err ocean -continent transition. It shows the position of the upper and lower serpentinite units within the former ocean-continent transition and summarises the field relationships between fault structures, continental rocks, exhumed mantle rocks and intrusive and extrusive mafic rocks (Schaltegger et al. 2002, Terra Nova).

Tectonically-driven deformation of the lithosphere leads to strain localisation through the formation of ductile shear zones, and their development is responsible for lithosphere-scale deformation that controls the nature and distribution of Earth's tectonic plates. Divergent plate boundaries, such as ocean-continent transitions, are the perfect place to study mechanisms activated during extension leading to localisation of deformation. The Platta-Totalp massifs in the Eastern Central Alps (Grison, Switzerland) are a type example of a zone of exhumed continental mantle. Mapping and structural analysis of the nappes has produced a palinspastic reconstruction of a complete stratigraphic sequence of an ocean-continent transition (Fig. 1) that can guide sampling for a study of deformation processes.

The mantle rocks in these units are spinel lherzolites and harzburgites, into which gabbros and basaltic dykes were intruded (Fig. 2a). Mantle rocks close to the continent are spinel peridotite mixed with (garnet)-pyroxenite layers while the ultramafic rocks at some distance from the continent are pyroxenite-poor peridotite that equilibrated in the plagioclase stability field (Fig. 1). Two-pyroxene and single-orthopyroxene thermobarometric data from the Platta nappe show that the equilibration temperature (at 25-45 km depth) increases from 850±50 °C near to the continent to >1000 °C further oceanwards (*Desmurs, 2001, PhD*). The change in temperature is related to the exhumation of the massif during crustal thinning. Some peridotites contains garnet pyroxenite, indicating high-pressure formation within the spinel peridotite field (>45 km depth) in the mantle sequence.

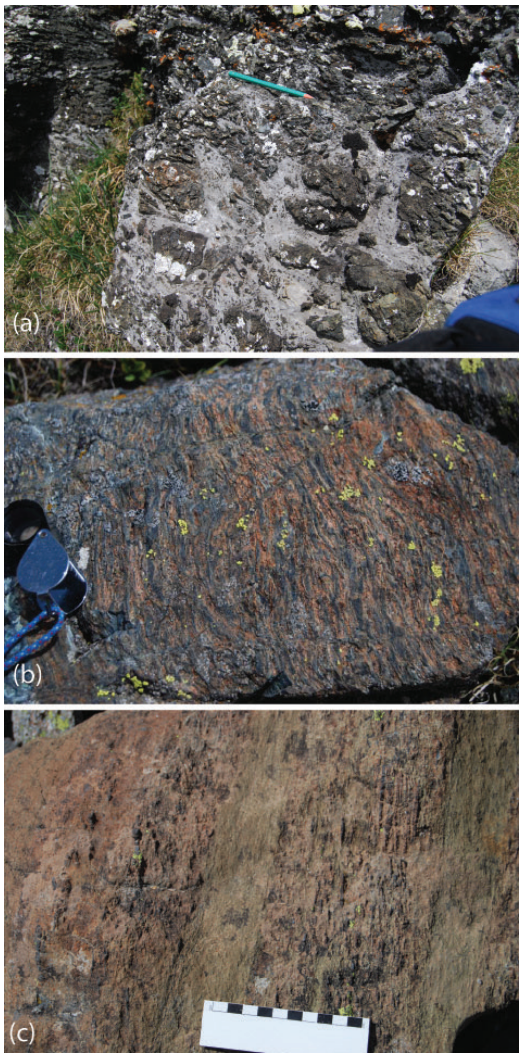

Fieldwork in the upper mantle part (Fig. 1) reveals heterogeneous distribution of deformation from lower to upper serpentinite units. The peridotite is deformed in both units, but is more deformed in the upper serpentinite unit (Fig. 2b). At a smaller scale, the deformation and the composition of the rock are heterogeneous. The peridotite shows dunitic and harzburgitic layers, and high-temperature shear zones at metre or centimetre scale (Fig. 2c and 3). Sampling across this sequence gives a spatial resolution of the deformation within an ocean-continent transition. A detailed study of the peridotite texture is being combined with the analysis of the crystallographic preferred orientation of minerals, using electron backscatter diffraction method (EBSD) to

Figure 2. (a) Ophicarbonate at the top of the mantle sequence; (b) Peridotite with foliation in the upper serpentinite unit; (c) Variation of the peridotite composition in the upper serpentinite unit.

determine the deformation mechanisms activated during extension. This study is coupled with thermometric calculations to constrain the temperature of the deformation. The study will constrain the localisation of the deformation related to decreasing temperatures and possible percolation within extensional settings such as ocean-continent boundaries.

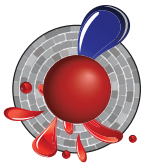

This project is part of CCFS Themes 2 and 3, Earth Evolution and Earth Today, and contributes to understanding Earth's Architecture and Fluid Fluxes.

Contacts: Mary-Alix Kaczmarek, Steve Reddy
Funded by: CCFS and Curtin University

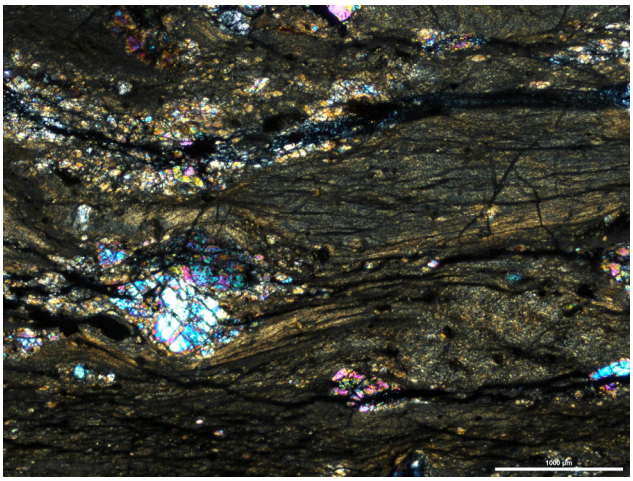

Figure 3. Crossed-nicol photomicrograph of an ultra-mylonitic peridotite.

Multistage refertilisation of an Archean peridotite massif (NE Tibet, China)

Peridotite massifs in orogenic belts and mantle xenoliths brought up by volcanic rocks both reveal the lithological and geochemical heterogeneity of the subcontinental lithospheric mantle (SCLM). Pyroxene-rich veins, secondary metasomatic phases and elemental and isotopic enrichments of Ca-, Al-rich minerals are common in orogenic peridotites. These fertile markers within the depleted host rocks suggest a complicated history of refertilisation. To sort out the sequence of multistage refertilisation in the SCLM is tricky, because of the overlapping of enrichment events and the rarity of useful dating targets. However, a study of elemental and isotopic (Sr-Nd-Hf-Os) compositions of minerals of the Shenglikou peridotite massif from the North Qaidam orogen (NE Tibet, China; Fig. 1) has revealed unusually clear details of the refertilisation history.

This ultramafic massif was scraped off from the Qilian continental-margin mantle wedge by the subducting Qaidam block during early Paleozoic assembly of the Tibetan plateau.

Refractory dunite and harzburgite formed the original lithologies, which enclose fertile garnet lherzolite zones, secondary clinopyroxene-rich lherzolite/wehrlite layers (Fig. 2) and rare garnet pyroxenite dykes. Re-Os isotopic analyses of Fe-Ni-sulfides from the peridotite give some ancient Re-depleted model ages (oldest ≈ 3.0 Ga), suggesting an Archean origin. Whole-rock oxide compositions show a linear mixing trend between the dunite and pyroxenite. Trace-element patterns imply the dunite-harzburgite protoliths were re-enriched by slab-derived fluids, and the lherzolite and wehrlite look like the products of reaction between the refractory peridotite and a pyroxenite melt with an arc signature.

However, mineral elemental and isotopic data argue against a single refertilisation by binary mixing. The initial Nd-Hf isotopic patterns (Fig. 3) indicate that the dunite-harzburgite protoliths, clinopyroxene-rich peridotites and pyroxenites record different isotopic evolution paths. Their Hf and Nd isotopes, compared with chondrite and depleted-mantle values, suggest that the Hf isotopes can record ancient events and are more immune to later metasomatism, but the Nd isotopes were largely shifted to less radiogenic values (Fig. 3) by subsequent enrichment events. Lu-Hf analysis of garnet and clinopyroxene from refractory garnet harzburgites away from the refertilised lithologies give an isochron age around 1.5 Ga (Fig. 4), consistent with their Hf depleted-mantle cont...

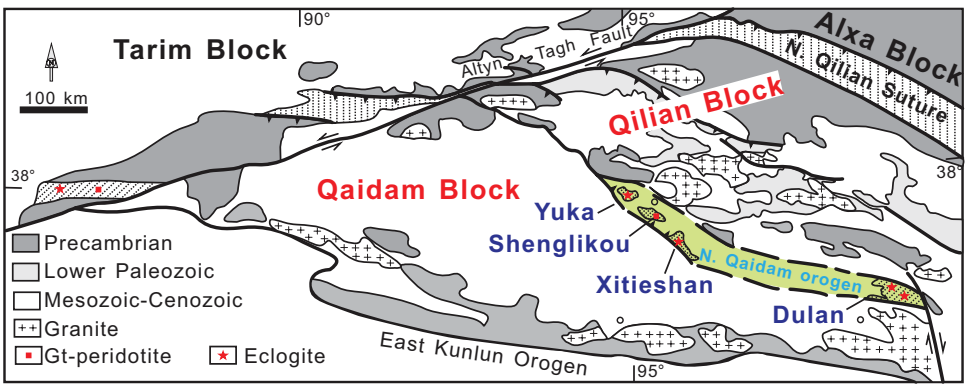

Figure 1. Tectonic units of the Northeastern Tibet area, China. The garnet peridotite massif is enclosed by ultrahigh-pressure (UHP) metamorphosed gneiss in the Shenglikou area, located at the western segment of the North Qaidam orogen. This orogen also exposes UHP rocks at the Yuka, Xitieshan and Dulan areas.

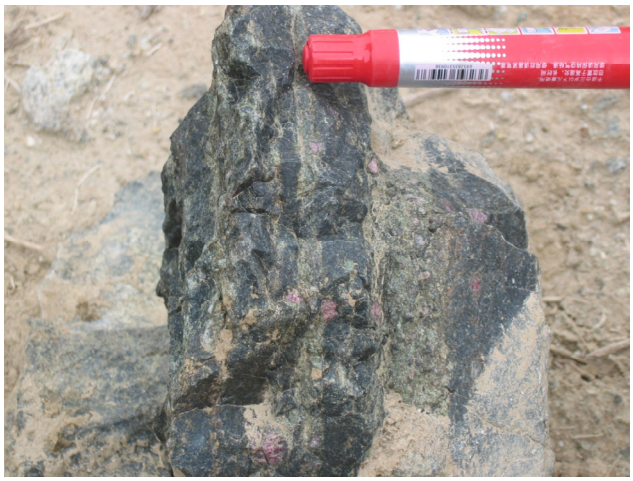

Figure 2. Clinopyroxene-rich garnet lherzolite/wehrlite (light green) inter-banded with garnet harzburgite host (dark green). The exposed pen is about 10 centimetres.

model ages; this suggests an early Mesoproterozoic refertilisation of this piece of Archean mantle. Garnet- and clinopyroxene-rich rocks (secondary layers and pyroxenite dykes) show Sm-Nd and Lu-Hf isochron ages of ~1.1-0.6 Ga. This time span may imply a refertilisation event at ~1.1-0.9 Ga (Xiong et al., 2010) that formed the secondary peridotite layers; then pyroxenite melts intruded the refertilised mantle before the incorporation of this mantle fragment into the subducting slab at ~430 Ma. Radiogenic Sr ($^{87}Sr/^{86}Sr$ initial=0.71266-0.71388), unradiogenic Nd isotopic data but near-DM Hf isotopes (Fig. 3) suggest the melt came from the asthenosphere, which nad been metasomatised by slab-derived material.

This work has shown that different incompatibilities and activities of isotopic pairs in rock-melt or rock-fluid systems can reveal different mantle events, and help us to clarify the sequence of multistage refertilisation in a volume of ancient SCLM.

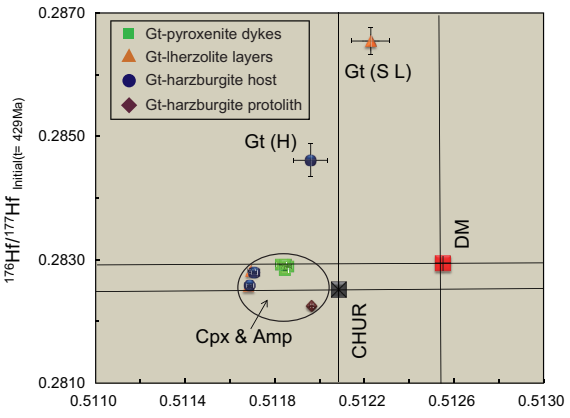

Figure 3. $^{143}Nd/^{144}Nd$ initial versus $^{176}Hf/^{177}Hf$ initial ratios of garnet, clinopyroxene and amphibole in different lithologies of the Shenglikou peridotite massif. Nd and Hf isotopic ratios are calculated back to 429 Ma, when the zircon formed in this massif by UHP metamorphism. Error bars are shown as ±1σ, and those of clinopyroxene and amphibole are smaller than the symbol size. "S L", secondary lherzolite; "H", harzburgite; "DM", depleted mantle; "CHUR", chondrite uniform reservoir; "Gt", garnet; "Cpx", clinopyroxene; "Amp", amphibole.

This project is part of CCFS Theme 2, Earth Evolution, and contributes to understanding Earth's Architecture and Fluid Fluxes.

Contacts: Qing Xiong, Sue O'Reilly, Bill Griffin, Norman Pearson, Jianping Zheng (China University of Geosciences, Wuhan)

Funded by: ARC Discovery (S.Y.O'R and W.L.G.), Centre of Excellence, NSFC (J.P.Z.)

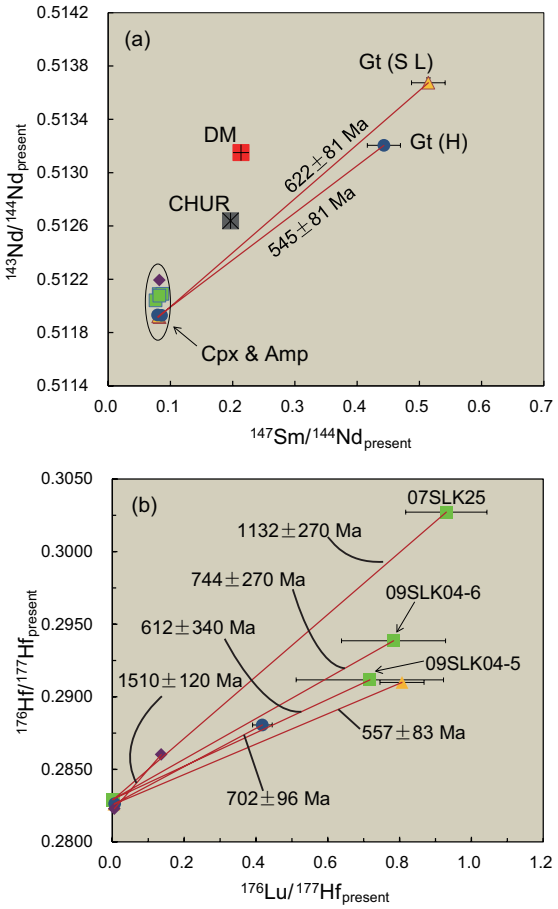

Figure 4. $^{147}Sm/^{144}Nd$ present versus $^{143}Nd/^{144}Nd$ present (a) and $^{176}Lu/^{177}Hf$ present versus $^{176}Hf/^{177}Hf$ present (b) diagrams of garnet, clinopyroxene and amphibole in different lithologies of the Shenglikou peridotite massif. Error bars are shown as ±1σ, and those of clinopyroxene and amphibole are smaller than the symbol size. Isochron ages (±2σ) are shown; the large uncertainties reflect the measurement of Lu/Hf ratios by LA-ICPMS and will be improved by further work. Abbreviations and symbols are the same as those of Figure 3.

Spurious Hadean ages in East Antarctica: the tribulations of moving Pb

Zircons from early Archean ortho- and paragneisses in the ultrahigh-temperature (UHT) metamorphic rocks of the Napier Complex of East Antarctica show very complex U-Th-Pb systematics. Published ages from the Mount Sones, Dallwitz Nunatak and Gage Ridge localities are scattered, and the oldest ages are reversely discordant (U/Pb ages older than $^{207}Pb/^{206}Pb$ ages). This problem attracted scientific attention several years ago, because $^{207}Pb/^{206}Pb$ ages are considered to be more robust than U-Pb ages in ancient rocks. Several different mechanisms were proposed to explain this phenomenon, but no satisfactory answer was forthcoming. Since uranium is strongly lattice-bound in zircon, it is unlikely to be mobilised, so the favoured explanation was "Pb gain", a mechanism opposite to Pb loss in normally-discordant data. However, the source of the "extra Pb" was not defined, and this problem has remained unresolved for more than 25 years.

We have used a novel high spatial resolution ion microprobe imaging technique to investigate the problem (*CCFS publication #276)*. Selected areas of 70 µm x 70 µm of Antarctic zircons were imaged using a small (~2 µm) rastered primary beam on the Cameca IMS 1280 at the National History Museum in Stockholm. The distribution of ^{48}Ti, ^{89}Y, ^{180}Hf, ^{206}Pb, (Fig. 1), ^{232}Th and ^{238}U was imaged in the single-collector mode and ^{204}Pb, ^{206}Pb, ^{207}Pb and ^{180}Hf in the multi-collector mode. Hafnium is evenly distributed in these zircons and served as a proxy matrix peak in both routines.

A zircon grain from a paragneiss from Mount Sones with a spot age of 3008±21 Ma ($^{207}Pb/^{206}Pb$ age) and U content of

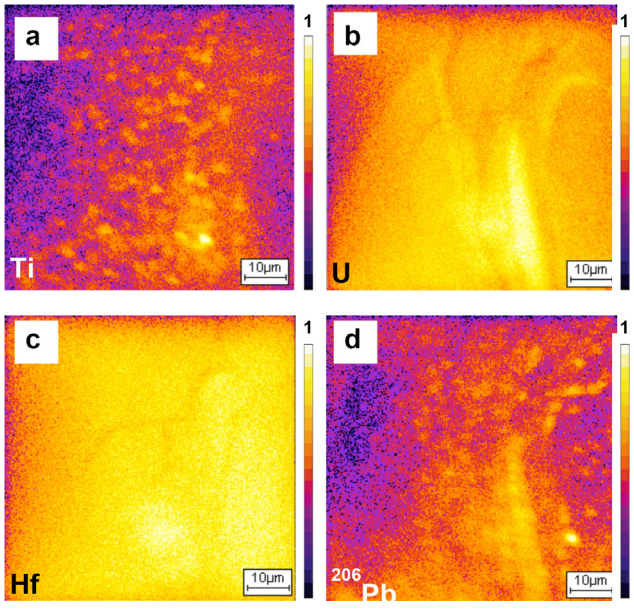

Figure 1. Scanning ion images of grain n3852-08 from Mount Sones sample 14178-2 using a single-collector routine: (a) ^{48}Ti, (b) ^{89}Y, (c) ^{180}Hf, (d) ^{206}Pb.

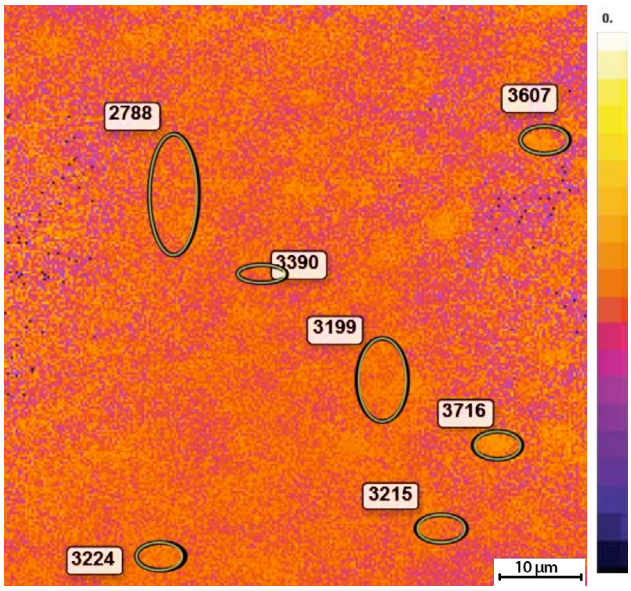

Figure 2. Multi-collector map of $^{207}Pb/^{206}Pb$. Ellipses show the areas used for $^{207}Pb/^{206}Pb$ age calculation. Field of view is 70 µm x 70 µm.

2561 ppm was one of those selected for investigation. The ion maps (Fig. 1b) reveal the distribution of selected elements. Cathodoluminescence (CL) images show that Yttrium, Th and U define a zonation. The Pb distribution, in contrast, shows an unusual patchiness (Fig. 1d). Although it broadly follows the U and Y zonation, there are bright patches with enhanced signals which do not correspond to any zones or to crystal imperfections (e.g. cracks). Ti also shows patchy distribution, but there is no direct correlation between patches of Pb and Ti.

In the multicollector mode, ^{206}Pb and ^{207}Pb isotopes exhibit similar patchiness. The ^{204}Pb image (not shown) is black, showing there is common Pb in the analysed area. Using the WinImage program, we produced maps of $^{207}Pb/^{206}Pb$ (Fig. 2), and these maps allow calculation of $^{207}Pb/^{206}Pb$ ages for spots of any size from ~2 μm^2 upward, within the frame of the picture (70 µm x 70 µm) and at any time after data collection. This is a new and unique method for obtaining age information from zircon, and new applications await.

These maps show areas of enhanced brightness where the $^{207}Pb/^{206}Pb$ ratio is higher and demonstrate that within these small areas (µm scale) the apparent $^{207}Pb/^{206}Pb$ age is older than in the rest of the crystal. Using these images, we have calculated $^{207}Pb/^{206}Pb$ ages ranging from 2.8 Ga up to 3.7 Ga (Fig. 2), both older and younger than the apparent SIMS age. Spuriously old $^{207}Pb/^{206}Pb$ ages in areas enriched in radiogenic Pb reflect a combination of supported and unsupported radiogenic Pb; Pb has indeed moved, but only within the grain, so there is no reason to invoke "extra Pb". In addition, the 'patchy' distribution of Ti has the potential to affect Ti-in-zircon thermometry, with implication for the accurate determination of zircon crystallisation temperatures.

Some of the ages measured in this zircon suite are Hadean (>4 Ga) and hence Pb redistribution of this type might have lead to the rocks being classified as samples of Earth's oldest crust. *cont...*

In the present example, the mobilisation and redistribution of Pb in Antarctic zircons probably occurred at ~2.5 Ga, the time of UHT metamorphism in the Napier Complex. This well-documented event reached temperatures >1100 °C, the highest recorded in Earth's continental crust.

All images are normalised to the HfO image to minimise the effect of enhanced ion emission from the original spot analysis crater. The colour-scale bars are relative intensity (i.e. do not correspond to ppm).

This project is part of CCFS Theme 1, Early Earth, and contributes to understanding Earth's Architecture.

Contacts: Monika Kusiak, Simon Wilde
Funded by: EU-FP7, Marie Curie Grant: CCFS Foundation Program 2

The glitter of gold 60 km beneath the Earth's surface

Glittering gold nugget!

Gold is a highly siderophile element (HSE) along with the platinum group elements (PGEs: Pt, Pd, Rh, Ru, Os and Ir) and Re. HSEs are elements that strongly prefer the metallic phase in comparison to silicate phases, and therefore are important tracers for differentiation events in Earth's history during the formation of the metallic core. However, our knowledge of gold abundance and its distribution in the mantle is limited. In this study, Au has been analysed along with major- and trace-elements in sulfides in fragments of the Earth's mantle (xenoliths) brought to the Earth's surface in basaltic magmas that formed Quaternary volcanoes in the Svalbard Archipelago (between north Norway and the North Pole). Combining these data with silicate data allows us to build a model of Au behaviour during mantle processes.

Analyses of the trace elements in clinopyroxene grains from the peridotite (olivine-rich) mantle xenoliths reveals there are three different types as seen by the contrasting patterns in Figure 1. There is an increase in the light rare-earth (LREE) elements progressing from Group I to Group II to Group III. This type of change in pattern can be due to the changing composition of fluids infiltrating the mantle rocks. These fluids change the composition of minerals in these rocks (metasomatism), and also progressively change their own composition through two-way reaction, a process similar to that in a chromatographic column. The strong enrichment in LREEs and Sr coupled is accompanied by a decrease in Ti and suggests that the metasomatic agent was a carbonatitic melt or fluid.

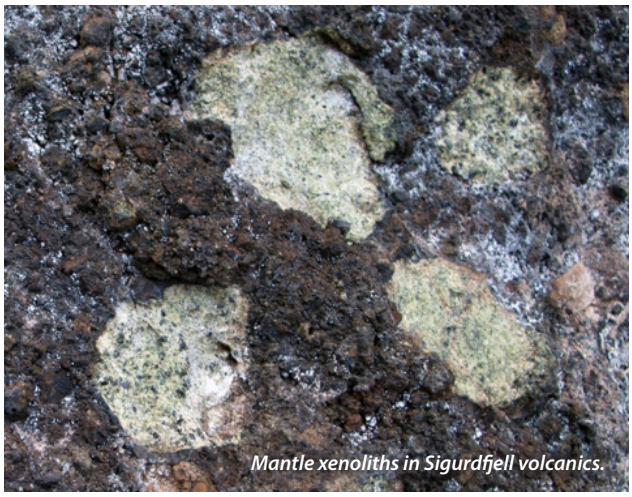

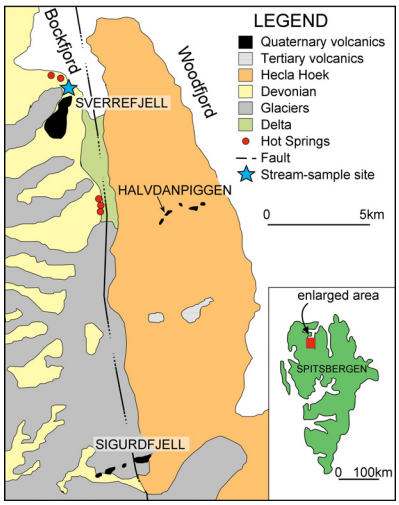

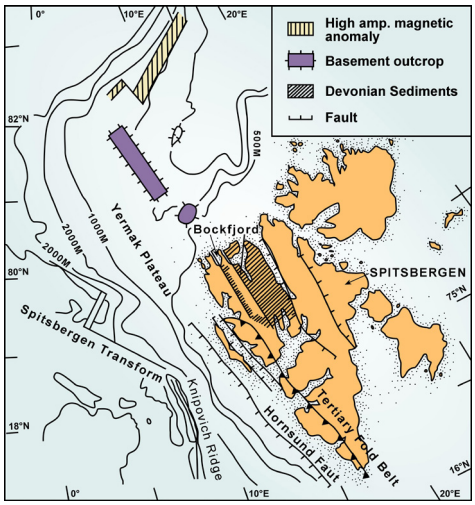

Locality maps: left shows the sample localities, right shows the broader geological context of Svalbard.

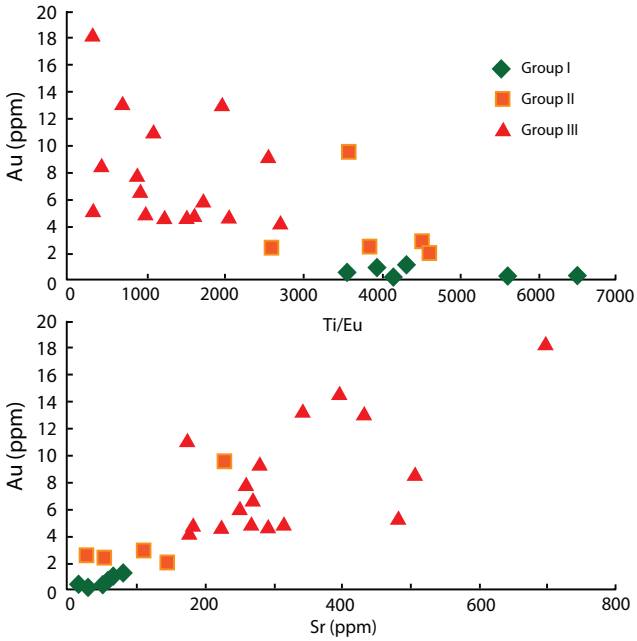

Figure 1. Svalbard metasomatism increase La/Yb and Sr, while decreasing Ti/Eu ratios – a typical signature of carbonatitic metasomatism.

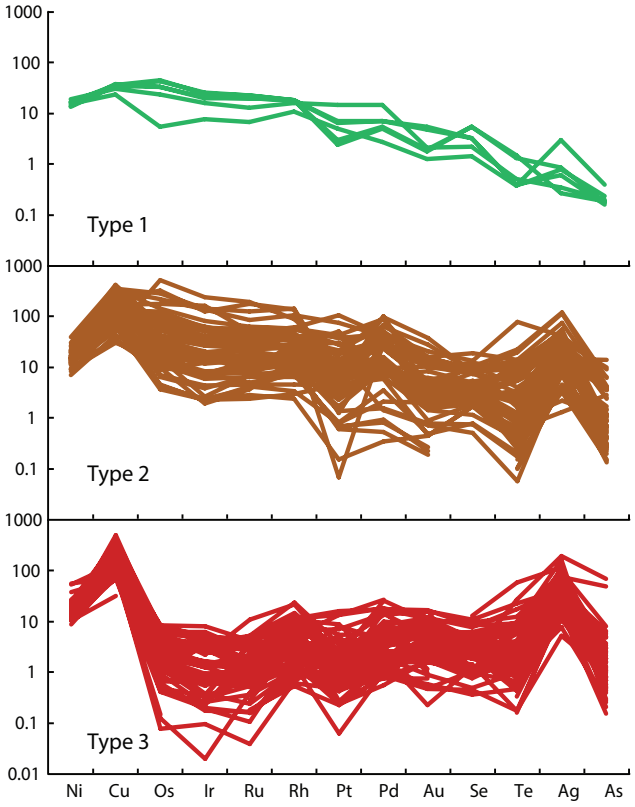

Figure 2. Trace element characteristics of sulfides in Svalbard xenoliths.

Sulfide grains are the residence site for platinum group elements in mantle rocks. Three distinct patterns for PGEs have been observed in the Svalbard sulfides (Fig. 2). The PGEs can be divided into two groups: the PPGEs (Pt, Pd and Rh), which are incompatible and therefore removed during melting, and the IPGEs (Ir, Os and Ru), which are left behind with the residue during mantle melting. Type 1 sulfides are residual sulfides, with average (PPGE/IPGE)n = 0.53; Type 3 sulfides were introduced during metasomatism with average (PPGE/IPGE)n = 3.61; Type 2 sulfides fall in between with average (PPGE/IPGE)n = 0.80. The Type 2 sulfides represent a mixing between a residual sulfide and the metasomatic agent that introduced the Type 3 sulfides. The gold content across all three sulfide types is remarkably consistent, and overlaps completely between the three types of sulfides (average AuType1 = 0.41±0.25 ppm; AuType2 = 0.84±1.00 ppm; AuType3 = 0.69±0.58 ppm). This is within the range of peridotite hosted sulfides from south-eastern Australia, and south-eastern China (Fig. 3). The sulfide types are not limited to any one group, but the relative amount of each sulfide type does change, with Group III having more Type 3 sulfides, while the Groups I and II samples are dominated by Type 2 sulfides. The Group I samples are the only ones that contain any Type 1 sulfides.

The sulfide chemistry broadly reflects changes in the metasomatic history defined by the clinopyroxene. There is also an increase in the absolute abundance of sulfides with increasing metasomatism, with a corresponding decrease in the average Au content in the sulfides. This indicates the gold was scavenged locally rather than introduced from an external source. However, there is a lack of correlation between La/Yb in clinopyroxene and Au/Ir or Pd/Ir in sulfides. This is typical for other sample sets (e.g. south-eastern China, south-eastern Australia, and Kaapvaal Craton), indicating a global decoupling sulfide and silicate metasomatism (Fig. 3).

This project is part of CCFS Themes 2 and 3, Earth Evolution and Earth Today, and contributes to understanding Earth's Fluid Fluxes.

Contacts: Ed Saunders, Norman Pearson, Sue O'Reilly, Bill Griffin
Funded by: CCFS Foundation Program 1, APA, MQPGRF

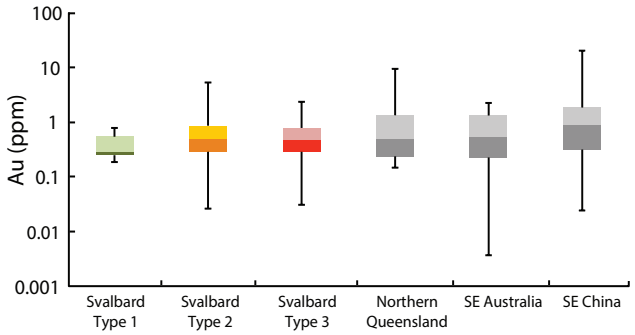

Figure 3. Gold content in Svalbard sulfides compared to other xenolith suites. Metasomatism has little effect on the average Au concentration within mantle sulfides.

Nickel sulfide deposits in the deep Earth - The future of mining?

Figure 1. Field work in the Ivrea-Verbano Zone of Northwest Italy.

Many world-class magmatic nickel sulfide deposits formed close to Earth's surface and there are probably few easily accessible deposits left to be discovered. The opening of new "exploration space" is essential to guarantee a steady metal supply in the future. One promising approach involves exploration for magmatic nickel-copper sulfide deposits that are hosted in the deep lithosphere, possibly at the crust-mantle boundary. However, very little is known about their genesis because such deep-seated deposits are rarely obducted to near-surface levels. The first step in developing exploration models for metal deposits in the deep Earth is to understand how metals are transported and concentrated at sub-crustal levels: an issue addressed by the CCFS project 'Metal Sources and Transport Mechanisms in the Deep Lithosphere'.

This project includes two detailed case studies: the first is the Ivrea-Verbano Zone of Italy (Fig. 1) and the second is the Archaean Thrym Complex of southeastern Greenland: these are among the few known areas where magmatic nickel-copper sulfide deposits occur in rocks that came from the deep lithosphere. How many more are there? Nobody knows, because the current dominant ore-genesis models, are largely focused on terrains that contain rocks from the upper crust while neglecting areas with outcropping deep lithosphere.

The formation of magmatic nickel-copper sulfide deposits in rocks from the deep lithosphere appears to be directly linked to the occurrence of metasomatic fluids, which are most evident in the Ivrea-Verbano Zone as a series of peridotitic, pipe-like intrusions up to 300 metres in diameter. These pipes contain water-rich magmatic minerals, such as phlogopite and amphibole, which are closely associated with nickel, copper and iron sulfides (Fig. 2). These minerals have isotopic signatures indicative of a mantle source, so the Ivrea-Verbano Zone is an excellent natural laboratory to investigate the role of fluids in the transport and concentration of metals in the deep Earth.

Trace-element data (LA-ICPMS) for amphibole and phlogopite from several pipes in the Ivrea-Verbano Zone suggest that juvenile, carbonate-rich hydrous fluids played an important role in the genesis of the pipes. The metasomatic fluid carried nickel, iron and copper and caused the parental rock to partially melt. The resulting melts evolved into the volatile-rich, pipe-like intrusions that reached sulfide-saturation during their emplacement, forming the sulfide deposits that we see today.

The Thrym Complex of southeastern Greenland is part of the North Atlantic Craton and is made up of migmatitic orthogneiss, narrow bands of mafic granulite, ultramafic and possible meta-sedimentary rocks, and alkaline-carbonatitic intrusive rocks. The narrow bands of mafic granulite are interpreted as mafic volcanic or gabbroic rocks from the lower crust. Ni-Cu-sulfide mineralisation can be found in the mafic granulite units and is most significant next to ultramafic bodies locally found within the mafic granulite bands. Sulfide mineralisation is also hosted in shear zones associated with the later part of the 2790-2700 Ma Skjoldungen Orogeny. The mafic and ultramafic rocks that host the mineralisation all show evidence for interaction with an incompatible-element-rich fluid at some point in their evolution.

This project is part of CCFS Theme 3, Earth Today and contributes to understanding Earth's Fluid Fluxes.

Contacts: Marek Locmelis, Marco Fiorentini
Funded by: CCFS Foundation Program 2a

Figure 2. Spectacular outcrops in Southeast Greenland.

Pink diamonds spotlight deep deformation

Deformation in the mantle is the cause of brown and pink colours in diamonds: brown diamonds are worth relatively little, while pink ones can bring very high prices indeed. The colour of brown and pink diamonds commonly is confined within {111} lamellae created during deformation, and this spatial phenomenon is commonly referred to in the gem trade as graining. Despite this inherent relationship between plastic deformation and pink colour in diamonds, the exact internal crystal defect responsible for the colour absorption has not yet been identified.

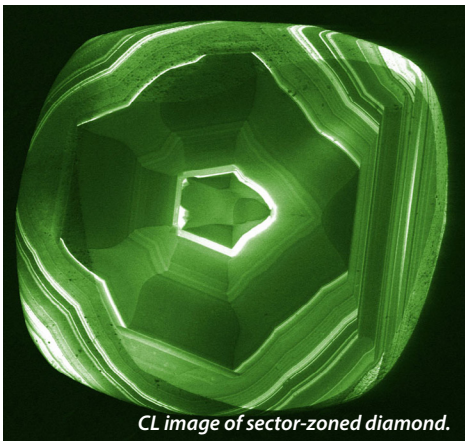
CL image of sector-zoned diamond.

Recent studies (*CCFS publication #211*) have identified the {111} deformation lamellae in natural pink and experimentally-deformed brown diamonds as micro-twins. However, we cannot assume that all brown and pink diamonds will contain micro-twins.

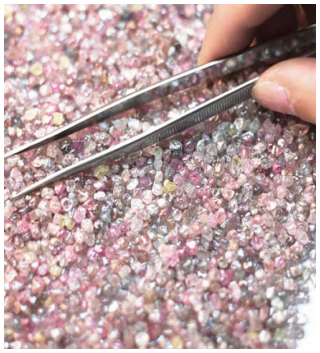

The Argyle diamond mine in Australia produces 90 to 95% of the world's pink diamonds. However, a recent study has shown that pink diamonds from Argyle have characteristics very different from the even rarer pink diamonds from other localities (Gaillou et al., 2010; *Diamond & Related Materials*). We have investigated these two groups of pink diamonds to better understand their differences and the processes of deformation in diamonds deep within the Earth.

Scanning electron microscope (SEM)-based electron backscatter diffraction (EBSD) is an ideal tool for investigating the deformation of diamonds and identifying the presence of micro-twins. We have used this technique available in the CCFS Geochemical Analysis Unit at Macquarie to study a set of diamonds provided by the Diamond Trading Company. Combining EBSD with cathodoluminescence (CL) imaging, another SEM-based technique, we have confirmed that pink diamonds from Argyle mine have a very unusual growth pattern, while pink diamonds from other localities have previously described growth patterns, where the {111} deformation lamellae cut across the growth stratigraphy (Fig. 1). Our work has confirmed that these {111} deformation lamellae are micro-twins, and that these features are not observed in the pink diamonds from Argyle. Work is ongoing to fully understand the mechanism by which the micro-twins form and what they tell us about the deformation environment experienced by the diamonds and their subsequent history deep within the Earth.


The Argyle Diamond Mine.

This project is part of CCFS Theme 2, Earth Evolution, and contributes to understanding Earth's Fluid Fluxes.

Contacts: Dan Howell, Bill Griffin
Funded by: CCFS Foundation Program 8

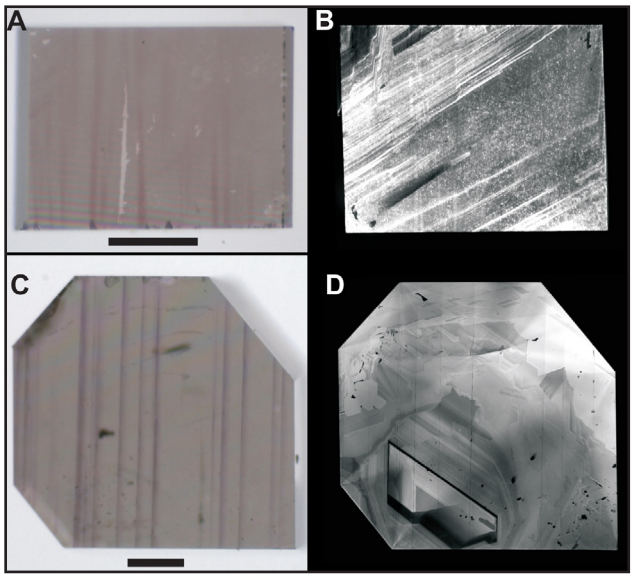

Figure 1. Images of two different pink diamonds. Images A & B are of an Arglye pink diamond, under plane light and CL respectively. The pink colour is less restricted to the {111} lamellae, and in the CL image the colour is very grained and does not correlate clearly with the {111} lamellae. Images C & D are from a pink diamond from South Africa. The plane light photo (C) shows the pink colour is very clearly retained in the {111} lamellae while the bulk of the diamond is colourless. These lamellae, shown to be micro-twins by EBSD analysis, are clearly picked out in the CL image (D), cross cutting the primary growth stratigraphy of the diamond. Scale bars represent 0.5mm.

Mechanisms of moving glaciers and ice sheets

Interpretation and prediction of past and future behaviour of polar and glacial ice is a major challenge, especially in view of changing climate. We performed unique deformation experiments to advance our knowledge of the effects of temperature changes and deformation rates on the flow properties of ice. In-depth knowledge of these properties is essential in order to develop reliable climate models incorporating the effects of polar and glacial ice mass flow and their reduction through time.

The team used a novel, world-first technique to investigate the deformation of ice. Heavy-water ice (D_2O) was used as a direct analogue for natural-water ice (H_2O). The use of heavy-water ice offers the unique opportunity to utilise neutron diffraction analysis in order to simultaneously monitor the flow properties, microstructure and orientation properties of ice. Laboratory grown polycrystalline samples were shortened up to 40% at variable temperatures and at three different constant deformation rates. Results show that ice exhibits a highly dynamic deformation behaviour. With deformation grain orientations change rapidly and distinctly. The processes that govern the flow properties of ice are changing with increasing temperature and amount of deformation. The competition of these processes is highly dynamic but predictable and this competition defines ice dynamics and needs to be incorporated in ice mass modelling.

Within this ongoing project the research team will expand the analysis to so called "dirty" ice, ice which is mixed with rock powder. The behaviour of "dirty" ice is not well understood, despite it's growing importance as ice masses become more and more rock powder laden in responce to climate change.

This project is relevant to CCFS theme 3, Earth Today and contributes to understanding Earth's Fluid Fluxes.

Contact: Sandra Piazolo
Funded by: ARC Furture Fellowship, Bragg Institute, ANSTO Lucas Heights

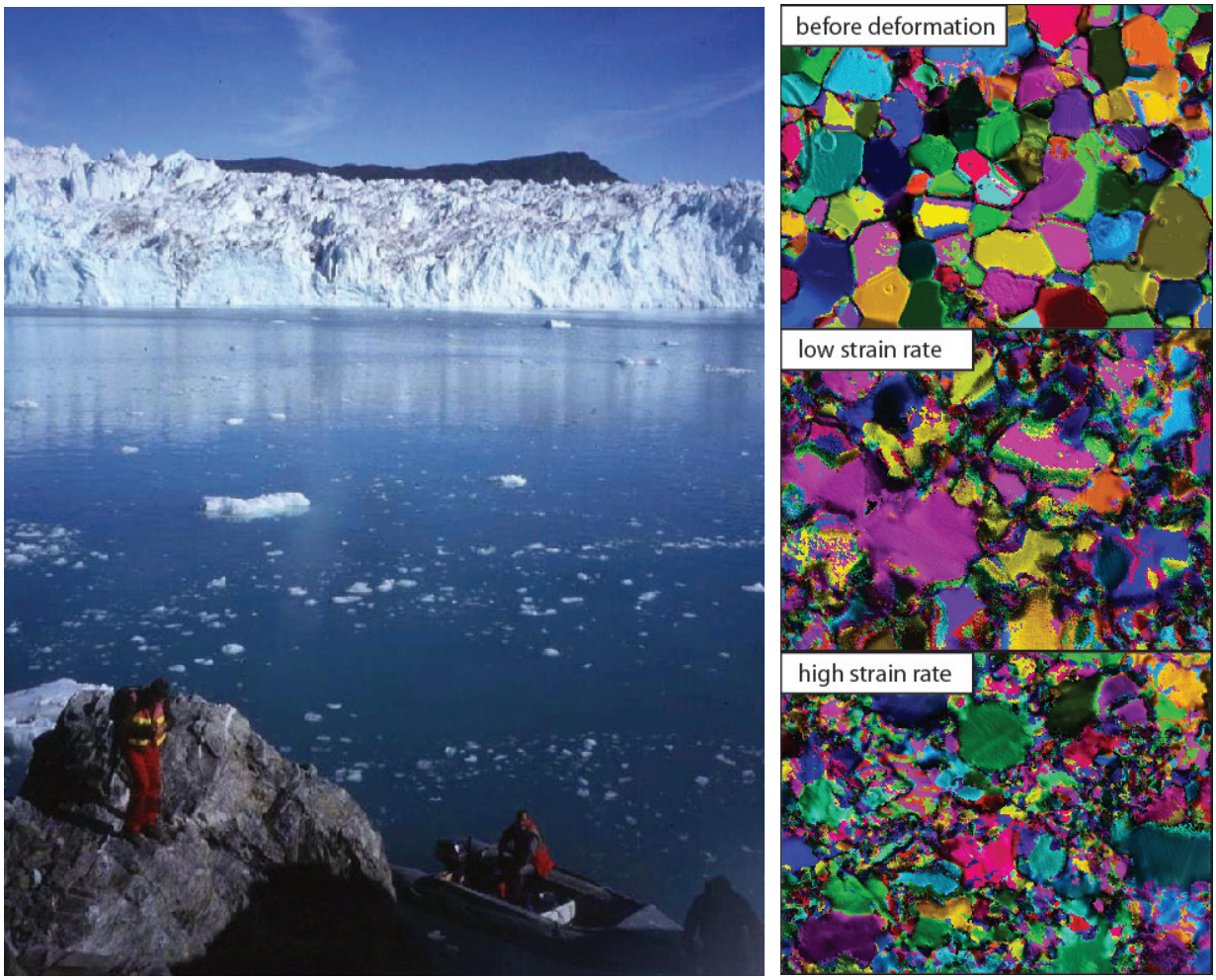

Figure 1. (left) Studying a rapidly flowing glacier which drains the Greenland ice cap, West Greenland. The rapid flow is a direct effect of elevated temperatures. Understanding the underlying principles of ice mass flow is essential for the prediction of climate change effects. (right) Experimental ice microstructures before deformation (top), after 10% deformation at low strain rates (middle) and high strain rates (bottom); optical micrographs where different colours signify different orientations, width of image is 4.8 mm.

Research highlights 2013

Contents

The GLAMour of mineral exploration

Giant magma-related ore systems are prime targets for modern mineral exploration – but how do they form? The Global Lithospheric Architecture Mapping (GLAM) project undertaken with industry collaboration has delivered an integrated model for more efficient global targeting of some key magma-related ore deposits. The magmas responsible for several types of ore deposit must pass through the stagnant subcontinental lithospheric mantle (SCLM) on their way to the surface - so how much control does the SCLM exert on the formation and localisation of the ores? GLAM has demonstrated that the 3D architecture of the SCLM influences the emplacement and fertility of such magmas. The GLAM outcomes to date are summarised in an invited article in Nature Geoscience (*CCFS Publication #207*), where we present evidence that the structure and evolution of the SCLM is directly relevant to the genesis and localisation of several types of major ore deposits, including diamond, Ni-Cu-(PGE), PGE and (Cu-)Au deposits.

Primary diamond deposits occur in dikes and pipes of kimberlites or lamproites, generated by low-volume melting; they pick up diamonds from the deep SCLM (>150 km) during their eruption. Blocks of cratonic SCLM can now be robustly identified in seismic tomography (e.g. *CCFS Publication #334* and references therein) and magnetotelluric (MT) surveys as volumes with high seismic velocity and high electrical resistivity. On the large scale (Fig. 1a), kimberlites are concentrated near the edges of cratonic blocks. High-resolution tomography (Fig. 1b) shows an even more obvious picture; most kimberlites cluster around high-velocity domains in the deep SCLM. These patterns reflect the geochemical requirements for diamond formation, and the structural requirements for magma emplacement. Diamond formation requires the metasomatic introduction of carbon into the depleted SCLM, typically accompanied by Ca, Al, K, Na and Fe, and such refertilised zones have lower seismic *cont...*

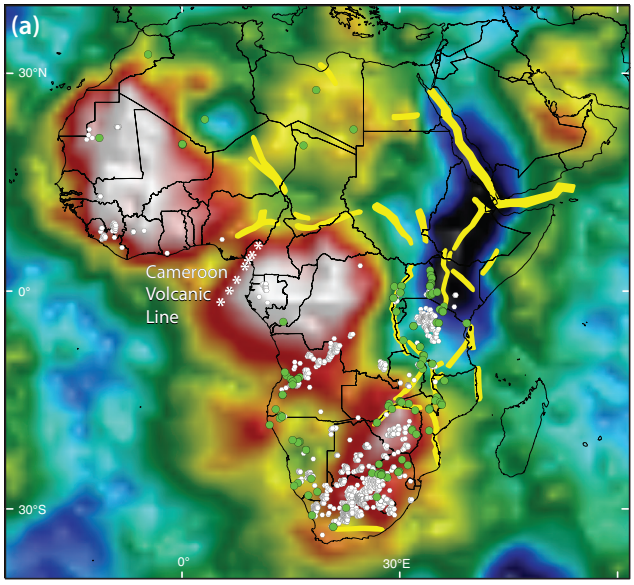

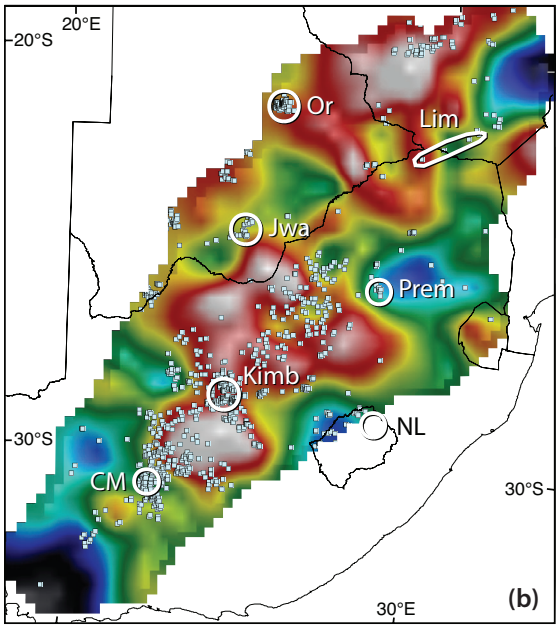

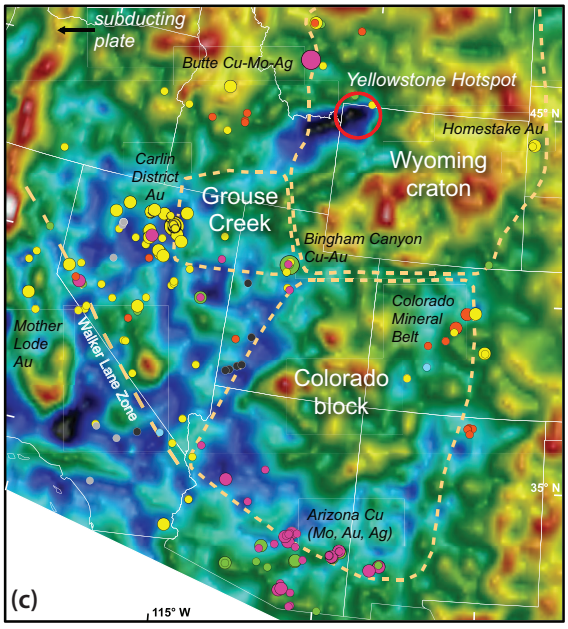

Figure 1. (Full references and sources given in Griffin et al., 2013, Nature Geoscience: CCFS Publication #207) Vs tomography (100-150 km) of the lithospheric mantle. Red to white colours indicate high Vs; blue colours low Vs.

(a) Africa, showing distribution of low-volume magmatic rocks along the boundaries of high-velocity blocks. Young rift basins shown in yellow.

(b) Detailed seismic tomography over part of the Kaapvaal craton, showing kimberlites around the margins of high-velocity volumes. Major kimberlite provinces: Kimb, Kimberley district; NL, Northern Lesotho; Prem, Premier; Jwa, Jwaneng district; Or, Orapa district; Lim, Limpopo Belt, including kimberlites such as Venetia.

(c) Vp tomography (90 km depth, of western USA, showing major (magmatic-) hydrothermal ore deposits by size (largest, supergiant; medium, giants; smallest, majors) and dominant metals (yellow, Au; green, Cu-Au; orange, Mo; light blue, REE; light grey, W(-Sn); dark grey, Fe). Significant lithospheric blocks, defined at sub-crustal depths from multi-disciplinary data, are outlined. Note deposits concentrate along prominent lithospheric structures, particularly in lower-velocity regions or on the flanks of highs, where lower velocities reflect refertilisation of the SCLM and/or higher temperature.

velocities. The weak zones on the margins of cratonic blocks, and in fractures within these blocks, provided channels for the C-bearing fluids, and later controlled the emplacement of the kimberlites.

Major Ni-Cu-(PGE) sulfide deposits are genetically linked to Large Igneous Provinces and komatiites, and the accumulation of metal-rich immiscible sulfide melts in mafic or ultramafic magmas (some likely scavenged from sulfides in lithospheric mantle e.g. *Zhang et al., E Sci Rev* 2008). The required high-T, low-P melting occurs only in areas of relatively thin lithosphere, and melts access the crust via major faults. This combination of factors is typical of tectonically active craton margins, where most large Ni-Cu-(PGE) deposits are found.

Ultramafic (High-MgO; generally komatiitic to picritic lavas and intrusions) magmas erupt at the surface where plume melting was focused by a transition from thick to thinner SCLM. High-MgO deposits are commonly found in pericratonic basins, which contain the S-rich sediments essential to S-saturation.

Low-MgO mafic (generally gabbro/norite intrusions) systems are also associated with trans-lithospheric faults at cratonic margins, but not with pericratonic basins. They are intrusion-hosted, and occur where magma ascent was hindered by thick crust or a compressive tectonic environment, and melt fractionation and chemical interaction with the lithosphere are enhanced.

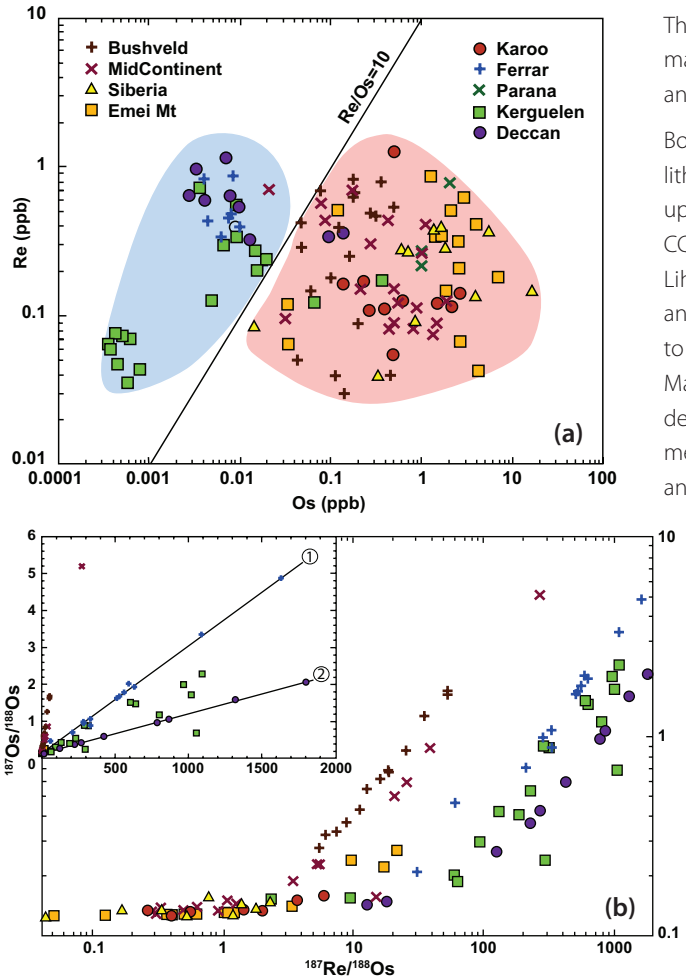

The structural role of the SCLM in focusing magma intrusion is clear, but its compositional role is less obvious. The orthodox view is that the SCLM contributes essentially nothing to magmas, and that most mantle magmas are equally endowed in Ni, Cu and PGEs, so the genesis of an ore deposit simply reflects local factors. However, melt modelling does not explain the high PGE levels in some magmas (e.g. Bushveld Complex), or the provinciality of PGE enrichment in both Ni-Cu-PGE and PGE reef deposits. Interestingly, Large Igneous Provinces and komatiites intruded into areas without (ancient) SCLM roots are not known to contain significant deposits.

"Fertile" (mineralised, continental) flood basalts show a distinctive high-Os signature (Fig. 2a) and our isotopic studies show that these LIPs have interacted with ancient metasomatised SCLM, with high Rb/Sr and low Sm/Nd and Re/Os. Several major LIPs yield Re-Os "isochrons" reflecting their eruption ages, with initial $^{187}Os/^{188}Os$ below that of the asthenospheric mantle, implying derivation of the Os from older SCLM (Fig. 2b). The SCLM thus may be a critical component in the genesis of Bushveld-type PGE- bearing intrusions.

There is strong evidence that SCLM metasomatised by hydrous melts/fluids above subducting slabs is essential in producing gold-rich (magmatic-) hydrothermal deposits, including Cu-Au porphyries. In seismic images these (and other magma-related) deposits coincide with medium- and lower- velocity SCLM (Fig. 1c). This suggests a model embracing three common features: a mantle source region carrying (Cu-) Au, trans-lithospheric faults, and a tectonic±thermal trigger.

Both the asthenosphere (ca 1ppb Au) and non-refertilised lithospheric mantle are depleted in Au relative to refertilised upper mantle, such as the Lanzo and Ronda peridotite massifs. CCFS research has shown that arc-related mantle near the giant Lihir gold deposit (Melanesia) is metasomatically enriched in Cu and Au, and SCLM xenoliths in China carry up to 14 ppb Au (up to 5 ppm Au in sulfide minerals; see *Research highlight p. 93*). Mantle gold enrichment can be related to trapping of low-degree melts; gold behaves as an incompatible element during melting. Even such metasomatised SCLM is relatively durable, and may store (Cu-)Au until a later melting event is triggered.

On balance, the evidence supports an important role for the SCLM in the genesis of some types of major ore deposits (Fig. 3). Lithospheric architecture controls the localisation of some types of ore deposits, and some types of magmas have picked up ore-forming components (e.g. diamonds,

Figure 2. Re-Os data for LIPs and other magmas
(a) Re and Os contents of mafic rocks from provinces with known Ni-Cu(-PGE) sulfide deposits (red field) and provinces lacking known deposits (blue field). (After Zhang et al, E. Sci Rev 2008) (b) $^{187}Re/^{188}Os$ vs $^{187}Os/^{188}Os$ in flood-basalt suites. Main figure, log-log scale; inset in linear scale. The "isochrons" in the inset correspond to (1) Ferrar dolerites; 65.6±0.3 Ma, intercept 0.12843 (γOs = 1.5±0.3), (2) Deccan Traps; 177±2 Ma, intercept 0.125±0.033 (γOs = -0.6±0.26).
Data: CCFS Publication #334, reference [30].

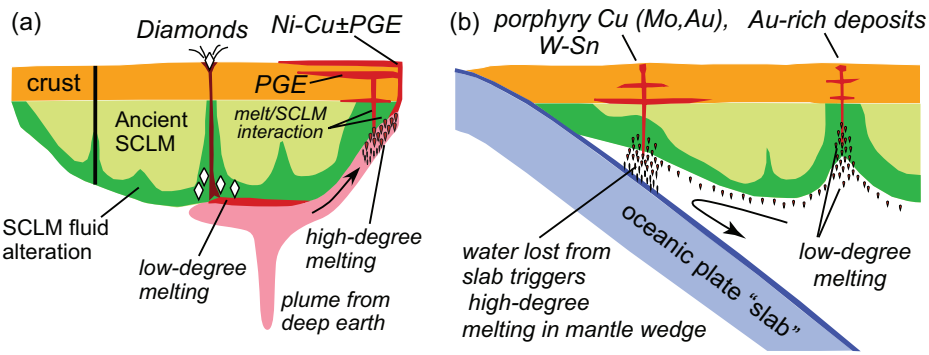

Figure 3. Interactions between magmas and the SCLM.
(a) Plume triggers kimberlite formation and flows to area of thinner SCLM where melting is focused. Variable interaction of melts with crust and SCLM influences Ni-Cu and PGE deposit genesis.
(b) Generalised convergent-margin setting. Au-poor magmatic-related deposits form from dominantly asthenospheric or crustal melts (e.g. Cu-rich or W-Sn porphyry, respectively). Low-degree melting of asthenosphere, particularly in retro-arc settings, can produce Au-rich metasomatic refertilisation of the SCLM. Subsequent melting (which may be much later) contributes Au to magmatic systems, forming deposits of porphyry Cu-Au, Epithermal Au, Iron Oxide Cu-Au, Intrusive-Related Orogenic Au, and possibly also Carlin-type Au and classic orogenic Au.

gold, PGEs) during their passage through the mantle lithosphere. A lithosphere-scale whole-system approach encompassing asthenospheric to crustal processes, with special attention to the structure, composition (fertility) and evolution of the SCLM, can produce better models for deposit genesis, and help build effective exploration models.

This project is part of all CCFS Themes 1, 2 and 3, Early Earth, Earth Evolution and Earth Today, and contributes to understanding Earth's Architecture and Fluid Fluxes.

Contacts: Bill Griffin, Graham Begg, Sue O'Reilly
Funded by: CCFS

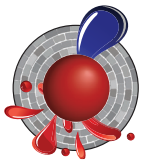

Youanmi seismic survey a milestone on the quest to unravel the Yilgarn's past

The Neoarchean Yilgarn Craton and the Proterozoic orogens around its margins are one of Earth's greatest mineral treasure troves, including iron, gold, copper and nickel deposits. Although the Yilgarn Craton is one of the best studied Archean cratons, its enormous size and limited outcrop make it hard to understand what controls the distribution of these vast resources and which geodynamic processes were involved the tectonic assembly of this part of the Australian continent.

In 2013, significant steps have been taken to address these outstanding questions, including the release of deep seismic reflection and MT surveys over the Youanmi, South Carnarvon, and Yilgarn Craton–Officer Basin–Musgrave Provinces, the holding of a CCFS project definition meeting, targeted field work in several locations in the Yilgarn Craton, and the planning and partial deployment of passive seismic arrays.

Three individual seismic lines (YU1, YU2 and YU3) and complementary magnetotelluric data were acquired across the northern Yilgarn Craton in 2010. Acquisition, processing and interpretation were managed by Geoscience Australia. The lines cross the northern part of the Yilgarn Craton from the Narryer Terrane in the northwest, across major bounding and internal structures of the Youanmi Terrane and into the Kalgoorlie Terrane of the Eastern Goldfields Superterrane. The north-western end of YU1 is east of the southern end of line CP3 from the 2010 Capricorn seismic survey. The two surveys are linked by the Southern Carnarvon (SC) Basin seismic survey, acquired by Geoscience Australia in 2011. The eastern end of YU2 crosses major structures on the western side of the Eastern Goldfields Superterrane that were also *cont...*

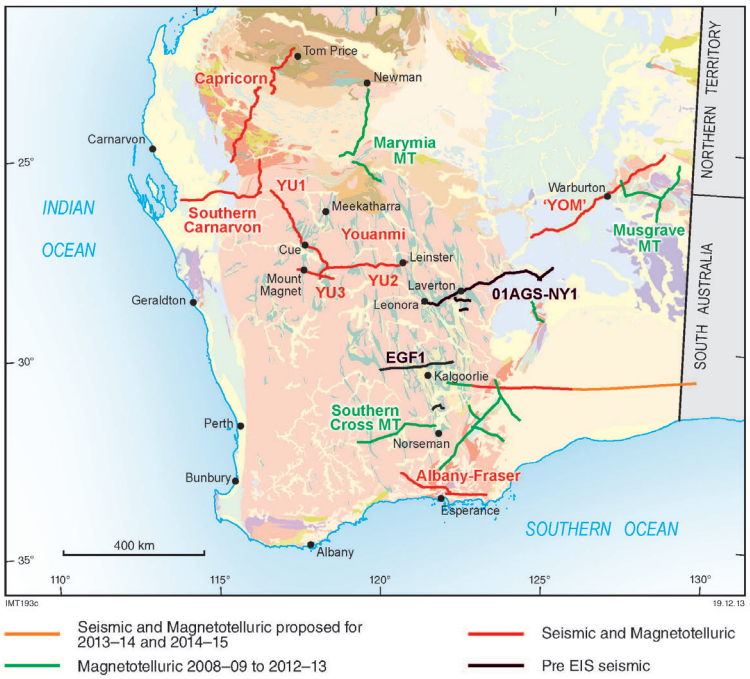

Figure 1. Location of seismic and magnetotelluric surveys funded through the Western Australian Government's Exploration Incentive Scheme (EIS).

Figure 2. Outcrop of Meeberrie gneiss in the Narryer Terrane.

imaged by the 2001 Geoscience Australia seismic line (01AGS-NY1), about 120 km to the southeast. The YU, SC and YOM surveys add to the existing network of deep-crustal seismic surveys, and have closed a data gap in the crustal structure of Western Australia, providing a c. 1800 km traverse across almost the entire southern half of Western Australia, from near the west coast to within about 80 km of the border with the Northern Territory.

Nd-isotope data suggest that the Youanmi Terrane has behaved as a coherent crustal block since at least 3000–2900 Ma ago. The Youanmi Terrane is bounded by crustal-scale fault zones that dip away from the nucleus, towards the west and northwest on the northwestern side, and towards the east on the eastern side. The accretion of the Eastern Goldfields Superterrane, which may be either an exotic terrane or an extended margin of the Youanmi Terrane, marked the amalgamation of the composite Yilgarn Craton by about 2655 Ma ago. The Narryer Terrane is generally interpreted to have accreted onto the Youanmi Terrane in the northwest, but further work may be required to better define the nature of the Narryer Terrane–Youanmi Terrane boundary.

In the CCFS Project-definition meeting held on 4 July 2013 at GSWA in Perth more than 20 scientists from within CCFS and collaborating institutions contributed to discussions on the direction of collaborative research on the lithospheric evolution and the related significant mineralisation of the Yilgarn Craton and its margins, specifically on geochemistry and geochronology, geodynamics and modelling, and lithosphere imaging.

It was agreed that to improve the geochemical and geochronological map of the Yilgarn Craton, U-Pb, Hf, and Nd isotope studies should be continued in the NE Yilgarn Craton, and extended to the SW Yilgarn Craton. To determine the relative roles of juvenile mantle and continental lithosphere in mafic/ultramafic rocks it was recommended to collect Os and Nd isotope data to develop a mantle-signature database that will supplement ongoing and future crustal isotopic mapping.

As a priority of geodynamics and modelling it was suggested that previously published geodynamic concepts that have been put forward for the Yilgarn Craton should be tested, starting with relatively well-described events such as aspects of the 2800–2600 Ma tectonic evolution in the eastern Yilgarn Craton.

A craton-scale 3D seismic passive-source deployment was proposed to improve lithospheric imaging. Passive-source techniques such as ambient- noise imaging and receiver-function CCP stacking have intermediate resolution in the crust compared with active-source studies, but unprecedented resolution in the cratonic lithosphere.

The success of the CCFS planning meeting is already evident, as some of the proposed ideas have influenced research proposals, while others have provided direction, focus and context to newly granted projects such as an ARC linkage project granted to the Australian National University and GSWA in 2013. This will fund a three-year passive-array deployment across the south-eastern margin of the Yilgarn. The 2014 deployment of a passive array within the Distal Footprint Science Investment and Education Fund project follows a similar approach for the Capricorn Orogen on the Yilgarn Craton's northern margin.

This project is part of CCFS Themes 1, 2 and 3, Early Earth, Earth Evolution and Earth Today, and contributes to understanding Earth's Architecture.

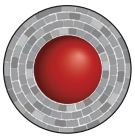

Contacts: Klaus Gessner, Ruth Murdie (GSWA), Huaiyu Yuan
Funded by: CCFS Foundation Program 10a, Western Australian Government's Royalties for Regions Exploration Incentive Scheme (EIS), Australian Research Council, SIEF

Publication: Youanmi and Southern Carnarvon seismic and magnetotelluric (MT) workshop, February 2013 (preliminary edition) on DigitalPaper: *http://geodocs.dmp.wa.gov.au/search.jsp?cabinetId=1101&Combined=N12BF*

Global komatiite sulfur dioxide degassing and the irreversible change of the late Archean atmosphere

This study has identified sulfur dioxide degassing from komatiite volcanoes as a single process that explains two major heretofore unrelated conundrums about the Archean earth system: (1) why are komatiite-hosted nickel deposits so well endowed? and; (2) why did the mass-independent record of S isotopes suddenly blossom 200 million years before the Great Oxidation Event? Although in hindsight sulfur dioxide degassing is an obvious process to call on, it has never before been proposed. This is because of disciplinary biases. First, the community studying komatiite-hosted nickel deposits focuses on how metals get into such systems, not how sulfur leaves. Second, the community studying mass-independent S isotopes focuses on sedimentary rocks, where signals are assumed to be larger, rather than igneous ones, where signals are assumed to be negligible. It took a strongly interdisciplinary approach to overcome these biases.

Komatiites are the hottest lavas that ever flowed on Earth. Most komatiite lavas erupted at temperatures of 1400-1600 °C as large submarine lava fields, rising from depths of >100 km in the Archean mantle. Upon emplacement, channelised lava flows and subvolcanic intrusions were sulfide-undersaturated and thermo-mechanically eroded their substrates. Through this process, komatiites incorporated sulfur (S) from volcanogenic exhalative sulfide lenses as well as sulfide-rich sediments that occurred close to volcanic vents, inducing the formation of an immiscible sulfide liquid. Elements such as nickel (Ni), copper (Cu) and the platinum group elements (PGEs) originally present in the komatiite magma strongly concentrated into the immiscible sulfide liquid, due to their high affinity for sulfidic and metallic phases. The progressive accumulation of immiscible sulfide liquid at the bottom of lava channels enabled prolonged partitioning of metals into the sulfide liquid from fresh parcels of komatiite magma, forming sulfide metal concentrations of potentially economic interest. However, this model does not explain the extreme variability in metal contents observed among and within different mineralised komatiites.

In this study we used sulfur isotope measurements on sulfides from komatiites and local volcanogenic and sedimentary country rocks to show that sulfur degassing was a critical component of the volcanic process. Data from variably mineralised komatiite units in the north Eastern Goldfields, Western Australia, indicate pervasive (>90%) sulfur loss from sulfide-saturated komatiite lavas, dominantly in the form of SO_2 gas. Rapid sulfur degassing associated with such voluminous and cataclysmic eruptions was most likely a contributing factor for economic mineralisation.

In fact, the total mass of Ni-bearing silicate melt that equilibrates with a sulfide liquid is thought to control the tenor of the resulting nickel-sulfide mineralisation. The high Ni tenors of mineralised komatiites seem to verify this proposal, since geological evidence indicates that large amounts of komatiite magmas interacted with relatively small sulfide reservoirs, leading to estimated silicate-sulfide mass ratios (R factors) of ~100-200. However, ~10- to 100-fold enrichments of Ni, Cu, and PGEs in the sulfide liquid are also a natural consequence of the sulfur loss process identified here. We suggest therefore that variable amounts of sulfur degassing may act in concert with elevated R factors to produce the wide range of nickel tenors observed across different komatiite-hosted nickel deposits.

The observed dramatic bloom in the sulfur mass-independent fractionation (S-MIF) record from sedimentary sulfides at ~2.7 billion years ago appears to reflect enhanced input of volcanic SO_2 to the atmosphere. However, the currently proposed volcanic sources of this SO_2 do not begin to dominate the global record until ~200 million years later. Our study identifies a new volcanic pulse of sulfur dioxide that fundamentally restructured the Earth's sulfur cycle in the late Archean and provides a solid geologically based hypothesis for the bloom in S-MIF at 2.7 Ga that contrasts with model-based suggestions of changing CH_4/O_2 ratios at this time. In fact, although komatiite volcanism occurred throughout much of the Archean eon, associated SO_2 degassing was probably maximised during the unique peak in komatiite-hosted nickel-sulfide mineralisation at ~2.7 billion years ago. Given the magnitude and brevity of degassing events associated with komatiite volcanism, we suggest that much of the SO_2 must have escaped direct sequestration in the marine environment, and, as recorded in the S-MIF archive, fundamentally altered the chemistry of the late Archean atmosphere.

This project is part of CCFS Theme 1, Early Earth, and contributes to understanding Earth's Fluid Fluxes.

Contact: Marco Fiorentini
Funded by: CCFS Foundation Program 5

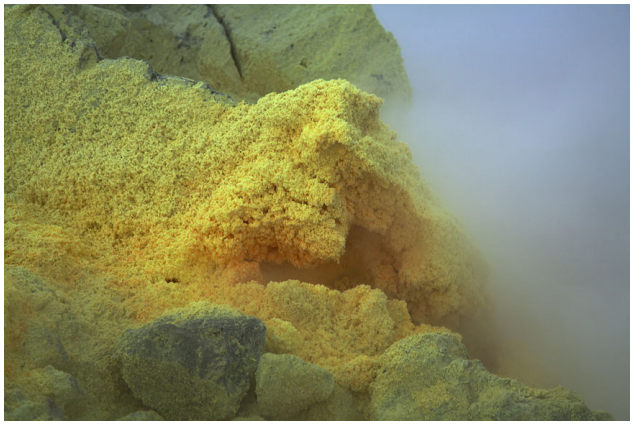

A degassing sulfur cone.

The Earth's thrumming uncovers the northward trek of the Tibetan Plateau

Tibet is a natural Earth laboratory where we can study the dynamics of continental deformation. The growth and maintenance of the enormously thick crust and high topography of this plateau are best explained by the channel flow model, which postulates the existence of a weak layer in the crust beneath the Plateau. Driven by the topographic loading, this weak layer flows to the surrounding areas of the Plateau where the crust is thinner. Geophysical features, including low velocity zones (LVZs) and highly conductive layers in southeastern Tibet, support this model. However, the distribution of LVZs in northern Tibet, which could be used to test the channel flow model, is unknown.

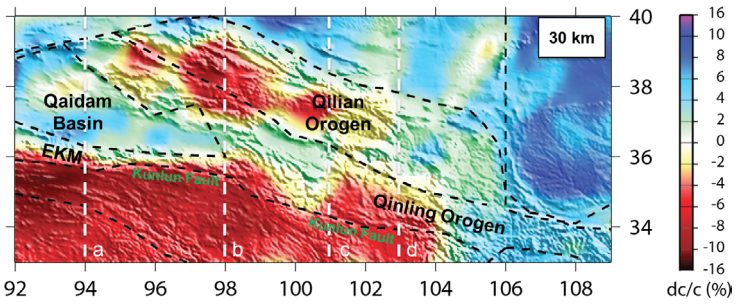

Figure 1. Vsv perturbation map at a depth of 30 km. The dashed lines indicate the four cross sections in Figure 2. EKM: East Kunlun Mountains.

By using ambient noise tomography and probabilistic inversion methods, we have constructed a 3D Vsv model of the north Tibetan crust with a resolution of ~50 km. Our 3D model (Fig. 1, 2) reveals strong LVZs at the middle crust between 20 and 40 km across northern Tibet. The LVZs show significant west-east variations along the Kunlun Fault compared to previous ambient noise tomography. In the western part (Fig. 2 left), LVZs are confined to the regions of the Kunlun Fault and the eastern Kunlun Mountains but are not observed beneath the Qaidam Basin. In the eastern part, beyond the eastern boundary of the Qaidam Basin (Fig. 2 right), LVZs extend and penetrate at least 100 km northward into the east Kunlun and Qinling Orogens. The strong contrast in the distribution of LVZs between the western and eastern parts of the study region mainly results from the distinct tectonic units neighboring northern Tibet. In the west, the strong crust of the Qaidam Basin blocks the penetration of LVZs but the predicted weaker crust in the Qinling Mountains allows the flow of LVZs.

Combined with the observations of strong radial anisotropy in the areas with strong LVZs, the existence of highly conductive layers and the high heat flow in northern Tibet, our Vsv model indicates that crustal channel flow may be occurring in northern Tibet and be responsible for the northward and outward expansion of the Tibetan Plateau. In addition to indicating that crustal flows do exist in northeastern Tibet, the distribution of LVZs from our research also defines the extent of the crustal flow, which is penetrating ~ 100 km beyond the Kunlun fault into the West Qinling Orogen.

This project is part of CCFS Theme 3, Earth Today, and contributes to understanding Earth's Architecture.

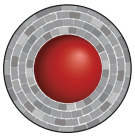

Contacts: Chengxin Jiang, Yingjie Yang

Funded by: ARC Discovery Project DP120103673, iMQRES Scholarship

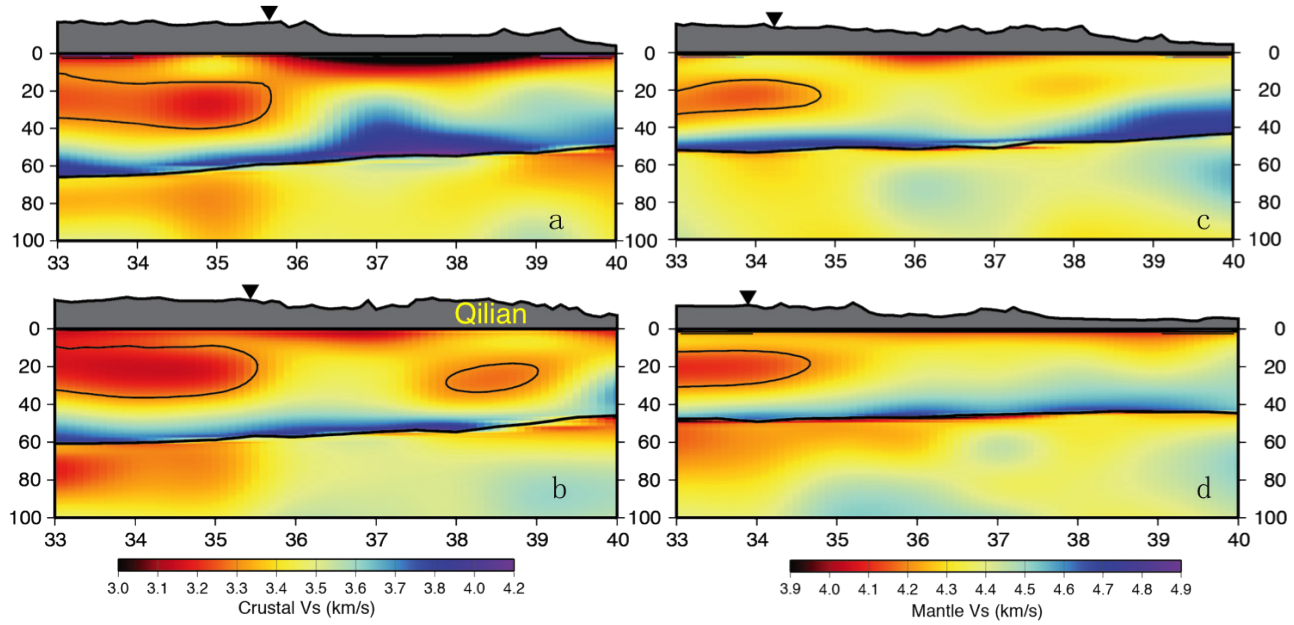

Figure 2. Four cross sections show the distribution of LVZs in north Tibet. All sections are plotted with absolute Vs values.

Microbial feasting on the early Earth

Tiny 1,900 million-year-old fossils from rocks around Lake Superior in Canada give the first ever snapshot of organisms eating each other and suggest what the ancient Earth would have smelled like.

Figure 1. Close up of ~1900 million year old Gunflint chert. The fossils are found in the black zones. Field of view is about 1 m.

While it was once thought that the earliest forms of life were based on photosynthesis from sunlight, much recent work on molecular evolution has shown that the most primitive life forms probably made do without light. Instead of carbon dioxide, such forms are thought to have broken down previously-formed organic matter, in the manner of feeding called 'heterotrophy'.

It has been more difficult, however, to find ancient fossil evidence for this heterotrophic mode of feeding. Our new research (*CCFS publication #321*) provides both physical and chemical clues to primitive heterotrophy in the ~1900 million year old Gunflint chert (Fig. 1), from the northern shore of Lake Superior.

We examined microscopic fossils (3-15 µm in diameter) from the Gunflint chert with a battery of high-spatial-resolution techniques including nano-scale secondary ion mass spectrometry (NanoSIMS), transmission electron microscopy (TEM) and focused-ion-beam milling combined with scanning electron microscopy (FIB-SEM). We found that one species of microfossil – a tubular form thought to be the outer sheath of a cyanobacterium called Gunflintia – was more perforated after death than other kinds, consistent with them having been eaten by other bacteria. Indeed, in some places, many of the tiny fossils had been partially or entirely replaced with pyrite (FeS_2) resulting from the activities of heterotrophic sulfate-reducing bacteria. We also found that these Gunflintia microfossils carried clusters of even smaller (~1 µm diameter) spherical and rod-shaped bacteria that were seemingly in the process of consuming their hosts (Fig. 2).

Comparable processes of heterotrophic consumption can still be seen going on today. Indeed they can often be detected by the whiffs they give off – because they give rise to the rotten-egg smell of hydrogen sulfide. Recent geochemical analyses have shown that such sulfur-based activities of bacteria probably can be traced back to 3500 million years or so (as we reported in *Nature Geoscience* in 2011). While the Gunflint fossils are only about half as old, they confirm that such bacteria were indeed flourishing by 1900 million years ago. This work also shows that they were also highly particular about what they chose to eat, appearing to prefer to snack on Gunflintia as a 'tasty morsel' in preference to another bacterium (Huroniospora).

This project is part of CCFS Theme 1, Early Earth, and contributes to understanding Earth's Fluid Fluxes.

Contacts: David Wacey, Mark Barley
Funded by: CCFS Foundation Program 5

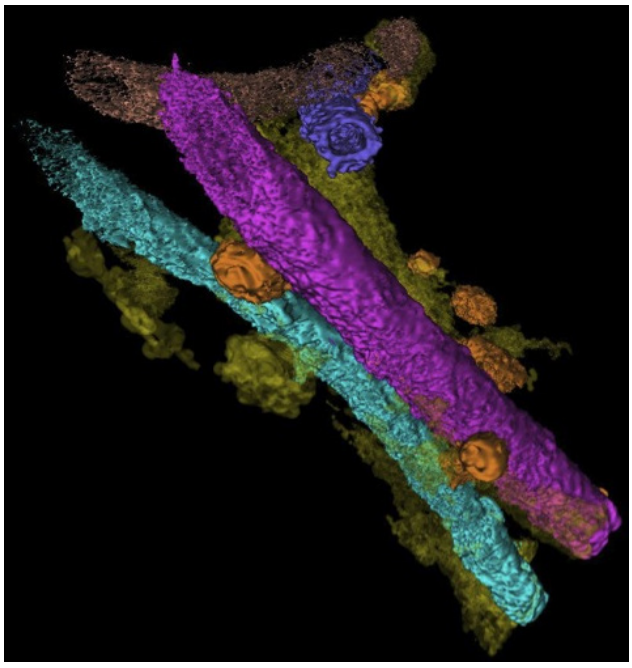

Figure 2. 3D reconstruction of tubular Gunflintia fossils being consumed by heterotrophic bacteria (orange spheres and rod-shapes that are about 1 µm in diameter).

Size matters for ion mobility in deformed Ni-sulfides

Most of the komatiite-hosted sulfide deposits in the Yilgarn craton have experienced some metamorphism and deformation. The signature of such events is well documented for the silicate phases, but what happens in the sulfides is often overlooked. This study focused on the Ni sulfides from three komatiite-hosted deposits: Silver Swan (Black Swan Ni-deposit, Kalgoorlie terrane), Perseverance (Agnew-Wiluna greenstone belt) and Flying Fox (Forrestania greenstone belt). These deposits experienced different degrees of metamorphism and deformation. The Silver Swan ore body recorded the least deformation and reached its peak metamorphic conditions at greenschist facies (*Hill et al. Min. Dep. 2004*) while Flying Fox, the most deformed, reached its peak metamorphic conditions in upper amphibolite facies (*Porter & McKay Econ. Geol, 1981*). This study *(CCFS Publication #373*) characterised the microstructures of three main sulfide phases; pyrrhotite (Fe_7S_8), pentlandite ($(Fe, Ni)_9S_8$) and pyrite (FeS_2). Electron backscatter diffraction analysis (ESBD) showed that pyrrhotite is commonly the most deformed phase. In the Silver Swan sample, pyrrhotite develops strain shadows around stronger pyrite, whereas in the Perseverance sample, pyrrhotite shows systematic parallel low-angle boundaries (Fig. 1a, b). In the Flying Fox sample, pyrrhotite contains deformation twins and strain localisation-induced low-angle boundaries (Fig. 2a). Unlike pyrrhotite, microstructures in pyrite and pentlandite are far more uniform. In all three samples, pyrite shows only minor lattice deformation whereas pentlandite locally develops a few low-angle boundaries.

Understanding the sulfide crystal lattice response to deformation leads to another question – are there compositional effects? We used two types of high-precision *in situ* analytical techniques to determine the trace-element concentrations: laser ablation

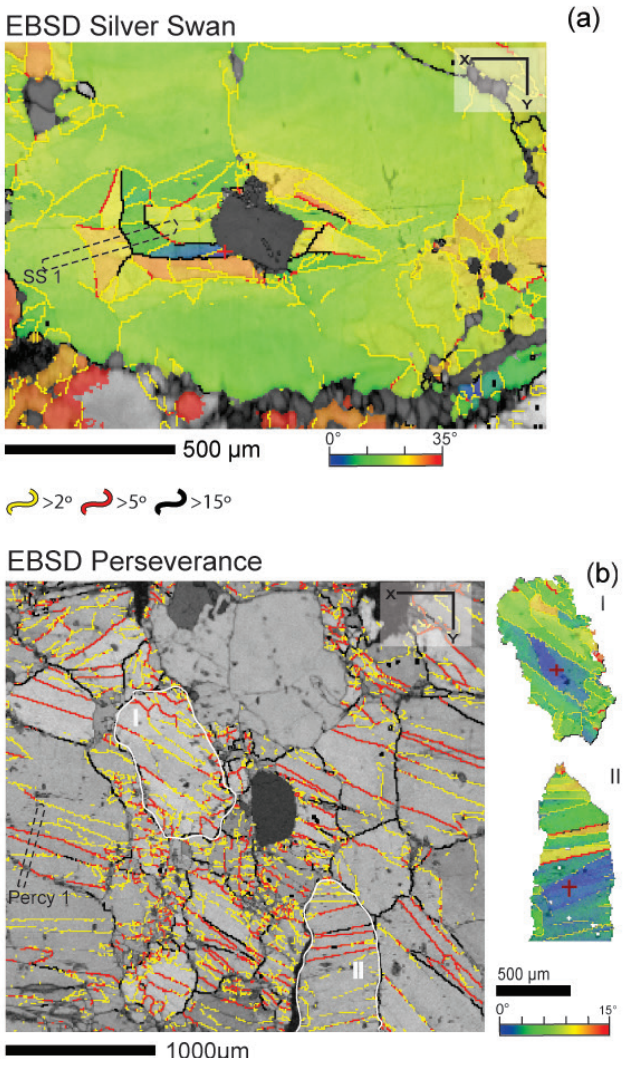

Figure 1. a) Electron backscatter diffraction (EBSD) data of Silver Swan massive sulfide. Band contrast–cumulative misorientation map for the pyrrhotite grain. Black dotted line SS1 shows the position of the ablated area from c). b) EBSD data of Perseverance massive sulfide. Band contrast– grain boundary map for the pyrrhotite grains. Black dotted line Percy 1 shows the position of the element profile from d). EBSD data shown for grains I and II indicate cumulative misorientation from the reference point (red cross). c) Laser ablation ICP-MS Pb profile along line SS1 from Silver Swan pyrrhotite. d) Laser ablation ICP-MS Pb profile along line Percy 1 from Perseverance pyrrhotite. Grey area on both c) and d) corresponds to the maximum local misorientation along the respective profile. Lead is plotted against the length in both c) and d).

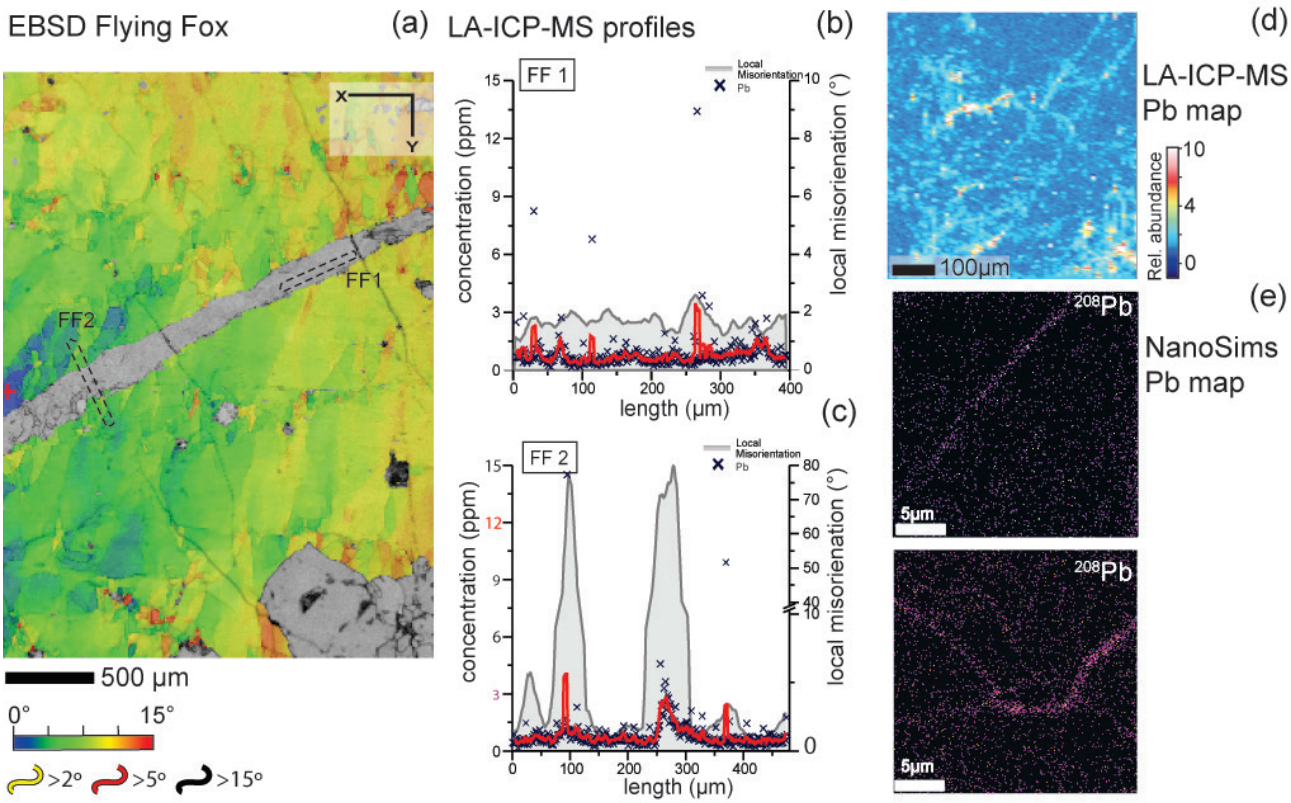

Figure 2. a) Electron backscatter diffraction (EBSD) data for Flying Fox massive sulfide show cumulative misorientation of the pyrrhotite. Black dotted lines show location of the laser profile from b) and c). b) Laser ablation ICP-MS profiles along line FF1 (b) and FF2 (c). Grey area on both b) and c) corresponds to the maximum local misorientation along the respective profile. d) Laser ablation ICP-MS element map for Pb, expressed in relative ppm abundance. e) NanoSims element maps for Pb. For location of the mapped area see CCFS publication #373.

inductively coupled plasma mass spectrometry (LA-ICP-MS) and Nano-scale secondary ion mass spectrometry (NanoSims). Both trace-element profiles and element maps were acquired using LA-ICP-MS (Fig. 1c, d and 2b-e). The results showed that particular trace-elements with large ionic radii (e.g. Pb) are more concentrated along high and low-angle boundaries as well as along twin boundaries (Fig.1c, d and 2b-e). Unlike Pb, the platinum group elements do not show such variations.

Element mapping with NanoSims has advantages relative to the LA-ICP-MS in terms of scale. Using NanoSims, we mapped an area of 25x25 µm around a twin boundary and detected increased values of Pb (Fig. 2e). It is important to note that these variations are not related to the presence of another phase, but only to the presence of particular dislocation arrays.

Two possible scenarios could explain the correlation between trace-elements and microstructures: 1) late hydrothermal fluid interaction with the sulfide phases and 2) intra-grain diffusion. In the first case, late hydrothermal fluids would play a role in introducing the elements (i.e. Pb) through fluid percolation and mineral–fluid reaction along preferential diffusion pathways such as low angle, grain and deformational twin boundaries. However, the hydrothermal fluid would need to be very similar in chemistry for three deposits hundreds of kilometres apart, so intra-grain diffusion seems the more likely mechanism. Intra-grain diffusion can occur during deformation and post-deformation. During deformation, dislocation cores move to form dislocation arrays. While they are moving, they may encounter large ions (i.e. Pb) and carry them along until they form a particular microstructure. In the case of post-deformation diffusion, intra-granular fluid (already present in the system) acts as a carrier and moves these large ions along high-diffusivity pathways (high and low-angle boundaries, and twin boundaries). At the moment we cannot distinguish between the two intra-grain processes.

Variation in trace elements is observed even in the samples from terrains that experienced metamorphic peak temperatures of no more than 350°C. This implies that the large ions still diffuse at relatively low temperatures. This revelation of strong within-grain trace-element variations, in particular for Pb, has huge implications in Pb geochronology. For more details on this work see *CCFS publication #373*.

This project is part of CCFS Themes 2 and 3, Earth Evolution and Earth Today, and contributes to understanding Earth's Fluid Fluxes.

Contacts: Zoja Vukmanovic, Steve Reddy, Marco Fiorentini

Funded by: (in part) CCFS Foundation Program 2

"Dirty" ice deformation – a peep-show for revealing properties of flowing rocks

Knowledge of the flow characteristics at the microscopic scale (rheological behaviour) of rock masses in the Earths' crust is essential to the quantitative understanding of plate tectonic processes at the global scale, such as plate movements, mountain building and the break-up of continents. The prediction of rock flow, based on in-depth understanding of the deformation mechanisms in such materials is fundamental to the accuracy of rheological models. Current geodynamic models commonly make the fundamental assumption that the rheology even of polyphase rocks can be approximated by that of a single, monomineralic rock type. However, experiments and field observations show that flow laws from monomineralic materials do not represent the true rheological behaviour of polymineralic rocks. Thus, constraining the rheology of anisotropic and multiphase materials making up the Earth is still a major challenge. Ice mixtures (ice containing another phase) represent such a material, and thus are very good analogues for understanding behaviours of multiphase rocks on Earth.

In nature, a significant percentage of ice is not pure H_2O but contains abundant air bubbles, porous hydrate crystals and second phases such as clays and fine grained rock '*powder*' i.e. '*contaminated/dirty*' ice. In both instances, these impurities may potentially represent the rheologically softest or hardest material. In nature, such "dirty" layers may govern movement on the large scale.

This project aims to advance our understanding of anisotropic polycrystalline material with more than one phase by using '*dirty ice*' for deformation experiments conducted at the Australian Nuclear Science and Technology Organisation (ANSTO). It represents a continuation of the pure-ice deformation work performed previously (*Piazolo et al. G3, 2013, CCFS/GEMOC publication number 342/901*).

Figure 2. Stress-strain curve for ice with different second phases, (bottom); cg. = coarse grained, fg. = fine-grained, DTHF2 = mixture between ice and gas-hydrate (analogue).

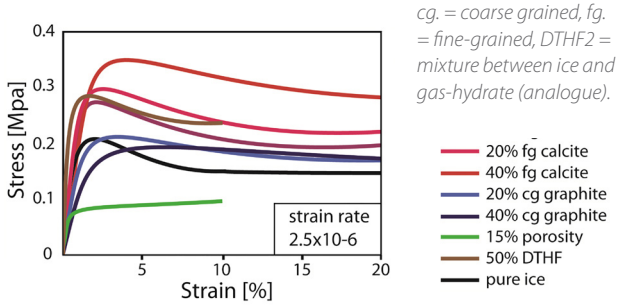

Our international research team chose to use heavy-water ice as D_2O provides a unique opportunity to use neutron diffraction analysis to simultaneously monitor the flow properties, microstructure and orientation properties of ice. Laboratory-grown polycrystalline '*dirty*' ice samples were shortened up to 20%. The results show that the rheology of ice is highly dependent on the nature of the second phases present, their shape, their relative volume and their grain size. A high proportion of second phases may stop ice from recrystallising and little to no crystallographic preferred orientation is produced. The material behaves like a Newtonian fluid with a linear relationship between stress and strain rate. This is markedly different to pure or near-pure ice, which typically shows an exponential relationship. Air bubbles as well as fluid brine significantly soften the material.

Based on these results, constitutive flow laws are being developed for mixed materials, which will be directly applicable to large-scale modelling of multiphase Earth materials.

This project contributes to the CCFS Goal "*to reach a new level of understanding of Earth's internal dynamics and fluid cycles, and how these have evolved* …" as well as CCFS Theme 3, Earth Today, and contributes to understanding Earth's Architecture.

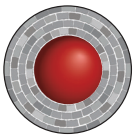

Contacts: Sandra Piazolo, Daria Czaplinska
Funded by: Bragg Institute, ANSTO, Lucas Heights, ARC DP120102060, FT1101100070

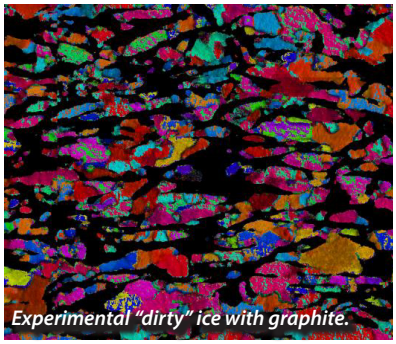

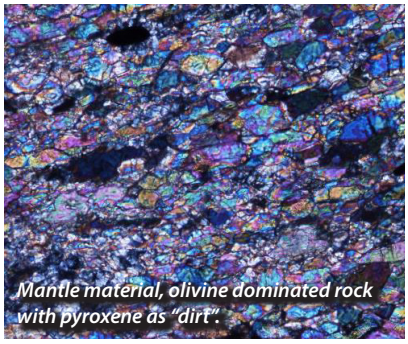

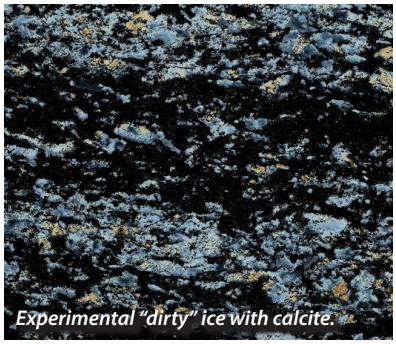

Figure 1. top left; optical photomicrographs of a typical mid-crustal rock - gneiss dominated by feldspar with amphibole as "dirt". Plane light, (courtesy of R. Gardner); top right; experimentally deformed D_2O ice with graphite after 10% deformation, cross polars; lower left; typical mantle material - deformed peridotite with pyroxene, cross polars, (courtesy of R. Gardner): lower right; experimentally deformed ice with calcite after deformation 10%, plane light. Field of view is 1 cm.

Mantle oddities: sulfate-dominated fluids in the Earth's mantle

Sulfur is the eleventh most abundant element in the silicate Earth, with an estimated primitive-mantle concentration of 250 ppm. It is a moderately incompatible volatile element that plays a pivotal role in transporting and concentrating chalcophile (= sulfur-loving) metals. In this regard, sulfide melts are enriched in metallic elements and sulfide and bisulfide anions complex with metallic cations dissolved in C–O–H–S fluids. However, the distribution and speciation of sulfur in the mantle remain poorly understood. CCFS Foundation Program 2 has addressed this issue by investigating S-bearing minerals in a global suite of mantle rocks. This has important implications for the formation of melts enriched in S and metals, which are ultimately involved in generating magmatic ore deposits.

Photograph of an off-cut of xenolith sample XM1/498. The off-cut was cut across a layer dominated by K-richterite with minor phlogopite (phl). The layer is pervasively cross-cut by creamy-coloured sulfate-rich veins (from Giuliani et al., 2013).

In the sub-continental lithospheric mantle (SCLM), sulfur is mainly stored in sulfide minerals in the reduced form S^{2-}. Mantle sulfides may have been deposited by immiscible sulfide melts that separated from silicate and/or carbonate melts at mantle depth, from S-bearing C–O–H fluids, and from sulfidation reactions between S-bearing fluids and silicate minerals. It has also been proposed that some sulfide minerals could be residual after the partial melting events that stabilised the lithospheric roots of continents.

In addition to sulfides, sulfur in the SCLM may also occur in the oxidised form SO_4^{2-}, in minerals such as apatite and amphibole, albeit in trace amounts. In addition, anhydrite ($CaSO_4$) has been reported as inclusions in diamond, barite ($BaSO_4$) in Cr-diopside from a peridotite xenolith, and alkali-rich sulfates in carbonate-rich inclusions hosted by ilmenite in a mantle polymict breccia. These occurrences attest to the presence of sulfate minerals in the mantle, even at depths within the diamond stability field (> 150 km). '*Daughter*' crystals of gypsum and barite have been reported in fluid inclusions hosted by mantle olivine, pyroxene and amphibole; this suggests that sulfate (SO_3) may be a more common component of some mantle fluids than previously recognised. The occurrence of sulfate compounds in mantle fluids is further supported by mass spectrometric analyses of crushed mantle xenoliths from southeast Australia, which showed the release of SO_2 during crushing. Finally, sulfates have been identified in metasomatised rocks from the mantle wedges above subduction zones, which are permeated by sulfate-rich oxidising melts.

Sulfates can crystallise from a range of chemically different fluids and are common constituents of carbonatitic rocks. Anhydrite has been shown to crystallise from silicate magmas of intermediate to acid composition. Strontium-rich barite and less commonly alkali-sulfate minerals occur in the groundmass of kimberlites. Celestine ($SrSO_4$) and aphthitalite [$(K, Na)_3Na(SO_4)_2$] have been found in melt inclusions hosted by kimberlitic olivine. Barite is a minor constituent of vein assemblages in mantle MARID (mica-amphibole-rutile-ilmenite-diopside) rocks and may have crystallised from kimberlite-related fluids.

There is also evidence for the occurrence of sulfate-bearing fluids in crustal rocks and documentation of sulfate melts from experimental simulations. However, despite increasing evidence for the occurrence of sulfate melts in crustal rocks, such fluids have never been documented in mantle rocks. Now, the occurrence of Ba-bearing celestine veins that also host abundant clinopyroxene and minor sphene, apatite, pectolite, phlogopite, barite and carbonates, in a mantle MARID xenolith sampled by the Bultfontein kimberlite (Kimberley, South Africa) has been documented (*CCFS publication #333*). On the basis of textures, mineral inclusions and mineral chemistry, and data for Sr and S isotopes in celestine and the other minerals in sulfate veins and the host MARID minerals, we suggest that the sulfate-rich veins were produced in the mantle from interaction between a sulfate-rich fluid and the MARID host rock. These celestine-bearing veins provide the first evidence for the occurrence of sulfate-dominated fluids in the Earth's mantle.

This project is part of CCFS Theme 3, Earth Today, and contributes to understanding Earth's Fluid Fluxes.

Contact: Marco Fiorentini

Funded by: CCFS Foundation Program 2a

The riddle of the origins of zircon in ophiolitic rocks: a case history from the Coolac Serpentinite Belt, southeastern Australia

An increasing number of studies are reporting U-Pb ages for zircons recovered from rocks of the mantle sections of the ophiolitic complexes and host peridotites. Were these zircons crystallised in the mantle from percolating metasomatic fluids or are they xenocrystic relics of crustal material recycled during subduction? What they mean in the framework of ophiolite and exhumed mantle rock genesis and evolution is controversial. The deciphering of this complexity requires integrated datasets that are not confined to zircon U-Pb data alone. Equally importantly, these data are integrated within a comprehensive geological framework. Our study of zircons from the Coolac Serpentinite Belt in southeastern Australia sends a cautionary message to the researchers who use ophiolitic zircon to unravel the past geodynamics of Earth's lithosphere and mantle.

The Coolac Serpentinite Belt (CSB) is part of the Tumut ophiolitic complex in the Lachlan Fold Belt, southeastern Australia (Fig. 1). The 63 km belt contains a high proportion of massive

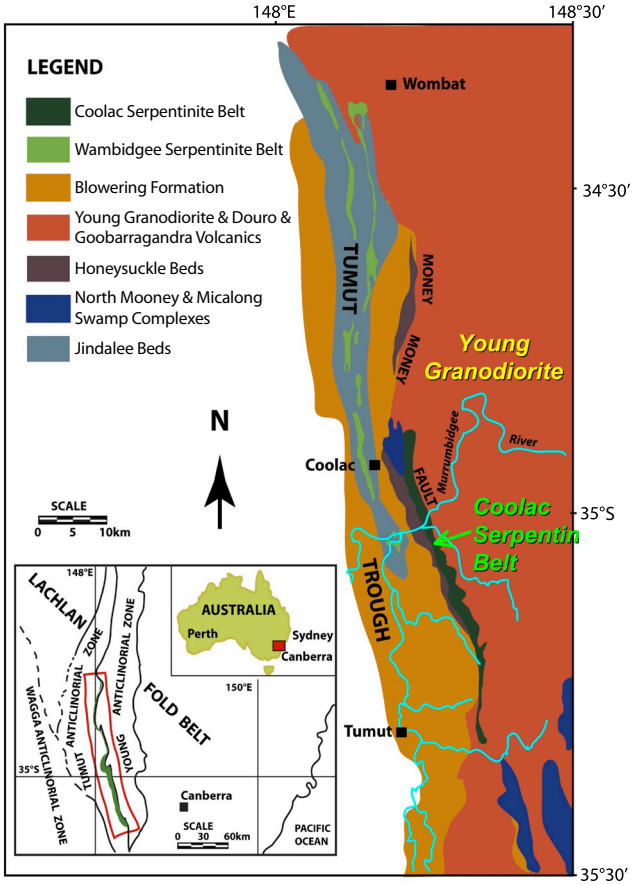

Figure 1. Map shows the location of the Tumut region within the Lachlan Fold Belt: the Coolac Serpentinite Belt (dark green) separates the Tumut and Young zones (after Graham et al., Geology, 24, 1996).

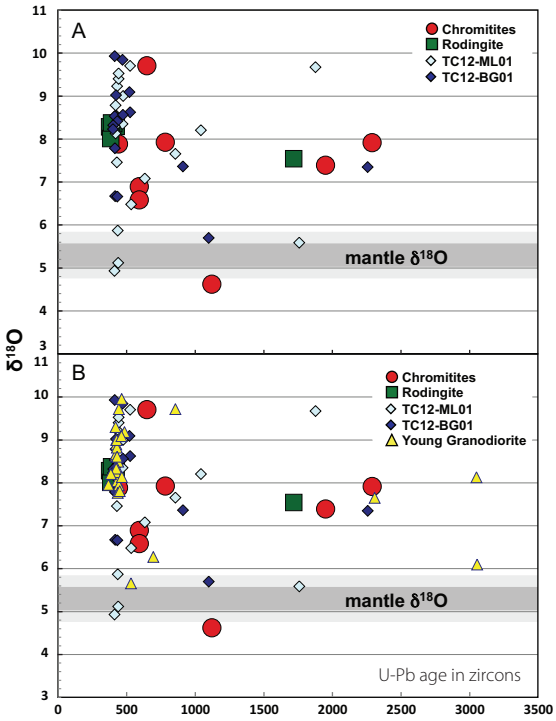

Figure 2. Plots of $\delta^{18}O$ versus U-Pb age in zircons from the Coolac Serpentinite Belt, including detrital 'TC' TerraneChron® (A) and comparison of those with zircon from the Young Granodiorite (B). The mantle values of 5.3‰ (Valley, 2003) are shown with 1σ and 2σ deviations as dark and light bands accordingly.

(unfoliated) ultramafic rocks that have undergone lower greenschist-facies metamorphism (e.g. Graham et al., Geology, 24, 1996). New U-Pb, Hf- and O-isotope, and trace-element data have been obtained for zircons from the rocks of the belt. These include zircons separated from two (high-Al and high-Cr) massive chromitites and rodingites in the Coolac Belt, and from detrital zircon grains recovered from gullies draining from outcrops consisting of mainly weakly serpentinised massive porphyroclastic harzburgite. The Belt is either faulted against, or intruded by, the S-type Young Granodiorite. Zircons from the Young granodiorite collected at the contact with the serpentinite belt were also studied to refine the tectonic relation and timing of the granitic magmatism.

The U-Pb age of the zircons from this serpentinite belt display a wide range, from Silurian to Paleo-Proterozoic, with the main age population clustering around 430 Ma (Fig. 2A). This main peak coincides, within analytical error, with the age obtained for plagiogranites from the Belt and with the age of the Young Granodiorite intrusion (427.6 ± 3.2 Ma). Moreover, the ages for the inherited zircon populations in the granodiorite correlate well with the older zircon populations from the Coolac ultramafic rocks (Fig. 2B).

Most of the Coolac zircons have negative εHf and heavy (>6) $\delta^{18}O$ indicative of a crustal origin. Combined with U-Pb age information, this implies that the zircons in the peridotites are xenocrystic (Fig. 2). One possibility is that zircons derived from subducted sediments were incorporated into the ophiolitic rocks

as in the Luobusa (Tibet) ophiolite (*Yamamoto et al., Island Arc, 22, 2013*). However, the similarity of the Coolac ophiolite-derived zircons with those from the Young Granodiorite may indicate that they were introduced into the Coolac peridotitic complex during the time of voluminous granitic magmatism that occurred in the region at ca 430 Ma ago. In the latter case, zircons carry no information on the origin of the Tumut ophiolitic rocks and only suggest that Coolac rocks had preceded granitic magmatism of the Lachlan Fold Belt.

Thus, our observations highlight that the collection of integrated information on zircons is critical for the adequate interpretation of the timing of the ultramafic rock formation, emplacement and subsequent tectonic implications in the context of regional geology. In cases of xenocrystic zircons, a clear understanding of their origin and relationships with the host ophiolitic rock would improve the probability of geological meaningful interpretation about the generation of ophiolites, and the subsequent dynamics of mantle-crustal interaction.

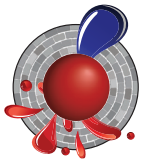

This project is part of CCFS Themes 2 and 3, Earth Evolution and Earth Today, and contributes to understanding Earth Architecture and Fluid Fluxes.

Contacts: Elena Belousova, José María González Jiménez, Bill Griffin, Sue O'Reilly, Norman Pearson

Funded by: ARC Future Fellowship, Macquarie University contribution to ARC FF and CCFS TARDIS

Metals flow in mantle streams

The capacity of aqueous fluids to selectively extract metals and incompatible elements from the Earth's mantle and thereby enrich its crust and lithosphere has long been inferred, but has been a challenging problem to investigate experimentally. By adopting an inverse approach, we have avoided many previously encountered difficulties and obtained detailed experimental data on the capacity of aqueous mantle fluids to transport a broad range of incompatible elements and metals. Rather than directly equilibrating water with mantle peridotite, we used a previously studied basanite as a proxy for a H_2O-saturated solidus melt (of peridotite) and determined the compositions of H_2O-rich fluids in equilibrium with the basanitic melt. The experimental conditions were 950-1200 °C and 1.0 to 4.0 GPa. In this way we were able to use mineral/melt partitioning data for the basanite to infer fluid/mineral partitioning for peridotite minerals. Our results were confirmed by one experiment in which we directly equilibrated an H_2O-fluid with a mica-amphibole-lherzolite assemblage.

At the lowest pressure and temperatures investigated (1.0 GPa, 950-1100 °C) H_2O-fluids have a limited capacity to transport most incompatible elements and metals (Figs. 1a, 2). But as pressure and temperature increase, the solubility of silicates and metals in H_2O-fluids increases dramatically. By 4.0 GPa there is complete miscibility between the H_2O-rich fluid and silicate melt (Fig. 1b). Relative to coexisting melts, the H_2O-rich fluids are enriched in silica, alkalis, Ba and Pb, and depleted in FeO, MgO, CaO and rare earth elements. Surprisingly they are not especially depleted in high-field-strength elements (Nb, Ta, Zr, Hf and Ti). These features are consistent with currently accepted ideas about the role of both H_2O-rich fluids and rutile in the development of arc magmas. They are also consistent with a role for H_2O-rich fluids in the development of incompatible-element enrichments in some samples of the deep mantle lithosphere as well as the lamproite magmas that bring such samples to the surface.

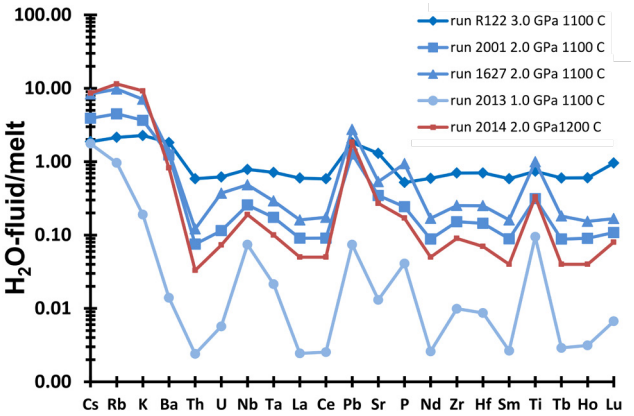

Figure 2. Partitioning of incompatible elements between H_2O-fluids and silicate melts.

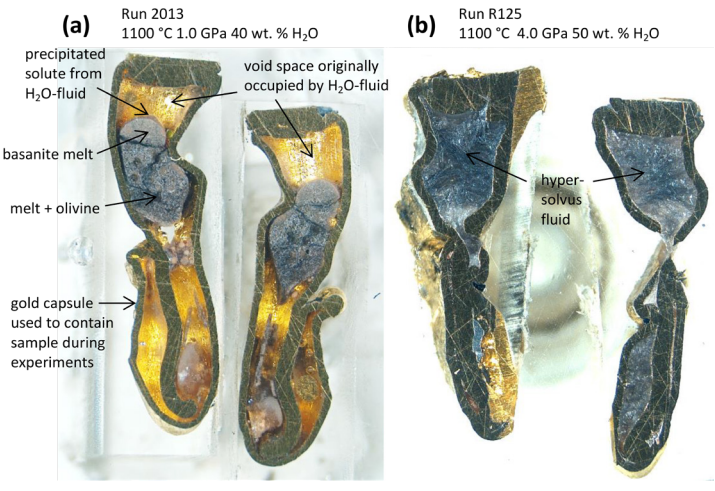

Figure 1. Longitudinal sections of sample capsules after experiments.

This project is part of CCFS Theme 3, Earth Today, and contributes to understanding Earth's Fluid Fluxes.

Contacts: John Adam, Tracy Rushmer, Marek Locmelis, Marco Fiorentini

Funded by: ARC CCFS

Supercontinent breakup clues in Yilgarn mafic dykes

The 1.21 Ga Marnda Moorn large igneous province (LIP) in the Yilgarn Craton (Fig. 1) recorded the final breakup of the Nuna (Columbia) supercontinent (see 2012 *Research highlight p. 53*). However, its petrogenesis has been poorly understood owing to the lack of geochemical data. Now, geochemical analyses of the Gnowangerup-Fraser Dyke Suite, a major part of the Marnda Moorn LIP, have begun to fill this gap (*CCFS publication #371*). The dykes are predominately tholeiitic and OIB-like dolerite (Type-1, high Ti), but there is one arc-like and more felsic dyke (Type-2, low-Ti) (Fig. 2). Type 1 samples have incompatible-trace-element compositions similar to those of tholeiitic Hawaiian plume-induced OIB and typical asthenospheric mantle-derived Nd isotopes with εNd(t) varying from +3.7 to +7.5, produced mainly within the spinel stability field (shallower than 75 km). Their source region most probably contains recycled oceanic crust. Samples from the Type 2 dyke have extremely unradiogenic Nd with εNd(t) of about -12, strong depletion of Nb-Ta-Zr-Hf-Ti, chondritic Nb/Ta ratios of 18–20, oversaturated silica, and strong deficiencies in CaO, FeOt, TiO_2, and Ni. This implies that the dyke was produced by partial melting of enriched sub-continental lithospheric mantle. The coexistence of OIB- and arc-like end-members but mainly Hawaiian OIB-like tholeiitic mafic dykes is interpreted to reflect large-scale asthenosphere upwelling in a very short time.

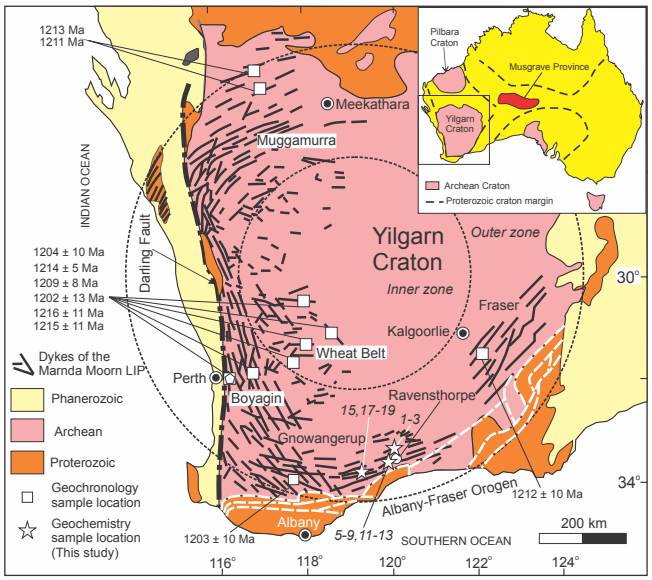

Figure 1. Simplified geology of the Marnda Moorn large igneous province. Thick black lines indicate general dyke trends. The inset map shows the location of the Musgrave Province, where ultrahigh-temperature events occurred at c. 1.21 Ga.

The geochemical and emplacement characteristics are attributed to relief of the lithosphere–asthenosphere boundary across the Yilgarn craton and a complex interplay between the plume, a heated lithosphere, normal asthenosphere, and recycled components. A two-stage melting model can explain the geochemical composition and emplacement of the Marnda Moorn LIP. This involves a mantle plume impinging on the base of the continental lithosphere beneath the Yilgarn craton at about 1.21 Ga. During the first stage, the root of the Yilgarn Craton would have deflected plume materials away from its centre in lateral flows, to pond beneath the cratonic margin. Heat from the underlying plume would enhance partial melting of enriched components of the SCLM to generate Type 2 dykes. At this stage, the recycled oceanic crust (pyroxenite and/or eclogite) would be extensively partially melted, further enhancing lateral flow of the plume materials and leading to significant erosion and destruction of the SCLM. The main phase of the Marnda Moorn LIP (OIB-type tholeiitic mafic rocks) was produced during the second stage by partial melting of ponded plume materials and newly formed pyroxenites, within the spinel stability field. Our plume-lithosphere interaction model is consistent with the occurrence of synchronous ultrahigh-temperature events in the Musgrave Province of central Australia and the large volume of mafic magma in the Marnda Moorn LIP.

This project is part of CCFS Theme 2, Earth Evolution, and contributes to understanding Earth's Architecture and Fluid Fluxes.

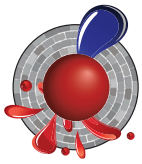

Contacts: Xuan-Ce Wang, Zheng-Xiang Li, Sergei Pisarevsky, Michael Wingate

Funded by: CCFS, CCFS ARC ECSTAR fund

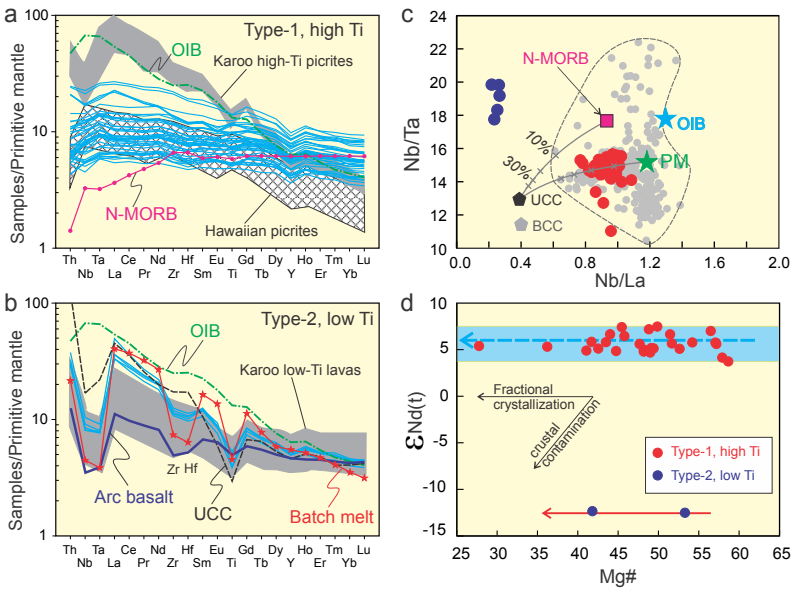

Figure 2. Primitive mantle-normalised incompatible trace-element distribution patterns (a and b) and plots of (c) Nb/Ta versus Nb/La and (d) Nd isotopes against Mg# for the samples of the Gnowangerup–Fraser Dyke Suite from the Marnda Moorn large igneous province.

Zircon: a prime witness to the Moon's early history

The first five hundred million years of Earth's history have seen most of the events that shaped it to its present form, such as differentiation into the core, mantle and crust and the formation of the atmosphere and hydrosphere. Unfortunately the later tectonic and hydrologic modifications of our planet have erased most records of these early events. The very early history of Earth is now only preserved in tiny zircon grains that survived the ca four billion years following their formation. However, due to their rarity and size they can provide only a glimpse of the early conditions on our planet. In contrast, the Moon was only geologically active for only about 1.3 billion years after its formation; the most recent basalt is about 3.2 billion years old. Therefore lunar rocks can reveal the early history of both Moon and Earth.

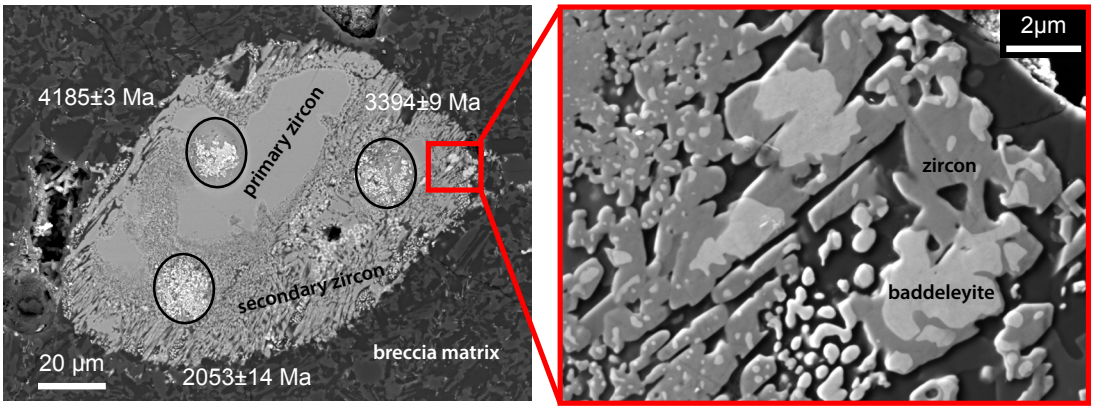

Figure 1. Left, is a back-scattered image of zircon from Apollo 15 breccia – circles indicate location of U-Pb analyses, with corresponding ages (Ma = million years). Right, a magnified view showing the relationships between zircon and baddeleyite in the zircon rim.

As on Earth, lunar zircon can be used for Uranium-Lead (U-Pb) dating, to give a timeline of early events in the differentiation of the Moon. In addition, zircon is chemically and physically robust: it can also survive meteoritic impacts and hence provide useful insight into the bombardment history of the early solar system. Our research focuses on deciphering both magmatic and impact features within tiny zircon grains to understand how these features affect their crystallography and chemistry and whether they can be used to date specific magmatic and impact events.

Since its formation, the Moon has been bombarded by countless meteorites, so that the lunar surface consists of a thick regolith covering the magmatic basement. Lunar zircons are found in impact breccias: mixtures of different rock and mineral fragments (clasts) welded together by impact-generated melts. Some zircon grains fortunately are found within their original magmatic rocks, which occur as minute clasts (up to a few centimetres) in the breccia. Lunar zircons can be classified into groups based on (i) their textural relationships with surrounding minerals in the host breccias, (ii) their internal microstructures as identified by small scale imaging and (iii) their U-Pb isotope systems as analysed in-situ by ion microprobe. Primary zircon has a magmatic origin and is unzoned or has sector and/or oscillatory zoning as identified in cathodoluminescence images. Its U-Pb age is concordant and consistent across its polished surface. Secondary zircon formed during an impact and usually shows internal structures overprinting primary features. Recrystallised or amorphous domains often yield internally consistent and close to concordant U-Pb ages that can be interpreted as dating impact events. Crystal-plastic deformation, planar deformation features and fractures, however, provide channels for Pb diffusion and result in partial resetting of the U-Pb isotopic systems.

A particular zircon with a complex structure was identified in one impact breccia sampled during the Apollo 15 mission. It has primary features preserved in its inner part while its outer rim has been transformed under high pressure and temperature during an impact. The inner part of the grain is crystalline and undeformed. The outer rim of the zircon is made of small zircon and baddeleyite (zirconium oxide) grains, formed by the breakdown of zircon [zirconium silicate] to baddeleyite and silica at pressures above 60 GPa and temperatures close to 1700°C, during impact. The age obtained for the primary inner core of the grain, although discordant, is in agreement with the age of other primary zircon grains from the same sample, at 4.33 billion years. This represents the age at which the zircon crystallised from a magma. The two other ages obtained on the outer rim of the grain are much younger and consistent with an impact that occurred 1.94 billion years ago. This zircon grain demonstrates that very small-scale microscopic imaging and precise in situ ion-probe dating can provide a wealth of information on the overall history of the Moon, and hence the Earth *(see CCFS publications #374, 423)*.

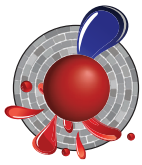

This project is part of CCFS Theme 1, Early Earth, and contributes to understanding Earth's Architecture and Fluid Flux

Contacts: Alexander Nemchin, Marion Grange
Funded by: CCFS, ARC Discovery Project #120102457 (Nemchin-Grange)

Detecting diamond distillation of nitrogen – frontiers of quantifying nitrogen mantle behaviour

Nitrogen is the most common impurity in diamonds, and the properties of nitrogen in the diamond lattice are an important part of standard diamond classification. Traditionally, the isotopic characteristics of this nitrogen have been analysed by bulk combustion methods. When modern *in situ* methods (secondary ion mass spectrometry, or SIMS) were first applied to carbon-isotope analysis of diamonds, it became obvious that bulk analysis is of limited value as it provides an averaged value, hiding the real variations in C-isotope composition that can be present in a single diamond. This is unfortunate, because these variations carry very interesting stories about the origins and growth histories of diamonds; we could expect similar revelations from *in situ* analysis of N isotopes in diamonds. However, until recently

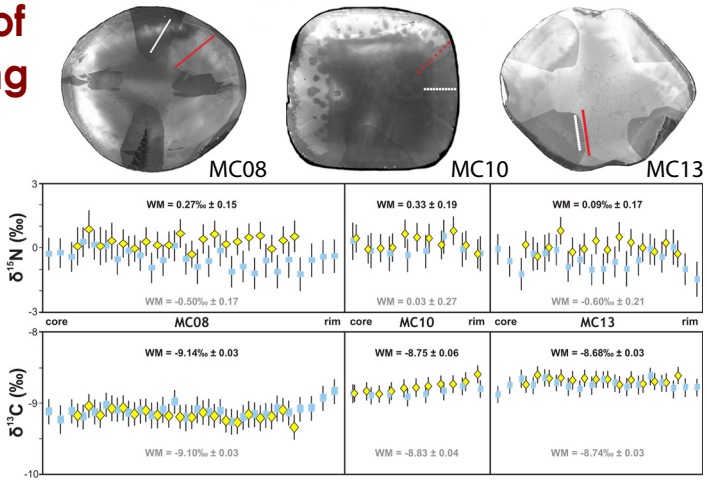

Figure 2. CL images of the three samples analysed by SIMS, showing where the data were collected. Red and white dots show analyses in the cuboid and octahedral sectors respectively. Each transect was repeated but slightly offset to obtain both C and N isotopic analyses. The data from both transects (Yellow diamonds = octahedral data, Blue squares cuboid data) are shown on the same graph, along with the weighted mean value (WM), to allow for easy sector comparison.

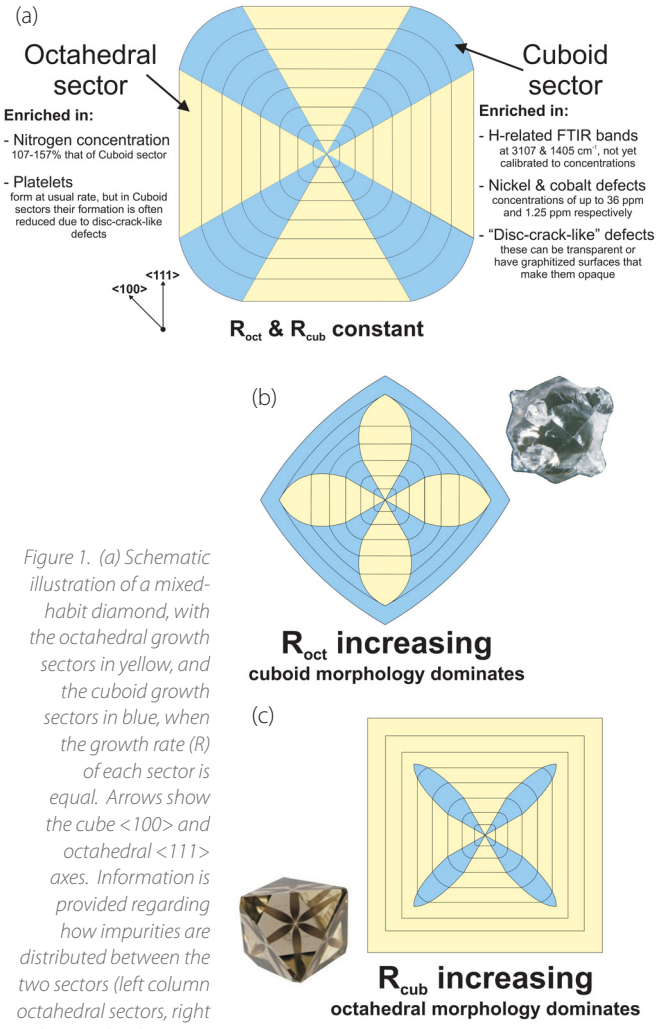

Figure 1. (a) Schematic illustration of a mixed-habit diamond, with the octahedral growth sectors in yellow, and the cuboid growth sectors in blue, when the growth rate (R) of each sector is equal. Arrows show the cube <100> and octahedral <111> axes. Information is provided regarding how impurities are distributed between the two sectors (left column octahedral sectors, right column cuboid sectors). Images (b) and (c) show examples of when the growth rate of one sector increases relative to the other. Inset are images of natural examples of these (courtesy of Tappert et.al. 2011 and G.M. Pearson).

SIMS analysis of nitrogen isotopes in diamond has faced large uncertainties due to issues with the methodology and the need for isotopically homogeneous reference material.

There have been two principal goals of this research (part of Foundation Program 8) that has the overarching goal of understanding the nature of deep Earth fluids. The first was the development of a suitable standard reference material for carbon and nitrogen isotopic analysis of diamond via SIMS in collaboration with Dr Richard Stern and Professor Thomas Stachel of the Canadian Centre for Isotopic Microanalysis (CCIM) at the University of Alberta. The CCIM is leading SIMS analysis of diamonds, and this expertise and knowledge is being used to establish such methodologies at the CCFS SIMS (CMCA) facility in UWA (see *Technology Development*, *2013 Annual Report*). The second goal of this work is to investigate the relationship between the nitrogen isotope systematics and the crystal growth mechanisms of diamond. In particular, we want to look at the relationship of these two and what roles they play in the growth of mixed-habit diamonds. This type of diamond has been the focus of some of the diamond research being carried out at CCFS (*CCFS publications #178, 180, 332*). They are unique crystals that exhibit periods of growth in which two competing growth mechanisms were occurring at the same time. These two growth mechanisms produce the characteristic smooth, flat octahedral growth, and the hummocky, rough cuboid growth (Fig. 1).

SIMS analysis of three previously-studied mixed-habit diamonds at the CCIM has shown that on the millimetre scale, the samples are homogeneous in terms of their carbon and nitrogen isotopes (Fig. 2). They therefore represent ideal standard reference materials for this type of analysis. The methodology that has been developed produces data with 2σ uncertainties of ~ ± 0.7 ‰

for $\delta^{15}N$ measurements. This is much better than the uncertainties of ± 8 ‰ that have been reported for $\delta^{15}N$ data from SIMS by other researchers in the past. Interestingly for the investigation of mixed-habit growth, all three samples show slightly elevated $\delta^{15}N$ values in the octahedral sectors compared to the cuboid ones (although this is only above uncertainty in two of the samples). This small fractionation is in stark contrast to that seen in synthetic diamonds, where the cube sectors have are $\delta^{15}N$ values that are 30 ‰ higher than the octahedral sectors. This work is showing an understanding of the growth mechanisms involved as well as the underlying crystallography is essential to interpreting and drawing conclusions from such commonly used data. Understanding isotopic distribution and possible fractionation is a first step in understanding the origin and significance of nitrogen in the mantle, especially the relative contributions from recycled and primordial sources.

This project is part of CCFS Themes 2 and 3, Earth Evolution and Earth Today, and contributes to understanding Earth's Fluid Fluxes.

Contacts: Dan Howell, John Cliff, Bill Griffin

Stretching, pushing or something else: A memory fragment in a continent lithosphere recalls its tectonic history

A link between the deformation of the upper mantle rocks and the directional dependence (anisotropy) of seismic wave speed is one of the mainstays of the modern structural seismology toolkit. It provides a means to "see" processes at depth that are suggested by observations of plate motion, by differences in absolute wave speed inferred from tomography, and by scenarios of past tectonic evolution. However, interpretations of seismic anisotropy beneath continents are challenging, because the peridotites that make up both the lithospheric mantle and the asthenosphere beneath it are likely to become anisotropic under strain. The early debates over where the anisotropy resides, and whether it reflects present or past deformation (Fig. 1), have been largely settled by the recognition that both volumes of olivine-rich rock will likely have systematic texture imparted onto them by past tectonic events and/or current plate motion, or both.

We have developed high-quality constraints on the vertical and lateral variation in anisotropy at three locations in eastern North America (NA), which we could then compare with structure predicted for this region by the large-scale NA surface wave model of Yuan and Romanowicz (*Nature, 466, 2010*). We use a combination of two complementary techniques, an anisotropy-aware receiver functions (RF) analysis and an inversion for multiple layers of anisotropy on the basis of directionally variable shear-wave. Compared with the regional surface-wave model, these two methods are capable of resolving anisotropy structure at the station scale. The combination of these two techniques is complementary because P-S mode conversion is primarily sensitive to vertical gradients in properties while birefringence in SKS phases is an integral measure of anisotropic properties along their near-vertical paths (Fig. 2).

Our findings are summarised in Figure 3, focusing on anisotropic symmetry axes predicted by SKS and RF observations at three stations, and fast axis directions predicted for the lithosphere and the asthenosphere in the surface wave continent-scale model. On the basis of the close agreement we see in the orientations of fast directions at different depths, we define two distinct anisotropic layers in the upper mantle: an upper lithospheric layer with a fast direction ~120° SE (Fig. 3a) and an asthenospheric layer with a fast direction ~50° NE (Fig. 3b). This is especially pronounced in the strength of anisotropy cont...

Funded by: CCFS Foundation Program 8

WHERE DOES SEISMIC ANISOTROPY RESIDE?

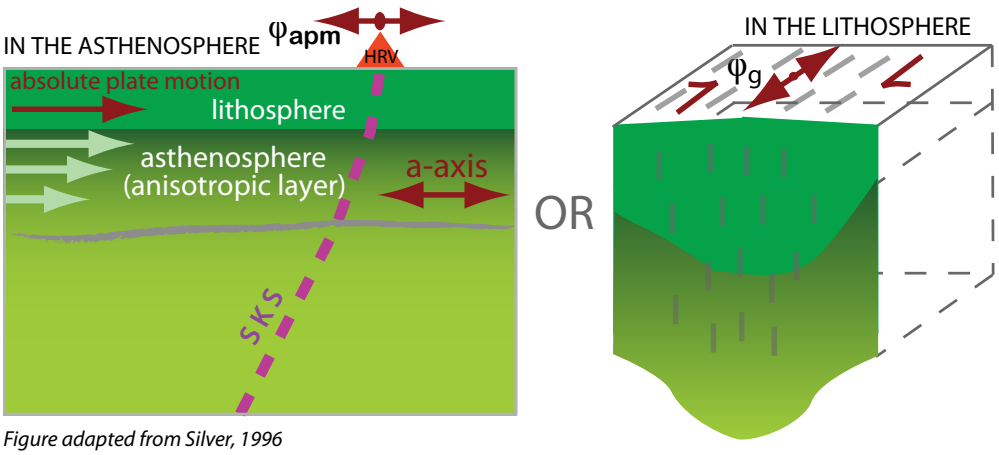

Figure adapted from Silver, 1996

Figure 1. Vertical variation of anisotropy in the shallow upper mantle. If anisotropic properties are restricted to a single layer (either frozen into the lithosphere or formed in the asthenosphere by current mantle flow), we can use observed polarisation of split shear waves as a representation of the past deformation (in the lithosphere) or current deformation (in the asthenosphere). φapm and φg: apparent fast axis directions inferred from SKS.

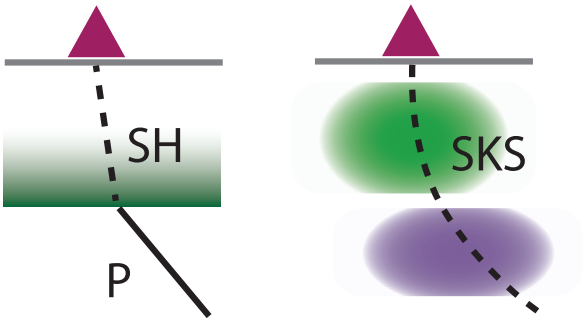

Figure 2. Depth sensitivity illustrated for receiver function analysis (left) and SKS modeling (right). Dashed lines indicated the shear wave (P-SH and SKS) paths. Preferred anisotropy depth distribution (shaded) is inferred from this study.

predicted in the lithospheric part of the *YR2010* model, which becomes progressively smaller inward from the coast. Nevertheless, the differences between these two layers are significantly stronger than the internal variation within each.

The close alignment of fast directions in the asthenosphere with the absolute plate motion (APM) vectors was anticipated. In eastern NA our observation favours the APM directions. Their apparent directional mis-match with the predictions of the YR2010 model or the APM direction is attributed to relatively small-scale lateral variation in upper mantle velocity (Fig. 3c). On the other hand, the inferred fast axis direction in the lithosphere is at a high angle to the strike of major tectonic units in the Appalachians, and is nearly identical over a broad region. This suggests that a regional deformation event affected a large area of the present-day northern Appalachians.

Several possible tectonic episodes in North America's history could have imparted the NW-SE oriented fabric to its mantle lithosphere. Deformation related to the assembly of the Appalachians from a set of terranes is not a plausible candidate. Numerous studies note near-parallel directions of tectonic units in compressive ("pushing") orogens and the fast direction of anisotropy, and have argued for orogen-parallel flow. Similarly, it is difficult to relate the broadly distributed sub-horizontal deformation to the rifting ("stretching") of the Atlantic, which was highly focused in the area presently offshore.

A scenario ("something else") that may explain the observed lithospheric anisotropy would involve the loss, on a regional scale, of the lower part of the lithosphere. This episode has to occur after the assembly of the Appalachians, to impact all the terranes involved. We considered a possibility of viscous instability that would lead to the development of "stretch marks" in the depth range where the lithosphere detaches. Given the broad areal extent of the lithospheric fabric, we believe that a "delamination" sensu stricto may be more probable.

The technique designed (*Yuan and Levin, JGR submitted*) serves as a toolkit that can be easily applied to Western Australia, which will pin-point the anisotropic lithospheric structure beneath local stations, complementary to a large-scale 3D tomographic inversion that is currently under development.

This project is part of CCFS Themes 2 and 3, Earth Evolution and Earth Today, and contributes to understanding Earth's Architecture and Fluid Fluxes.

Contact: Huaiyu Yuan
Funded by: CCFS Foundation Program 10a

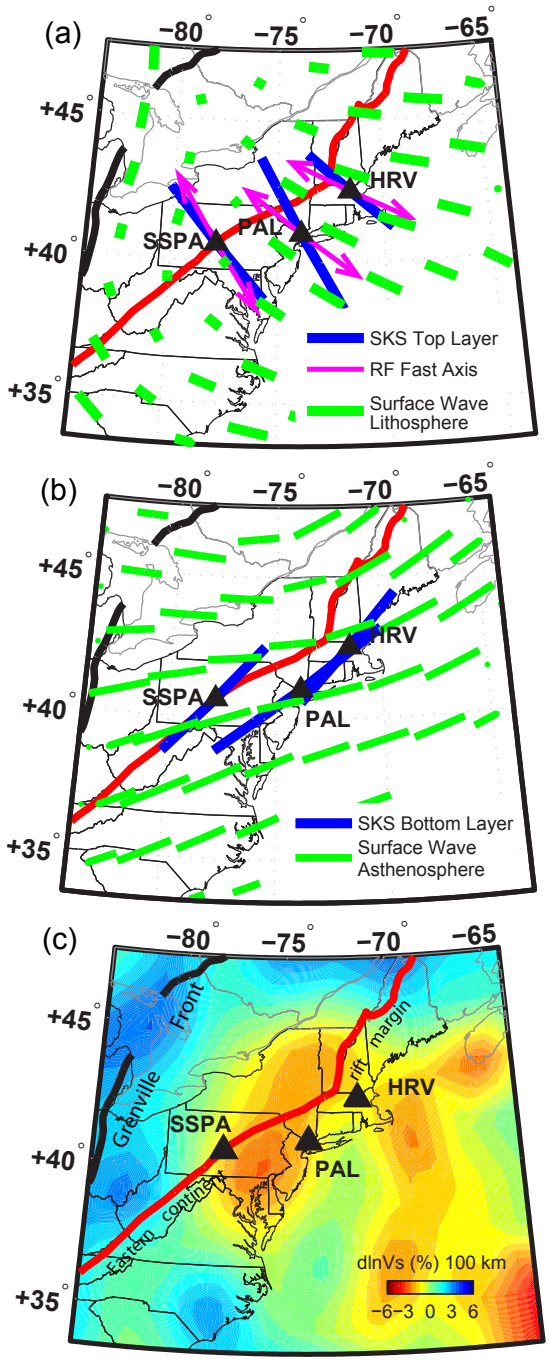

Figure 3. Map view showing the two-layer modeling results for the top layer (a) and bottom layer (b). The lithosphere anisotropy direction inferred from transverse receiver functions is also plotted as arrows in (a). Green sticks in (a) and (b) are equivalent two-layer (lithosphere and asthenosphere) model predicted from the 3D azimuthal anisotropy model of YR2010 model, maximum 1 s in the bottom layer). (c) Vs variation from Yuan et al. EPSL 2013 (http://dx.doi.org/10.1016/j.epsl.2013.11.057).

Mantle's golden secrets sparkle


Photo: Sigurdfjell sample locality

The upper mantle (convecting and lithospheric) plays an important role in the formation of major metallic ore deposits (e.g. Ni, Cr, diamonds; *CCFS publication #207*). However, the role of the mantle in the genesis of gold deposits is poorly defined and still widely debated. This is primarily because the ultra-low concentrations of gold in mantle rocks are very difficult to analyse.

The state-of-the-art instrumentation at CCFS has allowed us to tackle this problem from a new perspective. We have analysed the sulfide minerals, which naturally concentrate gold, in several suites of mantle peridotite (olivine-rich) xenoliths. These data can then be combined with the well-characterised alteration history of the samples to develop a model for how gold concentrations are modified during mantle processes. We also have compiled a large database of whole-rock gold analyses in mantle samples from the literature to compare with our analyses.

Our data indicate that gold concentration in the upper mantle is very heterogeneous. This is confirmed by a meta-analysis of the literature data. This heterogeneity is present on fractal scales. Using our techniques, we can observe it between grains hosted in a single sample, but it also occurs between samples from a single suite, and between localities globally.

The variation in gold contents shows a strong relationship with the degree of metasomatism the sample has experienced, as defined by rare earth element (REE) characteristics (Fig. 1). This relationship holds true using both our *in situ* analyses and in the compiled whole-rock dataset. The samples that show the *least* interaction with metasomatic agents (i.e. the samples with the lowest La/Yb ratios) have the *greatest* heterogeneity in the Au content, both among their individual sulfide grains and between xenoliths. Conversely, the samples that show strong interaction with metasomatic agents (i.e. samples with high La/Yb ratios) have relatively homogeneous gold contents among their individual sulfide grains as well as between samples. These strongly modified samples also typically have the lowest gold concentrations.

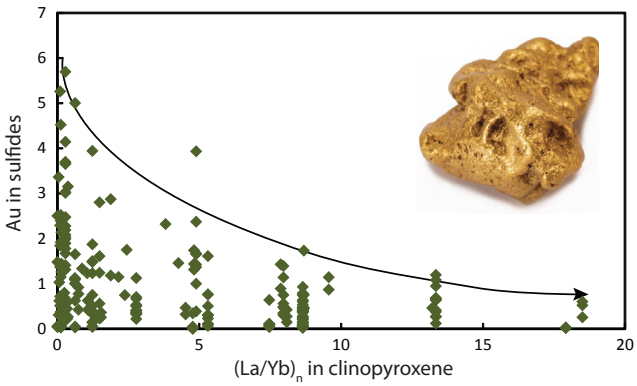

Figure 1. Au content in sulfides versus $(La/Yb)_n$ in coexisting clinopyroxene. Higher La/Yb ratios in clinopyroxene is indicative of a greater fluid flux. The samples that have experienced the greatest interaction with fluids have the lowest and the most homogenous gold contents.

This homogenisation and reduction of gold concentrations during metasomatism indicates that the samples that have experienced a high fluid flux have fully re-equilibrated with the metasomatic agent. During this process, gold has partitioned into the fluid phase and been partially removed from the system, resulting in overall lower gold concentrations. On the other hand, small fluid fluxes may introduce new sulfides into the samples but leave the previous generation of sulfides unmodified. As a result these "unmetasomatised" samples contain both residual and metasomatic sulfides.

These results have several major implications. Firstly, it indicates that gold is likely to be removed rather than added during major metasomatic modifications of the upper mantle. Contrary to what has previously been suggested, it is unlikely that there are regions of "gold-rich" metasomatised upper mantle.

Secondly, the heterogeneity of the sulfide phase in the otherwise "unmetasomatised" samples has implications for Os-isotope studies. Many previous studies have used whole-rock analytical techniques to determine the age of depletion of mantle samples. To exclude the effects of metasomatism, these studies often look at the REE characteristics of the samples and pick those that are "unmetasomatised". This study shows that these are the samples that are likely to have the greatest mixture of sulfide generations, and thus whole-rock techniques will not give a reliable age of depletion.

This project is part of CCFS Themes 2 and 3, Earth Evolution and Earth Today, and contributes to understanding Earth's Fluid Fluxes.

Contacts: Ed Saunders, Norman Pearson, Sue O'Reilly, Bill Griffin

Funded by: CCFS Foundation Program 1, APA, MQPGRF

How "super" was Nuna?

There has been a growing interest in the proposed pre-Rodinian supercontinent, variously called Nuna, Columbia, or Hudsonland. One of the main geological arguments used for this hypothesis is the presence of 2.1–1.7 Ga orogens in most continents around the world, which might have resulted from the assembly of this supercontinent. However, most reconstructions are highly speculative, mainly due to the lack of adequate high-quality paleomagnetic data to provide independent constraints. Our latest synthesis of paleomagnetic and geological data suggests that most of the 2.1-1.7 Ga orogens may have been related to the initial stage of a longer assembly process, during which some major building blocks of Nuna were formed. Those included: (i) West Nuna (Laurentia/Greenland, Baltica, Cathaysia, Rockall and possibly India); (ii) East Nuna (North, West and South Australia, Mawson Craton of Antarctica and North China) and (iii) Siberia and Congo-São Francisco cratons. According to our model, these three blocks amalgamated into a single supercontinent (Nuna) between 1.65 and 1.58 Ga. There were also some other continents, such as Amazonia/West Africa and Kalahari, which may or may not have been parts of the Mesoproterozoic supercontinent. Nuna may have broken apart at ca 1.45–1.38 Ma by the separation between Australia/East Antarctica and Laurentia. However, West Nuna, Siberia and possibly Congo/São Francisco were rigidly connected until after 1.27 Ga. The exact timing of their breakup is still uncertain.

Using a multi-disciplinary approach, we produced the first continuous global palaeogeographic animation for the half-billion years between 1.77 and 1.27 Ga (*CCFS publication #309*). Although our model may not be a unique solution, it is paleomagnetically permissible and is supported by a range of geological data. For example, reconstructions at 1.58 and 1.5 Ga (Fig. 1) demonstrate that the proposed position of the Mesoproterozoic mantle plume in South and West Australian cratons is in accord with a suggested hot spot track *(Betts et al., Terra Nova 2007)*. The connection between Siberia and Congo/São Francisco is supported by the recently discovered matching 1.505 and 1.38 Ga dyke swarms in these continents *(CCFS publication #221)*. The suggested time of the collision between East and West Nuna reflects the coeval orogenic events in western Laurentia and Northern Australia. Their separation may be related to the formation of the Belt-Purcell Basin in North America. The positions of parts of Australia and North China have been established in previous publications *(CCFS publications #117, 197)*. Connection between India and Baltica is also supported geologically *(CCFS publications #195, 309)*.

The relative positions of Laurentia, Baltica and India suggest a long-lived Mesoproterozoic active oceanic margin along their common ocean-facing edge (Fig. 1). Geological evidence for such a margin is found in all three continents (e.g. *CCFS publications #195, 309)*.

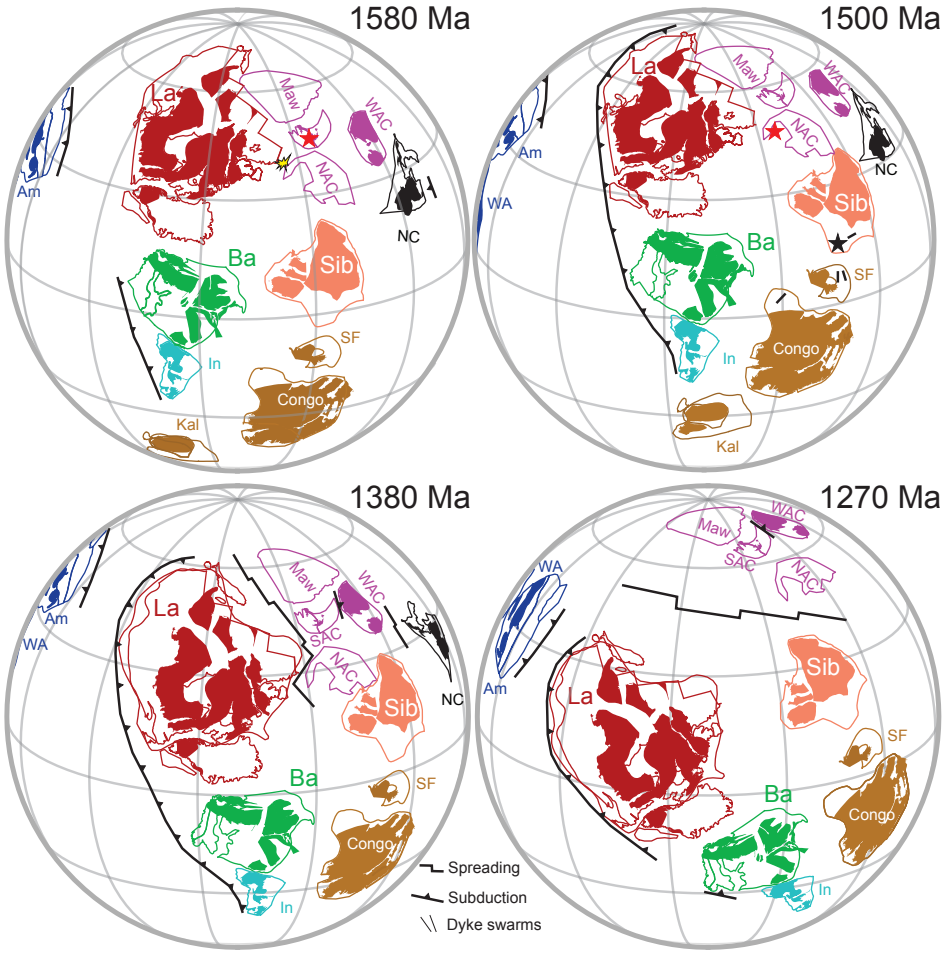

This project is part of CCFS Theme 2, Earth Evolution, and contributes to understanding Earth's Architecture.

Contacts: Sergei Pisarevsky, Zheng-Xiang Li
Funded by: CCFS Foundation Program 6

Figure 1. Mesoproterozoic global paleogeographic reconstructions. West Nuna: La = Laurentia, Ba = Baltica, In = India. East Nuna: NAC = North Australian craton, WAC = West Australian Craton, SAC = South Australian Craton, Maw = Mawson Craton, NC = North China. Si = Siberia, SF = São Francisco, Kal = Kalahari, Am = Amazonia, WA = West Africa. Filled areas represent Archean crust. Stars represent heads of mantle plumes.

Fluid-induced deformation during metamorphism

The deep-Earth water cycle is strongly coupled to the dynamics of Earth's interior. The amount of water carried into the deep mantle by descending oceanic crust is relatively small, but even a trace amount of water affects physical and chemical properties such as melting temperature, rheology, deformation mechanisms and electrical conductivity. Ophiolitic chromitites are commonly regarded as resistant to fluid-related processes, and have been used to track the evolution of Earth's mantle convection.

Chromitites occur in the Golyamo Kamenyane serpentinite, which is a part of a dismembered metaophiolite located in the Avren synform in the upper high-grade unit of the metamorphic basement of the Eastern Rhodopes crystalline massif in SE Bulgaria. These chromitites have been subjected to high-P metamorphism, but preserve evidence of fluid-rock interaction during metamorphism. The retrograde P-T exhumation path of the Golyamo Kamenyane chromitites allowed almost complete transformation of primary chromite into several types of secondary chromites, during amphibolite-facies deformation and fluid infiltration.

Detailed geochemical studies based on major element components (*Gervilla et al., 2012*) have classified the chromitites into four textural groups: partly altered chromite, porous chromite, non-porous chromite, and zoned chromite. According to their chemical modelling, chromitites reacted with two kinds of fluids during retrograde metamorphism: (1) Si-rich fluids with very low fO_2 that produced chlorite and partly altered and porous chromite, and (2) oxidising fluids that produced Fe^{3+}-rich chromite and formed non-porous and zoned chromite grains.

To investigate the chromite deformation and identify the slip systems, crystallographic orientation measurements were obtained by using the SEM-EBSD (Electron Back-Scattered Diffraction), in the CCFS Geochemical Analysis Unit at Macquarie. EBSD reveals significant crystal-plastic deformation, such as inter-crystalline deformation defined by low-angle boundaries (Fig. 1b, d). The homogeneous distribution of subgrain boundaries in zoned chromite indicates that chromite deformed after the chemical zoning had been established (Fig. 1b). Fluid percolation also produced recrystallisation of fine grains (Fig. 1d). The fine-grained aggregates of chromite probably formed by both dynamic recrystallisation and nucleation that were enhanced by reaction with oxidising fluids. However, there is no evidence of significant deformation in the partly altered chromite (Fig. 1a). Overall, fluid-rock interaction enhances deformation of chromites, which produces recrystallisation due to both dynamic recrystallisation and nucleation.

This project is part of CCFS Theme 2, Earth Evolution, and contributes to understanding Earth Architecture and Fluid Fluxes.

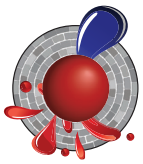

Contacts: Takako Satsukawa, José-María González-Jiminéz, Bill Griffin, Sue O'Reilly, Sandra Piazolo

Funded by: CCFS Foundation Program 1

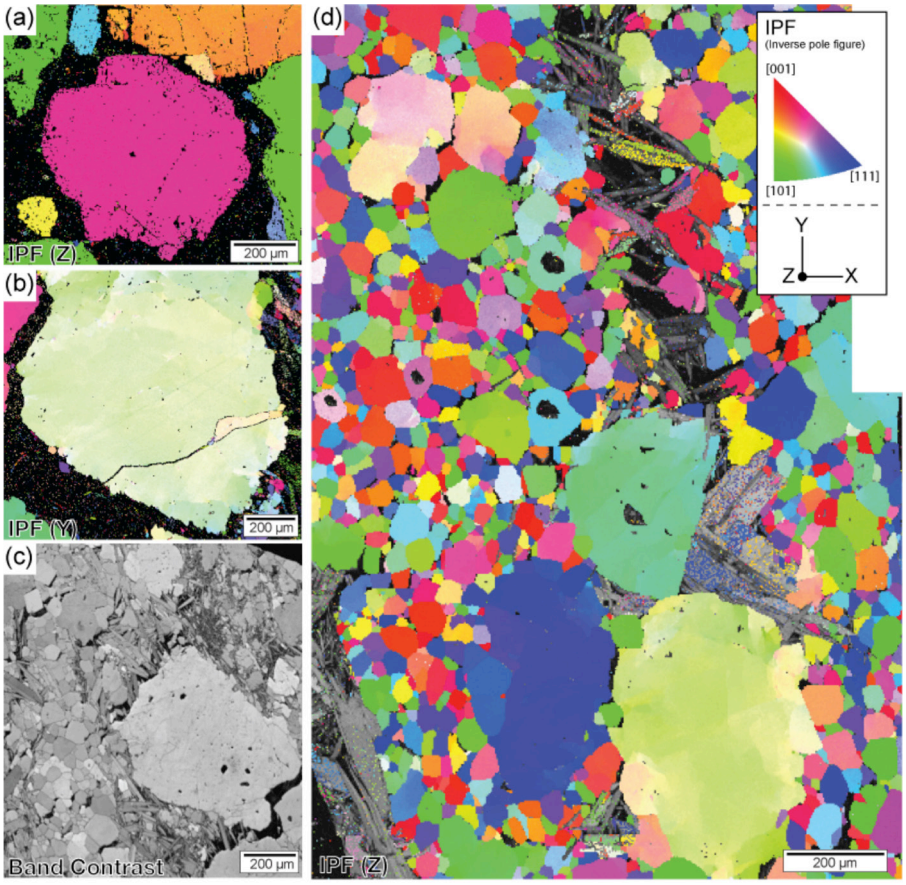

Figure 1. Crystallographic orientation maps of chromites from Golyamo Kamenyane. Rainbow scale in the maps indicated the Inverse pole figure (IPF) colour. (a) IPF map of partly altered chromite. (b) IPF map of zoned chromite. The presence of subgrain boundaries indicate crystal-plastic deformation. (c) Band contrast map of non-porous and zoned chromite. Euhedral chlorite grains fill in the chromites. (d) IPF map of non-porous chromite. Dynamic recrystallisation in coarse chromites by the development of subgrains in a matrix of recrystallised chromite.

New insights into Earth's early differentiation

To understand how Earth's mantle has evolved over time, we need to know the chemical composition and differentiation of the primordial silicate Earth. Planetary analogs (Mars and the Moon) suggest that Earth experienced large-scale melting soon after accretion, vigorous convection in the early mantle due to higher heat production from radioactive decay, core formation, and large impacts followed by crustal recycling. All this activity is generally thought to have efficiently mixed and homogenised the mantle, obliterating all signs of Earth's youthful exuberance. This implies that Earth started as a well-mixed homogeneous body that evolved progressively over geological time to form several chemically distinct domains. The isotopic and chemical heterogeneities observed in modern mantle-derived rocks thus are generally believed to reflect later production and recycling of oceanic and continental crust through geological time.

All that changed with the discovery of chemical and isotopic heterogeneities, which must have been generated ca 4.53–4.45 Ga ago, in high-magnesium lavas from Baffin Bay, which are only ca 60 Ma old (*CCFS publication #354*). Refractory lithophile elemental and isotopic evidence from less-evolved whole rock samples and olivine-hosted melt inclusions suggests a chemically heterogeneous source for the Baffin Bay lavas that contains enriched and depleted end-member components (Fig. 1a and b). Because the two end-members both have primitive Pb isotope compositions that plot within the geochrons of 4.53 to 4.40 Ga and coupled primitive He isotopes (Fig. 1c and d), the chemical heterogeneities likely formed in Earth's infancy. This implies that chemical effects of early differentiation can persist in mantle reservoirs to the present day. Figure 2a illustrates how global differentiation of the early silicate Earth from 4.55 to 4.40 Ga may have produced depleted and enriched types of dense melts in an undegassed deep Earth. The global differentiation of the bulk silicate Earth would have occurred in two independent layers at >1,800 km and ≤1,800 km depths. The density contrast would produce an enriched denser liquid phase at the core-mantle boundary. In contrast, within the upper layer (≤1,800 km) the residual liquid would rise buoyantly as crystallisation proceeded until a small fraction (≤1%) of melt ultimately formed a protocrust at the Earth's surface, resulting in depletion of 60% of the silicate Earth. The depleted dense melt may have been generated by high degree partial melting of peridotite at about 300-410 km depth, shortly after magma ocean crystallisation. These two types of dense melts would result in materials constituting the present-day thermo-chemical piles hosted within the two large low-shear-wave-velocity provinces above the core-mantle boundary, that have been protected from complete entrainment by subsequent mantle convection currents. We argue that, although such dense melts likely exhibit some 'primordial' geochemical signatures, they are not representative of the bulk silicate Earth. Such an early-formed dense chemical layer would continue to be sampled by mantle plumes (Fig. 2b). Our work links formation, preservation, and sampling of early chemical heterogeneities into a self-consistent

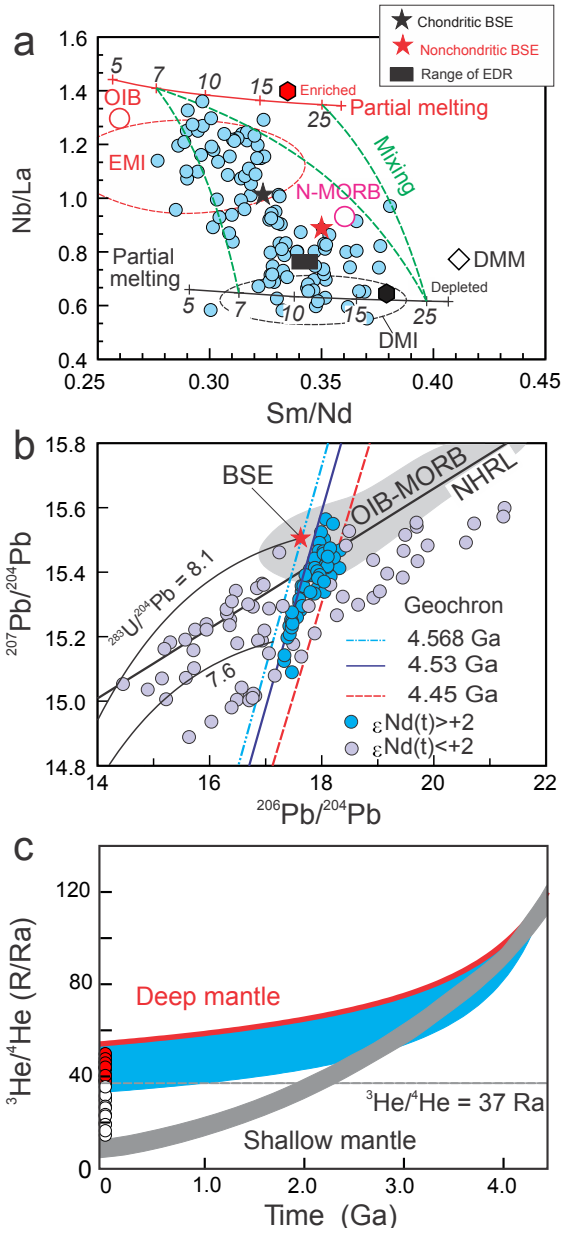

Figure 1. (a): EMI and DMI are the enriched and depleted types of melt inclusions from high $^3He/^4He$ BIWG picrites, compared to average normal-MORB (N-MORB), ocean island basalt (OIB), depleted MORB mantle (DMM). Lines indicate non-modal batch melting (solid lines with cross), binary mixing (green dashed lines); numbers in italics mark partial melt fractions (%). (b) Lead isotopes of Baffin Bay high-magnesium lavas. Black curves indicate evolution from the initial Pb-isotope composition of Canyon Diablo. Also shown are 4.568 Ga, 4.53 Ga, and 4.45 Ga geochrons. (c) Evolution of $^3He/^4He$ for the early formed dense chemical layer (blue) is based on the method of Class and Goldstein (2005) for an initial $^3He/^4He$ =120 RA, [^3He] ranging from 2.0×10^{11} to 0.8×10^{10} atomsg-1and U = 0.038 to 0.0028 ppm; Th = 0.0735 to 0.010 ppm. Evolution of deep mantle (red) and shallow mantle (grey) are from Lee et al (2010). The $^3He/^4He$ lower than 37 RA (open circles) were likely affected by post-eruption reduction of $^3He/^4He$ by ^4He accumulation.

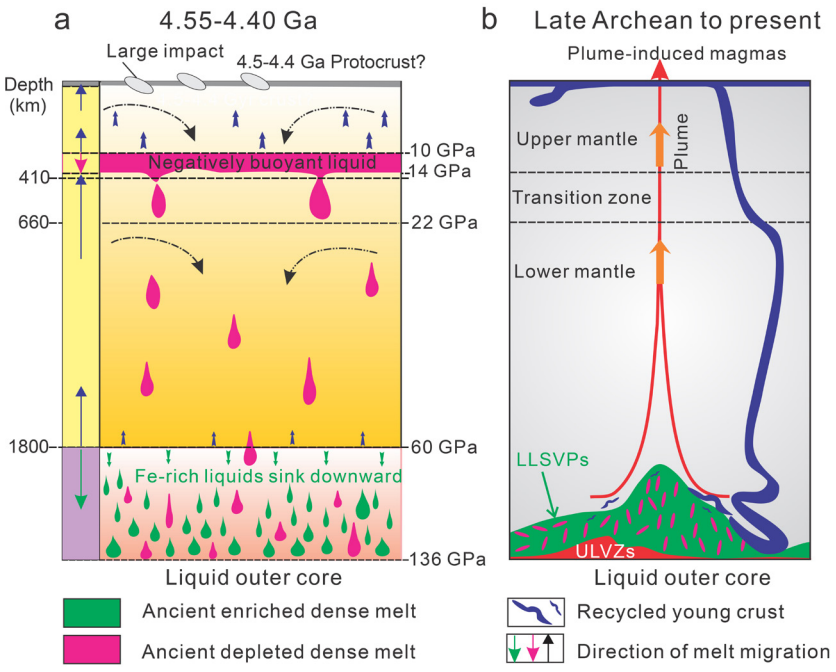

Figure 2. (a) Freezing of a magma ocean produced enriched dense melts below 1,800 km depth that accumulated at the CMB, and 60% depletion of the BSE occurred at above 1,800 km depths due to positive buoyancy of the residual melt. Shortly after magma ocean crystallisation, hot and deep melting of the upper mantle could have generated depleted dense melts at 410–300 km depth. The two types of dense liquids sunk and accumulated at the CMB to form a dense chemical layer. (b) In Late Archean and later times, melting was restricted to shallow depths. The dense chemical layer is likely hosted by large low-shear-wave velocity provinces (LLSVPs) and ultralow-velocity zones (ULVZs) and appears to have persisted for much of Earth's history.

geodynamic system and thus provides a strong case for mantle chemical heterogeneity being formed by a major differentiation event shortly after planet accretion rather than through the subsequent geodynamic evolution.

How such a dense chemical layer can be sampled and brought to the surface is another important question. Geological evidence related to supercontinent reconstructions shows that both the location and formation of superplumes were dominantly controlled by the first-order geometry of global subduction zones. Recent studies proposed that sinking subducted slabs not only can push the dense chemical layer upward, but at the same time also push the thermal boundary layer to form thermal-chemical domes, enhancing or triggering thermal instability (Fig. 2b). Our recent studies (*CCFS publication #336*) show that the late-Cenozoic less contaminated and synchronous basaltic samples from the Hainan-Leizhou peninsula, the Indochina peninsula and South China Sea seamount have primitive Pb isotopic compositions that lie on, or very close to, 4.5- to 4.4-Ga-old geochrons on a $^{207}Pb/^{204}Pb$ versus $^{206}Pb/^{204}Pb$ diagram, suggesting a mantle source that developed early in the Earth's history (4.5-4 Ga). These basalts occur above a seismically detected thermal plume adjacent to deep subducted slabs. Thus, they provide a strong case that the avalanches of subducted slabs to the CMB may have pushed up a thermal-chemical pile to form a thermal plume (Fig. 3; *CCFS publication #336*). The physical properties of mantle plumes also dictate that materials from the dense chemical layer near the CMB should only be a minor component of mantle plumes and thus can only be identified in the earliest phase of high temperature melts (picrites and komatiites). This implies that the ancient mantle reservoir could only be a dominant source component in the early stage of a plume magmatic event, which would then be diluted by recycled oceanic crust components as the plume magmatism continues.

This project is part of CCFS Theme 1, Early Earth, and contributes to understanding Earth's Fluid Fluxes.

Contacts: Xuan-Ce Wang, Zheng-Xiang Li
Funded by: CCFS ARC ECSTAR funds

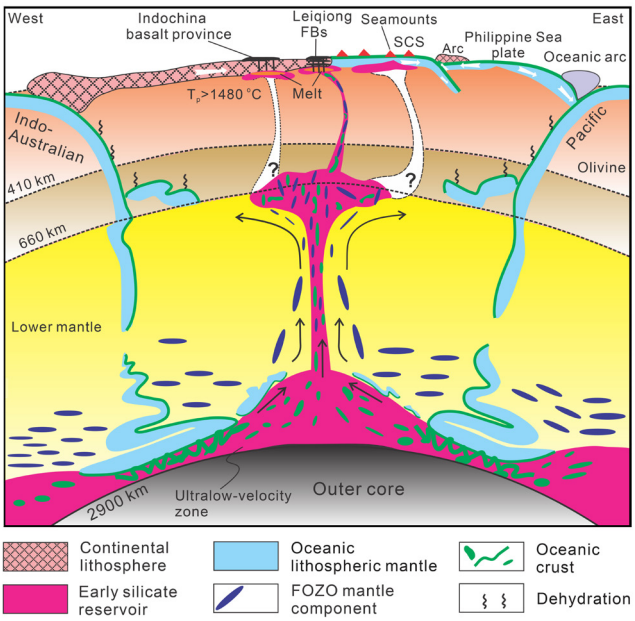

Figure 3. Formation of the Hainan plume. Broad low-velocity anomalies beneath the lithosphere and the transition zone are prominent, but the interpreted secondary plumes beneath the Indochina peninsula volcanic province and seamounts in the South China Sea (SCS) have not yet been reported by seismic tomography. Volcanism in the Indochina peninsula and the South China Sea may have been caused by thermal plumes or small-scale thermal upwellings from the edge of the broad anomaly. Early silicate reservoirs are recognised in plume-induced basaltic rocks

Zircon and baddeleyite fingerprint platinum, nickel and copper mineralisation processes at Noril'sk (Russia)

The ultramafic–mafic Noril'sk-1 intrusion in Polar Siberia (Russia; Fig. 1) hosts one of the world's major platinum group-element (PGE)-Cu/Ni sulfide deposits. Despite years of study there is still ongoing debate about the origin of the Noril'sk-type intrusions, especially about the sources of the silicate magmas and ore metals for individual lithological units. However, it is generally accepted that the mantle-derived ultramafic–mafic magmas and PGE–Ni/Cu deposits of the Noril'sk-Talnakh region in Russia are closely linked, implying that juvenile mantle-derived materials are intrinsic to their petrogenesis. It is also commonly assumed that the 'Noril'sk-type' intrusions are genetically linked to the 250 Ma Siberian flood-basalt volcanism.

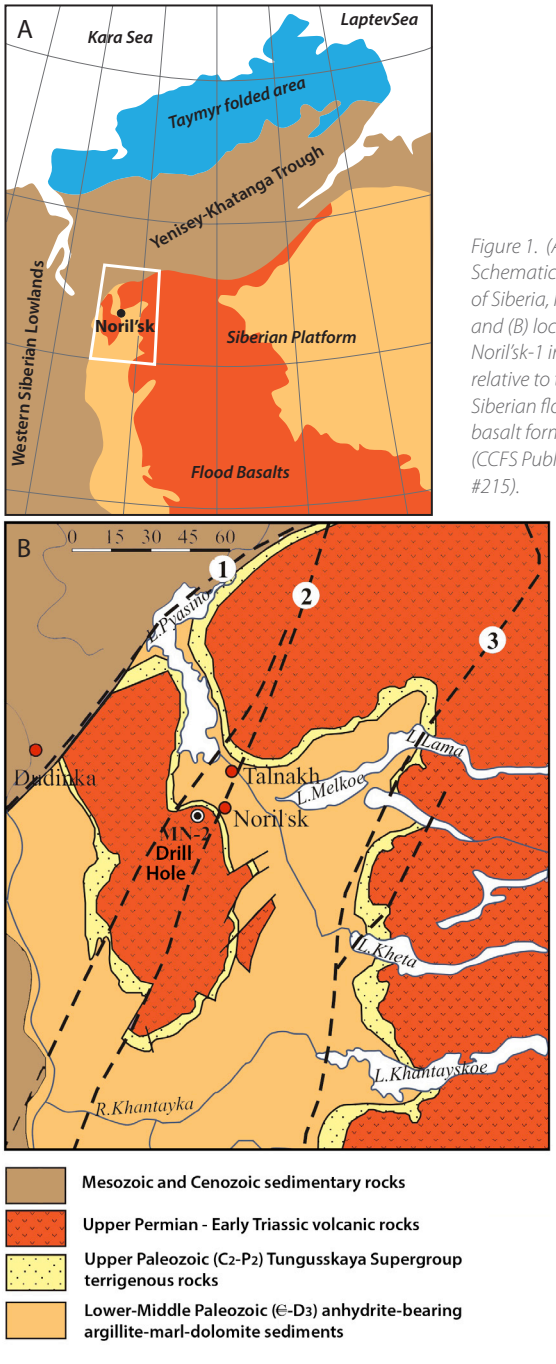

Figure 1. (A) Schematic map of Siberia, Russia and (B) location of Noril'sk-1 intrusion relative to the Siberian flood-basalt formation (CCFS Publication #215).

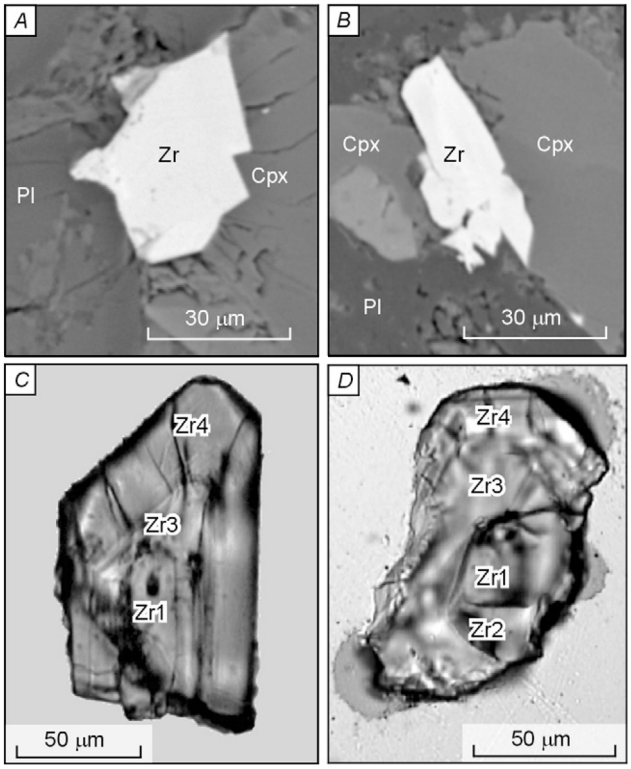

Figure 2. Examples of zircon in situ *in thin sections (A, B; in back-scattered electrons) and mineral separates (C, D; in transmitted light) from rocks of the Noril'sk-1 intrusion (GEMOC Publication #720). A, B, Assemblages of zircon and rock-forming minerals from olivine gabbro and taxitic pyroxene leucogabbro. Zr, zircon; Cpx, clinopyroxene; Pl, plagioclase. C, D, Inner structure of polyphase grains, composed of "cores" (Zr1 and Zr2) and "rims" (Zr3 and Zr4).*

Nd-Sr-Os-Pb isotopic studies of the main units of the economic Noril'sk-type intrusions and their ores have contributed to a better understanding of the origin of Noril'sk-type intrusive hosts and associated ores. The Os- and Pb-isotope compositions of the PGE–Cu/Ni sulfide ores preserve mantle-like values, and it has been suggested recently that staged chambers played an important role in the evolution of the Noril'sk-type deposits. Whole-rock Nd-isotope data represent the homogenised end product of these processes; they provide cumulative information and do not tell much about magma sources during the evolution of the ultramafic-mafic magmas. The wide variation of Hf-isotope values in zircon in rocks with homogeneous whole-rock Nd-isotope data has been documented previously (see *GEMOC publications #251, #491*), demonstrating that the zircon data provide superior constraints for end-member mixing components. This emphasises the usefulness of *in situ* analytical techniques, where the Hf-isotope composition of the zircon records the evolution of the magma chamber, with

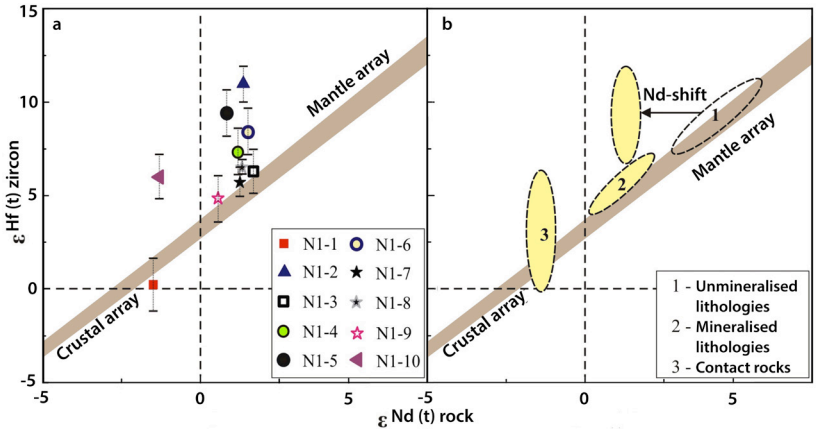

Figure 3. Plot of zircon εHf(T) versus whole-rock εNd(T), identifying three distinct clusters for the Noril'sk-1 intrusion. Mantle and crustal arrays according to Vervoort et al. (Geochim. Cosmochim Acta, 63, 1999).

input of magmas from different sources, and/or progressive contamination by country rocks.

However, there are few such data on zircon from the Noril'sk-type intrusions. To fill this gap we have explored the isotope systematics of Hf in zircon (Fig. 2) and baddeleyite from variously mineralised rocks of the economic Noril'sk-1 intrusion (*CCFS Publication #215*). *In-situ* Hf-isotope data of zircon and baddeleyite, combined with whole-rock Nd-isotope results, identify three distinct clusters of Hf-Nd isotope values (Fig. 3) typical of different lithological units (e.g. unmineralised gabbroic rocks, mineralised ultramafic and taxitic-textured rocks with disseminated PGE-Cu-Ni sulfide ores, and gabbro-diorite). These groupings suggest the interaction of three distinct magma sources during the protracted evolution of the Noril'sk-1 intrusion: (1) a juvenile source equivalent to the Depleted Mantle, (2) a subcontinental lithospheric mantle source and (3) a minor crustal component. It appears that the Hf-isotope composition of zircon and the Nd-isotope compositions of unmineralised lithologies were decoupled. These data also suggest that a prolonged period for concentration of the ore components in staged chambers during this interaction is a key factor for the formation of economic deposits, and that the zircons can fingerprint this process as a guide to exploration.

The zircon and baddeleyite from Noril'sk-1 show isotopic and geochemical features that are not usually expected for mafic and ultramafic rocks. Models for the origin of the Siberian flood basalts and their relationships to the Norilsk-type intrusions should be further investigated in light of new Hf-Nd isotopic constraints, which indicate a complex geological history for the economic ultramafic-mafic intrusions of the Noril'sk region.

This project is part of CCFS Themes 2 and 3, Earth Evolution and Earth Today, and contributes to understanding Earth Architecture and Fluid Fluxes.

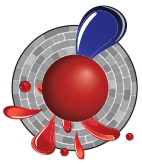

Contacts: Elena Belousova, Bill Griffin, Sue O'Reilly, Norman Pearson
Funded by: ARC Future Fellowship, Macquarie University contribution to ARC FT, CCFS Foundation Program 1

Giant porphyry copper deposits on the roof of the world flow from deep wet crust

The Gangdese porphyry copper belt in Tibet, the roof of the world, is the richest porphyry copper system known to have developed in a continental collision zone. Five porphyry copper – molybdenum (Cu-Mo) deposits are currently being mined in this province, accounting for an estimated 18 million tons (Mt) of contained copper-10.5 Mt of this in the giant Jiama deposit alone (Fig. 1). Seven additional prospects are under active exploration in the region, and it is clear that the potential of the belt has not been fully unlocked.

These porphyry Cu deposits developed in the Miocene, significantly post-dating the collision of India with Asia, so the most common model of porphyry copper genesis in association with oceanic subduction cannot be applied here. One of the most striking features of the metalliferous deposits is their close association with adakite-like intrusions, felsic igneous rocks with high Sr and Eu contents, and high Sr/Y ratios. These intrusions are widely attributed to dehydration melting (in the absence of free water) of garnet-amphibolite and/or eclogite facies rocks in the thickened crust below Tibet. However, the associated mineralised porphyries contain more than 9% water by weight, and cannot be derived through any simple evolution of melts originating from anhydrous high-grade metamorphic parent rocks. This presents a dilemma in explaining the development of this important endowed province.

To resolve this dilemma, we are looking at the wider regional context of these porphyries to produce an internally consistent model that can account for their key characteristics, and give a key to developing strategies for further exploration of the Gangdese belt.

In addition to the water problem, dehydration melting of amphibolites and/or eclogites does not produce melts with the chemical characteristics that match the inferred ore-forming magmas. Such melting would consume the hornblende in the source rocks before plagioclase began to melt, and *cont...*

Figure 1. The giant Jiama porphyry Cu deposit in Tibet. Photo taken from the elevation of 5000 m.

would not produce the adakite-like melts with high Sr and Eu contents and high Sr/Y. However, a high H_2O content in the starting material (and the resultant partial melt) stabilises hornblende to higher temperature and lowers the melting point of plagioclase. If significant amounts of water were added to the mafic lower crust, the chemical problems thus would be solved -- but how can large volumes of water be fluxed up into the lower crust in the Miocene, long after the cessation of oceanic subduction beneath this region?

We suggest that the coeval ultrapotassic lava flows of South Tibet provide the missing link in this puzzle. These mafic rocks are notably water-rich. Furthermore, the solubility of water in such ultrapotassic melts increases with increasing pressure, and therefore as the melts ascend, they release free water into the surrounding wall-rocks. Although they are rare at the surface, significantly larger volumes of ultrapotassic rocks are believed to occur at depth beneath the Tibetan lower crust, and underplating and crystallisation of these mantle-derived rocks may have provided the fluid required to catalyse the development of the fertile Tibetan porphyries in the Miocene.

This conceptual model is illustrated in Figure 2. We suggest that metasomatism of the lithospheric mantle and Jurassic underplating of arc melts below Tibet were essential to pre-condition the region for the subsequent development of the mineralised porphyries. In the Miocene, lithospheric thinning – probably due to convective removal of lithosphere during Himalayan orogenesis – caused melting of the water-rich metasomatised mantle domain, producing hydrous ultrapotassic-potassic melts. In the extensional conditions that prevailed across the western portion of the southern Lhasa subterrane, these mantle-derived magmas were able to ascend into the upper crust – and locally erupt. In the more compressive contemporary regime to the east of this subterrane however, the ultrapotassic-potassic magmas ponded in the lower crust. Release of water from the crystallising magmas then triggered melting of the overlying Jurassic arc material to produce the hydrous and adakite-like intrusions and associated porphyry Cu deposits.

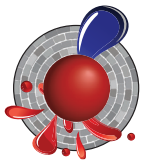

This project is part of CCFS Themes 2 and 3, Earth Evolution and Earth Today, and contributes to understanding Earth's Architecture and Fluid Fluxes.

Contacts: Yong-Jun Lu, Marco Fiorentini, Cam McCuaig
Funded by: CCFS Foundation Program 2a, 9, ARC CCFS ECSTAR funds

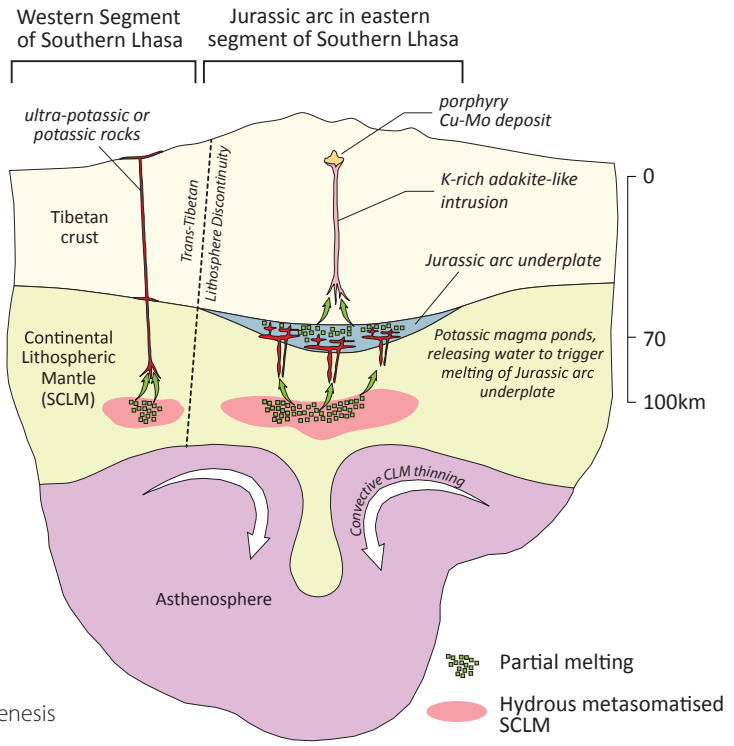

Figure 2. A conceptual model for the genesis of the hydrous fertile Tibetan porphyries, as outlined in the text.

Modelling multi-phase reactive flow in the mantle: a bottom-up approach

The physico-chemical processes that govern the evolution of continental lithosphere and its interaction with the sublithospheric upper mantle occur over very different spatial and temporal scales. The details of the interactions between these different scales and the resulting integrated macroscopic effects on the evolution of plates are still poorly understood. In order to understand these multi-scale (geological) processes, we need to be able to accurately simulate/model all the processes involved in natural multi-phase multi-component reactive systems. Unfortunately, although several groups are making progress towards this end, most modelling platforms available to the geodynamic community do not really deal with all these problems in an internally-consistent manner. It also can be difficult to scale them to a wide range of problems (e.g. from melting in cm-scale veins to mantle convection).

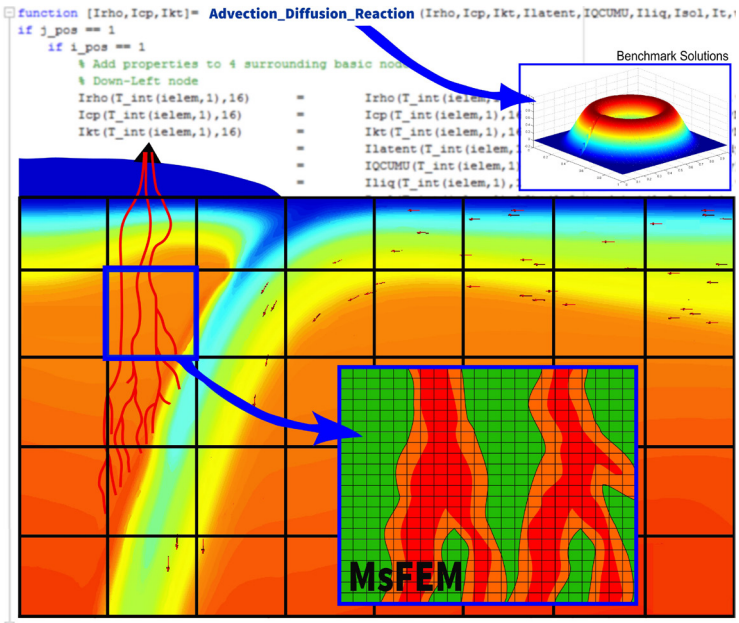

To bypass these limitations we take advantage of a novel numerical framework known as the Multi-scale Finite Element Method (MsFEM). The main idea is to capture the small-scale details of a problem and transfer them to the macro-scale through consistent and robust coupling of the micro- and macro-problems (back and forth). In particular, the MsFEM replaces the basis functions used in the traditional FEM, with a new set of micro-problem-dependent functions. This development provides a new numerical platform directly applicable to modelling geological phenomena such as the generation, migration and emplacement of magmas, chemical entrainment, transport of geochemical species, deposition mechanisms of sulfide liquids, the formation of ore bodies in hydrothermal systems, etc. Importantly, these "small-scale" processes are consistently coupled, in our numerical framework, to the large-scale driving tectonic processes, and that coupling allows us study the complex interactions between these different scales. So far, the MsFEM has been successfully applied and tested in fields such as composite materials, petroleum reservoirs and groundwater transport, but not yet in the large-scale analysis of the lithosphere-asthenosphere system.

Multi-phase reactive flow is governed by a multitude of balance and constitutive equations that need to be solved accurately with numerical methods. Ones of particular importance are the so-called "*advection-diffusion-reaction*" and the "*momentum*" equations, governing heat transfer and momentum transfer, respectively. Stability and accuracy analyses for these equations are well known and have been the subject of thousands of papers in the numerical community. Although there are many ways to solve these equations, not all of them are appropriate to a multi-scale approach. Moreover, the robustness, accuracy, and efficiency of many of these algorithms are still debatable when they are applied to geodynamic processes at different scales. This is due partly to poorly documented tests and benchmarks and partly to the geodynamics community's lack of any broad interest in multi-phase multi-component reactive flow .

As part of a larger CCFS Foundation Program 4, we are currently developing/testing a number of individual algorithms particularly designed to work under a multi-scale formalism for geodynamic problems. In particular, we have developed a new Lagrangian-Eulerian algorithm for advection-diffusion-reaction, which is proving to have remarkable accuracy, scalability, and generality. This finite-element algorithm combines the best features of fixed-mesh and marker-in-cell methods into a single conservative scheme that can accurately model processes in which there are large advective and reactive components together with isothermal and non-isothermal phase changes. We have also tested and improved existing multiscale algorithms that may be applicable to specific sub-problems. In parallel, we have implemented an efficient and fully compressible Lagrangian-Eulerian iterative solver (based on the "*Uzawa scheme*") for the momentum (and mass) equation and fast thermodynamic solvers for the computation of phase equilibria/component distributions. The internally-consistent combination of these three main components into a single thermo-chemical-mechanical algorithm will allow us to simulate a large variety of fluid-assisted geodynamic processes.

This project is part of CCFS Themes 2 and 3, Earth Evolution and Earth Today, and contributes to understanding Earth's Architecture and Fluid Fluxes.

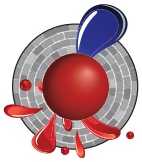

Contacts: Beñat Oliveira, Juan Carlos Afonso
Funded by: CCFS Foundation Program 4

Straining to transform from continent to ocean

The Grisons, in the Eastern Alps (Switzerland) have preserved an ocean-continent transition; numerous studies during the last decade provide an excellent structural framework. This area represents a section across a zone of exhumed continental mantle. Sub-continental spinel peridotite is exposed close to the continent (Totalp area) while the mantle further from the continent was infiltrated by melt and equilibrated in the plagioclase stability field (Platta area) (Fig. 1). The sequence includes highly deformed peridotites (ultramylonites) that allow us to study the evolution of deformation within an ocean-continent transition. A detailed study of the peridotite textures and geochemistry was combined with the analysis of the crystallographic orientation of minerals using the electron backscatter diffraction method (EBSD).

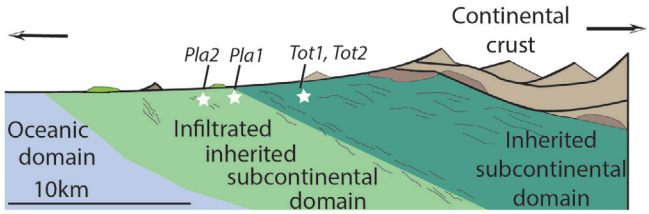

Figure 1. Schematic representation of an ocean-continent transition (after Peron-Pinvidic & Manatschal, 2009, Int.J.Earth.Sci, Muntener et al. 2010, J.Pet).

We sampled the Platta-Totalp massifs made of spinel lherzolites and harzburgites, intruded by gabbros and basaltic dykes, and partially covered by ophicarbonates. In Totalp, blocks of ultramylonites within a cataclastically deformed domain related to mantle exhumation, and ultramylonites parallel to the foliation of amphibole-bearing peridotites, were sampled.

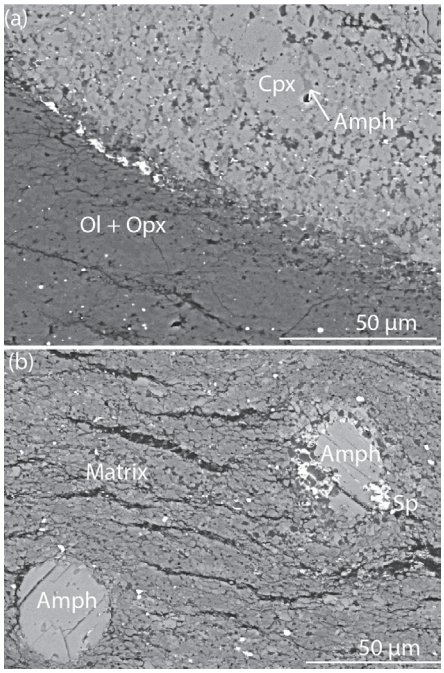

Figure 2. (a) Ultramylonite made by unmixed layers. Layers are clinopyroxene replaced by interstitial amphibole or olivine and orthopyroxene; (b) Ultramylonite contains round porphyroclasts of amphibole within a matrix of olivine, opx, cpx, amphibole and spinel.

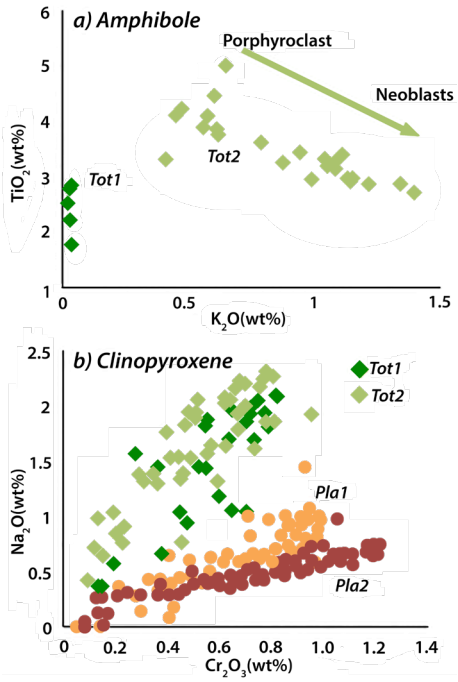

Figure 3. Chemical composition of amphibole (TiO_2 vs. K_2O wt%) and clinopyroxene (Cr_2O_3 vs. Na_2O wt%) from Totalp and Platta.

The ultramylonite blocks are formed by unmixed layers of olivine (ol) + orthopyroxene (opx) and clinopyroxene (cpx) + amphibole (Fig. 2a). Opx and ol grains are elongated, whereas the amphibole is interstitial and replaces the clinopyroxene. The ultramylonites have a fine-grained matrix (grain size 2-10 µm) composed of ol, opx, cpx, spinel and amphibole with rounded amphibole porphyroclasts (Fig. 2b). Pargasitic amphibole occurs in the former whereas kaersutitic amphibole characterises the latter. The kaersutite was related to pre-deformation metasomatism with K_2O enrichment from porphyroclasts to neoblasts during localisation of deformation (Fig. 3). The pargasite formed later than the kaersutite and was probably related to the exhumation of the mantle. The crystallographic preferred orientations of the kaersutite within the host peridotite are inherited from the porphyroclastic amphibole with a reorientation of <001> axes, to become parallel to the foliation. In the ultramylonitic matrix, the amphibole grains have elongated shapes and their <001> axes are parallel to the foliation, suggesting either a strong grain rotation or a dynamic recrystallisation.

The clinopyroxene composition has been analysed for Totalp and Platta samples. There is no distinct difference among the Totalp samples, but samples from Platta have lower Na_2O, suggesting melt percolation and crystallisation of plagioclase. Some Platta samples show slightly lower Na_2O suggesting less melt infiltration, and has a more continental affinity (Figs. 1 and 3). In porphyroclastic clinopyroxene from the host peridotite in Totalp, the activated slip is (010)[100], which is uncommon and marginal in peridotites because of using a large burger vector (Fig. 4a). In clinopyroxene porphyroclasts <100> axes are parallel to the foliation whereas the recrystallised grains show a reorientation with <001> axes more parallel to the foliation (Fig. 4b, c). Olivine porphyroclasts within the host peridotite show the activation of two slip systems within a single grain: (001)[100] and (100)[001]. In the fine-grained ultramylonitic matrix the dominant activated slip system is (001)[100] E-type.

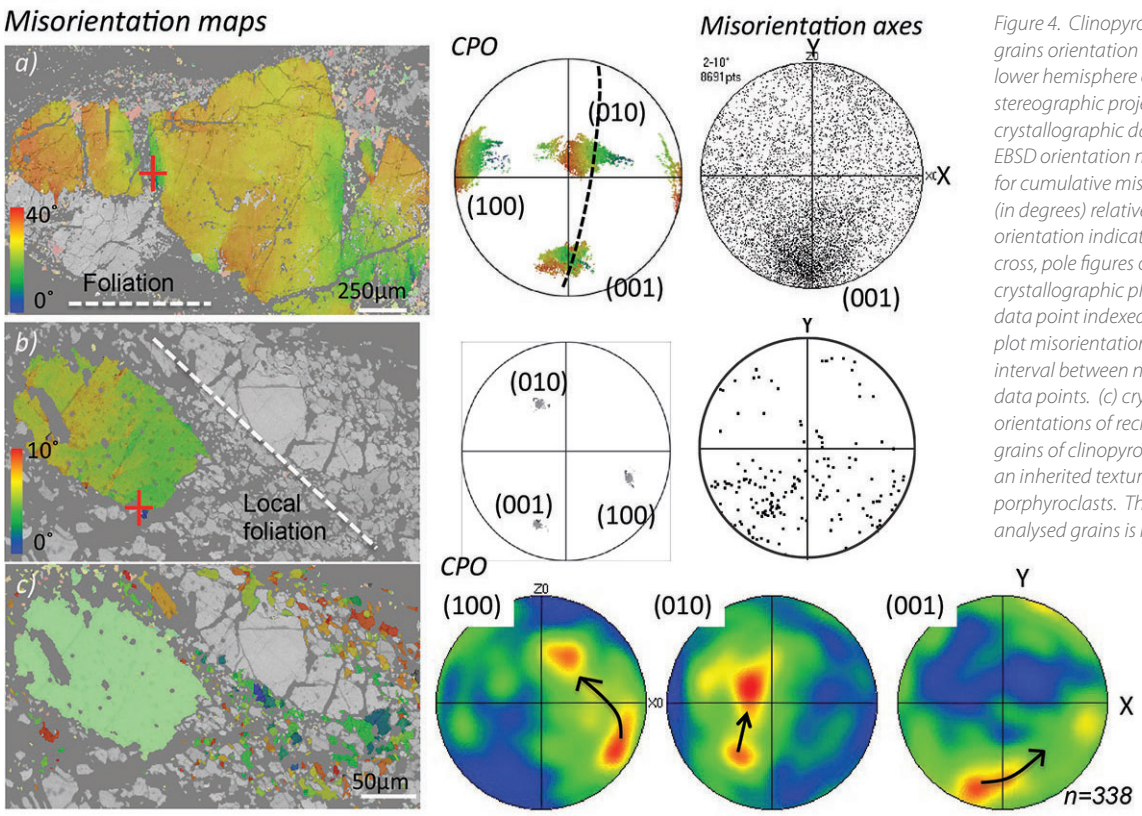

Figure 4. Clinopyroxene individual grains orientation maps and lower hemisphere equal area stereographic projections of crystallographic data. (a-b) EBSD orientation map colored for cumulative misorientation (in degrees) relative to reference orientation indicated by a red cross, pole figures of major crystallographic planes for every data point indexed on map, and plot misorientation axes for (2–10°) interval between neighbouring data points. (c) crystal preferred orientations of recrystallised grains of clinopyroxene showing an inherited texture from the porphyroclasts. The number of analysed grains is n=339.

The results obtained in 2013 show that the transition from subcontinental to infiltrated subcontinental mantle towards the ocean involved a compositional evolution and a change in deformation mechanisms. The presence of amphiboles testifies to fluid percolation before deformation, and tracks chemical evolution of the fluid during localisation of deformation. The amphibole and clinopyroxene crystal preferred orientations in the host peridotite are partially inherited from the primary texture, and overprinted by several mechanisms such as grain rotation, dynamic crystallisation and/or grain boundary sliding when the strain increases.

This project is part of CCFS Themes 2 and 3, Earth Evolution and Earth Today, and contributes to understanding Earth's Architecture and Fluid Fluxes.

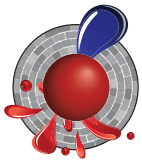

Contacts: Mary-Alix Kaczmarek, Steve Reddy
Funded by: CCFS, Curtin University (Perth), The Swiss National Foundation (SNF), The University of Lausanne

Mantle dynamics model constrained by plate history

The temporal evolution of the Earth's internal structure is very important to geoscience research, however this time-integrated evolution cannot be observed directly by available techniques. Mantle convection simulations are thus important tools to investigate this problem.

Subducting slabs descending deep into the mantle will carry, and subsequently release, water: this can promote partial melting in mantle rocks, resulting in volcanoes overlying deep, dewatering subducting slabs. Such volcanic activity can concentrate incompatible elements from Earth's interior at the surface, so models that can predict subduction dewatering pathways are of significant value to the mineral-exploration industry. However, plate boundaries have moved a lot in the past, obscuring the history of magmatism. We are developing dynamic models that can reconstruct the P-T-t path of minerals in subduction zones, and also the water content of subducting lithologies. Adopting mineral physics studies on the mantle solidus and partial melting, we will be able to calculate melting percentages and eruption rates to track the history of subduction zone volcanic activity through time, and provide quantitative and temporal maps of the generation and migration over the past few million years on a global scale.

In our approach, we use the open-source code ASPECT; this is a highly-parallelised and modularised code that uses the adaptive mesh refinement technique to achieve much better resolution than conventional approaches, at reasonable computational costs. It also supports temperature, pressure and composition - dependent simulation parameters, allowing us to adopt more realistic mineral physics models. Plate tectonics is the dominant control on the mantle flow pattern, and plate reconstructions from geophysical and geological data provide crucial *cont...*

constraints on surface motions in the past few hundred million years. In our mantle convection models, we use plate history as a time-dependent surface boundary condition.

Using this approach, our model successfully recovers the position of major subducting slabs and mantle upwellings, in accordance with present day seismological observations. Building such a model requires large amounts of computational power, and current models are running on a cluster with a few hundred CPUs, which may not be have the capacity to achieve the required resolution. A new resource allocation from Intersect, has delivered more computing power that will allow refinements of the current resolution over the next year.

This project is part of CCFS Theme 2 and 3, Earth Evolution and Earth Today, and contributes to understanding Earth's Architecture and Fluid Fluxes.

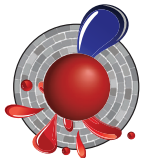

Contacts: Siqi Zhang, Craig O'Neill

Funded by: CCFS Foundation Program 4

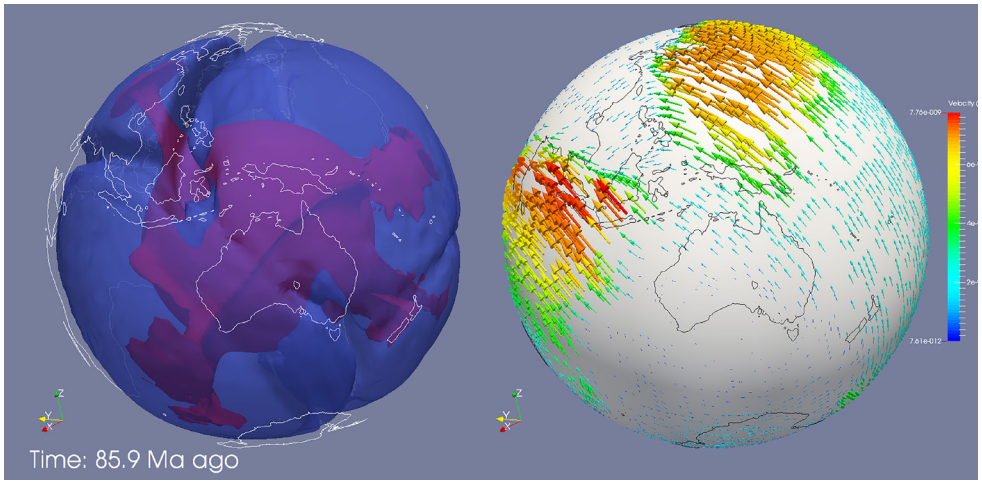

Figure 1. Snapshot at 85.9 Ma ago shows subducting slabs and plumes reconstructed by the mantle convection simulation constrained by plate history. In the left-hand figure, the transparent surfaces show contours of temperature; the present day coast-lines are shown in white. In the right-hand figure, the arrows show the surface motion constrained by plate reconstruction, and present-day coastlines are shown in black.

Zircon signposts for Gold

Multi-isotopic maps are a powerful tool for imaging lithospheric blocks of different age, and have been used in the Yilgarn Craton of Western Australia. Such maps combine *in situ* zircon U-Pb and Lu-Hf isotopic analyses with whole-rock Sm-Nd data. As the ancient lithospheric boundaries sometimes cannot be seen in modern seismic images, the isotopic mapping serves as a form of 'paleogeophysics' for imaging paleocraton margins through time.

There is a strong spatial correlation between lithospheric boundaries and the concentration of a variety of mineral deposit types; these isotopic boundaries mark lithosphere-scale structures that control magma and fluid flux, and thus the location of large mineral systems through time. However, the only available case study in the Archean is the Yilgarn of WA, and even that is only focused on the centre of the craton. Therefore, we have tested this hypothesis in the Wabigoon Subprovince in the western part of the Superior Craton of Canada.

The Wabigoon Subprovince previously has been subdivided into four terranes based on whole-rock Sm-Nd isotopic data (Fig. 1a; *Tomlinson et al. Prec. Res., 2004)*. Gold mineralisation is pervasive within the Wabigoon Subprovince, with numerous gold occurrences and prospects (Fig. 1a). The most economic gold mineralisation, i.e. gold mines represented by red stars, clusters mainly in the Eastern Wabigoon and Marmion gold camps (rectangles 1 and 2, respectively in Fig. 1a). However, no relationship between these important gold camps and the terrane boundaries is obvious in Figure 1a. For example, the terrane boundary in Eastern Wabigoon was assumed to trend E-W, whereas the gold mineralisation trends N-S. The Marmion gold camp trends NE, but is far away from the terrane boundary (Fig. 1a).

Figure 1b shows new mapping of Hf-isotope compositions in zircon, undertaken in this study. The warm colours represent relatively juvenile blocks with higher Epsilon (Hf) values, whereas the cold colours represent relatively ancient blocks with lower Epsilon (Hf) values. The boundaries of these isotopic domains are interpreted as lithospheric boundaries between different terranes. The revised terrane boundary in Figure 1b is mainly from *Stott, OGS, 2011*. It can be seen that the new zircon isotopic mapping results fit well with the revised terrane boundaries (Fig. 1b). In particular, the boundary between the Winnipeg River and Eastern Wabigoon Terranes now trends NE, consistent with the gold trend (rectangle 1 in Fig. 1b).

This coincidence supports the hypothesis that the terrane boundaries exert important controls on the location of significant gold mineralisation. A significant observation is that there are no gold mines within the ancient Winnipeg River Terrane, but instead the gold mines cluster within the Eastern Wabigoon Terrane, which is a juvenile block. This spatial relationship of gold with more juvenile rocks is similar to that observed in the Yilgarn Craton of Western Australia.

The Marmion gold camp is intriguing as it occurs along a NE-

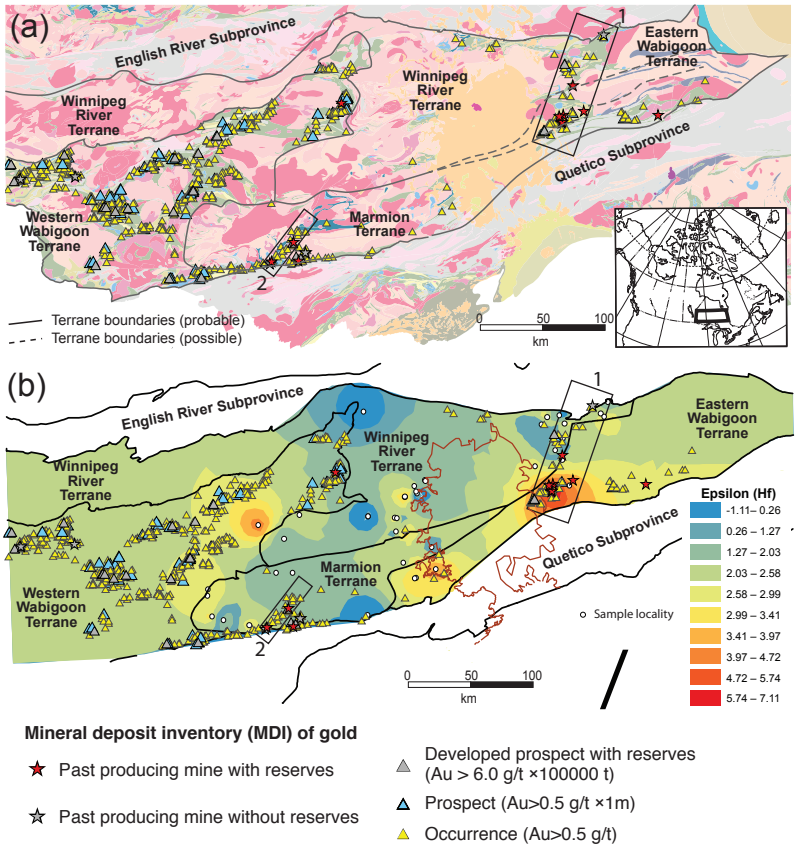

Figure 1. Spatial distribution of gold mineralisation and terrane boundaries within the Wabigoon Subprovince, Canada. (a) Geological map of the Wabigoon Subprovince showing terrane boundaries based on whole-rock Nd isotope data (Tomlinson et al., Precambrian Research 2004). Different colors represent different geological units. The inset shows the location of the study area. (b) Zircon Hf-isotope mapping of the Wabigoon Subprovince with the revised terrane boundaries after Stott, OGS, 2011. The contour bar shows the Epsilon Hf value of zircons studied. The rectangles labeled 1 and 2 highlight the two gold camps in Eastern Wabigoon and the Marmion terrane, respectively. The most economic gold mineralisation discovered to date is represented by red and grey stars.

trending zone within the Marmion Terrane (Fig. 1b). There are currently not enough zircon Hf data on both sides of this gold camp to reveal the isotopic signature of the lithosphere (Fig. 1b). However, Figure 2 shows a contrast in magnetic anomalies on both sides of this NE-trending structure within the Marmion terrane. The Hammond Reef deposit with 10 M oz of Au is close to this structure, highlighting the potential importance of this inferred terrane boundary (Fig. 2).

In summary, it appears that the spatial distribution of gold in the Wabigoon Subprovince is controlled by the terrane character (juvenile) and potentially their boundaries with ancient blocks (paleocraton margins), similar to the scenario in the Yilgarn Craton. Zircon isotopic mapping is a powerful tool to image the lithospheric boundaries and thus, can become a robust pathfinder to gold deposits.

This project is part of CCFS Themes 2 and 3, Earth Evolution and Earth Today, and contributes to understanding Earth's Architecture.

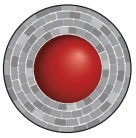

Contacts: Cam McCuaig, Yong-Jun Lu, Katarina Bjorkman
Funded by: ARC ECSTAR Fellowship, CCFS Foundation Program 9

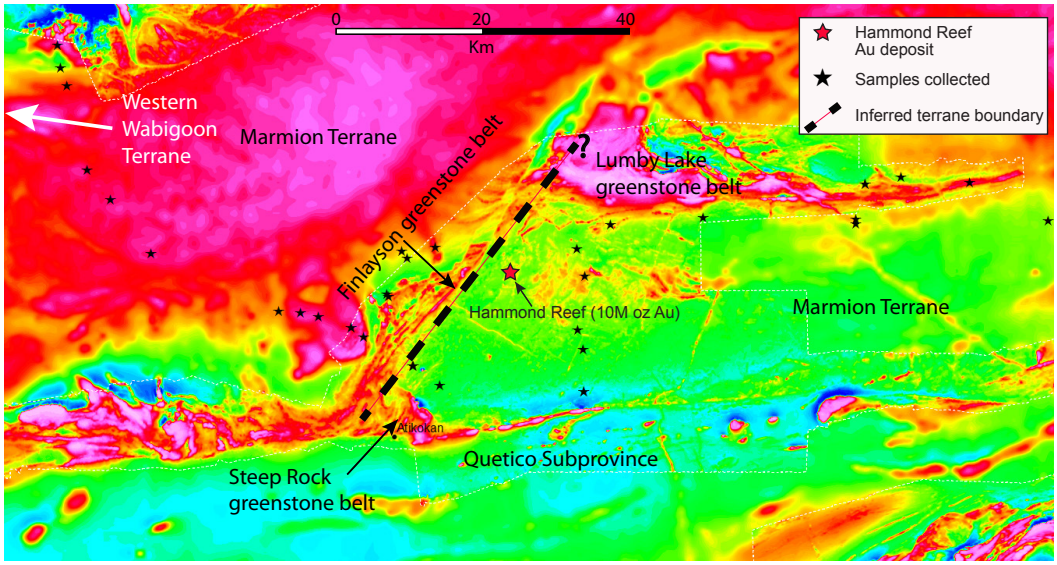

Figure 2. Residual total-field magnetic image of the Marmion Terrane. Warm and cold colors represent positive and negative magnetic anomalies, respectively. The magnetic character shows a marked change in the Marmion terrane across the NE-trending Finlayson greenstone belt, which can be inferred as a terrane boundary. The Hammond Reef deposit with 10 Moz Au is proximal to the inferred terrane boundary. However, this magnetic image probably only shows features down to about 20 km depth, and therefore does not image the deep lithosphere, unlike the isotopic data. The boundary between the Marmion and Western Wabigoon terranes is west of this map area, as indicated by the white arrow.

Diamond growth at the nanoscale – Mantle fluids at work

Diamondites are polycrystalline aggregates of diamond crystals with heterogeneous grain sizes and random orientation that formed in the Earth's mantle. They have a highly porous structure, which indicates that they precipitated from a volatile-rich medium strongly oversaturated in carbon. Gem-sized diamonds can contain a long history of growth and dissolution resulting in complex zonation patterns *(CCFS publication #168)*. In contrast, diamondites may form rapidly, presenting snapshots of diamond formation conditions that complement the information from slowly grown gem-sized diamond.

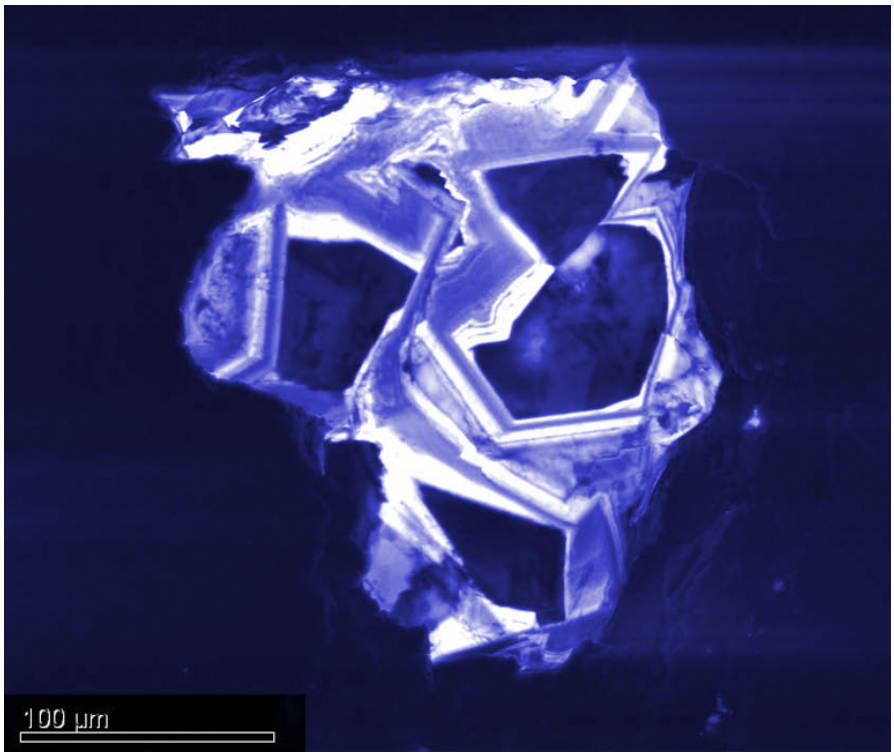

Figure 1. Cathodoluminescence image of diamondite showing complex zoning that most likely corresponds to episodic growth from a fluid dynamically changing in composition.

New microanalytical methods have allowed diamond studies to be carried to the next level, as submicron inclusions are now accessible, thus building on a solid foundation from studies of large inclusions, which are usually in the range of 200-300 µm. *In situ* analysis of diamonds and their inclusions is now able to span roughly six orders of magnitude in spatial resolution and draw critical complementary information from either end of this range. Large inclusions in diamondites are mostly intergrown with the diamond crystals rather than included. They record the general chemical environment of diamond formation, but can be subject to metasomatism that postdates diamond formation *(CCFS publication #210)*. In contrast, submicron-sized minerals included in the diamond crystals are shielded and contain the fluid from which the diamond precipitated.

To reveal more about the relationship between the diamond fluid and the growth mechanisms of the diamond crystals, we employed Transmission Electron Microscopy, enhanced with Focused-Ion Beam sample preparation, Transmission Kikuchi Diffraction Analysis and Nano-SIMS, enabling detailed analysis at the submicron scale and direct sampling of the diamonds' parental fluids included in the stones (*Jacob et al., Earth Science Reviews, in review*)

In situ sampling of diamond fluids reveals a large heterogeneity in redox conditions and chemical compositions at small scale, which is not reflected in the macro-inclusion suite. However, these fluids have compositions that correspond to the fluid end-members established by studies on fibrous diamonds; this suggests a universally important role for a limited number of basic ingredients, namely carbon, silicon, halogens and water.

Preliminary studies *(Rubanova PhD Thesis)* indicate that the crystals in diamondites may have grown not only by the octahedral (spiral/dislocation) mechanism, but also by cuboid (rough, adhesive type) growth. This suggests that other governing parameters, just beyond extreme carbon supersaturation, play an intrinsic role in their growth. Both growth mechanisms also occur in gem-sized diamonds, and the study of diamondites may tie these together in an integrated model and help define the impurities, oxygen fugacity, and episodic nature of these deep mantle fluids. Thus, diamondites could act as "Rosetta Stones" that can provide critical information about diamond growth and fluids in the Earth's mantle.

This project is part of CCFS Themes 2 and 3, Earth Evolution and Earth Today, and contributes to understanding Earth's Fluid Fluxes.

Contacts: Dorrit Jacob, Dan Howell, Bill Griffin, Sue O'Reilly, Sandra Piazolo
Funded by: CCFS

The leading edge in pits: the hole story for laser ablation ICP-MS

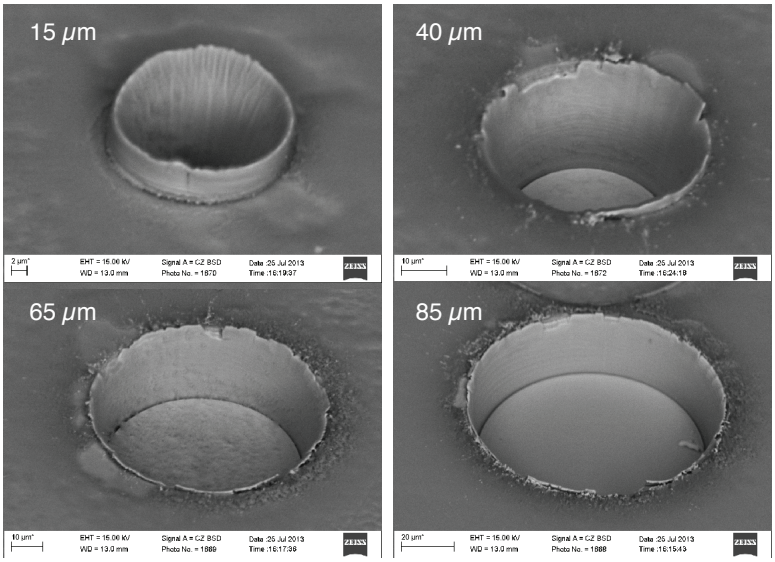

Figure 2. Back-scatter electron images of different laser spot sizes in GJ zircon. Note the marked development of the 'crown' of melt material on each pit, but especially the 15 μm diameter pit.

Conceptually, laser ablation is a simple process; material is removed from a solid (or liquid) sample by irradiation with a laser beam. In this sense laser ablation (LA) can be thought of as the micro-scale equivalent of taking a sledgehammer to an outcrop. However, the real power of laser ablation is that the sampled material can be directly transported into a plasma-source mass spectrometer, allowing rapid measurement of elemental abundances or isotope ratios. Researchers at Macquarie were among the pioneers in developing new analytical methods using laser ablation ICP-MS, and established early on, that the quantification of elemental abundances or isotope ratios is rather more complicated than a fantasy-world version of 'star-wars' mass spectrometry. As part of the development of leading edge analytical methods involving new laser hardware, CCFS researchers are revisiting the basics of how a laser beam interacts with minerals.

The ablation behaviour of different minerals for specific wavelengths of light is well-documented in the literature. The degree of coupling between the laser beam and different minerals is indicated by the amount of material removed from the hole; in quantitative elemental analysis this is corrected by use of an independently determined internal standard (an element of known concentration). A more significant issue is the progressive change in the ratios of measured signals of certain element pairs or isotope pairs as the laser drills into the sample. This is referred to as 'down-hole fractionation'. Elemental fractionation occurs because preferential ablation of some elements (low-volatility elements) in the sample results in non-stoichiometric sampling and analysis. Perhaps the best-documented example of laser-induced elemental fractionation is the changes in measured Pb/U and Pb/Th ratios in zircon as drilling proceeds.

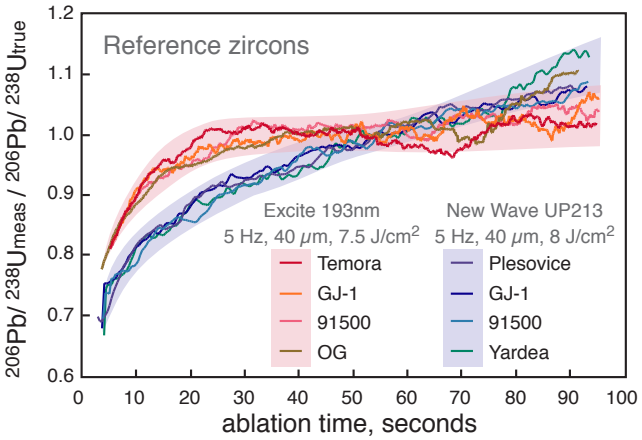

Figure 1. The plot of normalised $^{206}Pb/^{238}U$ (measured ratio relative to true ratio to remove the effect of age) vs time for selected reference zircons provides a comparison of 193 nm and 213 nm laser systems.

Down-hole laser-induced fractionation is one of the largest contributions to the uncertainty budget of LA-ICP-MS measurements of trace elements and isotope ratios. Efforts to improve the accuracy of analyses and to reduce the uncertainties associated with laser-induced fractionation have involved developments in both laser hardware and data-reduction software. Advances in cell design have improved the quantitative transport of material from the ablation site to the ICP, giving increased sensitivity and reduced fractionation. Rastering the laser, or using short acquisition times, are also commonly used to minimise downhole fractionation, but these compromise spatial resolution and depth information. Linear and exponential down-hole models are used in many data-reduction software packages and reflect the basic fractionation response for a wide range of laser specifications and operating conditions. In most models the fundamental assumption is that matrix-matched standards and samples ablate similarly with consistent time-depth relationships. However, further software advances are limited by our current understanding of the fundamental processes of ablation.

An investigation of the ablation characteristics of common minerals is part of the CCFS Foundation Program 'Frontiers in integrated laser-sampled trace-element and isotopic geoanalysis'. The aims are to assess the effect of laser wavelength, pulse width, spot size and fluence, in conjunction with laser-cell design and gas composition and flow rate. In the first phase of the study the focus has been on the ablation of zircon to establish the optimum set of hardware parameters and operating conditions to maximise spatial resolution, and to minimise ablation rate and U-Pb fractionation.

cont...

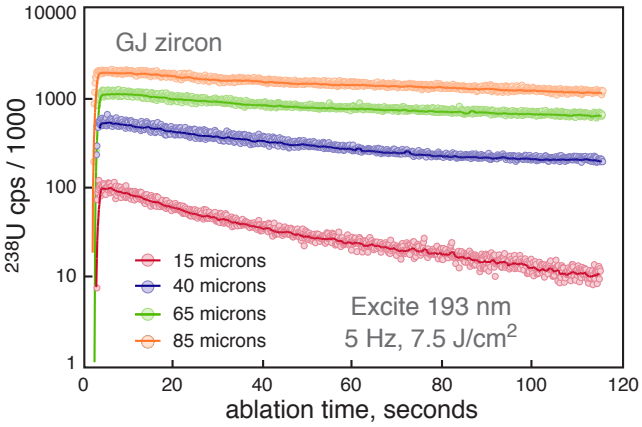

Figure 3. Plot of ^{238}U signal intensity (counts per second) versus time for 4 different spot sizes (15, 40, 65, 85 µm) in GJ zircon.

A distinctive down-hole fractionation of U and Pb is observed in ablation of zircon using 213 nm and 193 nm wavelength lasers (Fig. 1). The change in ratio from both systems is greatest in the first 150-200 laser pulses (20 to 30 seconds of ablation) but for the chosen operating parameters the 193 nm data show little further change with time, whereas the ratios produced by the 213 nm laser continue to increase with time.

Laser fluence and spot size have significant effects on ablation rate and fractionation. Ablation rate increases with fluence but more slowly for larger spot sizes. A series of images taken after a set number of laser pulses shows the development of a crater wall that forms from the initial laser pulse and grows in height with time by the addition of melt material extruded from the pit (Fig. 2). The development of this wall is more pronounced with small spot size and low fluence. There is also a significant decay in signal intensity with time, especially with small spot sizes, indicating that progressively less material is being removed from the hole and transported to the ICP (Fig. 3). The net effect is a greater fractionation of $^{206}Pb/^{238}U$ with small spot size due to the retention of melt and condensed material in and around the laser pit (Fig. 4).

One of the main drivers for investigating the fundamentals of the ablation process is to get higher spatial resolution but without compromising data quality. The results of the first stage of the study have produced a better understanding of how zircon ablates and the fractionation of U and Pb using a nano-second pulse laser system. This will form the benchmark for the next exciting experimental phase using the femto-second laser system.

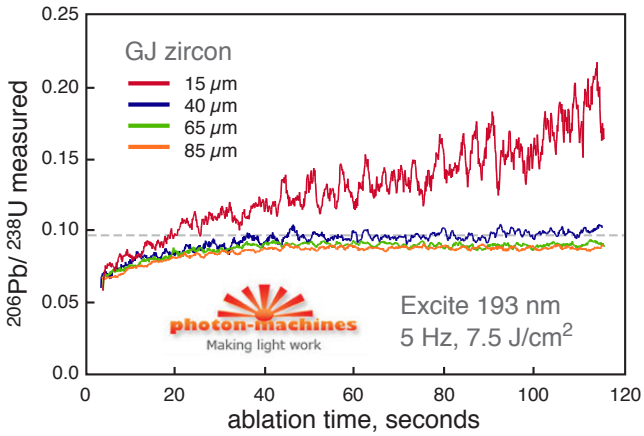

Figure 4. Plot of measured $^{206}Pb/^{238}U$ versus time for 4 different spot sizes (15, 40, 65, 85 µm) in GJ zircon.

This project is a Technology Development initiative in CCFS, contributes across all Themes (Early Earth, Earth Evolution and Earth Today), and contributes to understanding Earth's Architecture and Fluid Fluxes.

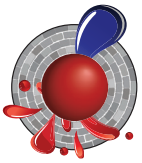

Contacts: Norman Pearson, Bill Griffin, Sue O'Reilly, Will Powell
Funded by: CCFS Foundation Program 'Frontiers in integrated laser-sampled trace-element and isotopic geoanalysis'

Are ancient zircon ages real, or due to ancient element movement?

Zircons from the Tula Mountains, Napier Complex (East Antarctica), attracted scientific attention because they come from some of the oldest rocks on Earth (*Black et al., CMP, 1986*), which experienced high-temperature metamorphism at 2.8 Ga and ultra-high-temperature metamorphism at 2.5 Ga, with temperatures estimated at over 1100 ºC (*Hokada et al., Prec. Res., 2005*), some of the highest temperatures recorded in Earth's crust. Isotopic disturbance of zircons >ca 3.4 Ga old from the Napier Complex has been recognised for many years (*Williams et al., CMP, 1984*). To investigate this phenomenon further, we analysed zircon grains from three samples: one orthogneiss (from Gage Ridge) and two paragneisses (one each from Mount Sones and Dallwitz Nunatak). The analysis included U-Pb geochronology, oxygen isotopes, REEs, Raman spectroscopy and scanning ion imaging. All samples yielded reversely discordant data; the zircons from Mount Sones are significantly younger than those from the other two samples with an age range from 3.0 Ga to 2.5 Ga. Detrital zircons from Dallwitz Nunatak yield ages between 3.5 Ga and 2.5 Ga. The Gage Ridge sample contains four age groups with concordant data between 3.6 Ga and 3.3 Ga (*Kusiak et al., 2013a*) and a discrete population of ca 3.8 Ga zircon with reversely discordant data. The REE distribution in zircon from all three samples is generally similar, with steep MREE to LREE trends, consistent with an igneous origin. However, such patterns are also present in metamorphic zircon that grew in the absence of garnet. The sample from Mount Sones

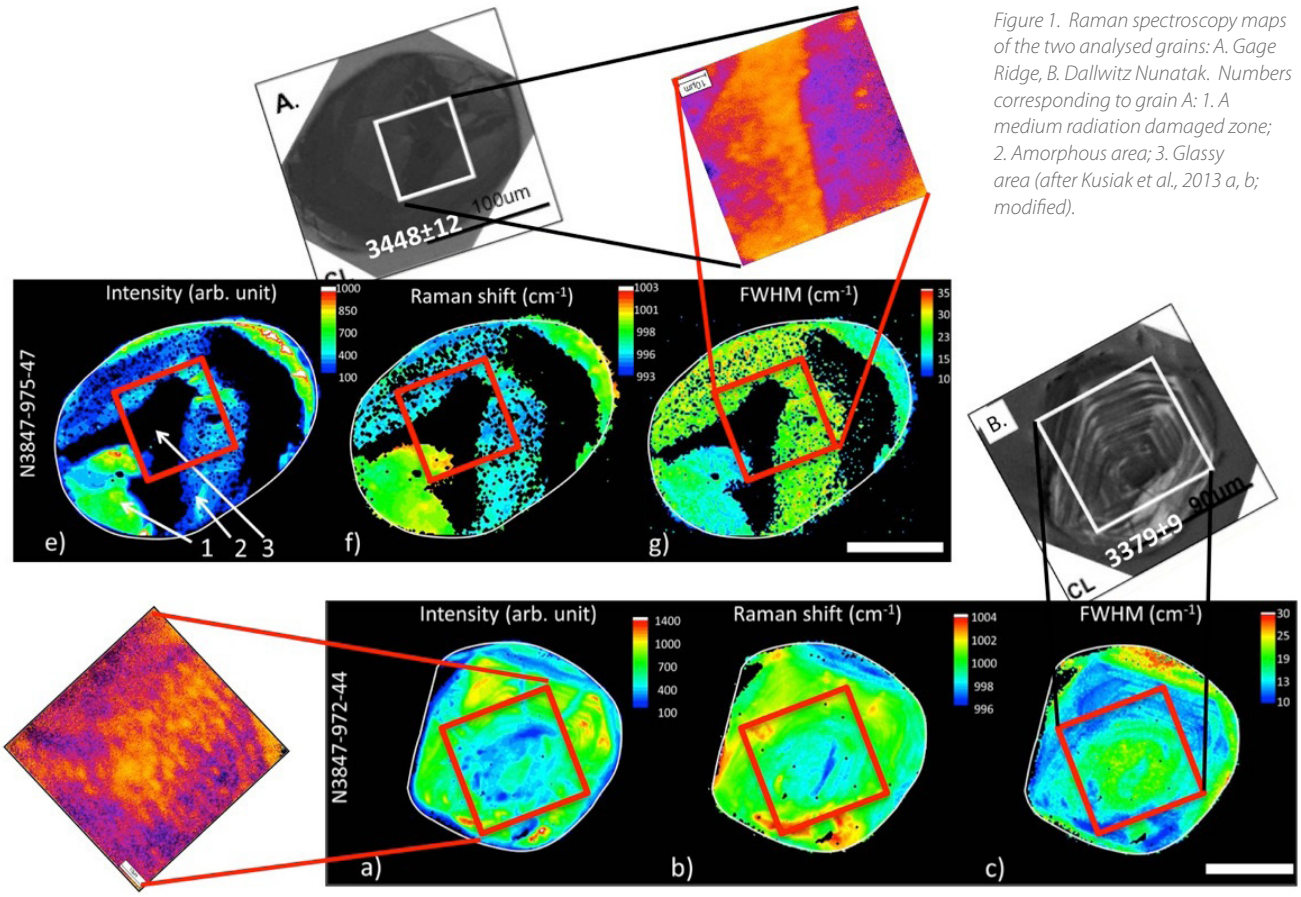

Figure 1. Raman spectroscopy maps of the two analysed grains: A. Gage Ridge, B. Dallwitz Nunatak. Numbers corresponding to grain A: 1. A medium radiation damaged zone; 2. Amorphous area; 3. Glassy area (after Kusiak et al., 2013 a, b; modified).

contains garnet that grew during ultra-high temperature (UHT) metamorphism (ca 2.5 Ga), and, like Kelly and Harley (*CMP, 2005*), we suggest that 2.8 Ga zircon grew during metamorphism under high-temperature and low-pressure conditions in the absence of garnet.

To test for U/Pb disturbance during metamorphism we analysed oxygen isotopes in zircon from all three samples. Igneous zircons from Gage Ridge have lower $\delta^{18}O$ values (4.7-6.8‰) than zircons from the paragneisses. However, the Dallwitz Nunatak zircons give a scattering of ages, and $\delta^{18}O$ varies from 6.8-8.0‰ (average $\delta^{18}O$ – 7.4‰), as might be expected for detrital zircons. Low scatter in $\delta^{18}O$ in zircons from the Mount Sones paragneiss, together with high values (7.2-8.9‰, average $\delta^{18}O$ – 8.1‰), are consistent with growth during the earlier metamorphism at 2.8 Ga.

A novel high-resolution ion-imaging technique using the Cameca 1280 SIMS was used to generate maps of Pb-isotopic "age" for selected zircons. These record patchy variations in the isotopic ratios that result in spurious ages, including some that are Hadean (>4.0 Ga). Raman spectroscopy was used to determine the degree of metamictisation in the same zircon domains previously imaged by SIMS (*CCFS Publications #407, 429*). From our results (Fig. 1), it is evident that there is no correlation and that Pb is patchily distributed regardless of the degree of crystallinity.

From these results we conclude that there is no evidence that oxygen isotopes or REE in zircon were disturbed during the UHT metamorphism at 2.5 Ga. The reverse discordance in zircon from Gage Ridge, Mount Sones and Dallwitz Nunatak is related to ancient mobilisation of Pb and the most likely cause was polymetamorphism under dry conditions - two metamorphic events, one low-pressure at ca 2.8 Ga and a UHT event at ca 2.5 Ga.

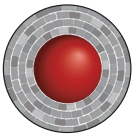

This project is part of CCFS Theme 1, Early Earth, and contributes to understanding Earth's Architecture.

Contacts: Monika Kusiak, Simon Wilde
Funded by: EU-FP7, Marie Curie grant

The enigma of chromitites in the upper mantle resolved

The mantle sections and the crust-mantle transition zones of many ophiolites contain bodies of chromitite, almost monomineralic concentrations of Cr- and Al-rich spinel. They are important economically as a source of chromium, and scientifically because these rocks encapsulate information on the nature of ancient upper mantle, young oceanic mantle, mantle melt formation and percolation processes, and on large-scale geodynamic emplacement mechanisms.

During the last four decades there has been a hot debate about the origin of these type of chromitites, yielding a huge number of studies with diverse and passionately defended hypotheses. Forensic-type studies of individual chromitite bodies in isolation have led to a profusion of genetic models indicating that chromitites from different localities formed by different mechanisms. These models can be grouped into three broad categories: (1) Fractional crystallisation of basaltic melts in magma chambers or conduits in the upper mantle or around the crust-mantle boundary. Variants of this model include changing the composition of the melt by an external process such as melt-rock reaction or assimilation of pre-existing mafic rocks. (2) Mixing or mingling of melts within dunite channels. (3) Separation of volatile-rich fluid phases with an important role for oxygen fugacity.

Among the questions that these models have been not able to resolve satisfactorily are: (1) how can chromium, a minor element in a peridotite-derived basaltic melt, be concentrated to produce large monomineralic bodies of chromite?; (2) how does a chromitite body start to nucleate and grow?; (3) what factors control the size of individual chromitite bodies?

A major breakthrough in our understanding of the genesis of the chromitites has come during the development of this research project, through the *in situ* analysis of Os isotopes by laser-ablation MC-ICPMS analysis of single tiny PGMs (and larger base-metal sulfides), which are usually found as inclusions in the chromitites. The Os-isotope composition of individual PGMs can now be directly related to their microstructural setting, internal structure and bulk composition (*CCFS Publications #198, 334, 348, 349*).

The observation that the primary Os-rich PGMs in the chromitites are highly heterogeneous in terms of Os-isotope composition, even at the scale of inclusions in an individual chromite grain, suggests that the chromitite formed by the mixing/mingling of multiple basaltic melts that sampled different mantle sources, and have undergone variable degrees of fractionation. In the exposed mantle sections of several ophiolites, meso- and micro-structures of chromite suggest that the intersecting melt-filled dunitic channels were draining ascending basaltic melts in a suprasubduction mantle. This is the ideal framework to produce chromitites by mixing of basaltic melts of different provenance and degrees of fractionation. In our new model, the formation of a chromitite body, its size and the type of chromitite microstructures, are inferred to reflect focused melt flow within these high-porosity and high-permeability networks of channels at different melt/rock ratios, and different temperatures of melts and host peridotite. Melt/rock ratio controls the amount of crystallising chromite and the chromitite microstructures. Moreover, the observation that many chromitites cross-cut their host peridotites suggest that mixing of melts at the intersection between melt-filled dunite channels is not the unique "physical" trap inducing crystallisation of chromitites. Also, in relatively

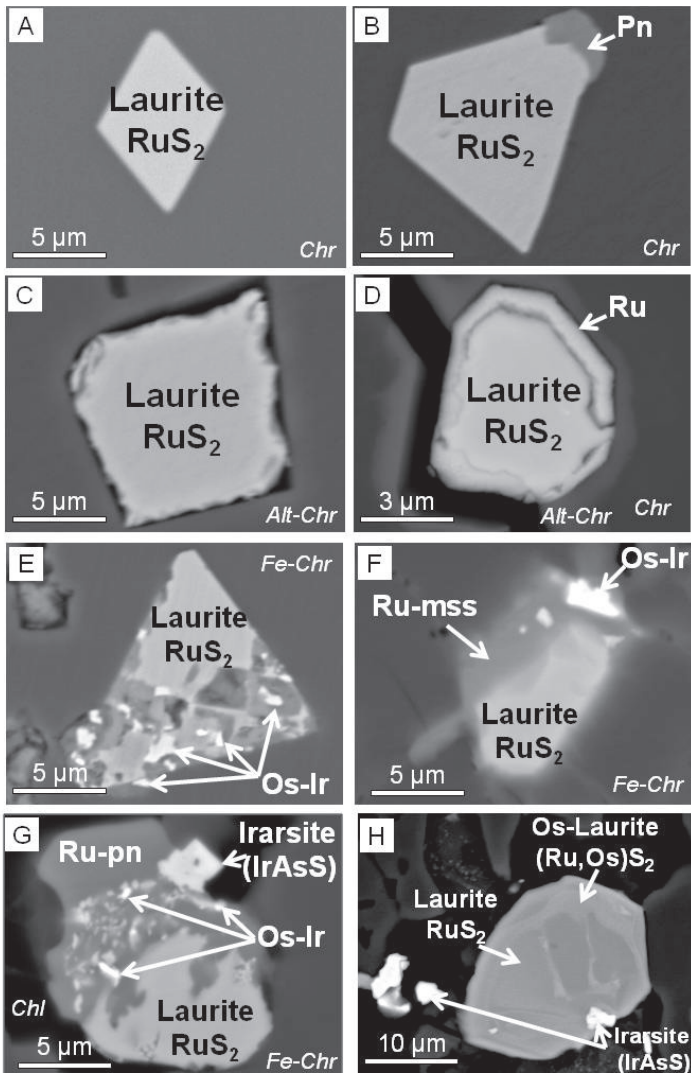

Figure 1. Backscattered electron images of Ru-Os sulfides and alloys from distinct microstructural positions in the Dobromirtsi chromitites. A and B: Primary (magmatic) laurite included in unaltered chromite. C and D: Partially corroded (secondary) laurite and Ru alloys in open fractures in chromite. E–G: Secondary assemblages showing distinct stages of alteration/replacement of laurite in ferrian chromite rims. H: Irregularly zoned laurite grain in the contact between a ferrian chromite rim and the interstitial matrix (for more details see CCFS publication #42).

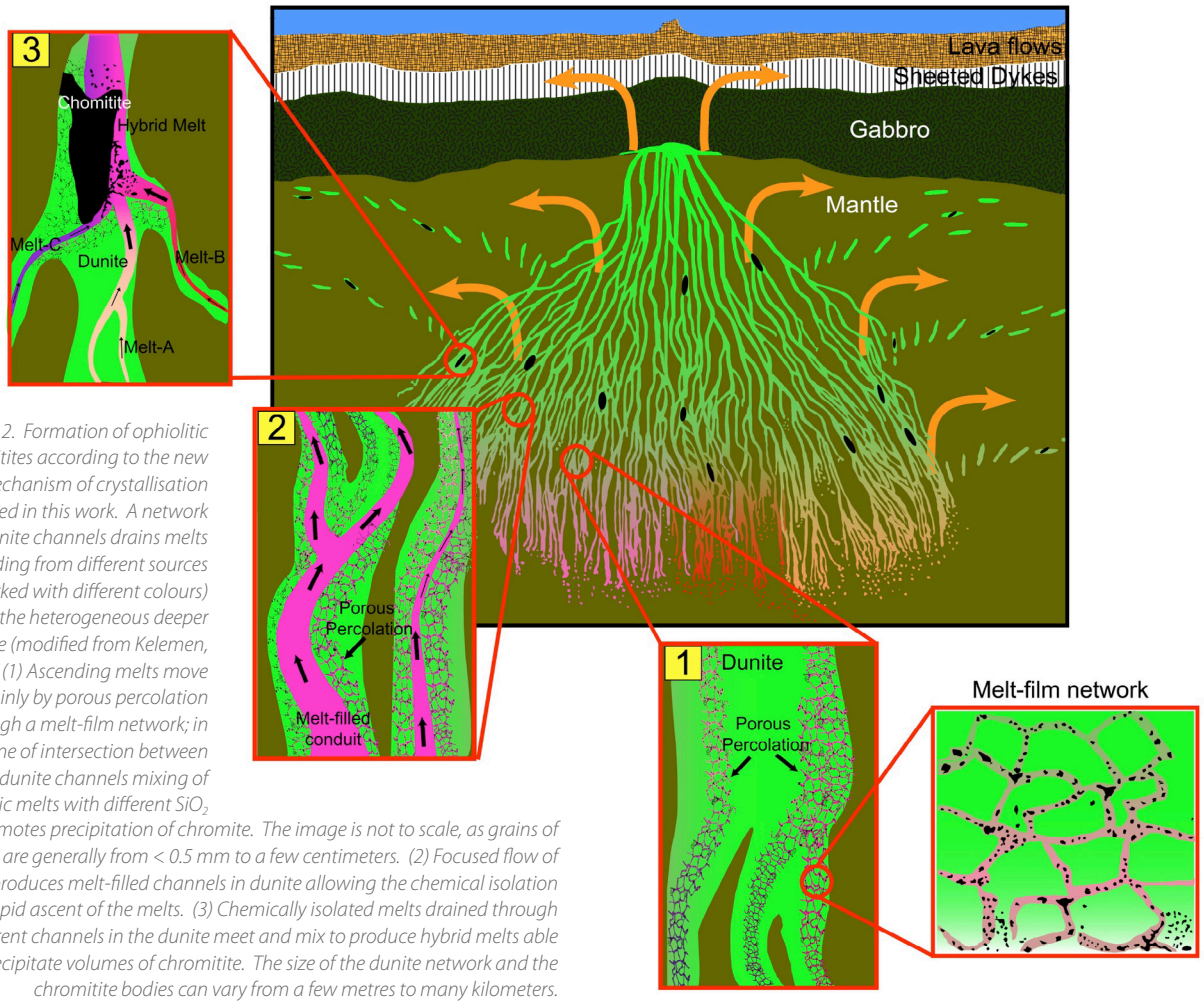

Figure 2. Formation of ophiolitic chromitites according to the new mechanism of crystallisation proposed in this work. A network of dunite channels drains melts ascending from different sources (marked with different colours) in the heterogeneous deeper mantle (modified from Kelemen, 2004). (1) Ascending melts move mainly by porous percolation through a melt-film network; in the zone of intersection between dunite channels mixing of basaltic melts with different SiO_2 promotes precipitation of chromite. The image is not to scale, as grains of olivine are generally from < 0.5 mm to a few centimeters. (2) Focused flow of melt produces melt-filled channels in dunite allowing the chemical isolation and rapid ascent of the melts. (3) Chemically isolated melts drained through different channels in the dunite meet and mix to produce hybrid melts able to precipitate volumes of chromitite. The size of the dunite network and the chromitite bodies can vary from a few metres to many kilometers.

cool mantle domains, chromitites may form in hydrofractures penetrating peridotites and infiltrated by interstitial chromite-bearing fluids. During these events of melt infiltration/injection, PGMs such as laurite or Os-Ir alloys already present in the mantle peridotite, or produced by the breakdown of PGE-bearing sulfides during the melt-rock reactions, can be also incorporated in a solid or crystal/melt mix into the parental melts of chromitites. This may explain why chromitites hosted in the mantle section of young ophiolites may contain PGM with Os-model ages > 2.5 Ga old.

On the other hand, the fact that some PGM grains in the chromitites are found along healed fractures cutting the primary chromite suggests that other populations of PGMs may have precipitated from metasomatic fluid/melts that infiltrated existing chromitites. The formation of this new generation of PGM can also explain the Os-isotopic heterogenity. The opening of the Os-isotopic system in PGMs associated with secondary chromite (produced by alteration of the magmatic chromite) also suggests that some PGMs that precipitated at mantle conditions, can be partly reacted and recrystallised during the infiltration of post-magmatic fluids. The recrystallisation of pre-existing PGM during polyphase metamorphism or "recycling" of the chromitite into deeper mantle levels can also explain the presence of micrometric PGMs with distinctly different Os-isotope compositions.

The results obtained in this project highlight the complex history that can affect the chromitites from their time of formation in the upper mantle, up to their surface emplacement. Chromitites may form at low pressures in the shallow mantle, but they can be later transported deep into the mantle (> 400 km) by subduction processes, and possibly integrated into the convecting mantle.

This project is part of CCFS Themes 2 and 3, Earth Evolution and Earth Today, and contributes to understanding Earth Architecture and Fluid Fluxes.

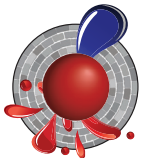

Contacts: José-María González-Jiminéz, Bill Griffin, Sue O'Reilly, Norman Pearson

Funded by: ARC CCFS ECSTAR Fellowship, CCFS Foundation Program 1

Transformation on Earth: the transition from ancient to modern Earth

Around 2.35 billion years ago (Ga), Earth's atmosphere and near-surface hydrosphere underwent perhaps the most fundamental revolution in Earth history since the Giant Moon-Forming Impact at 4.5 Ga: the rise in the concentration of atmospheric oxygen. This was a revolutionary event because of the effects it had on ocean chemistry and weathering: the oceans were scrubbed of iron (and soon after, manganese) and rusting of ferrous minerals in the continents released sulfate (and other elements) to the oceans through oxidative weathering. The resultant change in ocean chemistry is reflected in the rock record, with the disappearance of banded iron formations and the appearance of sulfates and phosphorites from 2.45-2.2 Ga. Eventually, the rise of atmospheric oxygen led to the evolutionary development (or at least, widespread flourishing) of eukaryotes, a more complex life form that depends on the extra energy available from oxygen. The rise of atmospheric oxygen coincided with climatic cooling to the extent that glacial deposits appear for the first time on many continents.

Only a few rock successions on Earth are preserved from across this period of Earth history, and almost all of those are plagued by an incomplete record with one or more unconformities, which are horizons of non-deposition, and/or erosion, where the history of change was not recorded, or preserved. However, there is one succession where a continuous sedimentary record is preserved across this interval of extraordinary change – the Turee Creek Group of Western Australia. In this succession, which is up to 4 km thick, we recently discovered the transition from ancient to modern Earth, recorded

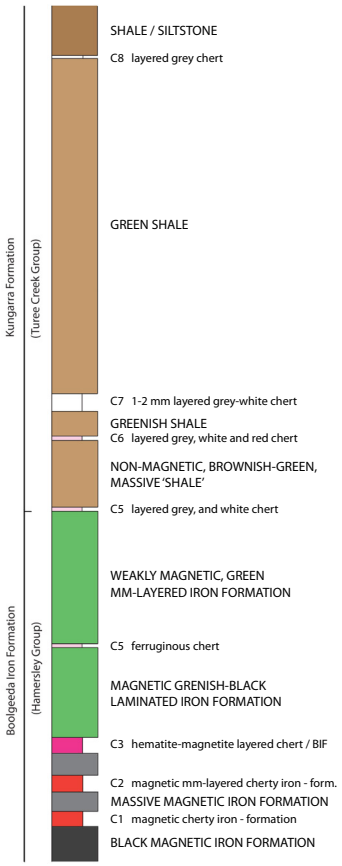

Figure 1. Stratigraphic section through the transition from the uppermost Boolgeeda Iron Formation of the Hamersley Group to the lowermost Kungarra Formation of the Turee Creek Group, here interpreted to occur at the base of the first non-magnetic unit. C1-C8 refers to chert layers from base to top across the section. (From Van Kranendonk et al., submitted).

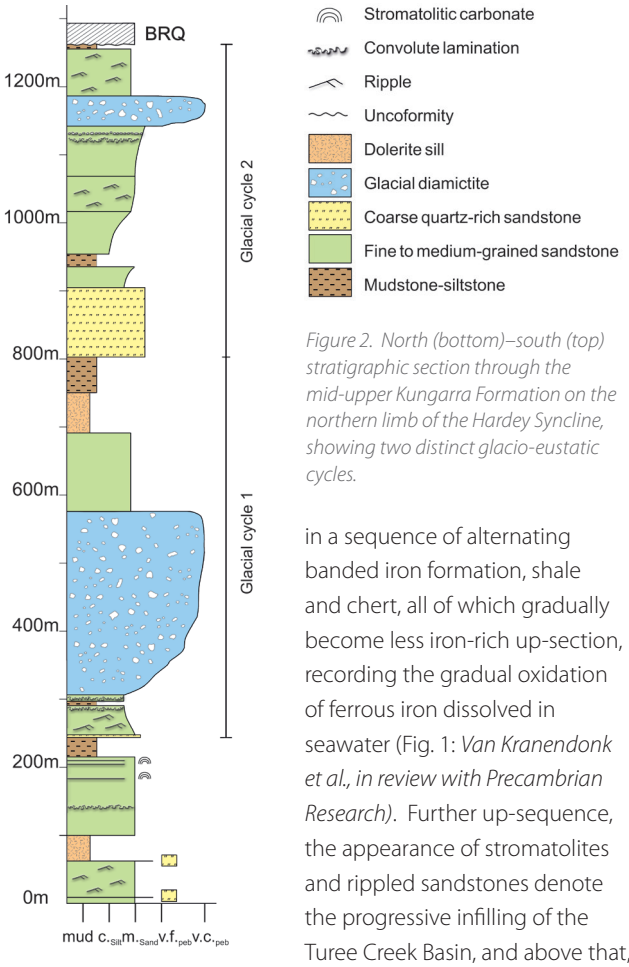

Figure 2. North (bottom)–south (top) stratigraphic section through the mid-upper Kungarra Formation on the northern limb of the Hardey Syncline, showing two distinct glacio-eustatic cycles.

in a sequence of alternating banded iron formation, shale and chert, all of which gradually become less iron-rich up-section, recording the gradual oxidation of ferrous iron dissolved in seawater (Fig. 1: *Van Kranendonk et al., in review with Precambrian Research)*. Further up-sequence, the appearance of stromatolites and rippled sandstones denote the progressive infilling of the Turee Creek Basin, and above that, we have discovered two glaciogenic successions, each marked by a period of rapid sea-level fall, when seawater volume was transferred into the developing ice sheets, followed by rapid sea-level deepening, as the glacial ice sheets melted (Fig. 2: *Van Kranendonk and Mazumder, in review with GSA Bulletin*).

In order to understand and quantify the nature of changes across this important interval, and to assess how the biosphere responded to this global climate change, Martin J. Van Kranendonk of the CCFS and his colleague from Paris, Professor Pascal Philippot, in collaboration with the Geological Survey of Western Australia, undertook a diamond drilling program to obtain fresh samples across each of the major transitions (Fig. 3). Three drill holes were obtained across different levels of the stratigraphy, including the basal contact with banded iron formations of the underlying Hamersley Group (ancient Earth), a full section through the lower of two glacial deposits and underlying stromatolites, and one through the upper part of the Turee Creek Group stratigraphy where the first sulfates might be expected to have been deposited, immediately above coastal to terrestrial sandstones of the Koolbye Formation (*Mazumder et al., in review, Precambrian Research*).

Preliminary results of drillcore inspection reveal that stromatolites have been intersected at several levels, and pyrite, of both authigenic and detrital origin, is common throughout the succession (Fig. 4). The basal transition from banded iron-

Figure 3. View looking over moderately dipping rocks of the Turee Creek Group, with the drillrig located on the flat ground in middle left. Lower slopes are glaciogenic diamictite.

formation to non-ferruginous chert was successfully recovered. A team of scientists from around the world will be analysing the cores to unlock their secrets and reveal more about the evolution of the ocean reservoir and the biosphere across the Great Oxidation Event.

This project is part of CCFS Theme 1, Early Earth, and contributes to understanding Earth's Architecture and Fluid Fluxes.

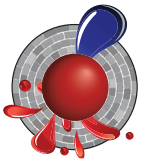

Contact: Martin J. Van Kranendonk, University of New South Wales m.vankranendonk@unsw.edu.au

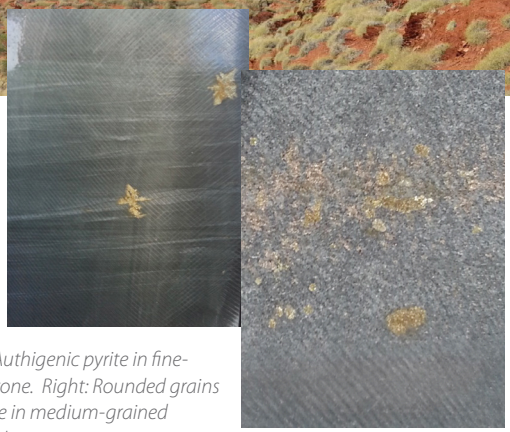

Figure 4. Left: Authigenic pyrite in fine-grained sandstone. Right: Rounded grains of detrital pyrite in medium-grained sandstone. Both views are 4 cm across.

Funded by: The University of New South Wales, Institute de Physique du Globe de Paris, the Agouron Institute

Isotopes reunite lost relatives in western Australia

The Arunta Orogen of central Australia (Fig. 1) comprises a large part of the southern margin of the North Australian Craton and records episodic tectonic and thermal activity spanning almost 1.5 billion years of Earth's history, from the Paleoproterozoic to the Devonian. The 1690–1630 Ma Warumpi Province forms the southernmost part of the Arunta Orogen and is separated from the older, 1860–1700 Ma Aileron Province to the north by the Central Australian Suture (Fig. 2a). Both are unconformably overlain by Neoproterozoic to Paleozoic basins.

The Warumpi Province has been considered to be exotic to the North Australian Craton. However, Hf-isotope evidence for mixing between 1690–1630 Ma mantle-derived melts and older sources indicates that the history of the Warumpi Province involved interaction with significantly older crust of at least Mesoarchean age (Fig. 2b).

The ages and Hf-isotope compositions of inherited zircons in the 1677 Ma Pollock Hills Formation are consistent with this older crust being part of the Aileron Province. This suggests that the Warumpi Province represents a slice of Aileron Province crust rifted away from the southern margin of the North Australian Craton at, or prior to, 1690 Ma. The Warumpi Province then acted as a locus for the voluminous production of mantle-derived (juvenile) 1690–1660 Ma crust, both outboard of the southern Aileron Province margin, and during its accretion back onto the Aileron Province during and following the 1640–1635 Ma Liebig Orogeny.

Detrital zircons from Neoproterozoic units, including the Amadeus and Murraba Basins, which unconformably overlie the Aileron and Warumpi Provinces in the west Arunta region, record a history of distinct changes in erosional sources during their early depositional histories. Changes in detrital age components with stratigraphic level in the >840 Ma Kiwirrkurra Formation, the 1040–820 Ma Heavitree Quartzite, and the probably younger Munyu Sandstone, demonstrate marked changes from Warumpi-dominated to Musgrave-dominated detritus. This change in provenance over time probably relates to changes in tectonism in the region during the Neoproterozoic, possibly associated with breakup of the Rodinia supercontinent. See *CCFS publication #436.*

cont...

Figure 1. a) Location of the Warumpi Province on the southern margin of the Arunta region.

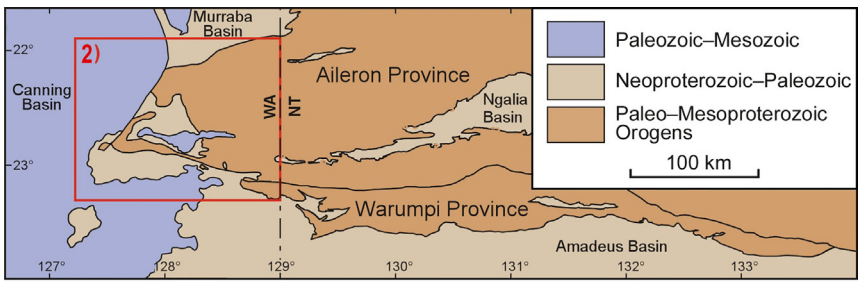

This project is part of CCFS Themes 2 and 3, Earth Evolution and Earth Today, and contributes to understanding Earth's Architecture.

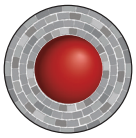

Contacts: Chris Kirkland, Michael Wingate
Funded by: CCFS, GSWA

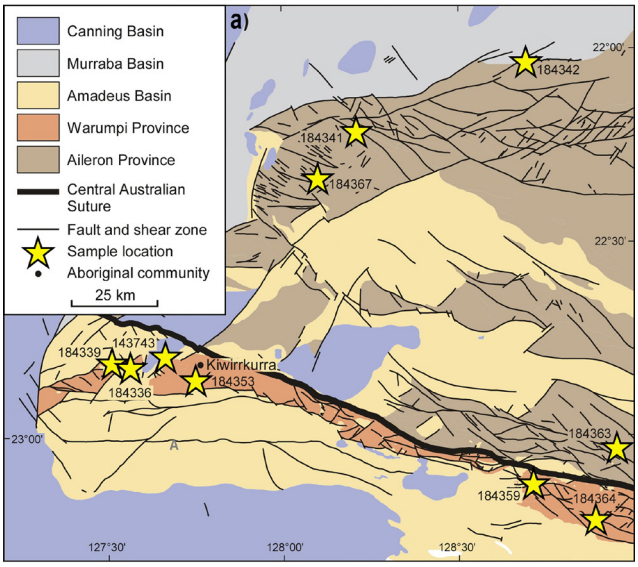

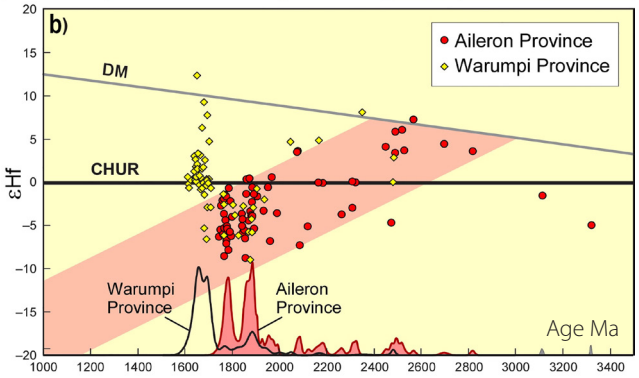

Figure 2. a) Simplified interpreted basement geology of the west Arunta region in Western Australia, showing the locations of analysed samples. b) εHf evolution diagram showing analyses of zircons from the Aileron (red circles) and Warumpi (yellow diamonds) Provinces. Probability density curves show the age distributions of Aileron Province (red) and Warumpi Province (unshaded) zircons. The light red field, which shows the crustal evolution of older components of the Warumpi Province, overlaps the compositional evolution of the Aileron Province, indicating a common source. See CCFS publication #436.

Tracking the birth and growth of the Central Asian Orogenic Belt

Most of the existing continental crust was generated by the end of the Archean (*CCFS Publication #342)*, and the production of new crust has decreased markedly since that time (*Belousova et al., Lithos 2010*), except for some sporadic bursts of activity. One of these is the Central Asian Orogenic Belt (CAOB), a complex tectonic collage of microcontinental blocks, island arcs, and remnants of oceanic crust between the Siberian Craton to the north and the Tarim and North China cratons to the south. The CAOB is the world's largest Phanerozoic accretionary orogenic belts and is the most important site for juvenile crustal growth in the Phanerozoic. The challenge is to unravel the major magmatic events in the generation of the juvenile crust from this Phanerozoic accretionary orogenic belt, and to answer several major questions.

Why was the CAOB the locus of such extensive juvenile crustal growth in Phanerozoic? Is this related to the massive amount of oceanic crust that was subducted during closure of the Paleo-Asian Ocean, to subduction of the Mongol-Okhotsk arcs, or to the Siberian mantle plume? What was happening at the different continental margins (e.g. Siberian margin and North China Craton margin)? Was the pre-existing Paleozoic accretionary crustal architecture modified largely by Mesozoic magmatism? Our recent work (*Li et al. Earth-Science Reviews, 2013, Wang et al. American Journal of Science, 2014*) is beginning to provide plausible answers to these questions, from detailed regional geological, petrological and geochronological studies on the subduction-related, collision-related and intraplate

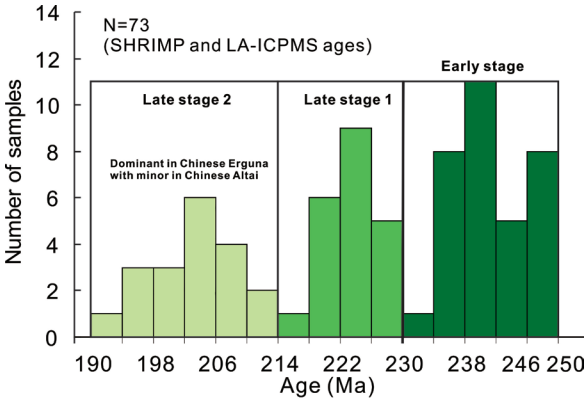

Figure 1. Histogram of Early Mesozoic zircon U-Pb ages in the CAOB. Only SHRIMP and LA-ICPMS zircon U-Pb data are used.

extensional magmatisms in the CAOB, tracing granite sources and origins to pinpoint crustal architecture and growth in the Early Mesozoic.

The numerous Early Mesozoic granitoids in the CAOB can be broadly classified into two groups on zircon U–Pb ages (Fig. 1): an early group from Early to Middle Triassic (250–230 Ma) and a late group emplaced during Late Triassic and Early Jurassic time (230-190 Ma). Early (250-230 Ma) granitoids are mainly distributed in the western Central Mongolia–Erguna Belt (CMEB), the western Altai Belt (AB), the South Mongolia–Xing'an Belt (SMXB) and the Beishan–Inner Mongolia–Jilin Belt (BIJB). They are mainly quartz-diorites, granodiorites and monzogranites, mostly of I-type, with minor mafic intrusions; some have adakite-like signatures and S-type features. Late (230-190 Ma) granitoids mainly occur in the North Mongolia–Transbaikalia Belt (NMTB), the eastern CMEB (Erguna massif) and the eastern Altai Belt (AB). They are mainly

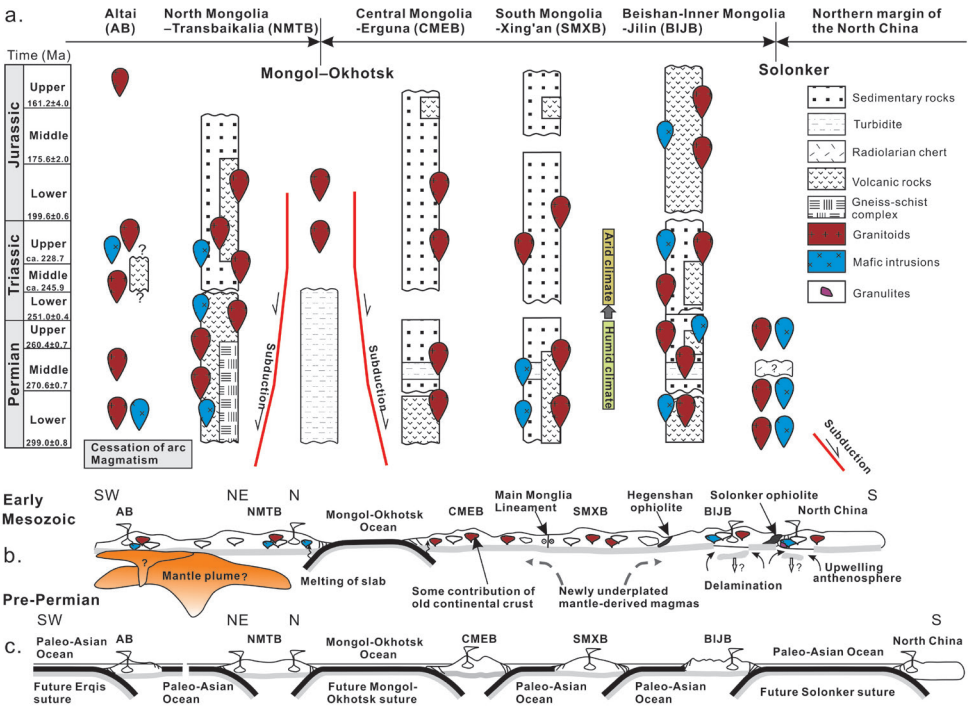

Figure 2. (a) Schematic space-time diagram showing major tectonic events affecting each belt in the CAOB. (b) Pre-Permian and (c) Early Mesozoic cross-section showing schematically the oceanic and arc/continent domains.

syenogranites, monzogranites and syenites, associated with many alkaline granites and mafic intrusions and are A-type and transitional I–A type or highly fractionated I-type granites.

Whole-rock Sr-Nd and zircon Hf isotopic data have been compiled for regional isotopic mapping. The $\varepsilon_{Nd}(t)$ values show large variations from −7.0 to +7.4 and Nd model ages (T_{DM}) from 0.46 Ga to 1.43 Ga; the initial Sr isotopic ratios (Sr_i) range from 0.7023 to 0.7174. The zircon $\varepsilon_{Hf}(t)$ values vary from -4.6 to +15.3 and give two-stage Hf model ages (T_{DM2}) from 0.30 Ga to 2.09 Ga. The extremely large variations of whole-rock Sr-Nd and zircon Hf isotopes imply heterogeneous source regions mainly dominated by juvenile components but with significant older crust as well. In the CAOB, the isotopic signatures (Nd-Hf) of the Early Mesozoic granitoids are similar to those of the Paleozoic granitoids in the same belt, indicating the Early Mesozoic crustal architecture retained its original Paleozoic continental signatures, which had not been modified by much juvenile mantle-derived material.

The older continental terrane was not thrust onto, or subducted beneath, the younger juvenile accretionary terranes, as seen in some collisional orogens. The crustal architecture in the CAOB is typical of an accretionary orogen that is characterised by horizontal accretion, not by vertical superposition of terranes. In contrast to the generation of massive juvenile crust in the Paleozoic accretionary stages of orogenic development, crustal recycling plays a more substantial role in the post-accretionary stages.

The generation of the Early Mesozoic granitoid magmas in the NMTB and the CMEB was dominated by the ongoing closure of the Mongol-Okhotsk Ocean and some were probably related to a mantle plume (Fig. 2). They may have been derived from melting of subducted materials or juvenile components with some probable contributions from ancient continental crust. Early Mesozoic granitoid magmas in the SMXB, the AB and the BIJB were generated in a post-/non-orogenic setting after the closure of the Paleo-Asian Ocean and were the results of partial melting of crustal components in response to underplating of mantle-derived magmas, most likely linked to lithospheric thickening, delamination and asthenospheric upwelling (Fig. 2). Early Mesozoic granitoid magmatism provides critical information on the Mesozoic post-accretionary tectonic evolution of the Paleo-Asian Ocean and transitional tectonic regimes from Early Mesozoic subduction to Late Mesozoic closure of the Mongol-Okhotsk Ocean as well as post-accretionary continental growth (Fig. 3).

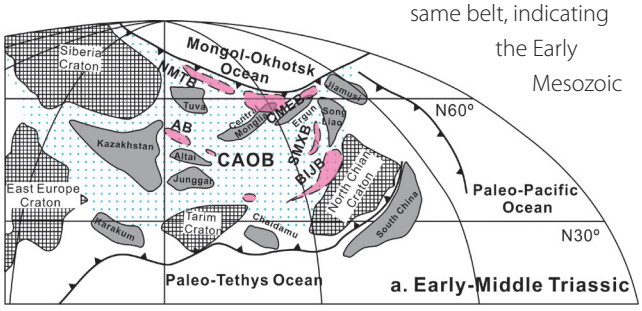

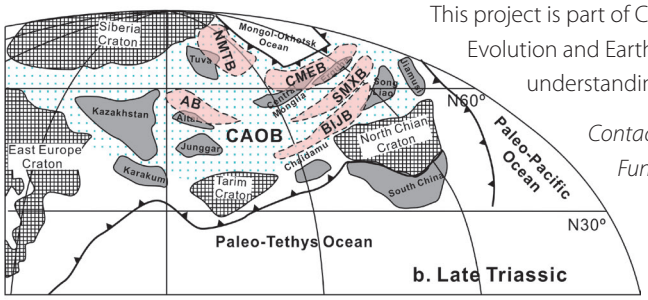

Figure 3. Schematic paleogeographic reconstruction of the Early Mesozoic ocean-continent framework of the CAOB and adjacent regions. The pink areas broadly represent the Early-Middle Triassic (a) and Late Triassic (b) granitoid belts in the CAOB.

This project is part of CCFS Themes 2 and 3, Earth Evolution and Earth Today, and contributes to understanding Earth's Architecture.

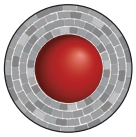

Contacts: Shan Li, Tao Wang, Simon Wilde

Funded by: National Basic Research Program of China, National Natural Science Foundation of China, China Geological Survey

Ghosts of oldest bacterial colonies haunt Western Australia

Identifying and reconstructing Earth's earliest biosphere is challenging. Earth's oldest sedimentary rocks are not only rare, but almost always have been heated and deformed by tectonic activity so that former signs of life are destroyed or modified beyond recognition. A new study, however, has revealed the well-preserved remnants of a complex bacterial ecosystem in a 3.5 Ga sedimentary sequence from the Pilbara region of Western Australia (*CCFS publication #365*).

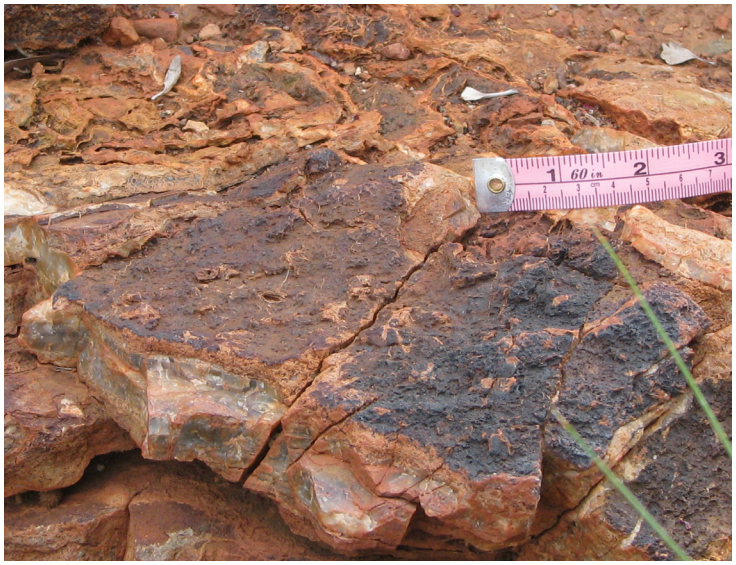

Figure 1. Microbial mat on rock surface from the 3.48 billion year old Dresser Formation, Pilbara, Western Australia.

The ancient core of the Pilbara terrane constitutes one of the rare geological areas that provide insights into the early evolution of life on Earth. Mound-like deposits (stromatolites) created by ancient bacteria, and rare microfossils of bacteria, have previously been described from this region. However, a phenomenon called microbially induced sedimentary structures, or MISS for short, had not previously been seen in rocks of this great age. Before our discovery the oldest MISS were ~ 3.2 billion years old.

MISS are created by communities of microorganisms, living in microbial mats, as they respond to changes in physical conditions such as erosion or sediment deposition in their immediate environment. A common example would be the binding together of sediment grains by microbes to prevent their erosion by water currents. MISS demonstrate not only the presence of life, but the presence of whole microbial ecosystems that could co-ordinate with one another and influence their environment.

MISS come in varied shapes and sizes. Some, such as crinkles and tufts on rock surfaces (Fig. 1), and eroded fragments of microbial mat, are on the millimetre to metre scale and can be seen with the naked eye. Other MISS are microscopic and typically include remnants of microbial filaments wrapping around sediment grains, or miniature versions of tufts (Fig. 2) and mat fragments. We have found at least ten distinct types of MISS from the 3.48 Ga Dresser Formation and demonstrated their close similarity in both morphology and preservation style to MISS found in the younger geological record. We also found that the structure and isotopic composition of carbon preserved in these MISS are consistent both with a biological origin and the known age of the samples.

As well as extending the geological record of MISS by almost 300 million years, our work shows that relatively complex mat-forming microbial communities probably existed almost 3.5 billion years ago. While it is arguable whether these MISS are the earliest signs of life on Earth, they certainly provide a new and robust source of evidence showing that large volumes of organisms were alive and well in these inhospitable conditions on the early Earth.

New discoveries of ancient life on Earth such as these can also be informative for the search for life on other planets, since the early histories of Earth and Mars are thought to have been similar. MISS could now be considered a prime target for Mars rovers, especially given that some MISS are of the centimetre scale and larger and may be visible to a rover camera.

This project is part of CCFS Theme 1, Early Earth, and contributes to understanding Earth's Fluid Fluxes.

Contact: David Wacey
Funded by: ARC CCFS CoE

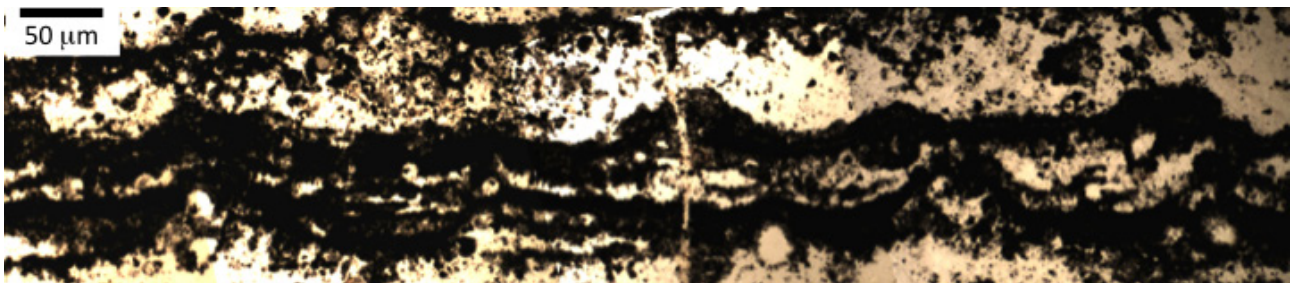

Figure 2. Cross-section through a tufted microbial mat from the Dresser Formation, viewed down the petrographic microscope. The black material is carbon and pyrite.

Trace elements in olivine are scouts for subducted continental crust in the source regions of magmas

Oceanic crust produced by sea-floor spreading at mid-ocean ridges is returned to the mantle by the process of subduction. This can be recognised by geophysical measurements that image sloping blocks of ocean crust beneath the surface, diving down beneath deep-sea trenches. For thirty years now, it has been debated how deeply these blocks are thrust into the mantle, and it is widely believed that some of this material reappears as chemical components in ocean islands such as Hawaii – thousands of kilometres from the position of any current subduction zone.

However, models for this recycling of crust usually deal with the basalts and gabbros that make up a thickness of about 7 km above the main mass of the ocean plate. It is much more difficult to characterise the recycling of the few hundred metres of sediments that were deposited on the ocean crust after its formation or during the collision process. Trace-element and isotopic compositions of volcanic rocks directly above the subduction zone indicate sediment subduction in some places, but in others the sediments are probably completely scraped off in the collision process, and do not follow the slab down into the subduction zone. The volumes of sediment involved are too small for the geophysical measurements to see.

Trace elements in olivine are a promising tool to solve this dilemma. Abundances of trace elements such as nickel, cobalt and manganese have been used to suggest the presence and melting of olivine-free rocks that originated from recycled oceanic crust beneath ocean islands (*Sobolev et al., 2007, Science*), but alternative explanations for these elements have also been put forward. No indicator for continental crust has been proposed as yet.

Our recent measurements in post-collisional volcanic rocks in the Mediterranean area have changed this. Many crustal blocks around the Mediterranean formed by a different subduction process, one that involved the collision and scrunching together of small ocean basins and blocks of continental crust – there is no deep subduction involved. These blocks are imbricated together and, after the lateral collision stops, the crust and lithosphere rise and melt, resulting in volcanoes that erupt 20-40 million years after collision ceases. These volcanic rocks contain large olivine crystals; some crystallised as the first minerals from the melts, and others were already present in the mantle and were torn off by the passing melt. These olivines have high concentrations of lithium and zinc (Fig. 1) - ten times as much lithium as is typical for mantle olivines, but similar to abundances seen in continental sediments. Coupled with previous results for lead isotopes in the volcanic rocks, which indicated input from continental crust, these lithium analyses in olivine clearly demonstrate the involvement of subducted continental sediments in the source regions of the melts. This process is widespread; the yellow points in Figure 1 are from Spain in the western Mediterranean, whereas the green points are from as far east as Turkey.

We will be pursuing research on this theme in the CCFS. The next questions are: [1] What are the olivines really "seeing"? We suspect that the lithium is concentrated by the formation of a different, intermediate rock type rich in mica and pyroxene, and this is what the olivines are really scouting for. [2] How important was subduction of continental crust earlier in Earth history? The suspicion here is that the accretionary type of collision involving small oceans and continental blocks, now seen in areas such as the Mediterranean and Indonesia, was much more widespread in the Archean, before all the continents had been formed.

This project is part of CCFS Theme 2, Earth Evolution, and contributes to understanding Earth's Fluid Fluxes.

Contact: Stephen Foley
Funded by: Geocycles Research Centre, University of Mainz - State of Rhineland Palatinate (Germany)

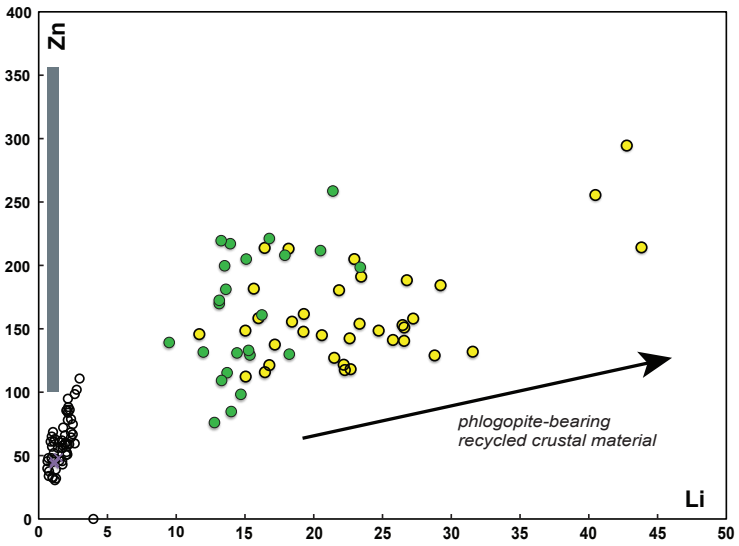

Figure 1. Both Li and Zn are enriched in olivines in Mediterranean post-collisional volcanic rocks (yellow and green circles) from source regions containing recycled continental crust, which is present in the source as phlogopite-bearing assemblages. Hawaiian olivines from sources containing recycled ocean crust lie in the grey box with variable Zn but low Li (1-2 ppm). Mantle olivines have almost exclusively less than 6 ppm lithium. From Foley, Prelevic, Rehfeldt and Jacob (2013) Earth and Planetary Science Letters Frontiers.

Auditioning zircons for perfecting performance

Zircon is a common U-rich accessory mineral recognised as a key geochronometer and premier geochemical tracer in terms of Hf and O isotopes because of its resistance to alteration and post-magmatic metamorphism. However, zircons with high uranium (U) contents commonly yield anomalous older apparent ages in ion microprobe analysis (commonly called the "high-U matrix effect") (*White and Ireland, Chem Geol, 2012*). Moreover, zircons with such discordant U-Pb ages usually also have disturbed oxygen-isotope compositions (Booth, GCA, 2005). Although these isotopic disturbances are commonly considered to be due to zircon metamictisation (the destruction of the crystal lattice by radiation damage), the discussion of data quality has mostly been qualitative. It is difficult to define a specific minimum U content that causes the "high-U matrix effect" or metamictisation, because the radiation damage is accumulated through time. This qualitative evaluation also has led most workers to overlook the different stability of zircon's U-Pb isotope system and oxygen-isotope system. For zircons in which the U-Pb system remains apparently undisturbed, the robustness of the oxygen isotope data is rarely questioned.

Raman spectra show that zircons with increasing degrees of radiation damage have gradually changing peaks and higher values of half-width height (Fig. 1), and the effects of radiation damage can be quantified, as displacements-per-atom, Ddpa (*Palenik, Am Mineral 2003*). We have used this technique to assess the effect of varying U contents on the ion microprobe U-Pb and oxygen isotopic signatures of zircon-quartz pairs from the U-rich A-type granites of Suzhou (southern China). The results show that zircons with U concentrations ([U]) greater than 1500 ppm show a negative correlation between [U] and $\delta^{18}O$ values, while zircons with [U] greater than 3000 ppm show a positive correlation between [U] and U-Pb ages (Fig. 2). Oxygen-isotope analyses of coexisting quartz provide constraints for interpretation of zircon oxygen-isotope values, because the isotopic partitioning between quartz and zircon is well known. This relationship allows us

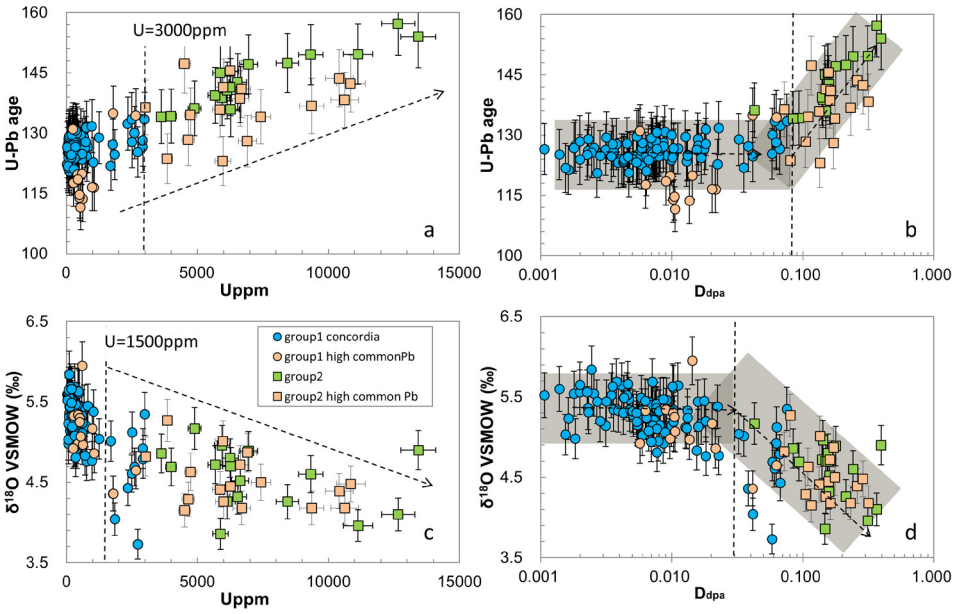

Figure 2. Plot of zircon U (or Ddpa) vs $^{206}Pb/^{238}U$ age (or $\delta^{18}O$); In-situ zircon U-Pb age and $\delta^{18}O$ data are obtained from SIMS analysis.

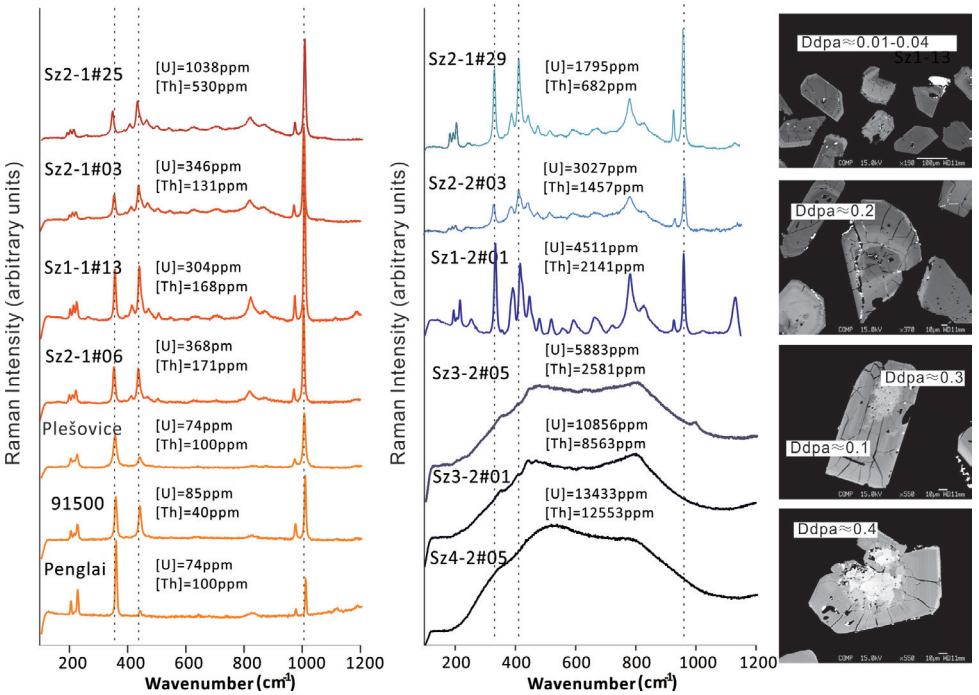

Figure 1. Raman spectra of zircons with different Ddpa values.

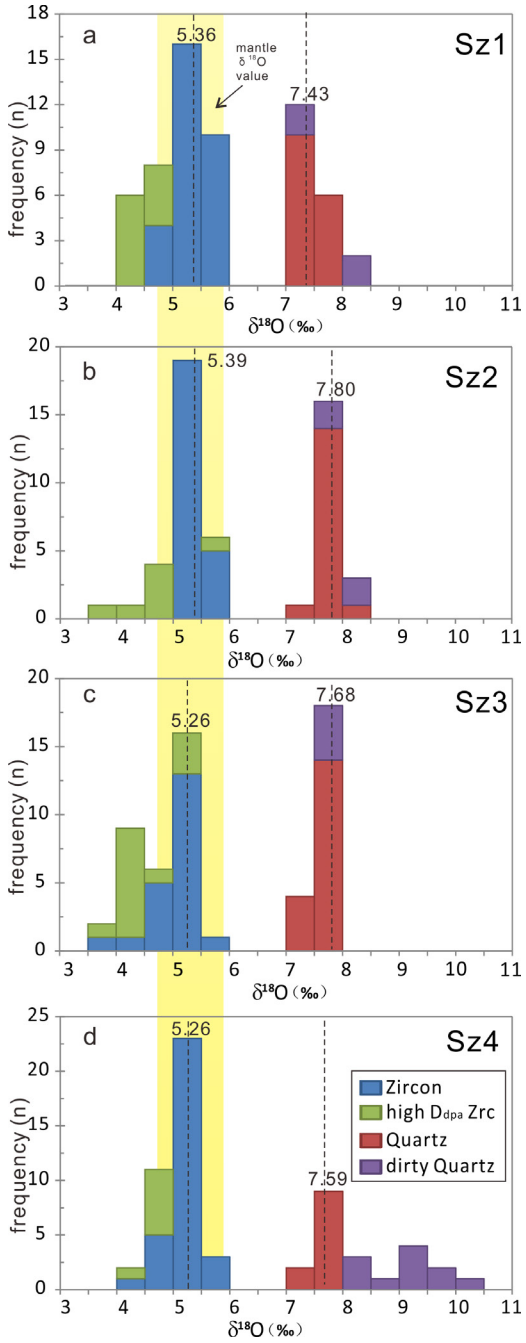

Figure 3. Histograms of $\delta^{18}O$ values for zircon-quartz pairs from the four representative Suzhou granite samples

to recognise anomalous $\delta^{18}O$ values (Fig. 3), which are clearly common in high-U zircons.

The high U contents of the zircons thus produce two independent effects, linked by the radiation damage. Anomalously high SIMS U-Pb ages are a direct result of the matrix effect caused by metamictisation, whereas the low $\delta^{18}O$ values result from interaction with infiltration of OH-bearing fluid and fluid-facilitated diffusion in the radiation-damaged areas. Previous oxygen-isotope studies of bulk zircon separates from the Suzhou granites reported low $\delta^{18}O$ ratios; it is now clear that these represent anomalous values due to effects of radiation damage to the zircons.

This study shows how essential it is to evaluate the degree of radiation damage before/after carrying out dating or oxygen-isotope analysis on zircons with high U contents. Raman spectroscopy can be used to measure the degree of radiation damage of zircons, but, it is not always available, especially for pre-existing data and data from the literature. In the absence of Raman spectra, Ddpa calculated from the [U], [Th] and age can be used to estimate the highest degree of radiation damage and screening for reliable zircon U-Pb geochronology and oxygen isotope analysis (Fig. 4). The results indicate that for the Suzhou pluton, Ddpa <0.03 is a robust discriminant threshold to identify zircons with primary oxygen-isotope ratios and Ddpa<0.08 is a robust discriminant to screen for reliable U-Pb dating. These different screening values reflect the evidence that oxygen-isotope compositions show disturbance at a lower level of post-crystallisation zircon lattice disturbance than does the U-Pb system.

This project is part of CCFS Theme 2, Earth Evolution, and contributes to understanding Earth's Architecture and Fluid Fluxes.

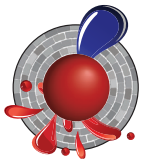

Contacts: Yuya Gao, Xian-Hua Li (P, IGGCAS, Beijing), Bill Griffin

Funded by: EPS postgraduate fund, iMQRES, MQ PGRF, CCFS, IGGCAS

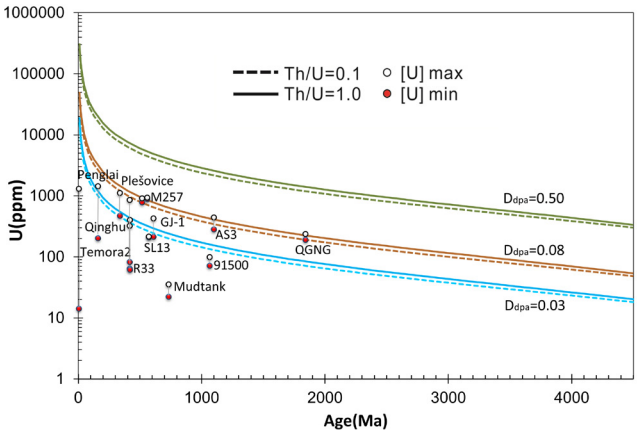

Figure 4. Correlation between U concentration and U-Pb ages, along with assigned Ddpa of 0.03, 0.08, and 0.5. Dashed lines Th/U = 0.1; solid lines Th/U = 1. The area between dashed and solid lines with same Ddpa, including all the zircons with Th/U = 0.1 ~ 1. Data sources for standard zircons: Penglai – Li, Geost. Geoan. Res, 2010; Qinghu – Li, Sci China Ser D, 2009; Plešovice – Slama, Chem Geol, 2008; Temora – Black, Chem Geol, 2003; R33 – Black, Chem Geol, 2004; M257 – Nasdala, Geost. Geoan. Res, 2008; SL-13 – Lee, Nature, 1997; GJ-1 – Jackson, Chem Geol, 2004; Mud tank – Black and Gulson, BMR J Aust Geol Geophys, 1978; 91500 – Wiedenbeck, Geostandards Newsletter,1995; AS3 – Paces and Miller, JGR,1993.

Why hasn't the Mediterranean Basin closed?

The Mediterranean Sea is the vestige of a large ocean that was closed by the northward movement of the African plate, creating the Alps as the leading edge of the African plate was subducted beneath Europe. But why did it stop there? Why does the Mediterranean exist at all? A growing body of data on U-Pb ages of magmatic zircons, Hf model ages of inherited zircons and whole-rock Nd model ages of crustal igneous and metamorphic rocks has provided many constraints on crustal evolution within the Mediterranean basin. However, there has been little robust information on the age of its underlying mantle, that would allow us to understand the deeper geological framework of the Mediterranean.

A synthesis of Re-depletion model ages (T_{RD}) for both whole-rock samples and *in situ* analyses of individual sulfides from mantle-derived rocks, including xenoliths and peridotite massifs that are widespread across the Mediterranean area, demonstrates the existence of different mantle domains *(CCFS Publication #234)*. A maximum T_{RD} age of 1.8 Ga is common to sulfides in mantle-derived peridotite xenoliths beneath Western Europe (Calatrava Volcanic Field, Spain; Languedoc and Massif Central, France) and to whole-rock samples from Azrou (North Africa) and the Pyrenees (France). A maximum at <1.4-1.3 Ga is seen in whole-rock samples from Central Europe (Bohemian and Rhenish Massifs) as shown in Figure 1.

In contrast, Os-bearing sulfides in xenoliths and sulfides and platinum-group minerals in peridotite massifs from the inner Mediterranean region (Hyblean Plateau in Sicily and Kraubath Massif in Austria) all show an oldest T_{RD} peak at ~ 2.3 Ga, equivalent to the oldest whole-rock T_{MA} of 2.2 Ga for rocks of Beni Boussera in northern Morocco and the 2.4 Ga peak in sulfides from peridotites of the internal Ligurides (Italy). A peak at 2.6 Ga is defined by sulfides in mantle xenoliths from the Tallante Volcanic Field in southern Spain.

These Re-Os data identify the existence of a common Paleo-Proterozoic (1.8 Ga) mantle on both sides of the Mediterranean realm, and an older (2.2-2.6 Ga) lithospheric mantle sitting inside the more recent Maghrebide-Appenine-Betic front generated during the Alpine-Betic orogeny. Thus, the Mediterranean basin may contain several buoyant Archean microplates, which could act like bollards, impeding the northward movement of Africa, and protecting the Mediterranean from closing.

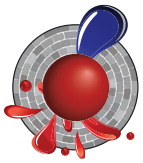

This project is part of CCFS Themes 2 and 3, Earth Evolution and Earth Today, and contributes to understanding Earth Architecture and Fluid Fluxes.

Contacts: José María González-Jiménez, Bill Griffin, Sue O'Reilly
Funded by: CCFS ARC ECSTAR funds

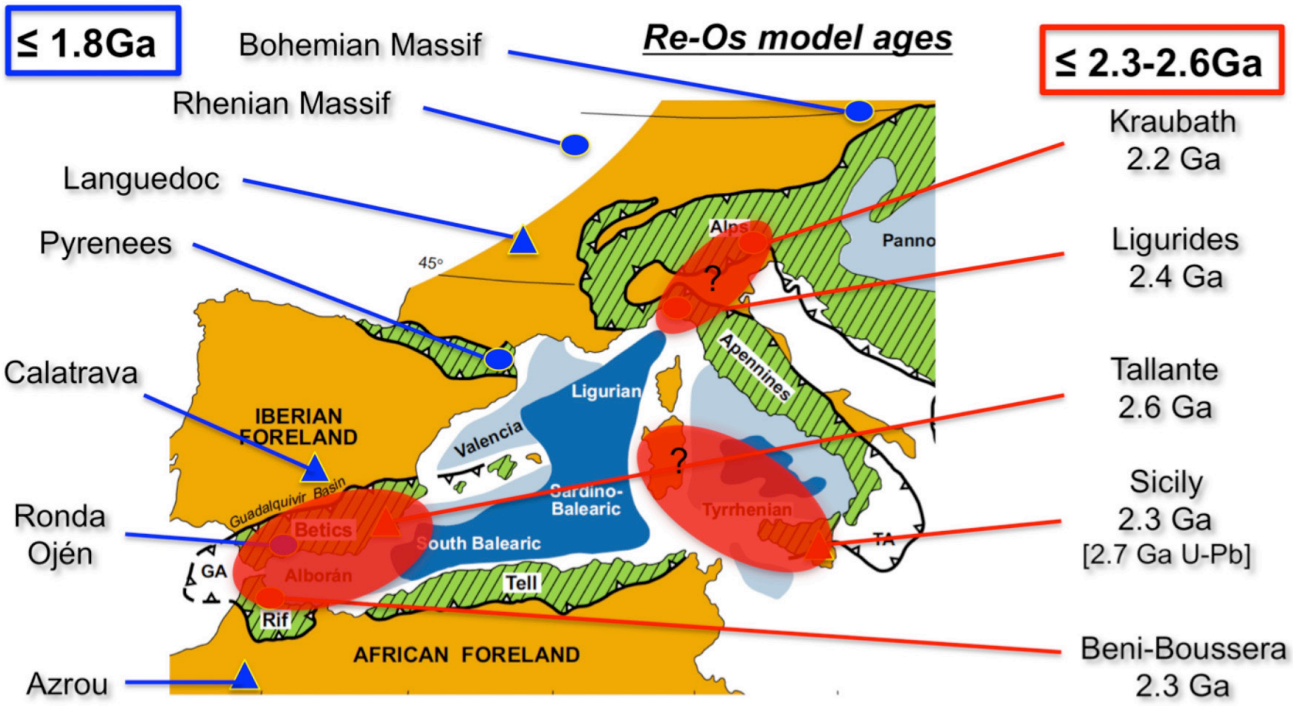

Figure 1. Distribution of maximum T_{RD} model ages across the Mediterranean region. The tagged line represents the Maghrebide-Appenine-Betic tectonic front. Red areas indicate possible Archean micro-plates.

Surface structures influence reaction rates of minerals

The rate at which minerals are dissolved and grow is crucial in our understanding of how Earth materials have changed in terms of physical and chemical properties through time. In recent years, it has been realised that many reactions that transform one mineral to another require fluid involvement. The first and often crucial step in this transformation is dissolution.

We have investigated the dynamics of dissolution and the time evolution of the (often assumed) parameter, dissolution constant, that determines at which rate a mineral dissolves under specific conditions. Classically, dissolution rates are calculated based on models of dissolution kinetics as a function of surface area, which is assumed to remain constant. However, this assumption ignores the changes occurring on the surface during the dissolution process. We examined how the topography of natural fluorite surfaces with different crystallographic orientations changed during up to 3200 hours of dissolution. The results were analysed in terms of changes in surface area, surface reactivity and dissolution rates.

We found that the dissolution rate is strongly time-dependent, while the value of the dissolution constant varies depending on the crystallographic orientation of the dissolving surface. All surfaces studied show rapid changes in topography and rapid dissolution rates during the initial 200 hours of dissolution. The factors controlling the development of topography are the stability of the step edges forming the initial surface and its inclination to the closest stable planes, which are specific for each surface orientation. The surface dynamics are accompanied by a significant decrease of dissolution rates after the initial rapid-dissolution regime. The time-dependent variation of dissolution rates is attributed to a decrease in the density of step edges on the surface and the continuously increasing exposure of more stable planes with time. During a second dissolution regime, some surfaces continue to show significant changes in topography, while on others the topography tends to remain approximately constant.

Our observations suggest that the development of topography during the initial dissolution regime is kinetically driven, and therefore the surface may only reach a metastable state. The height and size of the topographic features initially developed, and the types of planes and step edges that constitute them, determine the changes during the second dissolution regime. Dissolution transforms the metastable surfaces formed during the initial dissolution stage towards a more stable topography. Importantly, our results show that, contrary to classic theory, dissolution rates decrease even though the total surface area increases. Therefore, calculations of dissolution rates that assume dissolution rates are directly proportional to surface area are not valid for the surfaces studied. Instead, to develop accurate kinetic-dissolution models and more realistic stochastic dissolution simulations the surface reactivity, as determined by the relative stability of the planes and type of edges that constitute a surface, must be taken into account.

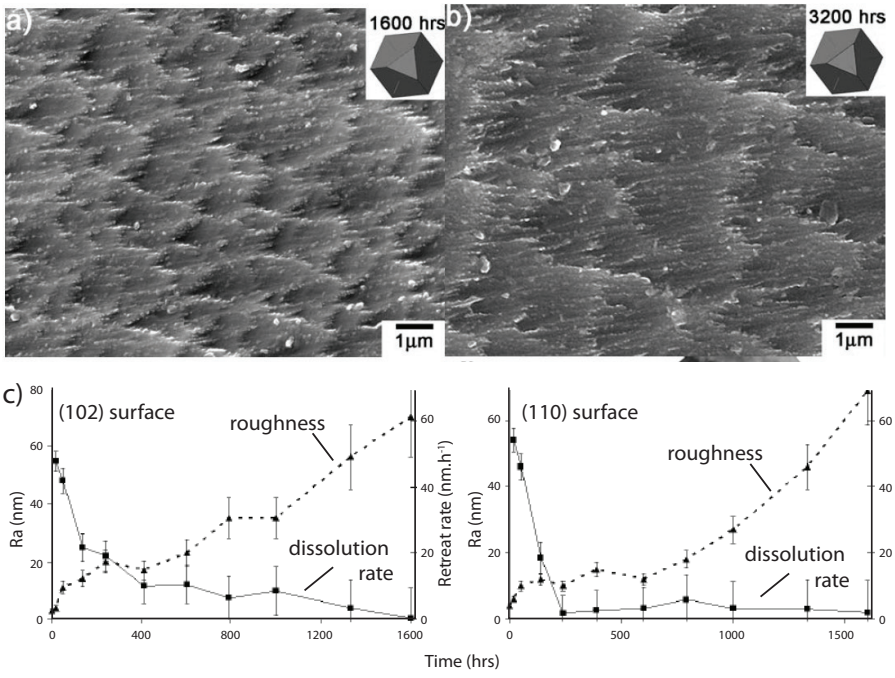

Change in dissolution rate, surface structure and topology / roughness as a function of time and surface orientation. (A) & (B) Examples of SE images showing topography of one studied surface after 1600 hrs and 3200 hrs dissolution. (C) Graphs showing that dissolution rates are initially high, while roughness/topography is low, subsequently dissolution rates decrease while roughness / topography increases. Two examples are shown, (left) surface (102), (right) surface (110).

Even though experiments were performed using fluorite, the same principles are predicted to hold for other crystal structures. This study may be the first step toward a quantitative characterisation of the often heterogeneous, fluid-mediated replacement of different minerals in the Earth's crust and Mantle (see *CCFS publication #364*).

This project contributes to the CCFS Theme 3, Earth Today, and furthers our understanding of Earth's Fluid Fluxes.

Contact: Sandra Piazolo

Funded by: ARC Future Fellowship, European Research Council

Different continent configurations around 800 – 500 million years ago give new clues about extreme climatic variations

The Neoproterozoic was one of the most dynamic times in Earth history, featuring the formation and breakup of the supercontinent Rodinia (e.g. *CCFS contribution #117*), repeated low-latitude glaciation at sea level (a Snowball Earth?), rapid oxidation of the atmosphere, and the end of the Precambrian explosion of complex life. To better understand the relationships between these dramatic events, we developed a set of revised global palaeogeographic maps for the 825–540 Ma time interval, accompanied by a compilation and graphical illustration of global data on sedimentary facies (*CCFS publication #314*; see Fig. 1 for examples). These maps form the basis for an examination of the relationships between known glacial deposits, paleolatitude, positions of continental rifting, relative sea-level changes and major global tectonic events such as supercontinent assembly, breakup and superplumes.

Our analysis reveals several fundamental palaeogeographic features that will help inform and constrain models for Earth's climatic and geodynamic evolution during the Neoproterozoic. First, whereas the latitudinal distribution of carbonate rocks appears to be in accord with a normal zonal global climate similar to that of the Phanerozoic (Fig. 2c), thus validating the palaeogeographic maps, glacial deposits at or near sea level appear to extend from high latitudes into the deep tropics for all three Neoproterozoic ice ages (720 Ma, ca 635 Ma, and ca 580 Ma), although the 580 Ma interval remains very poorly constrained in terms of both paleomagnetic data and global lithostratigraphic correlations (see Figs. 1 and 2b for latitudinal distributions of all three glacial events). This appears to be consistent with the predictions of the Snowball Earth model (e.g. Hoffman et al., 1998). Second, continental sedimentary environments were dominant in epicratonic basins within Rodinia (from >825 Ma to 750 Ma; Fig. 2a shows the low proportion of deep-marine facies for that time), possibly resulting from both plume/superplume dynamic topography and lower sea-level due to dominantly old oceanic crust. This was also the case at ca 540 Ma (Fig. 2a), but at that time the pattern reflects widespread mountain ranges formed during the assembly of Gondwanaland and the increasing mean age of global ocean crust. Third, deep-water environments were dominant during the peak stage of Rodinia break-up between ca 720 Ma and ca 580 Ma (Fig. 2a), probably indicating a higher sea level due to increased rate of production of newer oceanic crust, and perhaps the effect of continents drifting away from a weakening superplume. Such a geodynamic control of first-order global sea-level changes has also been observed during the evolution of the youngest supercontinent Pangaea (e.g. *Muller et al., 2008*), and agrees well with the hypothesised dynamic supercontinent-superplume coupling (see *Li and Zhong PEPI, 2009* for a review of the model). Finally, there is no clear association between continental rifting and the distribution of glacial strata, contradicting models that restrict glacial influence to those particular tectonic environments.

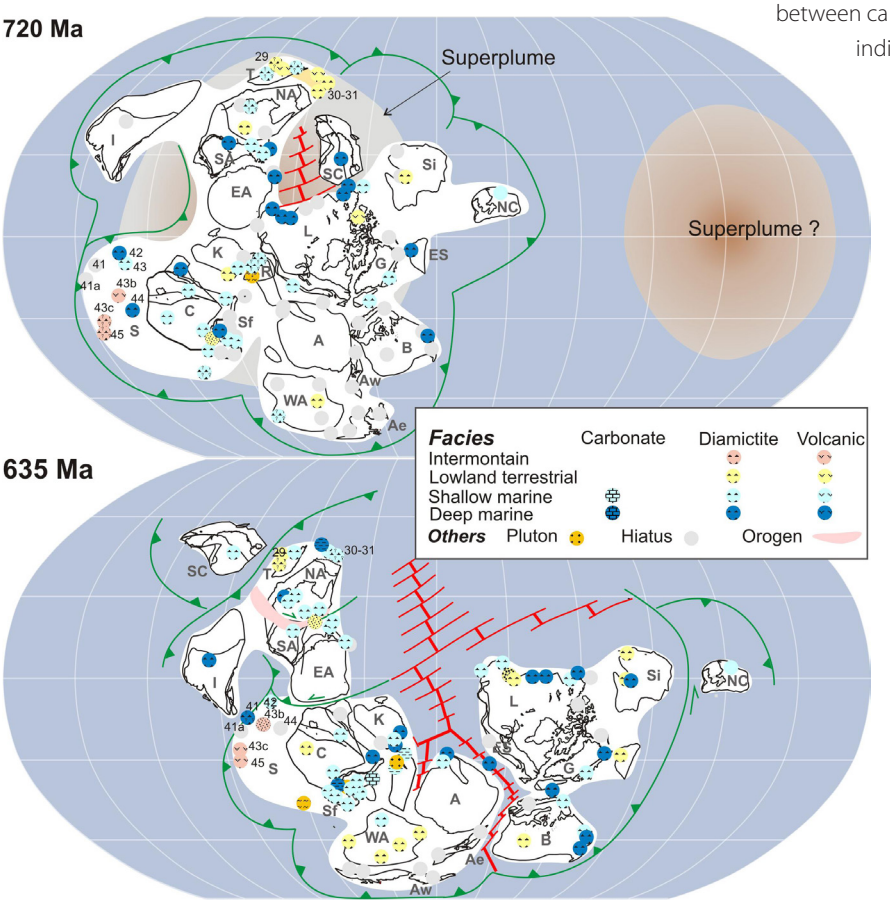

Figure 1. Revised global palaeogeographic reconstructions for 720 Ma and 635 Ma, with facies distributions featuring the occurrence of the "Sturtian" (ca. 720 Ma) and "Marinoan" (ca. 635 Ma) glaciations, respectively.

This project is part of CCFS Theme 2, Earth Evolution, and contributes to understanding Earth's Architecture.

Contact: Zheng-Xiang Li

Funded by: CCFS Foundation Program 6

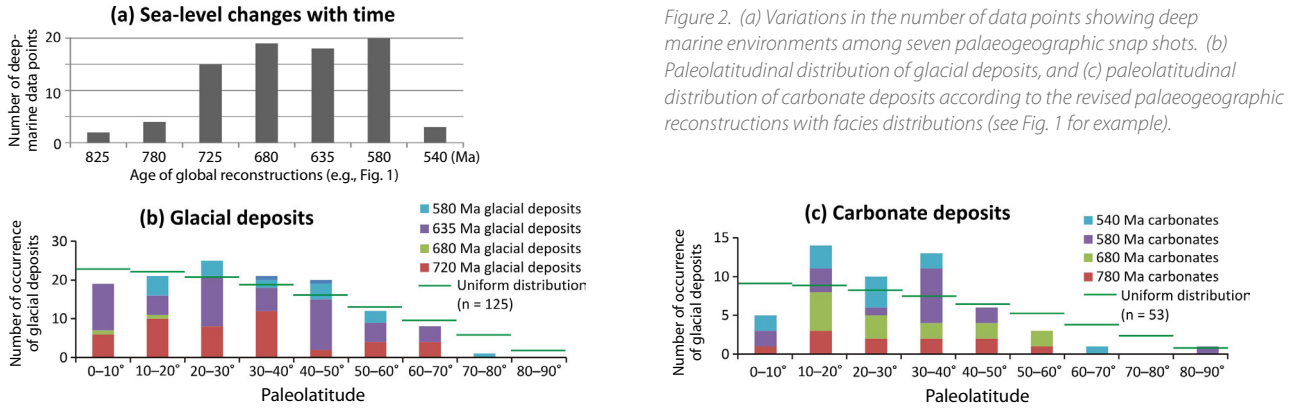

Figure 2. (a) Variations in the number of data points showing deep marine environments among seven palaeogeographic snap shots. (b) Paleolatitudinal distribution of glacial deposits, and (c) paleolatitudinal distribution of carbonate deposits according to the revised palaeogeographic reconstructions with facies distributions (see Fig. 1 for example).

The first Martian crust

Mars is the closest planet to Earth after the Moon and mankind has long speculated about possible life on Mars. The science-fiction novels from the 'fifties depicting human colonies on the red planet certainly fed this curiosity and contributed to the modern development of the small robots now roving the surface of Mars (like NASA's Opportunity and Curiosity). These remotely-controlled rovers have been providing stunning images and data from the Martian surface and have massively improved our knowledge of the planet. The other way we can study Mars is by finding and collecting meteorites, first launched from its surface during impacts, and then delivered to Earth. While the rovers and their range of high-tech instruments concentrate on the study of the surface, Martian meteorites provide insight into the deeper part of the planet. Most of them are mafic and ultramafic rocks originating either from the mantle or from the young volcanic plains covering the northern hemisphere of Mars. The southern hemisphere of Mars, known as the Southern Highlands, is believed to be much older and to hold clues to the planet's early differentiation. Yet, so far, no samples are available from this part of the planet.

A Martian meteorite recently recovered from the north-western African desert and called NWA 7533 is strikingly different from the other known Martian meteorites: it is a fragment of Mars' regolith breccia, comprising a fine mixture of fragments of igneous rocks and clast-laden impact melt. Superficially, it appears quite similar to some Apollo samples but has the unique Martian compositional signature (as identified by oxygen isotopes). It also contains (i) high abundances of meteoritic siderophile elements (like Ni and Ir) suggesting it formed as a result of impact and (ii) fine-grained material with composition similar to soil analysed from the Gusev crater by the Spirit rover, suggesting the meteorite mainly consists of soil particles; hence its classification as a regolith breccia. NWA 7533 also contains small magmatic clasts, enclosing zircon grains.

Our part in this exciting project was to image and date these zircon grains, achieved by in situ U-Pb dating using the SHRIMP (ion microprobe) in the John de Laeter centre at Curtin University. The small meteorite slab we studied contained seventeen zircon grains; ten were large enough to be dated, and seven grains, representing eighteen ion-microprobe analyses, could be combined to define a Discordia line. The upper intercept age at 4426 ± 23 Ma (million years) is interpreted as the crystallisation age of the zircon grains. The lower intercept age at 1718 ± 82 Ma represents the time where the U-Pb system was disturbed, most likely by an impact. The discovery of such ancient zircon grains on Mars implies that the planet's early crust differentiated at about the same time as the Earth and the Moon crusts (*CCFS Publication #370*). This is of particular interest as it may point toward a similar mechanism for the differentiation of terrestrial planets, regardless of their present shape and overall mass.

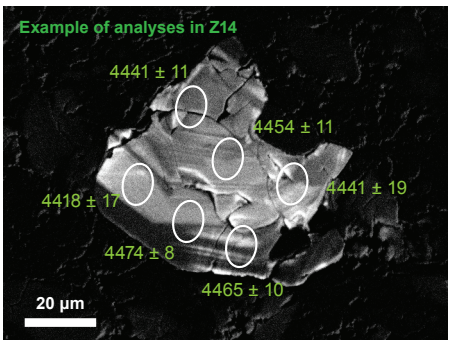

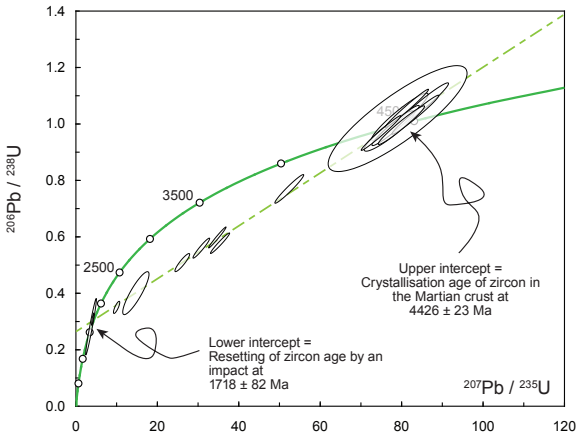

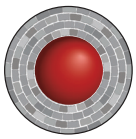

This project is part of CCFS Themes 1, Early Earth, and contributes to understanding Earth's Architecture.

Contacts: Alexander Nemchin, Marion Grange
Funded by: CCFS (Marion Grange salary)

Tracking deep fluid processes where continents collide: magmatic segregations in a Tibetan orogenic peridotite

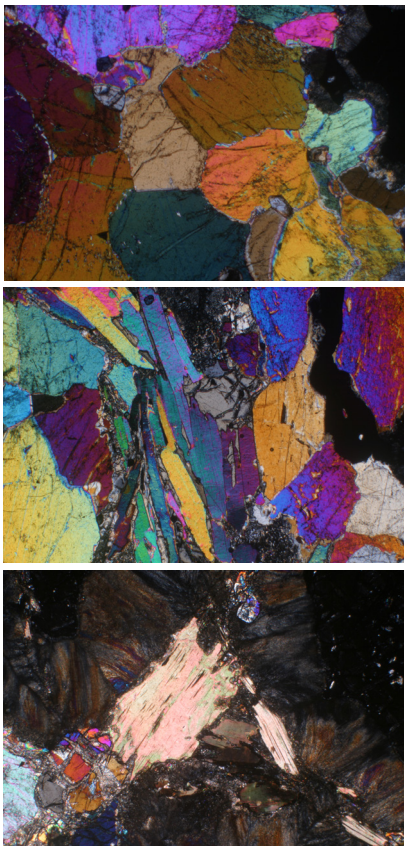

Figure 1. Thin-section photomicrographs of the Shenglikou pyroxenites, North Qaidam, NE Tibet.

Arc magmatism in subduction zones is a prime process controlling element recycling and continental growth at the convergent margins in the shallow Earth, but the early stages of magmatic processes at mantle depths remain unclear. Many previous studies have shown an andesitic average for the composition of the continental crust in contrast with the basaltic nature of primitive melts in plate collision zones, suggesting there is a complementary rock-type component at depth. Mafic to ultramafic pyroxenites hidden within the arc roots have been suggested as this complement (e.g. *Kay and Kay, GCA 1988; Dhuime et al., J Pet. 2009*). Thus, knowledge of the genesis and sources of these "hidden" pyroxenites is critical to understanding the dynamic processes of generation and migration of primitive arc magmas beneath active margins, and to linking the recycling of material between subduction slabs and erupted volcanics within a complete framework of plate convergence. This study examines the origin and history of pyroxenite dykes (interpreted to be magmatic segregations; Fig. 1) in the Shenglikou peridotite massif (North Qaidam Orogen, NE Tibet, China).

Major- and trace-element compositions of the pyroxenites indicate an origin as high-pressure (garnet-facies) cumulates and/or trapped melts, and the derivation of the parental magmas from the melting of a deep peridotite-dominated source. Bulk-rock trace-element patterns also show strong enrichment in fluid-mobile elements (Cs, Rb, Ba, U, Pb and Li) and marked negative anomalies in the high-field-strength elements relative to rare earth elements; overall they are geochemically similar to melts from a volatile-rich arc-type mantle. Initial Sr isotopic ratios (0.7152-0.7105) and Nd isotopic compositions (εNd(t) = -11.6 to -4.4) of clinopyroxene and garnet confirm the contribution of subducted sediments. However, the Hf isotopes of clinopyroxene, garnet and zircon show depleted-mantle isotopic values at 430 Ma; one garnet sample with depleted-mantle model age of 846 Ma shows minimum assimilation of the host peridotite during the pyroxenite intrusion. Oxygen isotopic signatures of garnet and zircon imply uncontaminated upper-mantle sources. These decoupled isotopic features further suggest that the melt source was a peridotite-dominated convective mantle wedge (controlling the Hf and O isotopes) that had been pervasively metasomatised by fluids from the subducted slab (controlling the Sr-Nd isotopes and highly-incompatible elements).

This study illustrates a detailed dynamic process of arc magmatism within the mantle wedge beneath an active continental margin (Fig. 2). A strongly metasomatised convective mantle moved as corner flow resulting from the early Cambrian subduction of the Proto-Tethys oceanic slab. The decompression and flux melting generated magmas that intruded into the overlying lithospheric mantle wedge as pyroxenite dykes. We suggest this is a significant process to allow the mafic-ultramafic complements of continental-arc lavas to escape delamination back to the convective mantle.

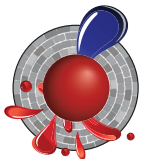

This project is part of CCFS Theme 2, Earth Evolution, and contributes to understanding Earth's Architecture and Fluid Fluxes.

Contacts: Qing Xiong, Sue. O'Reilly, Bill Griffin, Norman Pearson, Jian-Ping Zheng (China University of Geosciences, Wuhan)

Funded by: ARC Discovery , Centre of Excellence Grants (S.Y.O'R and W.L.G.), NSFC (J.P.Z.), CSC scholarship, IMQRES, MQ PGRF, EPS postgraduate fund

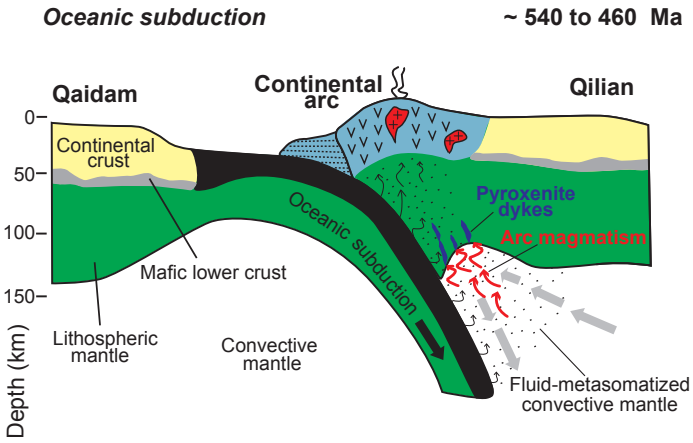

Figure 2. Cartoon representing our interpretation of the formation and evolution processes of the Shenglikou pyroxenite dykes within a tectonic framework of an early Paleozoic active continental margin, NE Tibet.

How soft is the lower crust? More ingredients to test the "*jelly sandwich*" model

Today, ancient rifting environments are important zones for the production of oil and minerals. Observations of rifted basement rocks, under the sediments that accumulate in the rifts, show they have experienced both shearing and extensional strain, often at lower-crustal depths. This project aims to develop a quantitative tool to determine the relative viscosity or "*resistance to flow*" of different rock types at lower-crustal levels. For such a study, "*boudins*" (French: a specific type of sausage; elongate sausage-shaped pieces of one rock layer aligned like a chain of pearls) can be used. Boudins occur where a harder, more competent layer in a weaker matrix is deformed by pure and/or simple shear, and at microscopic to landscape scales; they develop a variety of symmetric and asymmetric shapes. The temperature and pressure in the lower continental crust mean the rocks can flow and deform in ways unseen at the Earth's surface, and different rock types have different physical characteristics, melting temperatures, hardness, flow characteristics and viscosity. Our study adds more information about the rheological characteristics of the lower crust and will provide new data to assess details of the "*jelly sandwich*" model (e.g. Jackson GSA Today, 2002).

In this project, we combine detailed field work with numerical simulations. The Anita Shear Zone (ASZ) in Fiordland, New Zealand has been chosen as a field example; it is an excellent example of landscape scale, asymmetric ultramafic boudins formed at depth. The boudins are surrounded to the east by the Milford Orthogneiss and to the west by the Thurso Paragneiss. In the field, the first-order relative viscosities of the lithologies were determined, where the ultramafic layer is inferred to be the most viscous, followed by orthogneiss and then paragneiss. Field work uncovered a ~160m "*soft*", high-strain zone between the orthogneiss and the ultramafics and a much wider high-strain zone between the paragneiss and the ultramafics.

To investigate the impact of viscosity on boudin formation we used the Underworld software (*Moresi et al., J. Comp. Phys, 2003*) with, initially, three layers undergoing Newtonian flow with pure (extensional) shear, keeping the ultramafic:orthogneiss viscosity ratio at 5:3 and varying the paragneiss viscosity. Boudins started to form where the ultramafic:paragneiss viscosity ratio was 5:1, with better boudins forming as the ratio increased (5:0.5, 5:0.25 etc.). Subsequently, high-strain zones with a viscosity of 0.5 were added on either side of the more viscous ultramafic layer and the width of the high-strain zone on the orthogneiss side was varied. Boudin shapes similar to those of the ASZ were developed when the width of the paragneiss:orthogneiss high-strain zone was 4:1.

In general, the simulations show that individual boudins are more asymmetric where the paragneiss:orthogneiss high strain zone ratio is wider (4:1 cf 2:1) and the viscosity is asymmetric either side of the more viscous, boudinaging layer. A wider symmetric high-strain zone formed fewer, longer, more symmetrical boudins. This study highlights the importance of both high-strain zones and the relative viscosity of the lithologies for asymmetric boudin formation. Comparison of the symmetry and length of boudins measured in the field and those developed in numerical models allows quantitative determination of the relative viscosity ratio of the matrix and boudinaging layers.

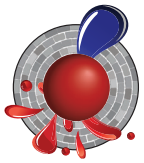

This project is part of CCFS Theme 3, Earth Today, and contributes to understanding Earth's Architecture and Fluid Fluxes.

Contacts: Robyn Gardner, Sandra Piazolo
Funded by: ARC Future Fellowship (Piazolo), MQ infrastructure funding, MQRES

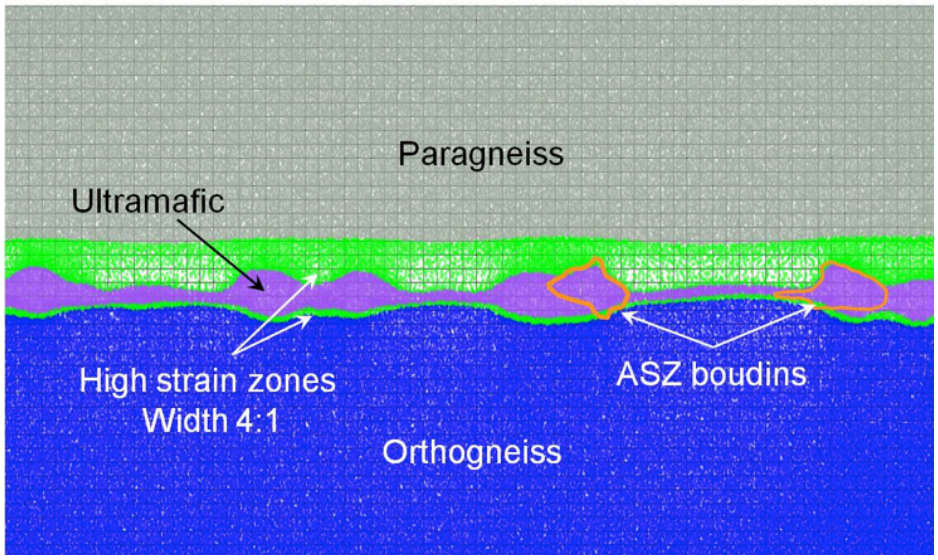

Simulated boudin formation where paragneiss:ultramafic:orthogneiss viscosity ratio is 1:5:3 with high strain zones with viscosity of 0.5 and paragneiss to orthogneiss zone width ratio of 4:1. The ASZ ultramafic boudins digitised from Google earth have been overlaid onto the simulated ultramafic boudins for comparison showing good agreement with the simulated shapes.

Is the Moho the Crust-Mantle Boundary? Evolution of an idea

The concept that the Mohorovicic Discontinuity (Moho) detected seismically does not necessarily coincide with the base of the continental crust as defined by rock-type compositions was introduced in the early 1980s (see *Griffin and O'Reilly, Geology 1987* and references therein). This had an important impact on understanding the nature of the crust-mantle boundary by integrating information from geophysics and the petrology and geochemistry of deep-seated samples brought to the surface either as fragments in magmas (xenoliths) or by tectonic activity.

The use of empirically-determined xenolith geotherms to plot the locus of the pressure-temperature curve with depth for specific lithospheric sections demonstrated that there is a variety of geotherms depending on tectonic environment. These geotherms range from very high near rift zones, through highly inflected but lower geotherms in active tectonic regions with basaltic volcanism (higher than "oceanic" geotherms), to very low geotherms in the most ancient cores of coherent cratons. These xenolith geotherms provided a robust framework for the construction of lithological sections through the lower crust and lithospheric mantle and revealed that the crust-mantle boundary is commonly transitional, over a depth range of 5 - 20 km or more, in off-craton regions. Early seismic-reflection data revealed that layering is common near the Moho and this correlates well with the petrological observation of multiple episodes of basaltic intrusion around the crust–mantle boundary. Petrologically, the crust-mantle boundary is defined as the depth at which peridotitic (mantle) wall rocks become dominant over mafic granulites and other deep-seated crustal rock types, and this boundary commonly lies 5 - 15 km above the seismically defined Moho, especially in off-craton regions.

Recent developments in seismological techniques, petrophysical laboratory measurements on natural rocks, and experimental petrology have refined interpretation of the formation of lower crust and uppermost mantle domains. The expansion of *in situ* geochronology (especially U-Pb ages and Hf-isotope composition of zircon and Os-isotope compositions of mantle sulfides) has allowed the recognition of linked tectonic events that have affected whole crust-mantle sections. These types of data reveal that the crust-mantle boundary has commonly changed in depth and thickness through time (*CCFS Publication #235*).

The main process effecting Moho depth variation is over- and under-plating of basaltic magmas at this major rheological boundary between peridotite and lower crustal rock types. This process is responsible for major crustal growth, resulting in a juvenile lower crust of mafic composition (which can then

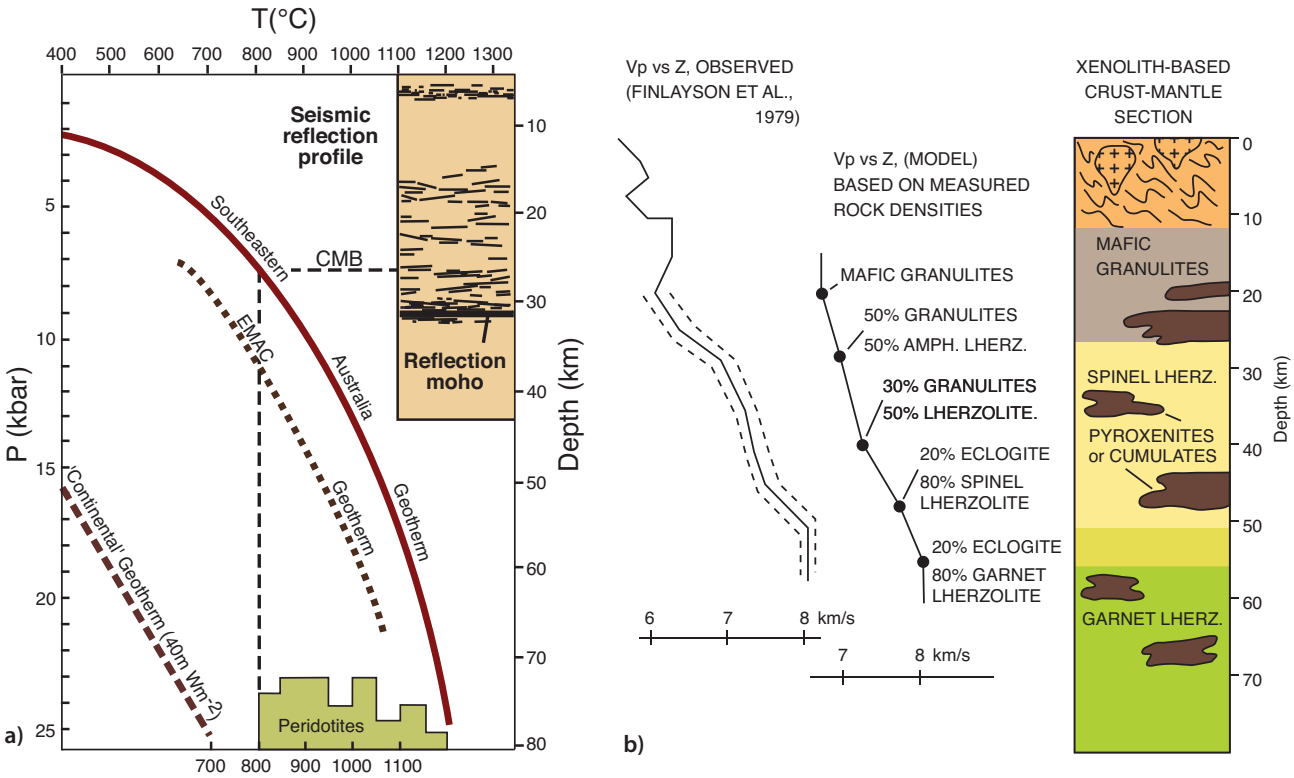

Figure 1. The geotherm generated by data from garnet+two-pyroxene xenoliths in alkali basalts of Eastern Australia. (a) Distribution of mantle peridotites beneath western Victoria, compared with the seismic reflection profile across the area (O'Reilly and Griffin, Geology, 1994); the crust-mantle boundary, as defined by the lowest temperature/depth estimates of abundant peridotite xenoliths, lies in the middle of the package of reflectors above the "reflection Moho" "EMAC" is the Eastern Margin of the Australian Craton. (b) Crust-mantle stratigraphy reconstructed from xenoliths and thermobarometry calculations beneath the Bullenmerri locality, compared with the seismic-velocity profile of Finlayson et al. (BMR Jnl. 1979).

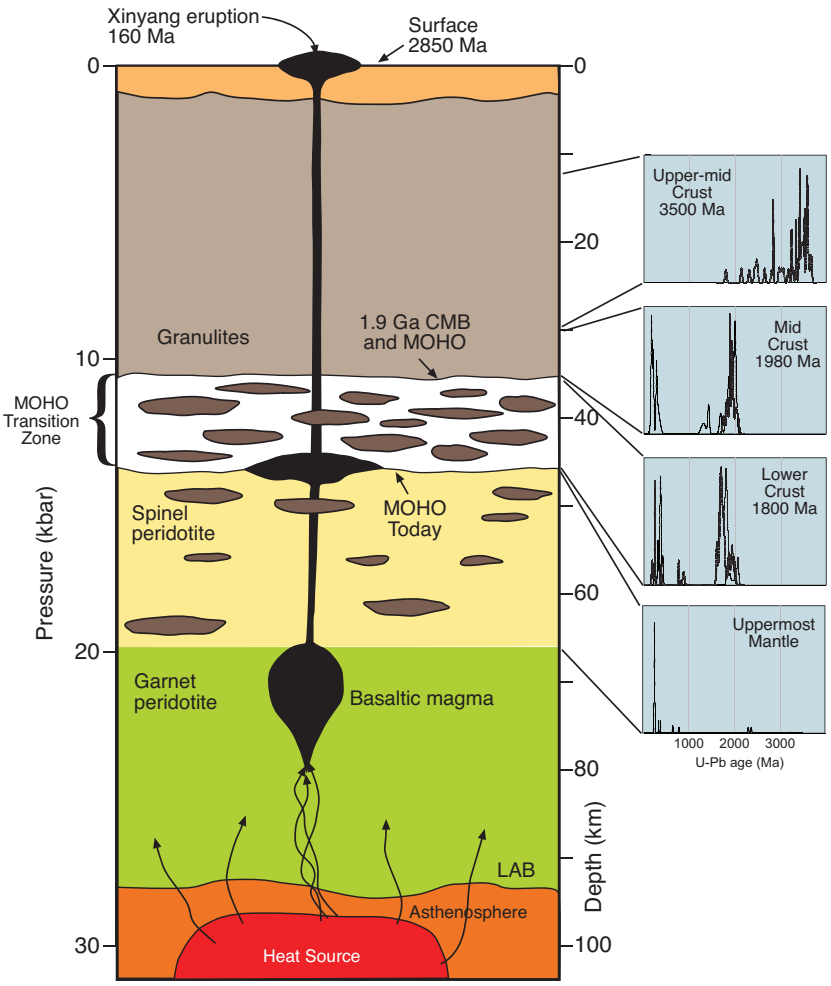

Figure 2. Crust-mantle section beneath the Xinyang area, on the southern edge of the North China Craton (after CCFS Publication #163). Histograms show U-Pb ages of zircons extracted from granulite, pyroxenite and peridotite xenoliths. The original 3.5 Ga crust was overplated at ca 2.85 Ga, and then underplated by mafic magmas at 1.9-2.0 Ga, and again at ca 1.6-1.8 Ga, lowering the crust-mantle boundary by ca 15 km. This lower crust and the subjacent upper mantle have been repeatedly intruded by mafic magmas from Paleozoic to Cenozoic time.

undergo melting and reworking to produce granitic magmas). In the alkali-basalt province of SE Australia the accumulated addition is approximately 5 km thick and occurred at a rate of about 900 m/Ma. This magma input is responsible for producing the characteristically high and inflected geotherm associated with such basaltic provinces before thermal decay occurs over about 30 million years.

However, the nature of the crust-mantle boundary in cratonic regions still remains enigmatic, mainly due to lack of key xenolith samples or exposed sections.

The observation that the Moho defined by seismic data may lie significantly deeper than the crust-mantle boundary has important implications for modelling the volume of the crust, especially in off-craton regions. Mapping of this crust using seismic techniques alone, without consideration of the petrological problems, may lead to an overestimation of crustal thickness by 15 – 30% and up to 50% in some areas. This will propagate to large uncertainties in the calculation of elemental mass balances relevant to crust-formation processes and the composition of the convecting mantle. For more details, refer to *CCFS Publication #235*.

This project is part of CCFS Themes 2 and 3, Earth Evolution and Earth Today, and contributes to understanding Earth's Architecture.

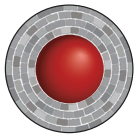

Contacts: Sue O'Reilly, Bill Griffin
Funded by: CCFS Foundation Program 1

Revised conceptual framework

Following the conceptual framework outlined on *page 4* of the 2014 CCFS Annual Report, these Research Highlights are identified as contributing to understanding Earth's Architecture (the '*roadmap*' for fluids) and/or Fluid Fluxes (the '*traffic report*'), with logos for easy attribution. For a full description of the new Flagship Programs, see the *2014 CCFS Annual Report Appendix 1*.

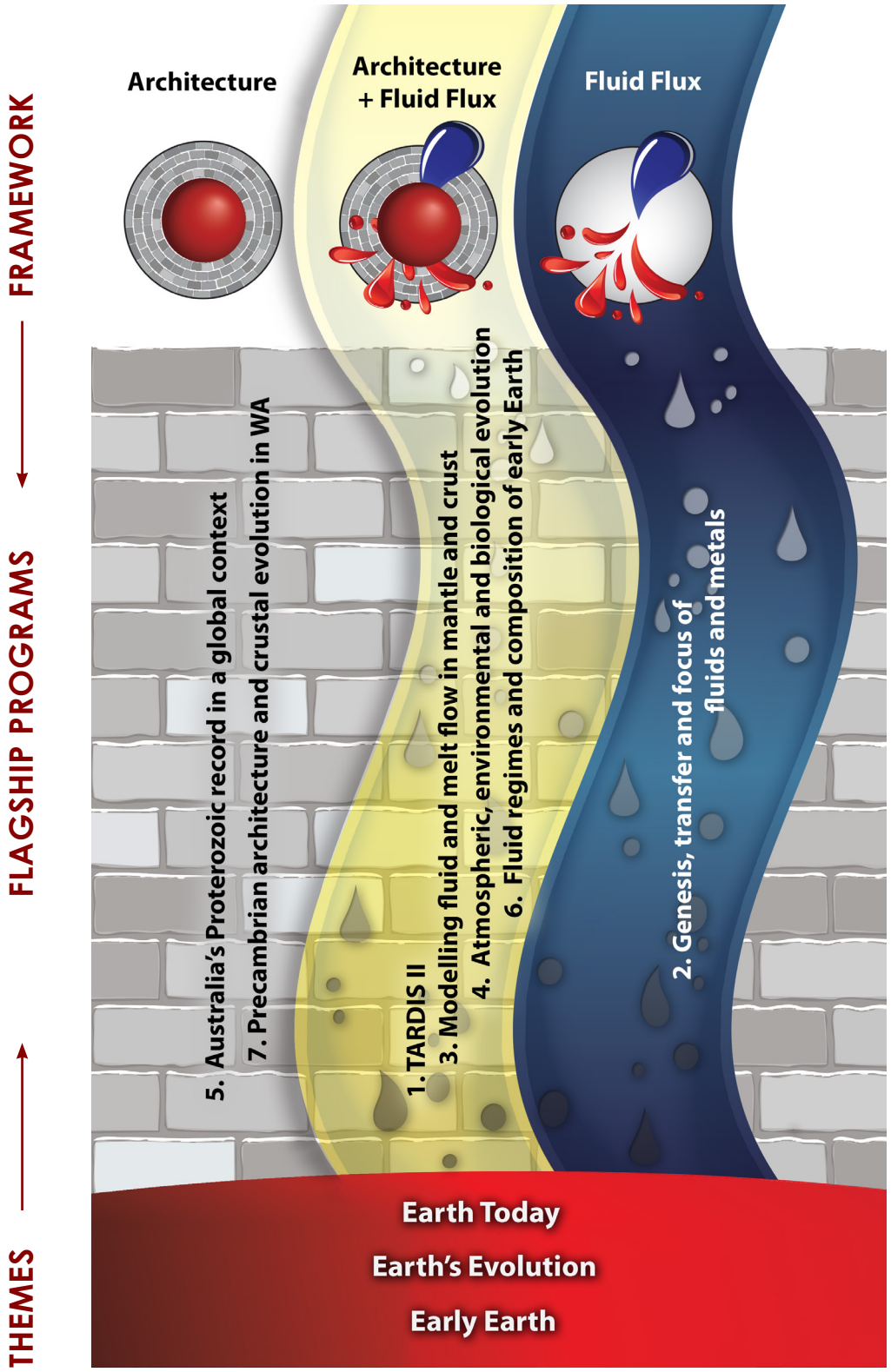

Research highlights 2014

Contents

Mineral exploration - Out of this world

Evaluating whether magmatic sulfide mineralisation exists on Mars can enhance our fundamental understanding of the processes that govern the evolution of such mineral systems on Earth - thus improving the scientific foundation upon which mineral exploration models are built. Understanding how and where potential ore-forming processes occurred on Mars is relevant both to long-term planning for future missions to the planet, and to designing exploration criteria for certain sample-return programs.

Widespread volcanic activity, showing striking mineralogical, petrographical and chemical similarities to terrestrial komatiites and ferropicrites, reshaped and buried the primary Martian crust. We have evaluated (CCFS *publication #508*) whether this igneous activity may have led to the formation of orthomagmatic Ni-Cu±(PGE) sulfide mineralisation similar to that associated with terrestrial komatiites and ferropicrites. Particular emphasis was focused on two different components of the Martian Ni-Cu±(PGE) sulfide mineral system: 1) the potential metal and sulfur fertility of mantle sources and derived melts, and 2) the physicochemical processes that enable sulfide supersaturation and batch segregation of metal-rich sulfide liquids.

We found that potentially metal-rich Martian mantle melts probably reach sulfide saturation within 30 wt% crystal fractionation. This value is comparable to that calculated for the mineralised ferropicrites at Pechenga, Russia. However, most known world-class Ni-Cu±(PGE) sulfide deposits associated with terrestrial komatiites and ferropicrites originated due to the assimilation of crustal sulfur-rich substrates. This assimilation promoted sulfide supersaturation and batch segregation of metal-rich sulfide liquids during the early stages of magma evolution. Given the high sulfur inventory of Martian crustal reservoirs, ranging from sulfide-bearing magmatic rocks to sulfate-rich soils, regoliths and sedimentary deposits, mantle-derived melts could have assimilated significant amounts of crustal sulfur during ascent and emplacement. We therefore have proposed that channelled lava flows, which were potentially emplaced on and incised into sulfur-rich crustal lithologies, may have led to the formation of orthomagmatic Ni-Cu±(PGE) sulfide mineralisation on Mars.

This project is part of CCFS Theme 1, Early Earth, and contributes to understanding Fluid Fluxes.

Contact: Marco Fiorentini
Funded by: CCFS Flagship Program 4

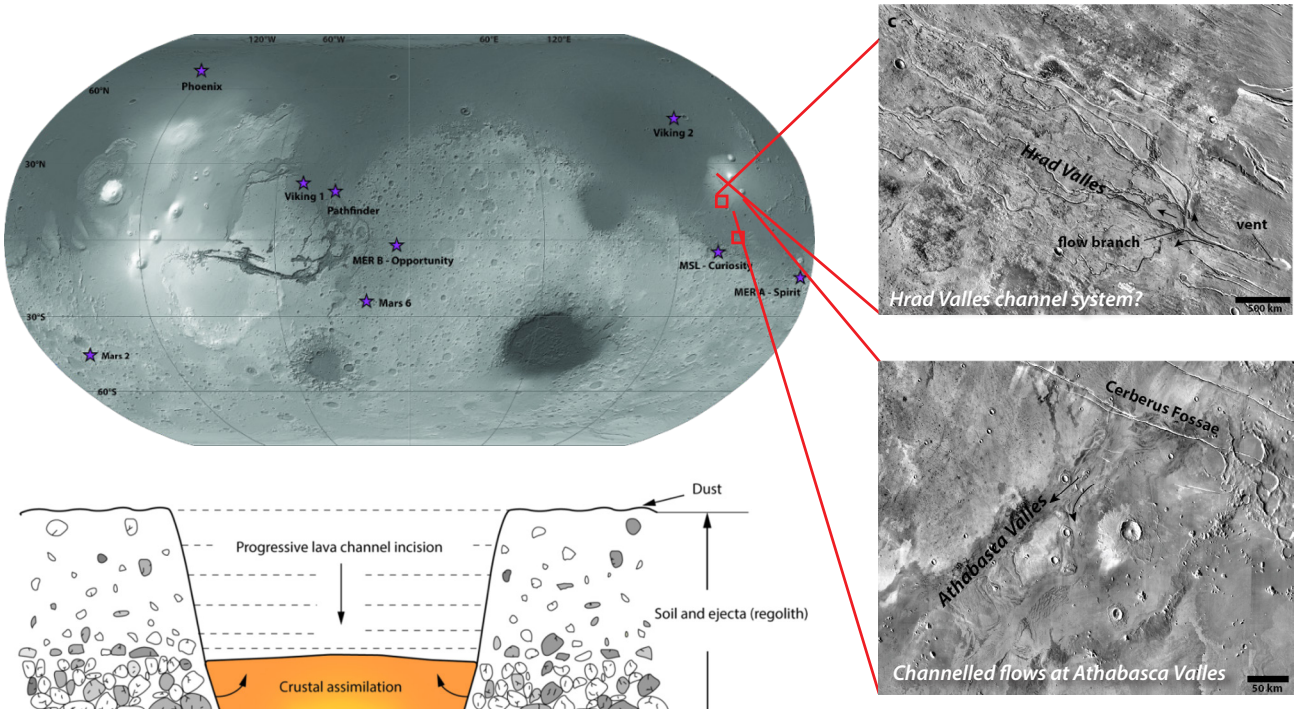

Figure 1. Sulfur Assimilation - Erosive Emplacement of Lava.

Cross Section through a Martian Lava Channel.

Scoping heat and composition in the depths below Central-Western US

Despite many geological and geophysical studies, the tectonic evolution of the Central-Western US region remains contentious. One of the major questions is the cause and timing of the uplift of the Colorado Plateau. Does the Plateau reflect mainly deep processes (e.g. large-scale dynamic topography) or shallow convection and heating? At least part of the controversy stems from the fact that studies of very different types (i.e. inversion does not inspire confidence in our understanding of important features of the Earth's interior. This raises the question as to what extent different models are actually supported or required by independent geophysical, geological, and geochemical evidence.

Here we apply an innovative 3D multi-observable probabilistic inversion method ("thermochemical tomography") using high-quality geophysical, geochemical and geological datasets to image the thermochemical structure of the Central-Western US. Working within this internally and thermodynamically consistent framework allows us to move beyond traditional methods and jointly use P-wave and S-wave teleseismic arrival times, Rayleigh wave phase dispersion data, Bouguer anomalies,

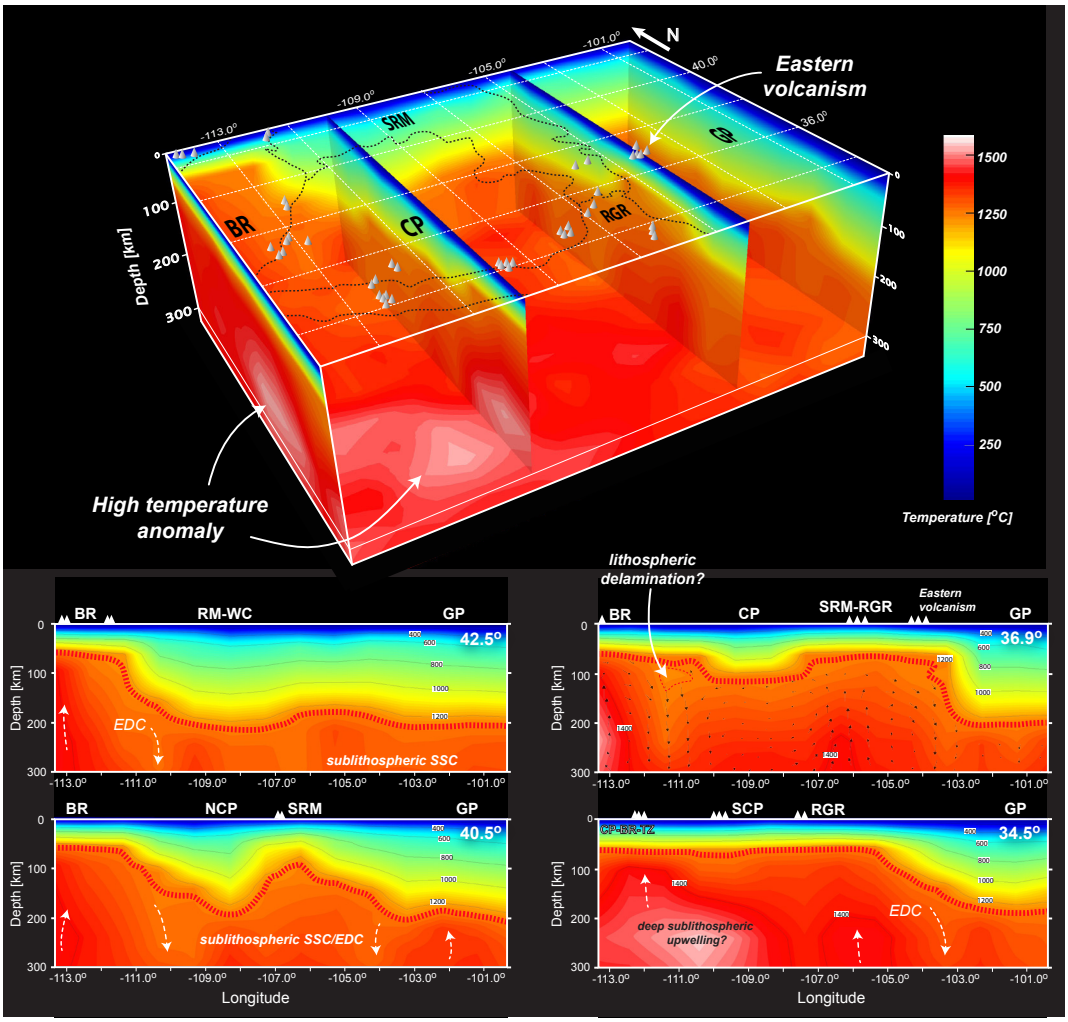

Figure 1. Top: Three-dimensional rendering of the thermal structure beneath Central-Western US. Major volcanic localities are indicated as white cones. Bottom: Temperature structure along four transects. The LAB is indicated by the thick red dashed line. Clear indications of both edge-driven convection (EDC) and sublithospheric small-scale convection (SSC) are visible in these transects. Cross-section at 36.9° includes the full instantaneous sublithospheric flow (as transparency); a clear downwelling is imaged beneath the western edge of the CP. SRM-WC = Southern Rocky Mountains-Wyoming Craton; NCP = Northern Colorado Plateau; SCP = Southern Colorado Plateau; BR = Basin and Range; RGR = Rio Grande Rift; GP = Great Plains.

of seismic data, numerical simulations, geochemical studies, electromagnetic studies), with different resolutions and sensitivities to the thermochemical structure of the Earth's interior have been used in isolation to explain the same observations. There is no *a priori* reason, however, why the results from these diverse studies should be strictly comparable, consistent or compatible, despite the fact that they all sample the same structure. Vastly different mechanisms can explain some observations (e.g. plateau elevation) equally well, and this long-wavelength gravity gradients, geoid height, absolute (local and dynamic) elevation, and data on surface heat flow. In our methodology, all physical and chemical parameters controlling model predictions are linked together by fundamental thermodynamic relations; the only independent variables in the inversion are therefore temperature, pressure and major-element composition. Accordingly, traditional tomographic images and models (e.g. S-wave velocity) are a by-product of our inversion rather than the main result.

We emphasise here that the thermal (and compositional) structure outcome is driven entirely by the constraining datasets. Thus, although we solve the 3D Stokes equations to obtain the instantaneous mantle flow and dynamic pressures arising from specific thermochemical structures required by data fits, small-scale convection patterns emerge only from the inversion of data, and are not imposed by flow computations. That makes it remarkable that cells of small-scale upwelling and downwelling (particularly beneath the Colorado Plateau region) with wavelengths of 200-300 km are recovered in the inversion (Fig. 1). These are the natural wavelengths of convection cells in the upper mantle. Our results demonstrate that the edges of the Colorado Plateau are being eroded by delamination and/or edge-driven downwellings. These downwellings transfer material from the lower parts of the lithospheric mantle to the upper sublithospheric mantle, changing its mean temperature and composition. This explains why the highly depleted nature of the uppermost lithospheric mantle becomes more obvious in regions where the Colorado Plateau lithosphere has been thinned or eroded by downwellings without associated volcanism.

Most of the present-day elevation in the Colorado Plateau area can be explained by a combination of lithosphere composition, crustal thickness and density structure, and thermal state, with only moderate localised contributions from sublithospheric upper-mantle convection. This analysis does not preclude the existence of deeper dynamic components, but it shows that large dynamic effects are not required to explain the available data. Our results therefore support models that require a net gain of lithospheric buoyancy since Laramide times.

The results reported here demonstrate that multi-observable thermochemical tomography described here, offers a robust method to characterise the fine-scale thermochemical structure of the lithosphere and upper mantle and opens new opportunities for deep-Earth imaging. The probabilistic nature and internally-consistent use of a number of key constraining datasets, all linked through a thermodynamic framework, gives the new method a unique sensitivity to thermal and chemical signatures that are otherwise difficult to assess unambiguously. This method allowed us to capture the complex interaction of structure and processes responsible for the present-day elevation of the Colorado Plateau, as well as directly imaging the dynamic behaviour of the upper mantle beneath the Central-Western US which, until now, has only been speculated upon, based on indirect proxies.

The intricate thermochemical structure of the lithospheric mantle seems to be linked more closely to interactions with the sublithospheric mantle via small-scale convection, melt production, and refertilisation of the lithospheric mantle rather than to physiographic or surface structures. Such interactions are likely to be key global and recurrent factors controlling the tectonic evolution of continental interiors and intra-plate epeirogenesis.

This project is part of CCFS Theme 3, Earth Today, and contributes to understanding Earth's Architecture and Fluid Fluxes.

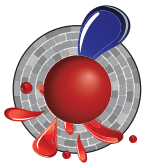

Contacts: Juan Carlos Afonso, Yingjie Yang
Funded by: ARC Discovery Project (DP120102372)

Giant porphyry copper deposits on the roof of the world

The Gangdese porphyry copper belt in southern Tibet, the roof of the world, is the most metal-rich porphyry copper system known from a continental collision zone. Numerous porphyry copper-molybdenum-gold (Cu-Mo-Au) deposits in this region contain over 20 million tons (Mt) of copper.

These porphyry Cu deposits are genetically associated with dacitic-rhyolitic (SiO_2>63 wt%) magmas with unusually high Sr/Y ratios (>40), which have been attributed to dehydration melting (no free water) of garnet amphibolites in a thickened lower crust beneath Tibet. To test this hypothesis and examine the hydration state of these magmas, we developed a geohygrometer for granitoid rocks, combining zircon-saturation thermometry and H_2O-dependent phase equilibria (Fig. 1).

The results show that the Tibetan high-Sr/Y ore-forming magmas had dissolved H_2O contents >10 wt% (Fig. 1). This is far more water than can be supplied by dehydration melting of basaltic amphibolites (maximum of 6.7 ± 1.4 wt%; Fig. 2).

cont...

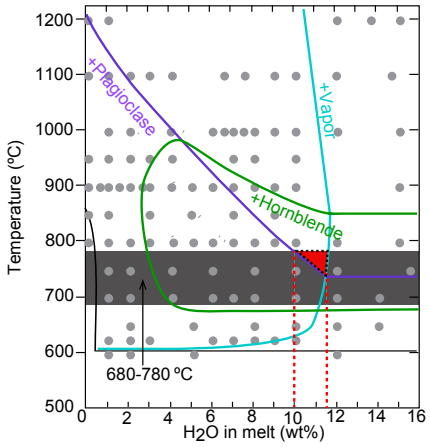

Figure 1. Temperature vs H_2O plot. Each grey circle represents an experiment in which the stable mineral phases were identified in run products by Naney (1983; American Journal of Science, 283, 993-1033). Only the plagioclase (blue), hornblende (green) and vapour (turquoise) saturation curves are shown for clarity. The grey band is the range of zircon-saturation temperatures for Tibetan ore-forming high Sr/Y porphyries and the dashed red triangle is the field of the Tibetan ore-forming dacitic porphyries. The H_2O contents in these ore-forming magmas are thus estimated to be at 10-12 wt% (red dashed lines).

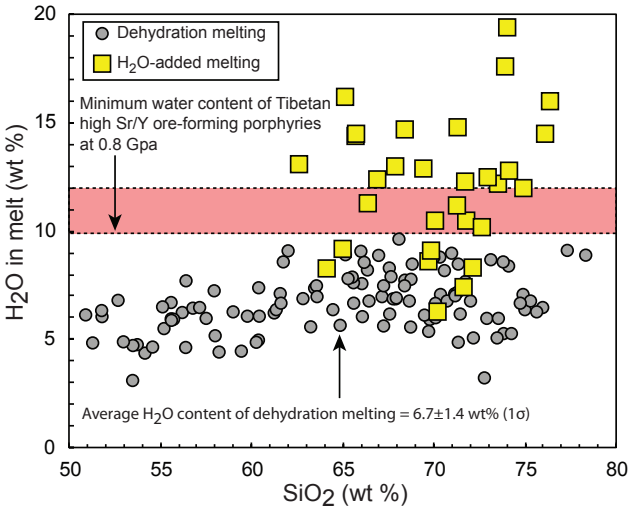

Figure 2. H_2O vs SiO_2 (wt %) in melts from H_2O-absent and H_2O-added experimental melting of basaltic amphibolite. The pink band highlights the minimum water content (10-12 wt %) of Tibetan copper-ore-forming porphyries.

Melting basaltic amphibolites in the presence of H_2O can produce high Sr/Y hydrous dacitic-rhyolitic melts (Fig. 2), but only with lower Mg# (>50), MgO and Cr contents than the Tibetan ore-forming porphyries (Fig. 3). Mafic microgranular enclaves (MMEs) have been reported from several Miocene porphyry Cu-Mo deposits in southern Tibet, which have much higher Mg#, MgO and Cr contents than partial melts of mafic lower crust (Fig. 3). These cognate enclaves, derived from metasomatised Tibetan mantle, represent quenched mafic magmas, injected into the porphyry-forming felsic magmas. They typically define fractionation trends and Sr-Nd-Hf isotopic compositions that relate them to the Tibetan ore-forming porphyries.

These observations suggest an alternative model for the genesis of copper-rich high-Sr/Y magmas: they are residually H_2O-enriched, high-pressure differentiation products of hydrous mafic partial melts of Tibetan mantle. The mid-Miocene stress regime was more compressive in the eastern portion of the Gangdese belt (where these porphyry copper deposits form) than in the western parts, where Miocene N-S trending rifts are abundant. The mafic magmas thus would tend to underplate the crust and differentiate and assimilate there until relatively silicic, hydrous residual melts have acquired sufficient buoyancy to overcome the compressive stress regime. During the high-pressure differentiation of mafic magmas, the resultant felsic magmas become rich in copper and water, so when they eventually reach the upper crust, they can form giant copper deposits.

Our new model implies that porphyry Cu deposits in continental collision zones have similar origins to those in other tectonic settings such as the circum-Pacific magmatic arcs. Therefore, a universal exploration model may be applied to search for porphyry deposits all over the world.

This project is part of CCFS themes 2 and 3, Earth Evolution and Earth Today, and contributes to understanding Earth's architecture and fluid fluxes.

Contacts: Yongjun Lu, Marco L. Fiorentini
Funded by: ARC CCFS ECSTAR funds, CCFS pilot project.

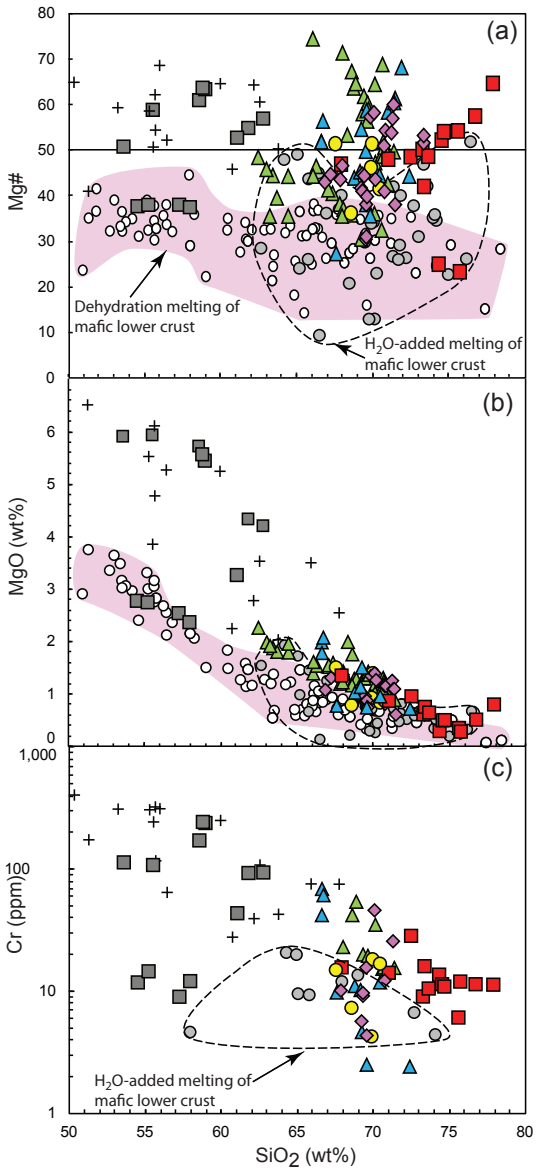

Figure 3. (a) Mg# vs SiO_2, (b) MgO vs SiO_2, and (c) Cr vs SiO_2 plots for high Sr/Y Cu-ore-forming porphyries in southern Tibet.

A tale of two rheologies - deformation with and without fluid

Although the amount of free fluid in the Earth's crust is very small, it plays a fundamental role in many geodynamic and geochemical processes. Field studies demonstrate that fluid circulation through the crust mainly occurs through localised sites of intense deformation, such as faults and shear zones. Although in recent years fluid-rock interaction during deformation has been much studied, it is still one of the least understood aspects in crustal tectonics.

The hydrated mid-crustal shear zones in the Wyangala Granite (SE Australia) displays a very localised infiltration of external syn-tectonic fluids, limited to the central domains, while the shear zone margins have remained relatively "*dry*" during the deformation allowing identification of the particular effects fluid exert on the rock rheology (flow behaviour during deformation).

Two cases can be distinguished: (1) the "*fluid-deprived*" shear zone margins preserve many similarities with the wall rock granite, chemically, mineralogically and structurally. The most deformed mineral in these domains is quartz displaying crystallographic preferred orientation and dynamic recrystallisation microstructures, which indicate the dominance of dislocation creep regime (described by a power-law function), which is consistent with the predictions of current theoretical models for the Earth's crust. (2) In the highly hydrated central domains of the shear zone, the granitic host rock is transformed into a fine grained quartz-muscovite phyllonite. During deformation feldspar breaks down into fine-grained muscovite-quartz-epidote aggregates, deformation occurs by pressure-solution creep and grain boundary sliding in the feldspar reaction products, as well as basal slip of muscovite, while remaining quartz porphyroclasts experienced very little deformation. All of these processes are facilitated by fluid and are characterised by a linear creep function resulting in extreme softening and strain localisation.

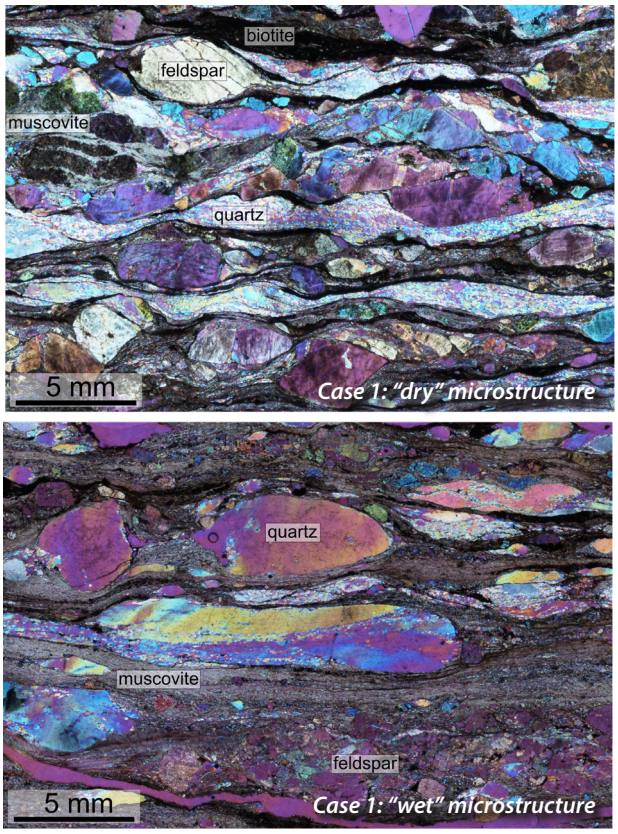

Figure 2. Optical photographs (through gypsum plate) of microstructures developed in a case of (1) "dry" deformation on the shear zone margins and (2) "wet" deformation in the shear zone centre.

This study demonstrates the dramatic softening fluids induce on rock rheology, and points out the limited applicability of theoretical models based on dry rheologies for deformation in the Middle crust, where metasomatic fluids are common.

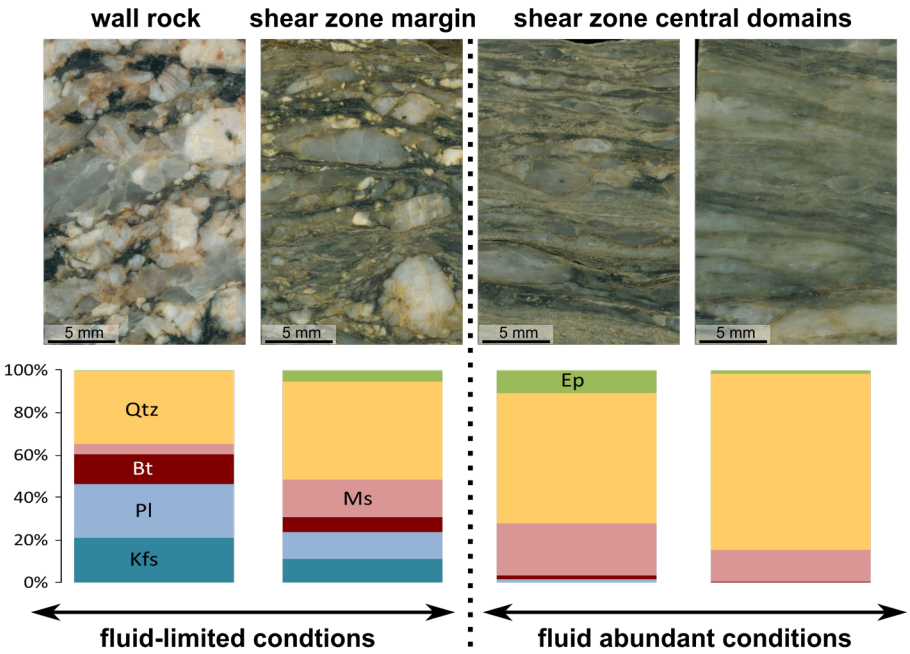

Figure 1. The structural and mineralogical evolution of fabrics across the shear zone.

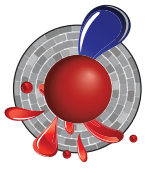

This project is part of CCFS Theme 2, Earth Evolution, and contributes to understanding Earth's Architecture and Fluid Fluxes

Contacts: Liene Spruzeniece, Sandra Piazolo

Funded by: ARC Discovery Project (DP120102060)

Dating kimberlites and mantle evolution below southern Africa

Kimberlite magmas represent our best source of information on the composition and evolution of the deep continental lithosphere, but extracting that information can be difficult, because kimberlites typically are jumbled mixtures of the original magma and debris carried up from the mantle. However, perovskite ($CaTiO_3$, with extensive substitution by Sr, U and REE) occurs in many kimberlites as a groundmass phase, early-crystallising in most cases. Its chemistry allows not only U-Pb dating of the kimberlite's emplacement, but Sr- and Nd isotopes carry information on the source(s) of the magma (*CCFS Publication #466*). We have dated groundmass perovskite by LA-ICPMS U-Pb techniques in 135 kimberlites and related

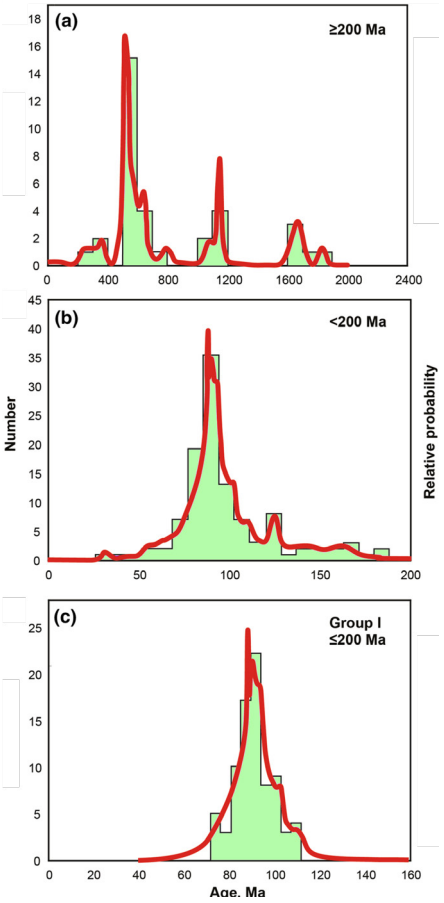

Figure 1. Cumulative-probability plots and histograms for U-Pb ages on perovskites. (a) ages >200 Ma; (b) ages <200 ma, showing buildup to main peak; (c) Group I kimberlites with ages <110 Ma (main pulse) showing abrupt cut-off at <80 Ma.

rocks from 110 localities across southern Africa. Sr and/or Nd isotopes have been analysed by LA-MC-ICPMS in a subset of these; combined with published data this gives ^{89}Sr-age datasets and ^{85}Nd-age datasets. The age distribution (Fig. 1) shows peaks at 1600-1800 Ma, 1000-1200 Ma, 500-800 Ma and 50-130 Ma. The major "bloom" of Group I kimberlites at ~90 ±10 Ma was preceded by a slow buildup in magmatic activity that began at ~70 Ma. The main pulse of the cluster of kimberlites at 120-130 Ma (called "Group II") was a distinct major episode within this buildup.

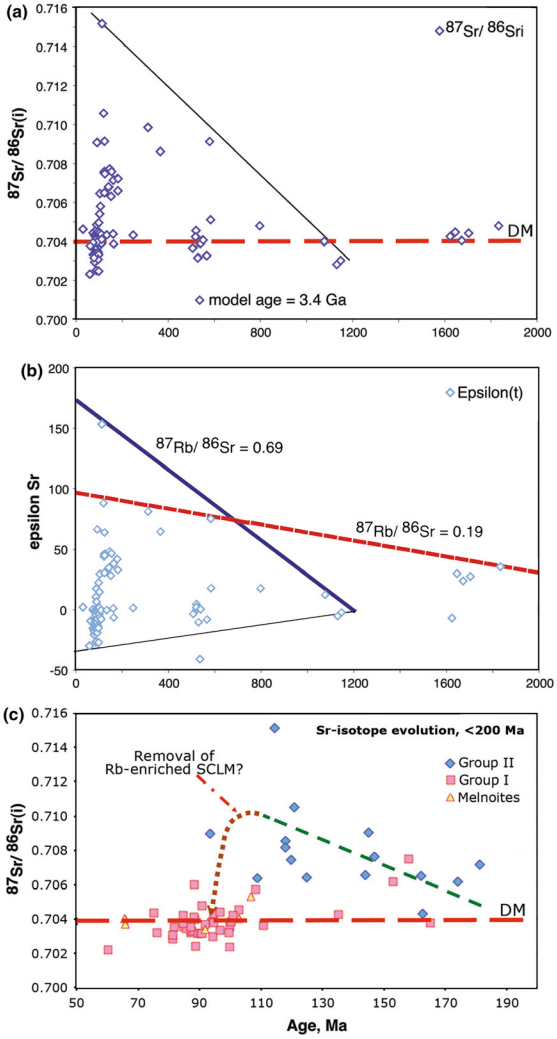

Figure 2. Sr-isotope data for perovskite in the analysed kimberlites, plotted vs time, to show the increased variability of the isotopic signatures of kimberlites toward the present. Heavy lines in (b) show the evolution of the radiogenic Reservoir 1 that could have contaminated the younger kimberlites, assuming that the necessary metasomatism occurred at ca 1.2 Ga or ca 2.0 Ga. Light line in (b) shows the depletion in Rb/Sr (relative to DM) that would be required to produce Reservoir 2 with low $^{87}Sr/^{86}Sr$. (c) shows details of the data for the last 200 Ma, with an interpretation of the data in terms of the destruction of reservoir (1).

The Sr- and Nd-isotope data (Figs. 2 and 3) show that the subcontinental lithospheric mantle (SCLM) sampled by the younger kimberlites was isotopically heterogeneous, and that this heterogeneity reflects a metasomatic refertilisation that may have begun as early as 1.2 Ga ago, but probably was episodic. This metasomatically modified mantle was sampled extensively by the Group II kimberlites that erupted at 120-130 Ma. However, the latest major bloom of Group 1 kimberlites (~90 ±10 Ma) sampled a much more strongly metasomatised mantle.

Figure 4 shows the spatial distribution of εNd and εSr overlain on the seismic-tomography image of southern Africa generated by the Kaapvaal Seismic Project (*Fouch et al., 2004*). The most striking observation from these maps is that the samples with the lowest εNd and the highest εSr are concentrated in three areas: around the low-Vs feature that marks the intrusion path

of the Bushveld Complex, along the Kimberley belt, and in the off-craton "tail" of kimberlites. The geochemical signature implies long-term geochemical enrichment in the LREE relative to the HREE (and hence low Sm/Nd) and high Rb/Sr. There is an

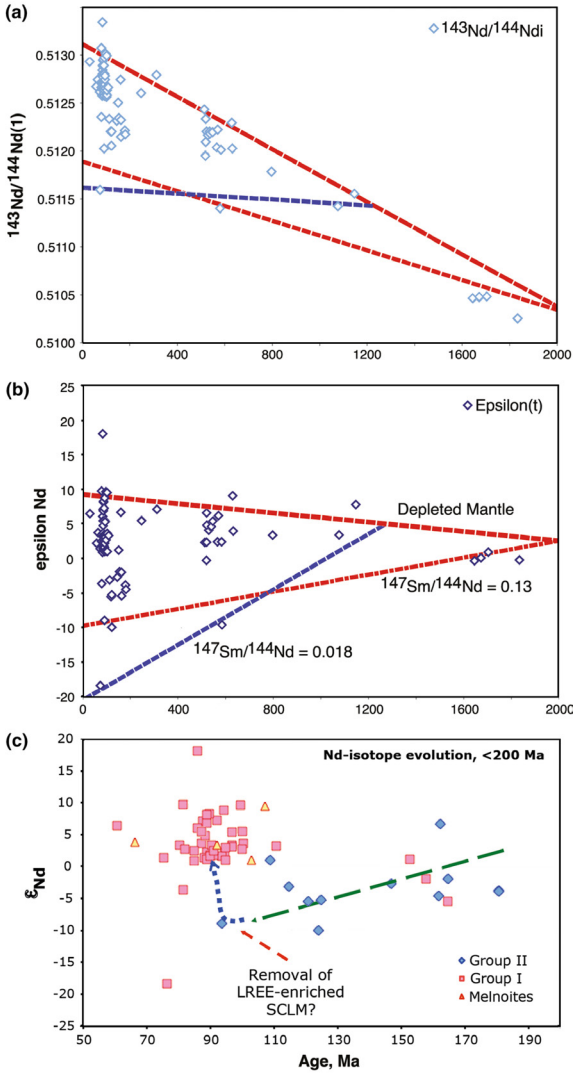

Figure 3. Nd-isotope data from perovskite in the analysed kimberlites, plotted against intrusion age. Dashed lines show the evolution of the depleted mantle, and of volumes metasomatised at ca 1.2 Ga or 2.0 Ga, labeled with the Sm/Nd ratio that would be needed for these volumes to evolve unradiogenic Nd-isotope compositions like those seen in some of the samples. (c) shows details of the data for the last 200 Ma, with an interpretation of the data in terms of the destruction of reservoir (1).

obvious correlation between this clearly metasomatic signature and low Vs, as would be predicted from studies of xenoliths, where this type of trace-element enrichment is associated with higher Fe/Mg, Ca and Al, and lower calculated seismic velocities (*Griffin et al. 2009*).

These maps suggest that volumes of metasomatised SCLM with very low εNd and high $^{87}Sr/^{86}Sr$, (the characteristic isotopic signature of Group II kimberlites (~120-130 Ma)), were confined to low-Vs zones along trans-lithospheric structures. These include the locus of the Bushveld intrusion, major faults and craton boundaries. Such metasomatised zones existed as early as 1800 Ma, but were only sporadically tapped until the magmatic buildup began at ca 170 Ma, and apparently were mostly gone by ca 110 Ma. We suggest that these metasomatised volumes resided mainly in the deep SCLM, and that their low-melting-point components were "burned off" by rising temperatures, presumably due to an asthenospheric upwelling that led to SCLM thinning and a well-documented rise in the ambient geotherm between 120 Ma and 90 Ma. The younger Group I kimberlites therefore rarely interacted with such SCLM, but had improved access to shallower volumes of differently metasomatised, ancient SCLM with low $^{87}Sr/^{86}Sr$ and intermediate εNd (0-5). The kimberlite compositions therefore record the slow evolution of the SCLM of southern Africa, from 1.8 Ga through a refertilisation event around 1 Ga ago, and a major thermal and compositional change at ca 110 Ma.

This project is part of CCFS Theme 2, Earth Evolution and contributes to understanding Earth's Architecture and Fluid Fluxes.

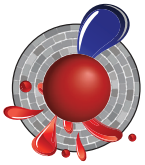

Contact: Bill Griffin
Funded by: CCFS

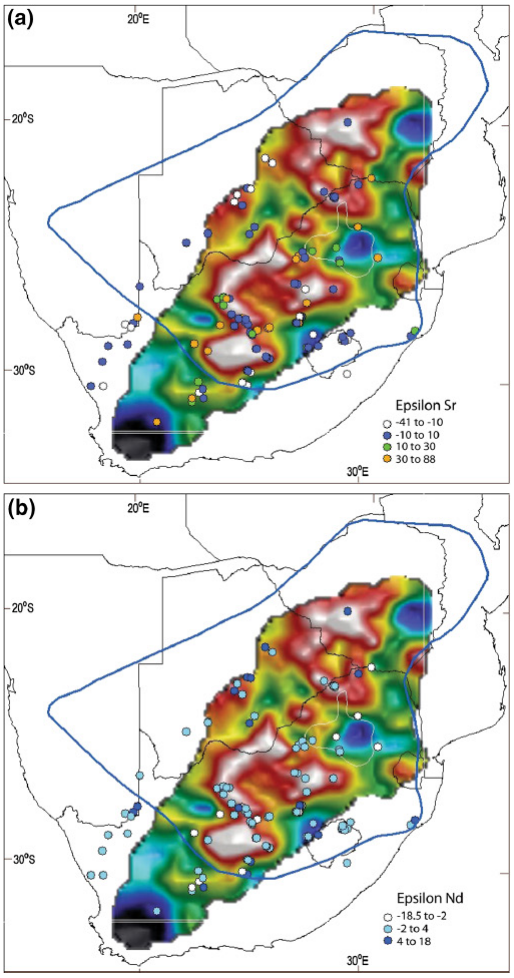

Figure 4. Values of εSr (upper) and εNd (lower) superimposed on the Vs tomography for the 150 km depth slice (after Begg et al., 2009), illustrating the association of metasomatic signatures (high εSr and low εNd) with low-Vs zones and trends. See Figure 2 for discussion of the velocity scales and interpretation of major tomographic features.

The growth of the Tibetan Plateau: the last 25 Myr

The spectacular topography of the Tibetan Plateau (Fig. 1) is the result of collision between India and Eurasia over some 50 Myr, but how did the plateau grow to its present size? Previous work along the eastern Longmenshan margin (LM in Fig. 1) of the Tibetan Plateau suggests a two-stage uplift (thus growth of the plateau) since ~30 Myr: one from 30-25 Myr, and another from

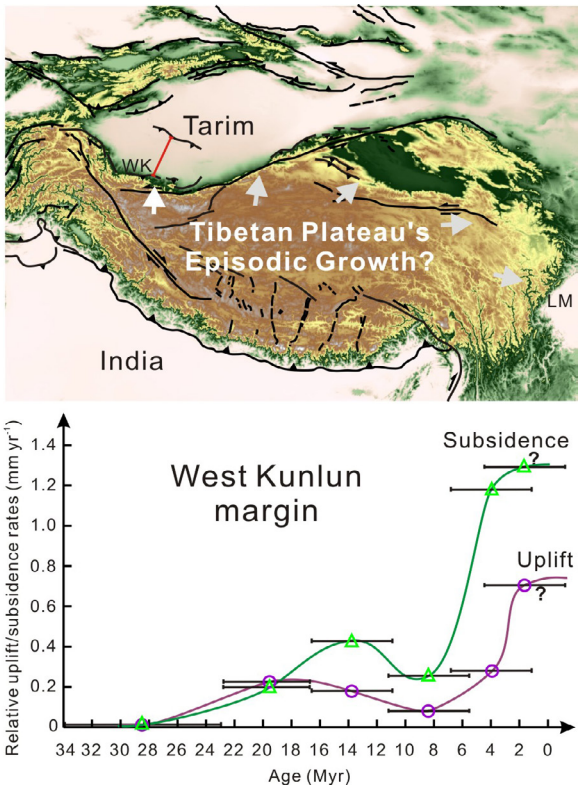

Figure 1. Location of the West Kunlun Range (WK) at the northwestern margin of the Tibetan Plateau, and time variations in estimated relative subsidence and uplift rates. The location of the seismic profile is shown as a red line. LM - the Longmenshan Range.

15-10 Myr. Was this just a local feature, or does it reflect plateau-wide episodic lateral growth? We have used high-resolution seismic reflection and drill core data from the southern Tarim Basin to analyse the pattern of plateau growth along the West Kunlun margin (WK in Fig. 1) of the northwestern Tibetan Plateau. The work was carried out through collaboration with Professor Xiao-Dian Jiang of Ocean University of China and published in *Nature Communications* (*CCFS contribution #496*).

The continental lithosphere of the Tarim Block underthrusted northern Tibet to its south, with up to 12 km of Cenozoic foreland basin deposits accumulated along the southern Tarim due to the loading of the plateau. These deposits provide a unique record of the history of the mountain building. Seismic reflection and drill hole data were acquired in the foothills of the West Kunlun Range and the southwestern Tarim foreland basin by the Shengli Oilfield Company (location of seismic profile shown by red line in Fig. 1), and were made available for our research. The change in sedimentary environment from a marine carbonate platform in the Oligocene to a clastic tidal flat in the early Miocene marks the beginning of foreland-basin development due to the formation of the proto-West Kunlun Range at the northern edge of the proto-Tibetan Plateau. The temporal variation in the deposition/subsidence rate is taken as reflecting changes in the orogenic loading on the lithosphere of the Tarim Block, which would have resulted in isostasy-driven surface uplift at the present northwestern margin of the Tibetan Plateau. Rate estimates for the depocentre (green curve in Fig. 1) indicate that there have been two episodes of rapid uplift along the West Kunlun Range: one in the mid-Miocene (~16-11 Myr), and the in the last ca 5 Myr; the latter has been significantly faster. Using the differences in thickness between strata on the two sides of a frontal thrust, we calculated the relative uplift rate on the hanging wall as a function of time; this analysis also indicates two episodes of rapid uplift (purple curve in Fig. 1).

Our data thus suggest that the uplift of northern Tibet started from near sea level at ~23 Myr; the first episode ended by ~10 Myr, followed by rapid uplift along the present plateau margin over the last 5 Ma. The contrast in the intensity of the two episodes probably indicates that during the first episode, the front of the proto-West Kunlun orogen at the edge of the plateau was off from its present position, and it only propagated to its present position during the second episode. This two-episode uplift history is comparable to that reported along the eastern margin of the Tibetan Plateau, suggesting that the growth of the Tibetan Plateau after the Eocene likely has been episodic in nature, and near-synchronous along both eastern and northern margins.

Recent work on both margins also suggests that brittle thickening of the upper crust plays the dominant role in plateau propagation along those margins (see *CCFS publication #223*). There is thus a case for synchronous episodic plateau expansion, dominantly through brittle thickening of the upper crust rather than mechanisms like crustal channel flow.

This project is part of CCFS Theme 2, Earth's Evolution, and contributes to understanding Earth's Architecture.

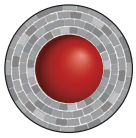

Contact: Zheng-Xiang Li

Funded by: NSFC (40772124 and 41176038), CGS (GZH200900504)

Modelling mantle melting: New horizons

One of the great goals of Geosciences is the explanation of geochemical data consistent with models of the Earth. Models are constrained by physical laws, so successful modelling explanations not only give multifaceted support to our stories about the formation and evolution of rocks, but simultaneously constrain the properties of the deep Earth from which they originate. Our project attempts to develop a new generation of detailed models for grain-scale microstructural evolution and chemical transport in the framework of classical irreversible thermodynamics. We have so far applied the current version of the models to the explanation of Rare-Earth Elements (REE) and Uranium-series isotopes in Ocean Island Basalts (OIB's). Figure 1a illustrates an example of the microstructure showing the 2D distribution of 5 phases (olivine, opx, cpx, garnet, and melt) around the garnet transition, and Figures 1b and 1c show the corresponding distributions of Sm/Yb and $^{228}Ra/^{232}Th$ ratios throughout the microstructure. Because different trace elements are characterised by different partition and diffusion coefficients, very different diffusive features can be seen.

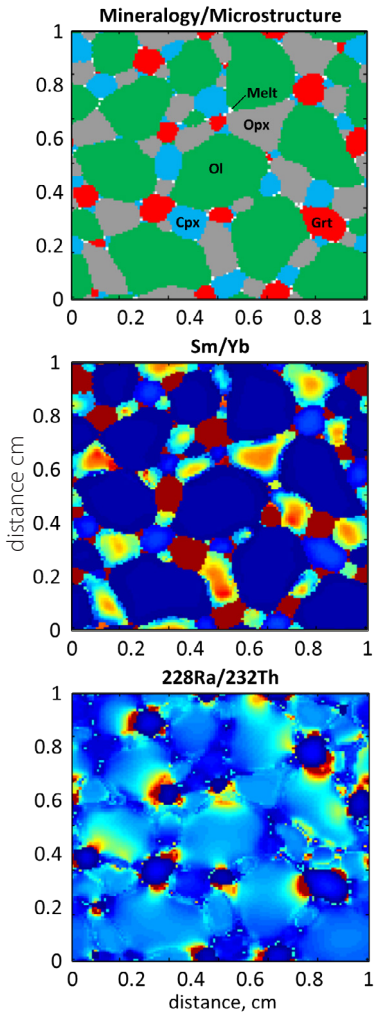

Figure 1.

One success of our modelling efforts is the explanation of REE ratios in OIBs. As shown in Figure 2, if REE ratios are plotted against the age of the lithosphere on which OIB's are erupted, we see step-like features in La/Sm and Sm/Yb ratios, separating low values over young (thin) lithosphere, and higher values on old (thick) lithosphere. The thin black line is a moving average of the data and the bold green line is our best model compared to the data. The fit is impressive, and by inspection of the properties of the model, we can infer the origin of the step-like feature. The step in La/Sm is caused by the onset of anhydrous melting, where melt productivity as a function of depth substantially increases. Sm/Yb, on the other hand, reveals a garnet signature: when oceanic lithosphere is about 15 million years old, it is ~50 km thick, which happens to be the depth at which garnet is stable. As garnet preferentially holds heavy rare earth elements (e.g. Yb) during melting, Sm/Yb is high in magmas derived by melting beneath older lithosphere, and low otherwise.

An interesting consequence of these explanations is that the source of OIB must be at a temperature <1400°C, about the temperature of ambient mantle. If the source were warmer, the models cannot fit the data. In other words, thermal mantle plumes do not appear to be consistent with our analysis. On the other hand, classical thermal plumes may be a rare source of intra-oceanic volcanism.

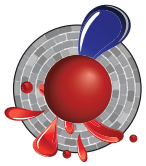

This project is part of CCFS Theme 2, Earth Evolution, and contributes to understanding Earth's Architecture and Fluid Fluxes.

Contacts: Chris Grose, Juan Carlos Afonso
Funded by: ARC Discovery Project (DP120102372), ARC IPRS

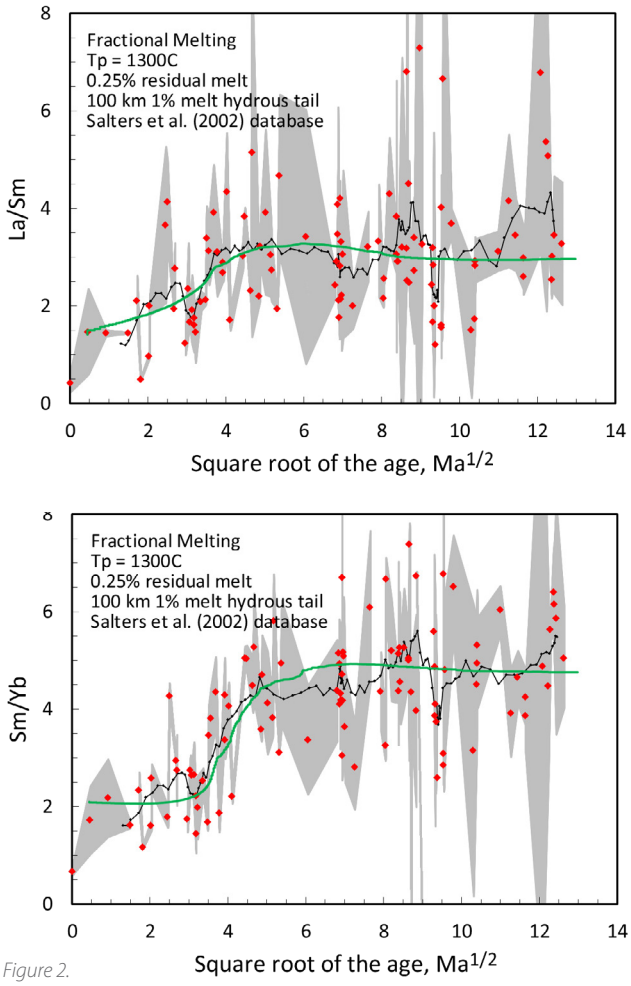

Figure 2.

Mesozoic flat-slab subduction and the opening of the South China Sea - clues from thermochronology

The South China Block (SCB) constitutes a major continental segment in the Western Pacific region (Fig. 1). Revealing the tectonothermal history of the region is fundamental to establishing the timing and kinematics of flat-slab subduction, foundering, and the opening of a marginal South China Sea.

We have carried out the first comprehensive thermochronological analysis of four areas in the southeastern SCB, making up a SE-NW traverse from the coast to the inland (A-D in Fig. 1). Late Triassic muscovite and biotite $^{40}Ar/^{39}Ar$ ages (220-200 Ma) in the northwest are clearly older than the Late Jurassic ages from the southeast (165-155 Ma; Fig. 2a). Among forty-one zircon (U-Th-[Sm])/He ages, four ages are pre-Middle Jurassic (253, 245, 220 and 176 Ma) and the remaining ages range from the Late Jurassic (152 Ma) to the Late Cretaceous (75 Ma). The four pre-Middle Jurassic ages are all from the northwest (area D) and the southeast is dominated by Cretaceous ages (Fig. 2b). Apatite fission track ages cluster at 70-30 Ma; two older ages (90 Ma) are from samples in the northwest (Fig. 2c). Like the apatite fission- track dates, apatite (U-Th-[Sm])/He ages form a tight Late Cretaceous-Eocene cluster at 70-30 Ma (Fig. 2d).

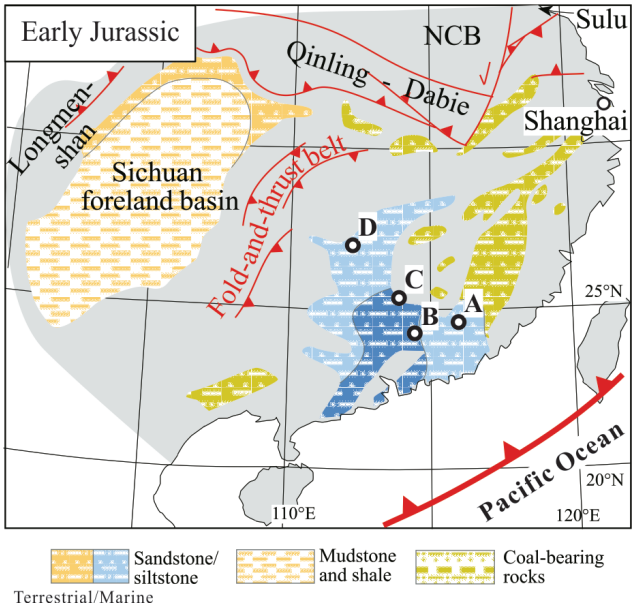

Figure 1. Paleogeographic map of the southeastern South China Block (SCB) showing areas studied in this project.

According to the time-temperature trajectories extracted from both forward and inverse modelling of thermochronological data, area D records rapid cooling related to orogenic uplift and related erosion during the Late Triassic. This orogenic uplift is

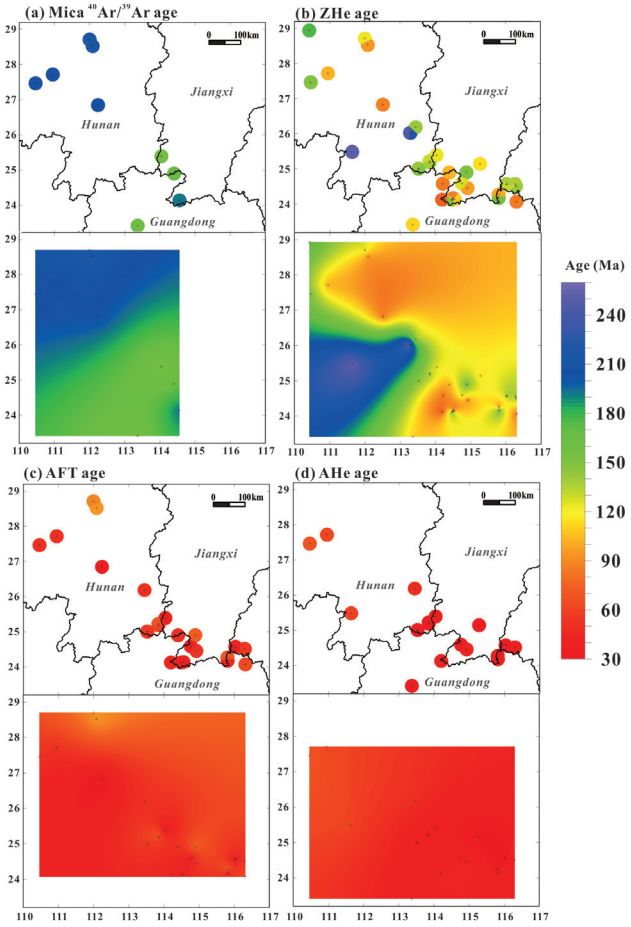

Figure 2. Database of new thermochronological ages in the southeastern SCB from this project. X-axis is longitude and y-axis is latitude. Mica $^{40}Ar/^{39}Ar$ = muscovite and biotite $^{40}Ar/^{39}Ar$ ages, ZHe = zircon (U-Th-[Sm])/He, AFT = apatite fission track ages, AHe = apatite (U-Th-[Sm])/He. Ages are expressed in Ma as circles; age values are indicated by the colour of circles. The pattern of ages was obtained by interpolation and smoothing of the data set. Previous data points are shown as black crosses in interpolated maps. Note that linking between areas without data points is by interpolation. The maps show the spatial distribution of ages and general trends; geology and faults are ignored.

interpreted as a result of the approaching flat subduction of a paleo-Pacific oceanic plateau from the southeast. At the same time, regions to the southeast were sagging and receiving terrestrial and shallow-marine sediments during the Late Triassic and Early Jurassic (Fig. 1 and 3). This may have resulted from the gravitational pull of the eclogitised oceanic flat slab (*Li and Li, 2007*, Fig. 3). Significant magmatic reheating occurred first in area B in the Middle Jurassic and generated a thermal peak of ~300 °C. Subsequently, in the Late Jurassic, a thermal peak of 250-300 °C was recorded in areas C and A, to the northwest and east of area B, respectively. This spatial distribution of Jurassic reheating is consistent with slab break-off as in a flat-slab model (Fig. 3).

The southern SCB was subjected to slow exhumation and cooling during the Cretaceous. The relatively quiescent, low temperature (200-100 °C) conditions reflect long-term thermal relaxation after the Middle-Late Jurassic magmatic heating. Such a protracted slow cooling is consistent with lithospheric rebound

in the flat-slab model. Intensive Cretaceous magmatism in the coastal regions during the Cretaceous, interpreted as reflecting the roll-back of the remaining paleo-Pacific oceanic slab (Fig. 3; e.g. *CCFS Publication #16*), can account for the reheating recorded in area A.

The Pacific subduction zone had migrated to the south of the present continental margin of SCB by ~90 Ma (Fig. 3; e.g. *CCFS Publication #31*). Rapid cooling from ~150 °C to surface temperatures started as early as latest Cretaceous time and lasted until the late Eocene, coinciding with rifting in the southeastern SCB that has been linked to the rollback of the subducting western Pacific oceanic plates. This rifting event ultimately led to the opening of the South China Sea (Fig. 3; e.g. *CCFS Publication #31*).

This project is part of CCFS Theme 2, Earth Evolution, and contributes to understanding Earth's Architecture.

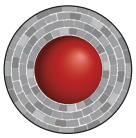

Contacts: Ni Tao, Zheng-Xiang Li
Funded by: CCFS, ARC Discovery Project (DP110104799)

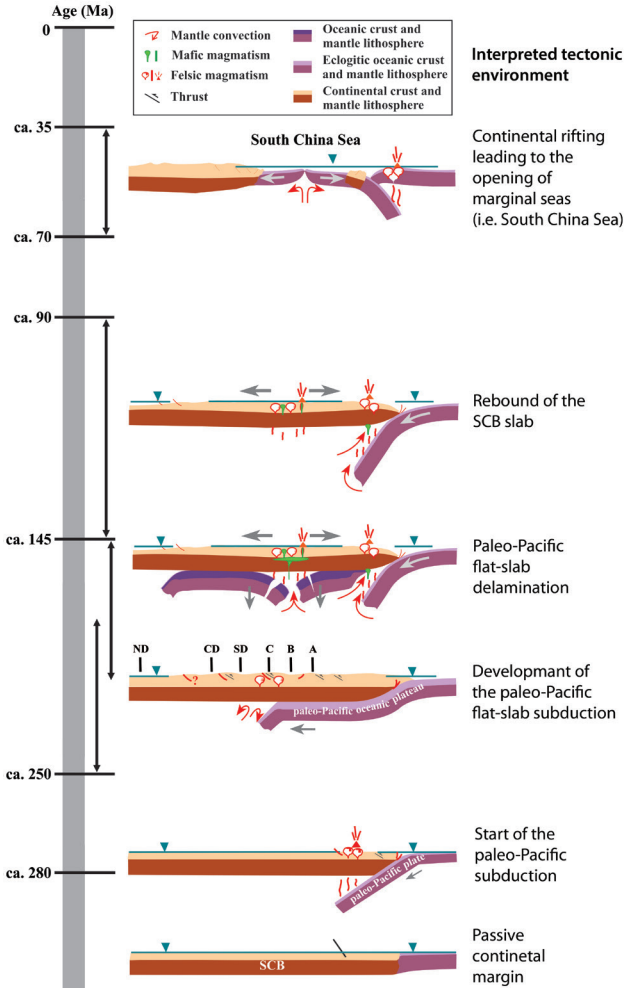

Figure 3. Schematic diagram showing the tectonic evolution of southeastern SCB, modified from Li and Li (2007); Li et al. (2012). Arrow bars on the left show the heat/cooling ages. ND = northern area D; CD = central area D; SD = southern area.

Migrating ridges link the deep and shallow mantle

It has long been recognised that mid-ocean ridges (MORs) migrate in an absolute sense relative to the underlying mantle. Present-day MOR migration rates affect seafloor morphology and the physical state of the upper mantle, and these migration rates correlate with asymmetric seafloor spreading, lava generation at ridge crests, asymmetry in melting depths and geochemical discontinuities, and ridge morphology. However, the effects of long-term variations in MOR migration and the resulting non-uniform sampling of the upper mantle have not been studied, although there is growing evidence from MORB geochemistry and upper mantle seismic tomography, mantle convection simulations and laboratory models, to supporticlose linkages between slowly migrating MORs and plumes in the present oceans.

Here, we use Large Igneous Provinces (LIPs) that have formed since the Early Cretaceous to demonstrate that ridge-plume interactions can continue for up to 180 Ma and strongly influence ridge migration rates. These long-standing MOR migration patterns and ridge-plume interactions influence the thermal structure of the upper mantle and the geochemistry of the ocean crust vs spreading segments (Fig. 1a) and their full spreading rates. To assess the relationships of slowly migrating ridges caused by plume-ridge interactions to the thermal structure of the upper mantle, we have developed and implemented a novel methodology to construct a global map of the relative volume of upper mantle material extracted through partial melting at MORs since the Early Cretaceous. Our map (Fig. 1b) is a proxy for the Volume of Extracted Mantle (VEM) and is calculated as a function of the residence time (i.e. the duration for which a MOR lies above an area of upper mantle) of the global MOR system and the rate at which material is extracted from the mantle (i.e. spreading rate).

Regions with high VEM values indicate prolonged melt extraction and mantle focusing/processing by a relatively stationary MOR system with moderate to fast spreading rates, e.g. the Eastern Pacific. In contrast, rapid MOR migration, even with rapid spreading rates, does not result in high

cont...

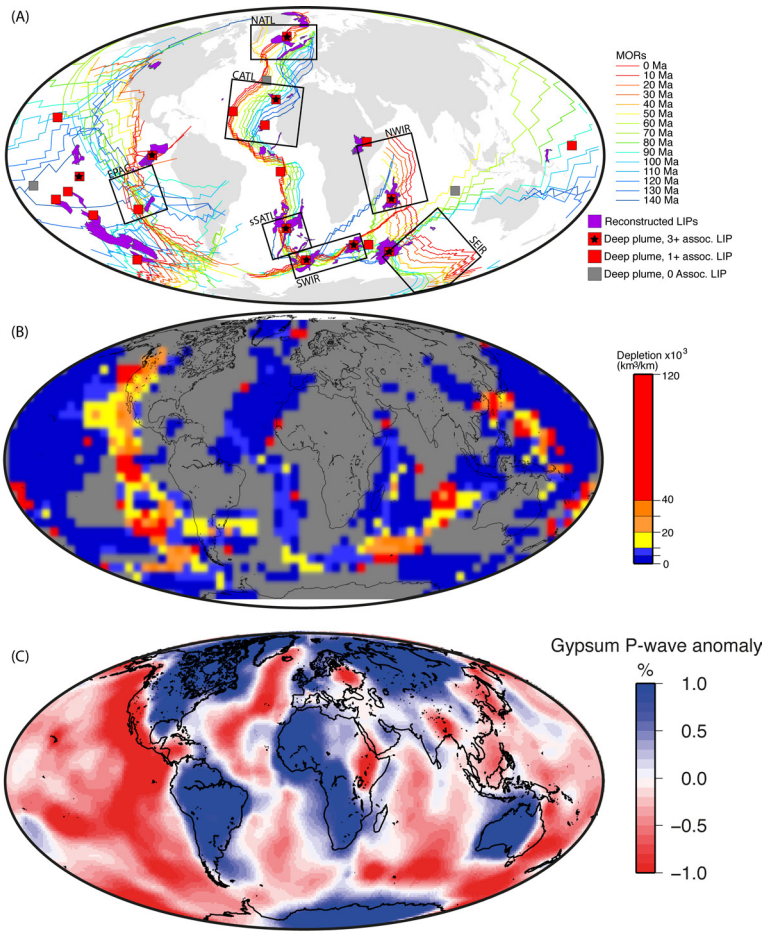

Figure 1. (A) Reconstructed mid-ocean ridges for the past 140 Myr in 10 Myr intervals. Black boxes show regions where ridge migration distances were computed along flow lines. CATL - Central Atlantic, EPAC - East Pacific Rise, NATL - North Atlantic, NWIR - Northwest Indian Ridge, SEIR - Southeast Indian Ridge, sSATL - southern South Atlantic, SWIR - Southwest Indian Ridge. LIP formation locations (purple) cluster around hotspots coinciding with slow ridge migration rates. (B) Estimated upper mantle VEM (km³/km of ridge). (C) 100-175 km S-wave velocities.

VEM values. We observe particularly slow MOR migration rates over the past 100 Ma at three ridges that currently exhibit ridge-plume interactions, namely the East Pacific Rise, the Southwest Indian Ridge, and the southern South Atlantic Ridge. On average, these three MOR systems have migrated <500 km in an absolute sense in the last 100 Ma, compared with absolute migration distances of >1500-2000 km for the Central and North Atlantic, and Northwest and Southeast Indian Ridges. We see evidence for higher upper mantle temperatures beneath slowly migrating ridges through global correlations between VEM and perturbations in both P- and S-wave velocity at depths 100-200 km. This is consistent with recent observations of higher upper mantle temperatures beneath spreading ridge segments located near deeply-sourced plumes. Together, patterns of MOR migration, LIP formation, and correlations of VEM with seismic tomography and MOR basalt geochemistry suggest a strong feedback between the dynamics of slowly migrating ridges and deeply-sourced plumes at global scale, which produce a self-sustained system over time scales up to 180 Ma.

In our proposed model, ridges at intermediate distances from plumes best represent the feedback mechanism. On the one hand, plume material will preferentially flow laterally towards areas with shallower lithosphere-asthenosphere interfaces (i.e. beneath MORs), with the effect of stabilising the MOR segment. On the other hand, the suction effect produced by the MOR will drain hot material from the plume and help stabilise the deeply-sourced plume.

These interactions result in a perturbation of the isotherm directly beneath the MOR, as hotter mantle is drawn towards the surface, a model supported by correlations between VEM, MOR basalt geochemistry and seismic tomography. Ridge segments located farther from the ridge-plume interaction are not affected by the ridge-plume interaction and are able to migrate more rapidly. These rapidly-migrating MORs do not perturb the upper mantle structure to any significant extent, nor focus large volumes of upper mantle towards the MOR. The plumes we have identified as participating in long-standing ridge-plume interactions are probably sourced from Large Low Shear Velocity Provinces. If these provinces are stable for very long periods of geological time, then it is possible that the relationships we observe between plume ridge interactions and slow MOR migration, and their effect on the thermal structure of the upper mantle are similarly stable. The stabilisation of MOR over time periods >180 million years, facilitated by ridge-plume interactions has significant implications for the way we model the plate-mantle system, and for understanding observed patterns of ridge morphology and geochemistry.

This project is part of CCFS Theme 3, Earth Today, and contributes to understanding Earth's Architecture and Fluid Fluxes.

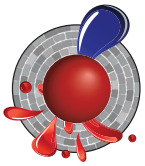

Contacts: J.C. Afonso, Jo Whittaker, Dietmar Muller
Funded by: CCFS Foundation Program 4

Deformation behaviour in polymineralic rocks

Deformation in rocks can be mainly localised in large ductile shear zones, broadly distributed into several smaller high-strain zones or dynamically change from one system to the other. One of the main reasons for strain localisation is a switch from Power-law flow, in which dislocation creep is a dominant deformation mechanism to Newtonian flow, in which deformation is dominated by diffusion or dislocation glide accommodated grain boundary sliding (GBS). A switch between these two types of flow will result in a marked weakening and strain localisation, because it lowers the effective viscosity of the rock by at least two orders of magnitude.

We have investigated the controls on the deformation behaviour of polymineralic rocks using a granitic pegmatite deformed at medium P and T conditions *(CCFS Publication #501)*. The chosen sample is an example of a mesoscale system where several minerals with different rheological behaviour were deformed together and strain was localised in a complex system of high-strain zones at different scales.

The sample shows visible zonation in the distribution and grain size of the minerals (Fig.1a). In the initially coarse-grained, K-feldspar-dominated lower part of the sample, several microscale shear zones developed; two mesoscale shear zones separate this zone from the upper, quartz-rich part of the sample and the wall rock (Fig. 1b).

Microstructural observations, and chemical and EBSD data, show that mesoscale shear zones form at the boundary between zones with different mineral assemblages, especially between the initially K-feldspar-rich and quartz-rich zones. Microscale shear zones in the initially coarser-grained, feldspar-rich zone form by (i) intense recrystallisation in originally smaller grains of plagioclase, next to initially large K-feldspars deformed in the brittle regime; (ii) fracturing coupled with grain-size reduction through the interface-coupled dissolution and reprecipitation replacement of coarse-grained K-feldspar by fine-grained albitic plagioclase. Strain is localised in the newly formed, fine-grained plagioclase and causes advanced recrystallisation of adjacent K-feldspar.

Once the grain size is sufficiently small, grain-boundary sliding becomes the dominant deformation mechanism. Consequently, once micro- and mesoscale high-strain zones are interconnected, the rheology of the rock is controlled by Newtonian flow. Phase mixing and continuous high strain rates help to maintain small enough grain sizes to allow Newtonian flow over long periods, "*stabilising*" the high-strain zones.

Our study shows that, in polymineralic rocks, the variation in initial and developing grain size, as well as mineral distribution, governs the dynamic rheological behaviour of the rock as a whole.

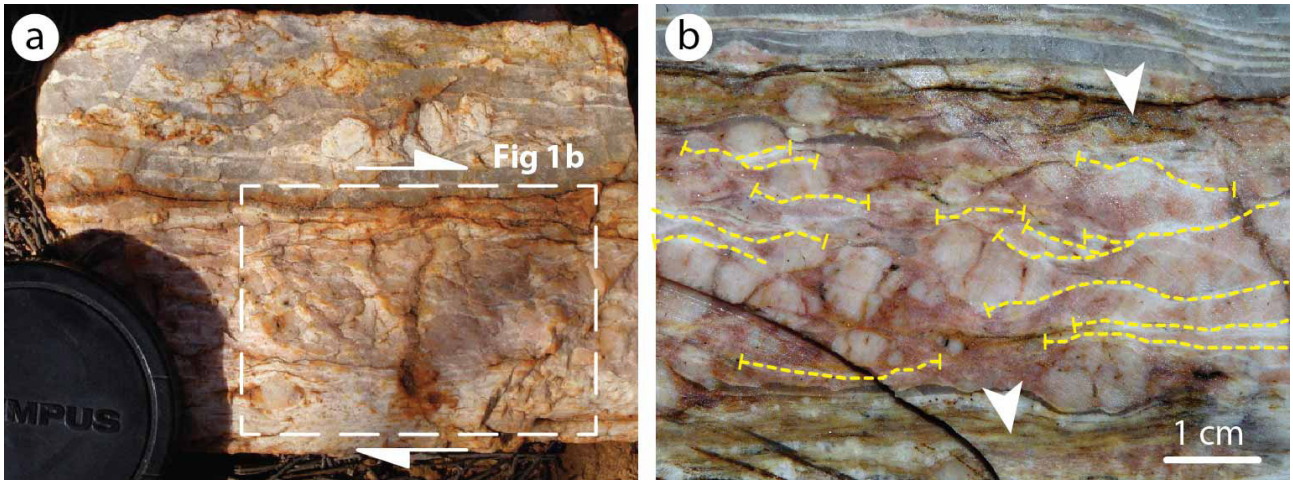

Figure 1. General characteristics of the studied sample: (a) hand specimen showing two main domains in pegmatite; (b) close-up of zone dominated by K-feldspar (pink) with several discontinuous microscale shear zones (yellow dashed lines) and two mesoscale zones of strain localisation below and above (white arrows).

This project is part of CCFS Theme 2, Earth Evolution, and contributes to understanding Fluid Fluxes.

Contacts: Daria Czaplinska, Sandra Piazolo
Funded by: ARC Discovery Project (DP120102060), Future Fellowship to Sandra Piazolo

Tibetan chromitites: Excavating the slab graveyard

Large peridotite massifs are scattered along the 1500 km length of the Yarlung-Zangbo Suture Zone (southern Tibet, China), the major suture between Asian and Gondwana-derived terranes. Diamonds occur in the peridotites and chromitites of several massifs, together with an extensive suite of trace phases that indicate extremely low fO_2 (SiC, nitrides, carbides, native elements) and/or ultra-high pressures (diamond, possible stishovite, coesite). Physical and isotopic (C, N) studies of the diamonds confirm they are natural, crystallised in a disequilibrium environment, and spent only a short time at

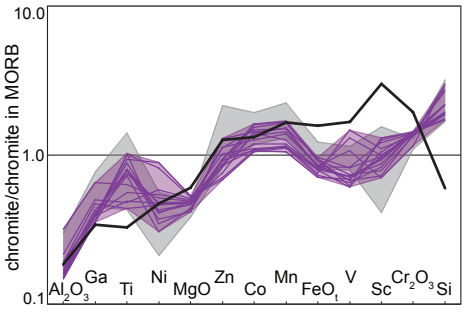

Figure 1. Major element oxide and minor/ trace-element plot (normalised to MORB chromite (Page and Barnes 2009)) for chromites from Luobusa, Tibet (purple), the Antalya ophiolite complex, Turkey (grey), and chromite hosted in boninite-lavas from Bonin Island (black; Pagé and Barnes, 2009). Luobusa (Tibet) chromites have Cr# from 0.60-0.78 and Mg# 0.58-0.73; Antalya (Turkey) chromites have Cr# from 0.59-0.73 and Mg# from 0.55-0.69.

mantle temperatures before exhumation and cooling (*Howell, Griffin et al., submitted*). These constraints are difficult to reconcile with previous models for the history of the diamond-bearing rocks. However, new investigations are providing evidence that these peridotite massifs have experienced a remarkable journey in time and space (*CCFS Publication #522*).

We have uncovered evidence that strongly suggests some of these peridotites have undergone metamorphism in or near the upper part of the Transition Zone, around 400-600 km deep. This includes the discovery that many of the chromites contain exsolved pyroxenes and coesite, consistent with inversion from the high-pressure polymorph (calcium-ferrite structure) of chromite, which is stable in the Mantle Transition Zone. This high-P polymorph structure, unlike the normal spinel structure of chromite, can accommodate ions such as Ca^{2+} and Si^{4+}; however, these elements are ejected (exsolved) when chromite is emplaced at shallow, (lower pressure) levels. This evidence, and the presence of diamonds, coesite and other high-pressure phases recorded in both the peridotites and the chromitites, suggest that the peridotite bodies have indeed risen from the Transition Zone. But how did they get there?

An answer comes from CCFS' extensive work on the trace-element geochemistry of chromites from many different geotectonic settings. The trace-element data for the Luobusa chromitites (Fig. 1) show that they are typical of chromitites formed above subduction zones by magma mixing, at shallow depths (tens of km) in the oceanic mantle. Euhedral, oscillatory-zoned zircons in the chromitites (Fig. 2), formed in this magma-mixing environment, give U-Pb ages of 376 ±7 Ma, εHf = 9.7±4.6, and $\delta^{18}O$ = 4.8 to 8.2; the isotopic data are consistent with mingling of magmas derived from the oceanic mantle and a subducting slab. Os-Ir nuggets in the chromitites have Re-Os model ages (TRD) of 234±3 Ma, while TRD of in situ Ru-Os-Ir sulfides range from 290-630 Ma, peaking at ca 325 Ma. All of these ages are significantly older than the emplacement of the peridotites into the Yarlung-Zangbo suture zone (ca 130 Ma).

A proposed P-T-t path (Fig. 3) traces the original formation of chromitites in mantle-wedge harzburgites, subduction of these harzburgites at ca 375 Ma, residence in the upper Transition Zone for >200 Ma, and rapid exhumation at ca 130 Ma. The Os-isotope data suggest that the subducted mantle consisted of previously depleted subcontinental lithosphere, dragged down by a subducting oceanic slab. Thermo-mechanical modeling (Fig. 4) shows that rollback of a younger subducting slab would produce a high-velocity channelised upwelling that could exhume

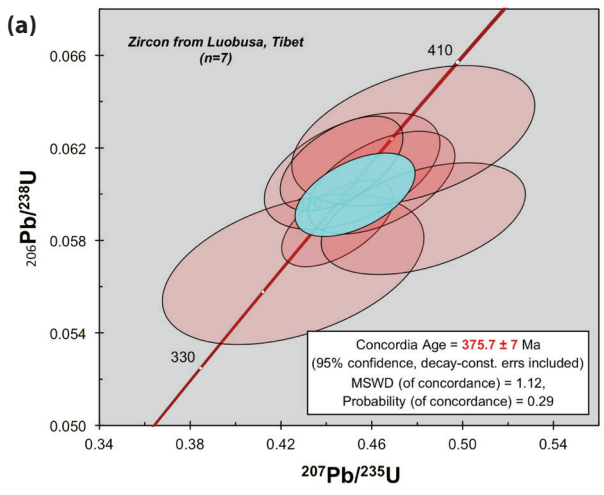

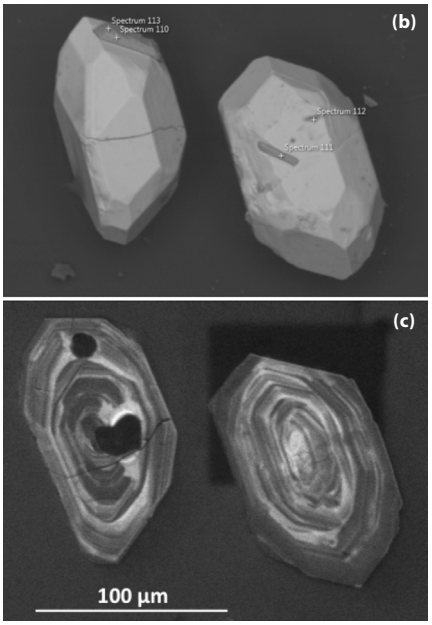

Figure 2. (a) Inverse $^{206}Pb/^{238}U$ vs $^{207}Pb/^{235}U$ concordia plot for zircon from Luobusa ophiolite, Tibet (n=7). Zircons from a Luobusa chromitite: (b) BSE image; (c) CL image. Dark inclusions are F-apatite; prisms of apatite are visible on both grains in (a).

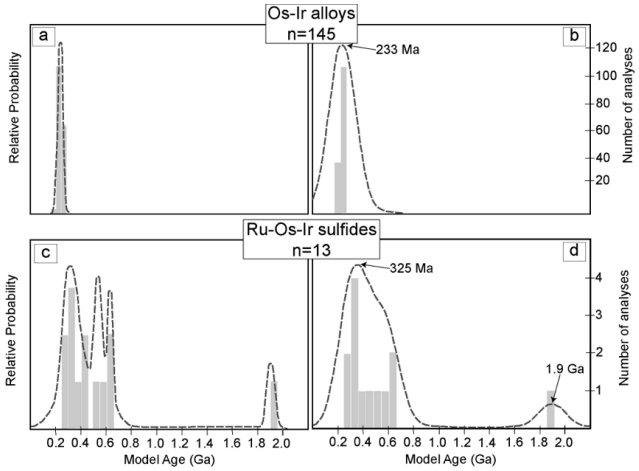

Figure 3. Model age ranges for b) Os-Ir alloys (Shi et al., 2007), and d) laurite. (a) and (c) show the data with the analysed analytical errors; in (b) and (d) the uncertainties have been expanded to a uniform 0.1 Ga.

the buoyant harzburgites (and their chromitites) from the Transition Zone in <10 Ma. This rapid upwelling could be the mechanism that brought some massifs to the surface in back-arc basins, forming parts of the oceanic crust basement. This model reconciles many apparently contradictory petrological and geological datasets. It also introduces a previously unrecognised, geodynamic process that may have operated in large collisional zones.

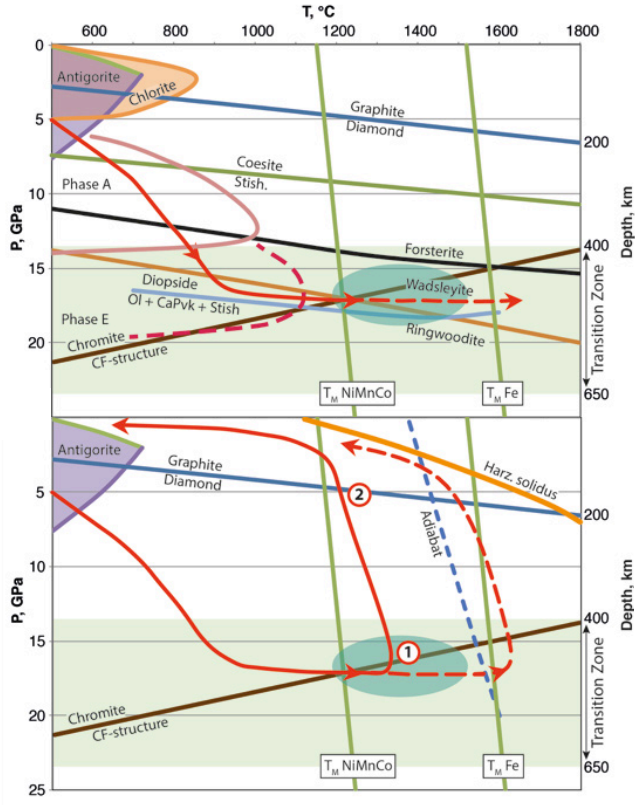

Figure 4. Reconstructed P-T-t path for the Luobusa-Kangjinla peridotite body. (a) stability fields of hydrous phases, and curves for relevant reactions and T constraints (see text); green oval outlines a probable P-T region for coexistence of wadsleyite, CF-structured chromite, and majoritic garnets. Red arrow illustrates subduction of mantle-wedge material into the Transition Zone, followed by heating to at least 1300 °C (constrained by the melting point of alloy inclusions in diamonds at TZ depths), or to >1500 °C (melting point of Fe). (b) Two end-member (low-T, high-T) adiabatic uplift paths are illustrated. Formation of diamonds is possible at point (1), but formation near point (2) would be more consistent with the lack of nitrogen aggregation in the diamonds.

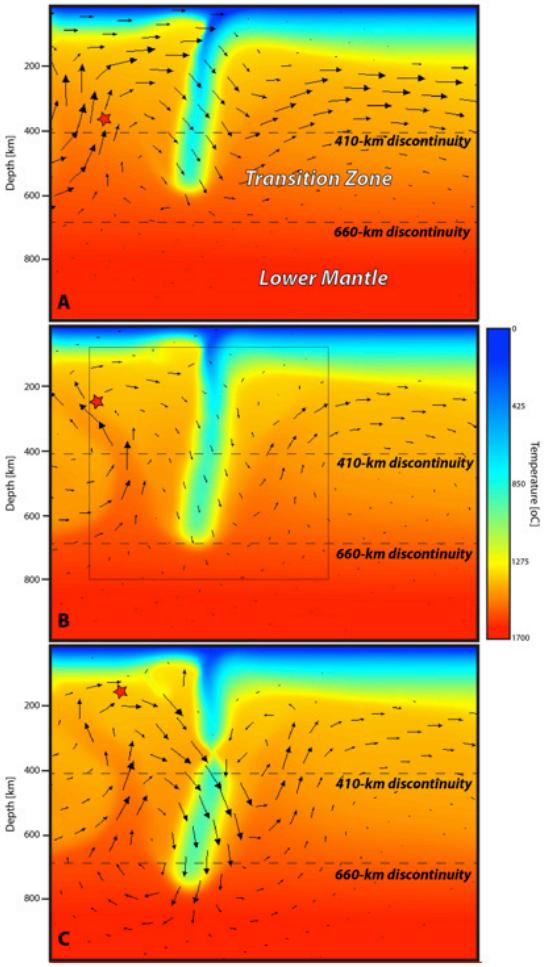

Figure 5. Ascent of TZ material in a thermo-mechanical simulation of continental collision involving slab roll-back and break-off. The simulation begins with a 400 km-long slab subducting at an angle of 45°. No boundary conditions are imposed on velocities, which are controlled entirely by the balance between internal forces (e.g. buoyancy, shear resistance, etc). More details can be found in Afonso & Zlotnik (2012). A) The verticalisation of the slab under the action of gravity generates a large-scale upwelling down to the TZ. B) This broad upwelling evolves into a narrower "channel" (favoured by a non-linear rheology) with velocities of 3-8 cm yr^{-1}. C) Once the continental plate arrives at the trench, subduction slows down and a slab break-off occurs. At this point, material from the TZ has been brought up to lithospheric depths in <10Ma, to become part of smaller-scale lithospheric tectonic processes. Red star indicates the path of a low-density passive tracer, which is at a depth of 520 km at the beginning of the simulation.

This project is part of CCFS Theme 2, Earth Evolution, and contributes to understanding Earth's Architecture and Fluid Fluxes.

Contacts: Nicole McGowan, Bill Griffin

Funded by: CCFS Foundation Program 1, APA, MQ PGRF

New Ce-Nd separation techniques improve our ability to detect early silicate differentiation of planetary bodies

Sm and Nd have two different radiogenic decay systems that can be useful for evaluating the hypothesis that the Earth and chondrites have the same Sm/Nd ratio: ^{146}Sm decays to ^{142}Nd (T1/2 = 68 Ma) and ^{147}Sm decays to ^{143}Nd (T1/2 = 106 Ga). The short-lived ^{146}Sm-^{142}Nd radioactive nuclides are ideal tools for constraining the early silicate differentiation of planetary bodies and the early history of the Earth's mantle. Because of its low initial abundance, ^{146}Sm is effectively extinct after 4-5 half-lives, so that ^{142}Nd/^{144}Nd anomalies can only be related to the differentiation of silicate reservoirs during the first few hundred million years of Earth's history. However, ^{142}Nd anomalies are expected to be extremely small (less than 40 ppm) and require ultra-precise measurements because the variation of ^{142}Nd/^{144}Nd is very small (<50 ppm). New-generation thermal-ionisation mass spectrometry (TIMS) has produced published reproducibilities of ^{142}Nd/^{144}Nd ca 5 to 7 ppm (2 RSD). For ultra-high-precision ^{142}Nd/^{144}Nd isotopic measurements the complete separation of Nd from the matrix and the isobaric interfering elements Ce and Sm is indispensible. During TIMS analysis, ^{140}Ce/^{144}Nd and ^{147}Sm/^{144}Nd must be lower than 0.000010.

A rapid solid-phase microextraction technique, using HEHEHP resin, has been developed to completely separate Ce from rare earth element (REE) mixtures, including Nd (Fig. 1), and has been applied to ultra-high-precision measurement of ^{142}Nd/^{144}Nd in geological materials (Fig. 2). In contrast to the traditional liquid-liquid micro-extraction technique, the benefits of the SPME tandem column techniques are high Nd recovery, low residual Ce (Ce/Nd <10-6), and ease of operation. A single HEHEHP resin column, replacing the traditional two-column scheme (AG 50W + HDEHP resins), is used to further purify Nd by removing Na salt and Sm isobaric interferences. All mean values of ^{140}Ce/^{144}Nd of geological samples after separation are <0.000010, even though the Ce/Nd ratio of geological materials is >3.0. Thus, ^{142}Ce interferences on ^{142}Nd never exceed 1.3 ppm. Ultra-high-precision TIMS analyses of silicate standards show that the internal precision of all runs is better than 4 ppm (2 RSD) for ^{142}Nd/^{144}Nd values. Values of ^{142}Nd/^{144}Nd for JNdi-1, JR-3, and BCR-2 have external precisions of ±4.8, ±4.4, and ±3.9 ppm (2 RSD), respectively. The external reproducibility is sufficient to resolve 5 ppm anomalies in ^{142}Nd/^{144}Nd.

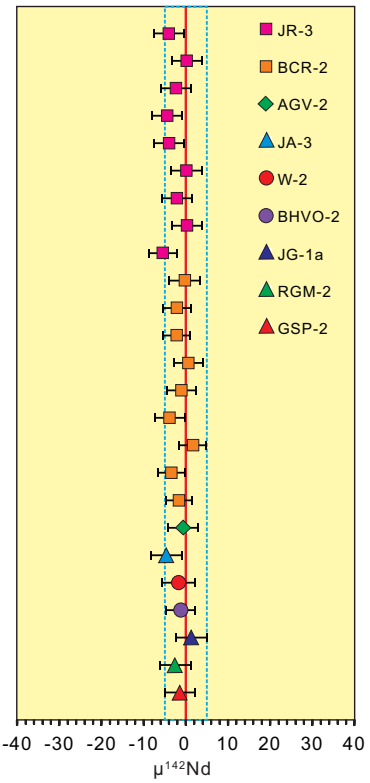

Figure 2. ^{142}Nd/^{144}Nd data for the CRM samples are plotted as deviations in ppm (μ^{142}Nd) from the JNdi-1 standard relative to the terrestrial Nd standard JNdi-1. $\mu^{142}Nd = (((^{142}Nd/^{144}Nd)_{sample}/(^{142}Nd/^{144}Nd)_{JNdi\text{-}1}) \times 106$, where the ^{142}Nd/^{144}Nd value of JNdi-1 is the average value in this study (1.1418367 ± 0.0000055, 2 SD, n = 37). The dashed lines delimit the external error of 5 ppm (2 RSD) of the repeated measurements of the JNdi-1 standard (n = 37). Error bars are 2 SE errors of individual measurements.

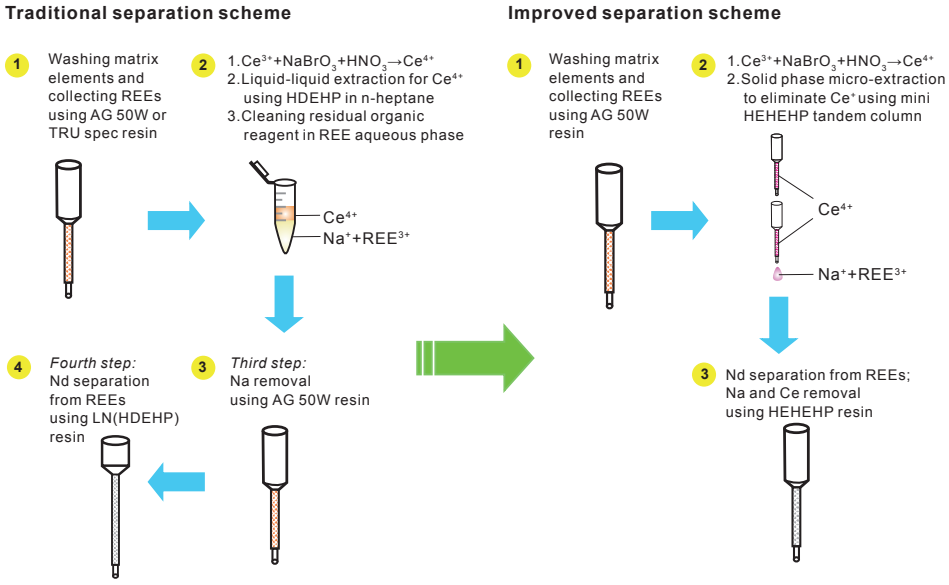

Figure 1. The new rapid solid-phase microextraction technique separation protocol compared with traditional methods.

Compared to the traditional methods, the new separation procedure has advantages in terms of simplicity, Nd recovery, and miniaturisation.

This project is part of CCFS Theme 1, Early Earth

Contacts: Xuan-Ce Wang, Chao-Feng Li (IGGCAS)
Funded by: National Science Foundation of China (No. 41373020)

The thermochemical structure of the lithosphere and upper mantle beneath South China

South China is an ideal natural Earth laboratory for testing ideas about lithospheric structure and evolution. South China experienced major changes in the thermochemical structure of its lithospheric mantle throughout the Phanerozoic. Existing lithospheric models for this region are inconsistent with each other, but recently, abundant geophysical data (topography, geoid, surface heat flow and dense regional seismic arrays) and petrological/geochemical data on mantle-derived xenoliths have become available, and we have used these new data to test the competing lithospheric models.

By jointly inverting Rayleigh-wave dispersion data, geoid height, topography and surface heat flow with a probabilistic (Bayesian) Monte Carlo method, we have defined the thermal and compositional structure of South China. Our inversions show marked differences in the depth to the lithosphere-asthenosphere boundary between the eastern and western regions of South China. The lithosphere is thin (85-150 km) beneath the South China Fold system and thickens beneath the Yangtze Craton, reaching maximum thicknesses of up to 250 km beneath the Sichuan Basin. The average lithospheric composition predicted by our inversion is significantly fertile (Mg# ~88-90), in agreement with independent geochemical observations on mantle xenoliths in the volcanic rocks of East China. Such fertile compositions, together with the relatively thin lithosphere thickness, point towards a widespread metasomatism/refertilisation event. We suggest, as others have, that a flat-subduction episode and subsequent slab removal may have triggered both the delamination of the lowermost part of the subcontinental lithosphere and the generation of asthenospheric melts that metasomatised (refertilised) the remaining lithospheric mantle. Inconsistencies among geophysical observations and the anomalously fertile compositions derived from the Sichuan Basin indicate that this region may currently be affected by small-scale convection or delamination processes. Alternatively, the anomalous observations may be associated with the eastward push of Tibetan lithosphere beneath the Yangtze Craton.

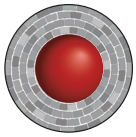

This project is part of CCFS Theme 3, Earth Today, and contributes to understanding Earth's Architecture.

Contacts: Bin Shan, Juan Carlos Afonso, Yingjie Yang

Funded by: ARC Discovery Project (DP120102372)

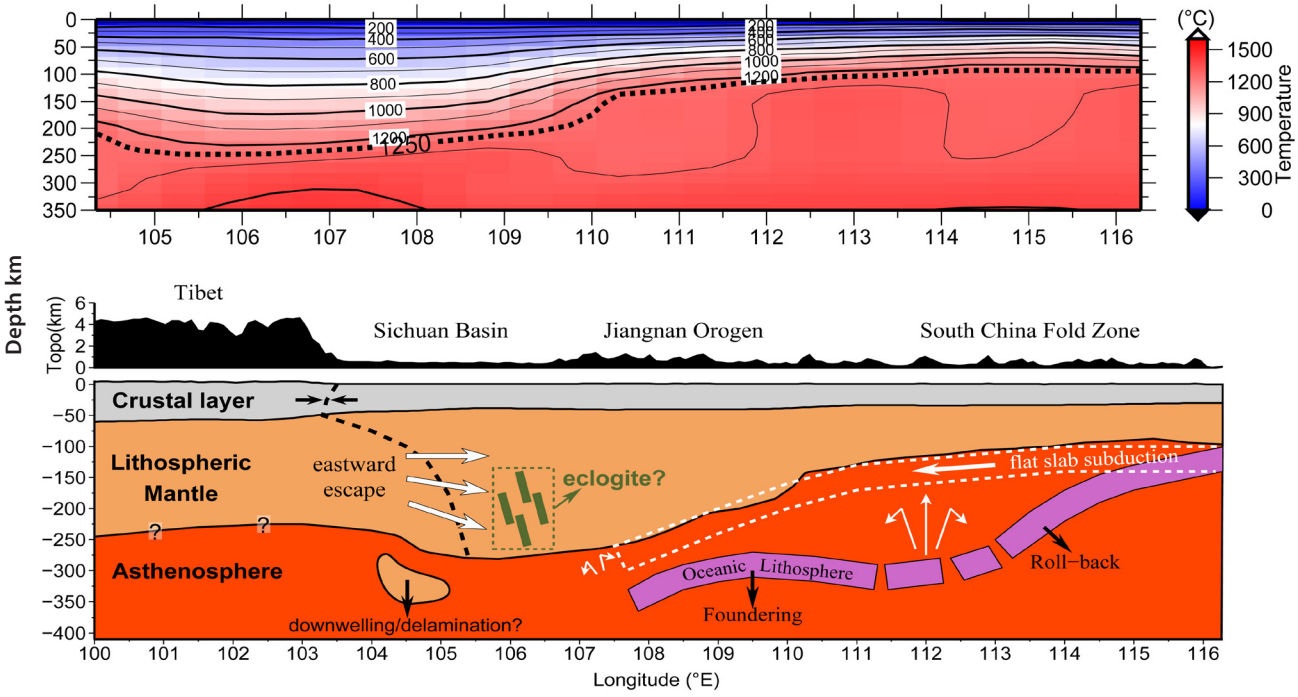

Figure 1. Temperature cross section obtained by interpolating the 1-D temperature structures; b) Cartoon illustrating a possible scenario for the thermochemical evolution of South China.

South China's collision with northern India 580-470 million years ago to join Gondwanaland

The position of the South China Block (SCB) relevant to Gondwanaland during late Precambrian and early Palaeozoic remains a challenge to geoscientists. One peculiar observation has been that prior to the Ordovician-Silurian Wuyi-Yunkai intraplate orogeny, the Yangtze half of the SCB was dominated by platform carbonate deposits whereas the Cathaysia half received almost exclusively siliciclastic deposition. What caused such contrasting depositional environments over the same continent?

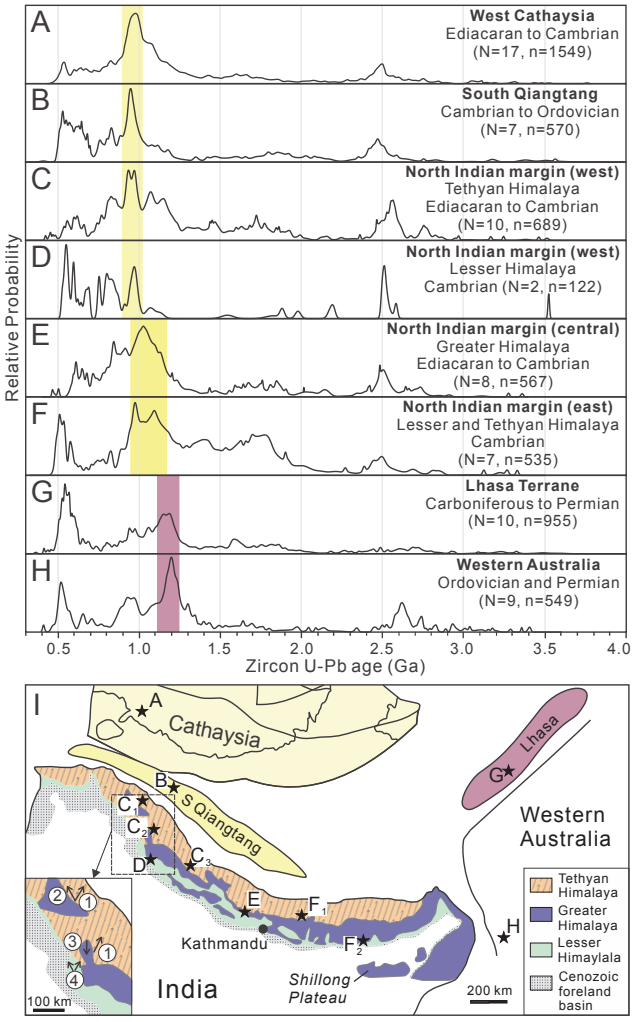

Figure 1. Provenance variations of Ediacaran-Cambrian sedimentary rocks along the northern margin of India, and comparisons with southwestern South China and adjacent terranes. Age spectra in (A)-(H) correspond to data points A-H in the location cartoon (I), where data points C1-C3 and D represent the western North Indian margin, data points E represent the central North Indian margin, and data points F1 and F2 represent the eastern North Indian margin. Sources of detrital zircon age spectra can be found in Yao et al. (2014; Am. J. Sci.).

LA-ICP-MS U-Pb dating of detrital zircons from Cambrian sedimentary rocks in southwestern South China has revealed four major age populations with a predominant peak at 980 Ma (*CCFS publication #366*). Zircon Hf-O isotopes suggest three Precambrian episodes of juvenile crustal growth for the source areas, with major crustal reworking at 580 Ma. The source provenance as defined by the U-Pb and Hf-O analyses is distinctly different from the known tectonomagmatic record of the SCB, hinting at an external source. The sedimentary facies and modal composition of the Cambrian clastic rocks further show that the clastics were derived from a source southeast of the present-day South China mainland.

Possible candidates for this source, such as western Australia and western Laurentia fail to match the zircon U-Pb patterns of the South China rocks. In contrast, zircon U-Pb patterns and Hf isotopes of Ediacaran-Cambrian clastic sedimentary rocks and granites in northwestern Indian Himalaya match well with those of the South China clastic rocks (Fig. 1). In addition, the strongest provenance connection with the SCB, which started from 580 million years ago, appears to be with northwestern India, and weakens eastward along the Himalaya toward western Australia (Fig. 1). Terranes such as Qiangtang and Lhasa show provenance affinities with the Indian and Australian sections of the Gondwana margin, respectively.

Together with a regional tectonostratigraphic analysis, our new results lead to a reconstruction of the tectonic evolution of the NE Gondwana margin for the late Neoproterozoic and earliest Paleozoic (Fig. 2). We propose that after breaking away from central Rodinia, South China started to approach northern

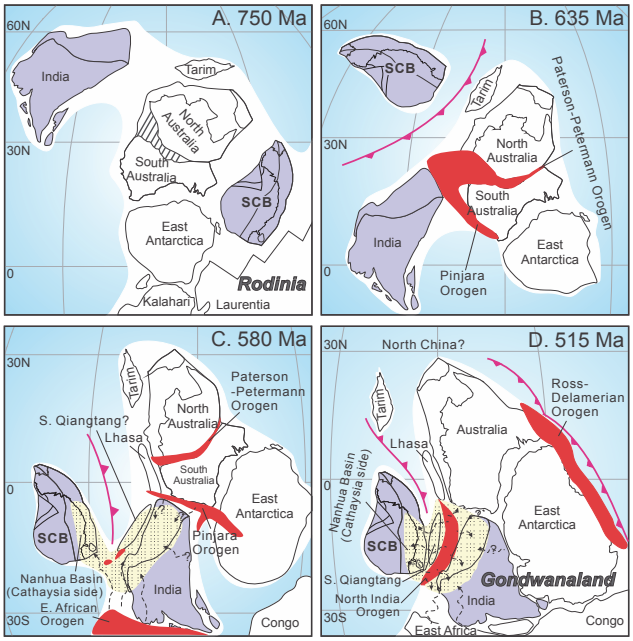

Figure 2. Paleogeographic reconstructions showing the position of South China (A) before the break-up of Rodinia in the mid-Neoproterozoic (750 Ma); (B) after Rodinia broke up, but prior to its collision with India during the assembly of Gondwanaland (635 Ma); (C) beginning of collision with NW India at ca 580 Ma during the assembly of Gondwanaland; (D) colliding with India to join Gondwanaland (515 Ma).

India at about 580 million years ago during the assembly of Gondwanaland. Continental collision occurred between 580 and 440 million years ago, causing not only the so-called "Pan-African" orogeny at the northern margin of India but also the intraplate Wuyi-Yunkai orogeny in South China. The collision started with northwestern India, and finished with northestern India. The resulting orogens shed vast amounts of Ediacaran-Cambrian clastic sedimentary rocks to an evolving foreland basin (the Nanhua foreland basin) in the SE South China Block.

This project is part of CCFS Themes 2 and 3, Earth Evolution and Earth Today, and contributes to understanding Earth's Architecture and Fluid Fluxes.

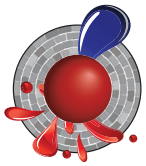

Contacts: Wei-Hua Yao, Zheng-Xiang Li
Funded by: CAS SAFEA(KZCX2-YW-Q04-06), NNSFC(41173039) and ARC Discovery Project (DP110104799). CCFS Foundation Program 5

Volatiles and mantle melting: An experimental study

Mineral/melt partitioning of volatiles (in particular H_2O) in the mantle is a first-order problem because of its influence on the distribution of melts and fluids in the mantle as well as the creation of the Earth's hydrosphere. Melts and fluids also play a key role in both fractionating and transporting metals and incompatible elements between the mantle and crust/hydrosphere. Thus, experimental data on the partitioning of volatile and non-volatile elements between peridotite minerals and melts can be related to the broader issues of the Earth's deep volatile cycle and its influence on mantle fractionation and evolution. The partitioning data generated within the framework of CCFS Foundation Program 2a define conditions under which relatively water-rich fluids and/or melts can exist in equilibrium with water-poor mantle host rocks. It also is relevant to the calculation of solidus temperatures for water-undersaturated mantle rocks.

Our new experimental data for the basanite UT-70489 include: H_2O-saturated liquidus and subliquidus phase equilibria (Fig. 2); H_2O-solubility data for 2.5 GPa, plus estimates of the 2.5 GPa liquidus of basanite under dry, and H_2O-saturated (~28 wt % dissolved H_2O) conditions (Fig. 3).

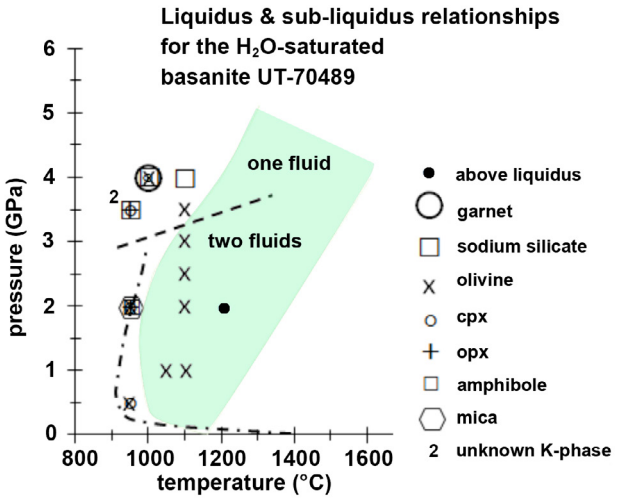

Figure 2. H_2O-saturated liquidus and subliquidus phase equilibria for basanite bulk composition.

These can be combined with published data for volatile-undersaturated basanite and for similar compositions (Fig. 3). The results fit to a polynomial that allows calculation of the effects of even small H_2O concentrations on liquidus temperatures. Initially this effect is large but then tails off as concentrations increase. This integrated information can be used to calculate solidus temperatures for H_2O-undersaturated mantle peridotites, which is probably the most common composition in the convecting asthenosphere.

Earlier studies have underplayed the role of low-degree melts in the asthenosphere. Earlier experiments on the liquidus of basanite showed that it is in equilibrium with garnet lherzolite at ~2.7 GPa and 1200 °C with 4.5 wt % of dissolved H_2O and 2 wt% of dissolved CO_2. These conditions are close to those estimated for oceanic geotherms. Using the D values for H_2O from this study, it is also possible to calculate a concentration of ~230 ppm H_2O for the residue. This is within the range of estimates for the MORB source. In this light, the presence of migratory solidus melts within the ordinary convecting asthenosphere seems both feasible and probable.

Currently, these results are being extended to 4.0 GPa by looking at liquidus equilibria for another potential primary melt composition (Laughing Jack Marsh melilitite). The initial results show that at 1400 °C, close to estimates of the mantle T at 4 GPa, *cont...*

this melilitite begins to melt with only 5 wt% of dissolved H_2O (plus a small but unknown amount of CO_2).

For H_2O-saturated conditions, the basanite results require greater interpretation. Olivine is the liquidus phase up to at least 3.5 GPa and T close to 1100 °C. This is ~100 °C above the water-saturated peridotite solidus. In this case, the basanite is not an exact match to the H_2O-saturated solidus melt. But from phase equilibria and mineral/melt partitioning, the H_2O-saturated melt can be predicted to be less olivine-normative, but more SiO_2- and Na_2O-rich than the basanite at the same pressure (2.7 GPa).
At pressures above those where complete miscibility occurs between basanitic melts and H_2O (~3.5 GPa at 1100 °C), conditions can also be bracketed (3.5-4.0 GPa and 950-1000 °C) for the equilibration of a basanite-like melt/fluid (containing ~50 wt% H_2O) with garnet lherzolite.

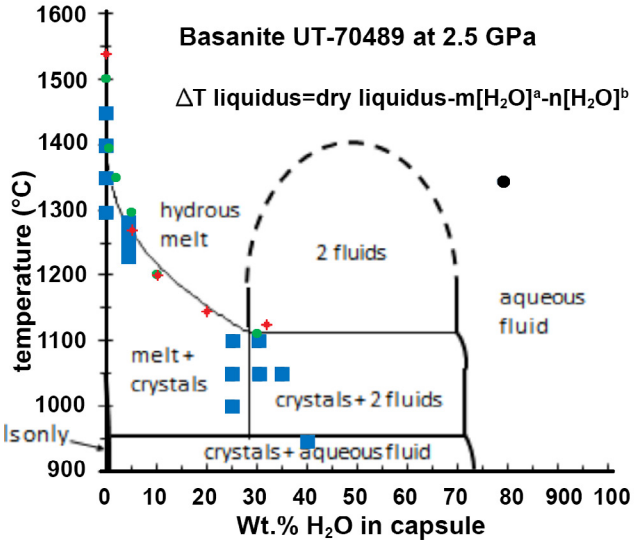

Figure 3. Water solubility at 2.5 GPa for basanite bulk composition in this study (blue squares) and the Mt. Leura basanite (red points) and Laughing Jack Marsh olivine melilitite (green points). See text for discussion.

Because of the strong influence of pressure on solute concentrations in hydrous fluids, our results favour relatively high temperatures for the water-saturated peridotite solidus (1000 °C at 2.0-3.0 GPa) rather than the very low temperatures advocated by some workers (as low as 850 °C at 2.0 GPa).

This project is part of CCFS Themes 2 and 3, Earth Evolution and Earth Today, and contributes to understanding Fluid Fluxes.

Contacts: John Adam, Tracy Rushmer
Funded by: CCFS Foundation Program; 2a Metal sources

Heterogeneous crust in the WA Craton

Recent seismic compilations show there is a global change in the characteristics of continental crust that was formed between 3.0Ga and 2.5Ga: older cratons have a thin, more felsic and less deformed crust with a very flat and sharp Moho; younger cratons have a thicker crust, more intermediate in composition and more deformed, usually with a diffuse Moho. These differences suggest a secular change in the processes of crustal growth in the late Archean.

Using the seismic receiver function technique, we have examined the crust in the Archean Western Australian (WA) Craton. We focused on its mean crustal properties and looked for possible links to its nearly 1 Ga history of early crustal formation. The crust in the constituent Pilbara and Yilgarn cratons is a typical mixture of plutonic rocks (granites) and supracrustal greenstone-facies rocks. The surface expression of these rocks are different across the two cratons: in the eastern and central Pilbara, granitoid domes and greenstone belts form a dome-and-keel pattern, while in the Yilgarn the granite-greenstone terranes are more elongated (Fig. 1), suggesting different tectonic processes during the growth and assembly of the two cratons.

Seismic records from available WA stations gave a fairly uniform coverage of the whole region. Receiver functions, the structural responses (functions) beneath a seismic station (receiver), were computed and stacked to derive the most coherent values for bulk crustal thickness (H) and the Vp/Vs ratio (k). The Vp/Vs ratio is closely related to crustal composition (Christensen, JGR 1996). It can be constrained robustly using the free-surface multiples of the Moho receiver function phase, which travel differently in P- and S-waves in the crust.

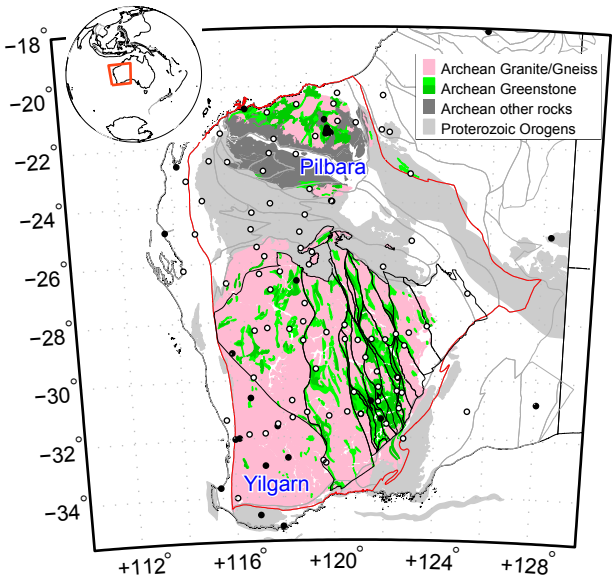

Figure 1. Seismic stations, rock ages and greenstone belts in the WA craton. Open and filled circles are temporary and permanent seismic stations. Red line contours the WA craton. Inset shows the location of the study region.

The crust in the WA craton is seismically heterogeneous (Fig. 2). While the Pilbara crust seems nearly uniform, the Yilgarn crust is spatially clustered into regions which correlate well with the surface tectonic units. The crustal density anomalies (*Aitken et al., Tectonophys. 2013*) and the mean crustal velocities (*Salmon et al., GJI 2013*) all indicate a similar pattern. The clustering in these observations indicates that the tectonic units in the WA craton are unique entities with deep-rooted geophysical signatures.

the crust substantially. Younger plumes in the Eastern Goldfields Superterrane, as evidenced by the 2.7 Ga komatiites along the western margin, may have dominated the thick and intermediate crust concentrated in this region.

Seismic observations show a heterogeneous crust in the WA Craton. The spatial correlation with the Archean tectonic domains indicates the spatial heterogeneity may be deeply

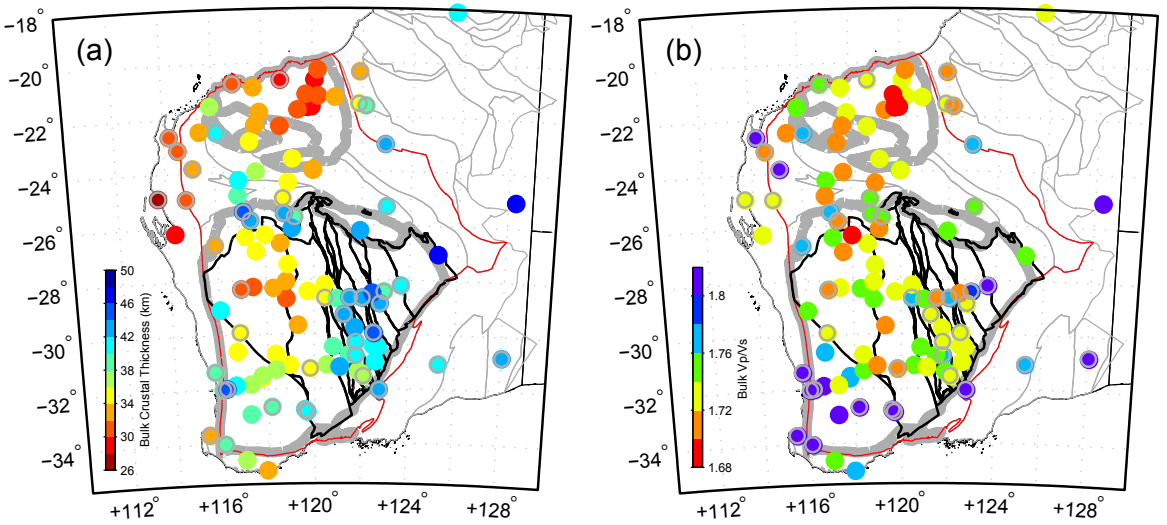

Figure 2. Bulk crustal properties in the WA craton. (a) Crustal thickness; (b) Vp/Vs ratio. Circles are stations.

Close inspection indicates that there is a weak correlation between the mean crustal thickness and the Vp/Vs ratio (Fig. 3), from the oldest crust in the Pilbara craton (formed ~3.6 Ga ago) to younger domains in the Yilgarn (<3.2 Ga). The Eastern Goldfields Superterrane, the youngest unit in the Yilgarn, is an outlier, which lies anomalously away from the trend.

Vertical tectonics has been proposed as responsible for the crustal structure of the Pilbara, especially in the >3.2 Ga mid- to eastern regions. The associated processes of plume impingement, melt differentiation, partial convective overturn, and delamination of lower crustal restites (*van Kranendonk et al., Geological Society London Special Publication 2014*), may have produced this extremely thin and felsic Pilbara crust.

Van Kranendonk et al. (2014) suspected that a transition towards accretional tectonics began about 3.2 Ga ago, as seen in linear trends of geological structures in the western Pilbara. In the Yilgarn. most crust is believed to have formed after 3.2 Ga (*Griffin et al., Precambrian Research 2004*). Most published crustal-genesis models favor arc accretion, as responsible for the elongated pattern defined by large-scale faults and greenstone belts. The processes associated with horizontal tectonics may have significantly contributed to the greater crustal thickness and more intermediate composition.

Much older crustal components (3.1-3.5 Ga; *Griffin et al. 2004*) have been recognised in the Murchison portion of the Yilgarn craton. These pieces of extraneous thin and felsic crust may have formed as in the Pilbara. Alternatively, late Archean plume activity in the region (*Ivanic et al., AJES 2010*) may have reworked rooted, extending through the whole cratonic lithosphere. The temporal correlation suggests that the early crustal-formation processes may have worked differently through time, but have left distinct seismic signatures in the crust.

This project is part of CCFS Themes 1 and 2, Early Earth and Earth Evolution, and contributes to understanding Earth's Architecture and Fluid Fluxes.

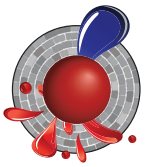

Contact: Huaiyu Yuan
Funded by: CCFS Foundation Program 10a

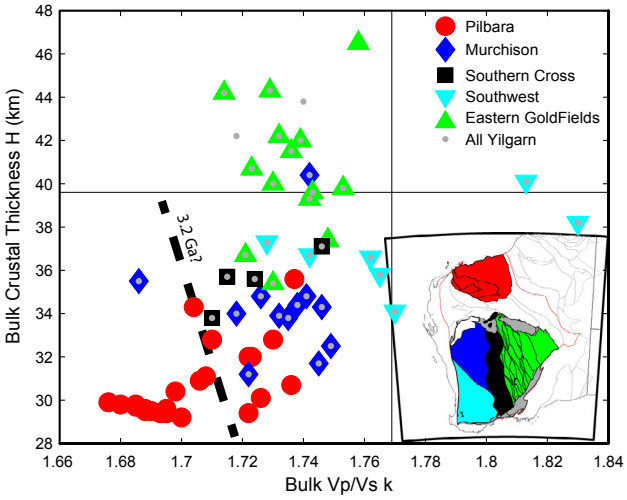

Figure 3. Clustering of bulk seismic properties in the WA crust. Thin lines show the global continental average. Thick dashed line shows a possible 3.2 Ga separation among all the measurements.

The origin of the Moon: spin-up during core formation?

The origin of the Moon is an ancient problem. The leading theory in recent decades has been a giant impact hypothesis, where a Mars-sized impactor - dubbed Theia - hit the protoEarth in a glancing impact in the late stages of accretion, ejecting a circum-planetary disk from which the Moon formed. The canonical models, however, predict that up to 60% of the Moon forms from material from the impactor Theia. However, the Moon and Earth's mantle have essentially identical oxygen and titanium isotopic signatures, distinct from any other planetary body, so a large contribution from Theia seems unlikely.

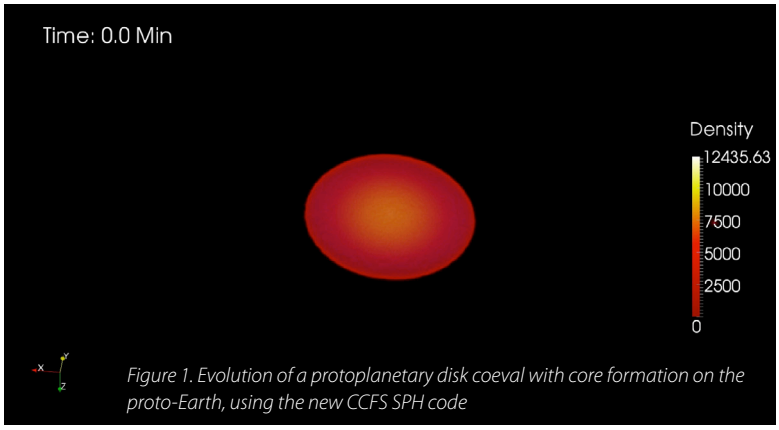

Figure 1. Evolution of a protoplanetary disk coeval with core formation on the proto-Earth, using the new CCFS SPH code

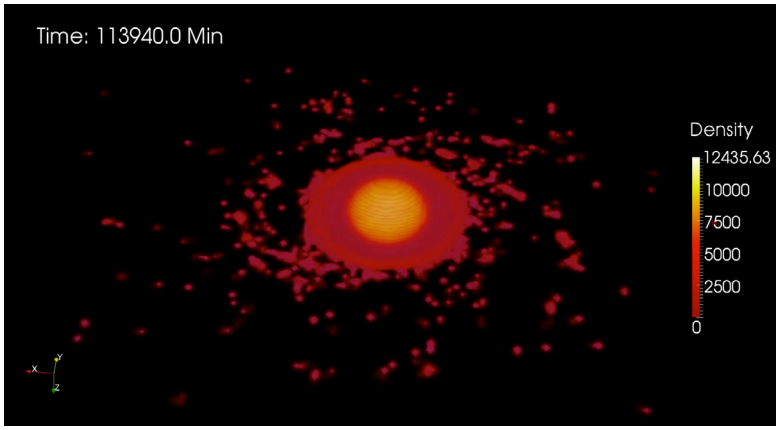

As a result, the impact community has moved towards special classes of impacts, with either a smaller impactor colliding with a rapidly-spinning proto-Earth, or two similarly-sized impactors in a head-on collision. Both require substantial loss of angular momentum in the Earth-Moon system and imply initial spin rates for the Earth of 1-4 hours, in line with recent accretion modeling.

We have developed an alternative scenario to explain the isotopic similarity of the Earth and Moon. Using parallel smoothed-particle hydrodynamic simulations, and a code developed within CCFS, we found that core formation in a rapidly rotating proto-Earth increases the angular momentum and results in a spin-up of the body. An analogy would be a twirling ice skater, increasing her rate of spin by pulling her arms in to her body. For fast initial rotations, this can result in mass being ejected along the equatorial plane. The magnitude of this effect depends on the initial spin, but for plausible rotation rates derived from accretion scenarios, the mass of disk ejected is between 0.2-3.5 lunar masses. The mass of the Moon predicted in the example shown is 0.6 Lunar masses, which compares well with the Moon. It also explains the Moon's low iron content, as the event was preceded by a major stage of core formation, removing much iron from the mantle. While the angular momentum is larger than in the current Earth-Moon system, modeling has shown this momentum would rapidlybe lost due to orbital resonance effects soon after Moon formation.

The timing is broadly consistent with the geochronology of the Moon and core formation - the oldest anorthosites on the Moon show that the Moon formed within the first 150 Myr of solar system history. Likewise Earth's core formation is constrained to be within the first 45-140 Myr by U-Pb systematics, or 70-100 Myr from Rb-Sr data. This timescale also is consistent with large-scale atmospheric blow-off ~100 Myr after solar system formation, as recorded in Xe- isotope systematics. Recent analysis of the water content of the Moon suggest up to 1410 ppm of water in mantle olivines; this is difficult to reconcile with a giant impact, but would be a natural consequence of this mechanism.

The Figure demonstrates the ejection of mass from the equatorial plane of a rapidly rotating proto-Earth, as a result of core formation. Using 50,000 interacting particles in a smoothed particle hydrodynamics simulation, we modelled the density re-distribution within a previously stable planet (top) during core formation, and track the increase in spin rate as a result of this, and the ejection of mass into a circum-planetary disk (bottom). The mass of this disk is sufficient to form Earth-sized Moons.

Finally, Venus has a slow retrograde rotation, and accretion modeling suggests this is a consequence of the last few large impacts in its accretion history. Despite these orbit-altering impacts, Venus does not have a moon, and has retained its primordial contingent of radiogenic noble gases, suggesting that the large-scale atmospheric blow-off that affected Earth did not occur. Our mechanism suggests that Venus' slow initial rotation made it difficult for core formation to spin the planet up enough to cause significant equatorial flattening. As a result, Venus never formed a Moon and did not experience the massive atmospheric loss expected during a mass spin-off event.

This project is part of CCFS Theme 1, Early Earth.

Contacts: Craig O'Neill, Siqi Zhang
Funded by: CCFS Foundation Program 4

Fluid-present deformation aids chemical homogenisation in chromite

The deep Earth water cycle is strongly coupled to the dynamics of Earth's interior. Oceanic crust descending into the deep mantle carries relatively little water, but even trace amounts of water affect physical and chemical properties, including melting temperature, rheology, deformation mechanism, electrical conductivity, etc. Ophiolitic chromitites are commonly regarded as resistant to fluid-related processes, and the chemical signatures of chromitites have been used to study processes in Earth's mantle. However, modification during deformation may have important implications for the interpretation of chemical signatures in chromite. We have studied how deformation promotes chemical homogeneity in chromite hosted in the serpentinite body of Golyamo Kamenyane, in south Bulgaria (*Gervilla et al., 2012; Colás et al., 2014*). These chromitites have undergone deformation together with fluid-rock interaction during metamorphism, and previous work suggested that these chromitites are one of the most chemically modified and deformed examples known (*Colás et al., 2014*). We have documented how chromite has deformed and homogenised under fluid-present amphibolite-facies conditions, providing new insights on the microstructural evolution of chromite during retrograde metamorphism.

We measured crystallographic orientation relationships using Electron Back-Scattered Diffraction (EBSD) and electron microprobe analysis. Chromites show porphyroclastic textures with coarse-grained porphyroclasts (ca 0.2 ~5 mm) and fine-grained neoblasts (< 200 µm) (Fig. 1a). Large chromite grains are chemically zoned in terms of major elements from core to rim, preserving an initial igneous feature (Cla, Clb), while outer rims show a metamorphic signature (Cll) (Fig. 1e). Large chromite grains also exhibit distinct intra-crystalline deformation including continuous crystal bending and subgrain boundaries, and chemical modification in their outer, deformed parts (Cll; Fig. 1a, d). Two types of fine-grained chromite, F1 and F2, are recognised. F1 exhibits a well-developed polygonal texture, straight grain boundaries and low intercrystal misorientation (<1º); F2 shows low-angle boundaries and significant intercrystalline misorientation (2 ~8º) (Fig. 1a). Both F1 and F2 have higher Fe^{3+} and Cr and lower Mg# values than the cores of large grains (Fig. 1e). We interpret F1 and F2 to represent chromite recrystallised by heterogeneous nucleation and subgrain rotation recrystallisation, respectively.

Crystallographic preferred orientation (CPO) and misorientation data on the well-developed low-angle (subgrain) boundaries in coarse grains and F2 grains indicate that deformation in chromite was accommodated mainly by dislocation creep, dominantly activating the {111}<100> slip system. The retrograde P-T exhumation path defined by thermodynamic and chemical modelling suggests that these fine-grained chromites were produced when the initial chromitites reacted with oxidising fluids during retrograde metamorphism (~1.0 GPa and 500-700 ºC). Our results show that deformation in the dislocation-creep regime in a chemically-open system induced chemical modification and homogenisation within chromite aggregates as well as strain localisation. This close physicochemical link offers new avenues for the interpretation of chemical signatures in chromites, linked to their microstructurally-controlled variation.

This project is part of CCFS Theme 2 Earth Evolution, and contributes to understanding Earth's Architecture and Fluid Fluxes.

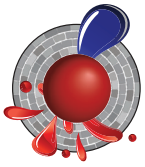

Contacts: Takako Satsukawa, Bill Griffin, Sue O'Reilly, Sandra Piazolo

Funded by: CCFS Foundation Program 1

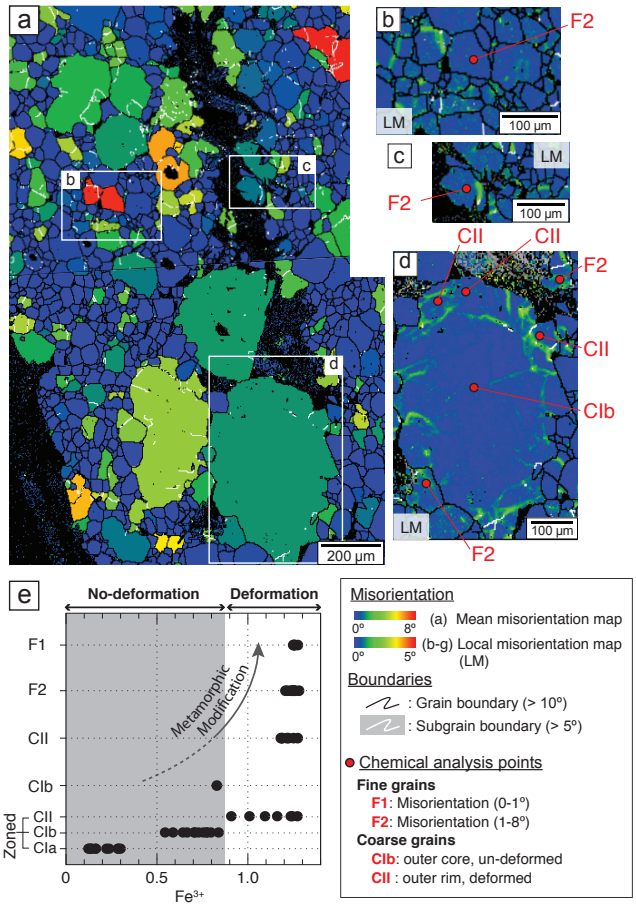

Figure 1. Orientation relationships as well as chemical composition of chromite porphyroclasts and adjacent fine grains. Step size of the map is 3 µm. (a) Colour coded EBSD map depicting the mean misorientation per grain (mean misorientation map). (b-d) EBSD maps showing local misorientations (LM) to identify crystal bending and subgrain boundaries below 5º. Fine grain types F1 and F2 are depicted. Chemical compositions at each red point are categorised according fine grain type (F1, F2) and coarse grain domain (CII, CIb). (e) Differences in chemical composition (Fe^{3+}) of different coarse-grained chr omite domains (CIa, CIb and CII) and fine chromite grain types (F1 and F2), note that coarse grains have a general Fe^{3+}-poor composition relative to the fine grains.

Mean plate velocity and the frequency of orogens: Secular changes in the supercontinent cycle?

We have used two sets of data for the last 2.5 Gyr to address the question of secular changes in the supercontinent cycle: the timing and locations of collisional and accretionary orogens, and average plate velocities as deduced from paleomagnetic and paleogeographic data. This analysis has been done in collaboration with Kent Condie (New Mexico Tech), Jun Korenaga (Yale University) and Steve Gardoll (Curtin University) (*CCFS publication #468*).

One of the main problems in counting orogens is: what constitutes a single orogeny? Collisional orogens of short strike length could be parts of a longer orogen, now displaced by supercontinent breakup. Therefore we have used "*orogen segments*" in our analyses. In some cases an orogen segment may represent a complete orogen, whereas in others, it may represent only part of a much more extensive orogen. We also have distinguished between collisional and accretionary orogens. Accretionary orogens do not always end with a continent-continent collision, but collisional orogens always do.

Paleomagnetic data provide a quantitative tool for paleogeographic reconstructions. However, the number of high-quality paleomagnetic results is limited, especially for the Early-Middle Paleozoic and the Precambrian. The most complete and reliable global paleogeographic reconstructions for the last 2 Gyr are constrained by both geological and paleomagnetic data. To calculate the average angular velocities of tectonic plates, we used published post-1800 Ma global paleogeographic reconstructions that fulfil the following criteria: (i) all major continental block positions are shown in the reconstructions; (ii) evolving block positions are known in time slices or animations; (iii) reconstructions are made using spherical geometry; and (iv) each reconstruction is made with Euler rotation parameters. Pre-1800 Ma paleogeographic reconstructions are rare and rather controversial. Unfortunately, only the paleomagnetic data from the Superior craton are sufficient for the estimation of mean angular velocities between 2500 and 1800 Ma. As the sizes of continents vary significantly, we calculated the mean angular velocity (in degrees/100 Myr) for each 100-Ma bin by normalising to continental area. We analysed only the movement of continental plates, because the data from oceanic plates are not available for most of the period of interest (≤2.5 Ga).

Peaks in the number of orogens, which probably reflect craton collisions, occur at 1850 and 600 Ma, with smaller peaks at 1100 and 350 Ma (Fig. 1). Distinct minima occur at 1700-1200, 900-700 and 300-200 Ma. Angular plate velocities as weighted by cratonic area vary greatly from about 20 to 80 deg/100 Myr with two peaks at 450-350 Ma and 1100 Ma (60-80 deg/100 Myr). However, the overall trend suggests a gradual speed up of plate tectonics with time. There is no simple relationship in the the frequency of cratonic collision or average plate velocity between supercontinent assemblies and breakups. The assembly of Nuna at 1700-1500 Ma correlates with very low collision rates, whereas the assembly of Rodinia and Gondwana at 1000-850 and 650-350 Ma, respectively, correspond to moderate to high rates. Very low collision rates occur during supercontinent breakup at 2200-2100, 1300-1100, 800-650, and 150-0 Ma. A peak in plate velocity at 450-350 Ma correlates with early growth of Pangea, and another at 1100 Ma with the initial stages of Rodinia's assembly following the breakup of Nuna.

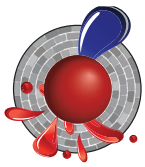

This project is part of CCFS Theme 2, Earth Evolution, and contributes to understanding Earth's Architecture and Fluid Fluxes.

Contact: Sergei Pisarevsky

Funded by: CCFS Foundation Program 6: Detecting Earth's rhythms: Australia's Proterozoic record in a global context

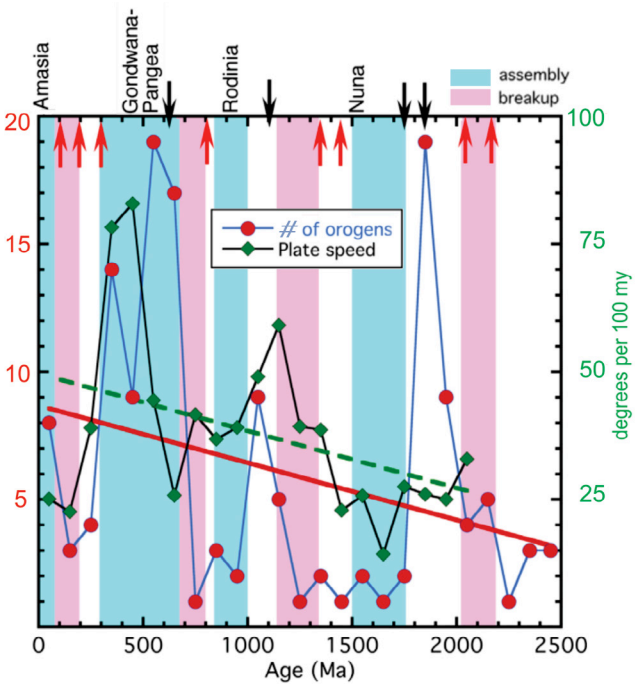

Figure 1. Secular changes in craton collision frequency and average area-weighted plate speed (deg/100 Myr). Collision frequency between cratons is expressed as number of orogen segments per 100-Myr bin moving in 100 Myr increments. Lines are linear regression analysis: n = 8.68-0.00224a, r = 0.287; s = 9.927-0.00223a, r = 0.393 (n, number of orogens; s, plate speed divided by five; a, age). Also shown are supercontinent assembly (blue stripes) and breakup (pink stripes) times. Major LIP (large igneous provinces) events: red arrows correspond to LIPs associated with supercontinent breakup, black arrows correspond to other LIPs.

Highly siderophile elements in the Emeishan LIP

Highly magnesian lavas (picrite) potentially preserve information about the origin and thermochemical state of the mantle sources of large igneous provinces (LIPs). We have carried out high-precision analysis of highly siderophile elements (HSE) in picrites from the ca 260 Ma Emeishan large igneous province

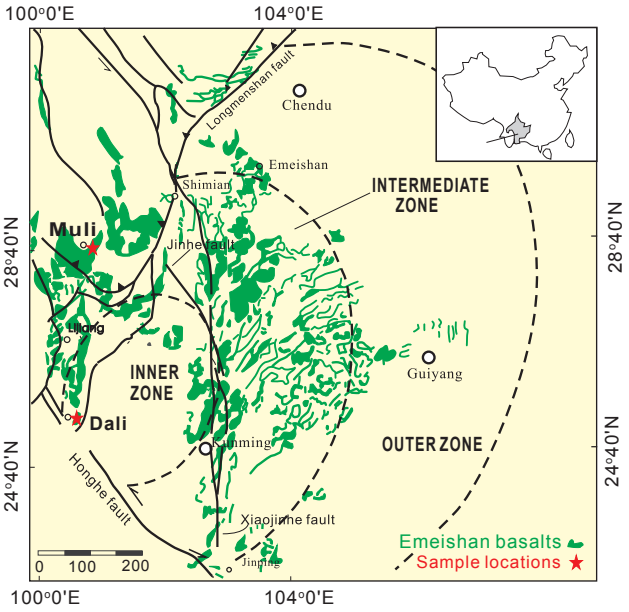

Figure 1. Distribution of the various components of the Emeishan Large Igneous Province, showing sample locations.

(Fig. 1). The absolute abundances of HSE in the Emeishan picrites are greater than those in MORB and in parental melts of Hawaiian picrites, and similar to the concentrations observed in komatiites (Fig. 2). The CI chondrite-normalised HSE patterns of the studied samples can be divided into two types (Fig. 3). Type 1, represented by the Muli picrites, is similar to that of the primitive upper mantle. Type 2, represented by the Dali picrites, has patterns similar to those of East Greenland and Iceland picrites; more fractionated Pt/Ir (8.6-34.5 with an average of 15.9 ± 8.4) and Pd/Ir (1.3-12.1 with an average 6.6 ±3.0) ratios relative to Type 1. The primary melt compositions of the studied samples were estimated using back addition of equilibrium olivine into selected whole rock compositions (Fig. 4). The estimated HSE

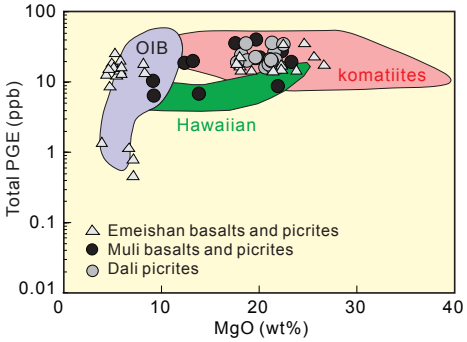

Figure 2. Total PGE contents versus MgO. The reference fields are after Ely and Neal, (2003), the Emeishan basalts and picrites data from Li et al. (2012).

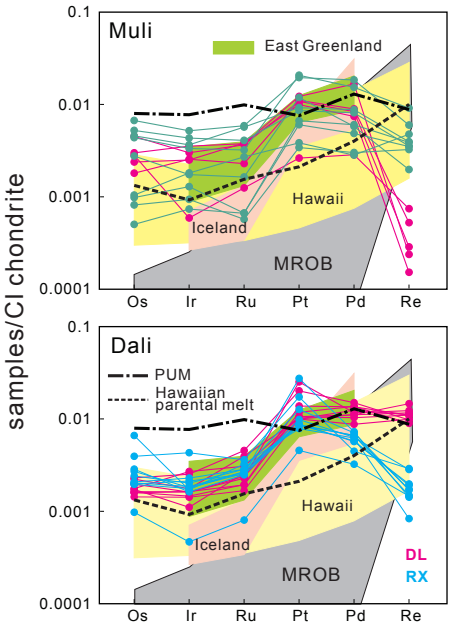

Figure 3. CI-chondrite normalised HSE patterns for (a) Muli and (b) Dali picrites. Primitive upper mantle (PUM) is thought to be representative of fertile peridotites, prior to the removal of material from the upper mantle (Becker et al., 2006). The reference MORB field is modified after Dale et al. (2008). The primitive melt for Hawaiian picrites is an average of individual suite parental melts (Ireland et al., 2009). The normalising values are from McDonough and Sun (1995). Data sources are as follows: east Greenland picrites are from Momme et al. (2006) and Momme et al. (1997); Iceland picrites from Momme et al., (2003); Hawaiian picrites from Bennett et al. (2000), Ireland et al. (2009) and Pitcher et al. (2009).

abundances in the parental melts of the Dali and Muli picrites are higher than estimates of Hawaiian parental melts. The large range of HSE abundances in the picrites reflects the integrated effects of source heterogeneity, plume-SCLM interaction, partial melting and early fractionation of olivine (± chromite). Together with existing isotopic data, this study shows that the source of the Emeishan plume mantle was chemically heterogeneous.

This project is part of all CCFS Theme 2, Earth Evolution, and contributes to understanding Earth's Architecture and Fluid Fluxes.

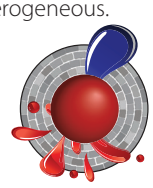

Contacts: Xuan-Ce Wang, Jie Li (GIGCAS, jieli@gig.ac.cn)

Funded by: National Science Foundation of China (No.40903007) and CCFS ESTAR Fellowship

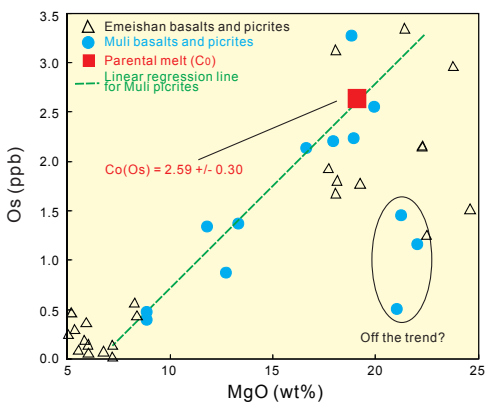

Figure 4. Example of how the HSE content in a parental melt was estimated, using Os abundances of the Muli picrites. The parental melt is assumed to contain 19 wt% MgO, and its Os abundance is determined by linear regression of the data. There are three samples that fall off the regression trend.

From core to ore: Localisation of Earth's hottest lavas

Volcanic eruptions are as old as the planet itself and have inspired awe, curiosity, and sometimes fear since the dawn of the first humans. These dynamic systems are the surface expression of the Earth's internal heat engine, and demonstrate that our planet is alive internally, as well as externally.

Despite the impressive impact of modern volcanoes, these eruptions and their flows pale in comparison to those that affected our planet in the past. The rarest and most evocative type of volcano is that of the ancient komatiites. These lavas are restricted to the early history of Earth around, 3.4-1.8 billion years ago when the mantle was much hotter. Erupted at temperatures above 1600 °C, they produced hose-like fire fountains, and lava flows that travelled at over 40 kilometres an hour as bluish-white, turbulent lava rivers. These crystallised to form some of the world's most spectacular igneous rocks, as well as giant nickel deposits, mainly in Western Australia and Canada.

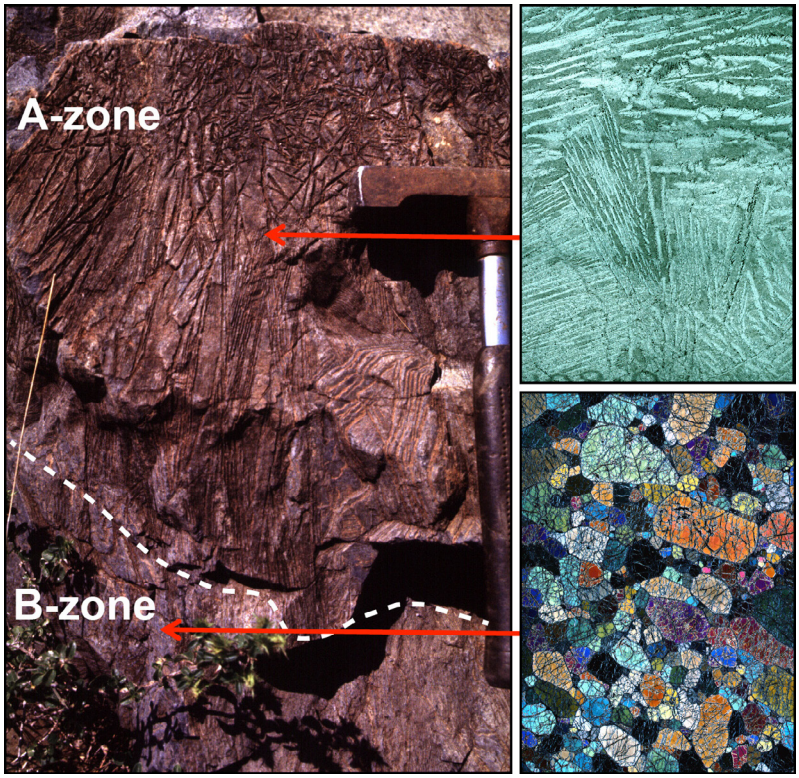

Figure 1. 3.4 billion year old komatiite flow from the Barberton greenstone belt in South Africa, where these ultra-high temperature lavas were first recognised. These lava flows consist of two zones; the A-zone (upper) is dominated by fine, needle-like crystals of olivine called 'spinifex texture', while the B-zone (lower) consists of a solid matrix of olivine crystals, which mark the base of the komatiite lava river.

These volcanic rocks have been studied for over 60 years and have been fundamental in developing our knowledge of the thermal and chemical evolution of the planet. However, until recently we did not understand why they formed where they did. Komatiites are found in ancient pieces of crust, called cratons, preserved from the Archean Eon 3.8-2.5 billion years ago. These cratons contain belts of preserved volcanic and sedimentary material, called greenstone belts. One of the largest cratons is Western Australia's Yilgarn Craton, which hosts most of the gold and nickel ever mined in Australia. This craton contains many greenstone belts but only a few contain major komatiite flows. The uneven distribution of ultra-high temperature lavas is not only a puzzling academic problem, but also is relevant to exploration for nickel ore deposits.

Previous research has demonstrated that komatiites form from mantle plumes - upwelling pipes of hot material that stretch from the outer core to the base of the crust; the modern equivalent is the mantle plume that is forming the Hawaiian island chain. Around 2.7 billion years ago, in a huge global event referred to as a 'mantle turnover', multiple mantle plumes formed, and one impacted the base of the Yilgarn Craton, forming the hottest lavas ever erupted on Earth. When plumes first hit the base of the lithosphere - the 50-250 km thick rigid outer shell of the Earth - they spread out into discs of hot material more than 1000 kilometres in diameter. If the plume covered such a large area, why are komatiites confined to specific linear belts?

CCFS researchers in collaboration with CSIRO and the Geological Survey of Western Australia, set out to answer this question, not by looking at the komatiites, but by studying the slightly younger granites that make up most of the craton. They used Hafnium isotopes in zircon to constrain the age of the rocks that were melted to form the granites and whether they had a mantle or a crustal source. Mapping out the isotopic compositions of the granites revealed a jigsaw pattern in the crust, defined by regions where the granites formed by melting pre-existing, much older crustal rocks, and younger areas where the crust was newly created from sources in the deeper mantle.

Comparing the nature and shape of the ancient continent with the location of the major komatiite events, we found a remarkable correlation. The major komatiite belts and their ore deposits are located at the edge of the older continental regions. This is because of the shape of the base of the ancient Australian continent. As the plume rises, it impacts the older lithosphere first; this is thick and as a result the plume cannot generate much magma. However, the plume flows upwards along the base of the lithosphere, into the shallower, younger areas. Here, huge volumes of magma are generated at the boundary between the old, thick and young, thin areas of the

lithosphere. Subsequently, komatiites, and their nickel deposits, are located at the margins of Earth's early continents.

This project is part of CCFS Theme 1, Early Earth, and contributes to understanding Fluid Fluxes.

Contact: Marco Fiorentini
Funded by: This study was started through ARC Linkage Projects (LP0776780, LP110100667) and finished within the framework of CCFS Flagship Program 2: Genesis, transfer and focus of fluids and metals.

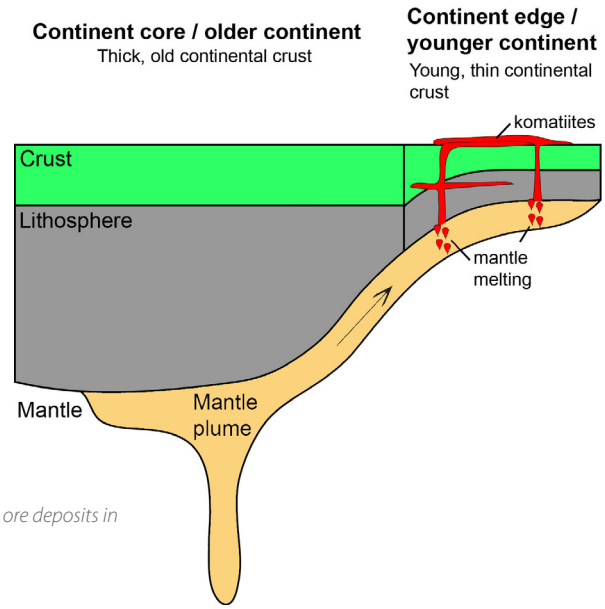

Figure 2. This cartoon demonstrates the main findings of our study. By imaging the older, thicker and younger, thinner areas of ancient lithosphere in the Yilgarn Craton, we were able to map the three-dimensional architecture of the craton and explain why komatiites are localised in specific belts. Plume melts are 'channeled' into the younger, thinner continental areas, resulting in a concentration of komatiites and their associated ore deposits in these areas.

Zircon signposts for base metals

Zircon multi-isotopic maps are a powerful tool for imaging lithospheric blocks of different age, and have been used in the Yilgarn Craton of Western Australia and the Superior Craton in Canada. Such maps combine *in situ* zircon U-Pb and Lu-Hf isotopic analyses. The isotopic mapping serves as a form of '*paleogeophysics*' for imaging ancient lithospheric architecture through time, even when it may not be visible in seismic data

There is a strong spatial correlation between lithospheric boundaries and the concentration of gold in Archean cratons. However, it is unknown whether this is the case for ore deposits in younger orogenic belts such as the world's largest - the Indo-Asian continental collision zone. Therefore, we have chosen the Lhasa Terrane in southern Tibet to examine the relationship between lithospheric architecture and various types of ore deposits in such orogens.

The Lhasa Terrane is the most metal-rich tectonic unit within the Indo-Asian collision zone with a variety of base metal deposits: copper, molybdenum, iron, lead and zinc (Fig. 1). It previously has been subdivided into northern, central, and southern subterranes, based on the differing sedimentary covers and metamorphic basements (Fig. 1). These three subterranes are separated by the Shiquan River-Nam Tso Melange Zone (SNMZ) and the Luobadui-Milashan Fault (LMF) (red lines on Fig. 1).

The zircon Hf-isotope mapping reveals more complex patterns than that defined by surface geology (Fig. 1). In the northern Lhasa subterrane, the western and eastern segments have high and low Epsilon Hf values, respectively, suggesting a juvenile block in the west and an ancient block in the east.

cont...

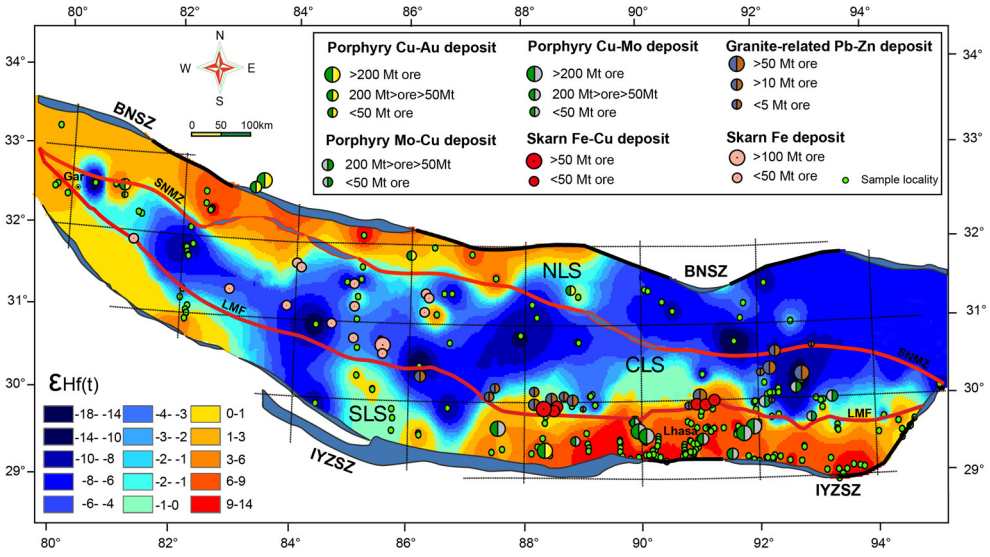

Figure 1. Zircon Hf isotopic mapping of the Lhasa Terrane in Tibet. The colour bands show the Epsilon Hf value of zircons studied. The ore deposits and zircon sample localities are also shown. The warm colours represent relatively juvenile blocks with higher Epsilon (Hf) values, whereas the cold colours represent relatively ancient blocks with lower Epsilon (Hf) values. Abbreviations: IYZSZ = Indus-Yarlung-Tsangpo Suture Zone; BNSZ = Bangong-Nujiang Suture Zone; LMF = Luobadui-Milashan Fault; SNMZ = Shiquanhe-Nam Tso Melange Zone; NLS = Northern Lhasa Subterrane; CLS = Central Lhasa Subterrane; SLS = Southern Lhasa Subterrane.

The central Lhasa subterrane is dominated by low Epsilon Hf values, consistent with it being an ancient Precambrian microcontinent. The southern Lhasa subterrane consists of two isotopically juvenile blocks in the west and east, withan ancient block in the middle (Fig. 1). A time slice map at 215-66 Ma, i.e. the period of orogenic accretion before India collided with Asia, reveals the same pattern for the Lhasa Terrane, suggesting that the lithospheric architecture of the Lhasa Terrane formed in the Mesozoic when two juvenile arcs accreted onto an ancient Precambrian microcontinent (Fig. 2a). A time slice map at 65-12 Ma, during the collision, shows that the eastern segment of the southern Lhasa subterrane is very juvenile, consistent with underplating of mantle-derived magmas generated during the Cenozoic collision (Fig. 2b).

The Mesozoic subduction-related porphyry Cu-Au deposits and Cenozoic collision-related porphyry Cu-Mo deposits are exclusively located in juvenile crust with high Epsilon Hf values (Figs. 1 and 2). The granite-related Pb-Zn deposits cluster in the oldest crustal regions or are developed along the margin of the old crustal block bounded by lithospheric faults (Fig. 1). The porphyry Mo-Cu deposits are localised along the reworked margins of the old crustal block. Skarn Fe-Cu ore deposits are typically localised along a terrane-boundary fault, through which crustally-derived felsic melts mixed with ascending Cu-rich mantle-derived mafic magmas. Skarn Fe deposits are exclusively located in the ancient crustal region (Fig. 1).

These zircon Hf-isotope maps show temporal-spatial relationships between lithospheric architecture and the location of ore deposits, and demonstrate that the structure, nature and composition of the lithosphere controlled the localisation of ore deposits and the migration of ore-forming metals into the crust. Zircon isotopic mapping is a powerful tool to image the lithospheric architecture of an orogenic terrane, and thus may become a robust pathfinder to base-metal deposits.

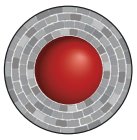

This project is part of CCFS Themes 2 and 3, Earth Evolution and Earth Today, and contributes to understanding Earth's Architecture

Contacts: Yongjun Lu, Zeng-Qian Hou, Cam McCuaig

Funded by: ARC ECSTAR Fellowship, CCFS Foundation Program 9: 4D Lithosphere evolution, CAGS

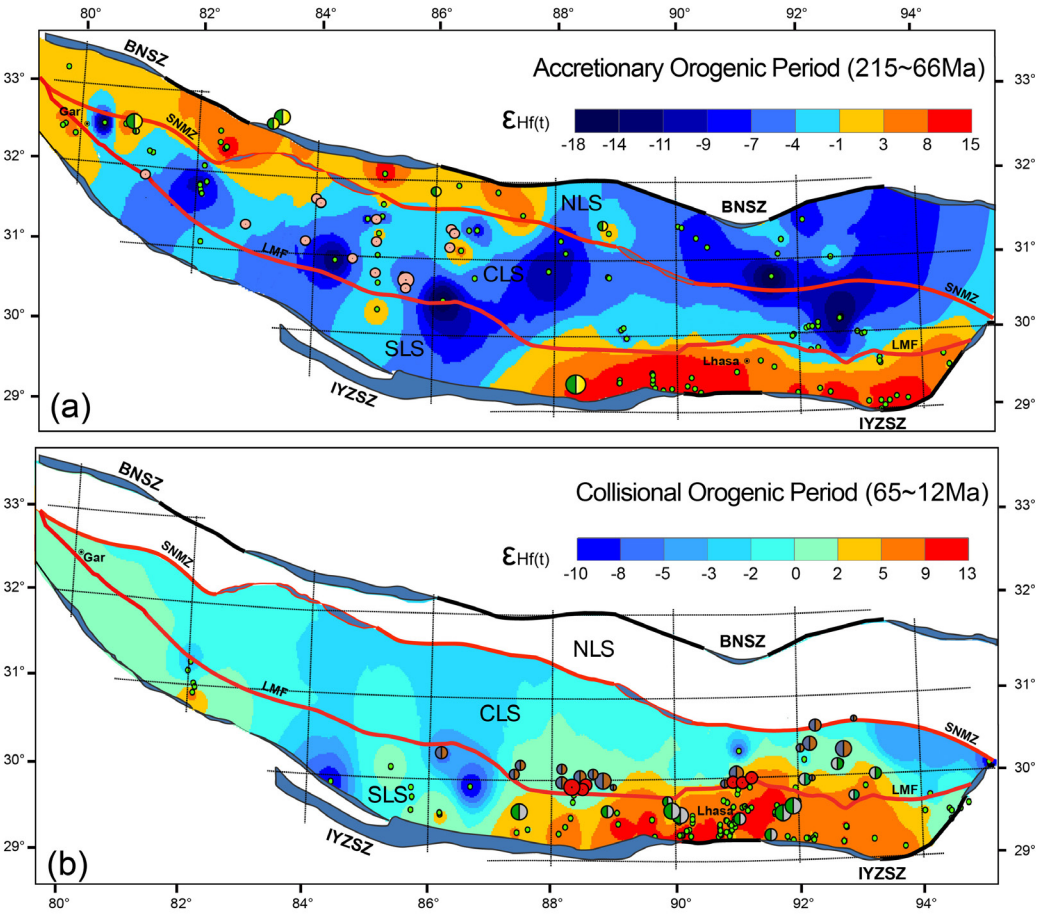

Figure 2. Time slices of zircon Hf isotopic mapping at 215-66 Ma (a) and 65-12 Ma (b). See Figure 1 for Legends.

Dissecting a continental collision with thermochronology

How are ultrahigh pressure metamorphic (UHM) rocks exhumed to the surface from mantle or lower-crustal depths? What happens after two continents collide? The clue could lie in the cooling history of UHP belts and the surrounding rocks, and one of the best-exposed and best-studied UHP terranes is the Dabie-Sulu orogenic belt in eastern China.

zircon (U-Th)/He dating to both the metamorphic rocks and syn- to late-orogenic granitic intrusions in the Sulu UHP belt and the adjacent Jiaobei region. $^{40}Ar/^{39}Ar$ and zircon (U-Th)/He data show that the UHP rocks experienced a prominent cooling event at ca 210-160 Ma (Fig. 1a). The Jiaobei region, underlain by the Archean basement of the NCB and located immediately north of the Sulu UHP belt, experienced a localised exhumation at ~260 Ma as well as a Jurassic (196 ± 9 Ma to 164 ± 7 Ma), westward-younging exhumation (Fig. 1b) that overlaps with the exhumation age of the Sulu UHP belt. The ca 260 Ma exhumation probably reflects tectonic erosion at the southern margin of the NCB in response to the initial continental collision, whereas the Jurassic exhumation may be related to an episode of NW-SE tectonic compression. Hence, the 210-160 Ma exhumation in both the Sulu UHP belt and the Jiaobei region is interpreted to reflect erosion in response to northward thrusting of the UHP rocks and the Jiaobei Archean basement. Overall, our results lend strong support to the continental-collision model of Li (1994) in which both the Sulu UHP rocks and the upper crust of the Jiaobei region moved northward along a mid-crustal detachment plane after the UHP rocks were exhumed to upper-crust levels (Fig. 2).

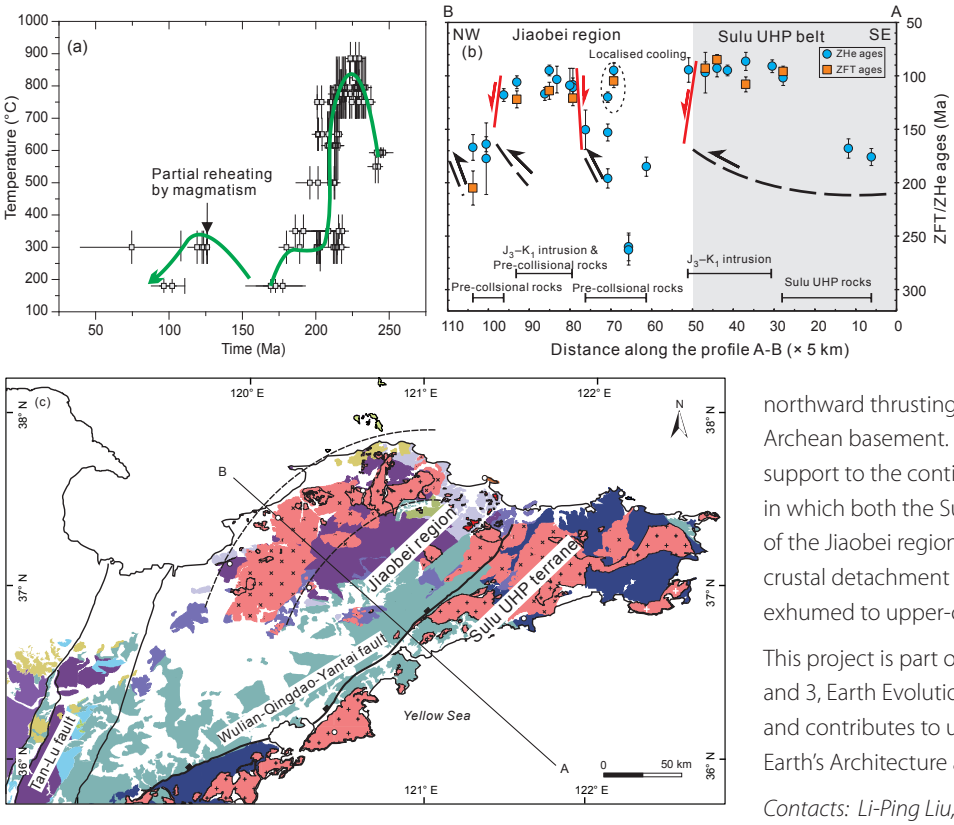

Figure 1. a) Temperature-time path based on zircon U-Pb, and hornblende and mica ^{40}Ar-^{39}Ar ages. b) Profile of ZHe and ZFT ages along the A-B cross section. Ages were projected along the dashed curves in Figure 1c. c) Geological map showing A-B section location.

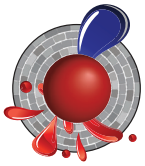

This project is part of CCFS Themes 2 and 3, Earth Evolution and Earth Today, and contributes to understanding Earth's Architecture and Fluid Fluxes.

Contacts: Li-Ping Liu, Zheng-Xiang Li

Funded by: ARC (DP110104799) and NSFC (41325009)

The Dabie-Sulu orogenic belt formed during the collision of the South China Block (SCB) with the North China Block (NCB) in early Mesozoic time. However, a lack of unambiguous kinematic constraints has made it difficult to verify competing models for the mechanisms of continental collision and exhumation of the UHP rocks. We have applied mica and hornblende $^{40}Ar/^{39}Ar$, zircon and apatite fission tracks, and

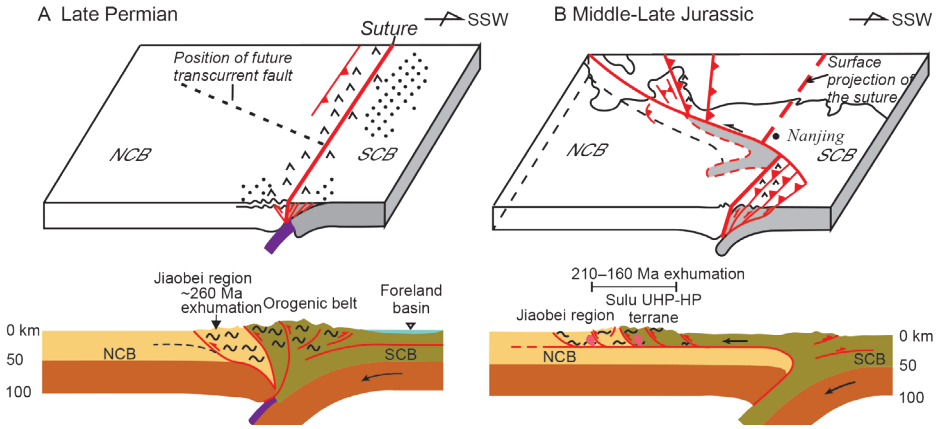

Figure 2. The crustal detachment model that is compatible with observed exhumation events. A) With initial continental collision at ~260 Ma, the Jiaodong region underwent crustal thickening and exhumation. B) By ~210 Ma, the UHP-HP rocks had been exhumed back from the mantle depths to crustal depths. Continuous compression led the UHP-HP rocks to detach from underlying SCB lower crust and move northward along a horizontal detachment until finally climbing the frontal thrust ramp at ~160 Ma. This movement also caused folding and thrusting in the Jiaobei region and exhumation of both the Sulu UHP rocks and the upper crust of the Jiaobei region.

Cryptic chemical fingerprints identify different origins for ancient regions of Western Australia

CCFS, through close collaboration with the Geological Survey of Western Australia, has produced a world-leading isotopic dataset that integrates U-Pb ages and Lu-Hf data from zircons with geological, geochemical, and geophysical information from across Western Australia. This expansive dataset has refined our understanding of the Proterozoic evolution of Australia. One of the most critical, yet controversial, issues relating to Proterozoic reconstructions of the Australian Continent is the nature, or even existence, of Mesoproterozoic links between the Musgrave Province and the Albany-Fraser Orogen.

The Musgrave Province lies between the North and South Australian Cratons, whereas the Albany-Fraser Orogen lies along the southern and southeastern margin of the Archean Yilgarn Craton. These two belts evolved through temporally similar Mesoproterozoic orogenies at 1345-1260 and 1215-1140 Ma, but on completely different basement. The West and North Australian Cratons amalgamated before the 1345-1260 Ma event, which is interpreted to result from the collision of those combined cratons with the South Australian Craton.

The Paleoproterozoic and Mesoproterozoic history of the Albany-Fraser Orogen involved the reworking of the Yilgarn Craton's margin, accompanied by significant juvenile mantle input. The orogen's profile of zircon ages and its Hf- and Nd-isotopic signature reveals an Archean component incorporated into rocks of all ages, which is unequivocally derived from the Yilgarn Craton. The age and isotopic signature of the Albany-Fraser Orogen thus suggests it is an indigenous component of the Yilgarn Craton, rather than an accreted terrane.

This program strand has produced well-defined Nd- and Hf-isotope arrays that track the evolution of the Musgrave Province, through distinct 1950-1900 and 1600-1550 Ma crustal-formation events. Rare non-radiogenic material in the Musgrave Province is only seen in detritus and in magmas that assimilated this material. This evolved detritus, derived from non-Yilgarn and reworked Archean sources, was added to sedimentary basins developed over the Musgrave Province basement from ca 1400 Ma onward. However, the pre-Mesoproterozoic isotopic composition and zircon-age profile for the Musgrave Province is distinctly different from that of the Albany-Fraser Orogen.

If the basement to the Musgrave Province is neither Archean nor part of the West Australian Craton, then what is it? The Madura Province, which lies south of the Musgrave Province, has a radiogenic signature similar to the Musgrave Province and the two provinces probably are contiguous beneath the younger cover sequences. We have found that the crust of the Madura Province contains zircons with 2.0-1.4 Ga mantle extraction ages, and is dominated by juvenile rocks related to oceanic crust that was consumed to the north of the South Australian Craton and east of the West Australian Craton. It appears that the Musgrave Province was formed by modification of Madura-Province crust along the edge of the North Australian Craton. Together, the Musgrave Province and the Madura Province represent Proterozoic Australia's most juvenile crustal remnant.

The new data indicate that the Musgrave Province developed on a juvenile substrate of Madura Province crust that was subducting beneath, and accreting to, the North Australian-West Australian Craton. During the Mount West Orogeny / Albany-Fraser Orogen at ca 1300 Ma, the Musgrave Province was not an along-strike equivalent of the Albany-Fraser Orogen. At that stage, the Musgrave was an active subduction zone, while the Albany-Fraser Orogen was undergoing orogenic collapse following the earlier accretion of the Loongana arc of the Madura Province to the West Australian Craton.

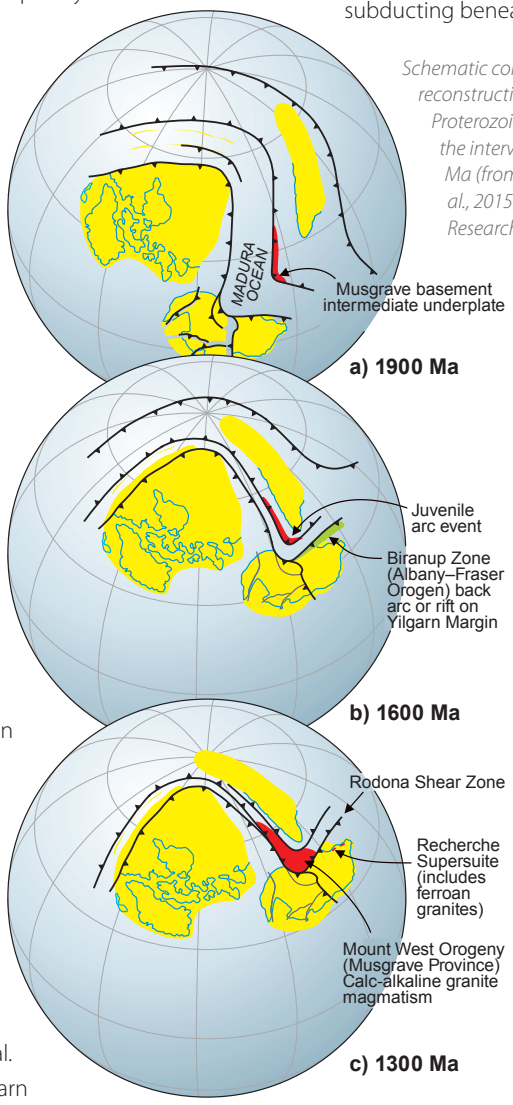

Schematic continental reconstruction of Proterozoic Australia for the interval 1900-1300 Ma (from Howard et al., 2015 Gondwana Research).

This project is part of CCFS Theme 2, Earth Evolution, and contributes to understanding Earth's Architecture.

Contacts: Chris Kirkland, Elena Belousova

Funded by: CCFS Foundation Program 10b.

Mobile lead and spurious zircon ages

Zircons from metasedimentary and metaigneous gneisses in the Napier Complex (East Antarctica) preserve zircon U-Pb ages greater than 3.8 Ga (*Black et al., 1986; Harley, 1997*). The complex underwent two metamorphic events; high-temperature metamorphism at ca. 2.8 Ga (*Kelly and Harley, 2005*) and ultra-high-temperature (T >1100 ºC) at ca 2550-2480 Ma (*Harley, 2000*). The earliest zircon SHRIMP (Sensitive High Resolution Ion MicroProbe) study of the Napier Complex (*Williams et al., 1984*) described isotopic disturbance of >3.4 Ga zircons, defined by reversely discordant analyses (i.e. U-Pb ages older than $^{207}Pb/^{206}Pb$ ages) and within-run instability of Pb during analysis. These results were confirmed recently by ion imaging utilising a Cameca ims 1280 (*CCFS Publications #407, 429*). These studies revealed the patchy distribution of Pb and Ti and identified the presence of unsupported Pb with anomalously high (>4 Ga) $^{207}Pb/^{206}Pb$ ages.

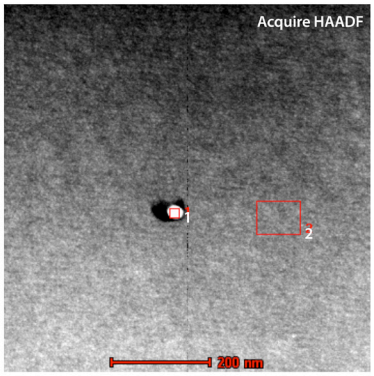

A.

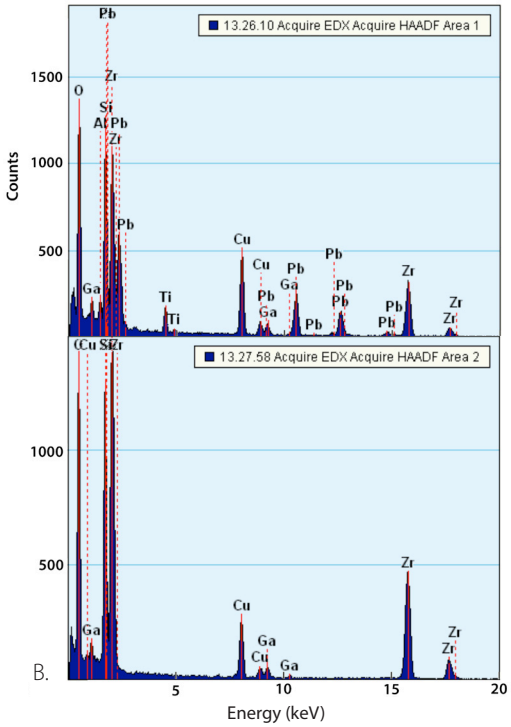

B.

Figure 1. A: High-angle annular dark-field TEM image showing Pb nanosphere. B: EDX spectra of nanosphere rich in Pb and Ti (top) and zircon (bottom).

Following this discovery, we analysed zircons from three samples: one orthogneiss (from Gage Ridge) and two paragneisses (one each from Mount Sones and Dallwitz Nunatak) by TEM (Transmission Electron Microscopy) applying the site-specific focused-ion-beam (FIB) technique at GeoForschungsZentrum (GFZ) Potsdam in Germany. TEM images revealed that zircon grains from the Napier Complex contain randomly distributed, spherical metallic lead nano-inclusions 5-30 nm in diameter (*Kusiak et al., under revision*). They occur either as individual droplets (Fig. 1) or together with unidentified phases rich in Ti and silica, which together constitute melt inclusions ca 20-80 nm in diameter. The occurrence of metallic Pb nanospheres in zircons that underwent UHT metamorphism explains the unusual U-Pb behaviour of such grains during SIMS (Secondary Ion Mass Spectrometry) analysis. Further studies are continuing to determine how the nanospheres may have formed. See *CCFS publications #407, 429.*

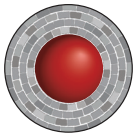

This project is part of CCFS Theme 1, Early Earth, and contributes to understanding Earth's Architecture.

Contacts: Monika A. Kusiak, Simon A. Wilde
Funded by: EU-FP7, Marie Curie grant

References:

Black, L.P., Sheraton, J.W., James, P.R. 1986. Late Archean Granites of the Napier Complex, Enderby Land, Antarctica - a Comparison of Rb-Sr, Sm-Nd and U-Pb Isotopic Systematics in a Complex Terrain. *Precambrian Research, 32, 4, 343-368.*

Harley, S.L., Black, L.P. 1997. A revised Archaean chronology for the Napier Complex, Enderby Land, from SHRIMP ion-microprobe studies. *Antarctic Science, 9, 74-91*

Harley, S.L., Motoyoshi, Y. 2000. Al zoning in orthopyroxene in a sapphirine quartzite: Evidence for >1120 ºC UHT metamorphism in the Napier Complex, Antarctica, and implications for the entropy of sapphirine. *Contributions to Mineralogy and Petrology, 138: 293-307.*

Kelly, N.M., Harley, S.L. 2005. Timing of zircon growth during highgrade metamorphism: Constraints from garnet-zircon REE. *Geochimica et Cosmochimica Acta, 69. 10, A22-A22.*

Kusiak, M.A. et al., under revision. Metallic lead nanospheres discovered in ancient zircons. *Proceedings of the National Academy of Sciences of the United States of America.*

Williams, I.S., Compston, W., Black, L.P., Ireland, T.R., Foster, J.J. 1984. Unsupported Radiogenic Pb in Zircon - a Cause of Anomalously High Pb-Pb, U-Pb and Th-Pb Ages. *Contributions to Mineralogy and Petrology, 88, 4, 322-327.*

The Hadean - Archean crust-mantle revolution: How should we divide the Archean?

When and how did the continents on which we live form and stabilise in the torrid early history of our evolving planet? We have used the mineral zircon as time capsules to record the history of events in the Earth's crust from trace-element and isotopic data (U-Pb and Lu-Hf). Sulfide minerals and metal alloys from mantle-derived samples (brought to the Earth's surface by magmas from 50 to 600 km deep), record the history of fluid, melting and formation events in the mantle using the Re-Os isotopic system. The combination of these two powerful tools allows time travel back to early Earth times and has produced some rare insights, changing our understanding of the timing of significant ancient upheavals that shaped Earth's crust.

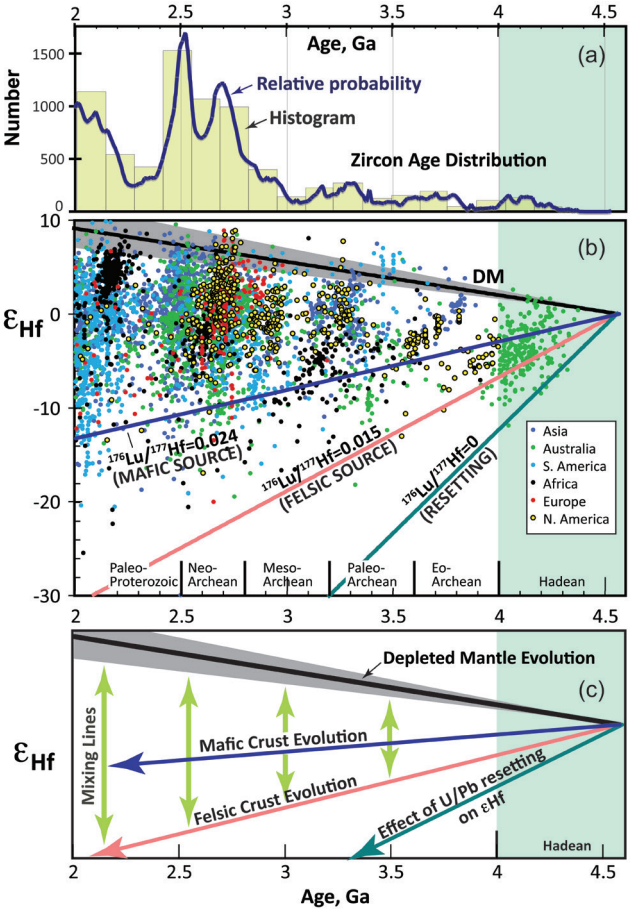

Figure 1. εHf vs age for zircons worldwide, divided by region. The database (n=6699) builds on the data of Belousova et al. (2010) updated with >2000 analyses published, and/or produced in our laboratories, after 2009. The conventional subdivision of the Hadean and Archean is shown along the X axis. (a) zircon age distribution shown as a histogram and a cumulative-probability curve. (b) distribution of Hf-isotope data. The "juvenile band", defined as ±0.75% of the εHf of the Depleted Mantle line at any time, is shown as a grey envelope. Evolution lines from 4.5 Ga are shown for reservoirs corresponding to typical mafic rocks ($^{176}Lu/^{177}Hf = 0.024$), the average continental crust ($^{176}Lu/^{177}Hf = 0.015$), and zircons, approximated by $^{176}Lu/^{177}Hf = 0$. (c) shows these evolution lines.

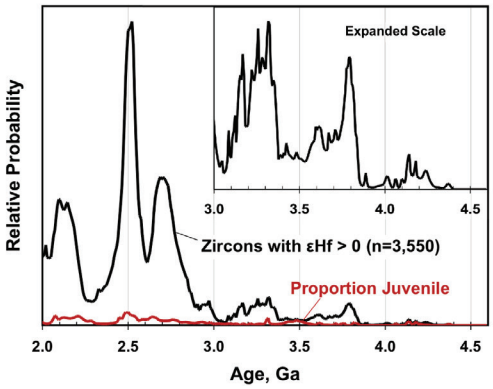

Figure 2. (a) Cumulative-probability curve and age histogram for all zircons with εHf falling within 0.75% of the Depleted Mantle curve in Figure 1. Inset uses an expanded scale to show detail in the oldest datasets.

We have integrated a worldwide compilation of the ages of crust and mantle events from 2 billion years ago until nearly the time of formation of planet Earth at ~4.5 billion years, allowing us to track patterns of evolution of the crust, and interaction between the mantle and crust. These data show that from about 4.5 to 3.4 billion years ago, the Earth's crust was essentially stagnant (like a lid on a hot cauldron), and was mainly basaltic in composition.

Data suggest that some zircons crystallised from magmas that were possibly generated by impact melting from bombarding planetary bodies (meteorites large and small). Pulses of magmatic activity at about 4.2, 3.8, and 3.3-3.4 billion years, possibly representing mantle convective overturns or rising mantle plumes, broke this quiescent state.

Between these pulses, there is evidence of resetting of zircon U-Pb ages (by impact?) but the Hf-isotope data (Fig. 1) allow us to see back through such events and imply that there was no further generation of new crust. There is thus no evidence of plate-tectonic activity, as described for the Earth in the state we know it today (i.e. through the Phanerozoic Era), before about 3.4 billion years ago. Previous modelling studies indicate that the early Earth may have been characterised by an episodic-overturn, or a stagnant-lid, regime. New thermodynamic modeling (*CCFS Publication #488*) confirms that an initially hot Earth could have a stagnant lid for ca 300 million years, and then experience a series of massive overturns at intervals on the order of 150 Ma, until the end of the EoArchean Period (earliest Archean time). The lack of older Os model ages (Fig. 2) suggests that subcontinental lithospheric mantle (SCLM) sampled on Earth today did not exist before about 3.5 billion years ago.

A lull in crustal production around 3.0 billion years coincides with the rapid buildup of Mg0-rich, buoyant SCLM, which peaked around 2.7-2.8 billion years; this pattern is consistent with one or more major mantle overturns. The generation of continental crust peaked later in two main pulses at about 2.75 and 2.5 billion years ago (*Belousova et al., 2010*). The age/Hf-isotope patterns of the crust generated from 3.0-2.4 billion years are similar to those in old tectonic regions of the Gondwana supercontinent, implying the existence of plate tectonics at the time of assembly of the ancient supercontinent (Kenorland)

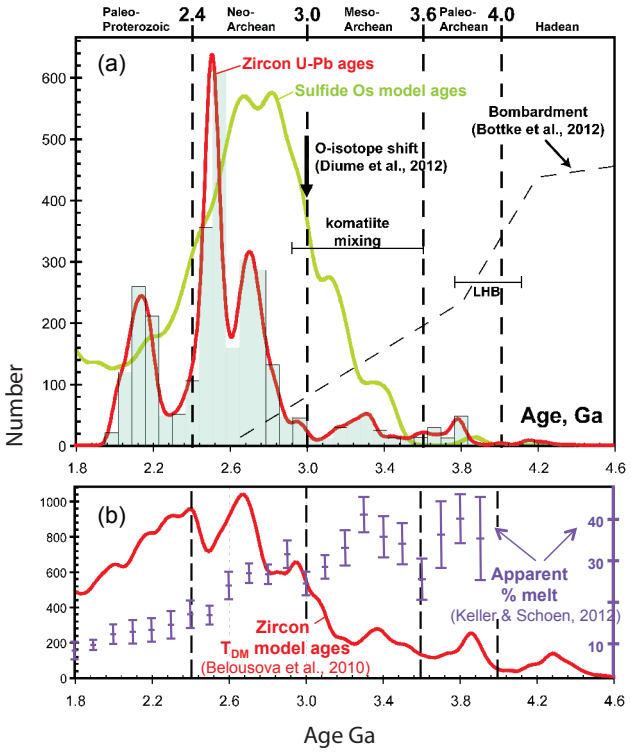

Figure 3. Summary of crust-mantle evolution. Grey histogram shows distribution of all zircons in the database for the time period shown; red line shows the probability distribution of these ages. Green line shows distribution of Re-Os TRD model ages for sulfides in mantle-derived xenoliths and xenocrysts. The revised distribution of meteorite bombardment intensity (Bottke et al., 2012) and a generalized summary of older interpretations of the "Late Heavy Bombardment" is shown as LHB. The homogenization of PGE contents in komatiites from 3.5-2.9 Ga (Maier et al., 2010) may mark the major mantle-overturn/circulation events discussed in the text. The O-isotope shift noted by Dhuime et al. (2012) marks the beginning of a quiescent period, or perhaps the destruction of the crust during the major overturns from 3.5-2.9 Ga.

ca 2.5 billion years ago. We have demonstrated a clear link in these data between the generation of the SCLM and the emergence of modern plate tectonics; we consider this link to be causal, as well as temporal.

The *International Geologic Time Scale* sets the Hadean-Archean boundary at 4.0 Ga and divides the Archean into four approximately equal time slices (Fig. 1): Eo-Archean (4.0-3.6 Ga (Ga = billion years ago)), Paleo-Archean (3.6-3.2 Ga), Meso-Archean (3.2-2.8 Ga) and Neo-Archean (2.8-2.5 Ga). There is no apparent evidence in the present datasets for these divisions, and we suggest a simplified subdivision, based on the changes in tectonic style (Fig. 3) at identifiable times.

In the absence of better data, we accept the Hadean-Archean boundary at 4.0 Ga, although we suggest that the stagnant-lid regime may have continued for another 500-800 million years. We propose that the term *Eo-Archean* be discarded, since there is little preserved evidence of magmatic activity between 4.2 and 3.8 billion years, and that the term *PaleoArchean* be used for the period 4.0-3.6 billion years; this timespan contains the oldest preserved crust, and inferred evidence for one major overturn. *MesoArchean* could be applied to the period 3.6-3.0 billion years, during which overturns became more prominent, ending with the buildup toward the major 2.8-2.55 billion years, magmatism that accompanied the building of the bulk of the Archean SCLM. NeoArchean can be usefully applied to the period 3.0-2.4 billion years, which marks a *new tectonic style* with frequent plume activity, the beginning of some form of plate tectonics, and the preservation of large volumes of continental crust. The zircon data suggest that this activity continued up to about 2.4 billion years ago, and then ceased quite abruptly, marking a natural end to the Neo-Archean period, and heralding a new geotectonic regime for Earth.

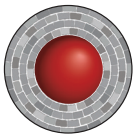

This project is part of CCFS Themes 1 and 2, Early Earth and Earth Evolution, and contributes to understanding Earth's Architecture.

Contacts: Bill Griffin, Elena Belousova, Suzanne O'Reilly
Funded by: CCFS Foundation Program; TARDIS: Tracking ancient residues distributed in the silicate Earth, Future Fellowship to Elena Belousova

Research highlights 2015

Contents

COPA: the Capricorn Orogen Passive-source Array

The SIEF Project

In 2013, a major Science and Industry Endowment Fund (SIEF) project, the "*UNCOVER Australia: Capricorn Distal Footprints Project*" was awarded to CSIRO, UWA, Curtin and GSWA. The SIEF project is one of the largest multi-method surveys attempted in Australia and aims to image the lithosphere from very shallow to its deeper levels. The project builds on current knowledge to deliver improved understanding of the evolution and controls on mineral systems in the Capricorn. The end goal is to apply these generic learnings elsewhere in order to develop a set of integrated large-scale geological and geophysical datasets that can assist in constraining whole lithosphere architecture and tectonic evolution and boost exploration discovery success in covered terrains in Australia

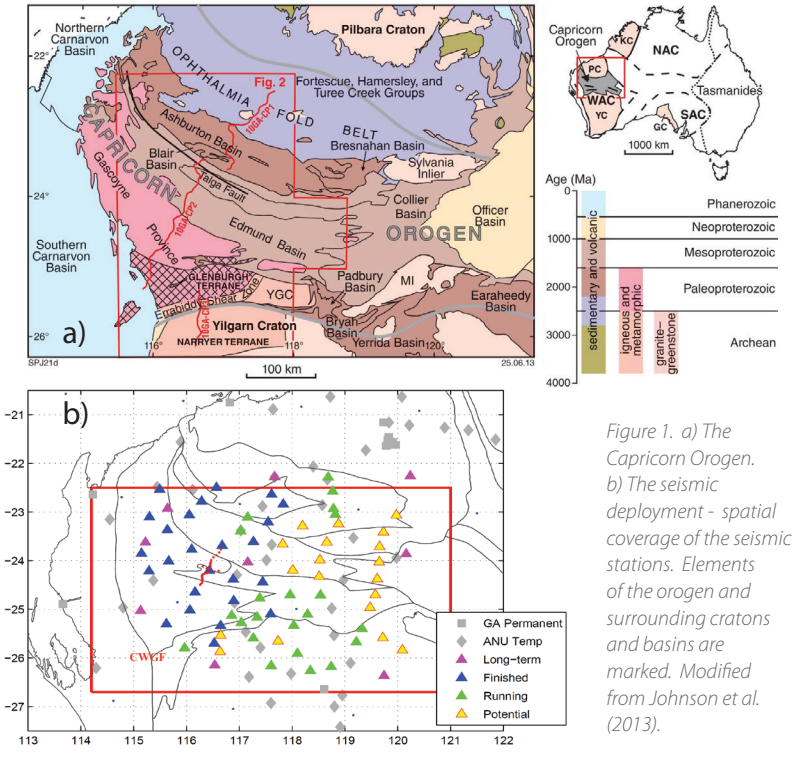

Figure 1. a) The Capricorn Orogen. b) The seismic deployment - spatial coverage of the seismic stations. Elements of the orogen and surrounding cratons and basins are marked. Modified from Johnson et al. (2013).

The Capricorn Orogen

The Capricorn Orogen of Western Australia is a 1000 km long, 500 km wide region of variably deformed rocks located between the Pilbara and Yilgarn Cratons (Fig. 1a, right). It records the Paleoproterozoic assembly of these cratons to form the West Australian Craton, and over one billion years of intracratonic reworking that followed. Owing to this reworking, the location of major crustal structures and the broad architecture of the orogen are poorly constrained. To improve the exploration potential of the region, a better understanding of the crustal architecture across the orogen is critical, especially identification the location and orientation of major crustal structures and craton edges, as well as any island arcs, or exotic accreted crustal material (*Johnson et al., Australian Journal of Earth Sciences, 2013*; Fig. 1a).

The COPA Deployment

The overall goal is to integrate other geological and geophysical datasets and produce 3D multiple-scale seismic images across the orogen. This will provide direct constraints on local geological models for the timing and kinematic evolution of faults and shear zones in the region and its 4D metallogenic history. We will also provide new insights on the tectonic amalgamation of the Western Australian craton. The main tools of the project are seismic tomography (body waves and surface wave/ambient noise) and receiver function CCP imaging. These two commonly used earthquake-seismology methods best fit the 2D design of the passive source project.

With a careful design of a 2D array that takes advantage of previous passive-source studies in the region, the proposed long-term and short-term deployments give us a 2D grid that spans a nearly 500 km by 500 km surface area. Station spacing is roughly 40 km and the 36 months in total deployment will guarantee enough data recording for 3D structure imaging using body wave tomography, ambient noise surface wave tomography and P- and S-wave receiver function Common Conversion Point (CCP) stacking techniques. 34 sets of seismometers loaned from the ANSIR national instrument pool (with 2 as backup) have been deployed in the western half of the orogen since March 2014.
In October 2014 a 25-site High-resolution Passive Source (HPS) array was also deployed, with varying 2, 4, and 8 km station spacing to focus on shallow crustal structure across the Collier Basin, Edmund Basin and the Gascoyne Province. The HPS array was deployed in October 2015.

Preliminary Results: Bulk Crustal Structure

In the passive-source studies, we will test several hypotheses that 1) distinct crustal blocks are seen continuously throughout the orogen (using ambient noise/body wave tomography); 2) distinct lithologies are present in the crust and upper mantle across the orogen (using receiver function CCP images); and 3) crustal and lithosphere deformation along craton margins in general follows '*wedge*' tectonics (e.g. subduction of juvenile blocks under the craton mantle, on craton-ward dipping sutures; *Snyder, Tectonophysics, 355, 7-22, 2002*).

Preliminary results of the crustal structure in the orogen are available from seismic receiver functions. A simple H-k stacking technique (*CCFS publication #649; Research highlight p. 196*) stacks available receiver functions to obtain an optimum pair of bulk crustal thickness (H) and Vp/Vs ratio (k; equivalent to Poisson's

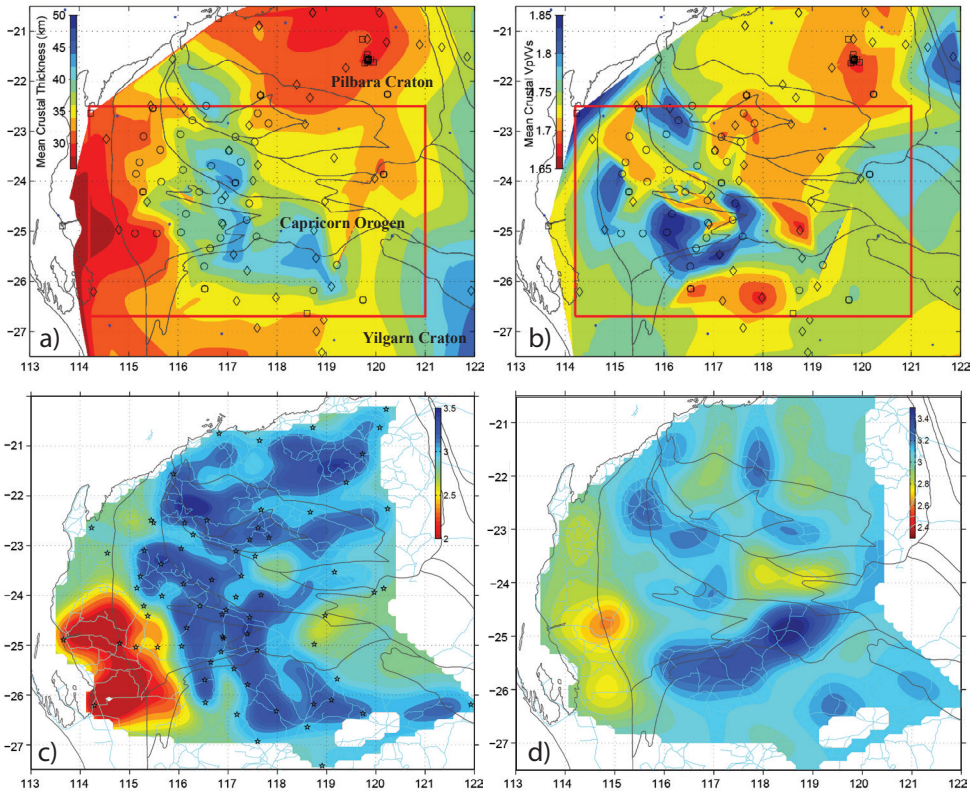

Figure 2. Preliminary results from the COPA deployment. a) and b), mean crustal thickness (in km) and Vp/Vs ratio. c) and d), shear wave velocity maps from ambient noise showing peak period at 2.5 s and 15 s, corresponding to maximum sensitivity at 3 and 20 km, respectively.

ratio; an indicator of crustal rock composition). The maps show bulk crustal thickness, Vp/Vs ratio, bulk crustal Vp velocity and the crustal density anomaly from gravity inversions. The western Capricorn Orogen is thicker, denser and higher-velocity, compared to the two cratons. Compositionally the western orogen is complex - it may indicate that different terranes of deformation processes were involved during the amalgamation of the WA craton in the Proterozoic. The northern margin of the Yilgarn Craton shows anomalously thicker, denser and higher velocity crust, and abrupt changes in the crustal conductivity are also observed in the MT study.

A tomographic inversion using ambient noise is currently being conducted to obtain shear wave velocities in a 3D volume of the orogenic crust. Available data for all possible station pairs are cross-correlated and stacked to obtain the empirical surface wave traveling between the station pair. Phase and group velocities can be measured for each station pair, which forms a path in a tomographic problem. Figure 2 shows the group velocity tomographic results at period 2.5 s (~3 km peak depth); and period 15 s (mid-crust). Significant structural differences are evident in the shallow and mid-crust. The high-velocity northern margin of the Yilgarn Craton is prominent, as seen previously in the receiver functions and MT images. The 3D tomographic model of shear velocity is under construction. More data are expected from the deployment to push the imaging capability to the lower crust, and to extend the horizontal coverage in the eastern Capricorn Orogen by April 2017.

cont...

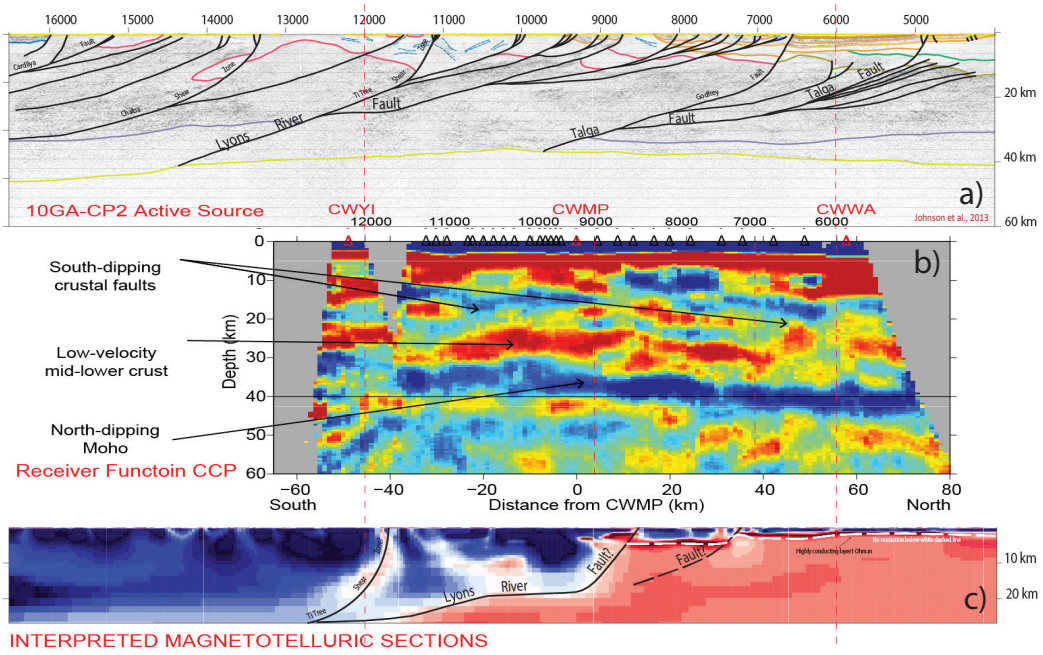

Figure 3. Comparison of the crustal scale results along the high resolution line from the active source (a; Johnson et al., 2013), the passive source CCP stack (b; this study); and the MT (c; Heinson et al., 2012). Note the prominent Moho interface, the truncations of crustal discontinuities, and the low-velocity mid- to lower crust inferred from the negative velocity contrast.

Preliminary Results: A High Resolution Crustal Cross-section

A receiver function CCP (common-conversion-point) stack is applied to the high resolution line (HPS) to reveal crustal discontinuities. The results show good correlation with the active source and magnetotelluric studies (*Johnson et al. 2013; Heinson et al., GSWA Report 2012*). The passive source CCP image shows comparable crustal structures: north-dipping Moho; and south-dipping crustal faults (truncated crustal discontinuities). A slow-velocity mid- to lower crust is inferred from the negative velocity gradients in the centre of the array, consistent with the ambient noise observations, and the highly conductive mid-crust in the MT image.

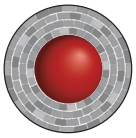

This project is part of CCFS Theme 3, Earth Today, and contributes to understanding Earth's Architecture.

Contact: Huaiyu Yuan
Funded by: CCFS Flagship Program 7, SIEF

The sulfur cycle in the Palaeoproterozoic Earth

The Earth's crust is a complex and dynamically evolving chemical interface between two convective fluid systems: the endosphere (linked core and mantle) and the exosphere (linked hydrosphere and atmosphere). The nature of the physical and chemical processes that occur on the surface of the planet are intimately linked by the energy available from the sharp chemical and thermal gradients that exist across this interface. On modern Earth, island/volcanic arcs are the direct consequence of subduction processes that occur at convergent plate boundaries, and are the factories where juvenile continental crust is formed and where explosive volcanic eruptions emit large quantities of gases into the atmosphere. There remains considerable uncertainty with respect to the key processes that occurred during the transition from the Archaean to the modern Earth. One of the key questions is whether ancient arcs behaved similarly to modern ones. The fragmented geological record of the Palaeoproterozoic (2.5-1.6 billion years ago) and Archaean (>2.5 billion years ago) eons makes it difficult to answer these questions with any certainty, allowing for a proliferation of inferences and unanswered questions.

A key insight into this knowledge gap comes from better understanding the shift in the isotopic signature of sulfur through time. Sulfur is a key volatile element that is cycled between the different crustal and mantle reservoirs during arc magmatism, and thus may be used as a tracer. However, the cycle of sulfur between the inner parts of our planet and the atmosphere in the Palaeoproterozoic remains poorly constrained. As a result, our understanding of the development of early life and many other earth processes in which sulfur plays a key role, including climate change, biological evolution and ore deposit genesis, have been hindered. We need isotopic markers that can trace the sources and map the path of this element through the uppermost layers of the upper mantle and crust (the lithosphere).

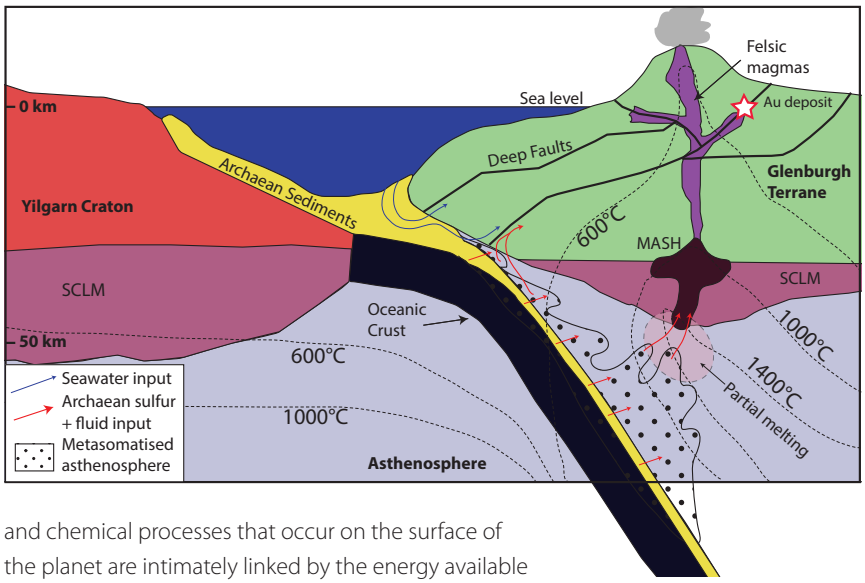

Figure 1. Schematic section through the Glenburgh continental arc system at ca 2.0 Ga, prior to collision between the Archean Glenburgh Terrane and Yilgarn Craton. This diagram highlights the development of a MASH (Melting, Assimilation, Storage, Homogenisation) zone where mafic magmas generated from partial melting of the metasomatised asthenosphere and subcontinental lithospheric mantle (SCLM) pool at their level of neutral buoyancy and differentiate into more buoyant felsic melts, which then ascend through the crust along major fault zones to produce the felsic magmatism, i.e. the Dalgaringa Supersuite, observed in the Glenburgh Terrane. Archaean sulfur and gold bearing fluids would also travel up these deep faults where they may interact with seawater, generating the observed sulfur isotope 'mixing line'.

The discovery of the presence of anomalous mass-independent fractionation of sulfur (MIF-S) signatures in Archaean sedimentary rocks provides a revolutionary way to probe the global sulfur cycle. These anomalies occur because in the ancient atmosphere, which lacked ozone, cosmic radiation could produce isotopes (such as ^{33}S) that are not formed now. This study focuses on the Palaeoproterozoic Glenburgh sulfur-bearing gold deposit, which is a natural laboratory ca 2 billion years old, hosted in the Glenburgh arc of Western Australia. Because this arc developed at the margin of a subducting Archaean block, we applied multiple sulfur isotope analysis as a chemically conservative tracer to test whether Archaean MIF-S sulfur could

be detected. Results show that Archaean sulfur can be traced throughout the Palaeoproterozoic Glenburgh arc (Fig. 1).

This is an extraordinary discovery as it provides key constraints on the sources of volatiles and metals in arc environments. This is still a heavily debated topic, as there is a mass-balance problem between the known concentrations of these elements in the mantle wedge below arc systems and the observed concentrations in arc magmas and associated mineralisation. Some workers have suggested that, particularly in the case of gold deposits formed in continental arcs, the ultimate source of gold is from subducted carbon-rich sedimentary rocks attached to the downgoing slab. In fact, since gold is insoluble in H_2O, it is thought that it may be mobilised in the form of Au sulfide complexes in fluids at high temperatures and pressures, such as those found in arc magmatic environments. Therefore, the isotopic composition of sulfide should also reflect a similar source, as is demonstrated in the dataset presented in this study.

The application of spatio-temporally constrained chemically conservative isotopic tracers such as MIF-S is critical for a better understanding of tectonic processes that drive fluid and metal transfer from Archaean cratons into their reworked margins and the operation of arc magmatism. At the Glenburgh deposit, mixing between sulfur isotope end-members (Paleoproterozoic seawater-derived sulfate and Archaean shale-derived pyrite; Fig. 2) is, in effect, recording the progressive closing of an ocean and a tectonic switch from subduction of oceanic crust to the onset of continent-continent collision with the Yilgarn Craton. Hence, multiple sulfur isotope data are able to image a process that is cryptic in most other currently available datasets, showing that sulfur cycling in arc settings occurs on very large scales, from the atmosphere-hydrosphere through to the lithosphere during crustal generation. If this happened in the Archean, it presumably could have happened throughout geological history, although we have no equivalent tracers for post-Archean processes.

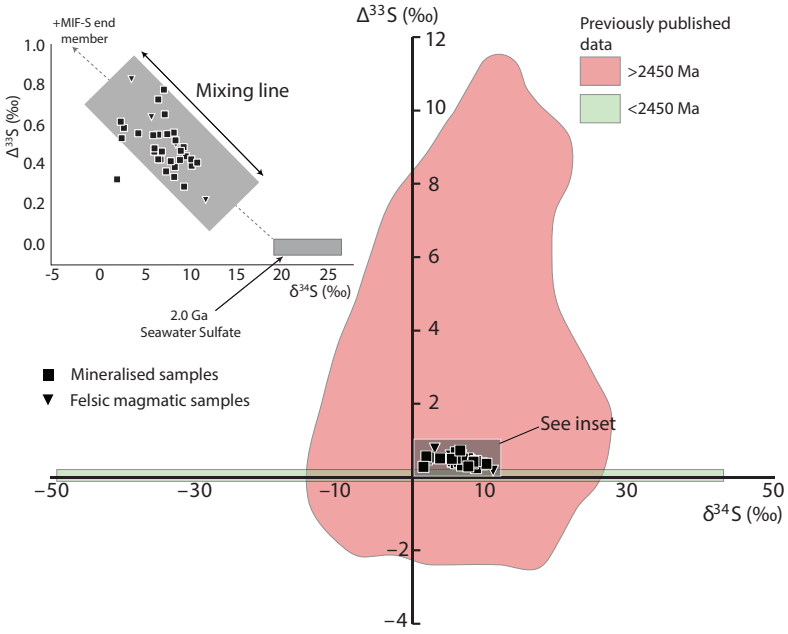

Figure 2. $\Delta^{33}S$ versus $\delta^{34}S$ from Glenburgh (this study) compared to previously published S-isotope data. Points shown have error bars smaller than the size of the points in all cases.

This project is part of CCFS themes 2 and 3, Earth's Evolution and Earth Today, and contributes to understanding Earth's Architecture and Fluid Fluxes.

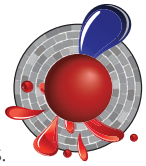

Contacts: Vikraman Selvaraja, Marco Fiorentini, Crystal LaFlamme, Boswell Wing

Funded by: MRIWA Distal Footprint Capricorn Study, umbrella of - but not funded by - CCFS Flagship Program 4

Primitive pyroxenites delaminated from ancient island arc

One of the major debates of modern petrology, known as the continental crust paradox, arises essentially from the discrepancy between the net basaltic output of modern arc magmatism and the average andesitic composition of the continental crust. If any post-Archean continental crust was to be made by arc magmatism, this paradox needs to be resolved. Among the potential explanations is that the mafic-ultramafic counterpart of the differentiated felsic crust had to be removed. After being postulated theoretically, and explained numerically and experimentally, the delamination (i.e. convective removal) of dense arc cumulates has been seismically evidenced. However, field evidence for this key geological process has been hard to find.

In north-western Spain, the Herbeira massif of the Variscan Cabo Ortegal Complex hosts one of Earth's rare exposures of sub-island-arc mantle. New field and petrographic investigations of this 600 m-thick mafic-ultramafic section have defined a crystallisation sequence of primitive cumulates (dunites ± chromitites, wehrlites and olivine websterites). Their particularly high CaO/Al_2O_3 (2.2-11.3), high concentrations of compatible elements and a signature of high large ion lithophile elements (LILE) / high field strength elements (HFSE) implies a origin from unusual arc magmatism. High-Ca parental melts of *cont...*

Figure 1. The Herbeira cliffs (621 m) of northern Galicia, Spain are the highest sea cliffs in continental Europe. They expose the largest mafic-ultramafic section of the Cabo Ortegal Complex, one of the only sub-island-arc mantle exposures in the world.

boninitic to picritic affinities were generated from shallow (<2 GPa) fluid-fluxed melting of a refractory lherzolite, involving carbonatite metasomatism. Following dynamic melt-rock interaction at shallower depths (<1.2 GPa), massive websterites and rare opx-rich websterites were produced. Chromatographic reequilibration accompanied the late magmatic migration of residual melts, which produced a wide range of rare-earth-element (REE) patterns.

Textural observations and preliminary electron back-scattered diffraction (EBSD) data indicate that Cabo Ortegal pyroxenites and their host peridotites record the development of sheath folds and mylonites during high shear-strain deformation, following high-temperature deformation. Peak metamorphism was reached under eclogite-facies conditions (1.6-1.8 GPa and 780-800°C) and exhumation into amphibolite-facies conditions then occurred. This complex tectonothermal record encapsulates delamination, high-pressure metamorphism, and exhumation of the arc root, which resulted from gravitational instabilities and subduction-channel processes.

The Herbeira massif thus may represent the first recognised piece of delaminated arc root, which originated as primitive boninitic to picritic cumulates in a peridotite matrix. It may offer insights into the problem of the '*andesitic*' continental crust.

This project is part of CCFS themes 2 and 3, Earth's Evolution and Earth Today, and contributes to understanding Earth's Architecture and Fluid Fluxes.

Contacts: Romain Tilhac, Hadrien Henry, Sue O'Reilly, Bill Griffin, Norman Pearson, Michel Grégoire, Georges Ceuleneer (Géosciences Environnement Toulouse, GET, France).

Funded by: Flagship Program 1, iMQRES scholarships, EPS postgraduate funds, CNRS funds (M. Grégoire, G. Ceuleneer). Two cotutelle programs between Macquarie and Paul Sabatier University, Toulouse, France have been established for the study of the Cabo Ortegal Complex.

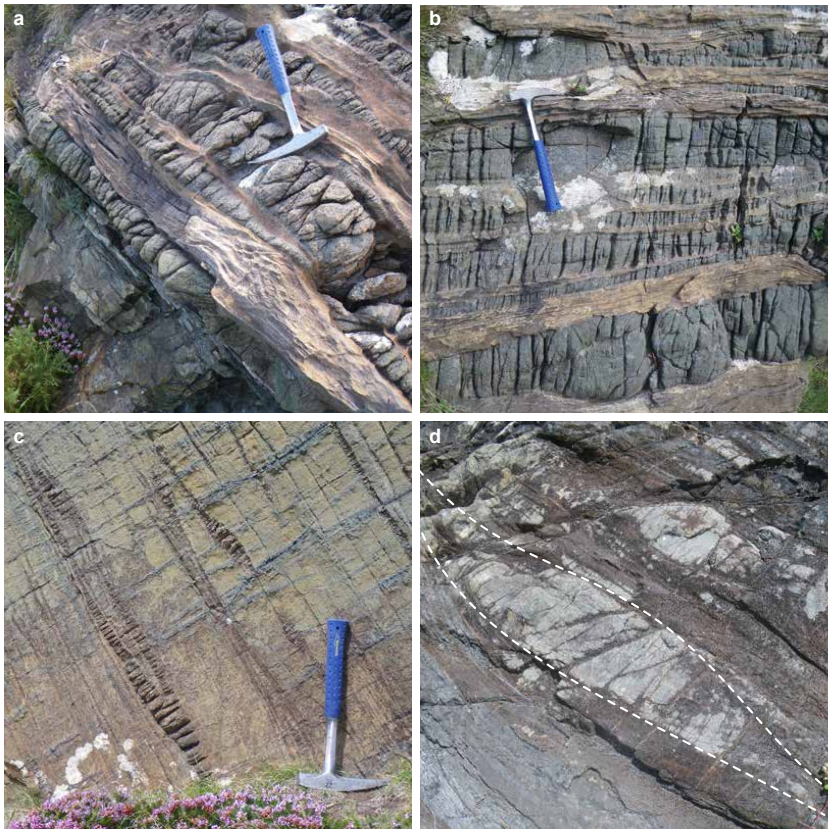

Figure 2. Typical exposures of Cabo Ortegal pyroxenites and dunites (a and b); individual pyroxenite layers may reach up to 3m thickness. Boudinaged pyroxenite layers in harzburgites bear witness to deformation under high-temperature conditions (c). The characteristic sigmoid shape of sheath folds developed from high shear strain of pyroxenites (d) and peridotites during delamination and subduction.

Extreme lithium isotopic fractionation in three zircon standards (Plešovice, Qinghu and Temora)

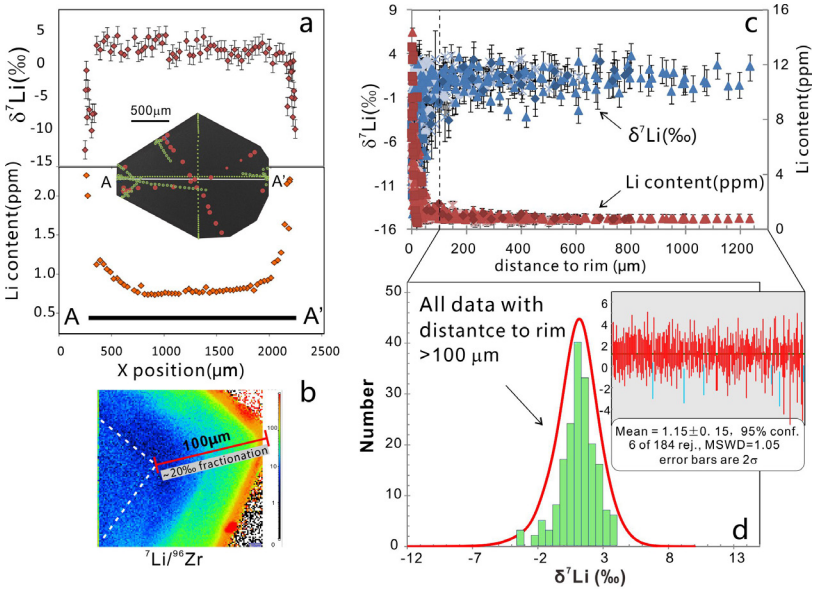

Figure 1. a) Trace outlines on the CL image of Plešovice-R show the position of the Li isotopic and [Li] measurements by SIMS; b) The ion image of the variation of Li and Y content (bright colours = higher concentration); c) δ^7Li and [Li] vs relative distance to the rim; d) Probability density plot and weighted average of analysed spots more than 100 μm from the rim.

Li isotopes in zircon are a new isotopic tracer for studying the origin and genesis of granitoid rocks and their implications for the early Earth evolution. However, there is still controversy as to whether Li isotopes in zircon retain their magmatic signatures or are modified by later processes. To understand Li behaviour in zircons, we have analysed Li isotopes and abundance in crystals of three zircon standards (Plešovice, Qinghu and Temora) commonly used for microbeam analysis of U-Pb age and O-Hf isotopes. We have also mapped Li concentration ([Li]) (image: 150 μm × 150 μm) on selected grains, using a Cameca 1280HR Secondary Ion Mass Spectrometer (SIMS). All zircon grains have a rim 5-20 μm wide in which [Li] is 5 to 20 times higher than the in core. Large isotopic fractionations (up to ~20‰) are observed in thin zircon rims (~50 μm) of single grains. The measured δ^7Li values range from -14.3 to +3.7‰ for Plešovice, -22.8 to 1.4‰ for Qinghu and -4.1 to 16.1‰ for the Temora zircon. The [Li] and δ^7Li are highly variable at the rims but relatively homogenous in the cores of the grains. From zircon rim to core, the [Li] decreases rapidly, while the δ^7Li increases, suggesting that the large isotopic variation of Li in zircons could be caused by diffusion. Our data demonstrate that areas with homogeneous δ^7Li in the cores of large zircon grains can retain the pristine isotopic signatures of the magmas, while analysis of bulk-rocks and/or mineral separates might produce false data: values representing mixing of rims and cores.

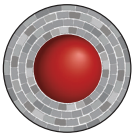

This project is part of CCFS Theme 2, Earth's Evolution, and contributes to understanding Earth's Architecture.

Contacts: Yu-Ya Gao, Xian-Hua Li, Bill Griffin, Yan-Jie Tang, Norman Pearson, Yu Liu, Mei-Fei Chu, Qiu-Li Li, Guo-Qiang Tang, Sue O'Reilly

Funded by: National Natural Science Foundation of China, Ministry of Science and Technology, MUIPRS, CCFS Flagship Program 1

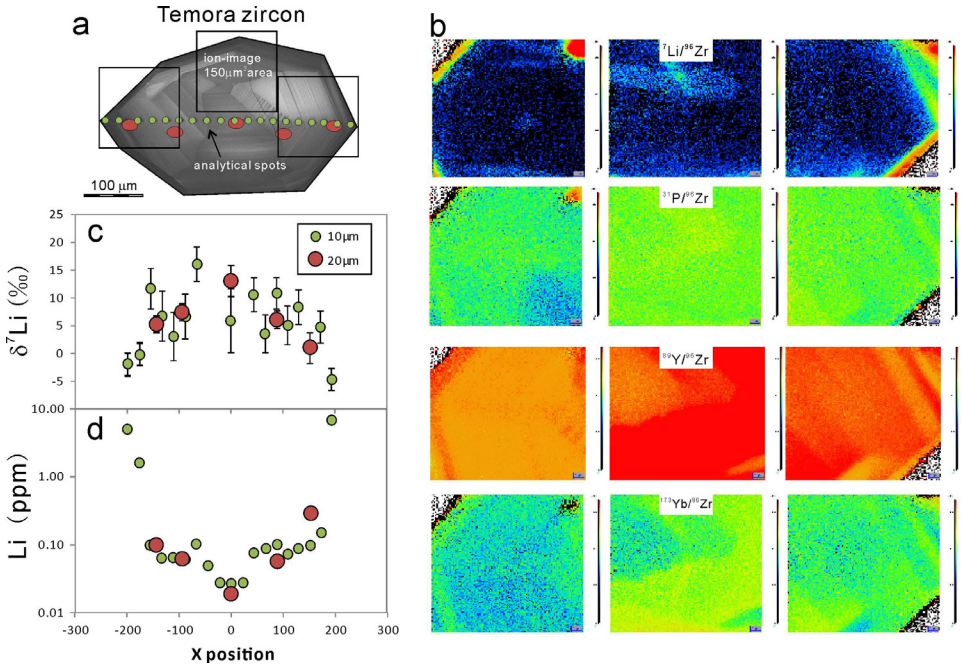

Figure 2. a) The CL image and analytical spots on the Temora zircon; b) ion images of Li, P, Y, and Yb; c) δ^7Li profile through zircon; d) [Li] profile through zircon.

Bridging the gap: using numerical modelling to better understand CO_2 transfer in subduction zones

When it comes to the chemical evolution of Earth, two volatile components stand out as the most geologically significant: water (H_2O) and carbon dioxide (CO_2). These volatiles play a crucial role in every facet of life. Both are key building blocks for organic life on Earth and H_2O has a profound impact on plate tectonics, where it is largely responsible for its mobility.

Volatile recycling in subduction zones, especially of H_2O, greatly affects the physicochemical properties of the overlying mantle (composed mostly of peridotite). As the mantle wedge hydrates, it loses its strength, density and viscosity, and it melts at lower temperatures, as a consequence of metasomatisation. On the other hand, the physicochemical effects of metasomatisation with a carbonic fluid are more subtle and enigmatic. Like H_2O, CO_2 decreases the melting temperature of peridotite. Interestingly, carbonate-rich melts are extremely mobile agents that can extract highly incompatible, heat producing elements (U, Th, and K). This can influence the long-term thermal budget of the mantle, and lead to thermal anomalies at different levels of the mantle. Carbon is also economically significant, important in its elemental form as either diamond or graphite. Lastly, the global carbon cycle and the habitability of our planet depend on the stability of carbon and its residence time in the mantle, the recycling efficiency in subduction zones, and rates of magmatic degassing.

Recently, much effort has been put into understanding the global carbon budget at depths greater than our atmosphere and the crust. Despite these efforts, estimates of carbon concentrations remain largely unconstrained. Experimental and thermodynamic models have been constructed to establish the amount of CO_2 recycled within subduction zones, but these have failed to give a conclusive number.

In this work, for the first time, a binary H_2O-CO_2 fluid has been coupled to a state-of-the-art geodynamic numerical modelling code (I2VIS). This allows us to study how dynamic effects, such as slab roll-back or sedimentary diapirism, lead to decarbonation, carbon recycling, and CO_2 metasomatism in a subduction zone.

This research bridges the dynamics gap, between static thermodynamic modelling and petrological experiments. We accomplished this by testing a wide range of subduction conditions to determine the key parameters that result in decarbonation in the context of a modern subduction zone. The results show that for different subduction regimes, distinctive degassing patterns are observed in time and space. For example, during stable subduction (Fig. 1) little, concentrated CO_2 release is observed, while in more dynamic models, decarbonation is more widely spread through the length of the subducting slab; this difference is a result of non-linear effects that are only seen during 3D and 4D modelling (x,y,z directions and time). We look to further extending our methods beyond decarbonation and to incorporate melting of subducted carbonated components to better understand recycling beyond subarc depths.

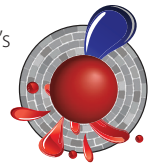

This project is part of CCFS themes 2 and 3, Earth's Evolution and Earth Today, and contributes to understanding Earth's Architecture and Fluid Fluxes.

Contacts: Christopher M. Gonzalez, Weronika Gorczyk
Funded by: ARC Linkage Project, UWA SIRF scholarship

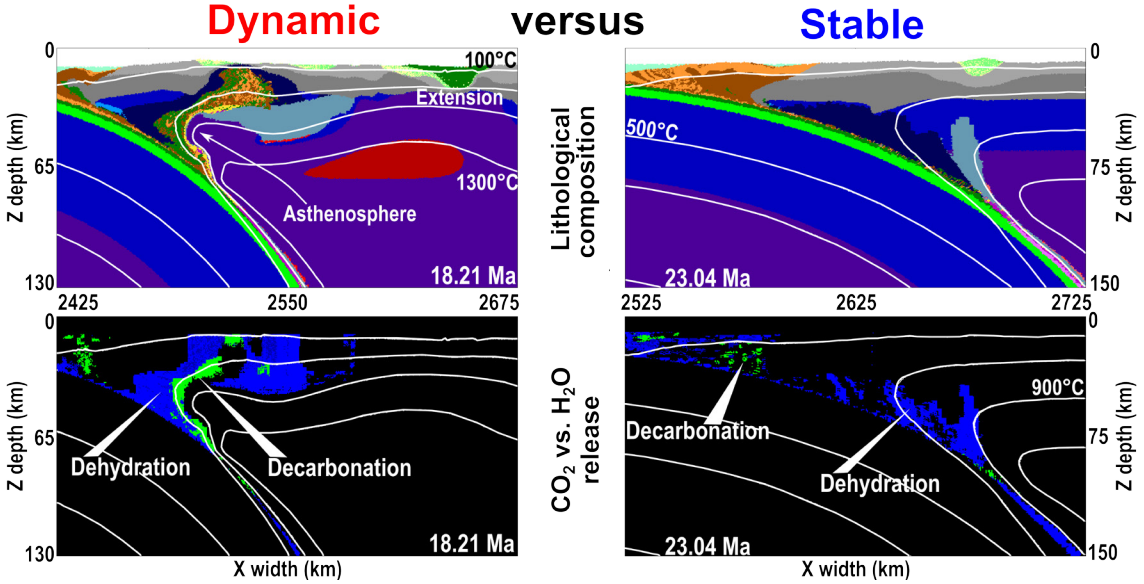

Figure 1. Image showing a comparison of a dynamic subduction zone with a stable subduction zone. In the stable subduction zone, there is neither extension nor sedimentary diapirism. In the dynamic subduction zone, the hot asthenosphere and low pressures result in the release of CO_2. Green and blue colours represent decarbonation and dehydration respectively. Fluids released are able to interact with and metasomatise the overlying lithospheric mantle.

In the deep between the WAC and the SAC

One way of determining the affinity of blocks of crust is to compare their Hf isotopic signatures. Flagship Program 7 aims to generate Lu-Hf isotopic data on previously dated zircon samples, and integrate this with geological, geochemical, and geophysical datasets of the Geological Survey of Western Australia. The research is focused in '*greenfields*' areas where little information presently exists. More than 9000 zircons, from 500 samples, have been analysed during the life of the project. Zircon samples have been selected from dated material in igneous, metamorphic, and sedimentary rocks of the Pilbara Craton, the Eastern Goldfields Superterrane and Murchison Domain of the Yilgarn Craton, the Albany-Fraser Orogen, the Musgrave Province, the Kimberley and Amadeus Basins, the Rudall Province, the Gascoyne Complex, and basement rocks beneath the Eucla Basin. This integrated approach, in which isotopic constraints are viewed in the context of geochemical information, geological mapping, and geophysical datasets has significantly enhanced our understanding of the geodynamics of Western Australia and provided a powerful new dataset to test models of tectonic evolution of the region. This work closely aligns with the UNCOVER initiative that seeks to provide an innovative, structured and nationally coordinated strategic plan to understand the deep geology of Australia, and thus bring competitive advantage to mineral exploration in Australia.

The Precambrian crystalline basement beneath the Eucla Basin represents a frontier '*greenfields*' region; very little is known about its age, composition, and geodynamic evolution. Recently the GSWA Exploration Incentive Scheme co-funded drilling of stratigraphic drill holes that have provided a unique sample set on which a range of cutting edge isotopic techniques has been applied in an effort to reveal its geological evolution and enhance its exploration potential. The exposed mineralised Gawler and Yilgarn cratons are separated by nearly one thousand kilometres of basement that represents a large prospective mineral province, but this region is buried beneath sedimentary basins formed during the development of Australia's southern margin. The mineral potential of this zone between the West Australian Craton (WAC) and the South Australian Craton (SAC) is demonstrated by recent onshore exploration success in both the Tropicana Zone (gold) and the Fraser Zone (nickel). Both these deposits lie in the Albany-Fraser Orogen, which reflects Proterozoic modification of the Yilgarn Craton. The basement substrate that lies further east between the exposed WAC and the SAC remains comparatively unknown.

Isotope geology is perhaps uniquely placed to see through overprinting events to expose both the timing and nature of early crustal formation processes. The Madura Province, the area of basement bounded by the Rodona Shear Zone and the Mundrabilla Shear Zone, lies adjacent to the Albany-Fraser Orogen but preserves a geological history startlingly different from its western neighbor. The Madura Province records two broad phases of magmatic activity. Zircon geochronology from intrusives (gabbros and granites) constrains one phase to 1411-1389 million years, whereas younger granites and gabbros have crystallisation ages of 1180-1125 million years.

Zircon crystals from all these magmatic rocks cluster along an apparent evolution array intersecting the depleted mantle at 1900-2000 million years ago. This suggests that these rocks all reflect dominant generation from a new piece of crust formed at this time. Scatter in this apparent evolution array is clear evidence of new mantle input during the initial phase of 1411-1389 million year magmatism. The isotopic signature of this *cont....*

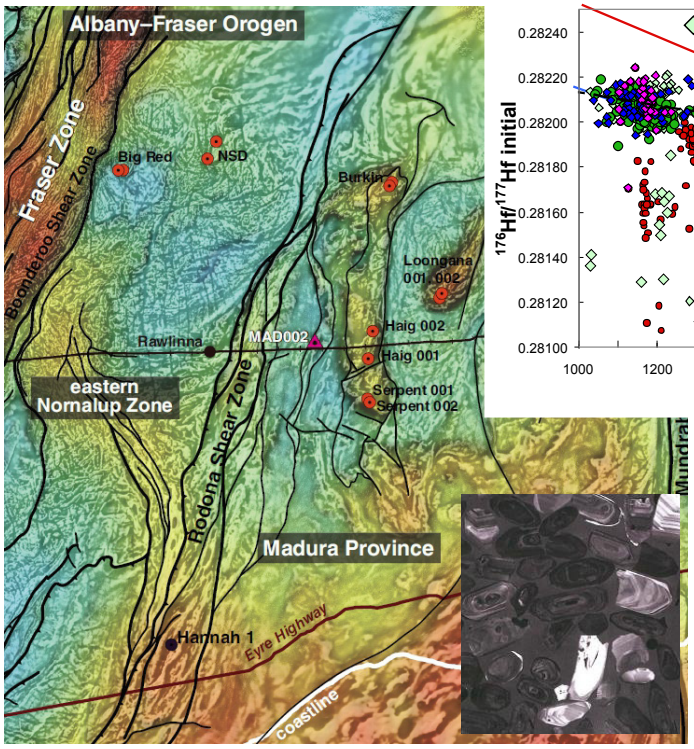

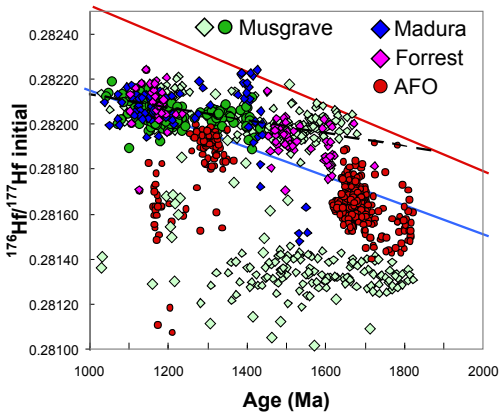

Figure 1. Map of drillhole locations in the eastern Albany-Fraser Orogen and Eucla basement superimposed on a gravity image with geology overlay. Stratigraphic drillholes (triangles) and other drillholes (circles) show the location of material from which Hf isotopes have been acquired. Inset: lower right, CL image of example zircon grains from granite within drillhole sample. Upper right; Hf isotopic evolution plot showing the change in isotopic signature through time and the projection back to a common mix of sources.

region is similar to that of intrusive rocks of the Musgrave Province in Central Australia. Although the age of magmatic crystallisation may be different, the timing of initial formation of crust is similar between the two provinces. In detail we interpret the 1900-2000 million year crustal-formation array to reflect a complex mix of oceanic magma sources with at least three components, including generation of new crust at 1900 million years and 1600-1200 million years, which also involved older Archean material. Such petrogenetic processes match aspects of oceanic arc magmatism and demonstrate that the Rodona Shear Zone was a fundamental suture separating reworked rocks of Yilgarn heritage from a new substrate of oceanic affinity lying between the older crustal blocks. These isotopic data, along with new geochemistry radically refine our understanding of the substrate between the Yilgarn and Gawler cratons, and suggest it reflects Proterozoic oceanic crust.

This project is part of CCFS themes 1 and 2, Early Earth and Earth's Evolution, and contributes to understanding Earth's Architecture.

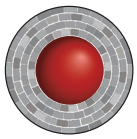

Contacts: Chris Kirkland, Michael Wingate, Yongjun Lu, Elena Belousova, Catherine Spaggiari, Hugh Smithies, Ed Saunders, Rosanna Murphy, Geological Survey of Western Australia

Funded by: Geological Survey of Western Australia

The hidden Archaean of Volgo-Uralia: a zircon tale

The amount of preserved Archean lithosphere and its global distribution are important for reconstructing Early Earth and to assess its subsequent evolution. However, only *ca* 20% of the presently remaining Archean crust is exposed at Earth's surface; the rest is hidden beneath polar ice sheets and the sedimentary cover of cratons, or forms minor fragments within Proterozoic and Phanerozoic orogenic belts.

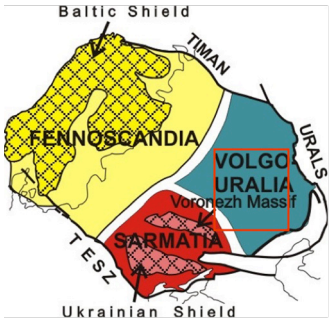

Figure 1. The three-segment subdivision of the EEC lithosphere. The red frame outlines the best-investigated part of Volgo-Uralia.

The protocontinent Volgo-Uralia (Fig. 1), which constitutes one-fourth of the East European Craton (EEC, "*Baltica*"), is covered entirely by thick sedimentary deposits. From geophysical studies and the examination of thousands of drillcores, the basement of Volgo-Uralia has been recognised as a vast high-grade terrain with a complex crustal history extending from the Paleoarchean to the Paleoproterozoic.

Our recent studies in Volgo-Uralia have been focused on looking for major events of the Archean crustal evolution employing Sm-Nd whole-rock analysis as well as the ion probe U-Th-Pb (SIMS) and Lu-Hf (LA-ICPMS) to analyse zircons. Particular attention was devoted to the widespread charnockitic rocks, which form large intrusions and contain zircon crystals with notably complex growth histories.

The zircons from one sample, an enderbite, have prismatic magmatic cores up to 2 mm across with oscillatory zoning, which enclose a few smaller zircon grains of an earlier generation (Fig. 2). The cores are surrounded by CL black-and-bright paired bands of curved metamorphic rims. The cores were notably fractured and fragmented prior to the metamorphic event.

The application of several methods of study (U-Pb SIMS/SHRIMP, ICPMS+TE, O- and Hf-isotopes in zircon) revealed (Fig. 3) that:

- The crystallisation age of the magmatic cores is between 3140 ± 7 Ma (SHRIMP) and 3127 ± 46 Ma (LA-ICPMS), while the metamorphic CL-bright rims formed at *ca* 1950 Ma (Fig. 3a and b). Intermediate ages are interpreted as resulting from various degrees of Pb loss caused by high-grade metamorphism.
- The metamorphic recrystallisation of the primary magmatic zircon correlates with depletion in REE, Pb and U which has been observed consistently in each analysed core-rim pair.

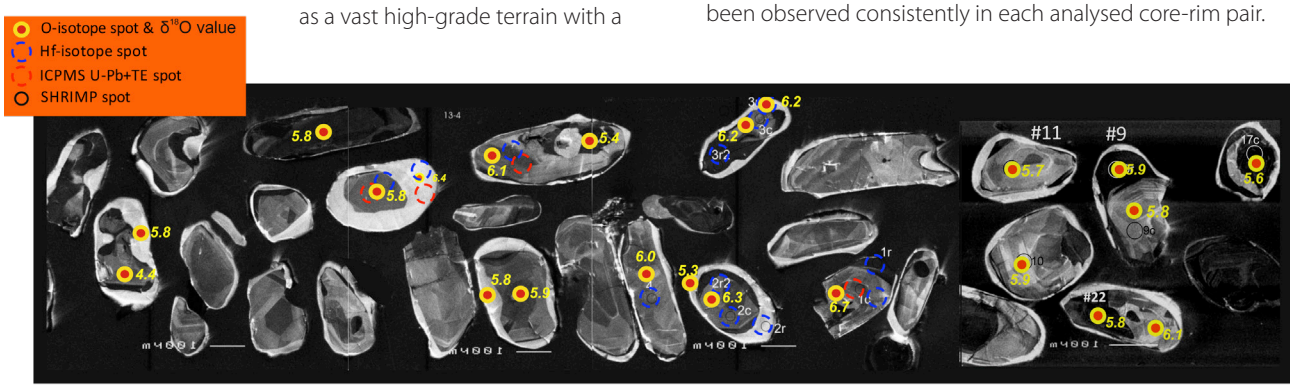

Figure 2. CL images of zircon from the studied enderbite. Gorbatovskaya 51 drill core (2896-2914 m depth), southern Volgo-Uralia.

Characteristically, the metamorphic rims are enriched in P and Hf. Variations of trace elements in the magmatic cores control those in the outermost metamorphic rims.

- The Hf-isotope compositions of the magmatic cores (-3 to -9 εHf) and metamorphic rims (-14 to -28 εHf), and their similar crustal model ages from 3.42 to 3.86 Ga, that the charnockitic magmas were derived by remelting of Eo- to Paleoarchean crust and very little, if any, juvenile material was added during the metamorphic event at *ca* 1950 Ma (Fig. 3c).
- No differences in O-isotopic composition have been detected between the cores and the rims; the $\delta^{18}O$ values vary from ca. 5 to 6.5 (Fig. 2), indicating that the Eo- to Paleoarchean crustal source of the magmas was originally mantle-derived.

From these results we conclude that the Mesoarchean (ca 3.1 Ga) granulitic crust in southern Volgo-Uralia was formed by the reworking of Eo- to Paleoarchean crust. Hf model crustal ages of up to 3.9 Ga found in this region as well as in central Volgo-Uralia suggest that Eo- to Paleoarchean continental crust was widespread throughout Volgo-Uralia. A back-arc setting along an active continental margin may explain the high-T, '*dry and ferroan*' magmatism of the studied charnockitoids. An alternative interpretation may be that deep mantle-plume activity at 3.1 Ga caused mantle underplating, extension of the Palaeoarchean crust and high-T magmatism.

This project is part of CCFS Theme 1, Early Earth, and contributes to understanding Earth's Architecture.

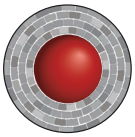

Contacts:
Svetlana Bogdanova (Lund University), Elena Belousova (CCFS)
Funded by: Belousova ARC Future Fellowship

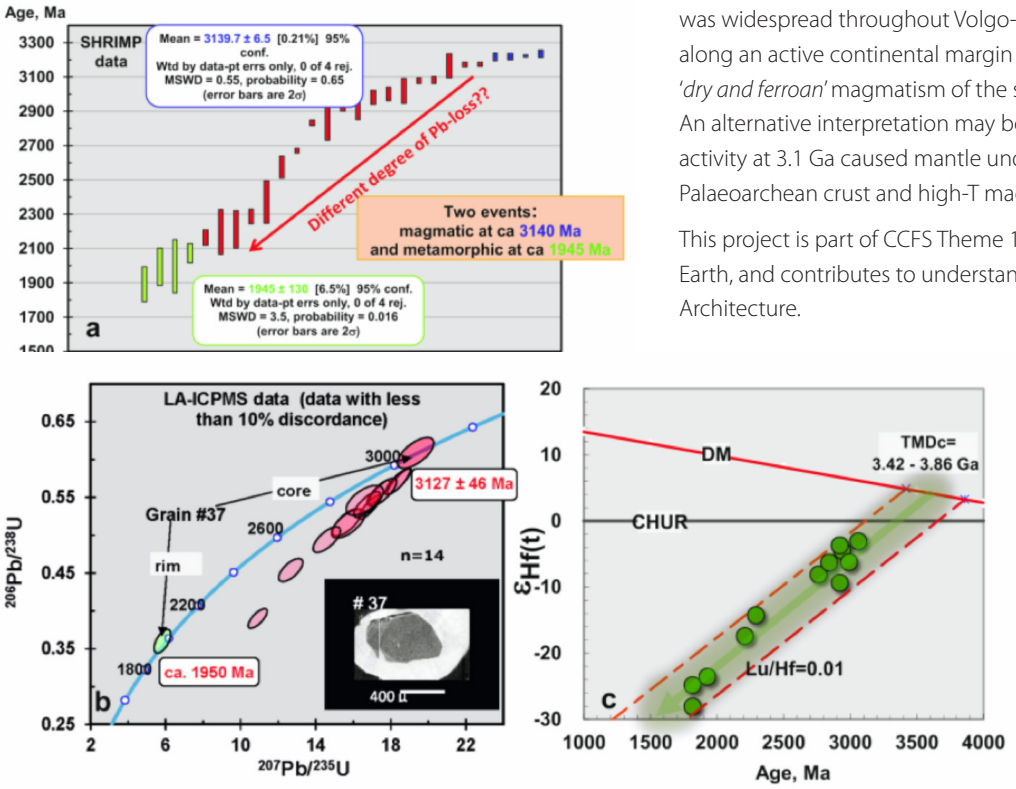

Figure 3. Results of the zircon studies.

Crustal volcanic plumbing systems follow lithospheric boundaries in the Newer Volcanics Province, SE Australia

Intraplate volcanism is a widespread phenomenon, which is generally regarded to be independent of plate tectonics due to its distance from plate boundaries. The Newer Volcanics Province (NVP) is the most recently active intraplate volcanism on the Australian continent. It includes more than 700 eruptions, with the earliest ~4 million years ago and the latest <5000 years ago. The erupted basaltic magmas cover a region more than 19,000 km^2, with an average thickness of less than 60 m. The origins of this intraplate-setting volcanism have drawn considerable attention from geoscientists. The latest research in the region suggests the NVP may originate from combined effects of localised mantle flow and shear flow, which are caused by the Australian plate's drift across a significant lithospheric step; while a nearby hotspot track - presumably fuelled by a plume - may have initiated the volcanism at ~4.5 Ma. However, important questions regarding how the magmas were stored and how they migrated through the crust to the surface remain unanswered, mainly due to the poor constraints on the crustal component of the NVP magmatic system.

In this study, we use ambient noise tomography and probabilistic inversion methods to construct the first local 3D crustal images of the NVP region (Fig. 1) with a general resolution of ~35 km. The images display distinct velocity features near the eastern and western margins of the NVP through the entire crust. This suggests the existence of a lithosphere-scale plumbing system for the migration of melt, associated with the boundary between the Delamerian Orogen and the Lachlan Orogen, which underlies the NVP. In particular, exceptionally high velocities are observed in the middle crust of the Delamerian Orogen, *cont....*

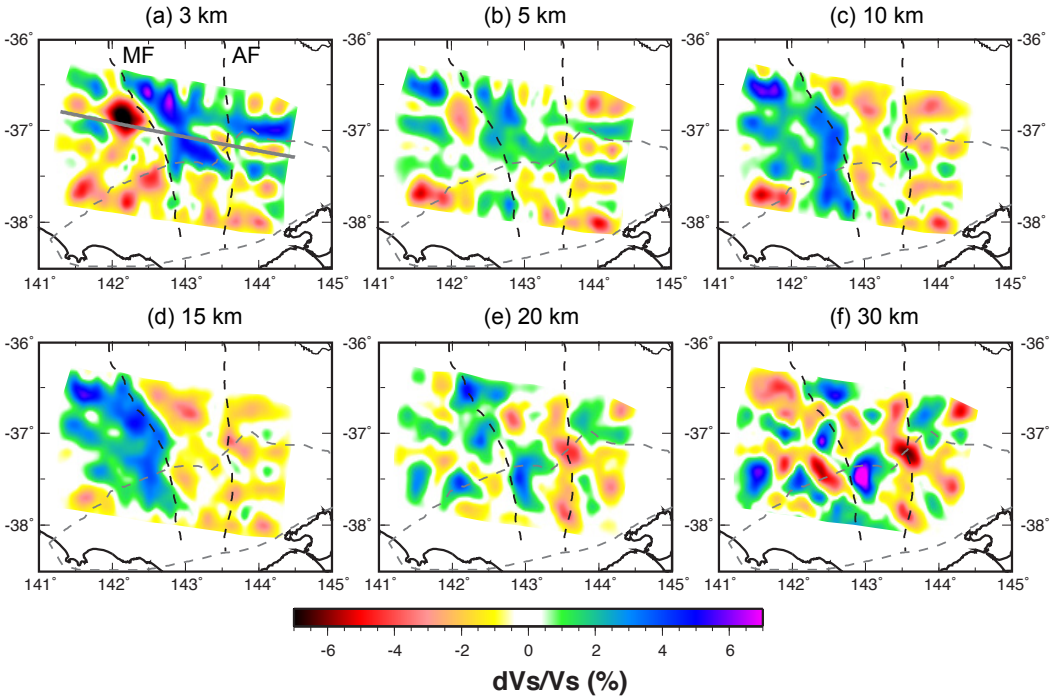

Figure 1. Vsv maps at depths of (a) 3, (b) 5, (c) 10, (d) 15, (e) 20 and (f) 30 km. All depths are relative to sea level. The solid grey line in figure (a) shows the profile location for Figure 2. Abbreviations: MF-Moyston Fault; AF-Avoca Fault.

which are best explained by buried magmatic arcs, resulting from subduction-accretion processes during the Delamerian Orogeny. The model also images small localised velocity reductions in the lower crust in the region where the two distinct lithospheric units meet. The low-velocity zone is spatially correlated with the top of a prominent lithosphere-scale low-resistivity zone, which we interpret to represent intruded magmatic sills with small proportions of melts. The minor volumes of erupted magmas and the small magmatic intrusion seen in the current lower crust indicate a much smaller magmatic plumbing system beneath the NVP (Fig. 2) than that of Yellowstone, which has a mantle-plume origin.

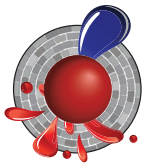

This project is part of CCFS Theme 3, Earth Today, and contributes to understanding Earth's Architecture and Fluid Fluxes.

Contacts: Chengxin Jiang, Yingjie Yang, Nick Rawlinson
Funded by: ARC Discovery Project, Yang ARC Future Fellowship, MQRES scholarship

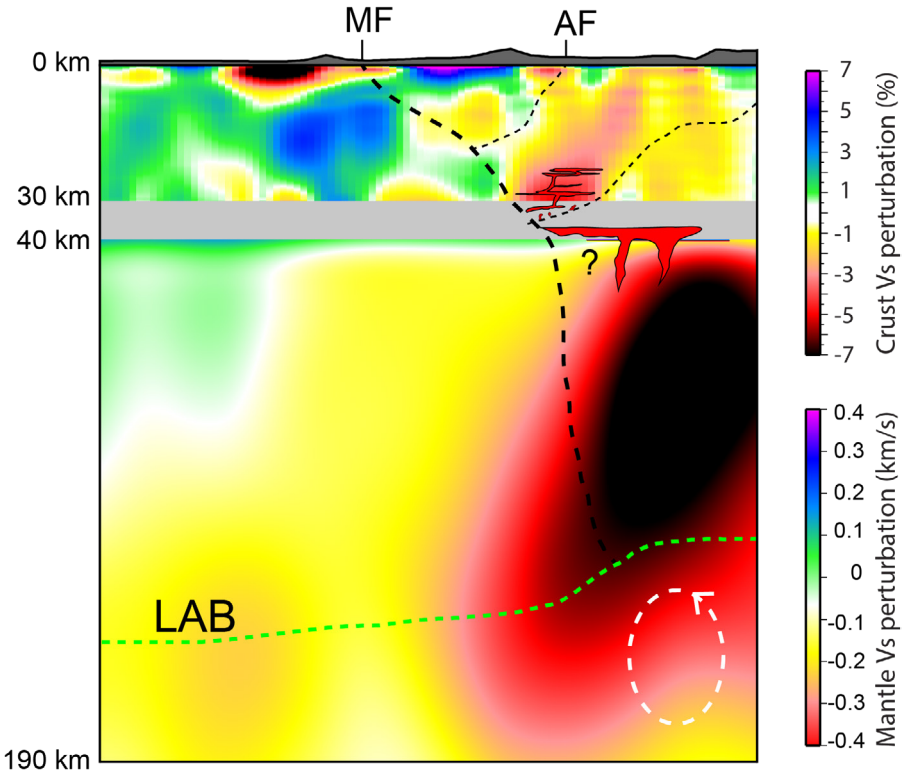

Figure 2. A cartoon to illustrate the accumulated magmatic intrusion in the lower crust beneath the NVP and its connection with the deep lithosphere. The crustal Vs perturbation is relative to the regional average from this study (0-30 km; two times exaggeration relative to the mantle part); while the mantle Vs perturbation is relative to the ak135 model [Kennett et al., 1995] in km/s from Rawlinson et al., [2016] (40-190 km). The white circle illustrates the edge-driven convection from the geodynamic model of D. Rhodri Davies and Rawlinson [2014]. The shaded area on the top of the section represents the real topography, and the depth of the LAB (Lithosphere-Asthenosphere boundary) is an approximation illustration based on the study of D. Rhodri Davies and Rawlinson [2014]. Abbreviations: MF-Moyston Fault; AF-Avoca Fault.

Trace elements in zircon, and the oxidation state of magmas

Many elements in silicate melts and crystalline rocks vary in ionic electric charge (also called ionic '*valence*' or '*oxidation state*'), depending chiefly on availability of oxygen as an electron acceptor; its availability is conventionally represented as '*oxygen fugacity*', fO_2. Such elements include iron as Fe^{2+} and Fe^{3+}, sulfur as S^{2-}, S^{4+}, and S^{6+}, cerium as Ce^{3+} and Ce^{4+}, europium as Eu^{2+} and Eu^{3+}, uranium as U^{4+}, U^{5+}, and U^{6+}, tin as Sn^{2+} and Sn^{4+}, vanadium as V^{3+}, V^{4+}, and V^{5+}, and molybdenum as Mo^{4+} and Mo^{6+}.

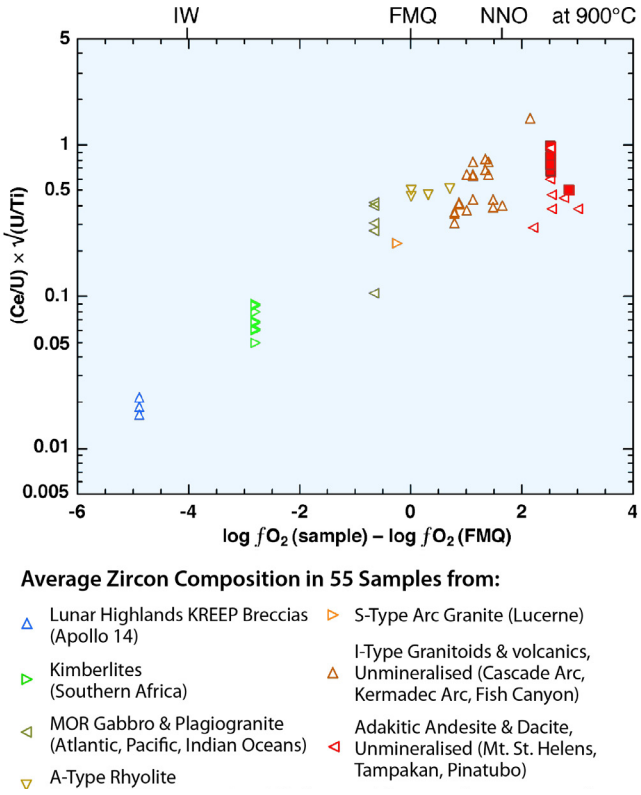

Figure 1. The average composition of several zircons in each of 55 samples is plotted against apparent oxidation state of the silicate melt from which the zircon crystallised. The abscissa variable is log units of oxygen fugacity above or below that of the reference mineral assemblage fayalite+magnetite+quartz, as given in publications that reported values of the oxidation state in the host rocks of the analysed zircons. Solid red symbols represent samples from igneous bodies related to copper ore deposits.

Whether or not a magma can produce an ore deposit of V, Sn, Mo, or Cu depends substantially on the valence of those elements in the magma. Major controversies surround the oxidation state of the early Earth's upper mantle and surface 4.5-2.3 billion years ago, and to what degree the oxidation state of Earth's mantle has been affected by cycling of materials from the surface into the planetary interior over the past 2.3 billion years, as Earth's surface became more oxidised due to production of oxygen by photosynthetic microbes.

Electron transfer among elements is fast, so all elemental oxidation/reduction couples in silicate melts are instantaneously interactive; therefore, a measure of the valence ratio of one element is, in principle, a constraint on the valence ratio of every other element. Zircon, $Zr^{4+}Si^{4+}O_4$, is a common minor mineral in igneous rocks and preserves a record of the oxidation state of its parent silicate melt and of the melt's source because (1) it takes in trace amounts of other elements of variable electric charge that substitute for Zr^{4+} and Si^{4+}, and (2) it is extremely resistant to chemical modification after crystallisation, so its record of oxidation state can be preserved for billions of years of deep burial at sub-magmatic temperatures. Over the past decade, scores of published papers have reported estimates of the relative oxidation state of magmas using the ratio Ce^{4+}/Ce^{3+} in zircon. Experimental studies demonstrate that Ce^{4+}/Ce^{3+} in silicate melts and zircon vary with magma oxidation state, but the ratio in zircon is even more sensitive to variation of temperature, because Ce^{3+} is 18% larger than Ce^{4+}, and 36% larger than Zr^{4+}, so substitution of Ce^{3+} represents a misfit in both size and charge. This requires coupled substitution of another misfit ion, usually either phosphorus P^{5+} for Si^{4+} or OH^{1-} for O^{2-}. Therefore, the Ce^{4+}/Ce^{3+} ratio in zircon is extremely sensitive to thermal contraction of the zircon crystal lattice, and the temperature dependence usually overwhelms the fO_2 signal being sought. We find that in nearly all publications in which zircon Ce^{4+}/Ce^{3+} was inferred to represent magmatic oxidation state, the variations in Ce^{4+}/Ce^{3+} were actually due almost entirely to variations in temperature.

To formulate a zircon sensor of the oxidation state of the parent magma that is relatively insensitive to temperature variation, the sensor ions need to have the same ionic charge and nearly the same size. The ratio Ce^{4+}/U^{4+} in zircon fits those requirements. However, the zircon inherits a distorted version of this ratio from its parent melt, biased by partition coefficients. As the parent melt crystallises, its Ce^{4+}/U^{4+} ratio decreases due to selective removal of some Ce^{4+} by other minerals that start crystallising before zircon. So the zircon indicator of magmatic oxidation state needs to account for the stage of chemical evolution of the parent magma. The ratio U/Ti in zircon works well as a qualitative indicator of the stage of chemical evolution of the parent magma. Figure 1 illustrates the potential of our new indicator of magmatic oxidation state, using our microbeam chemical analyses of zircons in eight igneous suites and many compiled from published literature. For each of these igneous suites, independent estimates of magmatic oxygen fugacity, fO_2, are available.

This study is an outcome from the ongoing Flagship Program 2.

This project is part of CCFS Themes 2 and 3, Earth's Evolution and Earth Today and contributes to understanding Fluid Fluxes.

Contacts: Robert Loucks, Marco Fiorentini, Yongjun Lu

Funded by: CCFS Flagship Program 2

Resolving the controversy of Earth's oldest fossils

A few 10 km outside Marble Bar in the Pilbara region of Western Australia lies one of the more famous sites for scientific research in Australia. Around a quarter of a century ago, UCLA palaeontologist JW Schopf discovered tiny filaments preserved within a ~3.5 Ga silica-rich rock, the so-called Apex chert. These were interpreted as the fossilised remains of primitive filamentous bacteria and thus thought to constitute the earliest known evidence for life on Earth.

With the technology available to researchers at that time this was a reasonable interpretation. The sizes of the filaments (mostly 1-20 µm in diameter) were comparable to known filamentous bacteria and they had an internal structure that resembled multiple cells joined in chains.

During the following decade these filaments became embedded in both the textbook and popular science literature as "*Earth's oldest microfossils*" and were also heralded as the standard against which other possible signs of ancient (or even extra-terrestrial) microbes should be judged.

Everything changed in 2002 when a team led by Oxford palaeobiologist Martin Brasier questioned the authenticity of the microfossils. Brasier and colleagues had re-interpreted the geological setting of the filaments, demonstrating that they were trapped in rocks that formed at high temperatures during volcanic activity, casting doubt on Schopf's initial interpretation.

Re-examination of the filaments under the microscope revealed that some appeared to branch and others followed the edges of mineral crystals. These new findings led the Brasier group to propose that the filaments were not microfossils, but merely bits of carbon, arranged in roughly filamentous patterns around crystal boundaries, probably formed by hot fluids.

In the ensuing decade or so the "*Apex microfossil debate*" has been intense. Although it is now accepted that the geological setting probably is hydrothermal, this has not diminished the Schopf group's belief in the authenticity of the microfossils. They now suggest that the filaments are fossils of heat-loving (thermophilic) bacteria, similar to those found around deep-sea hydrothermal vents today. On the other side of the debate, the Brasier group presented more detailed geological and microscopic analysis consistent with the filaments being non-biological artefacts. A scientific stalemate had been reached.

New work at CCFS led by ARC Future Fellow David Wacey in collaboration with the late Professor Brasier has finally ended the stalemate. Wacey and colleagues used high spatial resolution electron microscopy techniques to investigate the detailed structure and chemical composition of the filaments. This research, published in two parts in Proceedings of the National Academy of Sciences (*CCFS Publication #528*) and Gondwana Research (*CCFS Publication #663*) has confirmed that the Apex filaments are not microfossils, but instead are mineral artefacts, comprising stacks of silicate grains onto which later carbon was adsorbed.

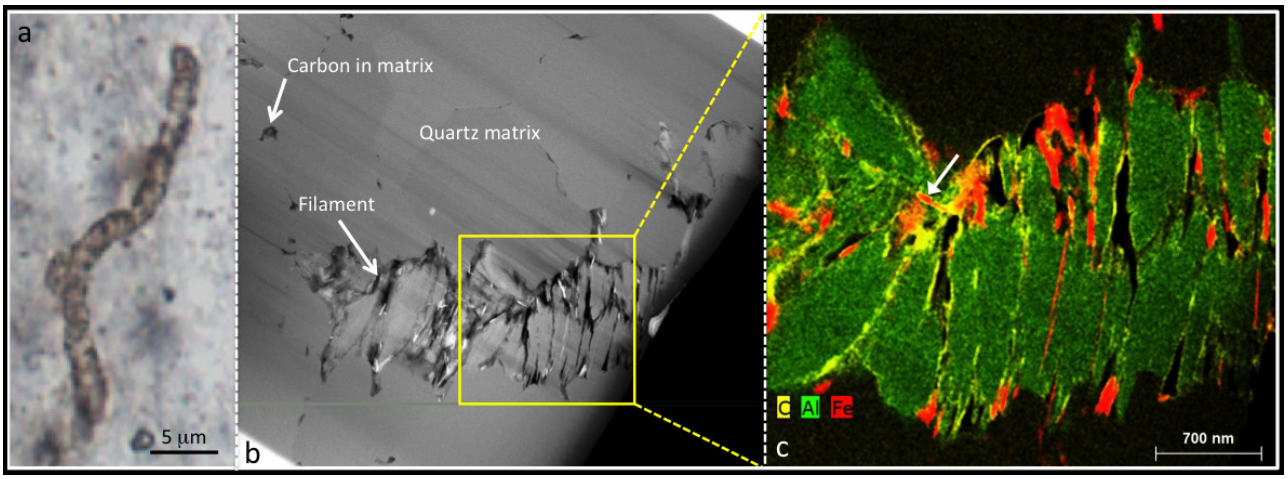

Figure 1. a) Typical filament from the 3.46 Ga Apex chert viewed using light microscopy. b) Transmission electron microscopy image of a filament from the Apex chert. c) False colour three-element overlay map of area boxed in (b). The filament comprises stacks of sheet-like phyllosilicate grains (green) with carbon (yellow) and iron (red) interleaved between some of the sheets. This distribution of phases is incompatible with a biological origin for the filament. In places, carbon completely coats the iron phase (arrow) suggesting carbon was the last phase to become associated with the filaments.

The new data provide a picture of the morphology and chemistry of the filaments at a spatial scale up to one hundred times better than previous studies. At this scale it becomes apparent that the filaments are made of hundreds of plate-like grains of a potassium and barium rich silicate mineral, similar in appearance to common mica. Although carbon is present in the filaments, its distribution is incompatible with any known biological morphology (Figs. 1 and 2).

Today mica-like minerals are used to clean up oil spills due to their very high capacity to adsorb hydrocarbons, and the carbon

in the Apex filaments probably was arranged by a similar process. While the lower-resolution techniques previously employed allowed a potential biological interpretation, the new high-resolution images show that the arrangement and distribution of the carbon within the minerals does not support the biological hypothesis.

This research does not really move the goalposts for when life first originated on Earth, since there are robust microfossils only a few million years younger than the Apex material. However, it emphasises that not everything that looks like life really is life. Perhaps most importantly it shows that microstructures that appear to tick all the boxes for biology when examined down to the micrometre scale, can fail some of these same criteria when examined at the sub-micrometre scale. This may usher in a new way of analysing possible signs of life in the future, on Earth or further afield.

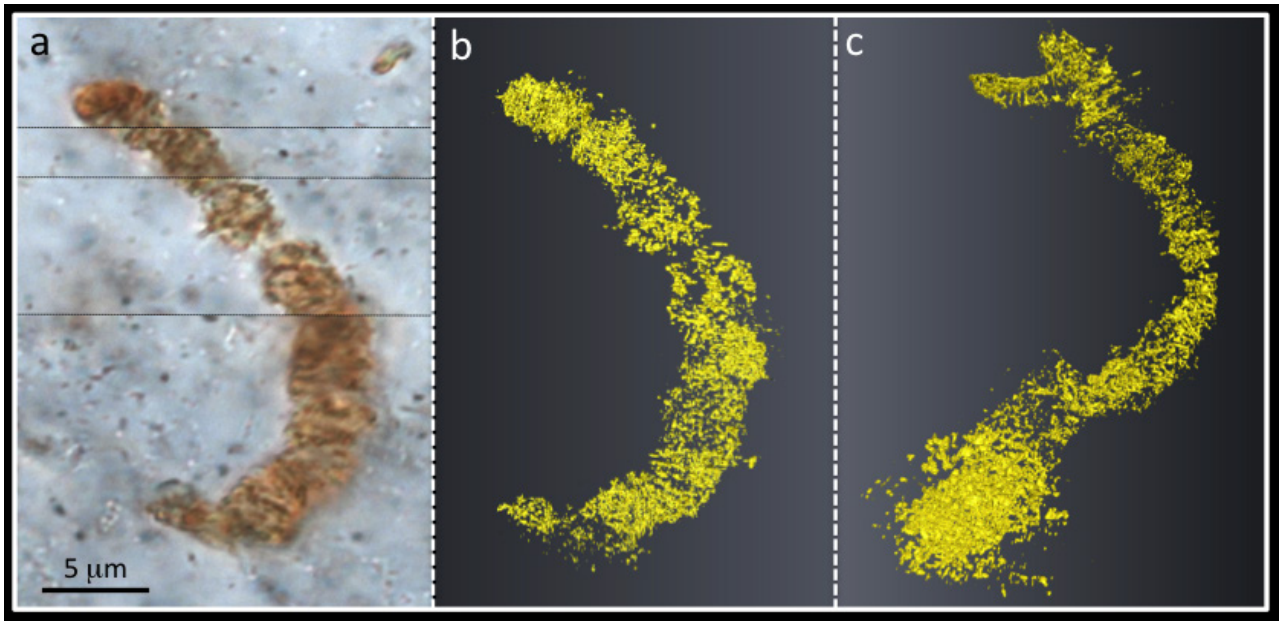

Figure 2. 3D reconstruction of an Apex filament. a) Transmitted light photomicrograph of chosen filament. b) 3D visualisation of carbon from nano-tomography images through the filament, shown in the same orientation as (a). c) 3D model rotated to show small branch extending down below the main body of the filament, not seen in (a-b), and incompatible with a primitive bacterial morphology.

Previously reported '*cellular compartments*' actually have very inconsistent lengths, and length/width ratios that match crystal growth patterns but are unlike any known microbial cells. The carbon is found to have entered the filaments after the formation of the surrounding minerals, again inconsistent with it being the *in situ* remains of bacteria (Fig. 1).

The field of early life research is fraught with difficulty. Data initially interpreted as biological in origin is often reinterpreted at a later date as having a geological explanation. As new analytical techniques become available, accepted paradigms may have to be questioned.

This project is part of CCFS Theme 1, Early Earth, and contributes to understanding Fluid Fluxes.

Contact: David Wacey
Funded by: ARC Future Fellowship

Mingling processes in Cretaceous Angolan kimberlites

Kimberlites are volcanic rocks which are best known as potential diamond mines. Indeed, it was the deep source of the kimberlitic magmas, as well as their rapid emplacement, that turned them into targets for diamond exploration. Angola is ranked fourth in Africa in terms of kimberlite abundance, but due to its recently troubled history, very little work has been carried out to characterise kimberlites in this country. Fortunately, a collaboration between University of Barcelona, Universidade Agostinho Neto (Luanda), CATOCA Company and CCFS has given access to several kimberlites of the Lunda Norte province (NE Angola) and allowed us to characterise them.

Kimberlites are heterogeneous rocks, with variable contents of groundmass minerals, xenocrysts and xenoliths entrained by the magmas during their ascent towards the surface. With this complex history, dating kimberlites and characterising their source is challenging. Perovskite ($CaTiO_3$) is a ubiquitous minor phase (<10%) in kimberlites and crystallises directly from the magma. It also is relatively resistant to weathering and *cont...*

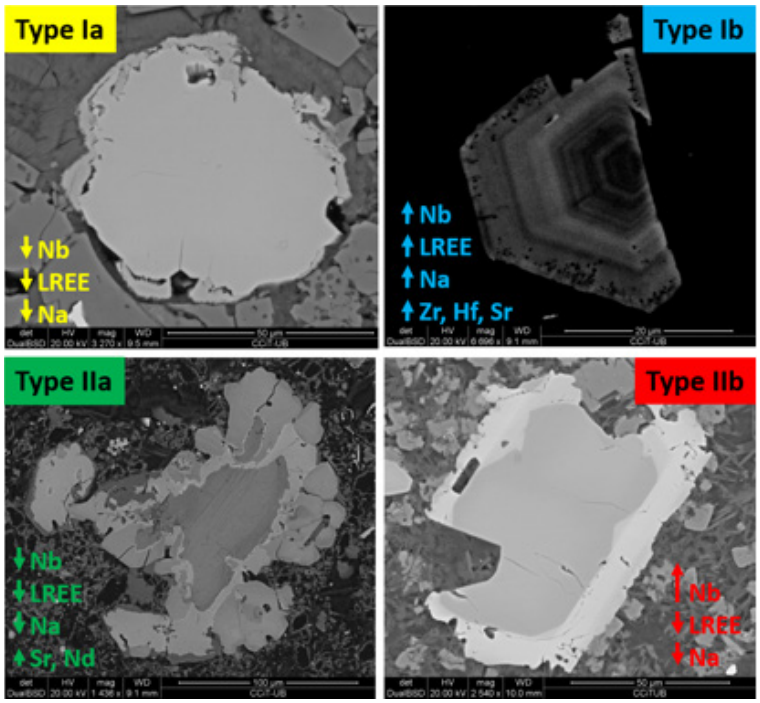

Figure 1. BSE-SEM images of the 4 textural types of perovskite found in the Angolan kimberlites, as well as their main compositional features. Primary perovskite (Type Ia) is typically unzoned, altered to TiO_2 and contains no inclusions. In contrast, primary perovskite (Type Ib) is commonly euhedral, shows oscillatory zoning, has tiny inclusions near the grain boundaries and remained unaltered. Secondary perovskite usually occurs as reaction-induced rims on ilmenite and other Ti oxides (IIa), although in some cases a fourth generation of perovskite was found as thin Nb-rich overgrowths (IIb) on previously crystallised perovskite.

a main carrier of U, Th, Sr and Nd. Therefore, over the last decade, perovskite has become widely used for both age determination and characterisation of the sources of kimberlitic magmas.

This study is the first work on *in situ* U-Pb geochronology and Sr-Nd isotope analysis of perovskite grains from Angolan kimberlites, and is based on a detailed petrographic and chemical study of perovskite from six pipes in the Lunda Norte province.

Four types of perovskite were identified, differing in texture, major- and trace-element composition, zoning patterns, type of alteration and the presence or absence of inclusions (Fig. 1). Primary groundmass perovskite is either as anhedral, Na-, Nb- and LREE-poor perovskite (Type Ia); or euhedral, strongly zoned, Na-, Nb- and LREE-rich perovskite (Type Ib). Secondary perovskite occurs as reaction rims on ilmenite (Type IIa) or as high-Nb (up to 10.6 wt% Nb_2O_5) rims on primary perovskite (Type IIb). The occurrence of these four types of perovskite reflects a complex, multi-stage process that involved mingling of compositionally different melts.

U-Pb dating of these perovskites yielded Lower Cretaceous ages for all the studied kimberlites: Mulepe 1 (116.2 ± 6.5 Ma), Mulepe2 (123.0 ± 3.6 Ma), Calonda (119.5 ± 4.3 Ma) and Cat115 (133 ± 10 Ma). Perovskite in the other two kimberlites shows higher alteration and Pb loss, and as a result only approximate ages could be obtained for the Lucapa 1 (135 Ma) and Lucapa 2 (156 Ma) kimberlites (Fig. 2).

Our results indicate that kimberlite magmatism in the Lunda Norte province (115-130 Ma) peaked around 120 Ma, coinciding with the breakup of the Gondwana supercontinent. Kimberlite emplacement was related to reactivation of NE-SW deep-seated faults (>300 km deep), or cryptic continental corridors, which represent the continuation of oceanic fracture zones. The Sr_i and εNd_i values reported in the perovskites are in good agreement with the published data for on- and off-craton South African Group I kimberlites, as well as with the petrological observations.

This work is part of CCFS Themes 2 and 3, Earth's Evolution and Earth Today, and contributes to understanding Earth's Architecture and Fluid Fluxes.

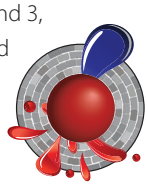

Contact: Montgarri Castillo Oliver

Funded by: SGR444 (Universitat de Barcelona), Fundació Pedro Pons (UB), CATOCA Company, CCFS Flagship Program 1

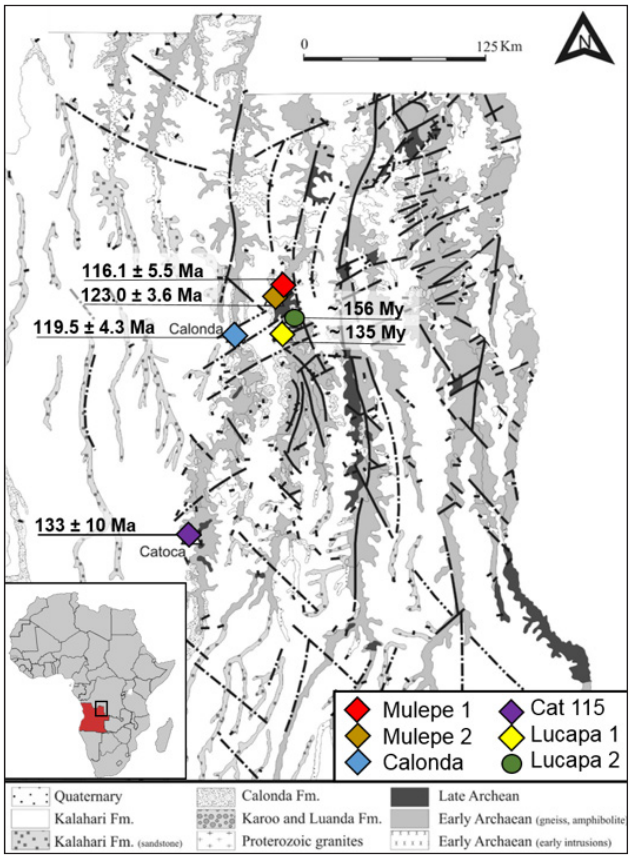

Figure 2. Location of the Angolan kimberlites studied in this work, as well as their emplacement ages.

In search of high flux magma conduits with new structural mapping tools

Magmatic Ni-Cu-PGE sulfide systems account for ~60% of world Ni production and include some of the most valuable mineral camps on earth such as Noril'sl-Talnakh (Russia), Voisey's Bay (Canada), and Jinchuan (China). There is consensus that Ni-Cu-PGE sulfide deposits are associated with high-flux magma channels that transport mantle-derived mafic and ultramafic melts into the crust. However, the mode of emplacement and self-organisation of these magma feeder systems remain poorly understood in the context of magmatic-sulfide systems.

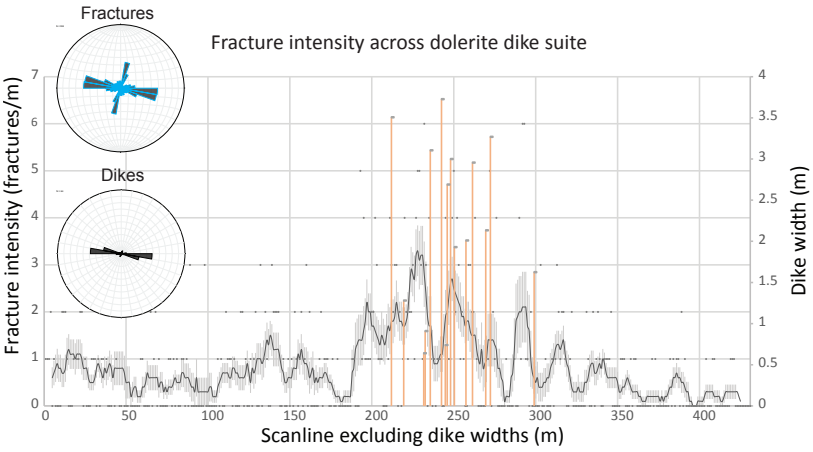

Figure 1. Moving average of fracture intensity surrounding a suite of dolerite dikes. Location of individual dikes shown in orange with dike widths on right-hand axis. Variance in average fracture intensity shown as standard error.

Important questions regarding magma emplacement include:
How is magma dispersed in large mafic systems?
How do propagating intrusions interact with country rocks at micro- to macro-scales?

As a first step toward addressing these questions, we examine how magma-carrying fracture networks develop and propagate. Where data is available for intrusion-hosted Ni-Cu-PGE deposits, host rock anisotropy has been shown to be a first-order control on intrusion geometry (Saumur et al., 2015). To further investigate magma-host rock interaction an innovative technique is employed using unmanned aerial vehicles and photogrammetry to map and structurally analyse a mafic intrusion network in 3D at very high resolution (1 cm to 1 pixel, or finer). Structural data are extracted from a digitally reconstructed outcrop model using a least squares regression analysis. The accuracy of structural measurements extracted from the model has been successfully validated with conventional field measurements. This method has the advantage of rapid and accurate data collection along spatially rectified traverses, referred to as scanlines.

The 3D mapping technique has been applied to a suite of 21 dolerite dikes emplaced in Mesoproterozoic granitic rocks along the south coast of Western Australia. The dikes are from <1 m to 5 m wide and closely spaced with a cumulative thickness of 33 m over an across-strike distance of 105 m. Dikes occupy vertical fractures that strike 075°-125°. Structural data is collected along scanlines oriented perpendicular to the mean strike direction of the dike suite. Scanline data reveal fracture intensity (number of fractures per fixed unit length) in granitic wall rocks within the dike suite to be on average 2.2 times higher than the background fracture intensity in the host rock. Though empirical data from other dike suites are not available, the fracture intensity difference is compatible with mechanical predictions of stress changes induced by propagation of an over-pressured blade-shaped intrusion (*Rubin and Pollard, 1988*). Such investigations of well exposed mafic intrusions are a first step toward understanding the mechanisms and dynamics of magma transport leading to the development of high-flux conduits.

This project is part of CCFS Theme 3, Earth Today, and contributes to understanding Earth's Architecture and Fluid Fluxes.

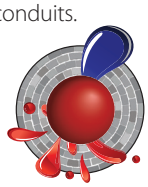

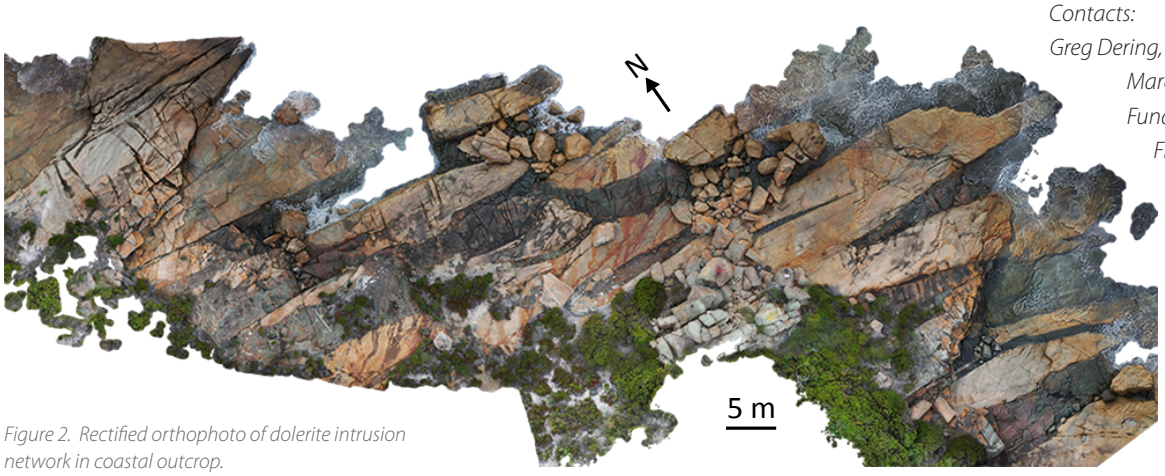

Figure 2. Rectified orthophoto of dolerite intrusion network in coastal outcrop.

Contacts: Greg Dering, Marco Fiorentini

Funded by: Fiorentini ARC Future Fellowship, CSIRO Mineral Systems Flagship, CCFS Flagship Program 2

The hot-and-cold Earth system

Controversy surrounds the evolution of planet Earth through deep time, specifically whether the crust has grown uniformly over time or in pulses associated with the supercontinent cycle. New research at CCFS has set out to investigate this problem by combining global datasets of geochemical proxies that reflect both the subduction process, and the production of magmas from juvenile mantle (non-subduction-related magmatism). Proxies include oxygen isotopes and incompatible trace elements of dated magmatic rocks (subduction-recycling proxy), and Hf-isotope compositions of dated zircon crystals (mantle magmatism proxy).

The results clearly show, in a statistically meaningful way, that the supercontinent cycle has been an important contributor to crustal growth since ca 3.2 billion years ago (Ga), when modern-style plate tectonics is now widely thought to have commenced (Fig. 1). More importantly, the supercontinent cycle appears to have evolved over the course of Earth history, with ever longer cycles and increasing amounts of crustal recycling up to 1 Ga, followed by decreasing amounts of crustal recycling thereafter. Periods of supercontinent formation were accompanied by widespread subduction of old, cold oceanic lithosphere and recycling of continental crust. Periods when supercontinents were amalgamated and then split apart were characterised by lower rates of crustal recycling and increased levels of juvenile mantle magmatism; the latter higher minima in Hf isotope values.

A key feature of the data that links with the geological record is that Earth operated in a '*Conditioned Duality*', with periods of rapid subduction and supercontinent amalgamation characterised by pulses of hot mantle magmatism and extensive crustal growth and rec-cling, followed by pulses of amalgamated and rifting supercontinents characterised by cool mantle and low rates of crustal growth and recycling (Fig. 2). Periods of warm mantle are characterised by the concentrated global eruption of mantle-derived melts (e.g., komatiites, and emplacement of large igneous provinces, such as the Bushveld magmatic province). But the widespread subduction of old cold oceanic lithosphere, and the associated piling-up of slab graveyards across the core-mantle boundary, led to mantle cooling when supercontinents were amalgamated. It was only after the mantle had warmed up again - through a combination of conduction from below and insulation from above - that the supercontinents were able to split apart and the next supercontinent cycle commence.

These pulses of rapid crust formation lead to the idea of '*crustal oversteps*', whereby too much crust forms during pulses of supercontinent formation relative to where the planet is in terms of overall heat loss. Thus, crustal recycling and renewed crustal

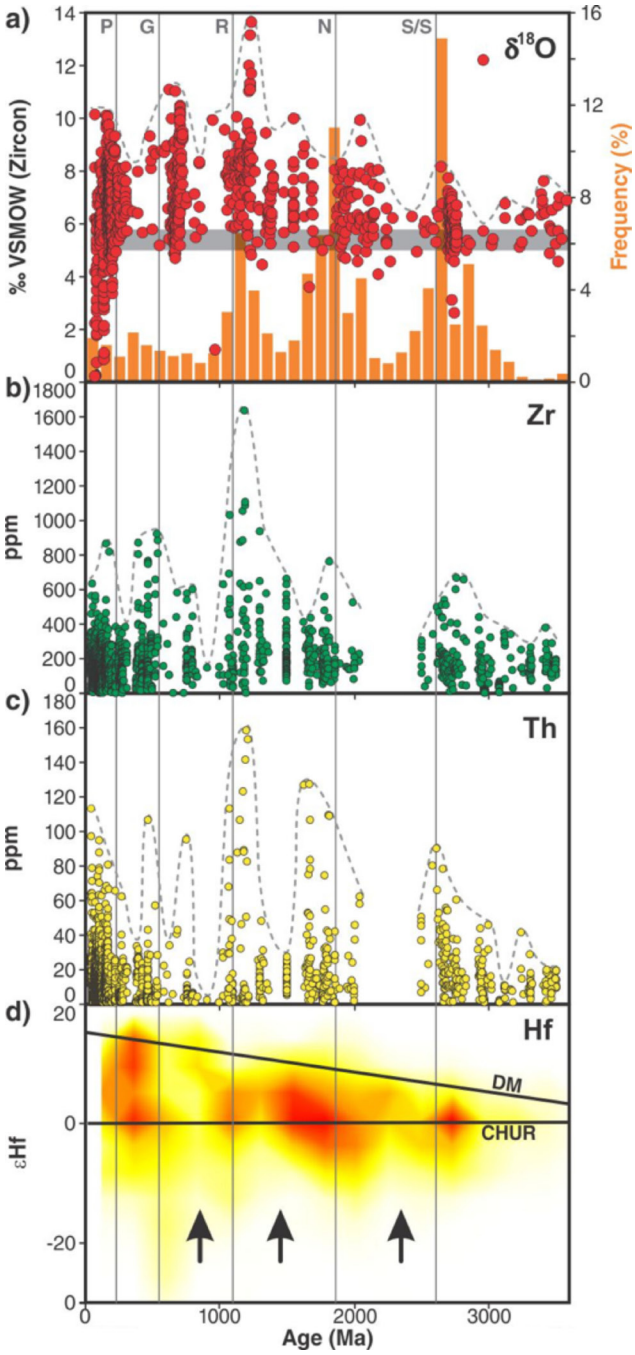

Figure 1. Evolution plots of isotopic and trace element geochemistry over time (age in millions of years (Ma)). A) $\delta^{18}O$(VSMOW) in zircon grains (red dots) from a global compilation plotted on a background of zircon ages of juvenile crust (data from Condie, 1998). Grey horizontal bar denotes average mantle values of oxygen isotopes in zircon (from Valley et al., 2005). B) and C) Concentrations of incompatible trace elements (Zr and Th) in dated igneous rocks from global geochemical datasets (from Van Kranendonk et al., 2015). D) Contour density plot of the number of Hf isotopic values of dated zircons from Belousova et al. (2010): CHUR = chondrite normalised uniform reservoir; DM = depleted mantle. Black arrows point to periods with minimum negative Hf isotopic values, representing pulses of minimal crustal recycling during times of supercontinent disaggregation. Red lines on the εHf vs time diagrams denote the variations in isotopic signature of crust, becoming highly negative during periods of supercontinent amalgamation as a function of increased crustal recycling, and returning to positive (juvenile) values during periods of renewed mantle magmatism accompanying supercontinent dispersals.

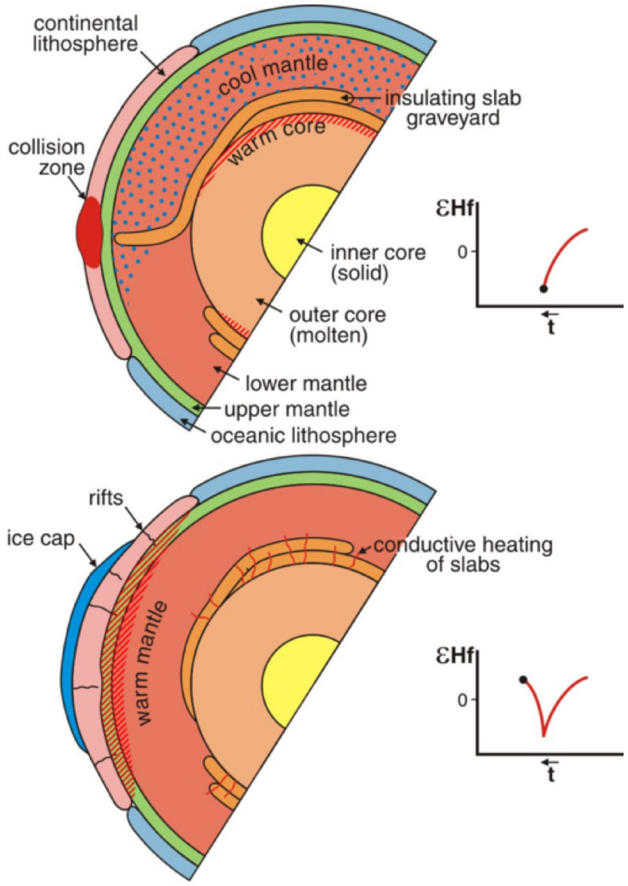

Figure 2. Schematic representation of the two-state Earth in hemispherical cross-sections. Top panel shows a period of supercontinent amalgamation, when widespread subduction causes mantle cooling through a combination of thermal cooling, arising from the introduction of cool oceanic lithosphere, and insulation of the mantle from core heat, through the presence of thick slab graveyards at the core-mantle boundary. Bottom panel shows a period of supercontinent disaggregation, when conductive heating from the core and supercontinent insulation cause mantle warming. Note that widespread glaciations (ice cap on bottom panel) lags behind mantle cooling is a function of the conductive cooling of the crust.

growth is delayed until the volume of crust matches the heat coming out of the mantle. With each stage of supercontinent assembly and related mantle cooling, the tessellation geometry changed in a stepwise manner, reflecting the overall decrease in planetary heat over time. Our current geometry of 12 plates matches a stable dodecahedral tessellation (T3 on Fig. 3), where-as previous steps included less stable geometries with more and smaller plates. However, in the Archean, a stable tessellation of N=32 plates existed as a truncated icosahedron of 12 pentagonal and 20 hexagonal plates of roughly equal size.

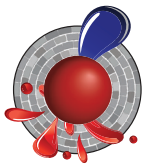

This project is part of CCFS Theme 2, Earth's Evolution, and contributes to understanding Earth's Architecture and Fluid Fluxes.

Contacts: Martin Van Kranendonk, Chris Kirkland
Funded by: CCFS Flagship Program 4, UNSW, Curtin University

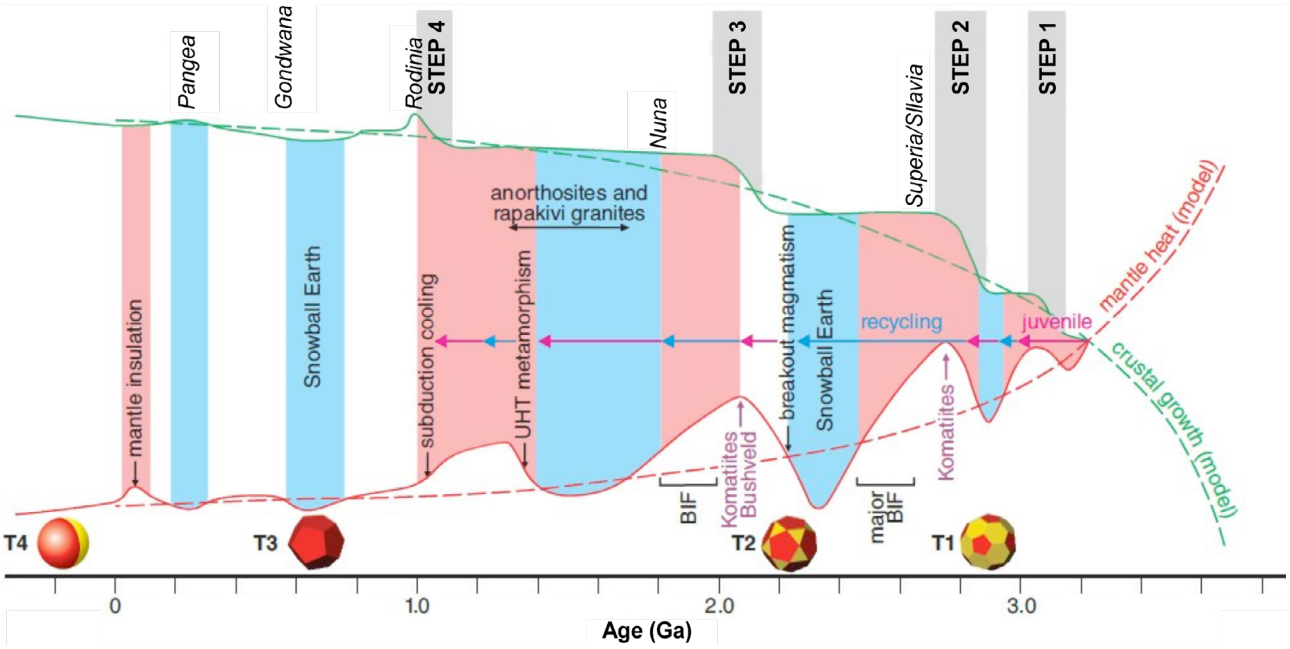

Figure 3. Schematic model of Earth evolution, showing modelled (dashed red curve) and inferred (smooth red curve) heat loss, idealised and inferred crust formation (dashed and smooth green curves, respectively) and tessellation states (T1 to T4). Crustal overstep events (Steps 1-4) are when the volume of continental crust exceeds the ideal volume for a given value of ideal heat loss, and occur immediately following supercontinent amalgamation events (names of supercontinents in italics above crustal growth curves). Heat loss is inferred to vary episodically above the idealised curve, with hot periods (coloured pink) identified by voluminous komatiite and Large Igneous Province (e.g., Bushveld) magmatism, and anorthosite-rapakivi granite magmatism, and cooler periods identified by ice ages (coloured blue). Pink arrows denote pulses of rapid juvenile magmatism; blue arrows periods of predominant crustal recycling. BIF = banded iron-formation; UHT = ultra-high temperature metamorphism.

Mineral exploration on Mars

The geology of Mars is surprisingly well documented. Orbiting satellites have surveyed the Martian surface via hyper-spectral imaging systems, Landers and Rovers have directly observed and analysed the Martian surface, and numerous Martian meteorites are available to the scientific community. The emerging picture is that the basaltic to ultramafic lavas that presently cover a large portion of the Martian surface may have had physical and chemical characteristics akin to the komatiites and ferropicrites that erupted on Earth during the Archean and Proterozoic eons.

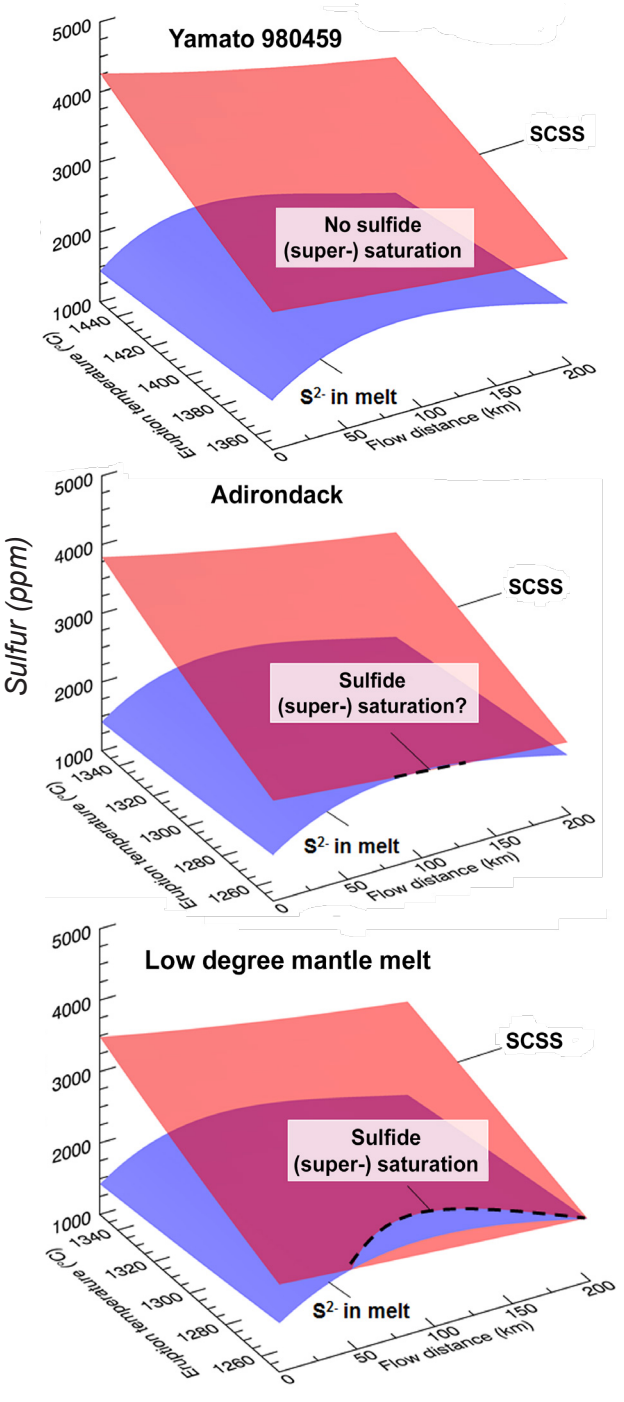

As komatiites and ferropicrites are significant hosts to high-grade Ni-Cu-PGE sulfide mineralisation, the question arises as to whether similar deposits can be found on Mars. Unfortunately, sulfides cannot be easily detected by means of remote sensing (e.g. via hyper-spectral imagery onboard satellites), and no evidence for significant sulfide enrichment has been found through the limited analysis of magmatic rocks at landing sites or through the study of Martian meteorites. Hence, we have investigated the potential loci for Ni-Cu-PGE sulfide mineralisation through the application of predictive mineral system targeting.

On Earth, komatiites and ferropicrites are thought to have been emplaced as turbulent lava flows along conduits and channels with high thermal and mechanical erosion rates. The erosion and assimilation of sulfur-rich substrates probably triggered batch segregation of sulfides and their accumulation in basal units. Similarly, a recent study carried out within the framework of CCFS Flagship Program 4 (*CCFS Publication #508*) has suggested that the thermal and mechanical erosion of widepsread sulfate-rich sedimentary substrates may have been a common mineralising process in erosive Martian lava flows. However, several mechanisms in this mineralisation model remain unconstrained. In fact, even if the erosive nature of some Martian lava flows is reflected in the occurrence of carved channels, recent numerical studies aimed at exploring their erosive capability did not consider the diverse array of eruption parameters and of potentially sulfate-rich sedimentary substrates, and focused on basaltic bedrock. Most importantly, both the efficiency of Martian lavas to assimilate and reduce sulfate (i.e., S^{6+}) to sulfide (i.e., S^{2-}), rather than the dissolving sulfur as S^{6+}, and the degassing of sulfur-bearing gases during lava emplacement (i.e., S_2, H_2S, SO_2), remain unconstrained.

Our ongoing study aims to refine existing mathematical lava-erosion simulations for turbulent flows, thermodynamic volatile degassing models, and formulations on the stability of sulfides, into a semi-quantitative model for sulfide batch segregation and the formation of komatiite-type sulfide mineralisation in Martian lava flows. We have examined a series of scenarios in which turbulent mafic to ultramafic melts (Fig. 1) with varied chemical

Figure 1. Modelling results for selected unidirectional, gravity-driven steady Martian lava flows in the turbulent flow regime, in the diagram flow distance from the vent (x-axis), eruption temperature (y-axis) and sulfur (i.e. sulfur capacity at sulfide saturation, SCSS, and actual sulfur in the melt). Lava cooling is simulated for convective heat loss to the base and top of the flow, as well as energy consumed due to thermal erosion of substrate and progressive crystallisation of the flow. Several algorithms are integrated to simulate the evolving flow characteristics (e.g., lava temperature, composition, Reynolds number, viscosity, heat transfer coefficient, mechanical and thermo-mechanical erosion rate) at incremental steps downstream. Batch segregation of sulfides may commences when the SCSS (red) and the sulfur in melt (blue) trajectory intersect. The lava types considered are selected Hesperian to Amazonian mantle melts constrained based on a) the study of the olivine-phyric Shergottite meteorite Y 980459, b) the Adirondack-class basalt at the Gusev Crater landing site, and c) low-degree melting experiments on the Martian mantle.

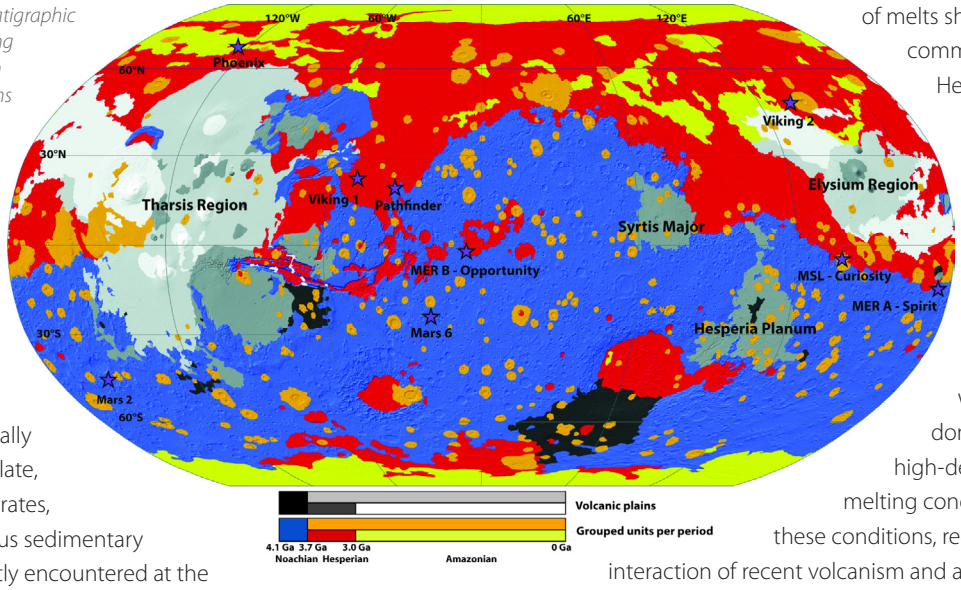

Figure 2. Chronostratigraphic map of Mars showing surfaces of common age. Volcanic terrains are subdivided separately in greyscale levels. Landing sites are highlighted with stars.

and physical characteristics are emplaced over, and potentially erode and assimilate, sulfate-rich substrates, such as the various sedimentary lithologies recently encountered at the Gale Crater and Meridiani Planum landing sites or documented from orbit.

Preliminary findings (Fig. 1) support the inference that sulfate assimilation is a potential trigger of sulfide batch segregation and consequent formation of Ni-Cu-(PGE) sulfide mineralisation. The liquidus temperature of the magma appears to be the key parameter in controlling the attainment of sulfide saturation. Therefore, only low-temperature lava flows corresponding to low-degree partial melts of the mantle are promising candidates for the presence of sulfide deposits on Mars (Fig. 2). These types of melts should be more common during the Hesperian (3.7-3.0 Ga) and especially during the Amazonian (<3.0 Ga), rather than during the Noachian, which is dominated by high-degree partial melting conditions. Given these conditions, requiring the interaction of recent volcanism and ancient sulfate-rich deposits, the window of opportunity for ore genesis on Mars may have been much tighter than on Earth, only rarely and sparsely allowing the formation of orthomagmatic mineral systems.

This project is part of CCFS Theme 1, Early Earth, and contributes to understanding Fluid Fluxes.

Contacts: Raphael Baumgartner, Marco Fiorentini, Fabrice Gaillard, David Baratoux
Funded by: CCFS Flagship Program 4

Messengers from the deep: Fossil wadsleyite-chromite microstructures from the Mantle Transition Zone

Seismological studies of Earth's mantle reveal three distinct changes in seismic velocity, at depths of 410, 660 and 2700 km; the interval between 410 and 660 km is termed the Mantle Transition Zone (MTZ). Investigations of the MTZ by deformation experiments and geophysical methods suggest that the MTZ has distinct rheological properties. However, their exact cause is still unclear, because actual samples of mantle rocks from deeper than 200 km are rare, and we still know little about the *cont...*

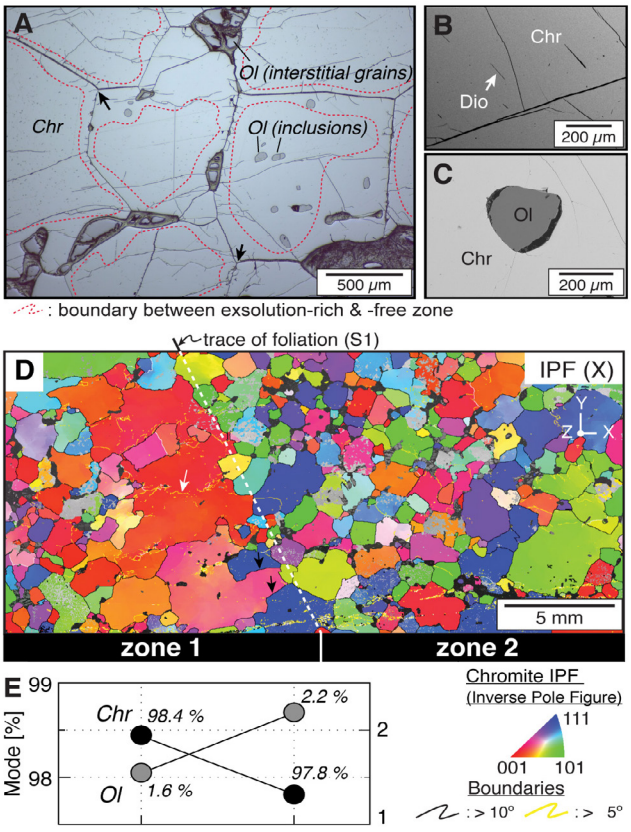

Figure 1. Microstructure of Luobusa chromitite. (A-C) Back-scattered electron (BSE). (A) Equilibrated microstructure of chromite with 120° triple junctions (black arrow) and smooth, nearly straight grain boundaries. Olivine occurs as inclusions and along grain boundaries. Interstitial grains are partially or completely serpentinised. (B) Exsolved diopside needles (Dio) in chromite (Chr). (C) Olivine inclusion (Ol) in chromite (Chr). (D) Colour coded EBSD map showing crystal orientation changes relative to the X direction of the sample reference frame. White and black arrows represent subgrain boundary and migrated grain boundary, respectively. (E) Modal composition of zone 1 and 2 in Figure 1(D).

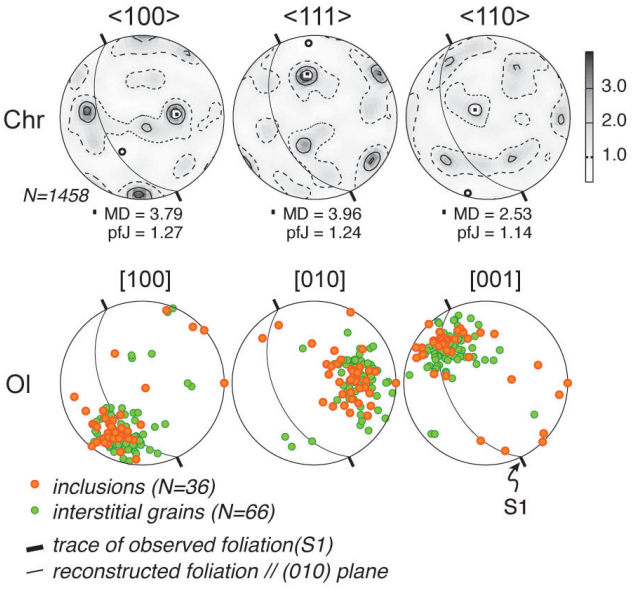

Figure 2. Crystallographic preferred orientation (CPO) of chromites (Chr) and olivines (Ol). Lower hemisphere, equal-area stereographic projections. MD: maximum density, pfJ: index of fabric intensity.

rheological properties and deformation behaviour of olivine polymorphs in the lower parts of the upper mantle.

Luobusa is one of several large peridotite massifs along the Yarlung-Zangbo suture zone of southern Tibet, which marks the boundary between the Indian and Asian blocks. The podiform chromitites in the Luobusa peridotite have received much attention because they include many ultra-high pressure (UHP) phases, such as microdiamonds (found in mineral separates and *in situ*), Si-rutile and coesite, as well as a range of highly reduced native elements, carbides and nitrides. Recently, a basic model for the subduction, MTZ UHP metamorphism and exhumation of the Tibetan peridotites has been presented (*McGowan et al., 2015, CCFS Publication #522*). These observations indicate that the Luobusa chromitites have experienced much higher pressures than the more common ophiolitic chromitites, whose history is restricted to the uppermost part of the mantle (*González-Jiménez et al., 2014, CCFS Publication #334*).

We have discovered the first direct evidence for crystal-plastic deformation by dislocation creep in the MTZ using a chromitite from the Luobusa peridotite. Chromite grains show exsolution of diopside and SiO_2 (Fig. 1A-B), suggesting previous equilibration as an orthorhombic polymorph in the MTZ. Olivine occurs both as inclusions in chromite and interstitially along grain boundaries (Fig. 1C). The grain-size difference between the enclosed and interstitial olivine grains is consistent with evidence for grain boundary migration, because grain boundaries can readily migrate across small grains but can be pinned by larger grains. A decrease in the rate of grain growth due to the presence of grains of a second phase also is consistent with the finer grain size and higher abundance of olivine in interior zone 2 relative to exterior zone 1 (Fig. 1D-E). The abundance of exsolved diopside needles in the cores of chromite grains, vs their absence in the rims, indicates that grain growth occurred after the transition from the orthorhombic high-pressure polymorph chromite to cubic chromite.

Electron backscattered diffraction (EBSD) analysis reveals that olivine grains co-existing with exsolved phases inside chromite grains and occurring on chromite grain boundaries have a single pronounced crystallographic preferred orientation (CPO) (Fig. 2). This suggests that olivine preserves the CPO of a high-pressure polymorph (wadsleyite), which implies the activation of the (011)[100] slip system in wadsleyite, before the high-pressure polymorph of chromite began to invert and exsolve. Chromite, a cubic phase also shows a significant CPO, suggesting that this was acquired while the chromite existed in the UHP orthorhombic polymorph. Thus, the fine-grained high-pressure phases were deformed by dislocation creep in the MTZ (Fig. 3). Significant grain-boundary migration under static conditions during passive exhumation produced an equilibrated microstructure. Grain growth masked at first sight its MTZ deformation history, but preserved the core-rim structure with exsolved diopside only in the cores, as well as the high-PT fabric. The relict olivine-chromite fabric of this Luobusa chromitite provides the first direct evidence of significant crystal-plastic

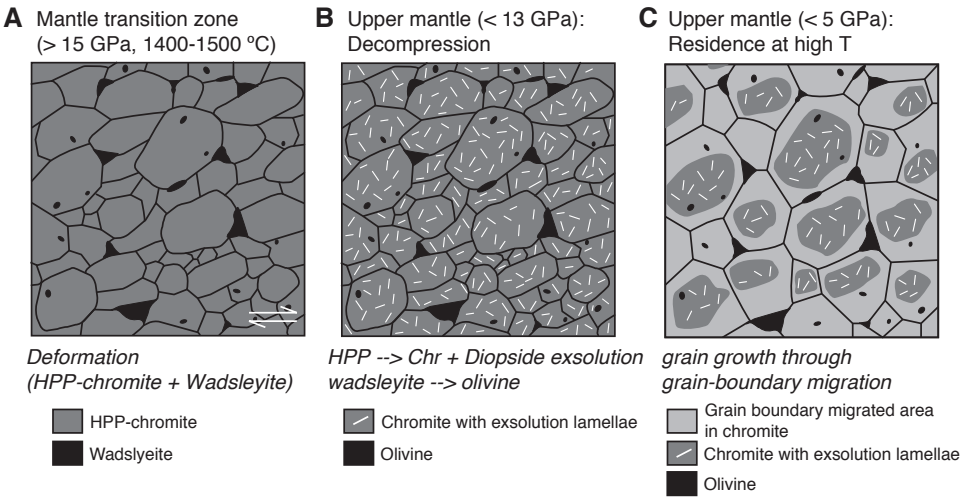

Figure 3. Schematic model of microstructural evolution in Luobusa chromitite. (A) Deformation of HPP (High Pressure Polymorph)-structured chromite and wadsleyite in Mantle Transition Zone. (B) Transformation from HPP structure to chromite; diopside/coesite exsolution; transformation of wadsleyite to olivine. (C) Grain growth through static grain-boundary migration to produce coarse equilibrated microstructure, with exsolution-rich cores and exsolution-free rims. Larger interstitial olivine grains pin the migrating boundaries.

deformation in the MTZ. These unique observations provide a window into the deep Earth, and constraints for interpreting geophysical signals and their geodynamic implications in a geologically robust context (*Satsukawa et al. 2015; CCFS Publication #673*).

This project is part of CCFS themes 2 and 3, Earth's Evolution and Earth Today, and contributes to understanding Earth's Architecture and Fluid Fluxes.

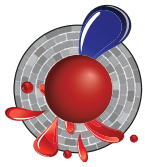

Contacts: Takako Satsukawa, Bill Griffin, Sandra Piazolo, Sue O'Reilly

Funded by: CCFS Flagship Program 1, ECSTAR

How kimberlites get to the surface (or not)

Kimberlites are economically and scientifically valuable because they are the major hosts to diamonds, entrain abundant mantle and crustal xenoliths and represent the deepest mantle-derived magmas (>150-200 km) that we can see at Earth's surface. Despite their importance, and at least 40-50 years of dedicated studies, several issues remain unresolved about kimberlite petrology, geochemistry, mineralogy and volcanology. These include: 1) the composition of kimberlite melts in the deep Earth and when they reach the upper crust; 2) the depth where kimberlite melts are generated; 3) the causes of the very fast ascent (several m/s) of kimberlite magmas; 4) the extent to which kimberlite rocks are modified by syn- and post-emplacement processes, such as ground-water alteration.

New research by ARC DECRA fellow Andrea Giuliani and his research group provides new insights into two of the above issues, namely the ascent mechanism(s) of kimberlite magmas and the evolution of kimberlite melts during their ascent through the lithospheric mantle.

The driving forces that promote the rapid ascent of kimberlite magmas are poorly constrained. For example, it has been proposed that exsolution of a CO_2-rich vapour phase at mantle depths provides the main propellant. However, this is hard to reconcile with the carbonate-rich nature of kimberlite matrices and, hence the parental magma(s); the CO_2 obviously has not escaped. In addition, many kimberlite magmas (e.g., magmatic dykes several km in length) have not been emplaced explosively. Finally, if magma ascent is not driven by volatile exsolution, we might expect the highly reactive kimberlite melts to be entirely consumed through reaction with mantle wall rocks. The ascent of kimberlite magmas to Earth's surface, therefore, requires unique conditions.

To investigate the evolution of kimberlite magmas, we need phases that preserve geochemical signatures of magma interactions during transport through the mantle and the crust. Phlogopite mica is a common mineral in kimberlites, where it spans a range in size from macrocrysts (~>0.5 mm; Fig. 1) to a groundmass phase (~<0.1 mm). It also preserves large compositional variations, a repository of information on the evolution of kimberlite and related melts.

In CCFS publication #680, Dr Giuliani and colleagues from the University of Melbourne and Tasmania, report new

cont...

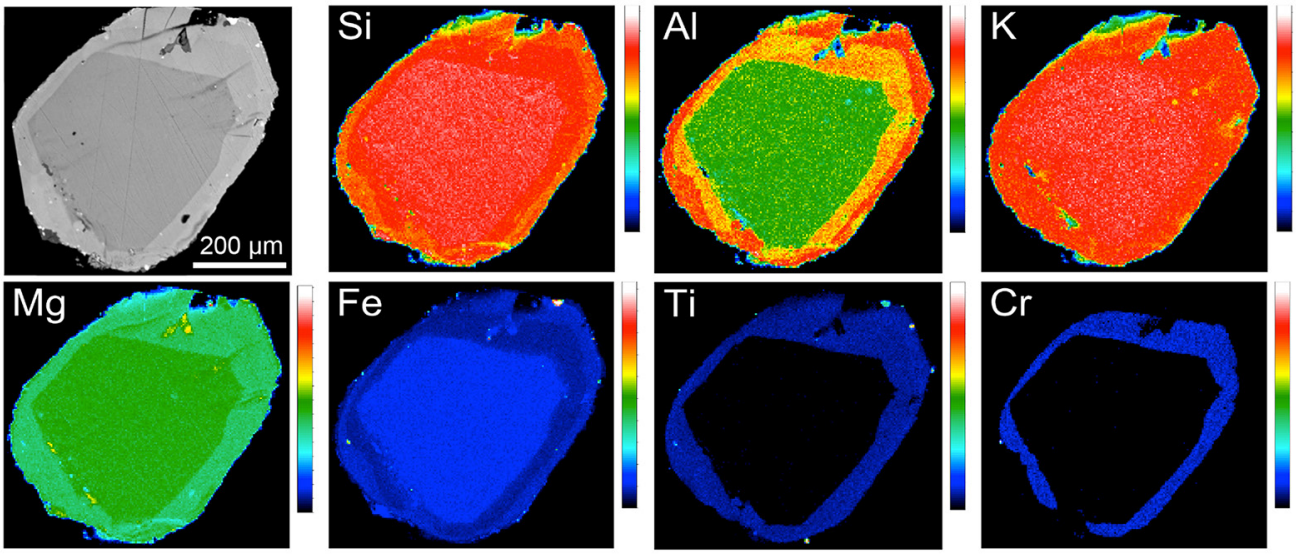

Figure 1. Scanning electron microscope (SEM), back-scattered electron (BSE) image and X-ray elemental maps of a typical concentrically-zoned phlogopite macrocryst from the Bultfontein kimberlite. The coloured scales on the right of each panel indicate the relative concentration of each element, i.e. 'cool' colours (blue, black) = low concentrations; 'warm' colours (red, orange) = high concentrations.

compositional data for phlogopite in the Bultfontein kimberlite (Kimberley, South Africa; the kimberlite type locality) and in mantle xenoliths entrained by the Kimberley kimberlites. Concentric zoning patterns in phlogopite macrocrysts in the Bultfontein kimberlite (Fig. 1) record a complex history of episodic crystal growth. Internal zones of macrocrysts and some cores in groundmass grains have Ti-Cr-rich compositions similar to overgrowth rims on phlogopite in mantle xenoliths from the Kimberley and other southern African kimberlites and matrix grains in polymict breccia xenoliths from Bultfontein. In mantle xenoliths, the phlogopite overgrowths have been previously interpreted as crystallising from kimberlitic fluids/melts, while polymict breccias are widely regarded as failed kimberlite intrusions at mantle depths. These results suggest that the Ti-Cr-rich zones of phlogopite in the Bultfontein kimberlite were produced in the mantle by reaction with one or more batches of kimberlite melt before phlogopite entrainment into the magma and transport towards the Earth's surface. Similar Ti-Cr-rich phlogopite cores were also identified in the groundmass of kimberlites from North America. Inner rims in phlogopite macrocrysts from the Aries kimberlites/orangeites and olivine macrocrysts and groundmass grains from kimberlites in Greenland, Canada, southern Africa and Russia have also been attributed to kimberlite metasomatism in the mantle.

This evidence, coupled with the occurrence of polymict-breccia xenoliths in South African and Russian kimberlites, indicates that '*failed*' kimberlite intrusions are probably a common phenomenon. Given the highly reactive nature of kimberlite melts towards mantle wall rocks, kimberlite magmas may only be able to reach the surface by ascent through a pathway created by multiple earlier magma pulses that metasomatise the conduit, insulating the later magmas from reaction with the surrounding mantle rocks (Fig. 2). This model might represent the fundamental ascent mechanism for kimberlite magmas.

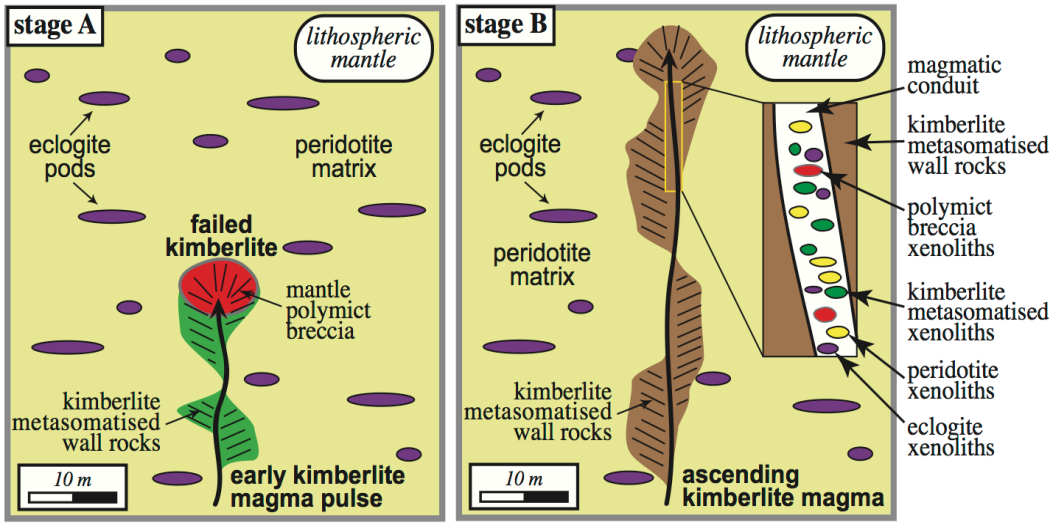

Figure 2. Conceptual model showing different stages in the evolution of a kimberlite magmatic system traversing the lithospheric mantle. Stage A: 'failed' kimberlite intrusion stalled at lithospheric mantle depths with the formation of polymict breccias and metasomatism of the conduit wall rocks. Stage B: the ascending kimberlite magma intrudes the pre-existing conduit and entrains wall rocks, including polymict breccias and previously metasomatised components (i.e. macrocrysts). The patchy occurrence of 'kimberlite-metasomatised wall rocks' illustrates that not all material entrained and transported to the surface is metasomatised, in agreement with the occurrence of abundant peridotite and eclogite xenoliths, that show minimal evidence of metasomatism by kimberlite magmas or related fluids. Other possible reasons for the abundance of non-metasomatised wall rocks include sampling of rocks several metres away from the metasomatised conduit, which could be incorporated into the conduit during the turbulent ascent of the larger kimberlite magma pulses and preferential melting and disaggregation of metasomatised wall rocks during kimberlite magmatic activity. The scale is based on a typical thickness of kimberlite dykes of about 0.5-1 m.

This study has also revealed that, in addition to the widely recognised magmatic and xenolithic components, kimberlite rocks host mantle-derived '*antecrysts*' (e.g., the high Ti-Cr zones of phlogopite grains), which are the products of '*failed*' kimberlite intrusions and were entrained by later kimberlite magmas. Mantle-derived antecrysts are an integral part of the kimberlite groundmass, where they occur as cores in groundmass grains. These antecrysts contribute to the bulk composition of kimberlites, and further complicate efforts to determine the composition of parental kimberlite melts by bulk-rock analysis.

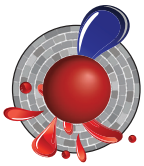

This project is part of CCFS Theme 2, Earth's Evolution, and contributes to understanding Earth's Architecture and Fluid Fluxes.

Contact: Andrea Giuliani

Funded by: ARC Discovery Early Career Researcher Award (DECRA)

A new zircon guide to copper-fertile igneous intrusions

The hunt for undiscovered mineral resources in igneous bedrock is increasingly reliant on *'halos'* - signals around an ore deposit that are much larger than the ore deposit itself. Stream sediments shed during erosion of an ore-bearing igneous complex can provide such a halo and can serve as guides to undiscovered ore upstream from the sediment sampling site.

CCFS research has identified several geochemical discriminants of granitic igneous rocks that produced magmatic-hydrothermal copper deposits. This type of deposit accounts for more than 75% of global copper production (*R. Loucks, Australian Journal of Earth Science, 2014*). Among the geochemical discriminants is the ratio europium/ytterbium, represented by the parameter (Eu/Eu*)/Yb. Eu/Eu* represents the *'Europium anomaly'* - the deviation of the measured abundance (Eu) from the abundance expected from the measured amounts of samarium and gadolinium (Eu*), which have atomic numbers just below and above, respectively, that of europium. Granitoid melts related to copper ores are distinguished from barren granitoid melts by unusually high values of Eu/Eu* and unusually low values of Y; the ratio (Eu/Eu*)/Yb magnifies the distinction of copper-ore-forming granitoid magmas from barren granitoid magmas.

Zircon, a ubiquitous trace mineral in granitic igneous rocks, takes in small amounts of Eu and Yb that substitute for some of the zirconium atoms in the zircon structure. We have discovered that zircon inherits a version of the (Eu/Eu*)/Yb ratio in its parent granitoid melt, warped by zircon's systematic preference for Yb relative to Eu. Europium atoms in the silicate melt can have an electric charge of +2 or +3; the granitoid melt's ratio of Eu^{2+}/Eu^{3+} is captured in the quantity Eu/Eu*. Zircon inherits a version of the parent granitoid melt's Eu/Eu*, warped by zircon's strong preference for Eu^{3+} relative to Eu^{2+}. Zircon also takes in small amounts of the elements cerium (Ce) and neodymium (Nd); magmas related to copper ores have unusually low abundances of Y, and zircon that crystallises from Y-depleted magmas inherits that feature as well.

Finally, zircons from copper-ore-forming granitoid magmas have distinctively high values of the ratio Ce/Nd, as compared to zircons from barren granitoids. The ratio (Ce/Nd)/Y in zircon thus magnifies the distinction between zircons from mineralised and unmineralised granitoid rocks.

We have measured (Eu/Eu*)/Yb and (Ce/Nd)/Y in hundreds of zircons from four major magmatic-hydrothermal ore deposits and nine barren igneous complexes, and compiled from the literature more than 2500 analyses of zircons from other copper-ore-bearing and barren igneous complexes. Figure 1 illustrates the efficacy of these parameters in discriminating zircons in copper-ore-bearing igneous complexes from zircons in barren reference suites. Because zircon is chemically and mechanically robust, it survives chemical alteration of its host rock and long-distance transport in streams. Our discovery allows the trace-element chemistry of zircon to be used by mineral exploration companies as a pathfinder to copper-fertile igneous complexes that may contain undiscovered ore. The analytical method used in our study, laser-ablation inductively-coupled plasma mass spectrometry, can do hundreds of analyses per day at a price that is cost-effective for mineral exploration.

This project is part of CCFS Themes 2 and 3, Earth's Evolution and Earth Today and contributes to understanding Fluid Fluxes.

Contacts: Robert Loucks, Yongjun Lu, Marco Fiorentini
Funded by: CCFS Flagship Program 2

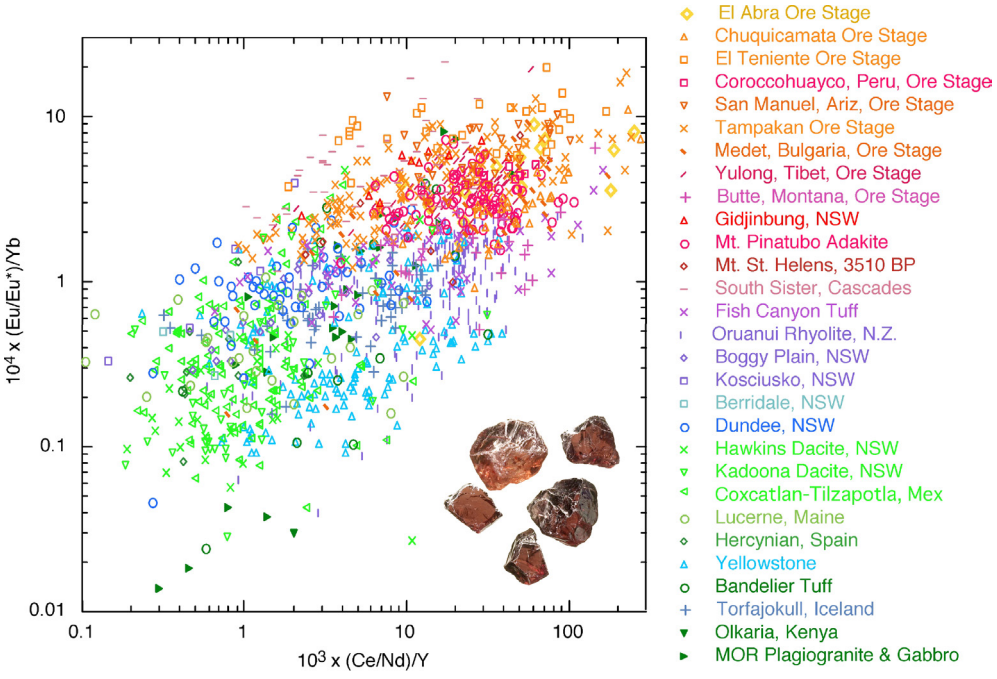

Figure 1. Trace elements in more than 3000 zircon crystals from copper-ore-bearing igneous complexes (red and orange symbols) and from unmineralised igneous complexes (violet, blue, green symbols). Because zircon robustly survives chemical alteration of its host rock and long-distance sedimentary transport, zircons in sediments can guide mineral exploration teams to copper-mineralised igneous complexes upstream from the sediment-sampling site.

Do continental flood basalts need plumes?

It has previously been postulated that the Earth's hydrous mantle transition zone may play a key role in intra-plate magmatism, but no confirmatory evidence has been reported. Here, we argue that high-temperature hydrothermally-altered subducted oceanic crust was involved in generating the Late Cenozoic Chifeng continental flood basalts of East Asia. This study combines oxygen isotopes with conventional geochemistry to provide the first evidence for an origin in the hydrous mantle transition zone.

The most striking observation in this study is that oxygen isotopes, $^{39}Ar/^{40}Ar$ ages, and other geochemical features of the Chifeng CFBs (SiO_2, Nb, Sm/Nd, and Ce/Pb) are correlated with their distance from the western edge of the stagnant Pacific slab (Fig. 1). In a westward direction, the lavas decrease in age, become progressively depleted in silica and have lower Sm/Nd ratios, whereas they show progressive enrichment in Nb and have higher Ce/Pb ratios. Importantly, the $\delta^{18}O$ values of olivine in the basalts increase westward away from the stagnant slab (Fig. 1). Thus the lavas immediately above the western edge of the stagnant Pacific slab are over-saturated in silica, and have the oldest eruptive ages, the lowest olivine $\delta^{18}O$ and possibly the highest fluid contents. The low-$\delta^{18}O$ lavas are characterised by enrichment of silica, high positive Sr anomalies, high Al_2O_3, and depletion in incompatible trace elements (Fig. 2), and Ce/Pb ratios like those commonly associated with subducted slabs (Fig. 3). Furthermore, the lower $\delta^{18}O$ is coupled with depletion in high field-strength elements (e.g., Nb; Fig. 2) and other incompatible elements, as evidenced by decreasing La/Sm ratios.

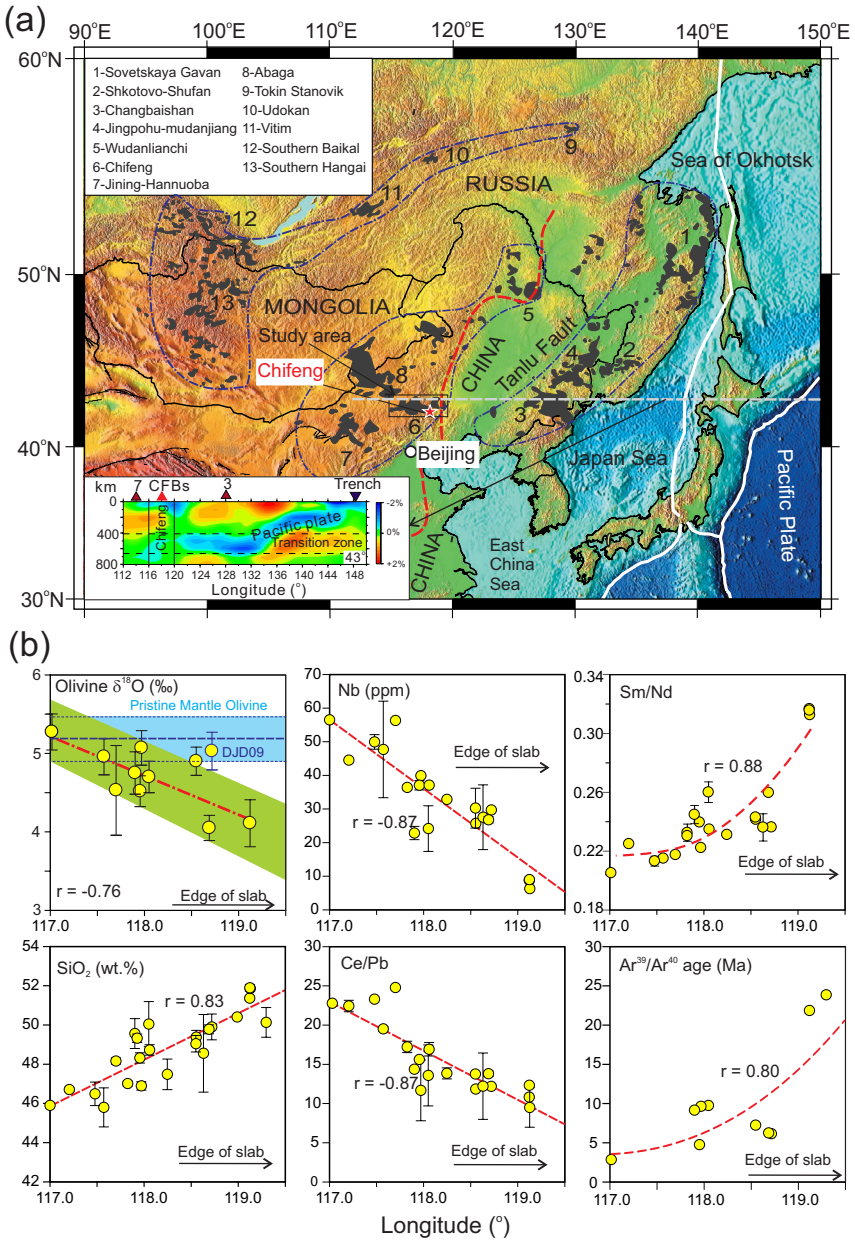

Figure 1. (a) Schematic map of the Late Cenozoic intraplate volcanic province in Central East Asia. (b) Covariations of olivine $\delta^{18}O$, major-trace elements, and $^{39}Ar/^{40}Ar$ ages as a function of eruptive longitude (for detail see text in X.C. Wang et al., 2015, Nature Communications, 6). Data points represent average of analysed whole-rock or olivine samples from individual Chifeng CFBs; error bars represent one standard deviation for each group of lava or olivine. r: correlation coefficient

This is confirmed by the studies of olivine-hosted melt inclusions from the south-eastern extremity of the Chifeng CFBs, erupted directly above the western edge of the stagnant Pacific slab. The melt-inclusion data imply that these CFBs were mainly derived from an olivine-free pyroxenite-dominated source with high water content (>450 ppm). These observations show that the low-$\delta^{18}O$ end-member melts most likely originated from hydrothermally-altered oceanic gabbros. Thus, the correlation of recycled oceanic gabbro-derived signatures with the inferred position of the stagnant Pacific slab within the hydrous MTZ provides an indirect, but important, constraint on the depth of the mantle source.

These observations lead us to propose an alternative model, whereby slab-triggered wet upwelling produces large volumes of melt that may rise from the hydrous mantle transition zone. This model explains the lack of pre-magmatic lithospheric extension or a hot-spot track

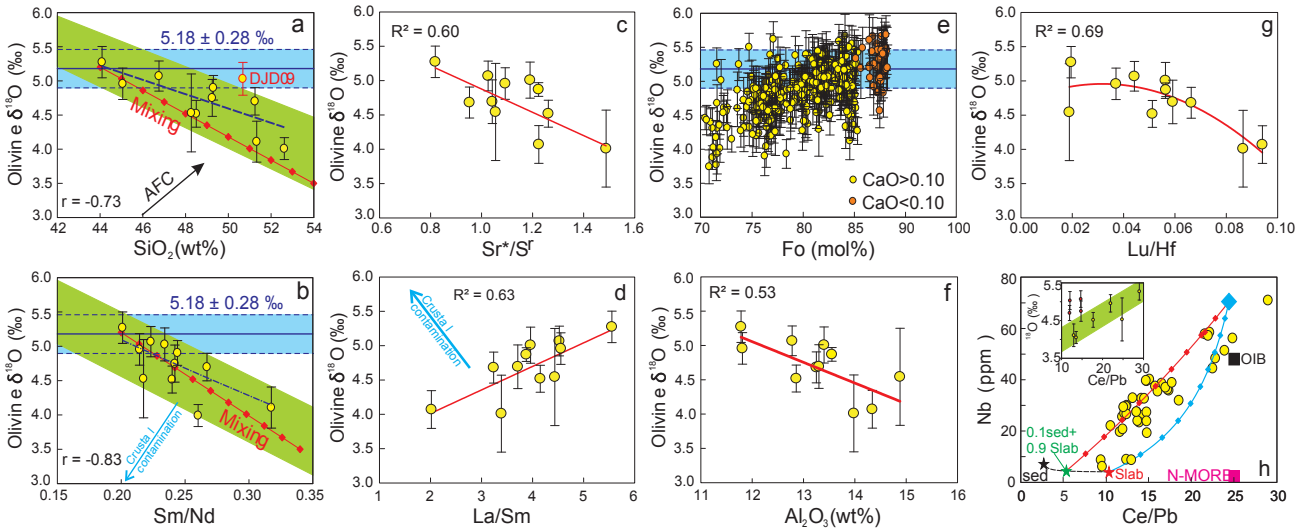

Figure 2. Correlation between average oxygen $\delta^{18}O$ values and (a) SiO_2, (b) Sm/Nd, (c) Sr/Sr, (d) La/Sm, (e) Fo contents, and (g) Al_2O_3, and (h) Lu/Hf and (f) Nb-Ce/Pb.*

and also the arc-like signatures observed in some large-scale intra-continental magmas. Deep-Earth water cycling, linked to cold subduction, slab stagnation, wet mantle upwelling, and assembly/breakup of supercontinents, can account for the chemical diversity of many continental flood basalts (Fig. 3).

This project is part of CCFS Theme 2, Earth's Evolution, and contributes to understanding Earth's Architecture and Fluid Fluxes.

Contacts: Xuan-Ce Wang, Simon Wilde

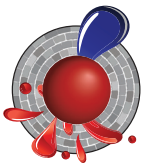

Funded by: Wang ARC Future Fellowship, National Natural Science Foundation of China (Grant No. 41222023 and 40803010) and the State Key Laboratory of Isotope Geochemistry at the Guangzhou Institute of Geochemistry, Chinese Academy of Sciences (Grant No. SKLIG-KF-13-07)

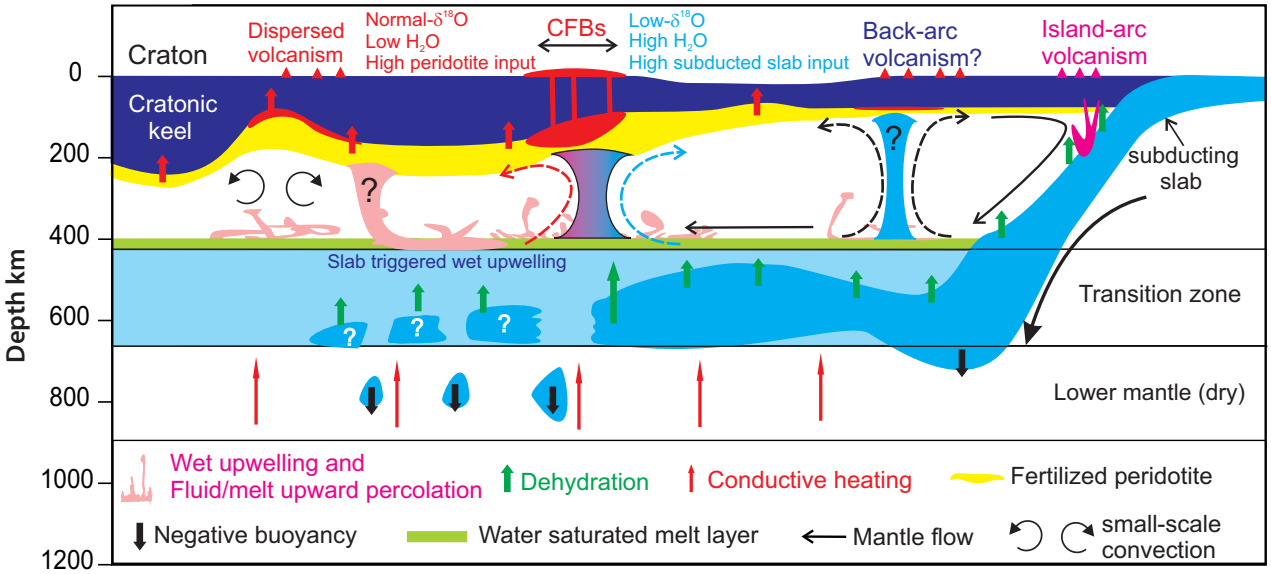

Figure 3. Effect of slab stagnation and water cycling (wet upwelling, upward percolation, and re-fertilisation) on the upper mantle thermochemical state. This model is mainly based on the strong spatial correlation of geochemical features with distance of eruptive lavas relative to the edge of the stagnant slab. It involves water partitioning in the Earth's mantle, behaviour of slab-triggered wet upwelling and upward percolation, hydrous mantle melting, the mantle wedge model, and upwelling from the hydrated mantle transition zone.

Ancient mantle lithosphere beneath the Khanka massif in Russian Far East: *In situ* Re-Os evidence

The Altaids (or Central Asian Orogenic Belt; CAOB) has been proposed as the world's largest site of juvenile crust formation during the Phanerozoic eon. Nevertheless, Kröner et al. (2014) documented that crustal evolution in the CAOB involved both addition of juvenile material from the mantle as well as abundant reworking of varying proportions of older crust throughout its accretionary history. Within the CAOB, several microcontinental blocks have been recognised, although it is still unclear if all of these truly predated accretion of the CAOB. This is also the case for the extreme eastern margin of the CAOB, which is composed of three microcontinental blocks: the Bureya, Jiamusi and Khanka massifs, located between the Siberia and North China cratons; the ongoing Pacific-plate subduction since the Mesozoic complicates the situation (Fig. 1).

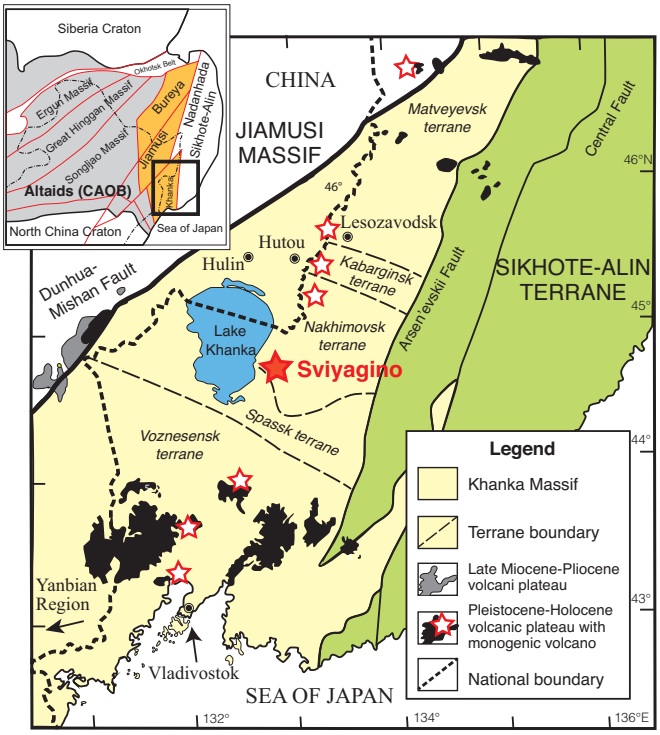

Figure 1. Tectonomagmatic map of the Khanka massif in relation to adjacent areas of NE China and Russia. Red stars: localities of individual volcanic domes; solid red star: locality of xenoliths from the Sviyaginsky volcano.

Lack of constraints has led to widely divergent views as to the origin and initial location of these blocks. It has been postulated that the Jiamusi-Khanka massif may be derived from a peri-Gondwana position, or be an exotic block of affinity to South China Block, or a fragment of the Siberian Craton.

Recent studies have demonstrated that Os model-age spectra from mantle xenoliths commonly show age peaks corresponding to the ages of thermal/tectonic events in the overlying crust. Thus, *in situ* analysis of Re-Os isotopic compositions by laser sampling of single sulfide grains makes it possible to test the existence of a Precambrian microcontinent within the eastern CAOB complex and clarify whether the Khanka massif has a tectonic affinity to the Siberian Craton. The Os isotope compositions of sulfides in mantle xenoliths hosted by late Miocene alkali basalts from the Sviyaginsky volcano, Russian Far East (Fig. 1), reveal the presence of Archean-Proterozoic subcontinental lithospheric mantle (SCLM) beneath the Khanka massif. Both their T_{MA} and T_{RD} model ages reveal similar peaks at 1.1 and 0.8 Ga suggesting later thermotectonic events in the SCLM, whereas T_{RD} model ages extend back to 2.8 ± 0.5 (2σ) Ga. The events recognised in the SCLM are consistent with those recorded in crust of the Khanka massif. The sulfide Os-isotope

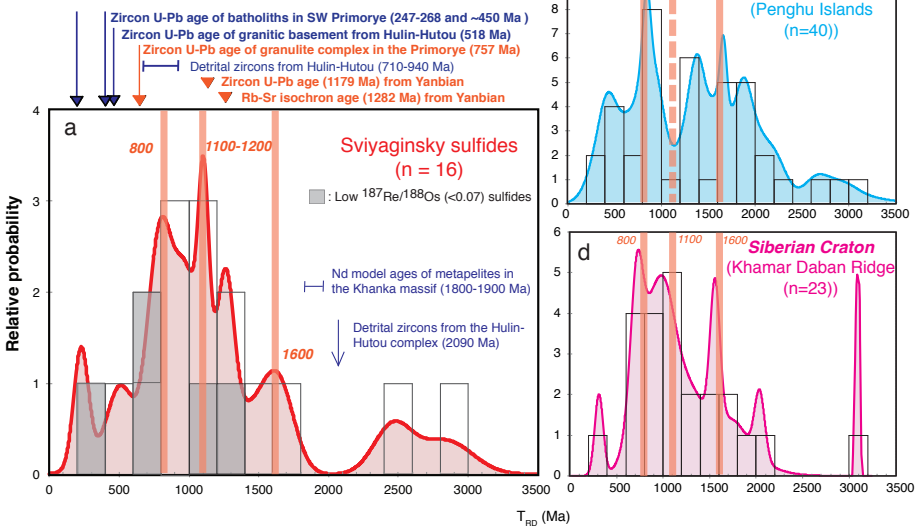

Figure 2. Cumulative probability diagrams (Ludwig, 2000) of T_{RD} model ages of sulfides from (a) the Sviyaginsky volcano; (b) the Turkana Depression in south Ethiopia on the Arabian-Nubian Shield (Wang et al., 2005); (c) the Penghu Islands in Taiwan at the margin of the South China Block (Wang et al., 2003, 2009a); and (d) the Khamar Daban Ridge in south Russian Siberia on the Slyudyansky terrane (our unpublished data). Thick line represents the distribution pattern of ages. The histogram of ages represented by thin grey lines is also shown. Grey bars indicate sulfides with low $^{187}Re/^{188}Os$ ratios (<0.07) having pristine characteristics without later modification. Corresponding crustal events are shown for comparison.

data show that the SCLM beneath the Khanka massif had formed at least by the Mesoproterozoic, and probably in the Archean, and was subsequently metasomatised during juvenile crustal-growth events related to the evolution of the Altaids. The peak Os model age pattern of the Sviyaginsky sulfides, compared to sulfide Os model ages from these terrains, provide further insights on the origin of the Khanka massif. In Figure 2, peak Os model age patterns of sulfides in mantle xenoliths from Turkana Depression in south Ethiopia on the Arabian-Nubian Shield (*Wang et al., 2005*), the Penghu Islands at the margin of South China Block (*Wang et al., 2003; 2009*), and the Khamar Daban Ridge in south Russian Siberia (Slyudyansky terrane; our unpublished data) are shown for comparison with the Sviyaginsky sulfides. Sulfides from south Ethiopia (Fig. 2b) do not have the Mesoproterozoic-Archean Os age record, and their peak Os age patterns are not consistent with the Sviyaginsky sulfides. The Sviyaginsky sulfides have pronounced peak ages at 1.1-1.2 and 0.8 Ga, while the Taiwan sulfides obviously do not have an age peak at 1.1-1.2 Ga (Fig. 2c). Only sulfides from the Slyudyansky terrane have peak age patterns similar to the Sviyaginsky sulfides (Fig. 2d). Thus the Khanka massif has tectonic affinities to the Siberian Craton and probably was derived from it, as proposed by Zhou et al. (2010).

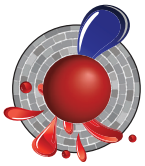

This project is part of CCFS themes 1 and 2, Early Earth and Earth's Evolution, and contributes to understanding Earth's Architecture and Fluid Fluxes.

Contacts: Kuo-Lung Wang, Sue O'Reilly, Bill Griffin

Funded by: Ministry of Science and Technology, Taiwan projects NSC 101-2923-M-001-001-MY3, NSC99-2116-M-001-017

Palaeoproterozoic Superia Supercraton: New insights from Yilgarn

The hypothesis of supercontinent cycles predicts the assembly of a supercontinent in Siderian time (2.5-2.3 Ga). Bleeker and Ernst (Dike swarms 2006) postulated the existence of the Superia supercraton at that time, which included the Superior, Karelia and Hearne cratons. Söderlund et al. (Precambrian Research 2010) provided some evidence that the Zimbabwe and Yilgarn cratons could also have formed part of Superia. To test this hypothesis we studied the Erayinia mafic dykes in the eastern part of the Yilgarn Craton. This study has been done in collaboration with Bert De Waele (SRK Consulting), Sarah Jones (St Barbara Limited), Ulf Söderlund (Lund University) and Richard Ernst (Carleton University) (*CCFS publication #508*).

Previously undated Erayinia dykes have been thought to belong either in the 2.42-2.41 Ga Widgiemooltha LIP or in the 1.21 Ga Marnda Moorn LIP. We dated Erayinia dykes at 2401 ± 1 Ma (U-Pb TIMS baddeleyite). The palaeomagnetic analysis isolated a stable primary remanence with steep downward direction similar, but not identical to that of the previously studied Widgiemooltha dykes. This slight directional difference and the opposite palaeomagnetic polarity suggest that Eryiania dykes are probably not related to the 10 m.y. older Widgiemooltha LIP. The comparison of Eryiania and Widgiemooltha palaeopoles suggest the angular velocity of the Yilgarn Craton between 2410-2420 and 2400 Ma at ~1°/m.y., which is comparable with similar estimations for the angular plate velocities in the Phanerozoic. The estimated amplitude of the geomagnetic secular variations at c. 2400 Ma is slightly higher than predicted by the existing models for the last 5 m.y. at the c. 64°latitude.

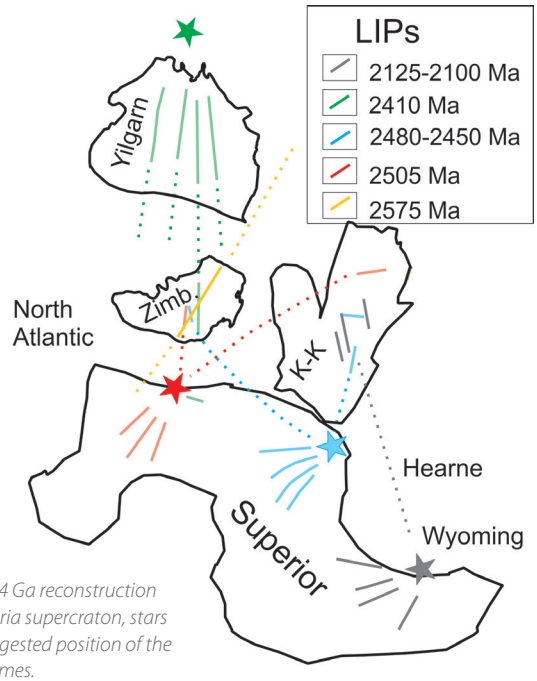

Figure 1. 2.4 Ga reconstruction of the Superia supercraton, stars denote suggested position of the mantle plumes.

New palaeomagnetic poles, together with previously published palaeopoles and with the analysis of Palaeoproterozoic LIPs distribution, led us to a modified reconstruction of the Superia supercraton at c. 2.4 Ga (Fig. 1) and confirmed the suggestion that the Superior, Yilgarn, Zimbabwe, Kola-Karelia, North Atlantic, Hearne and Wyoming cratons could be parts of this supercraton.

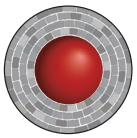

This project is part of CCFS themes 1 and 2, Early Earth and Earth's Evolution, and contributes to understanding Earth's Architecture.

Contact: Sergei Pisarevsky

Funded by: CCFS Flagship Program 5, LIPs - Supercontinent Reconstruction - Resource Exploration Project (www.supercontinent.org)

3D magma emplacement

Magma generation and emplacement is an important process of material transfer that shapes much of Earth's continental crust. Molten material generated below the lithosphere contributes to the growth of the continental crust, erupting as magmas in near-surface regions or large growing magma bodies at sub-crustal levels. Understanding the physical processes involved in the generation and emplacement of magma requires knowledge about the geochemical and physical properties of melt, magma (melt plus crystals) and host lithologies. Different magma sources, melting conditions and differentiation processes have been proposed to account for the basaltic and andesitic magmatism that operates on Earth's surface. However, it is becoming increasingly apparent that the evolution of magmas is intrinsically related to transport mechanisms, which control emplacement depths, structures and petrogenesis. Transport mechanisms that have been proposed in the past can be divided into two main groups, processes of diapiric-like emplacement and those that favour magma ascent in dikes. However, it seems that nature combines both processes, which may simultaneously or sequentially control ascent and emplacement. On the other hand, crustal heterogeneities, rheological anisotropy and local and far-field stresses are likely to play key roles in magma emplacement. Feedback between these processes will affect how and where magma is stored.

Despite the rapidly growing volume of geological, geophysical and experimental data on magma rheology, chemistry, structure and emplacement, numerical simulations on the dynamics of magma ascent and emplacement are comparatively rare. Numerical studies devoted to magmatism have instead mainly focused on the internal dynamics of magma chambers, and little is known about the visco-brittle/plastic interplay between magma and crust.

The new set of 3D numerical experiments demonstrates the first-order importance of host rock rheology upon emplacement; it is responsible for the variable shapes of the intrusions, such as cone shaped, saucer shaped, funnel shaped and tabular. Brittle parameters such as cohesion and friction angle, and especially the strain limit for fracture-related weakening are important. For example, with a fully mafic crust and strain hardening, the shape of the intrusion and the surrounding faults imitate the shapes of magmatic bodies observed in nature, such as '*ring complexes*' (Fig. 1a), which are incredible magmatic structures, and a rich source of information on magma transport and emplacement. On the other hand, with strain weakening the intrusion travels very rapidly through the crust and is of relatively small diameter without much deformation of the host rock.

This study also allows a glimpse into a long-standing debate on how and if magmas are controlled by extensional regimes or pre-existing shear zones (Fig. 1b).

It has been confirmed that pre-existing faults or shear zones control the development of the shape of the intrusion. Interestingly this control is better observed with mafic host rocks than with felsic rocks. In the first instance the shape of the intrusion strictly follows the pre-exisiting zones of weakness and flat dykes can be observed (Fig. 1b). On the other hand the boundaries of intrusions into felsic host-rocks do not sharply follow the pre-existing weak zones.

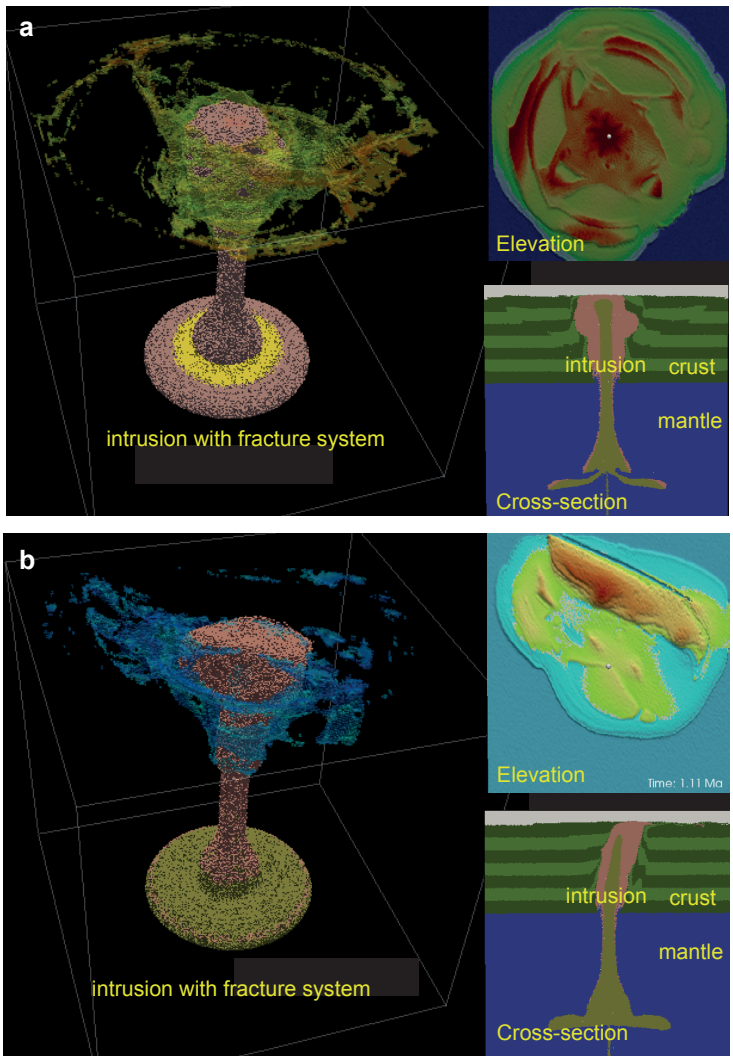

This project is part of CCFS Theme 2, Earth's Evolution, and contributes to understanding Earth's Architecture and Fluid Fluxes.

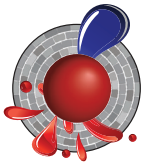

Contact: Weronika Gorczyk

Funded by: ARC Linkage Project, CCFS Flagship Program 2

Figure 1. 3D image represents an intrusion and the fracture system that develops around it. a) simulating a ring complex. b) simulating the directionality of the intrusion with a pre-existing weak structure, such as a fault. Top right (a, b): relative elevation: blue <0, red - >0, green = 0. Bottom right (a, b): cross-section through the middle of the intrusion showing rock composition.

Solving the "Ophiolite Conundrum"

Ophiolites record shallow plate-tectonic processes in oceanic basins, arcs and ocean-continent transitions on Earth; recent confirmation of natural ultrahigh-pressure and super-reduced phases (e.g., diamond, moissanite) from Tibetan ophiolites shows that these pieces of ancient lithospheric fragments can also provide new insights into the deep convective mantle and even the Transition Zone (410-660 km). However, a long-term global conundrum (supra-subduction-zone-type ophiolites with mid-ocean-ridge features) impedes further understanding of ophiolite formation and relevant geodynamic processes. We have carried out a systematic petrological and geochemical investigation of the Zedang ophiolite (outcrop area ~100 km_2) in the Yarlung Zangbo Suture Zone (South Tibet, China), which marks a tectonic boundary between the Indian and Asian continents.

In the Zedang ophiolite, detailed mineral chemical data reveal a two-layered lithospheric mantle structure: the harzburgite domain in the east [spinel Cr# (mole $Cr^{3+}/(Cr^{3+}+Al^{3+})$ = 0.62-0.33] is more depleted than the lherzolite domain in the west (spinel Cr# = 0.30-0.17) and shows much lower equilibration temperatures (differences of ~250-150 K) than the lherzolites. Clinopyroxene trace-element compositions indicate that the harzburgites underwent pervasive metasomatism after melt extraction, while the lherzolites did not.

New zircon U-Pb ages show that the harzburgites were intruded by dolerite dykes with clear chilled margins at ~130-128 Ma,

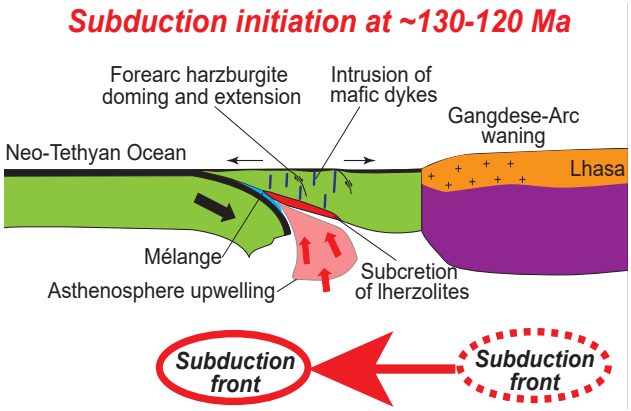

Figure 1. Cartoon illustrating the southward jump of the Neo-Tethyan subduction front at ~130-120 Ma, resulting in the subduction initiation and forearc lithosphere accretion as future Yarlung Zangbo ophiolites in South Tibet, China.

consistent with the widespread but minor mafic magmatism at ~130-120 Ma in the Yarlung Zangbo ophiolites. Nd-Hf isotopic data indicate that the Zedang lherzolites subcreted the pre-emplaced harzburgites concurrently with the intrusion of the dolerite dykes into the harzburgites, and that the lherzolites and dolerites both were derived from upwelling asthenosphere with minor slab input. Furthermore, available zircon geochronology and Hf-isotope data show that juvenile magmatism in the northern Gangdese Arc (southern part of the Lhasa microcontinent) almost ceased from ~130-120 Ma. These observations suggest a southward jump of the Neo-Tethyan subduction front from beneath the Gangdese subarc region (north) to the forearc oceanic lithosphere (south) during this short period. This jump may have been triggered by plate reorganisation related to the collision between the Lhasa *cont...*

Figure 2. Kang Wu, Xiaoxiao Huang, Qing Xiong and Xiaohan Gong climbing the Dazhuka Mountain, Xigaze ophiolite (S. Tibet).

and Qiangtang blocks, and the Gondwanaland breakup in the early Cretaceous.

We find that the relocation of the Tethyan subduction front caused the subduction initiation in front of the southern margin of the Gangdese Arc at ~130-120 Ma, and consequently resulted in asthenosphere upwelling, subcretion of lherzolites, doming and extension of the overlying harzburgitic forearc lithosphere and the intrusion of mafic dykes (Fig. 1). The extensional structure and MORB-type magmatism are similar to those usually observed in slow-spreading mid-ocean-ridges, and can be easily interpreted as formed during subduction initiation beneath pre-existing buoyant lithosphere, consistent with the geochemical evidence for a subduction-related evolution. Our multi-stage forearc accretion model provides a new solution to reconcile the global "*Ophiolite Conundrum*".

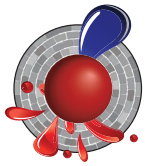

This project is part of CCFS Theme 2, Earth's Evolution, and contributes to understanding Earth's Architecture and Fluid Fluxes.

Contacts: Qing Xiong, Bill Griffin, Sue O'Reilly, Norman Pearson, Jian-Ping Zheng (China University of Geosciences, Wuhan)
Funded by: ARC Discovery Project, CCFS Flagship Program 1, NSFC (J.P.Z.)

Secular change in Archean crust formation recorded in Western Australia

The mechanisms that generated early Archean continental crust are controversial. Continental crust may have accumulated via horizontal accretion in modern-style subduction zones or via vertical accretion above upper mantle upwelling zones. However, the characteristics of the continental crust changes at the transition between the Archean and Proterozoic eons, suggesting that continental crust did not form in subduction zones until at least the late Archean.

In a manuscript (*Yuan, CCFS publication #649*) seismic receiver function data were used to analyse the bulk properties of continental crust in Western Australia (Fig. 1), which formed and stabilised over a billion years in the Archean. The analysis shows that the bulk seismic properties of the crust cluster spatially, with similar clusters confined within the boundaries of tectonic terranes (Fig. 2). This spatial clustering of the crustal properties is strongly indicative that these tectonic sub-units may have formed differently through time.

Local Archean crustal growth models suggest that both plume and subduction processes may have had a role in creating crust throughout the Archean. A correlation between crustal age and the bulk seismic properties of the crust reveals a trend: from about 3.5 Ga to the end of the Archean, the crust gradually thickened and simultaneously became more evolved in composition. A similar trend of Archean crustal thickening is also found in a global compilation by Keller and Schoener (*Nature, 2012*).

This trend probably reflects the transition between crust dominantly formed above mantle plumes, to crust formed in subduction zones - a transition that may reflect the secular cooling of Earth's mantle. Numerical simulations (*e.g. Johnson et al., Nature Geoscience, 2014*) show that such secular mantle cooling (decreasing mantle potential temperature (Tp), controls the overall efficiency of the Archean lower crustal delamination processes: higher Tp results in rapid and complete removal of the lower crust, while lower Tp makes the removal process less efficient. It is thus likely that the systematic crustal thickening in WA may simply reflect the secular mantle cooling process: more efficient lower crustal removal processes in the hotter Paleoarchean lead to a thin

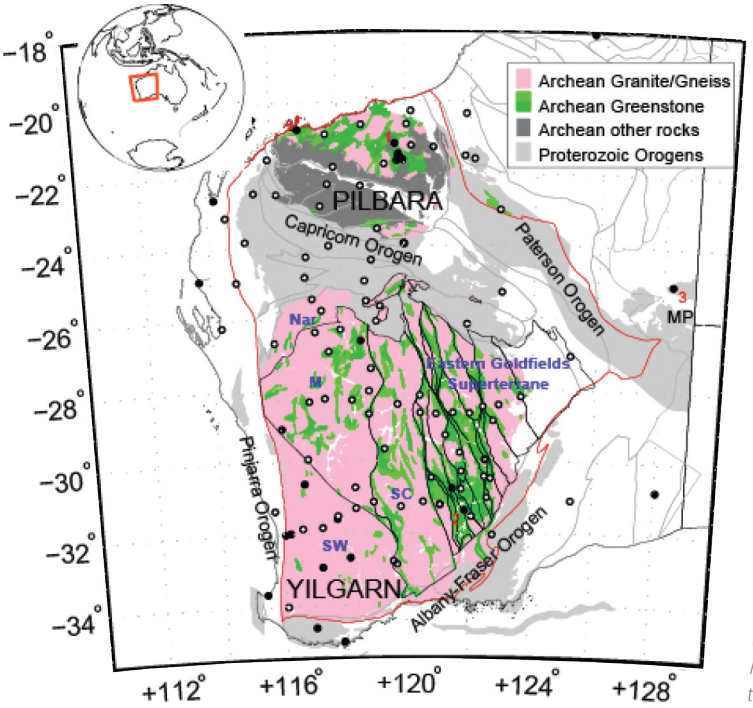

Figure 1. Simplified Archean and Proterozoic rock ages, crustal elements and seismic stations in Western Australia. Inset shows the location of the study region. Greenstone belts are shaded in green. Rock ages and large-scale crustal elements are based on 1:500k State Tectonic units map compiled by the GSWA. Terrane and domain boundaries in the Yilgarn follow Cassidy, et al. 2010. Seismic stations are shown by open (temporary deployment) and filled (permanent) circles. Labels are: Nar, Narryer terrane; M, Murchison domain; SW, Southwest terrane; SC, Southern Cross terrane; and MP, Proterozoic Musgrave Province.

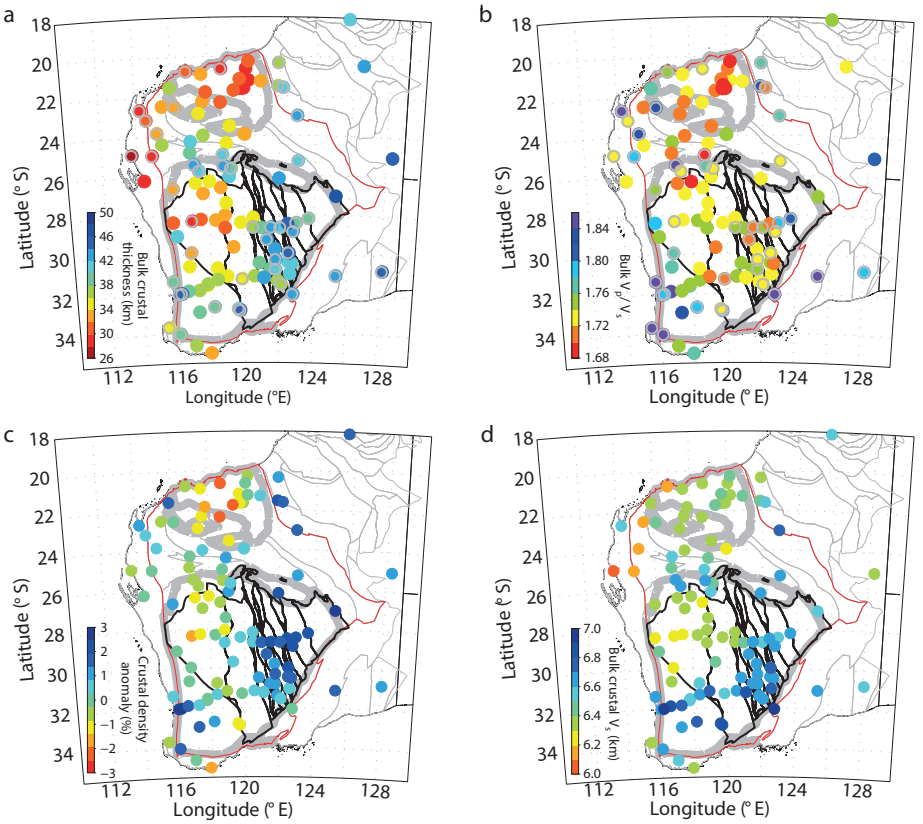

Figure 2. Spatial distribution of the crustal observations in the Western Australian craton. a-d, Bulk crustal thickness (a), Vp=Vs ratio (b), crustal density anomaly (c; Aitken et al., Tectonophysics 609, 467-479, 2013) and composite bulk crustal compressional wave (P-wave) velocity (d). The measurements are colour-coded and plotted at the seismic stations. The WA craton is contoured in red. The subdivisions of WA can be found in Figure 1.

Pilbara crust; towards the end of Archean, the delamination processes gets sluggish and less lower crust is delaminated, resulting in a gradually thickened crust.

The overall efficiency of the lower crustal delamination processes through time can also explain the age-progressive evolution of the WA crustal composition. In the Paleoarchean, the high mantle temperature and radiogenic crust, episodes of plume activity (*Van Kranendonk, CCFS publication #492*) and delamination-driven melts (*Bedard, Geochimica et Cosmochimica Acta, 2006*) are probably the key to generating the extremely felsic crust found in the Pilbara, by multi-stage crustal fractionation. In the late Archean, if more mafic lower crust is preserved, it would result in a bulk crustal composition that is more intermediate. By this time, crustal growth in WA may be in transition to a horizontal accretion regime.

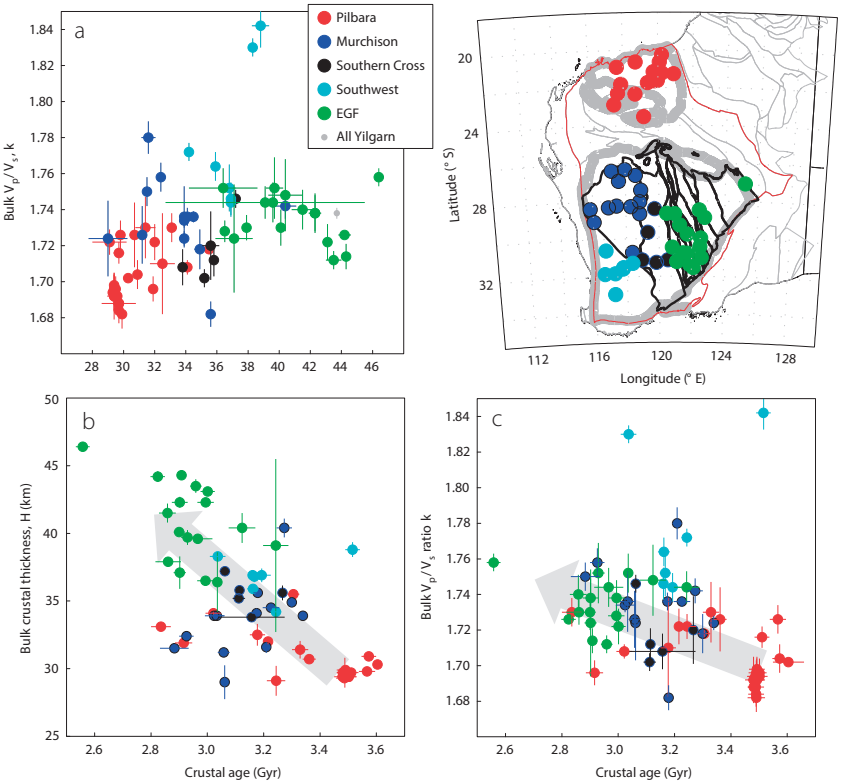

Figure 3. Clustering and temporal variations in the WA crust. a-c, Clustering in the seismic measurements (a), the age correlation of the bulk Vp=Vs ratio (b), and the bulk crustal thickness (c). Stations for each subdivision are marked on the map (inset) and labelled in a. The measurement errors of seismic observations and the errors associated with the isotopic ages are indicated. Note the large deviation of the Southwest terrane and the lack of robust measurements from the Narryer terrane, which are discussed in CCFS Publication #649.

As the mantle cooled, subduction eventually became more dominant in the late Archean (*Barley et al., Precambrian Research, 2008*); the subduction-related new magmas that were added to the continental crust may evolve to more intermediate composition (*Christensen and Mooney, Journal of Geophysical Research, 1995*).

This project is part of CCFS themes 1, 2 and 3, Early Earth, Earth's Evolution and Earth Today, and contributes to understanding Earth's Architecture.

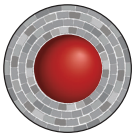

Contact: Huaiyu Yuan

Funded by: CCFS Flagship Program 7

The geometry and kinematics of hydrothermal vein emplacement in the 3.5 Ga Dresser Formation, North Pole Dome, Western Australia

Figure 1. Dense network of hydrothermal feeder veins to the Dresser Formation in the North Pole Dome.

The 3.5 Ga Dresser Formation in the Pilbara Craton of Western Australia is famous for hosting Earth's oldest convincing evidence of life, exposed in the North Pole Dome (see *Research highlight pp. 178-179*). The Dresser Formation is preserved as a ring of hills, up to 14 km in diameter, and dips shallowly away from the ca 3.46 Ga North Pole Monzogranite that was emplaced to the core of the dome as a sub-volcanic laccolith during eruption of the overlying (ca 3.45 Ga) Panorama Formation.

The Dresser Formation was previously considered to represent a quiet-water, shallow marine environment, but more recent studies suggest it was deposited in an active volcanic caldera floored by an extensive syn-depositional hydrothermal system (Fig. 1). Although the veins representing this system have been recognised as fracture fillings and syn-depositional growth faults (*e.g., Nijman et al., Precambrian Research, 1999*), no kinematic reconstruction of the offsets has previously been attempted. Such a reconstruction can constrain the regional tectonics and associated deformation: was there a regional stress field, or can the veins be related to processes directly related to magma supply and discharge within an evolving caldera system? Is there more than one vein set, and if so how do they relate to the developing caldera?

Answering these questions requires a better view of the structure of veins and their geometry and very detailed field studies of vein networks. This has involved detailed field mapping and structural analysis to define the 3-dimensional geometry of the network and the history of veining and fault-related offsets. In the field mapping phase we measured approximately 300 veins in the area (Fig. 2; B). Hydrothermal veins were measured for their strike and dip and geographic co-ordinates. As well, cross-cutting relationships between veins were documented where observed, to define the age relationships between the veins. The study area is divided into 10 separate structural blocks whose boundaries are defined by major faults (Fig. 2; A).

The measured veins in each structural block were analysed using the Dips and Stereonet computer programs. This allows determination of the principal orientation of the vein sets, the number of vein sets in each block, and the number of vein

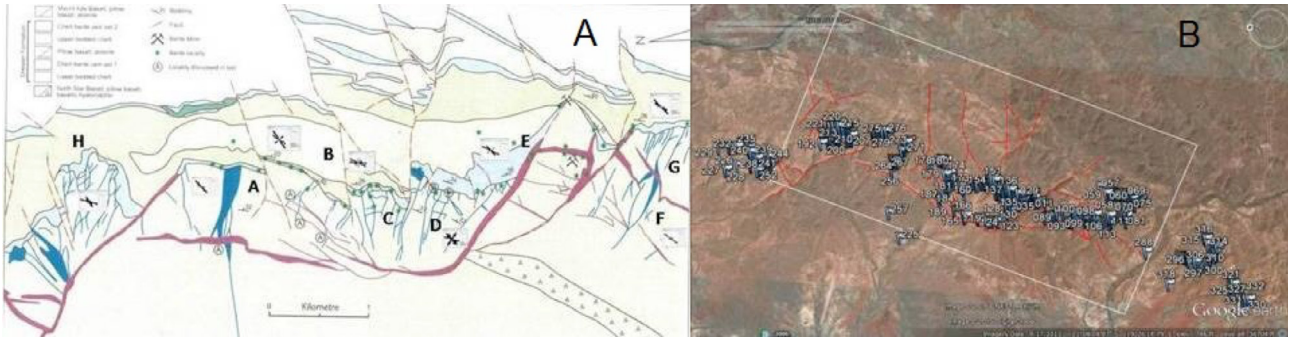

Figure 2. A) Geological map of part of the Dresser Formation, showing two sets of hydrothermal veins (dark blue and purple) and major structural blocks (A-H). Note that many veins occupy faults that offset bedded cherts (light blue) and volcanic rocks (green). B) Field stations in the study area. White rectangle outlines the area of represented in A.

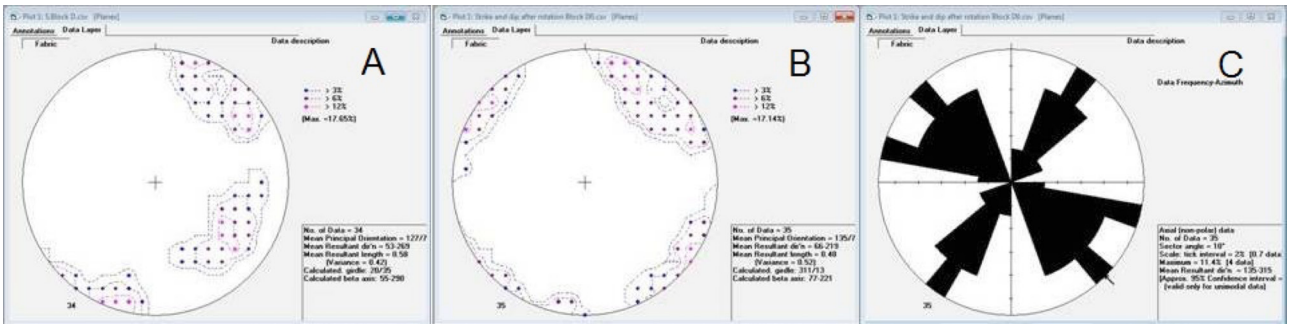

Figure 3. A) Measured orientations of veins in Block D. B) Back-rotated data of veins in block D, showing a NW-SE and NE-SW conjugate array of veins in this block prior to tilting. C) Rose Diagram of back-rotated vein data from block D.

systems in the whole of the study area. The measured data were back-rotated to horizontal by un-tilting the bedding, using the Stereonet program Georient. The back-rotated vein data thus represent the orientation of the veins in each structural block before regional tilting (Fig. 3).

This analysis indicates that almost all veins were vertical prior to tilting; therefore, Rose diagrams of each structural block were constructed, in order to identify the main direction of the veins in each block (Fig. 3; C).

The age relationships of the veins sets were studied in order to determine the relationship of the vein sets to regional deformation. The collected data also provide a better understanding of the history of events and geodynamic setting of the Dresser system. This information then will be used to develop a 4-dimensional understanding of the events that accompanied the flourishing of the earliest life on Earth.

This project is part of CCFS Theme 1, Early Earth, and contributes to understanding Earth's Architecture and Fluid Fluxes.

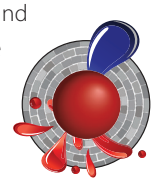

Contacts: Sahand Tadbiri, Martin Van Kranendonk
Funded by: CCFS Flagship Program 4

Unraveling the Baoule-Mossi secrets: U-Pb and Lu-Hf studies of detrital zircons from southern Mali, West African Craton

The West African Craton and in particular its southern portion represented by the Leo Man rise host a number of world class and base metal systems. The Leo Man is divided into the Archean Kénéma-Man in the western portion and the Baoulé-Mossi in the eastern region (Fig. 1). The Kénéma-Man domain is characterised by Archean age rocks and covers large portions of Sierra Leone, Liberia, Côte d'Ivoire, and Guinea. Its counterpart, the Baoulé-Mossi is characterised by Paleoproterozoic age rocks that are commonly referred to as the Birimian terranes. The Baoulé-Mossi covers most of the geology of Burkina Faso, Ghana, Mali, Niger, Côte d'Ivoire, and Guinea. The Birimian terranes *sensu lato* are comprised of relatively narrow volcano-sedimentary basins and linear or/and arcuate volcanic belts known as greenstone belts-basins; associated granitic-felsic intrusive terranes; the contemporaneous or slightly younger sedimentary basins, such as Kuasi, Siguiri, and Sunyani, and the late-basins such as the Tarkwa, and Bui.

cont...

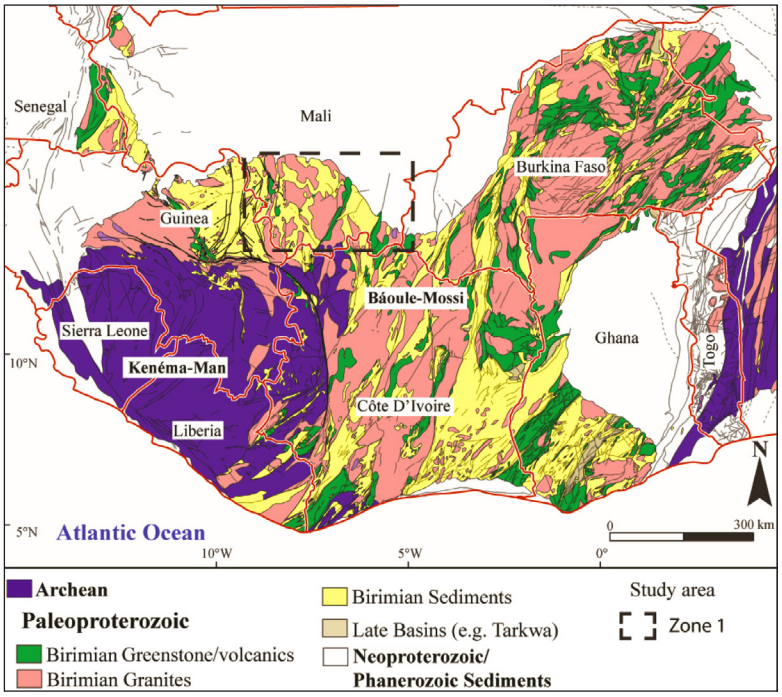

Figure 1. Simplified geological map of the Leo-Man rise (modified after the BRGM SIGAfrique map, (Milési et al., 2004) and the West African Craton (after Gueye et al., 2007).

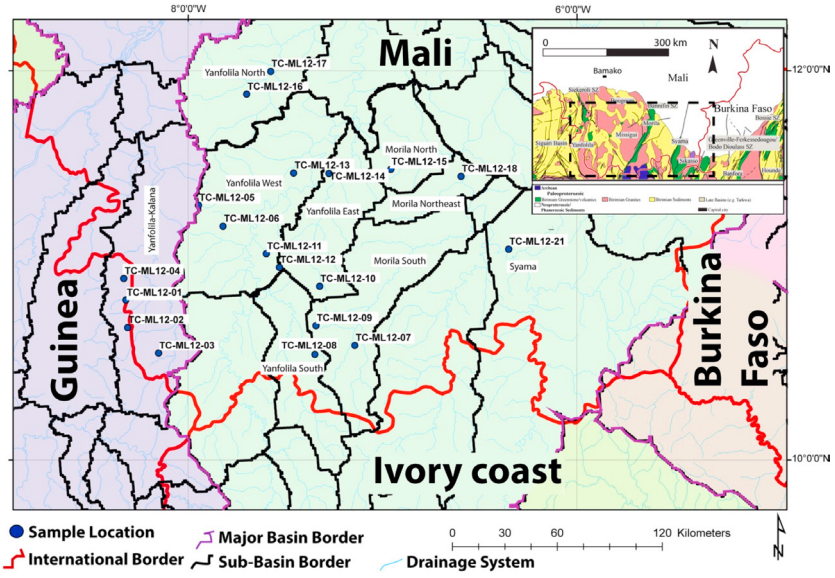

Figure 2. Sample distribution across southern Mali. Purple region represents the Niger River Basin while the light green region corresponds to the Bani River Basin. Basin and sub-basins after Lehner et al., 2006.

Despite the occurrence of a large number of mineral deposits, the region is still poorly understood and subject to much controversy. One of these controversies is the distinction between the Archean and Paleoproterozoic boundaries. It is also believed that the Paleoproterozoic Baoulé-Mossi is the result of mostly juvenile activity with limited interaction with older Archean material. In order to shed light onto the matter, this study analysed zircons collected from small streams, creeks and dry gullies in the area's modern drainage system. Zircons were collected from twenty sites across southern Mali covering the Niger and Bani river basins. The Niger River was sampled across 4 sites representing one sub-basin and the Bani River was sampled across eighteen sites representing 8 sub-basins (Fig. 2). A total of 599 zircons from the Niger River and 2254 zircons from the Bani River basin were selected as part of the study. U-Pb analyses were conducted on 295 zircons of the Niger River and 792 zircons of the Bani River, after which 92 zircons of the Niger River and 284 zircons from the Bani River were analysed for Lu-Hf isotopes.

The U-Pb results gave Paleoproterozoic ages between 2400 and 2070 Ma. This age range is in agreement with the historical record across southern Mali. These Paleoproterozoic age zircons are considered to be of magmatic origin and show limited metamorphic overprints. They yielded Hf-isotope compositions that indicate model ages between 2800 and 2100 Ma. The spread in Hf-isotope composition points towards a mixing between a juvenile source and a crustal source as old as 2800 Ma.

A second group of zircons yielded U-Pb ages between 3600 and 2100 Ma and Hf model ages between 3600 and 2800 Ma (Fig. 3). This second group presents characteristics that are congruent with long transport due to mostly sub-rounded to rounded crystal morphology. It is also likely that streams and small rivers transported zircons from the Archean Kénéma-Man domain to the Baoulé-Mossi domain because the basin drainage is mainly in a south-southwest to north-northeast direction. Multiple grains were analysed in both rims and suspected inherited cores and showed no variation in ages. Thus, no Proterozoic zircons with Archean age cores have been identified.

The identification of Archean zircons in the region suggests greater interaction between the Baoulé-Mossi and Archean Kénéma-Man domains. Although zircons of the Baoulé-Mossi domain generally confirm its juvenile origin, some of those Paleoproterozoic grains have Hf-isotope composition that indicate reworking of an older crust at a larger scale than previously recognised.

This project is part of CCFS Theme 2, Earth's Evolution, and contributes to understanding Earth's Architecture.

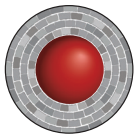

Contacts: Luis Parra-Avila, Elena Belousova, Marco Fiorentini, Lenka Baratoux, James Davis, John Miller, Cam McCuaig

Funded by: AMIRA International West Africa Exploration Initiative II (WAXI-II) Project (P934A), ARC Linkage Project, Geological Surveys and Departments of Mines in West Africa as sponsors in kind of WAXI; Fiorentini ARC Future Fellowship, CCFS Flagship Program 2

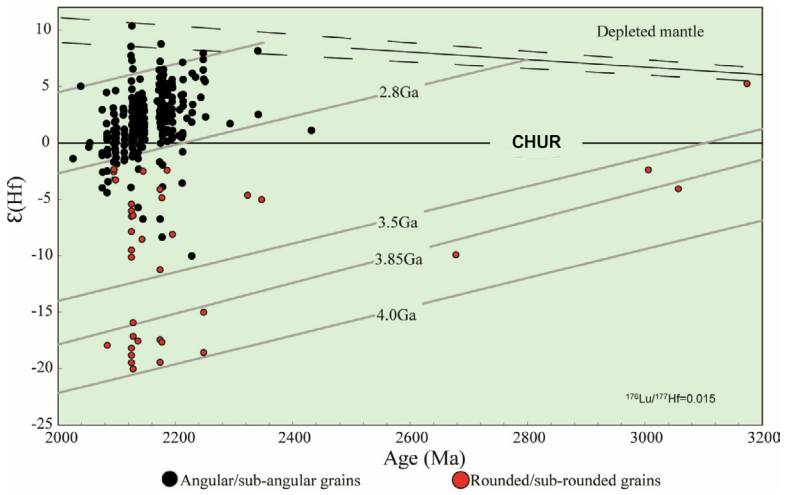

Figure 3. εHf vs. U-Pb age in Ma showing the distribution of the angular to sub-angular grains (black circles) and the sub-rounded to rounded grains (red circles).

Disequilibrium-induced initial Os isotopic heterogeneity: implications for dating and source tracing

The Re-Os isotopic system has been widely used to date a variety of materials ranging from mafic-ultramafic rocks and sulfides, to black shale, and even oil. Given their chalcophile and siderophile geochemical behaviour, both Re and Os have a strong affinity to trace phases (e.g. sulfides and alloys), and thus their budgets in these rocks are controlled mainly by these trace phases. The unequal distribution of these discrete trace phases (the nugget effect) leads to poor reproducibility of both Re and Os concentrations that limits applications of the isotopic system. However, its effect on the scale of initial Os isotopic heterogeneity is unclear. To clarify these uncertainties, it is necessary to investigate whether homogenisation of the Os isotopic composition was achieved in these rock systems during their formation.

Replicate analyses of gram aliquots of single basaltic powders (one of reference material BHVO-2 and three of the Hatu basalts from the western Junggar region, China) show large variations in both Os concentrations and isotopic ratios.

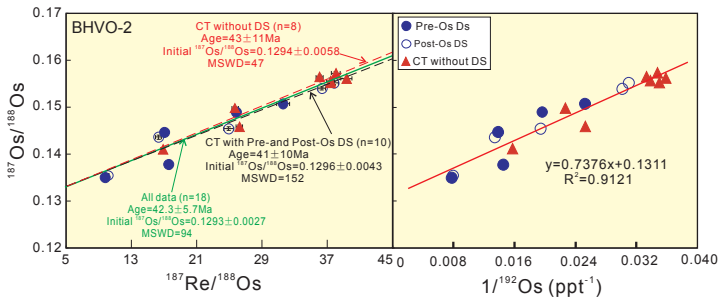

Figure 1. Measured $^{187}Re/^{188}Os$ vs $^{187}Os/^{188}Os$ (a) and inverse of ^{192}Os concentration vs $^{187}Os/^{188}Os$ (b) for BHVO-2 (true age <100 years). All regressions here were calculated using the program Isoplot 3.00 [Ludwig, 2003]- uncertainties - 2SE. The linear regression equation and R2 value are shown on the diagram here. These good positive covariations suggest binary component mixing.

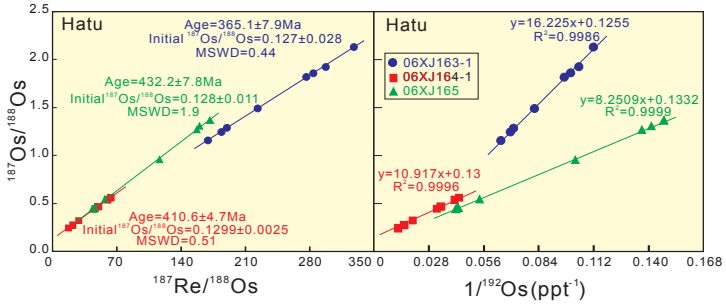

Figure 2. (a) Re-Os isochron diagram for replicate analyses (n = 8) of each of the three Hatu basalts (true age ca 315 Ma). The three samples exhibit three different apparent isochron ages with different initial $^{187}Os/^{188}Os$ ratios. (b) $^{187}Os/^{188}Os$ plotted against $1/^{192}Os$ for replicate analyses of the Hatu basalts. Error bars are shown when bigger than the symbols. All three samples show positive slopes with 06XJ163-1 having a steeper slope.

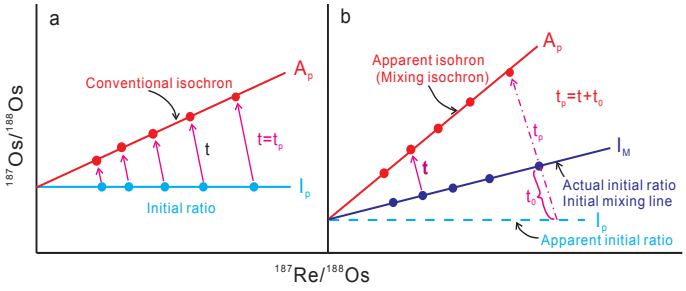

Figure 3. Illustration of the cases of binary mixing on the Re-Os isochron diagram, (a) K = 0; the initial Os isotopic ratios of the two mixing components were in equilibrium after diffusion during mixing (or the mixture was derived from a single homogeneous component). The isochron is a conventional isochron (Ap) with initial $^{187}Os/^{188}Os$ (Ip), and the observed apparent isochron age (tp) is equal to its formation age (t); (b) K ≠ 0; the initial Os isotopic ratios of the two mixing components were not in complete equilibrium after diffusion during mixing. The mixing line (Ap) represents the combination of an initial mixing line (IM) and the ingrowth of ^{187}Os since formation (t). Such an apparent isochron (AP) yields a geologically meaningless age (tp).

Duplicate analyses of a single powered whole-rock sample including both Hatu basalts and international reference rock (BHVO-2) defined good apparent Re-Os isochrons and linear trends between $1/^{192}Os$ vs $^{187}Os/^{188}Os$ (Fig. 1 and Fig. 2). These relationships signify disequilibrium-induced small-scale Re-Os heterogeneity and no individual analysis can represent the initial Os isotope composition of the whole-rock sample (their source composition). Because in most cases only one analysis was conducted on 1-2 g of a randomly selected aliquot of powdered whole-rock samples, this study raises the issue of whether an individual analysis can be representative of the source of the whole rock. This is especially true for rock units with large ranges of measured $^{187}Re/^{188}Os$ and $^{187}Os/^{188}Os$ ratios.

Apparent Re-Os isochrons can be generated through binary mixing without complete isotopic equilibrium at the time of formation, primarily due to limited diffusional exchange of Os isotopes between refractory Os-bearing inclusions, sulfides, their host minerals and the magma under mantle conditions (Fig. 3). The regressed initial Os isotopic composition may not represent the true value of the mantle source. Thus, when using the Re-Os isotopic system to date and to trace the source of basaltic rocks or other rocks with relatively low Os concentrations, it is necessary to consider whether the initial Os isotopic composition was heterogeneous or whether it had reached complete isotopic equilibrium. The results obtained in this study also pertain to Re-Os dating of low-temperature systems such as black shales, crude oil and bitumen.

This project is part of CCFS Theme 2, Earth's Evolution, and contributes to understanding Earth's Architecture.

Contacts: Xuan-Ce Wang, Jie Li

Funded by: Wang ARC Future Fellowship, National Natural Science Foundation of China (41173038)

Heaven on Earth: '*nebular*' mineral assemblages from Mt Carmel, Israel

The minimum oxygen fugacity (fO_2) of Earth's upper mantle probably is controlled by metal saturation, as defined by the Iron-Wüstite buffer reaction FeO→Fe + O. However, moissanite (SiC) is found in kimberlites worldwide, and an extensive suite of super-reduced minerals, including SiC, alloys and native elements, occurs in peridotite massifs in Tibet and the Polar Urals. These occurrences suggest that more reducing conditions (fO_2 = 5-6 log units below IW) must occur locally in the mantle. Unfortunately, these occurrences are known almost entirely from mineral separates, and thus lack spatial mineralogical context.

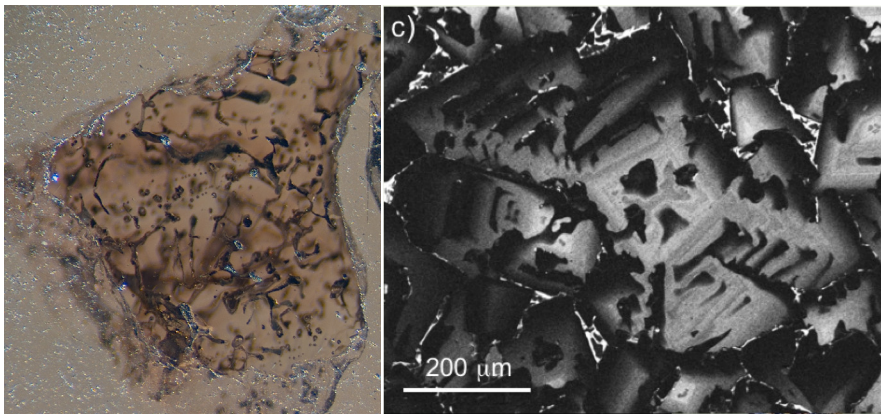

Figure 1. Left: transmitted-light image of 1-mm corundum grain from Mt Carmel, showing network of melt inclusions within and between corundum crystals. Right: cathodoluminescence image of corundum crystal showing skeletal/hopper growth; dark zones reflect high concentrations of Ti^{3+} in corundum, and darkest colours are adjacent to melt pockets.

In an ongoing collaborative research project with Shefa Yamim (A.D.M.) Ltd (Akko, Israel), we have found that aggregates of corundum crystals ejected from Cretaceous volcanos on Mt Carmel, North Israel, contain trapped melt pockets (Fig. 1) with high-temperature mineral assemblages that require extremely low fO_2 (IW -10). Over 65 different phases have been recognised; half of these have not been described previously as minerals.

The corundum crystals show spectacular variation in cathodoluminescence (CL), varying from light pink to dark pink to black, corresponding to a progressive increase in Ti content. Stoichiometry indicates that Ti is present as Ti^{3+}, i.e. a strongly reduced form. The CL images (Fig. 1) and EBSD studies show that most crystals are skeletal and grew as aggregates of hopper crystals, implying rapid crystallisation from melts supersaturated in Al_2O_3.

The pockets contain four basic types of melts. Type S (silicate), the most abundant, consists of crystalline phases, commonly including tistarite (Ti_2O_3), set in a matrix dominated by Ca-Al-Si-Ti-Zr-K oxides (Fig. 2). This matrix usually is either glass or very finely crystalline; it is amorphous in terms of Raman spectroscopy. Some inclusions show quench structures with radiating blades of anorthite and/or needles of unidentified REE-rich phases in the Ca-Al-Si glass, while in others the matrix has crystallised to an assemblage including anorthite and several undescribed Ca-K-Mg-Al silicates and oxides. None of the silicate or oxide phases in the Type-S melt pockets contain detectable levels of Fe or Ni.

Type A (alloy; Fig. 3) pockets were Fe-Ti-Si-C-P melts, and have crystallised to a range of phases, including gupeiite (Fe_3Si), FeTiSi, FeTi and TiC (khamrabaevite). Type N (nitride; Fig. 4) is represented mainly by osbornite (TiN with 12.5-16% N), intergrown with TiB_2; the identity of both phases has been confirmed by Dr Martin Saunders (UWA), using TEM electron diffraction. TiO has also been found together with TiN. Type N assemblages commonly occur in complex rectilinear

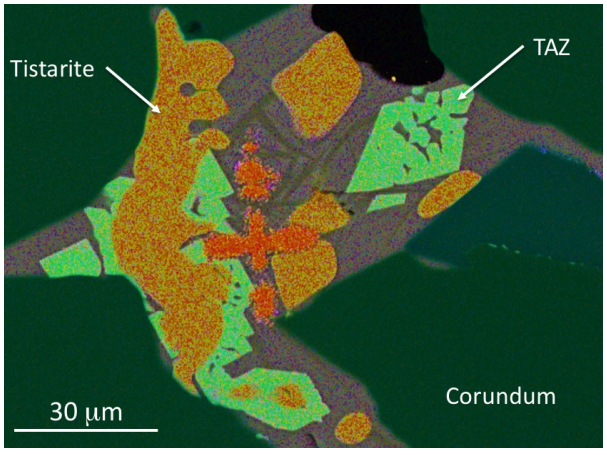

Figure 2. Tistarite and TAZ phase in melt pocket; dark matrix is Ca-Al-Si glass with darker quench needles of anorthite; red phase is TiN. Note euhedral corundum crystals forming boundaries to melt pocket.

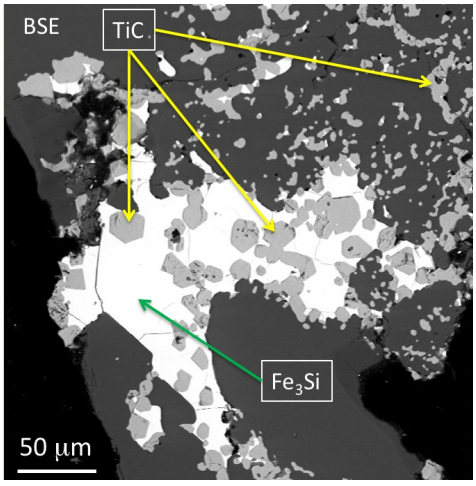

Figure 3. Type A melt pocket between euhedral corundum crystals; TiC crystallising from an Fe-Ti-Si-C melt have been trapped by the growth of the corundum crystals, confining the melt to the interstitial spaces.

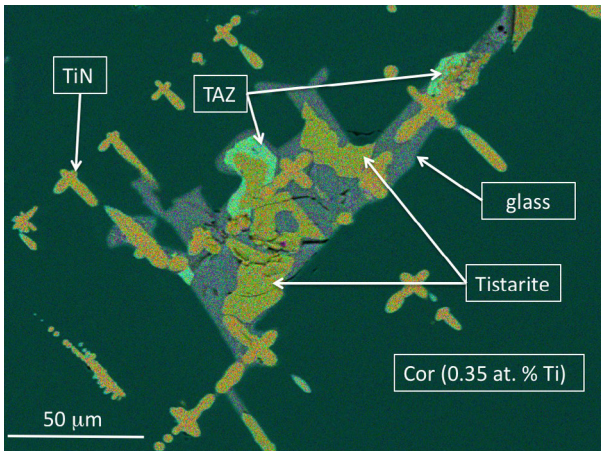

Figure 4. Type S and Type N melts; the TiN appears to fill rectilinear channels in the corundum, related to skeletal growth (Fig. 1).

3-D networks, which may cross Type S pockets (Fig. 4). Type D (desilicated; Fig. 5) pockets consist of phases with no Si, including native vanadium, grossite ($CaAl_4O_7$), hibonite ($CaAl_{12}O_{19}$) and fluorite.

The textural relationships in and among the melt pockets suggest that the different melts were mutually immiscible. They can be found in different areas of the same inclusion (especially where these are partially necked-down), and in separate inclusions in the same corundum grain; the apparent separation may simply reflect 2-D sectioning of complex 3-D structures (Fig. 1). The presence of glass with quench structures implies that the evolution of the melts was halted by eruption of the host magma. The peritectic crystallisation of corundum+melt → anorthite indicates crystallisation at depths of 30-100 km (i.e. within the lithospheric mantle) and temperatures in excess of 1450 °C. Available experimental data on other phases (usually at 1 atm. pressure) also indicate magmatic temperatures.

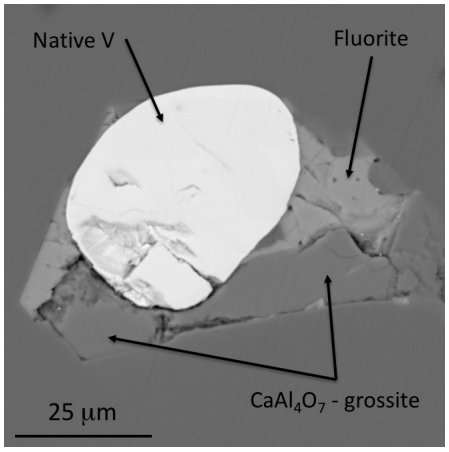

Figure 5. Type D (Si-free) melt pocket with native V, grossite and fluorite.

One of the most abundant phases in the Type S pockets is tistarite (Ti_2O_3), previously known only as a single grain (associated with TiC and corundum) from the Allende carbonaceous chondrite. These reduced phases are believed to have formed as high-T condensates during the early evolution of the solar nebula, when the fO_2 was 10^{-19}, ca 10 log units below the IW buffer (Fig. 6), because the solar wind consisted almost entirely of hydrogen.

Other '*nebular*' phases in the Mt Carmel assemblage include SiC, grossite, hibonite, osbornite, gupeiite and wassonite (TiS), all typically found in carbonaceous chondrites. Similar high-T, very low-fO_2 conditions must have existed locally in the Cretaceous upper mantle beneath Mt Carmel. We propose that the development of super-reducing conditions in Earth's upper mantle may reflect the mixing of deep-mantle CH_4+H_2 fluids with mafic magmas in volcanic plumbing systems. Such mixing can lead to desilication of the magma, oversaturation in Al_2O_3 and *'dumping'* of corundum in magma conduits. These remarkable samples represent a mantle environment, and a part of the global carbon cycle, that were previously unrecognised, and a process of fluid transfer that may be much more widespread.

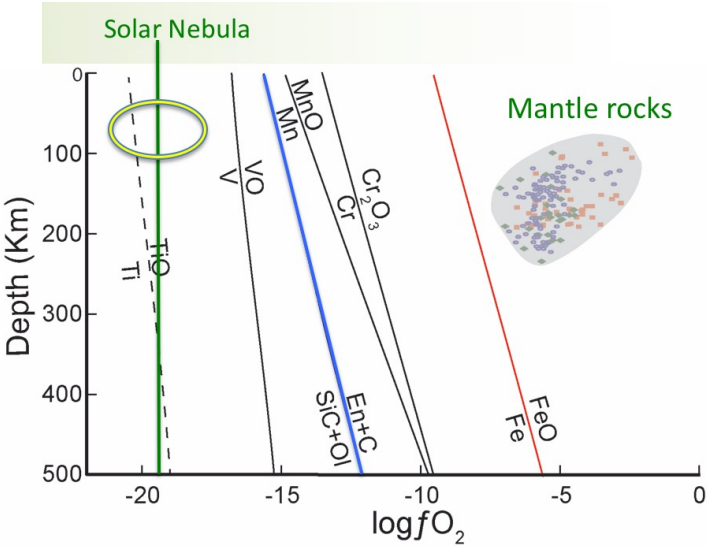

Figure 6. Some fO_2 buffer curves relevant to the assemblages in the melt pockets. The final conditions of crystallisation probably lie within the green oval, where fO_2 is similar to that in the early solar nebula. The grey field illustrates estimates of fO_2 in peridotite xenoliths derived from the lithospheric mantle.

This project is part of CCFS Themes 2 and 3, Earth's Evolution and Earth Today, and contributes to understanding Earth's Fluid Fluxes.

Contacts: Bill Griffin, Sue O'Reilly, Norman Pearson
Funded by: CCFS Flagship Program 1

Isotopic mapping of Archaean lithosphere to target orogenic gold and magmatic Cu-Ni-P

Steep penetrating lithospheric structures are pathways for focused mass and energy flow from mantle to crust. Mineralisation emplaced from the mantle into the crust is likely to be distributed along these pathways, a concept supported by empirical associations between mineral systems and lithospheric architecture. A large portion of today's continents (<70%) is thought to be underlain by Archaean continental lithospheric mantle, which may have been instrumental in localising much of the mineralisation of its time and in many succeeding events. As high-quality greenfield mineral discoveries decline, mapping the Archaean crust-mantle evolution through time and space has potential to highlight prospective lithosphere and aid in targeting mineral systems.

Despite a rich geological record of Archaean crust, conditions and geodynamic processes characterising the Archaean remain contentious. Interpretations inferred from petrological, geochemical and geophysical signatures are fraught with the prospect that these signatures reflect overprinting by deformation and metamorphism. An increasingly popular approach to interrogate the crustal record capitalises on the ability of the zircon lattice to concentrate useful radiogenic (Pb, Hf) and stable (O) isotopes and trace elements, and the mineral's resistance to subsequent resetting of these systems by tectonothermal reworking.

Results from *in situ* U Pb geochronology on igneous zircons of the Marmion Terrane (3.02 - 2.68 Ga), Wabigoon Superterrane, Western Superior Craton, Canada help constrain the cryptic growth of the crust across time and space. In conjunction with field-based studies, this has highlighted a shift in geodynamics at ~2.8 Ga, and allows us to explore relationships to mineral system distribution. As a uniquely preserved natural laboratory within the world's largest Archaean craton, insights gained

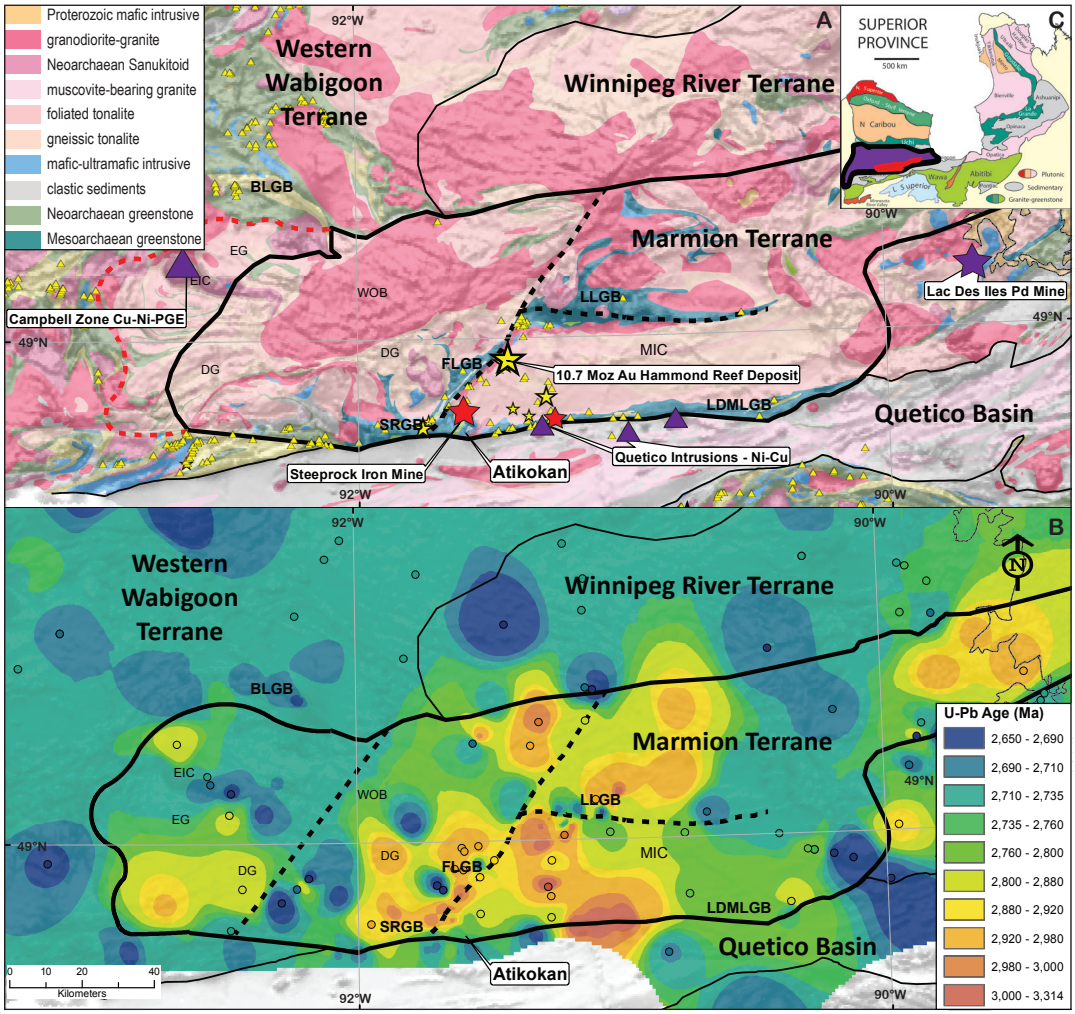

Figure 1. A. Geological map showing terrane boundaries of Stott (2011). Hatched boundaries are significant lithospheric structures. Red boundary is revised by this study. Triangles correspond to mineral occurrences, stars to past-producing mines (gold – yellow, iron – red, Ni-Cu-PGE – violet). B. Contour map based on U-Pb ages compiled from previous workers (mainly by TIMS) and this study by SHRIMP, shown in colour-coded circles corresponding to the colour scheme of the contours. Only ages interpreted as magmatic are included. C. Inset showing the location of the Marmion Terrane (red) within the Wabigoon Superterrane (violet) of the Superior Craton.

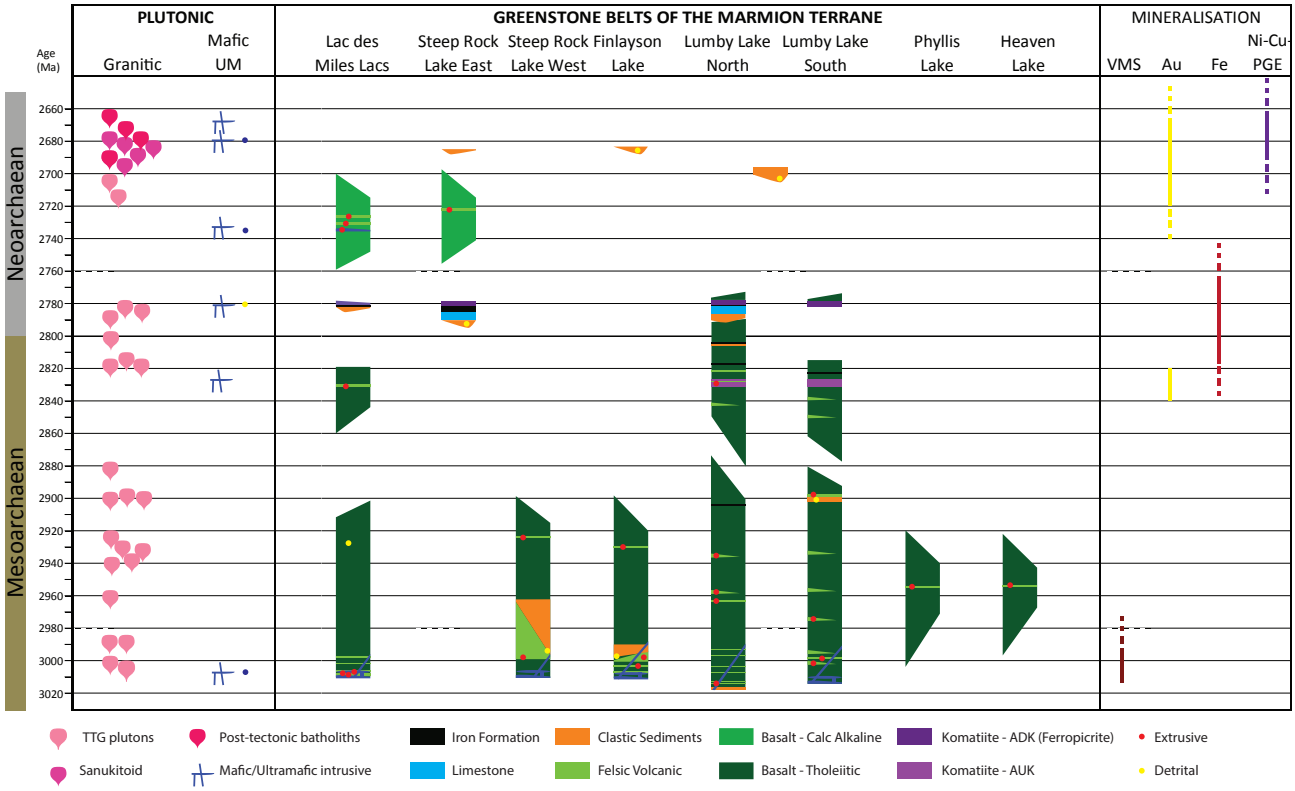

Figure 2. Stratigraphic compilation of the Greenstone belts within the Marmion Terrane. Ages are given by red (extrusive) and yellow (detrital) circles. Corresponding plutonic events are illustrated at the left. Age constraints on granitic intrusions are provided by U-Pb geochronology in zircons; blue circles indicate mafic events constrained by U-Pb geochronology in baddeleyite. Timing of mineralisation is constrained stratigraphically (VMS, Fe), by Pd-Pd ages in galena (Au) and by crystallisation ages (Ni-Cu-PGE).

here have potential to shed light on global crustal growth and geodynamics.

In the Western Superior, linear east-trending granite greenstone terranes are separated by highly metamorphosed and fault-bounded metasedimentary basins (Fig. 1c). The Marmion Terrane, with a western boundary revised by this study, stands out as the most coherent Mesoarchean block in the Wabigoon Superterrane. Isotopic patterns highlight a northeast-trending structure that is cryptic in the geology (western hatched line, Fig. 1b). Another northeast-trending structure, the Marmion Shear Zone (MSZ) appears to have controlled the significant gold deposits of the terrane (eastern hatched line, Fig. 1b). The focus of later tectonothermal events along these structures supports an interpretation of deep lithospheric structures in a northeast orientation.

Supracrustal rocks record a significant change across the Meso- to Neoarchaean boundary (Fig. 2). Cyclic tholeiitic volcanism with minor aluminum-undepleted komatiites dominates the 3.02 - 2.82 Ga record and provides evidence for high-degree partial melting of the mantle at depths above 8 GPa. The geochemistry of these rocks is analogous to those of oceanic plateaus, such as the Ontong Java Plateau. After 2.8 Ga the Marmion terrane was uplifted. Conglomerate channels were eroded into the granitic basement, and stromatolitic limestone and iron formations were deposited. Pyroclastic aluminum-depleted komatiite was then deposited, indicating much deeper mantle melting (Fig. 2). The uplift may reflect development of a depleted lithosphere which may be related to subsequent melting at greater depths.

Subsidence was followed by a shift to more calc-alkaline mafic to intermediate volcanism from 2.74 - 2.72 Ga on the southern margin of the terrane, reflecting melting of a fluid-fluxed mantle. Basin inversion accompanied ongoing transpression during the Kenoran orogeny and late Timiskiming-type sedimentation was localised in the synclinal axes of Mesoarchean greenstone belts and along the active southern margin of the terrane at 2.7 Ga. The main gold mineralisation was emplaced in the oldest tonalitic rocks at 2.7 Ga, along the steepest age gradients proximal to the reactivated MSZ and Quetico Fault, which marks the boundary between the Marmion Terrane and the Quetico basin to the south (Fig. 1). Gold mineralisation exploited a long-lived architecture during a time of favourable geodynamics.

This project is part of CCFS Theme 2, Earth's Evolution, and contributes to understanding Earth's Architecture.

Contacts: Katarina Bjorkman, Cam McCuaig, Yongjun Lu

Funded by: CCFS Flagship Program 2

The Ivrea Zone Pipes: new light on ore-forming processes in the deep continental crust

Our ability to discover new mineral resources is challenged today partly due to the limited predictive capability of the traditional approach based on analogue deposit models. Recently, a new conceptual framework, the mineral system approach, has been proposed, which enables more powerful predictive capability for mineral exploration. This project tests the hypothesis that the genesis of sizeable mineral deposits is the end product of self-organised critical systems operating from the scale of the planet all the way to the very focused environment where ore deposits can form. The mineral system approach represents a step change in the way we investigate ore-forming processes, whereby we look at the evolving relationship between the localised setting of anomalous metal resources and processes operating at the scale of the planet. Prior to the advent of this concept, single deposits were documented in detail as unique occurrences. However, this approach failed to focus on the commonalities among various occurrences and, more importantly, the larger-scale architectural framework that hosts them. The new rationale now takes on a more holistic approach acknowledging that the genesis of mineral occurrences required the conjunction in time and space of three main independent parameters: fertility, lithosphere-scale architecture, and favourable transient geodynamics.

This conceptual framework forms the basis of the present project, which focuses on a series of alkaline mafic-ultramafic pipes, rich in sulfides and hydrous minerals, that intruded the lower continental crust of the Ivrea-Verbano Zone in the Italian Western Alps (Fig. 1). The pipes are relatively small and primarily composed of a matrix of subhedral to anhedral amphibole (pargasite), phlogopite and orthopyroxene that enclose sub-centimetre-sized grains of olivine. The 1 to 5 m-wide rim portions of the pipes locally contain significant blebby and disseminated Fe-Ni-Cu-PGE sulfide mineralisation. Stratigraphic relationships, mineral chemistry, geochemical modelling and phase equilibria suggest that the pipes represent open-ended conduits within a large magmatic plumbing system. The earliest formed pipe rocks were olivine-rich cumulates, which reacted with hydrous melts to produce orthopyroxene, amphibole and phlogopite. Sulfides precipitated as immiscible liquid droplets that were retained within a matrix of silicate crystals and scavenged metals from the percolating hydrous melt, derived by partial melting of a metasomatised continental lithospheric mantle.

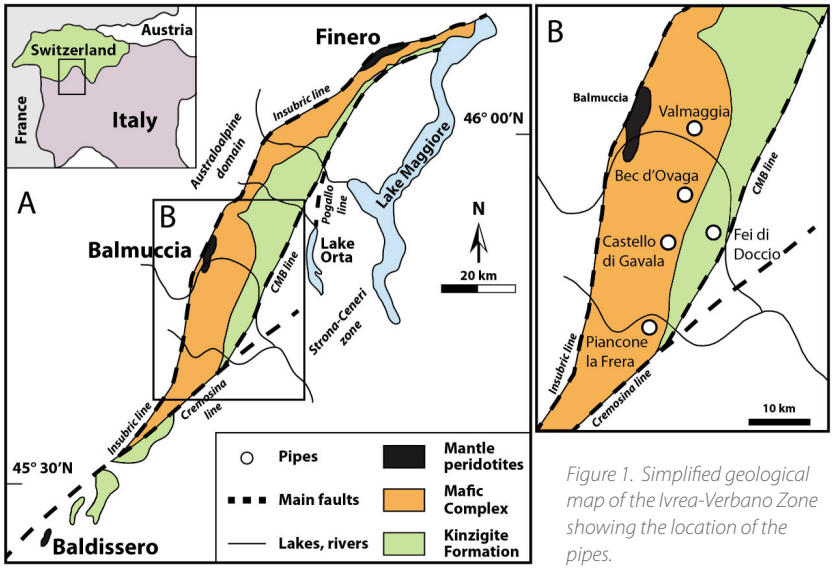

Figure 1. Simplified geological map of the Ivrea-Verbano Zone showing the location of the pipes.

New high-precision chemical abrasion TIMS U-Pb dating of zircons from one of the pipes indicates that these pipes were emplaced at ca 250 Ma, following partial melting of lithospheric mantle pods that were metasomatised during the Eo-Variscan oceanic to continental subduction (420-310 Ma). The thermal energy required to generate partial melting of the metasomatised mantle was most likely derived from crustal extension, lithospheric decompression and subsequent asthenospheric upwelling during the orogenic collapse of the Variscan belt (<300 Ma), as shown in Figure 2. If the pipes had been emplaced in an active compressional environment during the Variscan continental collision, as opposed to the extensional post-orogenic setting constrained through the high-precision geochronology presented in this study, their magmatic plumbing would have attained self-organising criticality with the establishment of high-flux conduits. This would have led to focused energy and mass flux transfer from the mantle into the crust, with the potential for the formation of sizeable orthomagmatic deposits, rather than the modest occurrences that actually formed.

In fact, rather than through a network of self-organised high-flux conduits, mantle-derived magmas trickled through a series of lower-energy pipes, producing a slow and persistent flux of magmas through the interface between the lithospheric mantle and the continental crust. In other words, the magmatic plumbing system that originated the pipes did not self-organise, with the result that high-flux networks were not established and no major ore-forming process occurred. However, even if this process of metal and volatile transfer from the lithospheric mantle to the base of the continental crust is not necessarily conducive to the synchronous genesis of economic mineral deposits, it can be a very effective mechanism to fertilise the

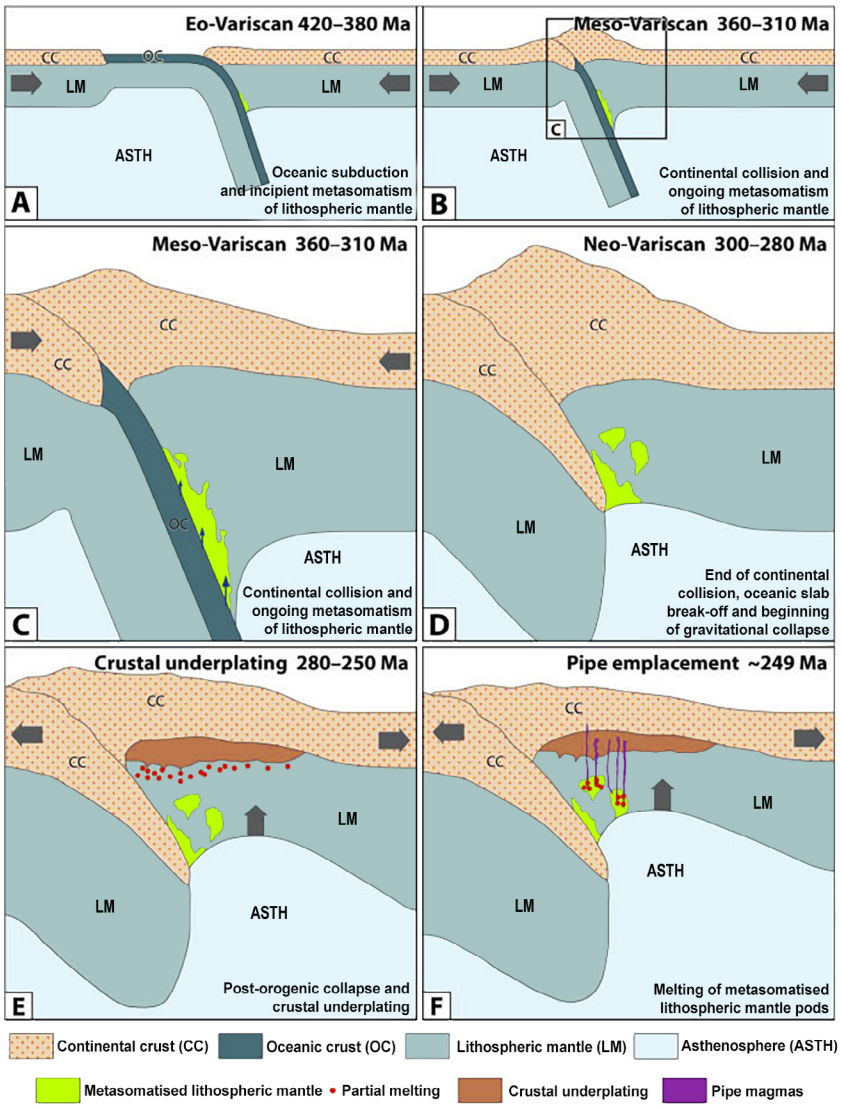

Figure 2. Schematic illustrations of the geodynamic evolution that facilitated the genesis of the pipes. (A) Early oceanic subduction in the Eo-Variscan (420-380 Ma) initiating metasomatism of the lithospheric mantle. (B, C) Continental collision and ongoing metasomatism of the lithospheric mantle in the Meso-Variscan (360-310 Ma) create pods of metasomatised mantle (cf. D). (D) End of the continental collision and beginning of the gravitational collapse in the Neo-Variscan (300-280 Ma). (E) Post orogenic collapse, crustal extension and asthenospheric rise cause decompression melting of the lithospheric mantle and initiate the underplating of the continental crust. (F) Further extension and asthenospheric rise cause partial melting of the metasomatised mantle pods, facilitating the intrusion of the pipe magmas into rocks of the upper lithospheric mantle and lower continental crust.

notably dry and restitic lower continental crust. Accordingly, even without necessarily generating significant syngenetic Ni-Cu-PGE mineralisation, this process has the potential to add metals and volatiles into the base of the continental crust, thus seeding the ground for the genesis of later mineral systems. This process could represent an effective mechanism to enhance the metal endowment of continental block margins and paleo-margins.

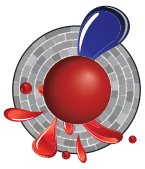

This project is part of CCFS Themes 2 and 3, Earth's Evolution and Earth Today and contributes to understanding Earth's Architecture and Fluid Fluxes.

Contacts: Marco Fiorentini, Marek Locmelis, Tracy Rushmer, John Adam, Steve Denyszyn, Ricardo Arevalo
Funded by: CCFS Flagship Program 2, Fiorentini ARC Future Fellowship

Research highlights 2016

Contents

Genesis of deposits of scandium, a promising rare metal

Rare metals play a critical role in the future of our society, through their use in the energy transition and information and communication technologies. However, this future depends on the supply of these metals. Among them, scandium is particularly interesting for a large range of applications, from medicine to electronics. The main driver for scandium demand lies in the mechanical properties and lightness this metal can add to high-performance alloys, vital to reduce carbon emissions in the transport sector. However, scandium deposits are rare and their genesis is poorly understood. Recently, promising concentrations have been found in tropical soils from Eastern Australia. In a collaborative research project with researchers from the University Pierre and Marie Curie (Paris, France) and Jervois Mining Ltd (Cheltenham, Victoria, Australia), we have determined the scandium-bearing minerals in such deposits and the nature of their association with Sc at the atomic scale. The results give a better understanding of the mechanisms of their formation, a fundamental step for exploration and exploitation of these deposits.

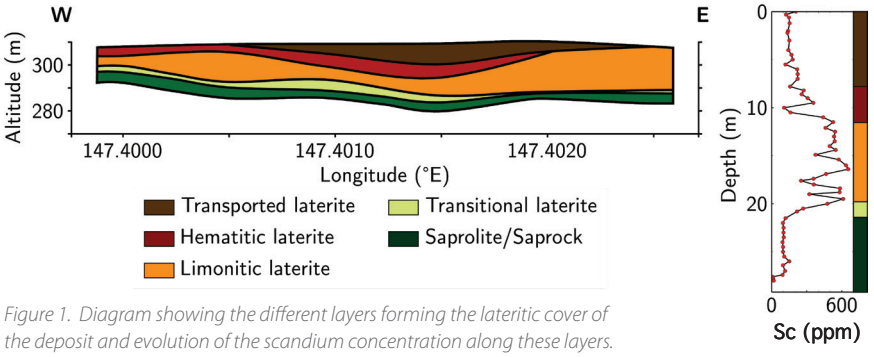

Figure 1. Diagram showing the different layers forming the lateritic cover of the deposit and evolution of the scandium concentration along these layers.

In Eastern Australia, volumes of ultramafic bedrock are frequently covered by a thick layer of residual rocks, called laterites. These formations developed during the Tertiary, under seasonally-dry humid tropical climatic conditions. These residual soils have been preserved by the geological stability of the Australian continent. Some areas are particularly enriched in scandium and constitute the richest deposits presently known for this metal. The samples studied come from the Syerston deposit, about 400 km west of Sydney. The wealth of this deposit provides a century-long resource for Sc at present levels of consumption.

The study of the parent rock, lying below the deposit, showed that it is already enriched in scandium compared to the Earth's crust. This rock is mainly composed of clinopyroxene accumulated in subvolcanic feeder conduit. The enrichment in scandium is the result of the affinity of this element for clinopyroxene, in which it is concentrated during their precipitation. The scandium concentration strongly increases in the lateritic cover, reaching outstanding levels for this element in particular, in one layer: the limonitic laterite (Fig. 1).
The mineralogical study of this layer showed the absence of scandium minerals. However, scandium is dispersed and correlated with the presence of iron oxides. These samples have been studied at the SOLEIL and ESRF synchrotrons in France using X-ray fluorescence mapping and X-ray absorption spectroscopy, confirming the close association between scandium and two particular iron oxides. Most of the scandium is adsorbed at the surface of goethite (FeOOH) while a minor part is incorporated into the crystal structure of hematite (Fe_2O_3) (Fig. 2).

This study has shown that the exceptional concentration of scandium in this deposit is the result of the initial fertility of the parent rock, and of its alteration in a tropical climate, leading to the release of Sc from the primary clinopyroxenes, and its trapping by newly formed iron oxides. Long time scales of alteration in the absence of major tectonic events explain the formation of this new type of scandium deposit. This development gives us the possibility to consider the development of new technologies based on the unusual properties of this metal.

This project is part of CCFS Theme 3, Earth Today, and contributes to understanding Fluid Fluxes.

Contacts: Mathieu Chassé, Bill Griffin, Sue O'Reilly
Funded by: CCFS Flagship Program 1

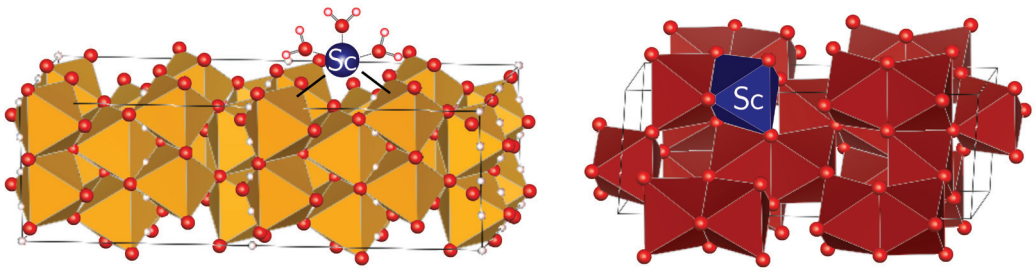

goethite (FeOOH)
80% of scandium (Sc)

hematite (Fe_2O_3)
20% of scandium (Sc)

Figure 2. Proportion of scandium associated with the scandium-bearing mineral species in the deposit and diagram showing the nature of the association at the atomic scale. Scandium is adsorbed at the surface of goethite and incorporated into the crystal structure of hematite.

Oldest Evidence of life on Earth discovered

A *Nature* paper has documented the discovery of the oldest evidence of life on Earth in the form of stromatolites preserved in 3700 million-year-old carbonate rocks from Western Greenland.

The discovery was made by a team led by Prof Allen Nutman (U. Wollongong), Prof Vickie Bennett (ANU), Prof Martin Van Kranendonk (UNSW and CCFS) and others in a set of newly exposed rocks within a low-strain pocket of the famous Isua supracrustal belt. Previously, the area had been covered by permanent snow, but heavy spring rain uncovered the rocks. The new exposures revealed a series of bedded, though metamorphosed, dolomite and calc-silicate rocks that preserved primary sedimentary structures, including cross-stratification in calc-silicate rocks, units of storm-generated sedimentary breccias, and bedded carbonates with low-amplitude coniform and domical stromatolites (Fig. 1). The rocks form part of a stratigraphic succession - together with pillow basalt and banded iron-formation - that can be mapped around a fold structure.

Additional evidence in support of these structures being stromatolites and not either abiogenic primary structures or post-depositional structural features includes:

1. The composition of the rocks, which is dolomite, a mineral well known from other fossiliferous Archean sedimentary deposits. This contrasts with siderite or ankerite, Fe-bearing carbonates that are demonstrably metamorphic in origin. The dolomite has characteristic seawater-like REE+Y patterns and $\delta^{13}C$ values (+1.2-1.5‰), characteristic of microbially-precipitated carbonate.
2. The geometry of the stromatolites, which clearly show upward growth from a flat (instigation) surface, and variable topographic morphology, as seen in other Precambrian, and living, examples. This precludes the structures being derived through boudinage, which produces symmetrical pinch-and-swell structures, or representing sedimentary flame structures, which have curved bases and show variation in sediment
grain size.
3. Onlap of sediment onto the topographic highs of the stromatolites, indicating the structures formed on, and grew up above, the seafloor at the time of sediment accumulation.
4. The fact that a metamorphic foliation could be discerned that transected the bedding at a high angle, showing the bedding was a primary feature.

The sedimentary features and composition of the bedded dolomite and calc-silicate rocks suggest stromatolite growth in a shallow marine environment. This discovery pushes back the record of life on Earth by 220 million years, the equivalent to nearly half the length of the Phanerozoic. The significance is twofold. First, it shows that life on Earth began relatively early, soon after the end of the late heavy meteorite bombardment, which ceased at c. 3.9 Ga. Second, because the coniform morphology is characteristic of stromatolites formed by phototrophic organisms and occurs in a shallow marine setting, it suggests that life had evolved a complex metabolism (phototrophy) and was able to inhabit seawater by 3.7 million years ago.

See *CCFS publication #837, Nutman et al., Nature, 537, 535-538.*

This project is part of CCFS Theme 1, Early Earth, and contributes to understanding Fluid Fluxes.

Contact: Martin Van Kranendonk
Funded by: ARC Discovery Project

Figure 1. 3,700 million-year-old stromatolites from Western Greenland.

Does the mantle move beneath Northeast China?

Intraplate volcanism on continents is an exception to the general model of Plate Tectonics, which states that most of the world's volcanoes both in oceans and on land occur at plate boundaries. Northeast China is an ideal place to study Cenozoic intraplate volcanism. Though located more than 2000 km west of the Japan trench, Northeast China hosts widely distributed Quaternary volcanism surrounding the Songliao Basin (SLB). Some of the most prominent volcanoes in the area include the well-known Changbaishan volcano in the southeast, the Jingpohu volcano in the east, the Wudalianchi volcano in the north, and two lesser known volcanoes, Abaga and Halaha, in the west (Fig. 1a). These Quaternary volcanoes are situated hundreds of kilometres apart with the SLB at the centre, which was formed by tectonic rifting in the late Mesozoic. Although it is generally agreed that the flat stagnation of the subducting Pacific slab in the Mantle Transition Zone has played an important role in the formation of Cenozoic volcanism in NE China, there is still little consensus about the mechanism responsible for the intraplate volcanism.

In order to understand the mantle processes responsible for the widespread magmatism in NE China, we constructed a high-resolution seismic model of the crust and upper mantle beneath NE China using seismic data recorded by the newly deployed NECESSArray. Our model reveals low-velocity anomalies in the upper mantle: one strong low-velocity anomaly beneath Changbaishan volcano in the east and relatively weak low-velocity anomalies beneath the Abaga and Halaha volcanos in the Xinmeng belt, surrounding a high-velocity anomaly beneath the SLB (Fig. 1 and 2). These low-velocity anomalies in the upper mantle are closely correlated with the distribution of young volcanic fields in NE China.

The widespread low velocity zone beneath Changbaishan has been interpreted as a large volume of upwelling hot asthenospheric materials that escape upward through a gap in the Pacific slab. The slowest velocity occurs at depths of 80-160 km (~-6% to -8%) (Figs. 2a and 2b), which may suggest the depths where partial melting mainly takes place, producing the magmas that feed the Changbaishan volcano. Cenozoic potassic basalts from the Changbaishan volcano and surrounding regions are interpreted to be derived by mixing of melts from the lithospheric mantle and the asthenosphere.

The most intriguing feature is the high velocity anomaly in the uppermost mantle beneath the SLB, which extends at least to 200 km depth. The overlying crust of the SLB has undergone considerable extension during the late Mesozoic, and as a consequence, it seems unlikely to have preserved such a thick lithosphere. The S-wave receiver-function study also indicates that the lithospheric thickness beneath SLB is between 80 and 100 km. If the lithospheric thickness beneath SLB is about 100 km, then a question arises: what causes the uppermost mantle high velocity anomaly down to ~200 km beneath SLB?

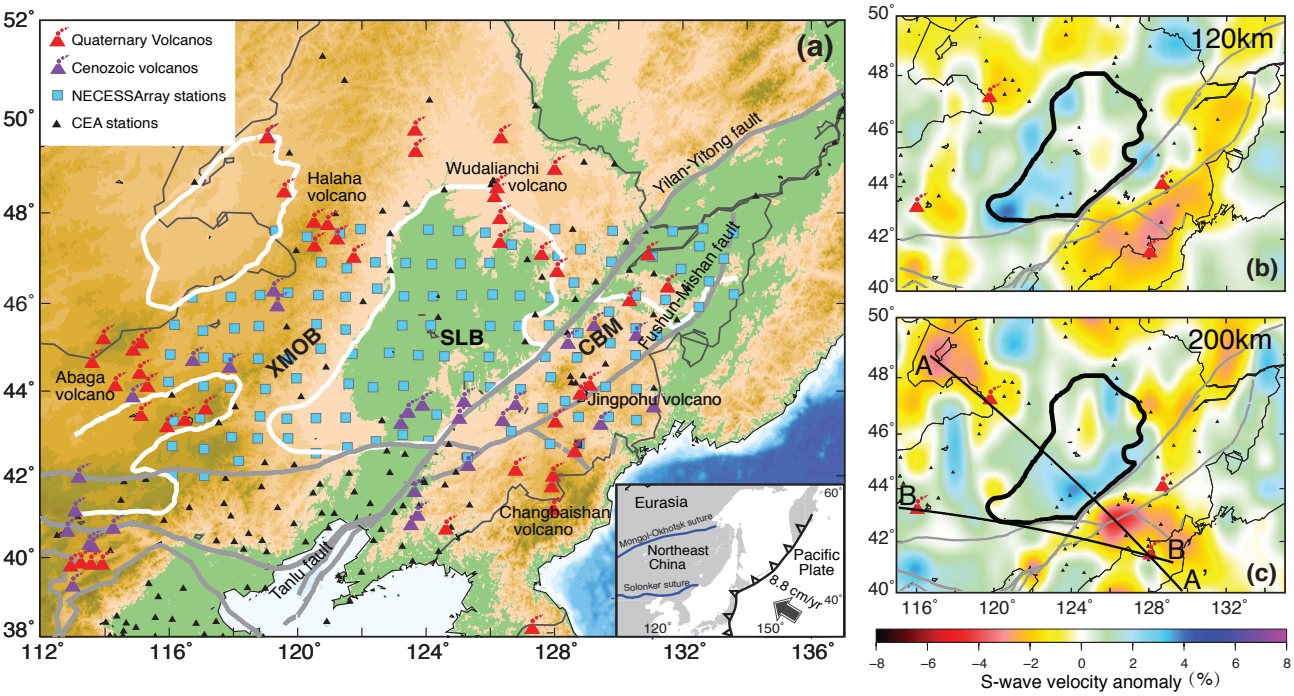

Figure 1. (a) Stations distribution and geological setting. Blue squares indicate 127 NECESSArray stations and black triangles denote 120 CEA stations. NE China is comprised of the Xing'an-Mongolia orogenic belt (XMOB), the Songliao basin (SLB) and the Changbai mountain region (CBM). Red and purple volcanic symbols are Quaternary and Cenozoic volcanoes in NE China. White lines outline major Mesozoic basins in NE China. CBV: Changbaishan volcano; JPHV: Jingpohu volcano; WDLCV: Wudalianchi volcano; HLHV: Halaha volcano; ABGV: Abaga volcano. NCC: North China Craton China, respectively. (b) and (c) S wave velocity anomaly from surface wave tomography at 120 and 200 km, respectively.

Based on our results, we propose a sub-lithosphere mantle convection model to explain both the deep upper-mantle high velocities beneath the Songliao basin, and the volcanism in the Xinmeng belt. As illustrated in the 3D cartoon (Fig. 2c), a plume-like upwelling with a large volume of hot mantle material has ascended through the upper mantle beneath Changbaishan. This mantle upwelling may also feed magma to the Quaternary Jingpohu volcano, which is located east of the SLB. If this is the case, a mantle downwelling beneath the SLB could be induced by the mantle upwelling from the mantle transition zone beneath the Changbaishan. The high velocity beneath the SLB may thus correspond to a downwelling limb of a larger upper mantle convective system. The downwelling beneath the Songliao basin would further induce secondary local convection within the asthenosphere to the west, leading to local upwelling beneath the Abaga and Halaha volcanoes (Fig. 2c), which are also imaged here as mantle low-velocity zones, but weaker and shallower than the one beneath the Changbaishan volcano (Figs. 1 and 2).

This project is part of CCFS Theme 3, Earth Today, and contributes to understanding Earth's Architecture and Fluid Fluxes.

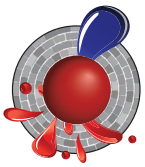

Contacts: Zhen Guo, Yingjie Yang, Juan Carlos Afonso

Funded by: DP120102372, ARC Future Fellowship FT130101220, CCFS Flagship Program 3

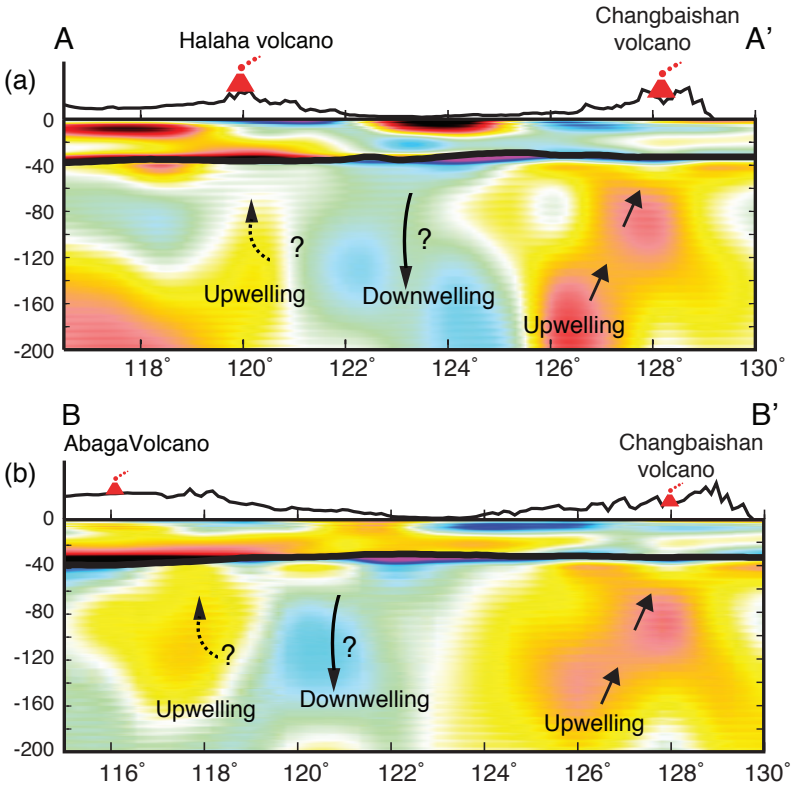

Figure 2. (a) and (b) Vertical cross-sections of S-wave velocities along A-A' and B-B'. Locations of these profiles are shown in Figure 1c. Arrows illustrate the possible upper mantle upwelling/downwelling beneath NE China. Crustal thicknesses are denoted as black bold lines. (c) Schematic model for small-scale mantle convection in NE China.

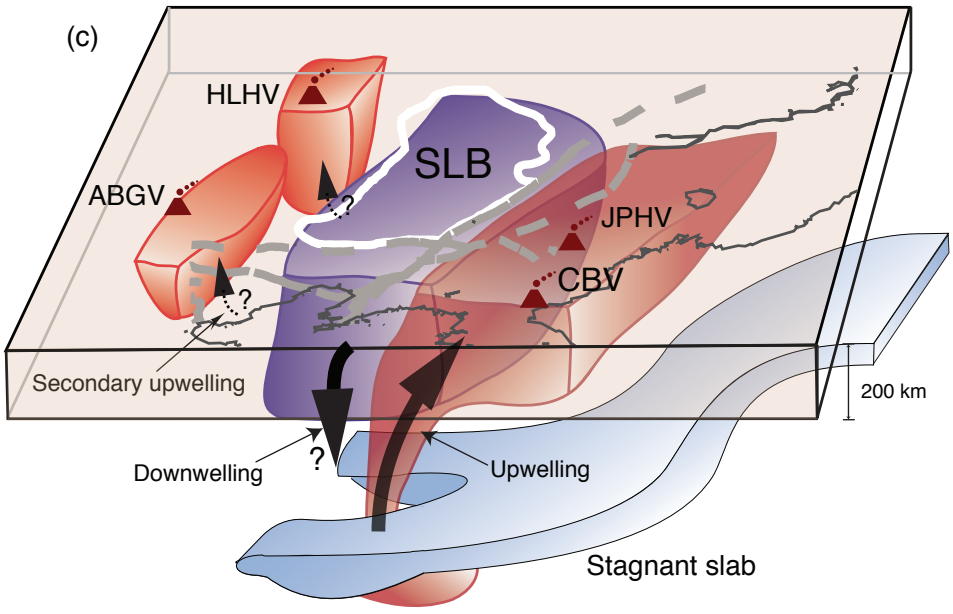

Unveiling the early history of crust in Western Australia

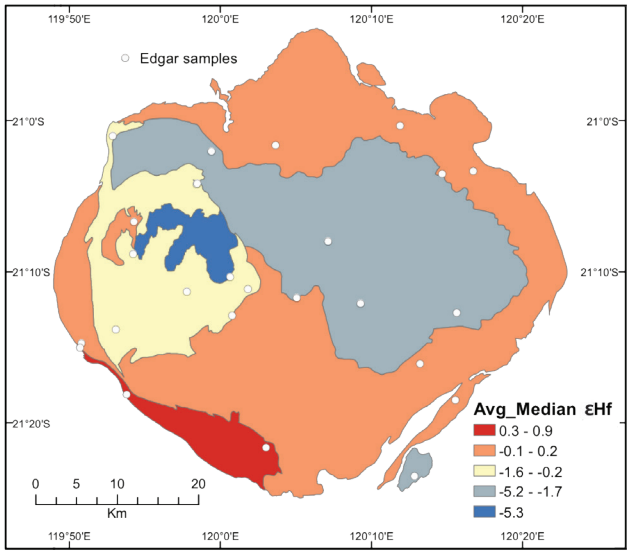

Figure 1. εHf isotopic map for the Mount Edgar Dome, East Pilbara Terrane, showing rim to core 3.5-2.8 Ga magmatism with increasingly evolved Hf signatures (From Gardiner et al. 2017, Precambrian Research, in review)

The Geological Survey of Western Australia (GSWA) in collaboration with CCFS and Curtin University has a major program for the acquisition and interpretation of Lu-Hf isotopic data, based on previously-dated zircon samples from GSWA's extensive sample holdings. The research is focused in '*greenfields*' areas where little information presently exists. More than 10,580 zircons, from 668 samples, have been analysed during the life of the project to date, including 56 samples and 1535 zircons in 2016. Zircon samples have been selected from dated material in igneous, metamorphic, and sedimentary rocks of the Pilbara Craton, the Eastern Goldfields Superterrane and Murchison Domain of the Yilgarn Craton, the Albany-Fraser Orogen, the Musgrave Province, sedimentary basins across Western Australia, the Rudall Province, the Gascoyne Complex, and basement rocks beneath the Eucla Basin. The project has addressed questions on the affinity of crustal blocks, helped map major lithospheric structures, and elucidated the timing of mantle input into the crust. The isotopic datasets produced have provided a powerful tool to understand fundamental components of mineral systems.

Recent results of note include the first major Hf-isotope dataset from the East Pilbara, with a unique focus on the magmatic evolution of a single granite dome. The East Pilbara Terrane is the archetypal granite-greenstone belt, and studies of East Pilbara have informed many ideas regarding early Earth geodynamic processes. Hf isotopes, with their sensitivity to magmatic source, have the potential to add significantly to this debate. Using this Hf dataset, important interpretations regarding: (a) the geodynamic operating model of pre-3.2 Ga Earth, (b) the existence of a ca 3.7 Ga sialic protocrust in the East Pilbara, and (c) the change in geodynamic style post-3.2 Ga can be made. Specifically, results from the East Pilbara indicate that reworking of existing tonalite-trondhjemite-granodiorite (TTG) dominated late Paleoarchean magmatism, which supports a vertical tectonic geodynamic regime for the Pilbara prior to 3.2 Ga.

Other notable outputs in 2016 include a combined oxygen- and Hf-isotope study from the Capricorn Orogen of Western Australia. This data set was used to understand the process of cratonisation in which the *in situ* chemical differentiation of continental crust produced a stable crust. Zircon Hf and O isotopes in granites from this region reflect multi-component sources and shallow crustal processes associated with magma emplacement. An increase in the Th/U ratio of magmatic zircon tracks crustal differentiation in this orogen. Cratonisation processes in the Capricorn Orogen led to shallow parts of the crust, dominated by granitic rocks, with high Th/U magmatic zircons and elevated levels of heat producing elements, becoming more susceptible to reworking.

New oxygen- and Hf-isotope data from sodic Sr-enriched magmas in the Rudall Province have proved important to understanding the crustal evolution and magmatic petrogenesis of this region. These magmas, although Proterozoic in age, are helpful to understand geochemically similar Archean magmatic rocks. Hf isotopes are sensitive to magmatic source compositions through time, and O isotopes are sensitive to the interaction of magmas with surface processes. The isotopic results from the Rudall magmatic rocks show that, despite the

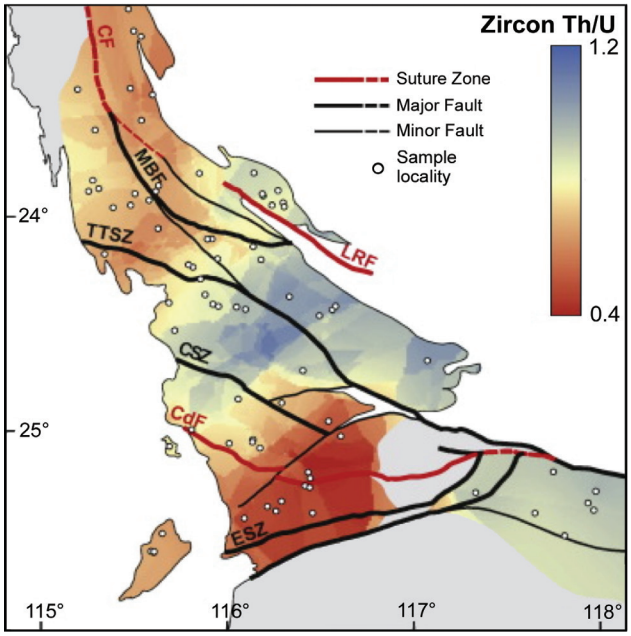

Figure 2. Gridded map of western part of the Capricorn Orogen in Western Australia showing the median Th/U ratio of magmatic zircon from U-Pb SHRIMP dated samples. Hot colours highlight areas dominated by juvenile rocks, whereas cool colours highlight magmatic rocks dominated by crustal reworking at the time of emplacement. The data highlight broad regions of crustal addition in the south and crustal differentiation and recycling in the central part (from Johnson et al., 2017; Lithos 268-271, 76-86).

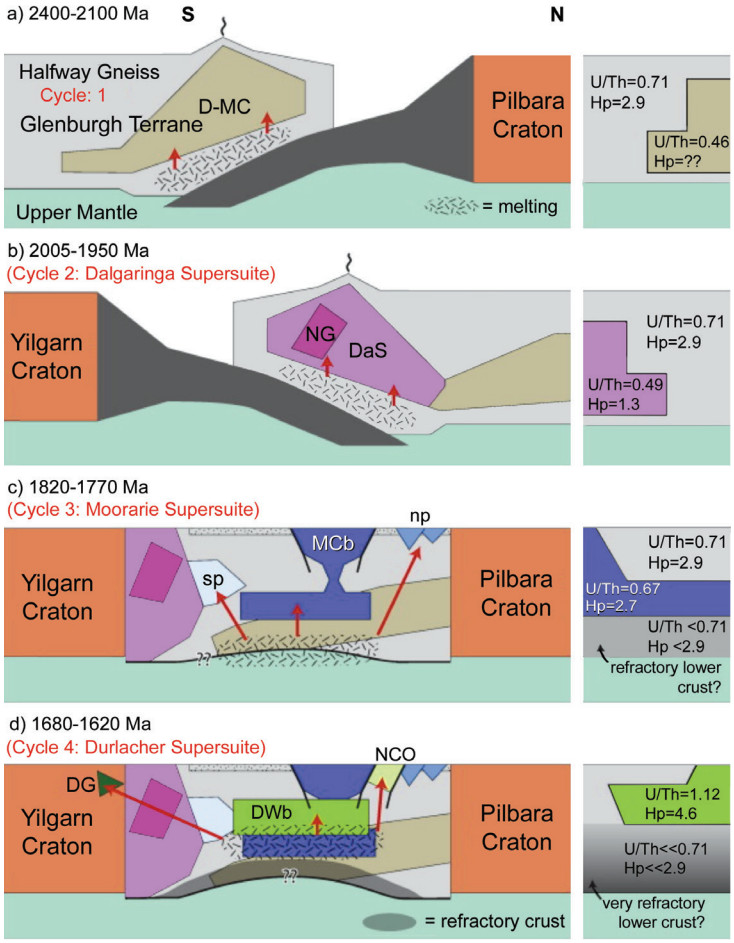

Figure 3. Schematic diagrams illustrating the tectonomagmatic evolution of the Capricorn Orogen as derived from the isotopic data. Panels on the right-hand side provide a summary of the median Th/U ratio of magmatic zircon as well as the present-day heat production (from Johnson et al., 2017; Lithos 268-271, 76-86).

TTG-like compositions, some magmas have highly-evolved Hf-isotope compositions, implying that their source was not young subducting oceanic lithosphere. Furthermore, mantle-like O-isotope compositions in these rocks suggest negligible components from a near-surface environment. This magmatic process implies the thickening of mafic source regions to generate melt that formed the crust. Given the geochemical similarity of these specialised Proterozoic melts to Archean TTG rocks, this mafic thickening and extraction of felsic melts could be a viable method to generate early Earth crust.

This project is part of CCFS Themes 1 and 2, Early Earth and Earth Evolution, and contributes to understanding Earth's Architecture and Fluid Fluxes.

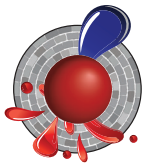

Contacts: Chris Kirkland, Yongjun Lu, Michael Wingate, Nick Gardiner, Simon Johnston, Hugh Smithies, Elena Belousova, Ed Saunders, Rosanna Murphy, GSWA

Funded by: CCFS Flagship Program 7, GSWA

Mantle xenoliths from a young European extensional basin

The study of mantle rocks in young off-craton environments provides insights into the physico-chemical properties of the upper mantle during tectonic processes. The Pannonian Basin in Central Europe, located between the Alps, Carpathians and Dinarides, was geodynamically active throughout the Cenozoic. Its crustal structure and surface processes have been extensively studied, but we still have little knowledge about how the upper mantle there evolved.

Mantle xenoliths occur in five areas within the Carpathian-Pannonian region, hosted by late Miocene-Pleistocene alkaline basalts. The focus area of this study, the Nógrád-Gömör Volcanic Field (NGVF) is located in the northern margin of the Pannonian Basin (Fig. 1). The host basalt at this locality is calculated to have reached the surface in ~36 hours, so the entrained xenoliths are considered to closely reflect the conditions in the upper mantle beneath the area. Thus they provide an excellent base for reconstructing geochemical processes.

Two major rock series have been identified among the NGVF xenoliths: lherzolitic and wehrlitic (Fig. 1). The lherzolitic group, which is the focus of this research, has a wide range of geochemical compositions; four subgroups were distinguished based on the Mg# of olivine and LREE/HREE ratios in pyroxenes. Each of these subgroups records a different metasomatic process or processes, which overprint the chemical signature of an ancient melt extraction event with removal of between 5 and 30% melt. Modal metasomatism is reflected by the presence of amphiboles, which have trace element contents matching those of clinopyroxenes in each xenolith where they appear (Fig. 2a). Thus two types have been distinguished, a Nb-poor type with a suprasubduction origin, and a Nb-rich type (Fig. 2b) which is inferred to have formed as mafic melts percolated through the upper mantle prior to the eruption of the host basalt. Such melts were responsible for causing enrichment in LILE-LREE to different extents in a group of the lherzolitic xenoliths, and a further addition of Fe, Mn and Ti in another. This latter group represents a transition towards the wehrlitic series, which is characterised by the lack of modal orthopyroxene, and contains secondary clinopyroxene, exhibiting Fe-Mn-Ti-LREE enrichment.

Equilibrium temperatures have been calculated with different thermometers, and a discrepancy of ~50-100°C was found between values obtained by major-element based and REE-based methods (Fig. 2c, d). Since trivalent REEs have higher

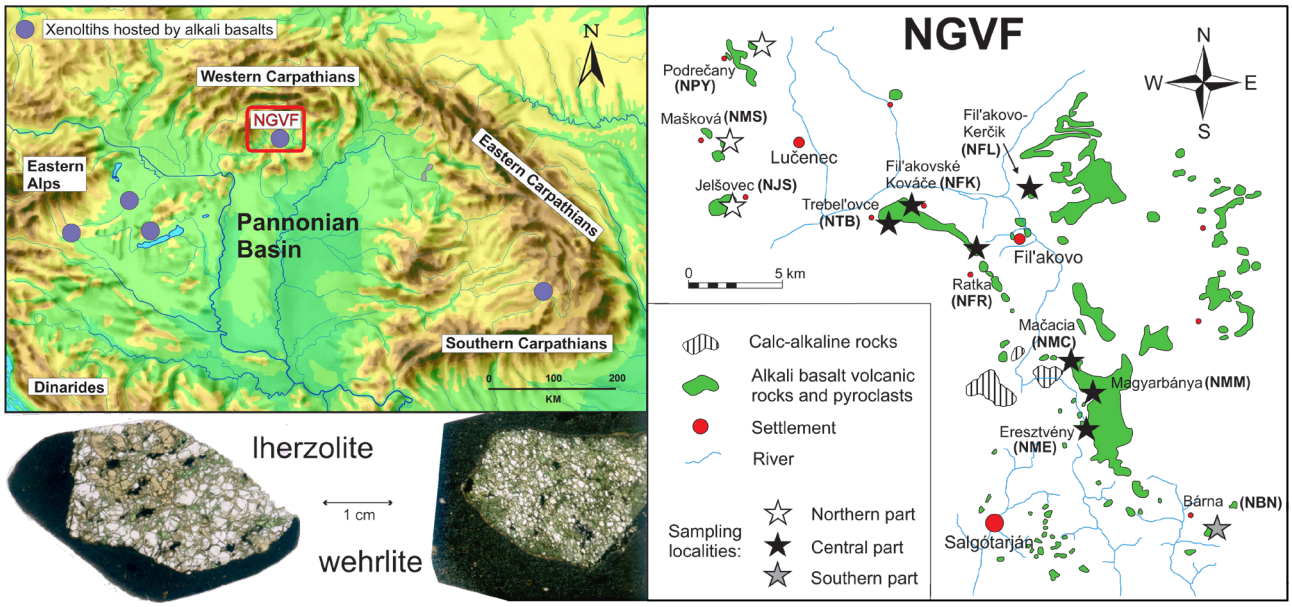

Figure 1. Top left: Alkali basalt-hosted xenolith occurrences in the Carpathian-Pannonian region. Right: Distribution of basalt outcrops and sampling localities in the NGVF. Bottom left: samples from the lherzolitic and wehrlitic series.

closing temperatures than the divalent major elements used by conventional thermometers, this difference can be explained by a major thermal event in the recent history of the NGVF mantle. It is assumed that the higher temperatures from REE-based thermometers reflect the heating by the extension and asthenospheric upwelling in the Pannonian Basin, whereas lower temperature values represent thermal relaxation and cooling following extension.

The distribution of textural types and crystal-preferred-orientation data acquired by EBSD (electron backscatter diffraction) analysis, as well as calculation of seismic properties, reveal that the three major domains of the NGVF (northern, central and southern) experienced different degrees of deformation. Xenoliths from the southern part represent a low-temperature, more equilibrated, fine-grained mantle domain, whereas the northern part is dominated by coarse-grained, high-temperature material with significant intragranular deformation. The strength of deformation and seismic anisotropy is highest in the central part, and is suspected to reflect a tectonic boundary beneath the area.

This project is part of CCFS Theme 2, Earth's Evolution, and contributes to understanding Earth's Architecture and Fluid Fluxes.

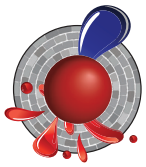

Contacts: Nora Liptai, Sue O'Reilly, Bill Griffin, Norm Pearson, Csaba Szabó, Levente Patkó (Eötvös University, Budapest, Hungary)

Funded by: Flagship Program 1, iMQRES, EPS postgraduate funds, Eötvös University postgraduate scholarship. This research is part of a cotutelle project between Macquarie and Eötvös University (Budapest, Hungary)

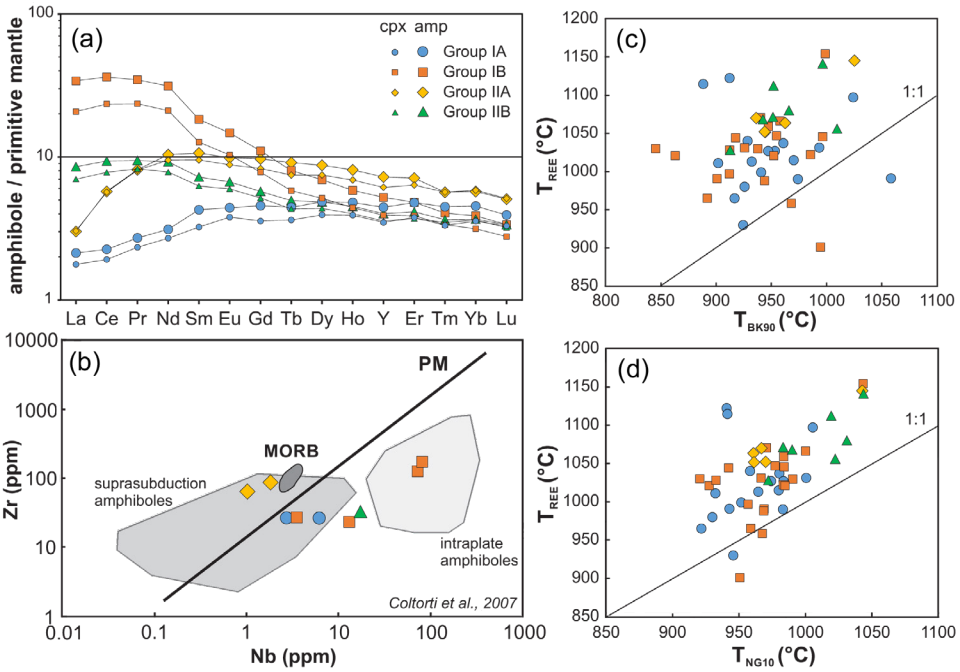

Figure 2. a) REE-distribution of clinopyroxenes and coexisting amphiboles. b) Nb-content based distinction of amphiboles from different environments. c-d) comparison of equilibrium temperatures calculated with REE-based (T_{REE}) and major element based thermometers (T_{BK90} = two-pyroxene method of Brey & Köhler, 1990; T_{NG10} = Ca-in-opx method of Nimis & Grütter, 2010).

Apatite - tracer for the evolution of porphyry systems

Analysis of the evolution of porphyry systems is key to better understanding how, when, and why fertile (i.e. metal-rich) igneous-hydrothermal systems develop. Accessory minerals, and in particular apatite, can serve as archives for the evolution of such systems. Apatite is ubiquitous in granitic rocks and can potentially record fluid evolution to lower temperatures (i.e. later stages) than zircon. Apatite hosts a range of trace elements, which can be used to establish the physical-chemical conditions of the magmatic system. Of particular interest are the REE, the halogen group elements (Cl, F, Br) and S, which provide constraints on the system's oxidation state, fluid source and metal transport capabilities. Previous studies have claimed that certain trace elements can be used to distinguish between fertile (i.e. ore-forming) and barren (ore-absent) porphyry systems. However, the proposed discrimination factors, based on trace element concentrations and ratios, are not universally applicable. In this study we will investigate porphyry systems of the Macquarie Arc (NSW) where several pulses of barren and fertile magmatism have been recognised. This igneous activity is spatially and geochronologically well-constrained, so the Macquarie Arc porphyries are an ideal case-study site.

The geochemistry of apatite will be combined with whole-rock data, which include the REE and isotopic tracers such as Sm-Nd. Whole-rock analyses and *in situ* mineral geochemistry of apatite will then be used to address the following fundamental questions:

- How representative is the geochemistry of apatite of its host rock?
- Can apatite be used to identify fertile igneous (porphyry) systems?
- Can metamorphic and igneous apatite be distinguished?

Solving the last question will be essential if apatite separates, such as detrital concentrates, are to be used to trace igneous systems in the prospective regions.

Preliminary results of quantitative EPMA element mapping (Fig. 1) show that apatite from mineralised systems often is distinctly zoned in terms of S concentrations, which is not observed in apatite from barren systems. This observation might give a first indication about the importance of S as a ligand for metals and related metal-melt-unmixing processes, which may be a key to mineralisation. In order to understand the source of S, we are currently developing a method to measure S isotopes *in situ* in apatite by SIMS. Sulfur-isotope ratios from apatite can then be coupled with Sm-Nd and other tracers to gain detailed insights into the geochemical evolution of porphyry systems.

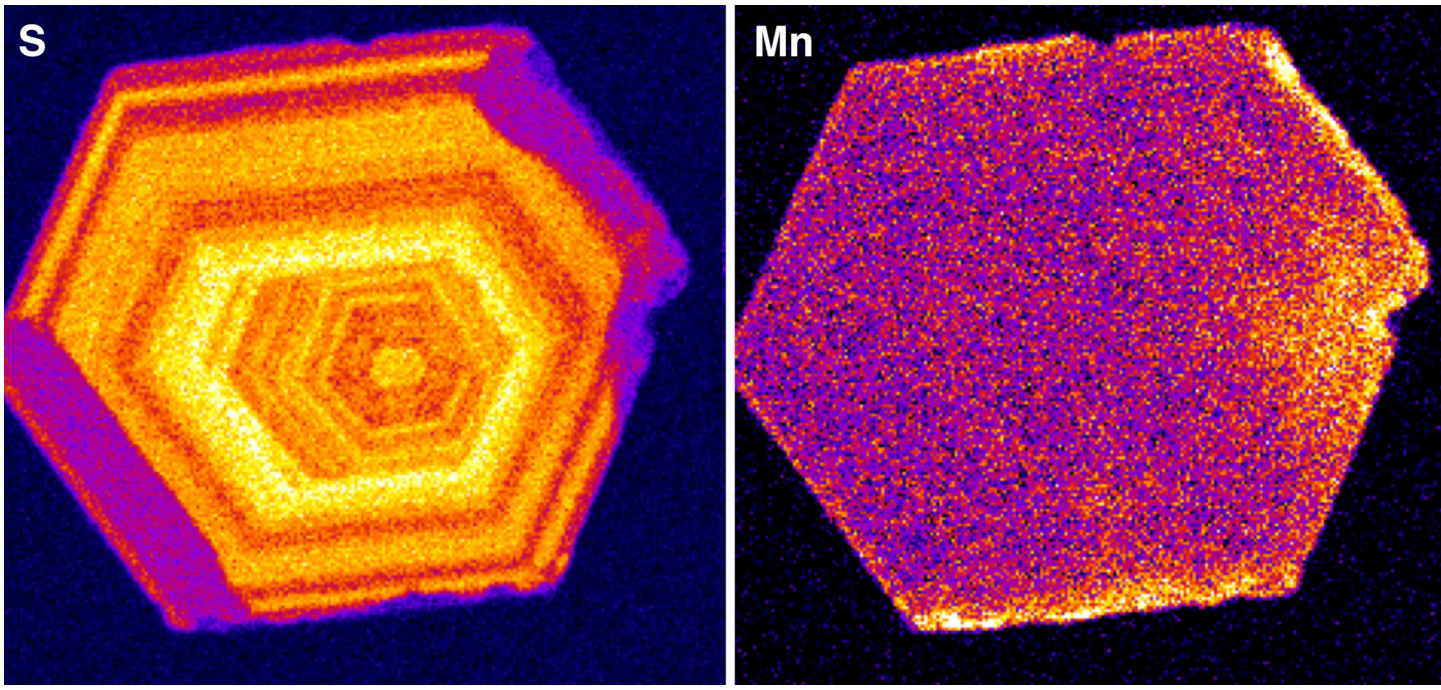

Quantitative EMPA maps of S and Mn in apatite from a mineralised porphyry system.

This project is part of CCFS Themes 2 and 3, Earth Evolution and Earth Today, and contributes to understanding Fluid Fluxes.

Contacts: Johannes Hammerli, Tony Kemp, Phillip Blevin, Marco Fiorentini
Funded by: CCFS Flagship Program 2

Hafnium isotopes record supercontinent cycles

We interrogated a large global Hf isotope dataset (>40,000 points), using a new statistical approach to track the most juvenile part of this dataset through time, linking secular variations with the supercontinent cycle. We statistically correlated supercontinent amalgamation intervals with episodes of evolved Hf, and breakup leading to re-assembly with episodes of juvenile Hf. Further, we found that the juvenile Hf signal is more sensitive to Pangaea and Rodinia assembly, its amplitude increasing with successive cycles to a maximum with Gondwana assembly, which may reflect enhanced subduction-erosion. We demonstrated that the juvenile Hf signal carries important information on prevailing global magmatic style, and thus tectonic processes.

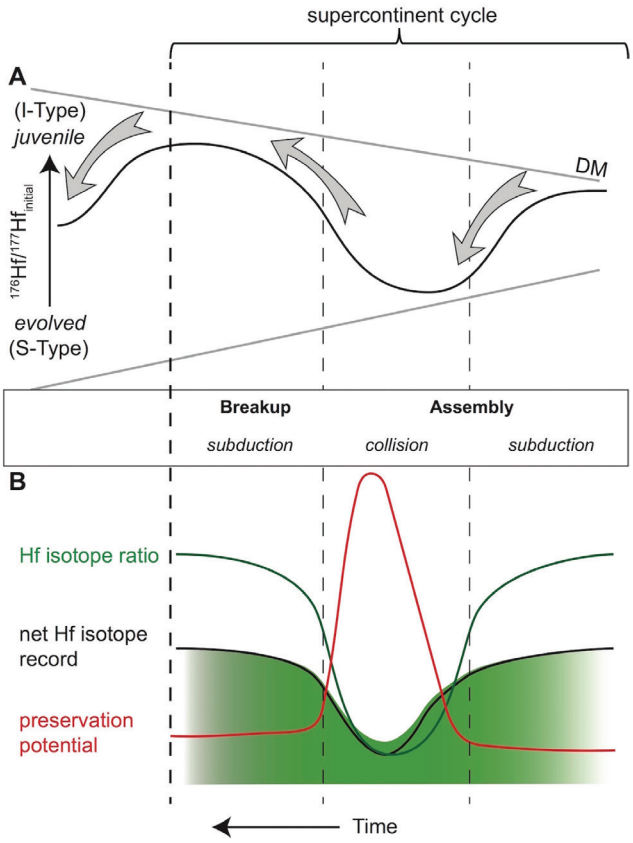

Figure 1. A. Schematic showing the conceptual evolution of initial $^{176}Hf/^{177}Hf$ ratios with respect to the stages of supercontinent assembly and breakup. B. Diagram showing the proposed effect of preservation bias on the Hf signal during a supercontinent cycle. Preservation curve and volume of generated magma retained in the geological record, and a lack of preservation will dilute global juvenile Hf signals towards a less radiogenic baseline, but will not affect the more evolved part of the record during continent collision. The net effect is to dampen but not remove the Hf isotope signal. The depth of shading reflects intensity of signal, based on number of analysis.

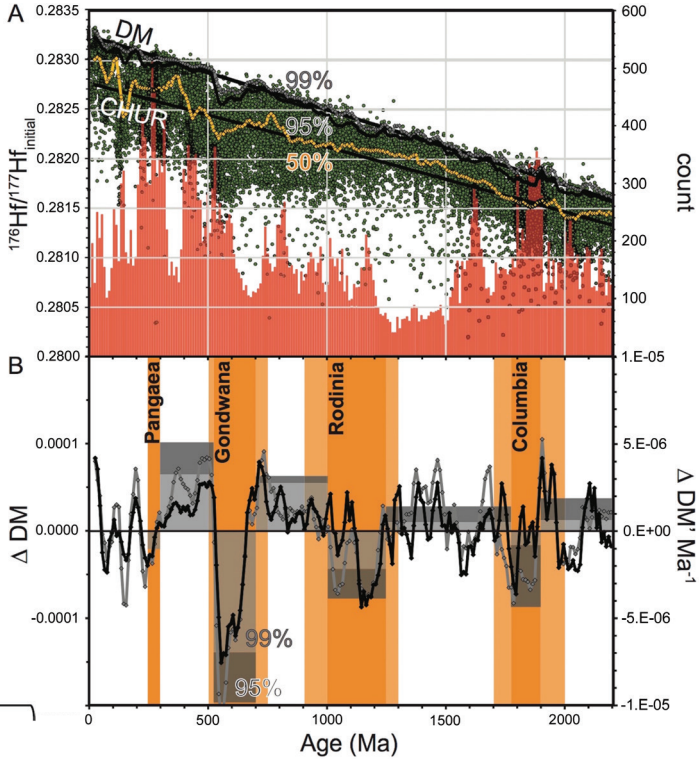

Figure 2. A. Global Hf dataset: initial $^{176}Hf/^{177}Hf$ versus U-Pb magmatic age from 0 to 2200 Ma. The 99th, 95% and median (50%) moving average time series are plotted. B. ΔDM (left scale) - a de-trended difference between DM and the Hf signal per 10 Ma; black = ΔDM95; grey = ΔDM99. A histogram of the ΔDM99 and ΔDM95 signals, the time-integrated difference for the periods within and between the indicated supercontinent assemblies (right scale). Periods of supercontinent assembly shown, with timeline A in dark orange and timeline B in lighter orange. Both from Gardiner et al. (2016), Scientific Reports 6, 38503 (CCFS publication #874).

This project is part of CCFS Theme 2, Earth's Evolution, and contributes to understanding Earth's Architecture and Fluid Fluxes.

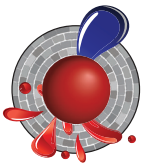

Contacts: Nick Gardiner, Chris Kirkland, Martin Van Kranendonk

Funded by: CET-Curtin internal funding

Strange mineral companions

Moissanite (SiC) is a rare mineral in terrestrial rocks. It can only form in environments with extremely low oxygen fugacity (fO_2) [at least 6-8 log units below the Iron-Wüstite (IW) buffer], which are not consistent with the normal fO_2 conditions (above IW) of the Earth's lithosphere. The occurrence of SiC and other very-reduced phases (e.g. native metal) in mantle rocks of the Tibetan ophiolites (e.g. Luobusa) has caused great concern about their formation and preservation mechanism in the Neo-Tethyan oceanic lithosphere. We report new observations of intergrown grains of SiC and associated oxidised phases from the Zedang ophiolite (close to the Luobusa ophiolite) in the Yarlung-Zangbo Suture Zone (South Tibet, China), and suggest a rapid dynamic process to isolate the host lithospheric fragment from ambient mantle.

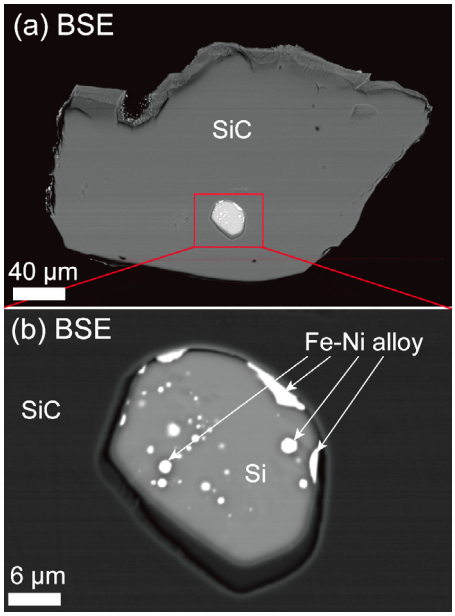

Figure 1. Back-scattered electron (BSE) images of a representative SiC grain (a) and its enclosed Si and Fe-Ni alloy (b), separated from harzburgite from the Zedang ophiolite (South Tibet).

SiC grains with diameters of ~100-500 μm have been separated from the Zedang harzburgite, chromitite and pyroxenite, all collected from the refractory harzburgite domain defined by Xiong et al. (*2016 EPSL, 438, 57-65, CCFS publication #691*). Combined imaging (optical microscopy and scanning electronic microscropy) and qualitative analyses (energy dispersive spectroscopy and laser Raman spectroscopy) have revealed that the SiC grains (mainly 6H polytype) contain droplet-shaped inclusions of Si metal and unmixing Fe-Ni-V-Ti-Mn-Si alloy (Fig. 1), suggesting formation at very high temperatures (≥~1400-1500 ºC) and ultra-reduced conditions (fO_2≤IW-6). Interestingly, some SiC grains are irregularly surrounded by K-rich silicate glasses, which contain inclusions of crystalline zircon. One SiC grain shows gradual oxidation from SiC, through Si and Si-C-O mixtures, to amorphous SiO_2, recording a complex reaction texture suggesting quenched glasses surrounding crystallised SiC (Fig. 2).

The coexistence of SiC and oxidised glasses, as well as the quenched texture, suggest that there must be a dynamic process (i.e. quenching) rapid enough to seal the extremely un-equilibrated phases and textures. Thermodynamic simulation of diffusive equilibration of SiC in an olivine matrix (Mg#=90) suggests that a SiC grain with a diameter of 300 μm will need ~1-10 million years to be consumed under temperatures of ~600-700 ºC (*Schmidt et al., 2014, PEPS, 1:27, 1-14*). These temperatures are consistent with those calculated from olivine-spinel pairs in the Zedang peridotites and chromitites. Therefore, to preserve these SiC grains and associated oxidised phases would require a rapid cooling process from peridotite solidus temperatures to ~600-700 ºC, within several million years. This process may reflect the very rapid ascent of the recycled peridotites and chromitites (host for the super-reduced phases) from the Mantle Transition Zone or deep upper mantle to lithospheric levels (*Griffin et al. 2016, J.Petrol. 57, 655-684. CCFS publication #704*) This rapid exhumation process has suppressed the thermodynamic consumption of SiC and other super-reduced phases with the host peridotites and chromitites, and eventually preserved them in the Neo-Tethyan oceanic lithosphere.

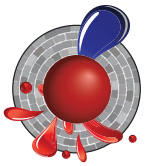

This project is part of CCFS Theme 2, Earth Evolution, and contributes to understanding Earth's Architecture and Fluid Fluxes.

Contacts: Qing Xiong, Bill Griffin, Jian-Ping Zheng (CUG Wuhan), Jin-Xiang Huang, Sarah Gain, Norman Pearson, Sue O'Reilly

Funded by: CCFS Flagship Program 1, NSFC

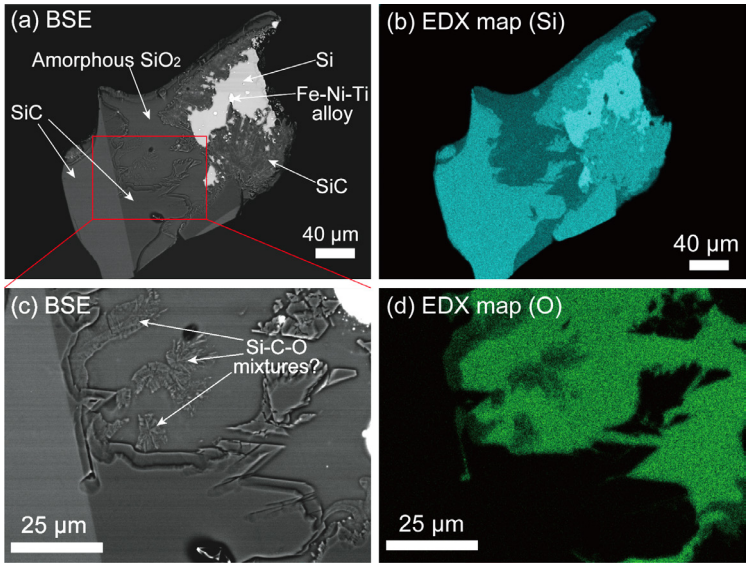

Figure 2. Back-scattered electron (BSE) images (a, c) and energy-dispersive X-ray (EDX) maps (b, Si; d, O) of a complex intergrowth grain of SiC with Si + Fe-Ni alloy (primary stage), reacted with oxygen-rich fluids/melts that formed amorphous SiO_2 and newly crystallised unknown Si-C-O mixtures (secondary products).

An Archean microcontinent lurking in the Capricorn Orogen

The Capricorn Orogen (Fig. 1a) formed during the Paleoproterozoic amalgamation of the Archean Pilbara and Yilgarn cratons to form the Western Australian Craton. Regional surveys involving geological mapping, geochemistry, and geophysics reveal a prolonged tectonic history of craton assembly and subsequent intracratonic reworking, which have significantly re-shaped the orogenic crust.

Using data from the on-going Capricorn Orogen Passive-source Array (COPA) stations and a high-density linear array embedded among the COPA stations (Fig. 1a), we conducted seismic receiver function and ambient noise studies targeting the Glenburgh Terrane, an exotic late-Archean to Paleoproterozoic crustal block previously inferred from distinct structural and isotopic characters in the core region of the terrane. The prominent Moho and intracrustal discontinuities vary across the

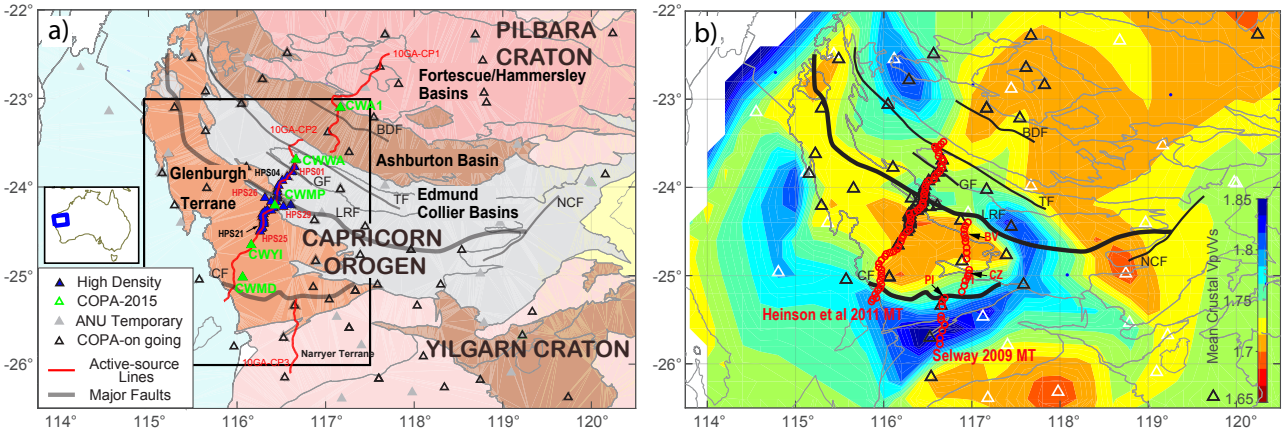

Figure 1. Crustal elements and seismic stations in the Capricorn region (a). The crustal element boundaries are simplified from the Geological map of Western Australia (2015). Red lines are the active source lines conducted by Geoscience Australia in 2010. The black and green (used in this study) triangles show the on-going Capricorn Orogen Passive-source Array (COPA). The High-density Passive Source (HPS) array is shown as the red triangles, which is partially collocated with active source line 10GA-CP2 (the middle one). Labels in a) are major faults: BDF Baring Downs Fault; TF, Talga Fault; GF, Godfrey Fault; LRF, Lyons River Fault systems; CF, Cardilya Fault; and NCF, Neds Creek Fault. (b) The seismic Vp/Vs ratio measurements which is indicative of an overall felsic composition of the Glenburgh Terrane bounded by major faults.

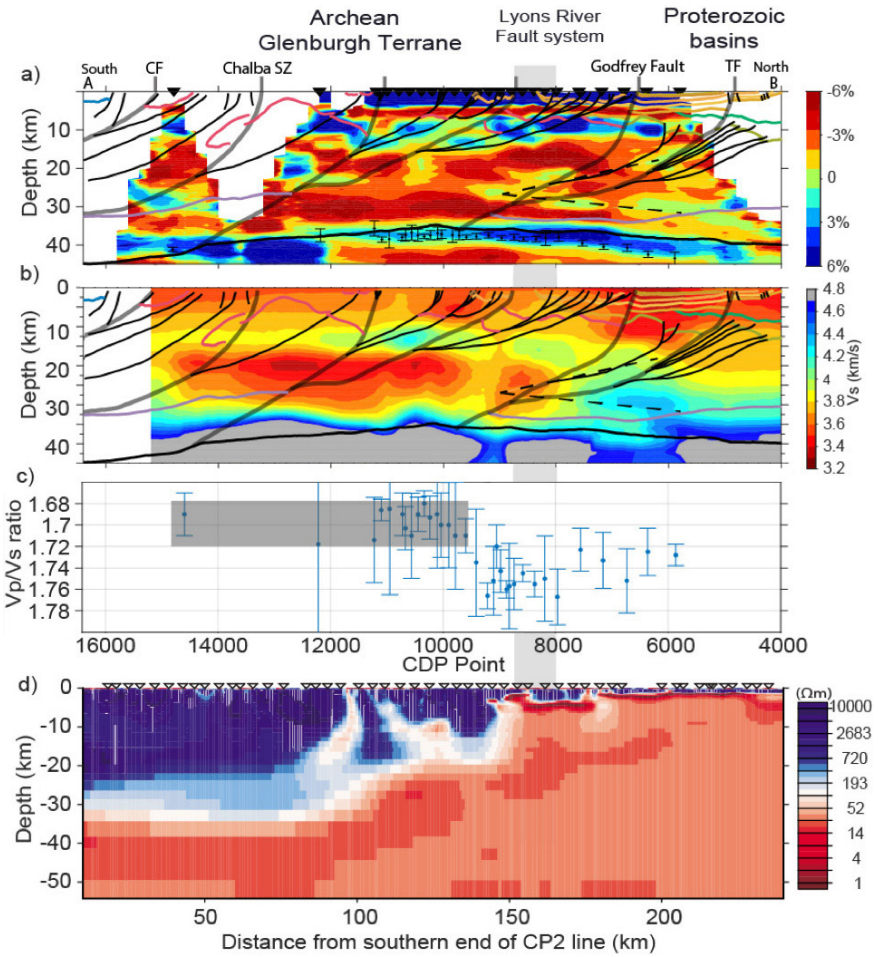

Figure 2. A compilation of available geophysical observations for the high density array, following the 10GA-CP2 line. a) Receiver function common-conversion-point stacking imaging showing the velocity gradient beneath the array. The active source interpretations are overprinted as lines. The vertical grey line shows the boundary of the Glenburgh Terrane and the Proterozoic basins. b) The shear-wave velocity model from the ambient noise inversion. Note the fast velocity shallow crustal layer which is also indicated in the receiver functions as a positive velocity gradient. c) The Vp/Vs ratio measurements. The small Vp/Vs ratios marked by the shaded region within the Glenburgh Terrane suggest a felsic bulk crustal composition, similar to that in the Archean Pilbara and Yilgarn and other global cratons. d) the 2010 magnetotelluric modeling image, showing the Glenburgh Terrane is resistive in shallow to middle crust, a common feature observed in Archean crust.

terrane boundary, showing a relatively thin crust (<40 km) with small Vp/Vs ratios (~1.70) in the Glenburgh terrane, compared with the thickened (>40 km) crust with elevated Vp/Vs ratios (>1.76) near the margins. Low Vp/Vs ratios (~1.70) are mapped terrane-wide (Fig. 1b), similar to what we have observed in the Archean Pilbara and Yilgarn cratons; they indicate a felsic bulk composition for the crust. Considering the available isotopic age data, and constraints from magnetotelluric and absolute shear wave velocity data (Fig. 2), the Glenburgh Terrane is interpreted as a microcontinent made in the Archean. A fast velocity is observed in the shallow crust (intraplating; Fig. 2), which suggests the crust was reworked during the assembly and cratonisation of the WAC and the subsequent intracratonic reworking/magmatic differentiation processes.

Our results illustrate that multi-disciplinary datasets bring complementary resolution and therefore may put tighter constraints on the tectonic processes that have affected the crust. See *CCFS publication #649, Yuan, 2015, Nature Geoscience 8, 808-103; Yuan et al., 2017, Crustal structure of the Glenburgh Terrane: the role of a microcontinent in the Paleoproterozoic craton assembly in Western Australia, submitted to JGR.*

This project is part of CCFS Themes 1, 2 and 3, Early Earth, Earth's Evolution and Earth Today, and contributes to understanding Earth's Architecture.

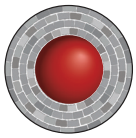

Contact: Huaiyu Yuan
Funded by: CCFS Flagship Program 7, SIEF Capricorn distal footprint

Magmatism lights up northern Gondwana 500-600 million years ago

Magmatism in continental arcs is often episodic, punctuated by high-volume magmatic flare-ups separated by lulls. Magmatic arcs commonly flare up every 30-70 Ma, which could be either a response to a tectonic event such as rapid slab retreat, change in dip angle and/or slab break-off; or could reflect a non-tectonic cause such as thermal runaway due to pooling of mafic magmas in the lower crust. Well-documented flare-ups are characterised by high-silica (felsic) rocks, with significant crustal inputs as indicated by high bulk-rock $^{87}Sr/^{86}Sr$, low εNd and high $\delta^{18}O$ and low εHf in zircon.

These ideas were developed for Cretaceous and younger continental arcs, where the igneous rocks are mostly exposed and include significant proportions of volcanic cover associated with plutonic rocks; these are the best places to define such magmatic episodicity and to consider its likely causes. These concepts also provide a new way to think about ancient continental arcs, where igneous rock exposures are more likely to be scattered, because most of the fossil continental arc is deeply eroded, buried by younger sediments, and disrupted by faulting. One way to explore ancient arc magmatic tempos is to complement direct sampling from scattered exposures with surveys of detrital zircons from the siliciclastic sediments derived from erosion of the nearby arcs. Recent improvements in U-Pb zircon dating and MC-ICPMS microanalysis of Hf isotopic compositions in the same grains provide powerful new tools for understanding the age of crystallisation, metamorphism and inheritance in igneous and sedimentary rocks.

Coupled Lu-Hf and O isotopic analyses of zircons and bulk-rock Nd-isotope compositions have proven particularly powerful for distinguishing juvenile (mantle) and recycled (older continental crust) components making up igneous rocks, especially where the rocks have been well-mapped, petrographically characterised, and analysed for major and trace element geochemical data. The use of all these tools in combination provides a powerful toolkit for constraining crustal growth and investigating magmatic flare-ups.

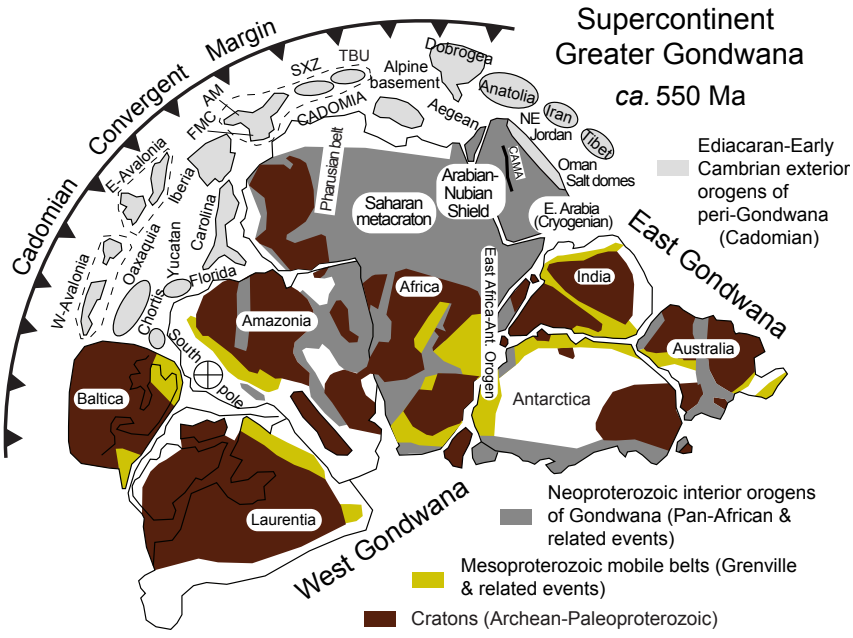

Figure 1. Paleogeography of the Cadomian - Avalonian active margin and related major peri-Gondwanan terranes at ~550 Ma. AM Armorican Massif, FMC French Massif Central, SXZ Saxo-Thuringian Zone (part of the Bohemian Massif), TBU Teplá-Barrandian Unit (part of the Bohemian Massif).

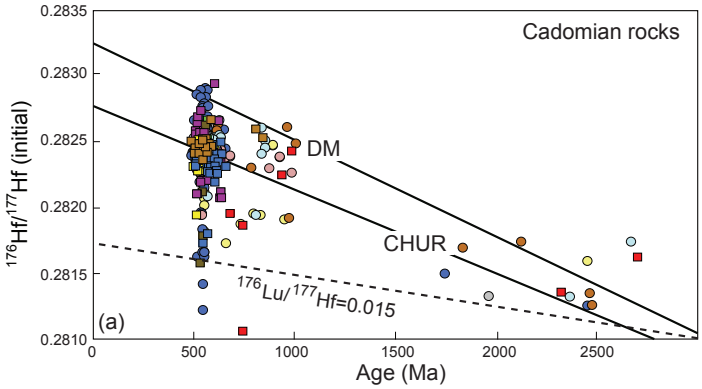

Figure 2. U-Pb age vs $^{176}Hf/^{177}Hf$ ratios for zircons from the Late Neoproterozoic-Cambrian rocks of Iran.

There is increasing evidence that a vigorous continental arc existed on the northern margin of the Greater Gondwana supercontinent during Late Ediacaran-Early Paleozoic time (500-600 Ma) (Fig. 1); this is referred to as the Cadomian orogen, although some segments, especially in the west, are called Avalonian. The Cadomian arc needs further study and this must use each of the outcrop areas that are now scattered across southern Europe and SW Asia. We are exploiting new zircon U-Pb-Hf-O as well as whole rock Sr-Nd isotopic data for a suite of Cadomian plutonic and volcanic rocks throughout Iran. Igneous rocks of the Cadomian arc were likely to have been dominated by development of calc-alkaline batholiths beneath thick sequences of felsic lavas, ignimbrites and arc-derived sediments, but these are rarely preserved. We are using these results to address the suitability of the magmatic flare-up model for understanding the Cadomian crust of this region and to address the thermal state of the Gondwana upper mantle and lower crust during that time span.

We have also analysed detrital zircons from a series of Late Neoproterozoic-Cambrian detrital sedimentary rocks to further unravel the role and extent of the Cadomian magmatism. Our results indicate that the Cadomian magmatism in Iran and surroundings, including Turkey, was a part of a ~100 Myr-long episode of subduction-related arc and back-arc magmatism at the northern margin of Gondwana. Zircon Hf isotope compositions (Fig. 2) show that during the Cadomian magmatic activity, juvenile arc magmas interacted with Archean crust to generate the Ediacaran-Cambrian igneous rocks. The hidden Archean crust is further evidenced by the occurrence of 2.5 Ga inherited zircons in the magmatic rocks and abundant magmatic, unrounded, Archean zircons in the sedimentary rocks (Fig. 3).

This project is part of CCFS Theme 2, Earth Evolution, and contributes to understanding Earth's Architecture.

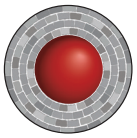

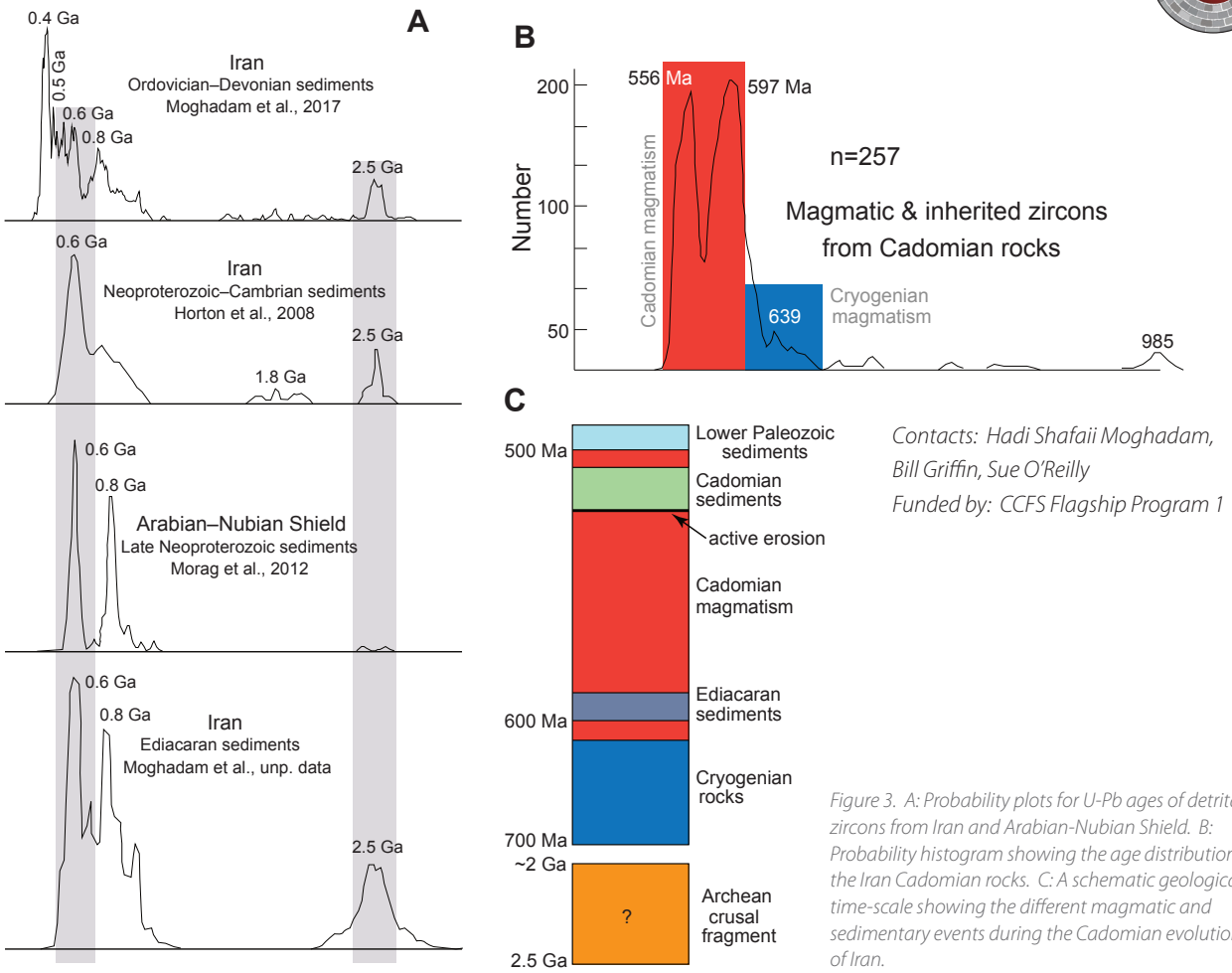

Figure 3. A: Probability plots for U-Pb ages of detrital zircons from Iran and Arabian-Nubian Shield. B: Probability histogram showing the age distribution of the Iran Cadomian rocks. C: A schematic geological time-scale showing the different magmatic and sedimentary events during the Cadomian evolution of Iran.

Contacts: Hadi Shafaii Moghadam, Bill Griffin, Sue O'Reilly

Funded by: CCFS Flagship Program 1

Isotopic canaries in zircon track Cu prospectivity across Southern Tibet

Porphyry deposits are the main source of copper and molybdenum worldwide and also an important source of gold and silver. Porphyry systems are found in both continental arcs and island arcs, e.g. circum-Pacific subduction zones, as well as continental collision zones, e.g. southern Tibet. Broadly, porphyry deposits are characterised by copper sulfide minerals in stockworks, disseminations and veinlets, commonly associated with porphyritic intrusions, affected by potassic, sericitic and in some cases, even argillic alteration (*Sillitoe, 2010*).

To gain new insights into the prospectivity and geologic setting of the Chongjiang (CJ), Gangjiang (GJ) and Bairong (BR) porphyry Cu prospects and the Tinggong (TG) porphyry Cu-Mo mine in the southern Lhasa terrane, southern Tibet, we use the new integrated approach published by Lu et al. (*2016*). The integrated approach includes the use of porphyry Cu fertility indicators based on traditional whole-rock geochemistry and new *in situ* zircon trace element analyses. Additional measurements included zircon U-Pb, Hf and O isotopes in order to better constrain magma sources and the petrogenetic evolution of the region.

Cu fertility indicators

Porphyry copper deposits are associated with hydrous and oxidised magmas at shallow crustal levels (*Sillitoe, 2010*). These hydrous magmas are characterised by high Sr/Y (>35), V/Sc (>10) and Al_2O_3/TiO_2 (>25) ratios. To complement the previously mentioned whole-rock indicators, Lu et al. (*2016*) took advantage of the remarkable resilience of zircon and its ability to record tectono-magmatic evolution. Under the new approach it is possible to distinguish between fertile and infertile magmatic suites and evaluate tectonic processes that are identified from whole rock geochemistry. The method includes *in situ* measurements of trace elements in zircons. The best indicators of Cu fertility based on zircon compositions are zircon Eu/Eu* (>0.3) and 10,000*(Eu/Eu*)/Y (>1), while zircon (Ce/Nd)/Y (>0.01) and Dy/Yb (<0.3) have proven to be moderately useful. In addition, the zircon O- and Hf- isotope data provide insights into the sources and petrogenetic evolution of the porphyry systems.

Southern Tibet Miocene porphyry copper deposits

The Himalayan-Tibetan orogeny is the result of the amalgamation of three distinct terranes, from north to south, the Songpan-Ganze, Qiangtang, and Lhasa terranes. The Lhasa terrane is further subdivided into three sub-terranes as shown in Figure 1 (*Hou et al., 2015*). The amalgamation of these terranes resulted from the Indo-Asian continental collision that started in the early Tertiary. The southern margin of the Lhasa terrane hosts Miocene porphyry copper deposits estimated at 18 Mt of Cu with a value of approximately 126 billion US$.

Preliminary results of the zircon U-Pb, trace element, Hf and O data indicate that the prospects CJ, BR, and GJ are fertile for Cu mineralisation and that they formed in a compression environment resulting from the continental collision of India and Asia at ca 55 Ma. The O and Hf data show that the samples are mostly of juvenile origin but after ca 55 Ma there is an increasing involvement of supra-crustal material in the magma genesis, possibly due to subduction of Indian continental sediments into the Tibetan mantle source.

See *CCFS publication #811, Lu et.al. Society of Economic Geologists Special Publ. 19, 329-347.*

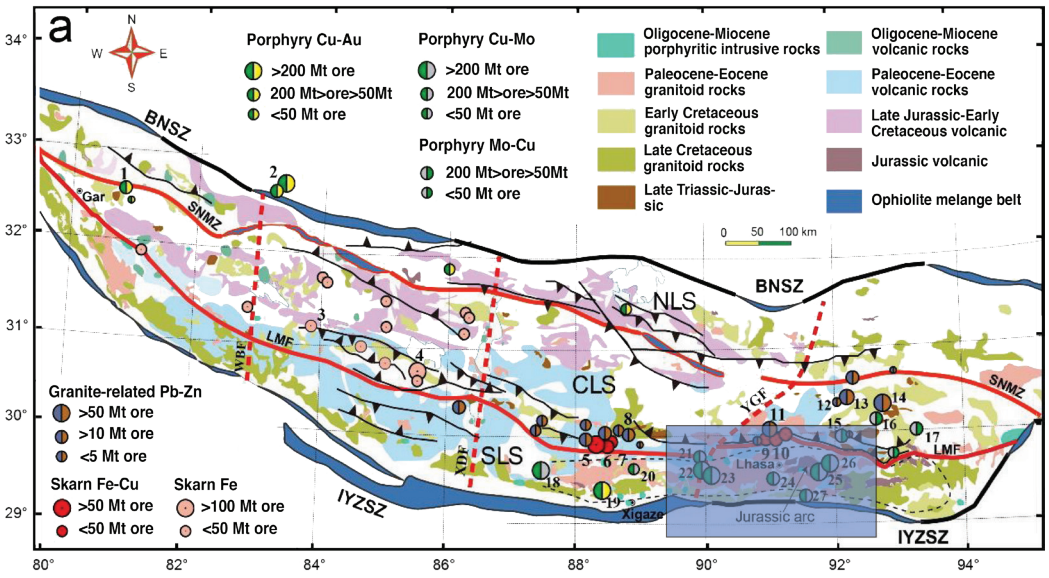

Figure 1. Simplified geological map of the Lhasa Terrane, and its sub-terranes, northern, central, and southern. Sub-terranes are cut by three Miocene normal fault systems: Wenbu, Xuru-Dangreyong, and Yadong-Gulu faults. Distribution of granitoid rocks and felsic volcanic rocks of the Lhasa terrane. Thick dashed red lines indicate N-S-trending normal fault systems. Thin dashed black line in eastern portion of the southern Lhasa sub-terrane indicates extent of a Jurassic magmatic arc (Hou et al., 2015). Blue box shows the location of the study area.

This project is part of CCFS Theme 2, Earth Evolution, and contributes to understanding Earth's Architecture and Fluid Fluxes.

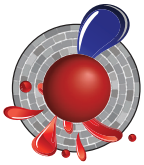

Contacts: Luis Parra-Avila, Yongjun Lu, Marco Fiorentini, Robert Loucks

Funded By: CCFS Flagship Program 2

Astrobiology *'Down under'*: Visualising early life on Earth

The advent of virtual reality technologies and multi-scale 3D modelling in combination with geological mapping has allowed perspectives of geological outcrops never before explored.

Over the past 30 years the world of virtual reality has emerged, not just for games but also for education and especially industry training. In recent years virtual reality has come back into the limelight and is better and cheaper than ever. Over the past 5 years, drones or Unmanned Aviation Vehicles (UAVs) have become relatively inexpensive and easy to use, with camera quality that reaches 4K. Meanwhile, point-and-shoot digital cameras provide easy-to-use, efficient, lightweight tools for capturing high-resolution images. These technologies provide an easy, inexpensive, way to collect and display visual data. This has significant applications in science, and especially for the visually-dependent disciplines such as the geosciences.

This research capitalises on the benefits of visual data capture, focusing on building a comprehensive virtual field trip (VFT) of a site that contains evidence for some of Earth's earliest life, the *ca* 3.48 Ga Dresser Formation North Pole Dome, Pilbara Craton, Western Australia. Extensive detailed mapping, along with petrological and geochemical data from the Dresser Formation has provided a plethora of paleoenvironmental evidence showing that life was living in and around volcanic hot springs much like those found in Yellowstone National Park or the North Island of New Zealand. Rock structures built by microbes almost 3.5 billion years ago can be found in the ancient deposits (Fig. 1).

The VFT includes immersive geological outcrop visuals and photogrammetric imaging (3D models), and integrates detailed scientific observations from the macro- to the micro-scale i.e. outcrop to microscopic view, respectively (Fig. 2). Results aim to: 1. Enhance the environmental model for the Dresser Formation, developing a better understanding of why some of Earth's earliest convincing evidence of life is in a volcanic hot-spring setting and; 2. Produce an interactive and immersive learning/educational tool - by way of a VFT - that can be used in online, face-to-face teaching, and as a research tool.

The principles and practices of the VFT can be applied to other geological sites, perhaps even Mars. The VFT serves as an educational tool and as a visual aid in communicating science and early life on Earth as well as providing assessment for the use of immersive environments in education and scientific research.

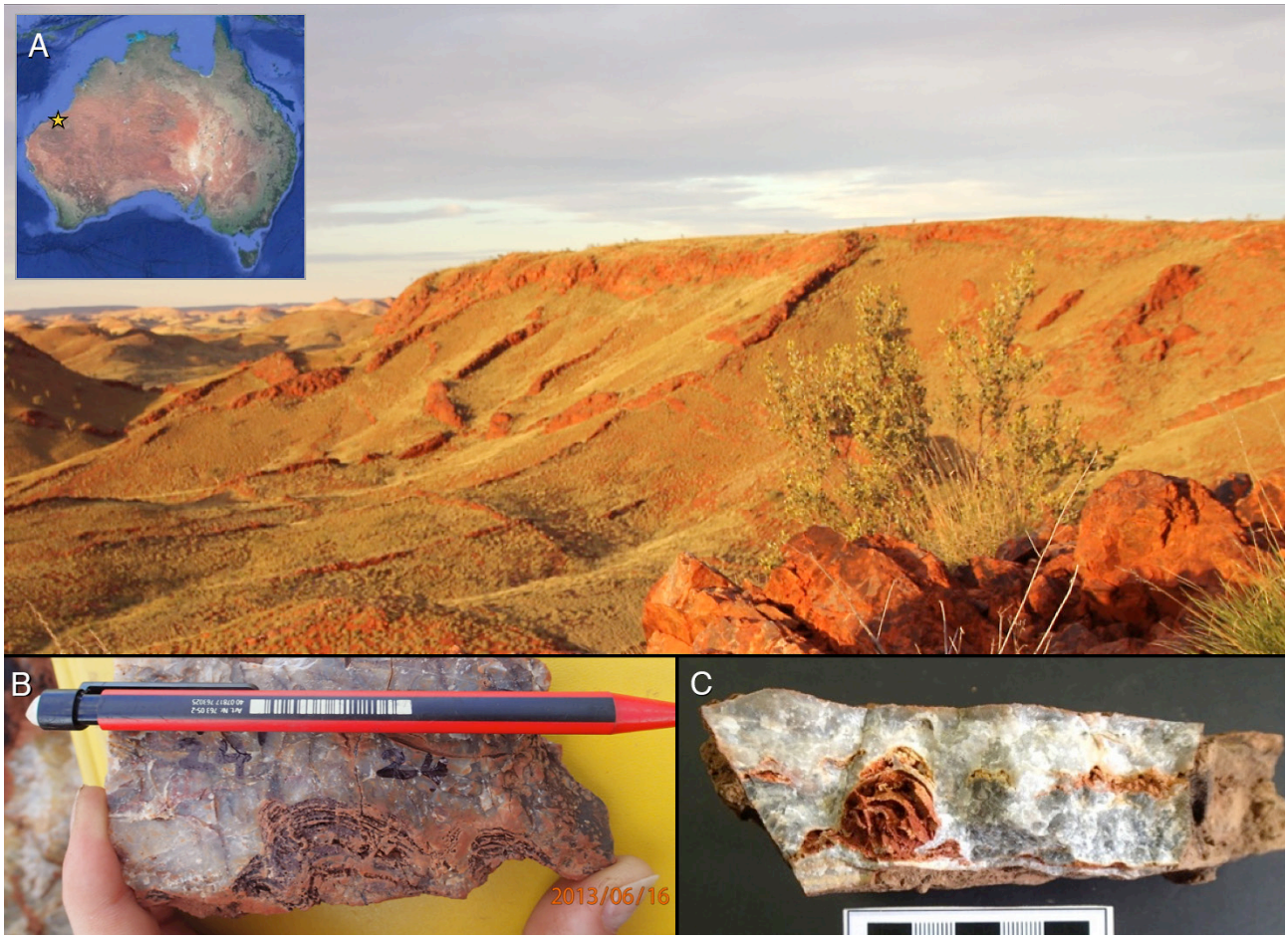

Figure 1. A. Location photo of the Dresser Formation. B-C. Signs of life: Stromatolites within the Dresser Formation - rock structures built by microbial life 3.5 billion yeas ago.

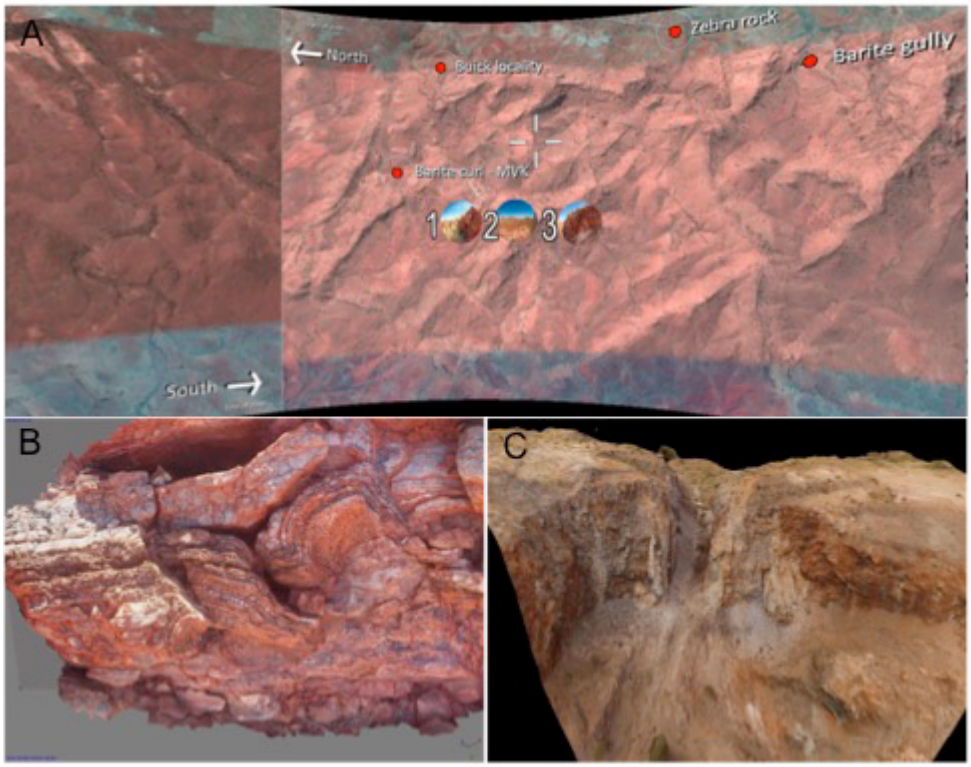

Figure 2. A. Map of the Dresser Formation within the Virtual Field Trip showing sites containing multiple 360° panoramas that contain detailed multimedia such as 3D models, photographs, micrographs and geo- chemical information. B. 3D model of stromatolites. FoV - 3 m. C. 3D model of local outcrop. FoV - 100 m.

In 2016, the Australian Centre for Astrobiology launched a pilot demonstration of the VFT at UNSW in the 3rd year astrobiology course (BEES6741: Life in the Universe). The students' task was to go through the Dresser Formation VFT and then create a table of evidence and a 3 minute video describing what they had observed and interpreted about the environment based on their experience. This has proven to be a successful and fun exercise. In 2017, we aim to develop and enhance the VFT and launch a second pilot program in this year's astrobiology course.

This project is part of CCFS Themes 1 and 2, Early Earth and Earth's Evolution, and contributes to understanding Fluid Fluxes.

Contacts: Tara Djokic, Martin Van Kranendonk
Funded by: CCFS Flagship Program 4

Mineral gymnastics track subduction zone processes

All around the world, sections of deep Earth material are exposed in ophiolitic complexes and allow geologists to take a direct look at the deep crust, the transition zone and the underlying upper mantle. In the Moho transition zone as well as in the upper mantle, we find a characteristic layering - dunites and pyroxenites entangled with each other. The physical and chemical properties of the dunites, the most volumetrically important fraction in the upper mantle, have been extensively studied. Pyroxenites, despite being geochemically significant, have not received much attention from the mineral-physics point of view and their influence on upper-mantle rheology still remains unclear.

In north-western Spain, the Cabo Ortegal massif makes up a spectacular field occurrence of deformed interlayered

Figure 1. Typical outcrop of massive pyroxenites in the Cabo Ortegal complex. Dunites (yellowish layers) are interlayered with massive pyroxenites (green-greyish layers). Deformation markers such as boudinage can be easily observed.

pyroxenites and dunites. Such outcrops constitute a fantastic natural laboratory to investigate how deformation affects a pyroxene-rich domain.

Field and geochemical evidence has defined four different types of pyroxenites: *type-1* are olivine-bearing clinopyroxenites enclosing dunitic lenses, and are interpreted as partial replacement of the host peridotite; *type-2* are massive websterites representing either more evolved products of the melt/rock interaction that led to *type-1* pyroxenites, or crystal cumulates in dykes and veins; *type-3* are foliated amphibole-rich clinopyroxenites with evidence of significant fluid percolation; and *type-4* represent the rare orthopyroxenites. We performed a petrological and textural characterisation of the different pyroxenites by Electron Backscatter Diffraction (EBSD). Combination of the results with field evidence revealed that at least two superimposed deformation events have been recorded by the Cabo Ortegal pyroxenites.

The most ancient event is suggested by the olivine and clinopyroxene fabrics and is likely to have occurred at temperatures greater than 1000°C in a hydrated environment. Such deformation conditions are consistent with the mantle wedge setting that has been already suggested by geochemical data. The second deformation event is recorded by the amphibole and occurred at lower temperature (500 to 800°C). This event is synchronous with the development of the spectacular sheath folds observed in the field and is consistent with close proximity to a slab.

Based on this new evidence, we argue that the Cabo Ortegal pyroxenites record mantle wedge deformation during the massive delamination of the arc root where it was generated. Our results are also consistent with the exhumation of the massif by its introduction into a subduction channel. Cabo Ortegal pyroxenites are therefore an incredible opportunity to have a look at the physical state of a piece of delaminated arc root and observe the impact of pyroxenes on the local rheology.

This project is part of CCFS Themes 2 and 3, Earth's Evolution and Earth Today, and contributes to understanding Earth's Architecture and Fluid Fluxes.

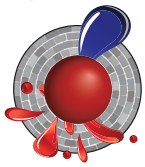

Contacts: Hadrien Henry, Romain Tilhac, Sue O'Reilly, Bill Griffin, Georges Ceuleneer (Géosciences Environnement Toulouse, GET, France)

Funded by: CCFS Flagship Program 1, Two iMQRES scholarships and cotutelle programs between Macquarie and Paul Sabatier University, EPS postgraduate funds, CNRS funds (G. Ceuleneer)

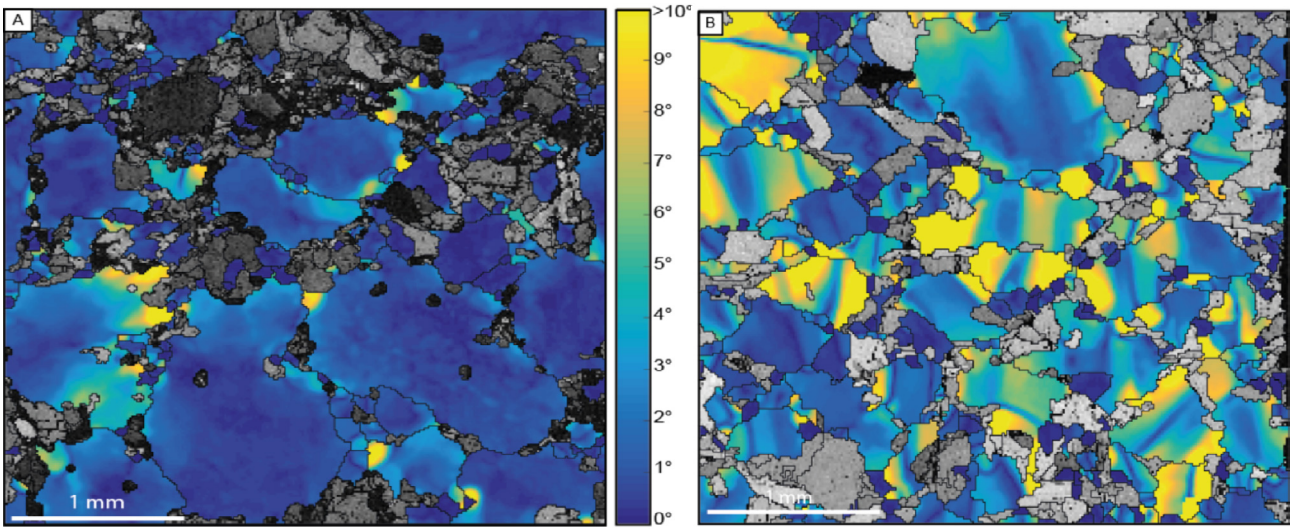

Figure 2. Microstructure of the pyroxenites plotted from EBSD data. These maps of misorientation to mean orientation indicate the angular deviation between each measurement (i.e. pixel) and the mean orientation of the grain it belongs to. A: Misorientation to mean orientation for clinopyroxenes. Misorientations are concentrated in the external part of the grain and at subgrain boundaries. B: Misorientation to mean orientation for orthopyroxenes. Misorientations are here concentrated in kink bands and form the spectacular undulose extinction one can see in thin sections.

Recognising where magma moves 40 km underground

Earth has a heterogeneous, layered crust that overlies a relatively homogeneous mantle. Every day, magma erupts from volcanoes around the world to form lava and other eruptive rock types. The geochemical signature of these volcanic rocks tells us that in most cases the source of the magma (i.e. the deep rocks that partially melted) includes both mantle and crustal components that are tens to even hundreds of kilometres deep in the Earth. Therefore, these partial melts must migrate from the deep Earth to the surface, yet geological pathways are difficult to recognise. Although some pathways are seen as dykes and shear zones, few are documented to be associated with mass transfer. Consequently, there must exist structures that are yet to be recognised as zones of substantial mass transfer.

Elongate bodies of rocks very rich in iron and magnesium, with low silica (< 45 wt%), are ubiquitous in exposures of the deep crust (exhumed from 25-50 km). Hornblendite bodies (rocks mainly comprising the mineral hornblende) of the Pembroke Valley, north of Milford Sound in New Zealand, are hosted within granulite-facies gabbroic gneiss and are typical of such occurrences. These examples have igneous grain shapes and mineral textures, in contrast with the metamorphic character of their host gneiss.

Both rock types have a common gabbroic parent; field relationships are consistent with modification to gabbroic gneiss and then into hornblendite. Although the hornblendite looks like a cumulate rock, where hornblende grains settled and concentrated in a magma chamber, the field relationships preclude this interpretation; these bodies are imposter cumulates. Instead, hornblendite formed when the host gabbroic gneiss was replaced because of channelled melt flux through the lower crust. High melt/rock ratios and disequilibrium between the migrating magma and the gabbroic gneiss induced dissolution (grain-scale magmatic assimilation) of the gneiss and crystallisation of hornblende from the migrating magma. The extent of this reaction-replacement mechanism indicates that such hornblendite bodies mark significant melt conduits. Accordingly, many of the ubiquitous elongate bodies rich in iron and magnesium of the lower crust probably map the '*missing*' mass-transfer zones.

The dissolution of plagioclase and pyroxene from the gabbroic gneiss and crystallisation of mainly hornblende marks a reactive period of melt-rock interaction. Once all the plagioclase and pyroxene of the host rock has reacted out of the channel of magma migration, it becomes an armoured channel.

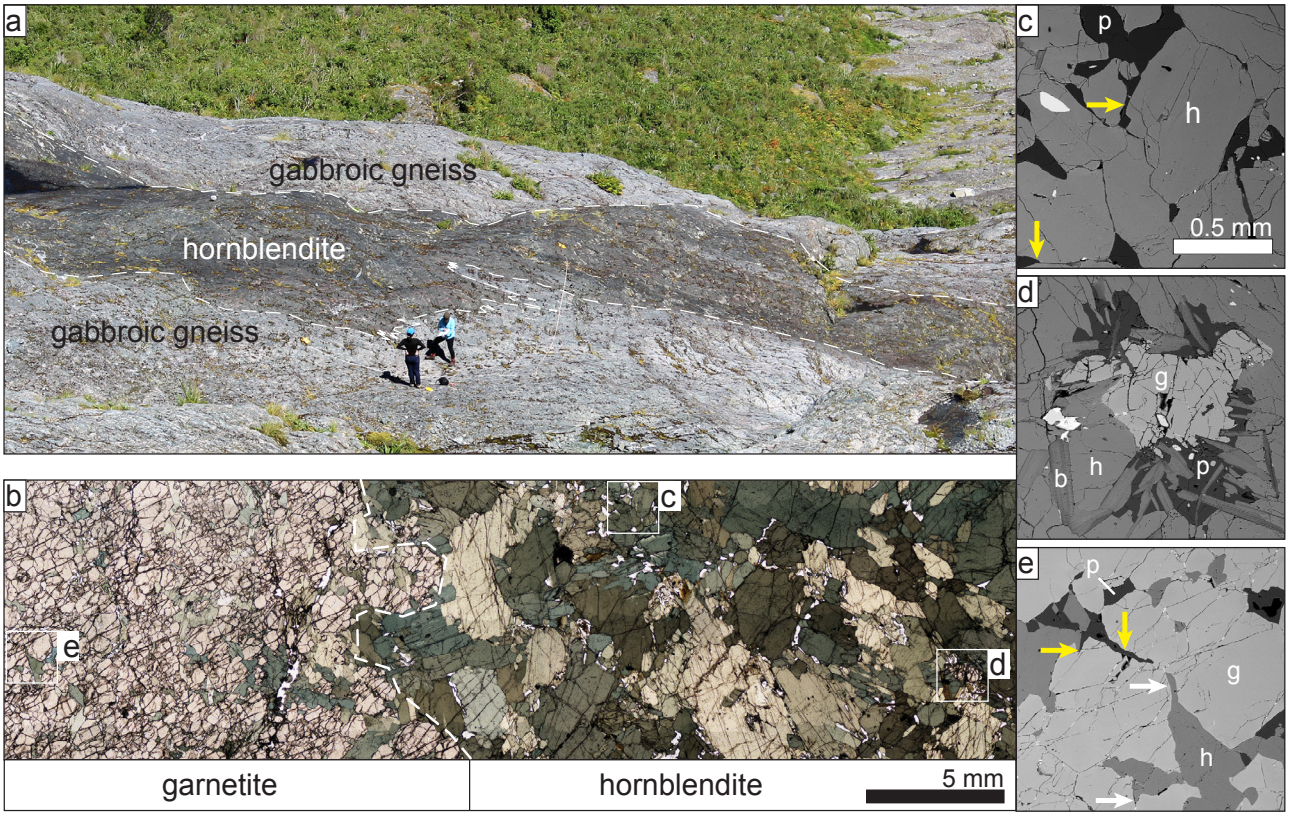

Figure 1. (a) Excellent exposure of an interpreted melt flux channel (30-40 m wide dark rock outlined by dashed lines, left to right) being mapped by Masters of Research students Uvana Meek and Victoria Elliott. (b) Photomicrograph of hornblendite (right) and garnetite stringer (left) from within the melt flux channel. (c-e) Back-scattered electron images of low dihedral angles, films along grain boundaries and small pockets representing the crystallsation of former melt, along with well-developed crystal faces at unlike mineral boundaries (e.g. plagioclase-hornblende boundaries in upper left of e). Mineral labels are plagioclase (p, yellow arrows), hornblende (h, white arrows), biotite (b) and garnet (g).

At this stage, magma can migrate through the channel without modification or chemical interaction with wall rocks. An indeterminate volume of melt could then use the channel, moving large volumes of melt through the crust.

See *CCFS publication #832, Daczko et.al., Scientific Reports, 2016, 6, 31369.*

This project is part of CCFS Theme 2, Earth's Evolution, and contributes to understanding Earth's Architecture and Fluid Fluxes.

Contacts: Nathan Daczko, Sandra Piazolo
Funded by: ARC DP (SP and ND), ARC Future Fellowship (SP)

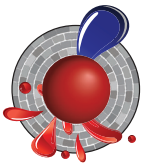

Ancient sulfur species recycled into younger igneous rocks

Cratonic margins are structurally and magmatically complex areas of the Earth's crust, and often have been affected by one or more orogenic cycles. Several studies (e.g. *Foley, 2008; Begg et al., 2010; Mole et al., 2014*) have argued that Archean lithospheric block margins exerted a first-order control on the ascent and focusing of mantle plumes that lead to the emplacement of hot magmas, host to orthomagmatic Ni-Cu-PGE deposits, and associated Au and base metal hydrothermal systems. The presence of trans-lithospheric faults along craton margins would help to focus fluids and metals, while mantle plumes provided a source of energy to drive ore-formation processes (e.g. *Mole et al., 2013*). Younger orogenic belts formed during the Proterozoic or Phanerozoic around Archean lithospheric blocks also are prospective for the presence of metal deposits (e.g. iron oxide Cu-Au, orogenic Au, porphyry Cu-Ag; *Groves et al., 2005*), suggesting that the cratonic margins continued to focus mineralisation. Therefore, it is important to elucidate the processes that drive volatiles and their associated metal cargoes into orogenic belts at the margins of reworked Archean Cratons.

Sulfur resides in the Earth's mantle, crust and hydrosphere but is locally concentrated in mineralised systems, where it acts as the primary complexing ligand in the formation of sulfide minerals. Mantle- and crustally-derived magmas have brought large quantities of economic metals from the Earth's interior to the near surface, and hydrothermal fluids have remobilised and re-precipitated these metals within the crust as different sulfides. The sulfur itself may be sourced from a variety of compositional reservoirs, each with distinct isotopic compositions. Mixing and interactions with the mantle, crustal magmas, hydrothermal fluids, country rocks, or meteoric waters imparts specific isotopic signatures, resulting in minerals with a range of isotopic compositions. Intra-grain and inter-grain chemical and isotopic variations in sulfur-rich mineralised systems record the interaction of these different reservoirs and offer unique insights

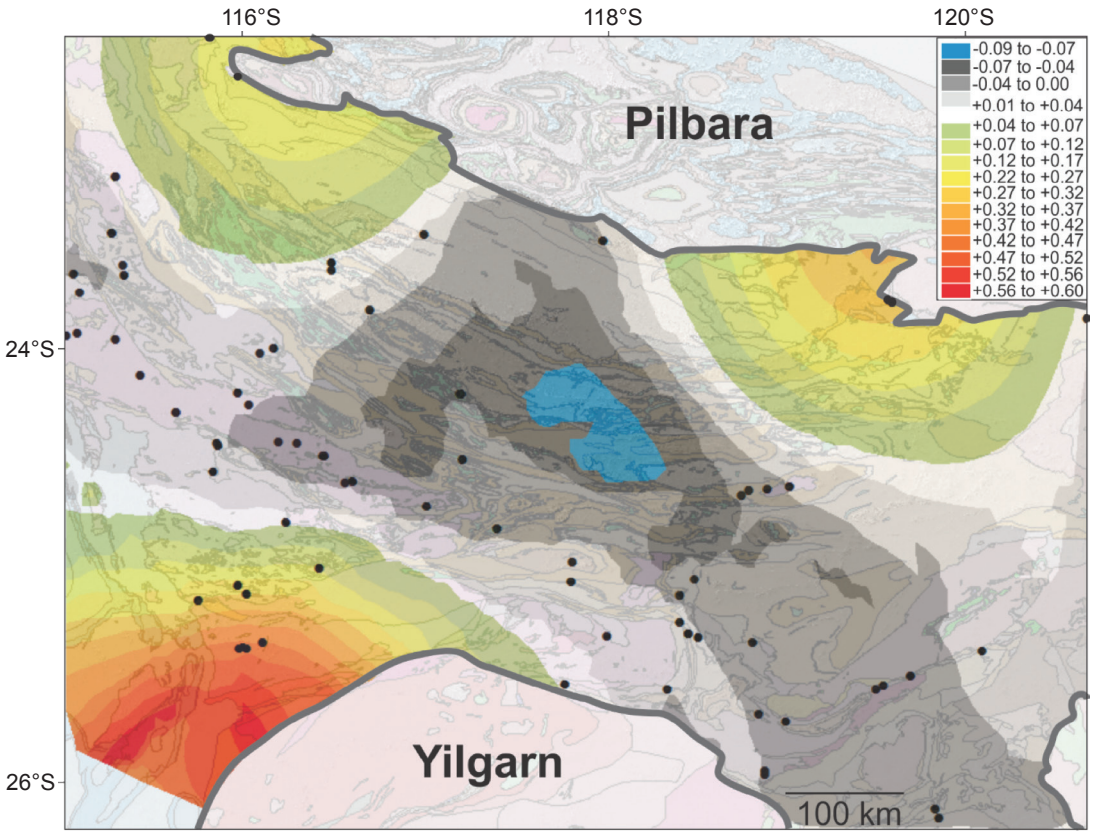

Figure 1. $\Delta^{33}S$ interpolated model of the Proterozoic Capricorn Orogen demonstrating MIF-S anomalies proximal to the Archean cratons.

into the complex fluid-rock interactions within mineral systems (*McCuaig et al., 2010*).

Understanding the cycling of sulfur and metals from Archean cratons into their margins can be explored using $\delta^{34}S$ - the isotopic tracer sensitive to physical processes of formation - and $\Delta^{33}S$ and $\Delta^{36}S$. The $\Delta^{33}S$ and $\Delta^{36}S$ anomalies express Mass-Independent Fractionation (MIF) - the production of sulfur isotopes by ultraviolet irradiation of a sulfur-rich atmosphere in Archean time, when Earth was not shielded by the oxygen and ozone in the atmosphere. These anomalies thus can be used as temporal tracers sensitive to the Archean-Proterozoic transition, like putting dye in watersheds to see how water travels.

The Capricorn Orogen is a natural laboratory to understand fluid, volatile and metal transfer to the margins of metal-endowed Archean cratons. The rocks making up the cratonic margins have long histories of deformation and hydrothermal fluid alteration. Results at the orogen-scale combined with detailed studies of ore deposits, help to track the mixing of geochemical reservoirs. The Proterozoic Capricorn Orogen records $\Delta^{33}S$ values that range from −0.07‰ to +0.80‰. Spatially, data from this study show that ancient sulfur, with geochemical signatures indicating formation by mass-independent fractionation, in the Capricorn Orogen occur in localised areas, especially near to the margins of Archean cratons (Fig. 1). We suggest that the spatially localised $\Delta^{33}S$ anomalies in Proterozoic samples, and the Archean $\Delta^{33}S$-$\Delta^{36}S$ array of -1 (Fig. 2) reflect a recycled MIF-Sulfur component, rather than a primary signature. This evidence indicates that MIF-Sulfur can be imparted to the Paleoproterozoic granitoid and hydrothermal record through tectonically-driven crustal formation processes.

The units hosting Archean-sourced MIF-Sulfur are dominantly magmatic (granitoids associated with collision and intraplate reworking) and hydrothermal (mineralised samples associated with faulting and veining). Other mineral deposits that preserve MIF-Sulfur anomalies occur in collisional (ca 2.0 Ga Glenburgh deposit; *Selvaraja et al. in review*) and intracontinental-reworking settings (ca 1.8 Ga Prairie Downs deposit; this study). Therefore, we propose that magmatic and hydrothermal events associated with collision and intracontinental reworking processes are responsible not only for recycling sulfur across terrain boundaries, but also for transferring metals from endowed Archean reservoirs into their younger margins.

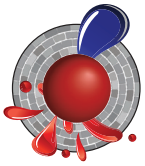

This project is part of CCFS Theme 2, Earth's Evolution, and contributes to understanding Earth's Architecture and Fluid Fluxes.

Contacts: Crystal LaFlamme, Marco Fiorentini, Boswell Wing, Mark Lindsay, Vikraman Selvaraja
Funded by: MRIWA

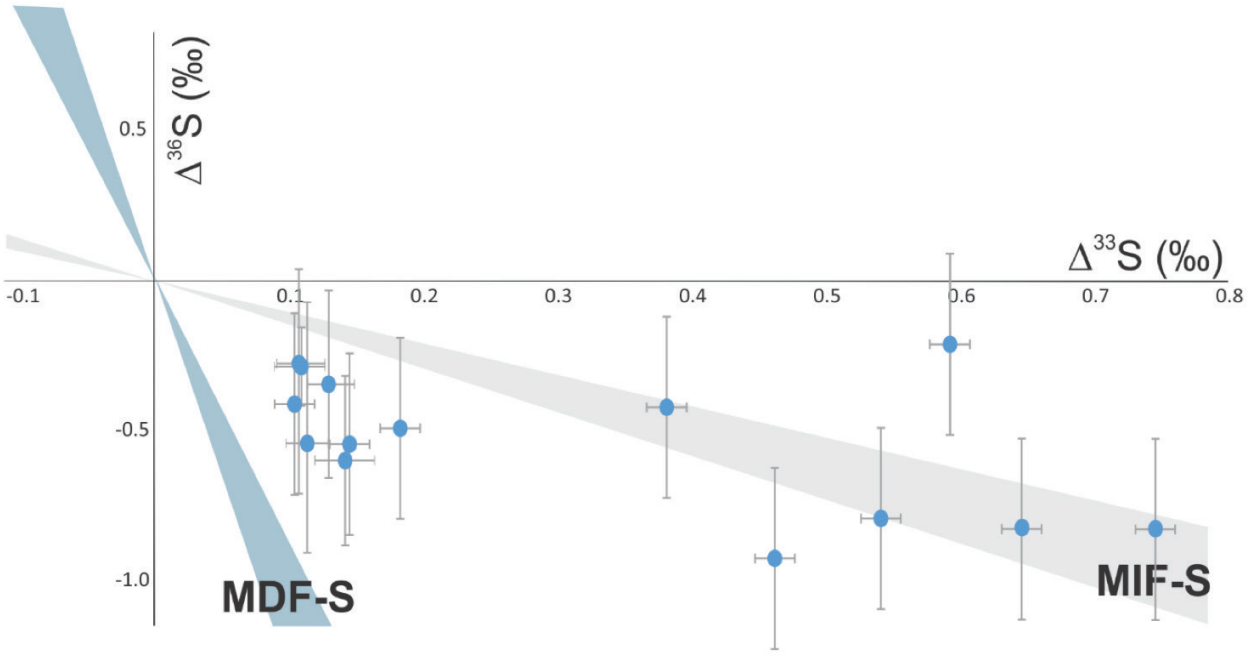

Figure 2. $\Delta^{33}S/\Delta^{36}S$ diagram for samples containing a $\Delta^{33}S$ anomaly (>0.1‰). Samples yield a $\Delta^{33}S$-$\Delta^{36}6S$ array with a slope of -1, typical of primary Archean sedimentary sulfur

Is the Ammassalik Intrusive Complex (South East Greenland) part of an ancient Ni-Cu magmatic province?

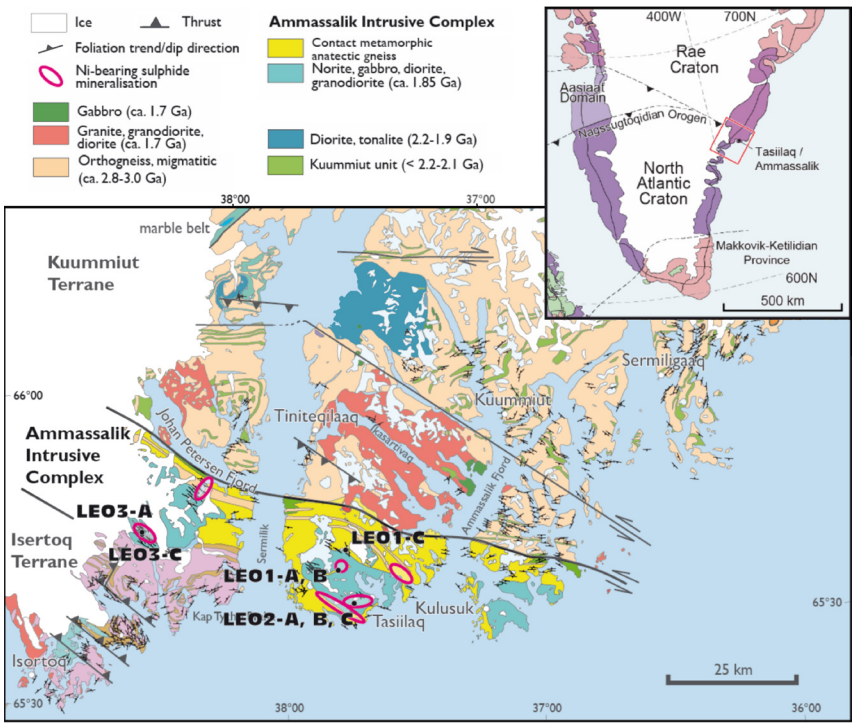

Figure 1. Detailed geology map of the Ammassalik Intrusive Complex. Geochronological samples are highlighted in black. Modified from Kolb (2014), Árting (2016) and Johannesen (2016).

The Paleoproterozoic Ammassalik Intrusive Complex formed during the Nagssugtoqidian orogeny, at the juncture of two Archean cratons, the Rae to the north, and the North Atlantic craton to the south (Fig. 1). The Ammassalik Intrusive Complex can be separated into three smaller complexes: the Johan Petersen, Tasiilaq and Kulusuk Intrusive Complexes, hosted in a ca ≤1990 Ma anatectic Bt-Gt paragneiss. The Ammassalik Intrusive Complex is interpreted to have been emplaced either as a dyke, later boudinaged, or as a series of pipes, at mid- to lower-crustal levels (granulite facies) in two successive pulses between ca 1915 and 1865 Ma.

Both the igneous rocks and the hosting Bt-Gt paragneiss show typical calc-alkaline and continental-arc signatures, including negative Ta, Nb and Ti anomalies. In addition, the fractionation of the MREE to HREE observed in the igneous samples, but not in the paragneiss, is consistent with a deep Gt-rich source. The igneous rocks of the Ammassalik Intrusive Complex can be sourced from partial melting of a Gt-lherzolite mantle, an eclogitic lithospheric mantle-wedge, or an eclogitic lower crust. However, each of these sources should have very different isotopic signatures.

Isotopic work on the igneous rocks of the Ammassalik Intrusive Complex suggests a mixture of sources. These sources represent mantle-derived magmas (from either the Gt-lherzolite mantle, or the lithospheric mantle-wedge) that assimilated and/or partially melted Paleoproterozoic to Archean supracrustal material on their way up through the mid- to lower crust. The host Bt-Gt paragneiss may have contributed to this supracrustal input and may be the source of the calc-alkaline and continental-arc geochemical signature of the igneous rocks. In detail, isotopic data (Fig. 2) show CHUR-like εHf values decreasing with time to around -10, interpreted to represent mixing of melts

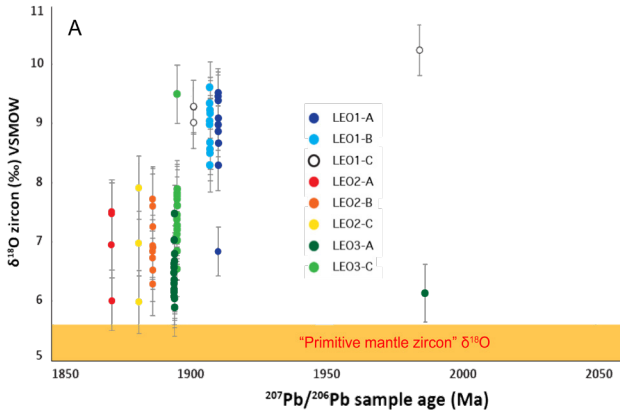

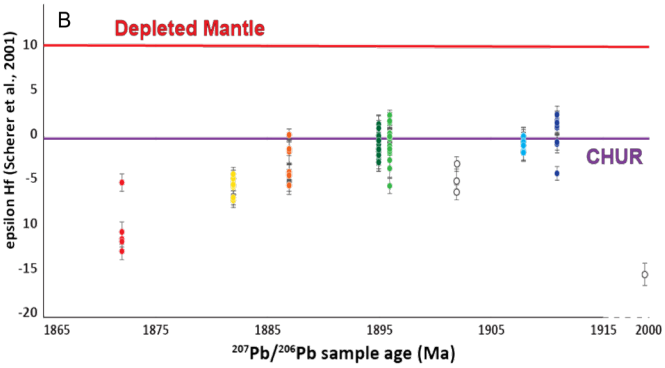

Figure 2. A) Diagram of the δ18O values for the igneous rocks from the Ammassalik Intrusive Complex, and Bt-Gt paragneiss. Primitive mantle zircon range from Valley et al. (2005). B) Lu-Hf data. CHUR: chondritic uniform reservoir.

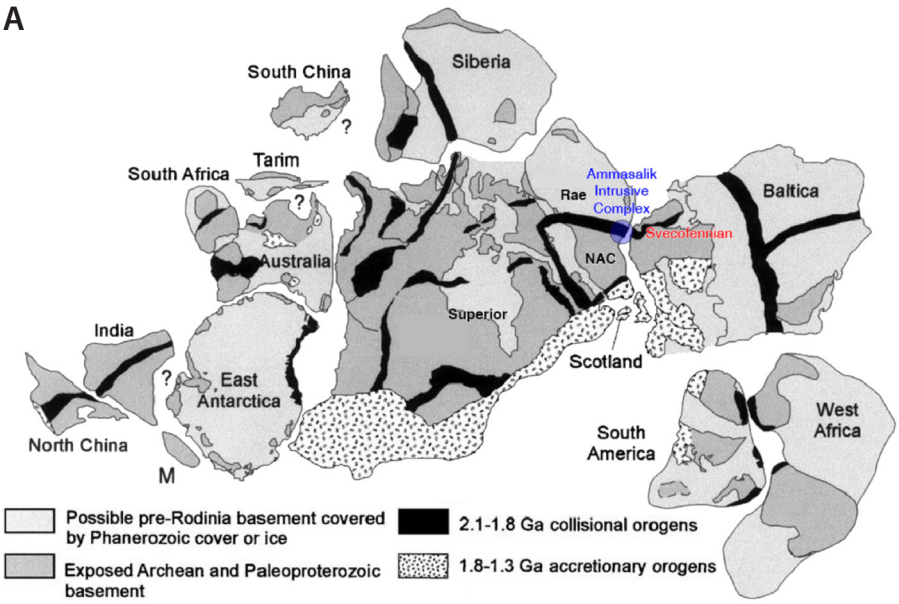

Figure 3. Reconstruction of A) the Columbia supercontinent showing the paleo-continuity between the Svecofennian Province and the Ammassalik region of south-eastern Greenland. Modified from Zhao et al. (2004). B) craton margins (modified from Bleeker, 2003) and associated Ni deposits highlighting the well-endowed Svecofennian Province and Kotalahti Ni belt and the link with south-eastern Greenland. Modified from Maier and Groves (2011).

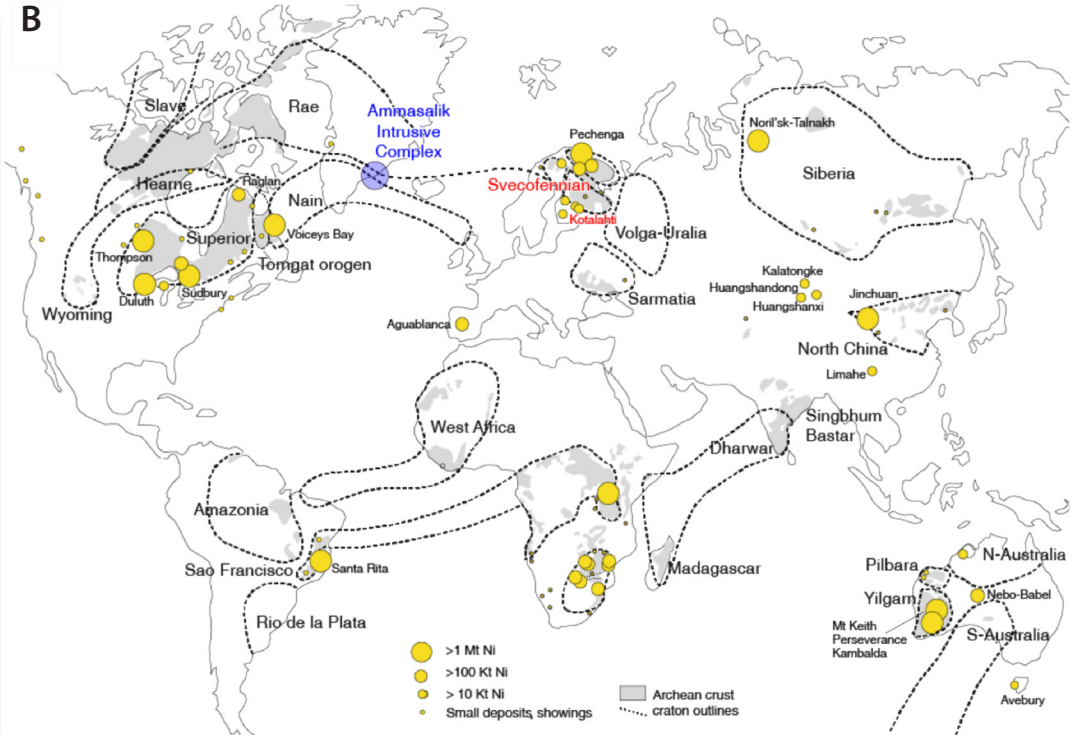

from a deep Gt-rich mantle with increasing partial melting and/or assimilation of Precambrian to Archean supracrustal material through time (T^{C}_{DM} for igneous rocks bracketed between 2320 and 3280 Ma). This mantle-crust mixing is further supported by bimodal supracrustal $\delta^{18}O$ values around 7 and 9‰, above the *'primitive mantle zircon'* range. The bimodal distribution may indicate a change through time in the type of supracrustal material involved. The isotopic composition of anatectic zircons in the Bt-Gt paragneiss also suggest that the Bt-Gt paragneiss was part of the supracrustal contribution.

The age bracket on the magmatism, between *ca* 1915 and 1865 Ma, overlaps with that of magmatism linked to the assembly of the Columbia supercontinent. This process was marked by the formation of numerous world-class Ni-Cu deposits around the world, some intrusive-hosted. Based on the age overlap and the paleoreconstruction of the supercontinent around 1.9 Ga, we interpret the Ammasalik Intrusive Complex and the south-eastern Greenland region as a direct continuation of the Svecofennian Province and the well Ni-endowed Kotalahti belt, along a circum-Rae magmatic province (Fig. 3). This conclusion highlights the high prospectivity of the south-eastern Greenland region for world-class intrusion-hosted Ni-sulfide deposits.

This project is part of CCFS Theme 2, Earth's Evolution, and contributes to understanding Earth's Architecture and Fluid Fluxes.

Contacts: Erwann Lebrun, Marco Fiorentini
Funded by: CCFS Flagship Program 2

Volcanic debris from up to 60 km beneath western Victoria tracks tectonic ups and downs

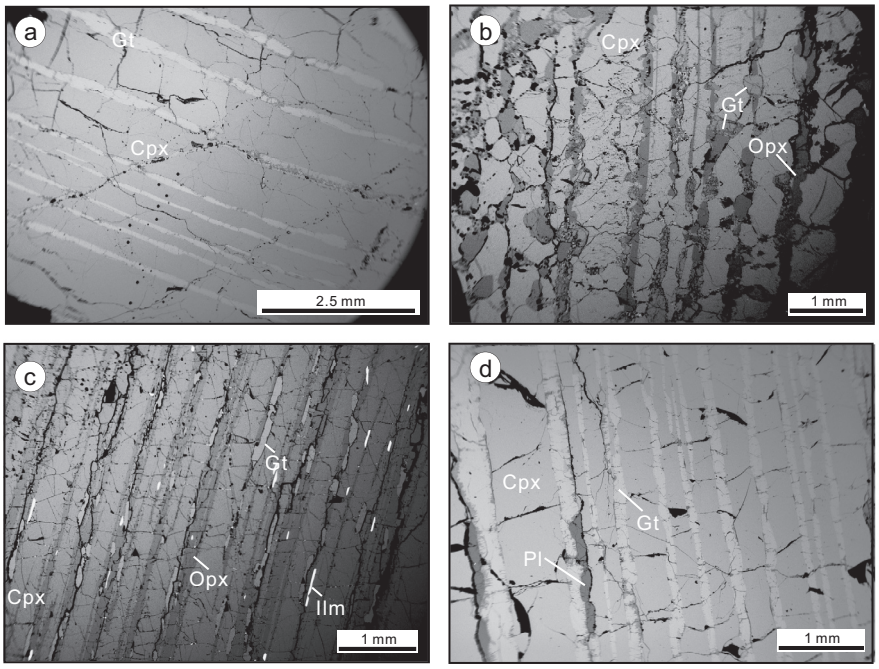

Figure 1. Backscattered electron (BSE) photomicrographs of clinopyroxene megacrysts with exsolution lamellae of garnet (Gt), orthopyroxene (Opx), ilmenite (Ilm) and plagioclase (Pl).

Subduction can draw surface, near-surface and shallow mantle materials (including volatiles) into the mantle and result in mantle/fluid interactions. The process plays a key role in cycling of volatiles and other elements and affects the composition and nature of Earth's deep interior. Pyroxenite xenoliths from ~30-60 km below the surface, provide a key tool to track these deep processes. The basanite tuffs of Bullenmerri and Gnotuk maars, southeast Australia, contain abundant garnet-bearing pyroxenite xenoliths. New petrographic, geochemical and isotopic investigations on these xenoliths reveal a picture of subduction-related magmatism at mantle depths.

Microstructural evidence of the exsolution of garnet (± orthopyroxene ± spinel ± plagioclase ± ilmenite) from complex clinopyroxene megacrysts suggest that all garnet pyroxenite xenoliths originally were clinopyroxene-dominant cumulates, modified by exsolution and recrystallisation during cooling to the ambient geotherm (Fig. 1). They can be divided into two types: Type I high-MgO garnet websterites, and Type II low-MgO garnet clinopyroxenites. The high-MgO garnet websterites have high Cr and low Al contents in both whole rock and clinopyroxene, relatively flat LREE patterns and homogeneous Sr-Nd-Hf isotopic compositions ($^{87}Sr/^{86}Sr$=0.70386-0.70657; $^{143}Nd/^{144}Nd$=0.51260-0.51283; $^{176}Hf/^{177}Hf$=0.28281-0.28305). These data suggest that they represent high-pressure cumulates from arc-related tholeiites, produced in the initial stages of partial melting of a mantle wedge due to slab dehydration. Conventional thermobarometry and thermodynamic modeling on the reconstructed clinopyroxene indicate that the primary clinopyroxenites crystallised at ~1420-1460 °C and 23-30 kb and finally equilibrated at ~982-1094°C and 14-17 kb.

Low-MgO clinopyroxenites have low Cr contents and variable REE patterns from LREE-depleted to LREE-enriched in the whole rock and clinopyroxene. They also show heterogeneous Sr-Nd-Hf isotopic compositions ($^{87}Sr/^{86}Sr$=0.70374-0.71548; $^{143}Nd/^{144}Nd$=0.51221-0.51355; $^{176}Hf/^{177}Hf$=0.28274-0.28396) in clinopyroxene but uncontaminated upper-mantle δ^{18}OV-SMOW in garnet (4.9-5.2 ‰), indicating that low-MgO pyroxenites may represent high pressure cumulates from an evolved magma derived from partial melting of hydrothermally altered oceanic crust with the addition of subducted sediments from the Paleozoic Lachlan orogenic belt. P-T calculations suggest that they crystallised at 1280-1400°C and 16-20 kb and finally equilibrated at 950-1050 °C and 12-17 kb.

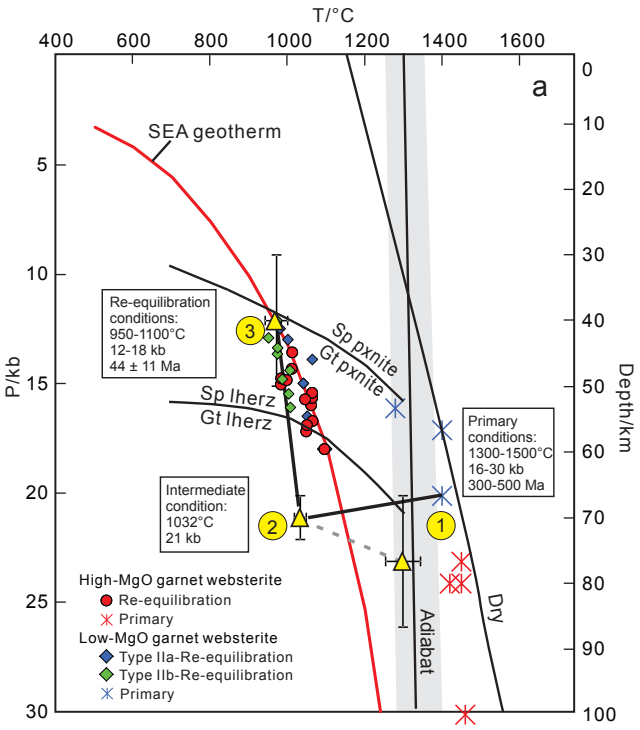

Figure 2. P-T-t path for the garnet pyroxenites from Lakes Bullenmerri and Gnotuk.

The preservation of fractionated trace-element patterns in multiple generations of garnet lamellae and their surrounding clinopyroxene indicates a decompresssional cooling path (1032 °C and 21 kb) before the xenoliths were entrained by the host basanite (Fig. 2).

These results imply that the protoliths of the garnet pyroxenite formed at a range of depths from ~50-100 km; back-calculation of the isotopic data suggests this primary crystallisation occurred about 300-500 m.y. ago. During, or shortly after cooling, they were tectonically uplifted to higher levels (~40-60 km; i.e. uplifted by at least 10~20 km) in Paleogene time (44 ± 11 Ma; Sm-Nd isochrons); this was accompanied by rifting associated with crustal inflation and thinning in southeast Australia.

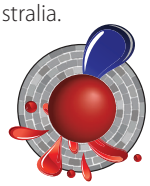

This project is part of CCFS Theme 2, Earth's Evolution, and contributes to understanding Earth's Architecture and Fluid Fluxes.

Contacts: Jianggu Lu, Bill Griffin, Sue O'Reilly, Qing Xiong, Jin-Xiang Huang, Norman Pearson, Jianping Zheng (China University of Geosciences, Wuhan)

Funded by: CCFS Flagship Program 1, IMQRES scholarships

Earth's magnetic switch activated in the deepest mantle

Earth scientists use paleomagnetism to establish a paleogeographic framework for continental blocks through Earth's history. Rapid changes in the geomagnetic field also provide critical information about Earth's long-term evolution and dynamics. In particular, dynamic activity at the core-mantle boundary impact on the behaviour of the geomagnetic field by changing the rate and geometry of the heat flux field. For instance, the lower mantle impacts on the geomagnetic reversal rate. It has also been suggested that heterogeneity in heat flux causes specific patterns of transitional paleomagnetic poles (or virtual geomagnetic poles - VGPs) during the reversal of the geomagnetic polarity. For example, transitional poles may be arranged on the rims of the large low shear velocity provinces (LLSVPs) near the core-mantle boundary. If proven, this relationship potentially can provide important constraints on the stability of LLSVPs over time, which has a direct influence on the concept of the supercontinent cycle.

In this study we investigated a sedimentary sequence from Armenia, where the two geomagnetic field reversals bounding the youngest normal-polarity subchron (the so called Jaramillo subchron with an age between 0.988 and 1.072 Ma), prior to the current Brunhes normal-polarity chron, have been recorded. The paleomagnetic signal in the sediments is of very high quality and, because these lake deposits accumulated very rapidly (~30 cm/ka), it was possible to study the field reversals over a thickness of ~2 m. We obtained standard, 1 inch diameter, paleomagnetic samples at intervals of less than 10 cm. Based on the paleomagnetic results we calculated, at each sample level, a geomagnetic pole assuming a dipole-dominated geomagnetic field (therefore virtual geomagnetic poles). Plotting these poles allowed us to investigate the appearance of the geomagnetic field during a polarity transition (or field reversal).

The obtained virtual geomagnetic pole (VGP) path indicates an oscillatory transitional field behaviour with four abrupt transequatorial precursory jumps across the Pacific (Fig. 1). The two records are strikingly similar to another high-quality paleomagnetic record (green points in

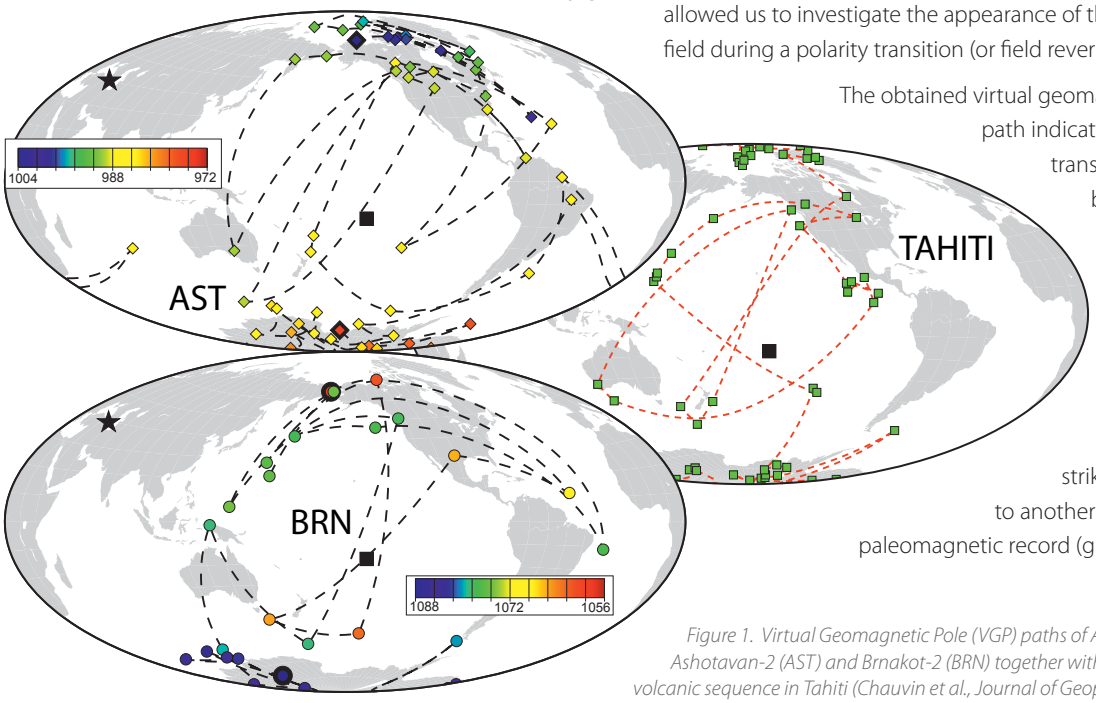

Figure 1. Virtual Geomagnetic Pole (VGP) paths of Armenian sections Ashotavan-2 (AST) and Brnakot-2 (BRN) together with the VGP path of volcanic sequence in Tahiti (Chauvin et al., Journal of Geophysical Research, 95, 1990). VGPs are colour coded with the inferred age in ka. Black star (square) indicates the location of the reversal records of this study (Tahiti).

Fig. 1), which is based on a volcanic sequence from Tahiti. The distribution of VGP positions of these three records clearly indicate regions of preferred occurrence (Fig. 2). Our results are in agreement with previously proposed bands of transitional VGP over the Americas and Australia/northwest Pacific zone, almost exclusively over the girdle of mantle downwelling between the two large provinces of low shear velocity (LLSVPs; Fig. 2).

Our observations imply a thermally stable zone within the outer core and below the LLSVPs, which persists throughout the polarity transition. This zone can generate a secondary radial dipole, which repels the transitional VGPs directly above this zone. As long as the LLSVPs are in place, all polarity transitions should look similar, as observed for the youngest polarity transitions.

Our work further demonstrates that there is an obvious link between the geometries of paleomagnetic reversals and lower-mantle structures. In future studies we may use this as a basis for investigating the temporal evolution of the lower mantle after identifying high-quality reversal records from older sequences. We show that with only three high quality records and a robust statistical analysis we can visualise an antipodal structure at the CMB. Such work will help us to evaluate how stable these features at the CMB actually are.

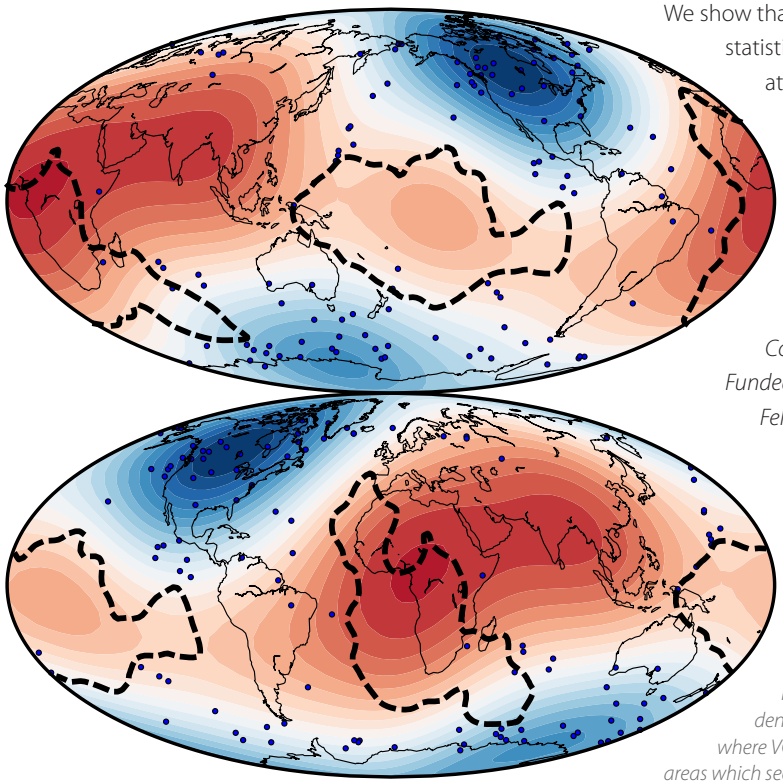

This project is part of CCFS Theme 2, Earth's Evolution, and contributes to understanding Earth's Architecture and Fluid Fluxes.

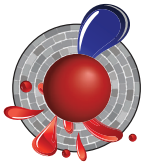

Contacts: Uwe Kirscher, Valerian Bachtadse
Funded by: CCFS Flagship Program 5, ARC Laureate Fellowship (FL150100133), DFG grant (Ba1210/14-1)

Figure 2. Stereographic projection of calculated VGPs of all studied samples (blue points) together with VGPs of a record from Tahiti (s.a.). Present day LLSVPs at the core-mantle boundary are outlines by black dotted lines. The reddish to bluish colour corresponds to a Gaussian kernel density estimate of the VGPs. Dark blue colours represent areas where VGPs are most likely to be found, while red colours represent areas which seem to be avoided by VPGs.

Sulfur isotopes reveal the evolution of mineralised Komatiites

Komatiites are ancient submarine lavas erupted over 2.5 billion years ago. Their ultramafic chemical compositions and the exceptionally high temperatures (~1600 ºC) of the lavas allowed them to form spectacular channelised lava flows that find present-day analogues in the Kilauea lava fields of Hawaii. Their high temperature and low viscosity let komatiites lavas flow turbulently and to mechanically and thermally erode and assimilate crustal substrates along their path.

Komatiites are economically important because they can host massive sulfide mineralisation enriched in Ni, Cu and platinum-group elements (PGE). Indeed, komatiite-hosted Ni-Cu-PGE deposits from the Yilgarn Craton, Western Australia, account for ca 20% of global Ni-sulfide resources. Current models suggest that the assimilation of crustal sulfur-rich material by komatiite-lava erosion was necessary for sulfide supersaturation and deposition of these deposits.

This study combined mineralogical and sulfur-isotope variations to evaluate magmatic processes involved in the evolution of the ore-bearing sequence at Wannaway (Eastern Goldfields). It also provides a perspective on the potential influence of such processes on the composition of the Archean atmosphere.

The mineralised successions comprise basal sufide-rich black shales overlain by komatiite-hosted sulfides manifested by gradual transitions from massive to matrix-textured and disseminated ores (Fig. 1). We analysed the S-isotope composition of samples taken at regular distances through the mineralised sequence and then correlated sulfur mass-dependent fractionation (MDF-S) signatures with recently

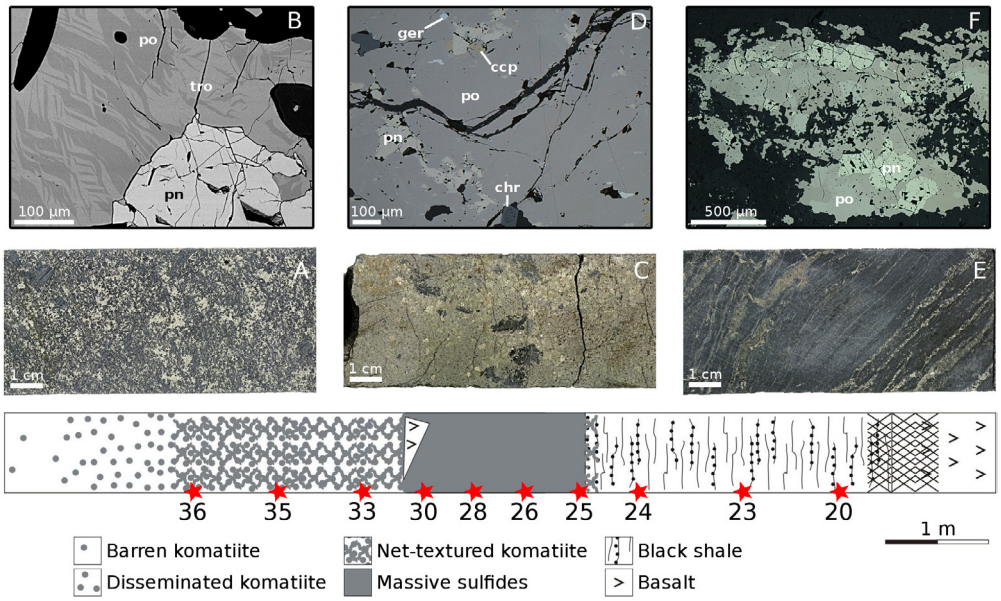

Figure 1. Scheme of the studied drillcore from the Wannaway Ni-Cu-PGE deposit, Western Australia. A) Drillcore section of net-textured komatiite; (B) BSE micro-image of net-textured sulfides; (C) Drillcore section of magmatic massive sulfides; (D) Optical reflected-light micro-image of massive sulfides; (E) Drillcore section of basal black shale; (F) Optical reflected-light micro-image of sedimentary sulfides.

discovered mass-independent fractionation (MIF-S) signatures to better constrain the effect of subsequent fractionation. The magmatic sulfides show a distinct positive MIF-S signature which indicates the assimilation of crustal material. The isotopic signatures of the sulfides are analogous to the sediments directly underlying the komatiite flows, suggesting that the assimilation occurred *in situ*. The data suggest that over 1/3 of the total sulfur in the deposit was assimilated from the country rocks.

In addition, the magmatic sulfides display a wide range in MDF-S signatures that gradually become lighter from the basal massive sulfides upwards. This isotopic drift is followed by the appearance of troilite (FeS) and a gradual decrease of pyrrhotite ($Fe_{1-x}S$) proportions. At stratigraphic levels where troilite becomes dominant, alabandite (MnS) appears; this is an unusual phase commonly related to strongly anoxic sedimentary environments and observed in meteorites. We argue that the combined upwards decrease in heavy sulfur isotopes along with the stability of troilite and alabandite is a consequence of magmatic devolatilisation and the release of SO_2-rich gasses during emplacement. The release of SO_2 would have stripped '*heavy*' sulfur from the komatiite magma, and caused local decreases in oxygen fugacity. This phenomenon, which is widely observed in present-day lava eruptions, has never been reported for Archean komatiites. This finding is particularly relevant to understanding the genesis and localisation of nickel sulfide systems with respect to the geodynamic setting of komatiite magmatism and associated sulfur degassing. A more detailed understanding of SO_2 devolatilisation processes during komatiite magmatism will shed new light on the processes that led to the oxygenation of early Earth's atmosphere.

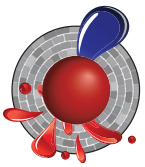

This project is part of CCFS Theme 1, Early Earth, and contributes to understanding Earth's Architecture and Fluid Fluxes.

Contacts: Stefano Caruso, Marco Fiorentini, Laure Martin

Funded by: GSWA, the Minerals Research Institute of Western Australia, UWA Scholarship for International Research Fees

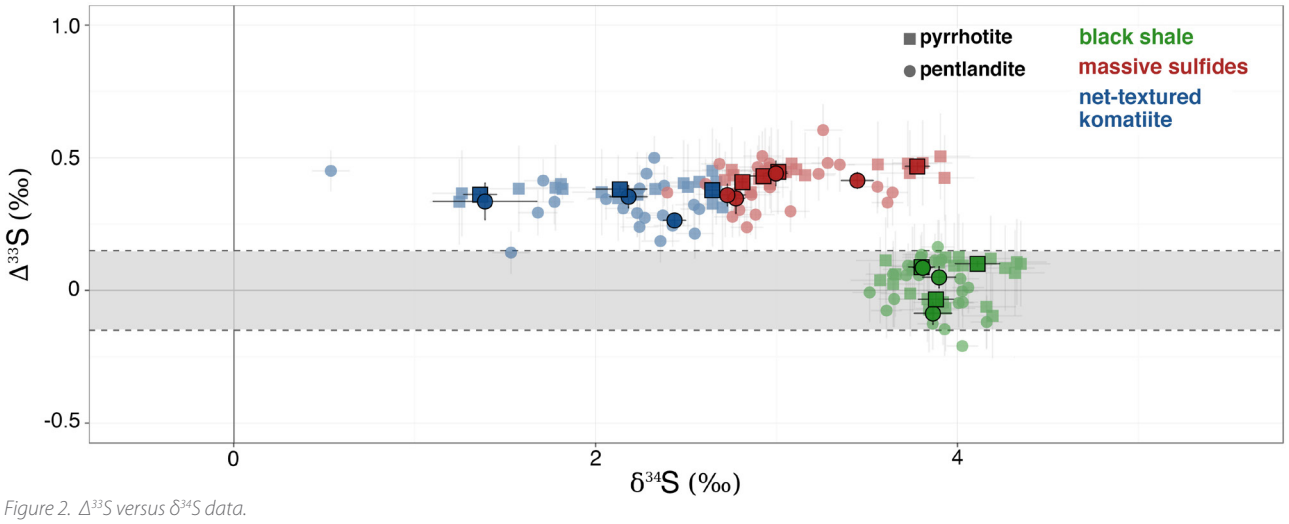

Figure 2. $\Delta^{33}S$ versus $\delta^{34}S$ data.

Ancient boron-rich, Himalayan cauldron - the soup for early life?

Figure 1. Luke Steller sampling active hot springs of the Puga Valley, India.

Darwin suggested that life may have started in "*…some warm little pond…*". What better place than hot springs, which today are known to host diverse microbial life, including not only phototrophic cyanobacteria, but also some of life's most primitive forms, chemotrophic archea. But can hot springs provide the right environments and critical elements for life to have originated there?

One of the key elements in prebiotic chemistry is Boron, which is a key catalyst in the polymerisation of organic molecules - i.e. the process that makes organic (carbon-bearing) molecules more complex. Boron is present in seawater in very dilute concentrations, but the problem with a marine environment for the origin of life is that there is no readily obvious mechanism for concentrating elements such as Boron and because many complex organic molecules cannot form just in the presence of water - they need the energy from wet-dry cycles to form. And so, hot springs!

Boron has been found in high concentrations in some hot springs, perhaps most notably from the Puga Valley of India, in the mountains of the Himalaya. Excitingly, Boron has recently been found concentrated in hot spring deposits 3.5 billion years old, intimately associated with some of the oldest evidence of life on Earth.

In July, UNSW Honours student Luke Steller, funded by CCFS Flagship Program 4, participated in a Spaceward Bound trip to the Puga Valley to collect samples of boron-bearing hot spring deposits (boratic sinter, muds and hot spring fluids) for compositional and boron isotopic analyses at the Pheasant Memorial Laboratory of Okayama University in Misasa, Japan. The aim was to compare the isotopic composition of boron in the active boratic hotspring deposits with that of 3.5 billion-year-old deposits. To our delight, the boron-isotope results from Puga Valley hot spring fluids were exactly the same as those from the ancient deposits, at -13‰, whereas muds and silicic crusts were fractionated to much more negative values.

These results support our recent observations (see *Research highlight p. 224*) that the 3.5 billion-year-old stromatolites flourished in a boron-rich hot spring environment. They also lend support to models of the origin of life in hot springs, as not only Boron, but other critical elements for prebiotic chemistry (P, C, H, Zn, O, S) have been found concentrated in these ancient rocks.

This project is part of CCFS Theme 1, Early Earth, and contributes to understanding Fluid Fluxes.

Contacts: Martin Van Kranendonk, Luke Steller
Funded by: CCFS Flagship Program 4

Zircon trace elements reveal oxidation signatures in ancient mantle

A major problem in understanding magmatic processes in the modern Earth and its evolution since planetary accretion is evaluation of the oxidation states of magmas and their source regions. In this study, we thermodynamically and empirically calibrate a novel method for determining magmatic oxygen fugacity (fO_2) in calc-alkalic, tholeiitic, adakitic and shoshonitic, metaluminous to moderately peraluminous and peralkaline melts as igneous zircon crystallised, to a precision of ±0.5 log unit fO_2, using only the easily measureable, redox-sensitive ratios Ce/U and U/Ti in zircon (nominally $ZrSiO_4$), without explicitly considering the ionic charge of Ce, U, or Ti, and without explicitly considering crystallisation temperature or pressure or silicate-melt composition (Fig. 1). Thermodynamic and empirical constraints indicate that our formulation is insensitive to variation of crystallisation temperature and pressure at lithospheric conditions. We use this new magmatic oxybarometer to illuminate the Hadean '*dark ages*' (4.0-4.6 Ga), for which detrital zircons are the only surviving witnesses of the period during which the Earth's proto-continental lithosphere developed.

We identify the oxidation states of magmas that produced Hadean and Eoarchean zircons in the Yilgarn, South China, Slave and Wyoming cratons (Fig. 2). Zircons in the 4375-3800 Ma age range from the Yilgarn Craton cluster in the fO_2 range of modern mid-ocean-ridge magmas, as do also most 3858-3200 Ma detrital

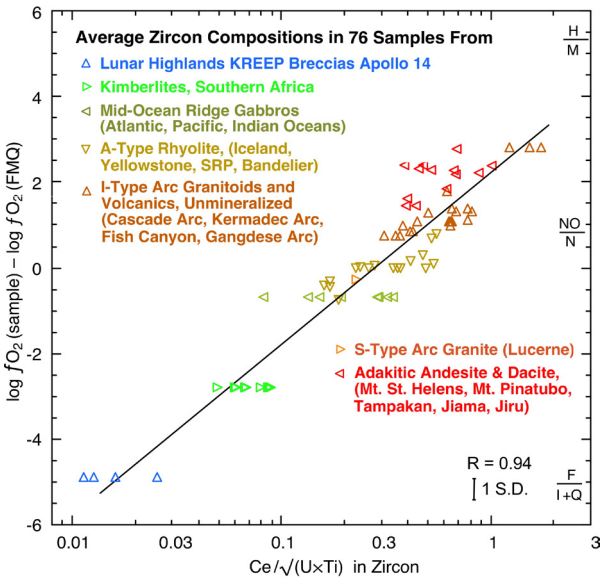

Figure 1. The average value of the parameter Ce/√(U×Ti) for the analysed zircon population in each rock sample is plotted against relative oxygen fugacity of the parent magma, as provided by independent constraints. The least-squares fit to the data (solid line) is ΔFMQ = 2.272 + 3.997 × log [Ce/√(U×Ti)], with a correlation coefficient R = 0.941 and a standard deviation of 0.495 log unit fO_2. 'SRP' denotes Snake River Plain, Idaho. Lucerne granite is in Maine, USA. Bandelier Tuff is in the Rio Grande Rift, New Mexico (USA).

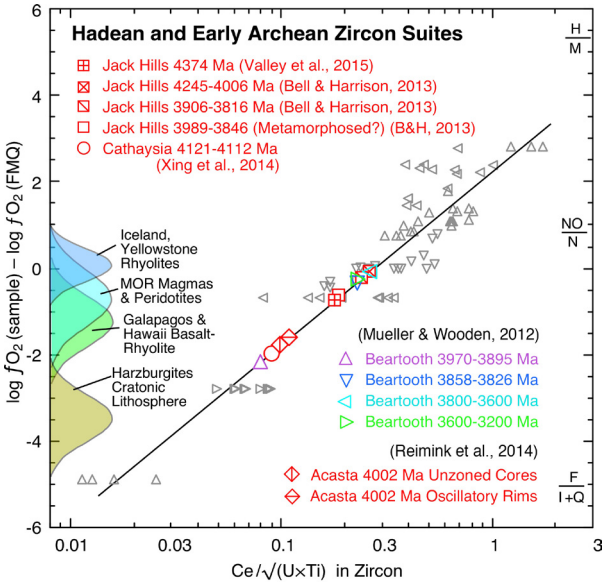

Figure 2. Average values of the parameter Ce/√(U×Ti) in suites of Hadean (4560-4000 Ma), Eoarchean (4000-3600 Ma), and Paleoarchean (3600-3200 Ma) zircons are plotted on the fO_2 calibration line and dataset from Figure 2 in order to infer oxidation states of the parental magmas. Hadean and early Archean zircons are binned by locality and by age subgroups, within which each population is relatively homogeneous. The Jack Hills locality is in the Yilgarn craton, Western Australia; the Cathaysia block is in the South China composite craton; the Acasta gneiss complex is in the Slave craton, Canada; the Beartooth Mountains are in the Wyoming craton, USA. Grey symbols are reproduced from Figure 1 for ease of reference to mid-ocean-ridge and mantle-plume-related suites. Colored curves at left represent Gaussian frequency distributions of magmatic oxidation states in various tectonic settings, based on log fO_2 data for mid-ocean ridge igneous suites and oceanic abyssal peridotites summarised from the literature.

zircons in the Wyoming Craton. More reducing conditions, about 2 log units lower fO_2, are represented by 3970-3896 Ma zircons in the Wyoming Craton and all analysed Hadean igneous zircons (4121-4002 Ma) from the Cathaysia Block of the South China Craton and from the Acasta Gneiss Complex in the Slave Craton. These data indicate that the secular evolution of the oxidation state of our planet may have not been linear and globally homogeneous. Oxidised and reduced domains co-existed in the early stages of the Earth evolution. However, the presence of early reduced suites, such as the ones from the South China and Slave cratons, imply derivation of parental mafic magmas or of re-melted mafic protoliths from sub-continental lithospheric mantle domains strongly depleted in ferric iron by prior episodes of basaltic/komatiitic melt extraction. These data indicate that by 4 Ga there may have already been a localised build up of chemically refractory, buoyant harzburgitic lithospheric mantle keels that shielded the underside of proto-continental crust from ablative loss by asthenospheric mantle convection, thus creating the conditions for the long-lived preservations of cratons.

This project is part of CCFS Theme 1, Early Earth, and contributes to understanding Fluid Fluxes.

Contacts: Robert Loucks, Marco Fiorentini
Funded by: CCFS Flagship Program 2

Potassium-rich magmas from a phlogopite-free source

Potassium-rich lavas are generally assumed to be produced by melting of mantle rocks that contain phlogopite, which is the source of the potassium. In the Mediterranean region, trace-element and isotopic compositions indicate that continental crustal material must be involved in the generation of many potassium-rich lavas. Melting occurs here in young lithosphere

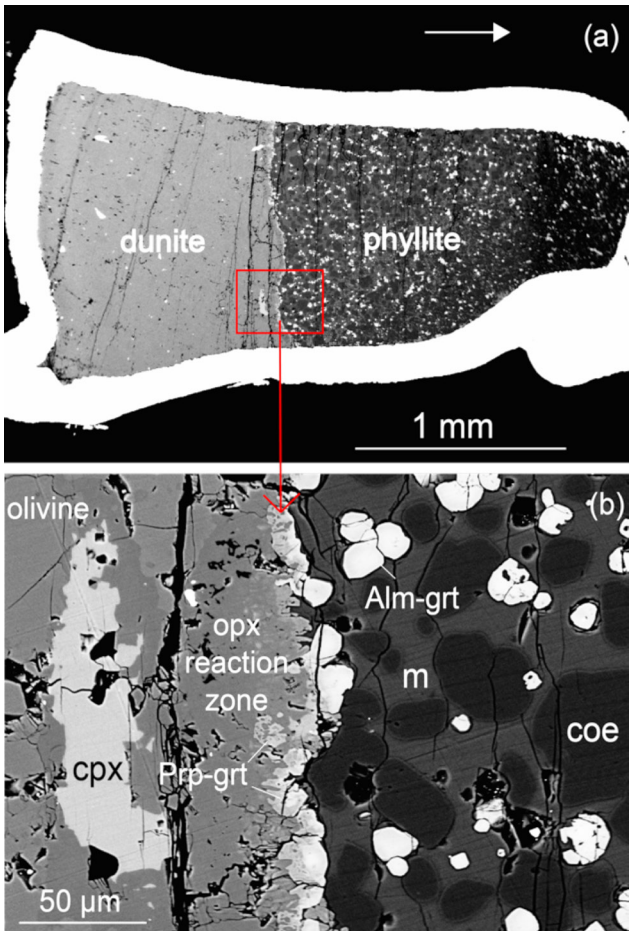

Figure 1. Representative back-scattered electron images of reaction run 139 (1000 °C, 3 GPa). Grt: garnet; Opx: orthopyroxene; Cpx: clinopyroxene; M: melt; Coe: coesite.

that was newly formed during the collision of small blocks and oceans, meaning that the continental crust was not stored for a long period of time in the mantle.

Few experimental studies have investigated the reaction between melts of continental crust and depleted peridotites, and so the reactions and the redistribution of trace elements during hybridisation and melting processes remains poorly constrained.

We have compared two types of experiments investigating the reaction between crust and mantle at depths of 60-100 km. In the first, continental crustal metasediment (phyllite) and depleted peridotite were juxtaposed as separate blocks, whereas in the second, the same rocks were ground together as a homogeneous powder. In the first series, a clear reaction zone dominated by orthopyroxene was formed but no hybridised melt could be analysed, whereas in the second series, analysable pools of hybridised melt were produced. Melt compositions from both experimental series show high abundances of Rb (100-220 ppm) and Ba (400-870 ppm), and consistent ratios of Nb/Ta (10-12), Zr/Hf (34-42) and Rb/Cs (28-34) similar to bulk continental crust.

The hybridisation process produces melts with $(Th/La)_N$ of ~2.5, higher than melts from the sedimentary rock alone (~1.7), accentuating the high Th/La already produced by other processes. High Th/La is a characteristic of potassium-rich lavas in these post-collisional environments. Melting of sedimentary rocks can strongly fractionate Sr from Nd, whereas hybridised melts show much less fractionation because of the diluting effect of the peridotite.

The trace-element patterns of hybridised melts produced in our experiments are remarkably similar to post-collisional K-rich volcanic rocks. Almost all trace elements exhibit almost identical arrays to the post-collisional K-rich volcanic rocks but with slightly lower concentrations, which is probably due

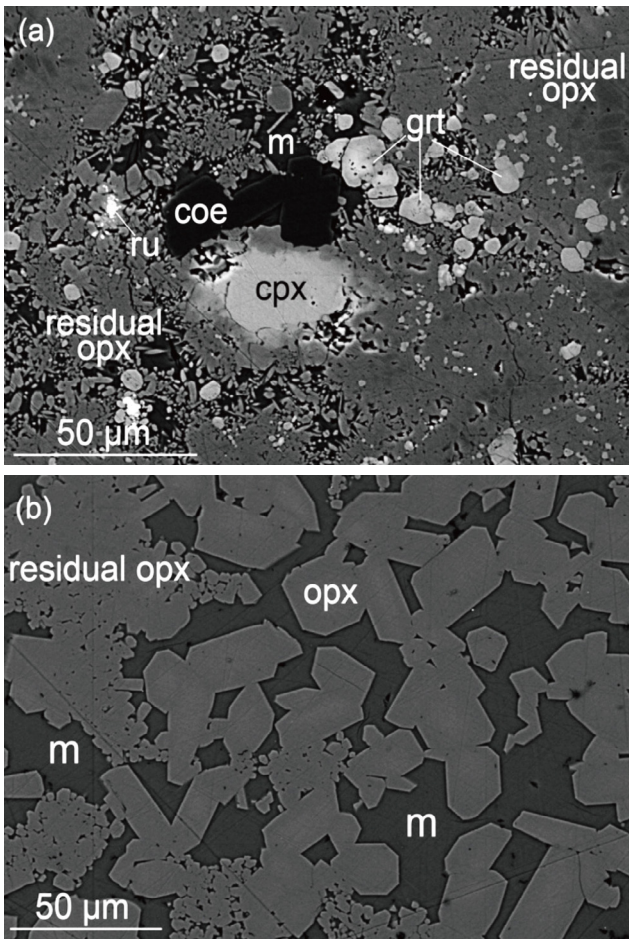

Figure 2. Representative back-scattered electron images of intimately mixed run products. Ru: rutile.

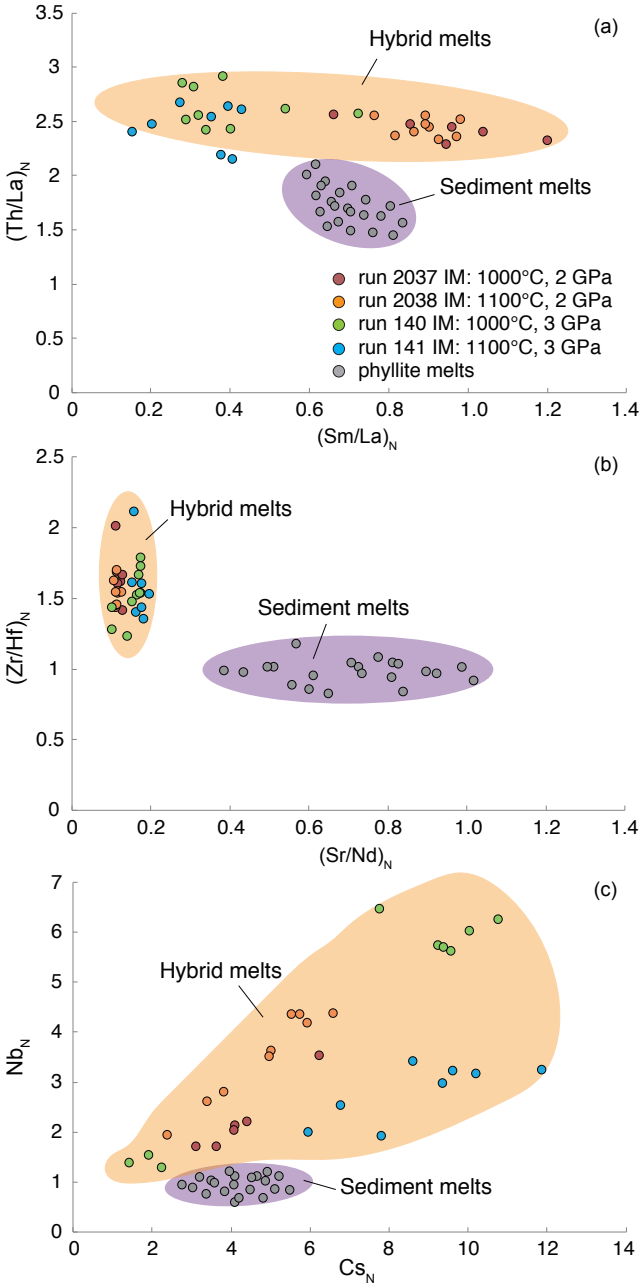

Figure 3. Variations of (a) $(Sm/La)_N$ versus $(Th/La)_N$; (b) $(Zr/Hf)_N$ versus $(Sr/Nd)_N$; (c) Cs_N (ppm) versus Nb_N (ppm) of the experimental melts. Subscript N denotes that the values have been normalised to their corresponding values in the starting materials in order to better reflect enrichment/depletion of key trace elements during melting in experimental runs. IM: intimately mixed runs.

to the higher sediment:peridotite mass ratio (1:1) used in the experiments.

A significant feature of our experimental results is the production of potassium-rich melts in the absence of residual K-rich minerals, which contrasts with most petrogenetic models that invoke phlogopite in the source of potassium-rich rocks. On the basis of previous experiments, phlogopite has been thought to form by interaction of melts with the mantle wedge due to slab-derived fluid/melt migration in the subduction zone.

Our study offers an alternative scenario that contradicts the widely held assumption that phlogopite is a required component in the source of potassium-rich magmas. Our experiments indicate that potassium may be exclusively incorporated in melts during hybridisation between sediment-derived melts and peridotite at shallow lithospheric depths.

The potassium content of these melts (~4-5% K_2O) is considerably enriched relative to that in the original phyllite (1.8 wt%) due to the breakdown of phengite in the phyllite, which is the only phase capable of providing a considerable amount of potassium to the whole-rock chemical inventory.

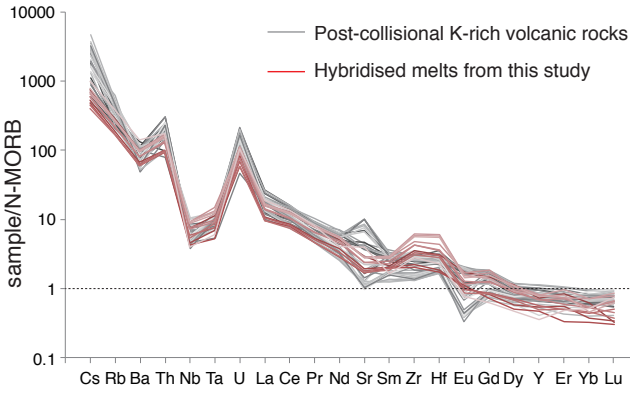

Figure 4. N-MORB normalised trace element compositions of hybridised melts in this study, compared to representative post-collisional K-rich volcanic rocks with K_2O of 3-5 wt%.

The strongly peraluminous (A/(CNK) > 1.25) composition of the hybrid melts may indicate that a phlogopite-free source is most likely for peraluminous K-rich volcanic rocks.

This project is part of CCFS Themes 2 and 3, Earth's Evolution and Earth Today, and contributes to understanding Earth's Architecture and Fluid Fluxes.

Contacts: Yu Wang, Stephen Foley, Dejan Prelević
Funded by: CCFS Flagship Program 3, iMQRES scholarships, EPS postgraduate funds, Deutsche Forschungsgemeinschaft (DFG)

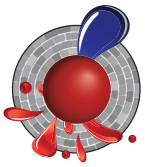

An increase in the complexity of life across Earth's Great Oxygenation Event

The Earth system fundamentally changed across the Archean-Proterozoic transition, not only the rate and mechanisms of crust formation, but also the composition of the atmosphere-hydrosphere. At about 2.4 Ga, the Great Oxygenation Event (or GOE), caused the irreversible oxygenation of Earth's atmosphere, producing a significant change in a variety of rock types and ore deposits. In addition, this first (but probably not last!), global pollution of the atmosphere by living organisms had a profound impact on life, resulting in the rise of eukaryotic life, with complex cell structures, and the adaptation of prokaryotic life (bacteria) to the new environmental conditions.

Perhaps the best (and only?) place to directly witness the adaptation of life across the GOE is in the Turee Creek Group of Western Australia. Here, a 350 m thick unit of stromatolitic shallow-water carbonate and microfossil-bearing deep-water black chert that was deposited in the immediate aftermath of the GOE contains a variety of evidence for a dramatic increase in the complexity of life. This includes a host of never-before described microfossils from a benthic, deep water, non-phototrophic, community. Previously documented forms are relatively large and filamentous, while the new microfossils include spherical aggregates of cells preserved in ultrafine-grained silica, and very fine filamentous forms that rim other microfossils and degraded organic material and appear to be organotrophs (organisms that harvest hydrogen or electrons from organic substrates).

In the shallow-water carbonate setting, stromatolites display a dramatic increase in morphological variation and complexity compared with any Archean example. This is the first appearance of complex branching forms, and the first occurrence of thick units of clot textured microbialites interbedded with stromatolites. This texture appears to have arisen when floating microbial communities suspended in the water column fell to the seafloor and were quickly cemented in place by coarse, radiating dolomite.

But perhaps the most exciting discovery is the small (up to 1 cm long), hollow, tube-like structures that surround finger-size columnar stromatolites in a unit 15 cm thick. The tube-like structures surround the stromatolites and are attached to them. They have thick, kerogen-rich rims, and hollow cores now filled by fine-grained silica (microquartz), carbonate, and an inner necklace of tiny framboids of highly fractionated ($\delta^{34}S = +22$ ‰) pyrite. These structures most closely resemble primitive calcareous sponges, although a eukaryotic origin has not been proven. Further work - funded by CCFS in 2017 - will investigate the kerogen in an attempt to document what may be the world's oldest eukaryote. See *CCFS publication #697 Barlow et al., Geobiology, 4, 317-343.*

This project is part of CCFS Theme 1, Early Earth, and contributes to understanding Fluid Fluxes.

Contacts: Erica Barlow, Georgia Soares, Brendan Nomchong, Martin Van Kranendonk
Funded by: CCFS Flagship Program 4

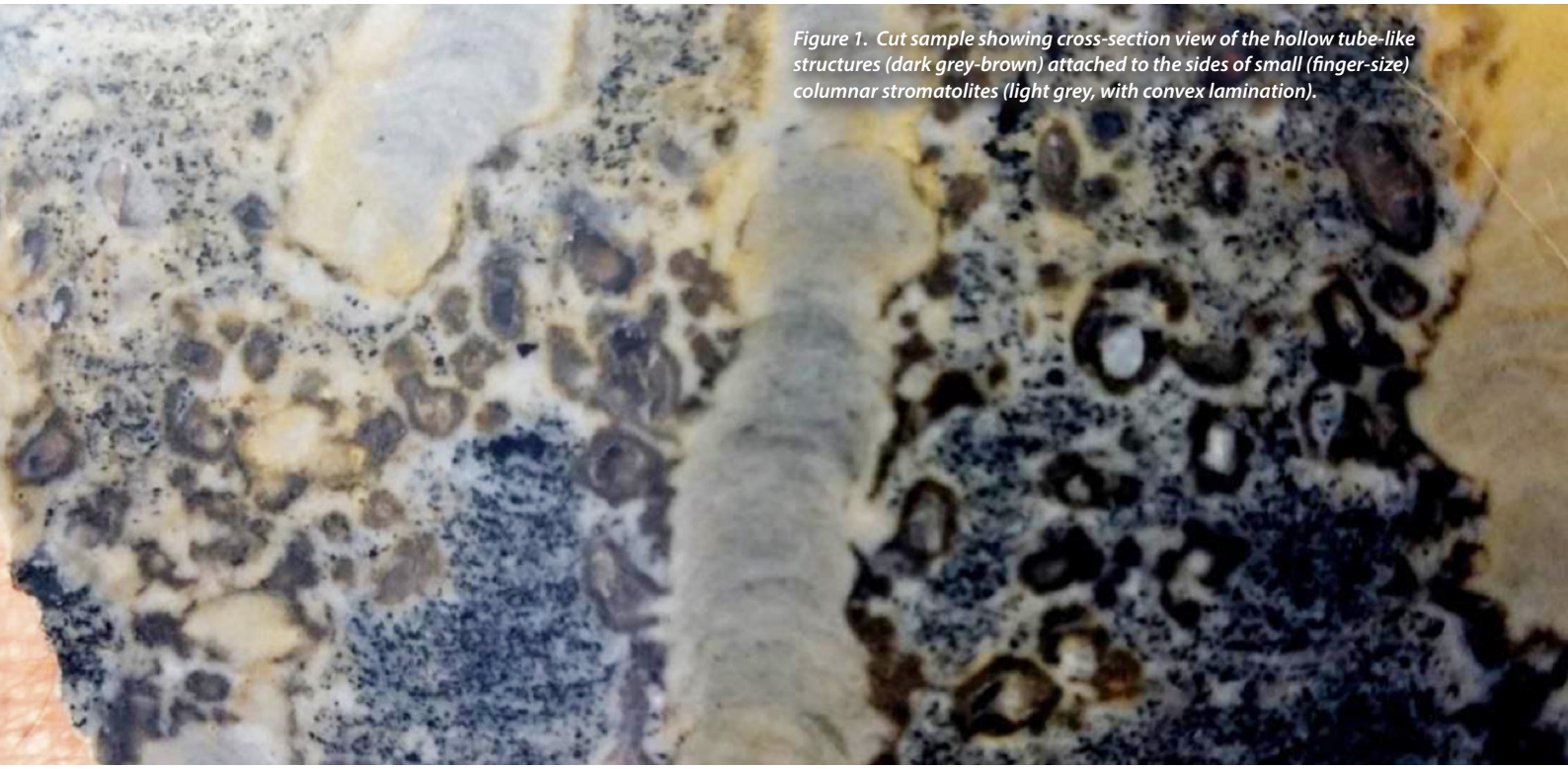

Figure 1. Cut sample showing cross-section view of the hollow tube-like structures (dark grey-brown) attached to the sides of small (finger-size) columnar stromatolites (light grey, with convex lamination).

What is the real S isotope composition of Earth's mantle?

Sulfur isotopes are a powerful geochemical tracer in high-temperature processes, but have rarely been applied to the study of the source and composition of fluids in the deep Earth. The only S-isotope data from the sub-continental lithospheric mantle (SCLM) for the mantle beneath cratons, the most ancient regions of Earth's continents, are from sulfide inclusions in diamonds. To provide new constraints on the S isotope composition of the SCLM and on the source(s) of mantle metasomatic fluids beneath the diamondiferous Kimberley region (South Africa), a research team led by ARC DECRA Fellow Andrea Giuliani and ARC Future Fellow Marco Fiorentini investigated the S isotope systematics of metasomatised (i.e. fluid-enriched) mantle xenoliths (i.e. fragments) transported to surface by the Bultfontein kimberlite (Kimberley, South Africa).

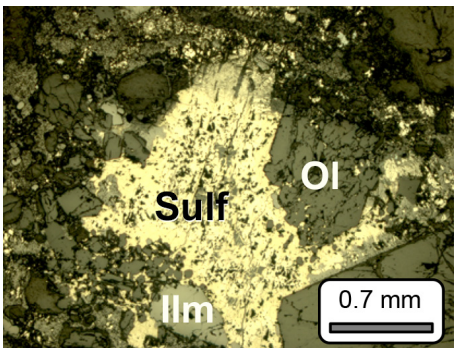

Figure 1. Photo-micrographs of sulfide aggregate in Bultfontein mantle xenolith.

Different types of sulfides (pentlandite and chalcopyrite) in these xenoliths were analysed by *in situ* secondary-ion mass spectrometry (SIMS), while bulk-rock material was analysed by gas source isotope ratio mass spectrometry techniques. Previous studies have shown that these xenoliths experienced different types of metasomatism at distinct times (~180 and ~90-80 Ma). Pentlandite grains are variably altered to heazlewoodite (Ni sulfide) + magnetite. The *in situ* S isotope analyses of pentlandite exhibit a relatively restricted range between -5.9 and -1.4‰ $\delta^{34}S$ (compared to VCDT), with no statistically meaningful differences between samples. Chalcopyrite only occurs in one sample and also shows $\delta^{34}S$ values between -5.4 and -1.0‰. The bulk-rock $S_{sulfide}$ isotope analyses vary between -3.4 and +0.8‰ $\delta^{34}S$. Importantly, the only sample hosting dominantly fresh sulfides shows a bulk-rock $\delta^{34}S$ value consistent with the mean value for the sulfides, whereas the other samples exhibit higher bulk $^{34}S/^{32}S$ ratios (i.e. higher $\delta^{34}S$ values). The differences between bulk-rock and average *in situ* $\delta^{34}S$ values are directly correlated with the degree of alteration of the sulfides. This indicates that the high $^{34}S/^{32}S$ ratios in the bulk samples are not due to the introduction of heavy S (commonly as sulfates)

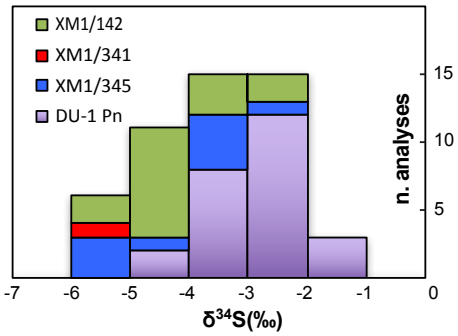

Figure 3. In situ sulfur isotope (‰ $\delta^{34}S$ relative to VCDT) analyses of pentlandite grains in Bultfontein mantle xenoliths. Different colors are used for each xenolith sample.

and are best explained by isotopic fractionation driven by the removal of light S during serpentinisation, when pentlandite is altered to S-poor mixtures of heazlewoodite and magnetite. Available bulk $S_{sulfide}$ isotopic data for SCLM peridotite xenoliths are dominated by positive $\delta^{34}S$ values, which contrasts with the negative values of the sulfides reported in this and previous studies. These results imply that the mantle S isotope values from bulk peridotite samples are commonly modified by isotopic fractionation during serpentinisation. Therefore, the S isotopic composition of the SCLM may require revision.

The limited isotopic variability shown by sulfides in the Bultfontein mantle xenoliths is probably due to intermittent tapping of fluids from a mantle source with a relatively restricted S isotope composition. While the asthenospheric mantle ($\delta^{34}S \leq$ -1.4‰; *Labidi et al., 2013 Nature, 501, 208-211*) is one candidate, $\delta^{34}S$ values as low as -5.9‰ suggest input from recycled crustal material in the mantle. This recycled material could be represented by the sulfur reservoir with negative $\delta^{34}S$ that is missing in the >500 Ma sedimentary record (*Canfield, 2004, American Journal of Science, 304: 839-861*), which was subducted and mixed with ambient material in the Earth's deep interiors. This study highlights the importance of S isotope geochemistry to trace the source of fluids in the mantle.

See *CCFS publication #789 Giuliani A., Fiorentini M.L., et al., Earth and Planetary Science Letters, 445, 114-124.*

This project is part of CCFS Theme 2, Earth's Evolution, and contributes to understanding Fluid Fluxes.

Contacts: Andrea Giuliani, Marco Fiorentini
Funded by: ARC DECRA, ARC Future Fellowship

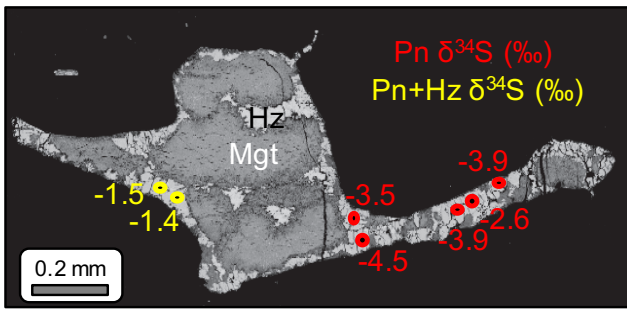

Figure 2. SEM-EDS image of sulfide grain in sample XM1/345 from Bultfontein showing $\delta^{34}S$ variations (as ‰ units) measured by SIMS. Values reported in yellow represent mixtures of pentlandite and heazlewoodite and are not considered quantitative because the instrumental fractionation factor for heazlewoodite is unknown. (Mgt: magnetite; Hz: heazlewoodite)

Zircon - a pathfinder for porphyry Cu ± Mo ± Au deposits

Porphyry Cu (±Mo ±Au) deposits supply nearly ~70% of the world's Cu, ~50% of its Mo, and ~25% of its Au. This type of mineral deposit mainly occurs in the circum-Pacific and Alpine-Himalayan mountain belts (Fig. 1). Discovery of new deposits is costly and challenging, and industry urgently needs tools for chemical fingerprinting or fertility assessment of potential exploration targets.

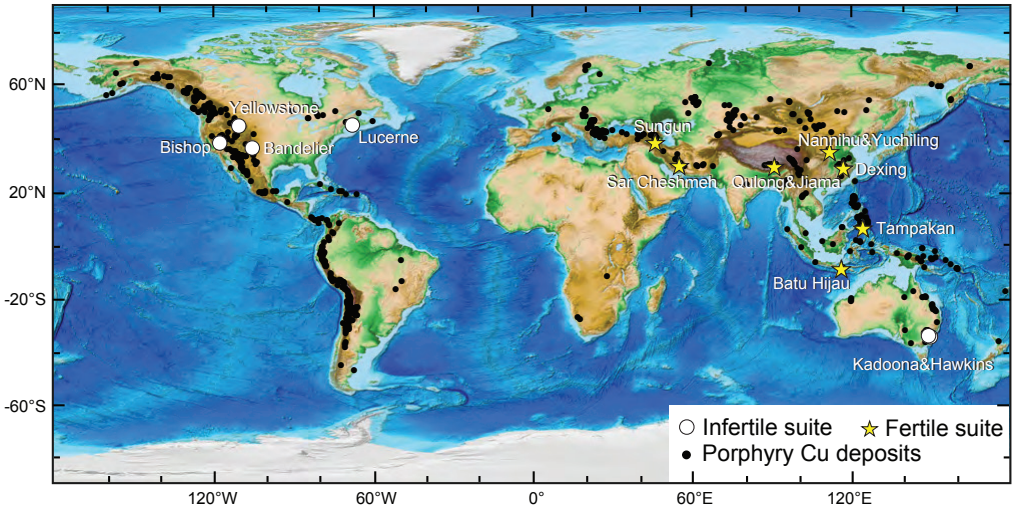

Figure 1. Map showing the worldwide distribution of porphyry Cu deposits, and the fertile and infertile magmatic suites investigated in this study.

Zircon ($ZrSiO_4$) is ubiquitous in Cu-ore-forming magmatic suites and records the compositional evolution and varying conditions of the parent melt. Zircon also survives intense hydrothermal alteration and weathering and long-distance detrital transport. It is now economically feasible to do rapid, precise characterisation of the chemistry of detrital zircons by Laser Ablation Inductively Coupled Plasma Mass Spectrometry (LA-ICPMS) to see whether a watershed contains eroding igneous rocks that might carry Cu ± Mo ± Au deposits.

We have investigated integrated LA-ICPMS U-Pb dating and trace-element analysis of zircon from infertile and fertile magmatic suites to see if there is a distinct zircon chemistry diagnostic of ore fertility of the parent magma (Fig. 1). The infertile suites are defined as magmatic rocks that have no mineralisation at any grade, whereas fertile suites refer to the intrusions related to porphyry-type ore deposits. The infertile suites are relatively reduced S- and A-type and relatively dry A- and I-type magmas, including the Yellowstone rhyolite (Wyoming), Bandelier rhyolite (New Mexico), Bishop tuff rhyolite (California), Lucerne reduced granite (Maine), and Hawkins S-type dacite and Kadoona I-type dacite (Lachlan belt, Australia). The fertile suites are more oxidised and hydrous and are selected from representative I-type intrusions related to porphyry and high-sulfidation epithermal Cu-Au deposits (Batu Hijau, Indonesia and Tampakan, Philippines), porphyry Cu-Mo-Au deposits (Sar Cheshmeh, Iran, Dexing, eastern China and Jiama, southern Tibet), porphyry Cu-Mo deposits (Sungun, Iran, and Qulong, southern Tibet), and porphyry Mo deposits (Nannihu and Yuchiling, central China).

The best fertility indicators are zircon Eu/Eu* and (Eu/Eu*)/Y ratios (Figs. 2 and 3). In particular, zircons from fertile magmatic suites have collectively higher zircon Eu/Eu* ratios (>0.3), 10,000*(Eu/Eu*)/Y (>1), and (Ce/Nd)/Y (>0.01) ratios than infertile suites. In fertile suites, zircon (Eu/Eu*)/Y ratios are positively correlated with (Ce/Nd)/Y ratios, but this correlation is absent in the infertile suites. These distinct trace element ratios are interpreted

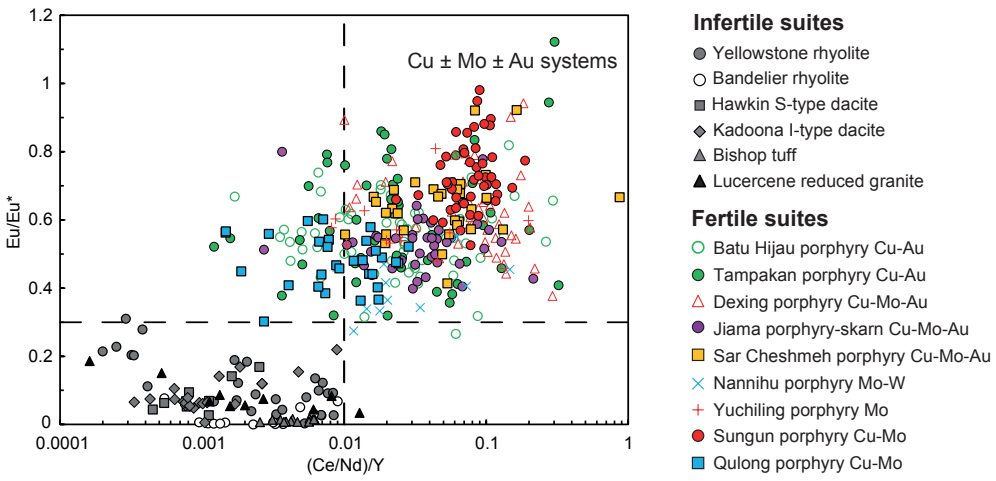

Figure 2. Zircon Eu/Eu versus (Ce/Nd)/Y plot. Eu/Eu* is europium anomaly, calculated as [Eu]/sqrt([Sm]*[Gd]) using concentrations already normalised to chondrite. Fertile suites have distinctly higher zircon Eu/Eu* values (>0.3) and (Ce/Nd)/Y ratios (>0.01) than infertile magmatic suites due to high magmatic water contents in the ore fertile suites.*

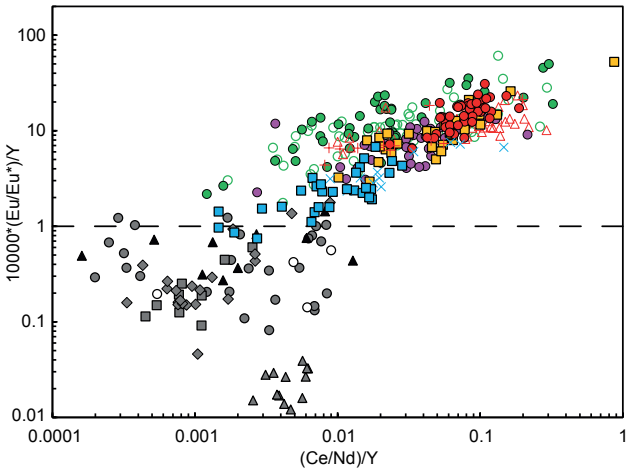

Figure 3. Zircon 10,000(Eu/Eu*)/Y versus (Ce/Nd)/Y plot. Fertile suites have distinctly higher zircon 10,000*(Eu/Eu*)/Y ratios (>1) and (Ce/Nd)/Y ratios (>0.01) than infertile magmatic suites due to high magmatic water contents in the ore fertile suites. See legend, Figure 2.*

to indicate a specific differentiation trend (suppression of plagioclase fractionation and enhanced early amphibole fractionation), the result of high magmatic water contents, which are a prerequisite for magmatic-hydrothermal (porphyry) ore formation. These zircon trace element ratios can identify magmatic suites that are potentially fertile for porphyry Cu-Au, porphyry Cu-Mo-Au, porphyry Cu-Mo, and porphyry Mo (-W) systems.

Combining all these zircon fertility indicators, it is possible to screen terranes or arc segments and distinguish those with unprospective A-, S-, and I-type granitoids from those with potentially mineralising I-type granitoids. Analysing detrital zircons from an area with little geologic information or poor outcrop could efficiently and cheaply identify drainages dominated by fertile I-type granitoids, so exploration could be focused on the most prospective areas.

This project is part of CCFS Themes 2 and 3, Earth's Evolution and Earth Today, and contributes to understanding Fluid Fluxes.

Contacts: Yongjun Lu, Robert Loucks, Marco Fiorentini, Cam McCuaig, Chris Kirkland, Luis Parra-Avila
Funded by: CCFS Flagship Program 2; CCFS Tibet pilot project

The giant sudoku of early Earth - a new solution?

The 2.0 - 1.8 Ga time interval in Earth's history is marked by globally widespread orogeny. These events accompanied the assembly of previously dispersed microcontinents and formed large cratons such as Laurentia (the cratonic part of North America), Baltica (East Europe), Siberia, Australia and Kalahari, and the accretionary growth of others (e.g. Amazonia). Most of these and other protocontinents then collided to form the Paleo-Mesoproterozoic supercontinent Nuna. The timing of the final assembly of Nuna is still debated, but broadly considered to be between 2.0 and 1.6 Ga.

Two key members of Nuna - Laurentia and Baltica, are proven to be mainly assembled and remained together between 1700 and 1270 Ma. Paleomagnetic data clearly indicate that Fennoscandia (the northern part of Baltica) joined Laurentia at about 1775 Ma, but the details of assemblies and eventual collision of these key members is still unclear. Our new 1975 Ma paleomagnetic data from Russian Karelia, together with previously published coeval paleopoles from Superior and Slave cratons (building blocks of Laurentia) throw some new light on this story.

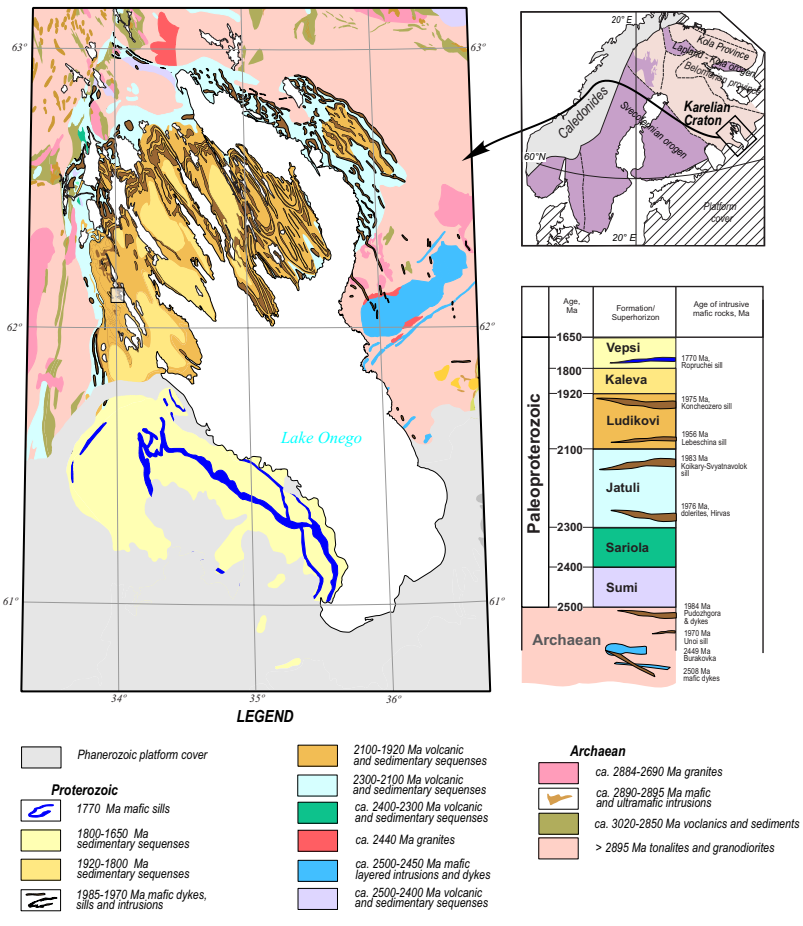

Figure 1. Geological map of the Onego Lake area.

Figure 2. 1975 Ma mafic dyke.

This study was done in collaboration with Natalia Lubnina (Moscow State University), Alexandra Stepanova and Svetoslav Sokolov (Karelian Research Center), and Svetlana Bogdanova (Lund University).

We studied well-dated 1785-1770 Ma mafic dykes and sills near the coast and on the islands of the Onego Lake in Russian Karelia (Figs. 1 and 2). Our study revealed a stable primary paleomagnetic remanence supported by several robust contact tests. Based on our new 1975 Ma Fennoscandian key paleopole and published poles from other cratons, we propose a paleomagnetically and geologically allowable 1975 Ma paleogeographic reconstruction of the Karelia (pre-Svecofennian Fennoscandia), Superior, Slave, Rae, Hearne and Amazonia cratons (Fig. 3). We conclude that at 1975 Ma all these cratons were widely separated by proto-oceans. In particular, the Karelia, Superior and Slave cratons were located at significantly different paleolatitudes, and their mutual azimuthal orientations require significant rotations before their final assembly at 1775 Ma (Fig. 3). This implies that the amalgamation of the Paleo-Mesoproterozoic supercontinent Nuna probably started after 1975 Ma.
See *CCFS publications #309, 882.*

This project is part of CCFS Themes 2 and 3, Earth's Evolution and Earth Today, and contributes to understanding Earth's Architecture.

Contact: Sergei Pisarevsky
Funded by: CCFS Flagship Program 5

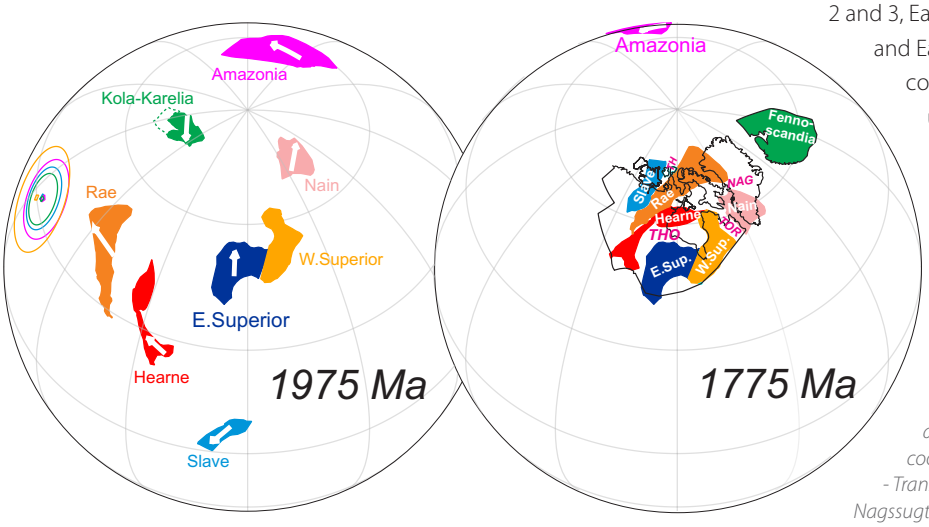

Figure 3. Paleogeographic reconstructions at 1975 Ma and 1775 Ma in Laurentian coordinates. 1.9-1.8 Ga orogens: THO - Trans-Hudson; 427 TOR - Torngat; NAG - Nagssugtoqidian; TH - Thelon.

Diamond formation caught *in flagrante delicto*

Gem-sized diamonds record a long history of growth and dissolution, resulting in complex zonation patterns that can be visualised by cathodoluminescence imaging. In contrast, polycrystalline diamonds form very rapidly, presenting snapshots of extreme conditions of diamond formation that complement our more time-integrated perspective of diamond growth derived from slowly grown gem-sized diamonds.

Polycrystalline diamonds are aggregates of diamond crystals with heterogeneous grain sizes and random orientation. They are found together with gem-sized diamonds in kimberlites in Africa and Siberia and can locally amount to *ca* 20% of the total diamond production.

The diamond aggregates can have up to 30% porosity, indicating they formed from a volatile-rich medium strongly oversaturated in carbon. Evidence from this diamond species emphasises the importance of redox gradients for the formation of diamond in the Earth's mantle. Recently we had the opportunity to study a sample from the Orapa Mine in Botswana using a novel microanalytical method called Transmission Kikuchi Diffraction. This method allows analysis of the structural and crystal orientation of mineral grains as small as some tens of nanometres (one nanometre is one billionth of a metre). It was the first time this method, developed in the material sciences, was applied to a natural rock sample.

A 150 nanometre thin foil, cut from the sample by Focused Ion Beam milling, transected one of the diamond crystals and the minerals included in that crystal (Fig.1). These inclusions were two iron sulfide crystals, one of which was rimmed by tiny grains

of iron oxide (magnetite, Fig. 2). Iron oxide also occurred as larger grains in other parts of this sample, but its association with iron sulfide was only revealed in this area.

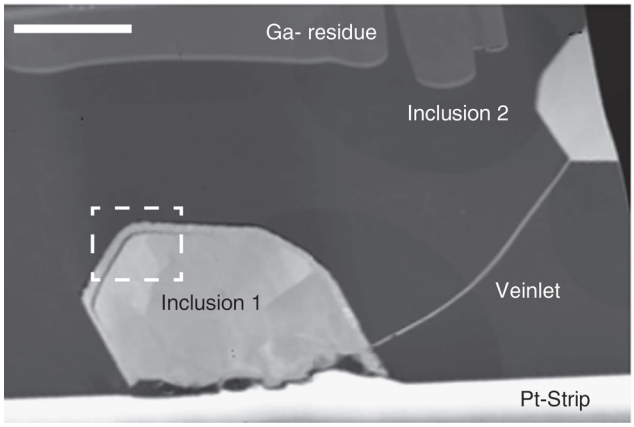

Figure 1. Overview of the iron sulfides included in diamond. A 150 nanometre thin foil cut by focused ion beam milling shows the host diamond with two iron sulfide inclusions connected by a veinlet of iron sulfide. The foil is covered by a protective Platinum strip (bottom) and displays some gallium residue from milling. Scale bar is 2µm.

Our Transmission Kikuchi Diffraction analyses showed that the crystal lattices of all three minerals, diamond host, iron oxide rim and iron sulfide grain, were systematically aligned. This phenomenon, termed epitaxy, is evidence that during their formation, each of the minerals nucleated and grew on the surface of the other. This is the first time the phenomenon has been documented in a diamond sample from the Earth's mantle and reveals that the trigger for the growth of the diamond lies in the redox (reduction-oxidation) reaction of carbonate (in a fluid) with iron sulfide to form iron oxide and diamond.

The most effective redox couple in the Earth's mantle is carbon and iron, which controls the onset of carbonate melting at depth by reduction of Fe^{3+} and oxidation of graphite or diamond. Conversely, oxidation of Fe^{2+} may lead to the freezing of mobile carbon species in the form of graphite or diamond. Iron (Fe^{2+}) sulfides in the Earth's mantle thus represent a reservoir with considerable redox potential. While sulfide is generally rare in the mantle, billions of years of subduction have created patches highly enriched in crustal material that contain abundant sulfides, carbon and volatiles and provide a very reactive environment in the Earth's mantle. One of these rarer patches seems to have been sampled by the kimberlites of the Orapa diamond mine.

Further investigation of the iron oxide grains rimming the iron sulfide could pin down the depth of this diamond-forming reaction to the base of the lithospheric root of the Kaapvaal craton (~180 km depth), because the grains preserve a '*memory*' of a phase transformation from a high-pressure modification of iron oxide.

Another important result from the use of the Transmission Kikuchi Diffraction method is that the iron sulfide grains were mechanically deformed, while the diamond hosting these inclusions was undeformed. This can only be explained if the iron sulfide grains were already crystallised and solid when the diamond included them, rather than liquid melt droplets. It appears therefore that pre-existing iron sulfide grains reacted with a carbonate-rich fluid or melt to form both a thin rim of iron oxide around the iron sulfides, and the enclosing diamond.

Unravelling the ages of diamonds relies entirely on the assumption that the inclusions in them, which are used for radiogenic isotope dating, are syngenetic to the diamond host. Our observations show that the iron sulfides predate the diamond and it is unclear how much time lies between the formation of the two minerals. This finding raises questions about some widely accepted concepts that need to be addressed in the future. See *CCFS publication #716, Jacob et al., Nature, 7, 11891, 2016.*

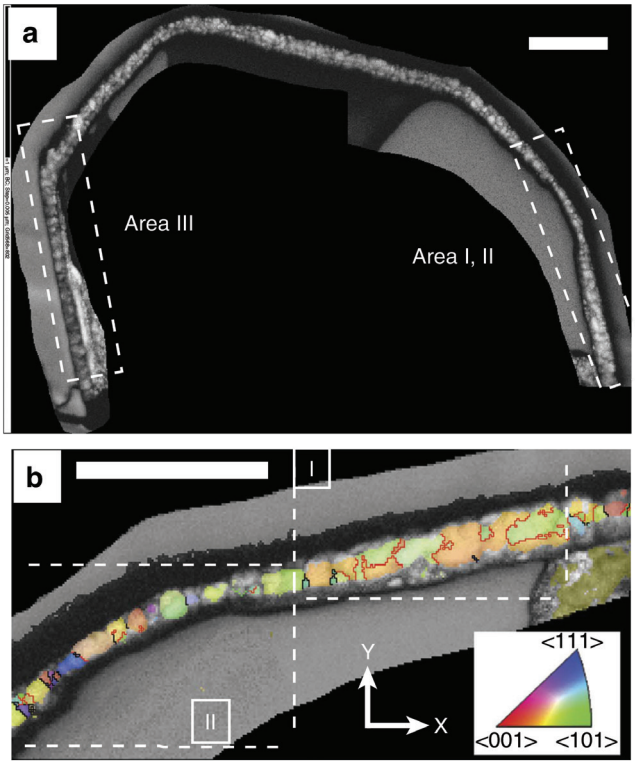

Figure 2. Crystallographic analysis of the iron oxide corona. Forescatter electron image of the iron oxide corona. Note that most of the iron sulfide was lost during re-thinning. The crystallography of areas I, II and III was further analysed. Scale bar is 0.5 µm.

This project is part of CCFS Theme 2, Earth's Evolution and contributes to understanding Fluid Fluxes.

Contact: Dorrit Jacob

Funded by: CCFS Pilot Project "Diamond growth at the nanoscale - Mantle fluids at work"

Birdshot on Mt Carmel: Immiscible metal, metal-oxide and silicate melts

Aggregates of hopper-formed corundum crystals (Carmel Sapphire) are common in Cretaceous pyroclastic ejecta exposed on Mt Carmel (Israel). Melt pockets trapped within and between corundum crystals contain mineral assemblages (SiC (moissanite), Fe-Ti-Zr silicides/phosphides, native V) that require high T and extremely low fO_2 (IW -10). Paragenetic studies suggest that the corundum and low fO_2 reflect interaction of mafic magmas with mantle-derived (CH_4+H_2) at high fluid/melt ratios, leading to progressive reduction and desilication of the magma, and ultimately to Al_2O_3-supersaturation, the rapid growth of corundum, and the deposition of abundant amorphous carbon. This evolution included several stages of liquid-liquid immiscibility.

Spherical to drop-shaped metal-rich pellets from <100 µm to several mm in diameter are common in the pyroclastics,

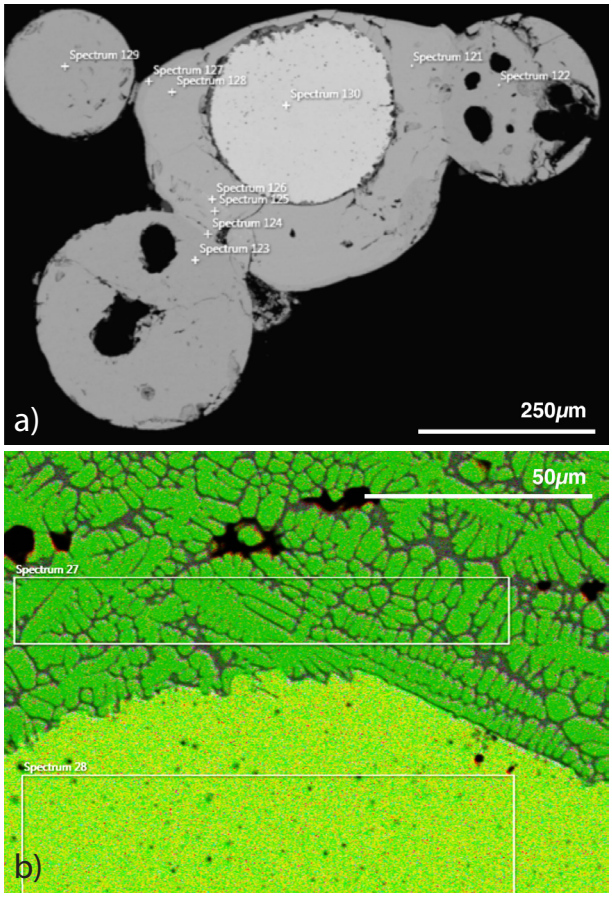

Figure 1. (a) Fe ball surrounded by shell of FeO-rich oxide melt; attached smaller balls are FeO-rich and TiO-rich melts with vesicles. (b) EDS image of Fe distribution at contact, showing dendritic crystals of FeO in a silicate-rich matrix (dark).

and appear to be melts separated from basaltic magma. They comprise Fe alloys, two types of metal-oxide melts, and a Fe-K-rich silicate melt. Pellets of different types and sizes may be stuck together (Fig. 1), suggesting the collision of melt droplets. Most pellets are vesicular, and in many a large central void makes up

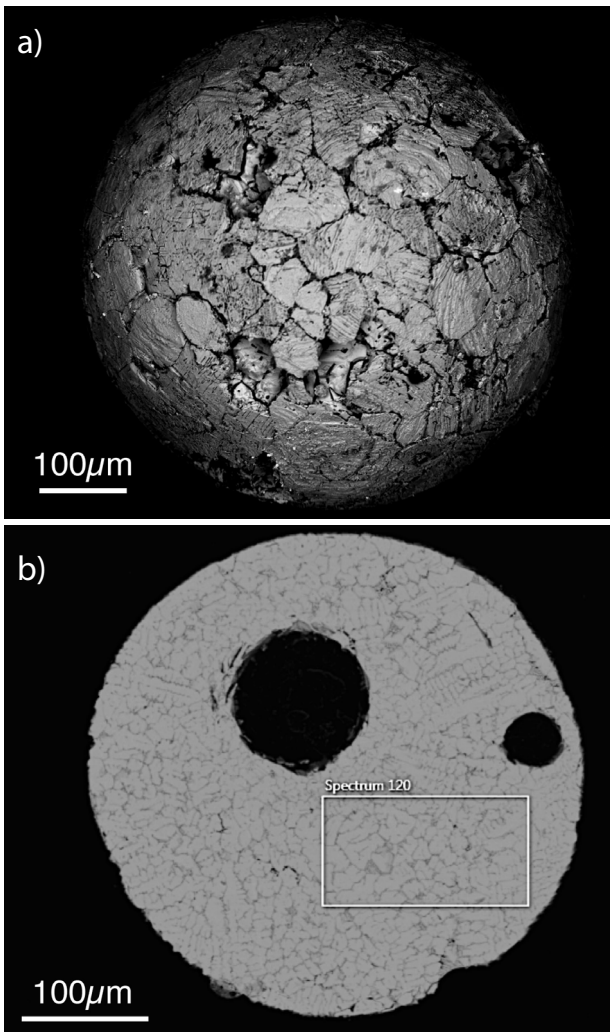

Figure 2. FeO-rich ball (a) surface showing plates made up of FeO crystals in matrix of glass richer in Si, Al, Ca; (b) polished section showing vescicles, and dendritic crystals of FeO in silicate-rich matrix.

most of the drop. These structures suggest that the initial melts contained high levels of volatiles (type unknown) that exsolved as the melts cooled, and were trapped inside the solidified outer shell. Four general types can be identified.

1. Fe melts: Generally ca 90% Fe, but some contain much higher Mn, Cr and Ni. Many contain micro-inclusions of type (2) below; they are typically rimmed by types (2-4) (Fig. 1, 4).
2. Fe-oxide melts: Example: SiO_2 6%, TiO_2 2%, Al_2O_3 2%, MgO 1%, FeO 87%, CaO 1.5 %. These typically consist of skeletal crystals of stoichiometric FeO (at % Fe= 50-55%), in a matrix enriched in Si, Al, Mg and Ca, apparently glassy; they commonly have a core of type 1 (Fig. 2).

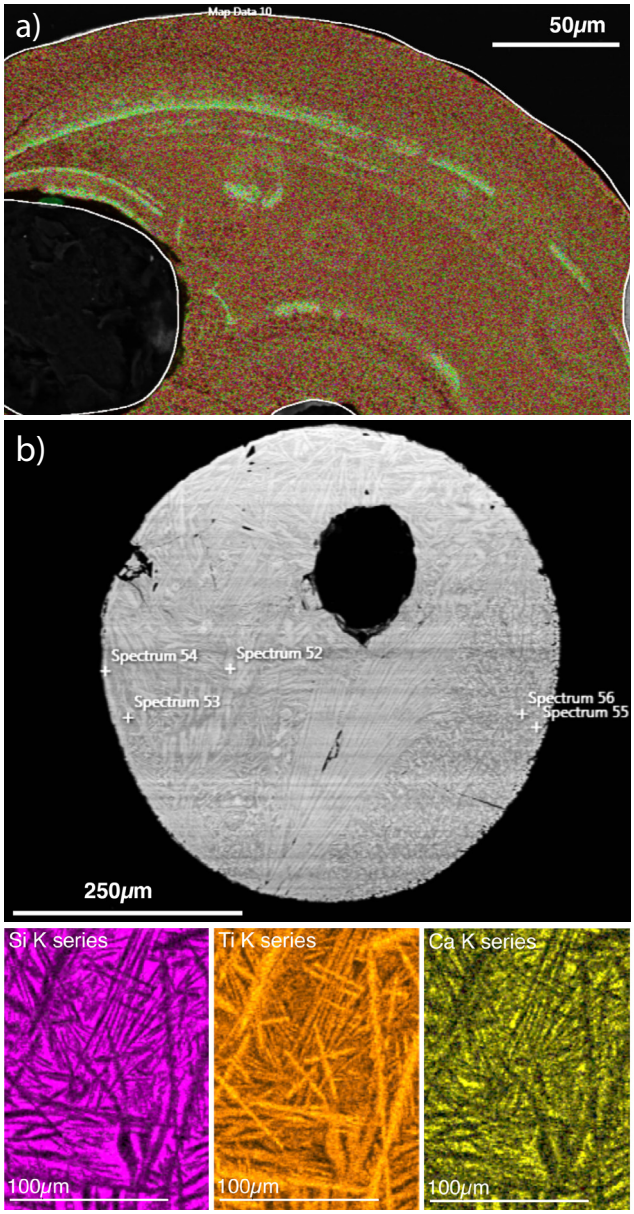

Figure 3. TiO-rich balls (a) EDS phase map of fine-grained ball, showing Liesegang-type zoning around vescicles. Light bands are rich in Ca and W. (b) TiO-rich ball with radiating crystals of $FeTi_2O_5$ (ferro-pseudobrookite) in Si-Ca-rich matrix.

3. Ti-oxide melts: Either very fine-grained, with internal bands suggestive of Liesegang rings (Fig. 3a) or quenched to long blades of $FeTi_2O_5$ in a matrix enriched in Si and Ca (Fig. 3b).

4. Iron-rich silicate glass: Extremely vesicular (Fig. 4), heterogeneous with Liesegang-ring zoning around vesicles and balls of types 1-3. Mean composition SiO_2 40%, TiO_2 1%, FeO 30%, MnO 11%, Na_2O 2%, K_2O 14%.

We suggest that these pellets were formed when fO_2 dropped to the Iron-Wustite boundary, resulting in the separation of mutually immiscible melts from the host magma. The vesicular nature of the oxide balls, coupled with the other data on the corundum system, suggests that mantle-derived methane ($\pm H_2$) provided both the reducing power, and the abundant gasses, through reactions such as 4FeO (melt) + CH_4 → 4Fe + CO_2 +$2H_2O$ and Fe_2O_3 + CH_4 → 2FeO +CO_2 +H_2O. This immiscibility played an important role in the further development of the Mt Carmel magmatic system toward final desilication and super-reduction: none of the silicate or oxide phases in the corundum aggregates contain Fe, because most of it had been removed earlier.

A similar model has been proposed by Grebnikov et al. (*2012; J. Volcanol. Seismol. 6, 211-229*) to explain Fe-cored Fe-oxide balls (our type 2) in Yakutian ignimbrites.

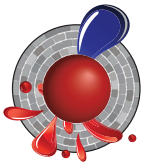

This project is part of CCFS Theme 2, Earth's Evolution and contributes to understanding Earth's Architecture and Fluid Fluxes.

Contacts: Bill Griffin, Sue O'Reilly, Jin-Xiang Huang, Sarah Gain
Funded by: CCFS Flagship Program 1 (TARDIS II)

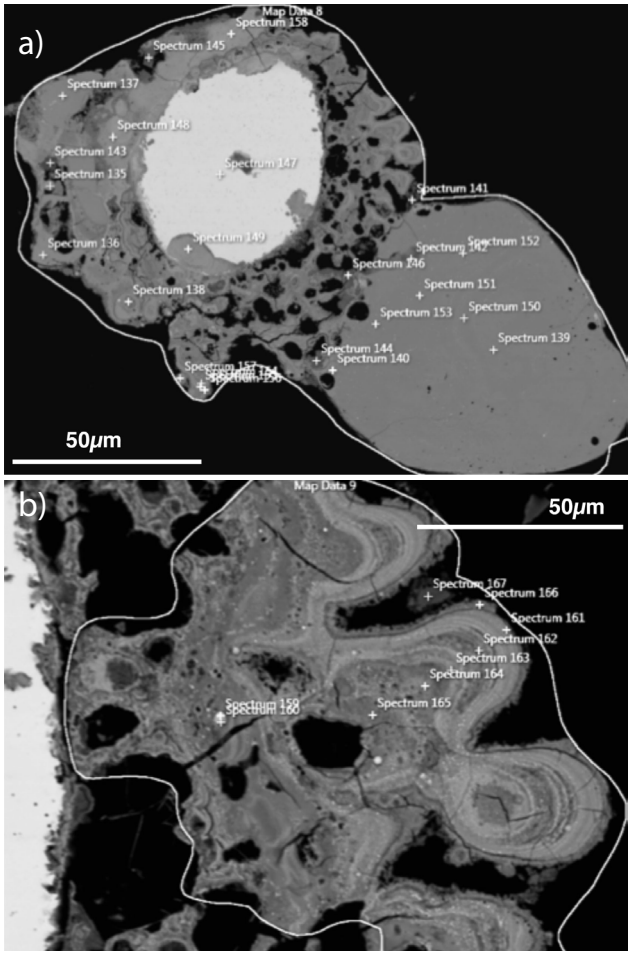

Figure 4. Silicate-metal-oxide melts. (a) BSE image, Fe ball surrounded by vesicular Fe-Mn-Si-K glass; attached ball is TiO-rich type 2. (b) Closeup of silicate glass, showing zoning around vesicles. Lighter bands are richer in Fe+Mn, lower in Si+K.

Sulfur-loving elements in meteorites from Mars probe the extra-terrestrial mantle?

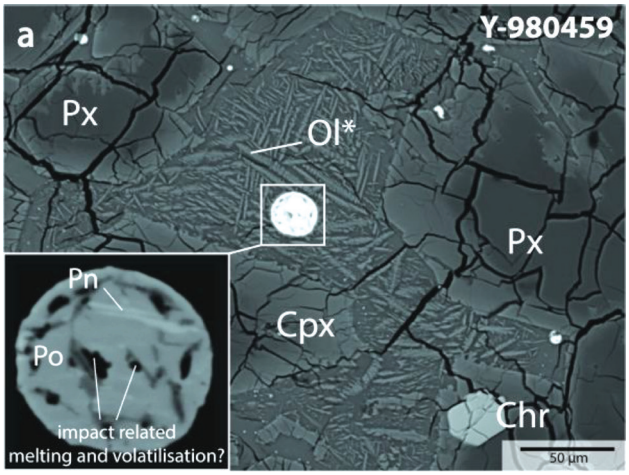

Figure 1. BSE image of a blebby (quench) sulfide assemblage in the fine-grained and plagioclase-free silicate mesostasis of Y-980459. Cpx = clinopyroxene, Chr = chromite, Ol = dendritic olivine, Po = pyrrhotite, Px = pyroxene.*

The Martian mantle is not available for direct sampling, but shergottite meteorites are thought to be derived from Mars; they can provide information on the chemical/petrological properties of Martian mantle reservoirs and igneous rocks. Whole-rock analysis of shergottites for Se and Te, as well as the highly siderophile elements (HSE) Au, Re, and PGE (Os, Ir, Ru, Rh, Pt, and Pd), led to the hypothesis that these elements were stripped from a magma ocean by Fe-Ni liquids at intermediate mantle pressures (~14 GPa).

Selenium, Te and HSE behave as chalcophile elements at redox conditions outside the stability field Fe-Ni metal. Hence, in Mars' mantle and derived magmas, sulfides may exert a major control on these elements, while PGE may also form discrete minerals (e.g. platinum group-minerals, PGM). However, the magmatic Fe-Ni-Cu sulfides contained in shergottites were not yet analysed by high-precision techniques, and no PGM were observed to date. Therefore, we acquired the first LA-ICPMS trace-element analyses on sulfides from selected high-Mg# olivine-phyric shergottites depleted in incompatible trace elements (ITE-depleted; Y-980459, DaG 476 and Dhofar 019), and one ITE-enriched, low-Mg# basaltic shergottite (Zagami).

The shergottite sulfides generally occur in spherical to ellipsoidal, and/or multiply lobed droplets usually ≤50 µm in size. Their pyrrhotite-dominated mineralogy (Fig. 1) is consistent with their *in situ* crystallisation from Ni- and Cu-poor immiscible sulfide melts, in which exsolution of Cu-sulfide and pentlandite was largely suppressed. However, magmatic characteristics have been variably masked by alteration on both Mars and Earth, as well as impact-related sulfide volatilisation during meteorite ejection. The small grain sizes and complex sulfide exsolution textures mean that individual sulfide phases cannot be resolved (Fig. 1), so the LA-ICPMS analyses represent the composition of the bulk sulfide.

The sulfide PGE-signatures mimic available whole-rock analyses, with CI-normalised patterns that increase in steepness with decreasing whole-rock Mg#, a signature of magmatic differentiation (Fig. 2a and Fig. 2b). While these variations suggest major sulfide controls, the Pt-depletions in sulfides may relate to the predominance of (nano-scale) Pt-Fe alloys in FeO-rich and reduced Martian magmas. Positive correlations exist between total Se, Te and HSE (particularly Pd) in sulfides, and whole-rock Mg# in the order Y-980459 >DAG 476 >Dhofar 019 (Fig. 3a). Notably, these trends are even preserved following recalculation to whole-rock concentrations on the basis of bulk sulfur analyses (Fig. 3b).

These results provide insights on siderophile-chalcophile element transfer in FeO-rich shergottite magmas. No whole-rock Te data exist to date, and previous whole-rock HSE concentrations have been questioned because of analytical issues (i.e., nugget effect) in the bulk-rock analyses of small

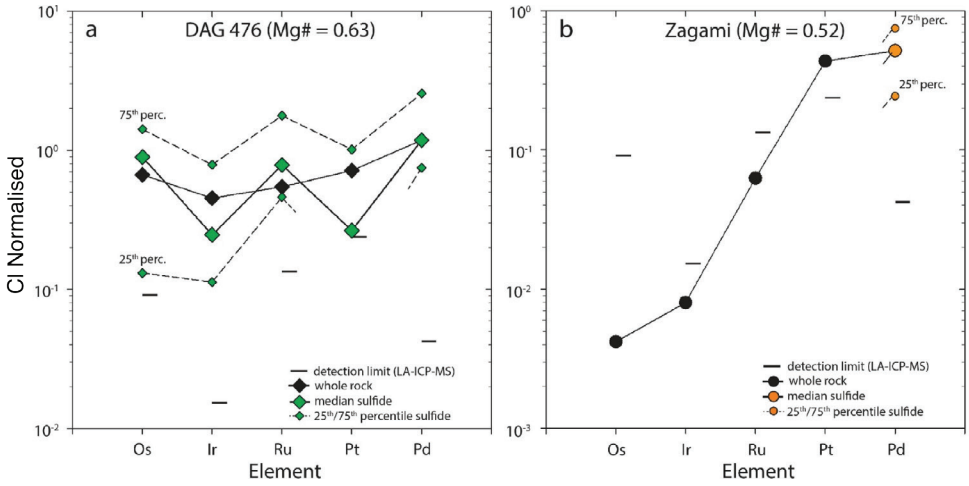

Figure 2. Chondrite-normalised concentration patterns for median PGE values in sulfides from DaG476 (a) and Zagami (b), compared to whole-rock data reported in Brandon et al. (Geochim. Cosmochim. Acta, 2012). The sulfide median and 25th/75th percentile values have been calculated from 22 and 35 single sulfide analyses from DaG 476 and Zagami. In order to improve data comparison, the whole-rock data are recalculated to the chondrite-normalised mean Pd concentrations in sulfides. The main deviations from the trends in whole-rock data are the Pt- (and Ir-?) deficiencies in sulfides, specifically in Zagami where no sulfide was found to contain Pt above detection limit.

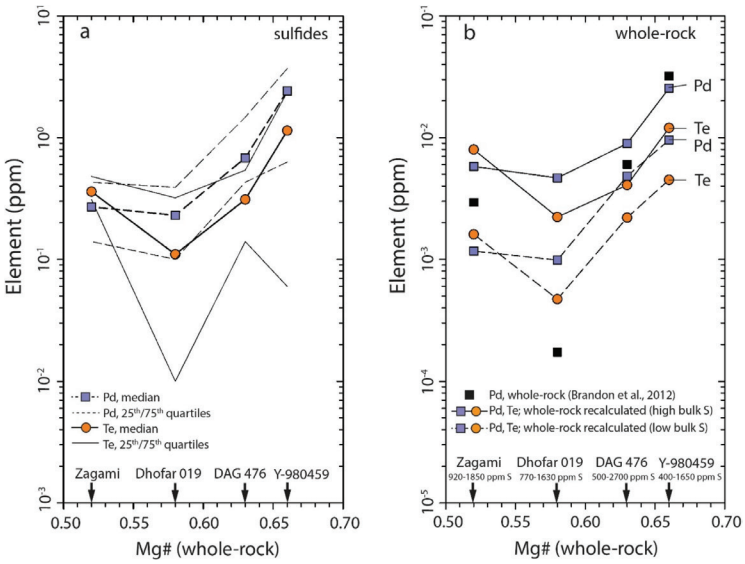

Figure 3. Concentrations of Te and Pd versus Mg# in the host rocks: a) sulfides, b) recalculated whole-rock concentrations. The latter are determined by Cwr=(Cs·Swr)/Ss, in which Cs are the median and 25th/75th percentile concentrations in sulfides, Swr is the whole-rock content of sulfur, and Ss is the sulfur content in bulk sulfides assuming troilite stoichiometry (FeS). The lower and upper whole-rock sulfur contents used for calculation are those reported/surveyed in Ding et al. (Earth Planet. Sci. Lett., 2015). Whole-rock concentrations of Pd for the analysed shergottites are taken from Brandon et al. (Geochim. Cosmochim. Acta, 2012).

sample masses. However, our data resolve distinct differences in PGE (particularly Pd) between the respective shergottites (Fig. 3b). Hence, provided that the analysed olivine-phyric shergottites relate to comparable mantle/magma sources, the positive correlations between Mg#, Se, Te and Pd may relate to sulfide immiscibility and fractionation during mantle melting, magma ascent or crystallisation.

In summary, our pilot study provides new insights into the behaviours of chalcogens and highly-siderophile elements in Martian magmas. More *in situ* analyses on sulfides from shergottite specimens may show whether the observed variations in sulfides are a general trend among (ITE-enriched and -depleted) olivine-phyric and basaltic shergottites, and if any such differences may lead to the more detailed understanding of sulfide stability and siderophile-chalcophile element transfer in igneous systems on both Mars and Earth.

This project is part of CCFS Themes 1 and 2, Early Earth and Earth's Evolution, and contributes to understanding Fluid Fluxes.

Contacts: Raphael Baumgartner, Marco Fiorentini
Funded by: CCFS Flagship Program 2

Use and misuse of ilmenite in diamond exploration

Ilmenite is a very common phase in kimberlites and related rocks and, as a consequence, is one of the main kimberlite indicator minerals (KIM) used to locate new targets. Because of its abundance in kimberlites, ilmenite has been investigated for diamond exploration, but its use as diamond indicator mineral (DIM) has been unsuccessful to date.

Complex crystallisation and replacement processes have been previously invoked to explain the compositional and textural variety of ilmenite found in kimberlites. The research presented here was carried out as a collaboration between CCFS, University of Barcelona and the Catoca mine (Angola) and it aims to shed new light on these processes, as well as their implications for diamond exploration. Petrographic studies were combined (for the first time) with major- and trace-element analyses to characterise the ilmenite populations found in xenoliths and as xenocrysts in two Angolan kimberlites (Congo-Kasai craton).

The study of mantle xenoliths already brought to light the complexity of the processes that can be involved in ilmenite formation at depth. In these xenoliths, ilmenite has a wide compositional range. It occurs either as thin veins or as small rounded grains, and may be accompanied by the crystallisation of a variety of metasomatic minerals (i.e. apatite, kaersutite, phlogopite and rutile).

However, ilmenite mainly occurs as individual xenocrysts in the kimberlitic matrix, where it can be found either as Mg-rich ilmenite nodules or as xenocrysts of ferrian ilmenite with hematite exsolution. Likewise, different types of secondary ilmenite were identified, in most cases replacing primary ilmenite grains and/or other titanium oxides: i) symplectitic ilmenite; ii) tabular ilmenite and iii) secondary Mn-rich ilmenite.

The trace-element analysis of ilmenite revealed that populations with the highest Mg contents (i.e. symplectitic, secondary Mg enrichment in the ilmenite nodules) typically show significantly higher contents of HFSE, Cr and V at a given Nb content, and thus diverge from the general trends described for most other ilmenites. These trace-element signatures in the ilmenite nodules, coupled with the co-crystallisation of perovskite, have been interpreted as a result of an interaction with the kimberlitic magma.

A multi-stage model has been proposed to describe the evolution of ilmenite in these pipes involving: i) Crystallisation of ilmenite under different conditions, both in crustal and metasomatised mantle domains; ii) Xenolith disaggregation

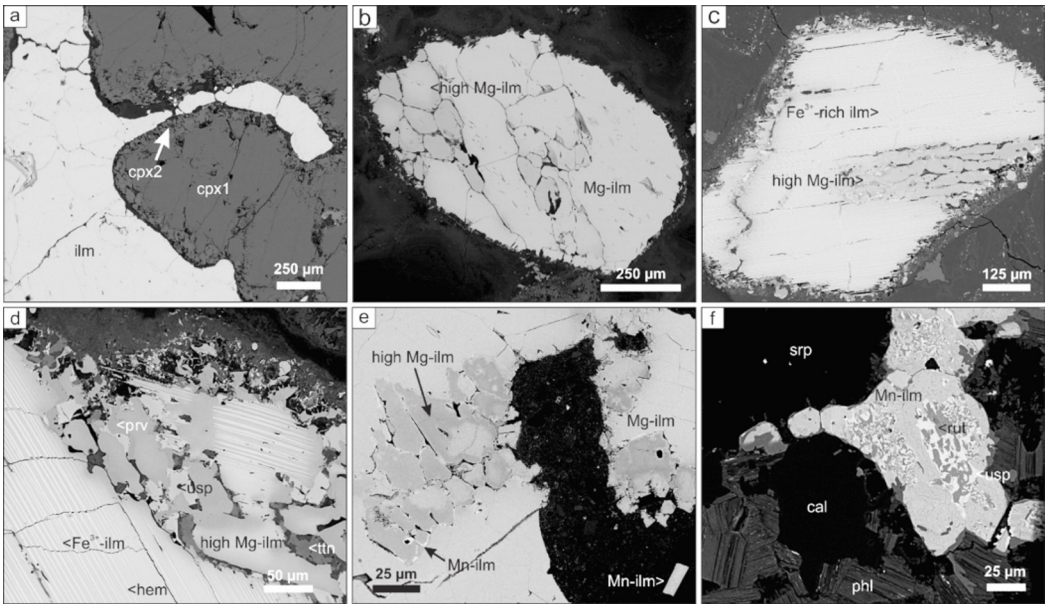

Figure 1. Textural types of ilmenite found in the Angolan kimberlites (BSE images). (a) metasomatic ilmenite in a mantle xenolith, associated with a secondary clinopyroxene (cpx2) replacing an early clinopyroxene (cpx1) and olivine; (b) ilmenite nodule showing recrystallisation and secondary enrichment in Mg set in the kimberlite matrix; (c) Fe^{3+}-ilmenite with fine hematite exsolutions replaced by symplectitic, darker Mg-rich ilmenite, which crystallises along fractures and grain boundaries. Detailed image (d) shows the complex replacement sequence of the symplectitic ilmenite: ulvöspinel (usp), perovskite (prv) and titanite (ttn); (e) nodular ilmenite replaced by Mg- and Mn-rich ilmenite along grain boundaries of the recrystallised grains, together with tabular Mn-rich ilmenite set in the kimberlite matrix; (f) late Mn-rich ilmenite, replacing previous rutile (rut) and ulvöspinel (usp), set in a matrix of serpentine (srp), calcite (cal) and phlogopite (phl).

producing at least two populations of ilmenite xenocrysts differing in composition (Fe^{3+}- and Mg-ilmenite nodules); iii) Interaction of both types with the kimberlitic magma during eruption, leading to widespread replacement by Mg-rich ilmenite along grain boundaries and fractures. These processes produced similar major-element compositions in ilmenites regardless of their primary origin, although in most cases the original enrichment in HSFE (Zr, Hf, Ta, Nb) observed in Fe^{3+}-rich crustal xenocrysts is preserved. Finally (iv) secondary Mn-ilmenite was formed by infiltration of late hydrothermal fluids, followed in some cases by subsolidus alteration in an oxidising environment.

This study has shown that ilmenite genesis is complex and may lead to misinterpretation of the diamond potential of a kimberlite during the exploration stage if textural and trace-element information is disregarded. Secondary Mg-enrichment of ilmenite xenocrysts is common and is unrelated to reducing conditions that could favour diamond formation/preservation in the mantle. Similarly, Mn-rich ilmenite should be disregarded as a diamond indicator mineral, unless textural studies can prove its primary origin.

This project is part of CCFS Themes 2 and 3, Earth's Evolution and Earth Today, and contributes to understanding Fluid Fluxes.

Contacts: Montgarri Castillo-Oliver, Bill Griffin, Norman Pearson, Sue O'Reilly
Funded by: CCFS Flagship Program 1

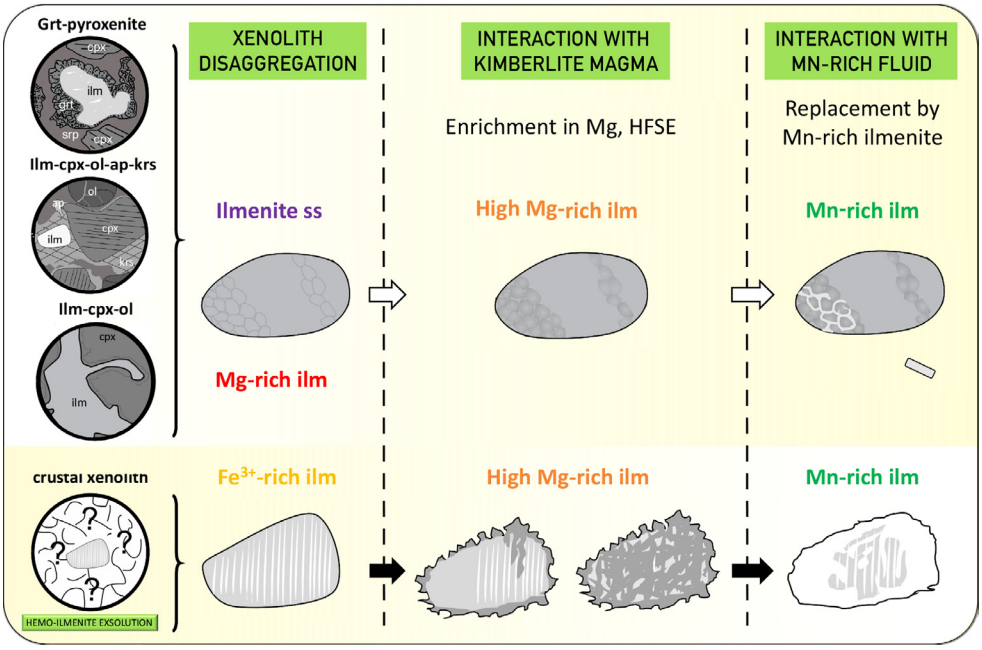

Figure 2. Schematic model of the multi-stage petrogenesis of ilmenite in the studied kimberlites, including the average composition of ilmenite at each stage. Mineral abbreviations: clinopyroxene (cpx), ilmenite (ilm), garnet (grt), serpentine (srp), apatite (ap), kaersutite (krs) and olivine (ol).

Cerium in zircon - serial tracking of mantle controls

Magmas emplaced deep in the Earth's crust cool slowly, and precipitate a sequence of mineral assemblages on the floor and walls of magma chambers. This crystallisation produces residual liquids that are depleted in many elements and enriched in others, relative to the parental silicate melt. In many cases, whether an element is sequestered in early minerals or accumulates in residual melts depends on the oxidation state of the melt, which enhances or hinders the ability of any given magma to produce ore deposits of many elements.

Oxidation/reduction couples that commonly are of petrologic and economic interest include Fe^{3+}/Fe^{2+}, $S^{6+}/S^{4+}/S^{2-}$, Eu^{3+}/Eu^{2+}, Ce^{4+}/Ce^{3+}, $U^{6+}/U^{5+}/U^{4+}$, Mo^{6+}/Mo^{4+}, Sn^{4+}/Sn^{2+}, $V^{5+}/V^{4+}/V^{3+}$, Ti^{4+}/Ti^{3+}, As^{5+}/As^{3+}, Se^{6+}/Se^{2-} and Mn^{3+}/Mn^{2+}.

Determination of the former oxidation state of a magma by chemical analysis of minerals in igneous intrusions is often hampered by subsolidus re-equilibration and/or alteration. The most sensitive and best-calibrated of the igneous mineral oxybarometers currently in use by petrologists - titanomagnetite-hemoilmenite pairs and chromite-bearing assemblages - re-equilibrate within days to weeks at near-solidus temperatures, and are reliable only when used on quickly-quenched volcanic rocks. A problem affects igneous amphibole oxybarometry and hygrometry; as magmas rise to depths <4-5 km, exsolution of H_2O from the silicate melt causes breakdown of amphibole to anhydrous minerals on timescales of days to weeks, and magmatic hornblende is not stable at shallower depths. Consequently, we need other equilibria to constrain fO_2. The potential appeal of a zircon oxybarometer is that chemical diffusion (re-equilibration) in zircon is extremely slow and zircon compositions are unaffected at granitoid magma temperatures at timescales on the order of 10^5-10^6 years.

The Ce^{4+}/Ce^{3+} ratio in zircon and the closely related Ce anomaly, which is commonly denoted Ce/Ce*, are widely used as proxies for the oxidation state of the zircon's parent silicate melt. The ratio U^{4+}/Pr^{3+} involves nearly the same ion sizes as Ce^{4+}/Ce^{3+} in zircon, so the two have similar temperature sensitivity, but opposite responses to redox variation in the parent melt. Plots of these ratio pairs in natural igneous zircon populations show strong positive correlations with slopes near unity, which invalidates their use as magmatic redox indicators (Fig. 1). We conclude that the Ce^{4+}/Ce^{3+} and Ce/Ce* ratios in zircon that are commonly referred to as oxybarometers actually vary in and among zircons chiefly in response to variations in the temperature at which zircon crystallised. Presently available zircon geothermometers are too imprecise to distinguish the small redox effect from the dominant temperature effect in most natural assemblages.

This project is part of CCFS Theme 3, Earth Today, and contributes to understanding Fluid Fluxes.

Contacts: Robert Loucks, Marco Fiorentini, Bruce Rohrlach (Avalon Minerals Ltd)
Funded by: CCFS Flagship Program 2

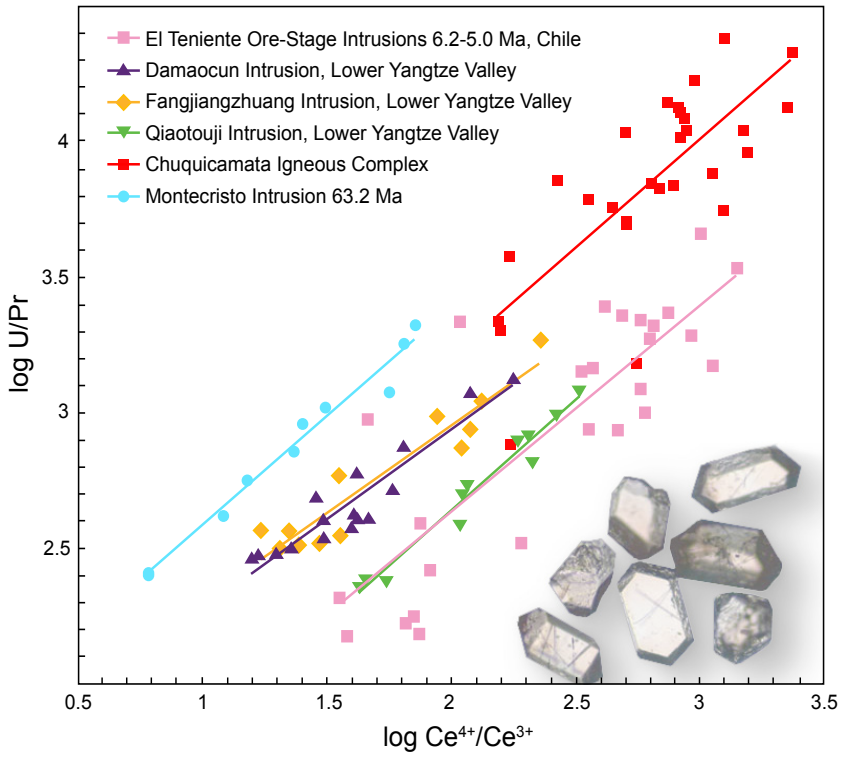

Figure 1. Zircon Ce^{4+}/Ce^{3+} values reported by authors of the source publications are plotted against the U/Pr ratios in those zircons. The zircon/melt partition coefficients of Ce and U respond oppositely to varying magmatic oxidation state, so these strong positive correlations prove that there is no resolvable component of the variation in zircon Ce^{4+}/Ce^{3+} that can be attributed to varying magmatic oxidation state.

Research highlights 2017

Contents

Origins of life: insights from the Pilbara

Currently, there are two principal environments considered as sites for the origin of life. The first is that life began in the ocean in hot vents – a theory that has been favoured since the 1977 discovery of hot seafloor vents thriving with microbial life. The second, and currently gaining traction, is that life began on land in a "*warm little pond*", i.e. hot springs on land - a theory first conceived by Charles Darwin.

The Pilbara is an ancient landscape that is barren and rather desolate today, but billions of years ago things were vastly different. The Dresser Formation, located in the East Pilbara, hosts some of the earliest evidence for life on Earth. Stromatolites, i.e. rock structures built by communities of microorganisms, were discovered there in the late 1970s and the site has been a place of interest for research into the early Earth and evolution ever since. Over the past 40 years, the environmental setting has been extensively debated. Original research suggested a quite shallow-water marine environment, resembling the modern Shark Bay, on the West Australian coast. However, since the late 1990s new evidence has pointed to a much more dynamic environment, that of an ancient volcano. What was still unclear about this volcanic setting was the link between life, i.e. stromatolites, and the hot circulating fluids that typically accompany volcanoes. In modern volcanic settings, hot fluids circulate in the underground rocks and manifest either as hot vents at the bottom of the salty ocean such as the black or white smokers, or as terrestrial hot springs where fresh rainwater falls on a land, such as those in Rotorua, New Zealand. This hot circulating water is full of elements liberated from the rocks and becomes a nutrient-rich environment, fertile grounds in which microbes can thrive.

Our recent work in the Pilbara has provided new and strong evidence that terrestrial hot springs had indeed existed within this ancient volcano and, more importantly, could be linked with life. A rock type called geyserite (opaline silica) was found alongside a suite of biological textures including stromatolites. Geyserite is only found in terrestrial hot spring pools and geysers on land. The accompanying biological signatures include a newly-identified microbial texture (called palisade fabric) that represents microbes that grew on the ancient sinter terraces – the rocks that form around hot spring pools. In addition, gas bubbles are inferred to be biological because the preservation of their bubble shape indicates that a sticky substance (microbial) was present that trapped them long enough to be entombed perfectly. All of these textures are almost identical to the fossil textures observed in modern terrestrial hot spring settings today.

Biochemical studies are now showing that some of the reactions necessary to form longer-chain polymers, the more complex molecules needed as ingredients for life, can only occur where dehydration and rehydration are allowed, i.e. in hot pools exposed to air on land.

The findings in the Pilbara provide a geological perspective that lends weight to an origin of life on land, as they extend the record of life living in hot springs on land back to 3 billion years, and indicate that life inhabited the land much earlier (by up to 580 million years) than previously thought.

This project is part of CCFS theme 2, Earth's Evolution, and contributes to understanding Fluid Fluxes.

Contacts: Tara Djokic, Martin Van Kranendonk
Funded by: CCFS Flagship Program 4, UNSW

Figure 1. The 3.5 billion year old Dresser Formation, Pilbara, Western Australia.

Figure 2. Cover art for Scientific American, August, 2017 issue relating to article containing Pilbara findings, CCFS publication #1070.

Detective work on stealthy processes in Earth's mantle solves continental survival, evolution and identity issues

Serial research on, and accumulation of diverse clues about, continental formation can now solve some fundamental questions about when, how, why and where deep processes shaped Earth's lithosphere.

The lithospheric mantle, the deep part of Earth's lithospheric plates up to 300 km below the surface, holds many layers of information about the fluids that have risen up from the convecting mantle, and the huge tectonic events that have shaped the outermost part of Earth's solid shell that we inhabit. It is a palimpsest - just like ancient manuscripts that have many layers of writing superimposed on, and obscuring, earlier messages. Unravelling such repeated fluid episodes from mantle materials brought to the surface as fragments in magmas, or tectonically thrust from depth on to the surface, and remotely sensing the physical properties of the hidden lithosphere with geophysical methods can help solve this great puzzle in deep time and deep space.

Interpreting this complex record and tracking specific episodes and processes is a key to reconstructing lithosphere evolution through time and the nature of volatile fluxes from the deep Earth. Convergence between datasets of Hf isotopic model ages for zircons (e.g., *Belousova et al., 2010, Lithos*) and Re-Os model ages for mantle sulfides (*CCFS publication #344*), reinforced by other geochemical and tectonic criteria, indicate that over 75% of the subcontinental lithospheric mantle (SCLM) and its overlying crust (now mostly lower crust) formed at 3.0-3.5 Ga, probably in global overturn events that marked a change in Earth's fundamental geodynamic behaviour (*CCFS publication #344*).

Pristine Archean lithospheric mantle, the roots of the Archean cratons up to >300 km deep, is not only more depleted (low in basaltic melt components) than younger lithospheric mantle, it is differently depleted. Proterozoic and Phanerozoic lithospheric mantle (xenoliths and orogenic massifs), as well as abyssal peridotites, ophiolitic peridotites, all have one important feature in common: as Al decreases, Fe (and Cr) contents show only a very narrow range (8±1 wt% FeO). In contrast, Archean peridotites have lower Fe at low Al contents, and may show a weak positive correlation between Fe (and Cr) and Al, suggesting that no Cr-Al phase (i.e. spinel or garnet) was present on the liquidus during the melting that produced Archean lithosphere. Garnet-peridotite suite rocks in cratonic mantle are thus now interpreted as products of the metasomatic introduction of garnet and clinopyroxene into original depleted harzburgite, thus '*refertilising*' the depleted residue.

Therefore, the traditional '*oceanic melting trend*' is now interpreted as a refertilisation trend, with the compositional trend arrow reversed (*Griffin et al., 2009, J Pet*). The cratonic roots in contact with the convecting part of the mantle (the asthenosphere) and outer margins in contact with repeated fluid and melt fluxes, are the most strongly modified domains through time, so cratonic root compositions show a general increase in fertility (e.g., increasing Fe, Ti, Ca, Al content and decreasing Mg content) with increasing depth.

Integration of geochemical and geophysical datasets, groundtruthed with petrophysical measurements and modelling for different mineral compositions and modes, has enabled us to interpret global (and regional) seismic tomographic results with an increasing degree of geological reality (Fig. 1).

Stealth metasomatism and its geophysical significance

Mantle metasomatism is the process, and the results, from the interaction of fluids with mantle rocks they pass through. This affects not only the geochemical characteristics of the

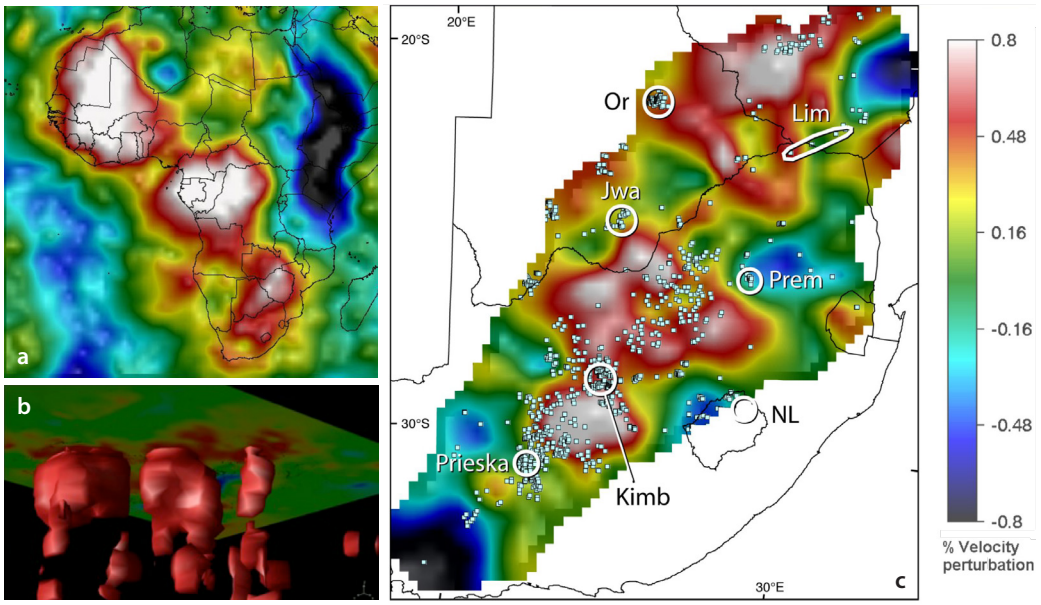

Figure 1. Vs tomography (100-150 km) of the lithospheric mantle. Red to white colours indicate high Vs; blue colours low Vs (modified from CCFS#207 and Begg et al., 2009, Geosphere). (a) Africa, showing distribution of the boundaries of high-velocity cratonic blocks with metasomatised (red) margins. (b) modelled high-Vs irregular volume of cratonic roots to ~350 km beneath each craton. (c) Detailed seismic tomography for Kaapvaal craton with kimberlites clustered at margins of high-velocity volumes. White circles show major kimberlite provinces.

lithospheric mantle, but also its physical parameters (and hence geophysical signatures) including density, seismic response and thermal and electrical characteristics. The concept of '*stealth*' metasomatism was introduced (*CCFS #5; http://ccfs.mq.edu.au/AnnualReport/12Report/ResHigh.html#Stealth*) to highlight the '*deceptive*' addition to lithospheric mantle rock-types of new minerals (e.g. garnet and/or clinopyroxene) indistinguishable mineralogically from common mantle-peridotite phase assemblages.

Recognition of stealth metasomatism reflects the increasing awareness of the importance of refertilisation (resulting in, for example, higher Fe, Ca and many minor- and trace-element contents) of ancient refractory mantle regions by deep-seated fluid fronts.

very depleted upper layer, becoming more metasomatised (evidenced by garnet peridotites) at depth, provides a solution to some important discrepancies between geophysical data and numerical models. A deep cratonic root made up mainly of garnet peridotites would imply a lower geoid and a much greater elevation than is observed for the Kaapvaal craton, and a mismatch in Vp/Vs ratios (*Afonso et al., 2010*), but a layered model with refertilisation increasing with depth, yields numerical models that fit the geophysical data.

Thermal changes are caused by advective transfer of heat by relatively hot metasomatising fluids and by the influx of heat-producing elements (K, U, Th) that accompanies some types of metasomatism. Radioactive decay of these elements can raise the local heat flow by 50-70% over normal reduced mantle heat

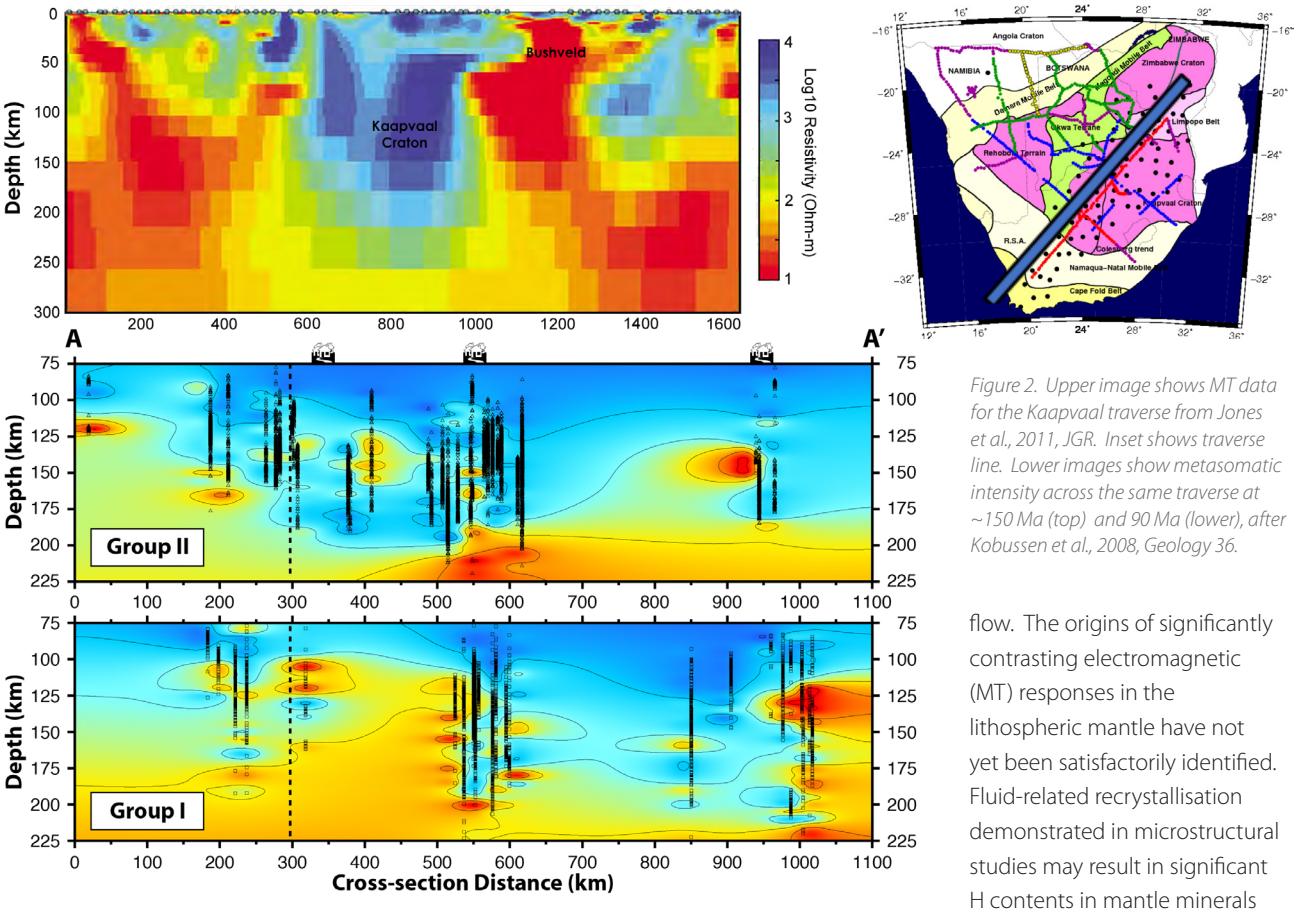

Figure 2. Upper image shows MT data for the Kaapvaal traverse from Jones et al., 2011, JGR. Inset shows traverse line. Lower images show metasomatic intensity across the same traverse at ~150 Ma (top) and 90 Ma (lower), after Kobussen et al., 2008, Geology 36.

flow. The origins of significantly contrasting electromagnetic (MT) responses in the lithospheric mantle have not yet been satisfactorily identified. Fluid-related recrystallisation demonstrated in microstructural studies may result in significant H contents in mantle minerals and may affect electrical conductivity. The key to understanding the electromagnetic signals from the mantle lies in identifying the nature of fluids, their oxidation state, and their distribution and thus is closely connected with a full understanding of metasomatic processes, grain sizes and fabrics, and fluid compositions and movement mechanisms in the mantle. Comparisons of high-resolution MT traverses with geochemical mapping traverses show a correlation of higher conductivity with more strongly metasomatised domains.

Understanding the timing and nature of stealth metasomatism is critical to understanding the geochemical and geodynamic evolution of different regions of the lithospheric mantle and also for assessing their metallogenic fertility.

Primitive Archean lithospheric mantle is highly magnesian (~49% MgO) with lower density (~3.31 g/cm^3) than fertile mantle (~3.37 g/cm^3). The resulting contrasts in seismic response become measurable if metasomatised regions are on the scale of tens to hundreds of km. Metasomatic refertilisation of the cratonic lithospheric mantle not only increases its density, but also strongly affects its rheology. The recognition that the cratonic lithospheric mantle may in general consist of a

The 2-D isotropic model of magnetotelluric response across the Kaapvaal Craton is shown in the top image, Figure 2 (*Jones et al., 2011, JGR*); the traverse locus is marked in the inset map. The lower

2 images show the contoured metasomatic intensity for domains beneath the same Kaapvaal traverse line in 2 time slices. This is measured using geochemical parameters of mantle-derived garnets carried to the surface in Group II kimberlites (upper panel) at around 150 Ma; the lower panel shows analogous results for garnets from Group I kimberlites (at around 90 Ma). Hotter colours show higher metasomatic intensity: the most highly metasomatised regions for the younger traverse (lower panel) coincide with regions of higher conductivity (lower resistivity).

Implications for metallogeny

Magma-related ore systems form economic deposits that underpin our human civilisation. The magmas related to metallic element redistribution derive from the asthenosphere, then traverse and interact to varying degrees with the subcontinental lithospheric mantle. The evolution of the original Archean lithospheric mantle has been the single largest influence on the formation of most of Earth's ore deposits (*CCFS publication #207*):

- the high degree of buoyancy of this ancient SCLM relative to the asthenosphere, results in the persistence today of low-density, rheologically coherent Archean domains and commonly, the preservation of old crustal (or at least lower-crustal) domains;
- the enduring (and volumetrically dominating) Archean lithospheric mantle domains are a reservoir for metasomatic enrichment over their long history, creating a potentially metallogenically-fertile mantle impregnated with critical elements (e.g., Au, Cu, Ni and PGEs; Fig. 3)
- the formation of Archean cratons provided an architectural mantle-scape of regions with contrasting rheology, composition and thickness. These cohesive Archean domains direct magma and fluid pathways around their margins and along old sutures between blocks, and may act as both sinks and sources for ore-forming elements depending on the geodynamic evolutionary stage;
- if the first stabilisation of lithospheric mantle at 3.0-3.5 Ga signalled the end of a mantle overturn regime (either uniquely, or intermittently with subduction), then this is when long-lived tectonic regimes conducive to mineralising systems (e.g., back-arc basins, passive margins, cratonic boundaries) became available (*http://ccfs.mq.edu.au/AnnualReport/13Report/ResHigh.html#GLAM*).

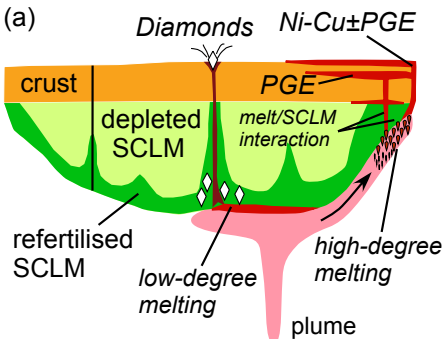

Figure 3. Interactions between magmas and the base and edges of cratonic roots. Plume magmatism triggers kimberlite formation and flows to areas of thinner SCLM where melting is focused. Variable interaction of melts with crust and SCLM influences Ni-Cu and PGE deposit genesis. Lithosphere-scale discontinuities and zones of weakness can focus the locus of kimberlite eruption. (Adapted from CCFS publication #207)

This project is part of CCFS theme 2, Earth's Evolution, and contributes to understanding Earth's Architecture and Fluid Fluxes.

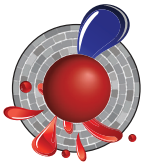

Contact: Sue O'Reilly
Funded by: CCFS Flagship Program 1

A piece of America lingers in northern Australia: Legacy of the 1.6-billion-year-old supercontinent Nuna

Throughout Earth's 4-billion-year history, as continents have shifted around the globe, they periodically have amalgamated to form supercontinents. Most recently this occurred about 300 million years ago to form the supercontinent Pangea, in which the southern continents (Africa, South America and Australia and Antarctica) were connected to Eurasia and North America. We now recognise that an earlier supercontinent termed Nuna formed about 1.6 billion years ago. Although previous researchers have speculated that north-east Australia was near North America, Siberia, or North China within the framework of Nuna, solid evidence has been hard to find.

Approximately two thirds of the Australian continent consists of basement rocks older than 600 million years. In North Queensland, rocks 1.7 billion years old are found in Mt. Isa and 500 km away in the Georgetown region. New sedimentological field data, in conjunction with new and existing geochronological data from both regions, have revealed an unexpected component of the Australian continent. As expected, Mount Isa rocks show strong resemblances to known Australian basement rocks. However, the age spectra of zircons from sedimentary rocks in the Georgetown area (Fig. 1) revealed signatures previously unknown in Australia. Instead, they show strong resemblance to spectra from sedimentary rocks in present-day Canada, sourced from American basement rocks (Fig. 2).

The simplest explanation for our findings is that 1.7 billion years ago, when the Georgetown rocks were deposited in a shallow sea, the area was part of North America. It was then rifted away from North America, and only collided with the Mt Isa region of northern Australia at around 1.6 billion-years ago when almost

Figure 1. Current ripple laminations in fine to medium grained sandstone sedimentary rocks in Georgetown indicate ancient shallow marine environments. Our data shows these sediments were deposited off the coast of North America adjacent to present-day Canada, and later transferred to Australia.

all continents on Earth at the time assembled to form the Nuna supercontinent (Fig. 2). When Nuna broke apart some 300 million years later, the Georgetown area remained permanently stuck to Australia.

In Mount Isa we find evidence of mountains being built as Georgetown collided with the rest of Australia. Interestingly, this mountain belt, in contrast to the Himalayas, would not have been as large. To explain this, we have evoked a double-sided subduction model. Another possibility is that the Earth during this period was hotter and was unable to support the immense mountain belts we see on the modern Earth.

This project is part of CCFS theme 2, Earth's Evolution, and contributes to understanding Earth's Architecture.

Contacts: Adam Nordsvan, Zheng-Xiang Li, Earth Dynamic Research Group, Curtin University
Funded by: ARC Laureate Fellowship ZX Li, Curtin University scholarship AR Nordsvan

See *CCFS publication #1043* (https://doi.org/10.1130/G39980.1)

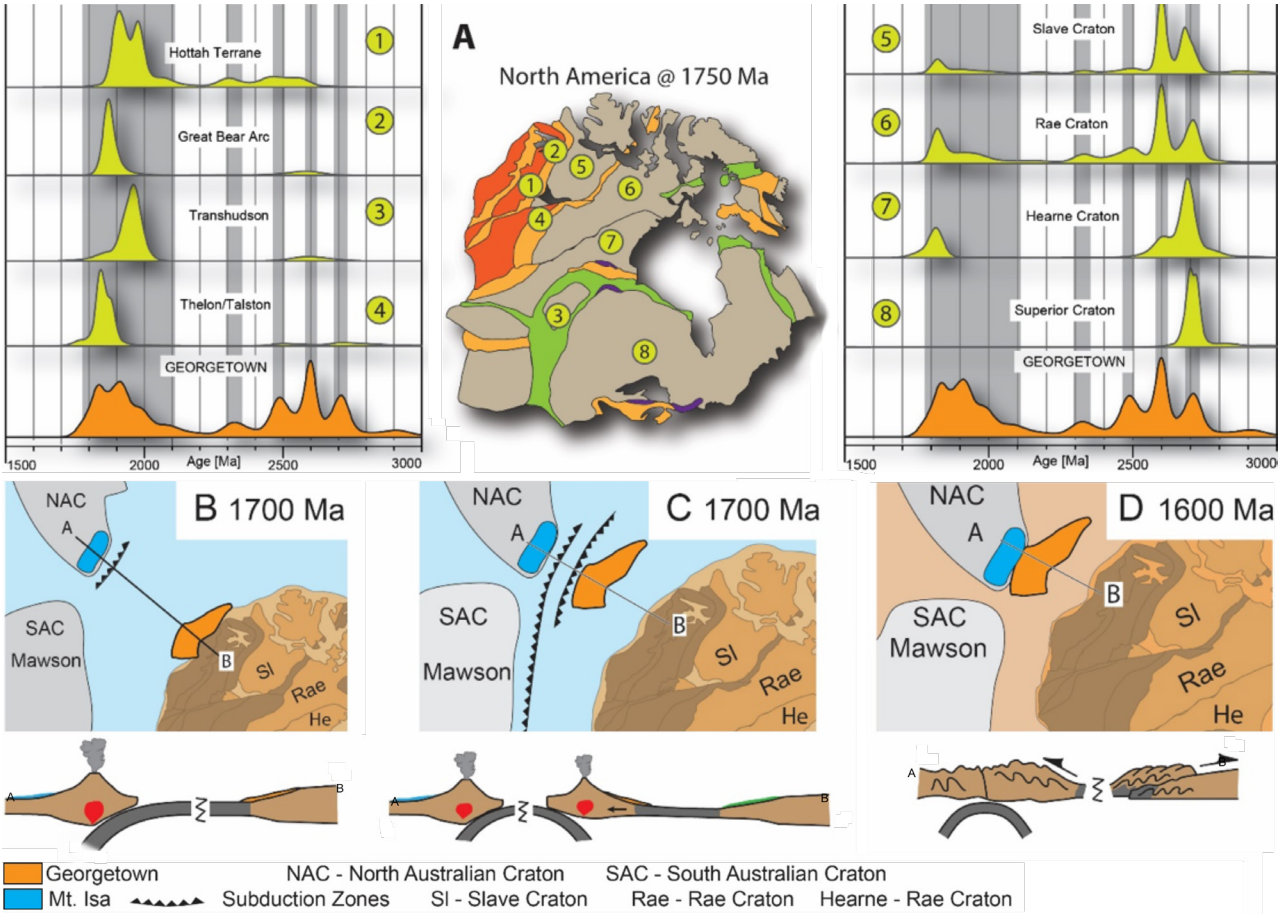

Figure 2. A) Detrital zircon spectra from the Georgetown sediments have multiple overlaps with magmatic ages from North America, suggesting an ancient link. B) Sediments now in Georgetown (orange) are believed to have been deposited off the coast of North America. C) An east-dipping subduction system caused Georgetown to be rifted away from North America about 1.7 billion years ago. D) Roughly 100 million years later, the Georgetown block was accreted to north-eastern Australia, and has stayed there ever since. This Australia-Antarctica-North America unification by ~1600 Ma signifies the completion of the assembly of Nuna.

Buoyant Ni-Cu-PGE-bearing magmas trapped deep in continental crust

The formation of magmatic Ni-Cu-PGE ore deposits depends on the ascent of high-degree partial melts from the mantle into the crust. Such deposits are commonly found along crustal-scale discontinuities that provide favourable pathways for mantle-derived magmas, such as translithospheric faults, sutures and rifts (*CCFS publication #207*). While this association has been demonstrated at the scale of tectonic plates, the mechanisms that govern magma flux within these zones of favourable structure remain poorly understood. Particularly little is known about the emplacement of ore-forming magmas in the deep crust because access to crustal roots is limited.

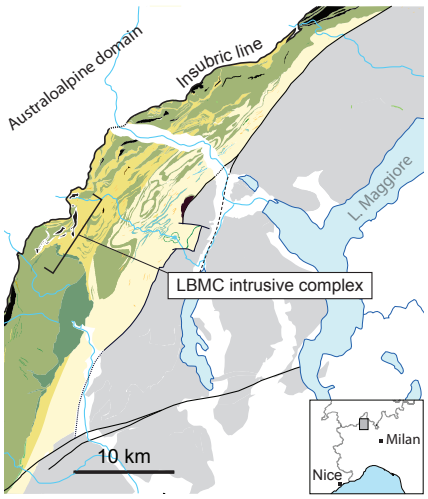

Figure 1. Generalised geologic map of the Ivrea Zone, showing the location of the LBMC intrusive complex within a section of lower continental crust that is tilted steeply SE, exposing amphibolite- to granulite-facies metasedimentary rocks (yellows) that are interleaved and intruded by mafic and minor intermediate igneous rocks (green).

The Ivrea Zone in the NW Italian Alps (Fig. 1) is a natural laboratory to examine mechanisms of magma ascent and arrest near translithospheric structures. Exhumation and tilting of continental crust has exposed a suite of mineralised mafic and ultramafic intrusions, the La Balma-Monte Capio (LBMC) intrusive complex, emplaced into host rocks at a paleodepth of 20-30 km. Collectively, these rocks preserve a continuous cross section of lower- to middle crust adjacent to a long-lived tectonic boundary between the Europe and Adria plates. The mineralised suite comprises several elongate ultramafic bodies, with a cumulative width of at least 9 km and thickness of 400 m, that are inferred to be the products of *in situ* differentiation of a high-Mg magma. Recent high-precision geochronology has revealed the mineralised bodies were emplaced at 200 Ma, overlapping with the onset of rifting at the plate boundary, and considerably later than the crystallisation of the host rocks.

A key finding is that the LBMC intrusive complex was emplaced at a rheological transition in lower continental crust, where granulite-facies gabbro is overlain by a package of paragneiss

Marco Fiorentini examines intrusive relationships between Ni-sulfide-bearing peridotite (bottom) and gabbros (centre) near the roof of the LBMC igneous complex (Photo: Greg Dering).

of similar metamorphic grade. Differences in bulk composition and mineralogy between the gabbros and overlying gneisses produce a significant density contrast at this transition. To evaluate the role of this pre-existing density contrast in trapping mafic and ultramafic magmas in the lower crust, we produced a 1D density model of the lower Ivrea Zone crust. The model incorporates published bulk densities for gabbros (n=40) and overlying granulite-facies gneisses (n=17). Densities were calculated for a range of estimated primary melt compositions (n=13) for the LBMC igneous complex, using Gibbs Free Energy minimisation and thermodynamic modelling based on empirically determined P-T parameters and the PerpleX software.

The results showed a significant range of overlapping densities at fixed P-T conditions for each of the three modelled components. Because this variation is the result of measured bulk rock compositions, it is probably representative of the natural variation in density within the lower crust. The mean calculated density of the La Balma parental melt (2810 kg/m^3) is less than the mean densities of both the footwall gabbros (3190 kg/m^3) and hanging wall felsic gneisses (2990 kg/m^3). Model results (Fig. 2) show that there is a 2.9-8.5% likelihood that estimated parental melt matches the calculated footwall

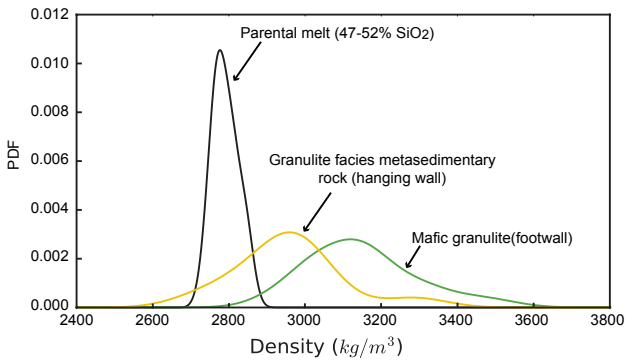

Figure 2. Kernel-density estimation for modelled physical densities of host rocks and parental melt compositions from the Ivrea Zone. The wide range of rock densities modelled for both metasedimentary and mafic granulites reflects heterogeneity in bulk composition found throughout the Ivrea Zone.

gabbro densities, and a 24.6% probability that bulk rock densities match those of the felsic wall gneisses. These results show that an emplacement scenario in which neutral buoyancy plays a role is only significant within areas characterised by particularly low-density granulite. In most scenarios covered by the model, parental melts maintain an internal vertical driving force that would be expected to carry the magma to significantly shallower crustal levels. The fact that the LBMC intrusive complex, and associated Ni-sulfide mineralisation, lies at this surprisingly deep level suggests that the internal buoyancy force of magma can be counteracted by mechanical and/or stress barriers over length scales of kilometres. Seismic velocity profiles indicate such physico-chemico transitions to be a relatively common feature of continental crust, particularly in extended terranes. Consideration of lower-crustal composition and structure should be incorporated into conceptual models of magma transport close to tectonic sutures; such models have historically emphasised sub-vertical pathways.

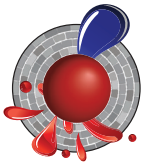

This project is part of CCFS theme 3, Earth Today, and contributes to understanding Earth's Architecture and Fluid Fluxes.

Contacts: Gregory Dering, Marco Fiorentini, Christopher Gonzalez, Jonathan Munnikhuis
Funded by: CCFS Flagship Program 2

Monitoring the evolution of gold-bearing fluids

$\Delta^{33}S$ anomalies ($\Delta^{33}S > \pm 0.2‰$) were formed in the Archean, largely through mass independent fractionation of sulfur isotopes (MIF-S) in an oxygen-poor atmosphere, and imparted to the Archean supracrustal rock record (as MIF-S). This indelible MIF-S0 signature can be used to trace sulfur pathways to orogenic gold deposits. Through this recycling process, the original MIF-S signal ($\Delta^{33}S \neq 0‰$) may be diluted by mixing between sulfur reservoirs to such an extent that it becomes undetectable ($\Delta^{33}S = 0 \pm 0.5‰$). In such cases, interpretation of the geological significance of such isotopic signatures may be compromised, mass-dependent isotopic fractionation of sulfur isotopes (MDF-S, recorded as $\delta^{34}S$) can yield small $\Delta^{33}S$ values (±0.2‰), often owing to biological reactions involving sulfur.

In this project, we have reassessed the quantification of $\Delta^{33}S$ due to MDF-S from the traditionally accepted 0±0.2‰ value (*Farquhar and Wing, Earth Planet Sci Letters, 2003*), and demonstrated that its magnitude is not constant but rather is directly linked to the degree of $\delta^{34}S$ fractionation. The analysis of these results and of a data compilation from ~2.65 Ga orogenic gold deposits of the Yilgarn Craton indicates that $\Delta^{33}S$ values are too large to be the result of purely MDF-S processes; at least some of the sulfur must be derived from Archean sedimentary rocks. A compilation of >3400 $\Delta^{33}S$ measurements of Archean sedimentary rocks shows highly variable positive and negative signals, whereas the gold deposits have remarkably constant $\Delta^{33}S$ values between 0 and +0.6‰. This strongly suggests that the auriferous fluids equilibrated at depth by mixing sulfur from Archean sedimentary rocks with sulfur from a reservoir with no MIF-S signature. These outcomes significantly enhance the power of MIF-S ($\Delta^{33}S$) as a tracer of sulfur pathways through the lithosphere.

Orogenic hydrothermal gold systems often show a large spread in $\delta^{34}S$ because sulfur isotopes are sensitive to changes in pH, *P, T,* fO_2, fS_2. We are focusing on harnessing this variation in a spatially and temporally constrained hydrothermal architecture to understand the precipitation mechanisms of metals carried in fluids. By monitoring the isotopic evolution of a hydrothermal fluid in space and time, we can better understand the changes in thermochemistry that lead to metal precipitation from a fluid, and apply this as a vector toward mineralisation. For example, at the 6 Moz Waroonga orogenic gold deposit of the Yilgarn Craton, both $\Delta^{33}S$ and $\delta^{34}S$ have been used to document that the source of sulfur in the system remained constant. The sulfide chemistry suggests that Au precipitation was driven by an abrupt change in the redox state of the ore fluid (captured in the $\delta^{34}S$ values of the mineralisation sequence).

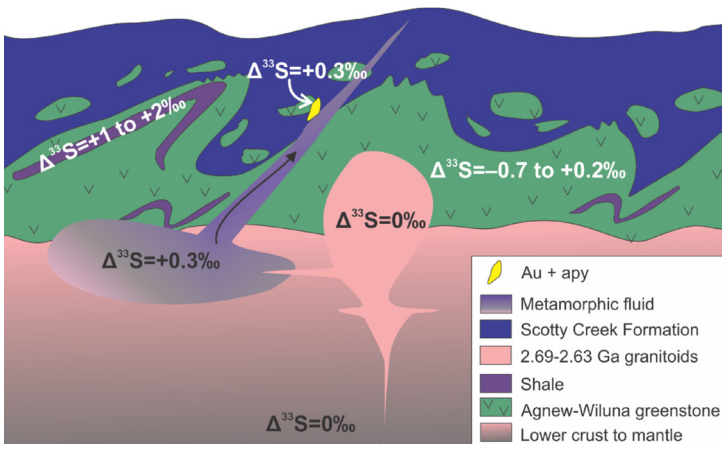

Figure 1. Schematic model demonstrating hypothesised sulfur reservoirs for Archean orogenic gold deposits in the Yilgarn Craton.

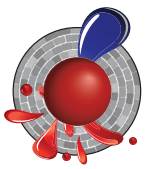

This project is part of CCFS theme 2, Earth's Evolution, and contributes to Understanding Earth's Architecture and Fluid Fluxes.

Contacts: Crystal LaFlamme, Nicolas Thebaud, Dennis Sugiono, Marco Fiorentini, Stefano Caruso, Heejin Jeon, Vikraman Selvaraja
Funded by: MRIWA

Southwestern Africa on the burner

Cenozoic volcanism is widespread in Africa; prominent examples are the Eastern African Rift System (EARS), the Cameroon Line, Darfur, Hoggar, Tibesti and the Moroccan Atlas (Fig. 1). The magmas commonly are derived from the mantle and range from carbonatitic and mafic alkaline to differentiated silica-rich magmas. A profound lithospheric control on intraplate volcanism is indicated by 1) association of volcanism with terrane boundaries and/or thin lithosphere; 2) cyclicity of magmatic activity in the same regions over >100 Myr; 3) synchronicity across the African plate; and 4) absence of clear age progression patterns. Conversely, a major role for mantle convection is supported by the coincidence of Cenozoic volcanism with regions of lithospheric uplift, positive free-air gravity anomalies and slow seismic velocities. With evidence for tectonic, lithospheric and convective controls, the ultimate trigger(s) of mantle-derived Cenozoic intraplate volcanism in Africa remains unresolved.

To improve constraints on the genesis of African volcanism, we and our colleagues at the University of Melbourne, Tasmania, Barcelona (Spain) and Luanda (Angola) have documented the age and isotopic composition of the Catanda Volcanic Complex (Figs 1 and 2), which hosts the only extrusive carbonatites in Angola. Apatite (U-Th-Sm)/He and phlogopite $^{40}Ar/^{39}Ar$ ages of Catanda lavas indicate eruption at ~500–800 ka (Fig. 3), >100 Ma after emplacement of abundant kimberlites and carbonatites in this region. The young age of the Catanda lavas is consistent

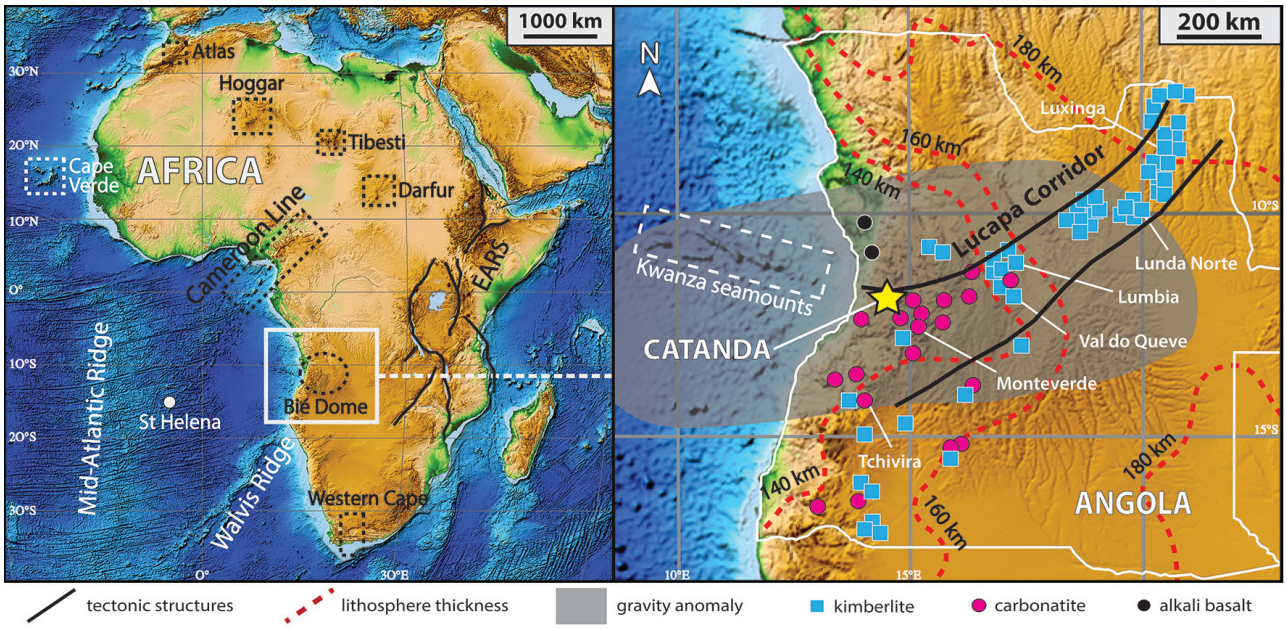

Figure 1. Elevation map of the African plate with inset showing location of the Catanda Complex and major Triassic and Cretaceous kimberlite, carbonatite and alkali basalt occurrences. Grey shaded area indicates free-air, crust-corrected gravity anomaly. Dashed red lines are estimates of the lithospheric thickness.

Figure 2. View of the Catanda Volcanic Complex (Angola).

with other evidence for recent volcanic and geothermal activity in the area, including well-preserved volcanic landforms (Fig. 2) and ongoing hydrothermal activity. These observations imply a recent resumption of volcanic activity in western Angola, some 90 Ma after emplacement of mafic alkaline dykes in the area. The lavas share HIMU-like Sr-Nd-Pb-Hf isotope compositions with other young mantle-derived volcanics from Africa (e.g., Northern Kenya Rift; Cameroon Line).

The position of the Catanda complex in the Lucapa corridor (Fig. 1), a long-lived extensional structure, coupled with recent seismic activity in the Catanda area suggests a possible tectonic trigger for the volcanism. The complex is also located on the Bié Dome (Fig. 1), a broad region (~1000 km in diameter; ~2500 m of elevation) of rapid Pleistocene uplift attributed to mantle upwelling. Seismic-tomography models indicate convection of deep hot material beneath regions of active volcanism in Africa, including Angola and northern Namibia. The rapid Pleistocene uplift, the occurrence of positive free-air gravity anomalies (Fig. 1), seismic tomography and mantle convection models all support active mantle upwelling beneath the area and make a purely tectonic trigger for mantle-derived magmatism unlikely. We suggest that rapid uplift of the Bié Dome and attendant Catanda carbonatitic volcanism in the Pleistocene might be related to a finger-like low-velocity structure, a branch of the South African Superplume that is rising beneath southwestern Africa. Thinned lithosphere beneath the Lucapa corridor and especially its western sector (Fig. 1) would provide a preferential pathway for focusing mantle upwelling.

While the Catanda complex and other expressions of late Cenozoic intraplate volcanism in Africa (e.g., EARS, Cameroon Line, Darfur, Hoggar, Tibesti, Moroccan Atlas) correlate with pre-existing lithospheric discontinuities, they also show evidence of being affected by active mantle upwelling. Therefore, intraplate carbonatitic and alkaline magmatism probably results from the complex interplay between multi-scale mantle convection and pre-existing lithospheric structures.

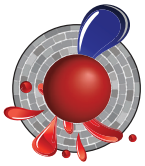

This project is part of CCFS theme 2, Earth's Evolution, and contributes to understanding Earth's Architecture and Fluid Fluxes.

Contacts: Andrea Giuliani, Juan Carlos Afonso
Funded by: ARC DECRA

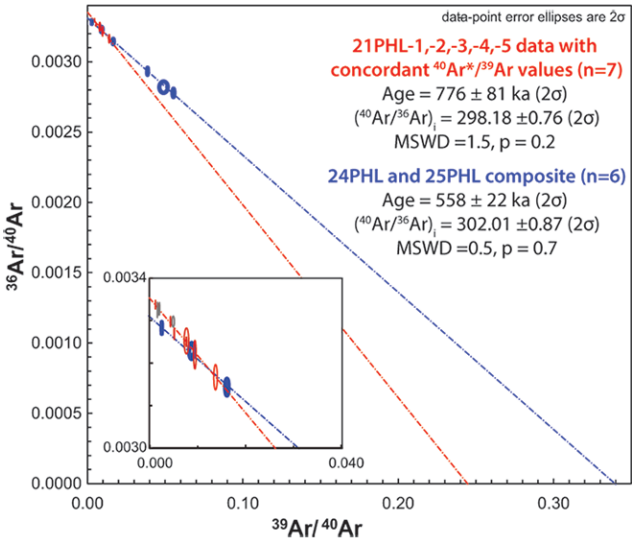

Figure 3. $^{40}Ar/^{39}Ar$ phlogopite inverse isochrons providing ages for the Catanda lavas.

A trapped fossil oceanic slab in NW China

The fate of subducted oceanic slabs can provide important clues to plate reconstruction through Earth history. However, an ancient oceanic slab, stalled in the lithosphere at the end of subduction, is unlikely to be well-preserved for long, due to the subsequent tecto-thermal events (magmatism in particular). The western Junggar region, situated in NW China (Fig. 1), is an ideal place to study the evolutionary history of the Central Asian Orogenic Belt (CAOB). This region is characterised by Paleozoic ophiolites, volcanic rocks and many valuable Cu-Au ore deposits, along with three large-scale NE-striking faults, the Hatu, Karamay-Urho and Darbut faults (Fig. 1). Particularly along the more than 200-km-long Darbut Fault and the hidden Karamay-Urho Fault, lenses of ophiolitic mélanges crop out. Extensive Late Paleozoic magmatism and deformation occurred in this region and across the entire CAOB. The tectonic origin of the western Junggar is believed to be related to either intracontinental or intra-oceanic arc-related subduction systems which developed in the early Paleozoic and ended in the late Paleozoic. However, the mode of subduction is still contentious. Based on geological and geochemical studies, several competing models of the subduction have been proposed, including northwestward subduction, a double-sided subduction and subduction of an oceanic ridge. These different models would predict different crustal structure. Thus, imaging the crustal structure at high resolution may help to discriminate among the competing models.

We have generated a shear wave velocity model of the crust in western Junggar based on data from an array of 31 portable broadband seismic stations. According to our model, large Vs contrasts are observed in the shallow crust between the Junggar basin and the Zaire mountain, with the boundary following the hidden Karamay-Urho Fault (K-U fault). Low-Vs anomalies dominate the upper crust beneath the Junggar basin with the velocity varying from ~1.5 km/s in the surface to ~3.0 km/s around 10 km depth. To the northwest of the K-U Fault, relatively high S-wave velocities (>3.5 km/s) are seen in the upper crust

beneath the Hongshan and Karamay intrusions. At depths of ~20 km, the patterns of shear velocities anomalies are very different from those in the upper crust. Very high S-wave velocities (3.7-4.1 km/s) occupy most of the area beneath the Junggar basin (Fig. 1c).

In our velocity model the body with high shear-wave velocity is nearly flat beneath the western Junggar basin and dips gently northwestward. This geometry probably reveals a SE-to-NW fossil subduction beneath the western Junggar, consistent with the interpretation of MT results (Xu et al., 2016). It appears that a fossil subducting oceanic slab and an intra-oceanic arc system are well preserved in the Darbut belt. The interpretation of the high velocity body as a remnant oceanic plate is also supported by our CCP imaging as shown in Fig. 2, where a clear Moho offset is visible slightly to the right beneath the Karamay-Urho fault. This Moho offset is likely to associated with the paleo-subduction interface, and the K-U fault can be interpreted as one of the major thrust faults separating the arc from the accretionary prism in the southeast. The zone without high velocities, between the western Junggar basin and the Zaire mountains, can be interpreted as the forearc accretion wedge, corresponding to the depression of the Moho interface. The distribution pattern of S-wave velocities strongly supports the model of a subduction zone which failed to be underthrust during the late Paleozoic and has been preserved ever since.

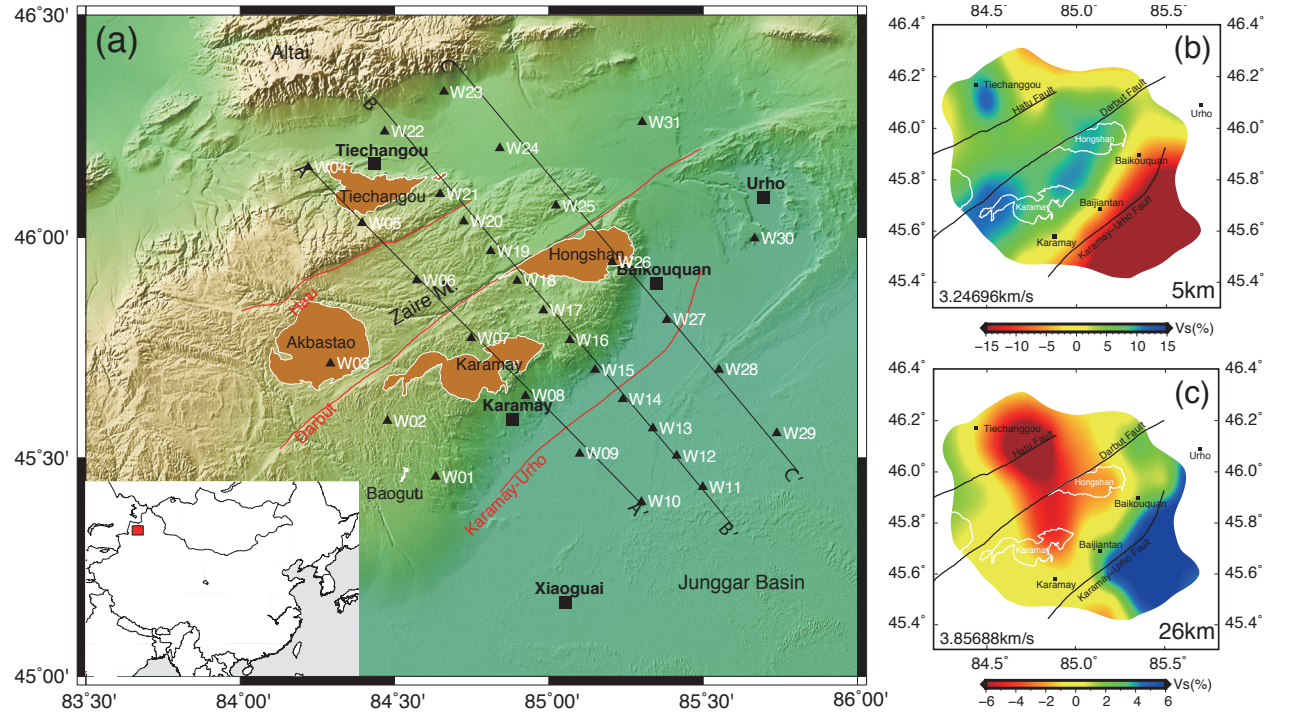

Figure 1. (a) Tectonic setting of the western Junggar region. The red lines indicate three major faults, black triangles indicate the locations of seismic stations, and the orange areas represent major intrusions. (b) and (c) S-wave velocity anomaly maps at 5 and 26 km depth from surface wave tomography with reference velocity of 3.247 km/s and 3.857km/s, respectively.

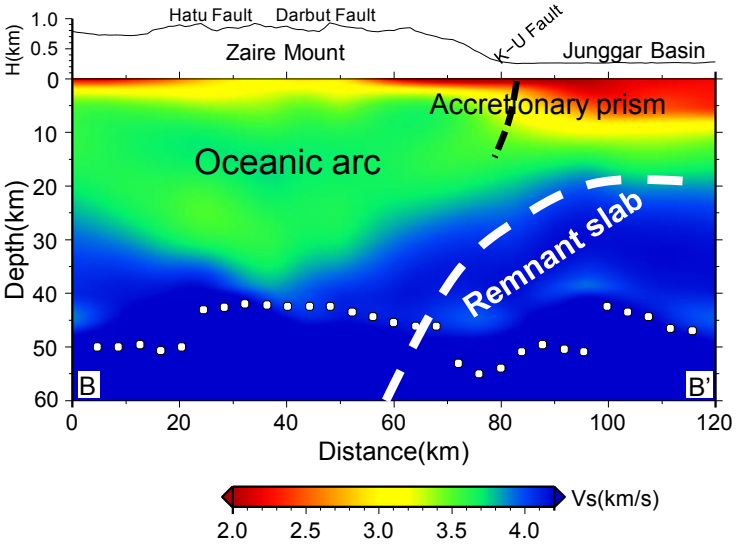

Figure 2. Vertical cross-section of S-wave velocities and our interpretation of a well-preserved fossil oceanic slab along BB' shown in Figure 1a.

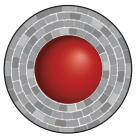

This project is part of CCFS theme 3, Earth Today, and contributes to understanding Earth's Architecture.

Contacts: Shucheng Wu, Yingjie Yang
Funded by: NSFC 41530319 and 41374079, CCFS Flagship Program 3

Distinctive aberrant geochemical fingerprints for Ancient SCLM in collision zones

Pyroxenites are more abundant in the lower crust of volcanic arcs and in sub-arc mantle than in most other mantle tectonic environments. The petrological processes responsible for their formation and evolution may play a key role in the development of chemical and isotopic heterogeneities in the mantle. However, their contribution has remained poorly constrained due to their complex petrogenesis and the uncertainty about the extent of their recycling. In the Cabo Ortegal Complex, Spain (Fig. 1A), abundant pyroxenites, associated with dunites and harzburgites, have formed by fractional crystallisation and melt/peridotite interaction after picritic and/or boninitic melts (Fig. 1B, C), probably in a sub-arc mantle.

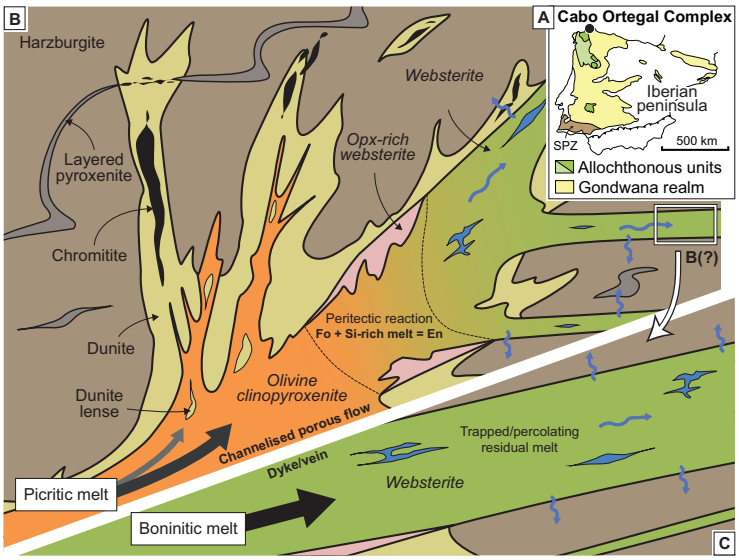

Figure 1. Location of the Cabo Ortegal Complex in the Variscan belt of the Iberian Peninsula (A) and conceptual petrogenetic model for Cabo Ortegal pyroxenites, dunites and chromitites, assuming an initially picritic (B) and boninitic melt (C).

Based on the availability of a robust tectonothermal, petrologic and geochemical background, we have applied Lu-Hf and Re-Os isotopic systematics to clinopyroxene, amphibole, and whole-rock samples from Cabo Ortegal pyroxenites and associated peridotites and chromitites. Our data show that the pyroxenites are characterised by uncorrelated $^{176}Lu/^{177}Hf$ and $^{176}Hf/^{177}Hf$ (0.2822-0.2855) and a wide range of $^{187}Re/^{188}Os$ and $^{187}Os/^{188}Os$ (0.16-1.44).

While Sm-Nd geochronology indicates that the pyroxenites probably formed during Cadomian arc magmatism (421-762 Ma), strikingly decoupled Nd- and Hf-isotope compositions (Fig. 2) along with EM I-like Sr and Nd signatures ($^{87}Sr/^{86}Sr_{(t)}$ = 0.7037-0.7045 and $\varepsilon_{Nd(t)}$ = 0.3-7.5) suggest a contribution from the sub-continental lithospheric mantle (SCLM), probably during the development of the arc on a continental margin. This is in good agreement with old Hf and Os (T_{MA}) model ages, and Re-Os (0.6-1.0 Ga) and Lu-Hf (1.1 Ga) isochron ages. In addition, cpx and amphibole exhibit a slight disequilibrium in terms of Hf isotopes, indicating a partial resetting of the system during amphibolitisation and the multi-stage nature of this process. Some amphibole growth is ascribed to the exposure of sub-arc mantle to a Devonian subduction zone, probably leading to sub-solidus reactions under granulite- to amphibolite-facies conditions, and to the remobilisation of Re, as evidenced by correlations between amphibole content, LREE enrichment and $^{187}Re/^{188}Os$.

Despite these isotopic perturbations, we show that different sections of a progressively LREE-enriched sample *preserve apparent Sm-Nd, Lu-Hf and Re-Os isochrons* that predate metamorphic amphibolitisation. This may reflect a relatively short distance of isotopic equilibrium arising from differential elemental and isotopic diffusivities during melt transport. We suggest that this transient phenomenon may be characteristic of (pyroxenite-forming) melt-peridotite interactions during the reworking of old continental lithosphere by arc magmatism. The recycling of arc pyroxenites may thus potentially account for the ubiquitous observation of decoupled Hf and Nd isotopes in the lithospheric mantle, consistent with the extensive preservation of Archean SCLM.

This project is part of CCFS themes 2 and 3, Earth's Evolution and Earth Today, and contributes to understanding Earth's Architecture and Fluid Fluxes.

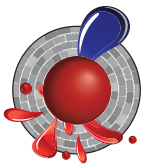

Contact: Romain Tilhac, Georges Ceuleneer (Géosciences Environnement Toulouse, GET, France), Sue O'Reilly, Bill Griffin

Funded by: CCFS Flagship Program 1

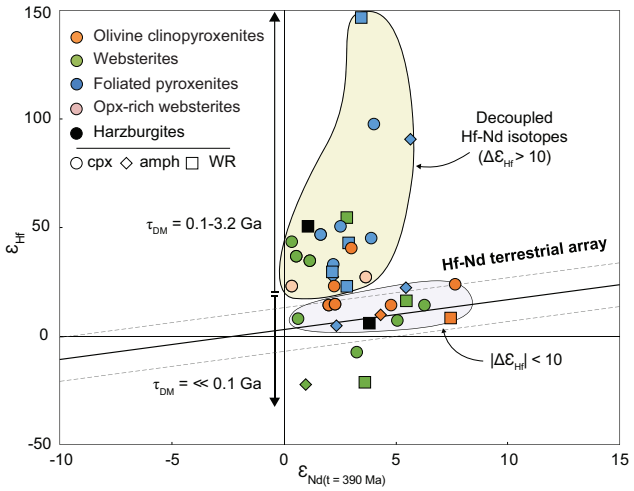

Figure 2. Decoupled Hf-Nd isotopes measured in Cabo Ortegal pyroxenites. $\Delta\varepsilon_{Hf}$ corresponds to the vertical distance to the terrestrial array in ε notation; corresponding Hf model ages (T_{DM}) are also shown.

Crustal Evolution of the Albany-Fraser Orogen

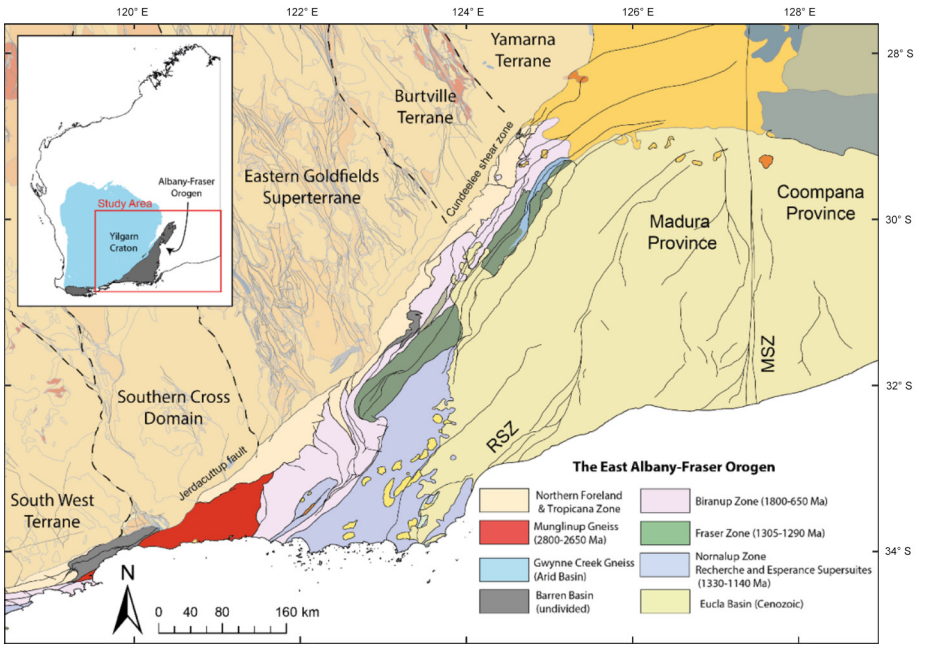

Figure 1. Geological Map of the Albany-Fraser Orogen showing the location of the study area.

The Albany-Fraser Orogen is a NE-SW trending Paleoproterozoic to Mesoproterozoic orogenic belt that lies wraps around the southern margin of the Yilgarn Craton (Fig. 1). Previous interpretations of the tectonic setting of the Albany-Fraser Orogen invoked the accretion of exotic or suspect terranes, but recent U-Pb geochronology, whole-rock geochemistry, Hf -and Nd-isotopic datasets have radically refined our understanding of the orogen. Recent work suggests that the Albany-Fraser Orogen contains no exotic components but formed through the episodic addition of juvenile magmas into the existing Archean crust of the Yilgarn Craton, in a series of events that overprinted but did not obliterate the original Archean signature.

Heterogeneity in the composition of granitic magmas is influenced by both large-scale lithospheric architecture and magma-generation processes (both related to geodynamic setting) as well as the composition of the crustal substrate. To test the influence of these processes on magma compositions we use zircon hafnium-isotopic compositions and whole-rock geochemistry from granitic rocks associated with a period of Paleoproterozoic magmatism called the Biranup Orogeny (1730-1650 Ma). A map of the median εHf of zircons from the Paleoproterozoic magmas of the Albany-Fraser Orogen shows a similar pattern to the variation in the large-scale structure of the Yilgarn Craton (Fig. 2). Sr/Y ratios of these granitic magmas are uniformly low along the length of the orogen, implying that crustal thickness was uniformly thin (ca 15 km) along the margin of the Yilgarn craton during this period in geological time (Fig. 3).

Thus, we conclude that the heterogeneity in the composition of zircons from the granitic rocks of the Biranup Orogeny largely reflects the regional-scale heterogeneity of the Archean basement terranes that were reworked to produce the Paleoproterozoic magmas, and not by large-scale variations in

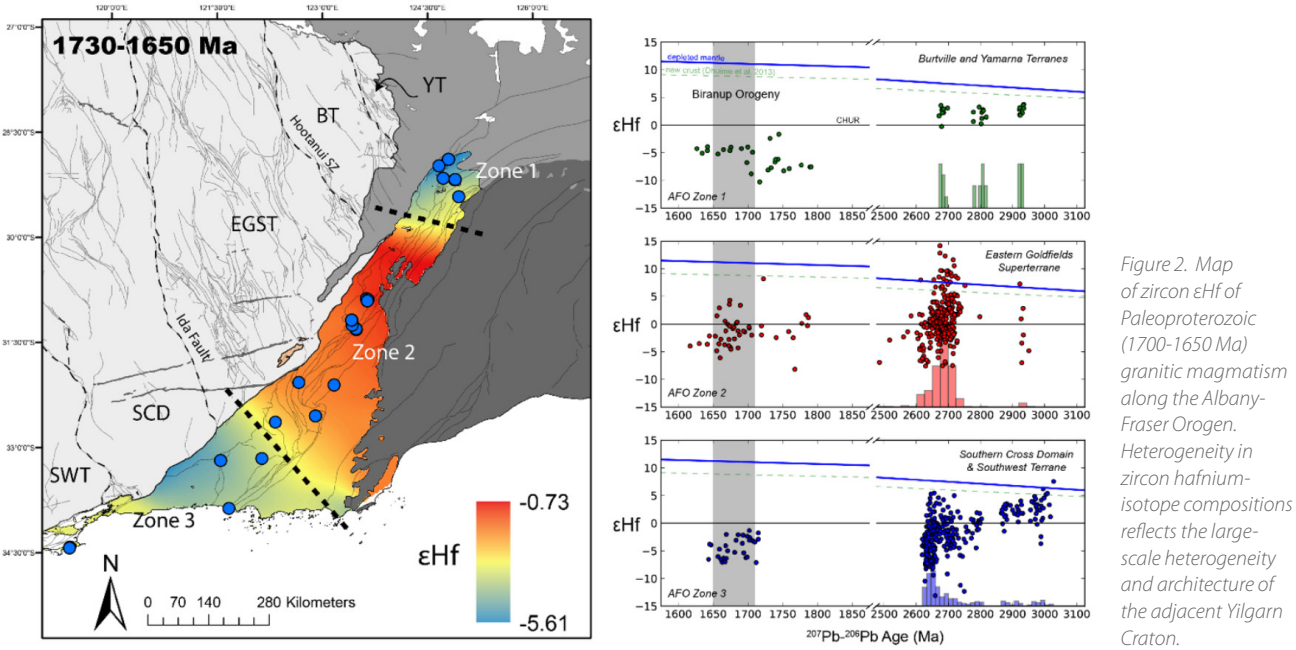

Figure 2. Map of zircon εHf of Paleoproterozoic (1700-1650 Ma) granitic magmatism along the Albany-Fraser Orogen. Heterogeneity in zircon hafnium-isotope compositions reflects the large-scale heterogeneity and architecture of the adjacent Yilgarn Craton.

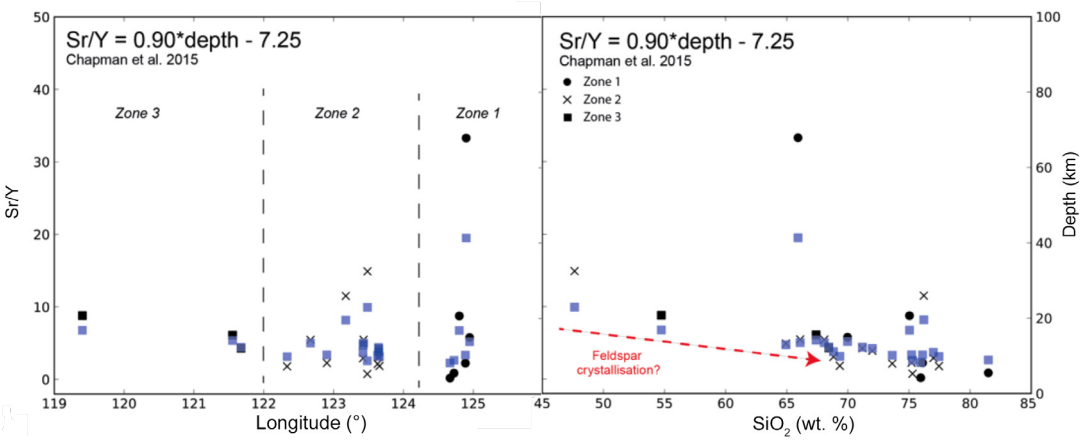

Figure 3. Plots of Sr/Y for the Paleoproterozoic magmas show uniformly low values along the length of the Albany-Fraser Orogen. This implies that crustal thickness was uniformly thin along the margin of the Yilgarn Craton during this period in time.

lithospheric architecture or crustal thickness. These data provide a means of visualising and tracking the influence of different basement terranes through space and time.

This project is part of CCFS theme 1, Earth's Evolution, and contributes to understanding Earth's Architecture.

Contacts: Michael Hartnady, Chris Kirkland, Chris Clark

Funded by: CCFS Flagship Program 7

El Dorado in El Indio Belt, Chile-Argentina

This project aimed to understand the structure of one of the most highly Au-endowed provinces of the Andes Cordillera: the Miocene El Indio Belt (EIB).

This 150 km x 100 km metallogenic camp located in the Chilean-Argentinean Andes Cordillera hosts >45 Moz Au, mostly in world-class Au-Ag epithermal deposits (Pascua-Lama, Veladero, El Indio-Tambo District and the most recent discovery, Alturas). It provides a natural laboratory to study the trans-lithospheric architecture that provided the magma/fluids/gold pathway and the architecture's geodynamic evolution related to metallogenic events.

The project is divided into several components, including surface structural mapping, geophysical (mainly magnetometry and gravity) reinterpretation, and geochemical analysis. Targeted geochronology and partial isotopic mapping (O-isotopes) using zircons help define the crustal architecture into which the Au deposits have been emplaced.

Both the Permian-Triassic granitic basement and Cenozoic intrusives or *in situ* domes (related to Au-Ag mineralisation) in Chile and Argentina were sampled for zircon analyses.

U-Pb SHRIMP-II geochronology, O-isotopes and Lu-Hf LA-ICP-MS analyses are being performed.

Preliminary results on the O-isotopes show a marked difference between zircons from Permian-Triassic basement rocks and zircons in Cenozoic magmas of the El Indio Belt. Basement zircons have high $\delta^{18}O$ (a crustal signature), and the oldest

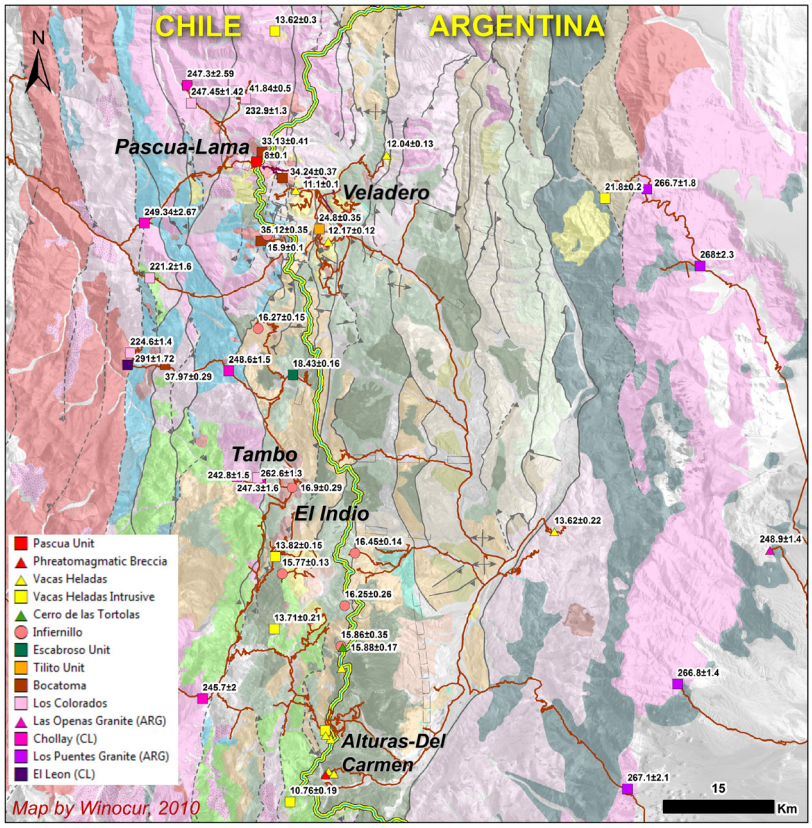

Figure 1. U-Pb zircon age of samples considered for zircon O-isotopes and Lu-Hf analyses on this project.

Fieldwork in the Argentinean Andes, El Indio Belt project (Constanza Jara).

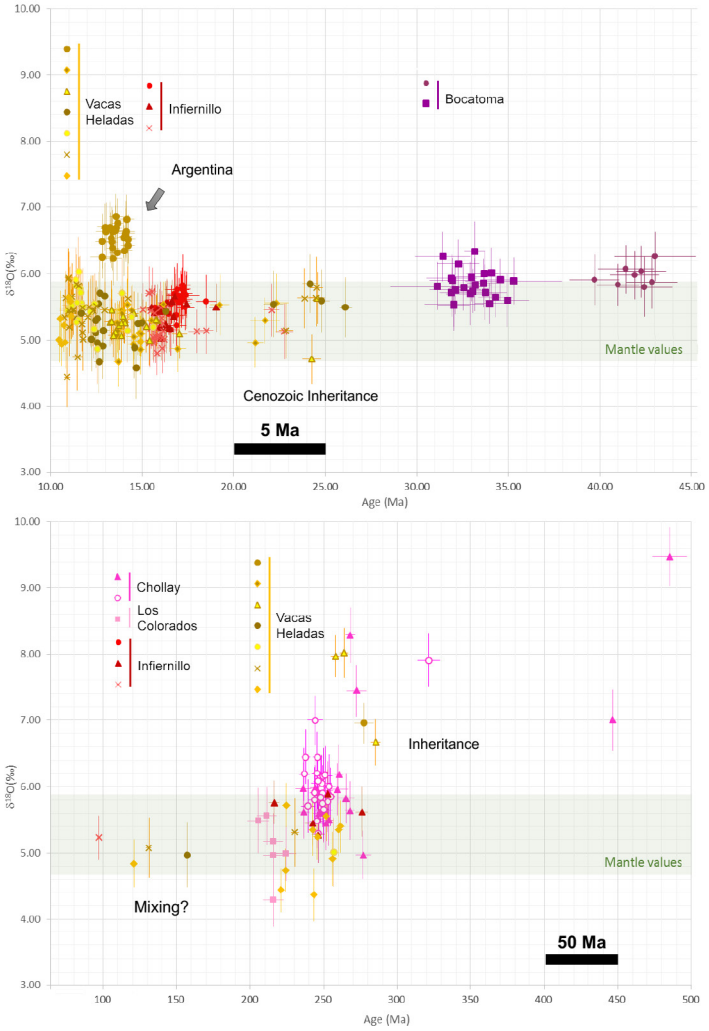

inherited cores of all samples show the highest crustal component. Zircons from early Cenozoic magmas all show a strong crustal component, but the zircon O-isotope signature becomes more mantle-like during the Oligocene to Miocene, with almost no crustal component in the later magmas.

Significant variations in age and O-isotopic signatures are observed between the E and W domains of EIB. Late magmas in the Argentinian area of the EIB show higher $\delta^{18}O$, probably indicating a greater degree of crustal involvement in the east, where the crust may be thicker and older. The preliminary data suggest a large N-S structure separates the two domains, and appears to survive the subsequent Cenozoic events.

The goals of this project are to stimulate new approaches to identifying new Au-rich provinces at early stages, by recognising key trans-lithosphere structures.

This project is part of CCFS theme 2, Earth's Evolution, and contributes to understanding Earth's Architecture.

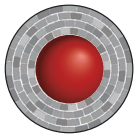

Contacts: Constanza Jara, John Miller (CSIRO), Marco Fiorentini, Heejin Jeon, Mark Fanning (ANU), Diego Winocur (UBA)

Funded by: Barrick Exploration

Figure 2. $\delta^{18}O$ vs U-Pb zircon age plot for each sample analysed spots. 10 to 500 Ma timespan, note change of timescale at 50 Ma. Error bar in 2σ.

Pyroxenite layering in the upper mantle and how to find it

Seismic waves reveal information on the interior of the Earth because their travel times reflect a complex combination of temperature, mineralogy, composition and the presence of melt or fluid along their trajectory. Because of the way minerals deform when subjected to stress, an alignment of the minerals develops during deformation and new bulk elastic properties arise. This process will give rise to a fast and a slow velocity direction for elastic waves travelling through the deformed rock (i.e., an anisotropy). Based on seismic data, seismologists can compute the anisotropy of the different seismic waves in the upper mantle domains. Their interpretation has been traditionally focused on the most volumetrically significant mineral (i.e., olivine) despite the fact that pyroxenites make up significant proportions in specific mantle domains. However, correctly understanding seismic data requires the determination of the seismic properties of a pyroxenite-rich domain to account for their effect on the resulting seismic signal. Following up on our previous research, we used the Herbeira massif, Cabo Ortegal, Spain as an example of a pyroxenite-rich domain from Earth's upper mantle. As the structure of Herbeira is not homogeneous, a new modelling protocol that incorporates the effects of this specific layered geometry was developed. This new calculation

Figure 1. Typical outcrop of layered pyroxenite in the Herbeira massif. The dark green layers (pyroxenites) alternate with brownish layers (dunites).

approach, combined with the data from Herbeira, allowed us to model a realistic supra-subduction upper mantle domain infiltrated by subduction-related melts.

The modelled seismic properties of a pyroxenite-rich domain similar to the Herbeira massif are comparable to that of common supra-subduction material (e.g., harzburgite xenoliths from the Kamchatka volcanoes) but will induce specific signal deviations in the anisotropic spectrum.

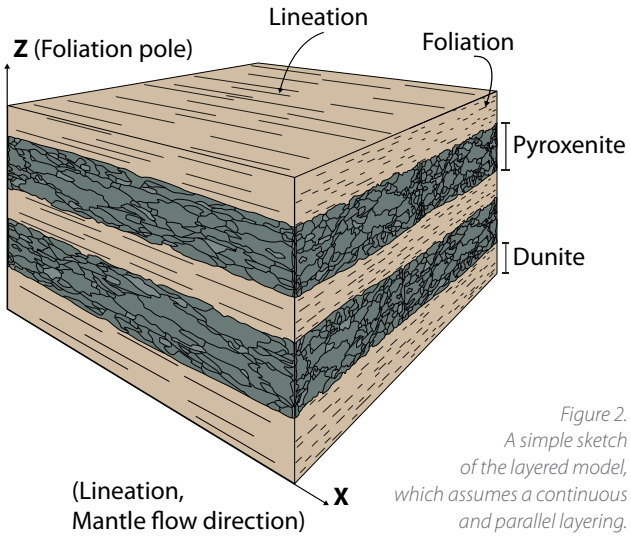

Figure 2. A simple sketch of the layered model, which assumes a continuous and parallel layering.

Along the volcanic front of subduction zones, down in the mantle wedge, a switch of the P-wave Fast-Velocity Direction (FVD) from trench-normal to trench-parallel is documented in seismic databases. Our model shows that the presence of layered pyroxenite complexes in this specific region is consistent with this large-scale observation. Although the model may not account for the whole switch, its observed sharpness could reflect the presence of pyroxenite. Large volcanic fronts can extend laterally for 200 km or more along the arc collision zone. Mantle pyroxenitic layering similar to that of Herbeira along this front, would delay P-waves travelling perpendicular to the arc strike by more than 0.4 sec, which is measurable.

We also have characterised the specific deviations that a layered pyroxenite-rich domain would have on the different shear waves and have recognised a seismic fingerprint for these kinds of domain, which potentially can be used to identify the presence of pyroxenites in subduction zones. This could be a starting point to bridge the gap between geophysical observations and isotope geochemistry in understanding the contribution of pyroxene-rich lithologies to the genesis of mantle-derived magmas in many tectonic environments, as well as potentially using seismic-velocity signatures to track paleo-subduction domains that have been infiltrated by fluids, thus forming pyroxenites.

This project is part of CCFS themes 2 and 3 and Earth's Evolution and Earth Today, and contributes to understanding Earth's Architecture and Fluid Fluxes.

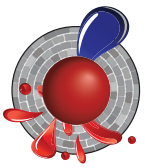

Contacts: Hadrien Henry, Beñat Oliveira, Romain Tilhac, Sue O'Reilly, Bill Griffin, Georges Ceuleneer (Géosciences Environnement Toulouse, GET, France)

Funded by: CCFS Flagship Program 1, iMQRES, EPS postgraduate funds, cotutelle program - Paul Sabatier University, CNRS

The oldest rocks formed by microbes: unexpected diversity

Microbialites are rocks produced by microbial life, and they commonly preserve fossils of some of Earth's earliest lifeforms – stromatolites. The microbialites of the 2.4 Ga Turee Creek Group, first reported in 2016, include the earliest known expression of clotted microbial growth in the rock record; clotted microbialites (or thrombolites) are preserved amongst stromatolites in a 300 m thick dolomite-carbonate reef. CCFS-funded research in 2017 has allowed for a more detailed examination, which has revealed that these clotted microbialites are far more diverse in both morphology and microtextures than previously realised.

Figure 1. Interconnected thrombolitic texture with the microbial framework (blue-grey colour, black arrows) surrounded by dolomite sand (tan colour, white arrows).

A total of three main types of clotted microbialite have been identified and described, two of which are new to the locality:

1. Clotted microbial aggregate: this texture is an aggregate of isolated fine-grained clumps of microbial carbonate, each enveloped by coarse carbonate cement, that appears to have buried stromatolites. These clumps contain preserved traces of kerogen, identified using Raman spectroscopy, which confirms their biological origin. The microbialite is not benthic but an aggregate that probably formed when clumps of microbial material settled out from the overlying water column and were rapidly cemented. This is the only clotted microbial texture that had previously been described from this locality.

2. Lobate thrombolites: these structures have the gross morphology of a stromatolite but lack internal layering. Preserved bedded sediment and marine precipitates fill the intercolumn space between individual thrombolites and indicate that primary textures have not been destroyed by diagenetic fluids; this indicates that the thrombolitic textures are also primary. These represent the earliest thrombolites with bioherm morphology, more than 400 Ma older than other examples.

3. Interconnected thrombolitic textures: these are comprised of an interconnected microbial framework of fine to medium carbonate with interstitial spaces filled by either carbonate sediment or marine cement. They are found in beds and mounds, and often have a gradational contact with stromatolitic units above and below. These thrombolites have morphologies that otherwise are only known from much younger (Neoproterozoic and Phanerozoic) rocks.

These discoveries add to the already diverse range of microbialites in the Turee Creek Group and supplement newfound diversity in deep-water microfossil communities and in problematic siliceous structures from shallow-water facies at the same locality. When considered alongside these other discoveries, the clotted microbialites of the Turee Creek Group represent just one facet of an apparent explosion in biotic complexity at 2.4 Ga, the driver of which is still under investigation.

This project is part of CCFS theme 1 Early Earth, and contributes to understanding Earth's Architecture and Fluid Fluxes.

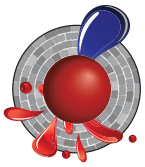

Contacts: Brendan Nomchong, Martin Van Kranendonk

Funded by: CCFS Flagship Program 4

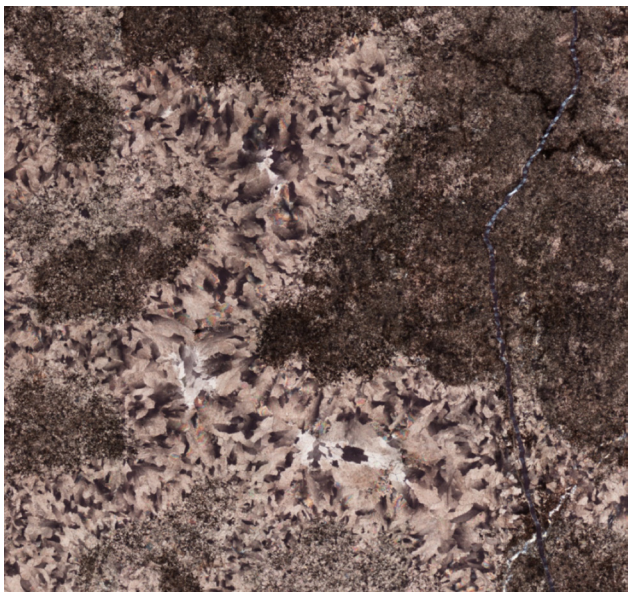

Figure 2. XPL image of interconnected thrombolitic texture. Microbial carbonate (dark, fine grained) is encased by a coarsely bladed marine cement. The microbial portion contains preserved kerogen. Image width: 1 cm.

Supercontinent Nuna formed in two stages

Figure 1. Sampling of the Hart Dolerite (low outcrop in the foreground) that intrudes the Paleoproterozoic Kimberley Group (cliff in the background) (Photo: Zheng-Xiang Li).

While there exists a general consensus regarding the configuration of the Earth's youngest supercontinent, Pangea, much uncertainty still surrounds that of arguably the oldest supercontinent, Nuna. Recent work suggests Nuna's final assembly was not completed until ca 1600 Ma, and that the preceding interval of ca. 2000-1700 Ma might represent a time when the building blocks of Nuna, including proto-Laurentia, proto-Australia and proto-Baltica, were assembled.

Current paleomagnetic constraints are still insufficient for establishing a detailed paleogeography for this assembly process. This is especially true for one of the key continent-continent connections in building Nuna, the speculated connection between western Laurentia and eastern proto-Australia. A 1976 preliminary study of the ca 1.8 Ga Hart Dolerite in the eastern Kimberley craton, north-western Australia, showed some promising results, although a subsequent study in 2008 in western Kimberly proved to be less successful. We undertook a meticulous sampling of the Hart Dolerite from the eastern Kimberley craton (Fig. 1), which yielded well defined paleomagnetic directions with dual polarities. A comparison of our resulting paleopole with other Australian poles for the period of 1800-1600 Ma indicates that proto-Australia, as a whole, underwent only very minor amounts of plate motion during that time. Our new results, along with existing data, also support the previously interpreted 40° intracontinental rotation between the North Australia and South Australia cratons during the Neoproterozoic (see *2011 CCFS Research highlight, p 16*).

A comparison of the Australian poles with that of Laurentia for the time between 1800 Ma and ~1400 Ma yielded more important findings: there are two distinct segments in the apparent polar wander paths (APWPs) of both continents for that time interval, suggesting similar movements of the two continents during these two time intervals. Comparable APWPs between 1800 Ma and 1730 Ma imply that the two continents were already close to each other then and shared similar plate motions (Fig. 2a). This was followed by a ca. 1000 km relative plate motion between them before ca. 1650 Ma, leading to the final assembly of Nuna by ca. 1600 Ma. The two continents as a core part of Nuna again shared common APWP after 1650 Ma that lasted at least until ~1400 Ma (Fig. 2b). We therefore suggest that there was a two stage assembly between Australia and Laurentia as part of the assembly of the supercontinent Nuna.

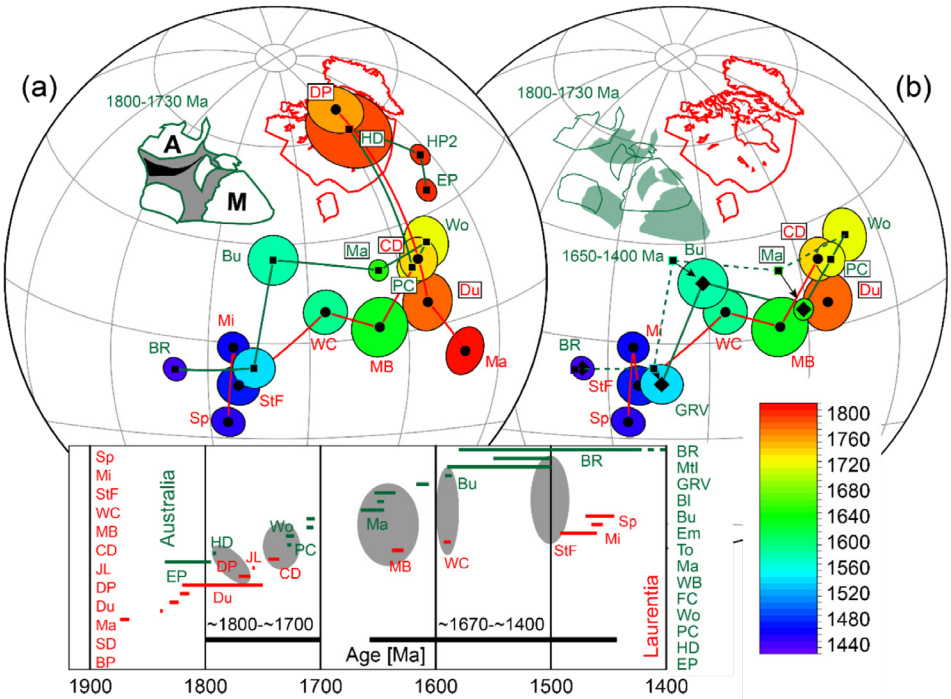

Figure 2. (a) Apparent polar wander paths of Australia (poles shown as squares and diamonds) and Laurentia (poles shown as black dots), colour coded with ages between 1900 and 1400 Ma after rotating proto-Australia to Laurentia to match their 1800-1730 apparent polar wander paths, or APWPs). (b) Proto-Australia rotated further to Laurentia, moving from the pre-1730 Ma position (green cratonic outlines) to its Nuna position after 1650 Ma (green shaded cratons), to match their APWPs for the1650-1400 Ma time interval, signalling the final assembly of the supercontinent Nuna soon after 1650 Ma.

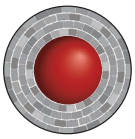

This project is part of CCFS theme 2, Earth's Evolution, and contributes to understanding Earth's Architecture.

Contacts: Uwe Kirscher, Zheng-Xiang Li
Funded by: CCFS Flagship Program 5, ARC Laureate Fellowship to ZXL, ARC LIEF grant to establish the new palaeomagnetism laboratory at Curtin University

Riding high on new wave model for southern California

Southern California, on the Pacific-North America plate boundary, is a tectonically active region where geological terranes are merged by major tectonic events during the evolution of the plate boundary. A 200-300 km wide zone of transpressive deformation (*Hauksson, 2000*) results from this interaction. These tectonic events have produced the complex 3D crustal structure of southern California, including terranes such as the Peninsular Ranges, Salton Trough, Transverse Ranges and southern Sierra Nevada Range (Fig. 1). Tape et al. (*2009, 2010*) generated a new 3-D crustal model M16 by applying adjoint tomography to a dataset of waveforms recorded at 203 stations from 143 local earthquakes. Their inversion used frequency-dependent travel-time measurements of three-component body waves and surface waves filtered at periods in the band 2-30 s.

In this study, we apply *adjoint tomography* to 5-50 s Rayleigh waves extracted from ambient noise to further improve the M16 model, especially in the lower crust. A spectral-element method was used to simulate wave propagation in M16 and successively updated the models.

The final model shows features generally in agreement with the initial model, especially at the shallowest depths (≤ 5 km). However, the new Vs model also reveals several new features in the mid-to-lower crust, including: (1) the mean speed of the lower crust is slowed down by about 6%; (2) high Vs anomalies (up to +4%) are observed throughout the crust in the Los Angeles Basin (LAB) and Central Transverse Ranges (CTR); (3) high Vs anomalies are observed in the lower crust beneath the westernmost Peninsular Range Batholith and Sierra Nevada Batholith; (4) an enhanced shallow high-velocity zone in the mid-crust is observed beneath Salton Trough Basin (STB). Our model also shows a refined lateral velocity gradient across PRB-SNB-SAF which provides constraints on the west-east compositional boundary of PRB-SNB, as well as the dip angle and the depth extent of SAF. As ambient noise cross-correlations are available between all station pairs, the new tomographic model we have obtained shows a better resolution than the initial one in areas not well-covered by event-station paths. Owing to the long-period features of ambient noise, the lower crust is much better illuminated through gradual fitting of long-period signals. The total misfit reduction, model validation from earthquake data, and a series of point-source resolution tests all confirm the robustness of our new tomographic model.

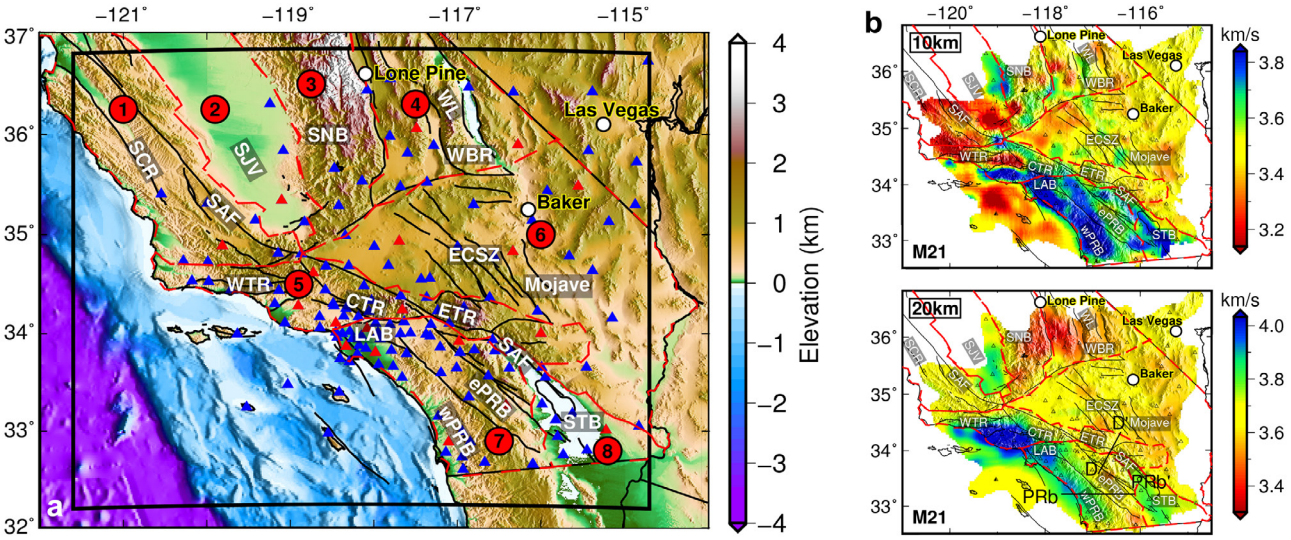

Figure 1. (a) Map of southern California with topography, bathymetry and active faults. The solid black outline defines the simulation region. The 148 stations used in this tomographic study are shown as triangles, out of which 19 are selected for the line search shown in red. Faults are indicated by bold black lines. Labels 1-8 denote eight geological provinces bounded by red dashed lines: 1. Coastal Ranges; 2. Great Central Valley; 3. Sierra Nevada; 4. Basin and Range; 5. Transverse Ranges; 6. Mojave Desert; 7. Peninsular Ranges; 8. Salton Trough. Geological features labeled in bold white letters as references for subsequent figures: SCR, southern Coast Range; SJV, San Joaquin Valley; SAF, San Andreas Fault; LAB: Los Angeles Basin; ePRB and wPRB: east and west Peninsular Ranges Batholith; SNB, Sierra Nevada Batholith; STB: Salton Trough Basin. (b) Horizontal slices of shear velocity for model M21 at 10 and 20 km.

We compared the initial model M16 and our final model M21 to two other models: one is Barak2015 from traditional ambient-noise tomography, and the other is CVM-S4.26 from a full waveform inversion of earthquake and ambient noise data. In general, the CVM-S.4.26 model contains more small-scale features than the other three models and has much higher velocities, perhaps due to the larger number of data used and iterations performed. Based on similar initial models and data sets, our final model shows velocity variations that are generally in agreement with those of Barak2015. However, our final model also differs from Barak2015 in several aspects, as shown in Figure 2. At the central section of SAF (profiles DD'), we observe a high-velocity zone in the middle crust that shows a slight NE dip, while Barak2015 shows it dipping into the lower crust. The high-velocity region in the lower crust beneath wPRB of our model is

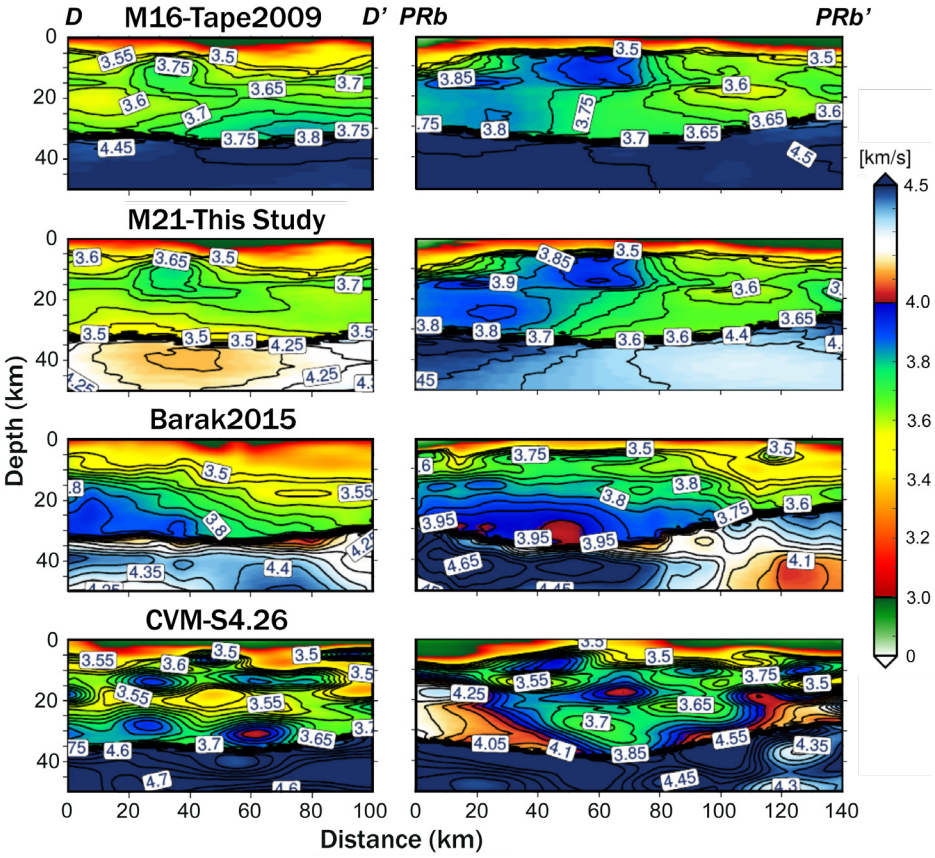

Figure 2. Comparison of model M16, M21, Barak2015 and CVM-S4.26 along DD' profile across SAF and PRbb' profile across PRB.

not as evident as that shown in Barak2015 and is only observed in the westernmost part (profile PRaa'). Our model shows that the southern boundaries of wPRB and ePRB have vertical-to-steep NE dips into lower crust, while Barak2015 shows only a slight NE dip in the middle crust (PRbb'). Moreover, our model shows increased shear velocities beneath LAB and CTR which are not identified in Barak2015.

Our study demonstrates the feasibility of applying adjoint tomography to ambient-noise data in southern California, which is complementary in coverage to the earthquake data used in previous studies. The numerical spectral-element solver used in adjoint tomography provides accurate structure sensitivity kernels through 3D model iterations, and hence generates more robust images than those produced by traditional ambient -noise tomography based on analytical methods.

This project is part of CCFS theme 3, Earth Today, and contributes to understanding Earth's Architecture.

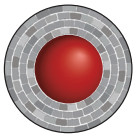

Contacts: Kai Wang, Yingjie Yang
Funded by: IMQRE 43887678, DP120102372, DP120103673

Mapping the basaltic underplate: plume-related zircons from Mt Carmel

Xenocrystic zircons from Cretaceous pyroclastic vents on Mt Carmel, N. Israel, document three major periods of earlier mafic magmatism: Permo-Triassic (285-250 Ma), Triassic (250-220 Ma) and Jurassic (210-160 Ma), which are only poorly represented in the local crustal record. Related alluvial deposits also contain these zircon populations, but most alluvial zircons are Cretaceous (118-80 Ma), or derived from much younger volcanic episodes (age peaks at 30, 13, 11, 9-10 and 4 Ma) (Fig. 1a, b). The Permo-Triassic-Jurassic zircons are typically large and glassy; they have irregular shapes and a wide variety of internal zoning patterns (Fig. 2). They appear to have grown from melts in the interstitial spaces of coarse-grained rocks (cumulates, peridotites); many show evidence of recrystallisation, including brecciation and rehealing by chemically similar zircon. Igneous-looking grains have mantle-like $\delta^{18}O$ (5.5±1 ‰), but recrystallisation leads to lower values (down to 3.1‰). Hf-isotope

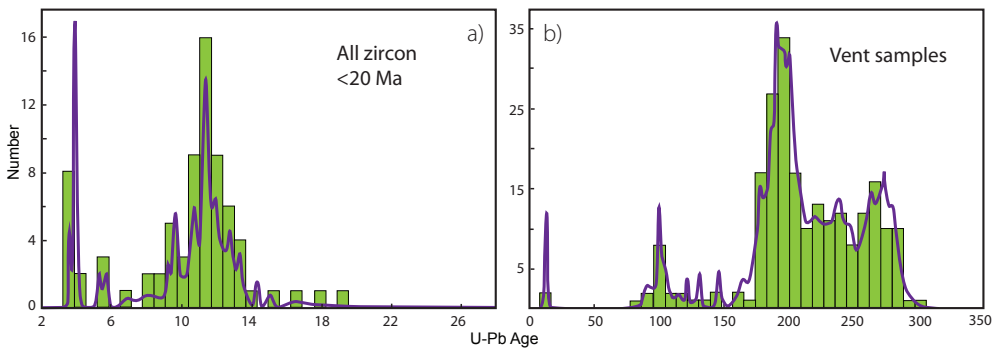

Figure 1. Age histogram/ cumulative probability curve for U-Pb data of a) Alluvial samples (0-20 Ma) and b) Vent samples (0-350 Ma).

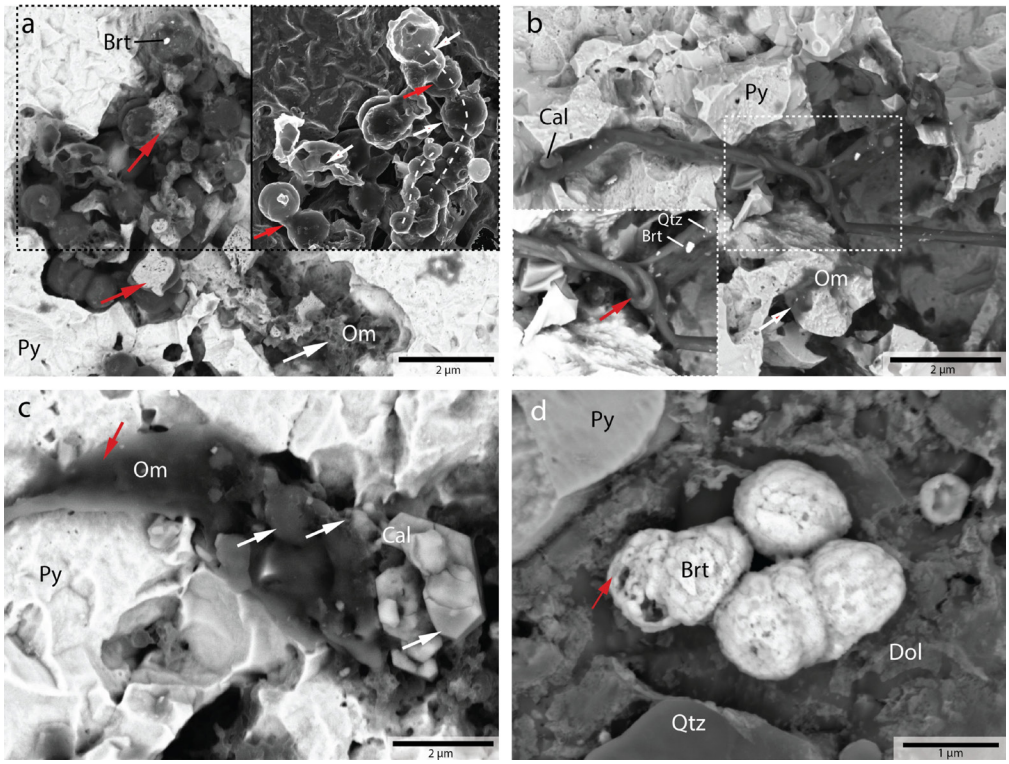

Figure 2. Images of Mount Carmel zircons. Scale bars are 200 microns. a. optical-microscope and cathodoluminescence 838 (CL) images of zircons showing corroded-prismatic shapes and core-rim zoning. b. Typical Mt Carmel-type zircons illustrating irregular shapes and internal structures. c. optical and CL images of large Mt Carmel-type zircon showing irregular form and internal brecciation. d. CL images of zoned Mt Carmel-type zircons, with brecciation.

compositions lie midway between the CHUR and Depleted Mantle (DM) reservoirs; Hf model ages suggest that the source region separated from DM in Neoproterozoic time (1000-1500 Ma). Most Cretaceous zircons have $^{176}Hf/^{177}Hf$ similar to those of the older zircons, suggesting they recrystallised in the Cretaceous thermal event. Calculated melts in equilibrium with the Permian to Cretaceous zircons are depleted in LREE and P, and have large positive Ce anomalies and negative Eu anomalies, variable Ti anomalies, and high and variable Nb, Ta, Th and U, consistent with the fractionation of monazite,

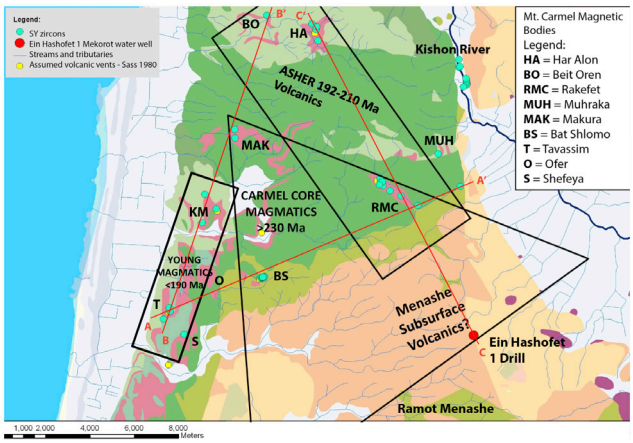

Figure 3. Map showing the distribution of zircon age populations in vents. Lines A-A', B-B', C-C' mark corresponding sections 1-3 in Figure 4.

zircon, apatite and Ti-bearing phases from the host magma. We suggest that these coarse-grained zircons crystallised from late differentiates of basaltic magmas, ponded near the crust-mantle boundary (ca 30 km depth), and were reworked repeatedly by successively younger igneous/metasomatic fluids.

The distribution of zircon populations in the Cretaceous volcanoes can be used to map the buildup of this basaltic underplate (Fig. 3). The Permian-Triassic (280-220 Ma) zircons are most abundant in the main central vents (Rakefet, Bat Shelomo, Makura) and the Ein Hashofet centre in the Ramot Menashe syncline. The Triassic-Jurassic zircons are found mixed with Permian-Triassic ones in Ein Hashofet and Rakefet, but make up the bulk of the sample in the northern bodies (BO, KM, and HA); the younger zircons are found mainly in KM, TAV and MH on the western side of Mt Carmel. This pattern suggests that the Permo-Triassic magmatism built up a *'pillow'* beneath the core of the Mt Carmel-Menashe area, so that the magmas of the younger episodes tended to intrude toward the margins of this central area (Fig. 4).

The trace element patterns of the Permo-Jurassic resemble those of zircons that crystallised from plume-related magmas (Iceland, Hawaii), and this is consistent with the compositions of Permian to Miocene basalts in the region. The zircon data support a published model that locates a fossil Neoproterozoic plume head beneath much of the Arabia-Levant region, which has been intermittently remelted to generate the volcanic rocks.
The Cretaceous magmas carry mantle xenoliths derived from up to 90 km deep, providing a minimum depth for the possible plume head. Post-Cretaceous magmatism, as recorded in detrital zircons from the area, shows distinct peaks at 30 Ma, 13 Ma, 11.4±0.1 Ma (a major peak; n=15), 9-10 Ma and 4 Ma, representing the Lower and Cover Basalts in the area. Some of these younger magmas tapped the same mantle source as the Permian-Jurassic magmatism, but many young zircons have Hf-isotope compositions extending up to DM values, suggesting derivation of magmas from deeper, more juvenile sources.

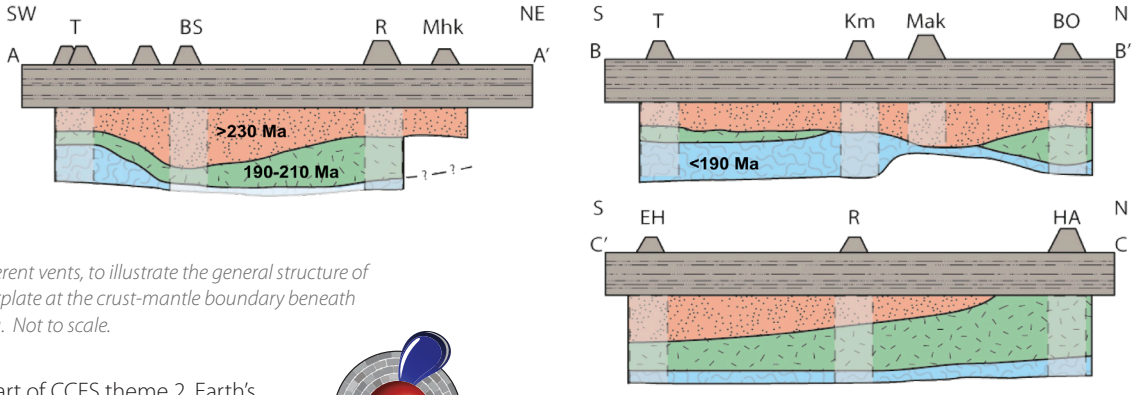

Figure 4. Cartoon showing the relative abundance of three zircon age populations in different vents, to illustrate the general structure of the gabbroic underplate at the crust-mantle boundary beneath the Mt Carmel area. Not to scale.

This project is part of CCFS theme 2, Earth's Evolution, and contributes to understanding Earth's Architecture and Fluid Fluxes

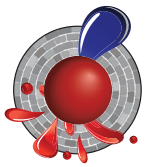

Contact: Bill Griffin

Funded by: CCFS Flagship Program 1

Seismic image of the Capricorn Orogen – revealing the crustal component

The Capricorn Orogen records the Paleoproterozoic amalgamation of the Archean Pilbara and Yilgarn cratons to form the Western Australian Craton. Regional surveys involving geological mapping, geochemistry, and geophysics reveal a prolonged tectonic history of craton assembly and subsequent intracratonic reworking, which has significantly re-shaped the orogenic crust.

To better understand the tectonic history, we targeted the seismic structure of the orogenic crust and sub-crustal lithosphere. We deployed a 76-station broadband array (COPA, Capricorn Orogen Passive-source Array) that covers the orogen in a 2D grid over nearly 500 km by 500 km surface area with roughly 40 km station spacing. The planned 36-month deployment could guarantee enough data recordings for 3D structure imaging using body wave tomography, ambient noise surface wave tomography and P- and S-wave receiver function Common Conversion Point (CCP) stacking techniques. Upon a successive instrument loan of 36 sets of seismometers from the ANSIR national instrument pool, 34 broadband seismometers (2 as backup) were first deployed in the western half of the orogen. In late 2015/early 2016, most stations were rolled over to the eastern half.

Here we report preliminary results from ambient noise tomography that focuses on the shear-wave velocity structure of the orogenic crust (Fig. 2). Some interesting results are noted.

1. Significant velocity differences are found between the western and eastern parts of the orogen;

2. The Glenburgh Terrane has slow velocities in the mid- to lower crust, similar to the bounding Pilbara and Yilgarn cratons.

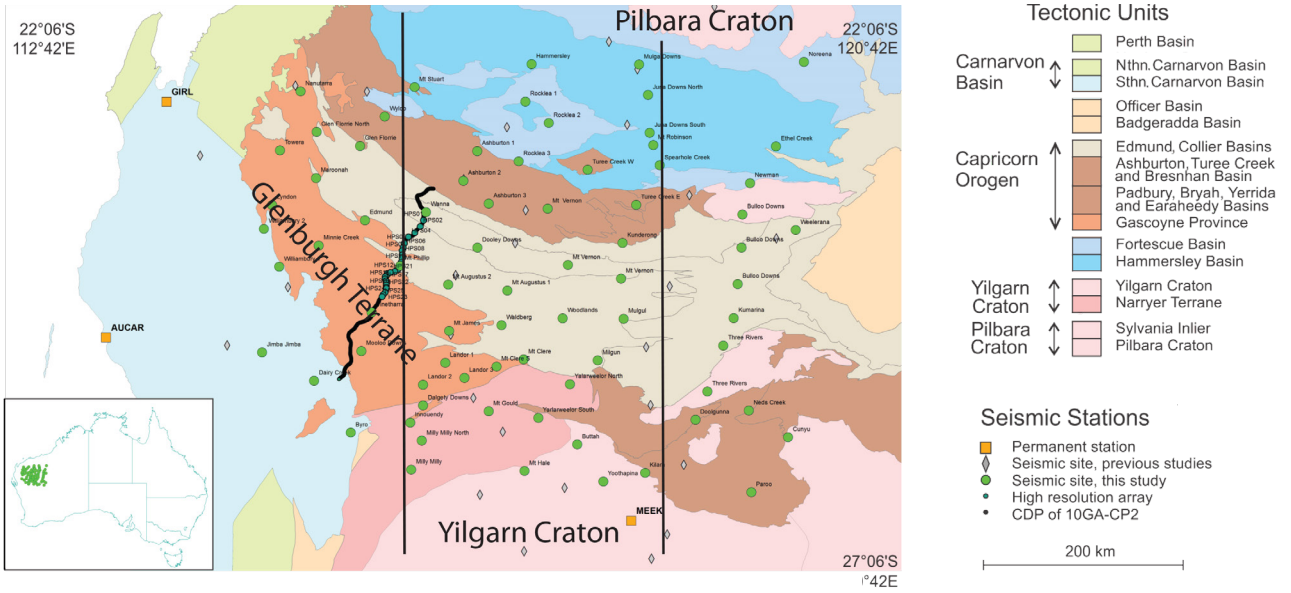

Figure 1. Capricorn seismic deployments and tectonic units. Green dots in the left panel are the 76 COPA stations from March 2014 to Nov 2017. Black line indicates the location of the 2010 active-source reflection line.

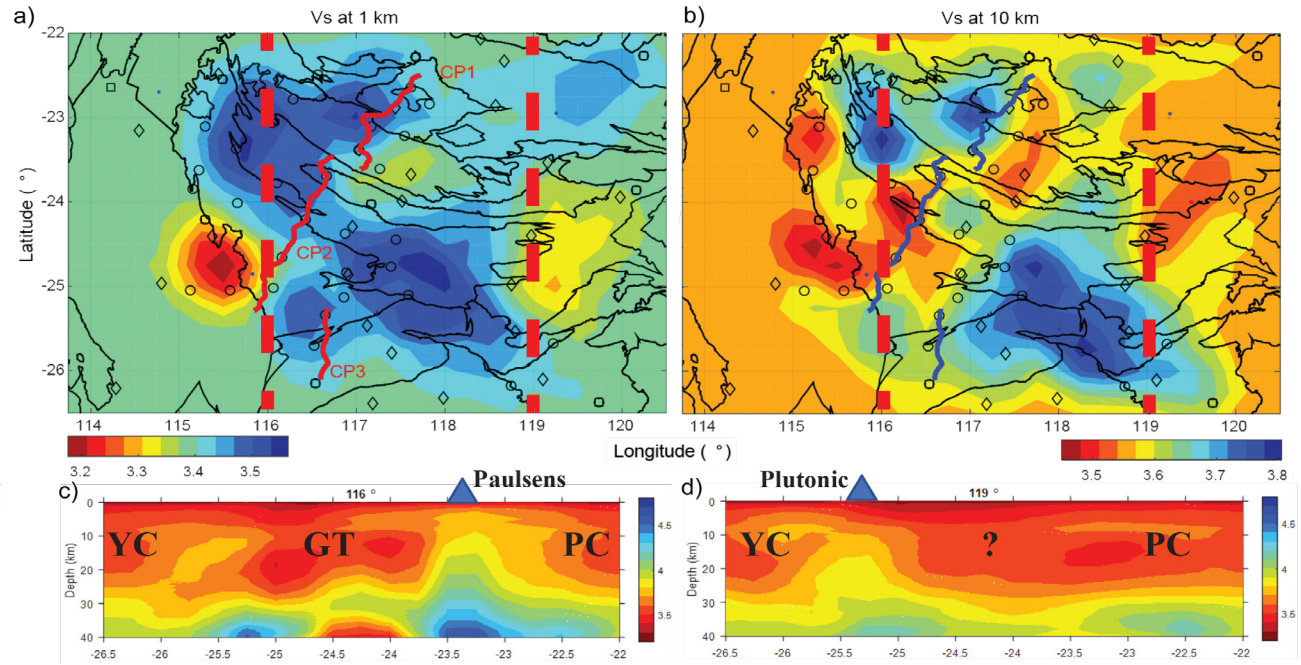

Figure 2. Initial ambient-noise tomography results for the orogen-scale COPA array. a) Vs at 1 km depth. b) Vs at 10 km depth. Stations used in the study are shown as open circles (deployed in this study) and open diamonds (early temporary deployments and permanent sites in the region). c) a cross-section for the western part of the orogen along 116° Longitude. d) a cross-section of the eastern part of the orogen along 119° Latitude. YC, Yilgarn Craton; GT, Glenburgh Terrane; PC, Pilbara Craton. The question mark indicates the region currently lacking station coverage. Blue triangles show the approximate locations of the Paulsens and Plutonic gold mines.

3. Clear Terrane boundaries may be marked by fast velocity lower crust that may represent mafic underplating associated with the 2.2 Ophthalmian and 2.0 Glenburgh Orogenies. These might represent the deep crustal sources of the mineral deposits (gold mines indicated in Fig. 2).

Combining our earlier crustal results (see *pp. 220-221, 2016 Research highlight "An Archean microcontinent lurking in the Capricorn Orogen"*), we can draw broader conclusions.

- Seismic signatures are found in the crust for the paleo-subduction associated with the 2.2 Ga Ophthalmian Orogeny, although there is no associated magmatic evidence at the surface.
- The Glenburgh microcontinent shares some crustal signatures (slow velocity, felsic composition, resistive crust) found in other Archean cratons, suggesting its formation may be associated with Archean vertical plume accretion.
- Significant reworking of the terrane crust left marks along the margins (lower crustal underplate, tectonic wedges), and inside the terrane (the fast-velocity upper crustal layer).

This project is part of CCFS themes 1, 2 and 3, Early Earth, Earth's Evolution and Earth Today, and contributes to understanding Earth's Architecture.

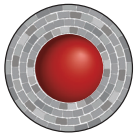

Contacts: Huaiyu Yuan, Klaus Gessner
Funded by: CCFS Flagship Program 7

Sulfidised stromatolites from the Pilbara: A new benchmark for oldest life on Earth

Definitive benchmarks for evidence of the oldest life on Earth remain controversial. Over the past decades, one has been the ~3.46 Ga Apex chert microfossil locality in the East Pilbara Terrane of Western Australia, but recent studies have convincingly shown that the filamentous structures in those cherts are abiotic artifacts rather than true microfossils. Claims for even older microfossil remains from Quebec, Canada, around 3.8 Ga, are even more contentious because they are less well-preserved in strongly metamorphosed rocks, and are not evidently composed of biological matter. Putative remains of microbial communities, generally known as stromatolites, have been reported from ~3.7 Ga old rocks of Greenland. However, stromatolite morphology – though compelling for most – remains contentious in the absence of microfossils, convincing biomineralisation, or chemical-based evidence. Here we report unequivocal microbial remains preserved in biologically precipitated stromatolitic sulfide (pyrite ± sphalerite, millerite and galena) laminae from the ~3.48 Ga old Dresser Formation, Pilbara Terrane, Western Australia. Although prone to recrystallisation and multiple stages of sulfide overgrowth, they preserve early-stage framboidal pyrite in nanoporous pyrite rich in organic matter, replicating textures known from *in situ* sulfidisation of modern biofilms. Furthermore,

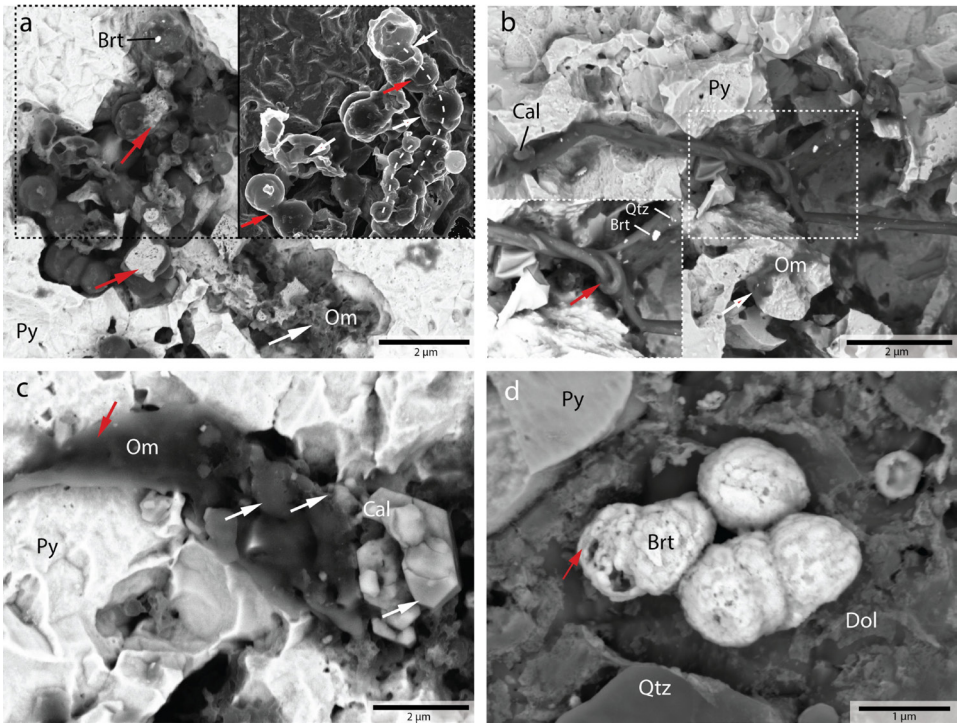

Figure 1. Backscattered electron- (BSE-) and secondary electron- (SE-) images of biomorphs rich in organic matter and barite mineralisation in stromatolitic sulfide laminae, observed following nitric acid etching. a. Irregularly-structured organic matter (white arrow), along with coccus-like hollow spheres and bulbous sheaths containing relict nanoporous pyrite cores (red arrow). The subfigure outlines the chain-like arrangement of coccus-like spheres and smaller irregular particles of organic matter (dashed lines), menisci of structureless organic matter (red arrows) interpreted as mineralised extracellular polymeric substance (EPS), as well as divided and bulbous arrangements of connected sphere (white arrows) suggestive of cell division (i.e., binary fission). b. Putative mineralised biofilm represented by a rope-like twisted and branched (red arrow) filament bundle speckled with quartz, calcite, and barite. c. Strand (white arrow) rich in organic matter yielding partly carbonatised (calcite) submicron-sized spheroids of organic matter (white arrows) occurring side by side with euhedral platy hexagonal calcite, replicating biofilm carbonatisation involving fossilisation of cocci bacteria. d. Agglomeration of submicron-scale barite spherulites in heavily etched dolomite. These barite textures are known from modern-day marine bioaccumulations, and have been replicated many times in laboratory experiments employing living strains of modern sulfur- oxidising marine bacteria. Brt = barite; Cal = calcite; Dol = dolomite; Om = organic matter; Py =Pyrite; Qtz = quartz.

we report candidate microfossils represented by spheres of organic matter that resemble coccus bacteria (Fig. 1a), as well as strands and filaments (Figs. 1b, c) interpreted as mineralised biofilms. Supporting evidence for a biological origin is derived from micromineralogy including spherulitic barite biomineralisation (Fig. 1d), as well as Micro-Raman Spectroscopy (MRS) analysis of organic matter (Fig. 2a) combined with Nanoscale Secondary Ion Mass Spectrometry (NanoSIMS) isotope mapping of elements necessary for life (carbon, nitrogen and oxygen; Fig. 2b, c). Collectively, the remarkable range of textural, mineralogical, and chemical biomarkers provides new definitive evidence of the

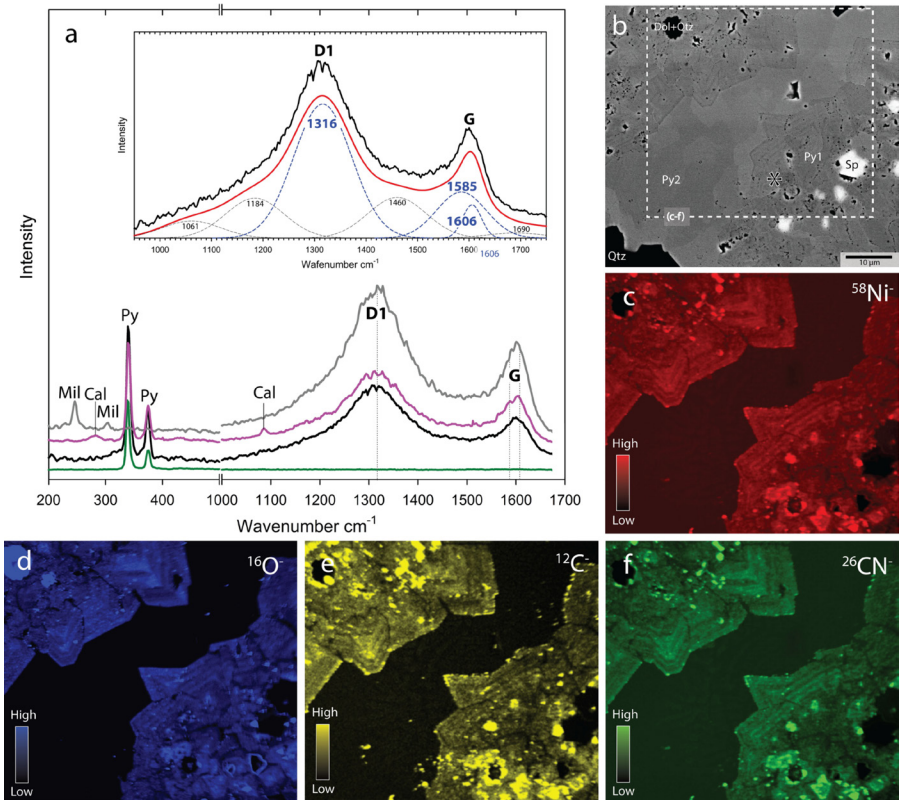

Figure 2. Molecular and isotopic analysis of organic-matter-rich sulfide (pyrite ± millerite) assemblages in stromatolitic sulfide laminae. a. Micro-Raman Spectroscopy (MRS) analyses of organic-matter-rich nanoporous pyrite and millerite compared with barren nonporous pyrite. Spectral deconvolution in the 900-1700 Δcm^{-1} range (subfigure) illustrates the immature kerogen-like nature of organic matter; i.e. predominance of molecular disorder (D1 band) relative to graphite-like order (G band). b-f. Backscattered electron (BSE-) image, and Nanoscale Secondary Ion Mass Spectrometry (NanoSIMS) maps of ^{51}Ni-, ^{16}O-, ^{12}C-, and ^{26}CN-, indicating coupled enrichments in nanoporous pyrite (Py1) relative to ubiquitous overgrowths of annealed nonporous pyrite (Py2). Cal = calcite; Dol = dolomite Mil = millerite; Py1 = nanoporous pyrite; Py2 = nonporous pyrite; Py = pyrite; Qtz = quartz; Sp = sphalerite.

oldest life on Earth at ~3.48 Ga, and points to a new taphonomy involving microbial sulfidisation that is important not only in the search for ancient life on Earth, but elsewhere in the solar system.

This project is part of CCFS themes 1 and 2, Early Earth and Earth's Evolution, and contributes to understanding Fluid Fluxes.

Contacts: Raphael Baumgartner, Martin Van Kranendonk, David Wacey, Marco Fiorentini, Stefano Caruso
Funded by: CCFS Flagship Program 4

Zircon morphology, isotopes and the magmatic fertility of porphyry Cu-Au deposits

Porphyry Cu-Au systems are associated with intrusive complexes made up of hydrous magmas related to continental and island arcs. These systems have a relatively well defined geodynamic framework. Increasing the understanding of the geologic processes and factors that lead to their formation will allow a better exploration success rate. Zircon compositions are powerful tools for unravelling the petrogenesis and magmatic evolution of Cu-ore-forming magmas. The Tampakan and Batu Hijau deposits (Fig. 1) are set in island-arc systems associated with subduction zones, and can be used to evaluate the importance of crustal contamination of the magmas.

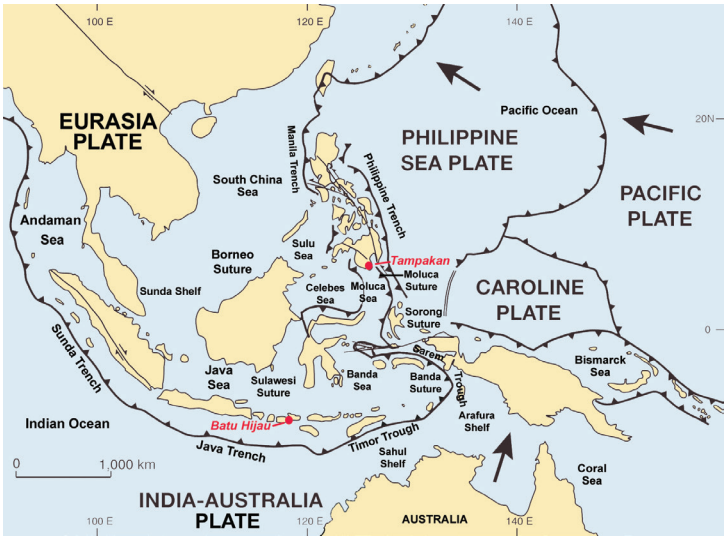

Figure 1. General plate boundaries across Indonesia, showing the most prominent trench and suture zones. Light grey shaded area represents the extension of the Sunda-Banda arc. Location of the Batu Hijau and Tampakan deposits represented by red dots. Modified after Metcalf (2009).

The Batu Hijau deposit sits along an arc system that has subducted older remnants of the Australian continental shelf (Figs. 1 and 3).

The Batu Hijau district (Fig. 1) contains 914 Mt of ore (0.53% Cu and 0.40 g/t Au). It is located on the island of Sumbawa along the Sunda-Banda volcanic arc segment between Wetar and Eastern Java. The arc consists of a succession of Miocene to Holocene units built over oceanic crust sitting close to the margin of the Sunda continental shelf. Parts of the Australian continental margin, with ages between ca 3200 and 500 Ma have been subducted along the arc, while parts of the fore-arc were dynamically uplifted.

The Tampakan district (Fig. 1) hosts giant high-sulfidation and porphyry Cu-Au deposits of Pliocene age, with estimated ore reserves of 12.5 million tonnes Cu and 500 tonnes Au. It lies at the northern end of the Miocene to Pliocene Sangihe volcanic arc on Mindanao Island, between crustal remnants derived from the Australian and Euroasian continental plates. This is a syn- to post-

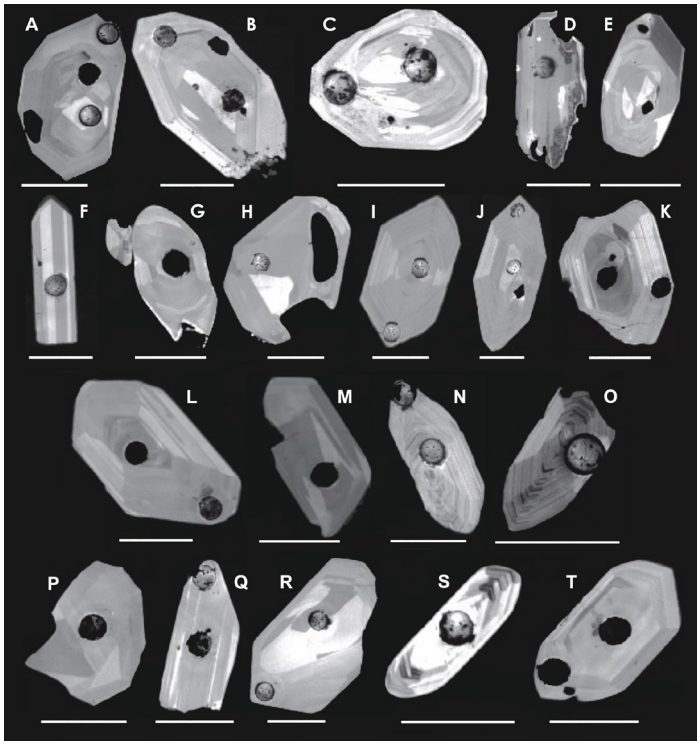

Figure 2. Morphologically, syn-ore zircons from the two studied deposits are characterised by unzoned cores surrounded by thin oscillatory zoned rims. Scale bars 100 µm.

collisional setting as the result of terrane accretion and arc collision. The geology of the region is dominated by a series of basalts and basaltic andesites of early to mid-Miocene age and related volcanoclastic sediments. The basaltic andesite unit is intercalated with a limestone unit. The package is unconformably overlain by the Tampakan Andesite Sequence. The Tampakan Andesite sequence represents an eroded stratovolcanic complex comprising 4 andesitic volcanic cycles lasting around 4.5 Myrs.

Zircon textural characteristics (Fig. 2) reflect two stages of magma emplacement. Unzoned cores suggest crystallisation within a long-lived, deep, hot magma chamber while the thin zoned rims suggest a relatively short residence time in the shallow crust, which may have prevented the loss of Cu metals. Preliminary O-isotope analyses show no sign of crustal contamination. I have had to infer that preliminary results show that zircons from pre- and post-ore samples, although not mineralised, display the same characteristics as syn-ore samples. The fact that all samples display such characteristics suggests that factors other than magma fertility played an important role in leading to mineralisation.

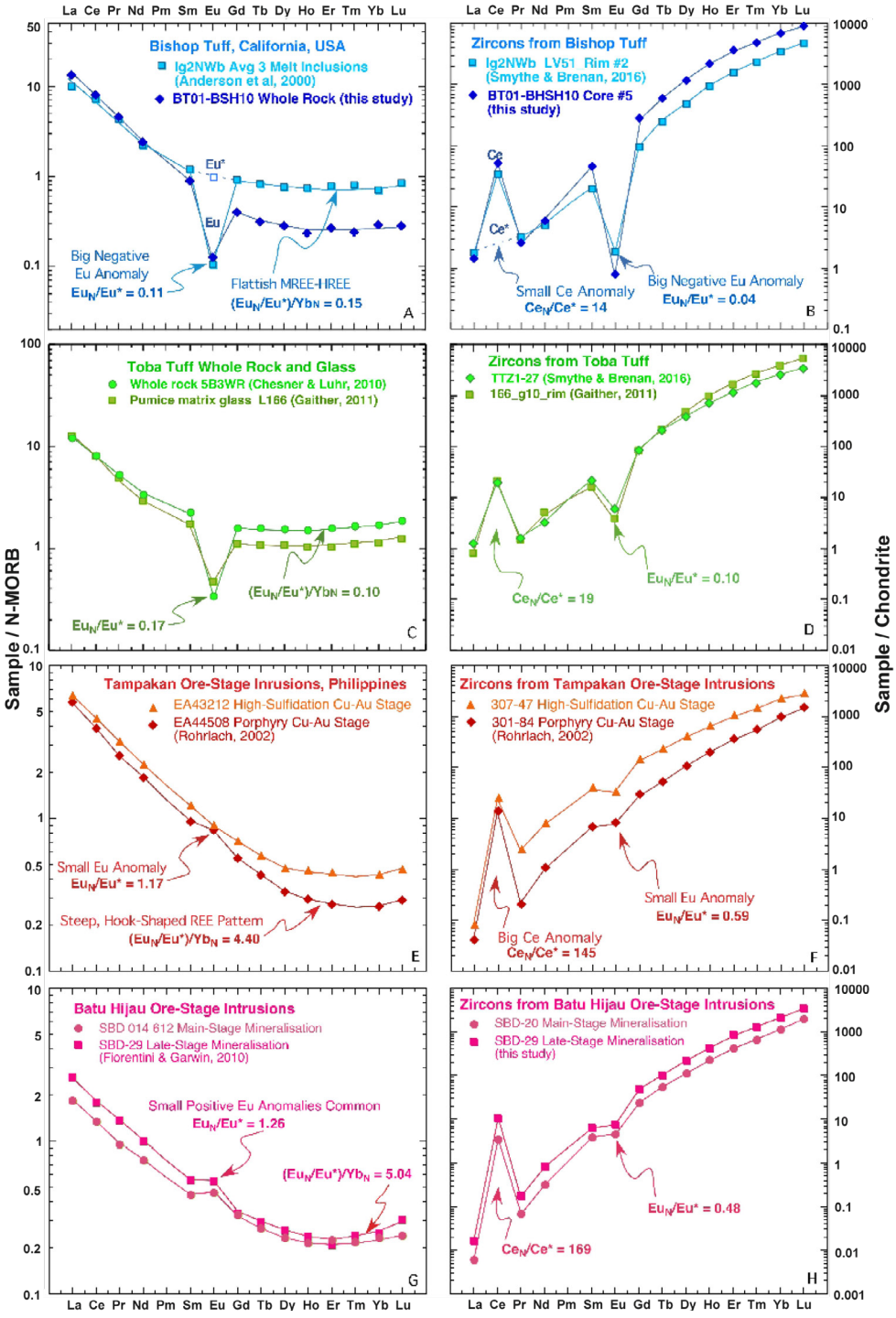

Figure 3. Whole rock (left) and zircon elemental data (right) display typical features of felsic arc magmas associated with magmatic-hydrothermal Cu ore deposits. These features include: steep, hook-shaped REE patterns, minimum around Er, and absence of a significant negative Eu anomaly.

This project is part of CCFS themes 2 and 3 and Earth's Evolution and Earth Today, and contributes to understanding Earth's Architecture and Fluid Fluxes.

Contacts: Luis Parra-Avila, Bob Loucks, Marco Fiorentini, Yongjun Lu
Funded by: GSWA

Porphyry Cu fertility in the Tibetan Plateau

Cenozoic porphyry Cu deposits in the Tibetan Plateau are typical of porphyry systems developed in continental collision zones. Understanding the temporal and spatial distribution of these deposits will help unravel the genesis of porphyry deposits in collision zones in general, and exploration targeting of porphyry deposits in similar orogenic belts.

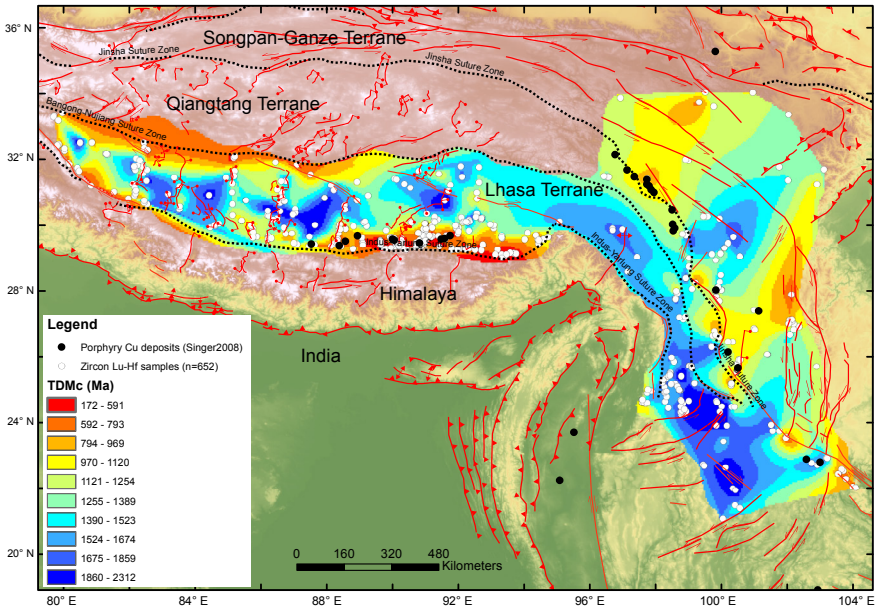

Figure 1. Contour map of zircon two-stage depleted mantle model ages (TDMc) for granitoid and felsic volcanic rocks in the Tibetan Plateau.

Results of zircon Lu-Hf isotopic mapping using 652 zircon samples from the Tibetan Plateau are shown in Figure 1. They demonstrate that most porphyry Cu deposits are associated with isotopically juvenile domains along the terrane-bounding Indus-Yarlung and Jinsha suture zones (Fig. 1). Such isotopic mapping can narrow the search space from over 2500 km scale to ~500 km scale.

Whole-rock geochemical mapping using ca 1200 samples across the Lhasa Terrane shows that all porphyry Cu deposits occur in domains of high 10000*(Eu/Eu*)/Y (>800; Fig. 2). Thus, the (Eu/Eu*)/Y ratio is the best whole-rock fertility indicator, and is interpreted to indicate extremely high magmatic water contents which induce early and prolific fractionation of hornblende and suppress early plagioclase crystallisation.

Zircon U-Pb and trace-element data were obtained from 66 igneous samples of Jurassic to Miocene age (181-11 Ma) in the eastern Gangdese belt. Both xenocrystic and magmatic zircons show systematic compositional evolution from Jurassic to Miocene. From ca 200 Ma to ca 55 Ma, zircon Eu/Eu* (0.1-0.4), 10000*(Eu/Eu*)/Y (0.1-10), and (Ce/Nd)/Y (0.001-0.05) ratios remain broadly similar. However, these zircon trace-element ratios increase rapidly after ca 55 Ma and peak at ca 13 Ma with Eu/Eu*, 10000*(Eu/Eu*)/Y, and (Ce/Nd)/Y up to 1, 70, and 2, respectively (Fig. 3). Similar temporal trends are also observed for whole-rock Sr/Y, La/Yb, and (Eu/Eu*)/Y, although whole-rock Eu/Eu* ratios appear to be similar throughout the Jurassic-Miocene period. In addition, Cretaceous samples show juvenile Hf-O isotopic signatures, whereas Eocene-Miocene intrusions show increasing zircon $\delta^{18}O$ values and decreasing epsilon Hf values, suggesting that increasing amounts of supracrustal materials were involved in magma genesis after c. 55 Ma.

Exploration is a scale-reduction process. Zircon Lu–Hf isotopic mapping is powerful in identifying juvenile crustal domains which are more prospective for porphyry Cu deposits. The combined mapping of zircon Hf isotopes and whole-rock 10 000*(Eu/Eu*)/Y ratio can help focus exploration on prospective areas.

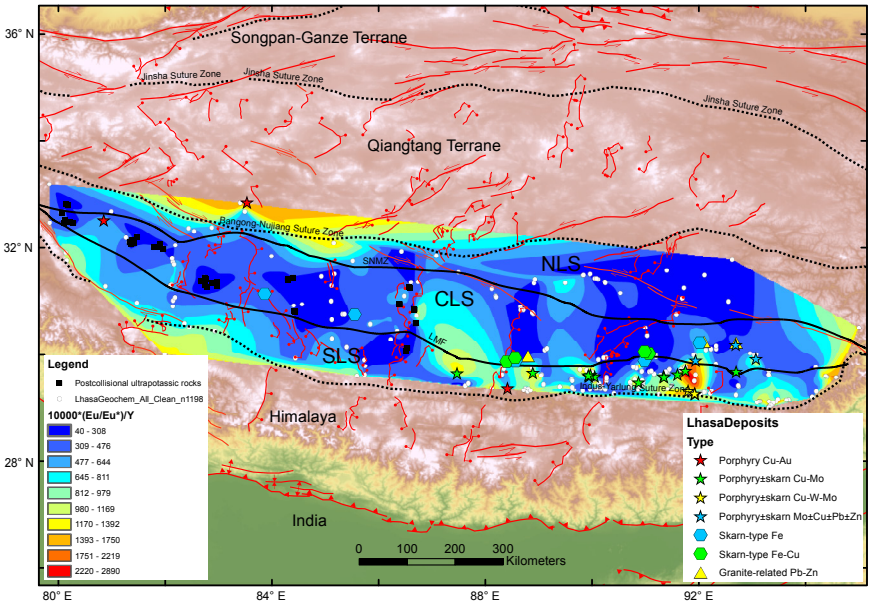

Figure 2. Contour map of whole-rock geochemical ratio of 10000(Eu/Eu*)/Y for mafic to felsic intrusive and volcanic rocks in the Lhasa Terrane, southern Tibet.*

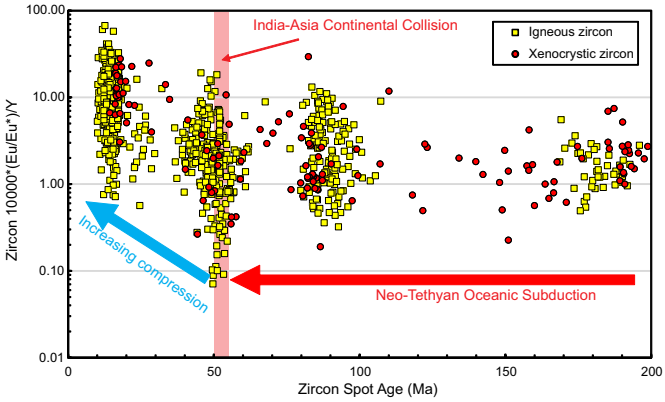

This project is part of CCFS themes 2 and 3 and Earth's Evolution and Earth Today, and contributes to understanding Earth's Architecture.

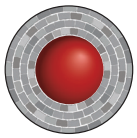

Contacts: Yongjun Lu, Zeng-Qian Hou, Zhi-Ming Yang, Luis Parra-Avila, Marco Fiorentini, Cam McCuaig, Bob Loucks
Funded by: CCFS Flagship Program 2

Figure 3. Zircon 10000 (Eu/Eu*)/Y ratio vs Age (Ma) for 66 magmatic rocks in the eastern Gangdese belt, Lhasa Terrane, southern Tibet.*

Following the tracks of carbon in the upper mantle

The mantle carbon cycle is an important, but largely unconstrained and debated problem in the deep Earth volatile cycle. The uncertainty derives from two main causes:

1) The location and conditions of carbonate melting in subduction slabs, along with the physical mechanisms by which carbon is removed from the slab into the overlying mantle wedge;

2) release of CO_2 from the downgoing slab causes changes in the chemical and physical properties of the lithospheric mantle by metasomatic interaction.

To better constrain these processes we have undertaken theoretical modelling to couple decarbonation reactions and experimentally-produced melting curves for carbonated basalts (MORB + CO_2) and sediments at pressures and temperatures relevant to upper mantle conditions.

The results confirm the hypothesis that carbon probably is likely filtered out at uppermost mantle conditions, suggesting a carbon increase in the lithospheric mantle over time. Carbonate melting in the mantle transition zone may provide an important component for organic-carbon signatures in diamonds. Lithospheric mantle enriched in CO_2 can be reactivated in subsequent tectonic events and lead to massive CO_2 release far from its original source – the subduction zone.

Overall, this study, though just beginning, is contributing to better understanding the deep carbon cycle and our ability to quantify the amount of CO_2 stored in the mantle.

This project is part of CCFS themes 2 and 3 and Earth's Evolution and Earth Today, and contributes to understanding Earth's Architecture and Fluid Fluxes.

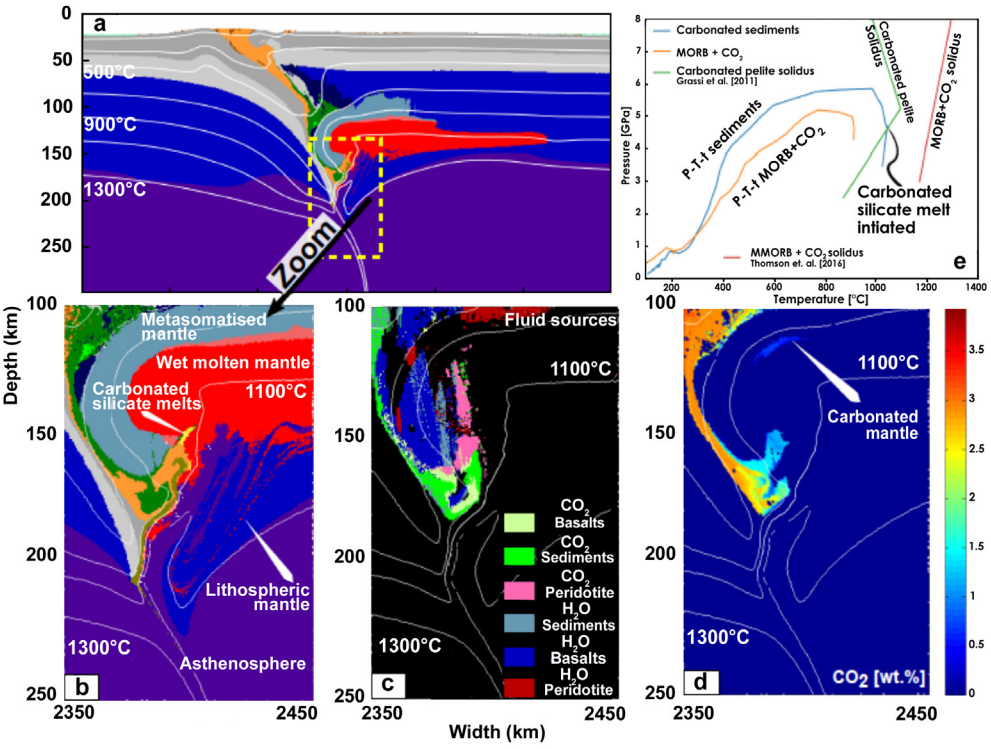

Contacts: Weronika Gorczyk, Christopher Gonzalez
Funded by: CCFS Flagship Program 2

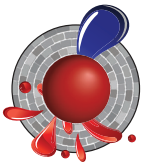

Figure 1. Model evolution for the initiation of carbonated silicate melts within a subarc region within the phase topology of a carbonated silicate melt: a) Model domain and evolution at 19.09 Ma. b) Enlarged area of carbonated silicate melting. c) CO_2 [wt. %] in rocks determined as stable by thermodynamic modelling. d) Devolatilised fluids at depth determined as unstable from thermodynamic modelling. e) Selected P-T paths of basalts and sediments crossing solidi determined by petrological experiments.

CO_2 released in continental rifts is "*fried lithospheric diamonds*"

Continental rifts around the world are characterised by a strong accumulation of carbonate-rich volcanoes, including carbonatites and ultramafic alkaline rocks. These rocks store enormous quantities of carbon that appears to have its source in the lower parts of the continental lithosphere. These rocks are well known for extremely runny and fast-flowing lavas at Oldoinyo Lengai in northern Tanzania, but are also important as the best examples of primary melts of the mantle from the lower cratonic lithosphere at depths of 120-180 km (known as ultramafic lamprophyres).

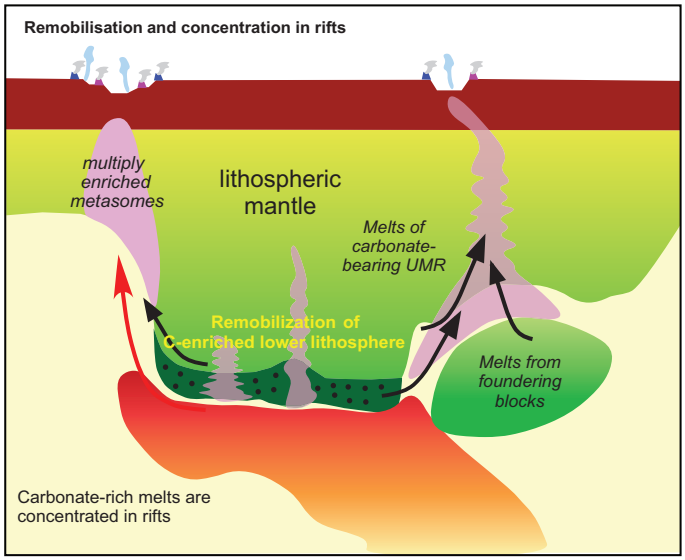

Figure 1. Stored carbon is reactivated by partial melting, concentrating the carbon in zones (purple; 150–240 Mt C km^{-3}) above which rifts may develop. Carbon escapes any foundering blocks, adding to the concentration in the sub-rift zones. Rift degassing thus involves carbon reactivated from an initially large volume. UMR, ultramafic rocks.

Studies of the release of CO_2 gas from continental rifts are being undertaken to assess the natural release of CO_2 into the atmosphere over time in order to compare and contrast it to levels of anthropogenic (man-made) carbon dioxide, which is accepted as being principally responsible for climate change. Measurements of CO_2 release have shown that even more carbon dioxide is released along rift faults and from volcanoes during their quiescent periods than volcanoes during eruptions.

Our interdisciplinary study brings together experts on degassing in continental rifts (Tobi Fischer of the University of New Mexico) and melting of the mantle (Stephen Foley, CCFS) in an attempt to understand where the carbon comes from, and whether we can explain how the concentration in continental rifts occurs. The result, published in *Nature Geoscience* in December 2017 (*CCFS Publication #995 Foley & Fischer, 2017, Nature Geoscience, 10, 897-902*), match the measured output of CO_2 gas in continental rifts to its capture, storage and remobilisation at the lithosphere base (150-200 km) within a factor of two – an excellent agreement in view of the great uncertainties involved.

The trapping and storage of carbon in the lower lithosphere was modelled as a three-stage process: (1) the original formation and stabilisation of the cratonic lithosphere, (2) gradual degassing from the mantle over time, and (3) carbon acquired from the passage of mantle plumes that contain carbon recycled into the mantle at subduction zones. When continental rifts form, this carbon, which has been stored for up to 3 billion years in the lithosphere, is remobilised by melting and focused into restricted zones beneath rifts, where deep fracture zones facilitate its concentration (Fig. 1).

Our calculations showed that the first step – the formation of the lithosphere itself – is insignificant in the deep carbon budget. The gradual degassing and release from mantle plumes were found to be similar in importance, with the latter slightly outweighing the former. To assess gradual degassing, we used similar models to those used for degassing at mid-ocean ridges, but modifying them for the depth zone relevant to sub-cratonic areas. Degassing from mantle plumes has been calculated before, because of the suspicion that mantle plumes may have caused the mass extinction of 96% of species at the end of the Permian. Here again, we used similar models, but modified the details for the pressure-temperature conditions and age ranges relevant to cratons.

The entrapment and release of carbon in the lower lithosphere is controlled largely by redox processes: carbonate-bearing melts freeze in the lithosphere because

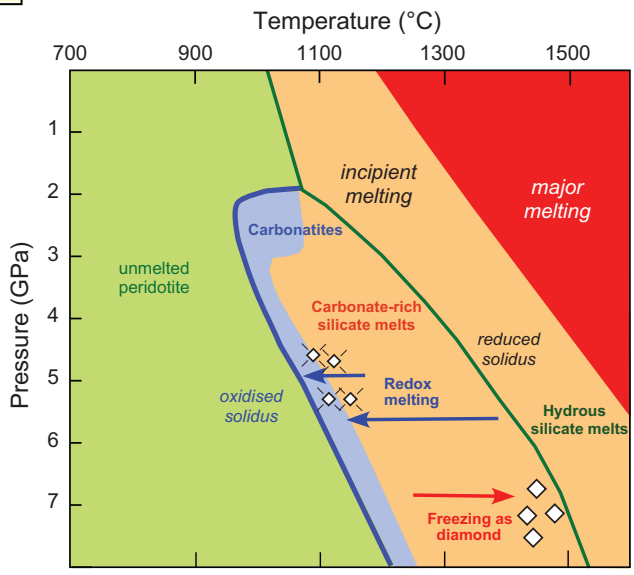

Figure 2. Melting curves of peridotite in reduced (green line) and oxidised (blue line) conditions in the incipient melting regime (blue to brown background). Carbon is immobilised in the reduced lower lithosphere by freezing to form diamond (red arrow) due to the change from blue to green melting curve. Later rifting and mantle upwelling causes access of oxidised melts to stored reduced carbon, depressing the solidus (redox melting; green line to blue line; blue arrows). Blue area indicates carbonatitic melts.

the environment there is more reduced, so that the carbon is stored as diamonds. Conversely, when melting occurs, the diamonds are oxidised and dissolve in the melts as carbonate (Fig. 2), enabling its transport and focusing into the zones beneath the rifts.

The values estimated for CO_2 release in rifts are 19 megatons of carbon per year (Mt/yr), and for time-integrated input into the lithosphere and focusing beneath rifts around 30 Mt/yr, just 50% higher. These values are closer than appears when one considers that much carbonate is not released into the atmosphere, but remains in igneous rocks near the surface.

However, this is a generalised model based on today's degassing pattern. At times in the past when supercontinents were breaking up, the total length of rifts was probably 3-5 times that on the Earth today. In these times, the amount of CO_2 released must have been correspondingly higher, so that natural CO_2 release may have directly affected the atmosphere to warm the climate.

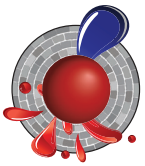

This project is part of CCFS themes 2 and 3, Earth's Evolution and Earth Today, and contributes to understanding Earth's Architecture and Fluid Fluxes.

Contact: Stephen Foley
Funded by: CCFS Flagship Program 3, USA National Science Foundation Grant EAR-11130660

Tiny droplets betray mantle melt origins

Melts in the upper mantle are commonly responsible for metasomatic reactions, which change the mineral and geochemical composition of the peridotite wall-rock. In most cases, the presence of an infiltrating melt is only evidenced by these characteristic compositional features in mantle rocks. However, on rare occasions, the melt can be '*caught in the act*' when trapped as primary silicate melt inclusions in newly-forming crystals.

Such an example was investigated in a metasomatically altered upper-mantle xenolith from the Nógrád-Gömör Volcanic Field, northern Pannonian Basin (Central Europe). Xenoliths from this locality have recently been shown to be affected by multiple metasomatic events (see *CCFS publication #1004*) the latest of which was caused by an intraplate mafic melt, resulting in clinopyroxene enrichment and elevated Fe contents. These metasomatic clinopyroxenes frequently host primary silicate melt inclusions (Fig. 1), which are about 10-20 µm in diameter and are partially crystallised, with several daughter minerals, residual glass and a gas bubble. The mineralogical, major- and trace-element compositions of several silicate melt inclusions were analysed to constrain the composition of the trapped melt.

We have used Raman spectroscopy to identify the daughter minerals, compromising clinopyroxene, apatite, anhydrite, barite, amphibole and mica. The gas bubbles are dominantly composed of CO_2. Subsequently, silicate melt inclusions were analysed by focused ion beam coupled scanning electron microscopy (FIB-SEM), a novel technique in nanoscale geological studies. The technique involves using the ion beam to slice through a small sample volume containing an inclusion, saving an image of each slice and carrying out *in situ* geochemical analyses on the exposed phases of the silicate melt inclusion (Fig. 2). Additional daughter phases were identified (spinel,

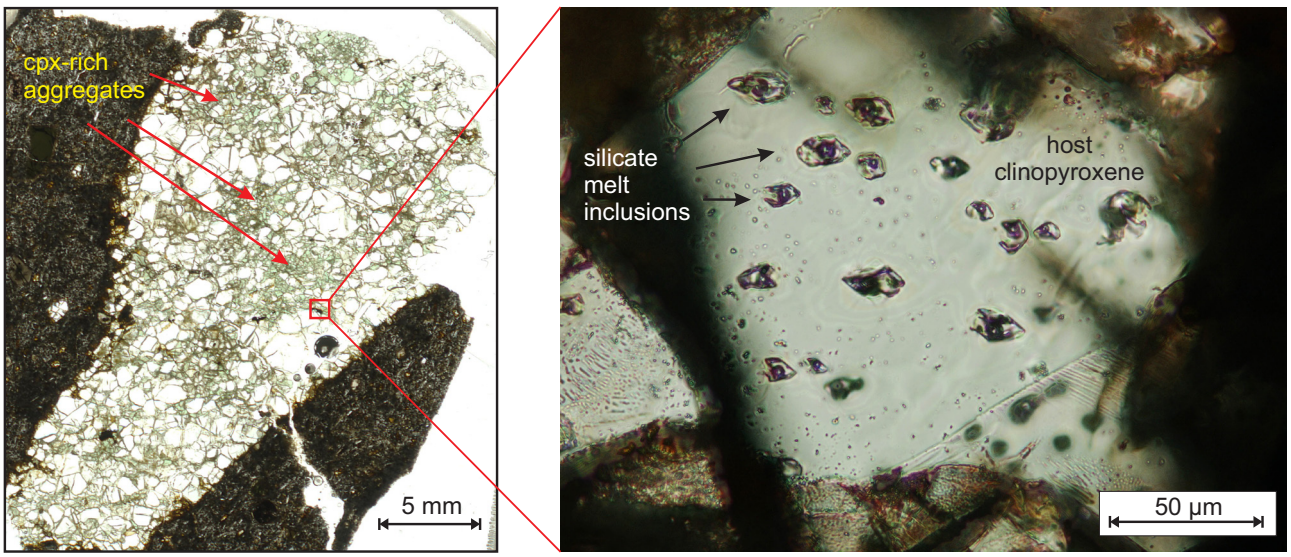

Figure 1. Left: clinopyroxene-rich, metasomatically altered xenolith. Right: merged image of plane- polarised photos, taken at different foci, of a clinopyroxene grain with primary silicate melt inclusions.

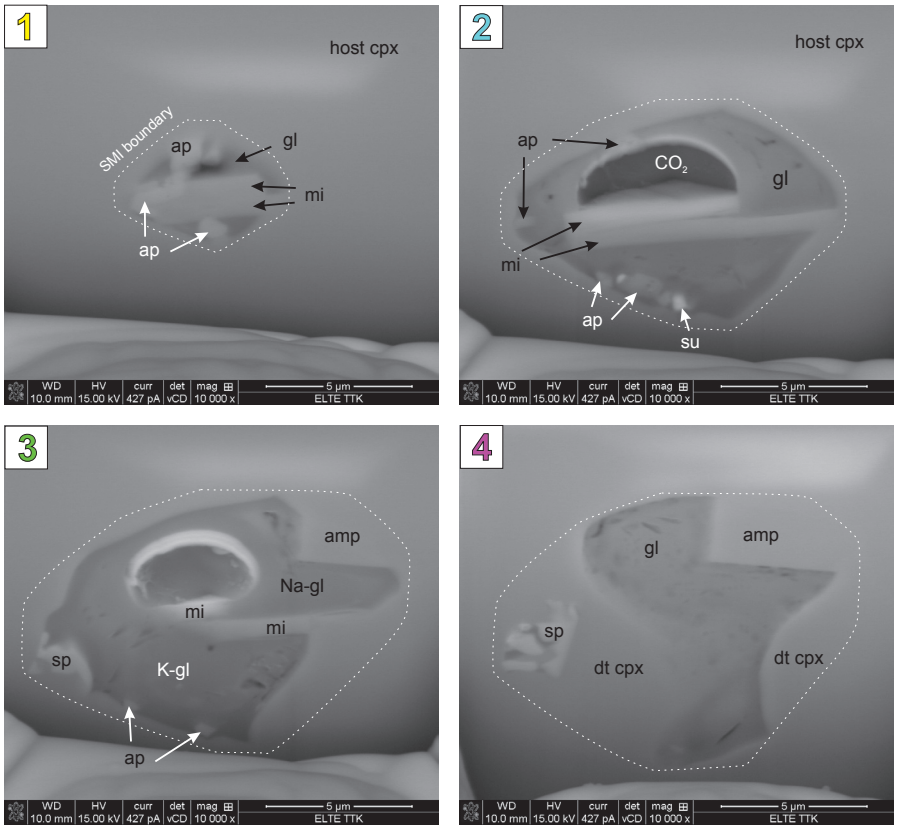

Figure 2. Plane-polarised light photomicrograph of a silicate melt inclusion and backscattered-electron images at different stages of the slicing process. Abbreviations of daughter phases: cpx – clinopyroxene, amp – amphibole, mi – mica, ap – apatite, sp – spinel, su – sulfide, gl – glass.

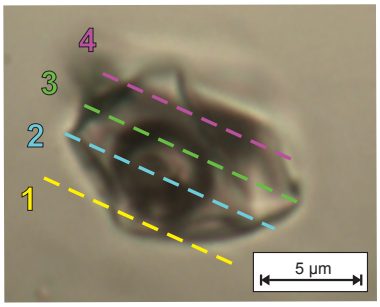

sulfide) by this technique, and a 3D phase map was constructed for the silicate melt inclusions, allowing calculations of the bulk modal and major-element compositions. Trace-element compositions then were determined using laser-ablation inductively coupled plasma mass spectrometry.

Bulk compositions lie within a narrow range for all the analysed silicate melt inclusions, indicating that they have trapped the same melt in similar conditions. This melt appears to be mafic in composition, with an enrichment in the most incompatible trace elements, like the host alkali basalt (Fig. 3). However, their high Fe contents verify that the trapped melt is the one linked to the latest metasomatic event in the studied locality. A simple geochemical model of Zajacz et al. (*2007, J. Petrology*) was applied, using the relationship of Nb and Y, to constrain the genesis of this melt (Fig. 3). The concentration of Y is commonly regarded as an indicator for the presence of garnet in the source, whereas Nb can be used to calculate the degree of partial melting. Based on the results, the metasomatising melt was generated by low-degree (~ 2%) partial melting of a garnet lherzolite, with slightly different composition than the source of the host magma.

Several post-entrapment processes can be reconstructed from the appearance and composition of the silicate melt inclusion daughter phases. The low density of the CO_2 bubble indicates that it was exsolved from the residual glass at shallow depths, most likely during ascent to the surface. Subsequently, secondary daughter minerals (sulfates, mica) crystallised on the boundary between the bubble and the glass, indicating the previous presence of S and H_2O in the volatile phase. Chemical heterogeneity in the glass may indicate a lack of equilibration before the '*freezing*' of the system under surface conditions.

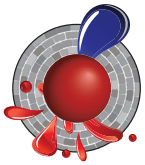

This project is part of CCFS theme 2, Earth's Evolution and contributes to understanding Earth's Architecture and Fluid Fluxes.

Contacts: Nora Liptai, Sue O'Reilly, Bill Griffin, Csaba Szabó, Márta Berkesi (Eötvös University, Budapest, Hungary)
Funded by: CCFS Flagship Program 1, iMQRES, EPS postgraduate funds. This project is part of a cotutelle PhD program between Macquarie University and Eötvös University in Budapest, Hungary.

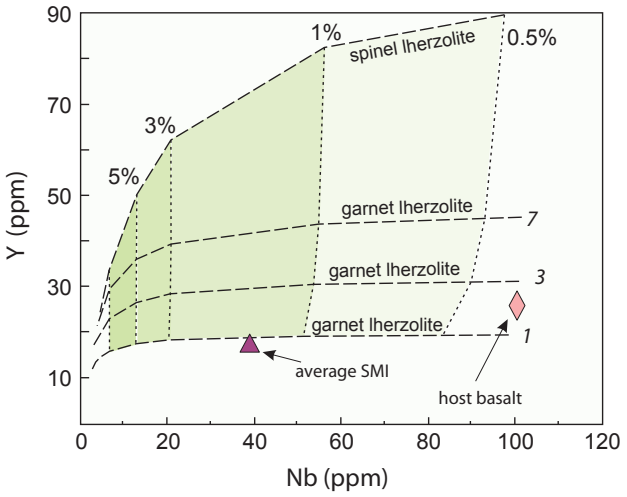

Figure 3. Nb vs Y diagram modelling the source composition and degree of partial melting for the genesis of the metasomatising melt. Dashed lines represent primitive mantle spinel- and garnet-lherzolite compositions; italic numbers refer to the clinopyroxene/garnet ratio in the source region. Dotted lines represent the degree of partial melting expressed in percentage.

Super-reducing conditions in a modern volcanic system: key to the redox evolution of cratonic lithosphere

Estimates of the oxygen fugacity (fO_2) of the cratonic subcontinental lithospheric mantle (SCLM) range from above the quartz-fayalite-magnetite (QFM) buffer to just above the iron-wustite (IW) buffer, and generally decrease with depth. Several lines of evidence suggest that the fO_2 of the sublithospheric mantle may be constrained by the IW buffer (the presence of metallic Fe), but there also is evidence that volumes of significantly lower fO_2 must exist within the SCLM, and perhaps within the deeper mantle. The remarkable super-reduced conditions in an off-craton volcanic setting (Mt Carmel, Israel; *Griffin et al., Geology 2016; CCFS #830*) may provide a key to the evolution of the redox state of the cratonic SCLM through time.

Aggregates of hopper-formed crystals of Ti-rich corundum are abundant in Upper Cretaceous basaltic pyroclastic rocks (vent breccias, tuffs) exposed on Mt Carmel near Haifa, Israel. Melt pockets trapped within and between corundum crystals contain mineral assemblages (SiC (moissanite), TiC, Fe-Ti-Zr silicides/phosphides and native V) that require P ≥ 1 GPa, T = 1500-1100 °C and extremely low fO_2 (10 to 12 log units below IW). Mineral parageneses suggest that the corundum and the low-fO_2 assemblages developed through interaction of basaltic magmas with mantle-derived (CH_4+H_2) at high fluid/melt ratios, leading to progressive lowering of fO_2.

A schematic illustration of the process is shown in Figure 1; this model envisions a magma chamber being flushed by a steady supply of CH_4±H_2, but other configurations are possible. The material described here comes from at least 8 different volcanoes, with eruptions spread over ca 10 Ma, sampling similar magmatic systems erupted at different stages of their evolution, and has been used to reconstruct the evolution of a single synthetic system. The early oxidation of CH_4 may have led to the precipitation of vesicular wustite (FeO) and abundant high-Mg calcite, found in the ejecta. The progressive lowering of fO_2 to the IW buffer is marked by the appearance of a suite of mutually immiscible melts: native Fe, Fe-oxide/silicate melt and Ti-oxide/silicate melt, coexisting with the host CaO-Al_2O_3-SiO_2 melt. This reaction appears to have removed most of the FeO from the system; none of the silicate phases in the trapped melts (see below) have significant contents of Fe. The removal of the Fe-FeO buffer would allow fO_2 to decline (rapidly?) to the levels (6 to 8 log units below IW) where silicide melts would separate and SiC could precipitate. This would remove SiO_2 from the melt (now dominated by CaO-Al_2O_3-MgO), driving it into Al_2O_3 –supersaturation which causes the rapid growth of corundum and the trapping of melt pockets. This desilication process

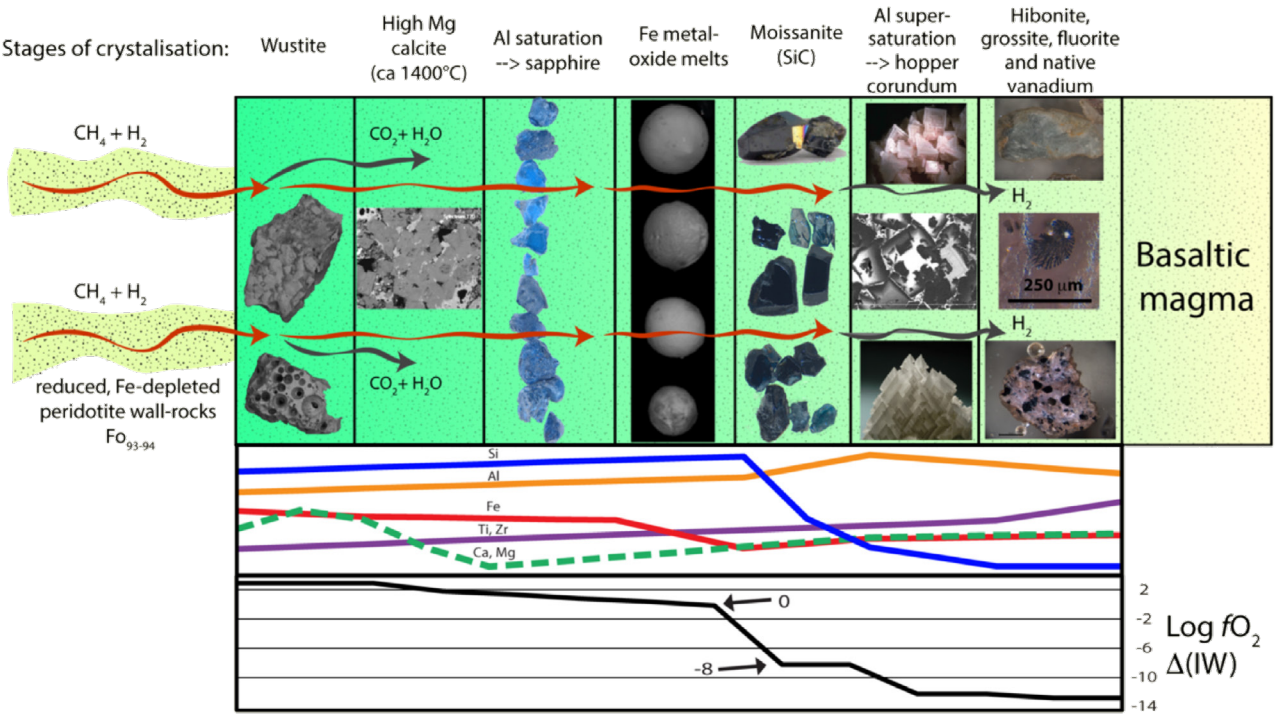

Figure 1. Model for the evolution of the Mt Carmel corundum-SiC system(s), as a progressive interaction between mantle-derived volatiles (CH_4±H_2) and a basaltic magma. The evolution of the melt composition and the fO_2 of the system is illustrated schematically in the lower panels; the curves for elemental abundance are not to scale. The most important aspects are the drop in Fe (especially FeO) at the IW buffer, the rapid desilication of the melt following the onset of SiC crystallisation, and the extremely low fO_2 required by the presence of abundant native V in the hibonite-grossite assemblage. The incongruent melting of anorthite suggests P ≥9 kb, while phase relationships in immiscible silicide melts indicate T = 1500-1200 °C. After Xiong et al., EJM 2017; CCFS#968).

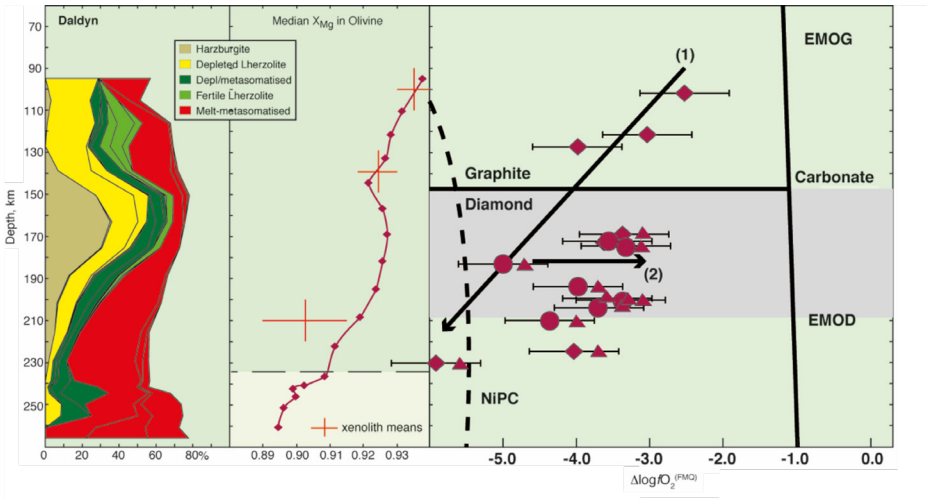

Figure 2. Left panel shows a lithospheric section of the SCLM beneath the Daldyn kimberlite field, constructed from garnet/chromite concentrates (Griffin et al., 1996) showing vertical distribution of rock types and metasomatic styles. The middle panel shows the median values of XMg in olivine, reconstructed from garnet compositions and temperature); note the inverse correlation between XMg and the degree of melt-related metasomatism. The right-hand panel (after Yaxley et al., 2012) shows estimated fO_2 based on $Fe_3+/\varepsilon Fe$; depleted samples define a trend of decreasing fO_2 with depth (Trend (1)), while metasomatised ones have experienced oxidation (Trend (2)). NiPC = Nickel Precipitation Curve.

apparently continued to near-completion, leading to a coarse-grained assemblage of hibonite ($CaAl_{12}O_{19}$) + grossite ($CaAl_4O_7$) + MgAl spinel + fluorite + native V, at $fO_2 \leq 11$ log units below IW. Many of the larger corundum aggregates are cut by breccia veins of amorphous (commonly vesicular) carbon, which also occurs in parallel-sided veinlets down to the sub-micron (TEM) scale, emphasising the important role of carbon in the evolution of these systems.

If this process reflects the rise of CH_4+H_2 from the sublithospheric mantle, much of that mantle probably is metal-saturated, consistent with observations of metallic inclusions in sublithospheric diamonds (e.g., *Smith et al., 2016*). Such fluids could penetrate up into a primitive depleted cratonic root, establishing the observed trend of decreasing fO_2 with depth (Fig. 2; *Yaxley et al., Lithos 2012*).

However, repeated metasomatism by silicic melts will raise the FeO content near the base of the craton, developing a carapace of oxidising material (Fig. 3). Oxidation of later CH_4-rich fluids in this carapace would release CO_2 and H_2O to drive metasomatism and low-degree melting in the SCLM. This model can explain the genesis of cratonic diamonds from both reduced and oxidised fluids, the existence of SiC as inclusions in diamonds, and the abundance of SiC in some kimberlites.

The recognition that $CH_4 \pm H_2$ may accompany melts rising from a deeper, metal-saturated mantle also suggests an explanation for the zones of high conductivity that mark the tracks of mantle-

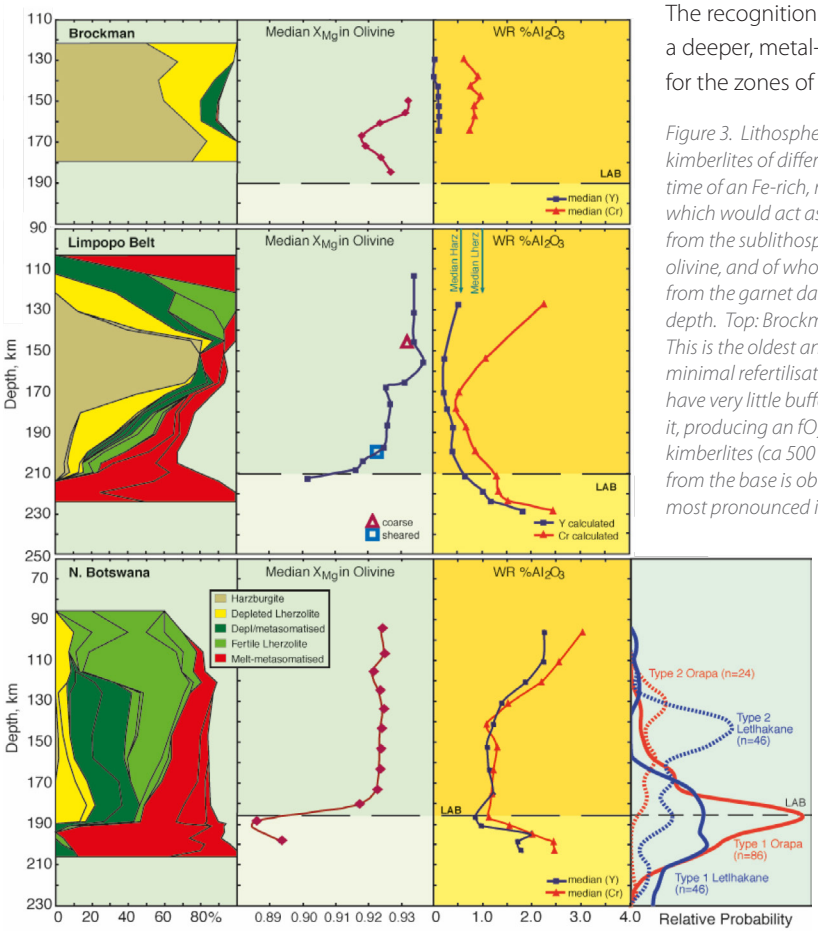

Figure 3. Lithospheric sections (as in Fig. 2) beneath three cratonic areas with kimberlites of different ages. The sections illustrate the development over time of an Fe-rich, melt-metasomatised carapace at the base of the SCLM, which would act as a filter to capture and oxidise (CH_4+H_2) rich fluids rising from the sublithospheric mantle. Estimates of the median Mg# of coexisting olivine, and of whole-rock Al_2O_3 content (based on two methods) are derived from the garnet data and illustrate the extent of metasomatism at each depth. Top: Brockman kimberlite (ca 1800 Ma), Pilbara Craton, W. Australia. This is the oldest and most primitive SCLM section known; it has experienced minimal refertilisation of the primary, highly depleted harzburgite. It would have very little buffering capacity and reduced fluids could penetrate well into it, producing an fO_2 gradient like that seen in Figure 2. Middle: Limpopo Belt kimberlites (ca 500 Ma), South Africa-Zimbabwe. The refertilisation of the keel from the base is obvious, but the changes in Fe content are moderate and most pronounced in a 10-15 km thick zone at the base. Mean compositions and P-T estimates are shown for two types of peridotite xenoliths.

Bottom: N. Botswana kimberlites (90-100 Ma). The metasomatic refertilisation has reduced the overall Mg# (and raised the Al content) of the whole section, but the most intense Fe-enrichment is concentrated in a 20-km thick zone at the base. Mean compositions and P-T estimates are shown for three types of peridotite xenoliths. There is a strong correlation of Fe enrichment with the distribution of eclogites, especially in the basal zone; Type I eclogites are typically heavily metasomatised. This Fe-rich basal barrier would represent a barrier to the passage of reduced fluids, and hence a source of CO_2 and H_2O for metasomatism and melt generation in this layer and above.

derived magmatic systems (from kimberlites to Bushvelds). The oxidation of CH_4 in rising fluids could propagate networks of microveinlets of amorphous carbon (even if later recrystallised to other forms), which might provide the fine-scale connectivity of conductive material in some mantle domains implied by the striking magnetotelluric images now becoming more widely available. See *CCFS publications #830 and #968*.

This project is part of CCFS theme 2, Earth's Evolution, and contributes to understanding Earth's Architecture and Fluid Fluxes.

Contact: Bill Griffin
Funded by: CCFS Flagship Program 1

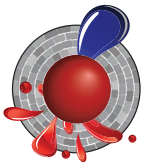

Phosphorites - Older than you think!

Figure 1. Float illustrating centimetre-scale stromatolites and attached millimetre-scale (red) branching structures (Photo: Martin Van Kranendonk).

Phosphorites (sedimentary rocks with high contents of Ca-phosphate) are direct evidence in the rock record of oxygenation within the oceans and atmosphere. Phosphorites thus are restricted in age, first appearing about 2.2 Gyrs ago. They generally form as the result of microbial processes and in the Paleoproterozoic record, only occur as thin, peritidal deposits parallel to shorelines. In 2017 evidence of an older phosphorite, phosphate-rich microbial mats and peloids, was documented within the 2.4-2.3 Ga Turee Creek Group. The same carbonate reef that contains this phosphorite, also has very diverse stromatolites, thrombolites and deep-water microbial communities. Field work in 2017 enabled greater mapping of the 150 cm unit containing the phosphorous-rich microbial mats and established that they are adjacent to stromatolites with attached complex branching structures (Fig. 1). The branching structures are unique to this site and could potentially represent a new form of complex life. Further work will investigate the potential relationship between oxygen in the water during the deposition of these rocks, and the increased complexity of structures within the reef, possibly as the result of life adapting to an oxygenated environment. Part of this work involves studying the range in morphology and the environment in which the branching structures developed, to determine whether these are a new form of complex life and whether there is a connection between their evolution and oxygen.

This project is part of CCFS theme 1 Early Earth, and contributes to understanding Fluid Fluxes.

Contacts: Martin Van Kranendonk, Georgia Soares
Funded by: CCFS Flagship Program 4

Figure 2. PhD Students Brendan Nomchong and Georgia Soares working hard in the field documenting the ridge (Photo: Martin Van Kranendonk).

Zircon signals mineralisation potential of Archean granites

Porphyry Cu deposits are major sources of Cu and Mo. They range in age from Archean to modern, although most are Jurassic and younger; porphyry deposits in Precambrian terranes are rare. Nevertheless, several porphyry-type Cu or Au deposits occur in the Superior Craton of Canada, and in the South West

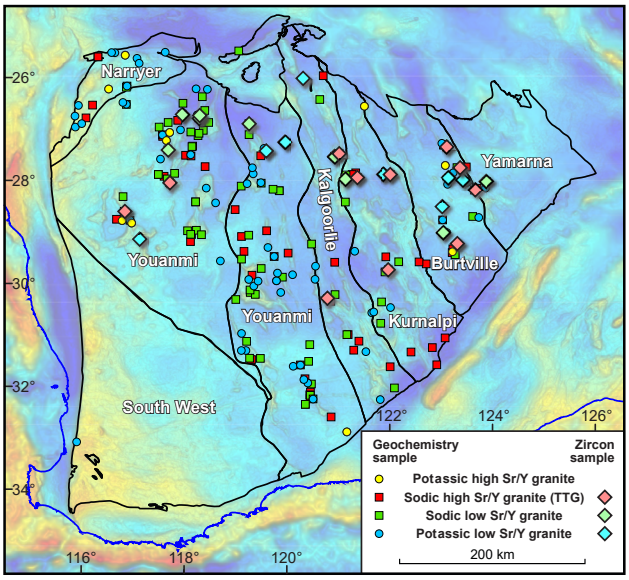

Figure 1. Granite whole-rock and zircon sample locations superimposed on a gravity image of the Yilgarn Craton, labelled by terrane.

Terrane of the Yilgarn Craton, suggesting that their potential in Archean cratons may not be fully recognised.

In Phanerozoic porphyry Cu systems, mineralised magmatic rocks have distinctive chemical fingerprints, including high Sr/Y, V/Sc, Eu/Eu*, and (Eu/Eu*)/Y ratios. Zircons in these rocks also have distinctive compositions, such as higher Eu/Eu* ratios. These signatures can be attributed to high magmatic water and sulfur contents and high oxidation states and can be used as indicators of ore fertility.

To test whether these fertility indicators can be applied to Archean granitic rocks across the Yilgarn Craton, we have compiled GSWA geochronology and geochemistry data for 230 unaltered and non-mineralised granites. The granitic rocks are divided into four groups (Fig. 1).

We also examined >2000 trace element analyses of zircons from 42 Yilgarn granite samples (Fig. 1).

We compared Yilgarn granites with well-characterised hydrous and oxidised Miocene Cu-mineralised granites in southern Tibet. The Tibetan granites crystallised from very hydrous magmas with >10 wt% water contents at depth, resulting mainly from high-pressure differentiation of hydrous mafic melts of Tibetan mantle.

Figure 2a shows that neither hydrous melting nor dehydration melting of mafic lower crust can produce melts with Mg# >50. Tibetan granites typically have Mg# >50 (Fig. 2a), consistent with input of primary mafic magmas through magma mixing. In contrast, most Yilgarn granites have Mg# <50, suggesting derivation mainly through crustal melting with limited mantle input.

Yilgarn high-Sr/Y granites are moderately- to strongly oxidised, whereas low-Sr/Y granites are moderately reduced to strongly oxidised (Fig. 2b). Tibetan Cu-mineralised granites are mainly strongly oxidised and tend to have higher Fe_2O_3/FeO at a given FeO_{total}, suggesting that Tibetan granites are generally more oxidised (Fig. 2b).

Most Yilgarn granites plot in the Cu-infertile field in a diagram of V/Sc vs SiO_2 (Fig. 2c), whereas all Tibetan Cu-mineralised

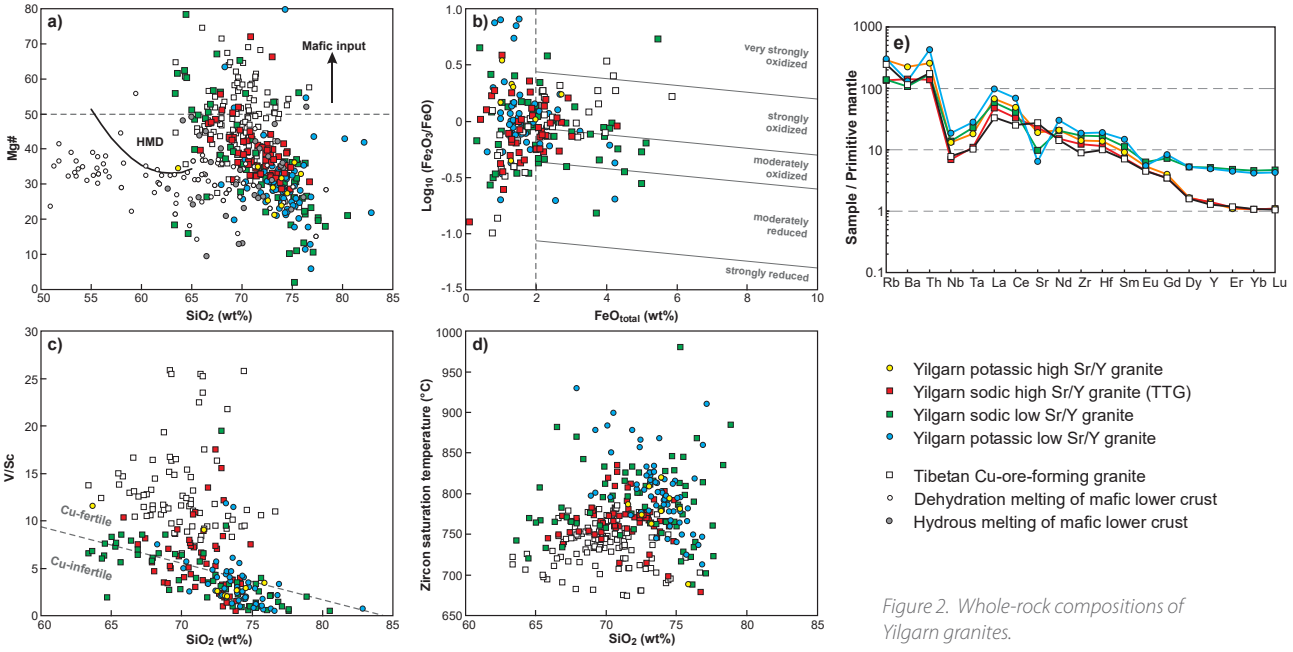

Figure 2. Whole-rock compositions of Yilgarn granites.

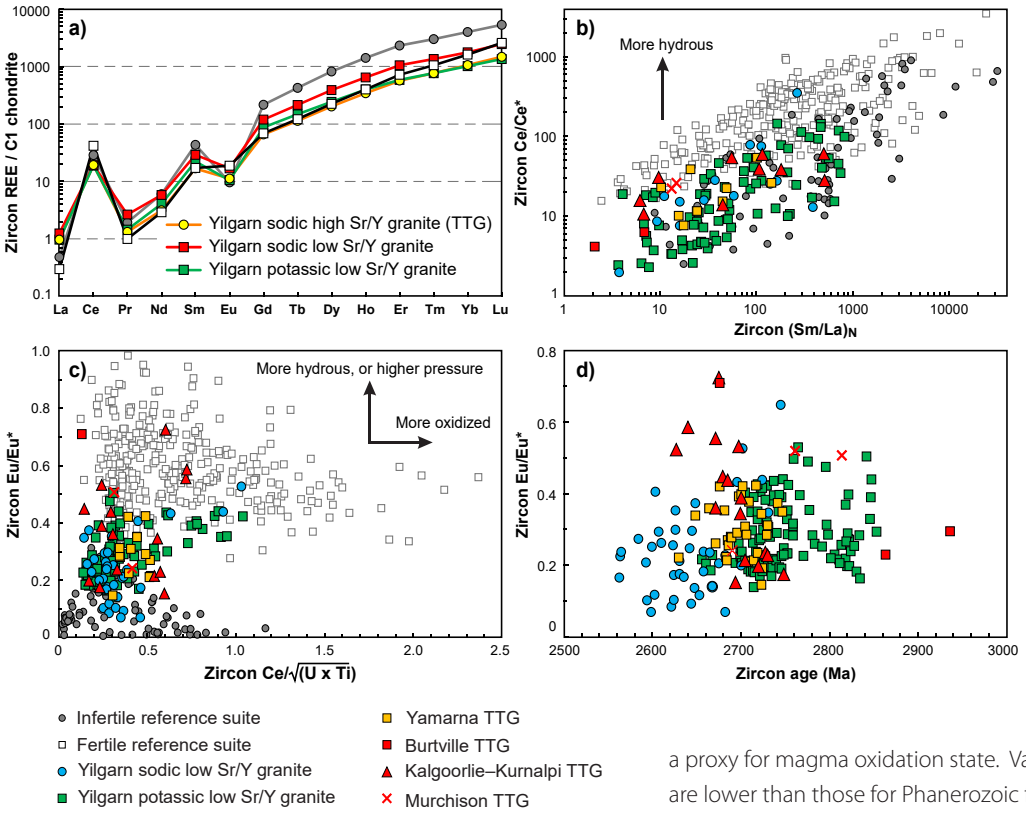

Figure 3. Compositions of zircons from Yilgarn granite.

granites plot in the Cu-fertile field. High V/Sc is caused by amphibole fractionation, which removes Sc, and by suppression of magnetite fractionation, which increases V in an oxidised and hydrous melt. The average V/Sc ratio for each group of Yilgarn granites is significantly lower, suggesting that Yilgarn granites are less fertile than Tibetan granites because the former are generally less oxidised and less hydrous. Zircon saturation temperatures indicate that Yilgarn granites crystallised at higher temperatures than Tibetan granites (Fig. 2d), which also suggests the magmas were less hydrous.

The trace-element patterns of Yilgarn high-Sr/Y and low-Sr/Y granites are distinctly different (Fig. 2e). High-Sr/Y granites are characterised by an absence of Sr and Eu anomalies, and depletion in heavy rare earth elements (HREE). Yilgarn low-Sr/Y granites have significant negative Sr and Eu anomalies and elevated HREE concentrations (Fig. 2e). These features suggest that Yilgarn high-Sr/Y granites were derived from high-pressure melting of mafic crust within the garnet stability field, whereas low-Sr/Y granites originated mainly from low-pressure melting of crust within the plagioclase stability field. Tibetan Cu-mineralised granites have similar HREE patterns to the Yilgarn high Sr/Y granites, but are more enriched in Sr and depleted in Zr (Fig. 2e), consistent with their derivation from high-pressure differentiation of more hydrous melts.

We also compared trace-element compositions of zircon in Yilgarn granites with those of reference suites from infertile and fertile granites. The zircon REE patterns of Yilgarn granites are similar to both Phanerozoic fertile and infertile suites (Fig. 3a). However, Yilgarn granites have consistently lower zircon Ce/Ce* and Eu/Eu* than Phanerozoic fertile suites (Fig. 3b, c), suggesting they were less hydrous than fertile suites.

Zircon Ce/√(U x Ti) was recently proposed as a proxy for magma oxidation state. Values for Yilgarn granites are lower than those for Phanerozoic fertile suites and similar to those of infertile suites. This also suggests that Yilgarn granites are less oxidised than Cu-fertile granites (Fig. 3c), and this is consistent with interpretations from whole-rock Fe_2O_3/FeO data (Fig. 2b).

Both whole-rock and zircon compositions indicate that many Yilgarn granites are less hydrous and less oxidised than Phanerozoic Cu-mineralised granites. The systematic difference in zircon chemistry between Archean granites and Phanerozoic fertile and infertile suites suggests that different processes were involved in forming Archean granites. We argue that Archean high-Sr/Y granites were formed mainly through intracrustal partial melting of mafic lower crust in the garnet stability field, whereas Phanerozoic fertile suites were formed by intracrustal amphibole-dominated fractionation of mafic magmas. Granites formed by the former process have lower potential for porphyry Cu mineralisation due to insufficient water and the absence of copper and sulfur accumulation in the melt.

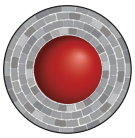

This project is part of CCFS theme 2, Earth's Evolution, and contributes to understanding Earth's Architecture.

Contacts: Yongjun Lu, Hugh Smithies, Michael Wingate, Noreen Evans, Paul Morris, David Champion, Cam McCuaig
Funded by: CCFS Flagship Program 7

Seismic image of the Capricorn Orogen – revealing the mantle component

The Proterozoic Capricorn Orogen in central Western Australia (Fig. 1) records the collisions of the Archean Pilbara and Yilgarn Cratons to form the West Australia Craton during two stages of Paleoproterozoic orogeny: 1) the 2.21-2.14 Ga

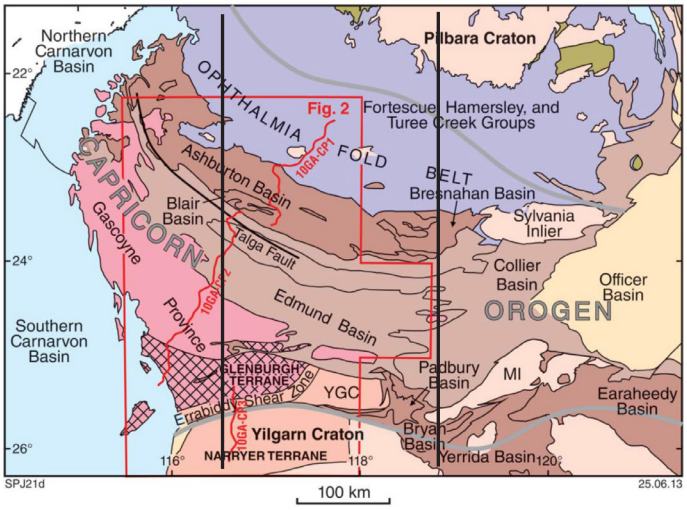

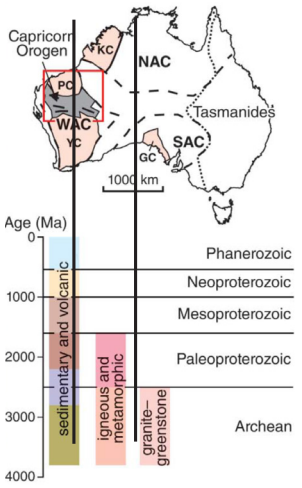

Figure 1. Tectonic map of the Capricorn Orogen modified from Johnson et al. (2013). Black N-S lines are the seismic transects shown in Figure 3.

Ophthalmian Orogeny, when the Glenburgh Terrane, a microcontinent between the Pilbara and Yilgarn, first collided with the Pilbara Craton; 2) the 2.00-1.95 Ga Glenburgh Orogeny, when the combined Pilbara Craton/ Glenburgh Terrane further collided with the Yilgarn Craton to form the West Australia Craton. After the final assembly, the Capricorn Orogen was affected by more than 1 billion years of episodic intracontinental reworking and reactivation processes.

To evaluate how these tectonic processes have imprinted the orogenic lithosphere, and thus shed light on the dynamics of early continental collision and stabilisation, we conducted a finite-frequency body-wave tomographic study, taking advantage of the new data recorded by a portable seismic array COPA (Capricorn Orogenic Passive-source Array, part of the SIEF program, Distal Footprint of Gigantic Ore systems - a Capricorn Case Study), which has been in the field since April 2013. We were able to extract travel-time information from 486 teleseismic events. We also incorporated data recorded during earlier field campaigns conducted by ANU.

Our provisional tomographic model reveals the following intriguing observations: 1) the Capricorn orogen is imaged clearly as a significant low-velocity anomaly, extending downwards to nearly 250 km depth, rather than a more typical high-velocity cratonic root. The low velocity may reflect the effects of punctuated lithospheric reworking and reactivation during the cratonisation processes; 2) the Glenburgh Terrane is underlain by a high-velocity anomaly ~150 km thick; 3) the northern edge of the Yilgarn Craton is characterised by a high-velocity anomaly that extends northwards to ~300 km depth beneath the Capricorn Orogen; and 4) the tomographic model captures likely remnant subducted slab pieces which are now part of the cratonic lithosphere.

This project is part of CCFS themes 1, 2 and 3, Early Earth, Earth's Evolution and Earth Today, and contributes to understanding Earth's Architecture.

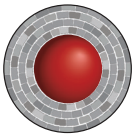

Contacts: Xiaobing Xu, Liang Zhao, Huaiyu Yuan
Funded by: CCFS Flagship Program 7

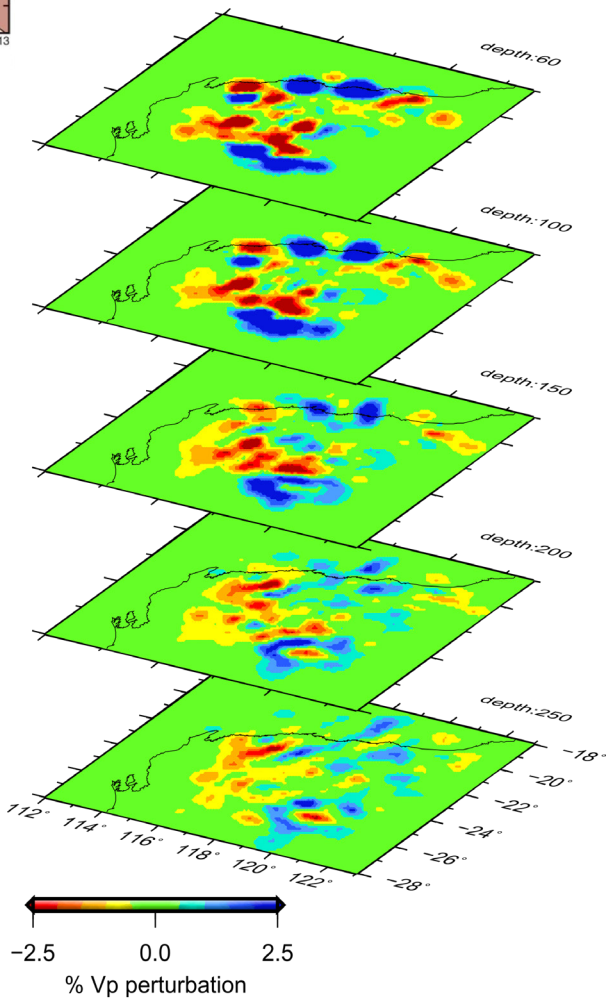

Figure 2. Map views of the preliminary P-wave velocity model.

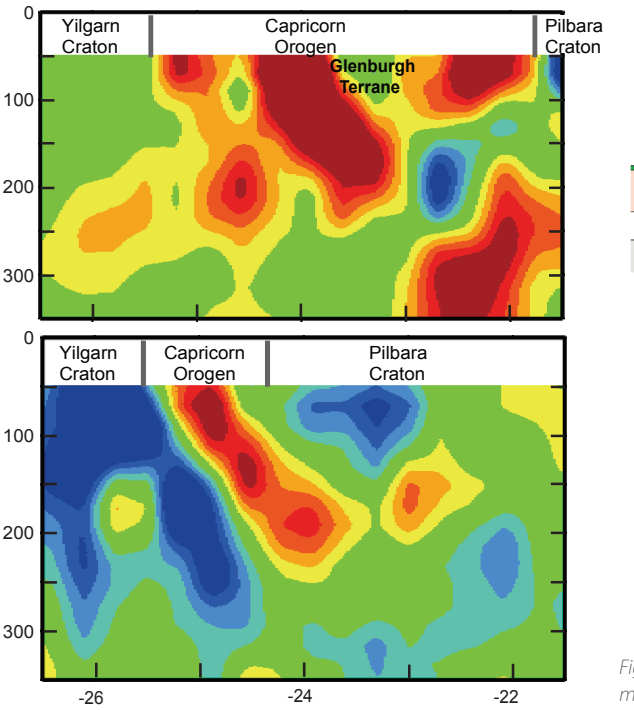

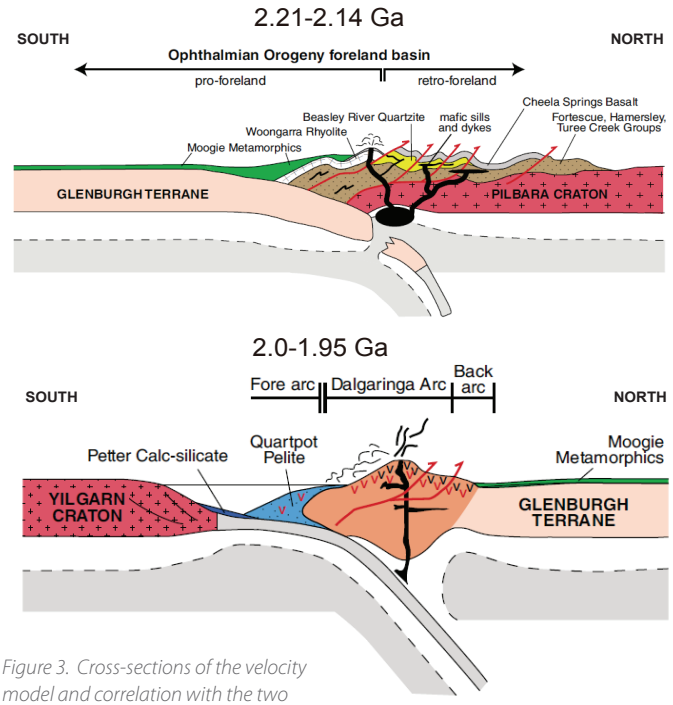

Figure 3. Cross-sections of the velocity model and correlation with the two Paleo-Proterozoic orogenies.

New petrogenetic model for the adakitic magmatism of Patagonia and the Austral Volcanic Zone

The '*Adakites*' from the Patagonian Cordillera and the Austral Volcanic Zone (AVZ) on the southwest margin of South America are widely regarded as true slab-melts, rare on Earth. These differ from ordinary calc-alkaline arc andesites and dacites by steeper REE patterns with low concentrations of HREE and Y, and high values of Mg#, Cr, Ni, and Sr for SiO_2 contents mainly in the range 56-63 wt%. The steep REE patterns have been interpreted as evidence for partial melting of eclogite in the subducting plate, by analogy with the '*adakites*' on Adak Island in the central Aleutian arc. However, an alternative interpretation of the type '*adakite*' by petrogenesis differentiation of hydrous magmas at high pressure and temperature is suggested by: 1) recognition of xenolith suites as cognate cumulates; 2) seismic evidence of a slab-mantle interface to at least 270 km depth under the central Aleutians, which means that slab temperature is less than 650°C under the volcanic front, too cool to be melted; and 3) along-arc variations of tectonic stress. This project will explore this alternative interpretation in the Plio-Holocene volcanic centres of the AVZ, as well as the mid-Miocene Patagonian '*adakites*'.

Why Patagonia? The western margin of Patagonia has experienced the subduction of the Chile Rise since ~22 Ma. A series of adakitic igneous complexes is correlated with the

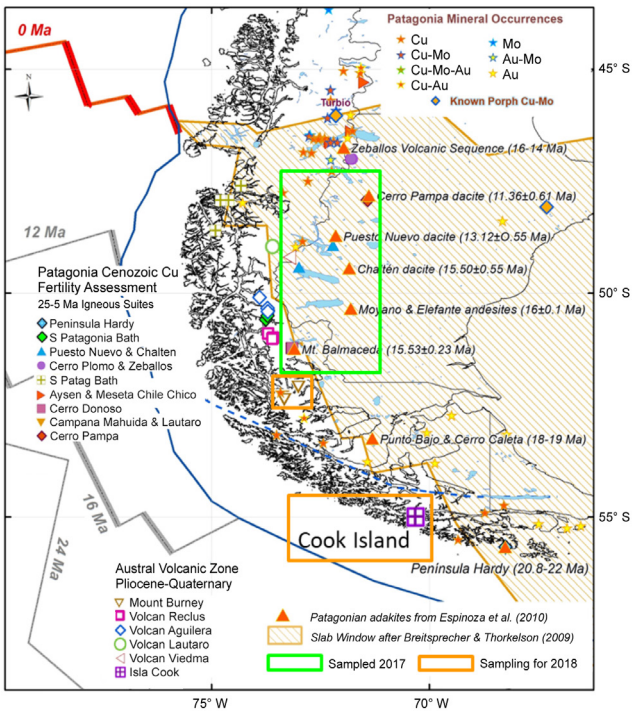

Figure 1. Distribution of the Miocene Patagonian Adakites and the Austral Volcanic Zone with Sampling Locations in this project.

northward-propagating compressive deformation wave, which seems to be associated with the young, warm and buoyant southern part of the subducted Nazca Plate. On the other hand, all six Holocene volcanic centres of the Andean AVZ (49-54°S), associated with subduction of the Antarctic Plate under the South American and Scotia Plates, have erupted exclusively adakitic andesites and dacites. The presence of these two

Gonzolo Henriquez enjoying the magnificent views during fieldwork in the Cerro Moyano, Patagonia - Argentina (Photo: Mario Coloma).

scenarios in one tectonic setting makes Patagonia a perfect location to understand the genesis of adakitic magmas.

The project integrates whole-rock geochemistry with U-Pb dating and trace-element analysis of zircons (*in situ* and detrital). Cathodoluminescence (CL) images will be used to search unzoned cores in zircon grains, which could imply deep, slow crystallisation of the plutonic rocks. We also will perform Al-in-hornblende (EPMA) barometry on hornblende phenocrysts in host rocks and plutonic enclaves at the CMCA (UWA).

Rock and stream sediments were taken from 5 mid-Miocene igneous centres, during 2017 in Patagonia (Chile and Argentina). Zircon separation and CL Imaging and geochemical sample preparation have already been done at the School of Earth Sciences and the CMCA (UWA). Over 2000 zircon LA-ICP-MS analyses were performed at QUT to November 2017, in addition to 15 whole-rock analyses (LabWest, Perth). Field work in 2018 will sample 2 adakitic volcanoes from the AVZ.

This project is part of CCFS theme 2, Earth's Evolution, and contributes to understanding Earth's Architecture and Fluid Fluxes.

Contacts: Gonzalo Henriquez, Marco Fiorentini, Bob Loucks

Funded by: CCFS Flagship Programs 2 and 3

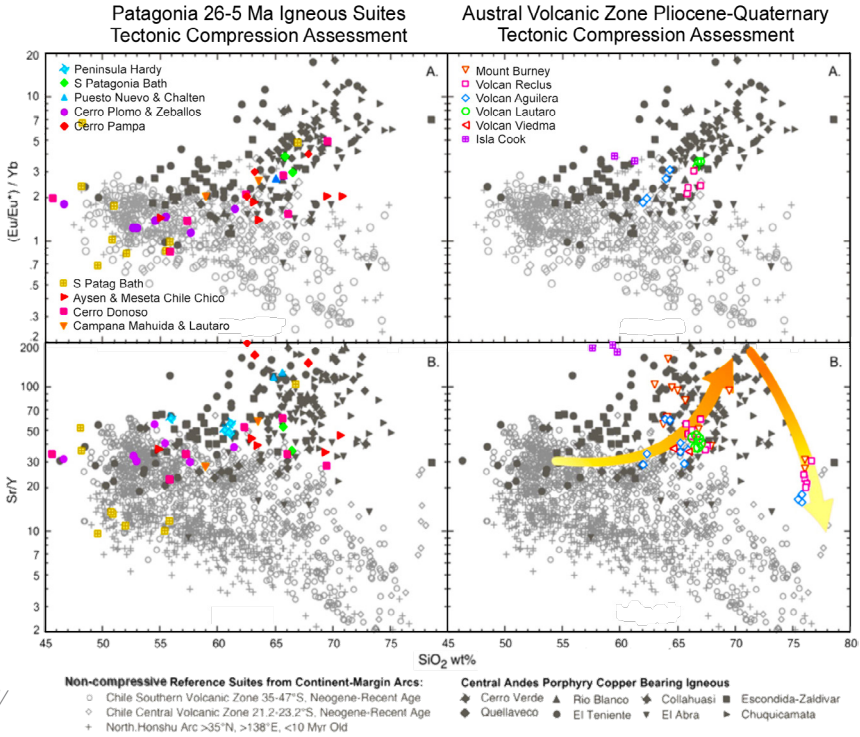

Figure 2. High-pressure magmatic evolution of Patagonian Igneous Centres exposed by use of Sr/Y and (Eu/Eu)/Yb ratios. Over ~400 geochemical analyses from the Patagonian region were compiled from literature and added to Robert Loucks' Global Data Base, according to 3 main criteria: Sr/Y > 35 and/or (Eu/Eu*)N/YbN > 1.9 and SiO_2 > 57 wt%.*

Research highlights 2018

Contents

At the end of the rainbow - Where is the pot of gold?

The nobility of gold, along with its high conductivity, ductility and especially its rarity have made it one of the most desired commodities in the history of humanity. Despite seven millennia of mining, the processes that locally enrich Au in the Earth are still enigmatic. Understanding these processes is becoming increasingly important as fewer new large gold deposits are being discovered, leading to claims that *'peak gold'* production has been reached. Most previous geological studies on Au have investigated crustal processes related to the formation of Au deposits. However, the ultimate source of the gold remains poorly constrained. Gold has been one of the least studied elements in the mantle. There are several reasons for this, including the fact that Au occurs in low levels in the mantle, making analysis difficult, and the mono-isotopic nature of Au makes isotope dilution, the technique commonly used to analyse the geochemically similar platinum group elements (PGE), impossible.

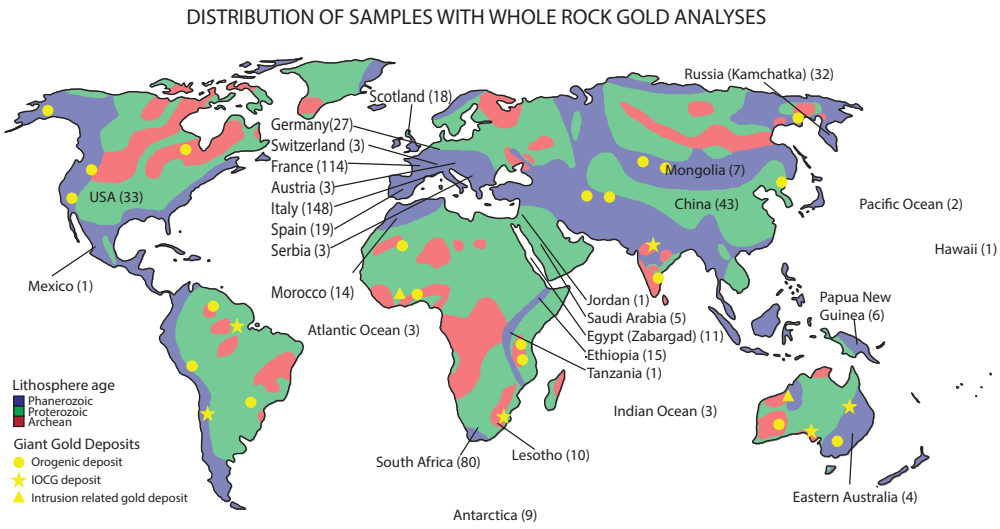

Figure 1. Global map showing distribution of upper mantle samples included in this study. Lithospheric ages simplified from the data in Artemieva (2006). Note: Location of giant gold deposits (classified as containing >500 t Au) from Groves et al. (2016).

We have compiled whole-rock analyses in mantle rocks (*CCFS publication #1206*) to investigate the abundance of gold in the lithospheric mantle, and how this distribution can be modified. This is the first time such an extensive database has been compiled for Au in mantle rocks, and several surprising results have emerged, including:

1. Modern lithospheric mantle has similar gold concentrations to the primitive upper mantle and the average continental crust, indicating that the lithospheric mantle has not been significantly depleted in Au over the course of Earth's history. This contrasts with previous suggestions that the primitive mantle was enriched in Au, making it a more fertile source for Au mineralisation in the Archean.

2. The lithospheric mantle has a relatively homogenous Au distribution, with the exception of the North China Craton, which appears to be anomalously enriched in Au. This enrichment is likely the result of the unique *'decratonisation'* event that the region underwent in the Mesozoic.

3. Au shows no systematic relationship with the LILE, and does not appear to be enriched by hydrous fluids in the mantle, which strongly contrasts with its behaviour in the crust. There is likewise no evidence that Au is enriched by carbonatitic metasomatism in the mantle. It may, however, be enriched by silicate melts in the mantle.

4. Au content of pyroxenites is commonly elevated relative to that of peridotites in the lithospheric mantle (median Au-in-pyroxenite = 2.0 ppb; median Au-in-peridotite = 1.2 ppb). The data indicate that the melts from which these pyroxenites have crystallised may be effective metasomatic agents within the lithospheric mantle. Such gold-rich pyroxenites and related magmas may play an important role in crustal mineralisation processes.

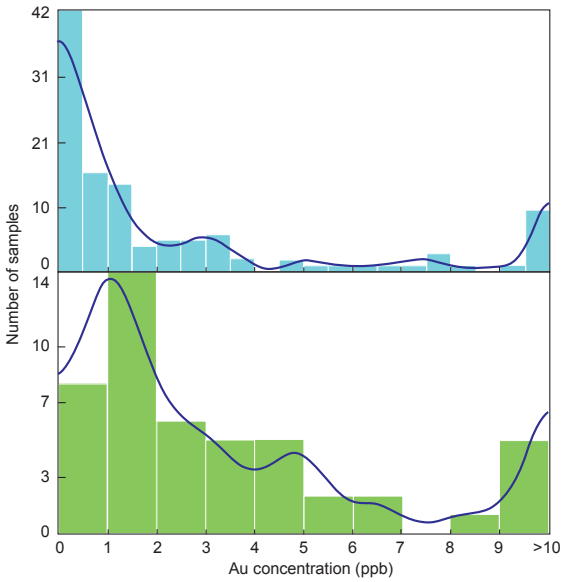

Figure 2. Histograms for Au concentrations in different lithologies: (a) dunite and harzburgite samples (n = 116); (b) pyroxenite samples (n = 48). All analyses >10 ppb have been included together on far right of histogram.

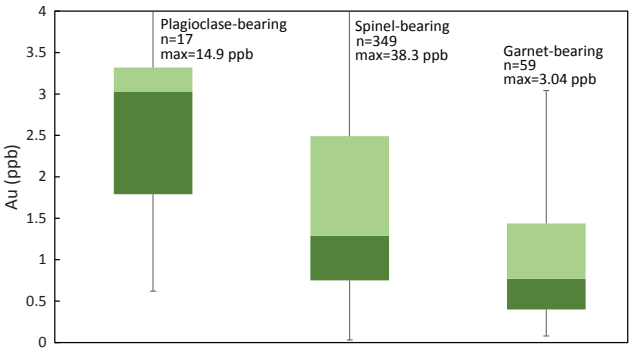

Figure 3. Box-and-whisker plots showing the decrease in Au with depth (from shallow, plagioclase-bearing peridotites on the left to deep, garnet-bearing peridotites on the right) in the lithospheric mantle.

In summary:

- Au contents in the subcontinental lithospheric mantle (SCLM), primitive upper mantle and crust are comparable, likely indicating efficient recycling through Earth history at least post-Archean
- The median Au contents in metasomatised, refertilised SCLM are higher than those in depleted and primitive SCLM
- Au is not sourced from subducted oceanic lithosphere but from asthenosphere
- Au is transported in silicate melts (evidenced by mantle pyroxenites), and not by *"fluids"*
- Shallow SCLM is most Au-enriched (indicating Au is upwardly mobile via silicate melt movement) in the lithospheric mantle

This project is part of CCFS themes 2 and 3, Earth's Evolution and Earth Today, and contributes to understanding Earth's Architecture and Fluid Fluxes.

Contacts: Ed Saunders, Sue O'Reilly, Bill Griffin
Funded by: TARDIS Flagship Program

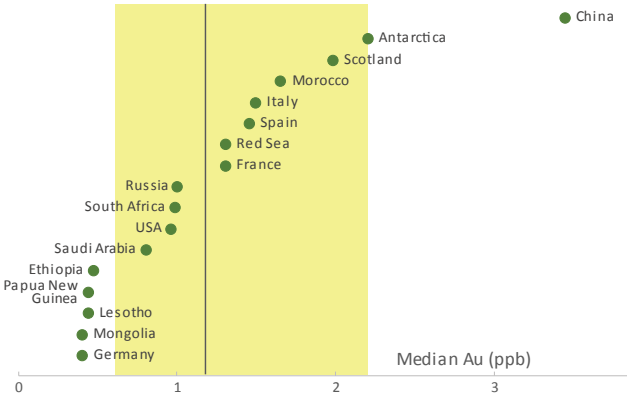

Figure 4. Median Au concentration in countries with five or more samples in the compiled database. Yellow box represents the 25-75th percentiles for upper mantle peridotites globally, dark grey line is median gold concentration for Au in upper mantle peridotites globally.

Atmospheric sulfur is recycled into the continental crust during supercontinent formation

The sulfur cycle across the lithosphere and the role of this volatile element in the metasomatism of the mantle at ancient cratonic boundaries are poorly constrained. We address these knowledge gaps by tracking the journey of sulfur in the assembly of a Proterozoic supercontinent using mass independent isotope fractionation (MIF-S) as an indelible tracer. MIF-S is a signature that was imparted to supracrustal sulfur reservoirs before the ~2.4 Ga Great Oxidation Event. The spatial representation of multiple sulfur isotope data indicates that successive Proterozoic granitoid suites preserve $\Delta^{33}S$ up to +0.8‰ in areas adjacent to Archean cratons. These results indicate that suturing of cratons began with devolatilisation of slab-derived sediments deep in the lithosphere. This process transferred atmospheric sulfur to a mantle source reservoir, which was tapped intermittently for over 300 million years of magmatism. Our work tracks pathways and storage of sulfur in the lithosphere at craton margins.

This project is part of CCFS themes 1 and 2, Early Earth and Earth's Evolution, and contributes to understanding Earth's Architecture and Fluid Fluxes.

Crystal LaFlamme and Marco Fiorentini (UWA) try to unravel the cryptic link between the global sulfur cycle and the genesis of world-class mineral deposits.

Contacts: Marco Fiorentini, Crystal LaFlamme
Funded by: SIEF, MRIWA, CCFS Flagship Program 2

The curious story of the uniqueness of Archean lithospheric mantle in the Earth: *Lithospheric mantle comes of age - dominant, persistent and widespread*

Continental crust on the modern Earth is underlain by a subcontinental lithospheric mantle (SCLM), consisting dominantly of variably depleted ultramafic rocks. It ranges from a few tens of kilometres thick beneath active rift zones, to >250 km beneath some Archean cratons, and is represented as dismembered buoyant blobs in ocean basins following intracratonic rifting (*CCFS publication #37*). Archean SCLM is both more depleted, and much more widespread, than previously understood. Its generation led to the formation of buoyant (and hence unsubductable) continental nuclei, which influenced the preservation of early crust and the nature of early plate tectonics. Its persistence has provided important constraints on the mechanisms and extent of growth of SCLM, including precluding growth by subcretion of subducted oceanic crust (e.g. *GEMOC publication #461*). The composition of the SCLM has changed through time (*CCFS publication #1183, Fig. 1*): SCLM thick enough to permit the formation of diamonds may only have formed uniquely in Archean time, lurking beneath some cratons ever since.

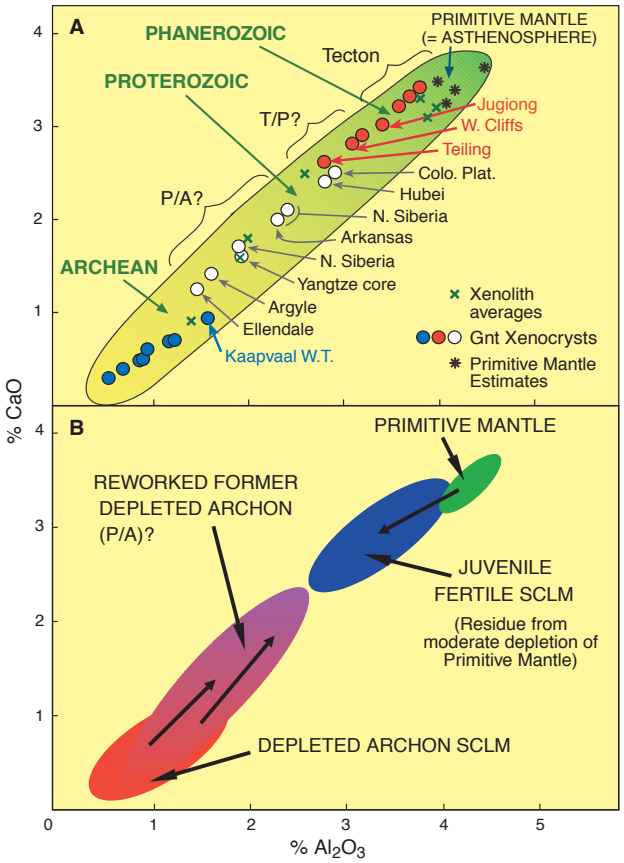

Figure 1. A. Estimates of the mean CaO and Al_2O_3 contents in subcontinental lithospheric mantle (SCLM) sections of different tectonothermal age based on the compositions of garnet xenocryst populations (circles) and xenolith populations (crosses) in volcanic rocks. B. Interpretation of the data in (A) in terms of depletion - refertilisation processes.

Archean SCLM is unique

The composition of the SCLM can be estimated from exposed orogenic massifs and from xenolith and xenocryst suites; each has its advantages and disadvantages. Most massifs represent relatively shallow SCLM sections, and have been strongly deformed during their emplacement, but exceptions may be found in some ultra-high-pressure zones, such as western Norway and in some orogenic domains in Tibet (*CCFS publication #704*). Xenolith suites sample larger vertical sections of the SCLM, but the relationships between different rock types are seldom obvious, and sampling (either by the volcano or by the geologist) may not be representative. Garnet xenocrysts in volcanic rocks can be used to estimate the composition of the SCLM, and this technique has provided a broader basis for mapping rock-type sections of the SCLM (*CCFS publications #1, 299, 303*).

How old is it?

The most robust isotopic system available for measuring the ages of SCLM peridotites is provided by the decay of ^{187}Re to ^{187}Os. During partial melting of the mantle, Re is extracted into the fluid phase, while Os remains concentrated in the residue; the removal of the melts from the system tends to freeze in the isotopic composition of the residual Os. The $^{187}Os/^{188}Os$ of the rock, or constituent minerals, can then be referred to a model for the evolution of Earth's Re-Os system to derive a model age that approximates the timing of the melt-extraction event. Detailed sulfide Re-Os data show a general overall decrease in model ages with depth beneath at least the Kaapvaal craton, but old sulfides and younger ones coexist in single hand specimens, reflecting the injection of multiple generations of sulfide.

Although the *in situ* sulfide dating method has been applied to a large range of lithospheric samples from different Archean cratonic regions, very few reliable model ages older than 3.6 Ga have been found (*CCFS publication #1183, Fig. 2.*); and the same is true for whole-rock data. While we do not have xenoliths of the SCLM from beneath areas that contain Hadean crustal rocks, the apparent lack of Hadean model ages beneath the oldest cratons seems to indicate that there was no Hadean SCLM. If the SCLM that we see today came into being only in Archean time, what does this tell us about the evolution of the early Earth?

How did it form?

A common model used to explain the formation of Archean SCLM is by the accumulation of subducted slices of oceanic mantle (*'lithospheric stacking'*). However, detailed seismic tomographic images of modern subducting slabs show that most descend steeply into the Earth, down to at least the 660 km discontinuity, rather than accumulating at shallow depths beneath the continents. In areas where shallow subduction is observed, the slab rarely extends far under the continents, and

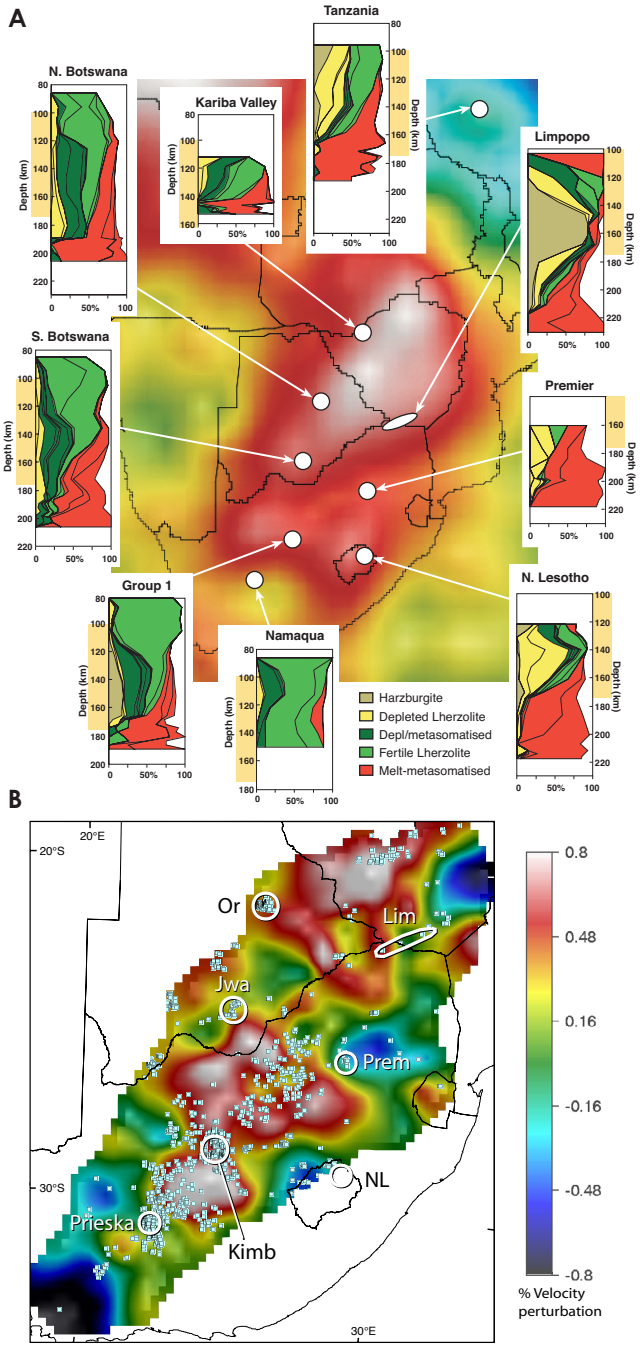

Figure 2. A. Seismic tomography image (100-175 km) of southern Africa, with location of well-documented xenolith suites and chemical tomography sections. White-pink colours indicate high seismic velocities, related to strong depletion and low geotherms; yellow-green colours indicate low velocities related to fertile compositions and higher geotherms. B. Detailed Vs tomography at 200 ± 50 km showing locations of known kimberlites. This emphasises that kimberlites tend to avoid blocks of best-preserved Archean subcontinental lithospheric mantle (white areas), instead following (and sampling) their more metasomatised, and hence lower-Vs, marginal zones. (Kimb, Kimberley area; NL, Northern Lesotho; Prem, Premier mine, Lim, Limpopo Belt; Jwa, Jwaneng; NB, Northern Botswana; Or, Orapa) (A) After Deen, T. et.al., 2006)., (B) After Fouch, M.J. et.al., 2004.

does not produce thick SCLM.

The composition of Archean SCLM as defined by xenolith suites is unique; the *'pristine'* Archean SCLM is even more highly depleted than previous estimates and new values for the major oxides have been calculated (*CCFS publication #1183*). Thus, the formation of these highly depleted volumes appears to be related to specifically Archean processes, and are inferred to include megaplumes or massive mantle overturns (*CCFS# 330; references therein*). It is also unlikely to be coincidental that the production of highly depleted Archean SCLM coincides in time with the large-scale production of komatiitic magmas, which probably reflect high degrees of partial melting, requiring rapid decompression and leaving a highly depleted residue. Cogent evidence for the contribution of plumes to the ancient SCLM is provided by mineral inclusions in diamonds of minerals that are stable only under ultradeep lower-mantle conditions (e.g. ferropericlase, CaSi- and MgSi-perovskites).

How extensive is Archean SCLM?

The Global Lithospheric Architecture Mapping (GLAM) project (*GEMOC publications #547, CCFS publication#75*) had produced maps of the rock types and ages of upper-lithosphere domains. These are blocks of crust and lithosphere generated or reworked at different times, and delineated by integrating regional tectonics and geochronology with all available geophysical data (magnetic, gravity, seismic) and geochemical datasets in a multi-dimensional database in a GIS environment (Fig. 3) The origins and evolution of the underlying lower-lithosphere domains are interpreted from a high-resolution global shear-wave tomographic model (*CCFS publication #75*), using thermal/compositional modelling (*CCFS publications #217, 218*) and xenolith/xenocryst data (compositions and ages) from volcanic rocks. This work has shown that most continents are assembled from Archean cratons and smaller cratonic fragments, stitched together and flanked by younger fold belts (e.g. *GEMOC publication #547; CCFS publications #75, 1183*). The larger cratons are underlain by geochemically depleted, buoyant and mechanically robust SCLM; these cratonic roots have steep sides, extending in some cases to more than 300 km.

The SCLM is not only widespread *geographically* beneath existing continents, but it also shows great *vertical* extent in at least some regions. High-resolution global seismic tomography (Vs) models reveal high-velocity domains beneath cratonic crust in Africa that extend to depths of 300-400 km (*GEMOC publication #576*). These high-velocity domains show a distinct contrast with the characteristics of *'normal'* asthenosphere and are interpreted as depleted, buoyant roots that formed in the Archean and have remained attached to the overlying ancient crust. Archean lithospheric mantle has also been inferred beneath the Atlantic oceanic crust from tomographic models and the world magnetic-anomaly map (GEMOC #575; *Korhonen et.al., 2007*) confirms that continental roots, overlain by thinned continental crust, locally extend well out under the deep Atlantic Ocean basin. However, such high-velocity domains are not confined to the Atlantic basin margins, but are scattered randomly through other basins. These high-velocity domains are interpreted to be remnant buoyant ancient lithospheric fragments isolated by disruption of continental cratonic regions during rifting. This

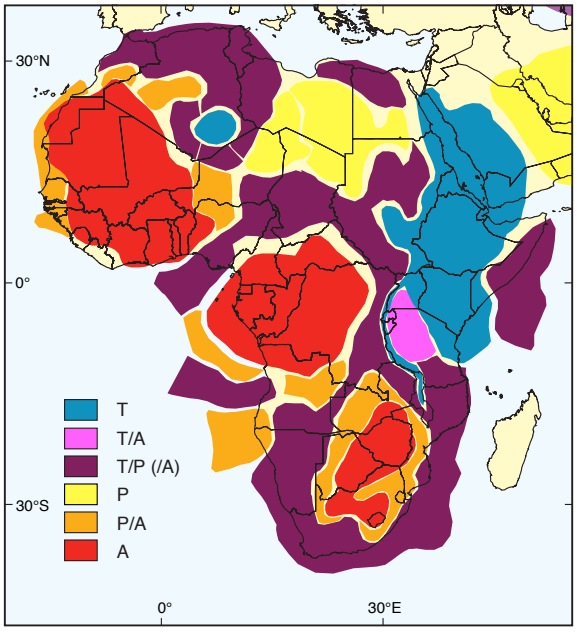

Figure 3. A Global Lithospheric Architecture Mapping interpretation of the subcontinental lithospheric mantle structure of Africa. A, Archon; P, Proton; T, Tecton (After Begg, et.al., 2009).

interpretation is supported by the old Os depletion ages of mantle peridotites from mid-ocean ridges and oceanic islands. (e.g. *GEMOC publication #576; CCFS publication #1183*).

This view of the secular evolution process emphasises the importance and uniqueness of the Archean SCLM. The formation of the Archean SCLM was one of the major events in Earth history, and the Paleoarchean-Mesoarchean period may have been a remarkable interregnum between the Hadean and a more modern Earth.

Implications for crustal evolution

If much of the present continental crust is underlain by SCLM produced in Archean time, then Archean crust may also be much more extensive than suggested by current outcrop patterns. Detailed studies of crustal xenoliths in basalts and kimberlites are now providing abundant evidence that ancient lower crust can be preserved while younger igneous rocks *'resurfaced'* it to form the upper crust. Such areas include localities in the North China Craton (*CCFS publication #95*), the Mediterranean region (*CCFS publication #234*), Spitsbergen (CCFS publication #37) and the Yangtze Craton (*CCFS publication #396*).

Our estimates based on the GLAM methodology indicate that more than 70% of SCLM has Archean heritage: it underlies most younger continental crust, and even some oceanic crust.

These advances in understanding the timing and mechanisms of SCLM formation have implications for models of crustal growth and recycling through time, which remain to be explored.

This project is part of CCFS theme 2, Earth's Evolution, and contributes to understanding Earth's Architecture and Fluid Fluxes.

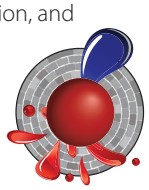

Contacts: Bill Griffin, Sue O'Reilly

Building the house from the basement: *in situ* isotopes in kimberlitic carbonates

Kimberlites are volcanic rocks, rich in volatiles (H_2O and CO_2), derived from a deep (>200 km) mantle source. As a consequence, they are often regarded as probes of the lithospheric mantle, providing unique insights of its structure, composition and evolution.

This project is focused on the study of *primary* kimberlitic carbonates, since they are considered good traps for the original CO_2 in kimberlite magmas and thus the best minerals to constrain the C and O isotope composition of the kimberlite parental melts. However, initial petrographic and compositional studies of kimberlites worldwide emphasised the complex petrogenesis of kimberlitic carbonates, involving both syn- and post-emplacement processes (i.e. magma crystallisation, hydrothermal alteration, crustal contamination, degassing or weathering). This heterogeneous nature explains why C-O isotope analysis of bulk carbonates in kimberlites yield inconclusive results about their origin. It clearly was necessary to develop a new approach that could correctly identify the origins of the different generations of carbonates described in the kimberlites. For the first time, textural and compositional studies were combined with *in situ* isotopic techniques (SIMS) to accurately measure the Sr, C and O isotope compositions of both primary and secondary carbonates.

A good example of the potential of this integrated methodology can be seen in our recent characterisation of the Benfontein kimberlite sills (South Africa). These three sills are well-known for their enrichment in carbonates, which show a variety of textures and compositions (e.g. laths, interstitial groundmass, veins) (Fig. 1 a-c). Another characteristic feature of the Benfontein kimberlite is the presence of calcite blobs or *'diapirs'* intruding the uppermost layers of the lowest of the three sills (Fig. 1 d-f). The origin of carbonate-rich sills associated with kimberlites has been a matter of debate since their discovery, and there is still no consensus about the origin of the *'diapirs'* at Benfontein. They have been related to carbonate-rich melt segregations from an evolved kimberlite magma; infilling of early gas cavities with a residual kimberlitic fluid; or crystallisation from hydrothermal, crustal-contaminated fluids.

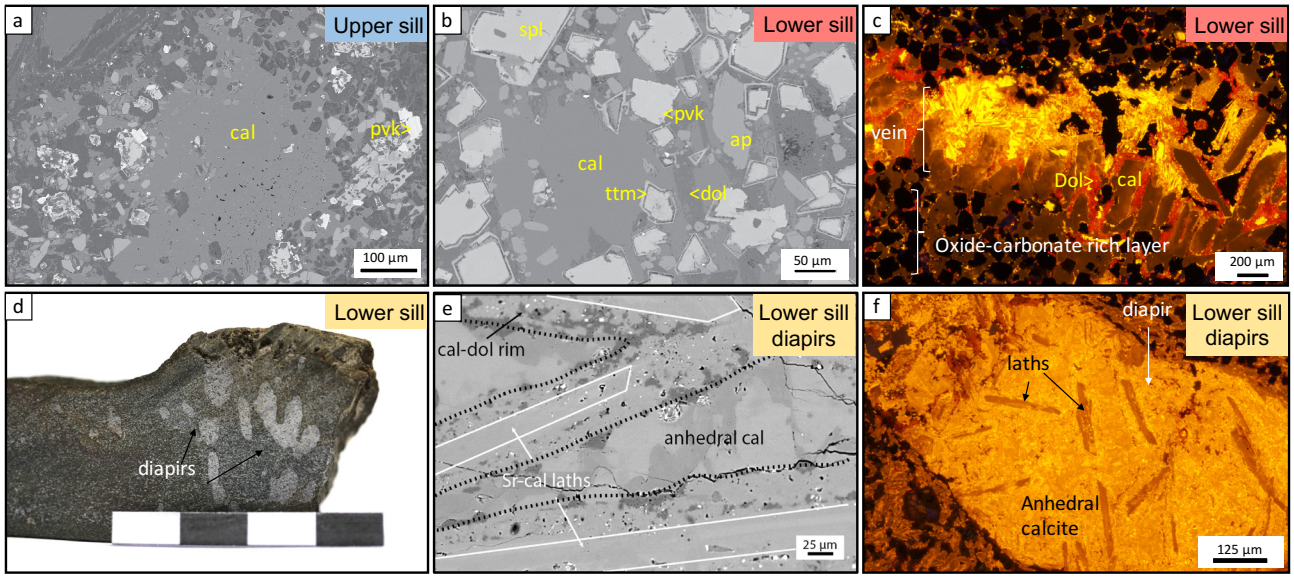

Figure 1. Carbonate petrography of the upper and lower sills in Benfontein. A) BSE-SEM image of the groundmass calcite (cal), interstitial to serpentinised olivine, with groundmass spinel and perovskite (pvk). B) BSE-SEM image of the oxide-rich layer, with abundant atoll spinel (spl) with a titanomagnetite rim (ttm), apatite (ap) and perovskite, with interstitial calcite and dolomite (dol). C) Cathodoluminescence (CL) image of the oxide-rich layer of the lower sill, crosscut by a carbonate-rich vein. (D-F) Hand sample, BSE-SEM and CL images of the diapirs of the lower sill. Note the different generations of carbonates: Sr-rich calcite laths, pure anhedral calcite of most of the diapir and a calcite-dolomite reaction rim.

Our multidisciplinary approach not only revealed the petrographic and geochemical complexity of carbonates in kimberlites in unprecedented detail, but also allowed confident identification of the processes that led to their formation. As shown in Figure 2, *in situ* C-O isotope studies, combined with Sr isotope analysis, have identified carbonates derived from: i. magmatic crystallisation of Sr-rich calcite laths and groundmass; ii. crystallisation of late groundmass calcite from hydrothermal fluids; and iii. variable degrees of crustal contamination in carbonate-rich diapirs and secondary veins. These diapirs most likely resulted from a residual C-O-H fluid or carbonate melt that had interacted with the local Dwyka shales, leading to higher $^{87}Sr/^{86}Sr$ and $\delta^{18}O$, but lower $\delta^{13}C$, than pristine magmatic calcite. Before coalescing into the diapiric segregations, they also variably entrained early-formed calcite laths and groundmass phases.

Comparison between *in situ* and bulk carbonate analyses (Fig. 2) confirms that C-O isotopic analyses of bulk carbonates from kimberlite rocks are not representative of the original C-O isotopic signature of the kimberlite magma. In contrast, calcite laths and most groundmass grains at Benfontein preserve isotopic values ($\delta^{18}O$ = 6 to 8‰ and $\delta^{13}C$ = -4 to -6 ‰), similar to those of pristine carbonatites, which therefore probably correspond to those of their parental melts. This narrow range suggests that the "*mantle carbonate*" box in Figure 2 could be more restricted than previously proposed.

This project is part of CCFS themes 1 and 2, Early Earth and Earth Evolution, and contributes to understanding Earth's Fluids.

Contacts: Montgarri Castillo-Oliver, Andrea Giuliani, Bill Griffin, Sue O'Reilly, Russell Drysdale, Adam Abersteiner, Emilie Thomassot, Xian-Hua Li

Funded by: CCFS Flagship Program 1, ARC DECRA to Andrea Giuliani (grant DE-150100009, European Science Foundation: Europlanet 2020 Consortium (project n. 16-EPN2-017)

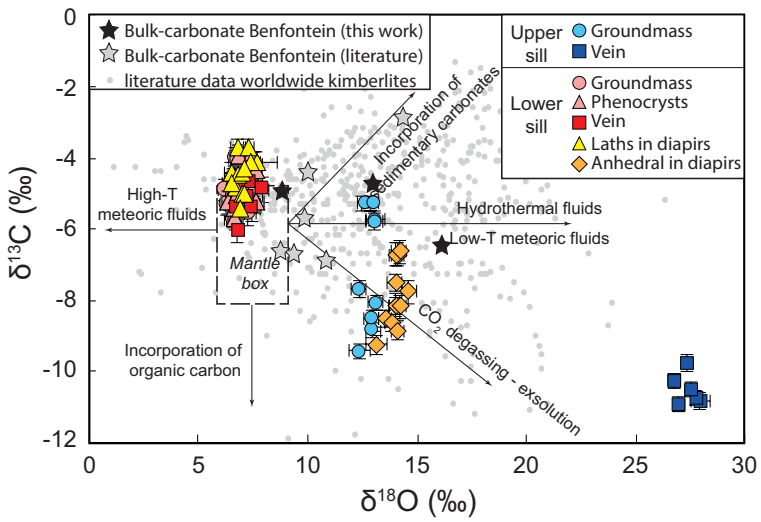

Figure 2. Plot of $\delta^{13}C$ (relative to VPDB) versus $\delta^{18}O$ (relative to VSMOW) showing the isotopic composition of different textural types of calcite from the Benfontein kimberlite analysed in situ by SIMS. Note that calcite in the groundmass, veins and diapirs (laths only) from the Lower sill plot in the "mantle box". Qualitative trends show how syn- and post-magmatic processes would modify the C-O isotope composition of magmatic carbonates.

The physics of recent earthquakes in southwest WA

On September 16, 2018, a magnitude 5.7 earthquake occurred near Lake Muir in southwestern Western Australia. The epicenter of the earthquake is located at the southwest corner of the SW Seismic Zone (Geoscience Australia 2018), where no quakes over magnitude 5 have ever been recorded before. After the mainshock, a sequence of aftershocks were recorded by the sparse regional seismic network. Obtaining reliable moment tensor solutions is important for revealing the seismogenic zones of the Lake Muir earthquake cluster, and to better understand the regional stress field that is important in regional hazard assessment.

In this study, we used a time-domain linear least-squares inversion method (*Lin et al. Tectonics 2018; CCFS contribution #1109*) to analyse the moment tensors of Lake Muir earthquakes and earlier regional earthquakes. Compared with other methods, this wave-form-based technique has a better control on the source parameters. We used long-period waveforms between 20 and 50 seconds, in the moment tensor inversion. For the smaller earthquakes or the noise waveforms, we also considered the long-period waveforms between 14.3 and 25 seconds or 10 and 25 seconds.

An important aspect in source-mechanism inversions is to have robust P- and S-wave velocity models. Taking advantage of the location of the Muir Earthquake being close to a permanent seismic station (RKGY), we constructed the S-wave velocity models by applying a transdimensional tomographic inversion technique (*Yuan and Bodin, Tectonics 2018; CCFS Contribution 1181*) to the dispersion datasets measured from station pairs between RKGY and other permanent stations. The P-wave model is approximated by using an active source reflection profile *(Dentith, Tectonophysics 2000).*

The solutions of the M5.7 Lake Muir earthquake and its M5.4 aftershock are shown in Figure 2 below. It is interesting is that the M5.7 main shock on Sept 16 (Fig. 2 left) shows mainly a thrust mechanism, but the two aftershocks, each occurring nearly a month apart on Oct 12 (M4.6) and Nov 08 (M5.4; righthand side in Fig. 2), show a gradual change in the solution towards strike-slip. We also inverted for source mechanisms for several recent earthquakes in southwestern WA. Some solutions were compared with that by the USGS (Figure 1) which show consistent results.

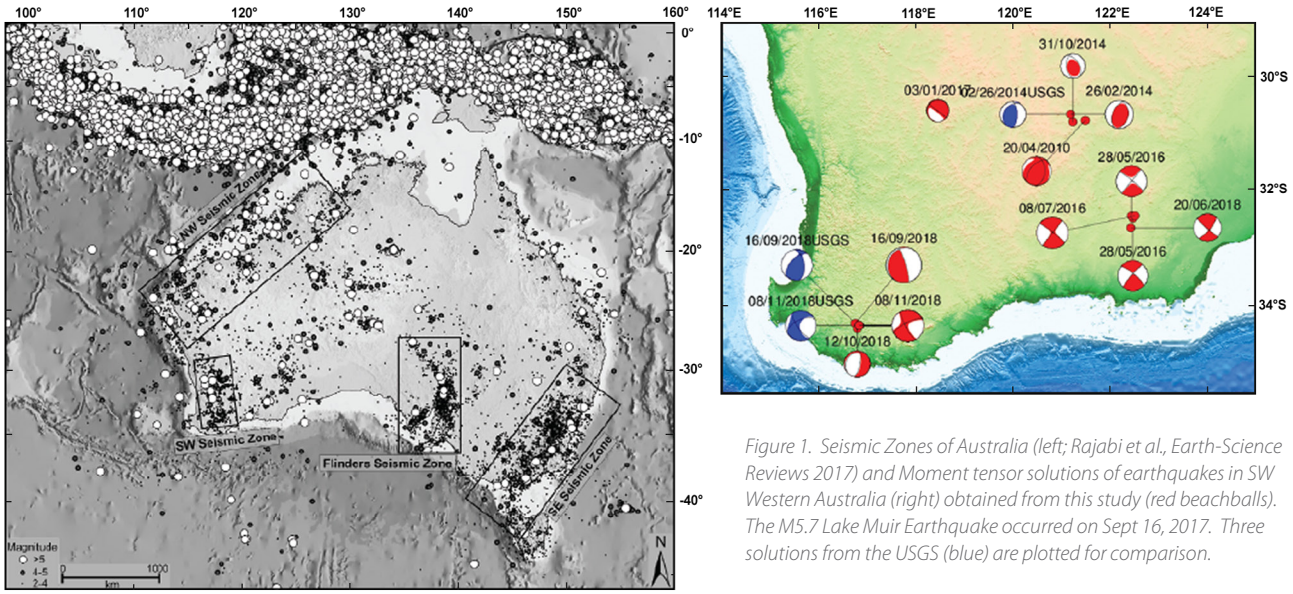

Figure 1. Seismic Zones of Australia (left; Rajabi et al., Earth-Science Reviews 2017) and Moment tensor solutions of earthquakes in SW Western Australia (right) obtained from this study (red beachballs). The M5.7 Lake Muir Earthquake occurred on Sept 16, 2017. Three solutions from the USGS (blue) are plotted for comparison.

The *regional stress field* indicates an east-west compression *(Rajabi et al., Earth-Science Reviews 2017)*, which explains the thrust-type mechanism of the M5.7 main shock, as well as of those earthquakes within the Yilgarn craton in the Kalgoorlie region. The change of the source mechanisms in the Lake Muir aftershocks may be attributed to a combined effect of complex stress release of the main shock in the complex local fault systems and triggering of new faults due to stress release of the main shock. Similar strike-slip solutions are found further east along the NE-SW trending craton margin in the east Albany-Fraser zone.

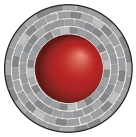

This project is part of CCFS theme 3, Earth Today, and contributes to understanding Earth's Architecture.

Contacts: Dr Xiangdong Lin (Beijing Earthquake Agency - visit sponsored by CCFS (2017-2018)) Huaiyu Yuan, Mike Dentith (GSWA), Ruth Murdie (GSWA), and Klaus Gessner (CCFS, GSWA)
Funded by: CCFS Flagship Program 7

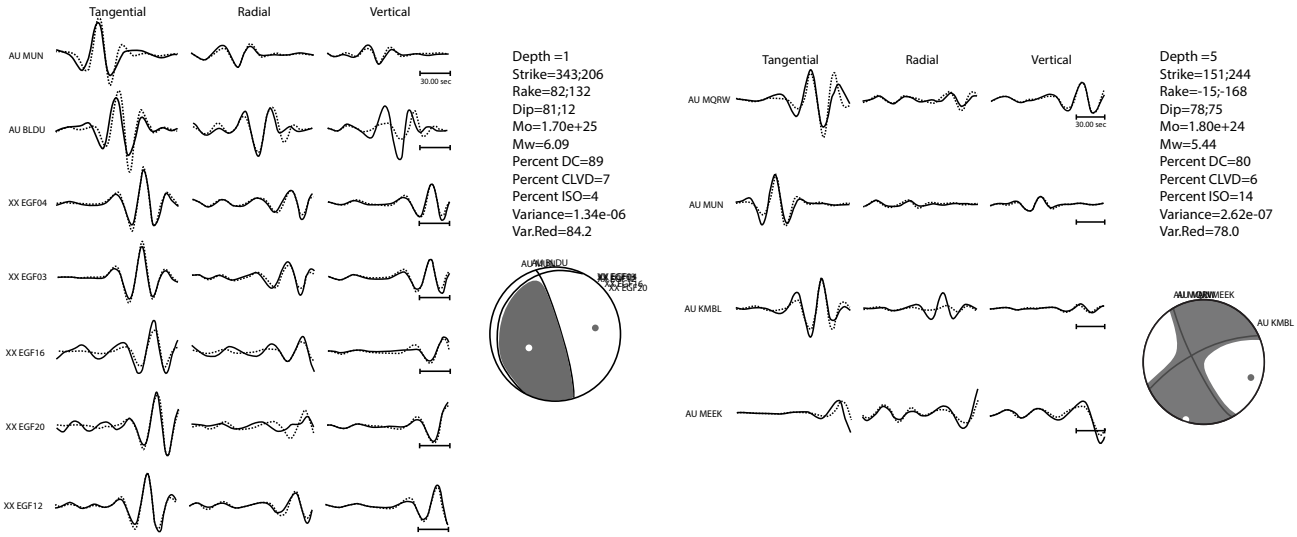

Figure 2. Source mechanism inversions for the M5.8 main shock (left) and the M5.4 aftershock (right) of the Lake Muir earthquake sequence.

CO_2 degassing - a new model approach to melting of mantle lithosphere

Reactivation of metasomatised mantle lithosphere may occur during continental extension, which is an important component of plate tectonics. The lower-most part of the metasomatised domains in the subcontinental mantle lithosphere can be locally enriched in CO_2. Therefore, partial melting of these metasomatised domains may play a crucial role in the global carbon cycle. However, little is known about this process and up until now few numerical constraints are available. Here we address this knowledge gap and use a 2-D high resolution petrological-thermomechanical model to assess lithospheric rifting, CO_2 degassing and melting. The numerical models fit well into natural rifting zones of the European Cenozoic Rift System for young (shallow) and of the North Atlantic Rift for old (thick) lithosphere.

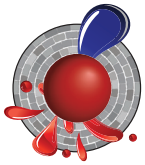

This project is part of CCFS theme 2, Earth's Evolution, and contributes to understanding Earth's Architecture and Fluid Fluxes.

Contacts: Weronika Gorczyk, Christopher Gonzalez
Funded by: CCFS Flagship 2

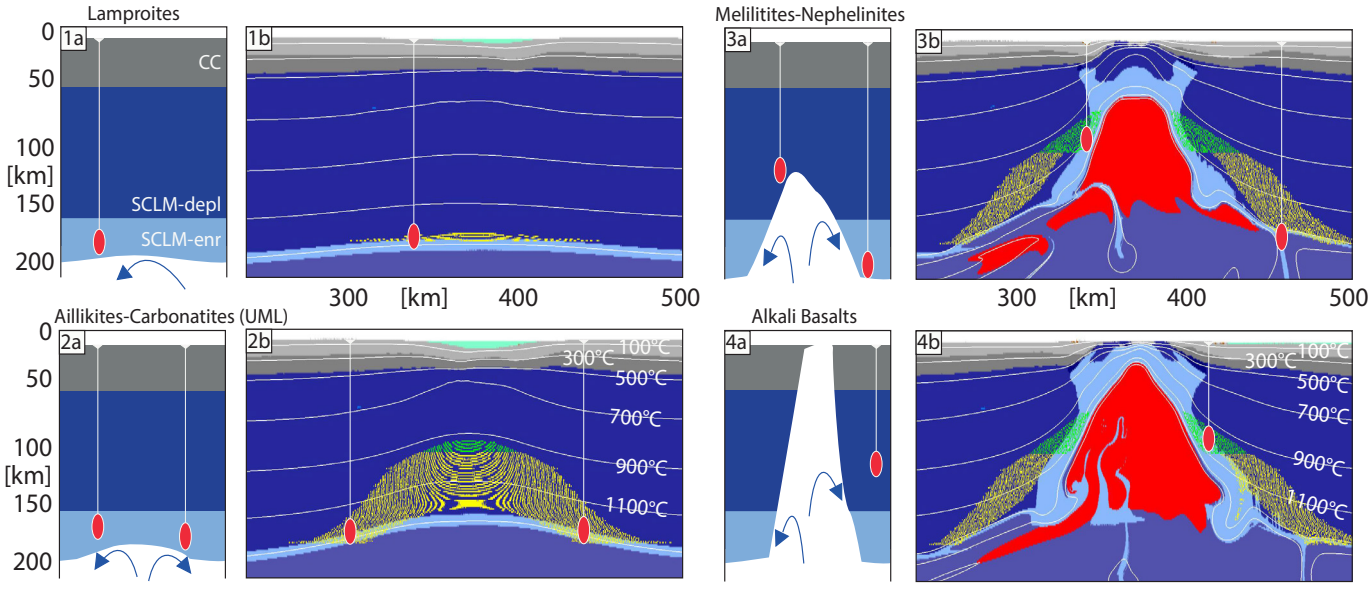

Figure 1. Comparison of tectonomagmatic model (plates [a]) of a segment of North Atlantic Craton close to the southern craton margin modified after Tappe et al. (2007), to numeral model 200 (plates [b]). Abbreviations: cc - continental crust, SCLM-depl - subcontinental lithospheric mantle - depleted, SCLM-enr - subcontinental lithospheric mantle - enriched in CO_2.

Olivine grains - new clues to the origin of diamondiferous kimberlites

Kimberlites are small-volume igneous rocks that have a unique role in the Earth sciences because they represent the primary host of diamond deposits; and derive from the deepest melts that occur at the surface of our planet. Despite decades of dedicated studies, the petrogenesis of kimberlites remains not fully understood. This is largely due to the complex hybrid nature of these rocks, including magmatic as well as abundant xenocrystic and alteration components. Olivine can provide unique insights into kimberlite origin and evolution, because it is the most abundant xenocrystic phase and a stable magmatic product over most of the crystallisation history of these magmas. Most olivine grains in kimberlites are compositionally zoned regardless of size and shape (Fig. 1). The zonation typically includes a core of variable composition that is overgrown by a rim characterised by relatively restricted Mg contents (Fig. 3), lower Ni and Cr, and higher Mn, Ca and Ti contents. One or more internal zones of variable composition may occur between core and rim of some grains (Fig. 1). The internal zones may be euhedral, diffuse or partially resorbed (embayments).

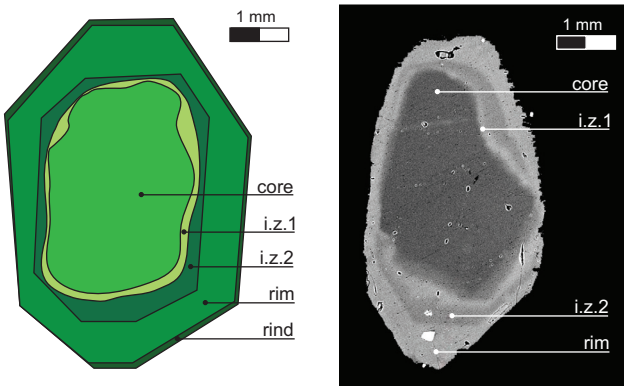

Figure 1. Cartoon showing the compositional zoning of an idealised olivine phenocryst, compared to a SEM back-scattered electron (BSE) image of a complexly zoned phenocryst from the Udachnaya-East kimberlite (Siberia).

A comparison between the compositions of olivine cores and olivine from mantle xenoliths (including megacrysts) entrained in kimberlites (Fig. 2), demonstrates that olivine cores are xenocrysts derived from disaggregation of mantle wall-rocks. This interpretation is consistent with the occurrence of mantle phases (i.e. orthopyroxene, clinopyroxene, garnet and Cr-spinel) as inclusions in olivine cores, and evidence of resorption (embayments) and abrasion (rounded shapes) of these cores. A variable proportion of olivine cores is sourced from mantle wall-rocks previously metasomatised kimberlitic magmas at mantle depths (including sheared peridotites and megacrysts), implying variable degrees of kimberlitic magma activity in the mantle before current kimberlite emplacement at surface.

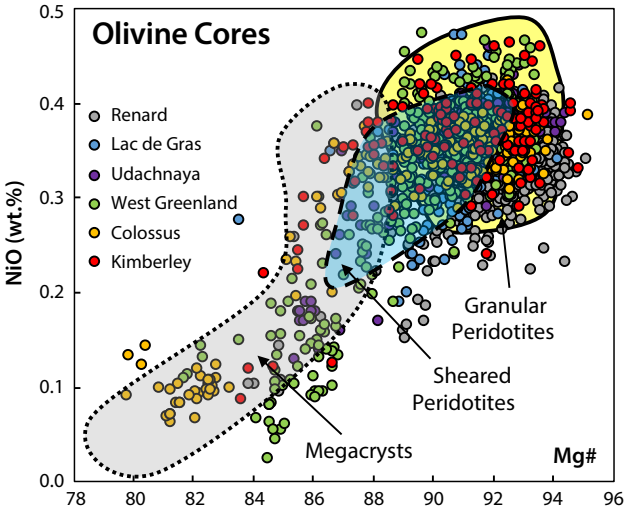

Figure 2. Mg#-NiO covariation diagram comparing the compositions of olivine cores in kimberlites with those of olivine in mantle lithologies sampled by kimberlite magmas, including megacrysts and peridotite xenoliths.

Olivine rims host inclusions of groundmass minerals (e.g. spinel, Mg-ilmenite, rutile), requiring a magmatic origin for the rims. There is a direct correlation between olivine rim and groundmass composition: high Mg/Fe rims are associated with carbonate-rich kimberlites, and lower Mg/Fe rims are correlated with increased phlogopite and Fe-bearing oxide modes (Fig. 4). With few exceptions, the compositions of olivine rims in each kimberlite locality, cluster (e.g. Kimberley) or form a compositional trend (e.g. Lac de Gras) within a restricted Mg# range (Fig. 3). This suggests that kimberlites within the same cluster derive from similar parental melts (and therefore sources), consistent with available radiogenic isotope results. Olivine rims in kimberlites from Lac de Gras, are compositionally indistinguishable from those occurring in rocks in hypabyssal root-zones, dykes and volcaniclastic units, thus indicating that such olivine crystallised during ascent, before different emplacement processes modified magma compositions. It can thus be inferred that the composition of (near-primitive) melt parental to olivine has

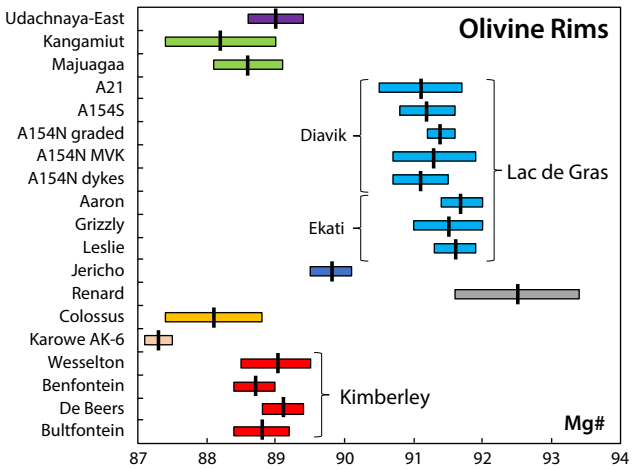

Figure 3. Average Mg# (± 2 s.d.) values of olivine rims in kimberlites worldwide. Note the similar compositions of rims within the same kimberlite cluster (i.e. Kimberley) and field (i.e. Lac de Gras).

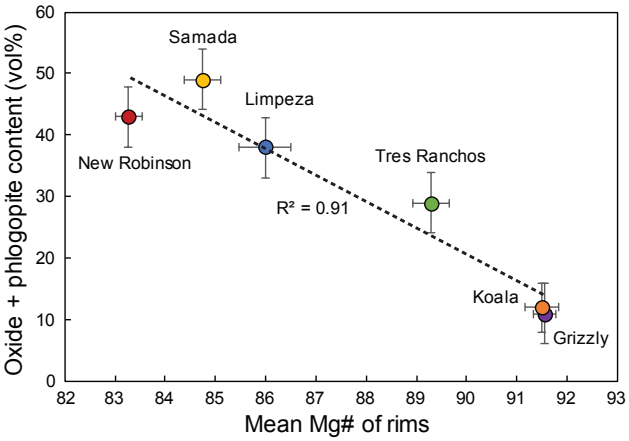

Figure 4. Comparison of mean Mg# value of olivine rims with the estimated abundance of phlogopite plus oxide minerals (spinel + Mg-ilmenite + perovskite) in the groundmass of kimberlites examined in this study. Note the statistical robustness of the inverse correlation between the two parameters (after Lim et al., 2018 Mineral Petrol).

minimal influence on kimberlite emplacement mechanism. Variations in the compositions of olivine rims in kimberlites from different areas relate to different parental melt compositions and contributions from a range of local processes (e.g. including olivine and spinel fractionation, assimilation of mantle material, CO_2 loss, melt oxidation) rather than variations in tectonic setting or emplacement mechanism.

Based on their compositional and textural features, three types of internal zones can be distinguished: 1) euhedral early liquidus olivine with higher Mg# and Ni than rims and hosting inclusions of magmatic chromite; 2) diffusional zones with compositions intermediate between those of cores and rims; 3) zones exhibiting resorption features that may be products of earlier kimberlite metasomatism at mantle depths.

In summary, olivine exhibits broadly analogous zoning in kimberlites worldwide. Olivine grains represent unique capsules that provide a potentially complete record of the evolution of kimberlite systems. Olivine cores store information on material entrained by kimberlites from the traversed mantle column, including evidence for early kimberlite metasomatism. Internal zones can show the effects of mantle metasomatism and/or record early kimberlite crystallisation at mantle depths. Rim compositions testify to the complex interplay of different processes during ascent and emplacement of kimberlite magmas. Ongoing research is exploring potential links between mantle-xenocrystic core and magmatic rim compositions to understand the effect of assimilation of mantle material on kimberlite melt composition; the oxygen isotopic composition of olivine to constrain the potential occurrence of recycled crustal material in the source of kimberlites; and the variability of olivine composition with time within kimberlite provinces to decipher the sources and evolution of different kimberlitic magma batches during protracted (10-30 Myr) magmatic episodes.

This project is part of CCFS theme 2, Earth's Evolution, and contributes to understanding Earth's Fluid Fluxes.

Contact: Andrea Giuliani
Funded by: ARC DECRA

Micro to global: microstructures reveal mantle secrets beneath the Pannonian Basin, Central Europe

Microstructures of mantle xenoliths can reveal the nature and behaviour of the upper mantle during tectonic processes. The characteristics of mantle-rock deformation are imprinted on the silicate minerals of the xenoliths, potentially identifying the tectonic history, as well as variables such as temperature, pressure, H ("*water*") content, and/or the interaction with melts/fluids. Physical properties of olivine, the most abundant upper mantle mineral, can be a proxy for the deformation processes that affected the xenolith-sampled mantle domain. Such parameters include orientation patterns of crystal axes, the strength of fabric expressed by the J-index (a dimensionless value that is a measure of the fabric strength, ranging from 1 (random orientation distribution) to infinity), and the grain orientation spread (a measure of the average amount of intragranular deformation).

The Pannonian Basin is a young back-arc basin located in Central Europe, surrounded by the Alps, Carpathians and Dinarides (Fig. 1). It has undergone significant extension during the Miocene then a compressional phase from ~8 Ma to recent times, resulting from the convergence of Adria and the European platform. Mantle-derived xenoliths were brought to the surface by late Miocene-Pleistocene alkali basalts in five areas (Fig. 1).

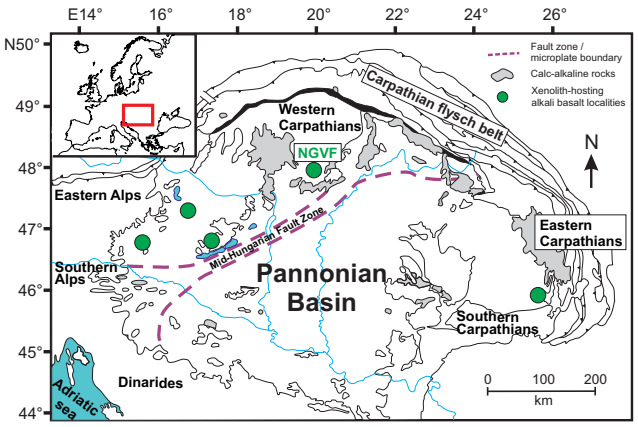

Figure 1. Locations of mantle xenolith-hosting alkali basalt outcrops within the Carpathian-Pannonian region. NGVF - Nógrád-Gömör Volcanic Field.

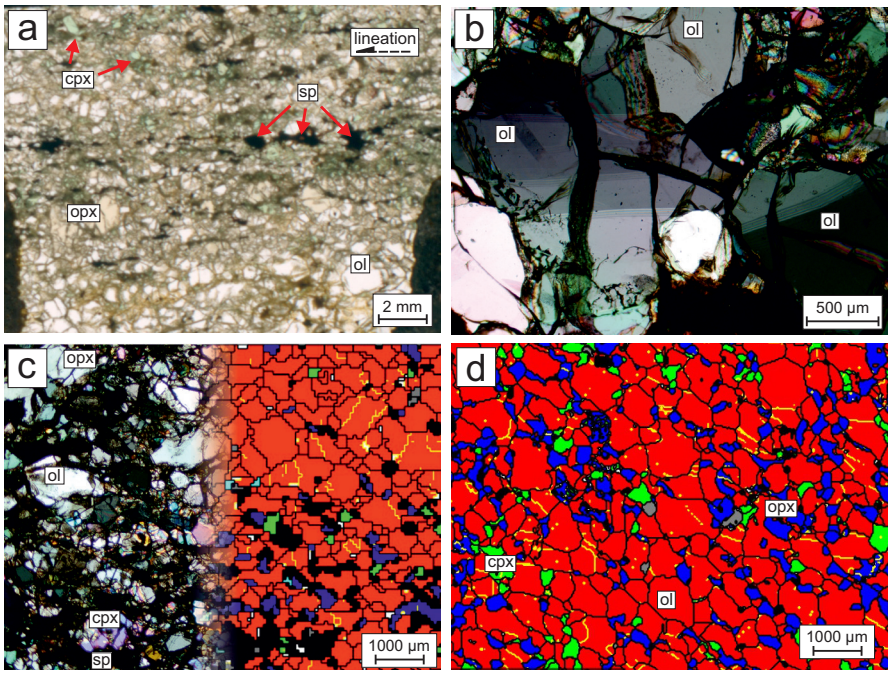

Figure 2. Characteristic microstructures in the studied Nógrád-Gömör xenoliths. a - lineation indicated by the distribution of spinel grains; b - subgrain boundaries in olivine; c - different olivine grain sizes in pyroxene-rich and pyroxene-poor domains; microphotograph (left) and electron backscattered diffraction (EBSD) phase map (right); d - EBSD map of equilibrated texture (straight grain boundaries, 120° triple junctions). Photomicrographs are transmitted light, plane-polarised in a, and cross-polarised in b and c. Colours on EBSD phase maps: red - olivine, dark blue - orthopyroxene, green - clinopyroxene, grey - spinel, light blue - amphibole. Abbreviations: ol - olivine, opx - orthopyroxene, cpx - clinopyroxene, sp - spinel.

The focus of this study is the xenoliths from the northernmost locality, the Nógrád-Gömör Volcanic Field, where crystal preferred orientations have not previously been described.

The xenoliths were analysed with a polarisation microscope and electron backscatter diffraction technique. Microstructural features indicating deformation include lineation outlined by spinel distribution (Fig. 2a) and elongated grain shapes, as well as common subgrain boundaries (seen as undulose extinction (Fig. 2b)). These deformation markers are commonly overprinted by annealing (static recrystallisation) resulting in grain growth of olivine (where olivine is not pinned by pyroxenes (Fig. 2c)), and straight grain boundaries with 120° triple junctions (Fig. 2d). Crystal preferred orientations of olivine reveal that most orientation patterns indicate deformation in a transpressional regime. This is consistent with the stress field generated by the convergent tectonics between the Adria microplate and the European platform.

Based on the positive correlation between the J-index and the equilibration temperatures (Fig. 3a) calculated from mineral compositions (*Liptai et al., 2017, J. Pet.; CCFS publication #1004*), the extent of deformation varies with depth. In addition, the extent of intragranular deformation is more dependent on the location, as it decreases from the northern part of the volcanic field towards the south (Fig. 3b). Post-kinematic annealing is linked to percolation of metasomatic mafic melts in the upper mantle of the NGVF before eruption of the host alkali basalt. Elevated equilibration temperatures in xenoliths from the central part of the volcanic field (Fig. 3b) are interpreted to derive from the youngest metasomatic event, which only shortly preceded the ascent of the host magma.

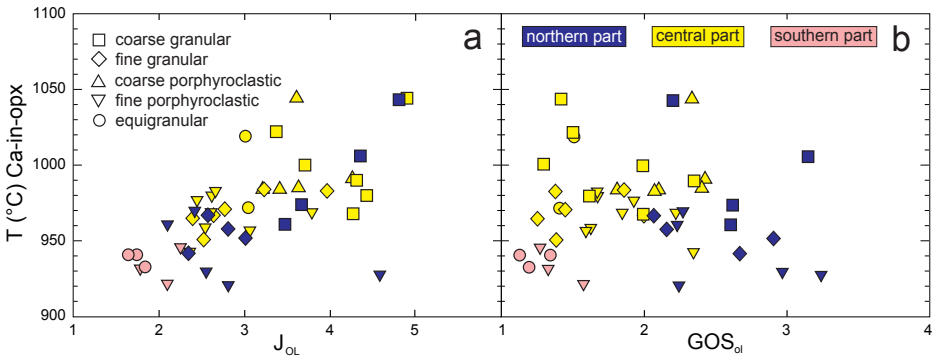

Figure 3. Olivine deformation features compared to calculated equilibration temperature (Ca-in-opx thermometer after Nimis & Grütter, 2010, CMP).

Crystal preferred orientation data also allow the calculation of seismic properties; combining that with measured shear wave splitting times in the area, the thickness of the anisotropic layer was estimated. The anisotropic thickness depends on the orientation of the foliation and lineation. The preferred model, on the available data, is horizontal lineation and vertical foliation. This is consistent with the recent tectonic regime, and also gives a minimum value for the thickness of the anisotropic layer. Some asthenospheric contribution may be needed to produce the observed shear wave splitting.

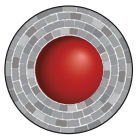

This project is part of CCFS theme 2, Earth's Evolution, and contributes to understanding Earth's Architecture.

Contacts: Nora Liptai, Sue O'Reilly, Bill Griffin, Csaba Szabó (Eötvös University, Hungary), Károly Hidas (University of Granada, Spain), Andréa Tommasi (University of Montpellier II, France)
Funded by: CCFS Flagship Program 1, iMQRES scholarship, EPS postgraduate funds. This project is part of a cotutelle PhD program between Macquarie University and Eötvös University, Budapest, Hungary.

A giant step towards a unified model for mantle magmatism

Mantle magmatism is a consequence of thermal discontinuities in, and one of the main mechanisms for the thermal evolution of, the Earth and other terrestrial planets. Encompassing partial melting, melt migration and mixing, melt-rock interaction and crystallisation, mantle magmatism can be modelled as a combination of phase changes (e.g. from solid to liquid), differential flow (e.g. of a fluid through a rigid matrix) and chemical reactions (exchange of chemical components). It can be described as a Muliti-Phase, Multi-Component, Reactive Transport system (MPMCRT) that can, in principle, be constrained experimentally and numerically modelled.

Over the past four decades specific aspects of MPMCRT, in the context of mantle magmatism, have been independently addressed by different communities (including petrologists, geochemists, geophysicists, computational geodynamicists). A new conceptual and numerical approach, integrating petrological, geochemical and geophysical considerations into a fully quantitative and comprehensive approach to mantle magmatism, bridges these traditional research silos.

This approach combines (1) a microstructural model for diffusion-controlled trace-element transport and (2) disequilibrium extensions of the multi-phase reactive transport model developed by *Oliveira et al.* (2018) (*CCFS Publication #1012*). In particular, chemical disequilibrium is accounted for by the novel thermodynamic formalism Dynamic Disequilibrium Melting (DDM, Fig. 1). DDM provides a versatile platform, not only able to study the dynamics and feedback of many magmatic systems over multiple scales but also rendering possible realistic comparisons between geophysical and geochemical datasets.

For example, the results of our MPMCRT model of mid-ocean ridges suggest that the modal, major- and trace-element compositions of abyssal peridotites could solely be accounted for by melt-extraction processes if disequilibria arising from

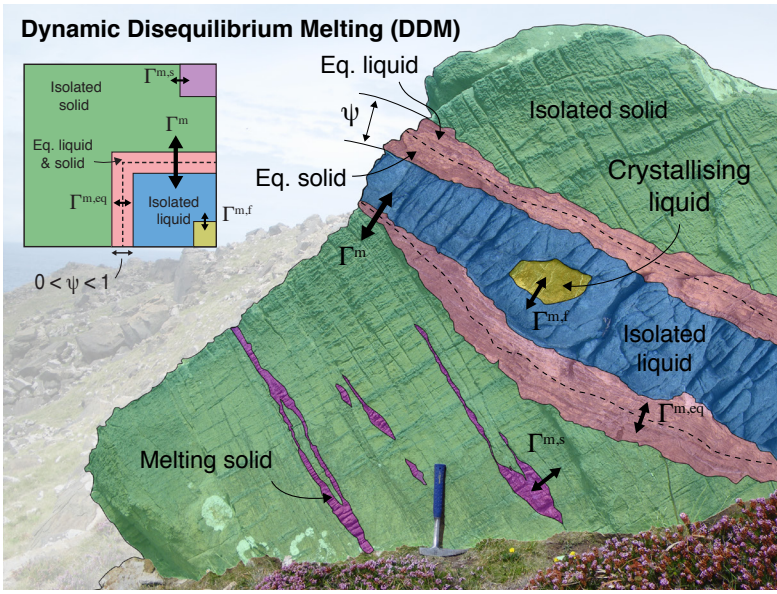

Figure 1. Schematic illustration (a) and projection (b) of the Dynamic Disequilibrium Melting model on a virtual outcrop of mantle rocks. Pink areas refer to fully equilibrated regions (e.g. dunitic reaction zone) and green and blue refer to chemically isolated solid (e.g. harzburgite) and liquid (e.g. basaltic melt), respectively. Each of the three regions has its own set of P-T-c^b conditions, and thus individual Gibbs free-energy minimisations are possible, allowing for independent crystallisation (yellow areas) and/or melting (purple areas) in the liquid and solid regions, respectively.

transport, phase changes and diffusion (Fig. 2) are accounted for. Similarly, local and global trends in MORB compositions could be reproduced using self-consistent tectonic scenarios. Application to lithospheric refertilisation processes is also particularly promising by introducing the properties for radiogenic isotope systems (currently under development).

This project is part of CCFS theme 2, Earth's Evolution, and contributes to understanding Earth's Architecture and Fluid Fluxes.

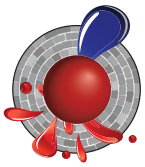

Contacts: Beñat Oliveira, Juan Carlos Afonso, Romain Tilhac

Funded by: CCFS Flagship Program 4, European Space Agency, La Caixa scholarship, iMQRES scholarships

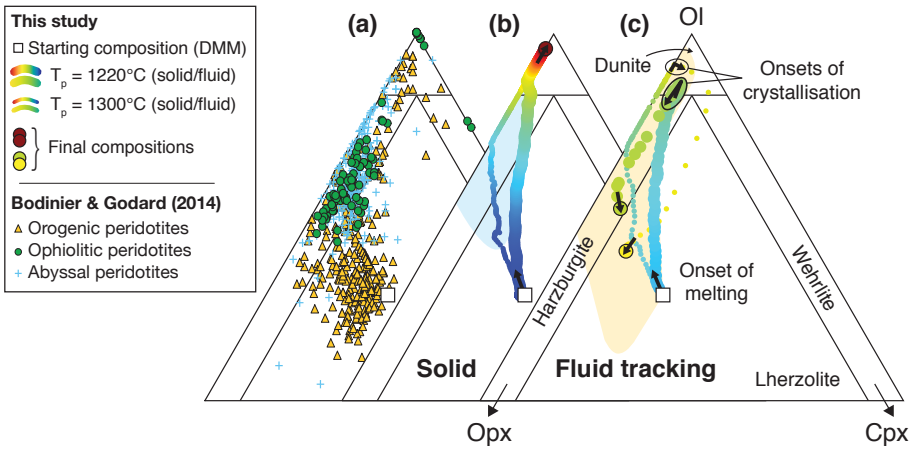

Figure 2. Comparison between modelled peridotites and the modal compositions of abyssal, ophiolitic and orogenic peridotites (a). Results were obtained while tracking either (b) an ascending mantle domain (solid tracking) or (c) a melt parcel (fluid tracking). Two scenarios are shown corresponding to a relatively cold (1220 ºC, bold lines) and hot (1300 ºC, bold lines) mantle potential temperature. Note that crystallisation occurs as the melts enter the thermal lithosphere (c), resulting in metasomatised peridotite compositions that overlap the field of orogenic peridotites. Colour code along the paths represent the evolution in time for each scenario.

Decoding Earth's supercycles

Repeated, and possibly cyclic, events of supercontinent assembly and breakup have been increasingly recognised over the past two decades. The latest of such events was the supercontinent Pangaea (ca 320-170 Ma), preceded by Rodinia (ca 900-700 Ma), and by Nuna (ca 1600-1400 Ma), implying a cyclicity of ~600 ± 100 Myr. A similar cyclicity, with a 50-100 Myr time lag, is found in global mantle plume intensity, leading to a geodynamic model of a coupled supercontinent-superplume cycle in Earth history. However, variations in global zircon Hf isotopic signatures and seawater Sr isotope ratios are both characterised by a longer-term variation trend with ca twice the wavelength of a typical supercontinent cycle. This billion-year variation trend (or supercycle) is also exhibited in global juvenile crust generation, and by the distribution of ages of certain global-scale mineral deposits (such as lead and zinc deposits and orogenic gold deposits), but why?

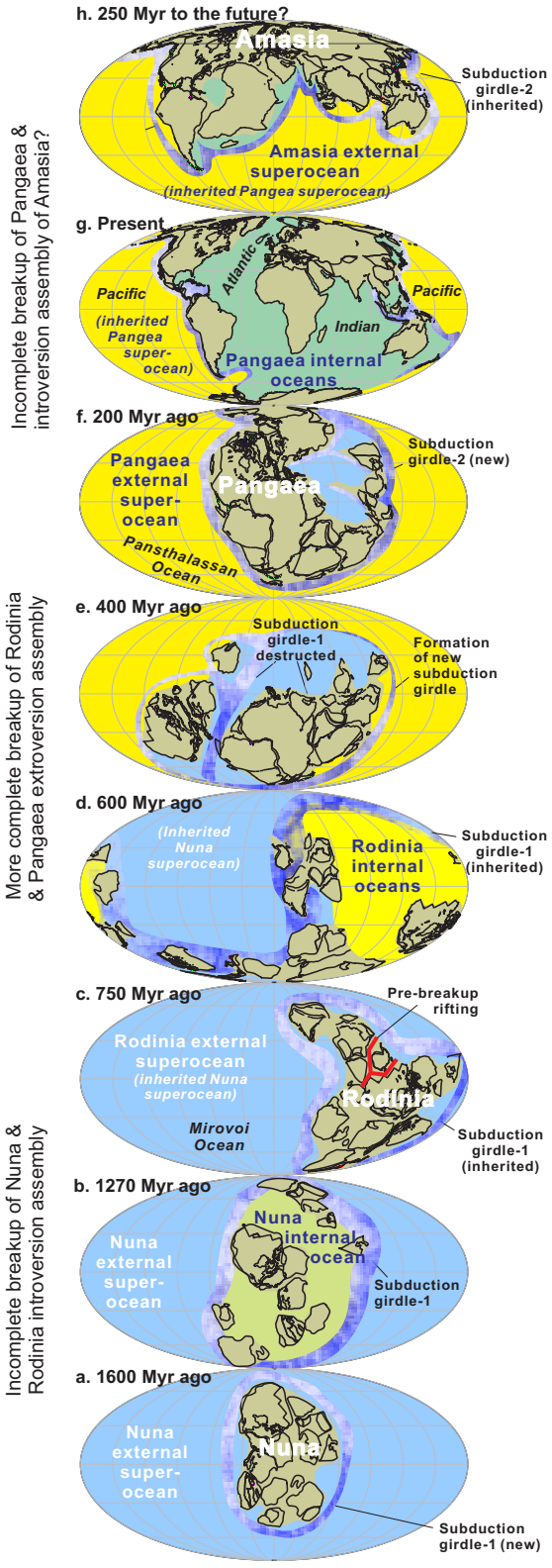

Li et al. (*CCFS publication #242*) suggested that the answer lies in the evolution of Earth's ocean basins. According to the model, supercontinents appear to assemble through two alternating pathways. One is extroversion (e.g. the assembly of Pangaea) where the previous supercontinent (Rodinia) was turned inside-out to form the new supercontinent, and in the process the superocean surrounding Rodinia was consumed (see Figures 1c to 1f). The other is introversion (e.g. the assembly of Rodinia), where the previous superocean surrounding Nuna survived the supercontinent cycle. In the latter case, the assembly of the new supercontinent occurred through the collapse of the internal oceans formed during the break-up of the previous supercontinent Nuna (Figures 1a to 1c).

More intriguingly, these two alternating methods of supercontinent assembly determine not only whether the superocean survives, but also whether the circum-superocean magmatism (e.g. the present-day Pacific Ring of Fire, which is scientifically referred to as the subduction girdle) survives. If this ring of fire survives along with the superocean, then the mantle structure maintains its pattern from the previous supercontinent cycle (the so-called degree-2 mantle structure; Fig. 2a). If not (in the case of extroversion supercontinent assembly), then the Earth's mantle structure is completely reorganised from a degree-2 pattern into a so-called degree-1 pattern (Fig. 2b), with the new supercontinent formed over a giant mantle downwelling (shown in blue). We speculate that such alternating pathways of supercontinent assembly (along with the survival or regeneration of the superocean and ring of fire) have produced an Earth cycle which is twice as long as the ca 600 Myr supercontinent cycle, influencing the formation of some of Earth's resources.

Figure 1. Survival of an external superocean over two supercontinent cycles as evidenced by global palaeogeography over the past 2000 Myr (a-h), and speculated corresponding mantle structures. Each major internal or external ocean system is colour-coded throughout the series of reconstructions. The assembly of Rodinia at 900 Ma (also future Amasia) is shown to be predominantly achieved through the closure of the internal ocean system formed as Nuna at 1400 Ma (or Pangaea at 170 Ma) fragmented (i.e. introversion), whereas the assembly of Pangaea was predominantly accomplished through the closure of the external ocean that surrounded Rodinia (i.e. extroversion).

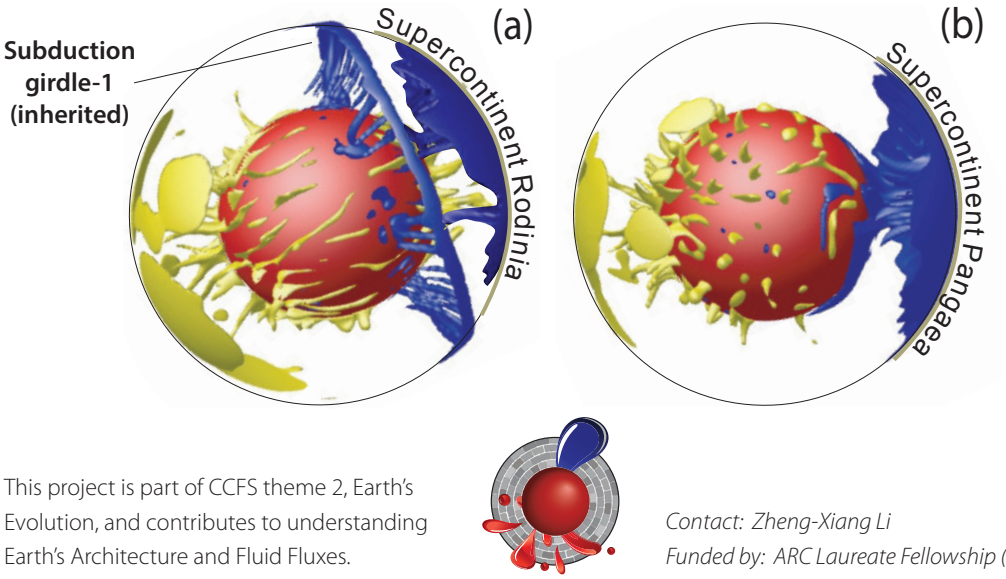

Figure 2. Different mantle structures related to the two different ways of supercontinent assembly. (a) A dominantly introverted supercontinent assembly inherits the pre-existing subduction girdle and degree-two mantle structure, along with the external superocean outside the subduction girdle. (b) A dominantly extroverted supercontinent assembly is accompanied by the destruction of the subduction girdle and the previous external superocean, where the new supercontinent forms above.

This project is part of CCFS theme 2, Earth's Evolution, and contributes to understanding Earth's Architecture and Fluid Fluxes.

Contact: Zheng-Xiang Li
Funded by: ARC Laureate Fellowship (ZX Li)

Volatile elements and metasomatism: how to move things around in the lithosphere

Volatile elements (C-H-N-S) are the chemical backbone for all essential organic molecules. They are also key to the planet's habitability and its geodynamic activity, including ore forming processes. Exchanges between Earth's interior and its exospheres (crust, hydrosphere, atmosphere) and biosphere occur during subduction and volcanism, but to what extent? What are the mechanisms and rates by which volatiles moves between deep and shallow reservoirs? What is the impact of mantle degassing on the secular evolution of the mantle and on the exospheres? As noted by the Deep Carbon Observatory (https://deepcarbon.net/) the inventory, cycles and behaviour of these key elements in the deep Earth are far from being constrained.

Because volatile elements have variable speciation they can be stored in the mantle in various ways: (i) as dissolved trace elements in the main silicate minerals (such as H in nominally anhydrous minerals: ol, opx, cpx); (ii) being a major element of specific/metasomatic phases, such as H in amphibole or C in carbonate, graphite and diamond; (iii) stored in melt/fluid inclusions; (iv) entering grain-boundary components. Therefore, their study requires a new approach integrating geochemical and mineralogical investigations at both whole-rock and mineral scales.

As a first step toward this aim, we have used an elemental analyser to determine whole-rock C, H, N and S contents in a series of alkali basalt-hosted peridotite xenoliths. Volatile contents vary widely (70-8000 ppm C; 50-485 ppm N, 90-1200 ppm H, 10-1500 ppm S). Eight well-characterised peridotite xenolith suites from alkali basalts were investigated, representing various degrees of melting and metasomatism. Correlations between C,H,N,S and melt-depletion criteria (e.g. Fo%, Al_2O_3WR) or metasomatic indicators (La/Sm) suggest that the variability in CHNS is not related to weathering or alteration but was mostly established during mantle processes. However, these relationships vary between suites. For example, the Ray Pic (RP) and Bullenmerri (BM) peridotites both contain amphibole. However RP xenoliths show H enrichment (up to ≈600 ppm), but low C contents (≈120±30 ppm) consistent with H_2O contents of

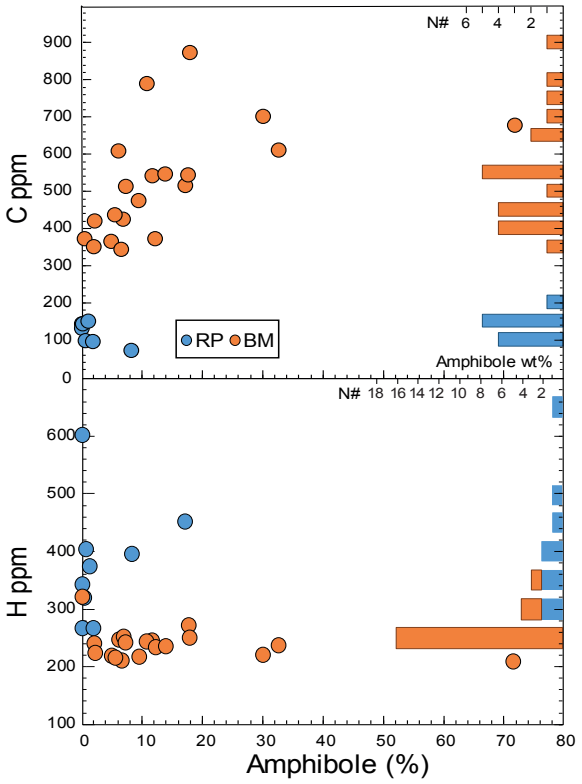

Figure 1. whole Rock C and H concentration (ppm) in amphibole bearing peridotite xenoliths from Ray-Pic (RP, Massif Central, France) and Bullenmerri (BM, Newer Volcanic Province, Au).

ca 1.4 wt% in the RP amphibole. BM xenoliths have in contrast low H contents (≈ 220 ppm) but clear enrichment in C (up to ≈700 ppm), well correlated with modal amphibole abundances (Figure 1). This difference in C and H behaviour is related to the distinctive trace-element patterns and amphibole compositions in each suite. In contrast, Borée peridotites, which contain no metasomatic amphibole, show high C and H contents (up to 1200 and 8000 ppm, respectively). Low H_2O contents in ol, opx and cpx obtained by FTIR (in collaboration with S. Demouchy, Géoscience Montellier, Fr) indicate that C and H enrichments in BO xenoliths are not related to the main silicate minerals. Spitsbergen xenoliths show both high C and S contents in agreement with their well-documented occurrence of sulfide and carbonate-bearing metasomatic-pockets.

Volatile elements have always been considered to be a key component of most metasomatic melts/fluids invoked for modal, cryptic and stealth metasomatism. While mantle petrologists and geochemists have defined various metasomatic agents (including carbonatitic, carbonated, hydrous) with specific geochemical fingerprints, the nature of, and ratios between, the various volatile elements in these melts/fluids are still highly debated. Our preliminary results suggest that it may be possible to more closely constrain the relative abundance and behaviour of volatiles during these metasomatic processes and investigate their effects on the transport and fractionations of trace elements including chalcophile elements.

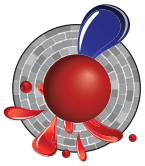

This project is part of CCFS theme 2, Earth's Evolution, and contributes to understanding Earth's Architecture and Fluid Fluxes.

Contacts: Ananuer Halimulati, Olivier Alard, Sue O'Reilly
Funded by: Olivier Alard ARC Future Fellowship, CCFS

The power of a systems approach to mineral and petroleum exploration in sedimentary basins

Petroleum systems and hydrothermal sedimentary rock-hosted copper, lead-zinc (clastic-dominated and Mississippi Valley-type), and uranium systems can be described in a common system framework comprising the critical processes of:

(1) establishing the fertility of source(s) of the commodity of interest and the transporting fluid,
(2) geodynamic triggers for commodity movement and accumulation,
(3) establishing an architecture for fluid movement,
(4) accumulation by deposition of the commodity, and
(5) preservation.

Consideration of these commodity systems in the context of the Earth's evolving atmosphere-hydrosphere-biosphere-lithosphere highlights the power of paleotectonic, paleogeographic, and paleoenvironmental reconstructions in the critical step of basin selection. Such consideration also highlights common gaps in understanding the commodity systems. These knowledge gaps constitute high-value research paths that would provide greatest leverage in area selection at the basin and play scales. These include improved knowledge of paleogeographic and paleoenvironmental reconstructions, basin hydrodynamics, and timelines of mass and energy flow through basins. For metal systems, better understanding is required of how metal extraction efficiency, solubility, mineral precipitation, permeability, and pressure and temperature gradients dynamically interact along flow paths during the evolution of basins. See *CCFS publication #1186.*

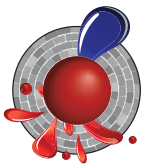

This project is part of CCFS themes 2 and 3, Earth's Evolution and Earth Today, and contributes to understanding Earth's Architecture and Fluid Fluxes.

Contact: Cam McCuaig
Funded by: BHP

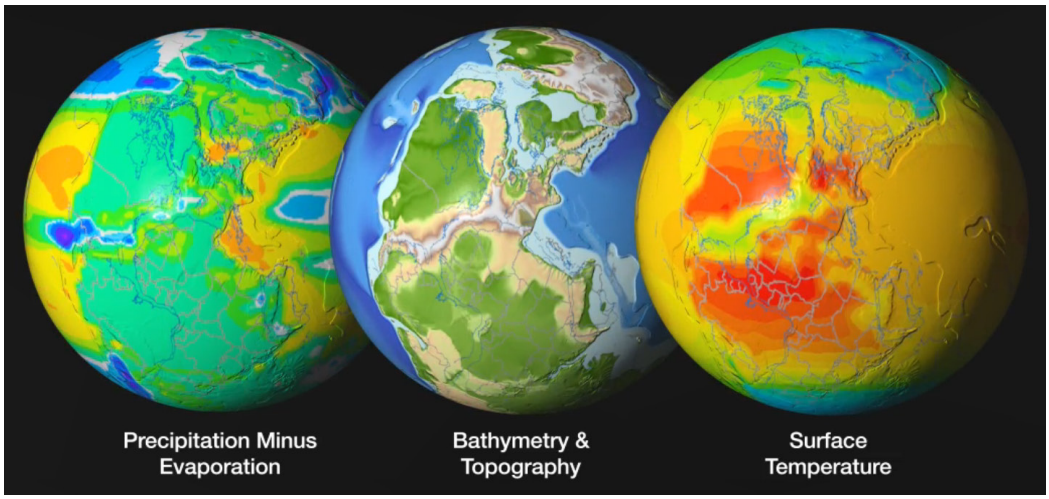

Figure 1. Getech (unpub. commercial software, 2015) paleogeographic reconstruction at 257 Ma. The figure illustrates how paleogeographic and paleotectonic reconstruction has the power to screen basins for fertility. The Late Permian, one of the world's great periods of deposition for petroleum source rocks, was also the time when the fertility for sedimentary rock-hosted copper and lead-zinc was established.

Can olivine's temperature diagnose the diamond potential of a kimberlite?

Kimberlite is the main volcanic host for transporting diamonds to the Earth's surface. Kimberlites also entrain fragments of rock (xenoliths) and disaggregated single grains from the lithospheric mantle (xenocrysts) which can provide valuable windows into the region from about 40 to 250 km beneath the surface.

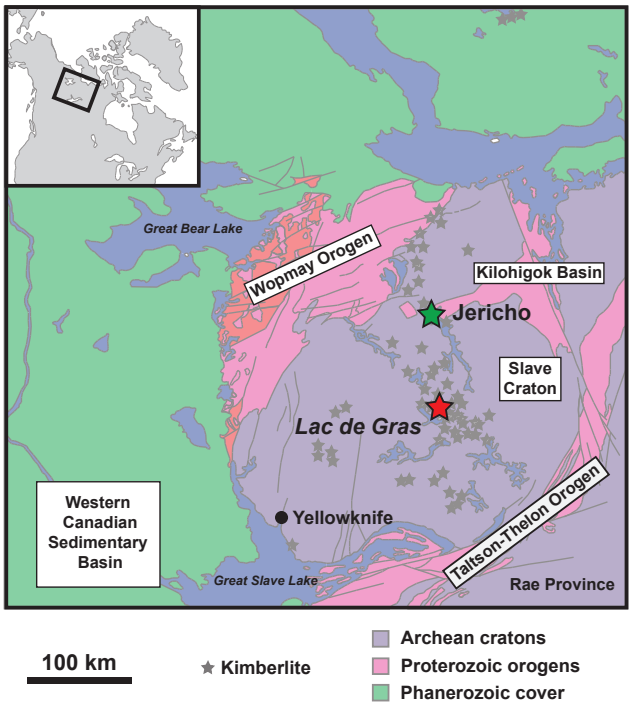

Figure 1. Map of the Slave Craton in northern Canada.

This study uses such xenoliths and xenocrysts from several kimberlite occurrences in the Cenozoic Lac de Gras kimberlite field in the Slave Craton, and the Jurassic (173 million years old) from northern Canada (Fig. 1). Geochemical data for abundant olivine xenocrysts in these two kimberlites are integrated to constrain their source depths. Olivine xenocrysts constitute about half the volume of these host rocks, and therefore their temperature profile may assist the identification of potential diamond occurrence, as diamond stability is limited to depths greater than ~140 km, equivalent to a temperature of 1000 °C. If the temperature of equilibration of at least some olivine xenocrysts indicate derivation from more than 140 km, diamond would be stable, and would have formed if there was sufficient carbon available.

Approximately 85% of the olivine xenocrysts studied here have compositions consistent with their derivation from mantle peridotites and pyroxenites. A new approach to single-grain olivine thermobarometry is being explored, based on the correlation between equilibration temperature, pressure and composition of olivine composition for the xenoliths from these localities.

A correlation between xenolithic olivine Mg# and pressure for most of these peridotitic and pyroxenitic bodies in the Jericho and Lac de Gras xenolith suites was observed. The relationship between xenolithic olivine Mg# and pressure thus may allow inferred estimates of the pressure (and by reference to the ambient geotherm, to the temperature) of xenocrysts assuming they derived from disaggregation of these source xenoliths.

Preliminary results suggest good agreement of the relative abundance of xenoliths and xenocrysts in the Lac de Gras pipes: both appear to be sourced predominantly from the deep lithospheric mantle (140-220 km; Fig. 2). At Jericho, xenoliths are sourced from as deep as 165 km, but xenocrysts appear to be exclusively above 140 km (Fig. 2).

The dominance of shallow material in the Jericho kimberlite may explain why the Jericho pipe has a lower concentration of diamonds than do the Lac de Gras mines

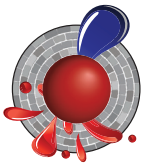

This project is part of CCFS theme 2, Earth's Evolution, and contributes to understanding Earth's Architecture and Fluid Fluxes.

Contacts: Stephanie Greene, Dorrit Jacob, Zsanett Pintér, Sue O'Reilly, Larry Heaman (University of Alberta, Canada)

Funded by: CCFS

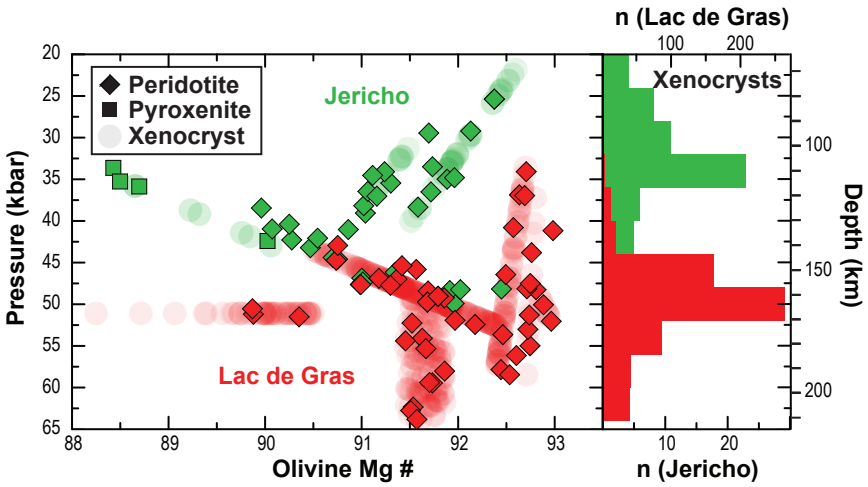

Figure 2. Pressure results for Jericho and Lac de Gras xenoliths compared to Mg# of olivine from xenoliths. Xenocrysts are projected onto the xenolith arrays and the depth profiles are expressed as a histogram.

In situ laser ablation split-stream (LASS-) MC-ICP-MS for simultaneous determination of Re-Os isotopes and siderophile-chalcophile elements in sulfides: Ablating away a Cornelian dilemma

In 1999, in an important World's first, GEMOC/GAU developed the techniques for *in situ* measurement of Re-Os isotopes in sulfides by LA-MC-ICPMS. It was then possible to date single *in situ* sulfide grains to infer the timing of melt-extraction events in the upper mantle. Since then the pioneering work of GEMOC/GAU demonstrated that elemental (e.g. PGEs) and isotopic *in situ* characterisations of (mantle) sulfides are powerful tools to unveil and date magmatic processes. Unfortunately, due to analytical and sample limitations (mantle sulfides Ø<100µm), investigators were left with the dilemma of choosing between trace elements or Re-Os isotopes.

20 years later, we report a 2nd World's first: we have now developed the capability to simultaneously measure *in situ* Re-Os isotopes and the concentrations of Platinum Group Elements (PGEs) in sulfides using laser ablation split stream (LASS) between a Nu Plasma II MC-ICPMS (Re-Os) and an Agilent 7700x Q-ICPMS (PGEs).

Owing to the considerable increase in sensitivity of the newer generations of Nu Instruments, and due to the ion counter inherent limitation, the amount of analyte sent to the Nu Plasma could be restricted, thus allowing us to divert the excess towards the ICP-MS for analysis of PGE and chalcophile trace element abundances. While the trace-element signal has been lowered by ≈50%, in contrast the implementation of the LASS was done without any loss of sensitivity (and thus precision) for the MC-ICP-MS. Although counting statistics are significantly lower (≈50%) for the ICP-MS, the accuracy and reproducibility for trace elements in reference materials (e.g. Po62, Ai3-W, FeS1) are satisfactory. For instance, Os content in Po62 is ca 1.67±0.06 ppm, while the Se content of AI3-W was found to be 168±1 ppm.

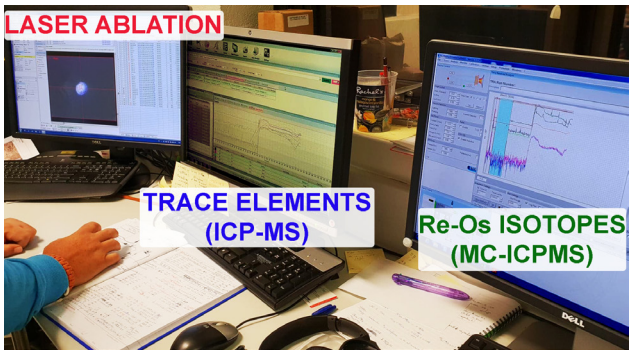

This technological breakthrough provides a significant increase in time efficiency as both measurements are now acquired in a single session. However the real advance resides in the ability to not have to choose between one or the other type of measurement. Therefore, this new methodology will enable us to build more comprehensive datasets offering better constraints on the systematics between the isotopic signatures and the trace-elements patterns of the sulfides, which will allow more accurate petro-geochemical understanding of the nature and timing of the processes occurring in the upper mantle.

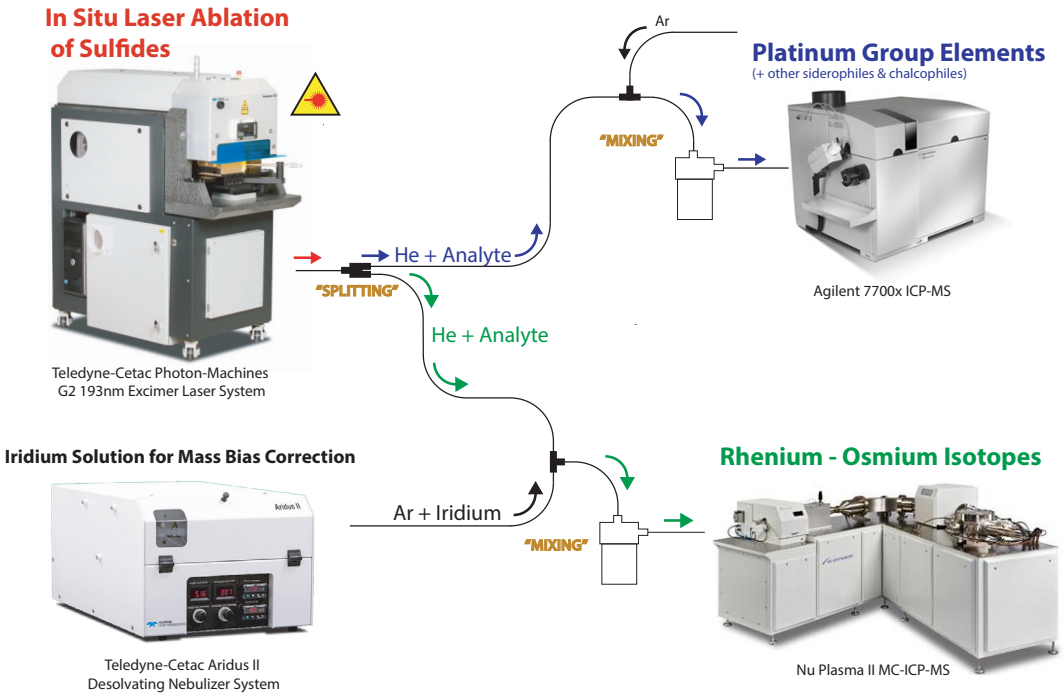

Contacts: Olivier Alard, Yoann Gréau
Funded by: CCFS

Holy hibonite! - *'meteoritic'* mineral assemblages in volcanic rocks

Hibonite ($CaAl_{12}O_{19}$) is a constituent of some refractory Calcium-Aluminum Inclusions (CAIs) in carbonaceous meteorites, commonly accompanied by grossite ($CaAl_4O_7$) and spinel. These phases are usually interpreted as having condensed, or crystallised from silicate melts, early in the evolution of the solar nebula. Both Ca-Al oxides are commonly found on Earth, but as products of high-temperature metamorphism of pelitic carbonate rocks. However, our ongoing studies of the ultra-reduced mineral assemblages in the ejecta from Cretaceous pyroclastic deposits on Mt Carmel, N. Israel have identified unique magmatic hibonite-grossite-spinel assemblages, crystallised from Ca-Al-rich silicate melts under conditions (high temperature, very low oxygen fugacity (fO_2)) comparable to those of their meteoritic counterparts.

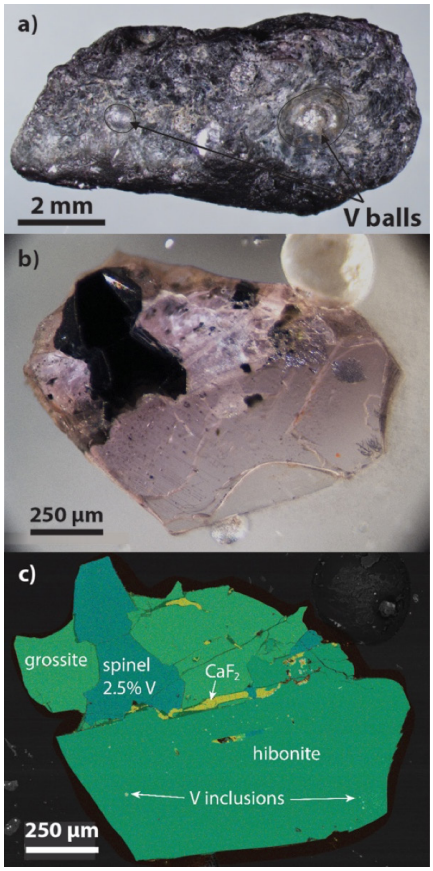

Figure 1. Hibonite-grossite aggregates. (a) large grain of hibonite-grossite aggregate with mm-size spheres of native V (V^0); (b) transmitted-light photo of transparent specimen, enclosing black spinel grain and rods of V^0; (c) phase map of (b) showing paragenesis of aggregates. Comparison of (b) and (c) shows that each tiny V^0 inclusion represents the end of a long rod or dendrite branch.

The Mt Carmel material includes aggregates of hopper/skeletal Ti-rich corundum, which have trapped melts that crystallised at fO_2 extending from 7 log units below the Iron-Wustite buffer (ΔIW= -7; SiC, Ti_2O_3, Fe-Ti silicide melts) to ΔIW ≤ -9 (native V, TiC, TiN). The assemblage hibonite + grossite + spinel + TiN first crystallised late in the evolution of the melt pockets; this hibonite contains % levels of Zr, Ti and REE, reflecting the concentration of incompatible elements in the residual melts as corundum continued to crystallise.

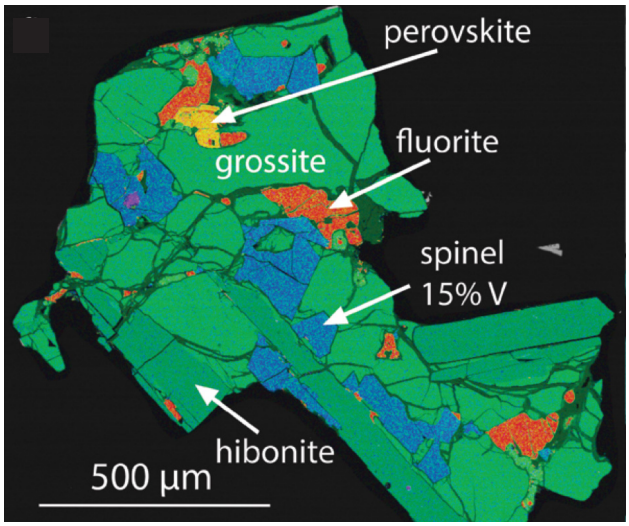

Figure 2. Hibonite-grossite aggregate illustrating crystallisation sequence. Resorbed corundum in hibonite reflects peritectic reaction L + Cor → Hib, followed by grossite + spinel ± krotite; fluorite and $Ca_4Al_6F_2O_{12}$ crystallise last.

A still later stage appears to be represented by coarse-grained (cm-size crystals) ejecta that show the crystallisation sequence: corundum + Liq → (low-REE) hibonite → grossite + spinel ± krotite ($CaAlO_4$) → $Ca_4Al_6F_2O_{12}$ + fluorite ± perovskite ($CaTiO_3$). This is the first reported terrestrial occurrence of krotite, which is otherwise found in CAIs. $Ca_4Al_6F_2O_{12}$ has been produced

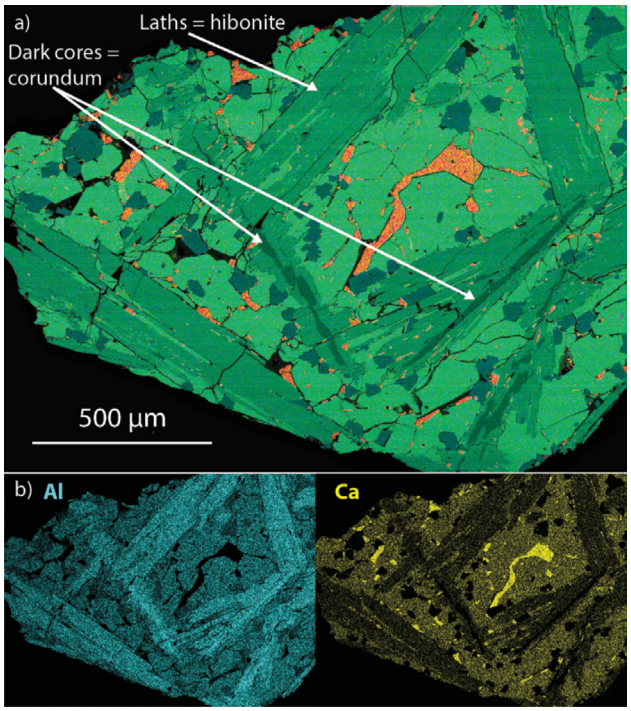

Figure 3. (a) Phase map of aggregate showing randomly-oriented hibonite plates, with narrow resorbed corundum cores, and hibonite + grossite intergrowths at edges of plates. Grossite (light green) is euhedral against CaF_2 (orange), the last phase to crystallise. Spinels (blue-green) are euhedral.

synthetically, but not previously found in nature; it is important because it is unstable below 1150 °C and constrains the temperature range of the assemblages. V^0 appears as spheroidal droplets, balls up to mm size, and spectacular dendritic growths, included in hibonite, grossite and spinel (see *Research highlight p. 315*). Spinels contain 10-16 wt% V in V^0-free samples, and <0.5 wt% V in samples with abundant V^0.

Ongoing paragenetic studies (see CCFS *Annual Report 2017*) suggest that the fO_2 evolution of the Mt Carmel magmatic system reflects interaction between OIB-type mafic magmas and mantle-derived $CH_4 + H_2$ fluids near the crust-mantle boundary. Temperatures estimated by comparison with 1-atm. phase-equilibrium studies range from ca 1500 °C down to 1200-1150 °C. When fO_2 reached ca ΔIW = -7, the immiscible segregation of Fe,Ti-silicide melts and the crystallisation of SiC and TiC effectively desilicated the magma, leading to supersaturation in Al_2O_3 and the rapid crystallisation of corundum, leading finally to the development of the hibonite-bearing assemblages.

The analogies to the mineralogy of CAIs suggest that this work is also relevant to studies of processes in the early Solar system. See *CCFS publication #1209*.

This project is part of CCFS theme 2, Earth's Evolution, and contributes to understanding Earth's Fluid Fluxes.

Contact: Bill Griffin
Funded by: CCFS Flagship program 1

Early cratonisation of the Yangtze Craton

The Earth is unique among terrestrial planets for its extensive regions of felsic crust, making up the continents. The felsic continental crust was largely generated during Archean time (>2.5 billion years ago), through tonalite-trondhjemite-granodiorite (TTG) magmatism, but exactly when and how such TTG-dominated crust formed and evolved into mature granitic compositions similar to modern upper crust is contentious.

The Yangtze Craton, southern China (Fig. 1) is one of the oldest blocks of continental East Asia, although the exact timing and evolution of, and the spatiotemporal relationships between these crustal provinces are not well understood.

Recent work has contributed to the recognition of several Archean crustal provinces (i.e. the Kongling Complex, the Yudongzi Complex, the Douling Complex, and the Zhongxiang Complex) in this Craton. The newly discovered Zhongxiang Complex in the northern Yangtze Craton (Fig. 1b) is among the known Archean crustal provinces and documents both sodic TTG and potassic granitic magmatism, providing a critical record of the evolving continental crust. An integrated study of petrology, zircon U-Pb geochronology and Hf-isotopes, and whole-rock geochemistry was conducted on the Zhongxiang Complex to better understand the crustal history. Our results revealed three major periods of Archean felsic magmatism in the Zhongxiang Complex: late Mesoarchean (2.90-2.87 Ga), early Neoarchean (2.77 Ga), and late Neoarchean (2.70-2.62 Ga). The 2.90-2.87 Ga magmatism is represented by monzogranites from the southern Zhongxiang Complex, which were derived from mixing of ancient and juvenile crustal components at relatively shallow crustal depths. This was followed by the emplacement of 2.77 Ga trondhjemitic

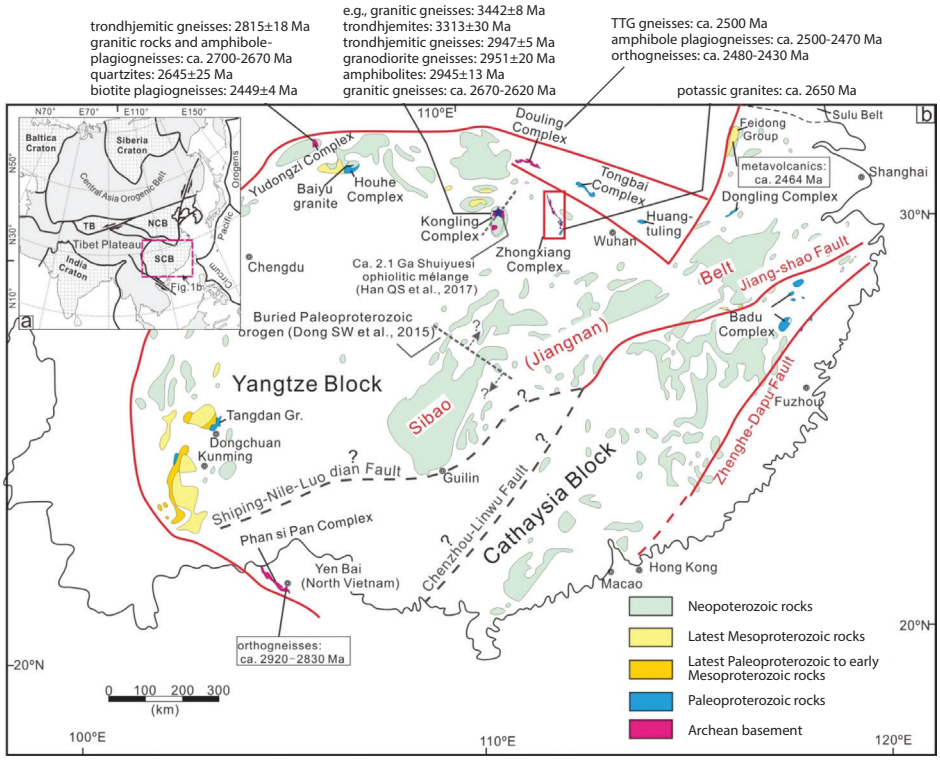

Figure 1. (a) Simplified tectonic map of Eurasia showing the major tectonic units and the location of SCB - South China Block, TB - Tarim Block, and NCB - North China Block. (b) A simplified geological map highlighting the Precambrian geological units of south China. Note the distribution of the Archean magmatic rocks along the northern and southern Yangtze margins.

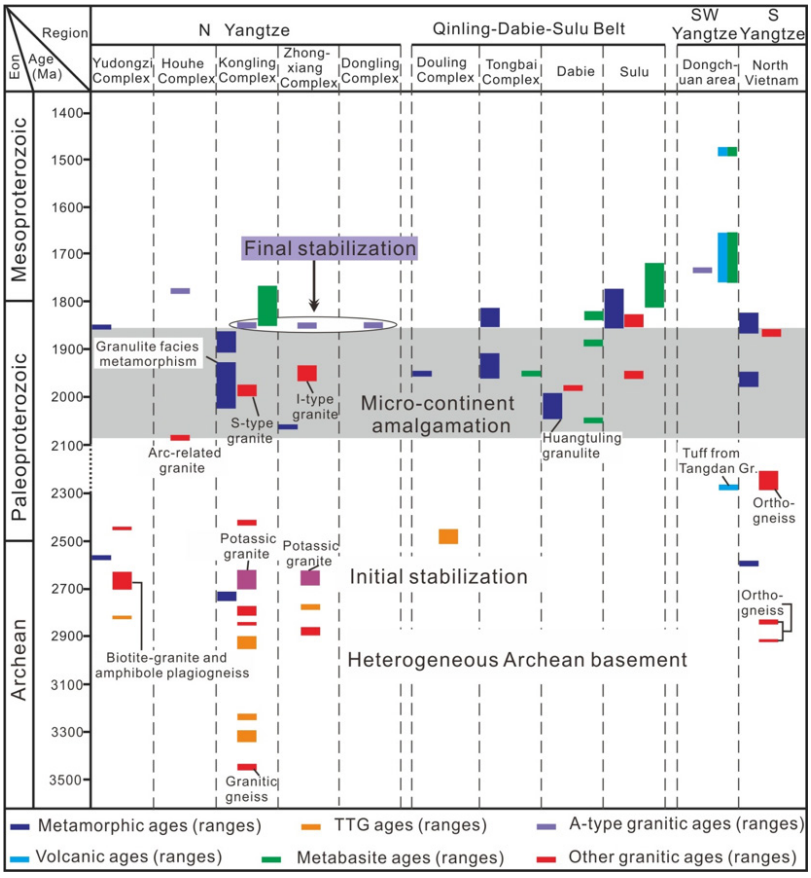

Figure 2. Time-space correlation chart of the Yangtze Craton illustrating the age ranges of principal Archean to early Proterozoic (>1.4 Ga) tectono-thermal events recorded in different parts of the Yangtze Craton. The compositionally variable Archean continental crust among different crustal domains of the Yangtze Craton, and their similar orogenic-related magmatic and metamorphic overprint during the late Paleoproterozoic point to the formation of a uniform Yangtze Craton by accretion of several crustal domains or terranes during the late Archean to Paleoproterozoic time. The concurrent emplacement of ca. 1.85 Ga A-type granites at different localities likely marked the final stabilisation of a coherent Yangtze Craton.

gneisses in nearby regions of the southern Zhongxiang Complex, which represent the only potential TTG with ages of 2.80-2.70 Ga in the Yangtze Craton. The trondhjemitic gneisses are typical of a medium-pressure TTG component and are interpreted as the products of partial melting of a basaltic source with appreciable involvement of pre-existing crustal components (i.e. tonalites). In contrast, the 2.67-2.62 Ga magmatism, represented by potassic granites from the northern Zhongxiang Complex, corresponds to high-temperature melting of meta-sedimentary source rocks in a within-plate extensional setting.

The transition of the felsic magma from Na-rich (2.77 Ga) toward K-rich (2.67-2.62 Ga) in the Zhongxiang Complex would have led to extensive removal of heat-producing elements from the lower crust, enabling the thermal stabilisation of the continental crust. This transition is broadly coeval with global TTG-granite and tectonic transitions related to thermo-mechanical and geodynamic changes of the continental crust at the end of the Archean, but appears to slightly postdate the TTG-granite transition in the nearby Kongling Complex (2.90-2.80 Ga) and to predate those in the Yudongzi Complex (2.70 Ga) and the Douling Complex (2.50 Ga), all of which are documented from the Yangtze Craton. Age and isotopic comparisons among the known Archean provinces further indicate a compositionally heterogeneous Archean Yangtze Craton, which likely comprises several Archean terranes that accreted to form the craton during the late Archean or even early Paleoproterozoic (Fig. 2).

This project is part of CCFS themes 1 and 2, Early Earth and Earth's Evolution, and contributes to understanding Earth's Architecture.

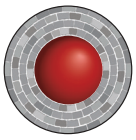

Contacts: Kai Wang, Zheng-Xiang Li, Earth Dynamic Research Group, Curtin University

Funded by: ARC Laureate Fellowship (ZX Li)

Sulfide aggregation in ophiolitic dunite channels amplifies Os-isotope mismatch between oceanic crust and mantle

Re-Os isotopic compositions of oceanic crust represented by fresh basaltic glasses from the mid-ocean ridges and primitive gabbroic cumulates in the ridge system are systematically more radiogenic than the normal values for Os isotopes [quartiles of γOs(t) with Q1= -4.1 and Q3= -0.6] of oceanic mantle, represented by abyssal peridotites and Os-Ir alloys from global ophiolites which are below the values for chondrites - i.e. '*sub-chondritic*'. Os isotopic decoupling between oceanic crust and mantle has been explained by radiogenic Os contributions from metasomatic sulfides and/or recycled pyroxenites in the convective mantle. However, the possible role of melt channels that regulate the flow of magmas feeding the oceanic crust at the crust-mantle boundary, have so far not been considered.

In situ Re-Os isotopic compositions of nearly 200 base-metal sulfide grains have been analysed from the ophiolitic low-Cr#

chromitites from Zedang (South Tibet) (*CCFS Publication #965*). These chromitites occur within dunite lenses, interpreted as interaction products between MORB-like melts and harzburgites. Thirty-eight analyses (mainly sulfide inclusions in chromite) show a wide range of $^{187}Os/^{188}Os$ (calculated at 130 Ma) from 0.1191 to 0.1702 with γOs(t) from -6.4 to +33.8. These values are similar to those of the oceanic crust and the Os-rich sulfides from the Oman low-Cr# chromitites. The initial $^{187}Os/^{188}Os$ ratios (0.1281-0.1296) of chromites from the Zedang chromitites are close to those for the Primitive Upper Mantle, but higher than those of the Zedang and other ophiolitic peridotites along the Yarlung Zangbo suture (South Tibet). This suggests that radiogenic Os components from asthenospheric or lithospheric mantle have been added to the dunite melt channels. The significant Os isotopic heterogeneity observed in the Zedang and Oman chromitites indicates that the Os-bearing phases were not well mixed, but aggregated together during the precipitation of chromite and monosulfide solid solution grains, when the dunite melt channels were produced in the oceanic crust-mantle transition zone. Such melt channels will affect the Os isotopic compositions of the migrating melts that ultimately generate the oceanic crust: and this process can explain the Os isotopic mismatch between oceanic crust and mantle (Fig. 1).

This project is part of CCFS theme 2, Earth's Evolution, and contributes to understanding Earth's Architecture and Fluid Fluxes.

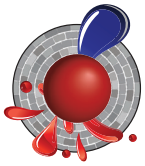

Contacts: Qing Xiong, José M. González-Jiménez, Jian-Ping Zheng, Bill Griffin, Sue O'Reilly

Funded by: NSFC (41520104003 and 41873032), CCFS Flagship Program 1

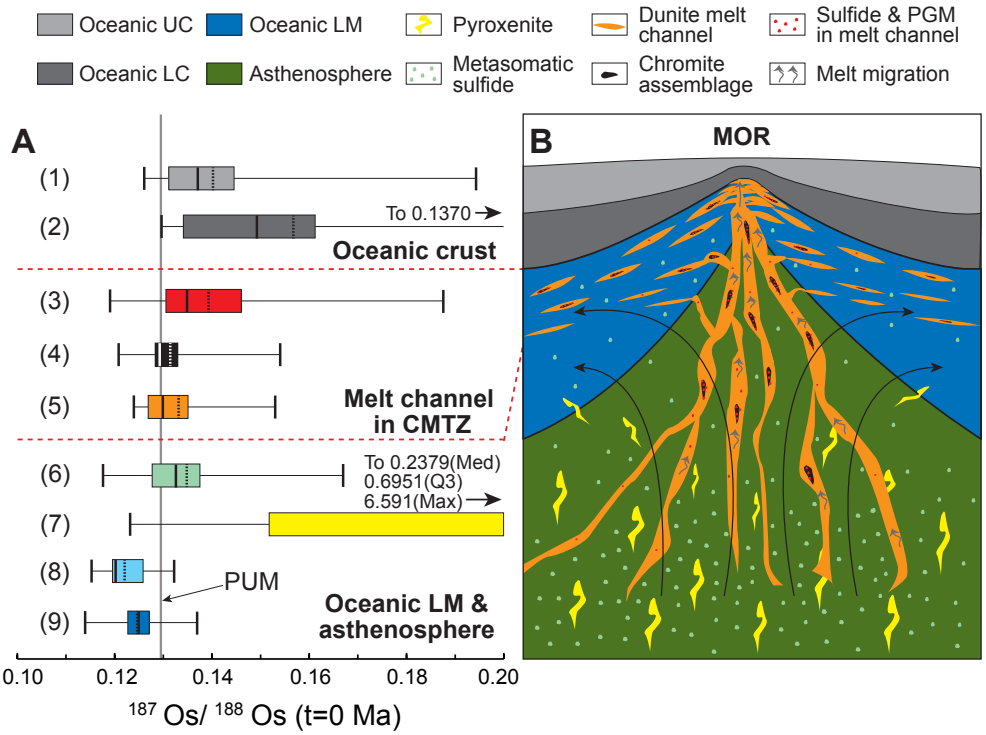

Figure 1. Comparison of box-whisker plots (A) for $^{187}Os/^{188}Os$ (t=0 Ma) ratios of oceanic crust, dunite melt channels and mantle. A schematic cartoon (B) shows the formation and distribution of dunite melt channels and relevant chromite assemblages beneath a mid-ocean ridge (MOR). Discrete Os components with heterogeneous Os isotopic compositions from the asthenosphere or lithospheric mantle were aggregated in the dunite melt channels, which regulate and contribute the Os isotopes of oceanic crust. Abbreviations: UC, upper crust; LC, lower crust; CMTZ, crust-mantle transition zone; LM, lithospheric mantle.

Pyroxenite microstructures help unlock deep Earth secrets

Seismic waves and their response to the mediums they travel through provide most of our knowledge of the structures and discontinuities of the deep Earth. Most minerals in Earth's mantle have strongly directional elastic properties, and thus the seismic waves passing through them will be slightly accelerated or decelerated depending on the incidence direction. Therefore, to improve the characterisation of the architecture of Earth's mantle, we need to be able to accurately interpret the geological significance of seismic dataset.

Olivine is the dominant mineral in Earth's upper mantle, but pyroxenes can be volumetrically dominant in specific geological contexts. A previous Research Highlight (*CCFS 2016 Annual Report, p. 225*) and *CCFS publication #969* examined the microstructure of deformed pyroxenites from the exhumed mantle terrane at Cabo Ortegal (Spain). In order to fully characterise the nature of deformation in pyroxenites, we also studied pyroxenites from the Trinity Ophiolite (USA), an undeformed analogue of the Cabo Ortegal pyroxenites.

Within the Trinity ophiolite, California, USA, the fossil magma chamber of Bear Creek contains abundant pyroxene-rich facies showing no evidence for plastic deformation. Down-section, the pyroxenite cumulates commonly alternate between

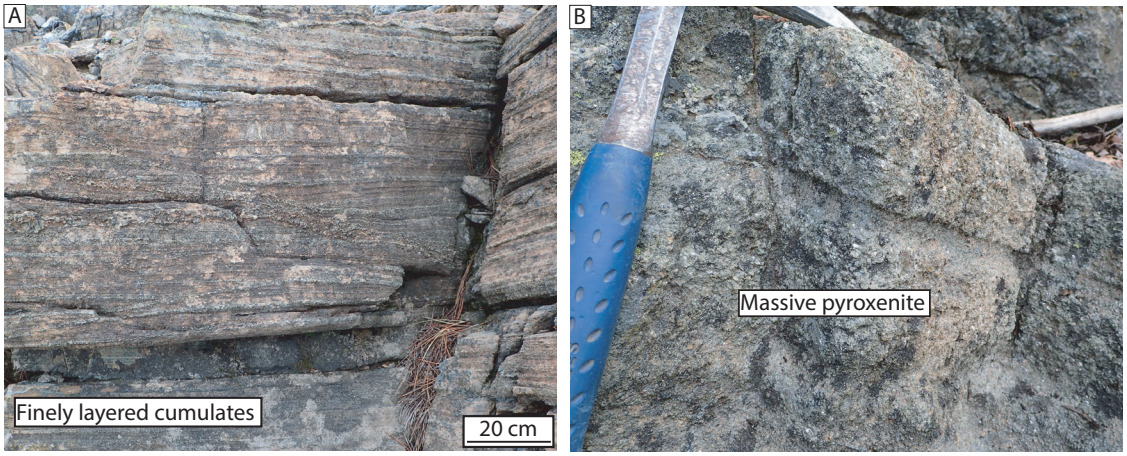

Figure 1. Field pictures of (A) the finely layered cumulates displaying the characteristic high-frequency layering and (B) Massive clinopyroxenites with significantly less olivine-rich layers.

olivine-rich and pyroxene-rich layers (Fig. 1B). Up-section, the frequency of olivine-rich layers decreases gradually until massive clinopyroxenites outcrop (Fig 1B).

Spatial orientations of the pyroxene and olivine grains in this cumulate suite were determined using the Electron Back-Scattered Diffraction (EBSD) technique. Our data demonstrate that magmatic processes in a magma chamber can cause strong preferred crystal orientation of the mineral grains. This preferred orientation is strongly planar, as observed in the field, but the grains have a cryptic preferred orientation within that plane (Fig. 2). We interpret this to be the result of the grains settling to the base of the magma chamber, oriented in a preferred crystallographic plane and/or as the result of compaction.

From a seismic perspective, fabrics from the Bear Creek cumulates show a distinctive anisotropy unique to such pyroxenite fabrics, and thus making them potentially seismically distinguishable from '*average*' lherzolitic upper mantle.

Our results further suggest that the pre-existing magmatic fabric could influence the behaviour of cumulate rocks during later deformation, because the pre-existing fabric will result in a favourably oriented set of slip systems that could be easily activated. This emphasises the caution required when interpreting deformation conditions based on slip system activation.

This project is part of CCFS themes 2 and 3, Earth's Evolution and Earth Today, and contributes to understanding Earth's Architecture and Fluid Fluxes.

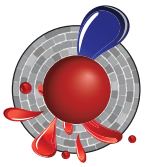

Contact: Hadrien Henry

Funded by: CCFS, Centre National de la Recherche Scientifique (CNRS), France

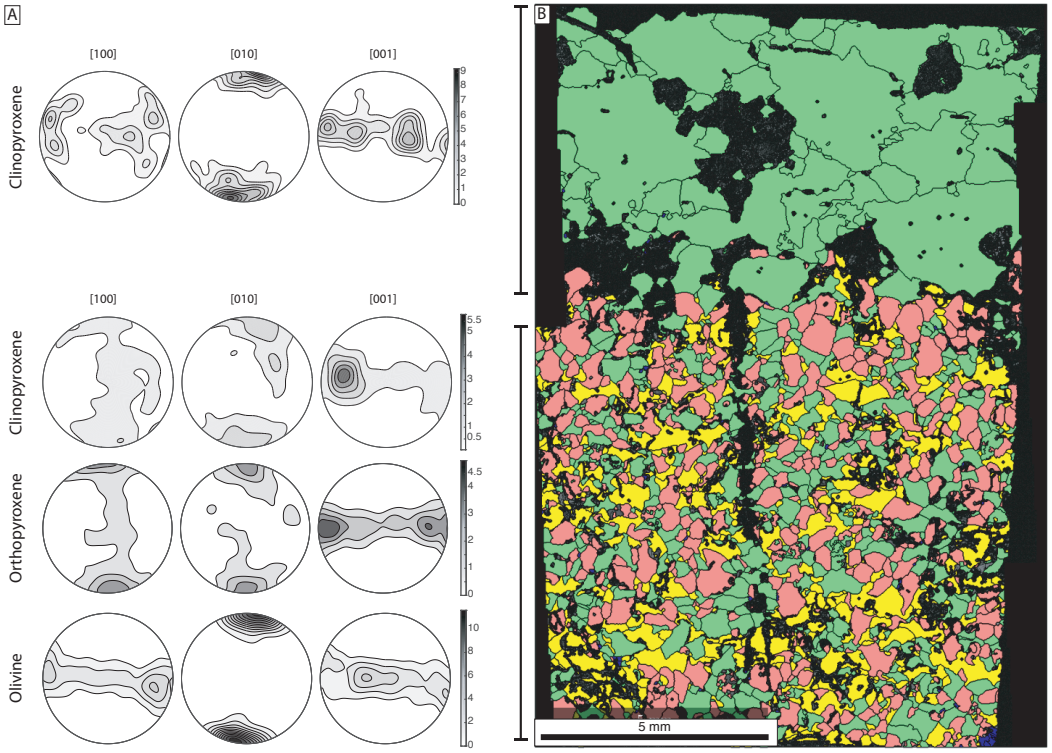

Figure 2. (A) Crystallographic preferred orientation of the rock-forming minerals along a sample where finely layered cumulates (bottom) and massive pyroxenites (top) are in contact. The strong planar feature is highlighted by the girdles formed by the [001] axis for all minerals. (B) Colour-coded map representing the distribution of the phases in the sample. Yellow codes for olivine, green for clinopyroxene and red for orthopyroxene. Black denotes non-indexed data.

Persistent ancient oceanic slab hovers in the upper mantle of western China?

Ancient oceanic slabs generally cannot be preserved in continental lithosphere for significant periods of time. Ancient subduction zones, which can provide important clues to the past tectonics, have rarely been imaged by geophysical techniques. However, the Junggar terrain (Fig. 1) appears to be an exception where a fossil oceanic slab has been well preserved since the late Paleozoic. The unique evolution history and the lack of subsequent thermal events in this region provide an undisturbed environment allowing the slab to remain until the present. Imaging the detailed geometry of the fossil subduction system in this region helps us to investigate the past tectonic process.

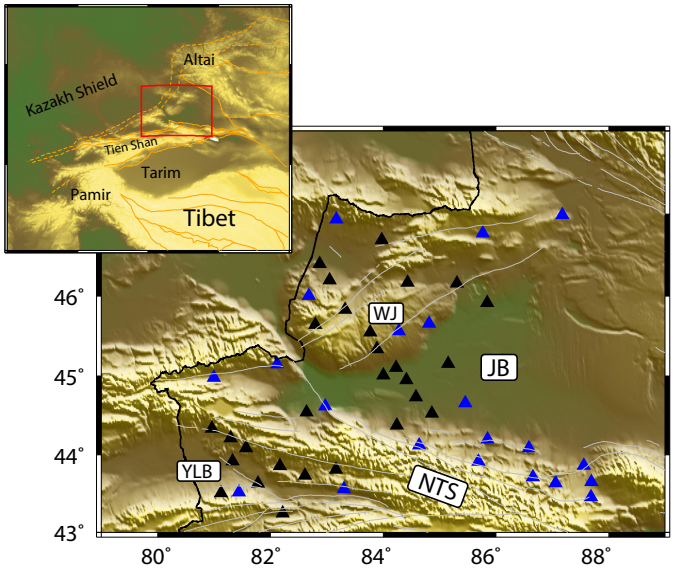

Figure 1. Location of the study region (red rectangle) and the broadband seismic stations. Blue triangles represent the 21 fixed stations from CEA and black triangles indicate the 28 deployed stations. Tectonic blocks around study region are outlined by orange lines, grey solid lines are the location of major faults, and the black solid line is the Chinese national border. WJ: West Junggar (or the Zaire mountains); YLB: Yili Block; JB: Junggar Basin or Dzungarian Basin; NTS: Chinese northern Tien Shan (or the Borohoro Mountains).

We deployed a seismic array occupying a larger spatial region across the Junggar Terrane (Fig. 1), in order to generate a high-resolution velocity model for the crust and upper mantle. This array consisted of 28 newly deployed broadband seismic stations from July 2016 to September 2017 along with 21 permanent stations from the China Earthquake Administration (CEA) Array. Based on data from this array, shear-wave velocity (Vs) models of the crust and upper mantle in the Junggar terrane are constructed using ambient noise and teleseismic surface-wave tomography techniques. According to our Vs model (Fig. 2), the patterns of velocity anomalies in the shallow crust agree well with the geological features in the surface. A large triangular-shaped low velocity zone dominates the entire Junggar Basin, corresponding to the thick sedimentary layer within the basin (~8-9 km in the north and over 10 km in the south). For the deeper structures, inverse velocity features compared to those observed for the shallow crust, characterise the study region with high velocities occupying the entire Junggar Basin.

One vertical profile (AA') is plotted in Fig. 3 to illustrate the vertical variations of velocity structures. This profile starts at the northern foothill of Northern Tien Shan and runs northwestward through the entire Junggar Basin and to the West Junggar. This ~400 km cross-section shows several interesting features. In the upper crust, the Junggar Basin is imaged as a prominent low Vs zone, with shear velocities much lower than 3.0 km/s. The thickest part of this low velocity body occurs beneath the southern margin of the Junggar Basin. At the depths of middle to lower crust, the Vs beneath Junggar Basin increases significantly, reaching ~3.9 km/s to ~4.0 km/s in the lowermost crust. The mid/lower crust high velocities extend into the NTS in the south, and dip toward northwest with depth underneath the

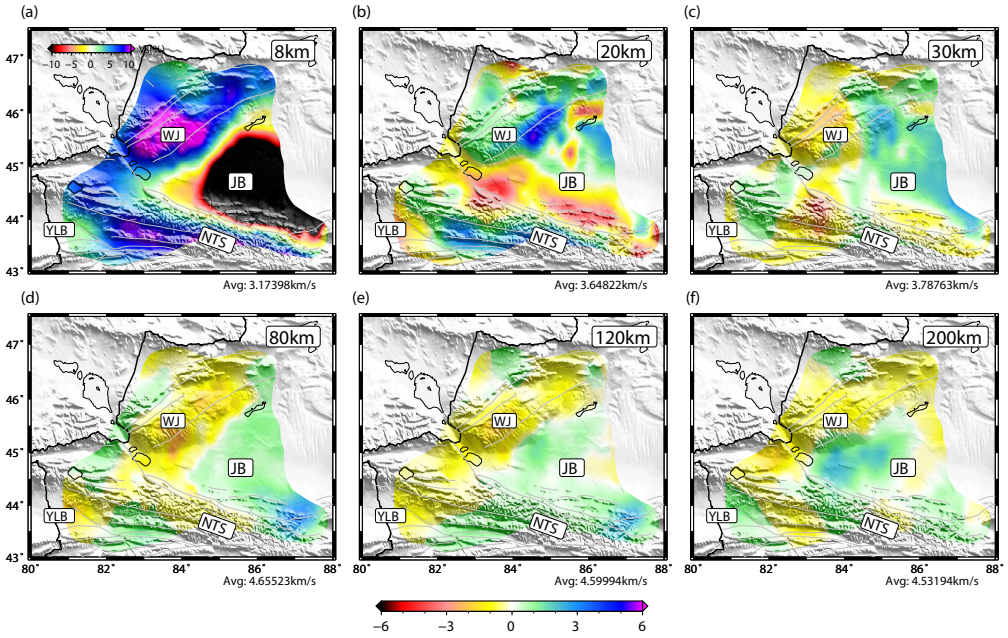

Figure 2. Vs perturbation maps at six different depths ranging from 8 km to 200 km. Colour pattern for the depth of 8 km is different from others and plotted in the top of (a). The average Vs is labelled at the bottom right of each subfigure.

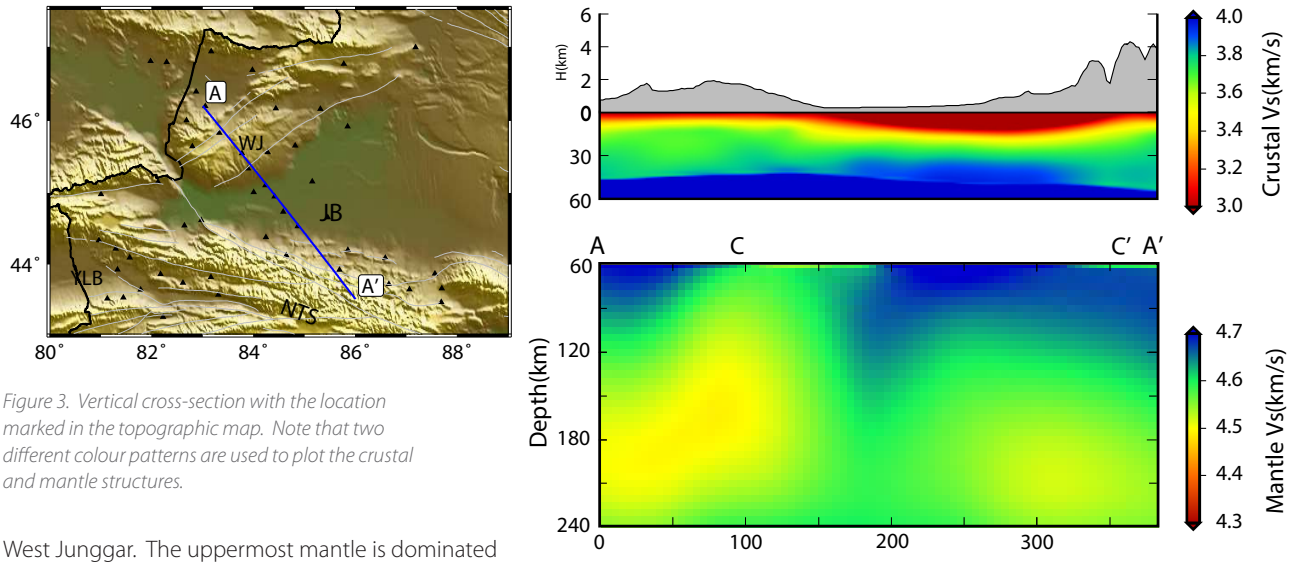

Figure 3. Vertical cross-section with the location marked in the topographic map. Note that two different colour patterns are used to plot the crustal and mantle structures.

West Junggar. The uppermost mantle is dominated by a high velocity body beneath Junggar Basin and Northern Tien Shan. The thickness of this high velocity layer is ~60 km with Vs higher than 4.65 km/s. In the margin between Junggar Basin and West Junggar, this high velocity domain slightly dips northwest, reaching a depth around 150 km. High velocity domains are also observed to the west part of West Junggar with a thickness of only ~30 km, thinner than the high velocity layer beneath the WJ and Northern Tien Shan. The uppermost mantle of West Junggar is dominated by a relatively low velocity anomaly extending to a depth of ~240 km.

Integration with previous magnetotelluric, geochemical, geochronological and geomagnetic studies in the Junggar Basin as the remnant of the ancient oceanic lithosphere beneath the ancient Junggar Ocean. In the AA′ profile beneath West Junggar, the upper mantle high velocity body slightly dips northwestward and then terminates at a depth of around 150 km. According to the geometry of the high velocity body, it is reasonable to deduce the polarity of the late Paleozoic subduction in the West Junggar is northwest. We then compare the current geothermal model in the Junggar region with the predicted oceanic slab half-space cooling model. The perfect match between them supports the hypothesis that the high velocity beneath the Junggar Basin at the lower crust and upper mantle depths, reflects the trapped Late Paleozoic oceanic slab. This finding is significant since very few ancient oceanic slabs can be preserved and imaged in continental collision zones worldwide. Also, the imaged, well-preserved subduction system in the Junggar terrane provides vital constraints for the past tectonics in this region.

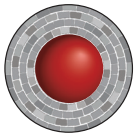

This project is part of CCFS theme 3, Earth Today, and contributes to understanding Earth's Architecture.

Contacts: Shucheng Wu, Yingjie Yang

Funded by: CCFS Flagship Program 3, NSFC 41530319, iMQRES 44659946

Vanadium melts reflect Earth's most reducing conditions

The pyroclastic ejecta of Cretaceous intraplate basaltic volcanoes exposed on Mt Carmel, in northern Israel, provide snapshots of unusual melt-fluid systems, sampled at different stages of their evolution. Now they have provided evidence of the most reducing conditions ever found on Earth, reflecting a hydrogen-dominated fluid phase.

Aggregates of skeletal corundum crystals found in the ejecta and secondary alluvial deposits contain melt pockets requiring high T (>1450-1200 °C), moderate P (ca 1 GPa) and extremely low oxygen fugacity (fO_2). Paragenetic studies (*Griffin et al., 2018, 2019a; Xiong et al., 2017*) suggest that the crystallisation of skeletal corundum and low fO_2 reflect the interaction of originally mafic magmas with $CH_4 + H_2$ at high fluid/melt ratios.

As the magmas were progressively reduced, the original silicate melts were depleted in Fe and Si by the exsolution of immiscible Fe-Ti-C-silicide melts that crystallised moissanite (SiC) and khamrabaevite (TiC). Still lower fO_2 is witnessed by inclusions of Ti^{2+}-bearing phases (TiB_2, TiN, TiC, TiO). The silicide melts efficiently scavenged Fe and heavier transition elements; no Fe-Ni-Co-bearing oxides or silicates are found in the melt pockets. The assemblages described here thus formed from residual melts, enriched in Ca, Al and minor elements (REE, Zr, Ti, V, Mn, Sc).

Hibonite ($CaAl_{12}O_{19}$) first appears together with corundum, Mg-Al spinel, TiN, Fe-Ti silicides, TiC and glass (see *Research highlight p. 309*). Coarser-grained (to cm-sized crystals) intergrowths of hibonite, grossite and spinel also occur as grains up to 2.5 cm across in placers of the Kishon and Yoqneam Rivers that drain

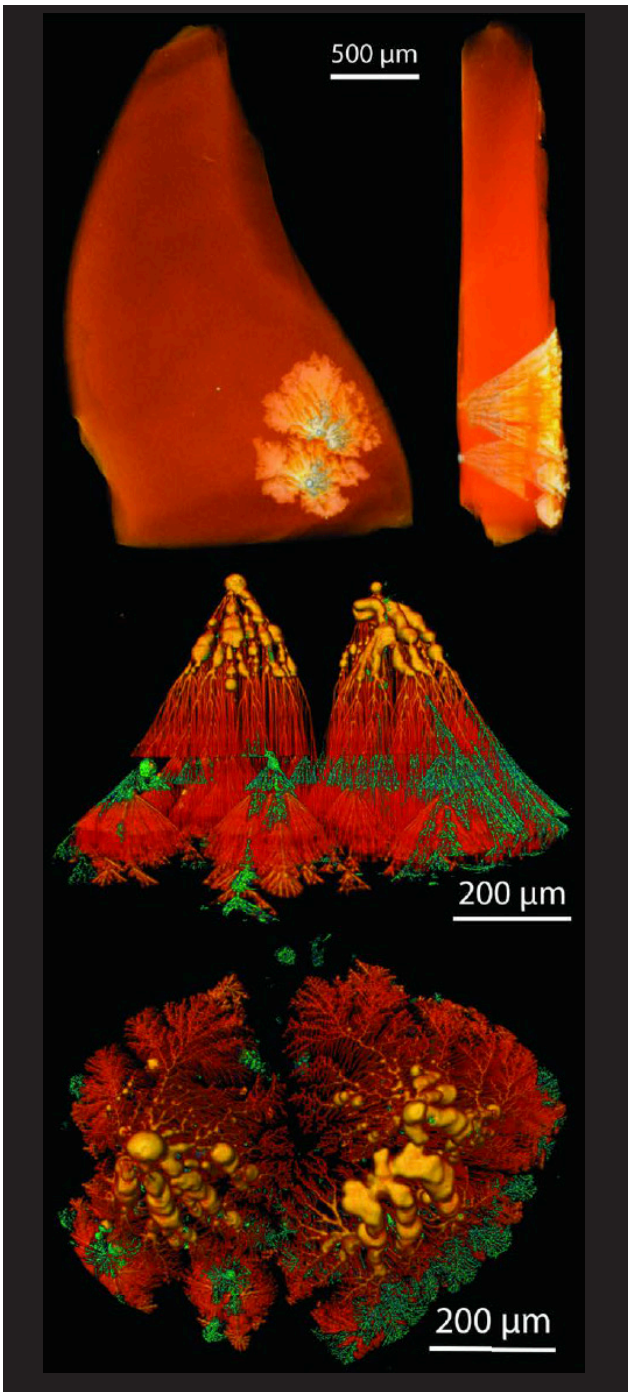

Figure 1. 3D-µCT images of dendritic native V in hibonite. a) low-resolution image of two dendrite clusters in a hibonite grain. b) magnified view, looking parallel to (0001) face; red to orange, vanadium; green, open cavities; (c) view from starting point, toward crystal face along c axis. Tendrils radiate off irregular clumps of V^0. Some consist of a series of joined balls that extend toward the crystal surface, then sprout into 3-D dendritic networks with clear breaks and restarts at intermediate crystal planes. The patterns suggest nucleation of V melts on the surface of growing crystals. Cover image.

Mt Carmel. They suggest that hibonite-bearing melts like those trapped in the corundum aggregates evolved even further beneath some volcanic centres.

In these xenoliths, native vanadium (V^0) and V-Al alloys occur mainly as spheroidal to amoeboid balls up to mm size in hibonite crystals. More commonly, V^0 forms droplets on (0001) planes, or rods normal to (0001) that commonly are necked down to produce linear trains of droplets. The inclusions are zonally distributed in some crystals.

Rare V^0 inclusions develop (Fig. 1) into *'dense branching structures'* (*Goldenfeld, 1989*). These grow roughly parallel with the c-axis of the host hibonite crystal, and each filament terminates in a single dendritic crystal. Clusters of fine branches terminate at planes parallel to (0001), suggesting a pause in the growth of the hibonite crystal. Some branches continued to grow when crystal growth resumed, but new droplets of V^0 also nucleated on the new crystal plane and grew independently of the older branches. In the example shown in Figure 1, this stop-start process occurred at least four times. 3D-µCT images (scan QR code, inside cover) show that the outer parts of many filaments are *'empty'*, even where they terminate well below the present crystal face.

The structures shown in Figures 1 and 2 are best explained by the nucleation of drops of molten vanadium on the faces of oxide crystals exposed to the silicate melt. These drops attracted more V^0 as the crystal grew, producing larger and elongated (sometimes hollow) inclusions. The formation of dense branching structures reflects diffusion-controlled interface motion, such as the growth of a crystal into a fluid, under conditions of mild to strong supercooling.

The melting point of vanadium is >1900 °C - so how could V^0 melts be present in this relatively low-T system? The answer lies in the reducing conditions. The fO_2 required for the presence of V^0 ($\leq\Delta$IW -9) implies a hydrogen-dominated environment, equivalent to the early solar nebula (*Grossman et al., 2008*). Analyses of hibonite grains have revealed hydrogen concentrations up to 0.5 wt%, suggesting that the '*voids*' are filled with H_2, and grains of VH_2 (the first natural metal hydride) occur among the V^0 balls (*Bindi et al., 2019*). In a hydrogen atmosphere, the melting point of vanadium can be lowered by >1000°C as H_2 dissolves in the melt, only to be expelled during solidification. We suggest that these hollow tubes and voids reflect the exsolution of H_2 from the solidifying V^0 melts in the inner parts of the structures, leading to the remelting and expulsion of V^0 in the outer parts, before the next layer of hibonite nucleated, and perhaps to production of the observed VH_2 phase.

The assemblages from Mt Carmel are interpreted to have crystallised late in the pre-eruption evolution of fO_2 in magma-fluid systems, ultimately leading to the most reducing conditions found on Earth, with free hydrogen as a volatile phase. The observed abundance of carbon in the assemblages suggests an important role for CH_4 in this process, and high fluid/rock ratios (Fig. 2). At Mt Carmel, such conditions existed for at least 10 m.y. and over an area of ca 150 km^2, in the uppermost part of a thin mantle lithosphere. This suggests the derivation of abundant $CH_4 \pm H_2$ fluids from the deeper mantle. We suggest that the sublithospheric mantle beneath this area was metal-saturated (i.e. fO_2 = IW), such that any C-O-H fluid issuing from it was

dominated by $CH_4 \pm H_2$. This conclusion has implications for understanding melting and metasomatic processes in the mantle. See *CCFS publications #1209 and 1160.*

This project is part of CCFS theme 2, Earth's Evolution, and contributes to understanding Earth's Architecture and Fluid Fluxes.

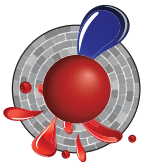

Contact: Bill Griffin
Funded by: CCFS Flagship program 1

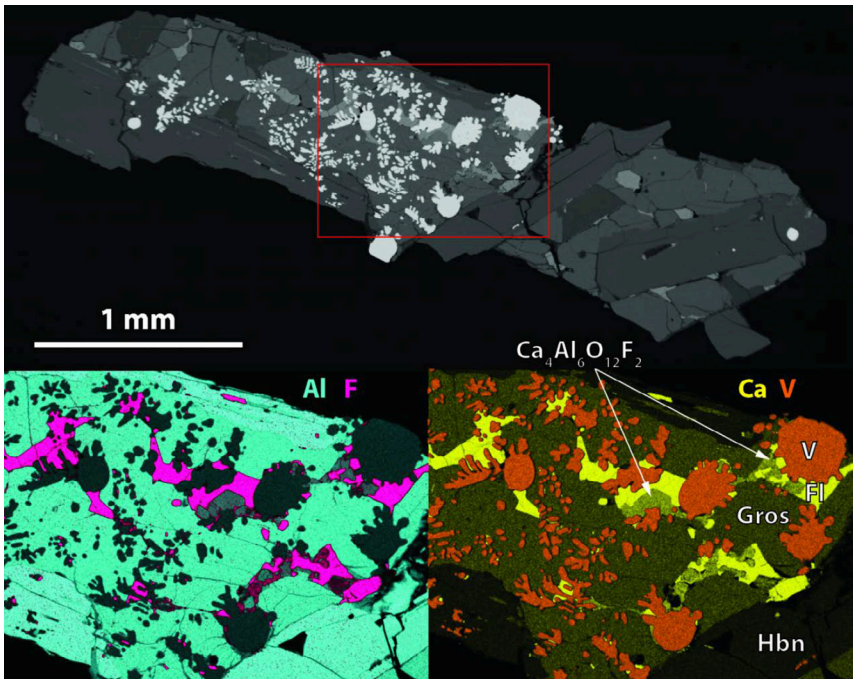

Figure 2. High-Al (mean 15 wt%) V balls in nest of grossulite between hibonite laths, with outlines suggesting they were fluid when trapped.

Revealing Gold Pathways in El Indio Belt, Chile-Argentina

This project to understand the structural architecture in one of the most highly Au-endowed provinces of the Andes Cordillera: the young Miocene El Indio Belt, is undertaken in collaboration with (and supported by) Barrick Exploration.

The El Indio Belt is a 150 km^2 metallogenic camp located in the Chilean-Argentinean Andes Cordillera. It hosts a resource of >45 Moz Au mostly in world-class Miocene Au-Ag epithermal deposits (Pascua-Lama, Veladero, El Indio-Tambo District and the most recent discovery Alturas). It provides a natural laboratory to study the trans-lithospheric architecture that acts as the pathway for magma/fluids/gold, and also the geodynamic evolution of the structural domains related to metallogenic events.

The project includes the reinterpretation of geophysical datasets (mainly aeromagnetometry, gravity and seismics) integrated with petrophysical data acquisition, as well as six months of surface structural mapping, all aimed to reveal the architecture of the El Indio Belt. This is coupled with cutting-edge techniques for zircon isotopic analyses, which have revealed the ancient nature of the El Indio Belt (see *CCFS Annual Report, 2017 p. 265*) and the magmatic evolution associated with the metallogenic processes.

Recent re-interpretation of the geophysical datasets has confirmed that the El Indio Belt is affected by a series of NW-SE- and NE-SW -ending structures

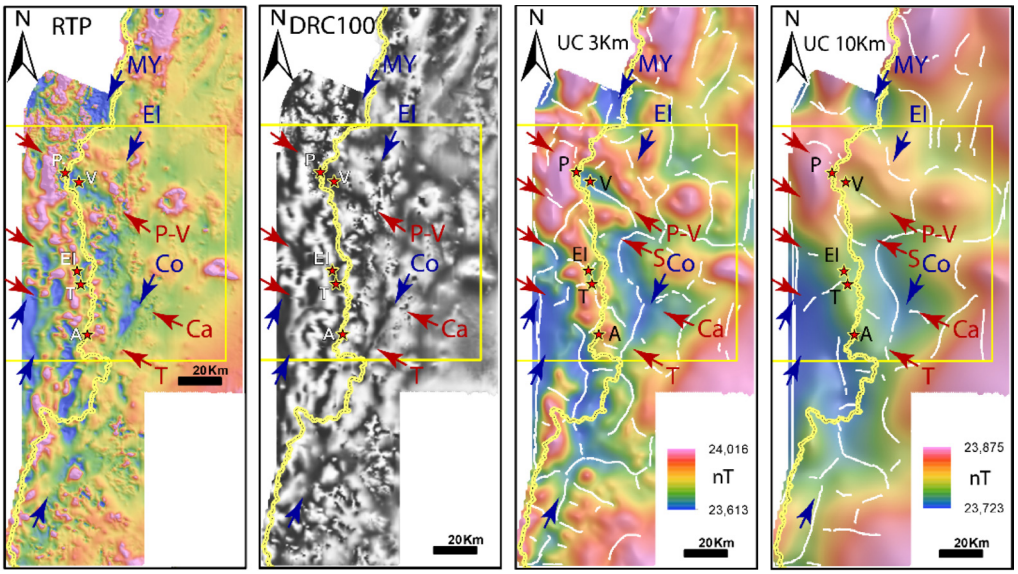

Figure 1. Different processing and enhancements on the EIB aeromagnetic surveys. RTP: Reduced to the pole. DRC: Dynamic Range Compression. UC: Upward continuation. Arrows show aeromagnetic lineaments, red correspond to NW-SE (P-V: Pascua-Veladero, S: Sancarron, Ca: Campana, T: Trapiche) and blue to NE-SW (MY: Molino Yaco, El: El Indio, Co: Colangüil). Yellow box indicates EIB working area. Stars correspond to Au-Ag HS epithermal deposits within the belt (P: Pascua, V: Veladero, El: El Indio, T: Tambo, A: Alturas). Yellow line is the international Chile-Argentina border.

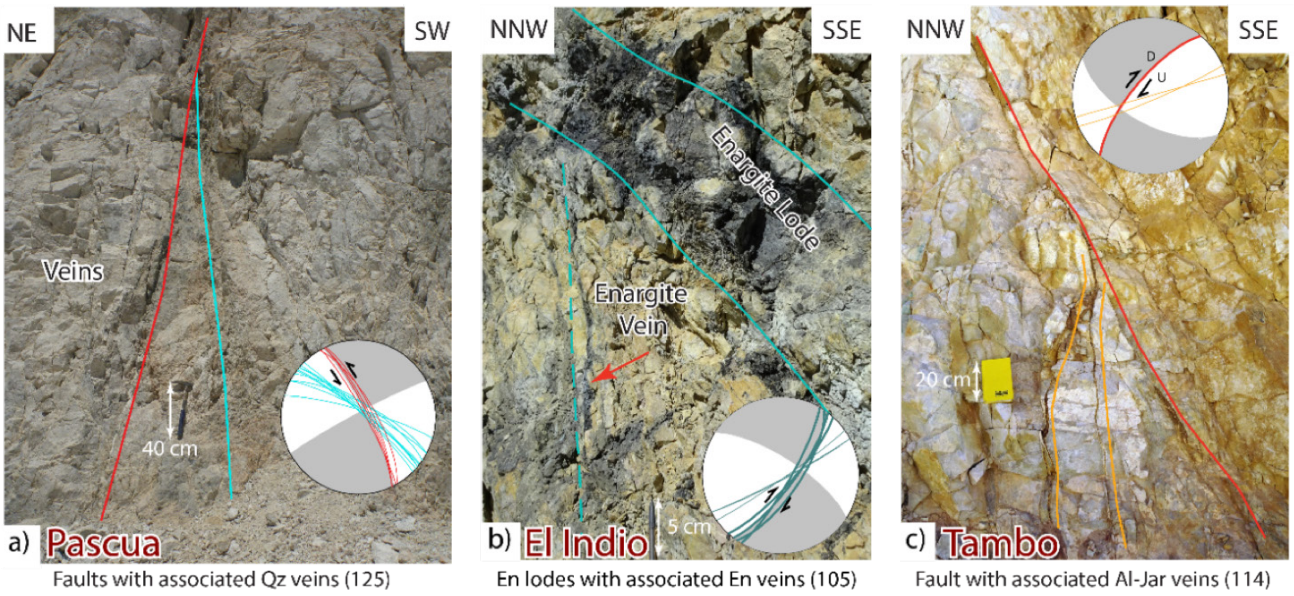

Figure 2. Altered and mineralised structures with kinematic indicators (tension veins and fractures) within the Miocene El Indio Belt (EIB), main Au-Ag deposits and minor prospects: a) Pascua fault with quartz (Qz) veins, b) El Indio enargite (En) lodes and veinlets, c) Tambo fault with alunite-jarosite (Al-Jar) veins. Numbers in parenthesis indicate station number.

that cross-cut the main N-S Andean trend. The Au-Ag deposits are located along the magmatic axis at the intersection of these structures, some of which penetrate at least 10 km into the crust (Fig. 1).

This deep-seated architecture has been corroborated in the field, where the NW-SE and NE-SW structures dominate in the areas within and around the deposits. These structures are '*old*', traceable in the pre-Cenozoic basement, and may have originated during the Upper Triassic when they focused the intrusion of mafic dyke swarms trending in the same orientations. They have indeed persisted from the basement to the overlying Miocene magmatic arc which produced the epithermal Au-Ag deposits. The structural orientations obtained for the mineralising events recorded around the El Indio Belt indicate that these deposits follow those trends. Furthermore, they originated mainly in a strike-slip regime, with dextral movement occurring along the NE-SW and sinistral movement in the NW-SE structures (Fig. 2). The magmatic signature of the ore-bearing magmas, however, denotes they were originated in a compressive setting, carrying high La/Yb in whole rock (previously found by *Bissig et al., 2001, IGR, 43: 4,312-340*) as well as low εHf ('*crustal-type*' signature) associated with '*mantle-like*' $\delta^{18}O$ signatures in zircon (this project, Fig. 3). This confirms that the main metallogenic period in the El Indio Belt took place in a change from a highly compressive tectonic setting to a more strike-slip environment, as previously reported by Giambiagi et al. (*2017, Tectonics, 36, 2714-2735*).

The combination of a favourable architecture (NW-SE and NE-SW cross-arc structures), with a proper geodynamic trigger (transition from compression to strike-slip), and Au-fertile magmatic suites (possibly generated during the compression event), have all been found in the El Indio Belt. They confirm the mineral systems hypothesis in the area, and provide a valuable insight into one of the most important Au-mineralisation events within the Andes.

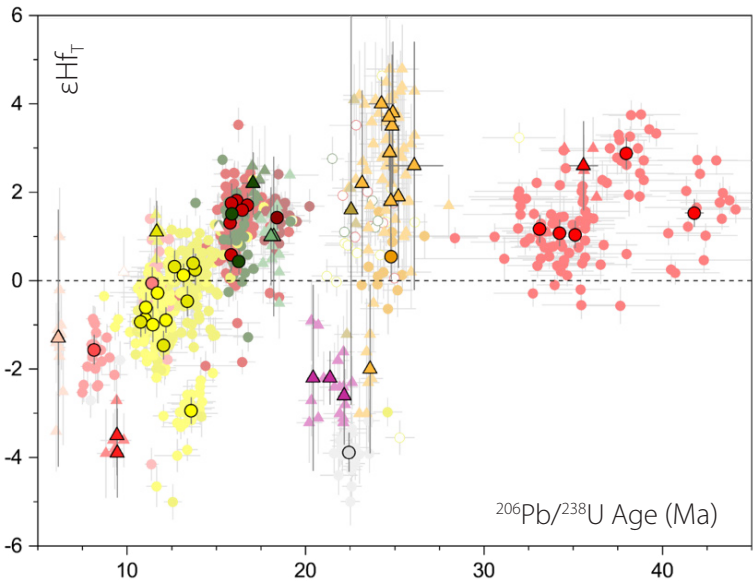

Figure 3. Age-εHf$_T$ signature for Cenozoic magmas of the EIB. *Between Eocene and Oligocene, the εHf$_T$ is relatively constant. Since ~20 Ma there is a sustained decrease in εHf$_T$ values towards lower values in the syn-mineralisation magmas (red stars), during the Upper Miocene compression.*

This project is part of CCFS theme 2, Earth's Evolution, and contributes to understanding Earth's Architecture.

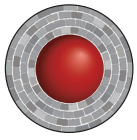

Contacts: Constanza Jara, Marco Fiorentini

Funded by: Barrick Exploration, CCFS Flagship Program 2

Oblique crustal structural grain in the crust beneath the Phanerozoic Perth Basin

The Perth Basin is a nearly 1300 km long north-northwest trending basin, located along the south-western margin of the Australian continent, formed during the breakup of Australia and Greater India in the Permian to Early Cretaceous. Extension and trans-tension deformations during the rifting processes led to the formation of deep (up to 15 km) rift basins and structurally complex crustal structure.

A 40-station 250 km long passive source linear array was deployed in 2017, to better define whole-crustal structural elements. The array is centred on the Perth Metropolitan region and is sub-parallel to the major structural boundary, the Darling fault, that separates the Yilgarn craton in the east. The array employed both 20-s and 120-s Trillium Compact sensors, operating variously from 6 months to a year to provide continuous recordings suitable for crustal receiver function and ambient noise analyses.

Here we present the crustal shear wave velocity model which was derived by applying a transdimensional inversion technique (*Bodin et al., JGR 2012*) to the dispersion group velocity dataset extracted using ambient noise (e.g. *Yang et al., JGR 2008*).

The technique treats the number of velocity layers as a free parameter (i.e. transdimensional), and therefore can recover high-resolution layered velocity variations in the crust (e.g. see *Yuan and Boding, Tectonics 2018, CCFS Contribution #1181*).

In the modelling area, the first 10-km of the crust is mostly covered by the thick Phanerozoic basin. This is consistent with previous active source reflection profiles that show 10-12 km basin thickness south of Perth. At 15 km depth, however, two relatively high-velocity crustal structures may be recognised, separated by a NW-SE trending slow velocity zone. This trend is at a high angle to the NS-striking Darling Fault that separates the Yilgarn Craton (east) and the Perth Basin (west). The deep structural trend seems to continue further into the mid- to lower-crust, where our dataset (<28 s) quickly loses depth sensitivity.

Our results illustrate that passive-source seismology provides powerful means (in this case crustal tomographic imaging) to delineate deep crustal domains. An important finding of this study is the NW-SE trending crustal structure under cover. Intriguingly the trend is parallel to the large-scale NW-SE trending fault systems at the southwestern corner within the Yilgarn Craton. The results may shed light on the complex local tectonics and help us better understand the craton evolution along its southwest margin.

This project is part of CCFS theme 3, Earth Today, and contributes to understanding Earth's Architecture.

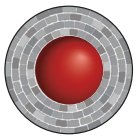

Contacts:
Dr Xiangdong Lin (Beijing Earthquake Agency - visit sponsored by CCFS (2017-2018)), Huaiyu Yuan, Mike Dentith (GSWA), Simon Johnson (GSWA), Ruth Murdie (GSWA), and Klaus Gessner
Funded by: Perth Basin Seismic (PBS) project (UWA-GSWA)

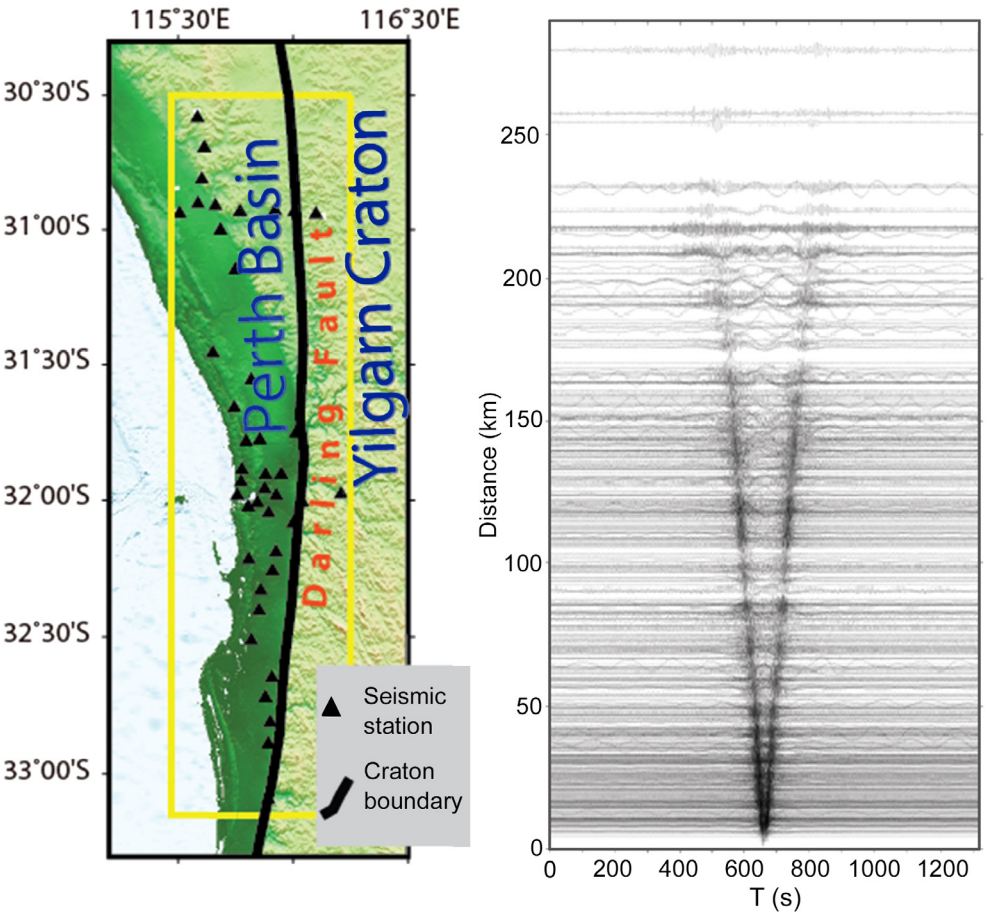

Figure 1. Perth Basin Seismic (PBS) array stations (left) and stacked cross-correlation functions (right) from ambient noise. Each trace shows equivalent surface wave signal traveling between a station pair. Craton boundary in the map is the Darling Fault separating at the surface the Yilgarn Craton (right) from the Perth Basin (left).

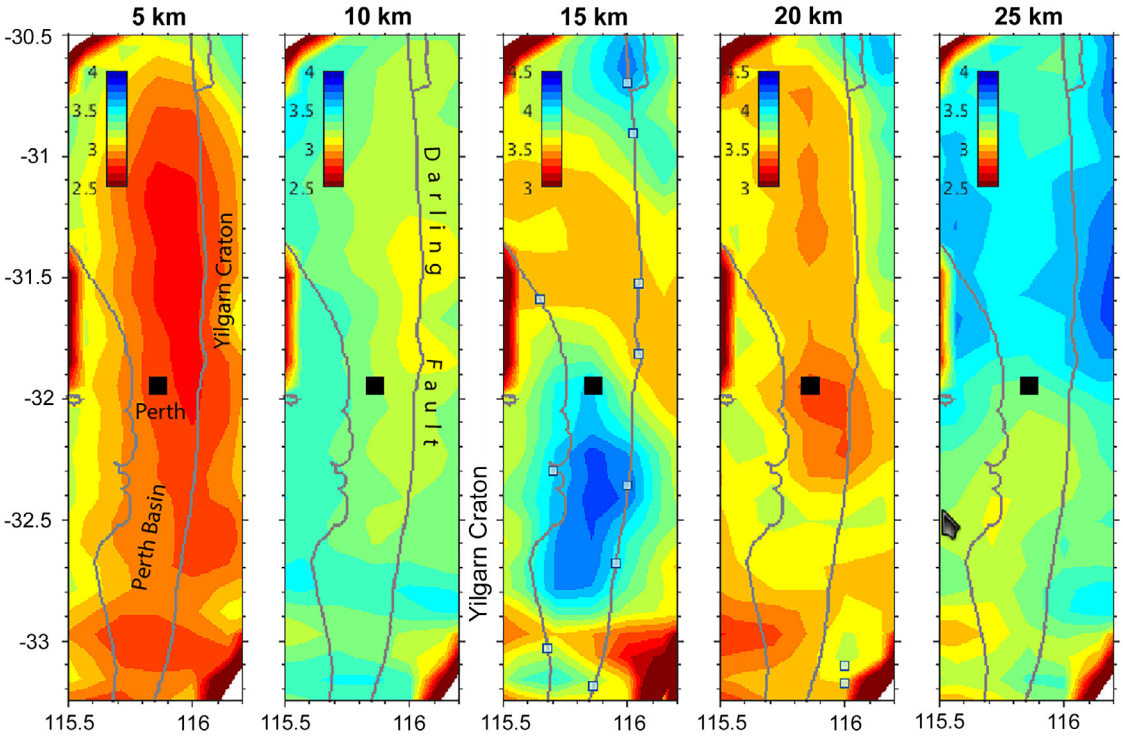

Figure 2. Map views of the shear-wave tomographic velocity model at various depths. Black square: Perth City.

A bigger tent for CAMP

New high-precision geochemical and isotopic data show that magmas related to the Central Atlantic Magmatic Province (CAMP) were emplaced at the base of the continental crust in the Ivrea Zone of northwest Italy (Fig. 1). These results significantly extend the known footprint of one of the largest examples of a large igneous province (LIP) on the planet. The La Balma-Monte Capio intrusion ranges from dunitic at the base to plagioclase-bearing pyroxenitic at the top. Zircons were extracted from two samples at different levels and dated using the chemical abrasion-isotope dilution-thermal ionisation mass spectrometry (CA-ID-TIMS) U-Pb method. The two weighted-mean $^{206}Pb/^{238}U$ ages at 200.5 ± 0.3 Ma and 200.1 ± 0.5 Ma indicate a short-lived magmatic system that fractionated in place. The timing of emplacement is different from that of all other mafic-ultramafic intrusions in the Ivrea Zone and is consistent with magmatism associated with the CAMP. We suggest that exposure in the Ivrea Zone provides a unique glimpse into the presently unknown character of LIP magmas at the base of the continental crust, where the emplacement of this intrusion was facilitated by its location at a lithospheric suture. See *CCFS publication #1188*.

This project is part of CCFS theme 2, Earth's Evolution, and contributes to understanding Earth's Architecture and Fluid Fluxes.

Contacts: Marco Fiorentini, Steve Denyszyn
Funded by: CCFS Flagship Program 2

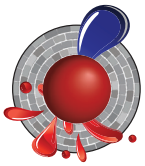

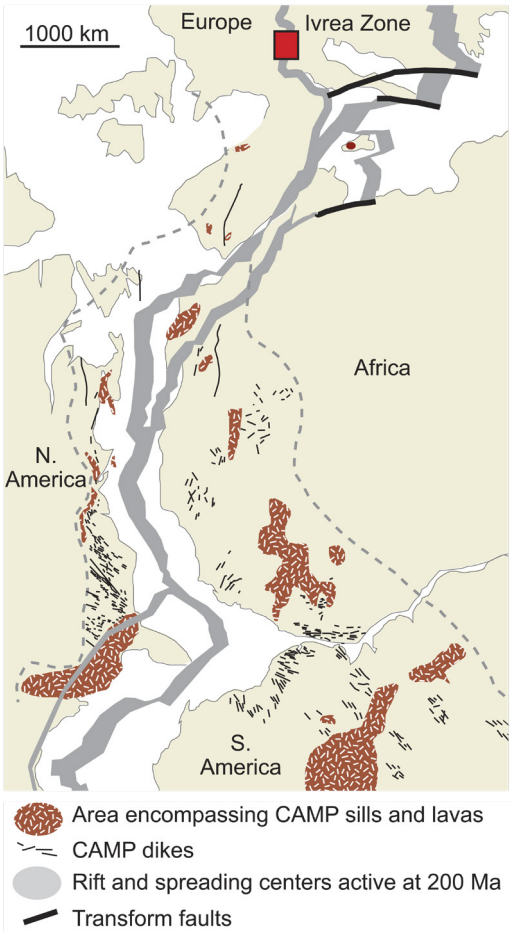

Figure 1. Reconstruction at ca. 200 Ma, with extent of intrusive and extrusive rocks of Central Atlantic Magmatic Province (CAMP) large igneous province (LIP). Star denotes location of La Balma-Monte Capio (LBMC) intrusion.

Langshan basalts record recycled Paleo-Asian oceanic materials beneath the northwest North China Craton

Crustal recycling is an important cause of mantle heterogeneity and can have significant control on basalt compositions. Recycled components from the subducted (Paleo-) Pacific slab have frequently been recognised in Cenozoic basalts from the eastern North China Craton (NCC). However, it still remains unclear if the subducted Paleo-Asian oceanic slab contributed to intraplate basalts in this Craton.

In a search of evidence for the recycled components from this slab, we have studied the Ar-Ar age, elemental and Sr-Nd-Pb isotope compositions of newly-discovered basalts from Langshan area and compiled a regional synthesis of Cenozoic alkali basalts from the northwest NCC (Fig. 1). This region is far from the Pacific domain but near the suture zone of the Paleo-Asian Ocean. With a Late Cretaceous eruption age (~89 Ma), Langshan basalts (Fig. 2) have low silica and high FeO, MgO and alkali contents, high incompatible elemental concentrations, positive Sr, Eu, Ba, Zr, Hf, Nb, Ta and negative Pb and Ti anomalies with subducted oceanic crust-like Ce/Pb, Nb/U, Rb/Sr and Ba/Rb ratios, superchondritic Zr/Hf ratios, and uniform radiogenic isotopes (εNd(t) = 2.32~2.64,

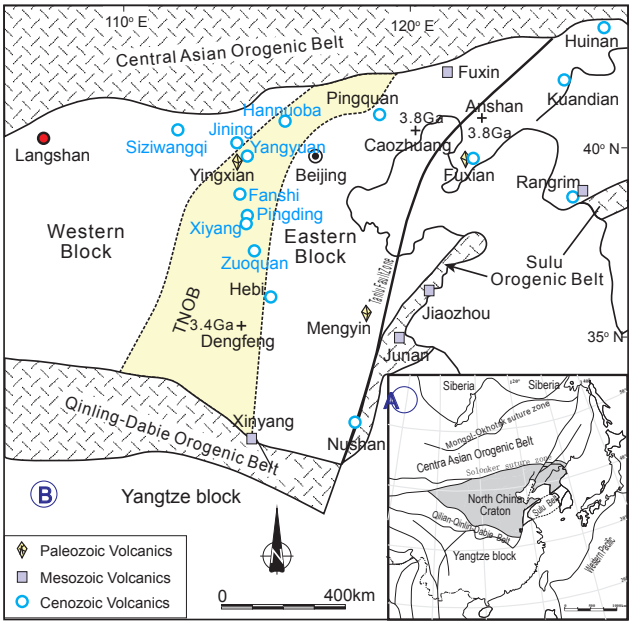

Figure 1. A) Simplified tectonic map of the North China Craton (Li et al., 2016). B) Tectonic sketch map of the NCC (Zhao et al., 2001, 2005; Kwon et al., 2009) with localities of mantle xenolith-bearing volcanics (Zheng et al., 2007; Yang et al., 2010; Xu et al., 2017; Dai et al., 2018). This craton is divided into eastern and western blocks with the Trans-North Orogenic belt in between according to Zhao et al. (2001). The compiled Cenozoic basalts in this study are from Siziwangqi and Jining in the western NCC, and Hannuoba, Yangyuan, Fanshi, Pingding, Xiyang, and Zuoquan in the TNOB. The term "northwest NCC" in this study refers to these localities and Langshan.

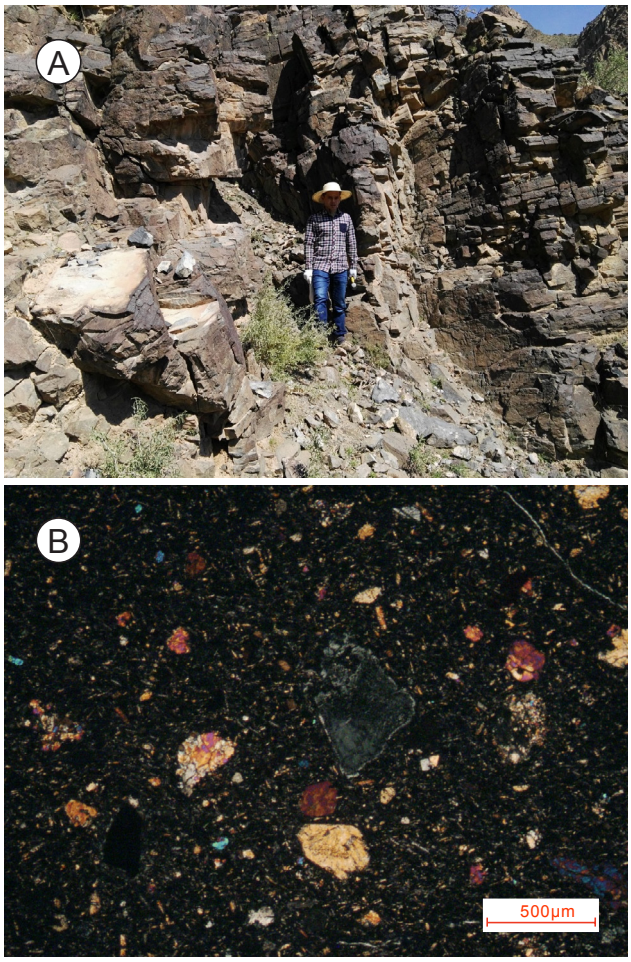

Figure 2. Field outcrop A) and microphotograph B) of the Langshan basalts. The man in A) is ~ 1.7 metres tall.

$^{87}Sr/^{86}Sr_i$ = 0.703796~0.704340, $^{206}Pb/^{204}Pb_i$ = 18.601~18.828, $^{207}Pb/^{204}Pb_i$ = 15.489~15.536, $^{208}Pb/^{204}Pb_i$ = 38.527~39.000). These compositional characteristics are shared by the compiled Cenozoic alkali basalts from northwest NCC.

The low silica and high MgO, FeO and alkali contents together with the positive Zr, Hf, Nb, Ta and negative Ti anomalies probably reflect silica-deficient garnet pyroxenites in their mantle source. The high Nb/U and Ce/Pb ratios and unradiogenic isotopes together with P-T estimates (P = ~2.5 GPa, T_p = 1300~1450 °C) collectively suggest an asthenosphere origin. The positive Sr, Eu, Ba, Zr, Hf, Nb, Ta anomalies and the canonical indices (high Ce/Pb, Nb/U and low Rb/Sr and Ba/Rb ratios) indicate the involvement of a subducted oceanic igneous slab. Considering 1) the particular tectonic setting of the study region (Fig. 1), 2) the inferred northward increase of silica-deficient pyroxenite in the mantle source of Cenozoic alkali basalts, 3) the evidence for strong lithospheric modification beneath the northwest NCC induced by slab-derived components, and 4) the longevity of subducted slab in convection mantle, the subducted Paleo-Asian oceanic materials could have introduced ubiquitous mantle heterogeneity beneath the northwest NCC and have played a significant role in generation of the Late

Cretaceous to Cenozoic intraplate alkali basalts there.

This project is part of CCFS theme 2, Earth's Evolution, and contributes to understanding Earth's Architecture and Fluid Fluxes.

Contacts: Hong-Kun Dai, Jian-Ping Zheng, Sue.

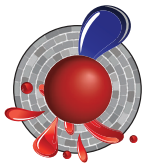

O'Reilly, Bill Griffin, Qing Xiong, Rong Xu, Yu-Ping Su, Xian-Quan Ping, Fu-Kun Chen

Funded by: National Key R&D Program of China (2016YFC0600403), NSFC (41520104003), CSC (201706415070), iMQRES, Outstanding Doctoral Dissertation of CUG, IGCP 622

Carmeltazite - The latest Mt Carmel sensation

One of the most common exotic phases in the ultra-reduced assemblages from Mt Carmel (see *Research Highlights pp. 309, 315, 329*) has now been recognised as a new mineral by the International Mineralogical Association. *Carmeltazite* has the idealised chemical formula $ZrAl_2Ti_4O_{11}$ and is named after the locality (Mt Carmel) and its dominant elements (Titanium, Aluminium and Zirconium).

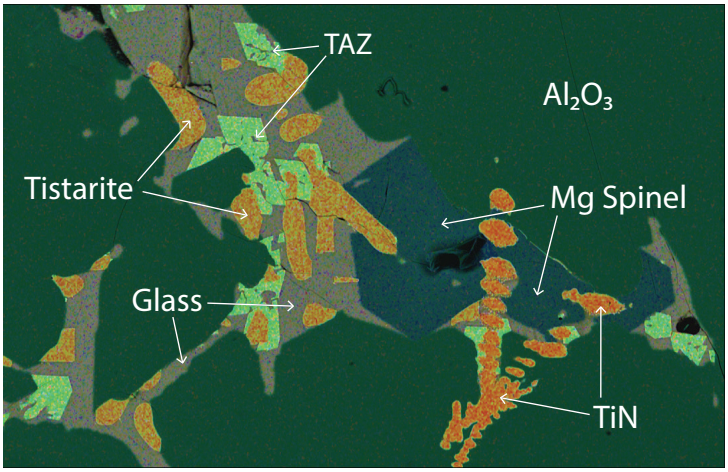

Figure 1. A typical melt pocket trapped in skeletal crystals of corundum (Al_2O_3). Euhedral crystals of carmeltazite (TAZ) surround locally resorbed crystals of tistarite (Ti_2O_3), set in a CaO-Al_2O_3-MgO glass. Image is 400 microns wide.

These unique mineral assemblages crystallised in melt pockets trapped in aggregates of corundum crystals (Carmel Sapphire™) found among the ejecta of small Cretaceous pyroclastic volcanoes on Mt Carmel. They are believed to have been crystallising in magma pockets trapped near the crust-mantle boundary, when they were entrained in basalts erupting from much deeper levels.

Carmeltazite typically crystallises after the earliest phases, tistarite (Ti_2O_3), TiN and spinel ($(Mg,Ti)(Al,Ti)_2O_3$) (Fig. 1). The assemblage is unusual on Earth, because Ti is present as Ti^{3+} instead of the common valence, Ti^{4+}, reflecting conditions in which oxygen fugacity lies 6 log units below the Iron-Wustite buffer ($fO_2 = \Delta IW$ -6) (see *Research Highlights pp. 309, 329*). Carmeltazite appears to crystallise at the expense of tistarite, but since both phases contain Ti^{3+}, there is no obvious change in fO_2 driving the crystallisation sequence. It is more likely that the crystallisation of tistarite and spinel served to further concentrate Zr to a critical level, leading to precipitation of carmeltazite.

Single-crystal X-ray diffraction studies were performed at Universita degli studi di Firenze, Italy, on fragments extracted from polished sections. The structure (Fig. 2) is orthorhombic, with space group Pnma. The refined X-ray formula can be written as $(Ti^{3+}_{3.75}\ Al_{1.94}\ Zr_{0.85}\ Mg_{0.22}\ Si_{0.14}\ Sc_{0.04}\ Ca_{0.03}\ Y_{0.02}\ Hf_{0.01})_{\Sigma=7.00}\ O_{11}$, in excellent agreement with that obtained from electron microprobe: $(Ti^{3+}_{3.60}\ Al_{1.89}\ Zr_{1.04}\ Mg_{0.24}\ Si_{0.13}\ Sc_{0.06}\ Ca_{0.05}\ Y_{0.02}\ Hf_{0.01})_{\Sigma=7.04}\ O_{11}$.

Over 130 different phases have thus far been recognised in the Carmel Sapphire™ provided by Shefa Yamim Ltd for this research. Most of these have not been found previously in Nature, and they will continue to provide insights into the evolution of this remarkable mineral system. See *CCFS publications #830 and 1229*.

This project is part of CCFS theme 2, Earth's Evolution, and contributes to understanding Earth's Fluid Fluxes.

Contacts: Bill Griffin, Luca Bind (University of Florence), Fernando Camara (University of Milan)

Funded by: CCFS

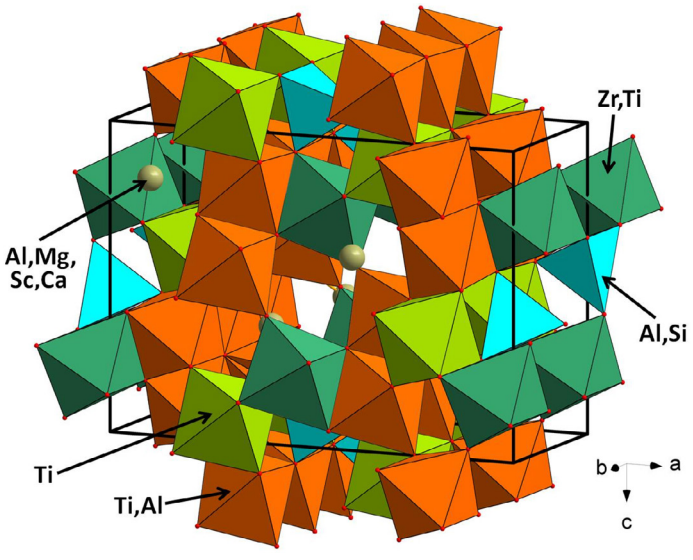

Figure 2. Structure of carmeltazite.

Putting the spin on Australia: First Precambrian palaeomagnetic data from the Mawson Craton (East Antarctica)

East Antarctica has been a key piece in Precambrian palaeogeographic reconstructions. As one of the most effective methods used to reconstruct supercontinents, palaeomagnetic studies have encountered great difficulties in East Antarctica due to inaccessibility, limited outcrops, and difficulties in conducting fieldwork in the Antarctic. There are only two Precambrian palaeomagnetic poles available from East Antarctica: the ca. 1130 Ma "BM" pole from the Borgmassif intrusions in Dronning Maud Land and the ca. 1100 Ma "CL" pole from Coats Land (Fig. 1). However, it is likely that neither the Dronning Maud Land nor Coats Land terranes joined the Mawson Craton until the final assembly of Gondwana at ca 520 Ma. Therefore, the BM and CL poles cannot be used to constrain the location of the Mawson Craton in pre-530 Ma palaeogeographic reconstructions. Additionally, for much of Precambrian time, the Mawson Craton is thought to have been a part of Australia, connected to the Gawler craton, which also lacks reliable pre-800 Ma palaeomagnetic constraints. We conducted a pilot palaeomagnetic study on the ca 1134 Ma Bunger Hills dykes of the Mawson Craton. Of the six dykes sampled, three gave meaningful results providing the first well-dated Precambrian palaeopole at 40.5°S, 150.1°E (A95 = 20°) for the Mawson Craton.

Although it is generally agreed that Precambrian Australia (west of the Tasman line; Fig. 1) is composed of three Archaean to Palaeoproterozoic cratons (the West, North, and South Australian cratons - WAC, NAC and SAC respectively), when and how the present-day configuration took form is still a matter of debate. In an effort to reconcile some mismatching coeval poles of

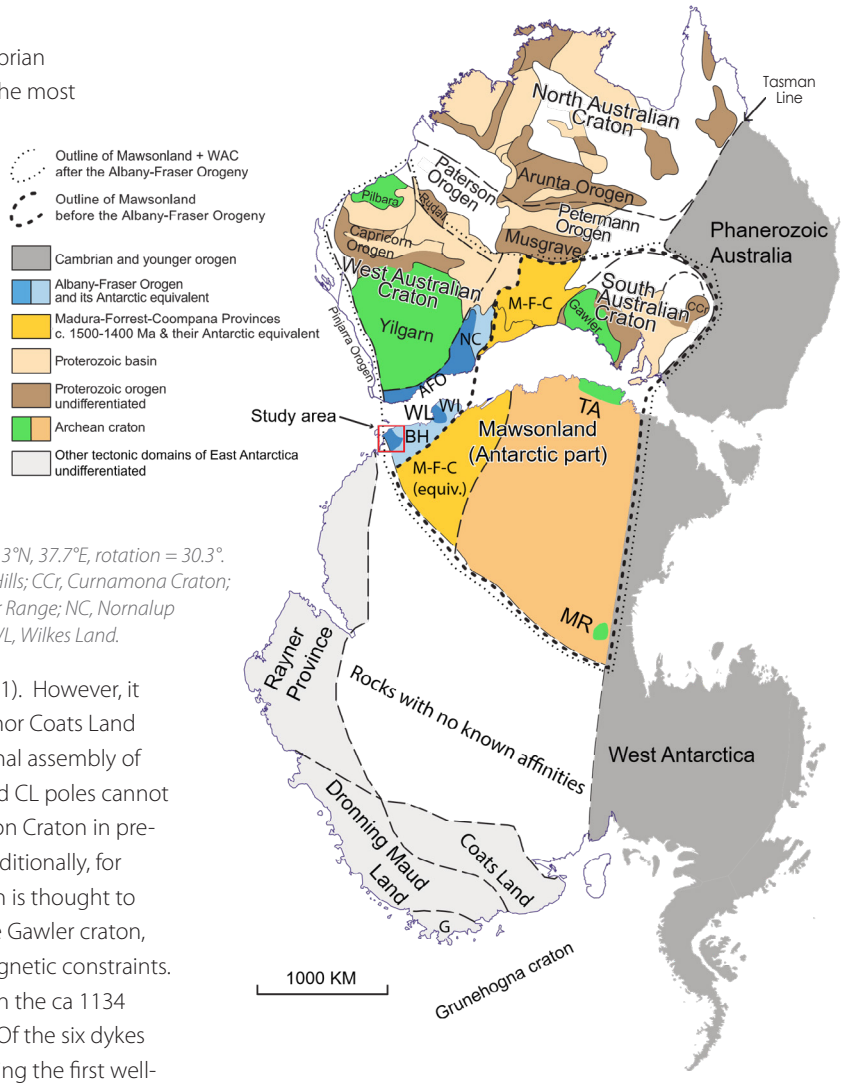

Figure 1. Tectonic map of Australia and Antarctica in a Gondwana configuration. Antarctica is rotated to Australia coordinates using a Euler pole7 at 1.3°N, 37.7°E, rotation = 30.3°. Abbreviations: AFO, Albany-Fraser Orogen; BH, Bunger Hills; CCr, Curnamona Craton; M-F-C, Madura-Forrest-Coompana Provinces; MR, Miller Range; NC, Nornalup Complex; TA, Terre Adélie craton; WI, Windmill Islands; WL, Wilkes Land.

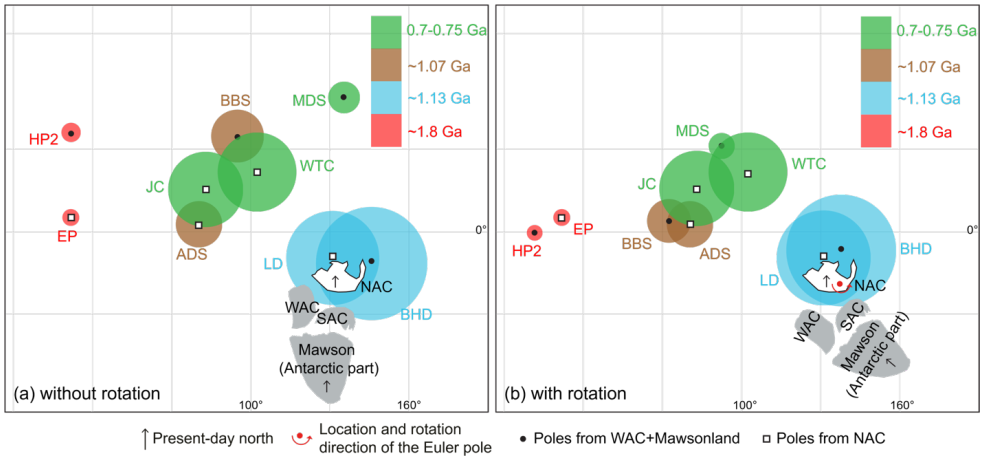

Figure 2. Four groups of coeval poles from the WAC + Mawson and NAC plotted in Mercator projection. Mawson (Antarctic Part) rotated to SAC in its Gondwana configuration using a Euler pole at 1.3°N, 37.7°E, rotation = 30.3°. (a) Australia in its present-day configuration; (b) WAC + SAC + Mawson rotated to NAC about a Euler pole at 20°S, 135°E, rotation = 40°. Poles from the NAC: EP - Elgee-Pentecost Formations; LD - Lakeview dolerite; ADS - Alcurra dykes and sills; JC - Johnny's Creek Member (Bitter Springs Formation); WTC - Walsh Tillite Cap Dolomite. Poles from WAC + SAC + Mawson: HP2 - Hamersley Overprint 2; BHD - Bunger Hills dykes; BBS - Bangemall Basin sills; MDS - Mundine Well dyke.

Australia, Li & Evans (2011, Geology) proposed that WAC + SAC (with Mawson) rotated ~40° relative to the NAC at ca 650-550 Ma to form the Precambrian part of Australia as we know it today (Fig. 1). Our new pole and the coeval Lakeview Dolerite pole make up another group of coeval poles from the NAC and WAC + SAC + Mawson, respectively, with which the intraplate rotation may be further tested. With the rotation applied, the area of overlap of the 95% confidence circles of the BHD and LD poles increases (Fig. 2), which constitutes a positive test for the relative rotation between WAC + SAC (+ Mawson) and NAC. The vast intracratonic rotation hypothesis not only reconciles discrepant coeval palaeopoles, but also provides a mechanism for the enigmatic Paterson and Petermann orogenies that account for significant mineralisation such as the massive Telfer Au deposit.

This project is part of CCFS theme 2, Earth's Evolution, and contributes to understanding Earth's Architecture.

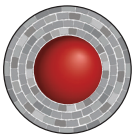

Contacts: Yebo Liu, Zheng-Xiang Li, Earth Dynamic Research Group, Curtin University
Funded by: ARC Laureate Fellowship (ZX Li), Australian Antarctic Science Project 4191

Sorting the wheat from the chaff in the source of Australian lamproites

Olivine is the main mineral in the Earth's upper mantle, but because of its very simple composition, it has been considered historically as being of little use as a tracer of mantle and magmatic processes. This has changed with recent advances in the analysis of minor and trace elements, which have made the low amounts of trace elements accessible by high-precision electron microprobe and Laser ablation-ICP-MS.

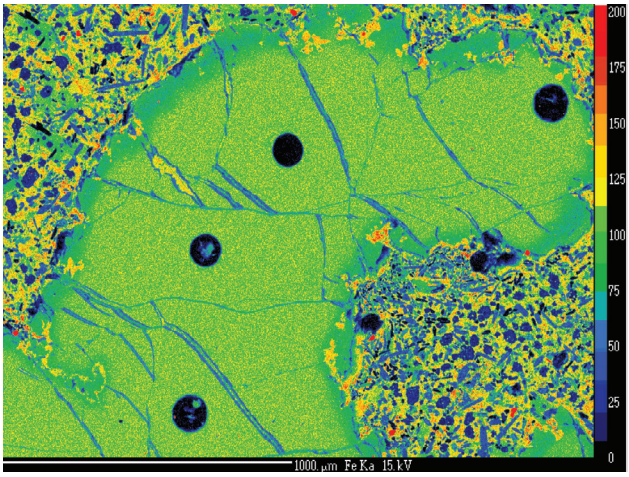

Figure 1. Main petrographic features of West Kimberley lamproite olivines. X-ray map (Fe Ka at 15 kV) of olivine xenocryst showing narrow reversely zoned rim.

As a result, minor and trace elements in olivine are used increasingly to identify the rocks present in the source, namely whether these are dominantly peridotite or contain significant amounts of other rocks, including material recycled into the mantle at subduction zones. Kimberlites are magmatic rocks with the deepest known origins (200-250 km), and a healthy debate has arisen recently as to how much of the olivine carried by them crystallised from the kimberlite melt and how much is entrained mantle material that may be related to part of the source.

The next deepest magmatic rocks are diamond-bearing lamproites, of which those of the Kimberley region of Western Australia (the name match is merely coincidental) are prime examples. We have investigated olivines from these lamproites and find many to have homogeneous cores with rims that crystallised at a late stage from the rising melt (Fig. 1). Phenocrysts - crystals that form directly from the melt - commonly show increasing Ca and Mn and decreasing Cr and Ni towards the rims. Xenocrysts - the entrained mantle material - are overgrown by rims of similar composition to all other rims. These rims are magnesium-rich (Mg# 91-92) and have compositions that show they formed from melts with 22-24 wt% MgO.

The xenocrysts are pieces of garnet peridotites from 115-190 km depth and show consistent variations in minor and trace element abundances with temperature and pressure of origin. The olivines from the deepest levels of the lithosphere have more Na, Al, P, Ti and Zr than shallower ones. This indicates that the mantle is more strongly depleted at shallower depths by previous melt loss, presumably in the first half of Earth history. However, this does not mean that this has always been the case: it is more likely that these shallower upper mantle levels escaped re-enrichment by later melts from below because the rising melts get stuck in the lower lithosphere.

Previous Pb isotope studies have shown that subducted sedimentary material was probably involved in the source of the West Kimberley lamproites. Our earlier studies of Mediterranean magmatic rocks showed that the presence of crustal material in the source is often flagged by the enrichment of lithium in olivines. However, we found that olivines in the West Kimberley lamproites are not enriched in lithium, which is thought to be due to its later loss in fluids or by diffusion during the long time period (around 2 billion years) between subduction and production of the lamproites in the relatively recent past. See *CCFS publications #1248.*

This project is part of CCFS theme 2, Earth's Evolution, and contributes to understanding Earth's Fluid Fluxes.

Contact: Stephen Foley
Funded by: CCFS Flagship Program 1

Reaction of subducted marine sediment with peridotite produces saline fluid inclusions in diamonds

Diamonds form in Earth's mantle at depths of greater than 150 km and are carried to the surface by volatile-rich magmas, the so-called kimberlites. Most of the non-gem quality and some gem-quality diamonds carry inclusions of other minerals or fluid phases. Commonly, the fluid inclusions are highly saline and carbonate-rich. They were previously explained as a proof of the recycling of sea-water to Earth's mantle within marine sediments and oceanic crust. However, the mechanism of their transport into the mantle remained unresolved.

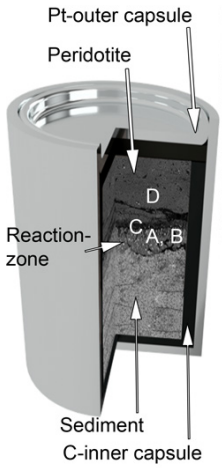

In this study, we melted oceanic sediment and reacted it with dunite in a 2-layer arrangement (Fig. 1) at pressures corresponding to depths of 90-180 km, where the sediment layer recrystallised to garnet and clinopyroxene (Fig. 1, A and B). The experiments also produced a reaction zone between the two rock types; in experiments at pressures at and above 4 GPa these reaction zones contain Na-K chlorides (Fig. 1, A, C, and D, Fig. 2). Most of the analysed chlorides contain 5-15 wt% Na and 30-45 wt% K, with K/Na ratios between 2 and 9 (Fig. 3).

In contrast, all reaction experiments at 3 GPa and the higher-temperature experiment at 4 GPa/1100 °C, as well as a sediment-melting experiment at 4 GPa/1000 °C are devoid of chlorides. In these experiments, potassium and sodium are contained in phengite, Mg-rich mica (phlogopite), and melt (Fig. 1, B, E, and F).

The crystallisation of Na-K chlorides is induced by the reducing conditions in the inner graphite capsule and a shift in fluid species which consumes H_2O following the reactions:

(1) $CH_4 + H_2O = 3H_2 + CO$ and (2) $2CO = C + CO_2$ (the CCO buffer).

Any oxygen fugacity (fO_2) equal to or below CCO will lead to chloride precipitation from an oversaturated solution: $Na/K^+(aq) + Cl^-(aq) = (Na,K)Cl$. Since the dehydration of the fluid (reaction (1)) is only observed in reaction experiments at >3 GPa, the sequence leading to chloride precipitation has to be as follows: (1) melting of the sediment and reaction with dunite, (2) total consumption of the melt phase by anhydrous phases (garnet and pyroxene) which drives all H_2O into a fluid phase, and (3) dehydration of the fluid by reaction

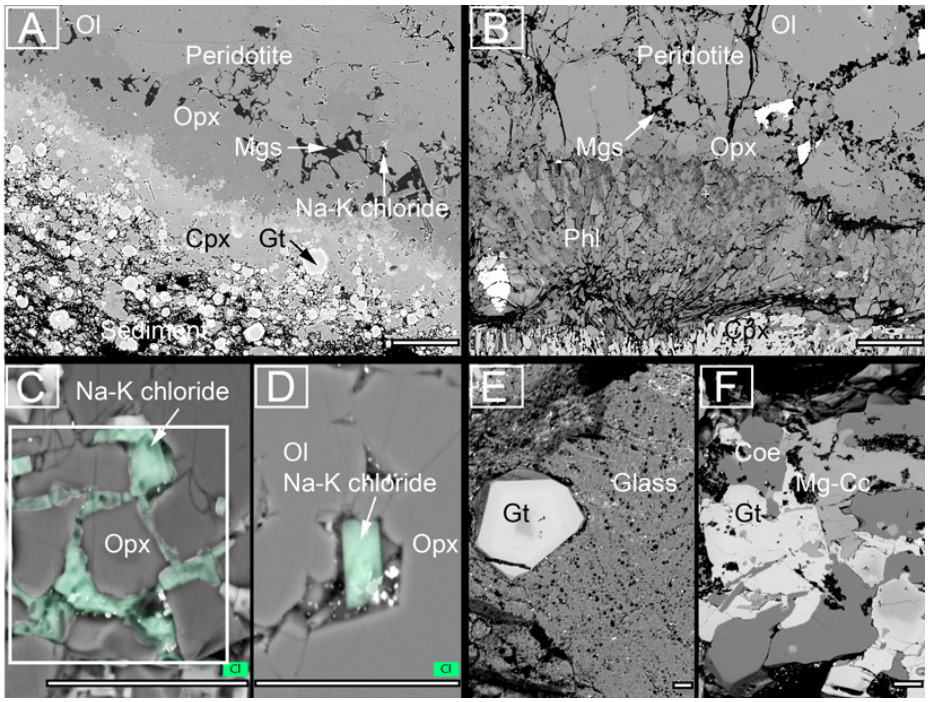

Figure 1. Backscattered electron images of experimental charges. Locations of images A-D from sediment-peridotite reaction experiments are schematically shown in capsule on left. A, C, D: reaction experiments at 5 GPa/1000 ºC with superimposed EDX maps of chlorine (green in C, D). The sediment half of two-layer experiments recrystallised to garnet and clinopyroxene, whereas orthopyroxene, magnesite (Mgs) and Na-K chlorides formed at the leading edge of the reaction zone against the peridotite. B: Peridotite layer in reaction experiment at 3 GPa/900 °C contained phlogopite behind the magnesite + orthopyroxene zone, and Na-K chlorides were absent. E, F: sediment melting experiment (no peridotite included) at 4 GPa/1000 °C showing silicate melt (E) in equilibrium with garnet, coesite, and mg-calcite shown in (F). Scale-bar in A, B = 100 µm and C, D, E, F = 20 µm.

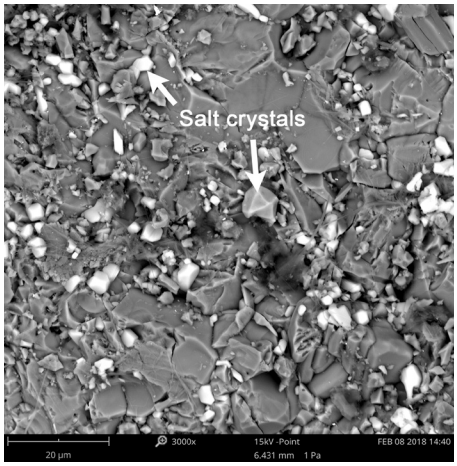

Figure 2. Secondary electron image of unpolished capsule showing idiomorphic salt crystals embedded in garnet and clinopyroxene.

(1) and precipitation of chloride from a fluid saturated in K, Na and Cl, and precipitation of carbon as graphite or diamond by reaction (2). If fO_2 is above CCO, Na-K chlorides will not precipitate, but instead be dissolved in highly saline hydrous fluids. The absence of hydrous crystalline phases such as mica in all chloride-bearing experiments is probably a direct result of the depletion of the fluid in H_2O.

Our results show that salt is a stable solid phase in the mantle below 110 km. The composition of the salts that form during the experiments are identical to the saline fluid inclusions in diamonds. We demonstrate that the processes that lead to the growth of salt and diamond crystals are driven by the recycling of oceanic sediments at subduction zones. The reaction products of our experiments also contain Mg-rich carbonates such as magnesite, which are necessary ingredients for the formation of kimberlite magmas that transport diamonds to Earth's surface.

This project is part of CCFS theme 3, Earth Today, and contributes to understanding Earth's Fluid Fluxes.

Contacts: Michael Förster, Stephen Foley, Horst Marschall, Olivier Alard, Stephan Buhre

Funded by: ARC grant FL180100134

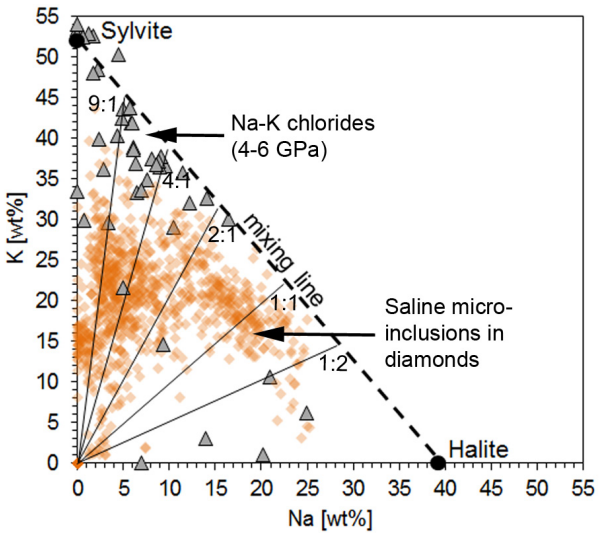

Figure 3. K/Na ratios of experimental chlorides and saline micro-inclusions in diamonds. Most saline micro-inclusions (orange diamonds) have a K/Na ratio between 1 and 9, similar to the ratios found in the experimental Na-K chlorides of this study (grey diamonds).

Pitfalls in the dating game: A cautionary tale

So when is a date not an age? This is an ongoing dilemma in U-Pb zircon geochronology and has led to a series of protocols being developed to potentially address this vexed question. But what if, even after doing all the '*correct*' things, you find that your date does not record the age of crystallisation? This is something that has been brought into clear focus in a recent paper published by our group (*Ge et al., Geology, 46, 303-306, 2018*).

But let us step back for a moment and briefly review the background to this problem; one that we have been working on since the inception of the CCFS. It had long been known that zircons in certain rocks can show reverse discordance, i.e. the result of either Pb gain or U loss (see *CCFS publication #738, Kusiak et al., PNAS, 112, 4958-4963, 2015* for a recent summary of this phenomenon). This appeared to be more prevalent when using secondary ion mass spectrometry (SIMS) techniques than either thermal ionisation mass spectrometry (TIMS) or laser ablation inductively-coupled mass spectrometry (LA-ICP-MS). During our re-investigation of high-grade gneisses from the Napier Complex in Antarctica it was evident, utilising the scanning ion-imaging capacity of a CAMECA IMS 1280, that radiogenic Pb had been locally mobilised and concentrated into micron- and nano-scale clusters. Further work using transmitted electron microscopy (TEM) established that, for the Napier Complex zircons, the Pb was concentrated into nanospheres of metallic Pb. The small size of these clusters, also established in related studies utilising atom probe tomography (APT), explains why this phenomenon was largely only detected by SIMS analyses, since the analysed volume is considerably smaller using this technique.

Mobility of Pb within zircon thus has the potential to affect the veracity of dates obtained from crystals showing this feature. However, it was generally considered that, owing to the small size of the clusters, their low concentration in areas showing this phenomenon, and their overall irregular distribution within the zircon crystals, that they were unlikely to have a major effect on the U-Pb ages obtained from such grains. It also appeared to be a feature affecting mainly high-grade gneisses that had undergone intense metamorphism and was therefore not a *'mainstream'* issue. Notwithstanding this view, since a large proportion of the oldest rocks on Earth are high-grade gneisses, it was evident that this needed to be carefully investigated.

The largest known inventory of Hadean zircons in the world resides in a conglomerate unit in the Jack Hills belt of Western Australia. Hence, this was the obvious place to see if Pb mobility was present and, if found, to test its nature and significance on the oldest ages recorded from Earth. A total of ~2500 detrital zircon grains were extracted from a sample collected at the original W74 discovery site and a large proportion of these was analysed rapidly by SIMS in order to identify Hadean crystals. From 215 identified Hadean crystals, a suite of 51 grains was finally selected as representing the most pristine grains based on multiple U-Pb SIMS dating, their lack of

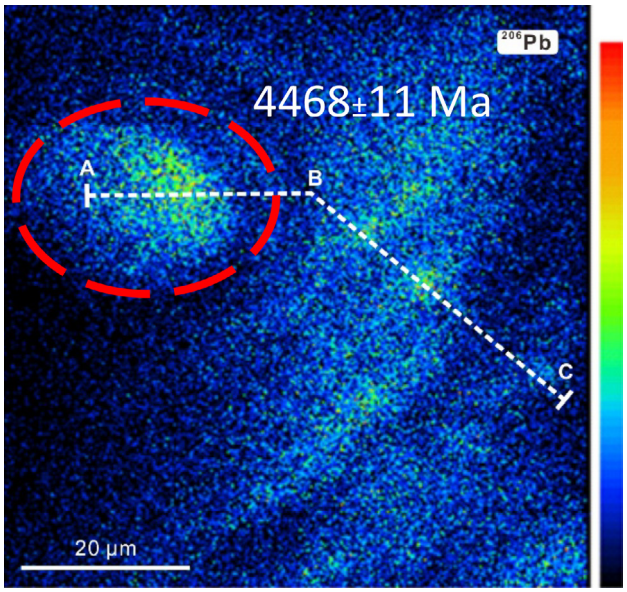

Figure 1. Site of SIMS analysis with date of 4468±11 Ma (2s), obtained on surface 2, projected onto scanning ion image of ^{206}Pb obtained on surface 5. The line A-B-C is a profile along which individual U and Pb isotopes were counted (see Ge et al., 2018 for details). The lighter areas in the figure indicate an increased Pb content.

imperfections and inclusions, and magmatic features evident in cathodoluminescence (CL) imaging.

One crystal (grain 14041) proved to be a stand-out. It recorded a concordia $^{207}Pb/^{206}Pb$ date of 4463 ± 17 Ma (2σ), the oldest zircon *'age'* ever recorded from Earth. This was established using multiple analyses and by re-polishing and re-analysing the same site. Indeed, a total of six dates revealed a range from 4486 ± 17 to 4425 ± 55 Ma (1σ): it met all the criteria for being an acceptable age for crystallisation of that zircon. However, knowing the potential for Pb mobilisation, it was imperative to test if this had affected grain 14041. Scanning ion imaging revealed a highly-significant phenomenon not previously recorded from zircon; an approximately 20-micron concentration of radiogenic Pb (Figure 1). Fortuitously, the SIMS site had been placed exactly over this circular zone of Pb-enrichment. Additional analyses and modelling established that the actual age of zircon grain 14041 was significantly younger at between 4.32 and 4.27 Ga, consistent with the 4277 ± 16 Ma (2σ) concordia age recorded by the majority of SIMS analyses in that crystal.

So what are the salutary lessons to be taken from this study? Firstly, it highlights that even concordant U-Pb ages can be spurious and up to 200 Ma older than the actual crystallisation age. This is an important finding, because dating the oldest zircons has major implications for crustal evolution on Earth, other terrestrial planets and the Moon. Secondly, it indicates the need to not only take multiple ages from the same zircon domain identified in CL images, but to also test this further by undertaking either scanning ion imaging or atom probe tomography to validate the findings. Finally, although Pb mobility has now been established in zircon in several parts of the world and in a variety of host rocks, the mechanism(s) remains elusive and is the subject of our ongoing investigations.

This project is part of CCFS theme 1, Early Earth, and contributes to understanding Fluid Fluxes.

Contact: Simon Wilde
Funded by: CCFS Flagship Program 6

A new mechanism for the formation of diamond-bearing eclogites?

The base of the cratonic lithosphere varies in its lithology: it consists mostly of highly depleted harzburgite as well as progressively modified metasomatised lherzolite, related to melt metasomatism. Melts rich in C, H and O originate from the underlying convecting mantle; they can infiltrate the cratonic lithosphere, where they are important in diamond formation and refertilisation (~150-200 km depth). These low-volume incipient melts can exist over a large temperature range (~300°C) in the upper mantle before major melting begins. They can form in reduced conditions dominated by $CH_4 + H_2O$ volatiles, or in oxidised conditions with hydrous carbonatitic affinity ($CO_2 + H_2O$).

Our experiments focused on the redox freezing of oxidised incipient melts as they encounter reduced depleted harzburgite at the bottom of the cratonic lithosphere. As oxidised incipient melts (predominantly CO_2 - H_2O) are unstable in the reduced cratonic lithosphere, reaction with surrounding mantle is inevitable and will result in the reduction of carbonate. The result is precipitation of diamond by a process known as *'redox freezing'*. Redox freezing deposits diamond in a reaction ($CO_2 = C + O_2$) that forms clinopyroxene-rich (omphacitic clinopyroxene, grossular-rich garnet) reaction zones (Fig. 1), in which mineral compositions are similar to those in eclogitic mantle xenoliths (Fig. 2).

The remaining reactive, hydrous and low-silica melt migrates further into the depleted reduced craton and consumes pyroxenes, precipitating olivine that is richer in Fe than in surrounding peridotites. The melt progressively increases its silica content by this process, becomes more 'oxidised', and finally precipitates hybrid, alkali-rich wehrlite veins with omphacitic clinopyroxenes and pyrope-rich (grospyditic) garnets similar to *'type A'* eclogites (Figure 1, 2). The formation of such eclogites has previously been explained by high-pressure metamorphic transformation of subducted oceanic crust, or by recrystallisation of high-pressure cumulates from mantle-derived melts.

In contrast, the redox freezing of alkaline, silica-undersaturated

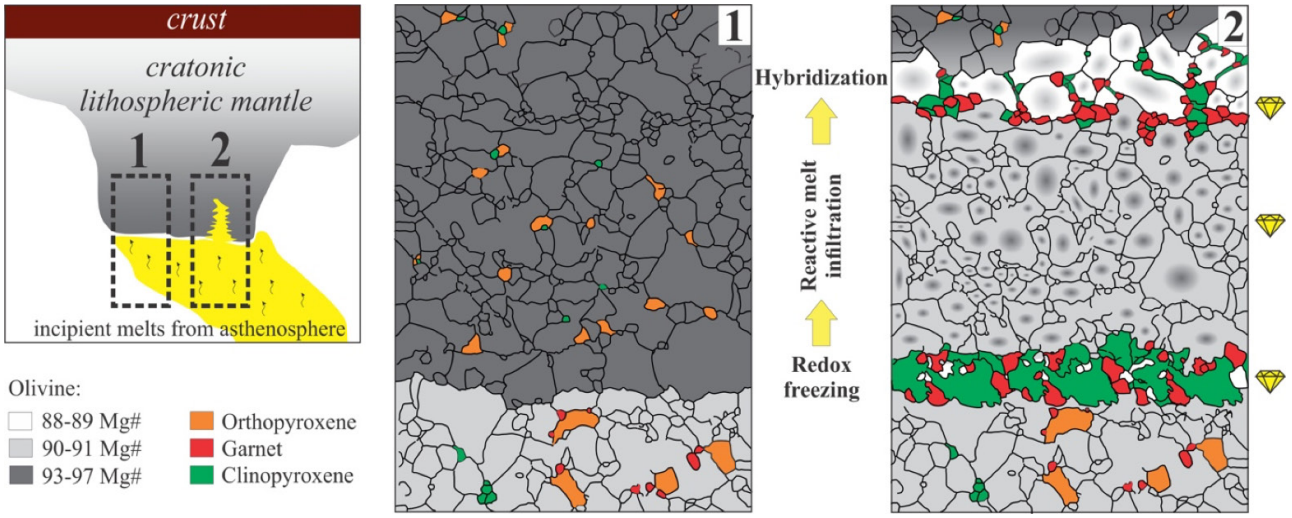

Figure 1. Hidden processes caused by redox freezing. The bottom of the depleted, reduced cratonic lithosphere is exposed to the infiltration of oxidised (CO_2-H_2O) silica-poor incipient melts (like ultramafic lamprophyre). Redox freezing forms a diamond-bearing eclogitic assembly. Remaining reactive hydrous melt infiltrates further into the cratonic lithosphere, forming dunites by consuming pyroxenes and precipitating Fe-richer olivines. The hybridisation reaction finally deposits the remaining melt as garnet-bearing wehrlite veins with adjacent Fe-rich olivines.

ultramafic lamprophyre-like incipient melts forms a diamond-bearing *'type C'* eclogitic assembly (also classically explained as subduction-related eclogites). Further hybridisation reactions precipitate the enigmatic *'type A'* wehrlite veins, usually linked to the crystallisation of more mafic (Mg-rich) melts in cratons. The redox reactions between reduced depleted cratonic rocks and infiltrating oxidised melts is more complex than previously assumed, and results not only in different types of bimineralic eclogitic rocks, but also in dunitic rocks (olivine with very minor pyroxenes) without high-degree melting of the cratonic lithosphere.

This project is part of CCFS themes 2 and 3, Earth's Evolution and Earth Today, and contributes to understanding Earth's Architecture and Fluid Fluxes.

Contact: Zsanett Pintér
Funded by: Flagship program 3

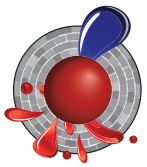

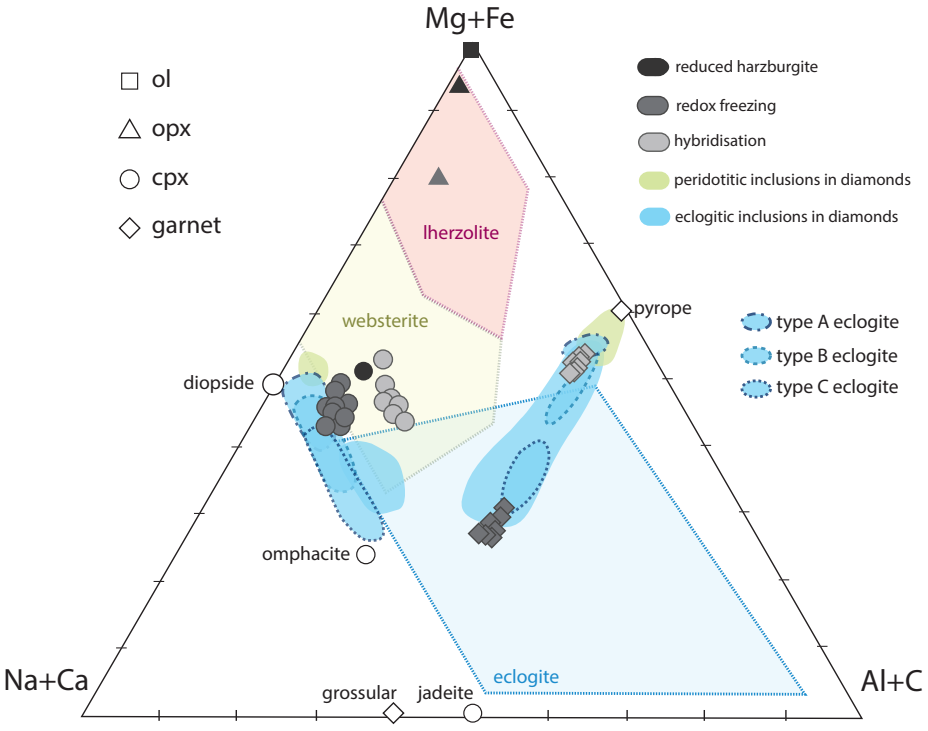

Figure 2. Ternary plot of mineral and rock compositions (defined by Mg + Fe, Ca + Na and Al + Cr) showing the complex nature of the redox freezing. Mineral end members for clinopyroxene and garnet are shown (diopside-omphacite, grossular-pyrope). Depleted, reduced harzburgite minerals are shown in black symbols. The reaction first precipitates grossular-rich garnets and omphacitic clinopyroxenes, proceeding to pyrope-rich garnets and Mg-rich omphacitic clinopyroxenes. Type A-B-C eclogites from Jacob 2004, Lithos 77, 295-316, diamond inclusions from Kiseeva et al., 2013, Geology 41 (8): 883-886.

Moissanite in the lithospheric mantle: Crystallisation from metallic melts

The redox state of Earth's mantle is a critical parameter in Earth processes, controlling the speciation of fluid and solid phases. The occurrence of moissanite (SiC) as xenocrysts in mantle-derived basaltic and kimberlitic rocks is a paradox in terms of the redox conditions of the mantle, since SiC can crystallise and remain stable only at fO_2 <ΔIW-6 (6 log units below the Iron-Wustite buffer) while the fO_2 of the lithospheric mantle is commonly considered to be much more oxidised (fO_2 ≥ΔIW-0).

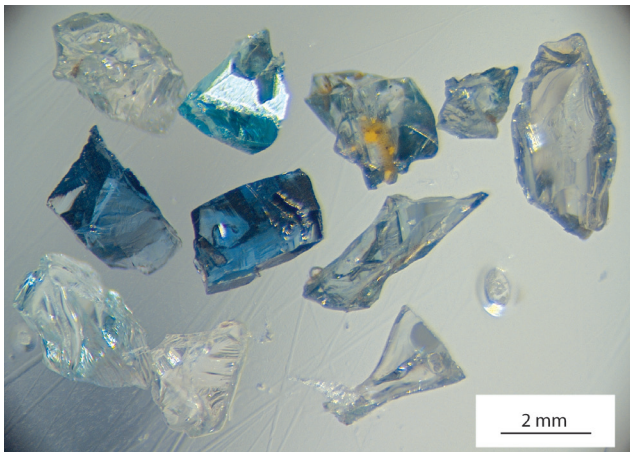

Figure 1. Moissanite grains from Mt Carmel, Israel.

Moissanite grains (Fig. 1) have been recovered from alkali basalts and related alluvial deposits at Mt Carmel, northern Israel, and from the Udachanaya and Aikhal kimberlites in Siberia. Most grains are fractured, but some partly preserve crystal faces. Grains from Mt Carmel are generally 0.5-2.0 mm in diameter, and range from black, blue, bluish-green to colourless. The Siberian samples are typically 0.4-1.0 mm in diameter; most are colourless, and some are bluish-green. 3D-CT scans of SiC grains reveal solid inclusions and elongated cavities; both tend to be aligned parallel to the c axis of the host crystal. Some cavities are associated with inclusions, but others are not. The inclusions in SiC (Fig. 2) typically have round to oval shapes, but some have straight boundaries, constrained by the crystal structure of the host grain, suggesting they were entrapped as melts. Each inclusion contains two or more phases with or without cavities. Native Si (Si^0) is usually the main phase and is always associated with one or more silicide phases, Si + Fe_3Si_7 ± $FeSi_2Ti$ ± $CaSi_2Al_2$ ± $FeSi_2Al_3$ ± $CaSi_2$. The existence of cavities suggests the former presence of a volatile phase during SiC crystallisation. These observations suggest that SiC crystallised in the lithospheric mantle from metallic melts (Si-Fe-Ti-C ± Al ± Ca), with dissolved carbon and H_2 derived from the sublithospheric mantle, which may be closely related to mantle plumes. SiC has been found in a melt pocket in corundum from Mt Carmel (see *Research Highlight, 2017*), suggesting genetic connections between SiC, corundum and their melt inclusions. Paragenetic studies of trapped melts in the associated corundum aggregates indicate that these silicide melts separated immiscibly from silicate melts following extended reduction of mafic magmas by $CH_4 + H_2$ fluids. When mafic/ultramafic magmas formed in the lithospheric mantle are fluxed with $CH_4 + H_2$ from depth, they can be progressively reduced, to a point where silicide melts become immiscible, and crystallise phases such as SiC.

The widespread occurrence of SiC in explosive volcanic rocks from different tectonic settings indicates that the delivery of $CH_4 + H_2$ from depth may commonly accompany explosive volcanism; this in turn implies that much of the sublithospheric mantle is metal-saturated, more than previously thought. The heterogeneity of redox states in the lithospheric mantle further influences geochemical reactions such as melting and geophysical properties such as seismic velocity and the viscosity of mantle rocks. The gases involved in SiC formation provide extra information on the degassing of the deep Earth.

This project is part of CCFS theme 2, Earth's Evolution, and contributes to understanding Earth's Architecture and Fluid Fluxes.

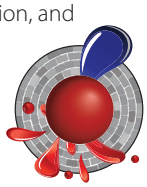

Contacts: Jin-Xiang Huang, Bill Griffin
Funded by: CCFS Flagship Program 1

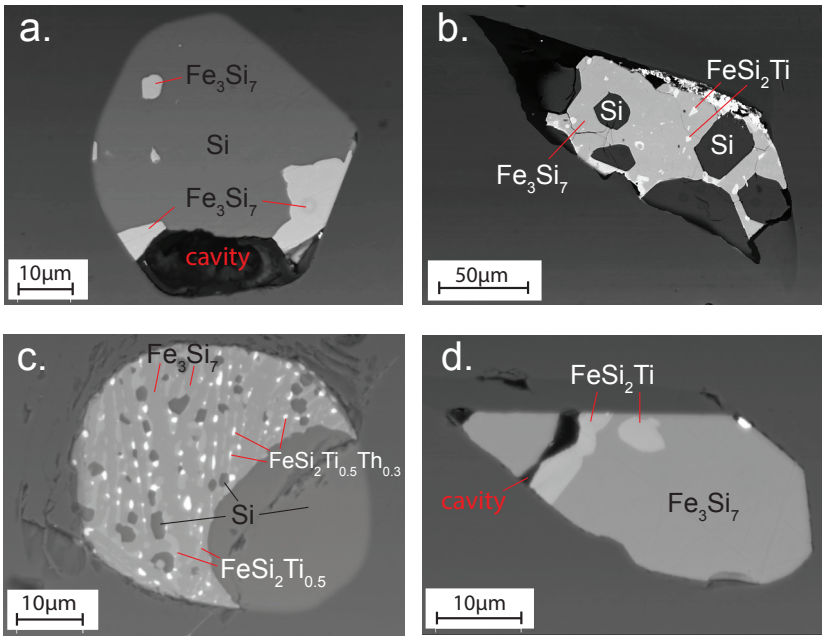

Figure 2. Back-scattered electron (BSE) images of inclusions in moissanite grains from Mount Carmel basalts and Yakutian kimberlites. a-b are Mt Carmel samples and c-d are Siberian samples.

Contact details

- **CCFS information is accessible at:**
  http://www.ccfs.mq.edu.au/

- **Contact CCFS via email at:**
  ccfs.admin@mq.edu.au

Read the full CCFS Annual Reports online:

http://ccfs.mq.edu.au/AnnualReport/

CCFS
ARC Centre of Excellence for
Core to Crust Fluid Systems
Administering Institution
Department of Earth and Planetary Sciences
Macquarie University NSW 2109
AUSTRALIA

Professor Suzanne Y. O'Reilly
Director
Phone: 61 2 9850 8362
Fax: 61 2 9850 8943
Email: sue.oreilly@mq.edu.au

Magdalene Wong-Borgefjord
Chief Operating Officer
Phone: 61 2 9850 1197
Fax: 61 2 9850 8943
Email: magdalene.wong-borgefjord@mq.edu.au

Sally-Ann Hodgekiss
Reporting and Communications Manager
Phone: 61 2 9850 6124
Fax: 61 2 9850 8943 or 6904
Email: sally-ann.hodgekiss@mq.edu.au

Australian Government
Australian Research Council

Australian Government
Australian Research Council

MACQUARIE
University

THE UNIVERSITY OF
WESTERN
AUSTRALIA

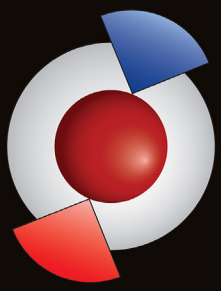

ARC Centre of Excellence for Core to Crust Fluid Systems

Delivering the fundamental science needed to sustain Australia's resource base